

Subsurface Ventilation Engineering.

Dedication: This work has been undertaken in fulfillment of a long-standing promise to my former teacher, mentor and dear friend,

Professor Frederick Baden Hinsley

The book is dedicated to his memory.

Subsurface Ventilation Engineering

Malcolm J. McPherson *
B.Sc., Ph.D., C.Eng., FIMinE, FIMM, Mem.AIME, Mem.ASHRAE

Emeritus Massey Professor of Mining Engineering and former
Associate Dean for Research and Graduate Studies,
College of Engineering,
Virginia Polytechnic Institute and State University.

Chairman, Mine Ventilation Services, Incorporated

*Formerly of the University of Nottingham, England
and the University of California, Berkeley.

Foreword to the Web version of the book.

In preparing this updated version of the textbook originally published in 1993 and under the title of Subsurface Ventilation and Environmental Engineering, the opportunity has been taken to update material that has seen significant change since the first version was written. The word 'Environmental' has been removed from the title as this term has increasingly come to refer to the surface environment. Several of the major changes are particularly applicable to developments in software that have taken place for planning the ventilation and condition of the underground environment.

The book remains a reference and text for professional engineers, researchers and teachers as well as for undergraduate and graduate students who have an interest in the planning and control of the environment in underground mines or other subsurface openings. Accordingly, the theoretical underpinnings of the subject are dealt with in some detail.

While the practical techniques of topics such as ventilation surveys or the use of computer software are included, this text is not intended specifically to be a ventilation officer's handbook. Such handbooks are best prepared within individual countries or institutions to reflect local methodologies, conditions and legislation.

In addition to printed copies, this updated text is available at no cost for downloading from the Internet address of Mine Ventilation Services, Inc. at: <http://www.mvsengineering.com/>

Contents

Preface
Acknowledgments
Unit conversion table

Chapter 1. BACKGROUND TO SUBSURFACE VENTILATION AND ENVIRONMENTAL ENGINEERING

- 1.1. Introduction
- 1.2. A brief history of mine ventilation
- 1.3. The relationships between ventilation and other subsurface systems

PART 1. Basic principles of fluid mechanics and physical thermodynamics

Chapter 2. INTRODUCTION TO FLUID MECHANICS

- 2.1. Introduction
- 2.2. Fluid pressure
- 2.3. Fluids in motion

Chapter 3. FUNDAMENTALS OF STEADY FLOW THERMODYNAMICS

- 3.1. Introduction
- 3.2. Properties of state, work and heat
- 3.3. Some basic relationships
- 3.4. Frictional flow
- 3.5. Thermodynamic diagrams

PART 2. Subsurface ventilation engineering

Chapter 4. SUBSURFACE VENTILATION SYSTEMS

- 4.1. Introduction
- 4.2. Mine systems
- 4.3. District systems
- 4.4. Auxiliary systems
- 4.5. Controlled partial recirculation
- 4.6. Underground repositories

Chapter 5. INCOMPRESSIBLE FLOW RELATIONSHIPS

- 5.1. Introduction
- 5.2. Atkinson's equation, the Square Law
- 5.3. Determination of friction factor
- 5.4. Airway resistance
- 5.5. Airpower
- A5 Shock loss factors.

Chapter 6. VENTILATION SURVEYS

- 6.1. Purpose and scope of surveys
- 6.2. Air quantity surveys
- 6.3. Pressure surveys
- 6.4. Organization of pressure-volume surveys
- 6.5. Air quality surveys

Chapter 7. VENTILATION NETWORK ANALYSIS

- 7.1. Introduction
- 7.2. Fundamentals of ventilation network analysis
- 7.3. Methods of solving ventilation networks
- 7.4. Ventilation network simulation packages

Chapter 8. MINE VENTILATION THERMODYNAMICS

- 8.1. Introduction
- 8.2. Components of the mine cycle
- 8.3. The complete mine cycle

Chapter 9. VENTILATION PLANNING

- 9.1. Systems analysis of the planning procedure
- 9.2. Establishment of the basic network
- 9.3. Airflow requirements and velocity limits
- 9.4. Planning exercises and time phases
- 9.5. Ventilation economics and airway sizing
- 9.6. Traditional method of ventilation planning

Chapter 10. FANS

- 10.1. Introduction
- 10.2. Fan pressures
- 10.3. Impeller theory and fan characteristic curves
- 10.4. Fan laws
- 10.5. Fans in combination
- 10.6. Fan performance
- 10.7. Booster fans

PART 3. Gases in the subsurface

Chapter 11. GASES IN SUBSURFACE OPENINGS

- 11.1. Introduction
- 11.2. Classification of subsurface gases
- 11.3. Gas mixtures
- 11.4. Gas detection and monitoring

Chapter 12. METHANE

- 12.1. Overview and additional properties of methane
- 12.2. The retention and release of methane in coal
- 12.3. Migration of methane
- 12.4. Emission patterns into mine workings
- 12.5. Methane drainage

Chapter 13. RADIATION AND RADON GAS

- 13.1. Introduction
- 13.2. The uranium series and radioactive decay
- 13.3. Radon and its daughters
- 13.4. Prediction of levels of radiation
- 13.5. Methods of monitoring for radiation
- 13.6. Control of radiation in subsurface openings

PART 4. Heat and humidity

Chapter 14. PSYCHROMETRY: THE STUDY OF MOISTURE IN AIR

- 14.1. Introduction
- 14.2. Basic relationships
- 14.3. The measurement of water vapour in air
- 14.4. Theory of the wet bulb thermometer
- 14.5. Further psychrometric relationships
- 14.6. Summary of psychrometric relationships
- 14.7. Deviations from classical theory
- 14.8. Psychrometric Charts
- A14 Derivation of the Clausius-Clapeyron equation

Chapter 15. HEAT FLOW INTO SUBSURFACE OPENINGS

- 15.1 Introduction
- 15.2. Strata heat
- 15.3. Other sources of heat
- A15.1 Carslaw and Jaeger solution to the heat conduction equation
- A15.2 Gibson's algorithm
- A15.3 Background theory of the heat transfer coefficient
- A15.4 Derivation of latent heat of evaporation at a wet surface

Chapter 16. SIMULATION OF CLIMATIC CONDITIONS IN THE SUBSURFACE

- 16.1. Background
- 16.2. Elements of mine climate simulation programs
- 16.3. Using a mine climate simulator.

Chapter 17. PHYSIOLOGICAL REACTIONS TO CLIMATIC CONDITIONS

- 17.1. Introduction
- 17.2. Thermoregulation of the human body
- 17.3. Physiological heat transfer
- 17.4. Indices of heat stress
- 17.5. Heat illnesses
- 17.6. Cold environments
- 17.7. Heat tolerance and
- 17.8. Effect of mine climate on productivity.
- A17 Listing of a thermoregulation computer model

Chapter 18. REFRIGERATION PLANT AND MINE AIR CONDITIONING SYSTEMS

- 18.1. Introduction
- 18.2. The vapour compression cycle
- 18.3. Components and design of mine cooling systems
- 18.4. Air heating

PART 5. Dust

Chapter 19. THE HAZARDOUS NATURE OF DUSTS

- 19.1. Introduction
- 19.2. Classifications of dust
- 19.3. Dust in the human body
- 19.4. The assessment of airborne dust concentrations

Chapter 20. THE AERODYNAMICS, SOURCES AND CONTROL OF AIRBORNE DUST

- 20.1. Introduction
- 20.2. The aerodynamic behaviour of dust particles
- 20.3. The production of dust in underground openings

20.4. Control of dust in mines

PART 6. Fires and explosions

Chapter 21. SUBSURFACE FIRES AND EXPLOSIONS

21.1. Introduction

21.2. Causes of ignitions

21.3. Open fires

21.4. Spontaneous combustion

21.5. Stoppings, seals and section pressure balances

21.6. The use of inert gases

21.7. Fire gases and their interpretation.

21.8. Explosions

21.9. Protection of personnel

21.10. Emergency procedures and disaster management.

PREFACE TO THE ORIGINAL TEXT

This book has been written as a reference and text for engineers, researchers, teachers and students who have an interest in the planning and control of the environment in underground openings. While directed primarily toward underground mining operations, the design procedures are also applicable to other complex developments of subsurface space such as nuclear waste repositories, commercial accommodation or vehicular networks. The book will, therefore, be useful for mining, civil, mechanical, and heating, ventilating and air-conditioning engineers involved in such enterprises. The chapters on airborne pollutants highlight means of measurement and control as well as physiological reaction. These topics will be of particular interest to industrial hygienists and students of industrial medicine.

One of the first technical applications of digital computers in the world's mining industries was for ventilation network analysis. This occurred during the early nineteen sixties. However, it was not until low-cost but powerful personal computers proliferated in engineering offices during the 'eighties that the full impact of the computer revolution was realized in the day-to-day work of most mine ventilation engineers. This book reflects the changes in approach and design procedures that have been brought about by that revolution.

While the book is organized into six parts, it encompasses three broad areas. Following an introductory background to the subject, chapters 2 and 3 provide the fundamentals of fluid mechanics and thermodynamics that are necessary for a complete understanding of large three-dimensional ventilation systems. Chapters 4 to 10, inclusive, offer a comprehensive treatment of subsurface airflow systems while chapters 11 to 21 deal with the airborne hazards that are encountered in underground openings.

Each chapter is self-contained as far as is practicable. The inter-related features of the topics are maintained by means of copious cross-references. These are included in order that practicing engineers may progress through a design project and be reminded of the wider repercussions of decisions that might be made. However, numerous cross-references can be a little distracting. The student is advised to ignore them during an initial reading and unless additional information is sought.

Many of the chapters are subdivided into theoretical and descriptive sections. Again, these can be read separately although a full understanding of the purpose and range of application of design procedures can be gained only through a knowledge of both. When used as a refresher or text by practicing engineers, it is suggested that the relevant descriptive section be consulted first and reference made back to the corresponding analysis or derivation when necessary.

The use of the book as an aid to teaching and learning can be moulded to suit any given curriculum. For the full education of a subsurface ventilation engineer, chapters 1 to 10 may be employed during a course on ventilation, i.e. airflow processes, leaving the chapters on gases, heat, dust, and fires and explosions for further courses. Alternatively, undergraduate courses may concentrate on the practical aspects of the subject, leaving the more theoretical analyses to graduate school. In any event the teacher may compile his or her own syllabus at any given level by choosing relevant sections from selected chapters.

In most countries, mining activities are regulated by specific state or national legislation. This book has been written for an international audience and reflects the author's experience of teaching and practice in a number of countries. While guideline threshold limit values are given, the reader is frequently reminded to consult the relevant local regulations for specific mandatory requirements and limitations on practical procedures. To reflect the international readership, Système Internationale (SI) units are employed and a comprehensive list of conversion factors is provided.

ACKNOWLEDGMENTS

There are many people without whose contributions the original edition of this book could not have been written. First, I thank Shirley, my wife, for her patience and understanding not only through the long hours of midnight oil burning that took place during the writing but, more particularly, for the extended periods, stretching over many years, when she was left alone to look after the home and family while I was deep under the surface of some faraway country.

I am grateful to former colleagues in the Department of Mining Engineering, University of Nottingham, England, for sowing seeds of ideas that later produced practical designs and procedures, many of which are reflected in this book; especially Ian Longson with whom I rediscovered the fascinations of thermodynamic logic, Leslie H. Morris, Dr. Jim R. Brown and, most of all, Professor F. Baden Hinsley to whom the book is dedicated. I am also privileged in having worked with excellent students from whom I learned a great deal, at Nottingham, the University of California, Berkeley, and at Virginia Tech.

Despite having been involved in numerous research investigations, my knowledge of subsurface ventilation and environmental engineering has been advanced primarily by working on feasibility studies and practical projects with mining engineers in many countries. Most of the case studies and examples in the book originated in such work. In particular, I am truly grateful for having had the opportunity of interacting with dedicated professional engineers in the United Kingdom, the countries of East and West Europe, South Africa, Australasia, India, South America, the United States of America and Canada.

I am indebted to the two ladies who shared typing the original manuscript. First, my daughter Alison D. McPherson who took great delight in correcting some of my mathematics, and Lucy Musante, my Secretarial assistant at Mine Ventilation Services, Inc. the most skilled and dedicated secretary with whom I have ever worked. Most of the initial reviews of chapters were undertaken by staff of Mine Ventilation Services, namely Daniel J. Brunner, Justus Deen, Martha O'Leary and, most particularly, Keith G. Wallace who willingly volunteered far more than his fair share of the work. Several chapters were reviewed by Dr. Felipe Calizaya, formerly at Berkeley and now at the University of Utah.

Some of the analyses described in the book arose directly out of funded research. The physiological model in chapter 17 was developed for the U.S. Department of Energy via Sandia National Laboratories as part of an investigation into climatic conditions in a deep geological repository for nuclear waste. Some of the heat transfer and climatic simulation studies in chapters 15 and 16, and investigations into the installation of booster fans outlined in chapter 9 were assisted by funding from the Generic Mineral Technology Center in Mine Systems Design and Ground Control, Office of Mineral Institutes, U.S. Bureau of Mines under Grant No. G1125151. I am indebted to those organizations for financing the work.

Finally, but also foremost, I thank the Good Lord for guiding my career to a point when I could prepare this book.

TABLE OF CONVERSION FACTORS BETWEEN IMPERIAL AND SI UNITS

Quantity	Imperial to SI			SI to Imperial		
Length	1 ft	= 0.304 8	m	1 m	= 3.280 8	ft
	1 yd	= 0.914 4	m		= 1.093 6	yd
	1 in	= 0.025 4	m		= 39.370 1	in
Area	1 ft ²	= 0.092 9	m ²	1 m ²	= 10.763 9	ft ²
	1 in ²	= 0.000 645	m ²		= 1550.003	in ²
Acceleration	1 ft/s ²	= 0.304 8	m/s ²	1 m/s ²	= 3.280 8	ft/s ²
Force	1 lbf	= 4.448 2	N	1 N	= 0.2248	lbf
	1 imp. ton f	= 9964.02	N			
Velocity	1 ft/s	= 0.304 8	m/s	1 m/s	= 3.2808	ft/s
	1 ft/min	= 0.005 08	m/s		= 196.85	ft/min
Volume	1 ft ³	= 0.028 32	m ³	1 m ³	= 35.315	ft ³
	1 yd ³	= 0.764 56	m ³		= 1.308	yd ³
	1 imp. gal	= 4.545	litre	1 litre	= 0.2200	imp. gal
	1 U.S. gal	= 3.785	litre	(0.001 m ³)	= 0.2642	U.S. gal
Volume Flow	1 ft ³ /s	= 0.028 32	m ³ /s	1 m ³ /s	= 35.315	ft ³ /s
	1 ft ³ /min	= 0.000 472	m ³ /s		= 2118.9	ft ³ /min
	1 imp gal/h	= 0.004 55	m ³ /h	1 m ³ /h	= 220.0	imp. gal/h
	1 imp gal/min	= 0.004 55	m ³ /min	1 m ³ /min	= 220.0	imp. gal/min
		= 4.545	litre/min	1 litre/min	= 0.220	imp. gal/min
		= 0.075 75	litre/s	1 litre/s	= 13.20	imp. gal/min
	1 U.S. gal/min	= 0.06313	litre/s		= 15.84	U.S. gal/min
Mass	1 lb	= 0.453 592	kg	1 kg	= 2.204 62	lb
	1 imp. ton (2240 lb)	= 1.016 05	t	1 t = 1000 kg	= 0.984 20	imp. ton
	1 short ton (2000 lb)	= 0.907 18	t		= 1.1023	short ton

Quantity	Imperial to SI			SI to Imperial		
Pressure, stress	1 lbf/ft ²	= 47.880	N/m ² = Pa	1 N/m ² = Pa	= 0.020 88	lbf/ft ²
	1 lbf/in ²	= 6894.76	N/m ²		0.000 145	lbf/in ²
	1 in w.g.	= 249.089	N/m ²		= 0.004 015	in w.g.
	1 ft w.g.	= 2989.07	N/m ²		= 0.000 3346	ft w.g.
	1 mm w.g.	= 9.807	N/m ²		= 0.101 97	mm w.g.
	1 in Hg	= 3386.39	N/m ²		= 0.000 2953	in Hg
	1 mm Hg	= 133.32	N/m ²		= 0.007 501	mm Hg
		= 1.333 2	mb		= 0.01	mb
	Note: The millibar (1 mb = 100 N/m ²) is included here as it is a familiar metric unit of pressure. It is not, however, an SI unit.					
Airway resistance	1 Atk	= 0.059 71	Ns ² /m ⁸	1 Ns ² /m ⁸	= 16.747	Atk
	1 PU	= 1.118 3	Ns ² /m ⁸		= 0.894 2	PU
Airway specific resistance	1 in w.g. per 10 000 ft ³ /min	= 22.366	Ns ² /m ⁸		= 0.044 7	in w.g. per 10 000 ft ³ /min
Friction Factor	1 lbf min ² /ft ⁴	= 1.8554 x 10 ⁶	kg/m ³	1 kg/m ³	= 539.0 x 10 ⁻⁹	lbf min ² /ft ⁴
Density	1 lb/ft ³	= 16.018 5	kg/m ³	1 kg/m ³	= 0.062 43	lb/ft ³
	1 imp. ton/yd ³	= 1328.94	kg/m ³		= 0.000 753	imp. ton/yd ³
	1 short ton/yd ³	= 1186.55	kg/m ³		= 0.000843	short ton/yd ³
Energy, work, heat	1 ft lbf	= 1.355 82	J	1 J	= 0.737 56	ft/lbf
	1Btu	= 1055.06	J		= 0.000 948	Btu
	1 cal	= 4.186 8	J		= 0.238 89	cal
	1 therm	= 105.506	MJ		= 0.009 478	μtherm
	1 kWh	= 3.6	MJ		= 0.000 278	Wh
Power	1 hp	= 745.700	W	1 W	= 0.001 341	hp
Heatflow	1 ft lbf/min	= 0.0226	W	1 W	= 44.254	ft lbf/min
	1 Btu/min	= 17.584	W		= 0.056 87	Btu/min
	1 RT Refrigeration (imp.) ton	= 3517	W		= 0.000 2843	RT

Quantity	Imperial to SI			SI to Imperial		
Specific energy	1 ft lbf/lb	= 2.989	J/kg	1 J/kg	= 0.3345	ft lbf/lb
Calorific value	1 Btu/lb	= 2326	J/kg	1 J/kg	= 0.000 430	Btu/lb
	1 therm/imp. ton	= 0.103 8	MJ/kg		= 9.634	μ therm/imp. ton
	1 therm/short ton	= 0.116 3	MJ/kg		= 8.602	μ therm/short ton
Gas constants	1 ft lbf/lb °R	= 5.380 3	J/kg K	1 J/kg K	= 0.185 9	ft lbf/lb °R
Specific heat	1 Btu/lb °R	= 4186.8	J/kg K	1 J/kg K	= 0.000 2388	Btu/lb °R
Specific entropy						
Specific volume	1 ft ³ /lb	= 0.062 43	m ³ /kg	1 m ³ /kg	= 16.018	ft ³ /lb
	1 ft ³ /imp. ton	= 0.027 87	m ³ /t		= 35.881	ft ³ /imp. ton
	1 ft ³ /short ton	= 0.031 21	m ³ /t		= 32.037	ft ³ /short ton
	Note: 1 metric tonne (t) = 1 000 kg					
Dynamic viscosity	1 lb/ft s	= 1.488 16	Ns/m ²	1 Ns/m ²	= 0.671 97	lb/ft s
	1 poise	= 0.1	Ns/m ²		= 10	poise
Kinematic viscosity	1 ft ² /s	= 0.092 903	m ² /s	1 m ² /s	= 10.763 9	ft ² /s
	1 stokes	= 0.000 1	m ² /s		= 10 000	stokes
Permeability	1 Darcy	= 0.98693x10 ⁻¹²	m ²		= 1.01324-12	Darcy
	1 md	= 0.98693x10 ⁻¹⁵	m ²		= 1.01324-15	md
Thermal conductivity	1 Btu ft/ft ² h °R	= 1.730 73	W/m K	1 W/mK	= 0.577 79	Btu ft/ft ² h °R
Thermal diffusivity	1 ft ² /s	= 0.092 303	m ² /s	1 m ² /s	= 10.764	ft ² /s
	1 ft ² /h	= 2.5806x10 ⁻⁵	m ² /s	1 m ² /s	= 38 750	ft ² /h

Quantity	Imperial to SI			SI to Imperial		
Thermal gradient	1 °F/ft	= 1.822 7	°C/m	1 °C/m	= 0.548 6	°F/ft
Moisture content	1 lb/lb	= 1	kg/kg	1 kg/kg	= 1	lb/lb
	1 gr/lb	= 0.000 1429	kg/kg		= 7000	gr/lb
Radiation	1 rad	= 0.01	Gray	1 Gray	= 100	rad
	1 Curie	= 37 x 10 ⁹	Bq	1 Bq	= 27 x 10 ⁻¹²	Curie
	1 rem	= 0.01	Sv	1 Sv	= 100	rem
	1 Roentgen	= 2.58 x 10 ⁻⁴	C/kg	1 C/kg	= 3876	Roentgen
Notes:	1 Gray	= 1 J/kg		1 Becquerel (Bq)	= 1 disintegration/s	
	1 Sievert (Sv)	= 1 J/kg		1 Coulomb (C)	= 1 amp.s	
Temperature	K	= °C + 273.15				
	°R	= °F + 459.67				
	For differential temperatures, 1 Centigrade degree = 1.8 Fahrenheit degrees.					
	For actual temperature, 1.8 x t(°C) + 32 = °F					
and	$\frac{t(^{\circ}\text{F}) - 32}{1.8}$	= °C				

Chapter 1. Background to subsurface ventilation and environmental engineering

1.1 INTRODUCTION	1
1.2 A BRIEF HISTORY OF MINE VENTILATION	1
1.3. THE RELATIONSHIPS BETWEEN VENTILATION AND OTHER SUBSURFACE SYSTEMS	6
1.3.1. The objectives of subsurface ventilation	6
1.3.2. Factors that affect the underground environment	6
1.3.3. The integration of ventilation planning into overall system design	8

1.1 INTRODUCTION

Ventilation is sometimes described as the lifeblood of a mine, the intake airways being arteries that carry oxygen to the working areas and the returns veins that conduct pollutants away to be expelled to the outside atmosphere. Without an effective ventilation system, no underground facility that requires personnel to enter it can operate safely.

The slaughter of men, women and children that took place in the coal mines of Britain during the eighteenth and nineteenth centuries resulted in the theory and art of ventilation becoming the primary mining science. The success of research in this area has produced tremendous improvements in underground environmental conditions. Loss of life attributable to inadequate ventilation is now, thankfully, a relatively infrequent occurrence. Falls of ground rather than ventilation-related factors have become the most common cause of fatalities and injuries in underground mines. Improvements in ventilation have also allowed the productivity of mines to be greatly improved. Neither the very first nor the very latest powered machines could have been introduced underground without an adequate supply of air. Subsurface ventilation engineers are caught up in a continuing cycle. Their work allows rock to be broken in ever larger quantities and at greater depths. This, in turn, produces more dust, gases and heat, resulting in a demand for yet better environmental control.

This opening chapter takes a necessarily cursory look at the long history of mine ventilation and discusses the interactions between ventilation and the other systems that, jointly, comprise a complete mine or underground facility.

1.2 A BRIEF HISTORY OF MINE VENTILATION

Observations of the movements of air in underground passages have a long and fascinating history. Between 4000 and 1200 B.C., European miners dug tunnels into chalk deposits searching for flint. Archaeological investigations at **Grimes Graves** in the South of England have shown that these early flint miners built brushwood fires at the working faces presumably to weaken the rock. However, those Neolithic miners could hardly have failed to observe the currents of air induced by the fire. Indeed, the ability of fire to promote airflow was rediscovered by the Greeks, the Romans, in medieval Europe and during the Industrial Revolution in Britain.

The **Laurium silver mines of Greece**, operating in 600 B.C. have layouts which reveal that the Greek miners were conscious of the need for a connected ventilating circuit. At least two airways served each major section of the mine and there is evidence that divided shafts were used to provide separate air intake and return connections to surface. Underground mines of the

Roman Empire often had twin shafts, and **Pliny (23-79 A.D.)** describes how slaves used palm fronds to waft air along tunnels.

Although metal mines were worked in Europe during the first 1500 years A.D., there remain little documented descriptions of their operations. The first great textbook on mining was written in Latin by **Georgius Agricola**, a physician in a thriving iron ore mining and smelting community of Bohemia in Central Europe. Agricola's "**De Re Metallica**", produced in 1556, is profusely illustrated. A number of the prints show ventilating methods that include diverting surface winds into the mouths of shafts, wooden centrifugal fans powered by men and horses, bellows for auxiliary ventilation and air doors. An example of one of Agricola's prints is reproduced in Figure 1.1.

Agricola was also well aware of the dangers of blackdamp, air that has suffered from a reduction in oxygen content, - 'miners are sometimes killed by the pestilential air that they breathe,' and of the explosive power of "firedamp", a mixture of methane and air "likened to the fiery blast of a dragon's breath." De Re Metallica was translated into English in 1912 by **Herbert C. Hoover and his wife, Lou**. Hoover was a young American mining engineer who graduated from Stanford University and subsequently served as President of the United States during the term 1929-1933.

From the 17th Century onwards, papers began to be presented to the **Royal Society** of the United Kingdom on the explosive and poisonous nature of mine atmospheres. The Industrial Revolution brought a rapid increase in the demand for coal. Conditions in many coal mines were quite horrific for the men, women, and children who were employed in them during the 18th and 19th centuries. Ventilation was induced either by purely natural effects, stagnating when air temperatures on the surface and underground were near equal, or by fire. The first **ventilating furnaces** of that era were built on surface but it was soon realized that burning coals suspended in a wire basket within the upcast shaft gave improved ventilation. Furthermore, the lower the basket, the better the effect. This quickly led to the construction of shaft bottom furnaces.

The only form of illumination until the early eighteen hundred's was the candle. With historical hindsight we can see the conjunction of circumstances that caused the ensuing carnage: a seemingly insatiable demand for coal to fuel the steam engines of the Industrial Revolution, the working of seams rich in methane gas, inadequate ventilation, furnaces located in methane laden return air and the open flames of candles. There are many graphic descriptions of methane and coal dust explosions, the suffering of mining communities, the heroism of rescue attempts and the strenuous efforts of mining engineers and scientists to find means of improving ventilation and providing illumination without the accompanying danger of igniting methane gas. Seemingly oblivious to the extent of the danger, miners would sometimes ignite pockets of methane intentionally for amusement and to watch the blue flames flickering above their heads. Even the renowned engineer, **George Stephenson**, admitted to this practice during the inquiries of a government select committee on mine explosions in 1835. A common method of removing methane was to send a "fireman" in before each shift, covered in sackcloths doused in water and carrying a candle on the end of a long rod. It was his task to burn out the methane before the miners went into the working faces.

John Buddle (1773-1843), an eminent mining engineer in the north of England produced two significant improvements. First, he introduced "**dumb drifts**" which bled sufficient fresh air from the base of a downcast shaft to feed the furnace. The return air, laden with methane, bypassed the furnace. The products of combustion entering the upcast shaft from the furnace were too cool to ignite the methane but still gave a good chimney effect in the shaft, thus inducing airflow around the mine. Buddle's second innovation was "panel (or split) ventilation". Until that time, air flowed sequentially through work areas, one after the other, continually increasing in methane concentration. Buddle originally divided the mine layout into discrete panels, with intervening barrier pillars, to counteract excessive floor heave. However, he found that by providing an intake and



A-MACHINE FIRST DESCRIBED. **B**-THIS WORKMAN, TREADING WITH HIS FEET, IS COMPRESSING THE BELLOWS. **C**-BELLOWS WITHOUT NOZZLES. **D**-HOLE BY WHICH HEAVY VAPOURS OR BLASTS ARE BLOWN OUT. **E**-CONDUITS. **F**-TUNNEL. **G**-SECOND MACHINE DESCRIBED. **H**-WOODEN WHEEL. **I**-ITS STEPS. **K**-BARS. **L**-HOLE IN SAME WHEEL. **M**-POLE. **N**-THIRD MACHINE DESCRIBED. **O**-UPRIGHT AXLE. **P**-ITS TOOTHED DRUM. **Q**-HORIZONTAL AXLE. **R**-ITS DRUM WHICH IS MADE OF RUNDLES.

Figure 1.1 A print from Agricola's "De Re Metallica"

(Reproduced by permission of Dover Publications)

return separately to each panel the ventilating quantities improved markedly and methane concentrations decreased. He had discovered, almost by accident, the advantages of parallel layouts over series circuits. The mathematical proof of this did not come until Atkinson's theoretical analyses several decades later.

The quest for a safe form of illumination went on through the eighteenth century. Some of the earlier suggestions made by scientists of the time, such as using very thin candles, appear quite ludicrous to us today. One of the more serious attempts was the steel **flint mill** invented in 1733 by **Carlisle Spedding**, a well known mining engineer, again, in the north of England (Figure 1.2). This device relied upon a piece of flint being held against a rapidly revolving steel wheel. The latter was driven through a gear mechanism by a manually rotated handle. The complete device was strapped to the chest of a boy whose job was to produce a continuous shower of sparks in order to provide some illumination for the work place of a miner. The instrument was deemed safer than a candle but the light it produced was poor, intermittent, and still capable of igniting methane.

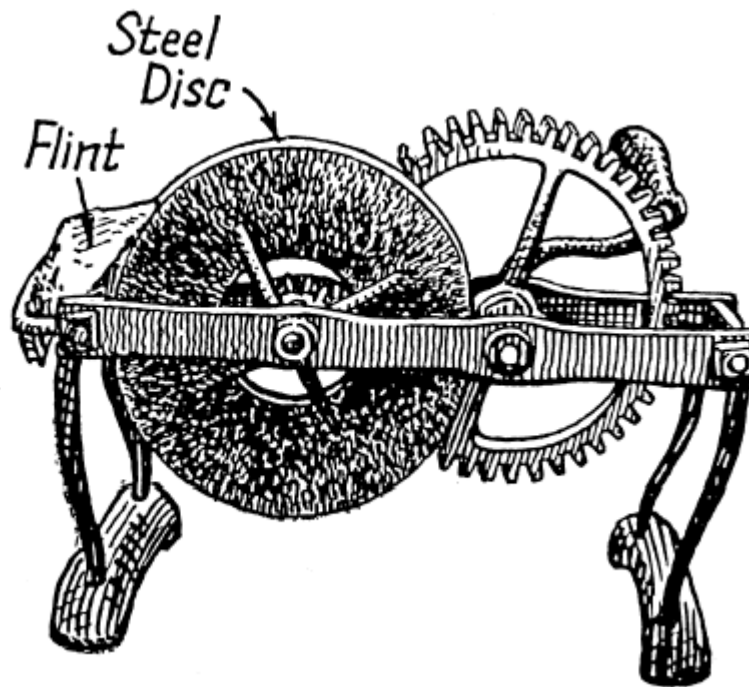


Figure 1.2 Spedding's Flint Mill (*Reproduced by permission of Virtue and Co., Ltd.*)

A crisis point was reached in 1812 when a horrific explosion at **Felling, Gateshead** killed 92 miners. With the help of local clergymen, a society was formed to look into ways of preventing such disasters. Contact was made with **Sir Humphrey Davy**, President of the Royal Society, for assistance in developing a safe lamp. Davy visited John Buddle to learn more of conditions in the mines. As this was well before the days of electricity, he was limited to some form of flame lamp. Within a short period of experimentation he found that the flame of burning methane would not readily pass through a closely woven wire mesh. The **Davy Lamp** had arrived (Figure 1.3).

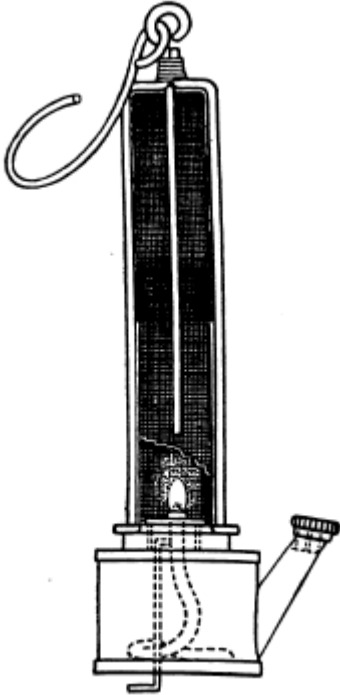


Figure 1.3 The original appearance of the Davy safety lamp. (reproduced by permission of Virtue and Co., Ltd.).

Buddle's reaction is best expressed in a letter he wrote to Davy.

"I first tried it in a explosive mixture on the surface, and then took it into the mine... it is impossible for me to express my feelings at the time when I first suspended the lamp in the mine and saw it red hot...I said to those around me, "We have at last subdued this monster."

The lamp glowed 'red hot' because of the methane burning vigorously within it, yet the flames could not pass through the wire mesh to ignite the surrounding firedamp.

Davy lamps were introduced into British mines, then spread to other countries. Nevertheless, in the absence of effective legislation, candles remained in widespread use through the nineteenth century because of the better light that they produced.

Perhaps the greatest classical paper on mine ventilation was one entitled "On the Theory of the Ventilation of Mines", presented by **John Job Atkinson** to the North of England Institute of Mining Engineers in December, 1854. Atkinson was a Mining Agent, an intermediary between management and the mine owners. He later became one of the first Inspectors of Mines. Atkinson appears to have been well educated in mathematics and languages, and

was clearly influenced by the earlier work of French hydraulic engineers (Chapter 5). He seems to have had some difficulty in having his paper accepted. Officers of the Institute decided, perhaps understandably, that the 154 page paper was too long to be presented at a meeting. It was, however, published and a meeting of the Institute arranged to discuss it. Despite publicity referring to the importance of the subject, attendance at the meeting was poor and there was little discussion. In this paper, Atkinson proposed and expanded upon the principles on which most modern mine ventilation planning is still based. However, the analytical reasoning and mathematical analyses that he developed in great detail were simply too much for engineers of the day. The paper was consigned to the archives and it was some sixty years after Atkinson's death that his work was "rediscovered" and put into practice.

During Atkinson's productive years the first power driven ventilators began to appear. These varied from enormous steam-driven piston and cylinder devices to elementary centrifugal fans.

The years around the turn of the century saw working conditions in mines coming under legislative control. Persons responsible for underground mining operations were required to obtain minimum statutory qualifications. Mine manager's examination papers concentrated heavily on ventilation matters until well into the twentieth century.

The nineteen twenties saw further accelerated research in several countries. Improved instrumentation allowed organized ventilation surveys to be carried out to measure airflows and pressure drops for the purposes of ventilation planning, although there was no practical means of predicting airflows in other than simple circuits at that time. Atkinson's theory was confirmed in practice. The first successful axial fans were introduced in about 1930.

In 1943, **Professor F. Baden Hinsley** produced another classical paper advancing understanding of the behaviour of airflow by using thermodynamic analyses. Hinsley also supervised the work at Nottingham University that led to the first practical use of **analog computers** in 1952 to facilitate

ventilation planning. This technique was employed widely and successfully for over a decade. The development of ventilation **network analysis programs** for digital computers in the early sixties rendered the analog devices obsolete. Initially, the network programs were written for, and required the power of mainframe computers. These were employed throughout the seventies. However, the nineteen eighties saw a shift to desktop computers and corresponding programs were developed. This is now the dominant method used for ventilation planning (Chapter 7).

The discipline of mine ventilation is an addictive subject for researchers of industrial history, full of lost discoveries and rediscoveries, excitement and despair, achievement and tragedy. It has been the subject of many papers and books. An excellent place to commence further reading is the text by Saxton serialized in Volume 146 of the Mining Engineer (Institution of Mining Engineers, U.K.), (1986-'87).

1.3. THE RELATIONSHIPS BETWEEN VENTILATION AND OTHER SUBSURFACE SYSTEMS

1.3.1. The objectives of subsurface ventilation

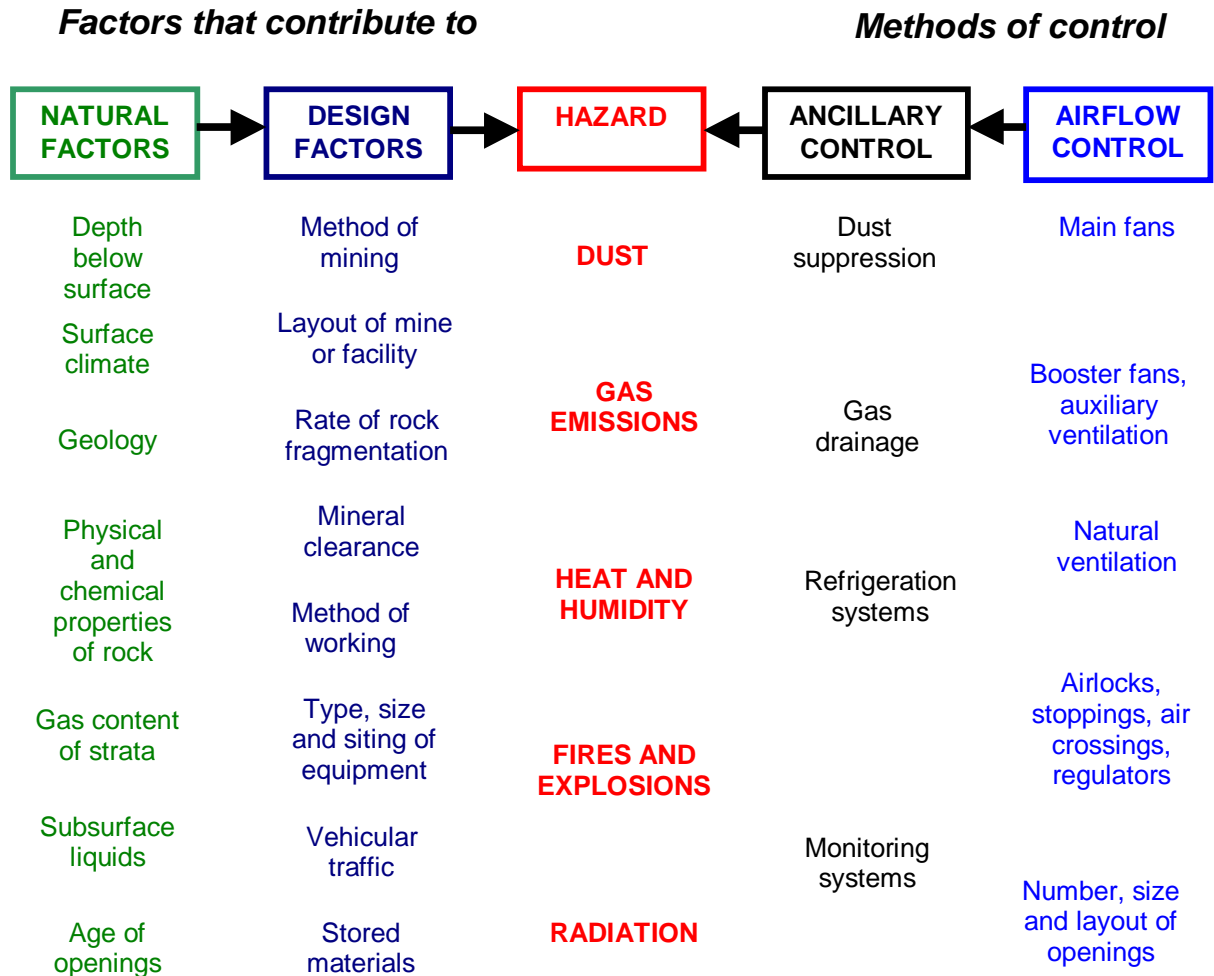
The basic objective of an underground ventilation system is clear and simple. It is to provide airflows in sufficient quantity and quality to dilute contaminants to safe concentrations in all parts of the facility where personnel are required to work or travel. This basic requirement is incorporated into mining law in those countries that have such legislation. The manner in which "quantity and quality" are defined varies from country to country depending upon their mining history, the pollutants of greatest concern, the perceived dangers associated with those hazards and the political and social structure of the country. The overall requirement is that all persons must be able to work and travel within an environment that is safe and which provides reasonable comfort. An interpretation of the latter phrase depends greatly on the geographical location of the mine and the background and expectations of the workforce. Personnel in a permafrost mine work in conditions that would be unacceptable to miners from an equatorial region, and vice versa, and neither set of conditions would be tolerated by factory or office workers. This perception of "reasonable comfort" sometimes causes misunderstandings between subsurface ventilation engineers and those associated with the heating and ventilating industry for buildings.

While maintaining the essential objectives related to safety and health, subsurface environmental engineering has, increasingly, developed a wider purpose. In some circumstances, atmospheric pressure and temperature may be allowed to exceed the ranges that are acceptable for human tolerance. For example, in an underground repository for high level nuclear waste, a containment drift may be sealed against personnel access after emplacement of the waste canisters has been completed. However, the environment within the drift must still be maintained such that rock wall temperatures are controlled. This is necessary to enable the drift to be reopened relatively quickly for retrieval of the nuclear waste at any subsequent time during the active life of the repository. Other forms of underground storage often require environmental control of pressure, temperature and humidity for the preservation of the stored material. Yet another trend is towards automated (manless) working faces and the possible use of underground space for in-situ mineral processing. In such zones of future mines, environmental control will be required for the efficient operation of machines and processes, but not necessarily with an atmosphere acceptable to the unprotected human physiology.

1.3.2. Factors that affect the underground environment

During the development and operation of a mine or other underground facility, potential hazards arise from dust, gas emissions, heat and humidity, fires, explosions and radiation. Table 1.1 shows the factors that may contribute towards those hazards. These divide into features that are imposed by nature and those that are generated by design decisions on how to develop and operate the facility.

Table 1.1 Factors that feature in the creation and control of hazards in the subsurface environment.



The major method of controlling atmospheric conditions in the subsurface is by airflow. This is produced, primarily, by main fans that are usually, but not necessarily, located on surface. National or state mining law may insist that main fans are sited on surface for gassy mines. While the main fan, or combination of main fans, handles all of the air that circulates through the underground network of airways, underground booster fans serve specific districts only. Auxiliary fans are used to pass air through ducts to ventilate blind headings. The distribution of airflow may further be controlled by ventilation doors, stoppings, air crossings and regulators.

It is often the case that it becomes impracticable or impossible to contend with all environmental hazards by ventilation alone. For example, increases in air temperature caused by compression of the air in the downcast shafts of deep mines may result in that air being too hot for personnel even before it enters the workings. No practical amount of increased airflow will solve that problem. Table 1.1 includes the ancillary control measures that may be advisable or necessary to supplement the ventilation system in order to maintain acceptable conditions underground.

1.3.3. The integration of ventilation planning into overall system design

The design of a major underground ventilation and environmental control system is a complex process with many interacting features. The principles of systems analyses should be applied to ensure that the consequences of such interaction are not overlooked (Chapter 9). However, ventilation and the underground environment should not be treated in isolation during planning exercises. They are, themselves, an integral part of the overall design of the mine or subsurface facility.

It has often been the case that the types, numbers and sizes of machines, the required rate of mineral production and questions of ground stability have dictated the layout of a mine without, initially, taking the demands of ventilation into account. This will result in a ventilation system that may lack effectiveness and, at best, will be more expensive in both operating and capital costs than would otherwise have been the case. A common error has been to size shafts that are appropriate for the hoisting duties but inadequate for the long term ventilation requirement of the mine. Another frequent, related problem is a ventilation infrastructure that was adequate for an initial layout but lacks the flexibility to handle fluctuating market demands for the mineral. Again, this can be very expensive to correct. The results of inadequate ventilation planning and system design are premature cessation of production, high costs of reconstruction, poor environmental conditions and, still too often, tragic consequences to the health and safety of the workforce. It is, therefore, most important that ventilation engineers should be incorporated as an integral part of a design team from the initial stages of planning a new mine or other underground facility.

REFERENCES

- Agricola, G. (1556). *De Re Metallica*. Translated from Latin by H.C. Hoover and L.H. Hoover. Modern publication by Dover Pub., Inc., New York (1950).
- Atkinson, J.J. (1854). On the theory of the ventilation of mines. *North of England Institute of Mining Engineers*, No. 3, p 118.
- Hartley, Sir Harold. "Humphrey Davy". S.R. Publishers Ltd.
- Hinsley, F.B. (1967). The control of atmospheric conditions in mines. 11th Cadman Memorial Lecture. *Mining Engineer* No. 77, pp 289.
- Hinsley, F.B. (1970). The development of the mechanical ventilation of coal mines, 1870-1940. *Univ. of Nottingham Mining Magazine* Vol. 22.
- Mason, E. (1954). *Practical Coal Mining*. Virtue and Co. Ltd. London.
- McPherson, M.J. (1964). Mine ventilation network problems, solution by digital computer. *Colliery Guardian* Vol. 209 No. 5392, pp 253-259.
- Saxton, I. (1986-1987). Coal mine ventilation from Agricola to the 1980's. Serialized in the *Mining Engineer* by the Inst. of Mining Engineers Vol. 146.
- Scott, D.R., Hinsley, F.B. and Hudson, R.F. (1953). A calculator for the solution of ventilation network problems. *Trans. Inst. Min. Engrs.* Vol. 112, pp 623.
- Wang, Y.J. and Hartman, H.L. (1967). Computer solution of three-dimensional mine ventilation networks with multiple fans and natural ventilation. *Int. J. of Rock Mech. and Min. SC.* Vol. 2, No. 2, pp 129-154.

Part 1

**Basic principles
of fluid mechanics
and physical
thermodynamics.**

Chapter 2. Introduction to Fluid Mechanics

2.1 INTRODUCTION	1
2.1.1 The concept of a fluid.....	1
2.1.2 Volume flow, Mass flow and the Continuity Equation.....	3
2.2 FLUID PRESSURE	3
2.2.1 The cause of fluid pressure.....	3
2.2.2 Pressure head.....	4
2.2.3 Atmospheric pressure and gauge pressure.....	5
2.2.4. Measurement of air pressure.....	5
2.2.4.1. Barometers.....	5
2.2.4.2. Differential pressure instruments	6
2.3 FLUIDS IN MOTION	8
2.3.1. Bernoulli's equation for ideal fluids	8
<i>Kinetic energy</i>	8
<i>Potential energy</i>	9
<i>Flow work</i>	9
2.3.2. Static, total and velocity pressures.	11
2.3.3. Viscosity	12
2.3.4. Laminar and turbulent flow. Reynolds Number.....	14
2.3.5. Frictional losses in laminar flow, Poiseuille's Equation.....	16
2.3.6. Frictional losses in turbulent flow.....	22
2.3.6.1. The Chézy-Darcy Equation	22
2.3.6.2. The coefficient of friction, f	25
2.3.6.3. Equations describing f - Re relationships.....	27
<i>Laminar Flow</i>	27
<i>Smooth pipe turbulent curve</i>	28
<i>Rough pipes</i>	29
Bibliography	31

2.1 INTRODUCTION

2.1.1 The concept of a fluid

A fluid is a substance in which the constituent molecules are free to move relative to each other. Conversely, in a solid, the relative positions of molecules remain essentially fixed under non-destructive conditions of temperature and pressure. While these definitions classify matter into fluids and solids, the fluids sub-divide further into liquid and gases.

Molecules of any substance exhibit at least two types of forces; an attractive force that diminishes with the square of the distance between molecules, and a force of repulsion that becomes strong when molecules come very close together. In solids, the force of attraction is so dominant that the molecules remain essentially fixed in position while the resisting force of repulsion prevents them from collapsing into each other. However, if heat is supplied to the solid, the energy is absorbed internally causing the molecules to vibrate with increasing amplitude. If that vibration becomes sufficiently violent, then the bonds of attraction will be broken. Molecules will then be free to move in relation to each other - the solid melts to become a liquid.

When two moving molecules in a fluid converge on each other, actual collision is averted (at normal temperatures and velocities) because of the strong force of repulsion at short distances. The molecules behave as near perfectly elastic spheres, rebounding from each other or from the walls of the vessel. Nevertheless, in a liquid, the molecules remain sufficiently close together that the force of attraction maintains some coherence within the substance. Water poured into a vessel will assume the shape of that vessel but may not fill it. There will be a distinct interface (surface) between the water and the air or vapour above it. The mutual attraction between the water molecules is greater than that between a water molecule and molecules of the adjacent gas. Hence, the water remains in the vessel except for a few exceptional molecules that momentarily gain sufficient kinetic energy to escape through the interface (slow evaporation).

However, if heat continues to be supplied to the liquid then that energy is absorbed as an increase in the velocity of the molecules. The rising temperature of the liquid is, in fact, a measure of the **internal kinetic energy** of the molecules. At some critical temperature, depending upon the applied pressure, the velocity of the molecules becomes so great that the forces of attraction are no longer sufficient to hold those molecules together as a discrete liquid. They separate to much greater distances apart, form bubbles of vapour and burst through the surface to mix with the air or other gases above. This is, of course, the common phenomenon of boiling or rapid evaporation. The liquid is converted into gas.

The molecules of a gas are identical to those of the liquid from which it evaporated. However, those molecules are now so far apart, and moving with such high velocity, that the forces of attraction are relatively small. The fluid can no longer maintain the coherence of a liquid. A gas will expand to fill any closed vessel within which it is contained.

The molecular spacing gives rise to distinct differences between the properties of liquids and gases. Three of these are, first, that the volume of gas with its large intermolecular spacing will be much greater than the same mass of liquid from which it evaporated. Hence, the density of gases (mass/volume) is much lower than that of liquids. Second, if pressure is applied to a liquid, then the strong forces of repulsion at small intermolecular distances offer such a high resistance that the volume of the liquid changes very little. For practical purposes most liquids (but not all) may be regarded as incompressible. On the other hand, the far greater distances between molecules in a gas allow the molecules to be more easily pushed closer together when subjected to compression. Gases, then, are compressible fluids.

A third difference is that when liquids of differing densities are mixed in a vessel, they will separate out into discrete layers by gravitational settlement with the densest liquid at the bottom. This is not true of gases. In this case, layering of the gases will take place only while the constituent gases remain unmixed (for example, see Methane Layering, Section 12.4.2). If, however, the gases become mixed into a homogenous blend, then the relatively high molecular velocities and large intermolecular distances prevent the gases from separating out by gravitational settlement. The internal molecular energy provides an effective continuous mixing process.

Subsurface ventilation engineers need to be aware of the properties of both liquids and gases. In this chapter, we shall confine ourselves to incompressible fluids. Why is this useful when we are well aware that a ventilation system is concerned primarily with air, a mixture of gases and, therefore, compressible? The answer is that in a majority of mines and other subsurface facilities, the ranges of temperature and pressure are such that the variation in air density is fairly limited. Airflow measurements in mines are normally made to within 5 per cent accuracy. A 5 per cent change in air density occurs by moving through a vertical elevation of some 500 metres in the gravitational field at the surface of the earth. Hence, the assumption of incompressible flow with its simpler analytical relationships gives acceptable accuracy in most cases. For the deeper and (usually) hotter facilities, the effects of pressure and temperature on air density should be taken into account through thermodynamic analyses if a good standard of accuracy is to be attained. The principles of physical steady-flow thermodynamics are introduced in Chapter 3.

2.1.2 Volume flow, Mass flow and the Continuity Equation

Most measurements of airflow in ventilation systems are based on the volume of air (m^3) that passes through a given cross section of a duct or airway in unit time (1 second). The units of volume flow, Q , are, therefore, m^3/s . However, for accurate analyses when density variations are to be taken into account, it is preferable to work in terms of mass flow - that is, the mass of air (kg) passing through the cross section in 1 second. The units of mass flow, M , are then kg/s .

The relationship between volume flow and mass flow follows directly from the definition of density, ρ ,

$$\rho = \frac{\text{mass}}{\text{volume}} \quad \frac{\text{kg}}{\text{m}^3} \quad (2.1)$$

and

$$\rho = \frac{\text{mass flow}}{\text{volume flow}} = \frac{M}{Q} \quad \frac{\text{kg s}}{\text{s m}^3}$$

$$\text{giving } M = Q \rho \text{ kg/s} \quad (2.2)$$

In any continuous duct or airway, the mass flows passing through all cross sections along its length are equal, provided that the system is at steady state and there are no inflows or outflows of air or other gases between the two ends. If these conditions are met then

$$M = Q \rho = \text{constant} \quad \text{kg/s} \quad (2.3)$$

This is the simplest form of the Continuity Equation. It can, however, be written in other ways. A common method of measuring volume flow is to determine the mean velocity of air, u , over a given cross section, then multiply by the area of that cross-section, A , (Chapter 6):

$$Q = u A \quad \frac{\text{m}}{\text{s}} \text{ m}^2 \text{ or } \frac{\text{m}^3}{\text{s}} \quad (2.4)$$

Then the continuity equation becomes

$$M = \rho u A = \text{constant kg/s} \quad (2.5)$$

As indicated in the preceding subsection, we can achieve acceptable accuracy in most situations within ventilation systems by assuming a constant density. The continuity equation then simplifies back to

$$Q = u A = \text{constant} \quad \text{m}^3/\text{s} \quad (2.6)$$

This shows that for steady-state and constant density airflow in a continuous airway, the velocity of the air varies inversely with cross sectional area.

2.2 FLUID PRESSURE

2.2.1 The cause of fluid pressure

Section 2.1.1 described the dynamic behaviour of molecules in a liquid or gas. When a molecule rebounds from any confining boundary, a force equal to the rate of change of momentum of that molecule is exerted upon the boundary. If the area of the solid/fluid boundary is large compared to the average distance between molecular collisions then the statistical effect will be to give a uniform force distributed over that boundary. This is the case in most situations of importance in subsurface ventilation engineering.

Two further consequences arise from the bombardment of a very large number of molecules on a surface, each molecule behaving essentially as a perfectly elastic sphere. First, the force exerted by a static fluid will always be normal to the surface. We shall discover later that the situation is rather different when the dynamic forces of a moving fluid stream are considered (Section 2.3). Secondly, at any point within a static fluid, the pressure is the same in all directions. Hence, static pressure is a scalar rather than a vector quantity.

Pressure is sometimes carelessly confused with force or thrust. The quantitative definition of pressure, P , is clear and simple

$$P = \frac{\text{Force}}{\text{Area}} \quad \frac{\text{N}}{\text{m}^2} \quad (2.7)$$

In the SI system of units, force is measured in Newtons (N) and area in square metres. The resulting unit of pressure, the N/m^2 , is usually called a Pascal (Pa) after the French philosopher, **Blaise Pascal (1623-1662)**.

2.2.2 Pressure head

If a liquid of density ρ is poured into a vertical tube of cross-sectional area, A , until the level reaches a height h , the volume of liquid is

$$\text{volume} = h A \quad \text{m}^3$$

Then from the definition of density (mass/volume), the mass of the liquid is

$$\begin{aligned} \text{mass} &= \text{volume} \times \text{density} \\ &= h A \rho \quad \text{kg} \end{aligned}$$

The weight of the liquid will exert a force, F , on the base of the tube equal to mass \times gravitational acceleration (g)

$$F = h A \rho g \quad \text{N}$$

But as pressure = force/area, the pressure on the base of the tube is

$$P = \frac{F}{A} = \rho g h \quad \frac{\text{N}}{\text{m}^2} \quad \text{or Pa} \quad (2.8)$$

Hence, if the density of the liquid is known, and assuming a constant value for g , then the pressure may be quoted in terms of h , the head of liquid. This concept is used in liquid type manometers (Section 2.2.4) which, although in declining use, are likely to be retained for many purposes owing to their simplicity.

Equation (2.8) can also be used for air and other gases. In this case, it should be remembered that the density will vary with height. A mean value may be used with little loss in accuracy for most mine shafts. However, here again, it is recommended that the more precise methodologies of thermodynamics be employed for elevation differences of more than 500 m.

2.2.3 Atmospheric pressure and gauge pressure

The blanket of air that shrouds the earth extends to approximately 40 km above the surface. At that height, its pressure and density tend towards zero. As we descend towards the earth, the number of molecules per unit volume increases, compressed by the weight of the air above. Hence, the pressure of the atmosphere also increases. However, the pressure at any point in the lower atmosphere is influenced not only by the column of air above it but also by the action of convection, wind currents and variations in temperature and water vapour content. Atmospheric pressure near the surface, therefore, varies with both place and time. At the surface of the earth, atmospheric pressure is of the order of 100 000 Pa. For practical reference this is often translated into 100 kPa although the basic SI units should always be used in calculations. Older units used in meteorology for atmospheric pressure are the bar (10^5 Pa) and the millibar (100 Pa).

For comparative purposes, reference is often made to standard atmospheric pressure. This is the pressure that will support a 0.760 m column of mercury having a density of 13.5951×10^3 kg/m³ in a standard earth gravitational field of 9.8066 m/s².

Then from equation (2.8)

$$\begin{aligned} \text{One Standard Atmosphere} &= \rho \times g \times h \\ &= 13.5951 \times 10^3 \times 9.8066 \times 0.760 \\ &= 101.324 \times 10^3 \quad \text{Pa} \\ \text{or} & \quad 101.324 \quad \text{kPa.} \end{aligned}$$

The measurement of variations in atmospheric pressure is important during ventilation surveys (Chapter 6), for psychrometric measurements (Chapter 14), and also for predicting the emission of stored gases into a subsurface ventilation system (Chapter 12). However, for many purposes, it is necessary to measure *differences* in pressure. One common example is the difference between the pressure within a system such as a duct and the exterior atmosphere pressure. This is referred to as *gauge pressure*.

$$\text{Absolute pressure} = \text{Atmospheric pressure} + \text{gauge pressure} \quad (2.9)$$

If the pressure within the system is below that of the local ambient atmospheric pressure then the negative gauge pressure is often termed the *suction pressure* or *vacuum* and the sign ignored.

Care should be taken when using equation 2.9 as the gauge pressure may be positive or negative. However, the absolute pressure is *always* positive. Although many quoted measurements are pressure differences, it is the absolute pressures that are used in thermodynamic calculations. We must not forget to convert when necessary.

2.2.4. Measurement of air pressure.

2.2.4.1. Barometers

Equation (2.8) showed that the pressure at the bottom of a column of liquid is equal to the product of the head (height) of the liquid, its density and the local value of gravitational acceleration. This principle was employed by **Evangelista Torricelli (1608-1647)**, the Italian who invented the mercury barometer in 1643.. Torricelli poured mercury into a glass tube, about one metre in length, closed at one end, and upturned the tube so that the open end dipped into a bowl of mercury. The level in the tube would then fall until the column of mercury, h , produced a pressure at the base that just balanced the atmospheric pressure acting on the open surface of mercury in the bowl.

The atmospheric pressure could then be calculated as (see equation (2.8))

$$P = \rho g h \quad \text{Pa}$$

where, in this case, ρ is the density of mercury.

Modern versions of the Torricelli instrument are still used as standards against which other types of barometer may be calibrated. Barometric (atmospheric) pressures are commonly quoted in millimetres (or inches) of mercury. However, for precise work, equation (2.8) should be employed using the density of mercury corresponding to its current temperature. Accurate mercury barometers have a thermometer attached to the stem of the instrument for this purpose and a sliding micrometer to assist in reading the precise height of the column. Furthermore, and again for accurate work, the local value of gravitational acceleration should be ascertained as this depends upon latitude and altitude. The space above the mercury in the barometer will not be a perfect vacuum as it contains mercury vapour. However, this exerts a pressure of less than 0.00016 kPa at 20 °C and is quite negligible compared with the surface atmospheric pressure of near 100 kPa. This, coupled with the fact that the high density of mercury produces a barometer of reasonable length, explains why mercury rather than any other liquid is used. A water barometer would need to be about 10.5m in height.

Owing to their fragility and slowness in reacting to temperature changes, mercury barometers are unsuitable for underground surveys . An aneroid barometer consists of a closed vessel which has been evacuated to a near perfect vacuum. One or more elements of the vessel are flexible. These may take the form of a flexing diaphragm, or the vessel itself may be shaped as a helical or spiral spring. The near zero pressure within the vessel remains constant. However, as the surrounding atmospheric pressure varies, the appropriate element of the vessel will flex. The movement may be transmitted mechanically, magnetically or electrically to an indicator and/or recorder.

Low cost aneroid barometers may be purchased for domestic or sporting use. Most altimeters are, in fact, aneroid barometers calibrated in metres (or feet) head of air. For the high accuracy required in ventilation surveys (Chapter 6) precision aneroid barometers are available.

Another principle that can be employed in pressure transducers, including barometers, is the piezoelectric property of quartz. The natural frequency of a quartz beam varies with the applied pressure. As electrical frequency can be measured with great precision, this allows the pressure to be determined with good accuracy.

2.2.4.2. Differential pressure instruments

Differences in air pressure that need to be measured frequently in subsurface ventilation engineering rarely exceed 7 or 8 kPa and are often of the order of only a few Pascals. The traditional instrument for such low pressure differences is the manometer. This relies upon the displacement of liquid to produce a column, or head, that balances the differential pressure being measured. The most rudimentary manometer is the simple glass U tube containing water, mercury or other liquid. A pressure difference applied across the ends of the tube causes the liquid levels in the two limbs to be displaced in opposite directions. A scale is used to measure the vertical distance between the levels and equation (2.8) used to calculate the required pressure differential. Owing to the past widespread use of water manometers, the millimetre (or inch) of water column came to be used commonly as a measure of small pressure differentials, much as a head of mercury has been used for atmospheric pressures. However, it suffers from the same disadvantages in that it is not a primary unit but depends upon the liquid density and local gravitational acceleration.

When a liquid other than water is used, the linear scale may be increased or decreased, dependent upon the density of the liquid, so that it still reads directly in head of water. A pressure head in one

fluid can be converted to a head in any other fluid provided that the ratio of the two densities is known.

$$p = \rho_1 g h_1 = \rho_2 g h_2 \quad \text{Pa}$$

$$\text{or} \quad h_2 = \frac{\rho_1}{\rho_2} h_1 \quad \text{m} \quad (2.10)$$

For high precision, the temperature of the liquid in a manometer should be obtained and the corresponding density determined. Equation (2.10) is then used to correct the reading, h_1 where ρ_1 is the actual liquid density and ρ_2 is the density at which the scale is calibrated.

Many variations of the manometer have been produced. Inclining one limb of the U tube shortens its practicable range but gives greater accuracy of reading. Careful levelling of inclined manometers is required and they are no longer used in subsurface pressure surveys. Some models have one limb of the U tube enlarged into a water reservoir. The liquid level in the reservoir changes only slightly compared with the balancing narrow tube. In the direct lift manometer, the reservoir is connected by flexible tubing to a short sight-glass of variable inclination which may be raised or lowered against a graduated scale. This manipulation enables the meniscus to be adjusted to a fixed mark on the sight-glass. Hence the level in the reservoir remains unchanged. The addition of a micrometer scale gives this instrument both a good range and high accuracy.

One of the problems in some water manometers is a misformed meniscus, particularly if the inclination of the tube is less than 5 degrees from the horizontal. This difficulty may be overcome by employing a light oil, or other liquid that has good wetting properties on glass. Alternatively, the two limbs may be made large enough in diameter to give horizontal liquid surfaces whose position can be sensed electronically or by touch probes adjusted through micrometers.

U tube manometers, or water gauges as they are commonly known, may feature as part of the permanent instrumentation of main and booster fans. Provided that the connections are kept firm and clean, there is little that can go wrong with these devices. Compact and portable inclined gauges are available for rapid readings of pressure differences across doors and stoppings in underground ventilation systems. However, in modern pressure surveying (Chapter 6) manometers have been replaced by the diaphragm gauge. This instrument consists essentially of a flexible diaphragm, across which is applied the differential pressure. The strain induced in the diaphragm is sensed electrically, mechanically or by magnetic means and transmitted to a visual indicator or recorder.

In addition to its portability and rapid reaction, the diaphragm gauge has many advantages for the subsurface ventilation engineer. First, it reflects directly a true pressure (force/area) rather than indirectly through a liquid medium. Secondly, it reacts relatively quickly to changes in temperature and does not require precise levelling. Thirdly, diaphragm gauges can be manufactured over a wide variety of ranges. A ventilation survey team may typically carry gauges ranging from 0 - 100 Pa to 0 - 5 kPa (or to encompass the value of the highest fan pressure in the system). One disadvantage of the diaphragm gauge is that its calibration may change with time and usage. Re-calibration against a laboratory precision manometer is recommended prior to an important survey.

Other appliances are used occasionally for differential pressures in subsurface pressure surveys. Piezoelectric instruments are likely to increase in popularity. The aerostat principle eliminates the need for tubing between the two measurement points and leads to a type of differential barometer. In this instrument, a closed and rigid air vessel is maintained at a constant temperature and is connected to the outside atmospheres via a manometer or diaphragm gauge. As the inside of the vessel remains at near constant pressure, any variations in atmospheric pressure cause a reaction on the manometer or gauge. Instruments based on this principle require independent calibration as slight movements of the diaphragm or liquid in the manometer result in the inside pressure not remaining truly constant.

2.3 FLUIDS IN MOTION

2.3.1. Bernoulli's equation for ideal fluids

As a fluid stream passes through a pipe, duct or other continuous opening, there will, in general, be changes in its velocity, elevation and pressure. In order to follow such changes it is useful to identify the differing forms of energy contained within a given mass of the fluid. For the time being, we will consider that the fluid is ideal; that is, it has no viscosity and proceeds along the pipe with no shear forces and no frictional losses. Secondly, we will ignore any thermal effects and consider mechanical energy only.

Suppose we have a mass, m , of fluid moving at velocity, u , at an elevation, Z , and a barometric pressure P . There are three forms of mechanical energy that we need to consider. In each case, we shall quantify the relevant term by assessing how much work we would have to do in order to raise that energy quantity from zero to its actual value in the pipe, duct or airway.

Kinetic energy

If we commence with the mass, m , at rest and accelerate it to velocity u in t seconds by applying a constant force F , then the acceleration will be uniform and the mean velocity is

$$\frac{0 + u}{2} = \frac{u}{2} \quad \frac{m}{s}$$

Then

distance travelled = mean velocity x time

$$= \frac{u}{2} t \quad m$$

Furthermore, the acceleration is defined as

$$\frac{\text{increase in velocity}}{\text{time}} = \frac{u}{t} \quad m / s^2$$

The force is given by

$$F = \text{mass} \times \text{acceleration}$$

$$= m \frac{u}{t} \quad N$$

and the work done to accelerate from rest to velocity u is

$$WD = \text{force} \times \text{distance} \quad Nm$$

$$= m \frac{u}{t} \times \frac{u}{2} t$$

$$= m \frac{u^2}{2} \quad Nm \text{ or } J \quad (2.11)$$

The kinetic energy of the mass m is, therefore, $m u^2/2$ Joules.

Potential energy

Any base elevation may be used as the datum for potential energy. In most circumstances of underground ventilation engineering, it is differences in elevation that are important. If our mass m is located on the base datum then it will have a potential energy of zero relative to that datum. We then exert an upward force, F , sufficient to counteract the effect of gravity.

$$\begin{aligned} F &= \text{mass} \times \text{acceleration} \\ &= m g \quad \text{N} \end{aligned}$$

where g is the gravitational acceleration.

In moving upward to the final elevation of Z metres above the datum, the work done is

$$\begin{aligned} \text{WD} &= \text{Force} \times \text{distance} \\ &= m g Z \quad \text{Joules} \end{aligned} \quad (2.12)$$

This gives the potential energy of the mass at elevation Z .

Flow work

Suppose we have a horizontal pipe, open at both ends and of cross sectional area A as shown in Figure 2.1. We wish to insert a plug of fluid, volume v and mass m into the pipe. However, even in the absence of friction, there is a resistance due to the pressure of the fluid, P , that already exists in the pipe. Hence, we must exert a force, F , on the plug of fluid to overcome that resisting pressure. Our intent is to find the work done on the plug of fluid in order to move it a distance s into the pipe.

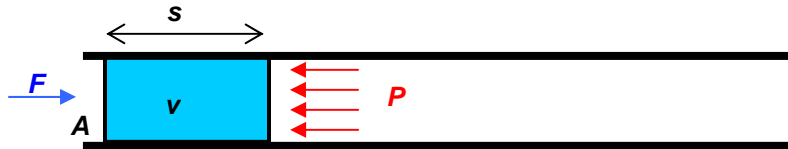


Figure 2.1 Flow work done on a fluid entering a pipe

The force, F , must balance the pressure, P , which is distributed over the area, A .

$$\begin{aligned} F &= P A \quad \text{N} \\ \text{Work done} &= \text{force} \times \text{distance} \\ &= P A s \quad \text{J or Joules} \end{aligned}$$

However, the product As is the swept volume v , giving

$$\text{WD} = P v$$

Now, by definition, the density is

$$\rho = \frac{m}{v} \quad \frac{\text{kg}}{\text{m}^3}$$

or

$$v = \frac{m}{\rho}$$

Hence, the work done in moving the plug of fluid into the pipe is

$$WD = \frac{Pm}{\rho} \quad \text{J} \quad (2.13)$$

or P/ρ Joules per kilogram.

As fluid continues to be inserted into the pipe to produce a continuous flow, then each individual plug must have this amount of work done on it. That energy is retained within the fluid stream and is known as the **flow work**. The appearance of pressure, P , within the expression for flow work has resulted in the term sometimes being labelled "pressure energy". This is very misleading as flow work is entirely different to the "elastic energy" stored when a closed vessel of fluid is compressed. Some authorities also object to the term "flow work" and have suggested "convected energy" or, simply, the " Pv work". Note that in Figure 2.1 the pipe is open at both ends. Hence the pressure, P , inside the pipe does not change with time (the fluid is not compressed) when plugs of fluid continue to be inserted in a frictionless manner. When the fluid exits the system, it will carry kinetic and potential energy, and the corresponding flow work with it.

Now we are in a position to quantify the total mechanical energy of our mass of fluid, m . From expressions (2.11, 2.12 and 2.13)

$$\begin{array}{rcccccc} \text{total mechanical} & & \text{kinetic} & & \text{potential} & & \text{flow} \\ \text{energy} & - & \text{energy} & + & \text{energy} & + & \text{work} \\ & & & & & & \\ & = & \frac{mu^2}{2} & + & mZg & + & m\frac{P}{\rho} & \text{J} \end{array} \quad (2.14)$$

If no mechanical energy is added to or subtracted from the fluid during its traverse through the pipe, duct or airway, and in the absence of frictional effects, the total mechanical energy must remain constant throughout the airway. Then equation (2.14) becomes

$$m \left\{ \frac{u^2}{2} + Zg + \frac{P}{\rho} \right\} = \text{constant} \quad \text{J} \quad (2.15)$$

Another way of expressing this equation is to consider two stations, 1 and 2 along the pipe, duct or airway. Then

$$m \left\{ \frac{u_1^2}{2} + Z_1g + \frac{P_1}{\rho_1} \right\} = m \left\{ \frac{u_2^2}{2} + Z_2g + \frac{P_2}{\rho_2} \right\}$$

Now as we are still considering the fluid to be incompressible (constant density),

$$\rho_1 = \rho_2 = \rho \quad (\text{say})$$

giving

$$\boxed{\frac{u_1^2 - u_2^2}{2} + (Z_1 - Z_2)g + \frac{P_1 - P_2}{\rho} = 0} \quad \frac{\text{J}}{\text{kg}} \quad (2.16)$$

Note that dividing by m on both sides has changed the units of each term from J to J/kg. Furthermore, if we multiplied throughout by ρ then each term would take the units of pressure. Bernoulli's equation has, traditionally, been expressed in this form for incompressible flow.

Equation (2.16) is of fundamental importance in the study of fluid flow. It was first derived by **Daniel Bernoulli (1700-1782)**, a Swiss mathematician, and is known throughout the world by his name.

As fluid flows along any closed system, Bernoulli's equation allows us to track the inter-relationships between the variables. Velocity u , elevation Z , and pressure P may all vary, but their combination as expressed in Bernoulli's equation remains true. It must be remembered, however, that it has been derived here on the assumptions of ideal (frictionless) conditions, constant density and steady-state flow. We shall see later how the equation must be amended for the real flow of compressible fluids.

2.3.2. Static, total and velocity pressures.

Consider the level duct shown on Figure 2.2. Three gauge pressures are measured. To facilitate visualization, the pressures are indicated as liquid heads on U tube manometers. However, the analysis will be conducted in terms of true pressure (N/m^2) rather than head of fluid.

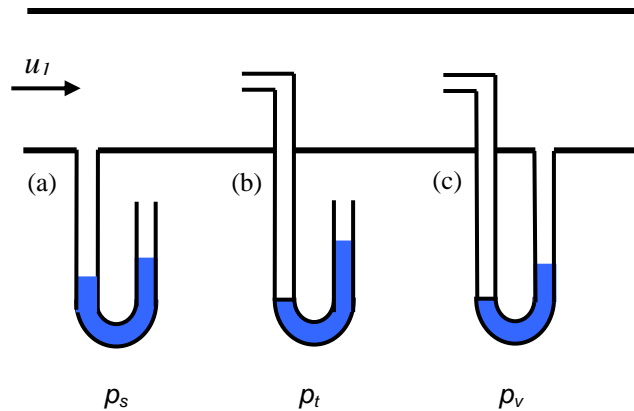


Figure 2.2 (a) static, (b) total and (c) velocity pressures

In position (a), one limb of the U tube is connected perpendicular through the wall of the duct. Any drilling burrs on the inside have been smoothed out so that the pressure indicated is not influenced by the local kinetic energy of the air. The other limb of the manometer is open to the ambient atmosphere. The gauge pressure indicated is known as the static pressure, p_s .

In position (b) the left tube has been extended into the duct and its open end turned so that it faces directly into the fluid stream. As the fluid impacts against the open end of the tube, it is brought to rest and the loss of its kinetic energy results in a local increase in pressure. The pressure within the tube then reflects the sum of the static pressure and the kinetic effect. Hence the manometer indicates a higher reading than in position (a). The corresponding pressure, p_t , is termed the total pressure. The increase in pressure caused by the kinetic energy can be quantified by using Bernoulli's equation (2.16). In this case $Z_1 = Z_2$, and $u_2 = 0$. Then

$$\frac{P_2 - P_1}{\rho} = \frac{u_1^2}{2}$$

The local increase in pressure caused by bringing the fluid to rest is then

$$p_v = P_2 - P_1 = \rho \frac{u_1^2}{2} \quad \text{Pa}$$

This is known as the velocity pressure and can be measured directly by connecting the manometer as shown in position (c). The left connecting tube of the manometer is at gauge pressure p_t and the right tube at gauge pressure p_s . It follows that

$$p_v = p_t - p_s$$

$$\text{or } p_t = p_s + p_v \quad \text{Pa} \quad (2.18)$$

In applying this equation, care should be taken with regard to sign as the static pressure, p_s , will be negative if the barometric pressure inside the duct is less than that of the outside atmosphere.

If measurements are actually made using a liquid in glass manometer as shown on Figure 2.2 then the reading registered on the instrument is influenced by the head of fluid in the manometer tubes above the liquid level. If the manometer liquid has a density ρ_1 , and the superincumbent fluid in both tubes has a density ρ_d , then the head indicated by the manometer, h , should be converted to true pressure by the equation

$$p = (\rho_1 - \rho_d)gh \quad \text{Pa} \quad (2.19)$$

Reflecting back on equation (2.8) shows that this is the usual equation relating fluid head and pressure with the density replaced by the difference in the two fluid densities. In ventilation engineering, the superincumbent fluid is air, having a very low density compared with liquids. Hence, the ρ_d term in equation (2.19) is usually neglected. However, if the duct or pipe contains a liquid rather than a gas then the full form of equation (2.19) should be employed.

A further situation arises when the fluid in the duct has a density, ρ_d , that is significantly different to that of the air (or other fluid), ρ_a , which exists above the liquid in the right hand tube of the manometer in Fig. 2.2(a). Then

$$p = (\rho_1 - \rho_d)gh - (\rho_d - \rho_a)gh_2 \quad \text{Pa} \quad (2.20)$$

where h_2 is the vertical distance between the liquid level in the right side of the manometer and the connection into the duct.

Equations (2.19) and (2.20) can be derived by considering a pressure balance on the two sides of the U tube above the lower of the two liquid levels.

2.3.3. Viscosity

Bernoulli's equation was derived in Section 2.3.1. on the assumption of an ideal fluid; i.e. that flow could take place without frictional resistance. In subsurface ventilation engineering almost all of the work input by fans (or other ventilating devices) is utilized against frictional effects within the airways. Hence, we must find a way of amending Bernoulli's equation for the frictional flow of real fluids.

The starting point in an examination of '**frictional flow**' is the concept of viscosity. Consider two parallel sheets of fluid a very small distance, dy , apart but moving at different velocities u and $u + du$ (Figure 2.3). An equal but opposite force, F , will act upon each layer, the higher velocity sheet tending to pull its slower neighbour along and, conversely, the slower sheet tending to act as a brake on the higher velocity layer.

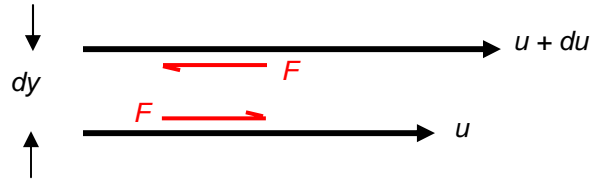


Figure 2.3 Viscosity causes equal but opposite forces to be exerted on adjacent laminae of fluid.

If the area of each of the two sheets in near contact is A , then the shear stress is defined as τ (Greek 'tau') where

$$\tau = \frac{F}{A} \quad \frac{\text{N}}{\text{m}^2} \quad (2.21)$$

Among his many accomplishments, **Isaac Newton (1642-1727)** proposed that for parallel motion of streamlines in a moving fluid, the shear stress transmitted across the fluid in a direction perpendicular to the flow is proportional to the rate of change of velocity, du/dy (velocity gradient)

$$\tau = \frac{F}{A} = \mu \frac{du}{dy} \quad \frac{\text{N}}{\text{m}^2} \quad (2.22)$$

where the constant of proportionality, μ , is known as the coefficient of dynamic viscosity (usually referred to simply as dynamic viscosity). The dynamic viscosity of a fluid varies with its temperature. For air, it may be determined from

$$\mu_{\text{air}} = (17.0 + 0.045 t) \times 10^{-6} \quad \frac{\text{Ns}}{\text{m}^2}$$

and for water

$$\mu_{\text{water}} = \left(\frac{64.72}{t + 31.766} - 0.2455 \right) \times 10^{-3} \quad \frac{\text{Ns}}{\text{m}^2}$$

where t = temperature ($^{\circ}\text{C}$) in the range 0 - 60 $^{\circ}\text{C}$

The units of viscosity are derived by transposing equation (2.22)

$$\mu = \tau \frac{dy}{du} \quad \frac{\text{N}}{\text{m}^2} \frac{\text{m}}{\text{m}} \frac{\text{s}}{\text{m}} \quad \text{or} \quad \frac{\text{Ns}}{\text{m}^2}$$

A term which commonly occurs in fluid mechanics is the ratio of dynamic viscosity to fluid density. This is called the *kinematic viscosity*, ν (Greek 'nu')

$$\nu = \frac{\mu}{\rho} \quad \frac{\text{Ns}}{\text{m}^2} \frac{\text{m}^3}{\text{kg}} \quad \text{or} \quad \text{Nm} \frac{\text{s}}{\text{kg}}$$

As $1 \text{ N} = 1 \text{ kg} \times 1 \text{ m/s}^2$, these units become

$$\text{kg} \frac{\text{m}}{\text{s}^2} \frac{\text{ms}}{\text{kg}} = \frac{\text{m}^2}{\text{s}}$$

It is the transmission of shear stress that produces frictional resistance to motion in a fluid stream. Indeed, a definition of an 'ideal fluid' is one that has zero viscosity. Following from our earlier discussion on the molecular behaviour of fluids (Section 2.1.1.), there would appear to be at least two effects that produce the phenomenon of viscosity. One is the attractive forces that exist between molecules - particularly those of liquids. This will result in the movement of some molecules tending to drag others along, and for the slower molecules to inhibit motion of faster neighbours. The second effect may be visualized by glancing again at Figure 2.3. If molecules from the faster moving layer stray sideways into the slower layer then the inertia that they carry will impart kinetic energy to that layer. Conversely, migration of molecules from the slower to the faster layer will tend to retard its motion.

In liquids, the molecular attraction effect is dominant. Heating a liquid increases the internal kinetic energy of the molecules and also increases the average inter-molecular spacing. Hence, as the attractive forces diminish with distance, the viscosity of a liquid decreases with respect to temperature. In a gas, the molecular attractive force is negligible. The viscosity of gases is much less than that of liquids and is caused by the molecular inertia effect. In this case, the increased velocity of molecules caused by heating will tend to enhance their ability to transmit inertia across streamlines and, hence, we may expect the viscosity of gases to increase with respect to temperature. This is, in fact, the situation observed in practice.

In both of these explanations of viscosity, the effect works between consecutive layers equally well in both directions. Hence, dynamic equilibrium is achieved with both the higher and lower velocity layers maintaining their net energy levels. Unfortunately, no real process is perfect in fluid mechanics. Some of the useful mechanical energy will be transformed into the much less useful heat energy. In a level duct, pipe or airway, the loss of mechanical energy is reflected in an observable drop in pressure. This is often termed the '**frictional pressure drop**'

Recalling that Bernoulli's equation was derived for mechanical energy terms only in Section 2.3.1, it follows that for the flow of real fluids, the equation must take account of the frictional loss of mechanical energy. We may rewrite equation (2.16) as

$$\frac{u_1^2}{2} + Z_1 g + \frac{P_1}{\rho} = \frac{u_2^2}{2} + Z_2 g + \frac{P_2}{\rho} + F_{12} \quad \frac{\text{J}}{\text{kg}} \quad (2.23)$$

where F_{12} = energy converted from the mechanical form to heat (J/kg).

The problem now turns to one of quantifying the frictional term F_{12} . For that, we must first examine the nature of fluid flow.

2.3.4. Laminar and turbulent flow. Reynolds Number

In our everyday world, we can observe many examples of the fact that there are two basic kinds of fluid flow. A stream of oil poured out of a can flows smoothly and in a controlled manner while water, poured out at the same rate, would break up into cascading rivulets and droplets. This example seems to suggest that the type of flow depends upon the fluid. However, a light flow of water falling from a circular outlet has a steady and controlled appearance, but if the flowrate is increased the stream will assume a much more chaotic form. The type of flow seems to depend upon the flowrate as well as the type of fluid.

Throughout the nineteenth century, it was realized that these two types of flow existed. The German engineer **G.H.L. Hagen (1797-1884)** found that the type of flow depended upon the velocity and viscosity of the fluid. However, it was not until the 1880's that Professor **Osborne Reynolds** of Manchester University in England established a means of characterizing the type of flow regime

through a combination of experiments and logical reasoning. Reynolds' laboratory tests consisted of injecting a filament of colored dye into the bell mouth of a horizontal glass tube that was submerged in still water within a large glass-walled tank. The other end of the tube passed through the end of the tank to a valve which was used to control the velocity of water within the tube. At low flow rates, the filament of dye formed an unbroken line in the tube without mixing with the water. At higher flow rates the filament of dye began to waver. As the velocity in the tube continued to be increased the wavering filament suddenly broke up to mix almost completely with the water.

In the initial type of flow, the water appeared to move smoothly along streamlines, layers or laminae, parallel to the axis of the tube. We call this **laminar flow**. Appropriately, we refer to the completely mixing type of behavior as **turbulent flow**. Reynolds' experiments had, in fact, identified a third regime - the wavering filament indicated a transitional region between fully laminar and fully turbulent flow. Another observation made by Reynolds was that the break-up of the filament always occurred, not at the entrance, but about thirty diameters along the tube.

The essential difference between laminar and turbulent flow is that in the former, movement across streamlines is limited to the molecular scale, as described in Section 2.3.3. However, in turbulent flow, swirling packets of fluid move sideways in small turbulent eddies. These should not be confused with the larger and more predictable oscillations that can occur with respect to time and position such as the vortex action caused by fans, pumps or obstructions in the airflow. The turbulent eddies appear random in the complexity of their motion. However, as with all "random" phenomena, the term is used generically to describe a process that is too complex to be characterized by current mathematical knowledge. Computer simulation packages using techniques known generically as **computational fluid dynamics (CFD)** have produced powerful means of analysis and predictive models of turbulent flow. At the present time, however, many practical calculations involving turbulent flow still depend upon empirical factors.

The flow of air in the vast majority of 'ventilated' places underground is turbulent in nature. However, the sluggish movement of air or other fluids in zones behind stoppings or through fragmented strata may be laminar. It is, therefore, important that the subsurface ventilation engineer be familiar with both types of flow. Returning to Osborne Reynolds, he found that the development of full turbulence depended not only upon velocity, but also upon the diameter of the tube. He reasoned that if we were to compare the flow regimes between differing geometrical configurations and for various fluids we must have some combination of geometric and fluid properties that quantified the degree of similitude between any two systems. Reynolds was also familiar with the concepts of "inertial (kinetic) force", $\rho u^2/2$ (Newtons per square metre of cross section) and "viscous force", $\tau = \mu du/dy$ (Newtons per square metre of shear surface). Reynolds argued that the dimensionless ratio of "inertial forces" to "viscous forces" would provide a basis of comparing fluid systems

$$\frac{\text{inertial force}}{\text{viscous force}} = \rho \frac{u^2}{2} \frac{1}{\mu} \frac{dy}{du} \quad (2.24)$$

Now, for similitude to exist, all steady state velocities, u , or differences in velocity between locations, du , within a given system are proportional to each other. Furthermore, all lengths are proportional to any chosen characteristic length, L . Hence, in equation (2.24) we can replace du by u , and dy by L . The constant, 2, can also be dropped as we are simply looking for a combination of variables that characterize the system. That combination now becomes

$$\rho u^2 \frac{1}{\mu} \frac{L}{u}$$

or

$$\frac{\rho u L}{\mu} = \text{Re} \quad (2.25)$$

As equation (2.24) is dimensionless then so, also, must this latter expression be dimensionless. This can easily be confirmed by writing down the units of the component variables. The result we have reached here is of fundamental importance to the study of fluid flow. The dimensionless group $\rho u L / \mu$ is known universally as Reynolds Number, Re . In subsurface ventilation engineering, the characteristic length is normally taken to be the hydraulic mean diameter of an airway, d , and the characteristic velocity is usually the mean velocity of the airflow. Then

$$Re = \frac{\rho u d}{\mu}$$

At Reynolds Numbers of less than 2 000 in fluid flow systems, viscous forces prevail and the flow will be laminar. The Reynolds Number over which fully developed turbulence exists is less well defined. The onset of turbulence will occur at Reynolds Numbers of 2 500 to 3 000 assisted by any vibration, roughness of the walls of the pipe or any momentary perturbation in the flow.

Example

A ventilation shaft of diameter 5m passes an airflow of 200 m³/s at a mean density of 1.2 kg/m³ and an average temperature of 18 °C. Determine the Reynolds Number for the shaft.

Solution

For air at 18 °C

$$\begin{aligned} \mu &= (17.0 + 0.045 \times 18) \times 10^{-6} \\ &= 17.81 \times 10^{-6} \text{ Ns/m}^2 \end{aligned}$$

$$\text{Air velocity, } u = \frac{Q}{A} = \frac{200}{\pi 5^2 / 4} = 10.186 \text{ m/s}$$

$$Re = \frac{\rho u d}{\mu} = \frac{1.2 \times 10.186 \times 5}{17.81 \times 10^{-6}} = 3.432 \times 10^6$$

This Reynolds Number indicates that the flow will be turbulent.

2.3.5. Frictional losses in laminar flow, Poiseuille's Equation.

Now that we have a little background on the characteristics of laminar and turbulent flow, we can return to Bernoulli's equation corrected for friction (equation (2.23)) and attempt to find expressions for the work done against friction, F_{12} . First, let us deal with the case of laminar flow.

Consider a pipe of radius R as shown in Figure 2.4. As the flow is laminar, we can imagine concentric cylinders of fluid telescoping along the pipe with zero velocity at the walls and maximum velocity in the center. Two of these cylinders of length L and radii r and $r + dr$ are shown. The velocities of the cylinders are u and $u - du$ respectively.

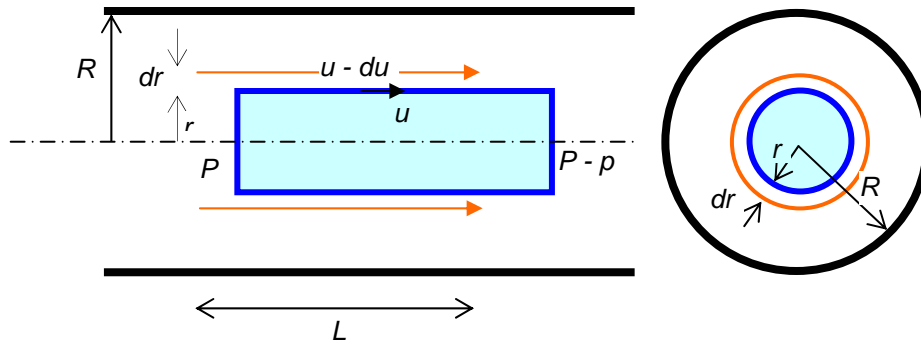


Figure 2.4 Viscous drag opposes the motive effect of applied pressure difference

The force propagating the inner cylinder forward is produced by the pressure difference across its two ends, p , multiplied by its cross sectional area, πr^2 . This force is resisted by the viscous drag of the outer cylinder, τ , acting on the 'contact' area $2\pi rL$. As these forces must be equal at steady state conditions,

$$2\pi r \tau L = \pi r^2 p$$

However, $\tau = -\mu \frac{du}{dr}$ (equation (2.22) with a negative du)

giving

$$-\mu \frac{du}{dr} = \frac{r p}{2 L}$$

$$\text{or } du = -\frac{p r}{L 2 \mu} dr \quad \frac{\text{m}}{\text{s}} \quad (2.26)$$

For a constant diameter tube, the pressure gradient along the tube p/L is constant. So, also, is μ for the Newtonian fluids that we are considering. (A Newtonian fluid is defined as one in which viscosity is independent of velocity). Equation (2.26) can, therefore, be integrated to give

$$u = -\frac{p}{L} \frac{1}{2 \mu} \frac{r^2}{2} + C \quad (2.27)$$

At the wall of the tube, $r = R$ and $u = 0$. This gives the constant of integration to be

$$C = \frac{p R^2}{L 4 \mu}$$

Substituting back into equation (2.27) gives

$$u = \frac{1}{4 \mu L} p (R^2 - r^2) \quad \frac{\text{m}}{\text{s}} \quad (2.28)$$

Equation (2.28) is a general equation for the velocity of the fluid at any radius and shows that the velocity profile across the tube is parabolic (Figure 2.5). Along the centre line of the tube, $r = 0$ and the velocity reaches a maximum of

$$u_{\max} = \frac{1}{4} \frac{\rho}{\mu} \frac{p}{L} R^2 \quad \frac{\text{m}}{\text{s}} \quad (2.29)$$

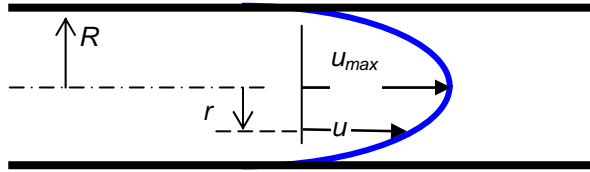


Figure 2.5 The velocity profile for laminar flow is parabolic

The velocity terms in the Bernoulli equation are mean velocities across the relevant cross-sections. It is, therefore, preferable that the work done against viscous friction should also be expressed in terms of a mean velocity, u_m . We must be careful how we define *mean velocity* in this context. Our convention is to determine it as

$$u_m = \frac{Q}{A} \quad \frac{\text{m}}{\text{s}} \quad (2.30)$$

where Q = volume airflow (m^3/s) and A = cross sectional area (m^2)

We could define another mean velocity by integrating the parabolic equation (2.28) with respect to r and dividing the result by R . However, this would not take account of the fact that the volume of fluid in each concentric shell of thickness dr increases with radius. In order to determine the true mean velocity, consider the elemental flow dQ through the annulus of cross sectional area $2\pi r dr$ at radius r and having a velocity of u (Figure 2.4)

$$dQ = u 2\pi r dr$$

Substituting for u from equation (2.28) gives

$$dQ = \frac{2\pi}{4\mu} \frac{\rho}{L} (R^2 - r^2) r dr$$

$$Q = \frac{2\pi}{4\mu} \frac{\rho}{L} \int_0^R (R^2 r - r^3) dr$$

Integrating gives

$$Q = \frac{\pi R^4}{8\mu} \frac{\rho}{L} \quad \frac{\text{m}}{\text{s}} \quad (2.31)$$

This is known as the **Poiseuille Equation** or, sometimes, the Hagen-Poiseuille Equation. **J.L.M. Poiseuille (1799-1869)** was a French physician who studied the flow of blood in capillary tubes.

For engineering use, where the dimensions of a given pipe and the viscosity of fluid are known, Poiseuille's equation may be written as a pressure drop - quantity relationship.

$$p = \frac{8 \mu L}{\pi R^4} Q$$

or

$$p = R_L Q \quad \text{Pa} \quad (2.32)$$

where $R_L = \frac{8 \mu L}{\pi R^4}$ $\frac{\text{Ns}}{\text{m}^5}$ and is known as the laminar resistance of the pipe.

Equation (2.32) shows clearly that in laminar flow the frictional pressure drop is proportional to the volume flow for any given pipe and fluid. Combining equations (2.30) and (2.31) gives the required mean velocity

$$u_m = \frac{\pi R^4}{8 \mu} \frac{p}{L} \frac{1}{\pi R^2} = \frac{R^2 p}{8 \mu L} \quad \frac{\text{m}}{\text{s}} \quad (2.33)$$

or

$$p = \frac{8 \mu u_m L}{R^2} \quad \text{Pa} \quad (2.34)$$

This latter form gives another expression for the frictional pressure drop in laminar flow.

To see how we can use this equation in practice, let us return the frictional form of Bernoulli's equation

$$\frac{u_1^2 - u_2^2}{2} + (Z_1 - Z_2)g + \frac{(P_1 - P_2)}{\rho} = F_{12} \quad \frac{\text{J}}{\text{kg}} \quad (\text{see equation (2.23)})$$

Now for incompressible flow along a level pipe of constant cross-sectional area,
 $Z_1 = Z_2$ and $u_1 = u_2 = u_m$
 then

$$\frac{(P_1 - P_2)}{\rho} = F_{12} \quad \frac{\text{J}}{\text{kg}} \quad (2.35)$$

However, $(P_1 - P_2)$ is the same pressure difference as p in equation (2.34).

Hence the work done against friction is

$$F_{12} = \frac{8 \mu u_m L}{\rho R^2} \quad \frac{\text{J}}{\text{kg}} \quad (2.36)$$

Bernoulli's equation for incompressible laminar frictional flow now becomes

$$\frac{u_1^2 - u_2^2}{2} + (Z_1 - Z_2)g + \frac{(P_1 - P_2)}{\rho} = \frac{8 \mu u_m L}{\rho R^2} \quad \frac{\text{J}}{\text{kg}} \quad (2.37)$$

If the pipe is of constant cross sectional area, then $u_1 = u_2 = u_m$ and the kinetic energy term disappears. On the other hand, if the cross-sectional area and, hence, the velocity varies along the pipe then u_m may be established as a weighted mean. For large changes in cross-sectional area, the full length of pipe may be subdivided into increments for analysis.

Example.

A pipe of diameter 2 cm rises through a vertical distance of 5m over the total pipe length of 2 000 m. Water of mean temperature 15°C flows up the tube to exit at atmospheric pressure of 100 kPa. If the required flowrate is 1.6 litres per minute, find the resistance of the pipe, the work done against friction and the head of water that must be applied at the pipe entrance.

Solution.

It is often the case that measurements made in engineering are not in SI units. We must be careful to make the necessary conversions before commencing any calculations.

Flowrate $Q = 1.6$ litres/min

$$= \frac{1.6}{1000 \times 60} = 2.667 \times 10^{-5} \quad \frac{\text{m}^3}{\text{s}}$$

Cross sectional area of pipe $A = \pi d^2 / 4 = \pi \times (0.02^2) / 4 = 3.142 \times 10^{-4} \text{ m}^2$

$$\text{Mean velocity, } u = \frac{Q}{A} = \frac{2.667 \times 10^{-5}}{3.142 \times 10^{-4}} = 0.08488 \quad \text{m/s}$$

(We have dropped the subscript m . For simplicity, the term u from this point on will refer to the mean velocity defined as Q/A)

Viscosity of water at 15 °C (from Section 2.3.3.)

$$\mu = \left(\frac{64.72}{15 + 31.766} - 0.2455 \right) \times 10^{-3} = 1.138 \times 10^{-3} \quad \frac{\text{Ns}}{\text{m}^2}$$

Before we can begin to assess frictional effects we must check whether the flow is laminar or turbulent. We do this by calculating the Reynolds Number

$$\text{Re} = \frac{\rho u d}{\mu}$$

where ρ = density of water (taken as 1 000 kg/m³)

$$\text{Re} = \frac{1000 \times 0.08488 \times 0.02}{1.138 \times 10^{-3}} = 1491 \quad (\text{dimensionless})$$

As Re is below 2 000, the flow is laminar and we should use the equations based on viscous friction.

Laminar resistance of pipe (from equation (2.32))

$$R_L = \frac{8 \mu L}{\pi R^4} = \frac{8 \times 1.1384 \times 10^{-3} \times 2000}{\pi \times (0.01)^4} = 580 \times 10^6 \quad \frac{\text{Ns}}{\text{m}^5}$$

Frictional pressure drop in the pipe (equation (2.32))

$$p = R_L Q = 580 \times 10^{-6} \times 2.667 \times 10^{-5} = 15\,461 \quad \text{Pa}$$

Work done against friction (equation (2.36))

$$F_{12} = \frac{8 \mu u L}{\rho R^2} = \frac{8 \times 1.1384 \times 10^{-3} \times 0.084\,88 \times 2000}{1000 \times (0.01)^2} = 15.461 \quad \frac{\text{J}}{\text{kg}}$$

This is the amount of mechanical energy transformed to heat in Joules per kilogram of water. Note the similarity between the statements for frictional pressure drop, p , and work done against friction, F_{12} . We have illustrated, by this example, a relationship between p and F_{12} that will be of particular significance in comprehending the behaviour of airflows in ventilation systems, namely

$$\frac{p}{\rho} = F_{12}$$

In fact, having calculated p as 15 461 Pa, the value of F_{12} may be quickly evaluated as

$$\frac{15\,461}{1000} = 15.461 \quad \frac{\text{J}}{\text{kg}}$$

To find the pressure at the pipe inlet we may use Bernoulli's equation corrected for frictional effects

$$\frac{u_1^2 - u_2^2}{2} + (Z_1 - Z_2)g + \frac{P_1 - P_2}{\rho} = F_{12} \quad \frac{\text{J}}{\text{kg}} \quad (\text{see equation (2.23)})$$

In this example

$$u_1 = u_2$$

$$Z_1 - Z_2 = -5 \text{ m}$$

and $P_2 = 100 \text{ kPa} = 100\,000 \text{ Pa}$

$$\text{giving } F_{12} = -5 \times 9.81 + \frac{P_1 - 100\,000}{1000} = 15.461 \quad \frac{\text{J}}{\text{kg}}$$

This yields the absolute pressure at the pipe entry as

$$P_1 = 164.5 \times 10^3 \quad \text{Pa}$$

or 164.5 kPa

If the atmospheric pressure at the location of the bottom of the pipe is also 100 kPa, then the gauge pressure, p_g , within the pipe at that same location

$$p_g = 164.5 - 100 = 64.5 \text{ kPa}$$

This can be converted into a head of water, h_1 , from equation (2.8)

$$p_g = \rho g h_1$$

$$h_1 = \frac{64.5 \times 10^{-3}}{1000 \times 9.81} = 6.576 \quad \text{m of water}$$

Thus, a header tank with a water surface maintained 6.576 m above the pipe entrance will produce the required flow of 1.6 litres/minute along the pipe.

The experienced engineer would have determined this result quickly and directly after calculating the frictional pressure drop to be 15 461 Pa. The frictional head loss

$$h = \frac{p}{\rho g} = \frac{15\,461}{1000 \times 9.81} = 1.576 \quad \text{m of water}$$

The head of water at the pipe entrance must overcome the frictional head loss as well as the vertical lift of 5 m. (An intuitive use of Bernoulli's equation). Then

$$h_1 = 5 + 1.576 = 6.576 \quad \text{m of water}$$

2.3.6. Frictional losses in turbulent flow

The previous section showed that the parallel streamlines of laminar flow and Newton's perception of viscosity enabled us to produce quantitative relationships through purely analytical means. Unfortunately, the highly convoluted streamlines of turbulent flow, caused by the interactions between both localized and propagating eddies have so far proved resistive to completely analytical techniques. Numerical methods using the memory capacities and speeds of supercomputers allow the flow to be simulated as a large number of small packets of fluids, each one influencing the behaviour of those around it. These mathematical models, using numerical techniques known collectively as **computational fluid dynamics (CFD)**, may be used to simulate turbulent flow in given geometrical systems, or to produce statistical trends. However, the majority of engineering applications involving turbulent flow still rely on a combination of analysis and empirical factors. The construction of physical models for observation in wind tunnels or other fluid flow test facilities remains a common means of predicting the behaviour and effects of turbulent flow.

2.3.6.1. The Chézy-Darcy Equation

The discipline of hydraulics was studied by philosophers of the ancient civilizations. However, the beginnings of our present treatment of fluid flow owe much to the hydraulic engineers of eighteenth and nineteenth century France. During his reign, **Napoleon Bonaparte** encouraged the research and development necessary for the construction of water distribution and drainage systems in Paris.

Antoine de Chézy (1719-1798) carried out a series of experiments on the river Seine and on canals in about 1769. He found that the mean velocity of water in open ducts was proportional to the square root of the channel gradient, cross sectional area of flow and inverse of the wetted perimeter.

$$u \propto \sqrt{\frac{A}{per} \frac{h}{L}}$$

where h = vertical distance dropped by the channel in a length L (h/L = hydraulic gradient)

per = wetted perimeter (m)

and \propto means 'proportional to'

Inserting a constant of proportionality, c , gives

$$u = c \sqrt{\frac{A}{per} \frac{h}{L}} \quad \frac{\text{m}}{\text{s}} \quad (2.38)$$

where c is known as the Chézy coefficient.

Equation (2.38) has become known as Chézy's equation for channel flow. Subsequent analysis shed further light on the significance of the Chézy coefficient. When a fluid flows along a channel, a mean shear stress τ is set up at the fluid/solid boundaries. The drag on the channel walls is then

$$\tau \text{ per } L$$

where per is the "wetted" perimeter

This must equal the pressure force causing the fluid to move, pA , where p is the difference in pressure along length L .

$$\tau \text{ per } L = A p \quad \text{N} \quad (2.39)$$

(A similar equation was used in Section 2.3.5. for a circular pipe).

But $p = \rho g h$ Pa (equation (2.8))

$$\text{giving } \tau = \frac{A}{per} \rho g \frac{h}{L} \quad \frac{\text{N}}{\text{m}^2} \quad (2.40)$$

If the flow is fully turbulent, the shear stress or skin friction drag, τ , exerted on the channel walls is also proportional to the inertial (kinetic) energy of the flow expressed in Joules per cubic metre.

$$\tau \propto \rho \frac{u^2}{2} \quad \frac{\text{J}}{\text{m}^3} = \frac{\text{Nm}}{\text{m}^3} \text{ or } \frac{\text{N}}{\text{m}^2}$$

$$\text{or } \tau = f \rho \frac{u^2}{2} \quad \frac{\text{N}}{\text{m}^2} \quad (2.41)$$

where f is a dimensionless coefficient which, for fully developed turbulence, depends only upon the roughness of the channel walls.

Equating (2.40) and (2.41) gives

$$f \frac{u^2}{2} = \frac{A}{per} g \frac{h}{L}$$

$$\text{or } u = \sqrt{\frac{2g}{f}} \sqrt{\frac{A}{per} \frac{h}{L}} \quad \frac{\text{m}}{\text{s}} \quad (2.42)$$

Comparing this with equation (2.38) shows that Chézy's coefficient, c , is related to the roughness of the channel.

$$c = \sqrt{\frac{2g}{f}} \quad \frac{\text{m}^{\frac{1}{2}}}{\text{s}} \quad (2.43)$$

The development of flow relationships was continued by **Henri Darcy (1803-1858)**, another French engineer, who was interested in the turbulent flow of water in pipes. He adapted Chézy's work to the case of circular pipes and ducts running full. Then $A = \pi d^2 / 4$, $per = \pi d$ and the fall in elevation of Chézy's channel became the head loss, h (metres of fluid) along the pipe length L . Equation (2.42) now becomes

$$u^2 = \frac{2g}{f} \frac{\pi d^2}{4} \frac{1}{\pi d} \frac{h}{L}$$

or

$$h = \frac{4fLu^2}{2gd} \quad \text{metres of fluid} \quad (2.44)$$

This is the well known **Chézy-Darcy equation**, sometimes also known simply as the Darcy equation or the Darcy-Weisbach equation. The head loss, h , can be converted to a frictional pressure drop, p , by the now familiar relationship, $p = \rho gh$ to give

$$p = \frac{4fL\rho u^2}{d} \quad \text{Pa} \quad (2.45)$$

or a frictional work term

$$F_{12} = \frac{p}{\rho} = \frac{4fL}{d} \frac{u^2}{2} \quad \frac{\text{J}}{\text{kg}} \quad (2.46)$$

The Bernoulli equation for frictional and turbulent flow becomes

$$\frac{u_1^2 - u_2^2}{2} + (Z_1 - Z_2)g + \frac{(P_1 - P_2)}{\rho} = \frac{4fL}{d} \frac{u^2}{2} \quad \frac{\text{J}}{\text{kg}} \quad (2.47)$$

where u is the mean velocity.

The most common form of the Chézy-Darcy equation is that given as (2.44). Leaving the constant 2 uncanceled provides a reminder that the pressure loss due to friction is a function of kinetic energy $u^2/2$. However, some authorities have combined the 4 and the f into a different coefficient of friction $\lambda (= 4f)$ while others, presumably disliking Greek letters, then replaced the symbol λ by (would you believe it?), f . We now have a confused situation in the literature of fluid mechanics where f may mean the original Chézy-Darcy coefficient of friction, or four times that value. When reading the literature, care should be taken to confirm the nomenclature used by the relevant author. Throughout this book, f is used to mean the original Chézy-Darcy coefficient as used in equation (2.44).

In order to generalize our results to ducts or airways of non-circular cross section, we may define a **hydraulic radius** as

$$\begin{aligned} r_h &= \frac{A}{per} && \text{m} && (2.48) \\ &= \frac{\pi d^2}{4\pi d} = \frac{d}{4} \end{aligned}$$

Reference to the "**hydraulic mean diameter**" denotes $4A/per$. This device works well for turbulent flow but must not be applied to laminar flow where the resistance to flow is caused by viscous action throughout the body of the fluid rather than concentrated around the perimeter of the walls.

Substituting for d in equation (2.45) gives

$$p = fL \frac{per}{A} \frac{\rho u^2}{2} \quad \text{Pa} \quad (2.49)$$

This can also be expressed as a relationship between frictional pressure drop, p , and volume flow, Q . Replacing u by Q/A in equation (2.49) gives

$$p = \frac{fL}{2} \frac{per}{A^3} \rho Q^2 \quad \text{Pa}$$

$$\text{or} \quad p = R_t \rho Q^2 \quad \text{Pa} \quad (2.50)$$

$$\text{where} \quad R_t = \frac{fL}{2} \frac{per}{A^3} \quad \text{m}^{-4} \quad (2.51)$$

This is known as the rational turbulent resistance of the pipe, duct or airway and is a function only of the geometry and roughness of the opening.

2.3.6.2. The coefficient of friction, f .

It is usually the case that a significant advance in research opens up new avenues of investigation and produces a flurry of further activity. So it was following the work of Osborne Reynolds. During the first decade of this century, fluid flow through pipes was investigated in great detail by engineers such as **Thomas E. Stanton (1865-1931)** and **J.R. Pannel** in the United Kingdom, and **Ludwig Prandtl (1875-1953)** in Germany. A major cause for concern was the coefficient of friction, f .

There were two problems. First, how could one predict the value of f for any given pipe without actually constructing the pipe and conducting a pressure-flow test on it. Secondly, it was found that f was not a true constant but varied with Reynolds Number for very smooth pipes and, particularly, at low values of Reynolds Number. The latter is not too surprising as f was introduced initially as a constant of proportionality between shear stress at the walls and inertial force of the fluid (equation (2.41)) for fully developed turbulence. At the lower Reynolds Numbers we may enter the transitional or even laminar regimes.

Figure 2.6 illustrates the type of results that were obtained. A very smooth pipe exhibited a continually decreasing value of f . This is labelled as the turbulent smooth pipe curve. However, for rougher pipes, the values of f broke away from the smooth pipe curve at some point and, after a transitional region, settled down to a constant value, independent of Reynolds Number. This phenomenon was quantified empirically through a series of classical experiments conducted in Germany by **Johann Nikuradse (1894-1979)**, a former student of Prandtl. Nikuradse took a number of smooth pipes of diameter 2.5, 5 and 10 cm, and coated the inside walls uniformly with grains of

graded sand. The roughness of each tube was then defined as e/d where e was the diameter of the sand grains and d the diameter of the tube. The advantages of dimensionless numbers had been well learned from Reynolds. The corresponding f - Re relationships are illustrated on Figure 2.6.

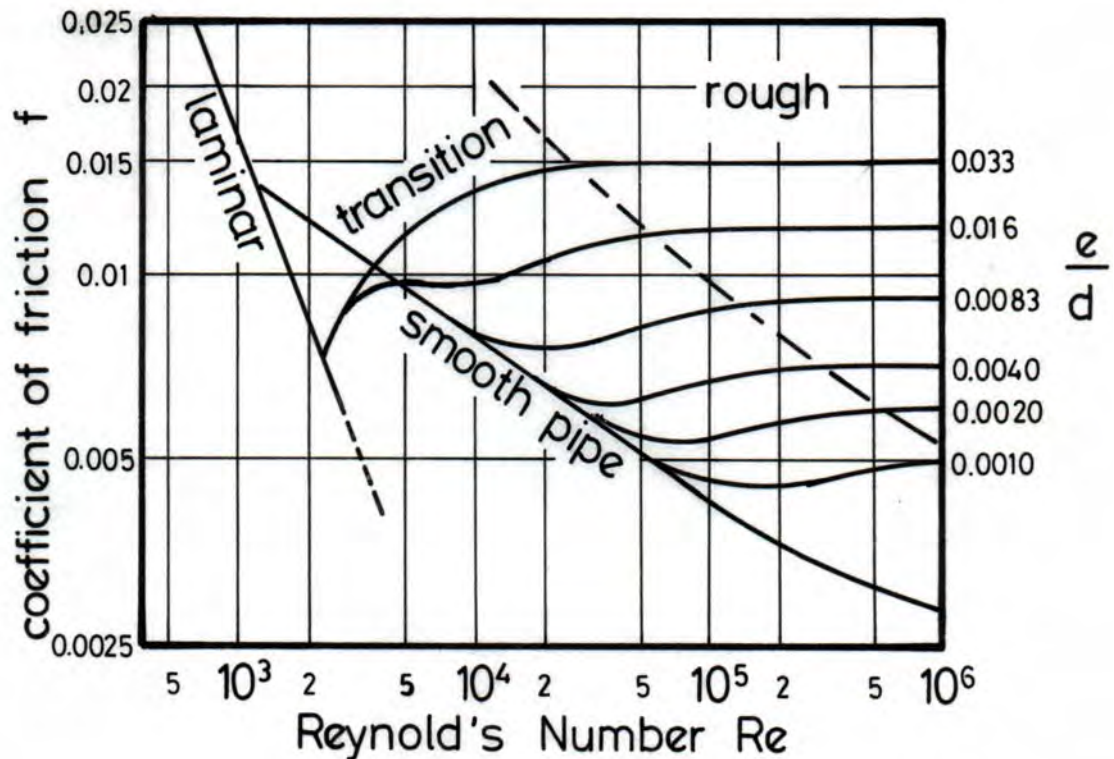


Figure 2.6 variation of f with respect to Re as found by Nikuradse

The investigators of the time were then faced with an intriguing question. How could a pipe of given roughness and passing a turbulent flow be "smooth" (i.e. follow the smooth pipe curve) at certain Reynolds Numbers but become "rough" (constant f) at higher Reynolds Numbers? The answer lies in our initial concept of turbulence - the formation and maintenance of small, interacting and propagating eddies within the fluid stream. These necessitate the existence of cross velocities with vector components perpendicular to the longitudinal axis of the tube. At the walls there can be no cross velocities except on a molecular scale. Hence, there must be a thin layer close to each wall through which the velocity increases from zero (actually at the wall) to some finite velocity sufficiently far away from the wall for an eddy to exist. Within that thin layer the streamlines remain parallel to each other and to the wall, i.e. laminar flow.

Although this **laminar sublayer** is very thin, it has a marked effect on the behaviour of the total flow in the pipe. All real surfaces (even polished ones) have some degree of roughness. If the peaks of the roughness, or asperities, do not protrude through the laminar sublayer then the surface may be described as "hydraulically smooth" and the wall resistance is limited to that caused by viscous shear within the fluid. On the other hand, if the asperities protrude well beyond the laminar sublayer then the disturbance to flow that they produce will cause additional eddies to be formed, consuming mechanical energy and resulting in a higher resistance to flow. Furthermore, as the velocity and,

hence, the Reynolds Number increases, the thickness of the laminar sublayer decreases. Any given pipe will then be hydraulically smooth if the asperities are submerged within the laminar sublayer and hydraulically rough if the asperities project beyond the laminar sublayer. Between the two conditions there will be a transition zone where some, but not all, of the asperities protrude through the laminar sublayer. The hypothesis of the existence of a laminar sublayer explains the behaviour of the curves in Figure 2.6. The recognition and early study of boundary layers owe a great deal to the work of Ludwig Prandtl and the students who started their careers under his guidance.

Nikuradse's work marked a significant step forward in that it promised a means of predicting the coefficient of friction and, hence, the resistance of any given pipe passing turbulent flow. However, there continued to be difficulties. In real pipes, ducts or underground airways, the wall asperities are not all of the same size, nor are they uniformly dispersed. In particular, mine airways show great variation in their roughness. Concrete lining in ventilation shafts may have a uniform e/d value as low as 0.001. On the other hand, where shaft tubing or regularly spaced airway supports are used, the turbulent wakes on the downstream side of the supports create a dependence of airway resistance on their distance apart. Furthermore, the immediate wall roughness may be superimposed upon larger scale sinuosity of the airways and, perhaps, the existence of cross-cuts or other junctions. The larger scale vortices produced by these macro effects may be more energy demanding than the smaller eddies of normal turbulent flow and, hence, produce a much higher value of f . Many airways also have wall roughnesses that exhibit a directional bias, produced by the mechanized or drill and blast methods of driving the airway, or the natural cleavage of the rock.

For all of these reasons, there may be a significant divergence between Nikuradse's curves and results obtained in practice, particularly in the transitional zone. Further experiments and analytical investigations were carried out in the late 1930's by **C.F. Colebrook** in England. The equations that were developed were somewhat awkward to use. However, the concept of "equivalent sand grain roughness" was further developed by the American engineer **Lewis F. Moody** in 1944. The ensuing chart, shown on Figure 2.7, is known as the Moody diagram and is now widely employed by practicing engineers to determine coefficients of friction.

2.3.6.3. Equations describing f - Re relationships

The literature is replete with relationships that have been derived through combinations of analysis and empiricism to describe the behavior of the coefficient of friction, f , with respect to Reynolds' Number on the Moody Chart. No attempt is made here at a comprehensive discussion of the merits and demerits of the various relationships. Rather, a simple summary is given of those equations that have been found to be most useful in ventilation engineering.

Laminar Flow

The straight line that describes laminar flow on the log-log plot of Figure 2.7 is included in the Moody Chart for completeness. However, Poiseuille's equation (2.31) can be used directly to establish frictional pressure losses for laminar flow without using the chart. The corresponding f -Re relationship is easily established. Combining equations (2.34) and (2.45) gives

$$p = \frac{8\mu uL}{R^2} = \frac{4fL}{d} \frac{\rho u^2}{2} \quad \text{Pa}$$

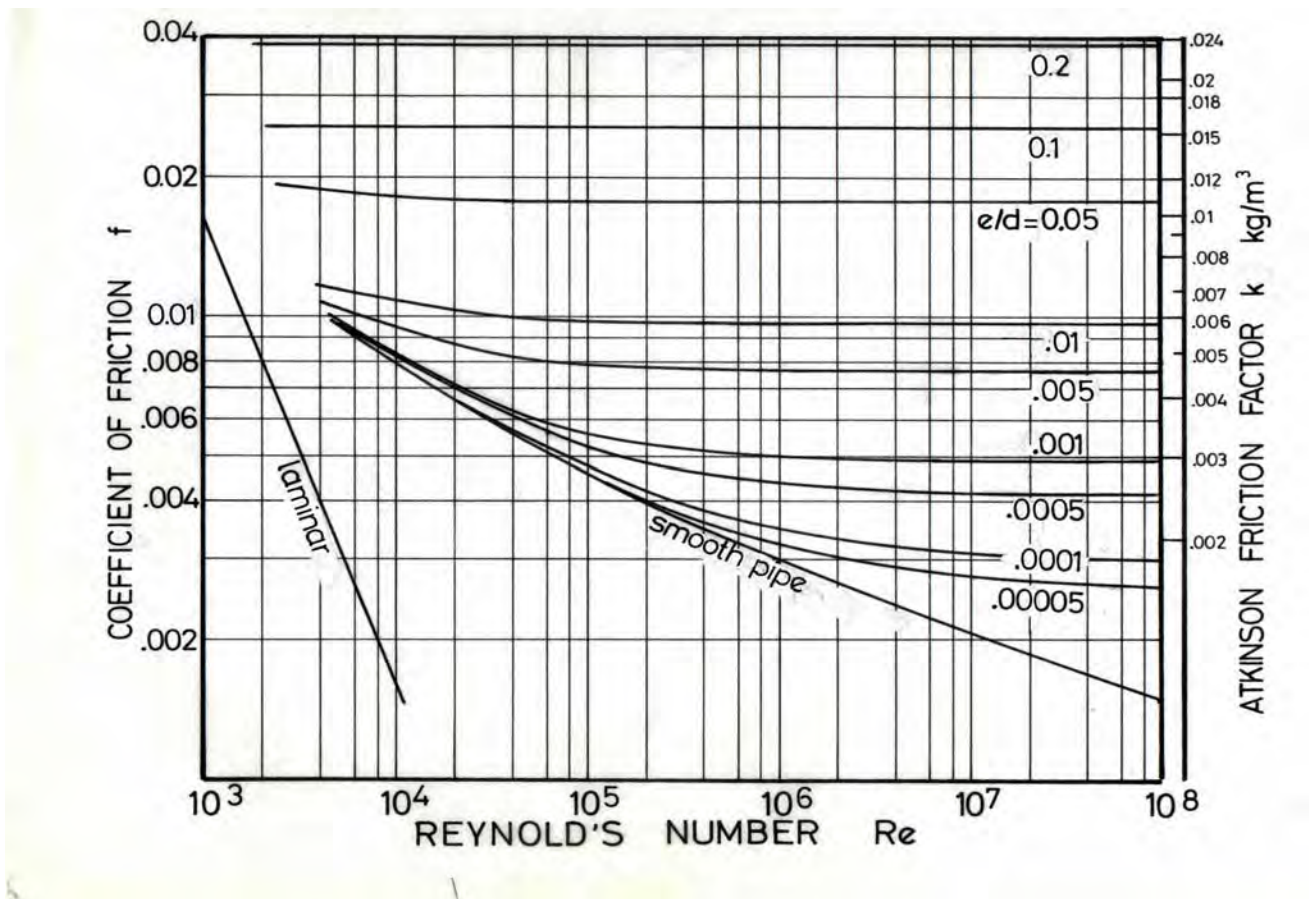


Figure 2.7 Type of chart developed by Moody.

Substituting $R = d/2$ gives

$$f = 16 \frac{\mu}{\rho u d}$$

or $f = \frac{16}{Re}$ dimensionless (2.52)

Smooth pipe turbulent curve

Perhaps the most widely accepted equation for the smooth pipe turbulent curve is that produced by both Nikuradse and the Hungarian engineer **Theodore Von Kármán (1881-1963)**.

$$\frac{1}{\sqrt{f}} = 4 \log_{10}(Re \sqrt{f}) - 0.4$$

This suffers from the disadvantage that f appears on both sides of the equation. **Paul R.H. Blasius (1873-1970)**, one of Prandtl's earlier students, suggested the approximation for Reynolds Numbers in the range 3 000 to 10^5 .

$$f = \frac{0.0791}{\text{Re}^{0.25}} \quad (2.54)$$

while a better fit to the smooth pipe curve for Reynolds Numbers between 20 000 to 10^7 is given as

$$f = \frac{0.046}{\text{Re}^{0.2}}$$

Rough pipes

When fully developed rough pipe turbulence has been established, the viscous forces are negligible compared with inertial forces. The latter are proportional to the shear stress at the walls (equation (2.41)). Hence, in this condition f becomes independent of Reynolds Number and varies only with e/d . A useful equation for this situation was suggested by Von Kármán.

$$f = \frac{1}{4(2\log_{10}(d/e) + 1.14)^2} \quad (2.55)$$

The most general of the f - Re relationships in common use is the **Colebrook White** equation. This has been expressed in a variety of ways, including

$$\frac{1}{\sqrt{4f}} = 1.74 - 2\log_{10}\left(2\frac{e}{d} + \frac{18.7}{\text{Re}\sqrt{4f}}\right) \quad (2.56)$$

and

$$\frac{1}{\sqrt{f}} = -4\log_{10}\left(\frac{e/d}{3.7} + \frac{1.255}{\text{Re}\sqrt{f}}\right) \quad (2.57)$$

Here again, f , appears on both sides making these equations awkward to use in practice. It was, in fact, this difficulty that led Moody into devising his chart.

The advantage of the Colebrook White equation is that it is applicable to both rough and smooth pipe flow and for the transitional region as well as fully developed turbulence. For hydraulically smooth pipes, $e/d=0$, and the Colebrook White equation simplifies to the Nikuradse relationship of equation (2.53). On the other hand, for high Reynolds Numbers, the term involving Re in equation (2.57) may be ignored. The equation then simplifies to

$$f = \left[4\log_{10}\left(\frac{e/d}{3.7}\right)\right]^{-2} \quad (2.58)$$

This gives the same results as Von Kármán's rough pipe equation (2.55) for fully developed turbulence.

Example

A vertical shaft is 400 m deep, 5 m diameter and has wall roughenings of height 5 mm. An airflow of $150 \text{ m}^3/\text{s}$ passes at a mean density of $1.2 \text{ kg}/\text{m}^3$. Taking the viscosity of the air to be $17.9 \times 10^{-6} \text{ N}\cdot\text{s}/\text{m}^2$ and ignoring changes in kinetic energy, determine:

- (i) the coefficient of friction, f
- (ii) the turbulent resistance, R_t (m^{-4})
- (iii) the frictional pressure drop p (Pa)
- (iv) the work done against friction, F_{12} (J/kg)
- (v) the barometric pressure at the shaft bottom if the shaft top pressure is 100 kPa.

Solution

For a 400 m deep shaft, we can assume incompressible flow (Section 2.1.1.)

$$\text{Cross-sectional area, } A = \frac{\pi \times 5^2}{4} = 19.635 \text{ m}^2$$

$$\text{Perimeter, } per = 5\pi = 15.708 \text{ m}$$

$$\text{Air velocity, } u = \frac{Q}{A} = \frac{150}{19.635} = 7.639 \text{ m/s}$$

In order to determine the regime of flow, we must first find the Reynolds Number

$$Re = \frac{\rho u d}{\mu} = \frac{1.2 \times 7.639 \times 5}{17.9 \times 10^{-6}} = 2.561 \times 10^6$$

(i) *Coefficient of friction, f :*

At this value of Re , the flow is fully turbulent (Section 2.3.4.). We may then use the Moody Chart to find the coefficient of friction, f . However, for this we need the equivalent roughness

$$\frac{e}{d} = \frac{5 \times 10^{-3}}{5} = 0.001$$

Hence at $e/d = 0.001$ and $Re = 2.561 \times 10^6$ on Figure 2.7 we can estimate $f = 0.0049$. (Iterating equation (2.57) gives $f = 0.00494$. As the friction coefficient is near constant at this Reynolds Number, we could use equation (2.55) to give $f = 0.00490$ or equation (2.58) which gives $f = 0.00491$).

(ii) *Turbulent resistance, R_t :* (equation (2.51))

$$R_t = \frac{f L per}{2 A^3} = \frac{0.0049 \times 400 \times 15.708}{2(19.635)^3} = 0.002036 \text{ m}^{-4}$$

(iii) *Frictional pressure drop, p :* (equation (2.50))

$$p = R_t \rho Q^2 = 0.002036 \times 1.2 \times (150)^2 = 54.91 \text{ Pa}$$

(iv) *Work done against friction, F_{12} :* (equation (2.46))

$$F_{12} = \frac{p}{\rho} = \frac{54.91}{1.2} = 45.76 \frac{\text{J}}{\text{kg}}$$

(v) *Barometric pressure at shaft bottom, P_2 :* This is obtained from Bernoulli's equation (2.47) with no change in kinetic energy.

$$(Z_1 - Z_2)g + \frac{P_1 - P_2}{\rho} = F_{12}$$

$$\begin{aligned} \text{giving } P_2 &= (Z_1 - Z_2)g\rho - F_{12} \rho + P_1 \\ &= (400 \times 9.81 \times 1.2) - 54.91 + 100\,000 \\ P_2 &= 104\,654 \text{ Pa} \quad \text{or} \quad 104.654 \text{ kPa} \end{aligned}$$

Bibliography

Blasius, H. (1913) Das Ähnlichkeitsgesetz bei Reibungsvorgängen in Flüssigkeiten. *Forsch. Gebiete Ingenieur.* Vol. 131

Colebrook, C.F. and White, C.M. (1937) Experiments with fluid friction in roughened pipes. *Proc. Royal Soc. (U.K.) (A)*, vol 161, 367

Colebrook, C.F. and White, C.M. (1939). Turbulent flow in pipes with particular reference to the transition region between the smooth and rough pipe laws. *Proc. Inst. Civ. Eng. (U.K.) Vol II*, 133

Daugherty, R.L. and Franzini, J.B. (1977). Fluid mechanics, with Engineering Applications (7th ed) *McGraw Hill*.

Lewitt, E.H. (1959) Hydraulics and fluid mechanics. (10th ed.) *Pitman, London*

Massey, B.S. (1968) Mechanics of fluids. *Van Nostrand, New York*.

Moody, L.F. (1944) Friction factors for pipe flow. *Trans. Am. Soc. Mech. Engr.* Vol. 66 p.671-84

Nikuradse, J. (1933) Strömungsgesetze in rauhen Röhren. *VDI-Forschungshft*, Vol 361

Prandtl, L. (1933) Neuere Ergebnisse der Turbulenz-forschung. *Zeitschrift des VDI*. No. 77, 105

Reynolds, O. (1883) The motion of water and the law of resistance in parallel channels. *Proc Royal Soc. London*, 35

Rohsenow, W.M and Choi H. (1961) Heat, Mass and Momentum Transfer. *International Series in Eng. Prentice-Hall*

Von Kármán, T. (1939) *Trans ASME Vol. 61, 705*

Chapter 3. Fundamentals of steady flow thermodynamics

3.1. INTRODUCTION	1
3.2. PROPERTIES OF STATE, WORK AND HEAT	2
3.2.1 Thermodynamic properties. State of a system.....	2
3.2.2 Work and heat	3
3.3. SOME BASIC RELATIONSHIPS	4
3.3.1. Gas laws and gas constants.....	4
3.3.2. Internal Energy and the First Law of Thermodynamics.....	7
3.3.3. Enthalpy and the Steady Flow Energy Equation.....	8
3.3.4. Specific heats and their relationship to gas constant.....	10
3.3.5. The Second Law of Thermodynamics.....	13
3.4. FRICTIONAL FLOW	14
3.4.1. The effects of friction in flow processes	14
3.4.2. Entropy	16
3.4.3. The adiabatic and isentropic processes	19
3.4.4. Availability.....	20
3.5 THERMODYNAMIC DIAGRAMS.....	23
3.5.1. Ideal isothermal (constant temperature) compression.....	24
3.5.2. Isentropic (constant entropy) compression	26
3.5.3. Polytropic compression	28
Further Reading	34

3.1. INTRODUCTION

The previous chapter emphasized the behaviour of incompressible fluids in motion. Accordingly, the analyses were based on the mechanisms of fluid dynamics. In expanding these to encompass compressible fluids and to take account of thermal effects, we enter the world of **thermodynamics**.

This subject divides into two major areas. Chemical and statistical thermodynamics are concerned with reactions involving mass and energy exchanges at a molecular or atomic level, while physical thermodynamics takes a macroscopic view of the behaviour of matter subjected to changes of pressure, temperature and volume but not involving chemical reactions. **Physical thermodynamics** subdivides further into the study of "closed" systems within each of which remains a fixed mass of material such as a gas compressed within a cylinder, and "open" systems through which material flows. A subsurface ventilation system is, of course, an open system with air continuously entering and leaving the facility. In this chapter, we shall concentrate on open systems with one further restriction - that the mass flow of air at any point in the system does not change with time. We may, then, define our particular interest as one of **steady flow physical thermodynamics**.

Thermodynamics began to be developed as an engineering discipline after the invention of a practicable steam engine by **Thomas Newcomen** in 1712. At that time, heat was conceived to be a massless fluid named 'caloric' that had the ability to flow from a hotter to a cooler body. Improvements in the design and efficient operation of steam engines, made particularly by **James Watt (1736-1819)** in Scotland, highlighted deficiencies in this concept. During the middle of the 19th century the caloric theory was demolished by the work of **James P. Joule (1818-1889)** in England,

H.L.F. Helmholtz (1821-1894) and **Rudolph J.E. Clausius (1822-1888)** in Germany, and **Lord Kelvin (1824-1907)** and **J.C. Maxwell (1831-1879)** of Scotland.

The application of thermodynamics to mine ventilation systems was heralded by the publication of a watershed paper in 1943 by **Frederick B. Hinsley (1900-1988)**. His work was motivated by consistent deviations that were observed when mine ventilation surveys were analyzed using incompressible flow theory, and by Hinsley's recognition of the similarity between plots of pressure against specific volume constructed from measurements made in mine downcast and upcast shafts, and indicator diagrams produced by compressed air or heat engines. The new thermodynamic theory was particularly applicable to the deep and hot mines of South Africa. Mine ventilation engineers of that country have contributed greatly to theoretical advances and practical utilization of the more exact thermodynamic methods.

3.2. PROPERTIES OF STATE, WORK AND HEAT

3.2.1 Thermodynamic properties. State of a system.

In Chapter 2 we introduced the concepts of fluid density and pressure. In this chapter we shall consider the further properties of temperature, internal energy, enthalpy and entropy. These will be introduced in turn and where appropriate. For the moment, let us confine ourselves to temperature.

Reference to the **temperature** of substances is such an everyday occurrence that we seldom give conscious thought to the foundations upon which we make such measurements. The most common basis has been to take two fixed temperatures such as those of melting ice and boiling water at standard atmospheric pressure, ascribe numerical values to those temperatures and to define a scale between the two fixed points. **Anders Celsius (1701-1744)**, a Swedish astronomer, chose to give values of 0 and 100 to the temperatures of melting ice and boiling water respectively, and to select a linear scale between the two. The choice of a linear scale is, in fact, quite arbitrary but leads to a convenience of measurement and simpler relationships between temperature and other thermodynamic properties. The scale thus defined is known as the Celsius (or Centigrade) scale. The older Fahrenheit scale was named after **Gabriel Fahrenheit (1686-1736)**, the German scientist who first used a mercury-in-glass thermometer. Fahrenheit's two "fixed" but rather inexact points were 0 for a mixture of salt, ice and water, and 96 for the average temperature of the human body. A linear scale was then found to give Fahrenheit temperatures of 32 for melting ice and 212 for boiling water. These were later chosen as the two fixed points for the Fahrenheit scale but, unfortunately, the somewhat irrational numeric values were retained. In the SI system of units, temperatures are most often related to degrees Celsius.

However, through a thermodynamic analysis, another scale of temperature can be defined that does not depend upon the melting or boiling points of any substance. This is called the **absolute** or **thermodynamic temperature scale**. **N.L. Sadi Carnot (1796-1832)**, a French military engineer, showed that a theoretical heat engine operating between fixed inlet and outlet temperatures becomes more efficient as the difference between those two temperatures increases. Absolute zero on the thermodynamic temperature scale is defined theoretically as that outlet temperature at which an ideal heat engine operating between two fixed temperature reservoirs would become 100 per cent efficient, i.e. operate without producing any reject heat. Absolute zero temperature is a theoretical datum that can be approached but never quite attained. We can then choose any other fixed point and interval to define a unit or degree on the absolute temperature scale. The SI system of units employs the Celsius degree as the unit of temperature and retains 0 °C and 100 °C for melting ice and boiling water. This gives absolute zero as -273.15 °C. Thermodynamic temperatures quoted on the basis of absolute zero are always positive numbers and are measured in degrees Kelvin (after Lord Kelvin). A difference of one degree Kelvin is equivalent to a difference of one Celsius degree. Throughout this book, absolute temperatures are identified by the symbol T and temperatures shown as t or θ denote degrees Celsius.

$$T = t(^{\circ}\text{C}) + 273.15 \quad \text{K} \quad (3.1)$$

The Kelvin units, K, are normally shown without a degree (°) sign. **Thermodynamic calculations should always be conducted using the absolute temperature, T, in degrees Kelvin.** However, as a degree Kelvin is identical to a degree Celsius, temperature differences may be quoted in either unit.

The state of any point within a system is defined by the thermodynamic properties of the fluid at that point. If air is considered to be a pure substance of fixed composition then any two independent properties are sufficient to define its **thermodynamic state**. In practice, the two properties are often pressure and temperature as these can be measured directly. If the air is not of fixed composition as, for example, in airways where evaporation or condensation of water occurs, then at least one more property is required to define its thermodynamic state (Chapter 14).

The **intensive or specific properties of state** (quoted on the basis of unit mass) define completely the thermodynamic state of any point within a system or subsystem and are independent of the processes which led to the establishment of that state.

3.2.2 Work and heat

Both work and heat involve the transfer of energy. In SI units, the fundamental numerical equivalence of the two is recognized by their being given the same units, Joules, where

$$1 \text{ Joule} = 1 \text{ Newton} \times 1 \text{ metre.} \quad \text{Nm}$$

Work usually (but not necessarily) involves mechanical movement against a resisting force. An equation used repeatedly in Chapter 2 was

$$\text{Work done} = \text{force} \times \text{distance}$$

$$\text{or} \quad dW = F dL \quad \text{Nm or J} \quad (3.2)$$

and is the basis for the definition of a Joule. Work may be added as mechanical energy from an external source such as a fan or pump. Additionally, it was shown in Section 2.3.1. that "flow work", Pv (J) must be done to introduce a plug of fluid into an open system. However, it is only at entry (or exit) of the system that the flow work can be conceived as a measure of force x distance. Elsewhere within the system the flow work is a point function. It is for this reason that some engineers prefer not to describe it as a work term.

Heat is transferred when an energy exchange takes place due to a temperature difference. When two bodies of differing temperatures are placed in contact then heat will "flow" from the hotter to the cooler body. (In fact, heat can be transferred by convection or radiation without physical contact.) It was this concept of heat flowing that gave rise to the **caloric theory**. Our modern hypothesis is that heat transfer involves the excitation of molecules in the receiving substance, increasing their internal kinetic energy at the expense of those in the emitting substance.

Equation (3.2) showed that work can be described as the product of a driving potential (force) and distance. It might be expected that there is an analogous relationship for heat, dq , involving the driving potential of temperature and some other property. Such a relationship does, in fact, exist and is quantified as

$$dq = T ds \quad \text{J} \quad (3.3)$$

The variable, s , is named entropy and is a property that will be discussed in more detail in Section 3.4.2.

It is important to realize that neither work nor heat is a property of a system. Contrary to popular phraseology which still retains reminders of the old caloric theory, no system "contains" either heat or work. The terms become meaningful only in the context of energy transfer across the boundaries of the system. Furthermore, the magnitude of the transfer depends upon the process path or particular circumstances existing at that time and place on the boundary. Hence, to be precise, the quantities dW and dq should actually be denoted as inexact differentials δW and δq .

The rate at which energy transfers take place is commonly expressed in one of two ways. First, on the basis of unit mass of the fluid, i.e. Joules per kilogram. This was the method used to dimension the terms of the Bernoulli equation in Section 2.3.1. Secondly, an energy transfer may be described with reference to **time**, Joules per second. This latter method produces the definition of **Power**.

$$\text{Power} = \frac{dW}{\text{time}} \text{ or } \frac{dq}{\text{time}} \quad \frac{\text{J}}{\text{s}} \quad (3.4)$$

where the unit, J/s is given the name **Watt** after the Scots engineer, James Watt.

Before embarking upon any analyses involving energy transfers, it is important to define a **sign convention**. Many textbooks on thermodynamics have used the rather confusing convention that heat transferred to a system is positive, but work transferred to the system is negative. This strange irrationality has arisen from the historical development of physical thermodynamics being motivated by the study of heat engines, these consuming heat energy (supplied in the form of a hot vapour or burning fuel) and producing a mechanical work output. In subsurface ventilation engineering, work input from fans is mechanical energy transferred to the air and, in most cases, heat is transferred from the surrounding strata or machines - also to the air. Hence, in this engineering discipline it is convenient as well as being mathematically consistent to regard all energy transfers to the air as being positive, whether those energy transfers are work or heat. That is the sign convention utilized throughout this book.

3.3. SOME BASIC RELATIONSHIPS

3.3.1. Gas laws and gas constants

An **ideal gas** is one in which the volume of the constituent molecules is zero and where there are no inter-molecular forces. Although no real gas conforms exactly to that definition, the mixture of gases that comprise air behaves in a manner that differs negligibly from an ideal gas within the ranges of temperature and pressure found in subsurface ventilation engineering. Hence, the thermodynamic analyses outlined in this chapter will assume ideal gas behavior.

Some twenty years before Isaac Newton's major works, **Robert Boyle (1627-1691)** developed a vacuum pump and found, experimentally, that gas pressure, P , varied inversely with the volume, v , of a closed system at constant temperature.

$$P \propto \frac{1}{v} \quad (\text{Boyle's law}) \quad (3.5)$$

where \propto means 'proportional to'.

In the following century and on the other side of the English Channel in France, **Jacques A.C. Charles (1746-1823)** discovered, also experimentally, that

$$v \propto T \quad (\text{Charles' law}) \quad (3.6)$$

for constant pressure, where T = absolute temperature.

Combining Boyle's and Charles' laws gives

$$Pv \propto T$$

where both temperature and pressure vary. Or, inserting a constant of proportionality, R' ,

$$Pv = R'T \quad \text{J} \quad (3.7)$$

To make the equation more generally applicable, we can replace R' by mR where m is the mass of gas, giving

$$Pv = mRT \quad \text{J} \quad (3.8)$$

or
$$P \frac{v}{m} = RT \quad \text{J/kg}$$

But v/m is the volume of 1 kg, i.e. the **specific volume** of the gas, V (m^3 per kg). Hence,

$$PV = RT \quad \text{J/kg} \quad (3.9)$$

This is known as the **General Gas Law** and R is the gas constant for that particular gas or mixture of gases, having dimensions of $\text{J}/(\text{kg K})$. The specific volume, V , is simply the reciprocal of density,

$$V = \frac{1}{\rho} \quad \text{m}^3/\text{kg} \quad (3.10)$$

Hence, the general gas law can also be written as

$$\frac{P}{\rho} = RT \quad \text{J/kg} \quad (3.11)$$

or
$$\rho = \frac{P}{RT} \quad \frac{\text{kg}}{\text{m}^3} \quad \text{giving an expression for the density of an ideal gas.}$$

As R is a constant for any perfect gas, it follows from equation (3.9) that the two end states of any process involving an ideal gas are related by the equation

$$\frac{P_1 V_1}{T_1} = \frac{P_2 V_2}{T_2} = R \quad \frac{\text{J}}{\text{kgK}} \quad (3.12)$$

Another feature of the gas constant, R , is that although it takes a different value for each gas, there is a useful and simple relationship between the gas constants of all ideal gases. **Avogadro's law** states that equal volumes of ideal gases at the same temperature and pressure contain the same number of molecules. Applying these conditions to equation (3.8) for all ideal gases gives

$$mR = \text{constant}$$

Furthermore, if the same volume of each gas contains an equal number of molecules, it follows that the mass, m , is proportional to the weight of a single molecule, that is, the molecular weight of the gas, M . Then

$$MR = \text{constant} \quad (3.13)$$

The product MR is a constant for all ideal gases and is called the **universal gas constant, R_u** . In SI units, the value of R_u is 8314.36 J/K . The dimensions are sometimes defined as $\text{J}/(\text{kg mole K})$ where one mole is the amount of gas contained in M kg, i.e. its molecular weight expressed in kilograms. The gas constant for any ideal gas can now be found provided that its molecular weight is known

$$R = \frac{8314.36}{M} \quad \frac{\text{J}}{\text{kgK}} \quad (3.14)$$

For example, the **equivalent molecular weight of dry air is 28.966**, giving its gas constant as

$$R = \frac{8314.36}{28.966} = 287.04 \quad \frac{\text{J}}{\text{kgK}} \quad (3.15)$$

Example.

At the top of a mine downcast shaft the barometric pressure is 100 kPa and the air temperature is 18.0 °C. At the shaft bottom, the corresponding measurements are 110 kPa and 27.4 °C respectively. The airflow measured at the shaft top is 200 m³/s. If the shaft is dry, determine

- the air densities at the shaft top and shaft bottom,
- the mass flow of air
- the volume flow of air at the shaft bottom.

Solution.

Using subscripts 1 and 2 for the top and bottom of the shaft respectively:-

$$(a) \quad \rho_1 = \frac{P_1}{RT_1} = \frac{100\,000}{287.04 \times (273.15 + 18)} = 1.1966 \quad \frac{\text{kg}}{\text{m}^3}$$

In any calculation, the units of measurement must be converted to the basic SI unless ratios are involved. Hence 100 kPa = 100 000 Pa.

$$\rho_2 = \frac{P_2}{RT_2} = \frac{110\,000}{287.04 \times (273.15 + 27.4)} = 1.2751 \quad \frac{\text{kg}}{\text{m}^3}$$

$$(b) \text{ Mass flow } M = Q_1 \rho_1 = 200 \times 1.1966 = 239.3 \quad \frac{\text{kg}}{\text{s}}$$

$$(c) \quad Q_2 = \frac{M}{\rho_2} = \frac{239.3}{1.2751} = 187.7 \quad \frac{\text{m}^3}{\text{s}}$$

Example.

Calculate the volume of 100 kg of methane at a pressure of 75 kPa and a temperature of 42 °C

Solution.

The molecular weight of methane (CH₄) is

$$12.01 + (4 \times 1.008) = 16.04$$

$$R(\text{methane}) = \frac{8314.36}{16.04} = 518.4 \quad \frac{\text{J}}{\text{kgK}} \quad \text{from equation (3.14)}$$

Volume of 100 kg

$$v = \frac{mRT}{P} = \frac{100 \times 518.4 \times (273.15 + 42)}{75\,000} = 217.8 \quad \text{m}^3 \quad \text{from equation (3.8)}$$

3.3.2. Internal Energy and the First Law of Thermodynamics

Suppose we have 1 kg of gas in a closed container as shown in Figure 3.1. For simplicity, we shall assume that the vessel is at rest with respect to the earth and is located on a base horizon. The gas in the vessel has neither macro kinetic energy nor potential energy. However, the molecules of the gas are in motion and possess a molecular or 'internal' kinetic energy. The term is usually shortened to **internal energy**. In the fluid mechanics analyses of Chapter 2 we dealt only with mechanical energy and there was no need to involve internal energy. However, if we are to study thermal effects then we can no longer ignore this form of energy. We shall denote the specific (per kg) internal energy as U J/kg.

Now suppose that by rotation of an impeller within the vessel, we add work δW to the closed system and we also introduce an amount of heat δq . The gas in the vessel still has zero macro kinetic energy and zero potential energy. The energy that has been added has simply caused an increase in the internal energy.

$$dU = \delta W + \delta Q \quad \frac{\text{J}}{\text{kg}} \quad (3.16)$$

The change in internal energy is determined only by the net energy that has been transferred across the boundary and is independent of the form of that energy (work or heat) or the process path of the energy transfer. Internal energy is, therefore, a thermodynamic property of state. Equation (3.16) is sometimes known as the non-flow energy equation and is a statement of the **First Law of Thermodynamics**. This equation also illustrates that the First Law is simply a quantified restatement of the general law of Conservation of Energy

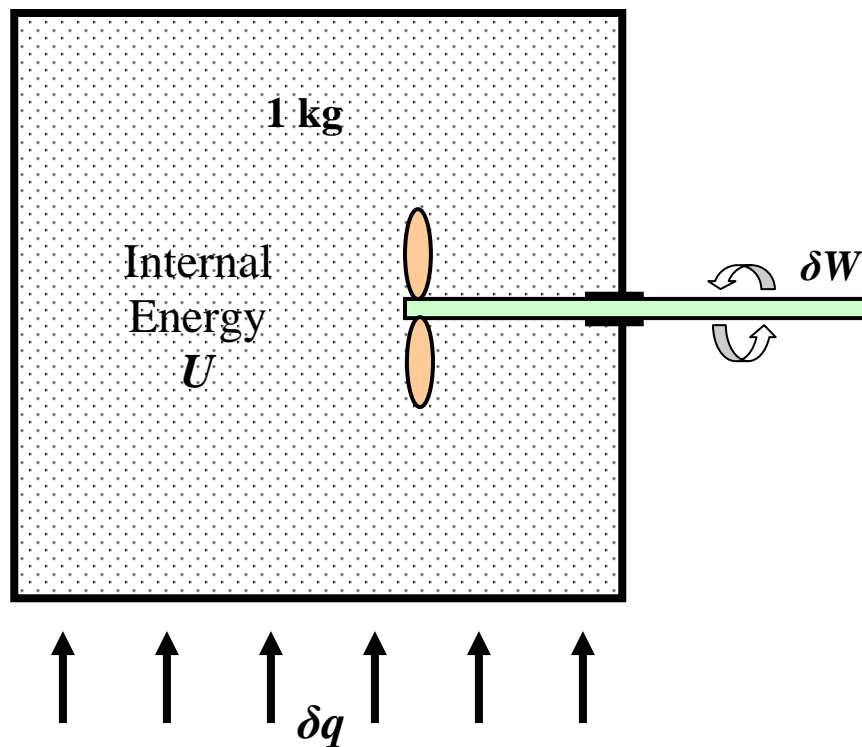


Figure 3.1. Added work and heat raise the internal energy of a closed system

3.3.3. Enthalpy and the Steady Flow Energy Equation

Let us now return to steady flow through an open system. Bernoulli's equation (2.15) for a frictionless system included mechanical energy terms only and took the form

$$\frac{u^2}{2} + Zg + PV = \text{constant} \quad \frac{\text{J}}{\text{kg}} \quad (3.17)$$

(where specific volume, $V = 1/\rho$).

In order to expand this equation to include **all** energy terms, we must add internal energy, giving

$$\frac{u^2}{2} + Zg + PV + U = \text{constant} \quad \frac{\text{J}}{\text{kg}} \quad (3.18)$$

One of the features of thermodynamics is the regularity with which certain groupings of variables appear. So it is with the group $PV + U$. This sum of the PV product and internal energy is particularly important in flow systems. It is given the name enthalpy and the symbol H .

$$H = PV + U \quad \text{J/kg} \quad (3.19)$$

Now pressure, P , specific volume, V , and specific internal energy, U , are all thermodynamic properties of state. It follows, therefore, that enthalpy, H , must also be a thermodynamic property of state and is independent of any previous process path.

The energy equation (3.18) can now be written as

$$\frac{u^2}{2} + Zg + H = \text{constant} \quad \frac{\text{J}}{\text{kg}} \quad (3.20)$$

Consider the continuous airway shown on Figure 3.2. If there were no energy additions between stations 1 and 2 then the energy equation (3.20) would give

$$\frac{u_1^2}{2} + Z_1g + H_1 = \frac{u_2^2}{2} + Z_2g + H_2 \quad \frac{\text{J}}{\text{kg}}$$

However, Figure 3.2 shows that a fan adds W_{12} Joules of mechanical energy to each kilogram of air and that strata heat transfers q_{12} Joules of thermal energy to each kilogram of air. These terms must be added to the total energy at station 1 in order to give the total energy at station 2

$$\frac{u_1^2}{2} + Z_1g + H_1 + W_{12} + q_{12} = \frac{u_2^2}{2} + Z_2g + H_2 \quad \frac{\text{J}}{\text{kg}} \quad (3.21)$$

This is usually rearranged as follows:

$$\frac{u_1^2 - u_2^2}{2} + (Z_1 - Z_2)g + W_{12} = (H_2 - H_1) - q_{12} \quad \frac{\text{J}}{\text{kg}} \quad (3.22)$$

Equation (3.22) is of fundamental importance in steady flow processes and is given a special name, the **Steady Flow Energy Equation**.

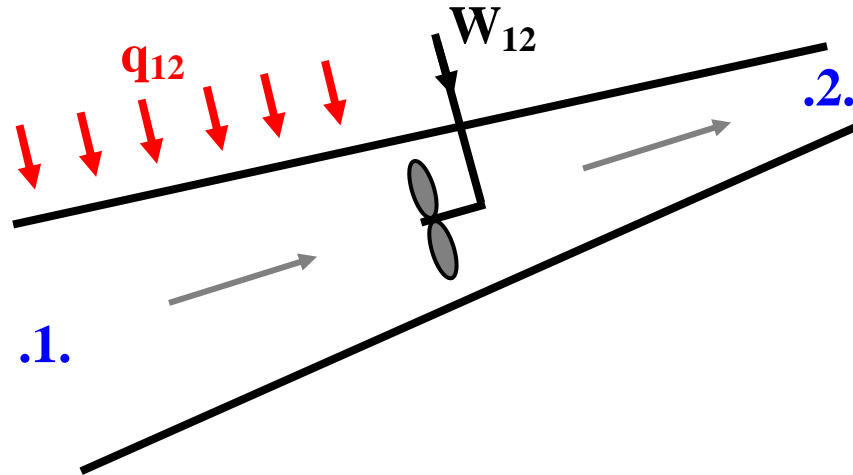


Figure 3.2. Heat and work added to a steady flow system.

Note that the steady flow energy equation does not contain a term for friction, nor does it require any such term. It is a **total energy balance**. Any frictional effects will reduce the mechanical energy terms and increase the internal energy but will have no influence on the overall energy balance. It follows that equation (3.22) is applicable both to ideal (frictionless) processes and also to real processes that involve viscous resistance and turbulence. Such generality is admirable but does, however, give rise to a problem for the ventilation engineer. In airflow systems, mechanical energy is expended against frictional resistance only - we do not normally use the airflow to produce a work output through a turbine or any other device. It is, therefore, important that we are able to quantify **work done against friction**. This seems to be precluded by equation (3.22) as no term for friction appears in that equation:

To resolve the difficulty, let us recall Bernoulli's mechanical energy equation (2.23) corrected for friction

$$\frac{u_1^2 - u_2^2}{2} + (Z_1 - Z_2)g + \frac{(P_1 - P_2)}{\rho} = F_{12} \quad \frac{\text{J}}{\text{kg}}$$

If we, again, add work, W_{12} , between stations 1 and 2 then the equation becomes

$$\frac{u_1^2 - u_2^2}{2} + (Z_1 - Z_2)g + \frac{(P_1 - P_2)}{\rho} + W_{12} = F_{12} \quad \frac{\text{J}}{\text{kg}} \quad (3.23)$$

(Although any heat, q_{12} , that may also be added does not appear explicitly in a mechanical energy equation it will affect the balance of mechanical energy values arriving at station 2).

We have one further step to take. As we are now dealing with gases, we should no longer assume that density, ρ , remains constant. If we consider the complete process from station 1 to station 2 to be made up of a series of infinitesimally small steps then the pressure difference across each step becomes dP and the flow work term becomes dP/ρ or VdP (as $V = 1/\rho$). Summing up, or integrating all such terms for the complete process gives

$$\frac{u_1^2 - u_2^2}{2} + (Z_1 - Z_2)g + W_{12} = \int_1^2 V dP + F_{12} \quad \frac{\text{J}}{\text{kg}} \quad (3.24)$$

This is sometimes called the steady flow mechanical energy equation. It is, in fact, simply a statement of Bernoulli's equation made applicable to compressible flow.

Finally, compare equations (3.22) and (3.24). Their left sides are identical. Hence, we can write an expanded version of the **steady flow energy equation**:

$$\frac{u_1^2 - u_2^2}{2} + (Z_1 - Z_2)g + W_{12} = \int_1^2 V dP + F_{12} = (H_2 - H_1) - q_{12} \quad \frac{\text{J}}{\text{kg}} \quad (3.25)$$

or, in differential form,

$$-u du - g dZ + dW = V dP + dF = dH - dq$$

Equation (3.25) is the starting point for the application of thermodynamics to subsurface ventilation systems and, indeed, to virtually all steady flow compressible systems. It is absolutely fundamental to a complete understanding of the behaviour of airflow in subsurface ventilation systems.

Students of the subject and ventilation engineers dealing with underground networks of airways should become completely familiarized with equation (3.25). In most applications within mechanical engineering the potential energy term $(Z_1 - Z_2)g$ is negligible and can be dropped to simplify the equation. However, the large elevation differences that may be traversed by subsurface airflows often result in this term being dominant and it must be retained for mine ventilation systems.

3.3.4. Specific heats and their relationship to gas constant

When heat is supplied to any unconstrained substance, there will, in general, be two effects. First, the temperature of the material will rise and, secondly, if the material is not completely constrained, there will be an increase in volume. (An exception is the contraction of water when heated between 0 and 4°C). Hence, the heat is utilized both in raising the temperature of the material and in doing work against the surroundings as it expands.

The specific heat of a substance has been described in elementary texts as that amount of heat which must be applied to 1 kg of the substance in order to raise its temperature through one Celsius degree. There are some difficulties with this simplistic definition. First, the temperature of any solid, liquid or gas can be increased by doing work on it and without applying any heat - for example by rubbing friction or by rotating an impeller in a liquid or gas. Secondly, if the substance expands against a constant resisting pressure then the work that is done on the surroundings necessarily requires that more energy must be applied to raise the 1 kg through the same 1 C° than if the system were confined at constant volume. The specific heat must have a higher value if the system is at constant pressure than if it is held at constant volume. If both pressure and volume are allowed to vary in a partially constrained system, then yet another specific heat will be found. As there are an infinite number of variations in pressure and volume between the conditions of constant pressure and constant volume, it follows that there are an infinite number of specific heats for any given substance. This does not seem to be a particularly useful conclusion. However, we can apply certain restrictions which make the concept of specific heat a valuable tool in thermodynamic analyses.

First, extremely high stresses are produced if a liquid or solid is prevented from expanding during heating. For this reason, the specific heats quoted for liquids and solids are normally those pertaining to constant pressure, i.e. allowing free expansion. In the case of gases we can, indeed,

have any combination of changes in the pressure and volume. However, we confine ourselves to the two simple cases of constant volume and constant pressure.

Let us take the example of a vessel of fixed volume containing 1 kg of gas. We add heat, δq , until the temperature has risen through δT . Then, from the First Law (equation (3.16)) with $\delta W = 0$ for fixed volume,

$$\delta q = dU$$

From our definition of specific heat,

$$C_v = \left[\frac{\delta q}{\delta T} \right]_v = \left[\frac{\delta U}{\delta T} \right]_v \quad \frac{\text{J}}{\text{kgK}}$$

As this is the particular **specific heat at constant volume**, we use the subscript v. At any point during the process, the specific heat takes the value pertaining to the corresponding temperature and pressure. Hence, we should define C_v , more generally as

$$C_v = \left[\frac{\partial U}{\partial T} \right]_v \quad (3.26)$$

However, for an ideal gas the specific heat is independent of either pressure or temperature and we may write

$$C_v = \frac{dU}{dT} \quad \frac{\text{J}}{\text{kgK}} \quad (3.27)$$

In section 3.3.2, the concept of internal energy was introduced as a function of the internal kinetic energy of the gas molecules. As it is the molecular kinetic energy that governs the temperature of the gas, it is reasonable to deduce that internal energy is a function of temperature only. This can, in fact, be proved mathematically through an analysis of Maxwell's equations assuming an ideal gas. Furthermore, as any defined specific heat remains constant, again, for an ideal gas, equation (3.27) can be integrated directly between any two end points to give

$$U_2 - U_1 = C_v (T_2 - T_1) \quad \frac{\text{J}}{\text{kg}} \quad (3.28)$$

Now let us examine the case of adding heat, δq , while keeping the pressure constant, i.e. allowing the gas to expand. In this case, from equation (3.19)

$$q = PV + U = H \quad \frac{\text{J}}{\text{kg}} \quad (3.29)$$

Therefore, the specific heat becomes

$$C_p = \left[\frac{\delta q}{\delta T} \right]_p = \left[\frac{\delta H}{\delta T} \right]_p \quad \frac{\text{J}}{\text{kgK}} \quad (3.30)$$

In the limit, this defines C_p as

$$C_p = \left[\frac{\partial H}{\partial T} \right]_p \quad \frac{\text{J}}{\text{kgK}} \quad (3.31)$$

Here again, for a perfect gas, specific heats are independent of pressure and temperature and we can write

$$C_P = \frac{dH}{dT} \quad \frac{\text{J}}{\text{kgK}} \quad (3.32)$$

or $(H_2 - H_1) = C_P (T_2 - T_1) \quad \frac{\text{J}}{\text{kg}} \quad (3.33)$

We shall use this latter equation extensively in Chapter 8 when we apply thermodynamic theory to subsurface ventilation systems. The same equation also shows that for an ideal gas, enthalpy, H , is a function of temperature only, C_p being a constant.

There is another feature of C_p that often causes conceptual difficulty. We introduced equations (3.29 and 3.30) by way of a constant pressure process. However, we did not actually enforce the condition of constant pressure in those equations. Furthermore, we have twice stated that for an ideal gas the specific heats are independent of either pressure or temperature. It follows that C_p can be used in equation (3.33) for ideal gases even when the pressure varies. For flow processes, the term specific heat at constant pressure can be rather misleading.

A useful relationship between the specific heats and gas constant is revealed if we substitute the general gas law $PV = RT$ (equation (3.9)) into equation (3.29)

$$H = RT + U \quad \text{J/kg}$$

Differentiating with respect to T gives

$$\frac{dH}{dT} = R + \frac{dU}{dT} \quad \frac{\text{J}}{\text{kgK}}$$

i.e. $C_P = \frac{dH}{dT} = R + C_V \quad \frac{\text{J}}{\text{kgK}}$

or $R = C_P - C_V \quad \frac{\text{J}}{\text{kgK}} \quad (3.34)$

The names "heat capacity" or "thermal capacity" are sometimes used in place of specific heat. These terms are relics remaining from the days of the caloric theory when heat was thought to be a fluid without mass that could be "contained" within a substance. We have also shown that temperatures can be changed by work as well as heat transfer so that the term specific heat is itself open to challenge.

Two groups of variables involving specific heats and gas constant that frequently occur are the ratio of specific heats (isentropic index)

$$\gamma = \frac{C_P}{C_V} \quad (\text{dimensionless}) \quad (3.35)$$

and $\frac{R}{C_p} \quad (\text{dimensionless})$

Using equation (3.34), it can easily be shown that

$$\frac{R}{C_p} = \frac{(\gamma - 1)}{\gamma} \quad (\text{dimensionless}) \quad (3.36)$$

Table 3.1 gives data for those gases that may be encountered in subsurface ventilation engineering. As no real gases follow ideal gas behavior exactly, the values of the "constants" in the table vary slightly with pressure and temperature. For this reason, there may be minor differences in published values. Those given in Table 3.1 are referred to low (atmospheric) pressures and a temperature of 26.7°C

Gas	Molecular weight M	Gas Constant $R=8314.36/M$ J/kg K	Specific heats		Isentropic index $\gamma = C_p/C_v$	$R/C_p = (\gamma - 1)/\gamma$
			C_p	$C_v=C_p-R$		
			J/(kgK)			
air (dry)	28.966	287.04	1005	718.0	1.400	0.2856
water vapour	18.016	461.5	1884	1422	1.324	0.2450
nitrogen	28.015	296.8	1038	741.2	1.400	0.2859
oxygen	32.000	259.8	916.9	657.1	1.395	0.2833
carbon dioxide	44.003	188.9	849.9	661.0	1.286	0.2223
carbon monoxide	28.01	296.8	1043	746.2	1.398	0.2846
methane	16.04	518.4	2219	1700	1.305	0.2336
helium	4.003	2077	5236	3159	1.658	0.3967
hydrogen	2.016	4124	14361	10237	1.403	0.2872
argon	39.94	208.2	524.6	316.4	1.658	0.3968

Table 3.1. Thermodynamic properties of gases at atmospheric pressures and a temperature of 26.7°C.

3.3.5. The Second Law of Thermodynamics

Heat and work are mutually convertible. Each Joule of thermal energy that is converted to mechanical energy in a heat engine produces one Joule of work. Similarly each Joule of work expended against friction produces one Joule of heat. This is another statement of the First Law of Thermodynamics. When equation (3.16) is applied throughout a closed cycle of processes then the final state is the same as the initial state, i.e. $\oint dU = 0$, and

$$\oint \delta W = -\oint \delta q \quad \frac{J}{kg} \quad (3.37)$$

where \oint indicates integration around a closed cycle .

However, our everyday experience indicates that the First Law, by itself, is incapable of explaining many phenomena. All mechanical work can be converted to a numerically equivalent amount of heat through frictional processes, impact, compression or other means such as electrical devices. However, when we convert heat into mechanical energy, we invariably find that the conversion is possible only to a limited extent, the remainder of the heat having to be rejected. An internal combustion engine is supplied with heat from burning fuel. Some of that heat produces a mechanical work output but, unfortunately, the majority is rejected in the exhaust gases.

Although work and heat are numerically equivalent, work is a superior form of energy. There are many common examples of the limited value of heat energy. A sea-going liner cannot propel itself by utilizing any of the vast amount of thermal energy held within the ocean. Similarly, a power station cannot draw on the heat energy held within the atmosphere. It is this constraint on the usefulness of heat energy that gives rise to the **Second Law of Thermodynamics**.

Perhaps the simplest statement of the Second Law is that heat will always pass from a higher-temperature body to a lower-temperature body and can never, spontaneously, pass in the opposite direction. There are many other ways of stating the Second Law and the numerous corollaries that result from it. The Second Law is, to be precise, a statement of probabilities. The molecules in a sample of fluid move with varying speeds in apparently random directions and with a mean velocity approximating that of the speed of sound in the fluid. It is extremely improbable, although not impossible, for a chance occurrence in which all the molecules move in the same direction. In the event of such a rare condition, a cup of coffee could become "hotter" when placed in cool surroundings. Such an observation has never yet been made in practice and would constitute a contravention of the Second Law of Thermodynamics.

The question arises, just how much of a given amount of heat energy can be converted into work? This is of interest to the sub-surface ventilation engineer as some of the heat energy added to the airstream may be converted into mechanical energy in order to help promote movement of the air.

To begin an answer to this question, consider a volume of gas within an uninsulated cylinder and piston arrangement. When placed in warmer surroundings, the gas will gain heat through the walls of the cylinder and expand. The piston will move against the resisting pressure of the surrounding atmosphere and produce mechanical work. This will continue until the temperature of the gas is the same as that of the surroundings. Although the gas still 'contains' heat energy, it is incapable of causing further work to be done in those surroundings. However, if the cylinder were then placed in yet warmer surroundings the gas would expand further and more work would be generated - again until the temperatures inside and outside the cylinder were equal. From this imaginary experiment it would seem that heat can produce mechanical work only while a temperature difference exists.

In 1824, while still in his twenties, **Sadi Carnot** produced a text "Reflections on the Motive Power of Fire", in which he devised an ideal heat engine operating between a supply temperature T_1 and a lower reject temperature, T_2 . He showed that for a given amount of heat, q , supplied to the engine, the maximum amount of work that could be produced is

$$W_{ideal} = \frac{(T_1 - T_2)}{T_1} q \quad \text{J} \quad (3.38)$$

In real situations, no process is ideal and the real work output will be less than the Carnot work due to friction or other irreversible effects. However, from equation (3.38) a maximum "**Carnot Efficiency**", η_c can be devised:

$$\eta_c = \frac{W_{ideal}}{q} = \frac{(T_1 - T_2)}{T_1} \quad (3.39)$$

3.4. FRICTIONAL FLOW

3.4.1. The effects of friction in flow processes

In the literature of thermodynamics, a great deal of attention is given to frictionless processes, sometimes called ideal or reversible. The latter term arises from the concept that a reversible process is one that having taken place can be reversed to leave no net change in the state of either the system or surroundings.

Frictionless processes can never occur in practice. They are, however, convenient metrics against which to measure the performance or efficiencies of real heat engines or other devices that operate through exchanges of work and/or heat. In subsurface ventilation systems, work is added to the airflow by means of fans and heat is added from the strata or other sources. Some of that heat may be utilized in helping to promote airflow in systems that involve differences in vertical elevation. An ideal system would be one in which an airflow, having been initiated, would continue indefinitely without further degradation of energy. Although they cannot exist in practice, the concept of ideal processes assists in gaining an understanding of the behaviour of actual airflow systems.

Let us consider what we mean by "friction" with respect to a fluid flow. The most common everyday experience of friction is concerned with the contact of two surfaces - a brake on a wheel or a tyre on the road. In fluid flow, the term "friction" or "**frictional resistance**" refers to the effects of viscous forces that resist the motion of one layer of fluid over another, or with respect to a solid boundary (Section 2.3.3). In turbulent flow, such forces exist not only at boundaries and between laminae of fluid, but also between and within the very large number of vortices that characterize turbulent flow. Hence, the effect of fluid friction is much greater in turbulent flow.

In the expanded version of the steady flow energy equation, the term denoting work done against frictional effects was F_{12} . To examine how this affects the other parameters, let us restate that equation.

$$\frac{u_1^2 - u_2^2}{2} + (Z_1 - Z_2)g + W_{12} = \int_1^2 VdP + F_{12} = (H_2 - H_1) - q_{12} \quad \frac{\text{J}}{\text{kg}} \quad \text{(from equation (3.25))}$$

But from equation (3.33) for a perfect gas

$$(H_2 - H_1) = C_p (T_2 - T_1) \quad \frac{\text{J}}{\text{kg}} \quad (3.40)$$

giving

$$\frac{u_1^2 - u_2^2}{2} + (Z_1 - Z_2)g + W_{12} = \int_1^2 VdP + F_{12} = C_p (T_2 - T_1) - q_{12} \quad \frac{\text{J}}{\text{kg}} \quad (3.41)$$

We observe that the friction term, F_{12} , appears in only the middle section of this three part equation. This leads to two conclusions for zero net change in the sum of kinetic, potential and fan input energy, i.e. each part of the equation remaining at the same total value. First, frictional effects, F_{12} , appear at the expense of $\int_1^2 VdP$. As F_{12} increases then the flow work must decrease for the middle part of the equation to maintain the same value. However, the conversion of mechanical energy into heat through frictional effects will result in the specific volume, V , expanding to a value that is higher than would be the case in a corresponding frictionless system. It follows that the appearance of friction must result in a loss of pressure in a flow system. A real (frictional) process from station 1 to station 2 will result in the pressure at station 2 being less than would be the case of a corresponding ideal process. The difference is the "**frictional pressure drop**".

Secondly, and again for a zero net change in kinetic, potential and fan energies, the lack of a friction term in the right hand part of equation (3.41) shows that the change in temperature ($T_2 - T_1$) is independent of frictional effects. In other words, the actual change in temperature along an airway is the same as it would be in a corresponding frictionless process. This might seem to contradict everyday experience where we expect friction to result in a rise in temperature. In the case of the steady flow of perfect gases, the frictional conversion of mechanical work to heat through viscous shear produces a higher final specific volume and a lower pressure than for the ideal process, but exactly the same temperature.

Returning to the concept of frictional pressure drop, the steady flow energy equation can also be used to illustrate the real meaning of this term. If we accept the usual situation in which the variation in density, ρ ($= 1/V$), along the airway is near linear, we can multiply equation (3.25) by a mean value of density, ρ_m to give

$$\rho_m \frac{(u_1^2 - u_2^2)}{2} + \rho_m (Z_1 - Z_2)g + \rho_m W_{12} = (P_2 - P_1) + \rho_m F_{12} = \rho_m (H_2 - H_1) - \rho_m q_{12} \quad \frac{\text{J kg}}{\text{kg m}^3} = \frac{\text{J}}{\text{m}^3} \quad (3.42)$$

(Note the new units of the terms in this equation. They still express variations in energy levels, (J), but now with reference to a unit volume (m^3) rather than a unit mass (kg). As it is the total mass flow that remains constant the steady flow energy equation (in J/kg) is the preferred version of the equation. (See also, Section 2.1.2). However, most of the terms in equation (3.42) do have a physical meaning. We can re-express the units as

$$\frac{\text{J}}{\text{m}^3} = \frac{\text{Nm}}{\text{m}^3} = \frac{\text{N}}{\text{m}^2} = \text{Pa} \quad (3.43)$$

As this is the unit of pressure, equation (3.42) is sometimes called the **steady flow pressure equation**. Furthermore,

$\rho_m \frac{(u_1^2 - u_2^2)}{2}$ is the change in velocity pressure (see equation (2.17))

$\rho_m (Z_1 - Z_2)g$ is the change in static pressure due to the column of air between Z_1 and Z_2

$\rho_m W_{12}$ is the increase in pressure across the fan

$(P_2 - P_1)$ is the change in barometric pressure, and

$\rho_m F_{12}$ is the frictional pressure drop, p , (equation (2.46)).

The **frictional pressure drop** may now be recognized as the work done against friction **per cubic metre of air**. As the mass in a cubic metre varies due to density changes, the disadvantage of a relationship based on volume becomes clear.

3.4.2. Entropy

In section 3.3.5. we discussed work and heat as "first and second class" energy terms respectively. All work can be transferred into heat but not all heat can be transferred into work. Why does this preferential direction exist? It is, of course, not the only example of 'one-wayness' in nature. Two liquids of the same density but different colours will mix readily to a uniform shade but cannot easily be separated back to their original condition. A rubber ball dropped on the floor will bounce, but not quite to the height from which it originated - and on each succeeding bounce it will lose more height. Eventually, the ball will come to rest on the floor. All of its original potential energy has been converted to heat through impact on the floor, but that heat cannot be used to raise the ball to its initial height. Each time we engage in any non-ideal process, we finish up with a lower quality, or less organized, state of the system. Another way of putting it is that the "disorder" or "randomness" of the system has increased. It is a quantification of this disorder that we call **entropy**.

Suppose we build a symmetric tower out of toy building bricks. The system is well ordered and has a low level of entropy. Now imagine your favorite infant taking a wild swipe at it. The bricks scatter all over the floor. Their position is obviously now in a much greater degree of disorder. Energy has been expended on the system and the entropy (disorder) has increased. This is entropy of position. Let us carry out another imaginary experiment. Suppose we have a tray on which rest some marbles. We vibrate the tray gently and the marbles move about in a random manner. Now let us vibrate the tray violently. The marbles become much more agitated or disordered in their movement. We have done work on the system and, again, the entropy level has increased. This is entropy of motion.

What has all this to do with heat transfer? Imagine that we have a perfect crystal at a temperature of absolute zero. The molecules are arranged in a symmetric lattice and are quite motionless. We can state that this is a system of perfect order or zero entropy. If we now add heat to the crystal, that energy will be utilized in causing the molecules to vibrate. The more heat we add, the more agitated the molecular vibration and the greater the entropy level. Can you see the analogy with the marbles?

The loss of order is often visible. For example, ice is an "ordered" form of water. Adding heat will cause it to melt to the obviously less organized form of liquid water. Further heat will produce the even less ordered form of water vapour.

How can we quantify this property that we call entropy? **William J.M. Rankine (1820-1872)**, a Scots professor of engineering showed in 1851 that during a reversible (frictionless) process, the ratio of heat exchanged to the current value of temperature, $\delta q/T$, remained constant. Clausius arrived at the same conclusion independently in Germany during the following year. Clausius also recognized that particular ratio to be a thermodynamic function of state and coined the name entropy, s (after the Greek work for 'evolution'). Clausius further realized that although entropy remained constant for ideal processes, the total entropy must increase for all real processes.

$$ds = \frac{\delta q}{T} \geq 0$$

When testing Clausius' conclusion, it is important to take all parts of the system and surroundings into account. A subsystem may be observed to experience a decrease in entropy if viewed in isolation. For example, water in a container that is placed in sufficiently colder surroundings can be seen to freeze - the ordered form of ice crystals growing, apparently spontaneously, on the surface of the less ordered liquid. The entropy of the water is visibly decreasing. Suppose the temperature of the water is T_w and that of the cooler air is T_a where $T_a < T_w$. Then for a transfer of heat δq from the water to the air, the corresponding changes in entropy for the air (sub-script a), and the water (subscript w), are:

$$ds_a = \frac{\delta q}{T_a}$$

and $ds_w = -\frac{\delta q}{T_w}$ (negative as heat is *leaving* the water)

Then the total change in entropy for this system is

$$ds_a + ds_w = \delta q \left[\frac{1}{T_a} - \frac{1}{T_w} \right] > 0$$

Using the thermodynamic property, entropy, we can now express the *combined* heat increase of a system, by both heat transfer and frictional effects, as dq_c

$$dq_c = T ds \quad \frac{\text{J}}{\text{kg}} \quad (3.44)$$

(see, also, equation (3.3)).

The symbol q_c , is used to denote the **combination** of added heat and the internally generated frictional heat.

Now to make the concept really useful, we must be able to relate entropy to other thermodynamic properties. Let us take the differential form of the steady flow energy equation (3.25).

$$VdP + dF = dH - dq \quad \frac{\text{J}}{\text{kg}} \quad (3.45)$$

Then $dF + dq = dH - VdP$

But the combined effect of friction and added heat is

$$dq_c = dF + dq$$

Therefore, equations (3.44) and (3.45) give

$$Tds = dH - VdP \quad \frac{\text{J}}{\text{kg}} \quad (3.46)$$

This is another equation that will be important to us in the thermodynamic analysis of subsurface ventilation circuits.

In order to derive an expression that will allow us to calculate a change in entropy directly from measurements of pressure and temperature, we can continue our analysis from equation (3.46).

$$ds = \frac{dH}{T} - \frac{VdP}{T} \quad \frac{\text{J}}{\text{kgK}}$$

But $dH = C_p dT$ (equation (3.32))

and $\frac{V}{T} = \frac{R}{P}$ (from the General Gas Law $PV = RT$)

$$\text{giving } ds = C_p \frac{dT}{T} - R \frac{dP}{P} \quad \frac{\text{J}}{\text{kgK}} \quad (3.47)$$

Integrating between end stations 1 and 2 gives

$$(s_2 - s_1) = C_p \ln\left(\frac{T_2}{T_1}\right) - R \ln\left(\frac{P_2}{P_1}\right) \quad \frac{\text{J}}{\text{kgK}} \quad (3.48)$$

This is known as the **steady flow entropy equation**.

3.4.3. The adiabatic and isentropic processes

An important thermodynamic process with which the ventilation engineer must deal is one in which there is no heat transfer between the air and the strata or any other potential source. This can be approached closely in practice, particularly in older return airways that contain no equipment and where the temperatures of the air and the surrounding rock have reached near equilibrium.

The steady flow energy equation for adiabatic flow is given by setting $q_{12} = 0$.

$$\text{Then } \int_1^2 VdP + F_{12} = (H_2 - H_1) \quad \frac{\text{J}}{\text{kg}} \quad (3.49)$$

The ideal, frictionless, or reversible adiabatic process is a particularly useful concept against which to compare real adiabatic processes. This is given simply by eliminating the friction term

$$\int_1^2 VdP = (H_2 - H_1) \quad \frac{\text{J}}{\text{kg}} \quad (3.50)$$

or $VdP = dH$

In Section 3.4.2, we defined a change in entropy, ds , by equation (3.46) i.e.

$$dq_c = Tds \quad \frac{\text{J}}{\text{kg}} \quad (3.51)$$

where q_c is the combined effect of added heat and heat that is generated internally by frictional effects. It follows that during a frictionless adiabatic where both q_{12} and F_{12} are zero, then dq_c is also zero and the entropy remains constant, i.e. an **isentropic process**.

The governing equations for an isentropic process follow from setting $(s_2 - s_1) = 0$ in equation (3.48). Then

$$C_p \ln\left(\frac{T_2}{T_1}\right) = R \ln\left(\frac{P_2}{P_1}\right) \quad \frac{\text{J}}{\text{kgK}}$$

Taking antilogs gives –

$$\frac{T_2}{T_1} = \left[\frac{P_2}{P_1}\right]^{R/C_p} \quad (3.52)$$

The index R/C_p was shown by equation (3.36) to be related to the ratio of specific heats $C_p/C_v = \gamma$ by the equation

$$\frac{R}{C_p} = \frac{(\gamma - 1)}{\gamma}$$

Then

$$\frac{T_2}{T_1} = \left[\frac{P_2}{P_1}\right]^{\frac{\gamma - 1}{\gamma}} \quad (3.53)$$

Values of the constants are given in Table 3.1. For dry air, $\gamma = 1.400$, giving the isentropic relationship between temperature and pressure as

$$\frac{T_2}{T_1} = \left[\frac{P_2}{P_1} \right]^{0.2856} \quad (3.54)$$

This is a particularly useful equation to relate pressures and temperatures in dry mine shafts where adiabatic conditions may be approached.

The isentropic relationship between pressure and specific volume follows from equation (3.53)

$$\frac{T_2}{T_1} = \left[\frac{P_2}{P_1} \right]^{1-\frac{1}{\gamma}} \quad (3.55).$$

But from the General Gas Law, (equation (3.12))

$$\frac{T_2}{T_1} = \frac{P_2 V_2}{P_1 V_1} \quad (3.56)$$

Combining equations (3.55 and 3.56) gives

$$\frac{P_2 V_2}{P_1 V_1} = \left[\frac{P_2}{P_1} \right]^{1-\frac{1}{\gamma}}$$

$$\frac{V_2}{V_1} = \left[\frac{P_2}{P_1} \right]^{-\frac{1}{\gamma}} = \left[\frac{P_1}{P_2} \right]^{\frac{1}{\gamma}}$$

$$\text{or } P_1 V_1^\gamma = P_2 V_2^\gamma = \text{constant} \quad (3.57)$$

3.4.4. Availability

In the context of conventional ventilation engineering, the energy content of a given airstream is useful only if it can be employed in causing the air to move, i.e. if it can be converted to kinetic energy. A more general concept is that of available energy. This is defined as the maximum amount of work that can be done by a system until it comes to complete physical and chemical equilibrium with the surroundings.

Suppose we have an airflow of total energy

$$\frac{u_2}{2} + Zg + H \quad \frac{\text{J}}{\text{kg}} \quad (\text{equation 3.20))}$$

The kinetic and potential energy terms both represent mechanical energy and are fully **available** to produce mechanical effects, i.e. to do work. This is not true for the enthalpy. Remember that enthalpy is comprised of PV and internal energy terms, and that the Second Law allows only a fraction of thermal energy to be converted into work. Suppose that the free atmosphere at the surface of a mine has a specific enthalpy H_o (subscript o for 'outside' atmosphere). Then when the mine air is rejected at temperature T to the surface, it will cool at constant pressure until it reaches the temperature of the ambient atmosphere T_o . Consequently, its enthalpy will decrease from H to H_o .

$$(H - H_o) = C_p (T - T_o) \quad \frac{\text{J}}{\text{kg}} \quad (3.58)$$

The process is shown on a temperature-entropy diagram in Figure 3.3. The heat rejected to the free atmosphere is represented by the area under the process line $\int_a^b T ds = \text{area } abcd$. However, for an

isobar (constant pressure), $\int_a^b T ds = \int_a^b dH = H - H_o$ (see equation (3.46) with $dP = 0$). Hence, the enthalpy change $H - H_o$ gives the heat lost to the atmosphere. Equation (3.58) actually illustrates the same fact, as heat lost is

$$\text{mass (1 kg) } \times \text{ specific heat } (C_p) \times \text{ change in temperature } (T - T_o)$$

for a constant pressure process.

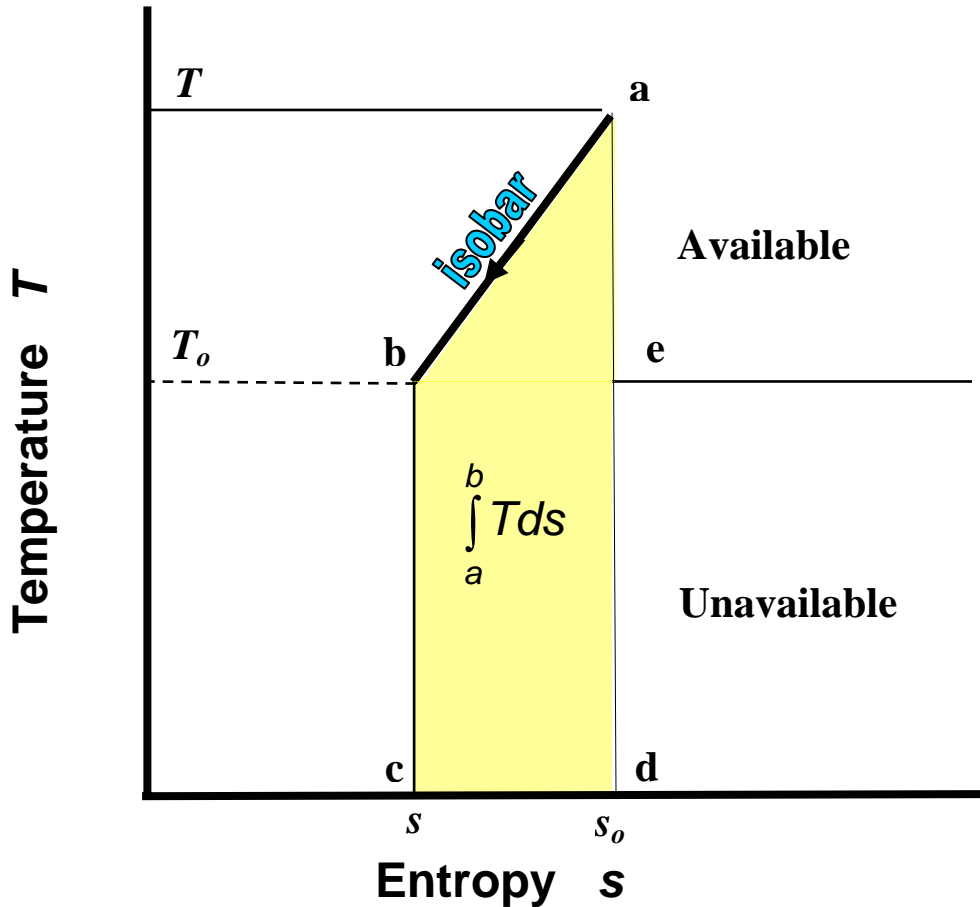


Figure 3.3. Temperature entropy diagram for constant pressure cooling

Now the Second Law insists that only a part of this heat can be used to do work. Furthermore, we have illustrated earlier that when a parcel of any gas reaches the temperature of the surroundings then it is no longer capable of doing further work within those surroundings. Hence, the part of the

heat energy that remains unavailable to do any work is represented by the $\int_e^b T ds$ area under the ambient temperature line T_o , i.e. $T_o (s - s_o)$ or area bcde on Figure 3.3. The only part of the total heat that remains available to do work is represented by area abe or $(H - H_o) - T_o (s - s_o)$.

The **available energy**, ψ , in any given airflow, with respect to a specified datum (subscript o) may now be written as

$$\psi = \frac{u^2}{2} + Zg + (H - H_o) - T_o(s - s_o) \quad \frac{\text{J}}{\text{kg}} \quad (3.59)$$

It should be made clear that **the available energy represents the maximum amount of energy that is theoretically capable of producing useful work**. How much of this is actually used depends upon the ensuing processes.

Let us now try to show that any real airway suffers from a loss of available energy because of frictional effects. If we rewrite equation (3.59) in differential form for an adiabatic airway, then the increase in available energy along a short length of the airway is

$$d\psi = u du + g dZ + dH - T_o ds$$

(H_o and s_o are constant for any given datum conditions).

This equation assumes that we do not provide any added heat or work. From the differential form of the steady flow energy equation (3.25) for adiabatic conditions and no fan work ($dq = dW = 0$),

$$u du + g dZ + dH = 0$$

$$\text{leaving } d\psi = -T_o ds \quad \frac{\text{J}}{\text{kg}} \quad (3.60).$$

Now, from equation (3.51), $ds = \frac{dq_c}{T}$

where q_c is the combined effect of friction, F , and added heat, q . However, in this case, q is zero giving

$$ds = \frac{dF}{T}$$

and

$$d\psi = -\frac{T_o}{T} dF \quad \frac{\text{J}}{\text{kg}} \quad (3.61)$$

As T_o , T and dF are positive, the change in available energy must always be negative in the absence of any added work or heat. This equation also shows that the loss of available energy is a direct consequence of frictional effects.

Available energy is a "consumable" item, unlike total energy which remains constant for adiabatic flow with no work input. During any real airflow process, the available energy is continuously eroded by the effects of viscous resistance in the laminar sublayer and within the turbulent eddies. That energy reappears as "low grade" heat or **unavailable energy** and is irretrievably lost in its capacity to do useful work. The process is illustrated in Figure 3.4.

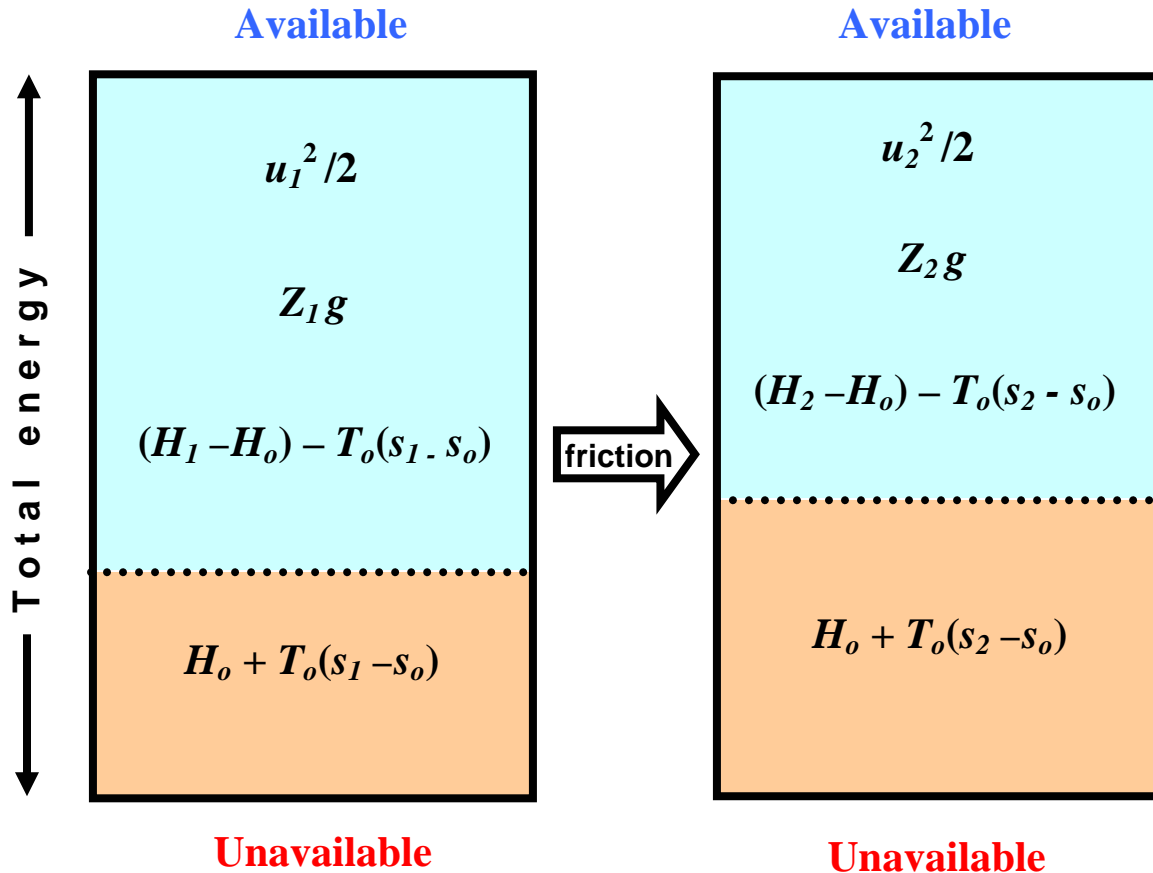


Figure 3.4. Available energy decreases and unavailable energy increases both by the amount $T_o (s_2 - s_1)$ when no heat or work are added.

3.5 THERMODYNAMIC DIAGRAM.

During any thermodynamic process, there will be variations in the values of the fluid properties. The equations derived in the preceding sections of this chapter may be used to quantify some of those changes. However, plotting one property against another provides a powerful visual aid to understanding the behaviour of any process path and can also give a graphical means of quantifying work or heat transfers where the complexity of the process path precludes an analytical treatment. These graphical plots are known as thermodynamic diagrams.

The two most useful diagrams in steady flow thermodynamics are those of pressure against specific volume and temperature against specific entropy. These diagrams are particularly valuable, as areas on the **PV diagram** represent **work** and areas on the **Ts diagram** represent **heat**. Remembering that simple fact will greatly facilitate our understanding of the diagrams. In this section, we shall introduce the use of these diagrams through three compression processes. In each case, the air will be compressed from pressure P_1 to a higher pressure P_2 . This might occur through a fan, compressor or by air falling through a downcast shaft. The processes we shall consider are isothermal, isentropic and polytropic compression. As these are important processes for the ventilation engineer, the opportunity is taken to discuss the essential features of each, in addition to giving illustrations of the visual power of thermodynamic diagrams.

3.5.1. Ideal isothermal (constant temperature) compression.

Suppose air is passed through a compressor so that its pressure is raised from P_1 to P_2 . As work is done on the air, the First Law of Thermodynamics tells us that the internal energy and, hence, the temperature of the air will increase (equation (3.16)). However, in this particular compressor, we have provided a water jacket through which flows a continuous supply of cooling water. Two processes then occur. The air is compressed and, simultaneously, it is cooled at just the correct rate to maintain its temperature constant. This is **isothermal compression**.

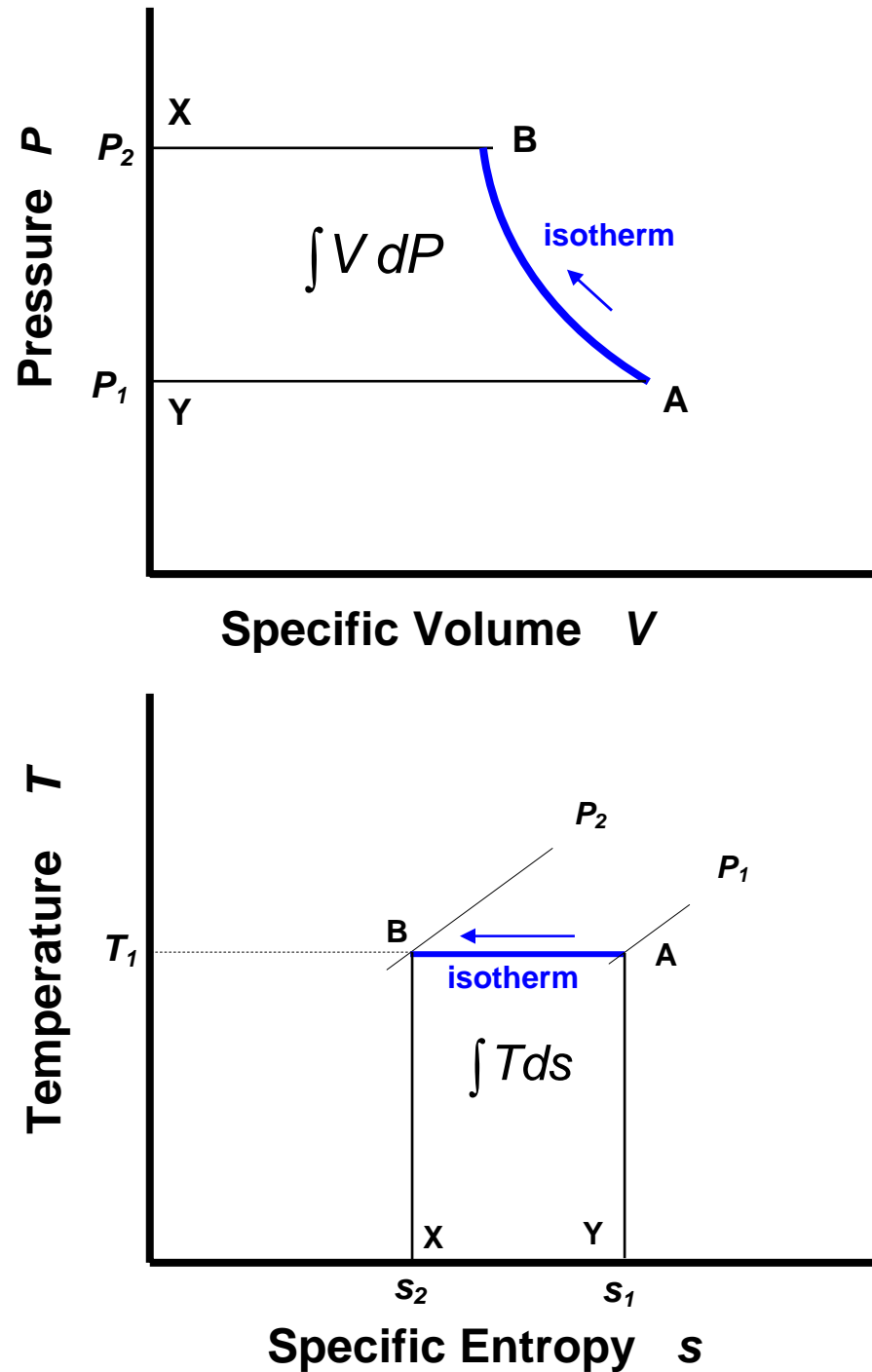
Figure 3.5. PV and Ts diagrams for an isothermal compression.

Figure 3.5 shows the process on a pressure-specific volume (PV) and a temperature-entropy (Ts) diagram. The first stage in constructing these diagrams is to draw the isobars representing P_1 and P_2 . On the PV diagram these are simply horizontal lines. Lines on the Ts diagram may be plotted using equation (3.48). Isobars curve slightly. However, over the range of pressures and temperatures of interest to the ventilation engineer, the curvature is small.

The process path for the **isothermal** (constant temperature) compression is shown as line AB on both diagrams. On the PV diagram, it follows the slightly curved path described by the equation

$$PV = RT_1$$

or
$$P = \frac{RT_1}{V} \quad \text{Pa} \quad (3.62)$$

On the Ts diagram, the isotherm is, of course, simply a horizontal line at temperature T_1 .

Let us first concentrate on the PV diagram. From the steady flow energy equation for a frictionless process, we have

$$\frac{(u_1^2 - u_2^2)}{2} + (Z_1 - Z_2)g + W_{12} = \int_1^2 VdP \quad \frac{\text{J}}{\text{kg}}$$

In this case we may assume that the flow through the compressor is horizontal ($Z_1 = Z_2$) and that the change in kinetic energy is negligible, leaving

$$W_{12} = \int_1^2 VdP \quad \frac{\text{J}}{\text{kg}} \quad (3.63)$$

The integral $\int_1^2 VdP$ is the area to the left of the process line on the PV diagram, i.e., area ABXY for the ideal compressor is equal to the work, W_{12} , that has been done by the compressor in raising the air pressure from P_1 to P_2 . We can evaluate the integral by substituting for V from equation (3.62).

$$W_{12} = \int_1^2 VdP = \int_1^2 \frac{RT_1}{P} dP = RT_1 \ln\left(\frac{P_2}{P_1}\right) \quad \frac{\text{J}}{\text{kg}} \quad (3.64)$$

as RT_1 is constant

This is **positive** as work is done **on** the air.

Now let us turn to the Ts diagram. Remember that the integral $\int Tds$ represents the combined heat from actual heat transfer and also that generated by internal friction. However, in this ideal case, there is no friction. Hence the $\int Tds$ area under the process line AB represents the heat that is removed from the air by the cooling water during the compression process. The heat area is the rectangle ABXY or $-T_1(s_1 - s_2)$ on the Ts diagram. In order to quantify this heat, recall the entropy equation (3.48) and apply the condition of constant temperature. This gives

$$-T_1(s_1 - s_2) = -RT_1 \ln\left(\frac{P_2}{P_1}\right) \quad \frac{\text{J}}{\text{kg}} \quad (3.65)$$

The sign is negative as heat is **removed** from the air.

Now compare the **work input** (equation (3.64)) with the **heat removed** (equation (3.65)). Apart from the sign, they are numerically identical. This means that as work is done on the system to compress the air, exactly the same quantity of energy is removed as heat during this isothermal process. [This result is also shown directly by equations (3.16) and (3.27) with $dU = \delta W + \delta q = C_v dT = 0$ giving $\delta W = -\delta q$ for an isothermal process].

Despite the zero net increase in energy, the air has been pressurized and is certainly capable of doing further useful work through a compressed air motor. How can that be? The answer lies in the, discussion on availability given in Section 3.4.4. All of the work input is **available energy** capable of producing mechanical effects. However, all of the heat removed is **unavailable energy** that already existed in the ambient air and which could not be used to do useful work. The fact that this heat is, indeed, completely unavailable is illustrated on the Ts diagram by the corresponding heat area $-T_1(s_1 - s_2)$ lying completely below the ambient temperature line.

This process should be studied carefully until it is clearly understood that there is a very real distinction between available energy and unavailable energy. The high pressure air that leaves the compressor retains the work input as available energy but has suffered a loss of unavailable energy relative to the ambient air. If the compressed air is subsequently passed through a compressed air motor, the available energy is utilized in producing a mechanical work output, leaving the air with only its depressed unavailable energy to be exhausted back to the atmosphere. This explains why the air emitted from the exhaust ports of a compressed air motor is very cold and may give rise to problems of condensation and freezing.

Maintaining the temperature constant during isothermal compression minimizes the work that must be done on the air for any given increase in pressure. Truly continuous isothermal compression cannot be attained in practice, as a temperature difference must exist between the air and the cooling medium for heat transfer to occur. In large multi-stage compressors, the actual process path on the Ts diagram proceeds from A to B along a zig-zag line with stages of adiabatic compression alternating with isobaric cooling attained through interstage water coolers.

3.5.2. Isentropic (constant entropy) compression

During this process we shall, again, compress the air from P_1 to P_2 through a fan or compressor, or perhaps by gravitational work input as the air falls through a downcast shaft. This time, however, we shall assume that the system is not only frictionless but is also insulated so that no heat transfer can take place. We have already introduced the **frictionless adiabatic** in Section 3.4.2 and shown that it maintains constant entropy, i.e. an **isentropic process**.

The PV and Ts diagrams are shown on Figure 3.6. The corresponding process lines for the isothermal case have been retained for comparison. The area to the left of the isentropic process line, AC, on the PV diagram is, again, the work input during compression. It can be seen that this is greater than for the isothermal case. This area, ACXY or $\int_1^2 V dP$, is given by the steady flow energy equation (3.25) with $F_{12} = q_{12} = 0$,

$$\text{i.e.} \quad \int_1^2 V dP = H_2 - H_1 = C_p (T_2 - T_1) \quad \frac{\text{J}}{\text{kg}} \quad (3.66)$$

On the Ts diagram, the process line AC is vertical (constant entropy) and the temperature increases from T_1 to T_2 . The $\int T ds$ area under the line is zero. This suggests that the Ts diagram is not very useful in further evaluating an isentropic process. However, we are about to reveal a feature of Ts diagrams that enhances their usefulness very considerably. Suppose that, having completed the isentropic compression and arrived at point C on both diagrams, we now engage upon an **imaginary**

second process during which we cool the air at constant pressure until it re-attains its original ambient temperature T_1 . The process path for this second process of isobaric cooling is CB on both diagrams. The heat removed during the imaginary cooling is the area $\int Tds$ under line CB on the Ts diagram, i.e. area CBXY. But from the steady flow entropy equation (3.47)

$$ds = C_p \frac{dT}{T} - R \frac{dP}{P} \quad \frac{\text{J}}{\text{kgK}}$$

and for an isobar, $dP = 0$, giving $ds = C_p \frac{dT}{T}$ or $Tds = C_p dT$

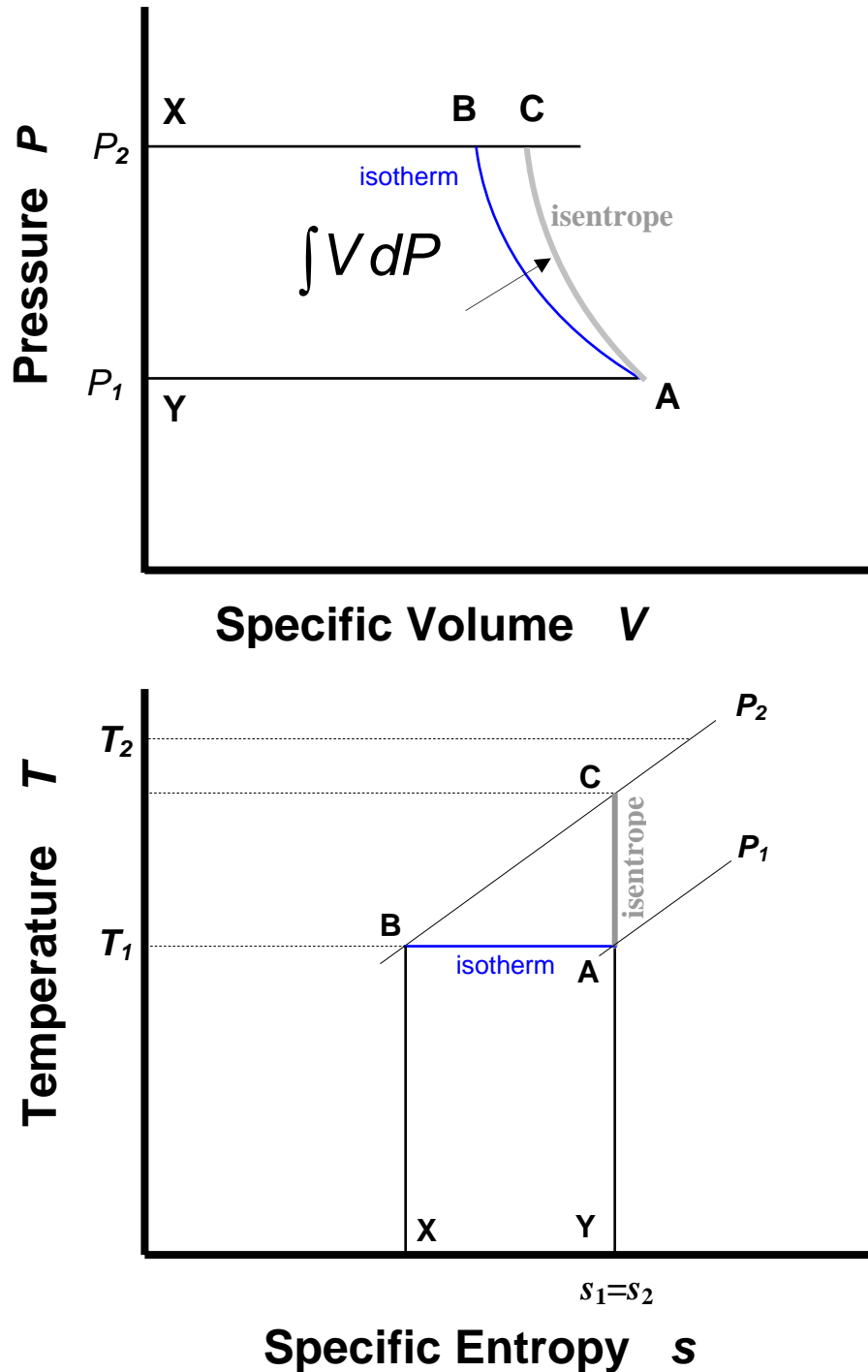


Figure 3.6. PV and Ts diagrams for an isentropic compression

Then heat removed during the imaginary cooling becomes

$$\int_2^1 T ds = - \int_1^2 T ds = - \int_1^2 C_p dT = -C_p(T_2 - T_1) \quad \frac{\text{J}}{\text{kg}} \quad (3.67)$$

Now compare equation (3.66) and (3.67). It can be seen that the heat removed during the imaginary cooling is numerically equivalent to the work input during the isentropic compression. Hence, the work input is not only shown as area ACBXY on the PV diagram but also as the same area on the Ts diagram. Using the device of imaginary isobaric cooling, the Ts diagram can be employed to illustrate work done as well as heat transfer. However, the two must never be confused - the Ts areas represent true heat energy and can differentiate between available and unavailable heat, while work areas shown on the Ts diagram are simply convenient numerical equivalents with no other physical meaning on that diagram.

3.5.3. Polytropic compression

The relationship between pressure and specific volume for an isentropic process has been shown to be

$$PV^\gamma = \text{constant} \quad (\text{equation 3.57})$$

where the isentropic index γ is the ratio of specific heats C_p/C_v . Similarly, for an isothermal process,

$$PV^1 = \text{constant}.$$

These are, in fact, special cases of the more general equation

$$PV^n = \text{constant}, C \quad (3.68)$$

where the index n remains constant for any given process but will take a different value for each separate process path. This general equation defines a polytropic system and is the type of process that occurs in practice within subsurface engineering. It encompasses the real situation of frictional flow and the additional increases in entropy that arise from heat transfer to the air.

Figure 3.7 shows the PV and Ts process lines for a polytropic compression. Unlike the isothermal and isentropic cases, the path line for the polytropic process is not rigidly defined but depends upon the value of the polytropic index n . The polytropic curve shown on the diagrams indicates the most common situation in underground ventilation involving both friction and added heat.

The flow work shown as area ADXY on the PV diagram may be evaluated by integrating

$$\int_1^2 V dP \quad \text{where } V = \left(\frac{C}{P}\right)^{1/n} \quad \text{from equation (3.68)}$$

$$\text{Then } \int_1^2 V dP = \int_1^2 \left(\frac{C}{P}\right)^{1/n} = C^{1/n} \frac{[P^{1-1/n}]_1^2}{1-1/n}$$

$$\text{or, as } C^{1/n} = P^{1/n} V$$

$$\int_1^2 V dP = \frac{n}{n-1} (P_2 V_2 - P_1 V_1) = \frac{n}{n-1} R (T_2 - T_1) \frac{J}{kg} \quad (3.69)$$

using the gas law $PV = RT$

This enables the flow work to be determined if the polytropic index, n , is known. It now becomes necessary to find a method of calculating n , preferably in terms of the measurable parameters, pressure and temperature.

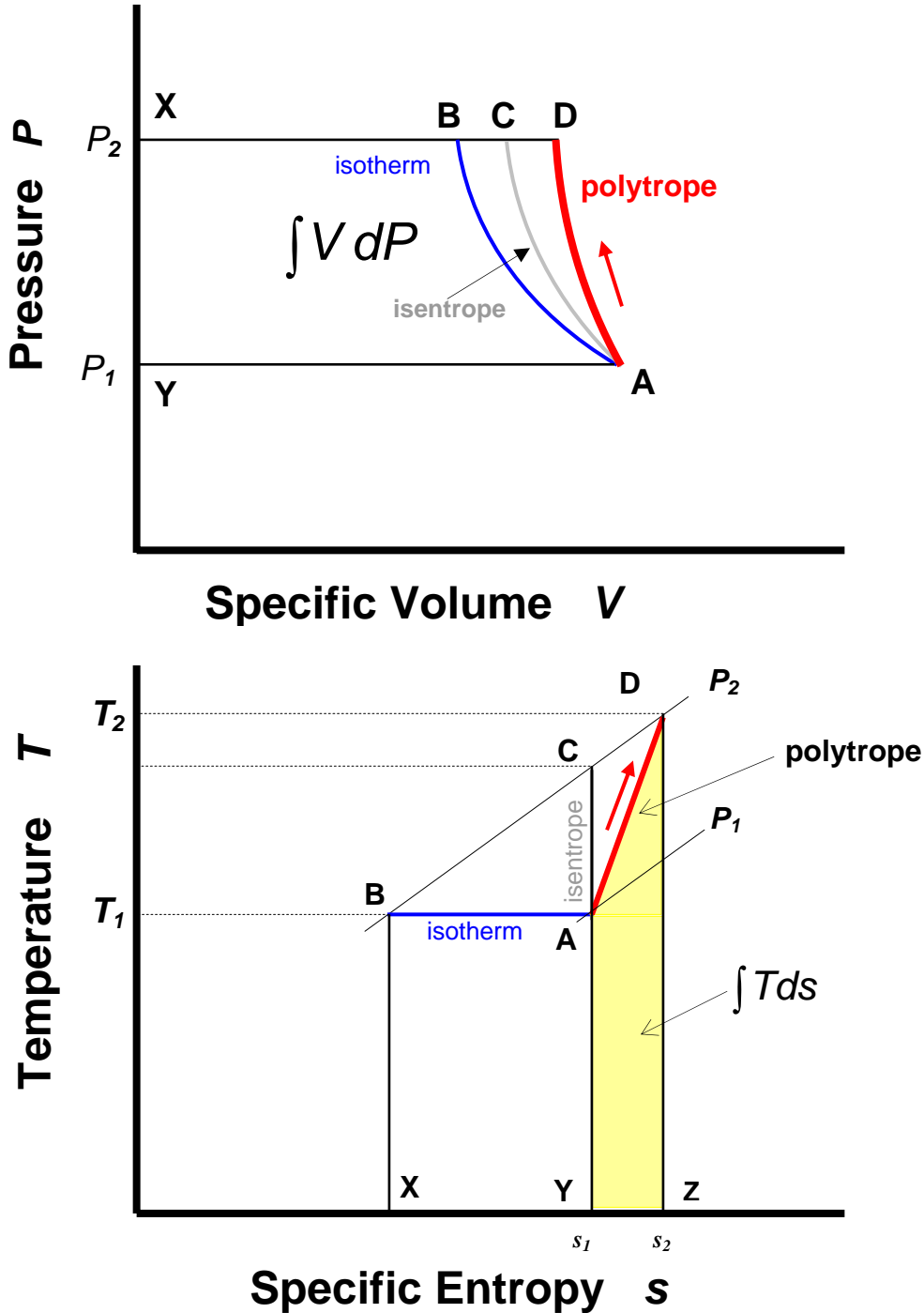


Figure 3.7. PV and Ts diagrams for a polytropic compression.

From the polytropic law (3.68) $P_1 V_1^n = P_2 V_2^n$ or $\frac{V_1}{V_2} = \left(\frac{P_2}{P_1}\right)^{1/n}$ (3.70)

and from the General Gas Law, (equation (3.12))

$$\frac{V_1}{V_2} = \frac{P_2 T_1}{P_1 T_2} \quad (3.71)$$

We have isolated V_1/V_2 in equations (3.70) and (3.71) in order to leave us with the desired parameters of pressure and temperature. Equating (3.70) and (3.71) gives

$$\left(\frac{P_2}{P_1}\right)^{1/n} = \frac{P_2 T_1}{P_1 T_2} \quad \text{or} \quad \frac{T_2}{T_1} = \left(\frac{P_2}{P_1}\right)^{1-1/n}$$

Taking logarithms gives

$$\frac{n-1}{n} = \frac{\ln\left(\frac{T_2}{T_1}\right)}{\ln\left(\frac{P_2}{P_1}\right)} \quad (3.72)$$

This enables the polytropic index, n , to be determined for known end pressures and temperatures. However, we can substitute for $n/(n-1)$, directly, into equation (3.69) to give the flow work as

$$\int_1^2 V dP = R(T_2 - T_1) \frac{\ln\left(\frac{P_2}{P_1}\right)}{\ln\left(\frac{T_2}{T_1}\right)} \quad \frac{\text{J}}{\text{kg}} \quad (3.73)$$

This is an important relationship that we shall use in the analysis of mine ventilation thermodynamics (Chapter 8).

Turning to the Ts diagram, the $\int T ds$ area under the polytrope AD, i.e. area ADZY, is the combined heat increase arising from internal friction, F_{12} , and added heat, q_{12} :

$$\int T ds = F_{12} + q_{12} \quad \frac{\text{J}}{\text{kg}} \quad (3.74)$$

But from the steady flow energy equation (3.25)

$$F_{12} + q_{12} = H_2 - H_1 - \int_1^2 V dP \quad \frac{\text{J}}{\text{kg}} \quad (3.75)$$

giving the area under line AD as

$$\int_1^2 T ds = H_2 - H_1 - \int_1^2 V dP \quad \frac{\text{J}}{\text{kg}} \quad (3.76)$$

We arrived at the same result in differential form (equation (3.46)) during our earlier general discussion on entropy.

As $(H_2 - H_1) = C_p (T_2 - T_1)$, and using equation (3.73) for the flow work, we can re-write equation (3.76) as

$$\int_1^2 T ds = C_p (T_2 - T_1) - R (T_2 - T_1) \frac{\ln(P_2/P_1)}{\ln(T_2/T_1)} \quad \frac{\text{J}}{\text{kg}}$$

$$= (T_2 - T_1) \left[C_p - R \frac{\ln(P_2/P_1)}{\ln(T_2/T_1)} \right] \quad \frac{\text{J}}{\text{kg}} \quad (3.77)$$

Now, using the same logic as employed in Section 3.5.2, it can be shown that the area under the isobar DB on the Ts diagram of Figure 3.7 is equal to the change in enthalpy $(H_2 - H_1)$. We can now illustrate the steady flow energy equation as areas on the Ts diagram

$$\underbrace{H_2 - H_1}_{\text{Area DBXZ}} = \underbrace{F_{12} + q_{12}}_{\text{Area ADZY}} + \int_1^2 V dP \quad \frac{\text{J}}{\text{kg}} \quad (3.78)$$

$$\text{Area DBXZ} = \text{Area ADZY} + \text{Area ADBXY}$$

Once again, this shows the power of the Ts diagram.

Example.

A dipping airway drops through a vertical elevation of 250m between stations 1 and 2. The following observations are made.

	Velocity u (m/s)	Pressure P (kPa)	Temperature t ($^{\circ}\text{C}$)	Airflow Q (m^3/s)
Station 1	2.0	93.40	28.20	43
Station 2	3.5	95.80	29.68	

Assuming that the airway is dry and that the airflow follows a polytropic law, determine

- the polytropic index, n
- the flow work
- the work done against friction and the frictional pressure drop
- the change in enthalpy
- the change in entropy and
- the rate and direction of heat transfer with the strata, assuming no other sources of heat.

Solution.

It is convenient to commence the solution by calculating the end air densities and the mass flow of air.

$$\rho_1 = \frac{P_1}{RT_1} \quad (\text{equation (3.11)})$$

$$= \frac{93\,400}{287.04 \times (273.15 + 28.20)} = 1.0798 \quad \frac{\text{kg}}{\text{m}^3}$$

$$\rho_2 = \frac{P_2}{RT_2} = \frac{95800}{287.04 \times (273.15 + 29.68)} = 1.1021 \quad \frac{\text{kg}}{\text{m}^3}$$

$$\text{Mass flow } M = Q_1 \times \rho_1 = 43.0 \times 1.0798 = 46.43 \quad \text{kg/s}$$

(a) *Polytropic index, n:*

From equation (3.72)

$$\frac{n-1}{n} = \frac{\ln\left(\frac{T_2}{T_1}\right)}{\ln\left(\frac{P_2}{P_1}\right)}$$

where $T_1 = 273.15 + 28.20 = 301.35$ and $T_2 = 273.15 + 29.68 = 302.83$ K

$$\frac{n-1}{n} = \frac{\ln\left(\frac{302.83}{301.35}\right)}{\ln\left(\frac{95.80}{93.40}\right)} = 0.1931$$

giving $n = 1.239$. This polytropic index is less than the isentropic index for dry air, 1.4, indicating that heat is being lost from the air to the surroundings.

(b) *Flow work:*

From equation (3.73)

$$\int_1^2 VdP = R(T_2 - T_1) \frac{\ln\left(\frac{P_2}{P_1}\right)}{\ln\left(\frac{T_2}{T_1}\right)} = 287.04(29.68 - 28.20) \frac{\ln\left(\frac{95.80}{93.40}\right)}{\ln\left(\frac{302.83}{301.35}\right)} = 2200.0 \quad \frac{\text{J}}{\text{kg}}$$

Degrees Celsius can be used for a difference ($T_2 - T_1$) but remember to employ degrees Kelvin in all other circumstances.

(c) *Friction:*

From the steady flow energy equation with no fan

$$\begin{aligned} F_{12} &= \frac{u_1^2 - u_2^2}{2} + (Z_1 - Z_2)g - \int_1^2 VdP \\ &= \frac{2^2 - 3.5^2}{2} + 250 \times 9.81 - 2200.0 \\ &= -4.1 + 2452.5 - 2200.0 = 248.4 \quad \text{J/kg} \end{aligned}$$

Note how small is the change in kinetic energy compared with the potential energy and flow work.

In order to determine the frictional pressure drop, we use equation (2.46):

$$p = \rho F_{12}$$

For this to be meaningful, we must specify the value of density to which it is referred. At a mean density (subscript m) of

$$\rho_m = \frac{\rho_1 + \rho_2}{2} = \frac{1.0798 + 1.1021}{2} = 1.0909 \quad \frac{\text{J}}{\text{kg}}$$

$$\rho_m = 1.0909 \times 248.4 = 271 \quad \text{Pa}$$

or, for comparison with other pressure drops, we may choose to quote our frictional pressure drop referred to a standard air density of 1.2 kg/m^3 , (subscript st) giving

$$p_{st} = 1.2 \times 248.4 = 298 \text{ Pa}$$

(d) *Change in enthalpy.*

From equation (3.33)

$$\begin{aligned} H_2 - H_1 &= C_p (T_2 - T_1) \quad \text{where } C_p = 1005 \text{ J/(kg K) for dry air (Table 3.1)} \\ &= 1005 (29.68 - 28.20) = 1487.4 \text{ J/kg} \end{aligned}$$

(e) *Change in entropy.*

From equation (3.51)

$$\begin{aligned} (s_2 - s_1) &= C_p \ln\left(\frac{T_2}{T_1}\right) - R \ln\left(\frac{P_2}{P_1}\right) \\ &= 1005 \ln(302.83/301.35) - 287.04 \ln(95.8/93.4) \\ &= 4.924 \quad - \quad 7.283 = -2.359 \text{ J/(kgK)} \end{aligned}$$

The decrease in entropy confirms that heat is lost to the strata.

(f) *Rate of heat transfer :*

Again, from the steady flow energy equation (3.25)

$$q_{12} = H_2 - H_1 - \frac{u_1^2 - u_2^2}{2} - (Z_1 - Z_2)g$$

(Each term has already been determined, giving

$$q_{12} = 1487.4 + 4.1 - 2452.5 = -961.0 \text{ J/kg}$$

To convert this to kilowatts, multiply by mass flow

$$q_{12} = \frac{-961.0 \times 46.43}{1000} = -44.6 \quad \text{kW}$$

The negative sign shows again that heat is transferred from the air to the strata and at a rate of 44.6 kW.

Further Reading

Hinsley, F.B. (1943) Airflow in Mines: A Thermodynamic Analysis. Proc. South Wales Inst. of Engineers Vol LIX, No. 2

Look, D.C. and Sauer, H.J. (1982) Thermodynamics. Published by Brooks /Cole Engineering Division, Monterey, California

Rogers, G.F.C and Mayhew, Y.R. (1957). Engineering Thermodynamics, Work and Heat Transfer. Published by Longmans, Green and Co.

Van Wylen, G. J. (1959). Thermodynamics. Published by John Wiley and Sons.

Chapter 4. Subsurface Ventilation Systems

4.1. INTRODUCTION	2
4.2. MINE SYSTEMS	2
4.2.1 General principles	2
<i>Fans</i>	3
<i>Stoppings and Seals</i>	3
<i>Doors and airlocks</i>	3
<i>Regulators</i>	4
<i>Air crossings</i>	4
4.2.2 Location of main fans	5
<i>Gas control</i>	5
<i>Transportation</i>	6
<i>Fan maintenance</i>	6
<i>Fan performance</i>	6
4.2.3. Infrastructure of main ventilation routes	7
<i>Mine resistance</i>	7
<i>Leakage control</i>	8
<i>Direction of airflow</i>	9
<i>Airflow travel distance and use of old workings</i>	10
4.3. DISTRICT SYSTEMS	11
4.3.1. Basics of district system design	11
4.3.2. Stratified deposits	12
<i>Longwall systems</i>	13
<i>Room (bord) and pillar systems</i>	14
4.3.3. Orebody deposits	17
4.4. AUXILIARY SYSTEMS	21
4.4.1. Line brattices and duct systems	21
4.4.2. Forcing, exhausting, and overlap systems	23
4.4.3. Air movers	25
4.5. CONTROLLED PARTIAL RECIRCULATION	25
4.5.1. Background and principles of controlled partial recirculation	25
4.5.2. Controlled recirculation in headings	26
4.5.3. District systems	29
<i>Positions of fans</i>	29
<i>Pollution levels</i>	31
4.6. UNDERGROUND REPOSITORIES	33
4.6.1. Types of repository	33
4.6.2. Ventilation circuits in repositories for nuclear waste	33
4.6.3. Additional safety features	35
BIBLIOGRAPHY	35

4.1. INTRODUCTION

Practically every underground opening is unique in its geometry, extent, geological surroundings, environmental pollutants and reasons for its formation - natural or man-made. The corresponding patterns of airflow through those openings are also highly variable. There are, however, certain features that are sufficiently common to permit classifications of structured ventilation systems and subsystems to be identified.

In this chapter, we shall discuss the essential characteristics of subsurface ventilation systems, first on the basis of complete mines and primary airflow routes. The opportunity is taken to introduce some of the technical terms used by ventilation engineers. The terms chosen are those that are in common use throughout the English speaking mining countries. Secondly, we shall look at district systems for more localized areas of a mine. These, in particular, vary considerably depending upon the geometry of the geologic deposit being mined. Although reference will be made to given mining methods, the treatment here will concentrate on principles rather than detailed layouts. In most countries, state or national mining law impacts upon the ventilation layout. System designers must, as a pre-requisite, become familiar with the governing legislation. In the absence of any relevant legislation applicable to the location of the mine, or where the engineer perceives it to be inadequate, then it is prudent to utilize the pertinent laws from another country that has a well-developed history of mining legislation.

Thirdly, auxiliary ventilation systems will be examined, these dealing with the ventilation of blind headings. The chapter also deals with the principles of controlled partial recirculation and the ventilation of underground repositories for nuclear waste or other stored material.

4.2. MINE SYSTEMS

4.2.1 General principles

Figure 4.1. depicts the essential elements of a ventilation system in an underground mine or other subsurface facility.

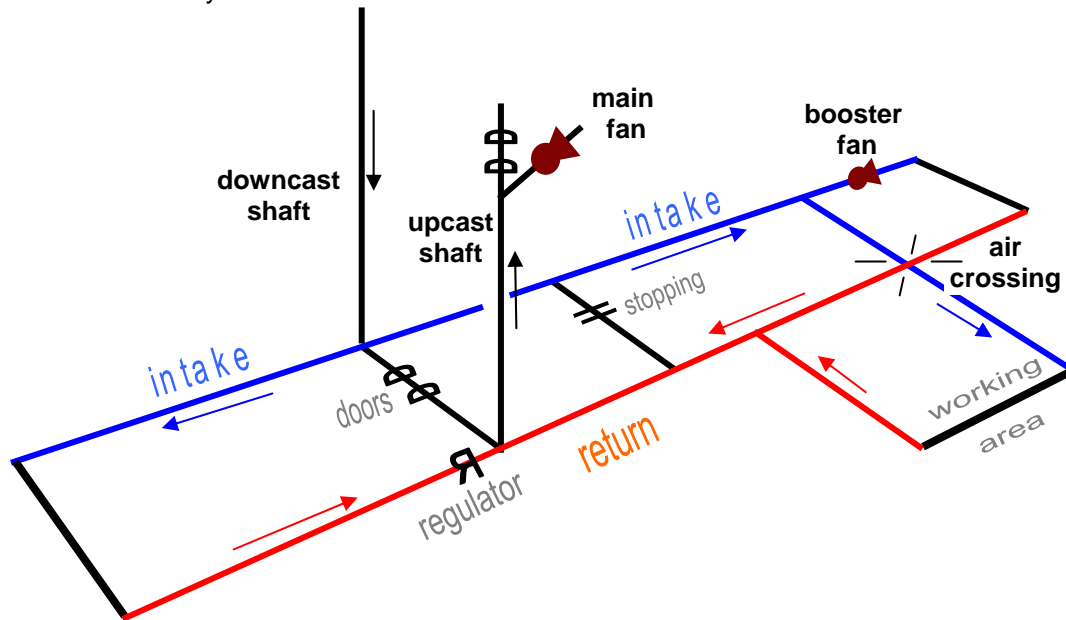


Figure 4.1. Typical elements of a main ventilation system

Fresh air enters the system through one or more **downcast shafts, drifts (slopes, adits)**, or other connections to surface. The air flows along **intake airways** to the working areas or places where the majority of pollutants are added to the air. These include dust and a combination of many other potential hazards including toxic or flammable gases, heat, humidity, and radiation. The contaminated air passes back through the system along **return airways**. In most cases, the concentration of contaminants is not allowed to exceed mandatory threshold limits imposed by law and safe for the entry of personnel into all parts of the ventilation system including return airways. The intake and return airways are often referred to simply as **intakes** and **returns** respectively. The return air eventually passes back to the surface via one or more **upcast** shafts, or through inclined or level drifts.

Fans

The primary means of producing and controlling the airflow are also illustrated on Figure 4.1. **Main fans**, either singly or in combination, handle all of the air that passes through the entire system. These are usually, but not necessarily, located on surface, either **exhausting** air through the system as shown on Figure 4.1 or, alternatively, connected to downcast shafts or main intakes and **forcing** air into and through the system. Because of the additional hazards of gases and dust that may both be explosive, legislation governing the ventilation of coal mines is stricter than for most other underground facilities. In many countries, the main ventilation fans for coal mines are required, by law, to be placed on surface and may also be subject to other restrictions such as being located out of line with the connected shaft or drift and equipped with **"blow-out" panels** to help protect the fan in case of a mine explosion.

Stoppings and Seals

In developing a mine, connections are necessarily made between intakes and returns. When these are no longer required for access or ventilation, they should be blocked by **stoppings** in order to prevent short-circuiting of the airflow. Stoppings can be constructed from masonry, concrete blocks or fireproofed timber blocks. Prefabricated steel stoppings may also be employed. Stoppings should be well keyed into the roof, floor and sides, particularly if the strata are weak or in coal mines liable to spontaneous combustion. Leakage can be reduced by coating the high pressure face of the stopping with a sealant material and particular attention paid to the perimeter. Here again, in weak or chemically active strata, such coatings may be extended to the rock surfaces for a few metres back from the stopping. In cases where the airways are liable to convergence, precautions should be taken to protect stoppings against premature failure or cracking. These measures can vary from "crush pads" located at the top of the stopping to sliding or deformable panels on prefabricated stoppings. In all cases, components of stoppings should be fireproof and should not produce toxic fumes when heated.

As a short term measure, fire-resistant brattice curtains may be tacked to roof, sides and floor to provide temporary stoppings where pressure differentials are low such as in locations close to the working areas.

Where abandoned areas of a mine are to be isolated from the current ventilation infrastructure, **seals** should be constructed at the entrances of the connecting airways. If required to be explosion-proof, these consist of two or more stoppings, 5 to 10 metres apart, with the intervening space occupied by sand, stone dust, compacted non-flammable rock waste, cement-based fill or other manufactured material. Steel girders, laced between roof and floor add structural strength. Grouting the surrounding strata adds to the integrity of the seal in weak ground. In coal mines, mining law or prudent regard for safety may require seals to be explosion-proof.

Doors and airlocks

Where access must remain available between an intake and a return airway, a stopping may be fitted with a ventilation door. In its simplest form, this is merely a wooden or steel door hinged such that it opens towards the higher air pressure. This self-closing feature is supplemented by angling the hinges so that the door lifts slightly when opened and closes under its own weight. It is also

advisable to fit doors with latches to prevent their opening in cases of emergency when the direction of pressure differentials may be reversed. Contoured flexible strips attached along the bottom of the door assist in reducing leakage, particularly when the airway is fitted with rail track.

Ventilation doors located between main intakes and returns are usually built as a set of two or more to form an airlock. This prevents short-circuiting when one door is opened for passage of vehicles or personnel. The distance between doors should be capable of accommodating the longest train of vehicles required to pass through the airlock. For higher pressure differentials, multiple doors also allow the pressure break to be shared between doors.

Mechanized doors, opened by pneumatic or electrical means are particularly convenient for the passage of vehicular traffic or where the size of the door or air pressure would make manual operation difficult. Mechanically operated doors may, again, be side-hinged or take the form of roll-up or concertina devices. They may be activated manually by a pull-rope or automatic sensing of an approaching vehicle or person. Large doors may be fitted with smaller hinged openings for access by personnel. Man-doors exposed to the higher pressure differentials may be difficult to open manually. In such cases, a sliding panel may be fitted in order to reduce that pressure differential temporarily while the door is opened. Interlock devices can also be employed on an airlock to prevent all doors from being opened simultaneously.

Regulators

A passive regulator is simply a door fitted with one or more adjustable orifices. Its purpose is to reduce the airflow to a desired value in a given airway or section of the mine. The most elementary passive regulator is a rectangular orifice cut in the door and partially closed by a sliding panel. The airflow may be modified by adjusting the position of the sliding panel manually. Louvre regulators can also be employed. Another form of regulator is a rigid duct passing through an airlock. This may be fitted with a damper, louvres or butterfly valve to provide a passive regulator or a fan may be located within the duct to produce an active regulator. Passive regulators may be actuated by motors, either to facilitate their manual adjustment or to react automatically to monitored changes in the quantity or quality of any given airflow.

When the airflow in a section of the mine must be increased to a magnitude beyond that obtainable from the system then this may be achieved by **active regulation**. This implies the use of a **booster fan** to enhance the airflow through that part of the mine. Section 9.6 deals with the subject of booster fans in more detail. Where booster fans are employed, they should be designed into the system such that they help control leakage without causing undesired recirculation in either normal or emergency situations. In some countries, coal mine legislation prohibits the use of booster fans.

Air crossings

Where intake and return airways are required to cross over each other then leakage between the two must be controlled by the use of an air crossing. The sturdiest form is a natural air crossing in which the horizon of one of the airways is elevated above the other to leave a sill of strata between the two, perhaps reinforced by roof bolts, girders or timber boards. A more usual method is to intersect the two airways during construction, then to heighten the roof of one of them and/or excavate additional material from the floor of the other. The two airstreams can then be separated by horizontal girders and concrete blocks, or a steel structure with metal or timber shuttering. Sealants may be applied on the high pressure side. Control of the airway gradients approaching the air crossing reduces the shock losses caused by any sudden change of airflow direction. Man-doors can be fitted into the air-crossing for access.

Completely fabricated air crossings may be purchased or manufactured locally. These can take the form of a stiffened metal tunnel. Such devices may offer high resistance to airflow and should be sized for the flow they are required to pass. They are often employed for conveyor crossings. Another type of air crossing used mainly for lower airflows and which requires no additional excavation is to course one of the airstreams through one or more ducts that intersect a stopping on

either side of the junction. An advantage of this technique is that the ducted airflow may be further restricted by passive regulators or up-rated by fans in the ducts.

In all cases, the materials used in the construction of air crossings should be fireproof and capable of maintaining their integrity in case of fire. Neither aluminium nor any other low melting-point or combustible material should be employed in an air crossing.

4.2.2 Location of main fans

In the majority of the world's mines, main fans are sited on surface. In the case of coal mines, this may be a mandatory requirement. A surface location facilitates installation, testing, access and maintenance while allowing better protection of the fan during an emergency situation. Siting main fans underground may be considered where fan noise is to be avoided on surface or when shafts must be made available for hoisting and free of airlocks. A problem associated with underground main fans arises from the additional doors, airlocks and leakage paths that then exist in the subsurface.

In designing the main ventilation infrastructure of a mine, a primary decision is whether to connect the main fans to the upcast shafts, i.e. an **exhausting system** or, alternatively, to connect the main fans to the downcast shaft in order to provide a **forcing or blowing system**. These choices are illustrated in Figure 4.2 (a and b).

From the time of the **shaft bottom furnaces** of the nineteenth century, the upcast shaft has, traditionally, been regarded as associated with the means of producing ventilation. Most mines are ventilated using the exhaust system. An examination of the alternatives continues to favour a primary exhaust system in the majority of cases. The choice may be based on the following four concerns.

Gas control

Figure 4.2 shows that air pressure in the subsurface is depressed by the operation of an exhausting main fan but is increased by a forcing fan. The difference is seldom more than a few kilopascals. As strata gases are, typically, held within the rock matrix at gauge pressures of 1000 kPa or more, it is evident that the choice of an exhausting or forcing system producing a few kilopascals will have little effect on the rate of gas production from the strata.

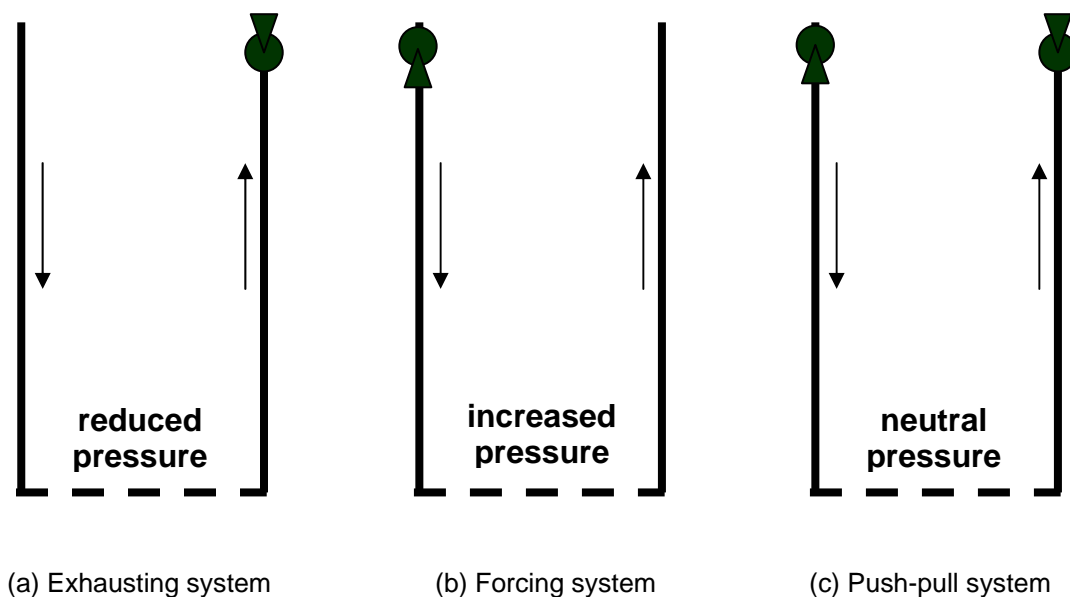


Figure 4.2 Possible locations of main fans

Unfortunately, much of the gas is not emitted directly into the ventilating airstream but collects in worked out areas, relaxed strata or in voidage that is connected to, but not part of the main ventilation system. Such accumulations of gas are at near equilibrium pressure with the adjacent airways. Hence, any reduction in barometric pressure within the ventilation system will result in an isothermal expansion of the accumulated gases and produce a **transient emission** of those gases into the ventilation system. This occurs naturally during periods of falling barometric pressure on the surface. In some countries, a mandatory record of surface barometric readings is updated at the beginning of each shift at coal mines. During a period of **falling barometric pressure**, unusually heavy emissions of methane or deoxygenated air may be expected. At such times, it is not wise to sit down for lunch against a seal or stopping beyond which are old workings.

Steady state operation of either exhausting or forcing fans will produce no changes of air pressure in the subsurface. However, consider the situation of the stoppage of a forcing fan. The barometric pressure throughout the ventilation system will fall rapidly. Accumulations of voidage gas will expand and flood into the workings at the worst possible time i.e. when the airflow is considerably diminished, causing a peak concentration of gas. Conversely, when a main exhausting fan stops, air pressure in the system increases, compressing accumulations of gas. Hence, no peak of general body gas concentration occurs within the airstream. It is true that when the main exhaust fan restarts, the sudden reduction in barometric pressure will then cause expansion and emission of accumulated gas. However, this occurs at a time of full ventilation and the peak of gas concentration will be much less than that caused by stoppage of a forcing fan. A consideration of strata gas control favours a primary exhausting system.

Transportation

The choice between main forcing and exhausting systems should take into account the preferred **routes for the transportation of mineral, personnel and materials**. Ideally, conveyors, locomotives or other modes of moving broken rock should not be required to pass through airlocks. Hence, a mine design that has mineral or rock transportation routes in main intakes and rock hoisting in a downcast shaft will favour an exhausting system. Alternatively, if there are good reasons to transport mineral in the returns and upcast shaft then a forcing system may be preferred. This could be necessary, for example, in evaporite mines producing potash or halite where the hygroscopic nature of the mineral could give ore handling problems if transported within the variable humidity of intake airways.

In American coal mines, **conveyors** are normally required to be located in **"neutral" airways**, ventilated by air that will neither pass on to working faces nor is returning from work areas. This system has the advantage that smoke and gases produced by any conveyor fire will not pollute the working faces. The major disadvantages are the additional potential for leakage and difficulties in controlling the air quantity along the conveyor routes.

Fan maintenance

An exhausting fan will pass air that carries dust, water vapour, perhaps liquid water droplets, and is usually at a higher temperature than that of the air entering the mine. The combined effects of impact and corrosion on impeller blades are much greater on main exhaust fans. Forcing fans handle relatively clean air and require less maintenance for any given duty. On the other hand, corrosive air passing up through the headgear of an upcast shaft can cause much damage. This can be prevented by drawing the air out the shaft into a near surface fan drift by means of a low pressure - high volume fan.

Fan performance

A forcing fan normally handles air that is cooler and denser than that passing through an exhausting fan. For any given mass flow, the forcing fan will pass a lower volume flow at a reduced pressure. The corresponding power requirement is, therefore, also lower for a forcing fan. However, the effect is not great and unlikely to be of major significance.

A counteracting influence is that forcing fans must be fitted with **inlet grilles** to prevent the ingress of birds or other solid objects. These grilles necessarily absorb available energy and result in an additional frictional pressure drop. Furthermore, the expanding evasee fitted to a main exhaust fan recovers some of the kinetic energy that would otherwise be lost to the surface atmosphere.

When air is compressed through a fan its temperature is increased. If the air contains no liquid droplets and there is insignificant heat transfer through the fan casing then the **temperature rise** is given as

$$\Delta T = \frac{0.286}{\eta} \frac{T_1}{P_1} \Delta P \quad ^\circ\text{C} \quad (4.1)$$

(see derivation in Section 10.6.1.2)

where η = fan isentropic efficiency (fractional)
 T_1 = Absolute temperature at inlet (K)
 P_1 = Barometric pressure at inlet (Pa) and
 ΔP = Increase in absolute pressure across the fan (Pa)

The rise in temperature through a forcing fan will be reflected by an increase in average temperature in the intake airways. However, heat exchange with the strata is likely to dampen the effect before the air reaches the work areas (Section 15.2.2.).

Figure 4.2(c) shows a combination of main forcing and exhausting fans, known descriptively as a **push-pull system**. A primary application of a main push-pull system is in metal mines practicing caving techniques and where the zone of fragmented rock has penetrated through to the surface. Maintaining a neutral pressure underground with respect to surface minimizes the degree of air leakage between the workings and the surface. This is particularly important if the rubbelized rock is subject to spontaneous combustion. In cold climates, drawing air through fragmented strata intentionally can help to smooth out extremes of temperature of the intake air entering the workings (Section 18.4.6.).

In the more general case of multi-shaft mines, the use of multiple main fans (whether exhausting, forcing or push-pull) offers the potential for an improved distribution of airflow, better control of both air pressures and leakage, greater flexibility and reduced operating costs. On the other hand, these advantages may not always be realized as a multi-fan system requires particularly skilled adjustment, balancing and planning.

4.2.3. Infrastructure of main ventilation routes.

Although the simplified sketch of Figure 4.1 depicts the main or **trunk** intakes and returns as single airways, this is seldom the case in practice other than for small mines. In designing or examining the underground layout that comprises a subsurface ventilation system, the following matters should be addressed:

Mine resistance

For any given total airflow requirement, the operational cost of ventilation is proportional to the resistance offered to the passage of air (Section 9.5.5.2.). This resistance, in turn, depends upon the size and number of the openings and the manner in which they are interconnected. Problems of ground stability, air velocity and economics limit the sizes of airways. Hence, multiple main intakes and returns are widely employed.

The mine resistance is greatly reduced and environmental conditions improved by providing a separate **split** of air to each working panel. The advantages of parallel circuits over series ventilation were realized early in the nineteenth century (Section 1.2).

Leakage control

The **volumetric efficiency** of a mine is defined as

$$VE = \frac{\text{Airflow usefully employed}}{\text{Total airflow through main fans}} \times 100 \text{ per cent} \quad (4.2)$$

where the 'Airflow usefully employed' is the sum of the airflows reaching the working faces and those used to ventilate equipment such as workshops, electrical gear, pumps or battery charging stations. The volumetric efficiency of mines may vary from 75 down to less than 10 per cent. The latter value indicates the large and, often, expensive amount of air leakage that can occur in a mine. It is, therefore, important to design a subsurface ventilation system to minimize leakage potential and to maintain the system in order to control that leakage. Whenever possible, intake and return airways, or groups of airways, should be separated geographically or by **barrier pillars** with a minimum of interconnections.

A prerequisite is that all doors, stoppings, seals and air crossings should be constructed and maintained to a good standard. A stopping between a main intake and return that has been carelessly holed in order to insert a pipe or cable, or one that has been subject to roadway convergence without the necessary repairs may be a source of excessive leakage. Unfortunately, if a large number of stoppings exist between an intake and adjacent return then the leakage may become untenable even when each individual stopping is of good quality. This can occur in workings that have been developed by room and pillar methods. The reason for this is the dramatic decrease in effective resistance to airflow when the flow paths are connected in parallel. For n stoppings constructed between two adjacent airways, their combined (**effective**) **resistance** becomes

$$R_{eff} = \frac{R}{n^2} \quad (\text{see section 7.3.1.1})$$

where R is the resistance of a single stopping.

Figure 4.3 shows the dramatic reduction in effective resistance that occurs as the number of stoppings increases. In such cases, it becomes important not only to maintain good quality stoppings but also to design the system such that pressure differentials between the airways are minimized.

Air pressure management is a powerful tool in controlling leakage and, hence, the effectiveness, volumetric efficiency and costs of a ventilation system. It is particularly important for mines that are liable to spontaneous combustion. Ideally, resistance to airflow should be distributed equitably between intakes and returns. In practice, one often observes return airways of smaller cross section than intakes and that have been allowed to deteriorate because they are less frequently used for travelling or transportation. This will increase the pressure differentials between intakes and returns. Similarly, local obstructions caused by falls of roof, stacked materials, equipment or parked vehicles will affect the pressure distribution and may exacerbate leakage. The positions and settings of booster fans or regulators also have a marked influence on leakage patterns and should be investigated thoroughly by network analysis (Chapter 7) during design procedures.

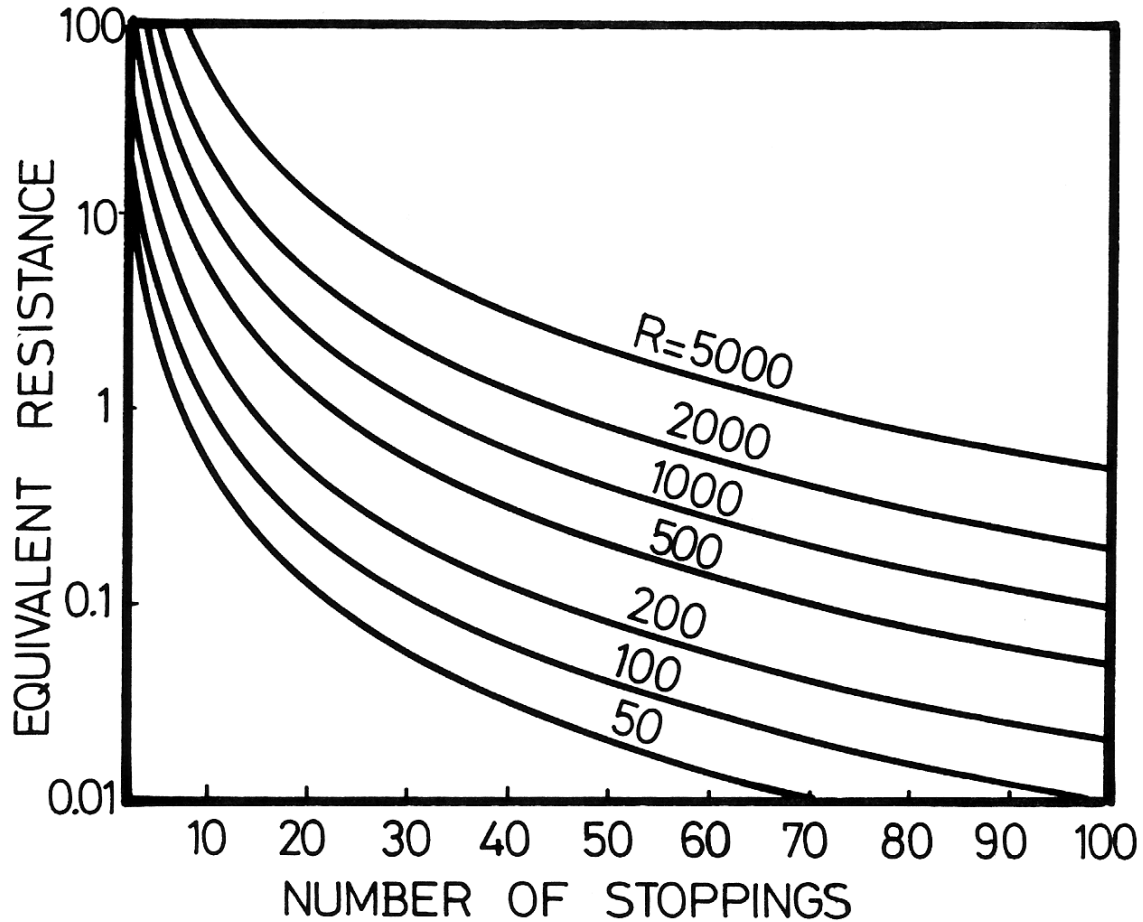


Figure 4.3. Equivalent resistance of sets of stoppings between a pair of adjacent entries.
 R = Resistance of one single stopping

Direction of airflow

There are two considerations regarding the direction of the airstream - first with respect to the transportation of the mined material. An **antitropical system** is one in which the airflow and transported rock move in opposite directions. Other than the "neutral" airways of American conveyor roads, this implies mineral transportation in intake airways. Conversely, a **homotropical system** is one in which the airflow and the fragmented rock move in the same direction. This implies mineral transportation in the return airways and is often associated with a main forcing system. The homotropical system ensures that any pollution generated from the fragmented rock along the transportation route passes directly out of the mine without affecting working faces. Such pollution may include dust, heat, humidity and gases issuing from the broken rock or equipment. The higher relative velocity between conveyed material and the airflow in an antitropical system can result in a greater entrainment of dust particles within the airstream. Furthermore, a homotropical system is preferable in the event of a fire occurring along the mineral transportation route. On the other hand, siting electrical or other equipment capable of igniting a methane-air mixture in a return airway may be inadvisable or, indeed, illegal for gassy mines.

The second concern in the matter of airflow direction is the inclination of the airway. An **ascentional** ventilation system implies that the airflow moves upwards through inclined workings. This takes

advantage of the natural ventilating effects caused by the addition of heat to the air (Section 8.3.1). In open stoping or mining layouts that involve multiple connections in inclined workings, ascensional ventilation may be the only technique capable of either controlling or utilising natural ventilating effects. **Descensional** ventilation may be employed on more compact mining systems such as longwall faces and normally then becomes also a homotropical system with both air and conveyed mineral moving downhill. However, this may cause difficulties in controlling the natural buoyancy effects of methane in waste areas. The advantage claimed for descensional ventilation is that because the air enters the workings at a higher elevation it is then cooler and drier than if it were first coursed to the lower end of the workings.

Escapeways

Except for blind headings, there should always be at least two means of egress from each working place in an underground mine or facility. Preferably, there should be two separate intake routes designated as escapeways in case of a fire or other emergency. Within this context the term "separate" is taken to imply that those airways have different and identifiable sources of intake air such that a source of pollution in one of them will not affect the other - either through leakage or series ventilation. Nevertheless, at least one return air route must always remain open and travelable without undue discomfort, to allow for an emergency situation where the working face itself becomes impossible to traverse.

Escapeways should be marked clearly on maps and by signs underground. Personnel should be made familiar with those routes through regular travel or organized escape drills. Mining legislation may dictate minimum sizes for escapeways and the frequency of their inspection.

*Airflow travel distance and use of **old workings***

The routes utilized for main intake and return airflows should be reviewed from the viewpoint of travel distance and corresponding time taken for a complete traverse by the air. For high strata temperatures, it is advantageous for intake air to reach the workings as quickly as possible in order to minimize the gain of heat and humidity. However, this is tempered by air velocity constraints and ventilation operating costs.

In mines located in **cold climates**, it may be preferable to encourage natural heating of the intake air by allowing it to take a circuitous and slow route in order to maximize its exposure to rock surfaces. Another situation occurs when variations in air humidity or temperature cause problems of slaking (sloughing) of strata from the roof or sides of the airways or workings. Here again, a case may be made for the natural air conditioning gained by passing the intake air through a network of older airways prior to reaching the current work areas (Section 18.4.6.).

The employment of old workings as an integral part of a ventilation system can result in significant reductions in mine resistance and, hence, the operating costs of ventilation. Furthermore, return air passing through abandoned areas will help to prevent buildup of toxic, asphyxiating or flammable gases. However, using old workings in this way must be treated with caution. It is inadvisable to rely upon such routes as they may be subject to sudden closure from falls of roof. Secondly, travelable intake and return airways must always be maintained for reasons of safety and, third, old workings liable to spontaneous combustion must be sealed off and the pressure differentials across them reduced to a minimum.

From a practical viewpoint where old workings can be employed safely for airflow then it is sensible to use them. However, during system design exercises they should not be relied upon to provide continuous airflow routes but, rather, as a bonus in reducing the costs of ventilation. In any event, as a mine develops, it becomes advisable to seal off old areas that are remote from current workings. Unless this is done, then overall management and control of the airflow distribution will become increasingly difficult.

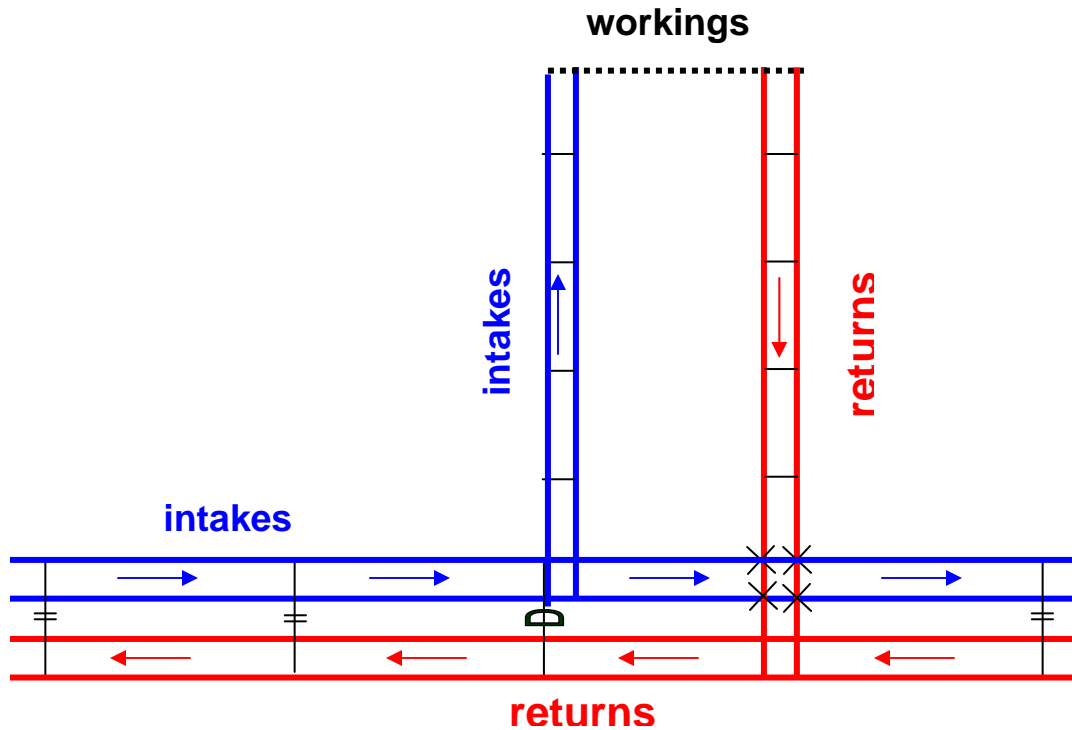


Figure 4.4 U-tube ventilation

4.3. DISTRICT SYSTEMS

4.3.1. Basics of district system design

Underground ventilation layouts serving one or more districts of a mine may be divided into two broad classifications, **U-tube** and **through-flow ventilation**. Each of these takes on a diversity of physical configurations depending upon the type of mine and disposition of the local geology.

As illustrated on Figure 4.4 the basic feature of U-tube ventilation is that air flows towards and through the workings, then returns along airways separated from the intakes by stoppings and doors. Room and pillar layouts and advancing longwalls tend to be of this type.

Figure 4.5 illustrates the alternative through-flow ventilation system. In this layout, primary intakes and returns are separated geographically. Adjacent airways are either all (or mainly) intakes or returns and, hence, reducing the number of leakage paths. There are far fewer stoppings and air crossings but additional regulation (regulators or booster fans) is required to control the flow of air through the work area. Practical examples of through-flow ventilation are the parallel flows from downcast to upcast shafts across the multilevels of a metal mine, or the back-bleeder system of a retreating longwall.

The simplest possible application of the U-tube system is for a set of twin development headings. Indeed, the U-tube method is the only one capable of ventilating pilot workings that are advancing into an unmined area. Through-ventilation requires the prior establishment of one or more connections between main intake and return airways. Once that has been accomplished then through-ventilation has several significant advantages. First, leakage of air from intake to return is greatly reduced. Hence, lower total airflows are required to provide any required ventilation at the

working face. Secondly, the parallel airways and, often, shorter total travel distance of the airstream give a lower district resistance - particularly for workings distant from the main shafts. This permits reduced ventilating pressures. The combination of lower total airflows and lower ventilating pressures leads to large reductions in ventilation operational costs. Furthermore, the fan duties will remain much more stable in a through-flow system than the escalating demands of an advancing U-tube layout.

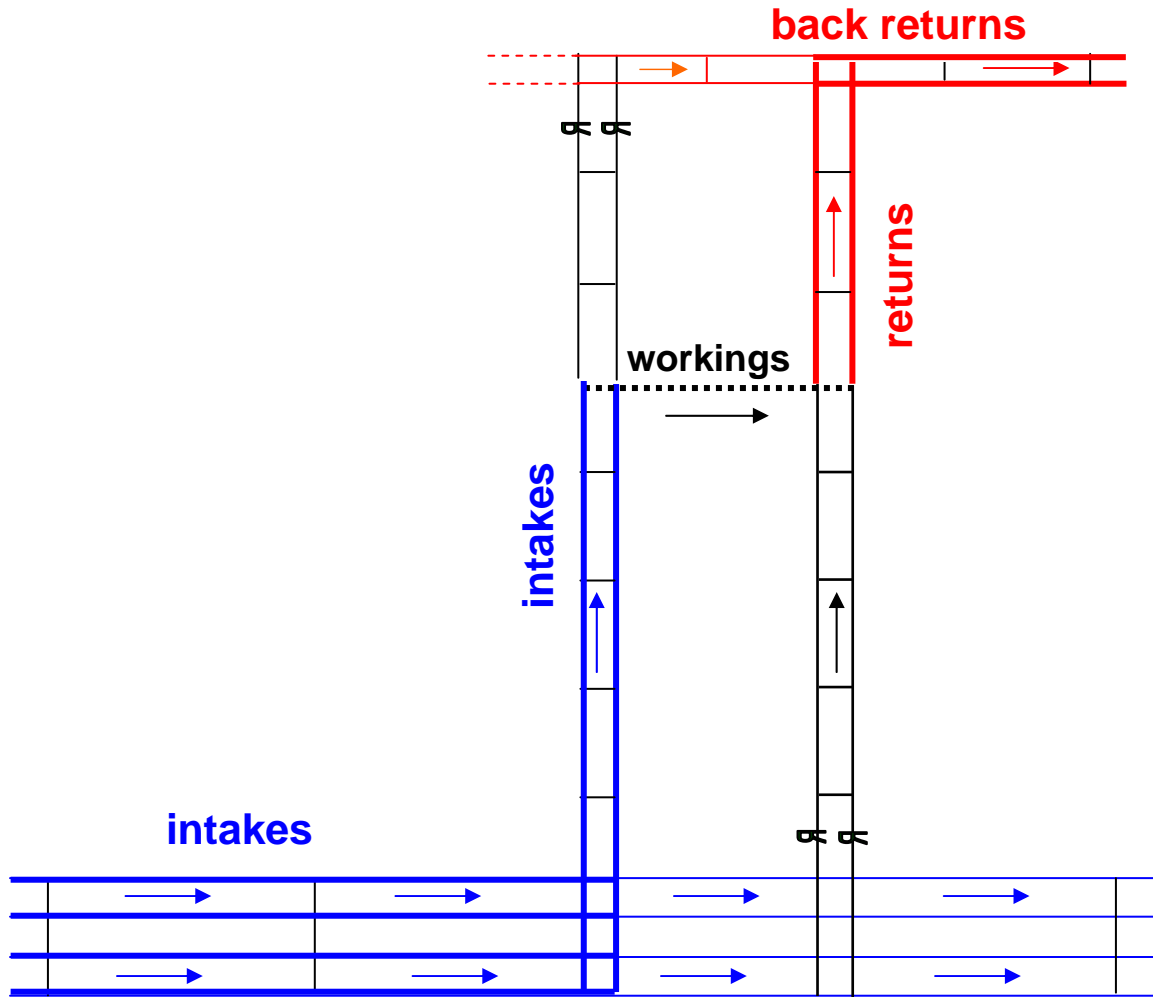


Figure 4.5 Through-flow ventilation system

4.3.2. Stratified deposits

The vast majority of underground mines extracting coal, evaporites or other tabular forms of mineral deposits normally do so by one of two techniques, **longwall or room and pillar** (bord and pillar) mining. While the actual layouts can vary quite significantly from country to country and according to geological conditions, this Section highlights the corresponding modes of airflow distribution that may be employed.

Longwall systems

The two major features of longwall mining that have influenced the design of their ventilation systems are, first, the control of methane or other gases that accumulate in the waste (gob) areas and and, second, the high rate of rock breakage on heavily mechanized longwalls that exacerbates the production of dust, gas, heat and humidity.

Figure 4.6 illustrates some of the ventilation layouts used on longwall districts. Single entry systems are employed primarily in European coal mines. Figures 4.6 (a and b) show the application of the U-tube principle to advancing and retreating longwalls respectively. With the advancing system, leakage of some of the intake air occurs through the waste area, controlled by the resistance offered by the roadside packing material and the distribution of resistance and, hence, air pressure around the district. This can give rise to problems of **gob fires** in mines liable to **spontaneous combustion**.

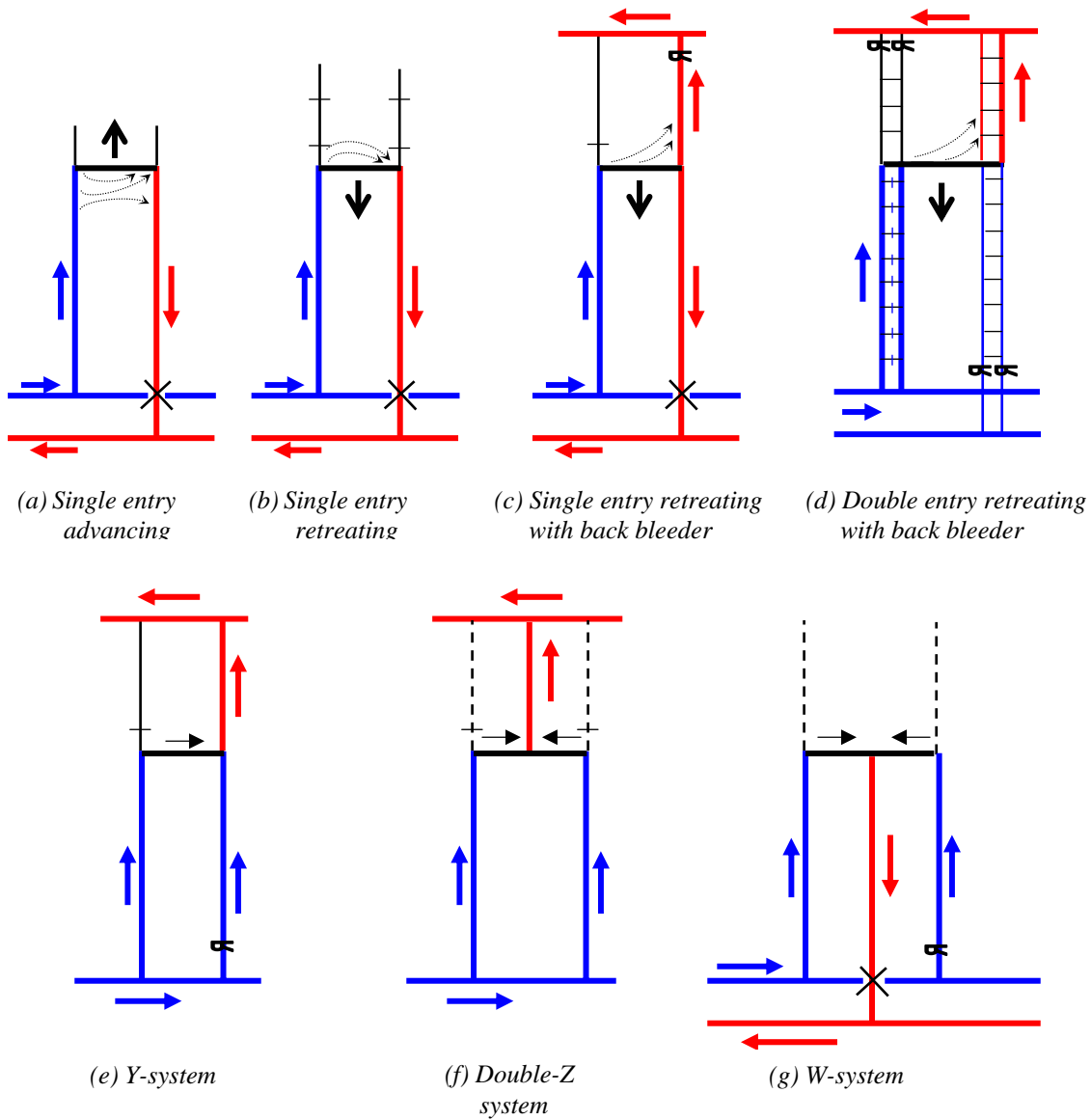


Figure 4.6 Classifications of longwall district ventilation systems.

Gases from the waste may also flush onto the face leading to unacceptable concentrations toward the return end. The same difficulty may arise to a lesser extent when the U-tube principle is applied to a retreating face, the abandoned airways being stopped off as the face retreats.

Figure 4.6(c) shows a single entry longwall with the back (or bleeder) return held open in order to constrain the gas fringe safely back in the waste area and, hence, prevent flushes of waste gas onto the face. The system illustrated in (c) is a combination of U-tube and through-flow ventilation.

Figure 4.6(d) illustrates the longwall system more often used in coal mining countries that have a tradition of room and pillar mining such as the United States, Australia or South Africa. Two or more entries are driven initially using room and pillar mining, these serving as the lateral boundaries of retreat longwall panels. Again, back bleeders are used to control waste gas.

Figures 4.6(e), (f) and (g) illustrate a classification of systems for longwall faces where the make of gas from the face itself is particularly heavy. The Y system provides an additional feed of fresh air at the return end of the face. This helps to maintain gas concentrations at safe levels along the back return airway(s). Figure 4.5(d) is, in fact, a double entry through-flow Y system. The double-Z layout is also a through-flow system and effectively halves the length of face ventilated by each airstream. The W system accomplishes the same end but is based on the U-tube principle. Both the double-Z and W systems may be applied to advancing or retreating faces, depending upon the ability of the centre return to withstand front abutment and waste area strata stresses. Again, in both the double-Z and W systems, the directions of airflow may be reversed to give a single intake and two returns (or two sets of multiple returns). This may be preferred if heavy emissions of gas are experienced from solid rib sides.

Room (bord) and pillar systems

Figure 4.7 shows two methods of ventilating a room and pillar development panel; (a) a **bidirectional or W system** in which intake air passes through one or more central airways with return airways on both sides, and (b) a **unidirectional or U-tube system** with intakes and returns on opposite sides of the panel. In both cases the conveyor is shown to occupy the central roadway with a **brattice curtain** to regulate the airflow through it. It is still common practice in room and pillar mines to course air around the face ends by means of **line brattices** pinned to roof and floor but hung loosely in the cross-cuts to allow the passage of equipment. An advantage of the bidirectional system is that the air splits at the end of the panel with each airstream ventilating the operational rooms sequentially over one half of the panel only. Conversely, in the unidirectional or U-tube system the air flows in series around all of the faces in turn. A second advantage of the bidirectional system arises from the fact that **rib side gas emission** is likely to be heavier in the outer airways. This can become the dominant factor in gassy coal seams of relatively high permeability necessitating that the outer airways be returns. In most coal mining countries, legislation requires that gas concentration in intake airways be maintained at very low levels.

Unfortunately, the bidirectional system suffers from one significant disadvantage. The number of stoppings required to be built, and the number of leakage paths created between intakes and returns, are both doubled. In long development panels, the amount of leakage can become excessive allowing insufficient air to reach the last open cross-cuts (Section 4.2.3). In such circumstances, attempts to increase the pressure differential across the outbye ends of the panel exacerbate the leakage and give a disappointing effect at the faces.

The unidirectional system has a higher volumetric efficiency because of the reduced number of leakage paths. However, in both cases, the line brattices in the rooms offer a high resistance to airflow compared with an open cross-cut. This is particularly so in the case of the unidirectional system where the useful airflow is required to pass around all of these high resistance line brattices in series.

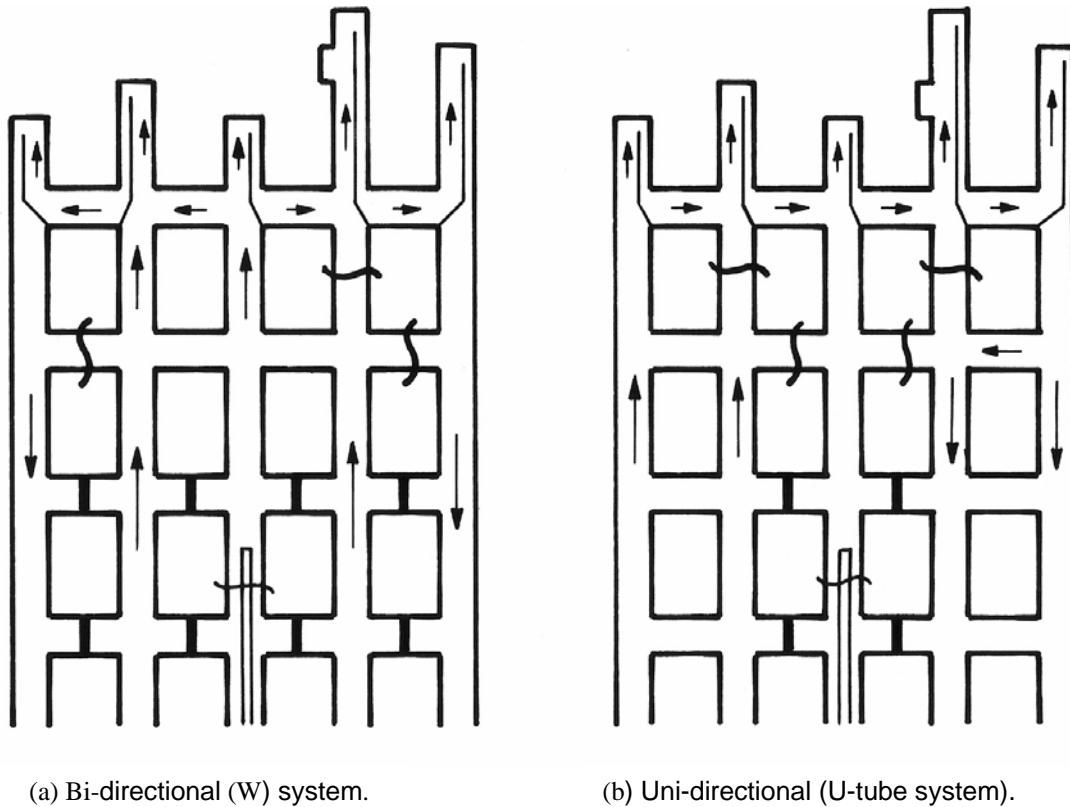


Figure 4.7 Room and pillar development with line brattices. These result in a high resistance for the face section.

The imposition of line brattice resistance at the most inbye areas of a mine ventilation system forces more air to be lost to return airways at all **leakage** points throughout the entire system. An analogy may be drawn with a leaky hosepipe. If the end of the pipe is unobstructed then water will flow out of it freely and dribble from the leakage points. If, however, the end of the pipe is partially covered then the flow from it will decrease but water will now spurt out of the leakage points.

The problem can be overcome by employing **auxiliary fans and ducts** either to force air into the rooms or exhaust air from them (Section 4.4). Figure 4.8 illustrates a room and pillar panel equipped with exhausting auxiliary ventilation. With such a system, the fans provide the energy to overcome frictional resistance in the ducts. The effective resistance of the whole face area becomes zero. Smaller pressure differentials are required between intakes and returns for any given face airflows and, hence, there is a greatly reduced loss of air through leakage. The electrical power taken by the auxiliary fans is more than offset by the savings in main fan duties.

A further advantage of employing auxiliary fans is that each room is supplied with its own separate and controllable supply of air. However, the fans must be sized or ducts regulated such that no undesired recirculation occurs.

The choice between auxiliary fan and duct systems and line brattices in room and pillar workings should also take into account the height and width of the airways, the size and required mobility of equipment, the placement of ducts or brattices, the extent of pollution from dust, gas and heat, fan noise, and visibility within the workings.

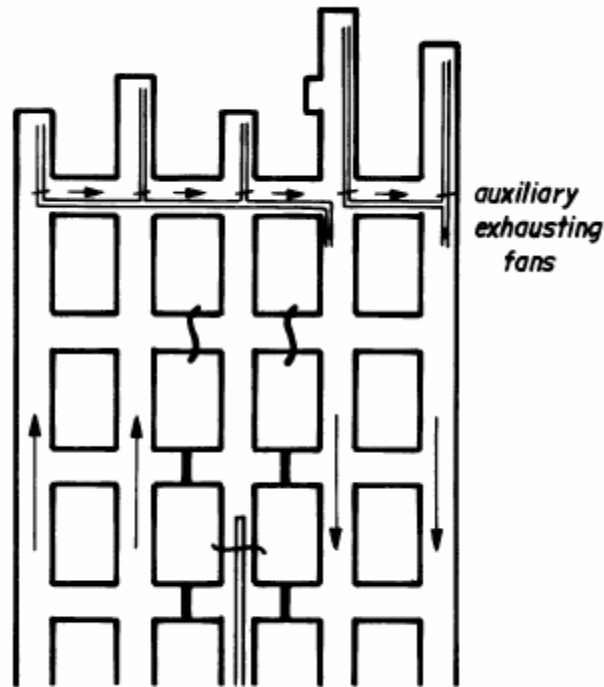


Figure 4.8 U-tube room and pillar development panel with auxiliary fans (zero face resistance)..

The systems shown on Figure 4.6 for longwalls each have their counterparts in room and pillar mining. An example of a retreating **double-Z** (through-flow) system applied to a room and pillar section is shown on Figure 4.9. There are, however, significant differences in the ventilation strategy between the two mining methods. The larger number of interconnected airways and higher leakage result in room and pillar layouts having lower resistance to airflow than longwall mines. It follows that room and pillar mines tend to require higher volume flows at lower fan pressures than longwall systems. Similarly, because of the increased number of airways and leakage paths it is particularly important to maintain control of airflow distribution paths as a room and pillar mine develops. It is vital that **barrier pillars** be left between adjacent panels and to separate the panels from trunk airway routes. Such barriers are important not only to protect the integrity of the mine in case of pillar failure but also to provide ventilation control points and to allow sealing of the panel in cases of emergency or when mining has been completed.

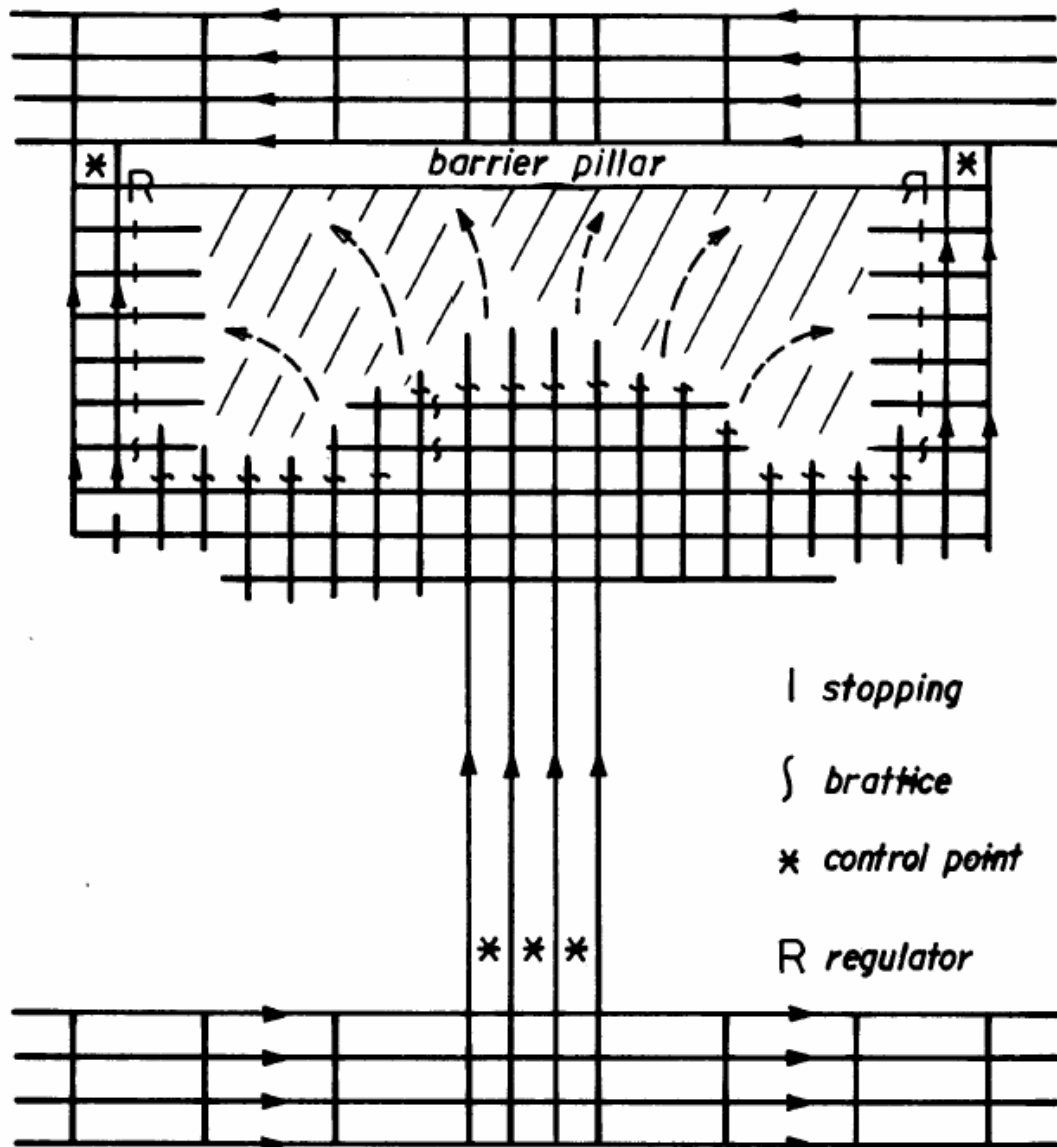


Figure 4.9 A retreating room and pillar district using a through-flow ventilation system

4.3.3. Orebody deposits

Metalliferous orebodies rarely occur in deposits of regular geometry. Zones of mineralization appear naturally in forms varying from tortuous veins to massive irregularly shaped deposits of finely disseminated metal and highly variable concentration. The mining layouts necessarily appear less ordered than those for stratified deposits. Furthermore, the combination of grade variation and fluctuating market prices results in mine development that often seems to be chaotic. The same factors may also necessitate many more stopes or working places than would be usual in a modern coal mine, with perhaps only a fraction of them operating in any one shift. Hence, the ventilation system must be sufficiently flexible to allow airflow to be directed wherever it is needed on a day-by-day basis.

Ventilation networks for metal mines, therefore, tend to be more complex than for stratified deposits and are usually also three dimensional. Figure 4.10 illustrates the ventilation strategy of many metal mines although, again, the actual geometry will vary widely. Air moves in a through-flow manner from a downcast shaft or ramp, across the levels, sublevels and stopes towards return raises, ramps or upcast shaft. Airflow across each of the levels is controlled by regulators or booster fans. Movement of air from level to level, whether through stopes or by leakage through ore passes or old workings tends to be ascensional in order to utilize natural ventilating effects and to avoid thermally induced and uncontrolled recirculation.

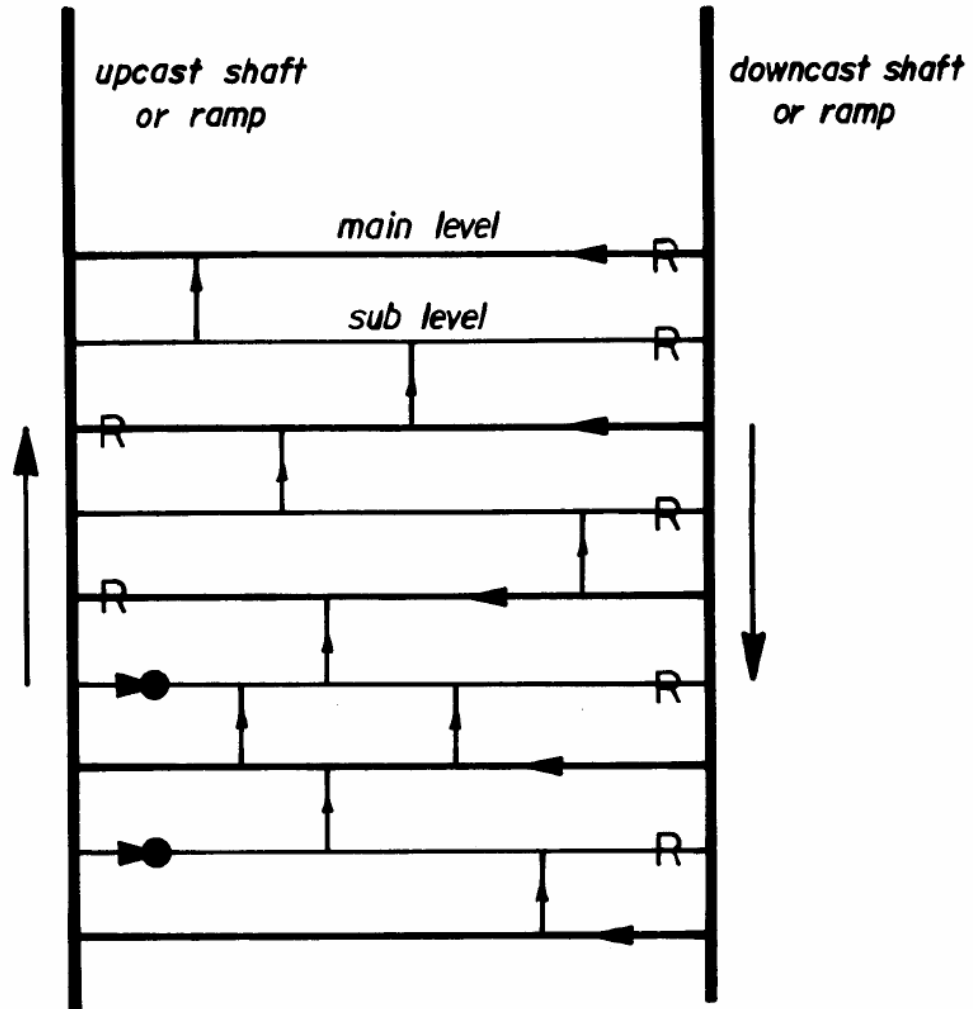


Figure 4.10 Section showing the principle of through-flow ventilation applied across the levels of a metal mine.

Airflow distribution systems for individual stopes are also subject to great variability depending upon the geometry and grade variations of the orebody. There are, however, certain guiding principles. These are illustrated in Figure 4.11 to 4.13 for three stoping methods. In the majority of cases, where controlled vertical movement of the air is required, stope airflow systems employ ascensional through-flow ventilation. Although auxiliary fans and ducts may be necessary at individual drawpoints, every effort should be made to utilize the mine ventilation system to maintain continuous

airflow through the main infrastructure of the stope. Series ventilation between stopes should be minimized in order that blasting fumes may be cleared quickly and efficiently.

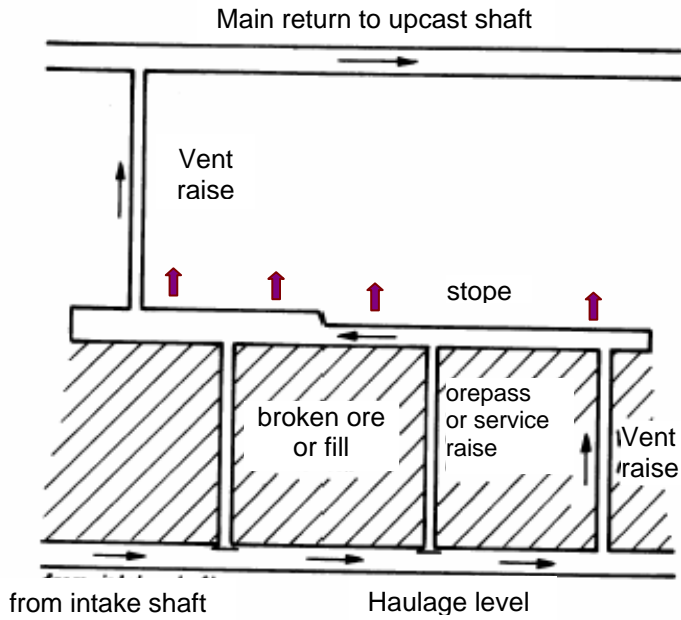


Figure 4.11 Simple ventilation system for shrinkage or cut-and-fill stopes.

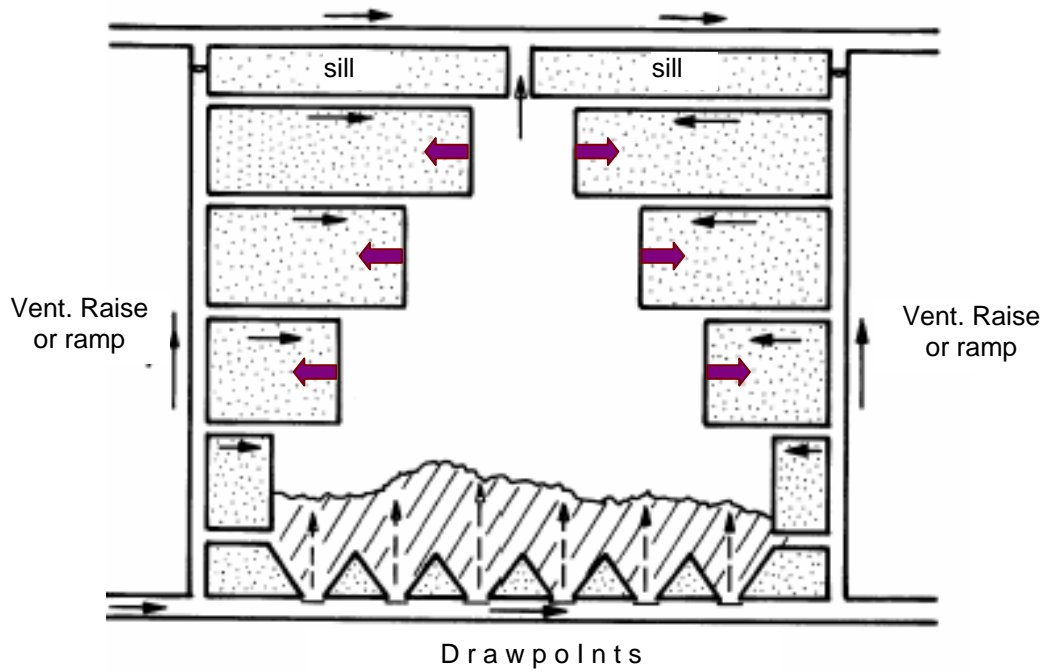


Figure 4.12 Ventilation system for sub-level open stopes

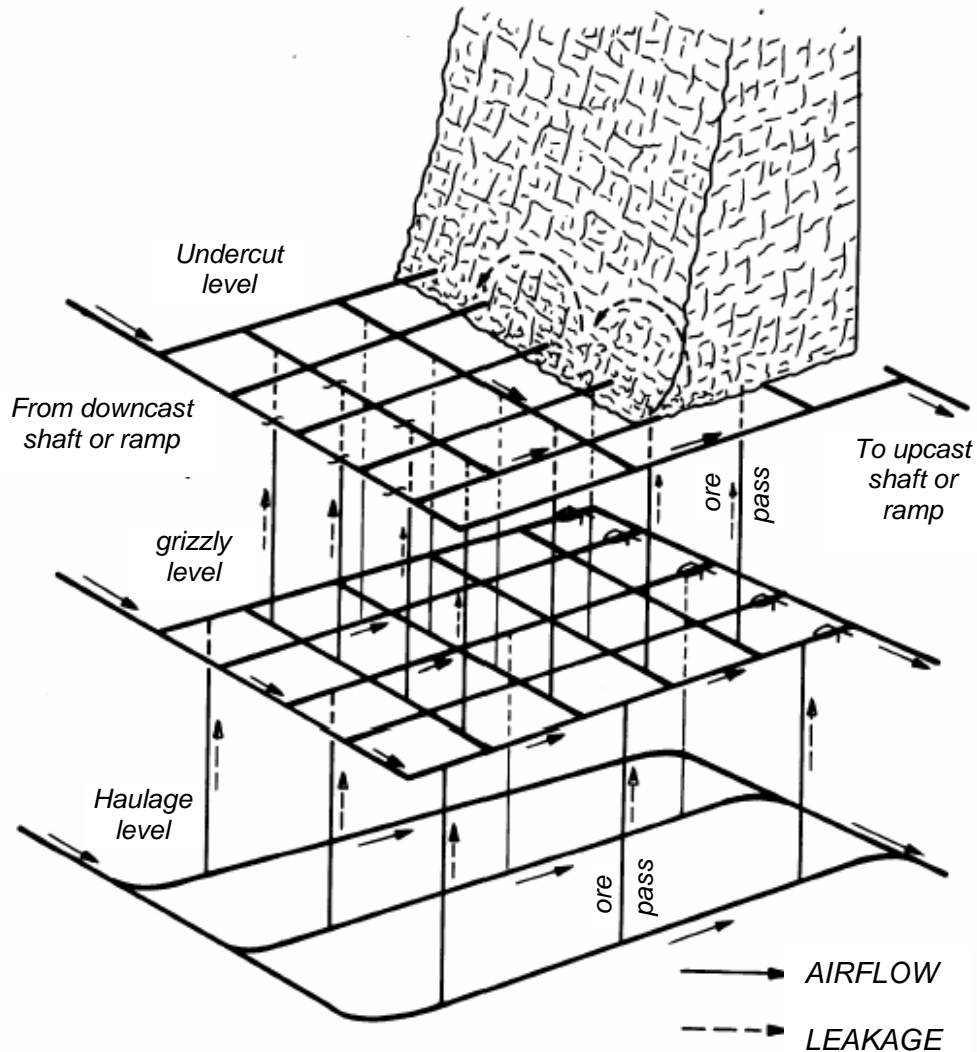


Figure 4.13 Typical ventilation system for a block caving operation.

Leakage through ore passes creates a problem in metal mines as the ore passes may often be emptied allowing a direct connection between levels. Airflows emerging from ore passes can also produce unacceptable dust concentrations. Closed ore chutes and instructions to maintain some rock within the passes at all times are both beneficial but are difficult to enforce in the necessarily production oriented activities of an operating mine. The design of the ventilating system and operation of regulators and booster fans should attempt to avoid significant pressure differences across ore passes. Maintaining an orepass at negative pressure by means of a filtered fan/duct arrangement can help to control dust at dumping or draw points. Attrition on the sides of ore passes often enlarges their cross-section and may produce fairly smooth surfaces. When no longer required for rock transportation, such openings may usefully be employed as low resistance ventilation raises.

Figure 4.13 for a block caving operation illustrates another guideline. Wherever practicable, each level or sublevel of a stope should be provided with its own through-flow of air between shafts, ventilation raises or ramps. While vertical leakage paths must be taken into account during planning exercises, maintaining an identifiable circuit on each level facilitates system design, ventilation management and control in case of emergency.

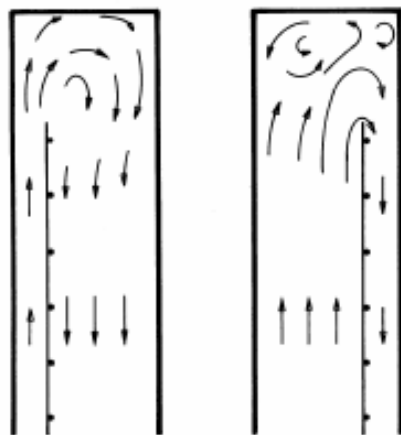
4.4. AUXILIARY SYSTEMS

Auxiliary ventilation refers to the systems that are used to supply air to the working faces of blind headings. Auxiliary ventilation may be classified into three basic types, line brattices, fan and duct systems, and "ductless" air movers. Ideally, auxiliary systems should have no impact on the distribution of airflows around the main ventilation infrastructure, allowing auxiliary ventilation to be planned independently from the full mine ventilation network. Unfortunately, this ideal is not always attained, particularly when line brattices are employed.

4.4.1. Line brattices and duct systems

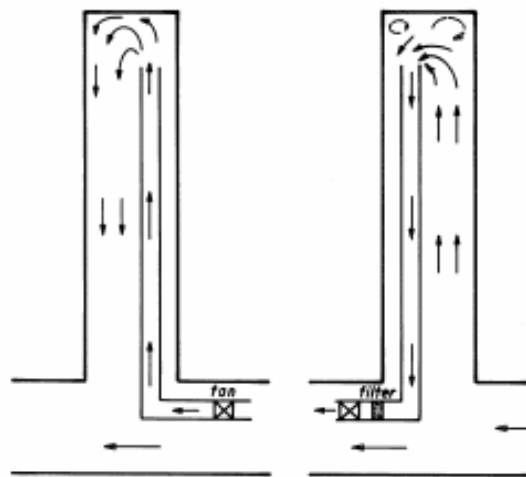
The use of line brattices was introduced in Section 4.3.2 (Figure 4.7) in relation to room and pillar workings where they are most commonly employed. It was shown that a major disadvantage of line brattices is the resistance they add to the mine ventilation network at the most sensitive (inbye) points, resulting in increased leakage throughout the system. This resistance depends primarily upon the distance of the line brattice from the nearest side of the airway, and the condition of the flow path behind the brattice. This is sometimes obstructed by debris from sloughed sides, indented brattices or, even, items of equipment put out of sight and out of mind, despite legislative prohibitions of such obstructions. In this section we shall examine the further advantages and disadvantages of line brattices.

Figure 4.14 shows line brattices used in the (a) forcing and (b) exhausting modes. The flame-resistant brattice cloth is pinned between roof and floor, and supported by a framework at a position some one quarter to one third of the airway width from the nearest side. This allows access by continuous miners and other equipment. Even with carefully erected line brattices, leakage is high with often less than a third of the air that is available at the last open cross-cut actually reaching the face. This limits the length of heading that can be ventilated by a line brattice. The need for line brattices to be extended across the last "open" cross-cut inhibits visibility creating a hazard where moving vehicles are involved. The advantages of line brattices are that the capital costs are low in the short term, they require no power and produce no noise.



Forcing Exhausting

Figure 4.14 Line brattices used for auxiliary ventilation.



Forcing Exhausting

Figure 4.15 Fan and duct systems of auxiliary ventilation.

Figure 4.15 shows the corresponding forcing and exhausting systems using auxiliary fans and ducting. In most cases, in-line axial fans are used although centrifugal fans are quieter and give higher pressures for the longer headings. The advantages of an auxiliary fan and duct are that they provide a more positive and controlled ventilating effect at the face, they cause no additional resistance to the mine ventilation system nor any consequential leakage throughout the network, and are much less liable to leakage in the heading itself. For headings longer than some 30 metres, auxiliary fans are the only practicable means of producing the required airflows. An exhausting duct also allows the air to be filtered, an advantage for dust control where series ventilation is practiced. The disadvantages involve the initial capital cost, the need for electrical power at the fans, the space required for ducts and the noise produced by the fans.

Care should be taken to ensure that the pressure-volume characteristics of the fan are commensurate with the resistance offered by the duct and the airflow to be passed. The latter is determined on the basis of the type and magnitude of pollutants to be removed (Chapter 9). The duct resistance is established as a combination of the wall losses within the duct, shock losses at any bend or change of cross section and at discharge. The equations employed are those derived for airway resistance in Section 5.4.

Example.

An airflow of $15 \text{ m}^3/\text{s}$ is to be passed through a 0.9m diameter fibreglass duct, 200m long, with one sharp right-angled bend. From manufacturer's literature, the friction factor for the duct is 0.0032 kg/m^3 . Calculate the total pressure to be developed by the fan and the fan power, assuming a fan efficiency of 60 per cent and an air density of 1.2 kg/m^3 .

Solution.

$$\text{Duct area } A = \pi \times 0.9^2 / 4 = 0.636 \text{ m}^2$$

$$\text{Perimeter } per = \pi \times 0.9 = 2.827 \text{ m}$$

Let us first determine the shock loss (X) factors for the system from Appendix A5 (Chapter 5).

Entry: (Section A5.4) In the absence of any inlet fitting, the shock loss factor is given as $X_{in} = 1.0$. This is caused by turbulence as the air enters the duct and should not be confused with the conversion of static pressure to velocity pressure at entry.

Bend: (Figure A5.1) For a sharp right-angled bend, $X_b = 1.2$

Exit: (Section A5.4) This is not really a shock loss but represents the kinetic energy of the air provided by the fan and lost to the receiving atmosphere. $X_{ex} = 1.0$

Total shock loss factor: $X_{sh} = 1.0 + 1.2 + 1.0 = 3.2$

Equivalent resistance of shock losses:

$$R_{sh} = \frac{X_{sh} \rho}{2 A^2} \quad \frac{\text{Ns}^2}{\text{m}^8} \quad (\text{See equation (5.18)})$$

$$= \frac{3.2 \times 1.2}{2 \times (0.636)^2} = 4.744 \quad \frac{\text{Ns}^2}{\text{m}^8}$$

Duct resistance:

$$R_d = \frac{k L per}{A^3} \quad \frac{\text{Ns}^2}{\text{m}^8} \quad (\text{see equation (5.4)})$$

$$= \frac{0.0032 \times 200 \times 2.827}{(0.636)^3} = 7.028 \quad \frac{\text{Ns}^2}{\text{m}^8}$$

Total resistance:

$$\begin{aligned} R_{tot} &= R_{sh} + R_d \\ &= 4.744 + 7.028 = 11.772 \quad \frac{\text{Ns}^2}{\text{m}^8} \end{aligned}$$

Required fan total pressure:

$$\begin{aligned} p_t &= R_{tot} Q^2 \quad (\text{see equation (5.5)}) \\ &= 11.772 \times 15^2 = 2649 \text{ Pa} \end{aligned}$$

The required fan power is $\frac{p_t \times Q}{\eta}$ where η = fan efficiency

$$\text{or} \quad \frac{2649 \times 15}{1000 \times 0.6} = 66.2 \quad \text{kW}$$

4.4.2. Forcing, exhausting, and overlap systems.

Figures 4.14 and 4.15 illustrate forcing and exhausting systems of auxiliary ventilation for line brattices and fan/duct systems respectively. The choice between forcing and exhausting arrangements depends mainly upon the pollutants of greatest concern, dust, gases or heat.

The higher velocity airstream emerging from the face-end of a forcing duct or, to a lesser extent, a forcing brattice gives a scouring effect as the air sweeps across the face. This assists in the turbulent mixing of any methane that may be emitted from fragmented rock or newly exposed surfaces. It also helps to prevent the formation of methane layers at roof level (Chapter 12). In hot mines, the forcing system provides cooler air at the face, even having taken the energy added by the fan into account. Furthermore, as the system is under positive gauge pressure, the cheaper type of **flexible ducting** may be used. This is also easier to transport and enables leaks to be detected more readily.

The major disadvantage of a forcing system is that pollutants added to the air at the face affect the full length of the heading as the air passes back, relatively slowly, along it.

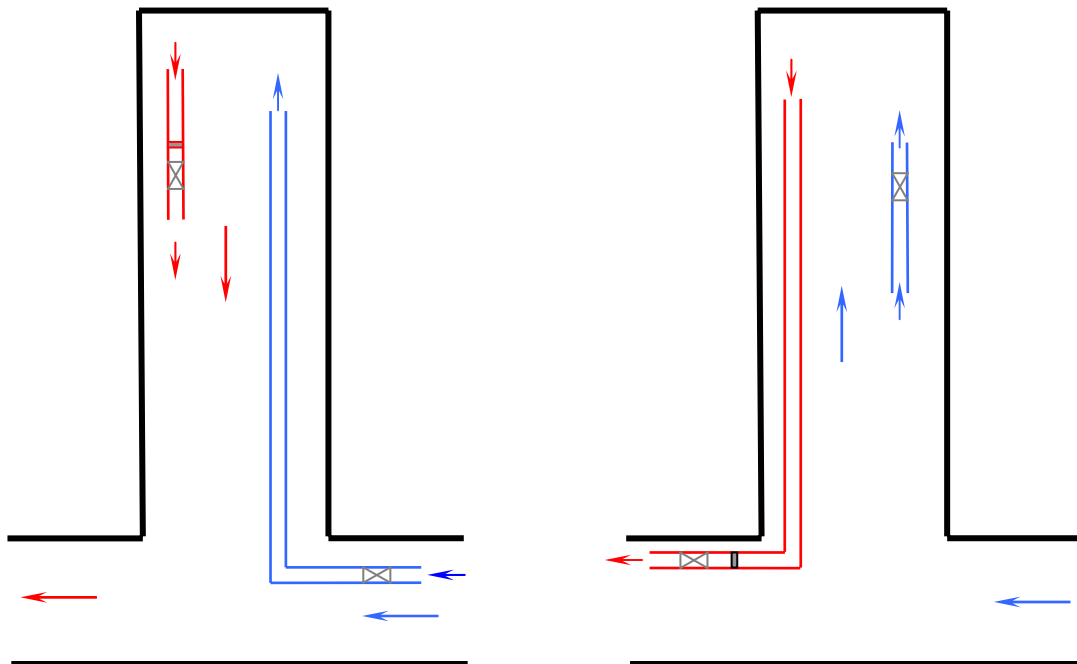
Where dust is the main hazard, an exhausting system is preferred. The polluted air is drawn directly into the duct at the face-end allowing fresh air to flow through the length of the heading. However, the lack of a jet effect results in poor mixing of the air. Indeed, unless the end of the duct or brattice line is maintained close to the face then local pockets of sluggish and uncontrolled recirculation may occur. In all cases, it is important that the ducting or brattice line be extended regularly so that it remains within some three metres of the face. This distance may be prescribed by legislation.

A further advantage of a ducted exhaust system is that a **dust filter** may be included within the system. In this case, the additional pressure drop across the filter must be taken into account in choosing the fan, and the filter serviced regularly in order that its resistance does not become excessive. Exhaust ducts must necessarily employ the more expensive rigid ducting or reinforced flexible ducting. If the exit velocity from an exhaust duct is high then an induction effect (Section 4.3.3), akin to a low pressure booster fan, can result in unexpected consequences including recirculation in the main entries.

For long headings, the resistance of the duct may become so great that **multiple fans** connected in series must be employed. If these are grouped as a cluster at the outbye end of the ducting then the high (positive or negative) gauge pressure will exacerbate leakage. It is preferable to space the fans along the length of the ducting in order to avoid excessive gauge pressures. The use of **hydraulic gradient diagrams** assists in the optimum location of fans and to prevent uncontrolled recirculation of leakage air. Multiple fans must be interlinked electrically and airflow or pressure monitors employed to detect accidental severing or blockage of the duct, in which case all fans inbye the point of damage must be switched off - again, to prevent **uncontrolled recirculation**.

It is clear that forcing and exhausting systems both have their advantages and disadvantages. Two-way systems have been devised that can be switched from forcing mode to exhausting for cyclic mining operations. These may employ a reversible axial fan or, alternatively, both a forcing and an exhausting fan, only one of which is operated at any one time with an appropriate adjustment of valves or shutter doors within the duct arrangement.

The more common methods of combining the advantages of forcing and exhausting ducts are **overlap** systems. Examples are shown on Figure 4.16. The direction and mean velocity of the air in the heading within the overlap zone clearly depends upon the airflows in each of the ducts. These should be designed such that the general body airflow in this region does not become unacceptably low. Where permitted by law, controlled recirculation may be used to advantage in overlap systems (Section 4.5.2). Where continuous miners or tunnelling machines are employed, the overlap ventilator may be mounted on the machine. In all cases, it is important that the fans are interlinked so that the overlap system cannot operate when the primary duct fan is switched off.



(a) Forcing system with exhaust overlap

(b) Exhausting system with force overlap

Figure 4.16 Overlap systems of auxiliary ventilation

4.4.3. Air movers

In addition to conventional ducted systems of auxiliary ventilation, a number of other techniques may be employed to enhance or control the movement of air within localized areas of a mine or tunnel.

Jet fans, sometimes known as ductless, vortex or **induction fans** are free standing units that produce a relatively high velocity outlet airstream. The jet of air produces two effects. First, the reach and integrity of the air vortex depends upon the velocity at the fan outlet, the size of the heading and whether the airway is a blind heading or part of a throughflow system. Satisfactory ventilation and turbulent mixing at the face of a large heading can be obtained from a jet fan sited 100 m outbye. Secondly, an induction effect occurs at the outer boundaries of the expanding cone of projected air. This entrains additional air from the surroundings producing a forward moving flow that is greater than the airflow through the fan itself. The conversion of velocity pressure into static pressure as the plume of air decelerates also generates a true ventilating pressure. This is seldom greater than some 20 Pascals but is sufficient to create significant airflows in large, low resistance airways. The induction effect inhibits excessive recirculation provided that incoming intake air is provided at the fan inlet. Jet fans have particular application in large room and pillar operations and may also be used in series to promote airflow through vehicular tunnels.

An airflow can also be generated by a spray of water giving rise to **spray fans**. Inertia from the motion of the water droplets is transmitted to the air by viscous drag and turbulent induction. Spray fans may be used very effectively to control the local movement of air around rock-winning machines such as continuous miners or longwall shearers. This assists in the rapid dilution of methane and in diverting dust-laden air away from operator positions. The effect depends upon the shape, velocity and fineness of the spray. Although dust suppression sprays also cause air induction it is usually necessary to add additional sprays if these are to be used for local airflow control. Provided that the service water is chilled, spray fans are also an efficient means of cooling the air in a work area.

Compressed air injectors are also induction devices. The compressed air is supplied through one or more forward pointing jets within a cylindrical or shaped tube. The best effect is obtained when the compressed air is supplied at the throat of a venturi. These devices are noisy and of much lower efficiency than fans. However, they have a role in areas where electrical power is unavailable. Mining law may proscribe the use of compressed air for the promotion of airflow in gassy mines as the high velocity flow of air through the jets can cause the build-up of an **electrostatic charge** at the nozzle. This produces the possibility of sparks that could ignite a methane-air mixture.

4.5. CONTROLLED PARTIAL RECIRCULATION

4.5.1. Background and principles of controlled partial recirculation

The idea of recirculating air in any part of a gassy mine has, traditionally, been an anathema to many mining engineers. Most legislation governing coal mines prohibits any ventilation system or device that causes air to recirculate. The background to such legislation is the intuitive fear that recirculation will cause concentrations of pollutants to rise to dangerous levels. A rational examination of controlled recirculation was carried out by **Leach, Slack and Bakke** during the 1960's at the Safety in Mines Research Establishment in England. Those investigators made a very simple and obvious statement but one that had, to that time, apparently been denied or ignored within the context of air recirculation. They argued that the general body gas concentration, C , leaving any ventilated region of a mine is given by

$$C = \frac{\text{Flow of gas into the region}}{\text{Flow of fresh air passing through the region}} \quad (4.3)$$

The value of C is quite independent of the flowpaths of the air within the region, including recirculation. It is true, of course, that if the through-flow of fresh air falls while the gas emission remains constant then the concentration of gas will rise. This would happen, for example, if the air duct serving a long gassy heading was dislocated while an inbye fan continued to run. This example illustrates a case of **uncontrolled recirculation**. The definition of a system of **controlled partial recirculation** is one in which a controlled fraction of the air returning from a work area is passed back into the intake while, at the same time, the volume flow of air passing through the region is monitored to ensure that it remains greater than a predetermined minimum value.

The advantages of controlled partial recirculation lie in the improved environmental conditions it can provide with respect to gases, dust and heat, as well as allowing mining to proceed in areas of a mine that are too distant from surface connections to be ventilated economically by conventional means.

As illustrated in Section 4.5.2., general body gas concentrations may actually be reduced by controlled recirculation. Furthermore, the higher air velocities that occur within a recirculation zone assist in the turbulent mixing of gas emissions, reducing the tendency to methane layering and diminishing the probability of accumulations of explosive methane-air mixtures.

As with gas, concentrations of **respirable dust** reach predictable maximum levels in a system of controlled recirculation and may be reduced significantly by the use of **filters**. The greater volume of air being filtered results in more dust being removed. The effect of controlled recirculation on climatic conditions is more difficult to predict. However, both simulation programming and practical observations have indicated the improvements in the cooling power of partially recirculated air for any given value of through-flow ventilation.

As workings proceed further away from shaft bottoms, the cost of passing air along the lengthening primary intakes and returns necessarily increases. Where new surface connections closer to the workings are impractical, perhaps because the workings lie beneath the sea or due to great depth then the cost of conventional ventilation will eventually become prohibitive - even when booster fans are employed. Using the air more efficiently through controlled partial recirculation then becomes an attractive proposition. If, for example, the methane concentration returning from a conventionally ventilated face is 0.3 per cent, and the safe mandatory limit is 1.0 per cent, then the through-flow provided from the main airways might be reduced to one half giving a methane concentration of 0.6 per cent while maintaining or increasing the face velocities by controlled recirculation.

During the 1970's the concept of controlled partial recirculation gained respectability and is now practiced by several of the world's mining industries operating, in some cases, by authorized exemptions from existing legislation.

The greatest disincentive against the introduction of controlled recirculation has been the risk of combustion gases from a fire being returned to working areas. Further potential problems arise from a consideration of **transient phenomena** such as blasting, or rapid changes in barometric pressure caused by the operation of doors or fans, and the possible resulting peak emissions of gases. The introduction of failsafe **monitoring systems** with continuous **computer surveillance** has revolutionized the situation (Section 9.6.3.). These self-checking systems involve monitoring the concentration of gases, air pressure differentials and airflows at strategic locations as well as the operating conditions of fans and other plant. Fans can be interlinked electrically to obviate the possibility of uncontrolled recirculation. Should any monitored parameter fall outside prescribed limits then the system will automatically revert to a conventional non-recirculating circuit. The introduction of reliable monitoring technology has allowed the advantages of controlled partial recirculation to be realized safely.

4.5.2. Controlled recirculation in headings

The most widespread application of controlled recirculation has been in headings. One of the disadvantages of the conventional overlap systems shown in Figure 4.16 is the reduction in general

body air velocity within the overlap zone. This can be overcome completely by arranging for the overlap fan to pass an airflow that is greater than that available within the heading, i.e. a system of controlled recirculation, accompanied by the corresponding monitoring system and electrical interlocks. This is particularly advantageous when applied to the scheme depicted in Figure 4.16(a) as filtered air is then available to machine operators as well as throughout the length of the heading.

Figure 4.17 shows two examples of a primary exhaust system configured for controlled recirculation. In both cases, an airflow Q_t (m^3/s) is available at the last open cross-cut and contains a gas flow of G_i (m^3/s). An airflow of Q_h passes up the heading where a gas emission of G_h is added.

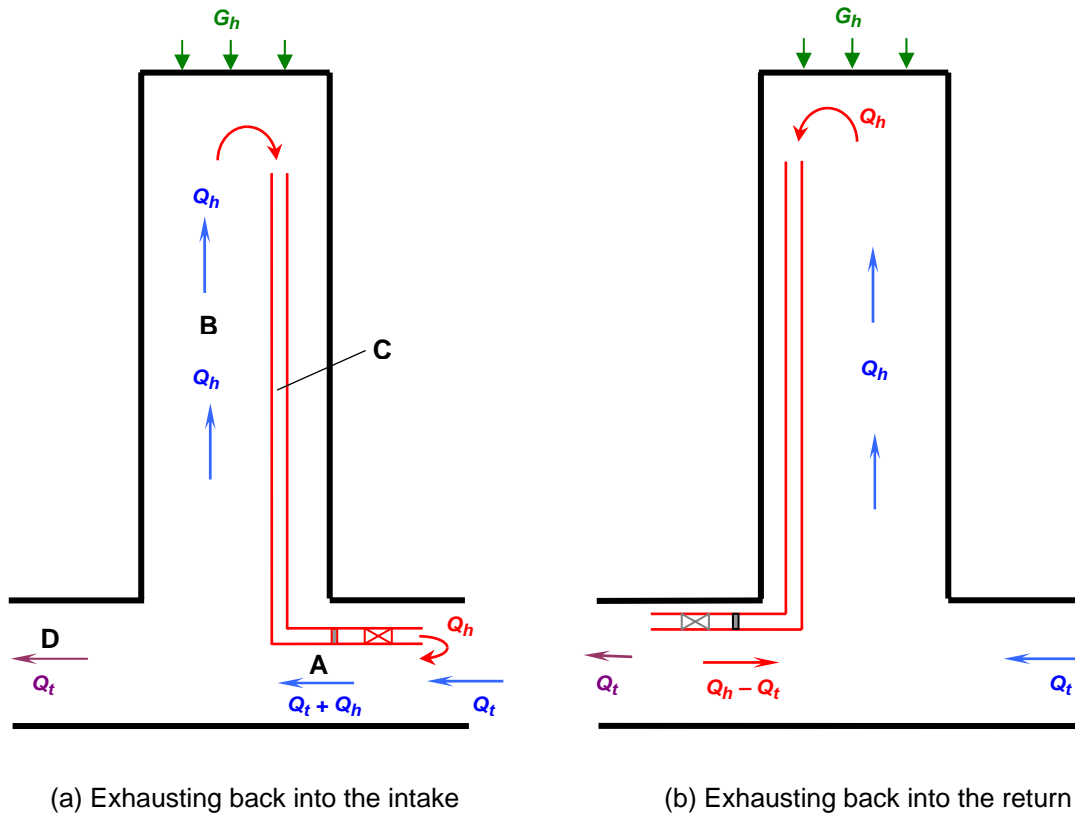


Figure 4.17 Controlled recirculation systems for headings.

Let us try to find the **maximum** general body gas concentrations that will occur in the systems. Referring to Figure 4.17(a) and using the locations A, B, C and D as identifying subscripts, the fractional gas concentration, C_g , at position D (leaving the system) must be

$$C_{gD} = \frac{G_i + G_h}{Q_t} \quad (\text{see equation (4.3)})$$

(In these relationships, it is assumed that the gas flow is much smaller than the airflow). However, inspection of the figure shows that this must also be the gas concentration at locations A and B. In particular,

$$C_{gB} = \frac{G_i + G_h}{Q_t}$$

But gas flow, $G = \text{Gas concentration} \times \text{airflow}$

$$G_B = \frac{(G_i + G_h)}{Q_t} \times Q_h$$

The gas flow in the duct, $G_C = G_B + G_h$, must then be

$$G_C = \frac{(G_i + G_h)}{Q_t} \times Q_h + G_h$$

Hence, the gas concentration in the duct,

$$\begin{aligned} C_{gC} &= \frac{G_C}{Q_h} \\ &= \frac{G_i + G_h}{Q_t} + \frac{G_h}{Q_h} \end{aligned} \quad (4.4)$$

This is the highest general body gas concentration that can occur anywhere within the system shown on Figure 4.17(a).

Examination of equation (4.4) shows that if the gas flows, G_i and G_h , are fixed and the fresh air supply, Q_t , remains unchanged then the maximum general body gas concentration, C_{gC} , must fall as Q_h is increased - that is, as the degree of recirculation rises. In the limit, at very high Q_h , the gas concentration in the duct tends toward that leaving the system at position D.

In a conventional non-recirculating system, the airflow taken into a heading is often limited to no more than half of that available at the last open cross-cut, i.e. $Q_h = 0.5 Q_t$. Applying these conditions to equation (4.4) gives

$$\begin{aligned} C_{gC} (\text{conventional}) &= \frac{(G_i + G_h)}{Q_t} + \frac{G_h}{0.5 Q_t} \\ &= \frac{G_i + 3G_h}{Q_t} \end{aligned} \quad (4.5)$$

Recirculation commences when $Q_h = Q_t$, giving

$$\begin{aligned} G_{gC} (\text{maximum, recirculating}) &= \frac{(G_i + G_h)}{Q_t} + \frac{G_h}{Q_t} \\ &= \frac{G_i + 2G_h}{Q_t} \end{aligned} \quad (4.6)$$

C_{gC} must be less than this at all greater values of Q_h , i.e. higher degrees of recirculation. Comparing equations (4.5) and (4.6) shows that in this configuration the maximum general body gas concentration is always less using controlled recirculation than with a conventional system. Turning to Figure 4.17(b), the analysis is even simpler. In this case, the maximum gas concentration (in the duct) must be the same as that leaving the system $(G_i + G_h)/Q_t$, provided that Q_h is equal to or greater than Q_t , i.e. controlled recirculation must exist. Here again, this is always less than would be attainable with a conventional non-recirculating system.

A similar analysis for dust concentration, C_d , on the system shown on Figure 4.17 but with no dust filter gives an analogous expression to that for gas.

$$C_{dC} = \frac{D_i + D_h}{Q_t} + \frac{D_h}{Q_h} \quad \frac{\text{mg}}{\text{m}^3} \quad (4.7)$$

Again it can be seen that the maximum concentration falls as Q_h is increased. For dust it is more pertinent to state the concentration at position B, i.e. in the main length of the heading: This becomes

$$C_{dB} = \frac{D_i + D_h}{Q_t} \quad \frac{\text{mg}}{\text{m}^3} \quad (4.8)$$

and is completely independent of the degree of recirculation.

If the filters shown in Figure 4.17(a) remove a fraction, η , of the dust in the duct then it can be shown that the corresponding concentrations become

$$C_{dC} = \frac{Q_h(D_i + D_h) + D_h Q_t}{Q_h(Q_t + \eta Q_h)} \quad \frac{\text{mg}}{\text{m}^3} \quad (4.9)$$

and

$$C_{dB} = \frac{D_i + (1 - \eta) D_h}{Q_t + \eta Q_h} \quad \frac{\text{mg}}{\text{m}^3} \quad (4.10)$$

These equations show that when filters are used, dust concentrations fall throughout the system. It has been assumed in these analyses that there is no settlement of dust.

Similar relationships can be derived for other configurations of controlled recirculation in headings.

4.5.3. District systems

The extension of controlled partial recirculation to complete areas of a mine has particular benefits in decreasing the costs of heating or cooling the air and for workings distant from the surface connections.

Positions of fans

Figure 4.18 shows simplified schematics illustrating three configurations of fan locations in a district recirculation system. In each case, the throughflow ventilation in the mains is shown as Q_m with Q_c passing from return to intake in the recirculation cross-cut, to give an enhanced airflow of $Q_m + Q_c$ in the workings. The ratio $F = Q_c / (Q_m + Q_c)$ is known as the **recirculation fraction**. The fan that creates the recirculation develops a pressure of p_r while the pressure differentials applied across the outbye ends for the three systems shown are p_{o1} , p_{o2} and p_{o3} respectively.

The simplest configuration is shown in Figure 4.18(a) with the recirculating fan sited in the cross-cut. This maintains the intakes and returns free for travel and unobstructed by airlocks. Locating the fan in this position will tend to decrease the throughflow, Q_m . Hence, if the total flow is to be maintained, the applied pressure differential must be increased from

$$p_{o1} = R_m Q_m^2 + R_w Q_m^2 \quad (\text{with no recirculation})$$

where R_m is the combined resistance of the intake and return mains

$$\text{to } p_{o1} = R_m Q_m^2 + R_w (Q_m + Q_c)^2 \quad (4.11)$$

with the recirculation shown on Figure 4.18(a). These equations are derived by summing the frictional pressure drops, p , around the path of the mains (subscript m) and workings (subscript w) - and by applying the square law $p = RQ^2$, where R = airway resistance (Section 5.2).

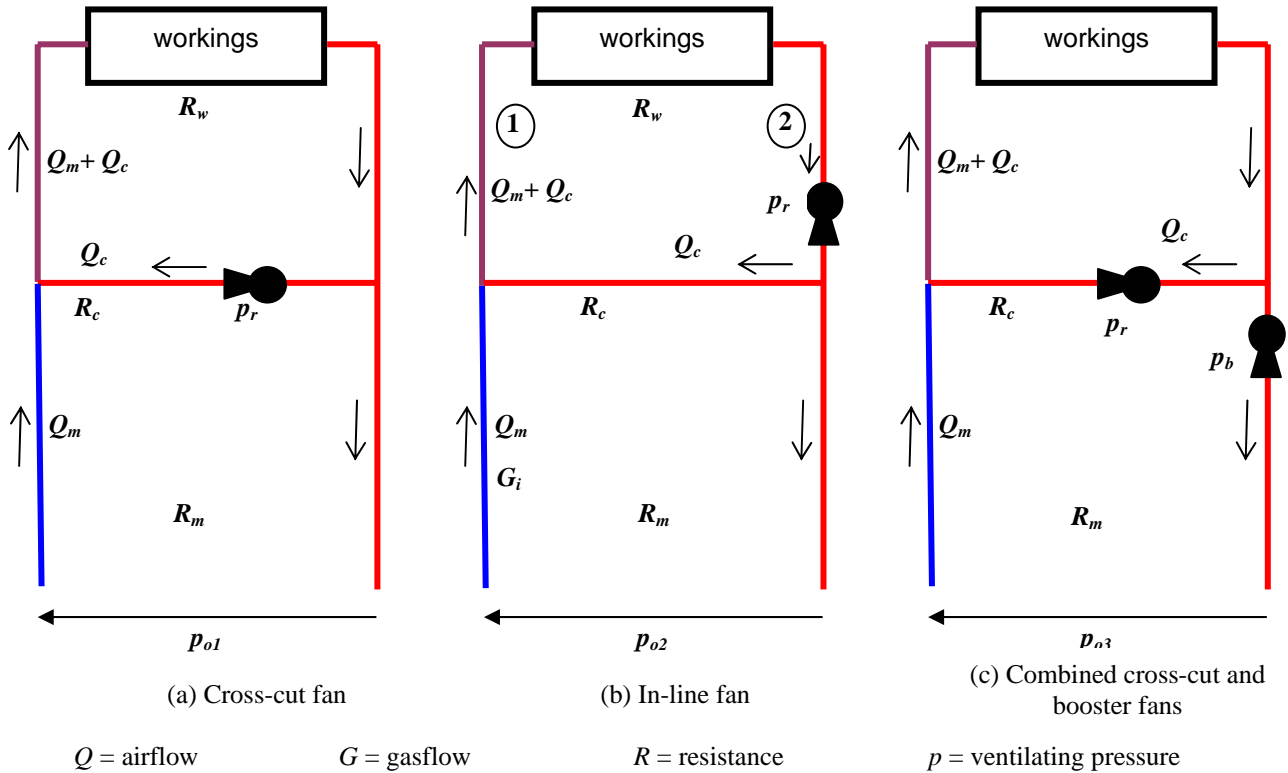


Figure 4.18. Schematics of district recirculation systems

Similarly, in all three cases (a), (b) and (c) the pressure required of the recirculating fan is given by summing the frictional pressure drops around the workings and cross-cut

$$p_r = R_c Q_c^2 + R_w (Q_m + Q_c)^2 \quad (4.12)$$

In system (b), the fan is located within either the intake or return inby the recirculation cross-cut. In this position, the fan acts as a district booster fan as well as creating the controlled recirculation. Hence, the throughflow, Q_m , will tend to increase. Alternatively, if the throughflow is to remain constant then *either* the outby pressure differential may be reduced to

$$p_{o2} = R_m Q_m^2 - R_c Q_c^2 \quad (4.13)$$

or a regulator can be introduced into either of the mains.

System (c) in Figure 4.18 combines a booster fan with a cross-cut fan and is the preferred configuration where recirculation is employed due to the workings being distant from the surface connections. In this system, the ventilating pressure applied across the district may be reduced by the magnitude of the booster fan pressure to maintain a constant Q_m , i.e.

$$p_{o3} = R_m Q_m^2 + R_w (Q_m + Q_c)^2 - p_b \quad (4.14)$$

The total **airpower** consumed within the systems is given as the sum of the pQ products for all airways. If corresponding airflows and the resistances are the same in each of the three systems then the required total airpowers must also be equal, irrespective of the locations of the fans. In practice, differences in the efficiencies of the fans will cause variations in the required total electrical input to the fan motors. This may, however, be of minor significance.

A major consideration in all designs of controlled partial recirculation is that in conditions of an emergency or plant stoppage, the system must fail-safe and revert to a conventional non-recirculating configuration. The airflows must then remain sufficient to allow personnel to evacuate the area safely and for the necessary ameliorative measures to be taken. The detection of such conditions is provided by monitoring the environmental parameters and the operation of the fans.

If the recirculating cross-cut fan in system (a) fails, then doors in the cross-cut must close automatically. The throughflow ventilation will increase, reducing the general body gas concentration in the return airways. However, the reduced air velocity in the working area will increase the probability of local accumulations of gas to that of a conventional non-recirculating system.

Stoppage of the in-line fan of system (b) is more serious. Again, doors in the cross-cut must be closed but the throughflow of air will decrease, resulting both in diminished airflows in the workings and also higher general body gas concentrations in the returns. However, this system is capable of better airflow control than the cross-cut fan. The degree of recirculation may be varied by modifying the duty of the fan installation (fan speed, vane settings or number of fans operating), regulating the airflow in either the intake or return inbye the cross-cut or by adjustment of a bypass path around the fan.

System (c) gives the greatest degree of flexibility. Stoppage of the cross-cut fan and closure of the corresponding doors will increase the throughflow, Q_m . However, should the booster fan fail, then electrical interlocks should close down the cross-cut fan. Reduced airflows throughout the system are maintained by the outbye pressure differential. Adjustment of the two fans allows a much greater degree of independent control of the airflow distribution than either of the systems (a) or (b).

Pollution levels

Although the general body gas concentration leaving any zone is independent of airflow distribution within the zone - recirculating or otherwise (Section 4.5.1), any airflow passed from a return to an intake airway may affect the quality as well as the quantity of the air in that intake.

Referring to Figure 4.18(b) suppose that the incoming intake air contains a gas flow of G_i (m^3/s) and a constant gas emission of G_w occurs in the workings. Let us derive expressions for the general body gas concentrations in the face return (position 2) and intake (position 1).

The return concentration must be the same as that leaving the complete district and in the cross-cut, assuming no other sources of gas emission:

$$C_{g2} = G_{gC} = C_g(\text{main return}) = \frac{G_i + G_w}{Q_m} \quad (4.15)$$

(see equation (4.3))

This is independent of the degree of recirculation.

To determine the gas concentration in the intake at position 1, consider first the gas flow passing through the cross-cut (subscript c)

$$\begin{aligned} G_c &= Q_c \times C_{gC} \\ &= Q_c \frac{(G_i + G_w)}{Q_m} \quad \text{from equation (4.15)} \end{aligned}$$

Now the gas flow at position 1 is

$$\begin{aligned} G_1 &= G_i + G_c \\ &= G_i + \frac{Q_c}{Q_m} (G_i + G_w) \end{aligned}$$

The corresponding concentration is given by dividing by the corresponding airflow, $Q_m + Q_c$, giving

$$C_{g1} = \frac{G_1}{(Q_m + Q_c)} = \frac{1}{Q_m} \left[\frac{G_i Q_m}{(Q_m + Q_c)} + \frac{Q_c}{(Q_m + Q_c)} (G_i + G_w) \right] \quad (4.16)$$

However, if we define the recirculation fraction as

$$F = \frac{Q_c}{(Q_m + Q_c)} \quad \text{where, also,} \quad 1 - F = \frac{Q_m}{(Q_m + Q_c)}$$

Then equation (4.16) becomes

$$\begin{aligned} C_{g1} &= \frac{1}{Q_m} [(1 - F)G_i + F(G_i + G_w)] \\ &= \frac{1}{Q_m} [G_i + FG_w] \quad (4.17) \end{aligned}$$

This verifies the intuitive expectation that as the degree of recirculation, F , increases then the gas concentration in the intake also increases. However, as F is never greater than 1, and comparing with equation (4.15), we can see that the intake, or face, gas concentration can never be greater than the return concentration. Hence, in a district recirculation system the general body gas concentration at no place is greater than the return general body concentration with or without recirculation. The maximum allowable methane concentrations in coal mine intakes may be prescribed by law at a low value such as 0.25 per cent. The value of F should be chosen such that this limit is not exceeded. Similar analyses may be carried out for **dust concentrations**. In this case, drop-out and the use of filters can result in significant reductions in the concentrations of dust in a system of controlled partial recirculation. However, the enhanced air velocities in the work area should not exceed some 4 m/s as the re-entrainment of settled particles within the airstream accelerates rapidly at greater velocities.

The **climatic conditions** within a system of controlled partial recirculation depend not only upon the airflows and positions/duties of the fans but also upon the highly interactive nature of heat transfer between the strata and the ventilating airstreams (Chapter 15). The locations, types and powers of other mechanized equipment, and the presence of free water also have significant effects. The only practicable means of handling the large numbers of variables is through a computer program to simulate the interacting physical processes (Chapter 16). Such analyses, together with practical observations, indicate that wet and dry bulb temperatures at any point may either increase or decrease when controlled partial recirculation is initiated without air cooling. The increased air velocities within the recirculation zone enhance the cooling power of the air on the human body for any given temperature and humidity. However, when controlled recirculation is practiced in hot mines, it is normally accompanied by cooling of the recirculated air. This is less expensive and more effective than bulk cooling the intake air in a conventional ventilation system and significant improvements in climatic conditions may be realized. Again, practical experience has shown that the higher airflows within a recirculation zone improves the effectiveness of existing refrigeration capacity.

In closing this section **the reader is reminded, once again, that air recirculation may be prohibited by the governing legislation.** The relevant statutes should be read, and/or enforcement agencies consulted before instituting a system of controlled partial recirculation.

4.6. UNDERGROUND REPOSITORIES

4.6.1. Types of repository

Underground space is increasingly being utilized for purposes other than the extraction of minerals or for transportation. The high cost of land, overcrowding and aesthetic considerations within urban areas encourages use of the subsurface for office accommodation, manufacturing, warehousing, entertainment facilities and many other purposes. The safety and stability of a well chosen geologic formation makes underground space particularly suitable for the storage of materials, varying from foodstuffs and liquid or gaseous fuels to toxic wastes. The design and operation of environmental systems in such repositories require the combined skills of mine ventilation engineers and HVAC (heating, ventilating and air-conditioning) personnel. The repositories must be constructed and operated in a manner that preserves the integrity of the stored material and also protects the public from hazardous emissions or effluents.

Perhaps the most demanding designs arise out of the perceived need to store **radioactive waste in deep underground repositories.** There are basically two types of this waste. First, there is the transuranic, or low level, radioactive waste such as contaminated clothing, cleaning materials or other consumable items that are produced routinely by establishments that handle radioactive materials. Such waste may be compressed into containers which may be stacked within excavated chambers underground. Secondly, there is the concentrated and highly radioactive waste produced from some defence establishments and as the plutonium-rich spent fuel rods from nuclear power stations. This waste may be packed into heavily shielded and corrosion resistant cylinders and emplaced within boreholes, about one metre in diameter, drilled from underground airways into the surrounding rock.

4.6.2. Ventilation circuits in repositories for nuclear waste

Figure 4.19 depicts the primary ventilation structure of a high level nuclear waste repository. As in the figures illustrating mining circuits shown earlier in the chapter, this sketch is conceptual in nature and is not intended to represent all airways.

During the operation of an underground repository two activities must proceed in phase with each other. One is the mining of the rooms or drifts where the material is to be placed, together with the excavation of transportation routes, ventilation airways and the other entire infrastructure required in an underground facility. This is referred to simply as the mining activity. Secondly, the

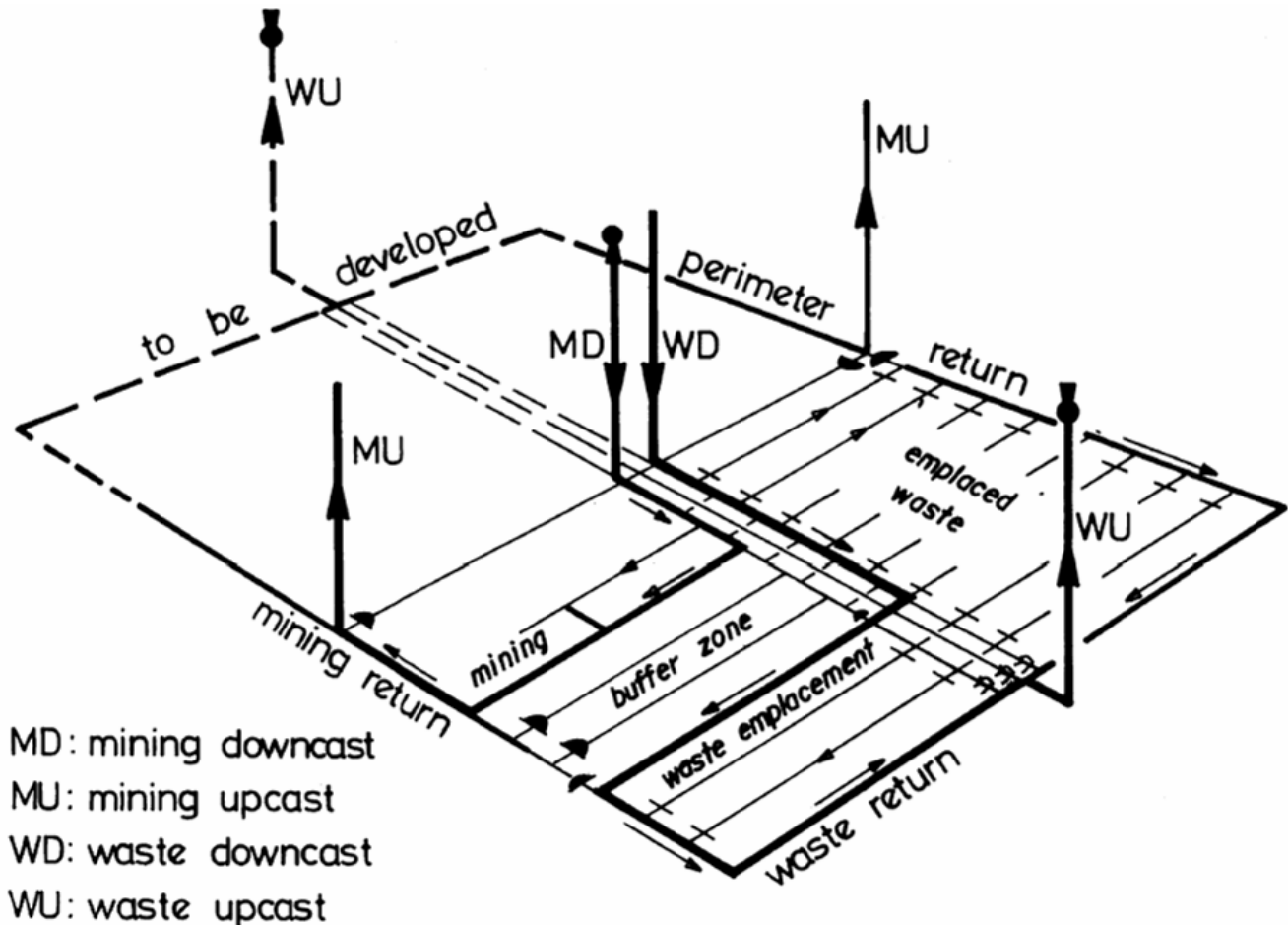


Figure 4.19 Example of primary ventilation circuits for an underground nuclear waste repository.

hazardous waste material must be transported through the relevant shafts and airways to the selected rooms for emplacement. Accordingly, this is known as the emplacement activity.

For reasons of environmental safety, the ventilation circuits for mining and emplacement activities in a nuclear waste repository must be kept separate. Furthermore, any leakage of air through doors or bulkheads between the two systems must always **leave** the mining zone and flow **into** the emplacement zone - even in the event of the failure of any fan. Figure 4.19 shows how this is achieved. The mining circuit operates as a through flow **forcing** system with the main fan(s) sited at the top of the mining downcast shaft(s). On the other hand, the emplacement circuit operates as a throughflow **exhaust** system with the main fans located at the top of the waste upcast shafts. It should be remembered that within the nomenclature of underground repositories, the term **waste** refers to the hazardous waste to be emplaced and not waste rock produced by mining activities. With this design, any accidental release of radionuclides into the underground atmosphere is contained completely within the emplacement circuit and will not contaminate the mining zones.

The shaft or surface-connecting ramp used for transporting the nuclear waste underground is not shown on Figure 4.19. This shaft will normally not form part of the main ventilation system but will have a limited downcasting airflow which passes directly into a waste main return. Similar arrangements may be made for the waste transportation routes underground, thus limiting the potential dispersion of radioactive contamination in the event of a waste container being damaged during transportation. Separate maintenance and repair shops are provided in the mining and emplacement circuits

When emplacement activities have been completed in any given room then the ends of that room may be sealed. In the case of high level nuclear waste, this may result in the envelope of rock surrounding the airway reaching temperatures in excess of 150 OC, depending upon the rate of heat emission from the waste, the distance of the canisters from the airway, the thermal properties of the rock, and thermal induction of water and vapour migration within the strata. If the drift is to be reopened for retrieval or inspection of any canister then a considerable period of cooldown by refrigerated air may be required before unprotected personnel can re-enter. To reduce the time and expense of the cooldown period, the emplaced room may not be completely sealed but allowed to pass a regulated airflow sufficient to maintain the rock surface temperature at a controlled level.

4.6.3. Additional safety features

Before any repository for hazardous waste is commissioned it must conform to the strictest standards of safety and quality assurance in order to protect both the workers and the general public from chemical or radioactive contamination. In the case of an underground repository, design safeguards commence with an extensive examination of the suitability of the geologic formation to act as a natural containment medium. This will involve the physical and chemical properties of the rock, the presence and natural migration rate of groundwater and the probability of seismic activity. Other factors that influence the choice of site include population density and public acceptance of the surface transportation of hazardous waste to the site.

In addition to continuous electronic surveillance of the quality of the atmosphere throughout the main ventilation routes of a nuclear waste repository, the fans, bulkheads and regulators must be monitored to ensure that they operate within design limits and that pressure differentials are maintained in the correct direction at all times. Regulators and doors may be fitted with electrical or pneumatic actuators suitable for both local and remote operation. Should airborne radioactivity be detected at any time and any location in the circuit then the air emerging from the top of the waste upcast shafts is diverted automatically through banks of **high efficiency particulate (HEPA) filters**. Separate or additional precautions should also be taken to protect surface buildings and shaft tops from tornadoes, floods or fall-out from volcanic activity.

Bibliography

- Burton, R.C., et al (1984) Recirculation of air in the ventilation and cooling of deep gold mines. **Trans. 3rd. International Congress on Mine Ventilation. Harrogate, England.**
- Dhar, N. and McPherson M.J. (1987) The effect of controlled recirculation on mine climate. **Proc. 5th Ann. Workshop. Generic Mineral Tech. Center, Mine Systems Design and Ground Control Alabama, USA pp. 139 - 151.**
- Hardcastle, S.G. (1985) Computer predicted airborne respirable dust concentrations in mine air recirculation systems. **Proc. 2nd U.S. Mine Ventilation Symp. Reno. pp. 239-248.**

Leach, S.J. and Slack A. (1969) Recirculation of Mine Ventilation Systems. **The Mining Engineer (U.K.) January, No. 100.**

Lee, R.D. and Longson, I. (1987) Controlled recirculation of mine air in working districts. **Jnl. Mine Ventilation Soc. of South Africa Vol. 40 No. 2, Feb.**

Longson, I, Lee, R.D., and Lowndes, I.S. (1985) The feasibility of controlled air recirculation around operating longwall coal faces. **Proc. 2nd U.S. Mine Ventilation Symp. Reno pp. 227-237.**

Robinson, R. (1989) Use of booster fans and recirculation systems for environmental control in British coal mines. **4th U.S. Mine Ventilation Symposium. Berkeley, CA, USA pp. 235-242.**

Wallace, K.G et al (1986) Impact of using auxiliary fans on mine ventilation efficiency and cost. **AIME meeting. New Orleans, March 1986.**

Wallace, K.G. (1988) Ventilation strategy for a prospective U.S. nuclear waste repository. **4th International Mine Ventilation Congress, Brisbane, Australia pp. 65-72. 4-33.**

Chapter 5. INCOMPRESSIBLE FLOW RELATIONSHIPS

5.1. INTRODUCTION	2
5.2. THE ATKINSON EQUATION AND THE SQUARE LAW	2
5.3. DETERMINATION OF FRICTION FACTOR.....	4
By analogy with similar airways.....	4
From design tables.....	5
From geometric data	5
5.4. AIRWAY RESISTANCE	7
5.4.1. Size of airway.....	8
5.4.2. Shape of airway	9
5.4.3. Airway lining.....	10
5.4.4. Air density	10
5.4.5. Shock losses.....	10
Shock loss factor	10
Equivalent length.....	11
5.4.6. Mine shafts.....	13
5.4.6.1. Shaft walls.....	14
5.4.6.2. Shaft fittings.....	14
<i>Longitudinal Fittings</i>	14
<i>Buntons</i>	14
<i>Form Drag and Resistance of Buntons</i>	14
<i>Interference factor</i>	16
5.4.6.3. Conveyances.....	17
<i>Resistance of a Stationary Conveyance</i>	17
<i>Dynamic Effects of a Moving Conveyance</i>	18
5.4.6.4. Entry and exit losses	22
5.4.6.5. Total shaft resistance	22
5.4.6.6. Methods of reducing shaft resistance	23
<i>Shaft walls</i>	23
<i>Buntons</i>	23
<i>Longitudinal Fittings</i>	23
<i>Cages and Skips</i>	23
<i>Intersections and loading/unloading stations</i>	24
5.5. AIR POWER	24
BIBLIOGRAPHY	25
APPENDIX A5.....	26
Shock loss factors for airways and ducts.....	26
A.5.1 Bends.....	27
A5.2 Changes in cross-section	29
A5.3 Junctions	29
A5.4 Entry and Exit	34
A5.5 Obstructions	35
A5.6. Interaction between shock losses	38

5.1. INTRODUCTION

In Chapter 2 we introduced some of the basic relationships of incompressible fluid flow. With the exception of shafts greater than 500m in vertical extent, changes in air density along individual airways may be ignored for most practical ventilation planning. Furthermore, in areas that are actively ventilated, airflows are turbulent in nature, other than in very large openings.

In this chapter, we shall confine ourselves to incompressible turbulent flow in order to develop and illustrate the equations and concepts that are most commonly employed in the practice of subsurface ventilation engineering.

Although the basic relationships that were derived in Chapter 2 may be employed directly for ventilation planning, **John J. Atkinson** introduced certain simplifications in his classical paper of 1854. These simplifications facilitate practical application but were achieved at the expense of precision. As the resulting "laws of airflow" remain in common use, they are introduced and discussed in this chapter. The important concept of airway resistance is further expanded by an examination of the factors that influence it.

5.2. THE ATKINSON EQUATION AND THE SQUARE LAW

In seeking to quantify the relationships that govern the behaviour of airflows in mines, Atkinson utilized earlier work of the French hydraulic engineers and, in particular, the **Chezy Darcy** relationship of the form expressed in equation (2.49)

$$p = f L \frac{\text{per}}{A} \rho \frac{u^2}{2} \quad \text{Pa}$$

It must be remembered that Atkinson's work was conducted in the middle of the nineteenth century, some thirty years before Reynold's experiments and long before Stanton, Prandtl and Nikuradse had investigated the variable nature of the coefficient of friction, f . As far as Atkinson was aware, f was a true constant for any given airway. Furthermore, the mines of the time were relatively shallow, allowing the air density, ρ , to be regarded also as constant. Atkinson was then able to collate the "constants" in the equation into a single factor:

$$k = \frac{f \rho}{2} \quad \frac{\text{kg}}{\text{m}^3} \quad (5.1)$$

giving

$$p = k L \frac{\text{per}}{A} u^2 \quad \text{Pa} \quad (5.2)$$

This has become known as **Atkinson's Equation** and k as the **Atkinson friction factor**. Notice that unlike the dimensionless Chezy Darcy coefficient, f , Atkinson's friction factor is a function of air density and, indeed, has the dimensions of density.

Atkinson's equation may be written in terms of airflow, $Q = uA$, giving

$$p = k L \frac{\text{per}}{A^3} Q^2 \quad \text{Pa} \quad (5.3)$$

Now for any given airway, the length, L , perimeter, per , and cross-sectional area, A , are all known. Ignoring its dependence upon density, the friction factor varies only with the roughness of

the airway lining for fully developed turbulence. Hence we may collect all of those variables into a single characteristic number, R , for that airway.

$$R = kL \frac{\text{per}}{A^3} \quad \frac{\text{Ns}^2}{\text{m}^8} \text{ or } \frac{\text{kg}}{\text{m}^7} \quad (5.4)$$

giving

$$\rho = RQ^2 \quad \text{Pa} \quad (5.5)$$

This simple equation is known as the **Square Law** of mine ventilation and is probably the single most widely used relationship in subsurface ventilation engineering.

The parameter R is called the **Atkinson's resistance** of the airway and, as shown by the Square Law, is the factor that governs the amount of airflow, Q , which will pass when a given pressure differential, ρ , is applied across the ends of an airway.

The simplicity of the Square Law has been achieved at the expense of precision and clarity. For example, the resistance of an airway should, ideally, vary only with the geometry and roughness of that airway. However, equations (5.1) and (5.4) show that R depends also upon the density of the air. Hence, any variations in the temperature and/or pressure of the air in an airway will produce a change in the Atkinson resistance of that airway.

Secondly, the **frictional pressure drop**, ρ , depends upon the air density as well as the geometry of the airway for any given airflow Q . This fact is not explicit in the conventional statement of the Square Law (5.5) as the density term is hidden within the definition of Atkinson resistance, R .

A clearer and more rational version of the Square Law was, in fact, derived as equation (2.50) in Chapter 2, namely

$$\rho = R_t \rho Q^2 \quad \text{Pa} \quad (\text{equation (2.50)})$$

where R_t was termed the rational turbulent resistance, dependent only upon geometric factors and having units of m^{-4} .

$$R_t = \frac{fL \text{ per}}{2A^3} \quad \text{m}^{-4} \quad (\text{from equation (2.51)})$$

It is interesting to reflect upon the influence of historical development and tradition within engineering disciplines. The k factor and Atkinson resistance, R , introduced in 1854 have remained in practical use to the present time, despite their weakness of being functions of air density. With our increased understanding of the true coefficient of friction, f , and with many mines now subject to significant variations in air density, it would be sensible to abandon the Atkinson factors k and R , and to continue with the more fundamental coefficient of friction f , and rational resistance, R_t . However, the relinquishment of concepts so deeply rooted in tradition and practice does not come about readily, no matter how convincing the case for change. For these reasons, we will continue to utilize the Atkinson friction factor and resistance in this text in addition to their more rational equivalents. Fortunately, the relationship between the two is straightforward.

Values of k are usually quoted on the basis of standard density, 1.2 kg/m^3 . Then equation (5.1) gives

$$k_{1.2} = 0.6 f \quad \frac{\text{kg}}{\text{m}^3} \quad (5.6)$$

and equations (5.5) and (2.50) give

$$R_{1.2} = 1.2 R_t \quad \frac{\text{Ns}^2}{\text{m}^8} \quad (5.7)$$

Again, on the premise that listed values of k and R are quoted at standard density (subscript 1.2), equations (5.3) to (5.5) may be utilized to give the **frictional pressure drop** and resistance at any other density, ρ .

$$\rho = k_{1.2} L \frac{\text{per}}{A^3} Q^2 \frac{\rho}{1.2} \quad \text{Pa} \quad (5.8)$$

$$R = k_{1.2} L \frac{\text{per}}{A^3} \frac{\rho}{1.2} \quad \frac{\text{Ns}^2}{\text{m}^8} \quad (5.9)$$

and $\rho = RQ^2 \quad \text{Pa} \quad (5.10)$

5.3. DETERMINATION OF FRICTION FACTOR

The surface roughness of the lining of an underground opening has an important influence on airway resistance and, hence, the cost of passing any given airflow. The roughness also has a direct bearing on the rate of heat transfer between the rock and the airstream (Chapter 15).

The coefficients of friction, f , shown on the Moody diagram, Figure 2.7, remain based on the concept of sand grain (i.e. uniformly distributed) roughness. Furthermore, as shown by equation (5.6), the Atkinson friction factor, k , is directly related to the dimensionless coefficient of friction, f . However, the k factor must be tolerant to wide deviations in the size and distribution of asperities on any given surface.

The primary purpose of a coefficient of friction, f , or friction factor, k , is to facilitate the prediction of the resistances of planned but yet unconstructed airways. There are three main methods of determining an appropriate value of the friction factor.

By analogy with similar airways

During ventilation surveys, measurements of frictional pressure drops, ρ , and corresponding airflows, Q , are made in a series of selected airways (Chapter 6). During major surveys, it is pertinent to choose a few airways representative of, say, intakes, returns, conveyor roadways or particular support systems, and to conduct additional tests in which the airway geometry and air density are also measured. The corresponding values of the friction factor may then be calculated, and referred to standard density from equations (5.9) and (5.10) as

$$k_{1.2} = \frac{\rho}{Q^2} \frac{A^3}{L \text{ per}} \frac{1.2}{\rho} \quad \frac{\text{kg}}{\text{m}^3} \quad (5.11)$$

Those values of k may subsequently be employed to predict the resistances of similar planned airways and, if necessary, at different air densities. Additionally, where a large number of similar airways exist, representative values of friction factor can be employed to reduce the number or lengths of airways to be surveyed. In this case, care must be taken that unrepresentative obstructions or blockages in those airways are not overlooked.

In practice, where the k factor is to be used to calculate the resistances of airways at similar depths and climatic conditions, the **density correction** $1.2/\rho$ is usually ignored.

Experience has shown that local determinations of friction factor lead to more accurate planning predictions than those given in published tables (see following subsection). Mines may vary considerably in their mechanized or drill-and-blast techniques of roadway development, as well as in methods of support., Furthermore, many modes of roadway drive or the influence of rock cleavage leave roughenings on the surface that have a directional bias. In such cases, the value of the friction factor will depend also upon the direction of airflow.

From design tables

Since the 1920's, measurements of the type discussed in the previous subsection have been conducted in a wide variety of mines, countries and airway conditions. Table 5.1 has been compiled from a combination of reported tests and the results of numerous observations made during the conduct of unpublished ventilation surveys. It should be mentioned, again, that empirical design data of this type should be used only as a guide and when locally determined friction factors are unavailable.

From geometric data

The coefficient of friction, f , and, hence, the Atkinson friction factor, k , can be expressed as a function of the ratio e/d , where e is the height of the roughenings or asperities and d is the hydraulic mean diameter of the airway or duct ($d = 4A/per$). The functional relationships are given in Section 2.3.6.3 and are illustrated graphically in Figure 5.1 (see, also, Figure 2.7).

For fully developed turbulent flow, the **Von Kármán equation** gives

$$f = \frac{k_{1.2}}{0.6} = \frac{1}{4 [2\log_{10}(d/e)+1.14]^2} \quad (\text{see equation 2.55})$$

Here again, the equation was developed for uniformly sized and dispersed asperities on the surface (**sand grain roughness**). For friction factors that are determined empirically for non-uniform surfaces, this equation can be transposed, or Figure 5.1 can be used, to find the equivalent e/d value. For example, a k factor of 0.012 kg/m^3 gives an equivalent e/d value of 0.063. In an airway of hydraulic mean diameter 3.5 m, this gives the effective height of asperities to be 0.22 m.

The direct application of the e/d method is limited to those cases where the height of the asperities can be measured or predicted. The technique is applicable for supports that project a known distance into the airway.

Example.

The projection of the flanges, e , in a tubed shaft is 0.152 m. The wall to wall diameter is 5.84 m. Calculate the coefficient of friction and Atkinson friction factor.

Solution.

The e/d ratio is

$$\frac{0.152}{5.84} = 0.026$$

From equation (2.55) or Figure 5.1, this gives

$$f = 0.0135 \text{ and } k_{1.2} = 0.0081 \text{ kg/m}^3$$

	Friction factor, k kg/m ³	Coefficient of friction, f (dimensionless)
Rectangular Airways		
Smooth concrete lined	0.004	0.0067
Shotcrete	0.0055	0.0092
Unlined with minor irregularities only	0.009	0.015
Girders on masonry or concrete walls	0.0095	0.0158
Unlined, typical conditions no major irregularities	0.012	0.020
Unlined, irregular sides	0.014	0.023
Unlined, rough or irregular conditions	0.016	0.027
Girders on side props	0.019	0.032
Drift with rough sides, stepped floor, handrails	0.04	0.067
Steel Arched Airways		
Smooth concrete all round	0.004	0.0067
Bricked between arches all round	0.006	0.01
Concrete slabs or timber lagging between flanges all round	0.0075	0.0125
Slabs or timber lagging between flanges to spring	0.009	0.015
Lagged behind arches	0.012	0.020
Arches poorly aligned, rough conditions	0.016	0.027
Metal Mines		
Arch-shaped level drifts, rock bolts and mesh	0.010	0.017
Arch-shaped ramps, rock bolts and mesh	0.014	0.023
Rectangular raise, untimbered, rock bolts and mesh	0.013	0.022
Bored raise	0.005	0.008
Beltway	0.014	0.023
TBM drift	0.0045	0.0075
Coal Mines: Rectangular entries, roof-bolted		
Intakes, clean conditions	0.009	0.015
Returns, some irregularities/ sloughing	0.01	0.017
Belt entries	0.005 to 0.011	0.0083 to 0.018
Cribbed entries	0.05 to 0.14	0.08 to 0.23
Shafts¹		
Smooth lined, unobstructed	0.003	0.005
Brick lined, unobstructed	0.004	0.0067
Concrete lined, rope guides, pipe fittings	0.0065	0.0108
Brick lined, rope guides, pipe fittings	0.0075	0.0125
Unlined, well trimmed surface	0.01	0.0167
Unlined, major irregularities removed	0.012	0.020
Unlined, mesh bolted	0.0140	0.023
Tubbing lined, no fittings	0.007 to 0.014	0.0012 to 0.023
Brick lined, two sides buntions	0.018	0.030
Two side buntions, each with a tie girder	0.022	0.037
Longwall faceline with steel conveyor and powered supports²		
Good conditions, smooth wall	0.035	0.058
Typical conditions, coal on conveyor	0.05	0.083
Rough conditions, uneven faceline	0.065	0.108
Ventilation ducting³		
Collapsible fabric ducting (forcing systems only)	0.0037	0.0062
Flexible ducting with fully stretched spiral spring reinforcement	0.011	0.018
Fibreglass	0.0024	0.0040
Spiral wound galvanized steel	0.0021	0.0035

Table 5.1 Average values of friction factors (referred to air density of 1.2 kg/m³) and coefficients of friction (independent of air density).

Notes: 1 See Section 5.4.6. for more accurate assessment of shaft resistance.

2. k factors in excess of 0.015 kg/m³ are likely to be caused by the aerodynamic drag of free standing obstructions in addition to wall drag.
3. These are typical values for new ducting. Manufacturer's test data should be consulted for specific ducting. It is prudent to add about 20 percent to allow for wear and tear.
4. To convert friction factor, k (kg/m³) to imperial units (lb. min²/ft⁴), multiply by 5.39×10^{-7} .

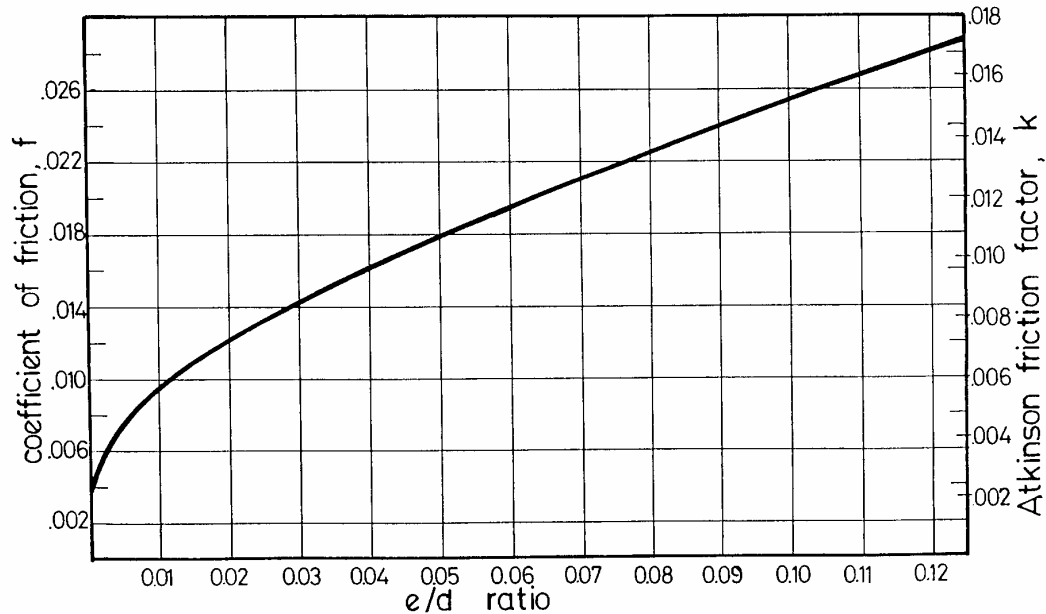


Figure 5.1 The coefficient of friction varies with the height of roughenings divided by the hydraulic mean diameter, e/d .

It should be noted that for regularly spaced projections such as steel rings, the effective friction factor becomes a function of the spacing between those projections. Immediately downstream from each support, wakes of turbulent eddies are produced. If the projections are sufficiently far apart for those vortices to have died out before reaching the next consecutive support, then the projections act in isolation and independently of each other. As the spacing is reduced, the number of projections per unit length of shaft increases. So, also, does the near-wall turbulence, the coefficient of friction, f , and, hence, the friction factor, k . At that specific spacing where the vortices just reach the next projection, the coefficient of friction reaches a maximum. It is this value that is given by the e/d method. For wider spacings, the method will overestimate the coefficient of friction and, hence, errs on the side of safe design.

The maximum coefficient of friction is reached at a spacing/diameter ratio of about 1/8. Decreasing the spacing further will result in "wake interference" - the total degree of turbulence will reduce and so, also, will the coefficient of friction and friction factor. However, in this condition, the diameter available for effective flow is also being reduced towards the inner dimensions of the projections.

5.4. AIRWAY RESISTANCE

The concept of airway resistance is of major importance in subsurface ventilation engineering. The simple form of the square law $p = R Q^2$ (see equation 5.5) shows the resistance to be a constant of proportionality between frictional pressure drop, p , in a given airway and the square of the airflow, Q , passing through it at a specified value of air density. The parabolic form of the square law on a p , Q plot is known as the airway resistance curve. Examples are shown on Figure 5.2.

The cost of passing any given airflow through an airway varies directly with the resistance of that airway. Hence, as the total operating cost of a complete network is the sum of the individual airway costs, it is important that we become familiar with the factors that influence airway resistance. Those factors are examined in the following subsections.

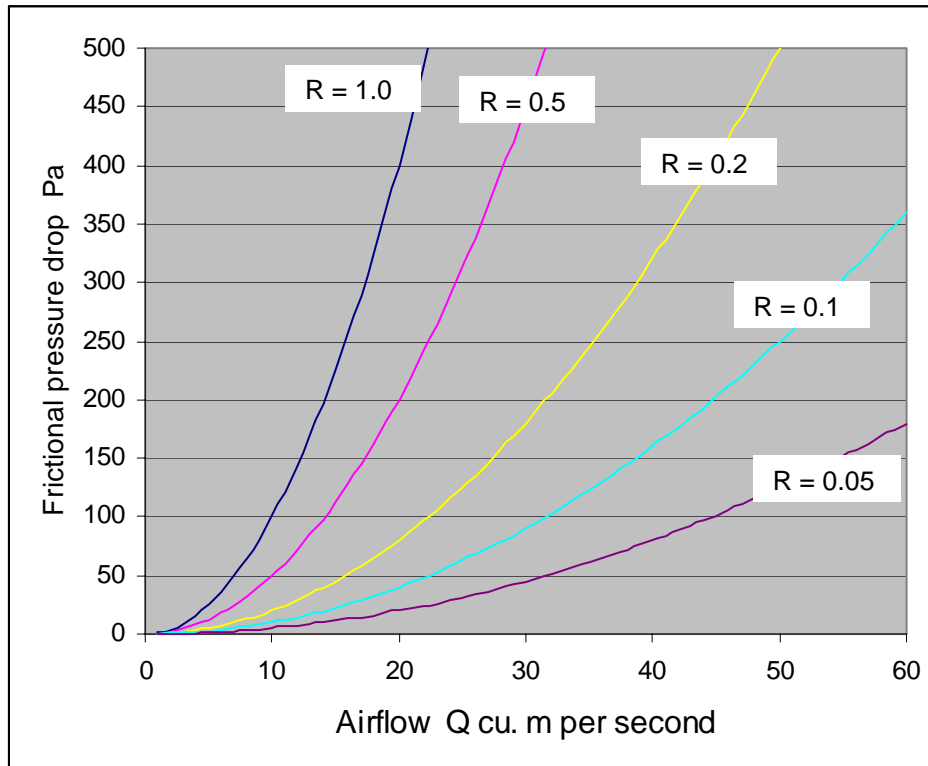


Figure 5.2. Airway resistance curves.

5.4.1. Size of airway

Equation (5.4) showed that for a given length of airway, L , and friction factor, k ,

$$R \propto \frac{per}{A^3} \quad \text{where } \propto \text{ means "proportional to".} \quad (5.12)$$

However, for any given shape of cross-section,

$$per \propto \sqrt{A} \quad (5.13)$$

Substituting for per in equation (5.12) gives

$$R \propto \frac{1}{A^{2.5}} \quad (5.14)$$

or, for a circular airway

$$R \propto \frac{1}{d^5} \quad (5.15)$$

These two latter proportionalities show the tremendous effect of airway size on resistance. Indeed, the cross-sectional area open for flow is the dominant factor in governing airway resistance. Driving an airway at only half its design diameter will result in the resistance being 2^5 or 32 times greater. Hence, for any required airflow, the cost of passing that ventilation through the airway will also increase by a factor of 32. It is clear that when sizing an underground opening that will form part of a main ventilation route, the resistance and ventilation operating costs must be taken into account. Airway sizing is considered further in Chapter 9.

5.4.2. Shape of airway

Again, for any given length of airway, L , and friction factor, k , the proportionality (5.12) can be rewritten as

$$R \propto \frac{\text{per}}{A^{1/2}} \frac{1}{A^{5/2}} \quad (5.16)$$

But for any given shape of cross section, $\frac{\text{per}}{A^{1/2}}$ is a constant (see proportionality (5.13)).

We term this parameter the **shape factor**, SF for the airway. Then if all other parameters remain constant, including cross-sectional area, A , the resistance of an airway varies with respect to its shape factor.

The planar figure having the minimum possible shape factor is a circle.

$$SF(\text{circle}) = \frac{\text{per}}{A^{1/2}} = \frac{\pi d}{d\sqrt{\pi/4}} = 3.5449$$

All other shapes have a greater shape factor than this value. For this reason, shape factors are usually normalized with respect to a circle by dividing by 3.5449 and are then quoted as **relative shape factor** (RSF) as shown in Table 5.2. The further we depart from the ideal circular shape then the greater will be the RSF and, hence, the airway resistance.

Shape of Airway	Relative Shape Factor
Circular	1.00
Arched, upright legs	1.08
Arched, splayed legs	1.09
Square	1.13
Rectangular width:height = 1.5 :1	1.15
2 :1	1.20
3 :1	1.30
4 :1	1.41

Table 5.2. Relative Shape Factors

In addition to demonstrating the effect of airway shape on its resistance to airflow, the purpose of relative shape factors in ventilation planning is now limited to little more than comparing the effect of shape for proposed airways of given cross-sectional area. It may also be useful as a correction factor for older nomograms relating airway resistance, area and k factor which were produced on the basis of a circular cross-section.

5.4.3. Airway lining

Equation (5.4) shows that airway resistance is proportional to the Atkinson friction factor, k , and, hence, is also directly proportional to the more fundamental coefficient of friction, f . The latter depends only upon the roughness of the airway lining for fully developed turbulent flow.

5.4.4. Air density

The Atkinson resistance, R , as used in the square law, $p = RQ^2$ depends upon the friction factor, k . However, equation (5.1) shows that k , itself, depends upon the density of the air. It follows that the Atkinson resistance also varies with the density of the air. On the other hand, the rational resistance, R_r , as used in the rational expression of the square law, $p = R_r \rho Q^2$ (equation (2.50)) is a function of the geometry and lining of the airway only and is independent of air density.

5.4.5. Shock losses

Whenever the airflow is required to change direction, additional vortices will be initiated. The propagation of those large scale eddies consumes mechanical energy (shock losses) and, hence, the resistance of the airway may increase significantly. This occurs at bends, junctions, changes in cross-section, obstructions, regulators and at points of entry or exit from the system.

The effects of shock losses remain the most uncertain of all the factors that affect airway resistance. This is because fairly minor modifications in geometry can cause significant changes in the generation of vortices and, hence, the airway resistance. Analytical techniques may be employed for simple and well defined geometries. For the more complex situations that arise in practice, scale models or computational fluid dynamics (CFD) simulations may be employed to investigate the flow patterns and shock losses.

There are two methods that may be used to assess the additional resistance caused by shock losses.

Shock loss factor

In text books on fluid mechanics, shock losses are often referred to in terms of the head loss or drop in total pressure, p_{shock} caused by the shock loss. This, in turn, is expressed in terms of 'velocity heads'.

$$p_{shock} = X \rho \frac{u^2}{2} \quad \text{Pa} \quad (5.17)$$

where ρ = air density (kg/m^3)
 u = mean velocity of air (m/s) and
 X = shock loss factor (dimensionless)

The shock loss factor can be converted into an Atkinson type of resistance, R_{shock} , by re-writing equation (5.17) as a square law

$$p_{shock} = \frac{X \rho Q^2}{2 A^2} = R_{shock} Q^2 \quad \text{Pa}$$

$$\text{where } R_{shock} = \frac{X \rho}{2 A^2} \quad \frac{\text{Ns}^2}{\text{m}^8} \quad (5.18)$$

If rational resistances (R_i) are employed then the density term is eliminated and the corresponding shock resistance becomes simply

$$R_{t,shock} = \frac{X}{2A^2} \quad \text{m}^{-4} \quad (5.19)$$

The major cause of the additional resistance is the propagation of vortices downstream from the cause of the shock loss. Accordingly, in most cases, it is the downstream branch to which the shock resistance should be allocated. However, for junctions, the cross-sectional area used in equations (5.18) and (5.19) is usually that of the main or common branch through which all of the local air-flow passes.

One of the most comprehensive guides to the selection of X factors is contained within the Fundamentals Handbook of the American Society of Heating, Refrigerating and Air Conditioning Engineers (ASHRAE). Similar design information is produced by corresponding professional societies in other countries.

An appendix is given at the end of this chapter which contains graphs and formulae relating to shock loss factors commonly required in subsurface ventilation engineering.

Equivalent length

Suppose that in a subsurface airway of length L , there is a bend or other cause of a shock loss. The resistance of the airway will be greater than if that same airway contained no shock loss. We can express that additional resistance, R_{shock} , in terms of the length of corresponding straight airway which would have that same value of shock resistance. This "equivalent length" of shock loss, may be incorporated into equation (5.9) to give an Atkinson resistance of

$$R = k(L + L_{eq}) \frac{\text{per}}{A^3} \frac{\rho}{1.2} \quad \frac{\text{Ns}^2}{\text{m}^8} \quad (5.20)$$

The resistance due to the shock loss is

$$R_{shock} = kL_{eq} \frac{\text{per}}{A^3} \frac{\rho}{1.2} \quad \frac{\text{Ns}^2}{\text{m}^8} \quad (5.21)$$

Equation (5.20) gives a convenient and rapid method of incorporating shock losses directly into the calculation of airway resistance.

The relationship between shock loss factor, X , and equivalent length, L_{eq} is obtained by comparing equations (5.18) and (5.21). This gives

$$R_{shock} = \frac{X\rho}{2A^2} = kL_{eq} \frac{\text{per}}{A^3} \frac{\rho}{1.2} \quad \frac{\text{Ns}^2}{\text{m}^8}$$

$$\text{or} \quad L_{eq} = \frac{1.2 X}{2k} \frac{A}{\text{per}} \quad \text{m}$$

The equivalent length can be expressed in terms of hydraulic mean diameters, $d = 4A/\text{per}$, giving

$$L_{eq} = \frac{1.2 X}{8k} d \quad \text{m} \quad (5.22)$$

leading to a very convenient expression for equivalent length,

$$L_{eq} = 0.15 \frac{X}{k} \quad \text{hydraulic mean diameters} \quad (5.23)$$

Reference to Appendix A5 for X factors, together with a knowledge of the expected friction factor and geometry of the planned airway, enables the equivalent length of shock losses to be included in airway resistance calculation sheets, or during data preparation for computer exercises in ventilation planning.

When working on particular projects, the ventilation engineer will soon acquire a knowledge of equivalent lengths for recurring shock losses. For example, a common rule of thumb is to estimate an equivalent length of 20 hydraulic mean diameters for a sharp right angled bend in a clean airway.

Example.

A 4 m by 3 m rectangular tunnel is 450 m long and contains one right-angled bend with a centre-line radius of curvature 2.5 m. The airway is unlined but is in good condition with major irregularities trimmed from the sides. If the tunnel is to pass 60 m³/s of air at a mean density 1.1 kg/m³, calculate the Atkinson and rational resistances at that density and the frictional pressure drop.

Solution.

Let us first state the geometric factors for the airway:

$$\begin{aligned} \text{hydraulic mean diameter,} \quad d &= \frac{4A}{per} = \frac{4 \times 12}{14} = 3.429 \text{ m} \\ \text{height/width ratio,} \quad \frac{H}{W} &= \frac{3}{4} = 0.75 \\ \text{radius of curvature/width ratio} \quad \frac{r}{W} &= \frac{2.5}{4} = 0.625 \end{aligned}$$

From Table 5.1, we estimate that the friction factor for this airway will be $k = 0.012 \text{ kg/m}^3$ at standard density ($f = 0.02$). At $r/W = 0.625$ and $H/W = 0.75$, Figure A5.2 (at end of chapter) gives the shock loss factor for the bend to be 0.75.

We may now calculate the Atkinson resistance at the prevailing air density of 1.1 kg/m³ by two methods:

- (i) Calculate the resistance produced by the shock loss separately:

For the airway, equation (5.9) gives

$$R = kL \frac{per}{A^3} \frac{\rho}{1.2} = \frac{0.012 \times 450 \times 14 \times 1.1}{12^3 \times 1.2} = 0.0401 \quad \frac{\text{Ns}^2}{\text{m}^8} \text{ referred to density of } 1.1 \text{ kg/m}^3$$

For the bend, equation (5.18) gives

$$R_{shock} = \frac{X\rho}{2A^2} = \frac{0.75 \times 1.1}{2 \times 12^2} = 0.00286 \quad \frac{\text{Ns}^2}{\text{m}^8} \text{ referred to density of } 1.1 \text{ kg/m}^3$$

Then for the full airway

$$R = R_{length} + R_{shock}$$

$$0.04010 + 0.00286 = 0.04296 \quad \frac{\text{Ns}^2}{\text{m}^8} \quad \text{referred to density of } 1.1 \text{ kg/m}^3$$

(ii) Using the equivalent length of the bend:

Equation (5.23) gives

$$L_{eq} = 0.15 \frac{X}{k} d = \frac{0.15 \times 0.75 \times 3.429}{0.012} = 32.15 \text{ m}$$

Then, from equation (5.20)

$$R = k(L + L_{eq}) \frac{\text{per}}{A^3} \frac{\rho}{1.2} = 0.012(450 + 32.15) \times \frac{14}{12^3} \times \frac{1.1}{1.2} = 0.04296 \quad \frac{\text{Ns}^2}{\text{m}^8}$$

and agrees with the result given by method (i).

If the coefficient of friction, f , and the rational resistance, R_t , are employed, the density terms become unnecessary and the equivalent length method gives the rational resistance as

$$R_t = f(L + L_{eq}) \frac{\text{per}}{2A^3} = 0.02(450 + 32.15) \times \frac{14}{2 \times 12^3} = 0.03906 \text{ m}^{-4}$$

.The Atkinson resistance at a density of 1.1 kg/m^3 becomes

$$R = \rho R_t = 1.1 \times 0.03906 = 0.04296 \quad \frac{\text{Ns}^2}{\text{m}^8}$$

At an airflow of $60 \text{ m}^3/\text{s}$ and a density of 1.1 kg/m^3 , the frictional pressure drop becomes

$$\rho = R_{1.1} \times Q^2 = 0.04296 \times 60^2 = 155 \text{ Pa}$$

or, using the rational resistance,

$$\rho = \rho R_t Q^2 = 1.1 \times 0.03906 \times 60^2 = 155 \text{ Pa}$$

5.4.6. Mine shafts

In mine ventilation planning exercises, the airways that create the greatest difficulties in survey observations or in assessing predicted resistance are vertical and inclined shafts.

Shafts are quite different in their airflow characteristics to all other subsurface openings, not only because of the higher air velocities that may be involved, but also because of the aerodynamic effects of ropes, guide rails, buntons, pipes, cables, other shaft fittings, the fraction of cross section filled by the largest conveyance (**coefficient of fill, CF**) and the relatively high velocity of shaft conveyances. Despite such difficulties, it is important to achieve acceptable accuracy in the estimation of the resistance of ventilation shafts. In most cases, the total airflow supplied underground must pass through the restricted confines of the shafts. The resistance of shafts is

often greater than the combined effect of the rest of the underground layout. In a deep room and pillar mine, the shafts may account for as much as 90 percent of the mine total resistance. Coupled with a high airflow, Q , the frictional pressure drop, p , will absorb a significant part of the fan total pressure. It follows that the operational cost of airflow (proportional to $p \times Q$) is usually greater in ventilation shafts than in any other airway.

At the stage of conceptual design, shaft resistances are normally estimated with the aid of published lists of friction (k) factors (Table 5.1), that make allowance for shaft fittings. For an advanced design, a more detailed and accurate analysis may be employed. An outline of one such method is given in this section.

The resistance to airflow, R , offered by a mine shaft is comprised of the effects of four identifiable components:

- (a) shaft walls,
- (b) shaft fittings (buntons, pipes etc.),
- (c) conveyances (skips or cages), and
- (d) insets, loading and unloading points.

5.4.6.1. Shaft walls

The component of resistance offered by the shaft walls, R_{tw} , may be determined from equations (5.9 or 2.51) and using a friction factor, k , or coefficient of friction, f , determined by one of the methods described in Section 5.3. Experience has shown that the relevant values in Table 5.1 are preferred either for smooth-lined walls or where the surface irregularities are randomly dispersed. On the other hand, where projections from the walls are of known size as, for example, in the case of tubbed lining, then the e/d method gives satisfactory results.

5.4.6.2. Shaft fittings

It is the permanent equipment in a shaft, particularly cross-members (**buntons**) that account, more than any other factor, for the large variation in k values reported for mine shafts.

Longitudinal Fittings

These include ropes, guide rails, pipes and cables, situated longitudinally in the shaft and parallel to the direction of airflow. Such fittings add very little to the coefficient of friction and, indeed, may help to reduce swirl. If no correction is made for longitudinal fittings in the calculation of cross-sectional area then their effect may be approximated during preliminary design by increasing the k factor (see Table 5.1). However, measurements on model shafts have actually shown a decrease in the true coefficient of friction when guide rails and pipes are added. It is, therefore, better to account for longitudinal fittings simply by subtracting their cross-sectional area from the full shaft area to give the "free area" available for airflow. Similarly, the rubbing surface is calculated from the sum of the perimeters of the shaft and the longitudinal fittings.

Buntons

The term "**bunton**" is used here to mean any cross member in the shaft located perpendicular to the direction of airflow. The usual purpose of buntons is to provide support for longitudinal fittings. The resistance offered by buntons is often dominant.

Form Drag and Resistance of Buntons

While the resistance offered by the shaft walls and longitudinal fittings arises from skin friction (shear) drag, through boundary layers close to the surface, the kinetic energy of the air causes the pressure on the projected area of cross-members facing the airflow to be higher than that on the downstream surfaces. This produces an inertial or "form" drag on the bunton. Furthermore, the breakaway of boundary layers from the sides of trailing edges causes a series of vortices to be propagated downstream from the bunton. The mechanical energy dissipated in the formation and maintenance of these vortices is reflected by a significant increase in the shaft resistance.

The drag force on a buntun is given by the expression:

$$Drag = C_D A_b \frac{\rho u^2}{2} \quad \text{N} \quad (5.24)$$

where C_D = coefficient of drag (dimensionless) depending upon the shape of the buntun,
 A_b = frontal or projected area facing into the airflow (m^2),
 u = velocity of approaching airstream (m/s), and
 ρ = density of air (kg/m^3).

The frictional pressure drop caused by the buntun is:

$$p = \frac{Drag}{A} = C_D \frac{A_b}{A} \frac{u^2}{2} \rho \quad \frac{\text{N}}{\text{m}^2} \quad (5.25)$$

where A = cross-sectional area available for free flow (m^2).

However, the frictional pressure drop caused by the buntuns is also given by the square law:

$$p = R_b Q^2 = R_{tb} \rho Q^2 = R_{tb} \rho u^2 A^2 \quad \frac{\text{N}}{\text{m}^2} \quad (5.26)$$

where R_b = Atkinson resistance offered by the buntun (Ns^2/m^8),
 R_{tb} = rational resistance of the buntun (m^{-4}), and
 Q = airflow (m^3/s).

Equating (5.25) and (5.26) gives:

$$R_{tb} = C_D \frac{A_b}{2A^3} \quad \text{m}^{-4}$$

If there are n buntuns in the shaft and they are sufficiently widely spaced to be independent of each other, then the combined resistance of the buntuns becomes:

$$R_{tn} = n R_{tb} = n C_D \frac{A_b}{2A^3} \quad \text{m}^{-4}$$

It is, however, more convenient to consider the **spacing**, S , between buntuns:

$$S = \frac{L}{n} \quad (5.29)$$

where L = length of shaft (m), giving,

$$R_{tn} = \frac{L}{S} C_D \frac{A_b}{2A^3} \quad \text{m}^{-4} \quad (5.30)$$

The effect of the buntuns can also be expressed as an additional coefficient of friction, f , or friction factor, $k_b = 0.6f_b$, since

$$R_{tn} = \frac{f_b L_{per}}{2A^3} \quad m^{-4} \quad [\text{from equation (2.51)}] \quad (5.31)$$

Equations (5.30) and (5.31) give:

$$f_b = \frac{C_D A_b}{S \times per} \quad (\text{dimensionless}) \quad (5.32)$$

Interference factor

The preceding subsection assumed that the buntons were independent of each other, i.e. that each wake of turbulent eddies caused by a buntion dies out before reaching the next buntion. Unless the buntions are streamlined or are far apart, this is unlikely to be the case in practice. Furthermore, the drag force may be somewhat less than linear with respect to the number of buntions in a given cross-section, or to A_b at connection points between the buntions and the shaft walls or guide rails. For these reasons, an 'interference factor', F , is introduced into equation 5.30 (Bromilow) giving a reduced value of resistance for buntions:

$$R_{tn} = \frac{L}{S} C_D \frac{A_b}{2A^3} F \quad m^{-4} \quad (5.33)$$

For simple wake interference, F is a function of the spacing ratio Δ ,

$$\Delta = \frac{S}{W} \quad (\text{dimensionless}) \quad (5.34)$$

where W = width of the buntion.

However, because of the difficulties involved in quantifying the F function analytically, and in evaluating the other factors mentioned above, the relationship has been determined empirically, (Bromilow) giving

$$F = 0.0035 \Delta + 0.44 \quad (5.35)$$

for a range of Δ from 10 to 40.

Combining equations (5.33), (5.34) and (5.35) gives:

$$R_{tn} = \frac{L}{S} C_D \frac{A_b}{2A^3} \left[0.0035 \frac{S}{W} + 0.44 \right] \quad m^{-4} \quad (5.36)$$

If expressed as a partial coefficient of friction, this becomes:

$$f_b = C_D \frac{A_b}{S \times per} \left[0.0035 \frac{S}{W} + 0.44 \right] \quad m^{-4} \quad (5.37)$$

Values of the coefficient of drag, C_D , measured for buntions in shafts are invariably much higher than those reported for freestanding aerofoil sections. Figure 5.3 indicates **drag coefficients** for the shapes normally used for buntions.















	2.75	direction of airflow ↓		1.82
	2.05			1.45
	2.05			1.98
	1.55			1.98
	2.00			1.40
	2.00			1.20
	1.55			1.06

Figure 5.3. Coefficients of drag, C_D , for buntions in a shaft.
(from information collated by Bromilow)

5.4.6.3. Conveyances

Resistance of a Stationary Conveyance

The main factors that govern the resistance of a stationary cage or skip in a mine shaft are:

- (a) The percentage of the free area in the cross section of the shaft occupied by the conveyance.
This is sometimes termed the “**coefficient of fill**”, C_F .
- b) The area and shape of a plan-view of the conveyance and, to a lesser degree, its vertical height.

The parameters of secondary practical importance include the shape of the shaft and the extent to which the cage is totally enclosed.

An analysis of the resistances offered by cages or skips commences by considering the conveyance to be stationary within the shaft with a free (approaching) air velocity of u_a (m/s). The conveyance is treated as an obstruction giving rise to a frictional pressure drop (shock loss) of X velocity heads:

$$p_c = X \frac{\rho u_a^2}{2} \quad \frac{\text{N}}{\text{m}^2} \quad (5.38)$$

where p_c = frictional pressure drop due to the conveyance (N/m^2) and
 u_a = velocity of the approaching airstream (m/s)
 ρ = air density (kg/m^3)

The effective rational resistance of the stationary cage, R_{tc} , can be expressed in terms of X from equation (5.19)

$$R_{tc} = \frac{X}{2A^2} \quad \text{m}^{-4} \quad (5.39)$$

where the free shaft area, A , is measured in square metres. The problem now becomes one of evaluating X .

One of the most comprehensive experimental studies on cage resistance was carried out by A. Stevenson in 1956. This involved the construction of model cages and measuring the pressure drops across them at varying airflows in a circular wind tunnel. From the results produced in this work, Figure 5.4 has been constructed.

All of the curves on Figure 5.4 refer to a cage whose length, L , is 1.5 times the width, W . A multiplying correction factor may be applied to the value of X for other plan dimensions. Hence, for a cage that is square in plan, $L/W = 1$ and the correction nomogram given also on Figure 5.4 shows that X should be increased by 12 per cent.

The shape of the curves indicates the dominant effect of the coefficient of fill, increasing rapidly after the cage occupies more than 30 per cent of the shaft cross section. The major cause of the shock loss is form drag and the resulting turbulent wake. Skin friction effects are relatively small. Hence, so also is the influence of the vertical height of the cage.

The curves refer to cages with covered roof, floor and sides, but open ends. In general, the effect of covering the ends is to reduce the shock loss. For totally enclosed skips, the value of X given by the curves should be reduced by some 15 per cent.

Dynamic Effects of a Moving Conveyance

In addition to the presence of a conveyance in a shaft, its motion will also influence the frictional pressure drop and effective resistance of the shaft. Furthermore, in systems in which two conveyances pass in the shaft, their stability of motion will depend upon the velocities of the airflow and the conveyances, the positions of the conveyances within the shaft cross section, their shape, and the coefficient of fill.

When two synchronized skips or cages pass, they will normally do so at mid-shaft and at the maximum hoist velocity. The coefficient of fill will, momentarily, be increased (doubled if the two cages have the same plan area). There will be a very short-lived peak of pressure drop across the passing point. However, the inertia of the columns of air above and below that point, coupled with the compressibility of the air, dampen out that peak quickly and effectively.

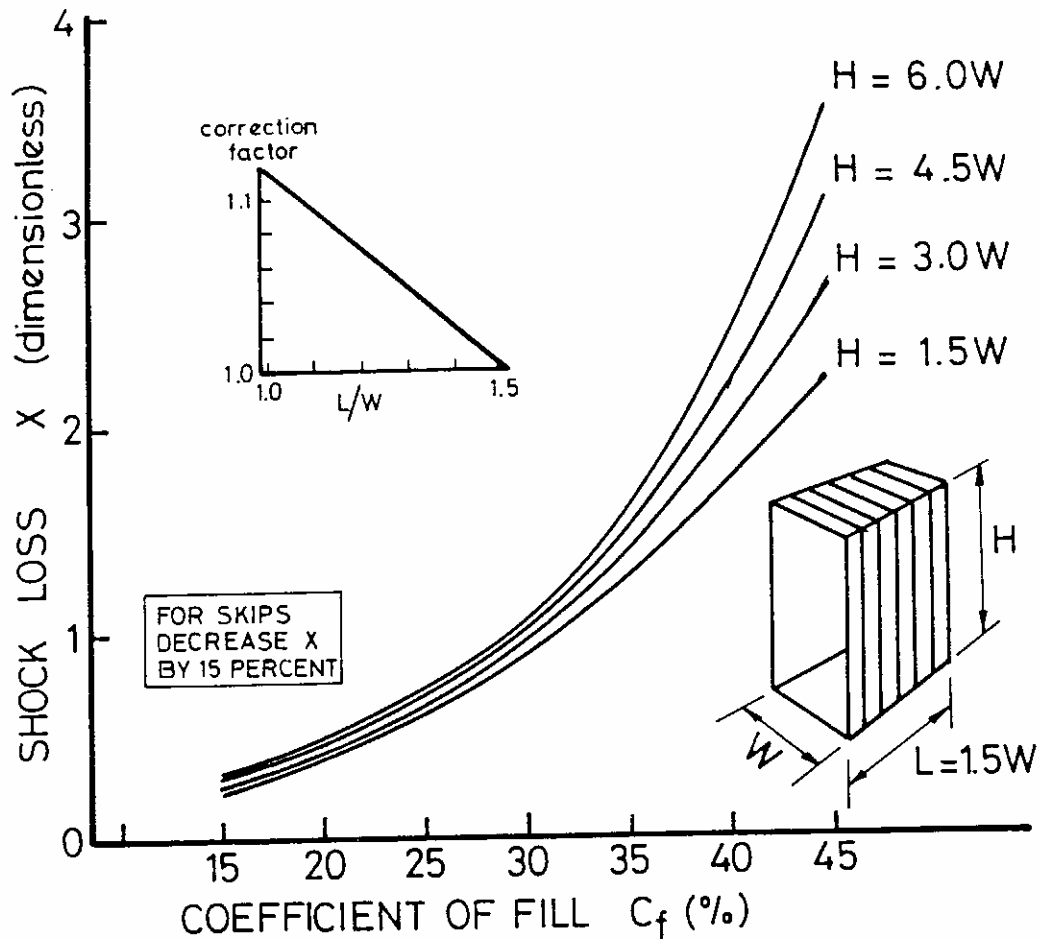


Figure 5.4. Shock loss factors for a conveyance in a mine shaft.

More important is the effect of passing on the **stability of the conveyances** themselves. They pass at a relative velocity of twice maximum hoisting speed, close to each other and usually without any continuous intervening barrier. Two mechanisms then influence the stability of the cages. First, thin boundary layers of air exist on the surfaces of each conveyance and moving at the same velocity. Hence, there will be a very steep velocity gradient in the space between passing conveyances. Shear resistance (skin friction drag) will apply a braking action on the inner sides of the conveyances and produce a tendency for the skips or cages to turn in towards each other. Secondly, the mean absolute velocity in the gap between the passing cages is unlikely to equal that surrounding the rest of the cages. There exists a variation in static pressure and, hence, an applied force on the four sides of each conveyance (the venturi effect). This again, will result in a tendency for lateral movement.

Passengers in conveyances will be conscious not only of the pressure pulse when the cages pass, but also of the lateral vibrations caused by the **aerodynamic effects**. The sideways motion can be controlled in practice by the use of rigid guide rails or, if rope guides are employed, by using a tensioned tail rope beneath the cages passing around a shaft-bottom pulley.

The aerodynamics of moving conveyances are more complex than for free bodies because of the proximity of the shaft walls. The total drag on the conveyance will reach a maximum when the vehicle is moving at its highest speed against the airflow. The apparent frictional pressure drop and resistance of the shaft will also vary and reach a maximum value at this same time. The opposite is also true. The drag, apparent frictional pressure drop, and apparent resistance of the shaft will reach a minimum when the conveyance is moving at maximum speed in the same direction as the airflow. The amplitude of the cyclic variation depends upon the resistance of the stationary cage (which in turn varies with the coefficient of fill and other factors as described in the previous subsection), and the respective velocities of the airflow and the cage.

In the following analysis, expressions are derived to approximate the effective pressure drop and effective resistance of a moving conveyance.

Consider a conveyance moving at its maximum velocity u_c against an approaching airflow of velocity u_a (Figure 5.5).

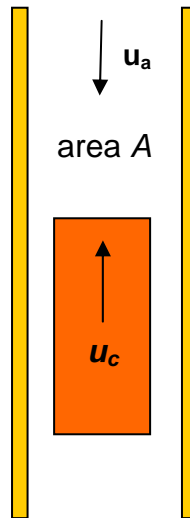


Figure 5.5. Moving conveyance in a shaft

If the rational resistance of the cage, when stationary, is R_{tc} (determined using the methodology of the previous section) then the corresponding pressure drop caused by the stationary cage will be:

$$p_c = R_{tc} \rho Q^2 = R_{tc} \rho u_a^2 A^2 \quad \frac{\text{N}}{\text{m}^2} \quad (5.40)$$

Now suppose that the cage were stationary in the shaft when the approaching airflow has a velocity of u_c . The corresponding pressure drop would be:

$$p'_c = \rho R_{tc} u_c^2 A^2 \quad \frac{\text{N}}{\text{m}^2} \quad (5.41)$$

This latter expression approximates the additional pressure drop caused by movement of the conveyance.

Adding equations (5.40) and (5.41) gives the maximum pressure drop across the moving conveyance.

$$\begin{aligned}
 p_{c\max} &= p_c + p'_c = \rho R_{tc} (u_a^2 + u_c^2) A^2 \\
 &= \rho R_{tc} u_a^2 A^2 \left[1 + \frac{u_c^2}{u_a^2} \right] \quad (5.42)
 \end{aligned}$$

$$= p_c \left[1 + \frac{u_c^2}{u_a^2} \right] \quad \frac{\text{N}}{\text{m}^2} \quad (5.43)$$

Similarly, the minimum pressure drop, occurring when the cage and airflow are moving in the same direction is given by:

$$p_{c\min} = p_c \left[1 - \frac{u_c^2}{u_a^2} \right] \quad \frac{\text{N}}{\text{m}^2} \quad (5.44)$$

Hence, the cyclic variation in frictional pressure across the shaft is:

$$\pm p_c u_c^2 / u_a^2 \quad \text{N/m}^2 \quad (5.45)$$

This variation occurs much more slowly than the pressure pulse caused by passing conveyances. The pressure drop due to a conveyance will:

- i. rise to $p_{c\max}$ as the conveyance accelerates to its highest speed against the airflow;
- ii. fall to p_c when the conveyance decelerates to rest;
- iii. drop further to $p_{c\min}$ as the conveyance accelerates to full speed in the same direction as the airflow; and again
- iv. rise to p_c when the cage comes to rest.

If two cages of equal dimensions are travelling in synchronization within the shaft, but in opposite directions, then the effect cancels out. Otherwise, the cyclic variation in pressure may be measurable within the ventilation network and, particularly, at locations close to the shaft. This is most likely to occur in a single conveyance shaft with a large coefficient of fill. A further effect will be to impose a fluctuating load on any fans that influence the airflow in that shaft.

The corresponding range of effective resistance for a conveyance moving against the airflow may also be determined from equation (5.42).

$$p_{c\max} = \rho R_{tc} (u_a^2 + u_c^2) A^2$$

However, if the effective resistance of the conveyance moving against the airflow is $R_{tc\max}$ then:

$$p_{c\max} = \rho R_{tc\max} Q^2 = \rho R_{tc\max} u_a^2 A^2 \quad (5.46)$$

Equating these two relationships gives:

$$R_{tc\max} = R_{tc} \left[1 + \frac{u_c^2}{u_a^2} \right] \quad \text{m}^{-4} \quad (5.47)$$

Similarly, when the airflow and conveyance are moving the same direction:

$$R_{tc\max} = R_{tc} \left[1 - \frac{u_c^2}{u_a^2} \right] \quad \text{m}^{-4} \quad (5.48)$$

It may be noted from equations (5.44) and (5.48) that when the conveyance is moving more rapidly than the airflow ($u_c > u_a$), and in the same direction, both the effective pressure drop and effective resistance of the conveyance become negative. In this situation, the conveyance is assisting rather than impeding the ventilation. *It should be noted that the approximation inherent in this derivation leads to unacceptable accuracy at low values of u_a .*

5.4.6.4. Entry and exit losses

In badly designed installations or for shallow shafts, the shock losses that occur at shaft stations and points of air entry and exit may be greater than those due to the shaft itself. Such losses are, again, normally quoted on the basis of X velocity heads, using the velocity in the free area of the shaft. The shock losses at shaft stations may be converted into a rational resistance:

$$R_{t,shock} = \frac{X}{2A^2} \quad (5.49)$$

The shock loss factors, X , may be estimated from the guidelines given in the Appendix to this chapter.

5.4.6.5. Total shaft resistance

Although interference will exist between components of shaft resistance, it is conservative to assume that they are additive. Hence, the rational resistance for the total shaft is:

$$R_t = R_{tw} + R_{tn} + R_{tc} \left\{ 1 \pm \frac{u_c^2}{u_a^2} \right\} + R_{t,shock} \quad \text{m}^{-4} \quad (5.50)$$

walls fittings conveyance(s) entries/exits

This may be converted to an Atkinson resistance, R , referred to any given air density in the usual manner:

$$R = R_t \rho \quad \frac{\text{Ns}^2}{\text{m}^8}$$

Having determined the total resistance of a shaft, the corresponding effective coefficient of friction, f , or friction factor k (at any given value of air density) may be determined

$$f = 2R_t \frac{A^3}{L_{per}} \quad (\text{dimensionless}) \quad (5.51)$$

and $k = \rho \frac{f}{2} \quad \text{kg/m}^3$

5.4.6.6. Methods of reducing shaft resistance

Shaft walls

A major shaft utilized for both hoisting and ventilation must often serve for the complete life of the underground facility. Large savings in ventilation costs can be achieved by designing the shaft for low aerodynamic resistance.

Modern concrete **lining of shafts** closely approaches an aerodynamically smooth surface and little will be gained by giving a specially smooth finish to these walls. However, if tubing lining is employed, the wall resistance will increase by a factor of two or more.

Buntons

A great deal can be done to reduce the resistance of buntons or other cross members in a mine shaft. First, thought should be given to eliminating them or reducing their number in the design. Second, the shape of the buntons should be considered. An aerofoil section skin constructed around a girder is the ideal configuration. However, Figure 5.3 shows that the coefficient of drag can be reduced considerably by such relatively simple measures as attaching a rounded cap to the upstream face of the bunton. A circular cross section has a coefficient of drag some 60 percent of that for a square.

Longitudinal Fittings

Ladderways and platforms are common in the shafts of metal mines. These produce high shock losses and should be avoided in main ventilation shafts. If it is necessary to include such encumbrances, then it is preferable to compartmentalize them behind a smooth wall partition. Ropes, guides, pipes, and cables reduce the free area available for airflow and should be taken into account in sizing the shaft; however, they have little effect on the true coefficient of friction.

Cages and Skips

Figure 5.4 shows that the resistance of a cage or skip increases rapidly when it occupies more than 30 per cent of the shaft cross section. The plan area of a conveyance should be as small as possible, consistent with its required hoisting duties. Furthermore, a long narrow cage or skip offers less resistance than a square cage of the same plan area. Table 5.3 shows the effect of attaching streamlined fairings to the upstream and downstream ends of a conveyance.

No. of Cage Decks	Shape of Fairing	Cage Without Fairings	Upstream Fairing Only	Downstream Fairing Only	Fairings at Both Ends
1	Aerofoil	2.05	1.53	1.56	0.95
4	Aerofoil	3.16	2.46	2.71	2.11
1	Triangular with ends filled	2.13	1.58	1.59	1.13
1	Triangular without ends filled	2.13	1.65	1.79	1.48
4	Triangular with ends filled	3.29	2.96	2.92	2.70
4	Triangular without ends filled	3.29	2.86	3.18	2.80

Table 5.3 Shock loss factor (X) for a caged fitted with end fairings in a shaft (after Stevenson).

This table was derived from a model of a shaft where the coefficient of fill for the cage was 43.5 per cent. The efficiency of such fairings is reduced by proximity to the shaft wall or to another cage. There are considerable practical disadvantages to cage fairings. They interfere with cage suspension gear and balance ropes which must be readily accessible for inspection and maintenance. Furthermore, they must be removed easily for inspection and maintenance personnel to travel on top of the cage or for transportation of long items of equipment. Another problem is that streamlining on cages exacerbates the venturi effect when two conveyances pass. For these reasons, fairings are seldom employed in practice. However, the simple expedient of rounding the edges and corners of a conveyance to a radius of about 30 cm is beneficial.

Intersections and loading/unloading stations

For shafts that are used for both hoisting and ventilation it is preferable to employ **air bypasses** at main loading and unloading stations. At shaft bottom stations, the main airstream may be diverted into one (or two) airways intersecting the shaft some 10 to 20m above or below the loading station. Similarly, at the shaft top, the main airflow should enter or exit the shaft 10 to 20m below the surface loading point. If a main fan is to be employed on the shaft then it will be situated in the bypass (fan drift) and an airlock becomes necessary at the shaft top. If no main fan is required at that location then a high-volume, low-pressure fan may be utilized simply to overcome the resistance of the fan drift and to ensure that the shaft top remains free from high air velocities. The advantages of such air bypasses are:

- they avoid personnel being exposed to high air velocities and turbulence at loading/unloading points.
- they reduce dust problems in rock-hoisting shafts.
- they eliminate the high shock losses that occur when skips or conveyances are stationary at a heavily ventilated inset.

At the intersections between shafts and fan drifts or other main airways, the entrance should be rounded and sharp corners avoided. If air bypasses are not employed then the shaft should be enlarged and/or the underground inset heightened to ensure that there remains adequate free-flow area with a conveyance stationary at that location.

5.5. AIR POWER

In Chapters 2 and 3, we introduced the concept of mechanical energy within an airstream being downgraded to the less useful heat energy by frictional effects. We quantified this as the term F , the work done against friction in terms of Joules per kilogram of air. In Section 3.4.2. we also showed that a measurable consequence of F was a frictional pressure drop, p , where

$$F = \frac{p}{\rho} \quad \frac{\text{J}}{\text{kg}} \quad (3.52)$$

and $\rho = \text{mean density of the air}$

The airpower of a moving airstream is a measure of its mechanical energy content. Airpower may be supplied to an airflow by a fan or other ventilating motivator but will diminish when the airflow suffers a reduction in mechanical energy through the frictional effects of viscous action and turbulence. The airpower loss, APL , may be quantified as

$$APL = FM \quad \frac{\text{J kg}}{\text{kg s}} \quad \text{or } W \quad (5.53)$$

where $M = Q\rho$ (kg/s) (mass flowrate)

Then $APL = FQ\rho$

But $F = p/\rho$ from equation (5.52), giving

$$APL = pQ \quad W \quad (5.54)$$

As both p and Q are measurable parameters, this gives a simple and very useful way of expressing how much ventilating power is dissipated in a given airway.

Substituting for p from the rational form of the square law

$$p = R_t \rho Q^2 \quad (\text{equation (2.50)})$$

$$\text{gives } APL = R_t \rho Q^3 \quad W \quad (5.55)$$

This revealing relationship highlights the fact that the power dissipated in any given airway and, hence, the cost of ventilating that airway depend upon

- (a) the geometry and roughness of the airway
- (b) the prevailing mean air density and
- (c) the cube of the airflow.

The rate at which mechanical energy is delivered to an airstream by a fan impeller may also be written as the approximation

$$\text{Air power delivered} = p_{ft} Q \quad W \quad (5.56)$$

where p_{ft} is the increase in total pressure across the fan. For fan pressures exceeding 2.5 kPa, the compressibility of the air should be taken into account. This will be examined in more detail in Chapter 10.

Bibliography

ASHRAE Handbook (Fundamentals) (1985) **American Society of Heating, Refrigerating and Air Conditioning Engineers** 1791 Tullie Circle, N.E., Atlanta, GA 30329.

Atkinson, J.J. (1854) On the Theory of the Ventilation of Mines. **Trans. N. of England, Inst. of Mining Engineers. Vol. 3 PP. 73-222.**

Bromilow, J.G. (1960) The Estimation and the Reduction of the Aerodynamic Resistance of Mine Shafts. **Trans. Inst. of Mining Engineers. Vol. 119 pp. 449-465.**

McElroy, G.E. (1935) Engineering Factors in the Ventilation of Metal Mines. **U.S. Bureau of Mines Bull. No. 385.**

McPherson, M.J. (1988) An Analysis of the Resistance and Airflow Characteristics of Mine Shafts. **4th International Mine Ventilation Congress, Brisbane, Australia.**

Prosser, B.S. and Wallace, K.G. (1999) Practical Values of Friction Factors. 8th U.S. Mine Ventilation Symposium. Rolla, Missouri, pp. 691-696.

Stevenson, A (1956) Mine Ventilation Investigations: (c) Shaft pressure losses due to cages. **Thesis, Royal College of Science and Technology, Glasgow, Scotland.**

Appendix A5

Shock loss factors for airways and ducts.

Shock loss (X) factors may be defined as the number of velocity heads that give the frictional pressure loss due to turbulence at any bend, variation in cross sectional area or any other configuration that causes a change in the general direction of airflow.

$$p_{shock} = X \rho \frac{u^2}{2} \quad \text{Pa} \quad \text{[equation (5.17)]}$$

where ρ = air density (kg/m³) and
 u = air velocity (m/s)

The shock loss factor is also related to an equivalent Atkinson resistance.

$$R_{shock} = \frac{X \rho}{2 A^2} \quad \frac{\text{Ns}^2}{\text{m}^8} \quad \text{[equation (5.18)]}$$

where A = cross-sectional area of opening (m²)

or rational resistance

$$R_{t,shock} = \frac{X}{2 A^2} \quad \text{m}^{-4} \quad \text{[equation (5.19)]}$$

This appendix enables the X factor to be estimated for the more common configurations that occur in subsurface environmental engineering. However, it should be borne in mind that small variations in geometry can cause significant changes in the X factor. Hence, the values given in this appendix should be regarded as approximations.

For a comprehensive range of shock loss factors, reference may be made to the Fundamentals Handbook produced by the American Society of Heating, Refrigerating and Air-Conditioning Engineers (ASHRAE).

Throughout this appendix, any subscript given to X refers to the branch in which the shock loss or equivalent resistance should be applied. However, in the case of branching flows, the conversion to an equivalent resistance $R_{sh} = X \rho / (2A^2)$ should employ the cross sectional area of the main or common branch. Unsubscripted X factors refer to the downstream airway.

A.5.1 Bends

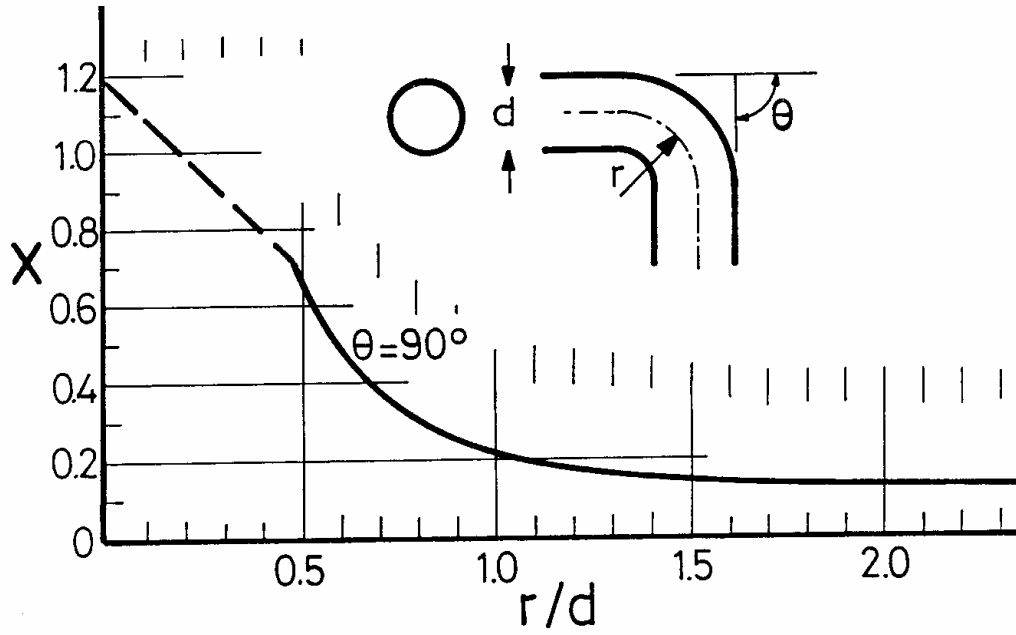


Figure A5.1. Shock loss factor for right angled bends of circular cross section

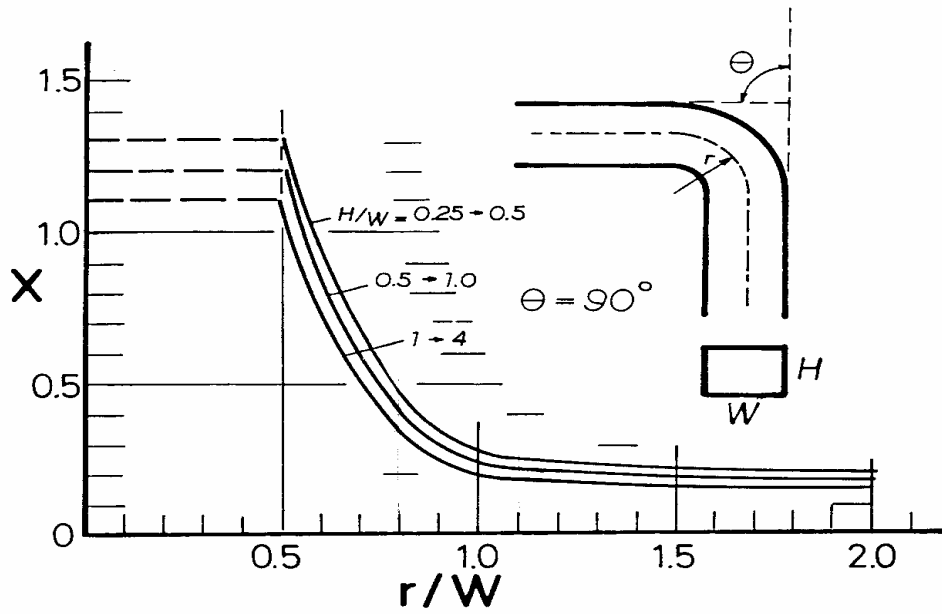


Figure A5.2. Shock loss factor for right angled bends of rectangular cross section.

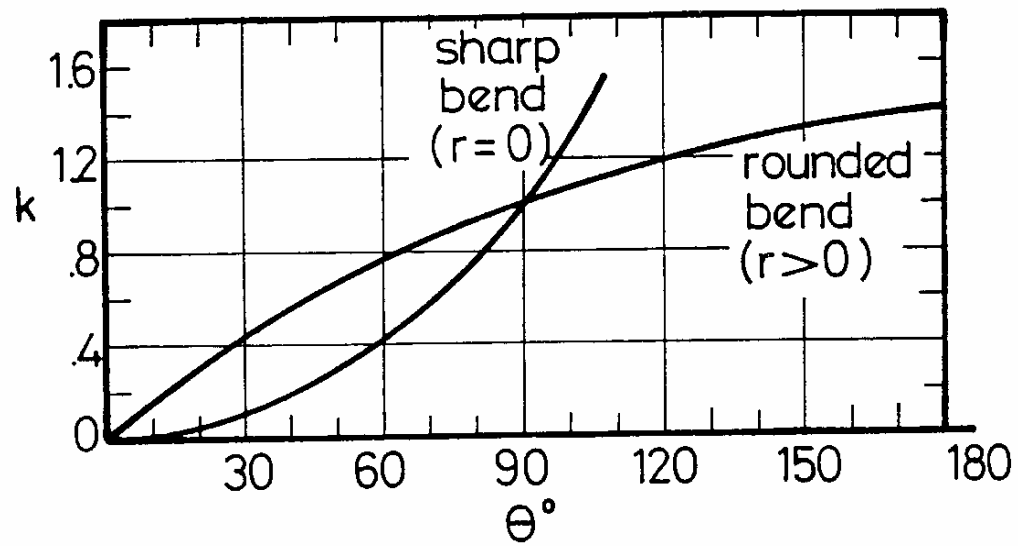


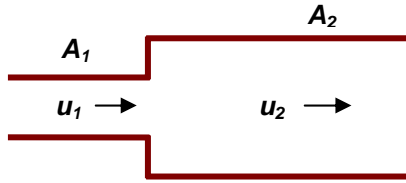
Figure A5.3. Correction to shock loss factor for bends of angles other than 90°

$$X_\theta = X_{90} \times k$$

Applicable for both round and rectangular cross sections

A5.2 Changes in cross-section

(a) Sudden enlargement:

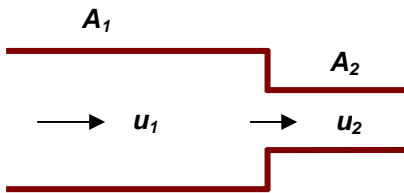


A = Cross sectional area
 u = Air velocity

$$X_2 = \left[\frac{A_2}{A_1} - 1 \right]^2 \quad \text{where } X_2 \text{ is referred to Section 2}$$

$$X_1 = \left[1 - \frac{A_1}{A_2} \right]^2 \quad \text{where } X_1 \text{ is referred to Section 1. (Useful if } A_2 \text{ is very large)}$$

(b) Sudden contraction:

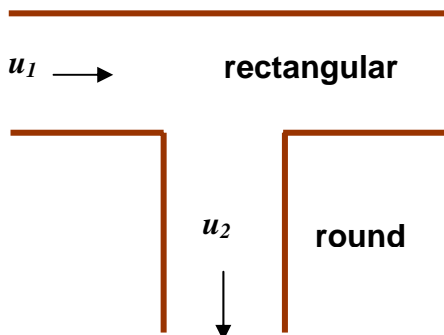


$$X_2 = 0.5 \left[1 - \frac{A_2}{A_1} \right]^2$$

A5.3 Junctions

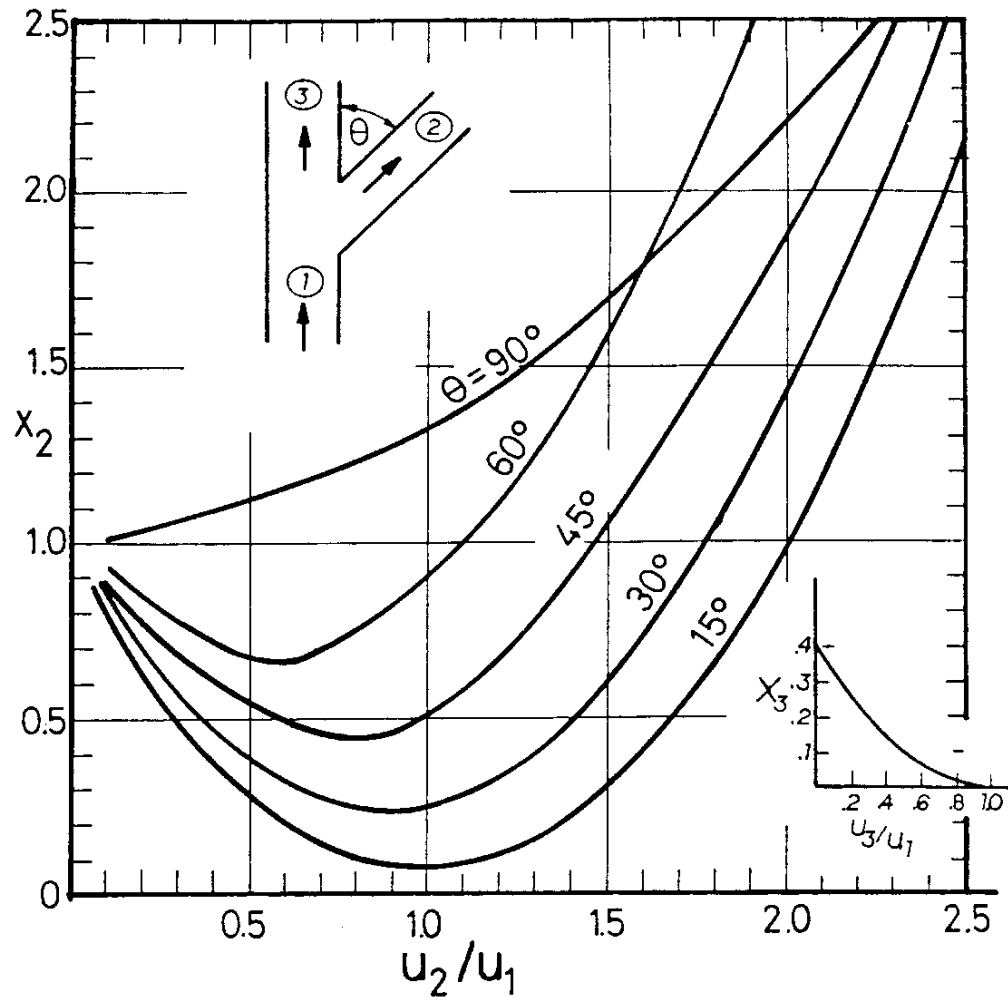
The formulae and graphs for shock loss factors at junctions necessarily involve the branch velocities or airflows, neither of which may be known at the early stages of subsurface ventilation planning. This requires that initial estimates of these values must be made by the planning engineer. Should the ensuing network analysis show that those estimates were grossly in error then the X values and corresponding branch resistances should be re-evaluated and the analysis run again.

(a) Rectangular main to diverging circular branch (e.g. raises, winzes)



$$X_2 = 0.5 \left[1 + 2.5 \frac{u_2}{u_1} \right]$$

$$R_{2,shock} = \frac{X_2 \rho}{2 A_1^2} \quad \frac{Ns^2}{m^8}$$



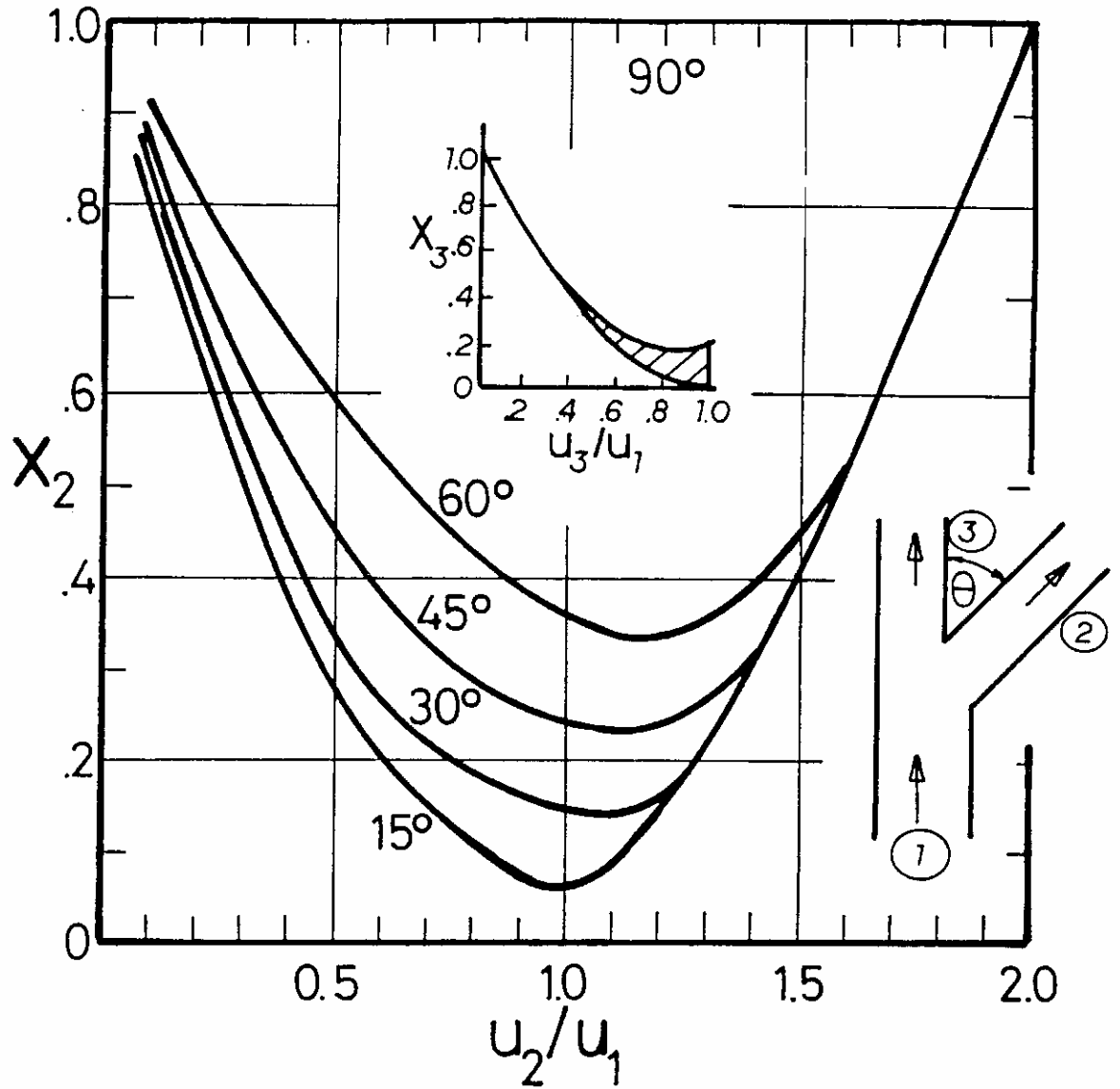
(b) Figure A5.4. Circular main to circular branch (e.g. fan drift from an exhaust shaft).

A = cross-sectional area (m^2): u = air velocity (m/s):

Condition: $A_1 = A_3$

$$R_{2,shock} = \frac{X_2 \rho}{2 A_1^2} \quad \frac{\text{Ns}^2}{\text{m}^8}$$

$$R_{3,shock} = \frac{X_3 \rho}{2 A_1^2} \quad \frac{\text{Ns}^2}{\text{m}^8}$$

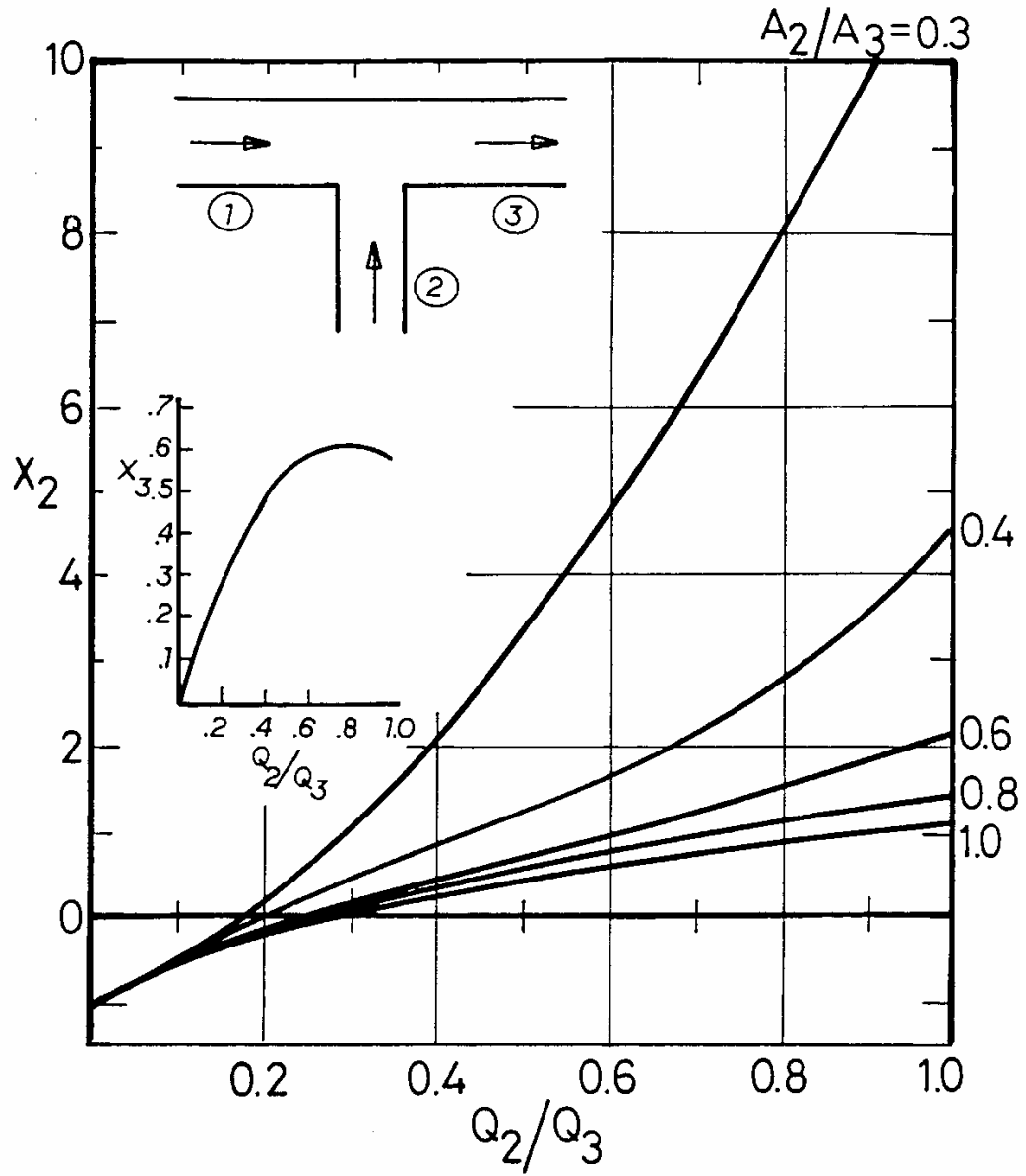


(c) Figure A5.5. Rectangular main to diverging rectangular branch

Condition: $A_1 = A_2 + A_3$

$$R_{2,shock} = \frac{X_2 \rho}{2A_1^2} \quad \frac{Ns^2}{m^8}$$

$$R_{3,shock} = \frac{X_3 \rho}{2A_1^2} \quad \frac{Ns^2}{m^8}$$



(d) Figure A5.6. Circular branch converging into circular main

A = cross sectional area (m^2):

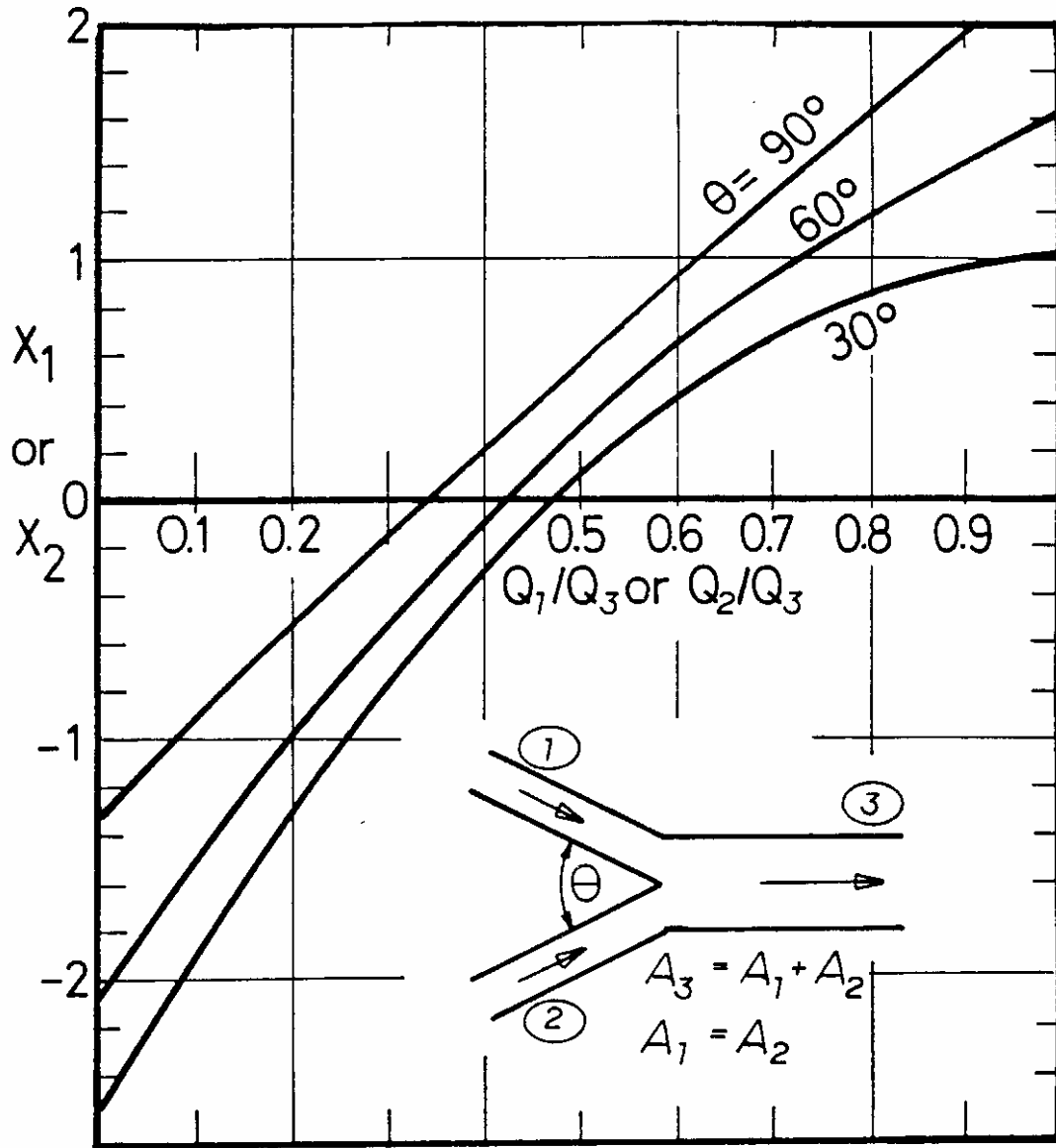
Q = airflow (m^3/s)

$$R_{2,shock} = \frac{X_2 \rho}{2 A_1^2}$$

$$\frac{Ns^2}{m^8}$$

$$R_{3,shock} = \frac{X_3 \rho}{2 A_1^2}$$

$$\frac{Ns^2}{m^8}$$



(e) Figure A5.7. Converging Y junction, applicable to both rectangular and circular cross-sections.
 (For a diverging Y junction, use the branch data from Figure A5.5.)

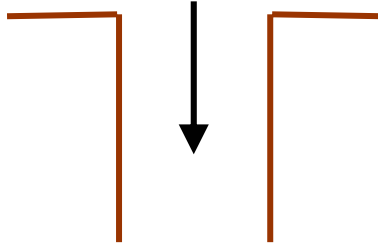
Conditions: $A_3 = A_1 + A_2$
 $A_1 = A_2$

$$R_{1,shock} = \frac{X_1 \rho}{2 A_3^2} \quad \frac{Ns^2}{m^8}$$

$$R_{2,shock} = \frac{X_2 \rho}{2 A_3^2} \quad \frac{Ns^2}{m^8}$$

A5.4 Entry and Exit

(a) Sharp-edged entry:



$$X = 0.5$$

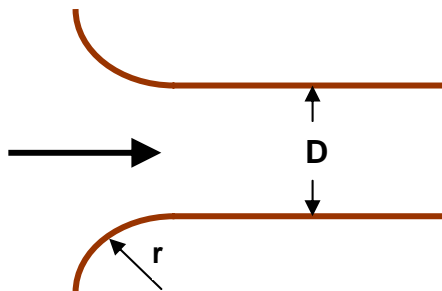
(b) Entrance to duct or pipe:



$$X = 1.0$$

(This is a real loss caused by turbulence at the inlet and should not be confused with the conversion of static pressure to velocity pressure)

(c) Bell-mouth:



$$X = 0.03 \text{ for } r/D \geq 0.2$$

(d) Exit loss: $X = 1.0$ (direct loss of kinetic energy).

A5.5 Obstructions

(a) Obstruction away from the walls (e.g. free-standing roof support).

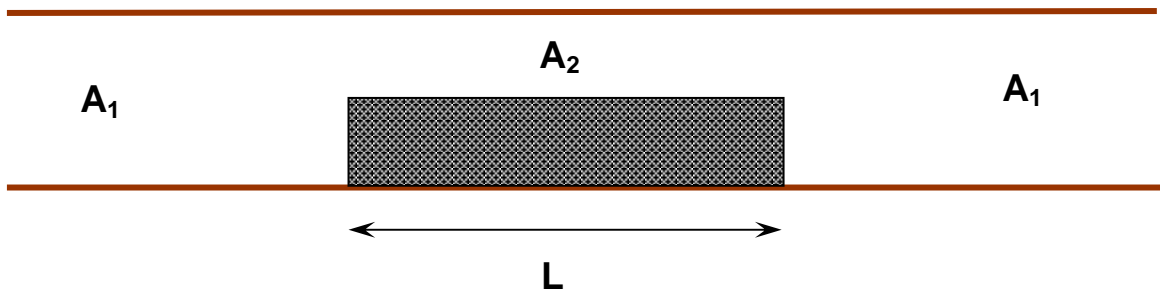
$$X = C_D \frac{A_b}{A}$$

where C_D = Coefficient of Drag for the obstruction (see Figure 5.3)

A_b = cross sectional area facing into the airflow

A = area of airway

(b) Elongated obstruction



A = cross sectional area open to airflow

Ignoring interaction between constituent shock losses, the effect may be approximated as the combination of the losses due to a sudden contraction, length of restricted airway and sudden enlargement. This gives

$$X_2 = 1.5 \left[1 - \frac{A_2}{A_1} \right]^2 + \frac{2kL \text{ per}_2}{\rho A^2}$$

or, when referred to the full cross-section of the airway,

$$X_1 = X_2 \left[\frac{A_1}{A_2} \right]^2$$

where k = Atkinson friction factor for restricted length (kg/m^3)

per_2 = perimeter in restricted length (m)

ρ = air density (kg/m^3).

(c) Circular and rectangular orifices (e.g. regulators, door frames)

$$X_1 = \frac{1}{C_c^2} \left\{ \left[\frac{A_1}{A_2} \right]^2 - 1 \right\}$$

where C_c = orifice coefficient (Figure A5.8)

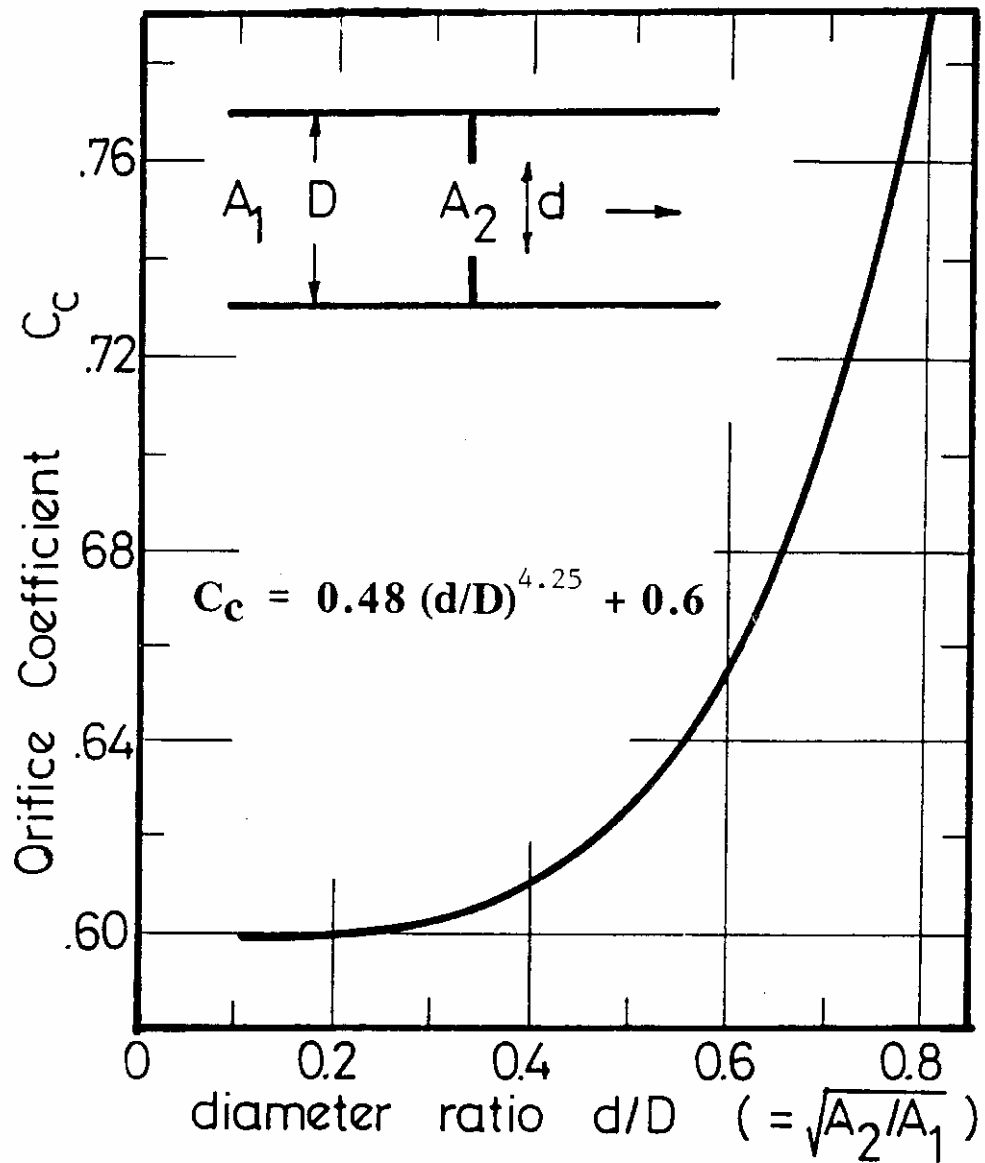
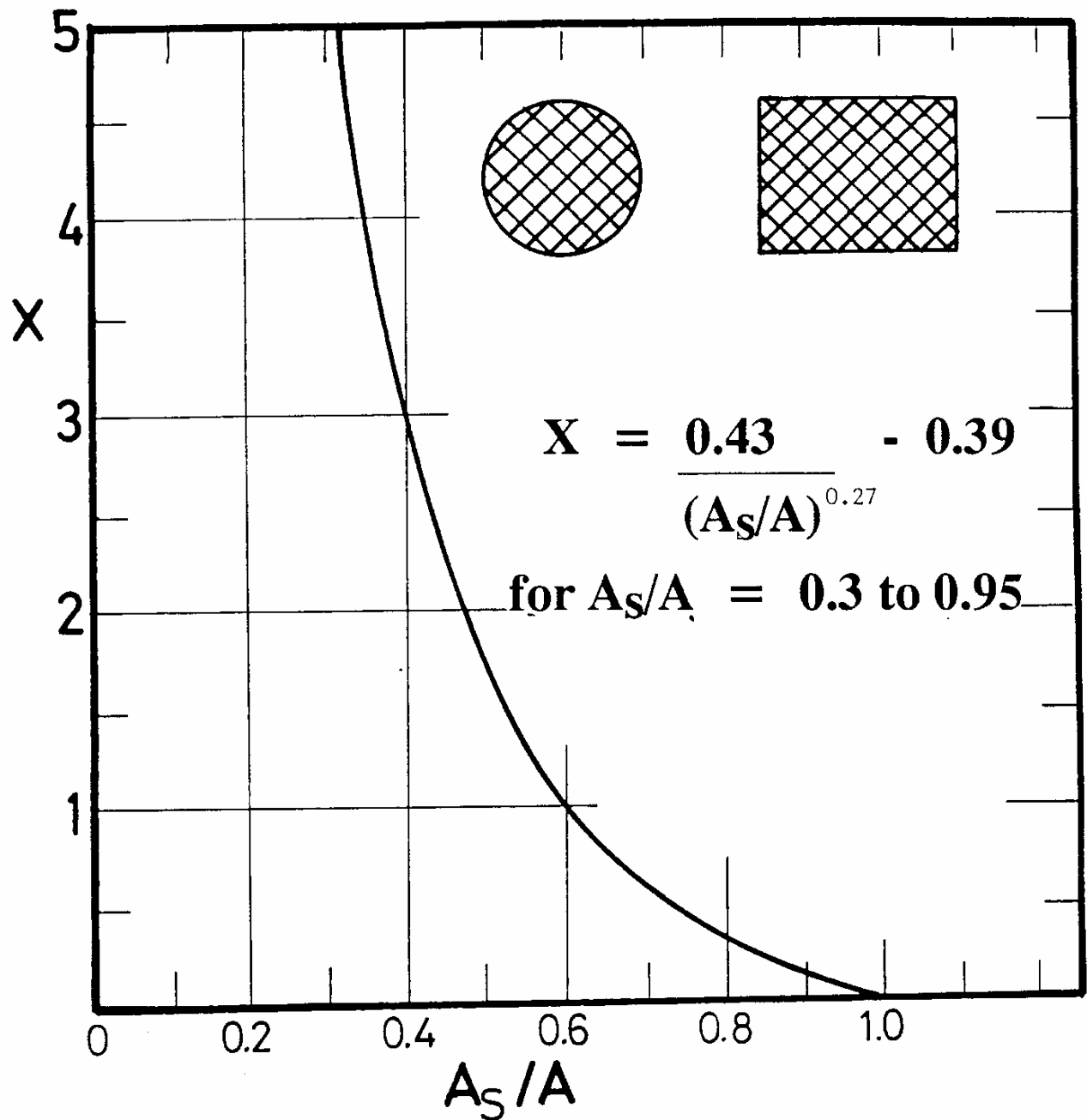


Figure A5.8. Orifice coefficients (of contraction) for sharp edged circular or rectangular orifices.



(d) Figure A5.9. Shock loss factor for screen in a duct.

A = full area of duct

A_s = open flow area of screen

A5.6. Interaction between shock losses

When two bends or other causes of shock loss in an airway are within some ten hydraulic mean diameters of each other then the combined shock loss factor will usually not be the simple addition of the two individual shock loss factors. Depending upon the geometrical configuration and distance between the shock losses, the combined X value may be either greater or less than the simple addition of the two. For example, a double bend normally has a lower combined effect than the addition of two single bends, while a reverse bend gives an elevated effect. Figure A5.10 illustrates the latter situation. This Figure assumes that the shock loss furthest downstream attains its normal value while any further shock within the relevant distance upstream will have its shock loss factor multiplied by an **interference factor**.

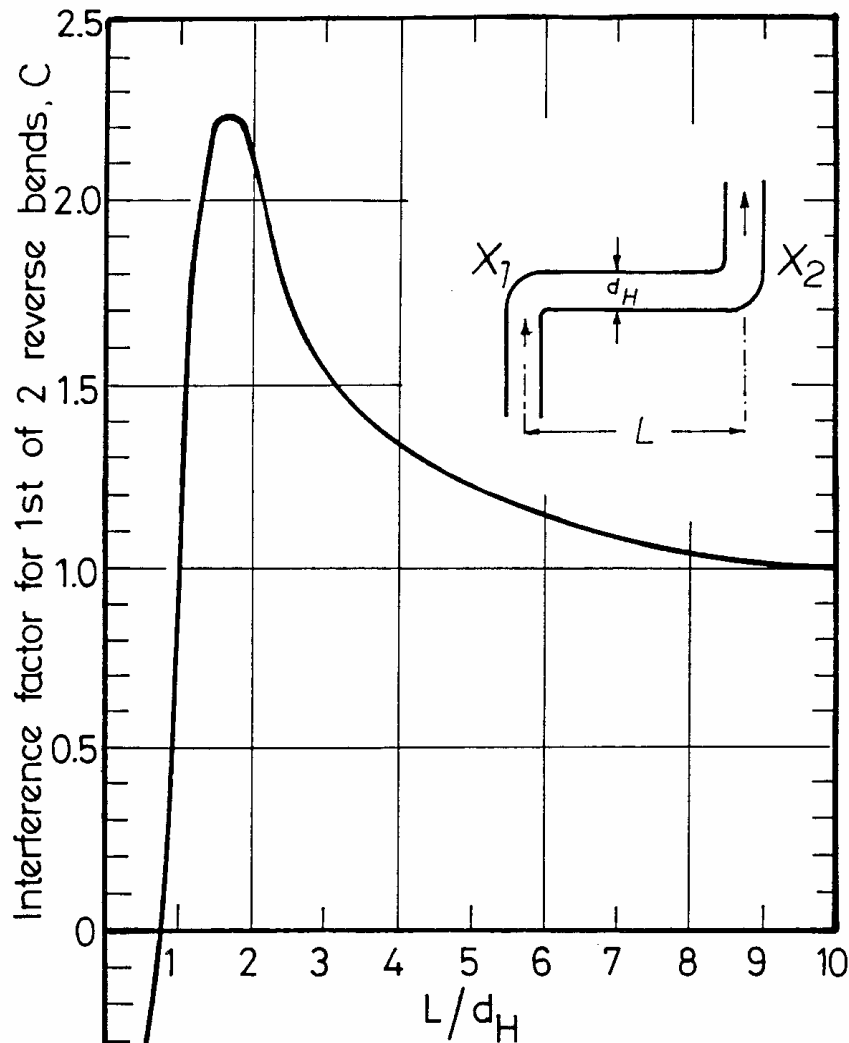


Figure A5.10 Correction (interference) factor for first of two interacting shock losses.

$$\text{Combined shock loss } X_{comb} = C X_1 + X_2$$

where X_1 and X_2 are obtained from the relevant graphs.

Chapter 6. Ventilation Surveys

6.1. PURPOSE AND SCOPE OF VENTILATION SURVEYS	2
6.2 AIR QUANTITY SURVEYS	3
6.2.1. Rotating vane anemometers	3
6.2.2. Moving Traverses	3
<i>The traverse</i>	4
<i>Booking</i>	5
6.2.3. Fixed point measurement	6
6.2.4. Density correction	6
6.2.5. Swinging vane anemometer (velometer)	6
6.2.6. Vortex-shedding anemometer	7
6.2.7. Smoke tubes	7
6.2.8. Pitot-static tube	7
6.2.9. Fixed point traverses	9
<i>Method of equal areas</i>	9
<i>Log-linear traverse</i>	12
<i>Velocity contours</i>	12
6.2.10. Hot body anemometers	13
6.2.11. Tracer gases	14
6.2.12. Measurement of cross-sectional area	16
6.3. PRESSURE SURVEYS	17
6.3.1. Gauge and tube surveys	17
<i>Theory</i>	17
<i>Practical Procedure</i>	19
6.3.2. Barometer and altimeter surveys	21
<i>Theory</i>	22
<i>Practical Procedure</i>	24
6.4 ORGANIZATION OF PRESSURE-VOLUME SURVEYS	25
6.4.1. Initial planning	25
6.4.2. Survey management	26
6.4.3. Quality assurance	26
6.5. AIR QUALITY SURVEYS	27
 BIBLIOGRAPHY	 28
 APPENDIX A6.	 29
Application of the gauge and tube method of measuring frictional pressure drops in cases of significant differences in elevation	29

6.1. PURPOSE AND SCOPE OF VENTILATION SURVEYS

A ventilation survey is an organized procedure of acquiring data that quantify the distributions of airflow, pressure and air quality throughout the main flowpaths of a ventilation system. The required detail and precision of measurement, and the rigour of the ensuing data analysis depend upon the purpose of the survey. Perhaps the most elementary observation in underground ventilation is carried out by slapping one's clothing and watching the dust particles in order to ascertain the direction of a sluggish airflow.

Measurements of airflow should be taken in all underground facilities at times and places that may be prescribed by law. Even in the absence of mandatory requirements, a prudent regard for safety indicates that sufficient routine measurements of airflow be taken

- (a) to ensure that all working places in the mine receive their required airflows in an efficient and effective manner,
- (b) that ventilation plans are kept up to date and
- (c) to verify that the directions, quantities and separate identity of airflows throughout the ventilation infrastructure, including escapeways, are maintained.

Similarly, routine measurements of pressure differentials may be made across doors, stoppings or bulkheads to ensure they are also maintained within prescribed limits and in the correct direction. The latter is particularly important in underground repositories for toxic or nuclear materials and where spontaneous combustion may occur.

One of the main differences between a mine ventilation system and ductwork in a building is that the mine is a dynamic entity, changing continuously due to modifications to the structure of the network and resistances of individual branches. Regular measurements of airflow and pressure differentials underground are necessary as a basis for incremental adjustment of ventilation controls.

During the working life of a mine or other underground facility, there will be occasions when major modifications are required to be made to the ventilation system. These circumstances include opening up new districts in the mine, closing off older ones, commissioning new fans or shafts, or interconnecting main sections of the mine. The procedures of ventilation planning are detailed in Chapter 9. It is important that planning the future ventilation system of any facility is based on reliable and verified data. Ventilation surveys that are carried out in order to establish a data base for planning purposes must necessarily be conducted with a higher degree of organization, detail and precision than those conducted for routine monitoring and control. This chapter is directed primarily towards those more accurate surveys.

A major objective of ventilation surveys is to obtain the frictional pressure drop, p , and the corresponding airflow, Q , for each of the main branches of the ventilation network. From these data, the following parameters may be calculated for the purposes of both planning and control:

- distribution of airflows, pressure drops and leakage
- airpower ($p \times Q$) losses and, hence, distribution of ventilation operating costs throughout the network (Section 9.5.4)
- volumetric efficiency of the system (Section 4.2.3)
- branch resistances ($R = p/Q^2$)
- natural ventilating effects
- friction factors (Equation 5.11)

While observations of airflow and pressure differentials are concerned with the distribution and magnitudes of air volume flow, other measurements may be taken either separately or as an integral part of a pressure/volume survey in order to indicate the quality of the air. These measurements may include wet and dry bulb temperatures, barometric pressures, dust levels and concentrations of gaseous pollutants.

6.2 AIR QUANTITY SURVEYS

The volume of air, Q , passing any fixed point in an airway or duct every second is normally determined as the product of the mean velocity of the air, u , and the cross-sectional area of the airway or duct, A

$$Q = u \times A \qquad \frac{\text{m}}{\text{s}} \text{ m}^2 = \frac{\text{m}^3}{\text{s}}$$

Most of the techniques of observing airflow are, therefore, combinations of the methods available for measuring mean velocity and cross-sectional area.

Prior to the invention of anemometers in the nineteenth century, the only practicable means of measuring rates of airflow in mines was to observe the velocity of visible dust or smoke particles suspended in the air. An even cruder old method was to walk steadily in the same direction as the airflow, varying one's pace, until a candle flame appeared to remain vertical. Modern instruments for the measurement of airspeed in mines divide into three groups depending upon (i) mechanical effects, (ii) dynamic (velocity) pressure of the airflow and (iii) thermal effects.

6.2.1. Rotating vane anemometers

The vast majority of airspeed measurements made manually underground are gained from a rotating vane (windmill type) anemometer. When held in a moving airstream, the air passing through the instrument exerts a force on the angled vanes, causing them to rotate with an angular velocity that is closely proportional to the airspeed. A gearing mechanism and clutch arrangement couple the vanes either to a pointer which rotates against a circular dial calibrated in meters (or feet) or to a digital counter.

The instrument is used in conjunction with a stopwatch and actually indicates the number of "metres of air" that have passed through the anemometer during a given time period. The clutch device is employed to stop and start the pointer or digital counter while the vanes continue to rotate. A zero reset lever is also incorporated into the instrument. Low range vane anemometers will typically have eight vanes, jewelled bearings and give repeatable readings for velocities in the range 0.25 to 15 m/s. High range instruments may have four vanes, low-friction roller or ball bearings and can be capable of measuring air velocities as high as 50 m/s. Digital vane anemometers indicate directly on an odometer counter, an illuminated screen, or feed an electronic signal into a data gathering system. Modern handheld instruments may also be fitted with a microprocessor to memorize readings, dampen out rapid variations in velocity or into which can be entered the cross-sectional area for the calculation of volume flow. Two types of vane anemometer are included in the selection of ventilation survey instruments shown on Plate 1.

In order to obtain a reliable measure of the mean air velocity in an underground airway, it is important that a recommended technique of using the anemometer is employed. The following procedure has evolved from a combination of experiment and practical experience.

6.2.2. Moving Traverses

The anemometer should be attached to a rod of at least 1.5m in length, or greater for high airways. The attachment mechanism should permit the options of allowing the anemometer to hang vertically or to be fixed at a constant angle with respect to the rod. A rotating vane anemometer is fairly insensitive to yaw and will give results that do not vary by more than ± 5 per cent for angles deviating by up to 30° from the direction of the airstream. Hence, for most

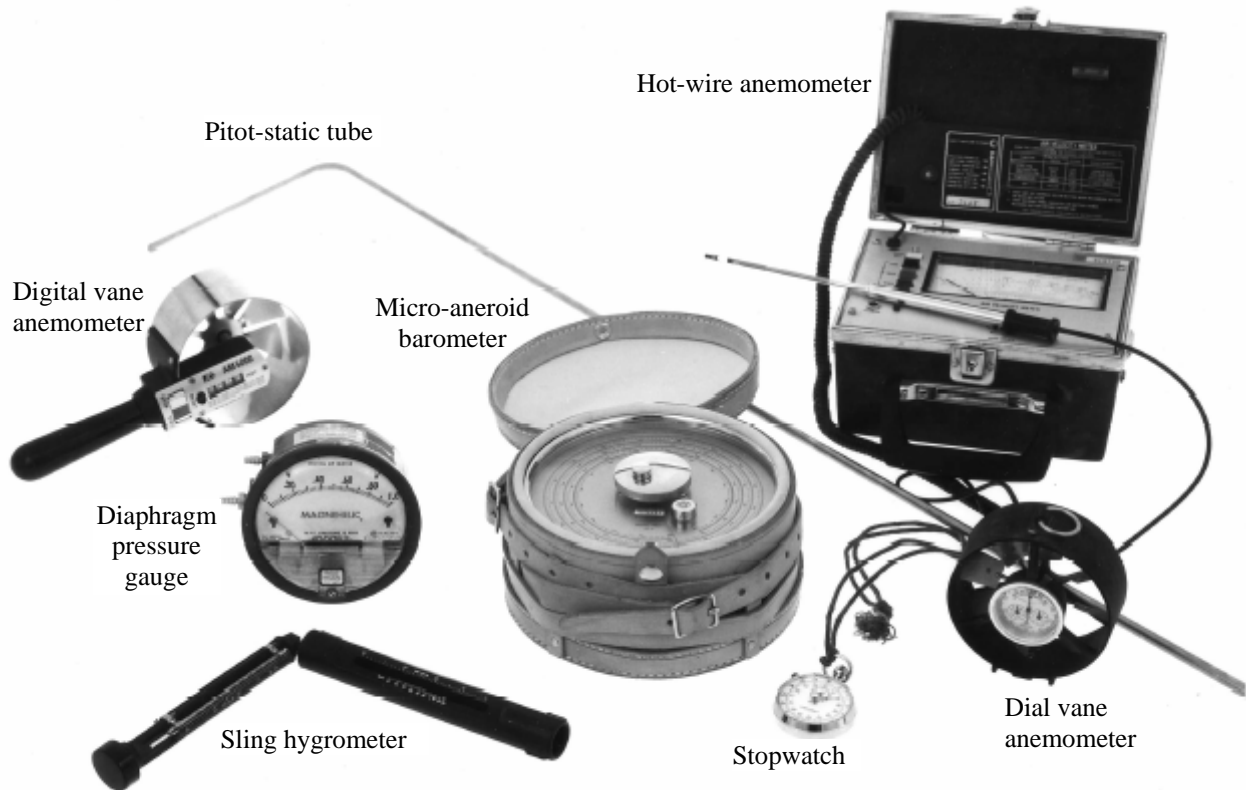


Plate 1. Selection of instruments that may be used in ventilation surveys

underground airways, allowing the anemometer to hang freely at the end of the rod will give acceptable results. For airways of inclination greater than 30° , the anemometer should be clamped in a fixed position relative to the rod and manipulated by turning the rod during the traverse such that the instrument remains aligned with the longitudinal axis of the airway.

The traverse

The observer should face into the airflow holding the anemometer rod in front of him/her so that the dial is visible and at least 1.5m upstream from his/her body. To commence the traverse, the instrument should be held either in an upper or lower corner of the airway, with the pointer or counter reset to zero, until the vanes have accelerated to a constant velocity. This seldom takes more than a few seconds. The observer should reach forward to touch the clutch control lever while a second observer with a stopwatch counts backwards from five to zero. On zero, the anemometer clutch is activated releasing the pointer and, simultaneously, the stopwatch is started.

The path of the traverse across the airway should be similar to that shown on Figure 6.1. The aim should be to traverse the anemometer at a constant rate not greater than about 15 per cent of the airspeed. Ideally, equal fractions of the airway cross sectional area should be covered in equal times. This is facilitated by the stopwatch observer calling out the elapsed time at ten second intervals. The complete traverse should take not less than 60 seconds and may be considerably more for large or low velocity airways. The final five seconds should be counted down by the stopwatch observer during which time the traverse person stretches forward to disconnect the clutch at the end of the time period. The length indicated by the anemometer is immediately read and booked, and the instrument reset to zero.

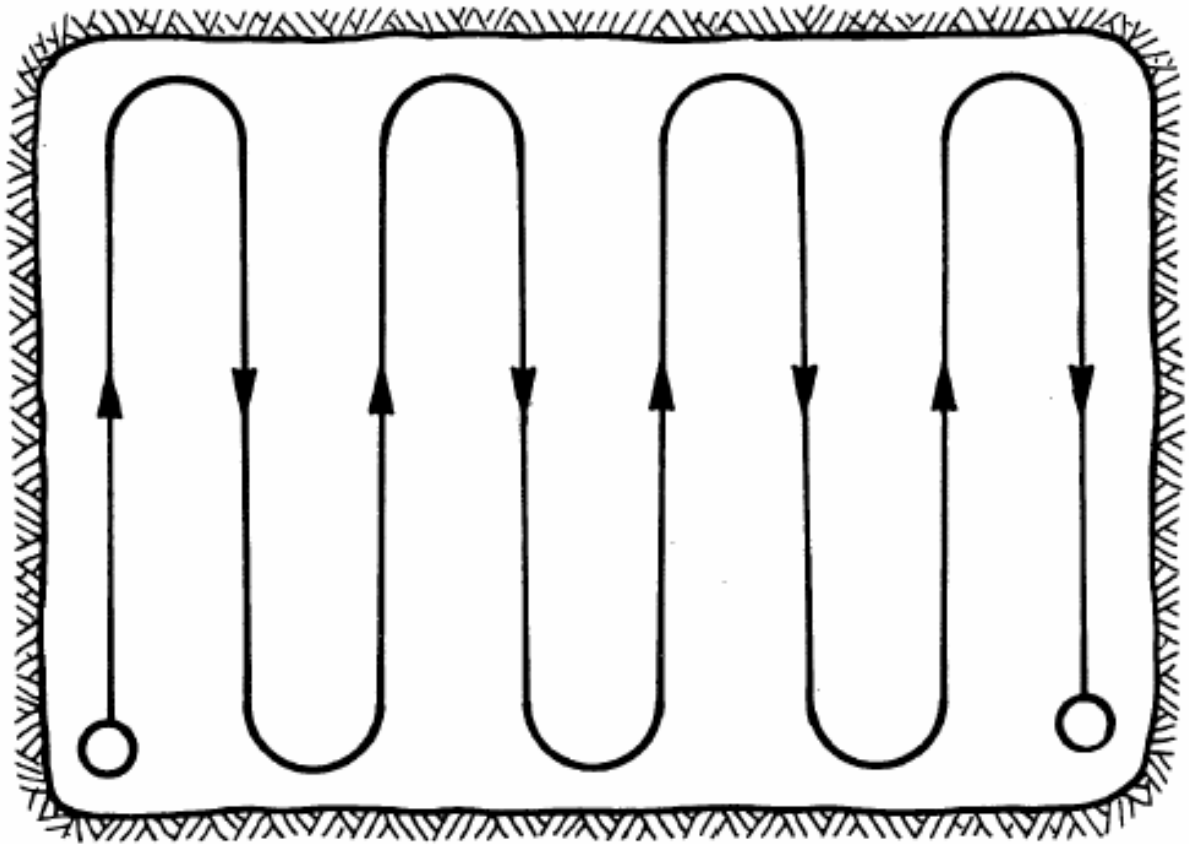


Figure 6.1. Path of a moving anemometer traverse

The procedure is repeated, traversing in the opposite direction across the airway. Traverses should be repeated until three readings are obtained that agree to within ± 5 per cent. In favourable steady state conditions, experienced observers will often achieve repeatability to within ± 2 per cent. Larger discrepancies may be expected in airways where there is a highly asymmetric variation in velocity across the airway, where the floor conditions are unstable, or when obstructions exist in the cross section. Measuring stations should be chosen to avoid such difficulties wherever possible. Another annoying cause of discrepancy is the opening of a ventilation door during the period of measurement. Two or more sets of traverses should be taken at different locations within each airway. Where cross-cuts or other leakage paths affect the airflow then a sufficient number of additional measurement points should be traversed in order to quantify the rate and direction of leakage.

Booking

The anemometer field book should be waterproof and laid out such that each double page has segments for

1. names of observers
2. the location of the measuring station, time, date,
3. anemometer readings and corrections
4. dimensioned sketch of cross-section
5. calculation of area
6. calculation of air volume flow.

The bookings are normally made by the stopwatch person. For each traverse, the anemometer reading is divided by the corresponding time to give the air velocity. The mean of these station velocities, ignoring any values outside the ± 5 per cent tolerance, gives the observed mean velocity. In most cases, the time of each traverse at a station is the same, allowing the anemometer readings to be averaged before calculating the mean velocity. The observed mean velocity must then be corrected according to the calibration chart or curve for the instrument (Section 6.4) to give the actual mean velocity, u .

The cross sectional area, A , is determined using one of the methods discussed in section 6.2.12. The calculation of airflow is then completed as

$$Q = u \times A \qquad \frac{\text{m}}{\text{s}} \text{m}^2 = \frac{\text{m}^3}{\text{s}}$$

Anemometer traverses may also be employed at the ends of ducts. However, it is recommended that the technique not be used for duct diameters less than six times that of the diameter of the anemometer.

6.2.3. Fixed point measurement

An estimate of duct airflow may be obtained by holding the anemometer at the centre of the duct and multiplying the corrected reading by a further correction factor of 0.8. A similar technique may be employed for routine check readings taken at well established measuring stations in airways. The reading obtained from a stationary anemometer at a known location within the cross-section should, initially, be compared with that given from a series of traverses in order to obtain a "fixed point" correction factor for that station. This is typically 0.75 to 0.8 for the fixed point located some one half to two thirds the height of the airway. Subsequent routine readings may be obtained simply by taking an anemometer reading at the fixed point and applying the appropriate calibration and fixed point corrections. Provided that the measuring station is well downstream of any bends or major obstructions and the airflow remains fully turbulent then the fixed point correction factor will stay near constant as the airflow varies.

6.2.4. Density correction

For precise work, anemometer readings may be further corrected for variations in air density:

$$u = u_i + C_c \sqrt{\frac{\rho_c}{\rho_m}} \qquad (6.1)$$

where

u = corrected velocity

u_i = indicated velocity

C_c = correction from instrument calibration curve or chart

ρ_c = air density at time of calibration

ρ_m = actual air density at time of measurement

Equation (6.1) shows that the density adjustment $\sqrt{\frac{\rho_c}{\rho_m}}$ is effectively applied only to the calibration correction and is ignored in most cases.

6.2.5. Swinging vane anemometer (velometer)

In its most fundamental form, the swinging vane anemometer (velometer) is simply a hinged vane which is displaced against a spring from its null position by a moving airstream. A connected

pointer gives a direct reading of the air velocity. The air enters a port at the side of the instrument. This port can be fitted with interchangeable orifices or probes to give a range of measurable velocities. Oscillations of the vane may be reduced by the eddy current damping produced when a metal strip connected to the vane moves between strong permanent magnets. The delicacy of the velometer together with its pronounced directional bias has limited its use in underground surveys. However, it can serve a useful purpose in giving spot readings as low as 0.15 m/s in gassy mines where hot wire probes are prohibited.

6.2.6. Vortex-shedding anemometer

For continuous monitoring systems, both rotating vane and swinging vane instruments with electrical outputs have been employed. However, they both require relatively frequent calibration checks when used in mine atmospheres. For this type of application, the vortex-shedding anemometer is preferred as it has no moving parts.

When any bluff object is placed in a stream of fluid, a series of oscillating vortices are formed downstream by boundary layer breakaway, first from one side of the body then the other. The propagation of the vortices is known as a Kármán street and can often be observed downstream from projecting boulders in a river. The rate of vortex production depends upon the fluid velocity. In the vortex-shedding anemometer, the vortices may be sensed by the pulsations of pressure or variations in air density that they produce. One apparent disadvantage noticed in practice is that when sited in a fixed location underground for monitoring purposes they require calibration for that specific location. They may also require electronic damping to eliminate large but short lived variations in signals caused by the passage of vehicles.

6.2.7. Smoke tubes

Smoke tubes are perhaps the simplest of the mechanical techniques employed for measuring airflows and are used for very low velocities. A pulse of air forced by a rubber bulb through a glass phial containing a granulated and porous medium soaked in titanium tetrachloride or anhydrous tin will produce a dense white smoke. This is released upstream of two fixed marks in the airway. An observer with a spot-beam cap lamp is located at each mark. The time taken for the cloud of smoke to travel the length of airway between the marks gives an indication of the centre-line velocity of the air. This must then be adjusted by a centre-line correction factor to give the mean velocity. The correction factor is usually taken to be 0.8 although a more accurate value can be calculated for known Reynold's numbers. The length of airway should be chosen such that at least one minute elapses during the progression of the smoke between the two marks. Dispersion of the smoke cloud often causes the downstream observer some difficulty in deciding when to stop the stopwatch. Due to the uncertainties inherent in the technique, smoke tubes are normally employed as a last resort in slow moving airstreams.

6.2.8. Pitot-static tube

In section 2.3.2 we discussed the concepts of total, static and velocity pressures of a moving stream of fluid. A pitot-static tube, illustrated on Figure 6.2, can be used to measure all three. This device consists essentially of two concentric tubes. When held facing directly into an airflow, the inner tube is subjected to the total pressure of the moving airstream, p_t . The outer tube is perforated by a ring of small holes drilled at right angles to the shorter stem of the instrument and, hence, perpendicular to the direction of air movement. This tube is, therefore, not influenced by the kinetic energy of the airstream and registers the static pressure only, p_s . A pressure gauge or manometer connected across the two tappings will indicate the difference between the total and static pressure, i.e. the velocity pressure:

$$p_v = p_t - p_s \quad \text{Pa} \quad [\text{from equation (2.18)}] \quad (6.2)$$

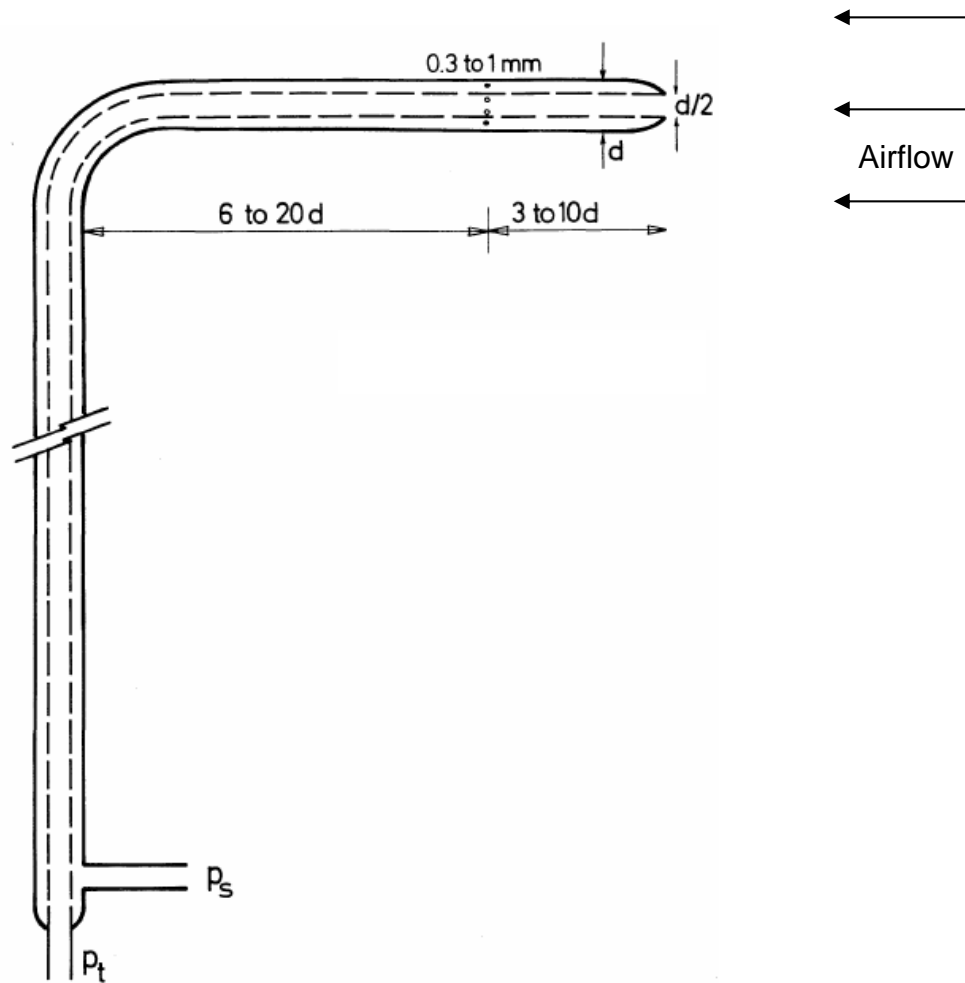


Figure 6.2 Pitot-static tube

Furthermore, the velocity head is related to the actual velocity of the air, u

$$u = \sqrt{\frac{2p_v}{\rho}} \quad \text{m/s} \quad [\text{from equation (2.17)}] \quad (6.3)$$

where

$$\rho = \text{actual density of the air (kg/m}^3\text{)} \\ \text{(see equation (14.52) for air density).}$$

Pitot-static tubes vary widely in overall dimensions. For measuring air velocities in mine airways or at main fans, the longer stem may be some 1.5m in length. Much smaller versions are available for use in ducts or pipes.

Modern pitot-static tubes reflect the total, static and velocity pressures of the airflow to an excellent degree of accuracy. Unfortunately, the precision of the measurement depends also upon the manometer or pressure gauge connected to the tappings. This imposes a practical restriction on the lower limit of air velocity that can be measured by a pitot-static tube in the turbulent airflows of an underground system.

Example

If a diaphragm pressure gauge can be read to the nearest ± 1 Pa, then the lowest pressure that will give 10 per cent accuracy in the pressure reading is 10 Pa. Calculate the air velocity corresponding to a velocity pressure of 10 Pa, assuming an air density of 1.2 kg/m^3 .

Solution

$$u = \sqrt{\frac{2 p_v}{\rho}} = \sqrt{\frac{2 \times 10}{1.2}} = 4.08 \quad \text{m/s}$$

As the great majority of underground openings have air velocities of less than 4 m/s, it is clear that the use of the pitot-static tube for the measurement of air velocity is limited to ventilation ducting and a few high velocity airways; primarily fan drifts and evasees, ventilation shafts, some longwall faces and trunk airways.

One of the difficulties of using a pitot-static tube for the spot measurement of pressures or velocities in a turbulent airstream is the oscillation in the readings. A small wad of cotton wool inserted into the flexible pressure tubing between the pitot-static tube and the pressure gauge damps out the short term variations. However, the cotton wool should not be so tightly tamped into the tubing that the gauge reaction becomes unduly slow. Electronic diaphragm gauges are often fitted with an internal damping circuit.

6.2.9. Fixed point traverses

The rotating vane anemometer is an integrating device, accumulating the reading as it traversed continuously across an airway or duct. Most other instruments for the measurement of air velocity, including the pitot-static tube, do not have this advantage but are confined to giving a single spot reading at any one time. In order to find the mean velocity in an airway from pitot-static tube readings it is, therefore, necessary to take spot measurements at a number of locations over the cross-section. This procedure is known by the contradictory sounding term "fixed point traverse". Differing techniques of conducting such traverses vary in the number of observations, locations of the instrument and treatment of the data. Three of these techniques are described here. In all cases, the fixed point traverse method assumes that the distribution of flow over the cross-section does not vary with time. For permanent monitoring stations, a grid of multiple pitot-static tubes may be left in place.

Method of equal areas

In this method, the cross-section of the duct or airway is divided into subsections each of equal area. Figure 6.3 shows a rectangular opening divided into 25 equal subsections similar in shape to the complete opening. Using a pitot-static tube or anemometer, the velocity at the centre of each subsection is measured. The mean velocity is then simply the average of the subsection velocities.

There are a few precautions that should be taken to ensure satisfactory results. First, if a pitot-static tube is employed then the velocity at each subsection should be calculated. Averaging the velocity pressure before employing equation (6.3) will not give the correct mean velocity. Secondly, it will be recalled that the velocity gradient changes most rapidly near the walls. Hence, accuracy will be improved if the velocities for the subsections adjacent to the walls and, especially, in the corners are determined from a number of readings distributed within each of those subsections. Third, the number of subsections should increase with respect to the size of the airway in order to maintain accuracy.

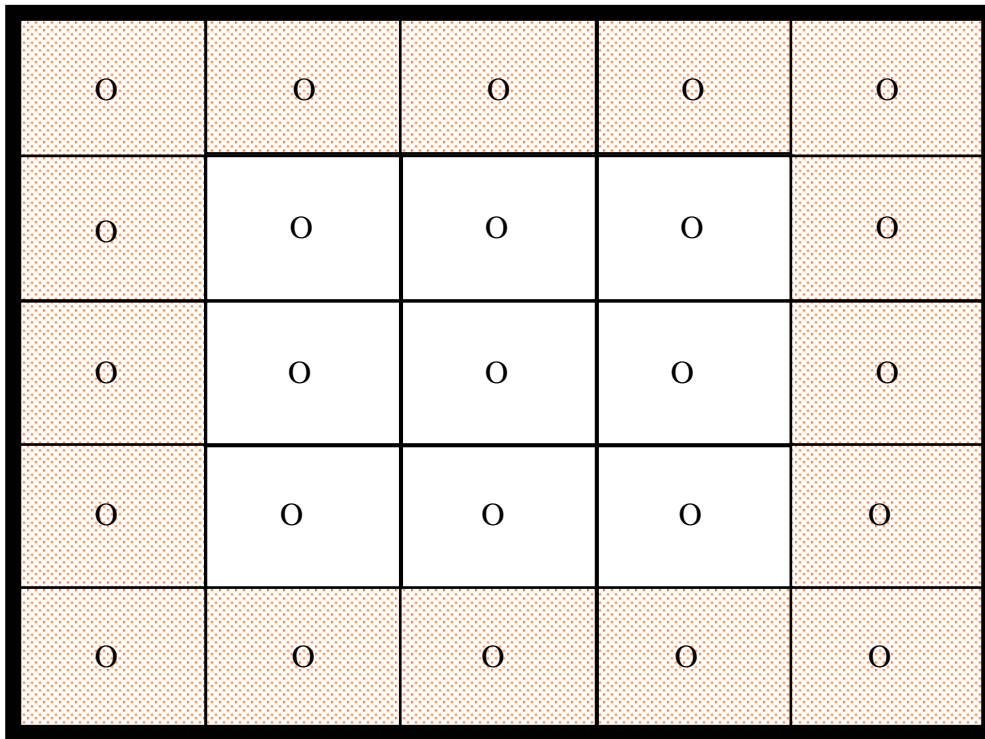


Figure 6.3 Measuring points for a fixed point traverse in a rectangular opening. The velocity in each shaded subsection should be averaged from several readings distributed over the subsection.

As a guide, the recommended number of points, n , for a rectangular opening may be estimated as

$$n = 100 e^{-8/A} + 23 \tag{6.4}$$

where e is the exponential exponent, 2.7183 and A is the cross-sectional area (m²)

The estimated number of points may then be rounded to a value that is convenient for subdividing the cross-sectional area but should never be less than 24. Correct positioning of the measuring instrument is facilitated by erecting a grid of fine wires in the airway to represent the subsections.

In the case of circular openings, the method of equal areas divides the circle into annuli, each of the same area. Readings should be taken at points across two diameters and the corresponding velocity profiles plotted. Should those profiles prove to be skewed then readings should be taken across two additional diameters. The number of measuring points recommended on each diameter is given in Table 6.1. Figure 6.4 illustrates an 8 point traverse on each of 4 diameters.

Diameter of duct (m)		< 1.25	1.25 - 2.5	> 2.5
No. of points		6	8	12

Table 6.1 Number of measuring points on each diameter of a circular opening.

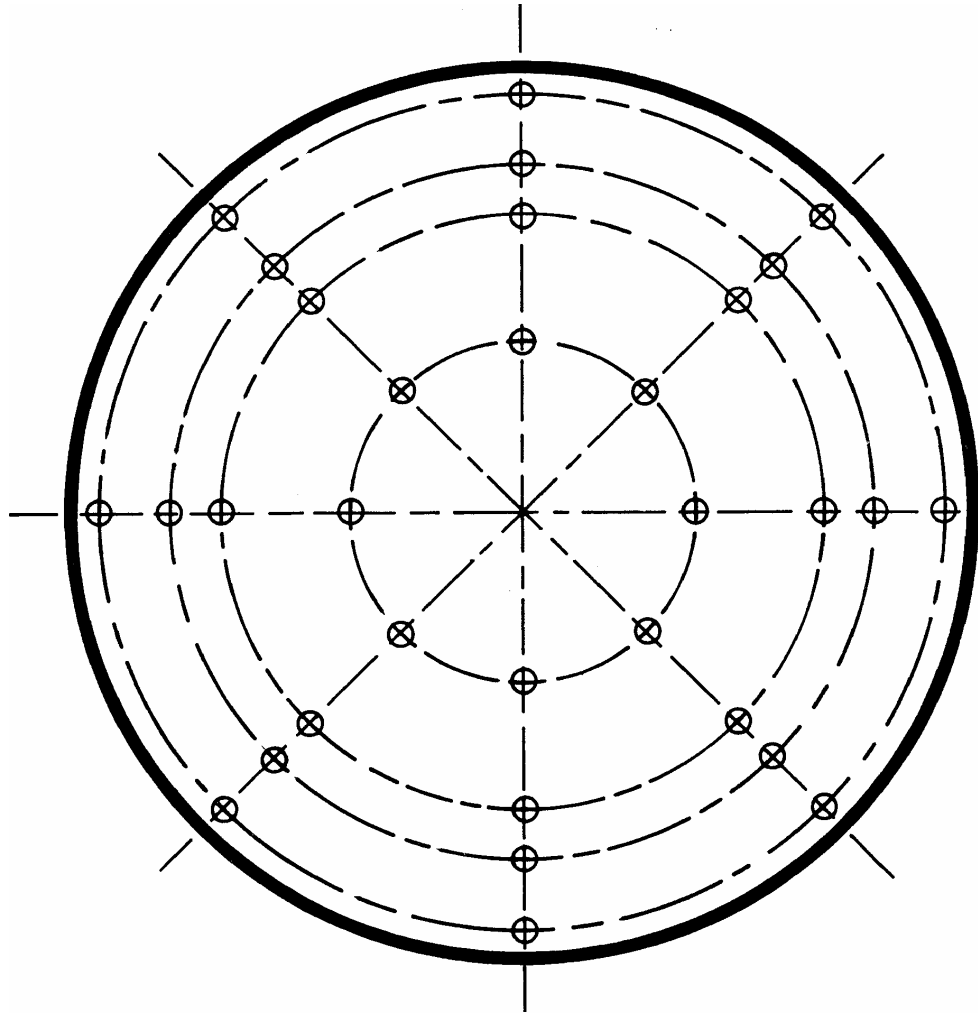


Figure 6.4 Measuring positions for a 8 point traverse on 4 diameters of a circular duct.

The locations of the points are at the centre of area of the relevant annulus on each diameter and may be calculated from

$$r = D \sqrt{\frac{2n-1}{4N}} \quad \text{m} \quad (6.5)$$

where

r	=	radius of point n from the centre
n	=	number of the point counted outwards from the centre
D	=	diameter of the duct (m)
N	=	number of points across the diameter

Table 6.2 gives locations of points for 6, 8, and 12 point traverses in terms of fractions of duct diameter measured from one side.

Where a pitot-static tube traverse is to be conducted across a duct from the outside then a clamping device should be attached to the outer surface of the duct to hold the pitot-static tube firmly in place. The positions of measurement should be marked on the stem of the instrument

using Table 6.2 or 6.3. After each relocation of the measuring head, the pitot-static tube should be yawed slightly from side to side until the orientation is found that gives the greatest reading of total or velocity pressure. The head of the instrument is then aligned directly into the airstream.

No. of measuring points on each diameter	Fractions of one diameter measured from side of duct												
	centre ▼												
6				0.044	0.146	0.296	0.704	0.854	0.956				
8			0.032	0.105	0.194	0.323	0.677	0.806	0.895	0.968			
12	0.021	0.067	0.118	0.177	0.250	0.356	0.644	0.750	0.823	0.882	0.933	0.979	

Table 6.2 Positions of measuring points in a circular duct using the method of equal areas.

Log-linear traverse

A more accurate method of positioning points of measurement along the diameters of a circular duct has been derived from a consideration of the logarithmic law equations that describe the velocity profile for turbulent flow. The effects of observational errors are minimized when the points are located according to this method, known as the log-linear traverse. The corresponding locations are given in Table 6.3.

No. of measuring points on each diameter	Fractions of one diameter measured from side of duct												
	centre ▼												
6				0.032	0.135	0.321	0.679	0.865	0.968				
8			0.021	0.117	0.184	0.345	0.655	0.816	0.883	0.978			
12	0.014	0.075	0.114	0.183	0.241	0.374	0.626	0.759	0.817	0.886	0.925	0.986	

Table 6.3 Log-linear traverse positions of measuring points in a circular duct.

Velocity contours

One of the difficulties that besets ventilation engineers in measuring large scale airflows is that conditions are often not conducive to good accuracy. "Textbook" advice is to choose measuring stations well away from obstructions, bends or changes in cross-section. Unfortunately, this is not always possible, especially when measuring airflows at the inlets or outlets of fans. It is not uncommon to find that longitudinal swirl in a fan drift or re-entry in an evasee causes the air to move in the wrong direction within one part of the cross-section. Similarly, in obstructed but high velocity airways underground such as many longwall faces, complex airflow patterns may exist.

A useful rule of thumb is that the averaging of spot velocities from a pitot-static tube traverse is acceptable if more than 75 per cent of the velocity pressures (p_v) are greater than the maximum p_v divided by 10.

For difficult cases, the construction of velocity contours can provide both a visual depiction of the flow pattern and also a means of quantifying airflow. A scale drawing of the measurement cross-section is made on graph paper. A grid of fine wires is constructed in the airway to define the points of measurement. The number of points should be not less than that recommended in the previous subsection. The greater the number of measurement points, the more accurate will be the result. The velocities at the corresponding points of measurement are entered on the graph paper and contour lines of equal velocity (isovels) are constructed. Figure 6.5 shows an example of velocity contours obtained on a longwall face.

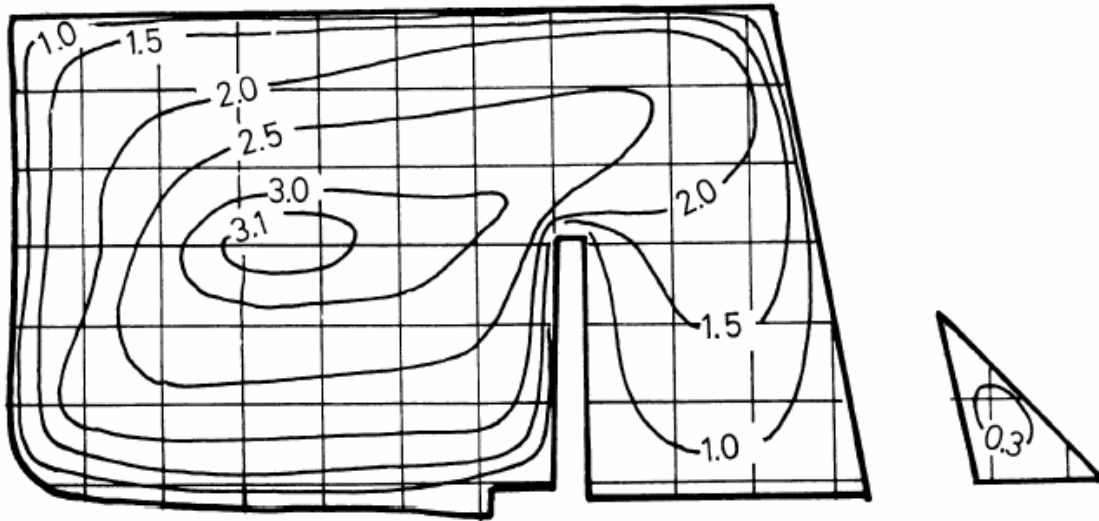


Figure 6.5 Example of velocity contours at an airflow measuring station on a longwall face

The area enclosed by each contour can be determined either by planimeter (if the scale drawing is large enough for good planimeter accuracy) or by the rudimentary method of counting squares on the graph paper. The construction of isovels and determination of the areas enclosed are greatly facilitated by the use of a computer software contouring package. Fully automated systems have been devised that scan the actual cross-section and produce quantified velocity contour diagrams. However, the expense of such systems is seldom justified other than in research and testing laboratories.

By difference, the area of the band between each contour is evaluated and may be multiplied by the mean of the bounding velocities and the area scale factor to give the airflow for that band. Provided that the outermost contour is close to the walls then the velocity at the walls may be taken as zero. The sum of all band airflows gives the total flow for the airway.

6.2.10 Hot body anemometers

When any heated element is placed in a moving fluid, heat energy will be removed from it at a rate that depends upon the rate of mass flow over the element.

In the hot wire anemometer a wire element is sited within a small open ended cylinder to give the instrument a directional bias. The element forms one arm of a Wheatstone bridge circuit. In most hot wire anemometers, the temperature of the element is maintained constant by varying the

electrical current passing through it as the air velocity changes. In other designs, the current is kept constant and the temperature (and, hence, electrical resistance) of the element is monitored. Modern hot wire anemometers are compensated for variations in ambient temperature and most also indicate dry bulb temperature. For precise work, readings should be corrected for air density:

$$u = u_i \frac{\rho_c}{\rho_m} \quad (6.5)$$

where u = true air velocity
 u_i = indicated air velocity
 ρ_c = air density at calibration (usually 1.2 kg/m³)
 ρ_m = actual air density at time of measurement.

Hot wire anemometers are particularly useful for low velocities and are reliable down to about 0.1 m/s. They are convenient for fixed point traverses in slow moving airstreams. If a hot wire anemometer is to be used in a gassy mine then a check should first be made on the permissibility of the instrument for use in potentially explosive atmospheres.

The **Kata thermometer**, described in Section 17.4.3.2 as a means of measuring the cooling power of an airstream, can also be used as a non-directional device to indicate low air velocities, typically in the range 0.1 to 1 m/s. The main bulb of the Kata thermometer is heated until the alcohol level is elevated above the higher of the two marks on the stem. When hung in an airstream, the time taken for the alcohol level to fall between the two marks, coupled with the Kata index for the instrument and the air temperature, may be used to determine the non-directional air velocity. The Kata thermometer is seldom used for underground work (except in South Africa) because of its fragility.

6.2.11. Tracer gases

The rate at which injected gases are diluted provides a means of measuring air volume flow without the need for a cross-sectional area. The method is particularly useful for difficult situations such as leakage flow through waste areas, main shafts and other regions of high velocity and excessively turbulent flow, or total flow through composite networks of airways.

Hydrogen, nitrous oxide, carbon dioxide, ozone, radioactive krypton 85 and sulphur hexafluoride have all been used with the latter particularly suitable for leakage or composite flows. The gas chosen should be chemically inert with respect to the mineralization of the strata.

There are two techniques of using tracer gases for the measurement of airflow. For high velocity airways, the tracer gas may be released at a monitored and steady rate M_g (kg/s). At a point sufficiently far downstream for complete mixing to have occurred, samples of the air are taken to establish the steady state concentration of the tracer gas. Then

$$C = \frac{q_g}{Q} = \frac{M_g}{\rho_g Q} \quad (6.6)$$

or

$$Q = \frac{M_g}{C \rho_g} \quad \frac{\text{m}^3}{\text{s}} \quad (6.7)$$

where q_g = volume flow of tracer gas (m³/s)
 Q = airflow (m³/s)
 C = downstream concentration of tracer gas (fraction by volume)
 ρ_g = density of tracer gas at ambient pressure and temperature (kg/m³)

It is assumed that the volume flow of tracer gas is negligible compared with the airflow.

In the case of sluggish or composite flows, a known mass of the tracer gas, M (kg), is released as a pulse into the upstream airflow. At the downstream station, the concentration of tracer gas is monitored and a concentration-time, $(C \text{ v } t)$, graph is plotted as shown on Figure 6.6. Now, the concentration C is given as the ratio of the volume flow rate of gas, q_g , and the airflow, Q .

$$C = \frac{q_g}{Q} \quad (\text{fraction, by volume})$$

$$\text{But } q_g = \frac{M_g}{\rho_g} \quad \frac{\text{m}^3}{\text{s}}$$

where M_g = mass flow rate of gas at the monitored downstream station (kg/s)
and ρ_g = density of gas at the prevailing temperature and pressure (kg/m³)

$$\text{giving } C = \frac{M_g}{\rho_g Q}$$

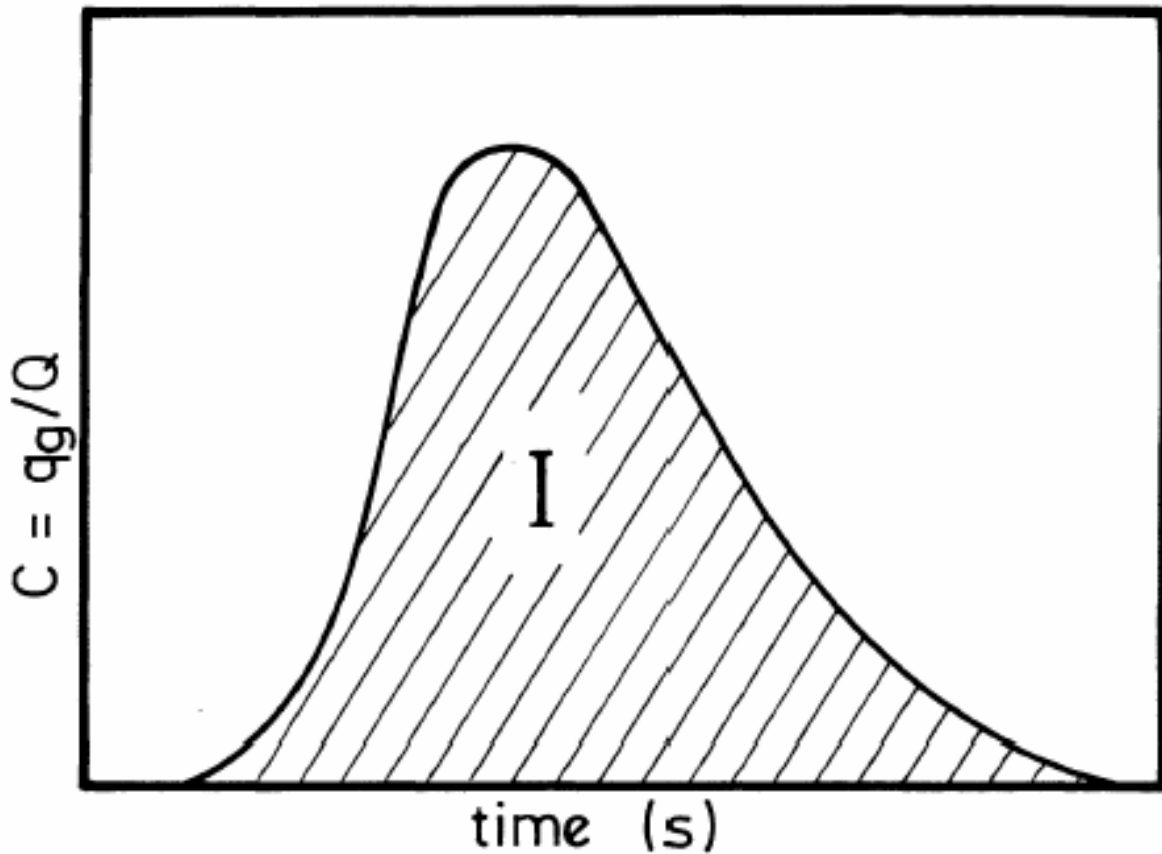


Figure 6.6 Concentration-time curve at a tracer gas monitoring station

Hence, the complete area under the curve of C against t ,

$$I = \int_0^{\infty} C dt \quad (\text{This equals the total volume of tracer gas that passed the station})$$

$$= \frac{1}{\rho_g Q} \int_0^{\infty} M_g dt$$

But the total mass of gas released, M , must also be equal to $\int_0^{\infty} M_g dt$ (assuming that all of the air passing the upstream station also passes through the downstream station).

giving $I = \frac{M}{\rho_g Q}$

or $Q = \frac{M}{I \rho_g} \quad \frac{\text{m}^3}{\text{s}} \quad (6.8)$

6.2.12 Measurement of cross-sectional area

As the vast majority of airflows are determined as the product of a mean velocity and a cross-sectional area, the accuracy of the airflow depends equally upon the measured velocity and cross-sectional area. There is little point in insisting upon meticulous procedures for the measurement of mean velocity unless the same care is applied to finding the cross sectional area.

By far the most common method of measuring airway area is by simple **taping**. This will give good results where the opening is of regular geometric shape such as a rectangle or circle. Airflow measuring stations should, wherever possible, be chosen where the airway profile is well defined. The frames of removed ventilation control doors can provide excellent sites for airflow measurement. Shapes such as arched profiles or trapeziums may be subdivided into simple rectangles, triangles and segments of a circle, and appropriate taped measurements taken to allow the area to be calculated.

Inevitably, there are many situations in which airflows must be determined in less well defined cross-sections. Several techniques are available for determining the corresponding cross-sectional area. For shapes that approximate to a rectangle, three or more heights and widths may be taped to find mean values of each. Care should be taken in such circumstances to make allowance for rounding at the corners. This often occurs due to spalled rock accumulating on the floor at the sides of airways.

A more sophisticated technique is the **offset method** in which strings are erected that define a regular shape within the airway. These strings are usually two vertical and two horizontal wires encompassing a rectangle. Taping from the wires to the rock walls at frequent intervals around the perimeter allows a plot of the airway profile to be constructed on graph paper.

The **profilometer** is a plane-table device. A vertical drawing board is attached to a tripod in the middle of the airway cross-section. Taped measurements made from the centre of the board to points around the rock walls may be scaled down mechanically or manually to reconstruct the airway profile on the drawing board. An electronic version replaces the tape by an ultrasonic distance measuring device although reflections of the beam can produce errors within the confines and rough surfaces of an underground airway.

The **photographic method** entails painting a white line around the perimeter of the measuring station. A linear scale such as a surveyor's levelling staff is fixed vertically within the defined

profile. A camera is located such that it is aligned along a longitudinal centre-line of the airway and with its lens equidistant from all points on the painted line. These precautions reduce perspective errors. The area within the white line may be determined by overlaying the resulting photograph with transparent graph paper.

Such time consuming methods tend to be employed for permanent measuring stations rather than for temporary survey stations. In all cases, the cross sectional area of conveyors, ducts or other equipment should be determined and subtracted from the overall area of the airway.

6.3. PRESSURE SURVEYS

The primary purpose of conducting pressure surveys is to determine the frictional pressure drop, p , that corresponds to the airflow, Q , measured in each branch of a survey route. There are essentially two methods. The more accurate is the gauge and tube or trailing hose method, in which the two end stations are connected by a length of pressure tubing and the frictional pressure drop measured directly. The second method, of which there are several variations, involves observing the absolute pressure on a barometer or altimeter at each station.

Although tradition within individual countries tends to favour one or other of the two methods, both have preferred fields of application. In general, where foot travel is relatively easy between measuring stations, the gauge and tube method can be employed. Where access is difficult as in multi-level workings or in shafts then the barometer method becomes more practicable.

6.3.1. Gauge and tube surveys

Figure 6.7 illustrates the principles of gauge and tube surveying. A pressure gauge is connected into a length of tubing whose other ends are attached to the total head tapping of pitot-static tubes sited at the end stations. In practice, of course, the tubing and instrumentation are all within the airway. Let us deal first with the essential theory of the method before discussing the practical procedure of gauge and tube surveying.

Theory

From the steady-flow energy equation (3.25) for an airway between stations 1 and 2, and containing no fan,

$$\frac{u_1^2 - u_2^2}{2} + (Z_1 - Z_2)g = \int_1^2 V dP + F_{12} \quad \frac{\text{J}}{\text{kg}} \quad (6.9)$$

where

u	=	air velocity (m/s)
Z	=	height above mine datum (m)
g	=	gravitational acceleration (m/s^2)
V	=	specific volume of air ($= 1/\rho$) (m^3/kg)
and F_{12}	=	work done against friction (J/kg)

If we assume a linear variation in air density between stations 1 and 2 then we can adopt an arithmetic mean value of density for the airway, $\rho_a = 1/V$. Furthermore, the frictional pressure drop referred to that density is given by equation (2.46) as

$$p_{12} = \rho_a F_{12} \quad \text{Pa} \quad (6.10)$$

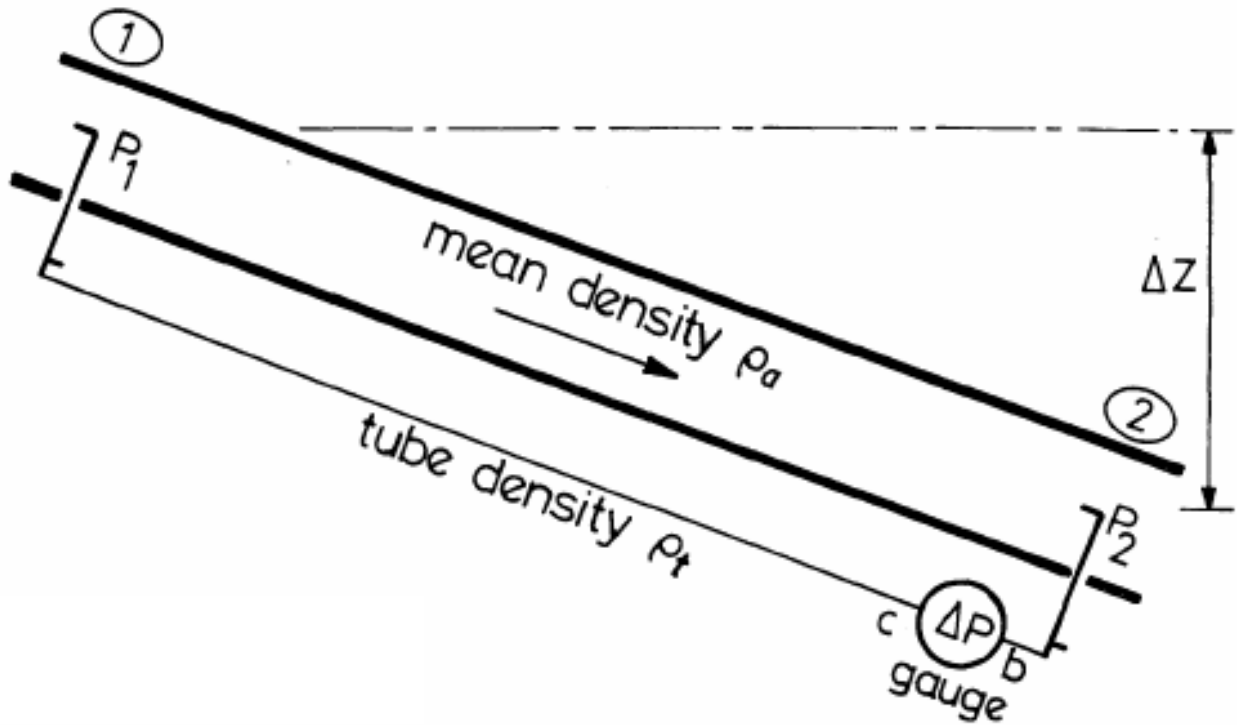


Figure 6.7 Measuring the frictional pressure drop between two stations by the gauge and tube method.

Applying these conditions to equation (6.9) gives

$$p_{12} = \rho_a F_{12} = \rho_a \frac{(u_1^2 - u_2^2)}{2} + \rho_a (Z_1 - Z_2)g - (P_2 - P_1) \quad \text{Pa} \quad (6.11)$$

(See section 3.4.1 for a fuller explanation of this equation.)

However, velocity pressure $p_v = \frac{\rho_a u^2}{2}$

and static pressure $p_s = \rho_a Zg + P$ when referred to the mine datum for elevation.

Hence, equation (6.11) may be written as

$$\begin{aligned} p_{12} &= (p_{v1} + p_{s1}) - (p_{v2} + p_{s2}) && \text{Pa} \\ &= p_{t1} - p_{t2} && \text{Pa} \end{aligned} \quad (6.12)$$

where $p_t =$ total pressure ($p_v + p_s$) as sensed by the total head tapping of a pitot-static tube.

This shows that the frictional pressure drop, p_{12} , referred to the mean density in the airway between the pitot-static tubes is given simply as the pressure gauge reading shown as ΔP in Figure 6.7. If that measured frictional drop is to be referred to a standard value of air density, ρ_{st} , in order to compare or compound it with frictional pressure drops measured in other airways then the correction is given as

$$\rho_{12} \text{ (standardized)} = \rho_{12} \frac{\rho_{st}}{\rho_a}$$

In the great majority of cases no further calculation is required. This explains why the gauge and tube technique is termed a direct method of measuring the frictional pressure drop in an airway. (But see Appendix A6 for situations where there is a significant difference in elevation between the two end stations)

Practical Procedure

The procedure for conducting a gauge and tube survey commences by assembling the equipment and calibrating the gauges. For convenience, a list of the required equipment is given here, together with some explanatory comments:

- 2 pitot-static tubes, approximately 1.25m in length. Shorter instruments may be employed for small airways or for use in ducts.
- An assortment of diaphragm pressure gauges ranging from a full scale deflection of not more than 100 Pa to the highest pressure developed by any fan in the system. The gauges should be calibrated in the horizontal position against a primary manometer immediately prior to an important survey. The use of diaphragm gauges rather than inclined manometers has greatly improved the speed of gauge and tube surveying.
- A continuous length of nylon or good quality plastic tubing between 100 and 200m in length. The tubing should be mechanically strong so that it can withstand being run over by rubber-tyred vehicles or being dragged under doors without permanent damage. An internal diameter from 2 to 3 mm is convenient. Larger tubing may become difficult to handle while the waiting time of transmission of a pressure wave may become unduly long if the tube is too narrow. The tube should be pressure tested before and after the survey.
- Short lengths of flexible tubing to connect the pitot-static tubes and gauge to the main tubing. Metal connectors and clamps should also be carried in case it becomes necessary to repair damage to the main tubing.
- 2 or 3 cans of spray paint for station marking. Chalk or industrial type crayons can also be used.
- 1 pocket barometer and 1 whirling hygrometer.
- 1 waterproof field book and pencils.
- 1 100m flexible measuring tape.
- Tool kit containing screwdrivers, adjustable spanners (wrenches) and a sharp knife.

The route of the traverse and sites of main junction stations should have been established before commencing the observations (Section 6.4). Two persons are required for a gauge and tube survey. It is helpful to have the lowest range gauge fixed within a box with a transparent top, and side holes for extended pressure tappings. Straps around the waist and neck of the observer hold the gauge in a horizontal position. This facilitates travelling and making observations for consecutive tube lengths along an airway.

The following procedure for making the observations is recommended:

1. At the starting station, the pressure tubing is unwound and laid out along the airway in the direction of the second main station. At the forward position, the zero setting of the gauge is checked and, if necessary, adjusted by connecting the high and low pressure tappings by a short length of tubing. The gauge is then connected in-line between the main tube and the total head tapping of the leading pitot-static tube as illustrated on Figure 6.7. At the rear position, the second pitot-static tube is similarly connected to the pressure tubing. The flexible tubing used for connections should be of an internal diameter that fits snugly on to the main tube, the gauge tappings and the pitot-static tube without requiring undue force.
2. To make the observation, both pitot-static tubes are held facing into the airflow, away from the body of the observer and at a position between one half and two thirds the height of the airway. The gauge is observed until the reading becomes constant. This may take two to three minutes depending upon the length and diameter of the main tube. Light tapping of the fingers may assist in overcoming any slight frictional resistance of the diaphragm or linkages within the gauge. On completing the gauge reading, the leading observer should indicate that fact to the trailing observer either by cap-lamp signals or by a tug on the tube. The barometric pressure, wet and dry bulb temperatures are also read and booked by the leading observer together with the distance between observers. In most cases this is the known length of the main tube. For shorter distances, the measuring tape or other means should be used to determine the actual length.
3. The final duty of the leading observer is to paint or chalk an indicator mark on the rail or airway side. A second tug on the tube or a cap-lamp signal indicates that it is time to move on. The leading observer walks forward, dragging the tube behind him. When the trailing observer reaches the indicator mark he simply stops, grasping the main tube firmly.
4. The procedure is repeated for each tube length until the next main (junction) station is reached.

The leading observer is kept busy while the trailing observer has little to do other than holding a pitot-static tube at each station or substation and walking forward. However, it is preferable that the observers exchange positions only in alternate shifts rather than during any one day. An experienced team can progress along a traverse route fairly quickly. Indeed, using modern equipment, it is usually the measurement of airflows by the accompanying airflow team rather than frictional pressure drops that dictates the overall speed of the survey (see section 6.4).

Each major junction of airways should be a main station within a gauge and tube traverse. At each of those junctions, the pitot-static tube should be held at the centre of the junction. If high turbulence causes excessive fluctuations on the gauge then the static tapping(s) on the pitot-static tube(s) may be employed. In this case, an anemometer should be held at the position of the pitot-static tube(s) to measure the local velocity. The corresponding velocity pressures should be calculated and applied as a correction to the gauge reading in order to determine the frictional drop in *total pressure*.

Care should be taken at all times to ensure that the pitot-static tubes do not become clogged by dust or other debris. Similarly, in wet conditions, it is vital to take precautions against water entering any tube. Pitot-static tubes or the open ends of pressure tubing should never be allowed to fall on to the floor during a traverse.

During the course of a pressure traverse, check readings should be taken of the pressure differences across doors between airways. It is convenient to carry a separate 10m length of flexible tubing for this purpose. It takes only a few seconds to attach a gauge of the required

range. If in doubt concerning the range, a high pressure gauge should be used first to establish an approximate pressure difference, then exchanged for a more appropriate instrument if necessary. It is usually sufficient to measure the static pressure across a door. Hence, the two ends of the tubing should be protected against the very local air velocities that sometimes occur from leakage close to a door. A practical way of doing this is simply to insert the end of the tube into one's pocket.

6.3.2. Barometer and altimeter surveys

If the absolute static pressures are measured on barometers at the two ends of a subsurface airway then the difference between those two measured pressures will depend upon

- the difference in elevation between the stations,
- the air velocities, and
- the frictional pressure drop between the two stations at the prevailing airflow.

As the elevations and velocities can be measured independently, it follows that the barometric readings can be used to determine the frictional pressure drop.

The concept of barometers was introduced in section 2.2.4.1. The instruments used for mine barometric surveys are temperature compensated microaneroid devices. The facia of the instruments are normally calibrated in kilopascals or other units of pressure. However, it will be recalled that pressure may be quoted in terms of the column of air (or any other fluid) above the point of measurement.

$$P = \rho g h \quad \text{Pa} \quad (6.22)$$

[see equation (2.8)]

If the air density, ρ , and gravitational acceleration, g , are regarded as constant then the pressure may be quoted in head (metres) of air, h . This relationship is utilized to inscribe the facia of some aneroid barometers in terms of metres (or feet) of air column.

$$h = \frac{P}{\rho g} \quad \text{m} \quad (6.23)$$

The instrument then indicates an approximate elevation or altitude within the earth's atmosphere relative to some datum and, accordingly, is then called an altimeter. For a more accurate elevation, the reading should be corrected for the difference between the actual values of ρ and g , and the standard values to which the altimeter has been calibrated. Some sophisticated altimeters have an inbuilt bias which compensates for changes in air density with respect to height. This allows a linear scale for altitude. For density compensated altimeters, the conversion takes the form:

$$\text{barometric pressure} = \exp(a - b \times \text{indicated altitude})$$

where the constants a and b depend upon the units of pressure and altitude, and factory settings of the altimeter.

In most mining countries, barometric pressure surveys are carried out using direct indicating barometers. In the United States, altimeters are commonly employed. However, if the altimeter readings are converted to pressure units then the two methods become identical.¹

¹ It would seem to have been the larger market (and, hence, readier availability) of altimeters together with the concepts of a head of air and a head of water that led to the early use of altimeters in the United States.

Theory

Again, we commence with the steady flow energy equation for an airway between stations 1 and 2, and containing no fan. In the usual case of polytropic flow, the energy equation gives the work done against friction as:

$$F_{12} = \frac{u_1^2 - u_2^2}{2} + (Z_1 - Z_2)g - R(T_2 - T_1) \frac{\ln\left(\frac{P_2}{P_1}\right)}{\ln\left(\frac{T_2}{T_1}\right)} \quad \frac{\text{J}}{\text{kg}} \quad (6.24)$$

(see equation (8.1))

or, for isothermal flow where $T_1 = T_2$

$$F_{12} = \frac{u_1^2 - u_2^2}{2} + (Z_1 - Z_2)g - RT_1 \ln\left(\frac{P_2}{P_1}\right) \quad \frac{\text{J}}{\text{kg}}$$

where

- P = barometric pressure (kPa)
- T = absolute temperature (degrees Kelvin)
- Z = elevation of barometer location (m)
- u = air velocity at the barometer (m/s)
- and R = mean gas constant (J/kg K) [from equation (14.14)]

As all parameters are measurable in these relationships, the work done against friction, F_{12} can be determined. This, in turn, can be converted into a frictional pressure drop, p_{12} , referred to any given air density, ρ_a .

$$p_{12} = \rho_a F_{12} \quad \text{Pa [see, also, equation (6.10)]}$$

A complication arises if the barometric pressures at the two stations are not read simultaneously. In this case, the surface atmospheric pressure may change during any time interval that occurs between readings at successive stations. If the atmospheric pressure at a fixed control station is observed to increase by ΔP_c during the time elapsed while moving from station 1 to station 2, then the initial value, P_1 , should be corrected to

$$P_1 + \Delta P_c \quad (6.25)$$

The correction, ΔP_c may, of course, be positive or negative. By assuming a series of polytropic processes connecting the control barometer (subscript c) to the traverse barometer (subscript 1), it can be shown that a more accurate value of the correction is given as

$$\Delta P_c \frac{P_1}{P_c} \quad (6.26)$$

Example

The following two lines are an excerpt from a barometer field book.

Station No.	Time	Traverse barometer P kPa	Temperatures		Elevation Z m	Velocity u m/s	Control barometer P_c kPa
			t_d °C	t_w °C			
1	13:42	103.75	15.6	13.0	2652	2.03	98.782
2	14:05	104.61	17.2	14.2	2573	1.52	98.800

Using the psychrometric equations given in section 14.6, the moisture contents of the air at stations 1 and 2 were calculated to be

$$X_1 = 0.008035 \text{ kg/kg dry air}$$

and $X_2 = 0.008536 \text{ kg/kg dry air}$

Equation (14.14) then indicates the corresponding gas constants as

$$R = \frac{287.04 + 461.5 X}{(1 + X)}$$

giving $R_1 = 288.431 \text{ J/kg } ^\circ\text{C}$ and $R_2 = 288.517 \text{ J/kg } ^\circ\text{C}$ with an arithmetic mean of $288.474 \text{ J/kg } ^\circ\text{C}$.

During the time period between taking barometer readings P_1 and P_2 the control barometer registered an increase in atmospheric pressure of

$$\Delta P_c = 98.800 - 98.782 = 0.018 \text{ kPa}$$

Equation (6.26) gives the corrected reading at station 1 as

$$\begin{aligned} & P_1 + \Delta P_c \frac{P_1}{P_c} \\ &= 103.75 + 0.018 \times \frac{103.75}{98.782} \\ &= 103.75 + 0.019 = 103.769 \text{ kPa} \end{aligned}$$

The steady flow energy equation (equation (6.24) then gives

$$F_{12} = \frac{u_1^2 - u_2^2}{2} + (Z_1 - Z_2)g - R(T_2 - T_1) \frac{\ln\left(\frac{P_2/P_1}{T_2/T_1}\right)}{\ln\left(\frac{T_2/T_1}{T_2/T_1}\right)} \quad \frac{\text{J}}{\text{kg}}$$

$$\begin{aligned} \text{where } T_1 &= 273.15 + 15.6 = 288.75 \text{ K} \\ \text{and } T_2 &= 273.15 + 17.2 = 290.35 \text{ K} \end{aligned}$$

$$\begin{aligned}
 F_{12} &= \frac{2.03^2 - 1.52^2}{2} + (2652 - 2573)9.81 - 288.474(17.2 - 15.6) \frac{\ln\left(\frac{104.61}{103.769}\right)}{\ln\left(\frac{290.35}{288.75}\right)} \quad \frac{\text{J}}{\text{kg}} \\
 &= 0.91 + 774.99 - 674.22 \quad \frac{\text{J}}{\text{kg}} \\
 &= 101.7 \quad \frac{\text{J}}{\text{kg}}
 \end{aligned}$$

and the frictional pressure drop referred to standard density becomes

$$\begin{aligned}
 p_{12} &= F_{12} \rho = 101.7 \times 1.2 \\
 &= 122 \quad \text{Pa}
 \end{aligned}$$

(See, also, sections 8.2.2. and 8.3.3. for further examples.)

Practical Procedure

A barometric survey can be conducted with one observer at each station although an additional person at the traverse stations facilitates more rapid progress. The equipment required is as follows:

- 2 microaneroid barometers (or altimeters) of equal precision
- 1 whirling or aspirated psychrometer
- 2 accurate watches
- 1 anemometer
- 1 2m measuring tape
- waterproof field books and pencils
- 2 or 3 cans of spray paint to mark station numbers.

The microaneroids should be calibrated against a primary barometer prior to an important survey. A calibration cabinet can be constructed with the internal pressure controlled by compressed air feeds and outlet valves. In addition to pressure calibration, the instruments should be checked for temperature compensation and creep characteristics. Modern instruments are stable over the range of temperatures normally encountered in mines and adapt to a change in pressure within a few minutes.

For an underground barometer traverse only the main junctions need be considered as measurement stations. Intermediate substations, as required in the gauge and tube technique, are normally unnecessary. However, for main ventilating shafts, the most accurate results are obtained by taking readings at intervals down the shaft (Section 8.2.2).

There are essentially two methods of handling the natural variations in atmospheric pressure that occur during the course of the survey. One technique is to maintain a barometer at a fixed **control station** and to record or log the readings at intervals of about 5 minutes. The second method is the **leapfrog** procedure in which both barometers are used to take simultaneous readings at successive stations. After each set of readings, the trailing barometer is brought up to the forward station where the two barometers are checked against each other and reset if necessary. The trailing barometer is then moved on to assume the leading position at the next station.

The traverse procedure commences with the observers synchronizing their watches. If the control station method is used, the control should be established in a location that is reasonably stable with respect to temperature and not subject to pressure fluctuations from fans, ventilation controls, hoists or other moving equipment. A location on surface near the top of a downcast shaft and shaded from direct sunlight is usually satisfactory. A recording barometer may be employed at the control station, but only if it provides a precision equivalent to that of the traverse barometer.

At each traverse station the following readings are logged:

- date, barometer identification and name of observer
- number and location of station
- time
- barometer reading
- wet and dry bulb temperatures
- anemometer reading at the position of the traverse barometer.

The location of each station should be correlated with surveyors' plans to determine the corresponding elevation. The traverse barometer should be held at the same height above the floor at each station in order that its elevation can be ascertained to within 0.5m.

The anemometer should be employed to measure the air velocity at the position of the barometer. There is no need to conduct an anemometer traverse. As shown in the example given in the previous subsection, the effect of air velocity is usually small compared with the other terms in the steady-flow energy equation.

6.4 ORGANIZATION OF PRESSURE-VOLUME SURVEYS

The preceding two sections have discussed the techniques of measuring volume flows, Q , and frictional pressure drops, p , separately. It will be recalled that the results of the two types of survey will be combined to give the resistance, $R = p/Q^2$, and airpower loss, pQ , of each branch. As airflows and, hence, frictional pressure drops vary with time in an operating subsurface facility, it follows that p and Q should, ideally, be measured simultaneously in any given airway. Typically, there are two observers measuring airflows and another two involved in the pressure survey. The two teams must liaise closely.

6.4.1. Initial planning

A pressure-volume survey should be well planned and managed. The practical work for a major survey commences a week or two before the underground observations by assembling, checking and calibrating the equipment. In particular, it is inadvisable to rely upon manufacturers' original calibrations of vane anemometers or diaphragm pressure gauges. If the equipment required for calibration is unavailable locally then the work may be carried out by a service organization or the instruments returned to the manufacturers for customized calibration. The calibration is normally produced as a table of corrections against indicated readings and taped to the side of the instrument or carrying case. Interpolation from the table can be carried out at the time of measurement so that the reading, correction and corrected observation can all be logged immediately.

The mine plan should be studied carefully and the routes of the survey selected. A full mine survey will include each ventilation connection to surface and the infrastructure of airways that comprise the primary ventilation routes. Subsidiary survey routes may be appended to include individual working districts or to extend a data bank that exists from previous surveys. The routes should be chosen such that they can be formulated into closed traverse paths or loops within the ventilation network of the mine. Branches that connect to the surface close through the pressure

sink of the surface atmosphere. A main loop in a large mine may take several days to survey. However, each main loop should be divided into smaller subsidiary loops each of which can be closed within a single day of surveying.

An initial reconnaissance of the mine should be carried out, travelling through all airways selected for the primary traverses and establishing the locations of main stations. These are normally at major junctions of the ventilation system. Where two or more airways are adjacent and in parallel - and the gauge and tube method is employed for the pressure measurements - then it is necessary to take those measurements in one of the airways only. However, to obtain the total airflow in that composite branch of the network, it will be necessary to take flow measurements at corresponding points in each of the parallel airways. Airflow measuring stations should be selected and marked on the plan and, also, on the walls of the airway.

The subsequent employment of survey data for ventilation network analysis and forward planning (Chapters 7 and 9) should be kept in mind during the management of ventilation surveys. The identification number assigned to each network junction should give an indication of the location of the junction within the mine. In multi-level workings, for example, the first integer of station numbers may be used to indicate the level.

A pre-survey briefing meeting should be held with all observers present. Each observer should be fully trained in survey procedures, use of the instruments and techniques of observation. The traverse routes and system of station identification should be discussed, together with an outline schedule covering the days or weeks required to complete the survey.

6.4.2. Survey management

During production shifts, the airflows and pressure drops in an underground mine are subject to considerable variation due to movement of equipment, changes in resistance in the workings and opening of ventilation doors. Hence, the best time for ventilation surveys is when the mine is relatively quiescent with few people underground. During the duration of a survey, the observers should be prepared to work at weekends and on night shifts.

Although the frictional pressure drop and corresponding airflow should, ideally, be measured simultaneously in each leg of the traverse, this is often not practicable. Nevertheless, the teams should stay fairly near to each other so that there is a minimum delay between the two sets of measurements in a given branch. With experienced observers the teams maintain close liaison, assisting one another and always being conscious of the activity of the other team. This avoids the infuriating situation of the pressure team opening doors to take a check reading while the airflow team is in the middle of an anemometer traverse. Friendships have been known to suffer on such occasions.

Immediately following each shift the two teams should check all calculations carried out underground, transcribe the results of that shift's work from the field books to clean log sheets and, also, to a large scale copy of a mine map. Positions of measured airflows and pressure drops should be reviewed by both teams to ensure compatibility of measurement locations and to correlate identification of station numbers. Any difficulties encountered during the shift should be discussed. The final half hour or so of each working day may be spent in reviewing the ground to be covered in the following shift and the allocation of individual duties.

6.4.3. Quality assurance

It is most important that control is maintained over the quality of all aspects of an important ventilation survey, from initial calibration of the instruments through to the production of final results. Field books or booking sheets should be laid out clearly such that persons other than the observers can follow the recording of observations and calculations carried out underground. All calculations should be checked by someone other than the originator. Most of the calculations

involved in ventilation surveys are quite simple and may be carried out on a pocket calculator. The exception is for barometric surveys where a verified program for a personal computer is very helpful. Commercially available spreadsheet software can readily be adapted for this purpose.

Adherence to Kirchhoff's Laws should be checked both at the time of observations wherever practicable and, also, during the data transposition at the end of each shift. These laws are discussed fully in Chapter 7. Briefly, Kirchhoff I requires that the algebraic sum of airflows entering any junction is zero. Kirchhoff II states that the algebraic sum of standardized pressure drops around any closed loop must also be zero, having taken fans and natural ventilation pressures into account. In a level or near level circuit, the closing error of a pressure loop may be expressed as the actual closure divided by the sum of the absolute values of the measured frictional pressure drops around the loop. This should not exceed 5 per cent. The check measurements of pressure differentials across doors are invaluable in tracing or distributing observational errors. In the case of loops involving significant changes in elevation such as shaft circuits, the sum of standardized pressure drops will be a combination of observational errors and natural ventilating effects. The latter may be determined independently from temperature and pressure measurements as discussed in section 8.3.

It is vital that good records be kept of each phase of a survey. The survey team leader should maintain a detailed journal of the activities and achievements of each working day. This should include the clean log sheets of results transcribed from the field books at the end of each shift.

The conclusion of a major survey should see the establishment of a spreadsheet type of data bank or the extension of an existing data bank, holding the frictional pressure drop and corresponding airflow for every branch included in the survey. Other details such as the dates of observations, names of observers, instrument identifications and dimensions of airways may be included. The data bank may then be used to calculate airway resistances, airpower losses and friction factors, and also provides a data base from which a computer model of the mine ventilation network can be generated (Chapter 9). Additionally, the resistances, resistance per unit length and airpower losses may be shown on a colour-coded map in order to highlight sections of airways that are particularly expensive to ventilate.

6.5. AIR QUALITY SURVEYS

While pressure-volume surveys are concerned with the distribution of airflow around a ventilation system, the subsurface environmental engineer must also maintain control of the quality of that air, i.e. the concentrations of gaseous or particulate pollutants, and the temperature and humidity of the air. Such measurements should be made at specified times and places to ensure compliance with mandatory standards and with a regard for the safety and health of the workforce.

Details of the techniques of measuring and quantifying levels of dust, gas concentrations and climatic conditions are given in Chapter 23, 11 and 14 respectively. In addition to mandatory measurements a set of such observations made in a systematic manner around a continuous path is known as an air quality survey. This procedure should be employed for two reasons. First, it provides a means of tracking and quantifying the variation in pollutant levels and, secondly, it enables zones of emission of gases, dust, heat and humidity to be identified. Measurements of gas concentration are often made as a normal part of a pressure-volume survey in a gassy mine. Similarly the observations of barometric pressure, wet and dry bulb temperature made during a pressure survey may be used to compute and plot the variations in psychrometric conditions throughout the traverse paths.

BIBLIOGRAPHY

Air Movement and Control Assoc. Inc. (1976). **AMCA Application Manual (Part 3)**. A guide to the Measurement of Fan System Performance in the Field.

American National Standard (1985). Laboratory Methods of Testing Fans for Rating. AMCA, 30 West University Drive, Arlington Heights, IL 60004.

ASHRAE Handbook (1985). Fundamentals Volume. ASHRAE, 1791 Tullie Circle, N.E. Atlanta, GA. 30329, USA.

British Standard 848 Part 1 (1963). Methods of Testing Fans for General Purposes. British Standards Institution, 2 Park St., London W.1.

Hartman H.L., Mutmansky, J. and Wang, W.J., (1982). **Mine Ventilation and Air Conditioning**. Wiley Interscience.

Hinsley, F.B., (1962). The assessment of energy and pressure losses due to air-flow in shafts, airways and mine circuits **The Mining Engineer, Vol 121. No. 23, pp. 761-777**.

Hinsley, F.B., (1964). An enquiry into the principles and mutual interaction of natural and fan ventilation. **The Mining Engineer, Vol 124. No. 49, pp. 63-78**.

McPherson, M.J., (1969). A new treatment of mine barometer surveys. **The Mining Engineer, Vol 129 No. 109, pp. 23-34**.

McPherson, M. J and Robinson, G. (1980). Barometric survey of shafts at Boulby Mine, Cleveland Potash Ltd., **Trans. Inst of Min. and Met. Vol 89 - reproduced Jnl. Mine Ventilation Society of S. Africa, Vol 9, No.3, Sept. 1980**.

McPherson, M.J., (1985). The resistance to airflow on a longwall face. **2nd U.S. Mine ventilation Symposium, Reno, NV. pp. 531-542**.

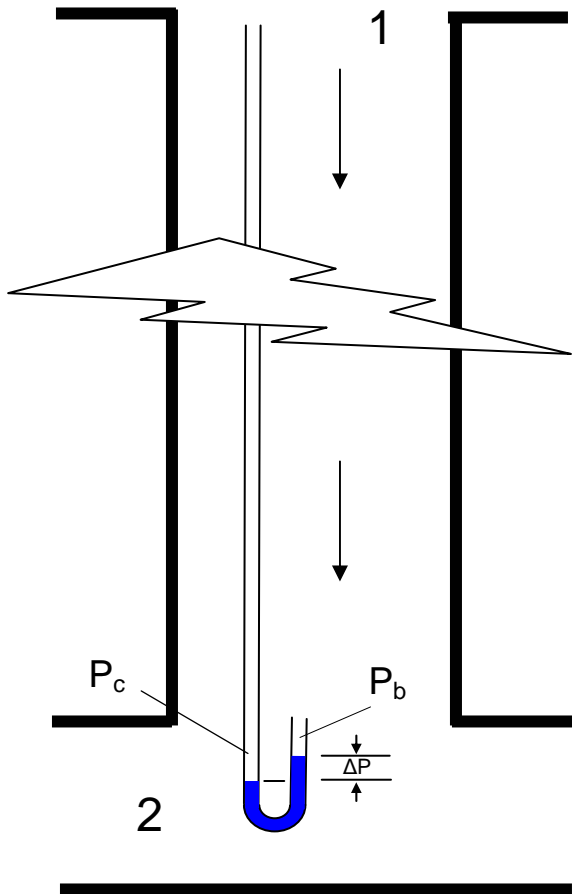
Mine Ventilation Society of South Africa, (1982). **Environmental Engineering in South African Mines. Mine Ventilation Society of S. Africa, Kelvin House, 2 Hollard St., Johannesburg, S. Africa**.

National Coal Board, U.K. (1979). **Ventilation in Coal Mines: A Handbook for Colliery Ventilation Engineers**.

Appendix A6.

Application of the gauge and tube method of measuring frictional pressure drops in cases of significant differences in elevation.

To this time, the gauge and tube technique has seldom been used for vertical shafts or highly inclined airways although the often difficult task of measuring shaft resistance would be greatly facilitated by leaving a length of small bore pressure tubing permanently in the shaft². Where the ends of the tube are at significantly different elevations a complication does, however, arise. It is found that in these circumstances, the reading depends upon the location of the gauge and increases as the elevation of the gauge decreases within the airway. This phenomenon occurs because the air within the tubing is stationary and, hence, not affected by friction. The pressure at all points within the tube differs from that outside the tube at the same elevation. For example, if the gauge is located at the bottom of a downcast shaft, as shown in Figure A6.1 the pressure in the tube will be higher than at a corresponding elevation outside the tube. If the temperature and moisture content inside and outside the tube are the same at corresponding points it follows that the mean density in the tube must be a little higher than that in the airway.



If the gauge is to indicate directly the frictional pressure drop referred to the mean density in the airway, ρ_a then it must be located at the position of mean density. In shafts or other airways of constant slope and resistance, this is very close to the midpoint. However, it is usually difficult to take measurements at this position and it is more practicable to site the pressure gauge either at the top or bottom of the shaft. A correction must then be applied to the reading in order to arrive at the frictional pressure drop referred to the mean air density.

We shall continue this analysis assuming the gauge to be at the base of a downcast shaft (Figure A6.1). The pressure in the tubing at the high pressure tapping is P_c and that at the low pressure tapping is P_b . The gauge reads $\Delta P = P_c - P_b$. However, the pressure P_c must equal the total pressure at station 1 plus the pressure due to the head of static air within the tube

$$P_c = P_1 + \frac{\rho_1 u_1^2}{2} + \Delta Z g \rho_t$$

where P = barometric (static) pressure
 u = air velocity
 ΔZ = depth of shaft
 and ρ_t = mean air density within the tube

And, at the low pressure tapping of the gauge

$$P_b = P_2 + \frac{\rho_2 u_2^2}{2}$$

Figure A6.1 Gauge at the bottom of a downcast shaft. The gauge is depicted as a manometer to show the direction of the pressure difference.

² Where such a tube is left in place permanently, it should be tested for leaks and internal condensate before being used for a frictional pressure drop observation. A disconnected compressed air pipe may be used as a temporary pressure tube.

Then

$$\Delta P = P_c - P_b = \frac{\rho_1 u_1^2 - \rho_2 u_2^2}{2} + \Delta Z g \rho_t + (P_1 - P_2) \quad (6.13)$$

Now, from equation (6.11), the frictional pressure drop in the airway, referred to the airway mean density, ρ_a , is given as

$$p_{12} = \rho_a \frac{u_1^2 - u_2^2}{2} + \Delta Z g \rho_a + (P_1 - P_2) \quad (6.14)$$

Hence, the "error" in the gauge reading becomes

$$\varepsilon = \Delta P - p_{12} = \frac{(\rho_1 u_1^2 - \rho_2 u_2^2) - (u_1^2 - u_2^2) \rho_a}{2} + \Delta Z g (\rho_t - \rho_a) \quad (6.15)$$

We can substitute for

$$\rho_a = \frac{\rho_1 + \rho_2}{2} \quad (\text{Mean density in airway})$$

$$\rho_t = \frac{\rho_1 + \rho_c}{2} \quad (\text{Mean density in tube})$$

where ρ_c = density in tube at position c.

$$\text{Now } \rho_c = \frac{P_c}{RT_2} \quad \text{and} \quad \rho_2 = \frac{P_2}{RT_2}$$

$$\text{giving } \rho_c - \rho_2 = \frac{P_c - P_2}{RT_2} = \Delta P \frac{\rho_2}{P_2} \quad (\text{ignoring the small effect of velocity pressure on the air density at position b.})$$

$$\text{or } \rho_c = \rho_2 + \frac{\Delta P}{P_2} \rho_2$$

Then, after some algebraic simplification, equation (6.15) becomes

$$\varepsilon = \frac{\Delta Z g \Delta P \rho_2}{2 P_2} - \frac{(u_1^2 + u_2^2)}{4} (\rho_2 - \rho_1) \quad (6.16)$$

giving

$$p_{12} = \Delta P - \varepsilon = \Delta P \left\{ 1 - \frac{\Delta Z g \rho_2}{2 P_2} \right\} + \frac{(u_1^2 + u_2^2)}{4} (\rho_2 - \rho_1) \quad (6.17)$$

This is the full form of the equation that allows the reading on the gauge at the base of the shaft or slope to be corrected to mean density for the airway.

The term $\frac{\Delta Z g \rho_2}{2 P_2}$

arises from the difference in mean air density between the airway and the tubing (equation (6.15),

while $\frac{(u_1^2 + u_2^2)}{4} (\rho_2 - \rho_1)$

is the result of converting the velocity pressures at ρ_1 and ρ_2 to the mean density ρ_a . To be precise, this latter term should be applied even when the airway is level. However, it is normally insignificant and may be ignored for practical purposes, giving the frictional pressure drop referred to the mean air density in the shaft as

$$p_{12} = \Delta P \left\{ 1 - \frac{\Delta Z g \rho_2}{2 P_2} \right\} \quad (6.18)$$

Equation (6.18) illustrates that the uncorrected reading, ΔP , on the shaft bottom gauge overestimates the actual frictional pressure drop.

Similar reasoning leads to the following equations for other configurations:

Gauge at the top of a downcast shaft

$$p_{12} = \Delta P(\text{top}) \left\{ 1 + \frac{\Delta Z g \rho_1}{2 P_1} \right\} + \frac{(u_1^2 + u_2^2)}{4} (\rho_2 - \rho_1) \quad (6.19)$$

Gauge at the base of an upcast shaft

$$p_{34} = \Delta P(\text{top}) \left\{ 1 - \frac{\Delta Z g \rho_3}{2 P_3} \right\} + \frac{(u_3^2 + u_4^2)}{4} (\rho_3 - \rho_4) \quad (6.20)$$

(Subscripts 3 and 4 refer to the bottom and top respectively of an upcast shaft.)

Gauge at the top of an upcast shaft

$$p_{34} = \Delta P(\text{top}) \left\{ 1 + \frac{\Delta Z g \rho_4}{2 P_4} \right\} + \frac{(u_3^2 + u_4^2)}{4} (\rho_3 - \rho_4) \quad (6.21)$$

Again, the kinetic energy term involving u values can usually be neglected.

Hinsley, in 1962 showed that for both downcast and upcast shafts the frictional pressure drops are given to a good approximation by the arithmetic average of the gauge readings at the top and bottom of the shaft.

Calculated Example

The following data³ were established for a downcast shaft fitted with a tube throughout its length. A pressure gauge can be connected to either the top or the bottom of the tube. Ignoring the small effects of air velocity, determine the frictional pressure drop, p_{12} , referred to the mean air density in the shaft.

Depth of shaft = 1219.2 m

	Top of shaft	Bottom of shaft
Barometric pressure, kPa	101.591	117.015
Air density, kg/m ³ (from psychrometric measurements – ref. Chapter 14, Section 6)	1.275	1.408
Pressure gauge when connected to top of tube, Pa	566	
Pressure gauge when connected to base of tube, Pa		655

Solution

(a) Using the pressure gauge reading at the top of the shaft, equation (6.19) applies. Ignoring the kinetic energy terms:

$$\begin{aligned}
 p_{12} &= \Delta P(\text{top}) \left\{ 1 + \frac{\Delta Z g \rho_1}{2 P_1} \right\} \\
 &= 566 \left\{ 1 + \frac{1219.2 \times 9.8066 \times 1.275}{2 \times 101591} \right\} = 608 \quad \text{Pa}
 \end{aligned}$$

(b) Using the pressure gauge reading at the bottom of the shaft equation (6.18) applies.

$$\begin{aligned}
 p_{12} &= \Delta P \left\{ 1 - \frac{\Delta Z g \rho_2}{2 P_2} \right\} \\
 &= 655 \left\{ 1 - \frac{1219.2 \times 9.8066 \times 1.408}{2 \times 117015} \right\} = 608 \quad \text{Pa}
 \end{aligned}$$

In both cases, p_{12} is referred to the mean air density in the shaft and, hence, give the same result. (In practice, it is to be expected that there will not be exact agreement between the results of shaft top and shaft bottom gauge locations because of observational errors.)

³ The given data are taken from Hinsley, F.B. (1962) on the basis of a frictional adiabatic process in a dry shaft. [“The Assessment of Energy and Pressure Losses due to Airflow in Shafts, Airways and Mine Circuits” (Section IV). The Mining Engineer, Vol.121, No. 23, August 1962.]

The arithmetic mean density in the shaft is

$$\rho_{mean} = \frac{1.408 + 1.275}{2} = 1.341 \quad \frac{\text{kg}}{\text{m}^3}$$

If corrected to standard air density ($\rho_{st}=1.2 \text{ kg/m}^3$) for comparison with other airways, the standardized frictional pressure drop becomes

$$\rho_{st} = \rho_{12} \times \frac{\rho_{st}}{\rho_{mean}} = 608 \times \frac{1.2}{1.341} = 544 \text{ Pa}$$

To check the approximate method of establishing the frictional pressure drop from the mean of the top and bottom gauge readings:-

The arithmetic mean of the pressure gauge readings at the top and bottom of the shaft is

$$\frac{566 + 655}{2} = 610.5 \quad \text{Pa}$$

showing that, in this case, the approximation is in excellent agreement with the calculated 608 Pa.

Chapter 7. Ventilation Network Analysis

7.1. INTRODUCTION	1
7.2 FUNDAMENTALS OF VENTILATION NETWORK ANALYSIS.....	3
7.2.1 Kirchhoff's Laws.....	3
7.2.2 Compressible or incompressible flow in ventilation network analysis	4
7.2.3 Deviations from the Square Law.....	6
7.3. METHODS OF SOLVING VENTILATION NETWORKS	6
7.3.1 Analytical Methods.....	6
7.3.1.1 Equivalent Resistances.....	6
7.3.1.2 Direct Application of Kirchhoff's Laws	10
7.3.2 Numerical Methods.....	12
<i>The Hardy Cross Technique.....</i>	13
(a) Mesh selection:	18
(b) Estimate initial airflows:.....	18
(c) Calculate mesh correction factors:.....	18
(d) Apply the mesh correction factor:.....	19
(e) Completion of mesh corrections.....	20
7.4. VENTILATION NETWORK SIMULATION PACKAGES.....	24
7.4.1 Concept of a mathematical model	24
7.4.2 Structure of a ventilation simulation package	25
7.4.3 Operating system for a VNET package	26
7.4.4 Incorporation of air quality into a network simulation package	27
7.4.5 Obtaining a ventilation simulation package	28
<i>Hardware requirements and size of network.....</i>	28
<i>Cost of software.....</i>	28
<i>Speed.....</i>	28
<i>Scope and ease of use.....</i>	28
<i>User's manual and back-up assistance.....</i>	28
7.4.6 Example of a computed network	29
REFERENCES	39

7.1. INTRODUCTION

A vital component in the design of a new underground mine or other subsurface facility is the quantified planning of the distribution of airflows, together with the locations and duties of fans and other ventilation controls required to achieve acceptable environmental conditions throughout the system. Similarly, throughout the life of an underground operation, it is necessary to plan ahead in order that new fans, shafts or other airways are available in a timely manner for the efficient ventilation of extensions to the workings. As any operating mine is a dynamic system with new workings continually being developed and older ones coming to the end of their productive life, ventilation planning should be a continuous and routine process.

The preceding chapters have discussed the behaviour of air or other fluid within an individual airway, duct or pipe. Ventilation network analysis is concerned with the interactive behaviour of airflows within the connected branches of a complete and integrated network. The questions addressed by ventilation network analysis may be formulated quite simply. If we know the resistances of the branches of a ventilation network and the manner in which those branches are interconnected then how can we predict, quantitatively, the distribution of airflow for given locations and duties of fans?

Alternatively, if we know the airflows that we need in specific branches of the network then how can we determine an efficient combination of fans and structure of the network that will provide those required airflows? **Ventilation network analysis** is a generic term for a family of techniques that enable us to address such questions.

In a given network there are a large number of combinations of airway resistances, fans, and regulators that will give any desired distribution of flow. Practical considerations limit the number of acceptable alternatives. However, the techniques of network analysis that are useful for modern industrial application must remain easy to use, and sufficiently rapid and flexible to allow multiple alternative solutions to be investigated.

Before the mid 1950's there were no practicable means of conducting detailed and quantitative ventilation network analysis for complete mine systems. Ventilation planning was carried out either using hydraulic gradient diagrams formulated from assumed airflows or, simply, based on the experience and intuition of the ventilation engineer. Attempts to produce physical models of complete mine ventilation systems using air or water as the medium met with very limited success because of difficulties from scale effects. Following earlier research in Holland (Maas, 1950), the first viable **electrical analogue computers** to simulate ventilation networks were produced in the United Kingdom (Scott et al, 1953) followed rapidly in the United States (McElroy, 1954). These analogues employed electrical current passing through rheostats to simulate airflows. Successive adjustment of the resistances of the rheostats enabled the linear Ohm's law for electrical conductors to emulate the square law of ventilation networks.

Linear resistance analogues became the main automated means of analyzing mine ventilation networks in the nineteen fifties and early 'sixties. Rapid advances in the electronics industries during that time resulted in the development of direct reading fluid network analogues that replaced the linear resistors with electronic components. These followed a logarithmic relationship between applied voltage and current, producing analogues that were easier to use and much faster in operation (Williams, 1964). However, by the time they became available, ventilation simulation programs for mainframe digital computers had begun to appear (McPherson 1964, Hartman and Wang 1967). These proved to be much more versatile, rapid and accurate, and their employment soon dominated ventilation planning procedures in major mining countries. Coupled with continued improvements in ventilation survey techniques to provide the data, ventilation network analysis programs resulted in hitherto unprecedented levels of flexibility, precision and economics in the planning, design and implementation of mine ventilation systems.

Throughout the 1970's network programs were developed for large centralized mainframe computers. Their initial use by industry tended to be inhibited by the often pedantic procedures of data preparation together with the costs and delays of batch processing. In the 1980's, the enhanced power and reduced cost of microcomputers led to the evolution of self-contained software packages that allowed very easy interaction between the user and the computer. These incorporated the use of graphics. Ventilation engineers could, for the first time, conduct multiple planning exercises on large networks entirely within the confines of their own offices. The complete processing of data from survey observations through to the production of plotted ventilation plans became automated. Personal computers, printers and plotters proliferated in mine planning offices. Together with the ready availability of software, these led to a revolution in the methodologies, speed and accuracy of subsurface ventilation planning.

In this chapter, we shall introduce the basic laws that govern the distribution of airflow within a network of interconnected branches. The analytical and numerical methods of predicting airflows will be examined before proceeding to a discussion of network simulation packages.

7.2 FUNDAMENTALS OF VENTILATION NETWORK ANALYSIS

Any integrated ventilation system can be represented as a schematic diagram in which each line (branch) denotes either a single airway or a group of openings that are connected such that they behave effectively as a single airway (Section 7.3.1.1). Only those airways that contribute to the flow of air through the system appear on the network schematic. Hence, sealed off areas of insignificant leakage, stagnant dead ends and headings that produce no induction effects (Section 4.4.3) on the main airflow need not be represented in the network. On the other hand, the tops of shafts or other openings to surface are connected to each other through the pressure sink of the surface atmosphere. The points at which branches connect are known simply as junctions or nodes.

7.2.1 Kirchhoff's Laws

Gustav R. Kirchhoff (1824-87) was a German physicist who first recognized the fundamental relationships that govern the behaviour of electrical current in a network of conductors. The same basic relationships, now known as Kirchhoff's Laws, are also applicable to fluid networks including closed ventilation systems at steady state.

Kirchhoff's first law states that the mass flow entering a junction equals the mass flow leaving that junction or, mathematically,

$$\sum_j M = 0 \quad (7.1)$$

where M are the mass flows, positive and negative, entering junction j .

However, it will be recalled that

$$M = Q\rho \quad \frac{\text{kg}}{\text{s}} \quad (7.2)$$

where Q = volume flow (m^3/s) and
 ρ = air density (kg/m^3)

$$\text{Hence } \sum_j Q\rho = 0 \quad (7.3)$$

In subsurface ventilation systems, the variation in air density around any single junction is negligible, giving

$$\sum_j Q = 0 \quad (7.4)$$

This provides a means of checking the accuracy of airflow measurements taken around a junction (Section 6.4.3).

The simplest statement of **Kirchhoff's second law** applied to ventilation networks is that the algebraic sum of all pressure drops around a closed path, or mesh, in the network must be zero, having taken into account the effects of fans and ventilating pressures. This can be quantified by writing down the steady flow energy equation (3.25), initially for a single airway.

$$\frac{\Delta u^2}{2} + \Delta Zg + W = \int V dP + F \quad \frac{\text{J}}{\text{kg}} \quad (7.5)$$

where u = air velocity (m/s)
 Z = height above datum (m)
 W = work input from fan (J/kg)
 V = specific volume (m^3/kg)
 P = barometric pressure (Pa) and
 F = work done against friction (J/kg)

If we consider a number of such branches forming a closed loop or mesh within the network then the algebraic sum of all ΔZ must be zero and the sum of the changes in kinetic energy, $\Delta u^2/2$, is negligible. Summing each of the remaining terms around the mesh, m , gives

$$\sum_m \int V dP + \sum_m [F - W] = 0 \quad \frac{\text{J}}{\text{kg}} \quad (7.6)$$

Now the summation of $-\int V dP$ terms is the natural ventilating energy, NVE , that originates from thermal additions to the air (Section 8.3.1). Hence, we can write

$$\sum [F - W] - NVE = 0 \quad \frac{\text{J}}{\text{kg}} \quad (7.7)$$

This may now be converted to pressure units by multiplying throughout by a single value of air density ρ .

$$\sum [\rho F - \rho W] - \rho NVE = 0 \quad \text{Pa} \quad (7.8)$$

However, $\rho F = p$ (frictional pressure drop, equation (2.46))
 $\rho W = p_f$ (rise in total pressure across a fan) and
 $\rho NVE = NVP$ (natural ventilating pressure, equation (8.32)),

each of these three terms being referred to the same (standard) density. The equation then becomes recognizable as Kirchhoff's second law:

$$\sum (p - p_f) - NVP = 0 \quad \text{Pa} \quad (7.9)$$

This is the relationship that is employed as a quality assurance check on a pressure survey (Section 6.4.3), or as a means of determining a value for the natural ventilating pressure (equation 8.51)).

7.2.2 Compressible or incompressible flow in ventilation network analysis

Kirchhoff's laws can be applied to fluid networks that conduct either compressible or incompressible fluids. In the former case, the analysis is carried out on the basis of mass flow. Equations (7.1) or (7.3) are employed for the application of Kirchhoff's first law and equation (7.7) for Kirchhoff's second law.

There is another set of equations that must be obeyed within ventilation networks. Those have already been introduced as the square law for each individual branch. When the flow is deemed to be compressible, then the rational form of the square law should be utilized

$$p = R_t \rho Q^2 \quad \text{Pa} \quad (\text{see equation (2.50)})$$

where $R_t =$ rational turbulent resistance (m^{-4})

But, as $p = F\rho$ (equation (2.46)),

$$p = F\rho = R_t\rho Q^2$$

$$\text{giving } F = R_t Q^2 \quad \frac{\text{J}}{\text{kg}} \quad (7.10)$$

Kirchhoff's second law for compressible flow (equation (7.7)) becomes

$$\sum_m [R_t Q^2 - W] - NVE = 0 \quad \frac{\text{J}}{\text{kg}} \quad (7.11)$$

As we progress from branch to branch around a closed mesh in a network then it is the algebraic values of the pressure drops, p , or losses of mechanical energy, F , that must be summed. These are both positive in the direction of flow and negative if the flow is moving against the direction of traverse around the mesh. Hence, equation (7.11) may, more appropriately, be written as

$$\sum_m [R_t Q |Q| - W] - NVE = 0 \quad \frac{\text{J}}{\text{kg}} \quad (7.12)$$

where $Q =$ airflow with due account taken of sign ($\pm \text{m}^3/\text{s}$)
and $|Q| =$ absolute value of airflow and is always positive ($+\text{m}^3/\text{s}$).

This device ensures that the frictional pressure drop or loss of mechanical energy always have the same sign as airflow.

In the case of incompressible flow, the application of Kirchhoff's laws becomes more straightforward. Equations (7.4) and (7.9) give

$$\begin{aligned} \sum_j Q &= 0 && \text{(Kirchhoff I)} \\ \text{and } \sum_m RQ|Q| - p_f) - NVP &= 0 && \text{(Kirchhoff II)} \end{aligned} \quad (7.13)$$

where $R =$ Atkinson resistance (Ns^2/m^8)

It will be recalled that the three terms of this latter equation should each be referred to the same (standard) value of air density, normally $1.2 \text{ kg}/\text{m}^3$.

Computer programs have been developed for compressible flow networks. These require input data (pressures, temperatures, elevations and air quality parameters) from which variations in air density and natural ventilation effects may be calculated. On the other hand, where compressibility and natural ventilating effects need to be taken into account, there are means by which these can be simulated to an acceptable accuracy by an incompressible flow network program. For these reasons, the great majority of subsurface ventilation planning employ the simpler and faster incompressible flow programs. The more sophisticated and demanding compressible flow programs are required for compressed air (or gas) networks or for specialized applications in subsurface ventilation systems.

The remainder of this chapter will concentrate on incompressible flow network analysis.

7.2.3 Deviations from the Square Law

The square law was derived in Section 2.3.6 from the basic Chezy Darcy relationship and further developed in Section 5.2. Both the rational form of the square law, $p = R_f \rho Q^2$, and the traditional form, $p = RQ^2$, apply for the condition of fully developed turbulence. Furthermore, both the rational resistance, R_f , and the Atkinson resistance, R , are functions of the coefficient of friction, f , for the duct or airway (equations (2.51), (5.4), and (5.1)). Hence, if the flow falls into the transitional or laminar regimes of the Moody chart (Figure 2.7) then the value of f becomes a function of Reynolds Number. The corresponding values of resistance, R_f , or R , for that airway then vary with the airflow. If the form of the square law is to be retained then the values of resistance must be computed for the relevant values of Reynolds Number.

However, many experimental researchers have found that plotting $\ln(p)$ against $\ln(Q)$ may give a slope that deviates slightly from Chezy Darcy's theoretical prediction of 2, even for fully developed turbulence. The relationship between frictional pressure drop, p , and volume flowrate, Q , may be better expressed as

$$p = RQ^n \quad \text{Pa} \quad (7.14)$$

where values of the index, n , have been reported in the range of 1.8 to 2.05 for a variety of pipes, ducts and fluids. Similar tests in mine airways have shown that n lies very close to 2 for routes along the main ventilation system but may be lower for leakage flows through stoppings or old workings. This effect is caused primarily by flows that enter the transitional or, even, laminar regimes. In the latter case, n takes the value of 1.0 and the pressure drop flow relationship becomes

$$p = R_L Q \quad (\text{see equation (2.32)})$$

where R_L = laminar resistance

In the interests of generality, we shall employ equation (7.14) in the derivations that follow.

7.3. METHODS OF SOLVING VENTILATION NETWORKS

There are essentially two means of approach to the analysis of fluid networks. The analytical methods involve formulating the governing laws into sets of equations that can be solved analytically to give exact solutions. The numerical methods that have come to the fore with the availability of electronic digital computers solve the equations through iterative procedures of successive approximation until a solution is found to within a specified accuracy.

In both cases, the primary processes of solution may be based on the distribution of pressures throughout the network or, alternatively, on the distribution of flows. The former may be preferred for networks that involve many outlet points such as a water distribution network. On the other hand, for networks that form closed systems such as subsurface ventilation layouts it is more convenient to base the analysis on flows.

7.3.1 Analytical Methods

7.3.1.1 Equivalent Resistances

This is the most elementary of the methods of analyzing ventilation networks. If two or more airways are connected either in series or in parallel then each of those sets of resistances may be combined into a single equivalent resistance. Although of fairly limited value in the analysis of

complete networks, the method of equivalent resistances allows considerable simplification of the schematic representation of actual subsurface ventilation systems.

In order to determine an expression for a **series circuit**, consider Figure 7.1 (a). The frictional pressure drops are given by equation (7.14) as

$$p_1 = R_1 Q^n, \quad p_2 = R_2 Q^n, \quad p_3 = R_3 Q^n$$

Then for the combined series circuit,

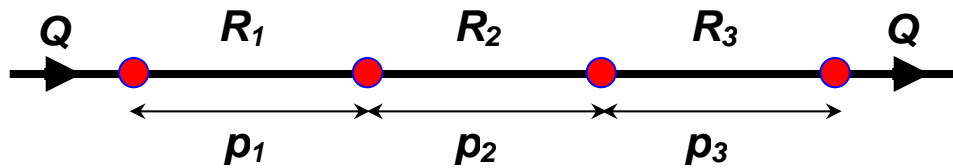
$$p = (p_1 + p_2 + p_3) = (R_1 + R_2 + R_3) Q^n$$

or $p = R_{ser} Q^n$ where $R_{ser} = R_1 + R_2 + R_3$

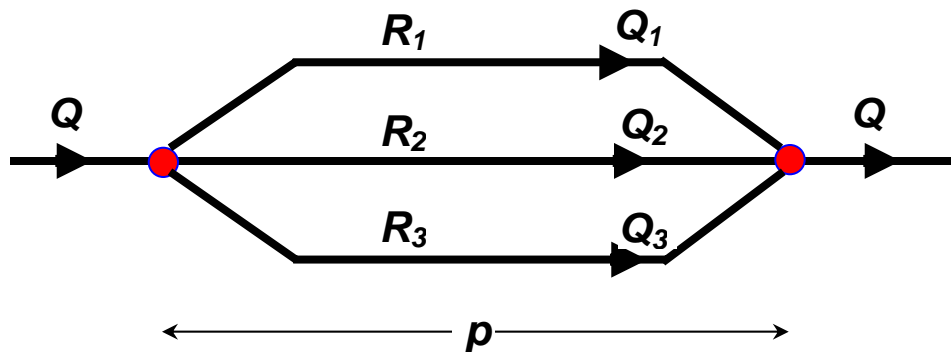
R_{ser} is the **equivalent resistance** of the series circuit.

In general, for a series circuit

$$R_{ser} = \Sigma R \quad (7.15)$$



(a) Resistances connected in series



(b) Resistances connected in parallel.

Figure 7.1 Series and parallel circuits.

In the case of a **parallel circuit**, Figure 7.1 (b) shows that each branch suffers from the same frictional pressure drop, p , between the common “start” and “end” junctions but passes differing airflows. Then

$$p = R_1 Q_1^n = R_2 Q_2^n = R_3 Q_3^n$$

$$\text{giving } Q_1 = (p/R_1)^{1/n}$$

$$Q_2 = (p/R_2)^{1/n}$$

$$Q_3 = (p/R_3)^{1/n}$$

The three airflows combine to give

$$Q = Q_1 + Q_2 + Q_3 = p^{1/n} \left\{ \frac{1}{R_1^{1/n}} + \frac{1}{R_2^{1/n}} + \frac{1}{R_3^{1/n}} \right\}$$

We may write this as

$$Q = \frac{p^{1/n}}{R_{par}^{1/n}}$$

where R_{par} is the equivalent resistance of the parallel circuit. It follows that

$$\frac{1}{R_{par}^{1/n}} = \left\{ \frac{1}{R_1^{1/n}} + \frac{1}{R_2^{1/n}} + \frac{1}{R_3^{1/n}} \right\}$$

or in general,

$$\frac{1}{R_{par}^{1/n}} = \sum \frac{1}{R^{1/n}} \quad (7.16)$$

In the usual case of $n = 2$ for subsurface ventilation systems,

$$\frac{1}{\sqrt{R_{par}}} = \sum \frac{1}{\sqrt{R}} \quad (7.17)$$

Example

Figure 7.2 illustrates nine airways that form part of a ventilation network. Find the equivalent resistance of the system.

Solution

Airways 1, 2, and 3 are connected in series and have an equivalent resistance of

$$\begin{aligned} R_a &= R_1 + R_2 + R_3 && \text{(equation (7.15))} \\ &= 0.6 + 0.1 + 0.1 = 0.8 && \frac{\text{Ns}^2}{\text{m}^8} \end{aligned}$$

This equivalent resistance is connected across the same two junctions, A and B, as airway 4 and, hence, is in parallel with that airway. The equivalent resistance of the combination, R_b , is given by

$$\frac{1}{\sqrt{R_b}} = \frac{1}{\sqrt{0.8}} + \frac{1}{\sqrt{0.3}} \quad \text{(equation (7.16))}$$

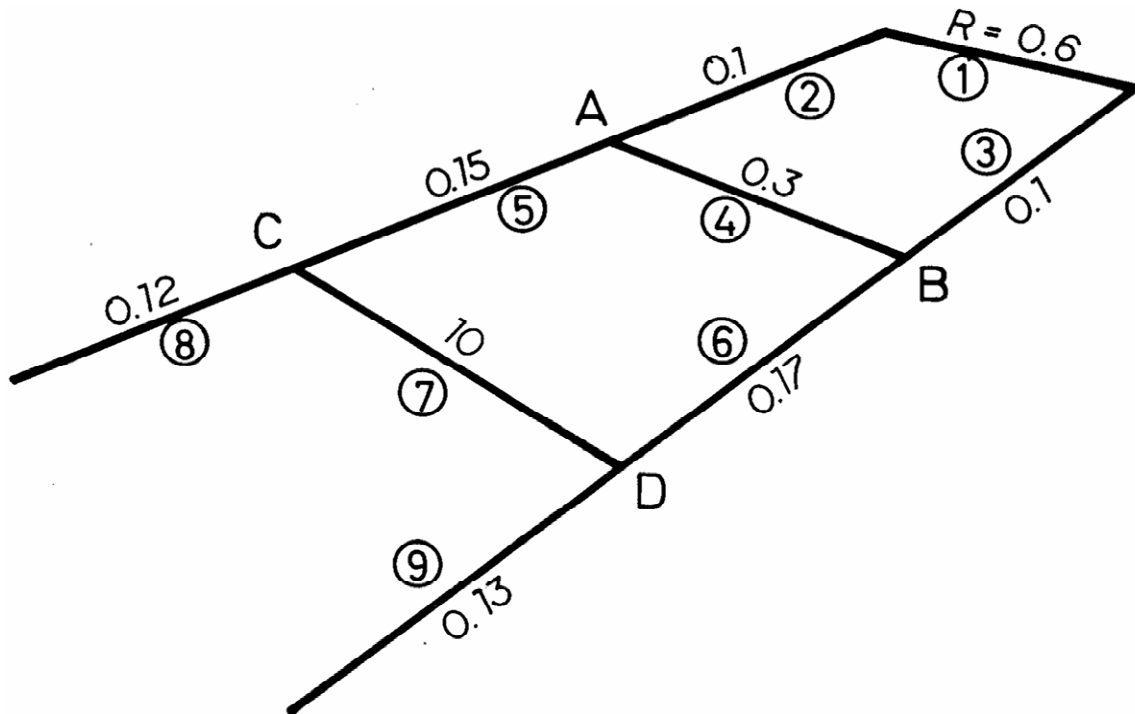


Figure 7.2 Example of a network segment that can be resolved into a single equivalent resistance

from which

$$R_b = 0.1154 \quad \frac{\text{Ns}^2}{\text{m}^8}$$

Notice that the equivalent resistance of the parallel circuit is less than that of either component (ref. Buddle, Section 1.2). Equivalent resistance R_b is now connected in series with airways 5 and 6 giving a new equivalent resistance of all paths in by junctions C and D as

$$R_c = 0.1154 + 0.15 + 0.17 = 0.4354 \quad \frac{\text{Ns}^2}{\text{m}^8}$$

Combining this in parallel with airway 7 gives

$$\frac{1}{\sqrt{R_d}} = \frac{1}{\sqrt{0.4354}} + \frac{1}{\sqrt{1.0}}$$

which yields $R_d = 0.298 \quad \frac{\text{Ns}^2}{\text{m}^8}$

The equivalent resistance of all nine airways, R_{equ} is then given by adding the resistances of airways 8 and 9 in series

$$R_{equ} = 0.298 + 0.12 + 0.13 = 0.548 \quad \frac{\text{Ns}^2}{\text{m}^8}$$

If it is simply the total flow into this part of a larger network that is required from a network analysis exercise then the nine individual airways may be replaced by the single equivalent resistance. This will simplify the full network schematic and reduce the amount of computation to be undertaken during the analysis. On the other hand, if it is necessary to determine the airflow in each individual branch then the nine airways should remain as separate resistances for the network analysis.

The concept of equivalent resistances is particularly useful to combine two or more airways that run adjacent to each other. Similarly, although a line of stoppings between two adjacent airways are not truly connected in parallel, they may be grouped into sets of five to ten, and each set represented as an equivalent parallel resistance, provided that the resistance of the stoppings is large compared with that of the airways. Through such means, the several thousand actual branches that may exist in a mine can be reduced to a few hundred, simplifying the schematic, reducing the amount of data that must be handled, and minimizing the time and cost of running network simulation packages.

7.3.1.2 Direct Application of Kirchhoff's Laws

Kirchhoff's laws allow us to write down equation (7.4) for each independent junction in the network and equation (7.9) for each independent mesh. Solving these two sets of equations will give the branch airflows, Q , that satisfy both laws simultaneously.

If there are b branches in the network then there are b airflows to be determined and, hence, we need b independent equations. Now, if the network contains j junctions, then we may write down Kirchhoff I (equation (7.4)) for each of them in turn. However, as each branch is assumed to be continuous with no intervening junctions, a branch airflow denoted as Q_i entering a junction will automatically imply that Q_i leaves at the junction at the other end of that same branch. It follows that when we reach the last junction, all airflows will already have been symbolized. The number of independent equations arising from Kirchhoff I is $(j - 1)$.

This leaves $b - (j - 1)$ or $(b - j + 1)$ further equations to be established from Kirchhoff II (equation (7.9)). We need to choose $(b - j + 1)$ **independent closed meshes** around which to sum the frictional pressure drops.

The direct application of Kirchhoff's laws to full mine circuits may result in several hundred equations to be solved simultaneously. This requires computer assistance. Manual solutions are limited to very small networks or sections of networks. Nevertheless, a manual example is useful both to illustrate the technique and assists in understanding the numerical procedures described in the following section.

Example

Figure 7.3 shows a simplified ventilation network served by a downcast and an upcast shaft, each passing $100 \text{ m}^3/\text{s}$. The resistance of each subsurface branch is shown. A fan boosts the airflow in the central branch to $40 \text{ m}^3/\text{s}$. Determine the distribution of airflow and the total pressure, p_b , developed by the booster fan.

Solution

Inspection of the network shows that it cannot be resolved into a series/parallel configuration and, hence, the method of equivalent resistances is not applicable. We shall, therefore, attempt to find a solution by direct application of Kirchhoff's laws.

The given airflows are also shown on the figure with the flow from A to B denoted as Q_1 . By applying Kirchhoff I (equation (7.4)) to each junction, the airflows in other branches may be expressed in terms of Q_1 and have been added to the figure.

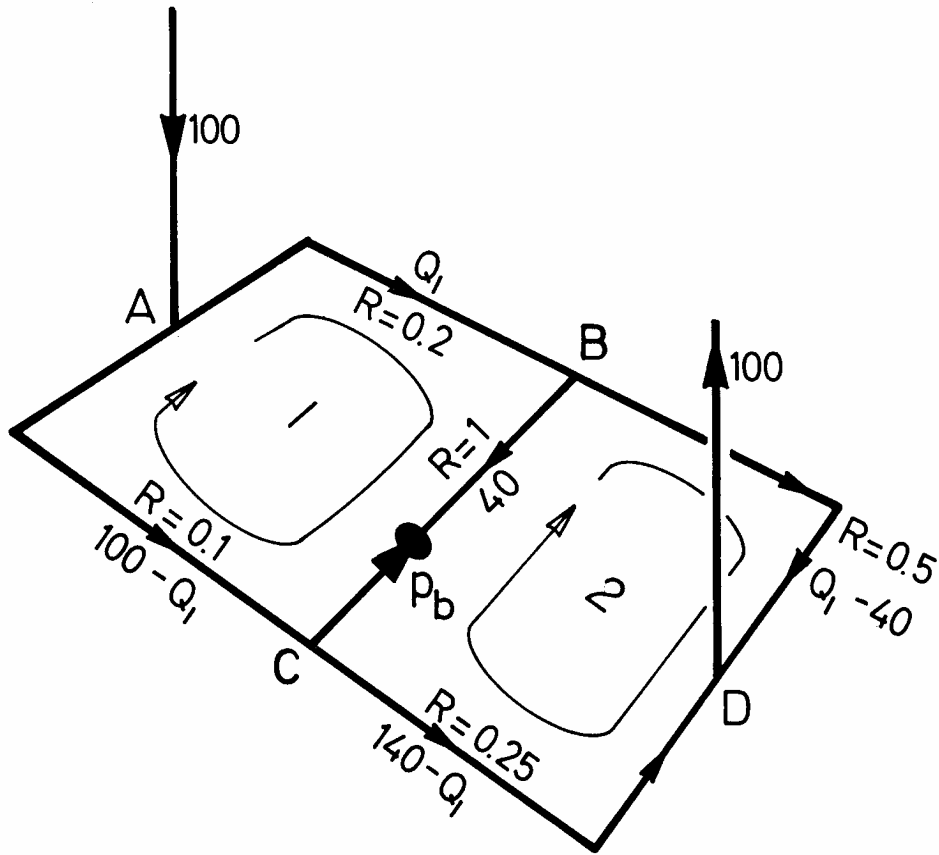


Figure 7.3. Example network showing two meshes and Kirchhoff I applied at each junction.

The shafts can be eliminated from the problem as their airflows are already known. In the subsurface structure we have 5 branches and 4 junctions. Accordingly, we shall require

$$b - j + 1 = 5 - 4 + 1 = 2 \text{ independent meshes}$$

In order to apply Kirchhoff II (equation (7.9)) to the first mesh, consider the pressure drops around that mesh, branch by branch, remembering that frictional pressure drops are positive and fan pressures negative in the direction of flow. Figure 7.3 shows that we may choose meshes along the closed paths ABCA and BDCB.

	Frictional pressure drop (RQ^2)	Fan
AB	$0.2 Q_1^2$	-----
BC	1.0×40^2	$- p_b$
CA	$- 0.1 (100 - Q_1)^2$	-----

Summing up these terms according to Kirchhoff II gives

$$0.2 Q_1^2 + 1600 - p_b - 0.1 (100 - Q_1)^2 = 0 \quad \text{Pa} \quad (7.18)$$

Collecting like terms gives

$$p_b = 0.1 Q_1^2 + 20 Q_1 + 600 \quad \text{Pa} \quad (7.19)$$

Inspection of Figure 7.3 and commencing from junction B, shows that the summation of pressure drops applied to the second mesh may be written as

$$0.5 (Q_1 - 40)^2 - 0.25 (140 - Q_1)^2 - 1 \times 40^2 + p_b = 0 \quad \text{Pa} \quad (7.20)$$

Notice that in this case, the direction of traverse is such that the pressure falls on passing through the fan, i.e. a positive pressure drop. Substituting for p_b from equation (7.19), expanding the bracketed terms and simplifying leads to

$$0.35 Q_1^2 + 50 Q_1 - 5100 = 0$$

This quadratic equation may be solved to give

$$Q_1 = \frac{-50 \pm \sqrt{50^2 + (4 \times 0.35 \times 5100)}}{2 \times 0.35} = 68.83 \text{ or } -211.69 \quad \frac{\text{m}^3}{\text{s}}$$

The only practical solution is $Q_1 = 68.83 \text{ m}^3/\text{s}$. The flows in all branches are then given from inspection of Figure 7.3 as

AB	68.83 m ³ /s
BD	28.83
BC	40.00
AC	31.17
CD	71.17

The required booster fan pressure, p_b , is given from equation (7.19) as

$$p_b = 0.1 (68.83)^2 + 20 (68.83) + 600 = 2450 \quad \text{Pa}$$

7.3.2 Numerical Methods

Although the analytical methods of ventilation network analysis were given considerable attention before the development of analogue computers in the 1950's, the multiple simultaneous equations that they produced could not readily be solved by manual means. As shown in the previous example, two mesh problems involve quadratic equations. A little further thought indicates that three mesh problems would involve polynomial equations in Q of order 4. Four meshes would produce powers of 8, and so on (i.e. powers of 2^{m-1} , where m = number of meshes).

Atkinson recognized this problem in his paper of 1854 and suggested a method of successive approximation in which the airflows were initially estimated, then adjusted towards their true value through a series of corrections. Although no longer employed, Atkinson's approach anticipated current numerical methods.

Since the mid 1960's, considerable research has been carried out to find more efficient numerical methods of analyzing ventilation networks. Y.J. Wang in the United States developed a number of algorithms based on matrix algebra and the techniques of operational research.

The method that is most widely used in computer programs for ventilation network analysis was originally devised for water distribution systems by Professor Hardy Cross at the University of Illinois in 1936. This was modified and further developed for mine ventilation systems by D.R. Scott and F.B. Hinsley at the University of Nottingham in 1951. However, it was not until digital computers became more widely available for engineering work in the 1960's that numerical methods became truly practicable.

The Hardy Cross Technique.

Figure 7.4 shows the system resistance curve for one single representative branch in a ventilation network. If the airflow, Q , is reversed then the frictional pressure drop, p , also becomes negative.

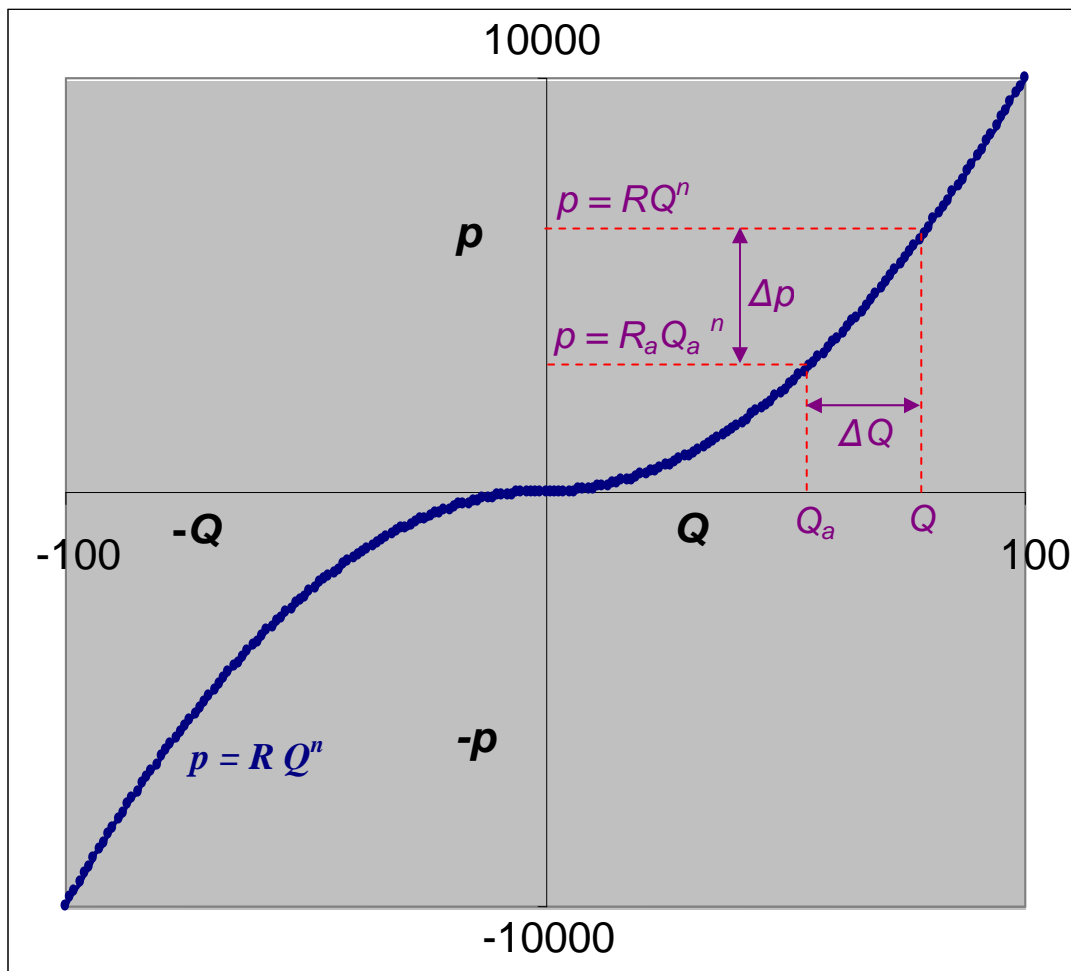


Figure 7.4 In the system resistance curve for an airway, p and Q always have the same sign. The p, Q slope remains non-negative.

Recalling that a primary purpose of ventilation network analysis is to establish the distribution of flow, the true airflow in our representative branch, Q , will initially be unknown. However, let us assume an airflow, Q_a , that is less than the true value by an amount ΔQ .

$$Q = Q_a + \Delta Q$$

The problem now turns to one of finding the value of ΔQ . We may write the square law as

$$p = R(Q_a + \Delta Q)^2 \quad (7.21)$$

or, more generally,

$$p = R(Q_a + \Delta Q)^n \quad (\text{section 7.2.3}) \quad (7.22)$$

Confining ourselves, for the moment, to the square law, equation (7.21) expands to

$$p = RQ_a^2 + 2RQ_a\Delta Q + R(\Delta Q)^2 \quad (7.23)$$

Furthermore, the frictional pressure drop corresponding to the assumed airflow is

$$p_a = RQ_a^2 \quad (7.24)$$

where the "error" in p is

$$\Delta p = p - p_a$$

Substituting from equations (7.22) and (7.23) gives

$$\Delta p = 2RQ_a\Delta Q + R(\Delta Q)^2 \quad (7.25)$$

If we can assume that $(\Delta Q)^2$ is small compared to $2Q\Delta Q$ then we may write the approximation as

$$\Delta p = 2RQ_a\Delta Q \quad (7.26)$$

Note that differentiating the square law,

$$p = RQ^2$$

gives the limiting case when $Q_a \rightarrow Q$. Then

$$\frac{\Delta p}{\Delta Q} \rightarrow \frac{dp}{dQ} = 2RQ \quad (7.27)$$

and corresponds with the difference equation (7.26)

Then

$$\Delta Q = \frac{\Delta p}{2RQ_a} \quad (7.28)$$

The technique of dividing a function by its first derivative in order to estimate an incremental correction factor is a standard numerical method for finding roots of functions. It is usually known as the **Newton or Newton-Raphson** method.

If the general logarithmic law is employed, equation (7.22) gives

$$p = RQ_a^n \left[1 + \frac{\Delta Q}{Q_a} \right]^n$$

Expanding by the Binomial Theorem and ignoring terms of order 2 and higher gives

$$p = RQ_a^n \left[1 + n \frac{\Delta Q}{Q_a} \right]$$

then

$$\Delta p = p - p_a = RQ_a^n n \frac{\Delta Q}{Q_a} \quad (\text{as } p_a = RQ_a^n)$$

giving

$$\Delta Q = \frac{\Delta p}{n RQ_a^{n-1}} \quad (7.29)$$

If we refer back to Figure 7.4, we are reminded that Δp is the error in frictional pressure drop that was incurred by choosing the assumed airflow, Q_a .

$$\Delta p = RQ^n - RQ_a^n \quad (7.30)$$

Hence, we can write equation (7.29) as

$$\Delta Q = \frac{RQ^n - RQ_a^n}{n RQ_a^{n-1}} \quad (7.31)$$

The denominator in this expression is the slope of the p, Q curve in the vicinity of Q_a .

So far, this analysis has concentrated upon one single airway. However, suppose that we now move from branch to branch in a consistent direction around a closed mesh, summing up both the Δp values and the p, Q slopes.

$$\begin{aligned} \Sigma \Delta p &= \Sigma (RQ^n - RQ_a^n) && \text{from equation (7.30)} \\ &= \Sigma RQ^n - \Sigma RQ_a^n \end{aligned}$$

and sum of p, Q slopes = $\Sigma (nRQ_a^{n-1})$

We can now write down a composite value of ΔQ for the complete mesh in the form of equation (7.31)

$$\Delta Q_m = \frac{\Sigma RQ^n - \Sigma RQ_a^n}{\Sigma(nRQ_a^{n-1})} \quad (7.32)$$

Note that ΔQ_m is no longer the correction to be made to the assumed airflow in any one branch but, rather, is the composite value given by dividing the mean Δp by the mean of the p, Q slopes.

Equation (7.32) suffers from the disadvantage that it contains the unknown true values of airflow, Q . However, the term ΣRQ^n is the sum of the corresponding true values of frictional pressure drop around a closed mesh and Kirchhoff's second law insists that this must be zero. Equation (7.32) becomes

$$\Delta Q_m = \frac{-\Sigma RQ_a^n}{\Sigma nRQ_a^{n-1}} \quad (7.33)$$

Another glance at Figure 7.4 reminds us that the pressure term in the numerator must always have the same sign as the airflow, while the p, Q slope given in the denominator can never be negative. Hence, equation (7.33) may be expressed as

$$\Delta Q_m = \frac{-\Sigma RQ_a |Q_a^{n-1}|}{\Sigma nR|Q_a^{n-1}|} \quad (7.34)$$

where $|Q_a^{n-1}|$ means the absolute value of Q_a^{n-1} .

There are a few further observations that will help in applying and understanding the Hardy Cross process. First, the derivation of equation (7.34) has ignored both fans and natural ventilating pressures. Like airways, these are elements that follow a defined p, Q relationship. Equation (7.34) may be expanded to include the corresponding effects

$$\Delta Q_m = \frac{-\Sigma(RQ_a |Q_a^{n-1}| - p_f - nvp)}{\Sigma(nR|Q_a^{n-1}| + S_f + S_{nv})} \quad (7.35)$$

where p_f and nvp are the fan pressures and natural ventilating pressures, respectively, that exist within the mesh,
and S_f and S_{nv} are the slopes of the p, Q characteristic curves for the fans and natural ventilating effects.

In practice, S_{nv} is usually taken to be zero, i.e. it is assumed that natural ventilating effects are independent of airflow.

For most subsurface ventilation systems, acceptable accuracy is achieved from the simple square law where $n = 2$, giving

$$\Delta Q_m = \frac{-\Sigma(RQ_a |Q_a| - p_f - nvp)}{\Sigma(2R|Q_a| + S_f + S_{nv})} \quad (7.36)$$

The **Hardy Cross procedure** may now be summarized as follows:

(a) Establish a network schematic and choose at least $(b-j+1)$ closed meshes such that all branches are represented (section 7.3.1.2). [b = number of branches and j = number of junctions]

in the network.] **Convergence** to a balanced solution will be improved by ensuring that each high resistance branch is included in only one mesh.

(b) Make an initial estimate of airflow, Q_a , for each branch, ensuring that Kirchhoff I is obeyed.

(c) Traverse one mesh and calculate the **mesh correction factor** ΔQ_m from equation (7.35) or (7.36).

(d) Traverse the same mesh, in the same direction, and adjust each of the contained airflows by the amount ΔQ_m .

(e) Repeat steps (c) and (d) for every mesh in the network.

(f) Repeat steps (c), (d) and (e) until Kirchhoff II is satisfied to an acceptable degree of accuracy, i.e. until all values of $-\sum(RQ_i |Q_i|^{n-1}) - p_f - nvp$ are close to zero, where Q_i are the current values of airflow.

A powerful feature of the method is that it is remarkably tolerant to poorly estimated initial airflows, Q_a . This requires some explanation as equation (7.28) and the more general equation (7.29) were both derived on the assumption that ΔQ was small compared to terms involving Q_a . In practice, it is observed that the procedure converges towards a balanced solution even when early values of ΔQ are large. There are two reasons for this. First, the compilation of a composite mesh ΔQ , tends to dampen out the effect of large ΔQ values in individual branches. Secondly, any tendency towards an unstable divergence is inhibited by the airway p, Q curves always having a consistent (non-negative) slope.

Another advantage of the Hardy Cross technique is its flexibility. Using equation (7.35) for the mesh correction factor allows a different value of the logarithmic index, n , to be used for each airway if required. For subsurface ventilation circuits, this is seldom necessary although special purpose programs have been written that allow either laminar ($n = 1$) or turbulent ($n = 2$) airflow in each branch.

A more general observation is that Kirchhoff's first and second laws are not interdependent. Kirchhoff I ($\sum Q = 0$) may be obeyed at every junction in a network that is unbalanced with respect to Kirchhoff II. Indeed, this is usually the case at the stage of selecting assumed airflows, Q_a . Furthermore, if one or more branches are to have their airflows fixed by regulators or booster fans, then those airways may be omitted from the Hardy Cross analysis as they are not to be subjected to ΔQ_m adjustments. Such omissions will result in Kirchhoff I remaining apparently violated at the corresponding junctions throughout the analysis. This does not affect the ability of the system to attain a balanced pressure distribution that obeys Kirchhoff II.

Example

Figure 7.5 (a) is the schematic of a simple network and gives the resistance of each branch. A fan produces a constant total pressure of 2000 Pa and the airflow in branch 3 is to be regulated to a fixed airflow of $10\text{m}^3/\text{s}$. Determine the distributions of airflows and frictional pressure drops, and the resistance of the regulator required in branch 3.

Solution

Although the Hardy Cross procedure is widely utilized in computer programs, its tedious arithmetic iterations ensures that it is seldom employed for manual application. For the purposes of illustration, in this example we shall follow the procedures that illustrate those employed in a typical ventilation network analysis software package.

(a) Mesh selection:

There are 10 branches labelled in the network. However, branches 1 and 5 are connected in series and may be considered as a single branch for the purposes of mesh selection. Furthermore, branch 3 has a fixed (regulated) airflow and, hence, need not enter into the Hardy Cross analysis. The effective number of branches is, therefore, $b = 8$ while there are $j = 6$ junctions, giving the required minimum number of meshes to be $b - j + 1 = 3$. An arrow is indicated to give each branch a positive direction. This is usually chosen as the direction in which the airflow is expected to move although either direction is acceptable. The branch arrow is merely a convenience to assist in traversing closed meshes within the network.

If we write down a list of branch resistances in order of decreasing value, then the three at the top of this list will correspond to branches 9, 10 and 7. We shall choose our first mesh commencing on branch 9 and close the mesh through a convenient route but without using branches 10, 7 or the fixed quantity, branch 3. Figure 7.5 (a) shows the loop starting on branch 9 and traversed by mesh 1. The second mesh commences on branch 10 and closes without traversing branches 9, 7, or 3. Similarly, the third mesh commences on branch 7 and involves no other high resistance or fixed quantity branch. The routes of the meshes so chosen are indicated on Figure 7.5 (a).

This technique of **mesh selection** is sometimes known as the **branch tree method** and leads to efficient convergence towards a balanced network as each high resistance branch appears in one mesh only.

A fourth mesh is selected, commencing on the fixed quantity (branch 3) and closing through any convenient route that does not include other fixed quantities, and irrespective of branch resistance values. This extra mesh will not be employed during the Hardy Cross analysis but will prove useful for the final calculation of the regulator resistance.

(b) Estimate initial airflows:

This is accomplished in two stages commencing from zero flow throughout the network. First, mesh 4 (the fixed quantity mesh) is traversed in a direction defined by the fixed airflow, adding a ΔQ_m of $10 \text{ m}^3/\text{s}$ (the required fixed airflow) to each branch around that mesh. As in all subsequent applications of mesh correction factors, ΔQ_m , the actual correction to each branch flow is ΔQ_m multiplied by +1 if the branch direction arrow coincides with the path of the traverse, or -1 if the branch direction arrow opposes the path of the traverse. This device gives the required airflow in the fixed quantity branch while ensuring that Kirchhoff I remains true at each junction. A similar procedure is followed in each of the three "normal" meshes, but employing a value of $\Delta Q_m = 1$. This merely ensures that the denominator of the mesh correction equation (7.35 or 7.36) will be non-zero during the first iteration. The airflows at this stage are indicated on Figure 7.5(a) and show the distribution at the commencement of the Hardy Cross procedure. It should be noted that if the method were to be applied manually then the number of iterations could be reduced by estimating a more realistic initial distribution of airflow.

(c) Calculate mesh correction factors:

Assuming the flow to be turbulent in each branch, we may utilize the square law and, hence, equation (7.36) to calculate the mesh correction factors. In this example, there are no natural ventilating pressures ($nvp = S_{nv} = 0$) and the fan is assumed to remain at a fixed pressure ($p_f = 2000 \text{ Pa}$ and $S_f = 0$).

Applying equation (7.36) for mesh 1 gives

$$\begin{aligned}\Delta Q_{m1} &= \frac{-(0.9 \times 1^2 - 0.3 \times 10^2 - 0.12 \times 0^2)}{2(0.9 \times 1 + 0.3 \times 10 + 0.12 \times 0)} \\ &= \frac{29.1}{7.8} = 3.73 \text{ m}^3/\text{s}\end{aligned}$$

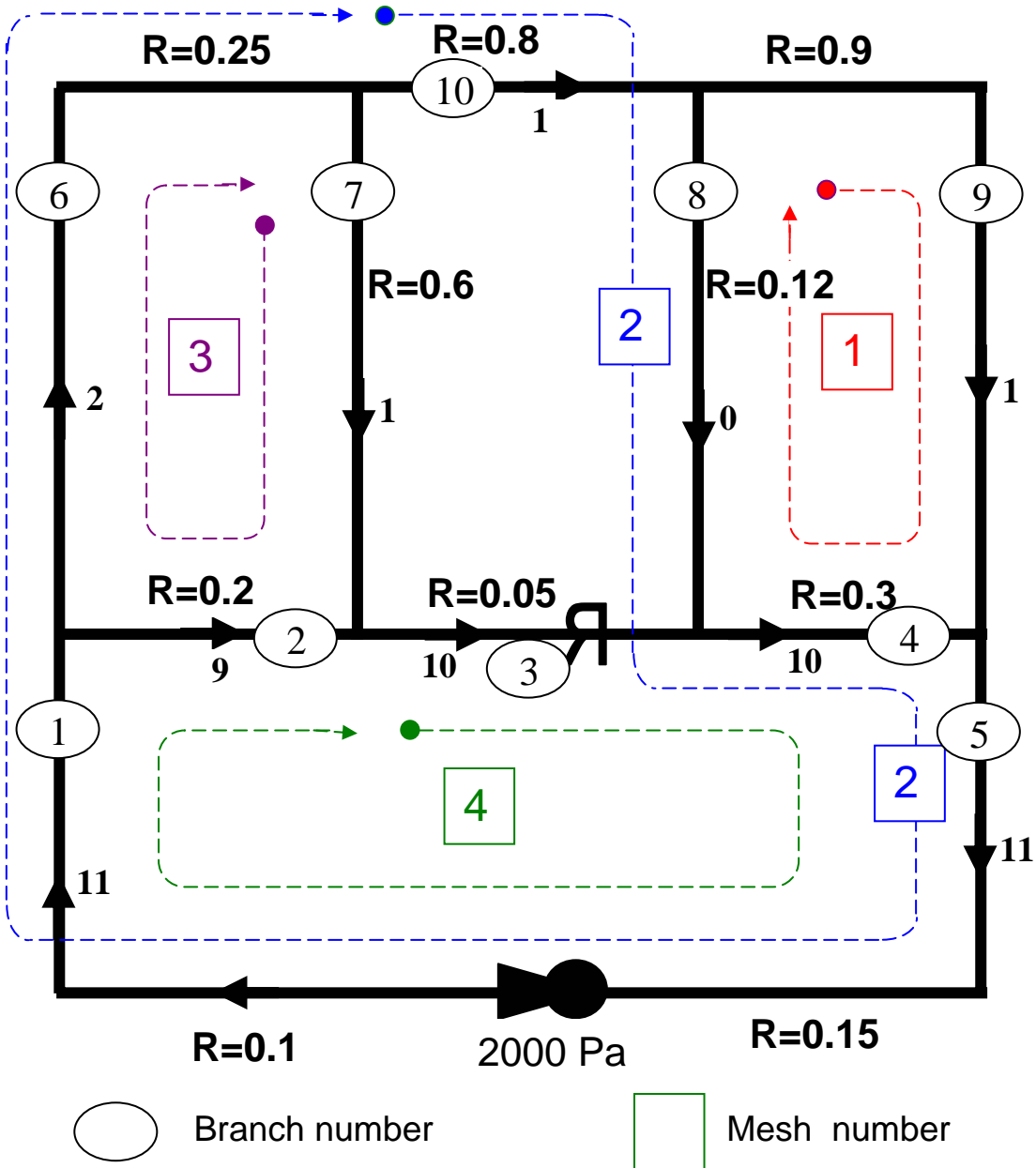


Figure 7.5(a). Example network showing airway resistances, initial assumed airflows and the meshes chosen.

(d) Apply the mesh correction factor:

Mesh 1 is traversed once again, correcting the flows algebraically by adding $\Delta Q_{m1} = 3.73$. The relevant branch flows then become:

Branch 9: $1 + (3.73 \times 1) = 4.73 \text{ m}^3/\text{s}$
 Branch 4: $10 + (3.73 \times -1) = 6.27 \text{ m}^3/\text{s}$
 Branch 8: $0 + (3.73 \times -1) = -3.73 \text{ m}^3/\text{s}$

Applying these corrections around mesh 1 gives the airflow distribution shown in Figure 7.5(b).

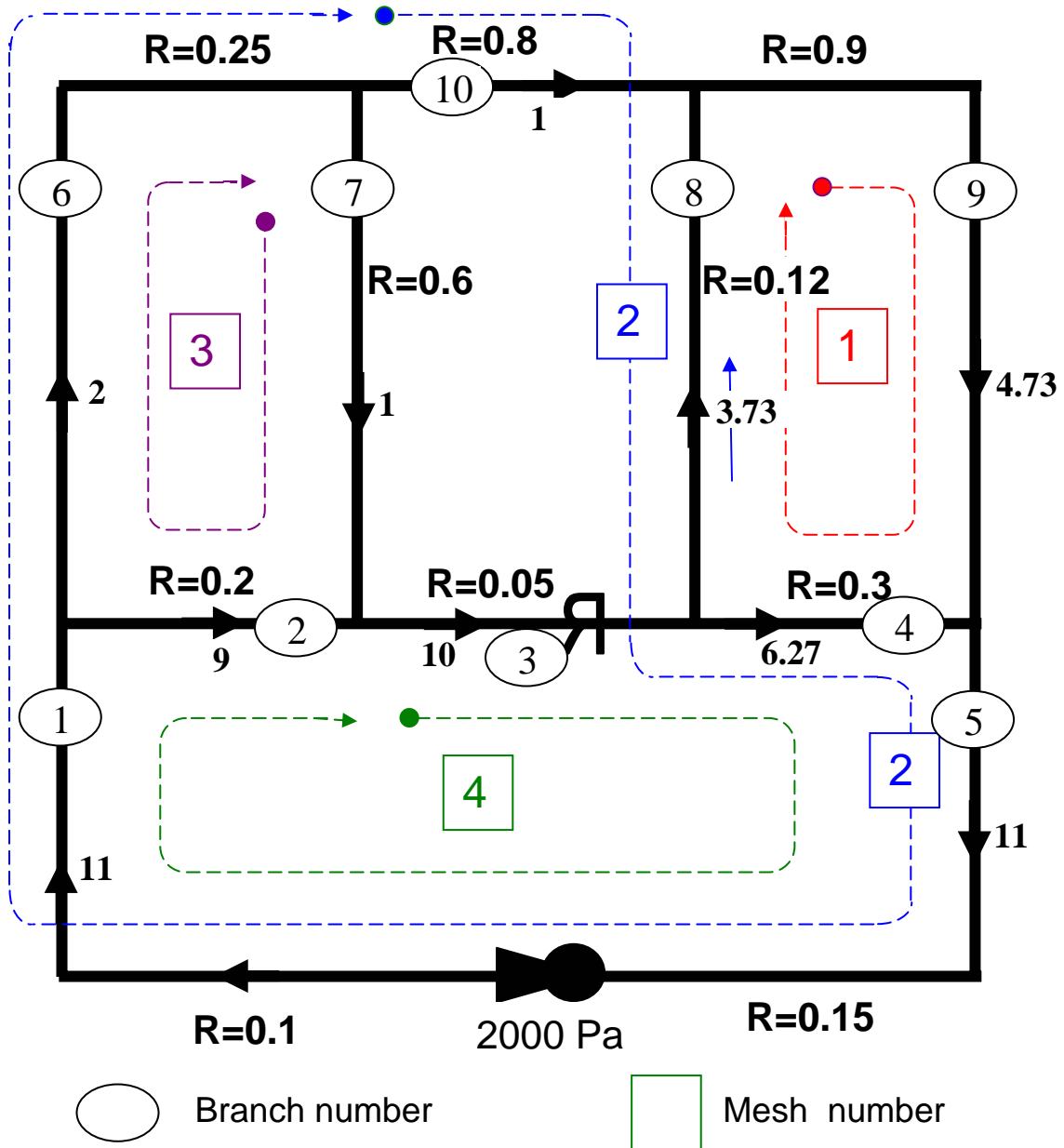


Figure 7.5(b). Example network showing airflows after $\Delta Q_{m1} = 3.73 \text{ m}^3/\text{s}$ has been applied to mesh 1.

(e) *Completion of mesh corrections*
Equation (7.36) for mesh 2 now gives

$$\Delta Q_{m2} = \frac{-(0.8 \times 1^2 - 0.12 \times 3.73^2 + 0.3 \times 6.27^2 + 0.25 \times 11^2 + 0.25 \times 2^2 - 2000)}{2(0.8 \times 1 + 0.12 \times 3.73 + 0.3 \times 6.27 + 0.25 \times 11 + 0.25 \times 2)} = 153.47 \text{ m}^3/\text{s}$$

and applying these corrections around mesh 2 gives the airflow distribution shown in Figure 7.5(c).

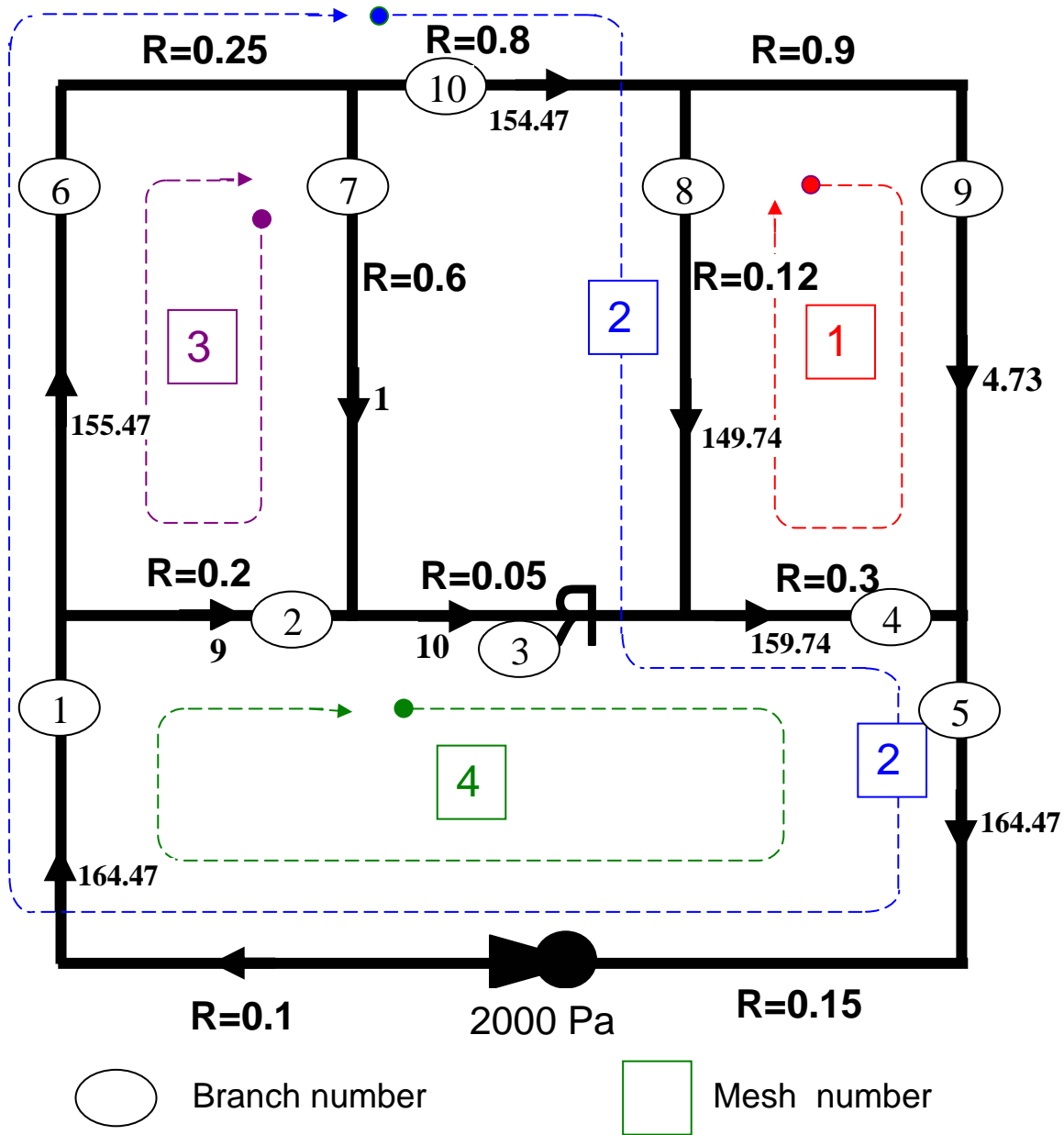


Figure 7.5(c). Example network showing airflows after $\Delta Q_{m2} = 153.47 \text{ m}^3/\text{s}$ has been applied to mesh 2.

Repeating the process for mesh 3 gives

$$\Delta Q_{m3} = \frac{-(0.6 \times 1^2 - 0.2 \times 9^2 + 0.25 \times 155.47^2)}{2(0.6 \times 1 + 0.2 \times 9 + 0.25 \times 155.47)} = -73.03 \text{ m}^3/\text{s}$$

and applying this correction around mesh 3 yields the airflow distribution shown on Figure 7.5(d), completing the first iteration for the network.

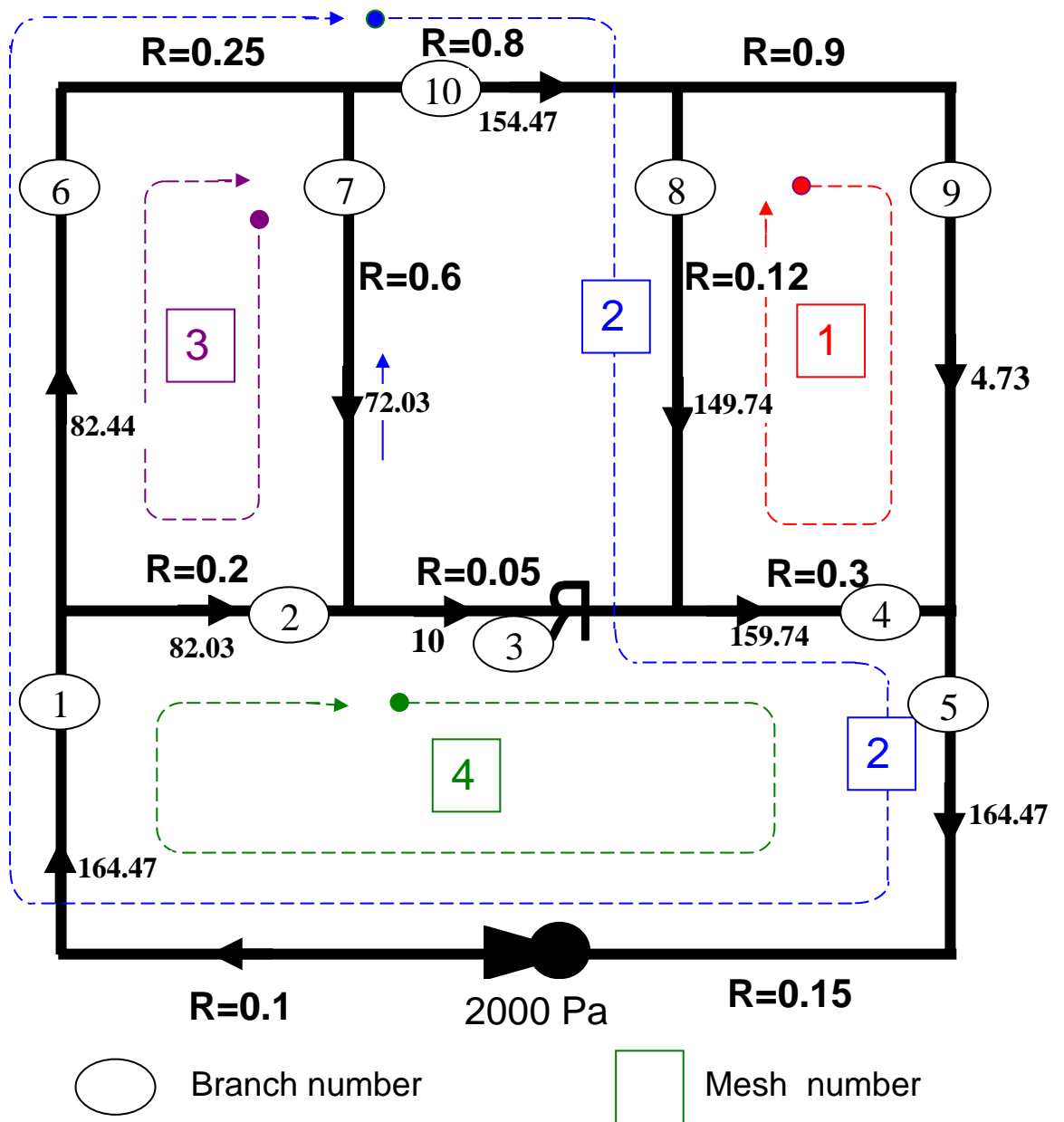


Figure 7.5(d). Example network showing airflows after $\Delta Q_{m3} = -73.03 \text{ m}^3/\text{s}$ has been applied to mesh 3 and completing the first iteration.

(f) The processes involved in (c), (d) and (e) are repeated iteratively until Kirchhoff's second law (numerator of equation (7.35)) balances to within a small closing error (say $\pm 1 \text{ Pa}$) for each mesh. The airflow correction factors and sums of pressure drops for each mesh are shown in Table 7.1. Notice how the initial large oscillations are followed by a controlled convergence towards zero despite the large opening values of ΔQ_m .

The final flow pattern arrived at after these nine iterations is given on Figure 7.5(e). The corresponding frictional pressure drops are each calculated as $p = RQ^2$ and shown in parentheses against each airflow.

Iteration	Sum of Pressure Drops Around Mesh Δp (Pa)			Mesh Correction Factor $\Delta Q_m(m^3/s)$		
	mesh1	mesh2	mesh3	mesh1	mesh2	mesh3
1	-29	-1958	6027	3.73	153.47	-73.03
2	-10326	28473	-4379	73.60	-64.63	34.17
3	5367	8810	-1231	-34.26	-33.36	16.66
4	1579	2524	-358	-16.49	-14.71	7.43
5	485	613	-91	-7.18	-4.69	2.40
6	128	114	-15	-2.25	-0.97	0.45
7	23	16	-2	-0.434	-0.143	0.056
8	3.2	2.0	0.2	-0.059	-0.017	0.007
9	0.4	0.2	-0.03	-0.007	-0.002	0.001

Table 7.1 Mesh correction factors and mesh pressure drops converge towards zero as the iterations proceed.

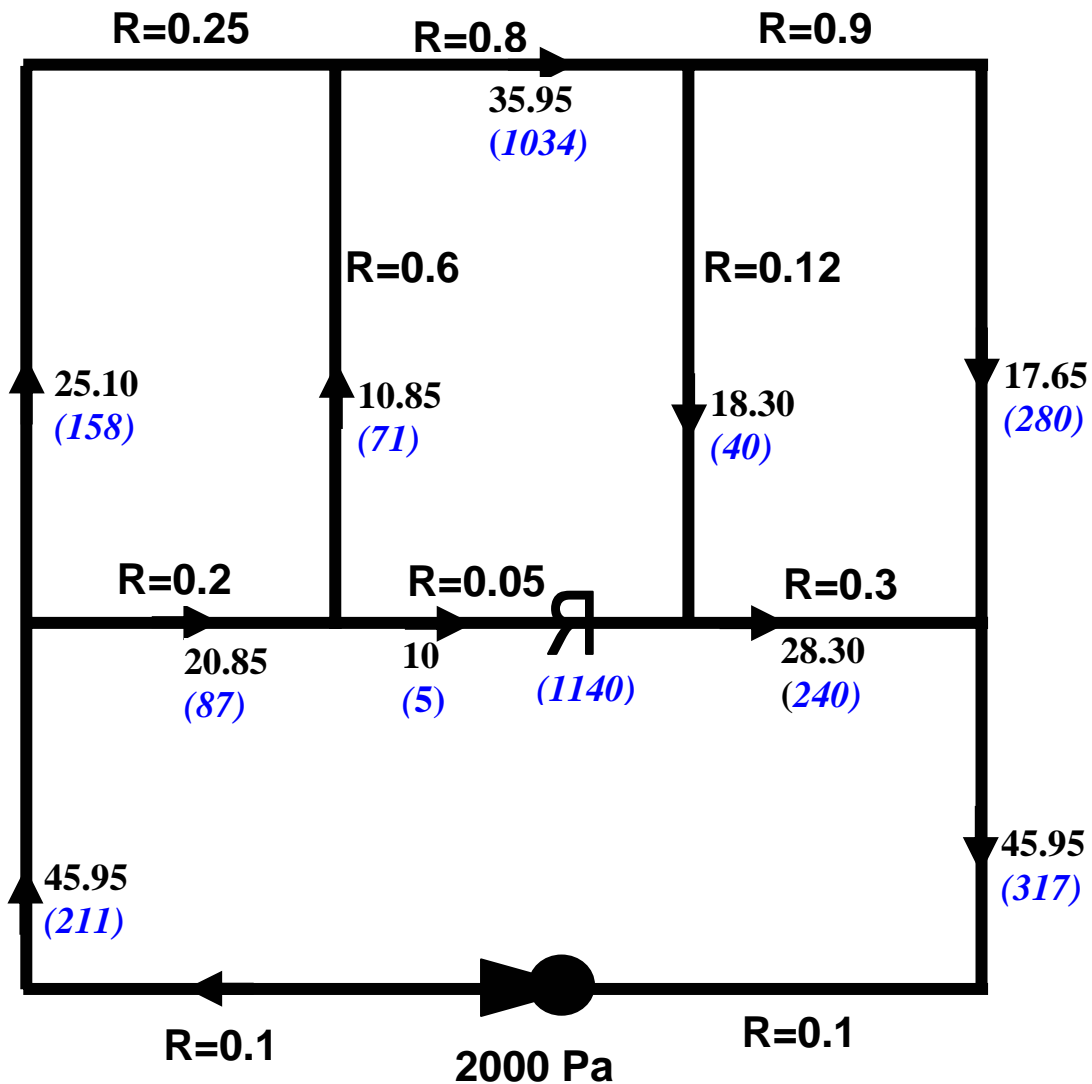


Figure 7.5(e). Final airflows and frictional pressure drops after nine iterations.

The pressure drop across the regulator, p_{reg} , in branch 3 can be determined from Kirchhoff's second law by summing the known pressure drops around mesh 4

$$p_{reg} = 2000 - (211 + 87 + 5 + 240 + 317) = 1140 \text{ Pa}$$

As the airflow through the regulator is known to be $10 \text{ m}^3/\text{s}$, the square law gives the regulator resistance as

$$R_{reg} = p_{reg}/10^2 = 11.4 \quad \text{Ns}^2/\text{m}^8$$

The actual dimensions of regulator orifice that will give this resistance may be determined using section A5.5 given at the end of Chapter 5.

7.4. VENTILATION NETWORK SIMULATION PACKAGES

Between the 1960s and the 1990s, the development and increasing sophistication of ventilation network simulation packages revolutionized the methodologies of mine ventilation planning. Ventilation engineers wishing to use modern software need give little conscious thought to what happens within the computer when they enter data or execute a simulation. Nevertheless, a grasp of the structure of a network package provides an understanding of the scope and limitations of the software, and promotes efficiency in its use. This section of the text provides an outline of how a ventilation network simulation package operates.

7.4.1 Concept of a mathematical model

Suppose that a vehicle leaves its starting station at time t_1 and travels for a distance d at an average velocity of u . The time at which the vehicle arrives at its destination, t_2 is given by

$$t_2 = t_1 + \frac{d}{u}$$

This equation is a trivial example of a mathematical model. It simulates the journey in sufficient detail to achieve the objective of determining the arrival time. Furthermore, it is general in that it performs the simulation for any moving object and may be used for any given values of t_1 , d and u . Different data may be employed without changing the model.

More sophisticated mathematical models may require many equations to be traversed in a logical sequence so that the result of any one calculation may be used in a later relationship. This logical sequence will often involve feed-back loops for iterative processes such as the Hardy Cross procedure.

A **simulation program** is a mathematical model written to conform with one of the computer languages. The basic ambition of a simulation program is to produce numerical results that approximate those given by the real system. There are three considerations that govern the accuracy of a simulation program; first, the adequacy to which each individual process is represented by its corresponding equation (e.g. $p = RQ^2$); secondly, the precision of the data used to characterize the actual system (e.g. airway resistances) and thirdly, the accuracy of the numerical procedure (e.g. the cutoff criterion to terminate cyclic iterations).

Many simulation programs represent not one but a number of interacting features comprising both physical systems and organizational procedures. In this case, several computer programs and data banks may be involved, interacting with each other. In such cases, the computer software may properly be referred to as a **simulation package** rather than a single program. This

is the situation for current methods of ventilation network analysis on desktop personal computers.

7.4.2 Structure of a ventilation simulation package

Figure 7.6 shows the essential structure of a ventilation network analysis package for a desktop or laptop computer. It includes a series of input files with which the user can communicate through a keyboard and screen monitor, either for new data entry or for editing information that is already held in a file. All files are normally maintained on a magnetic disk or other media that may be accessed rapidly by the computer.

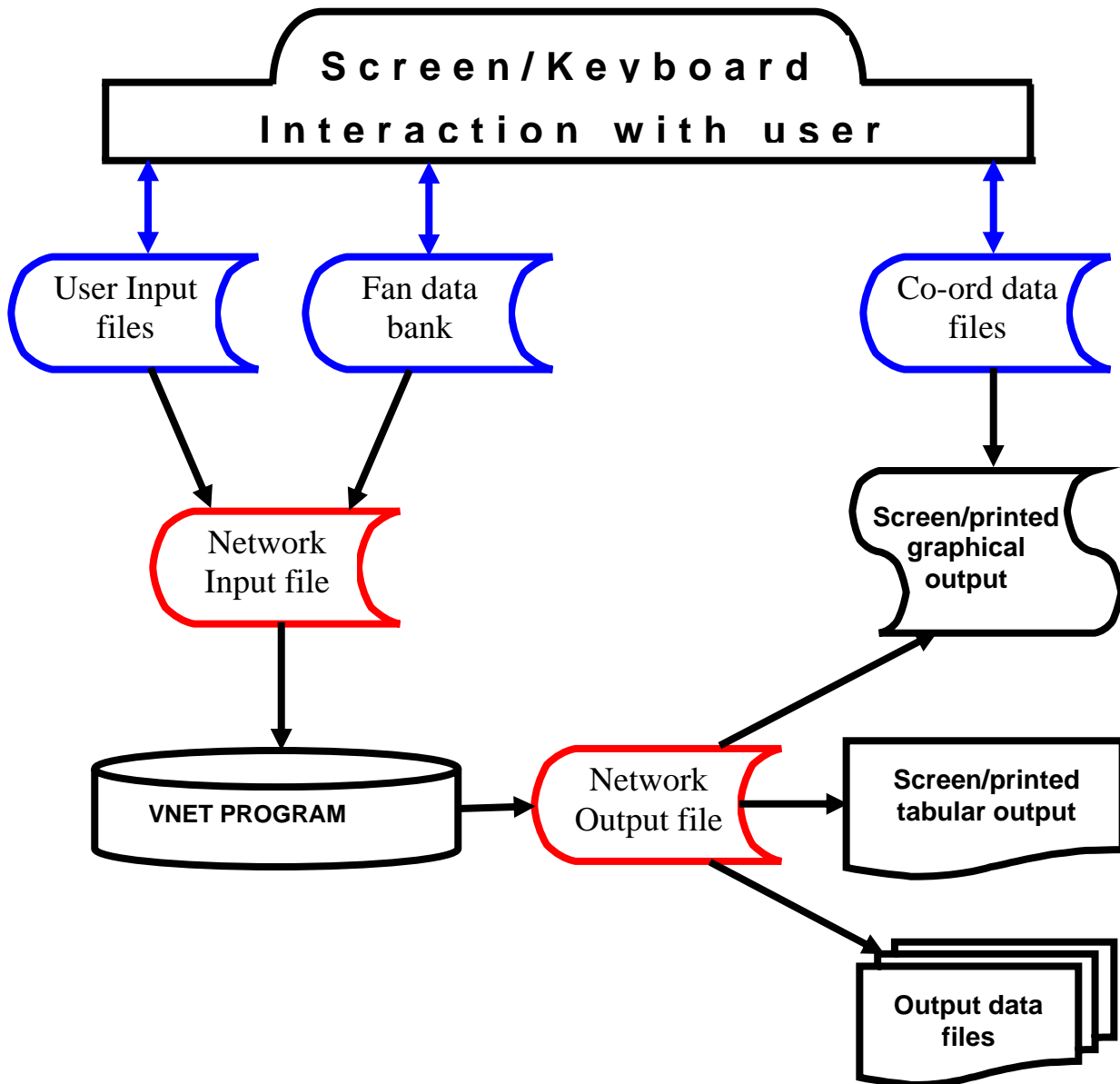


Figure 7.6 Data flow through a ventilation network analysis software package.

The **User Input Files** shown on Figure 7.6 hold data relating to the geometric structure of the network, the location of each branch being defined by a “from” and “to” junction number. This same file contains the type of each branch (e.g. fixed resistance or fixed [regulated] airflow) and information relating to branch resistances. The latter may be given (a) directly by the user, (b) defined as a measured airflow/pressure drop or (c) implied by a friction factor, airway geometry and an indication of shock losses. Additionally, the user may enter a value of **resistance per unit length of entry** that has been established from the mine records as typical for that type of entry (e.g. intake, return or conveyor). Although convenient, this facility should be used with caution as it is tempting to overlook the large effects of variations in the sizes of entries or shock losses arising from bends or obstructions. The User Input File allows entry of resistance data in whatever form they are available. User input files also allow the operator to enter the location and corresponding operating pressure of each fan in the network as well as natural ventilating pressures.

The **Fan Data Bank** is a convenient alternative means of storing the pressure/volume coordinates for a number of fan characteristic curves. Data from fan tests and manufacturers' catalogues can be held in the Fan Data Bank and recalled for use in the subsequent analysis of any network.

The ventilation network analysis program (denoted as **VNET** on Figure 7.6) in most commercial packages is based on the mesh selection process and Hardy Cross technique described and illustrated by example in Section 7.3.2. However, those procedures have been modified to maximize the rate of information flow, the speed of mesh selection and to accelerate convergence of the iterative processes. In order to achieve a high efficiency of data transfer, the VNET program may require that the network input data be specified in a closely defined format. However, this is contrary to the need for flexibility in communicating with the user. Hence, Figure 7.6 shows a Network Input File acting as a buffer between the user-interactive files and the VNET program. Subsidiary “management” programs, not shown on Figure 7.6, carry out the required conversions of data format and control the flow of information between files. Similarly, the output from the VNET program may not be in a form that is immediately acceptable for the needs of the user. Hence, that output is dumped temporarily in a Network Output File. Under user control it may then be (a) copied into an output data file for longer term storage, (b) displayed in tabular form on the screen or printer, (c) produced as a plotted network schematic on a screen or hardcopy printer or plotter and (d) transferred to other graphical software for incorporation into mine maps.

If graphical output is required then the user-interactive **Coordinate Data File** shown on Figure 7.6 must first be established. This contains the x, y, z coordinates of every junction in the network. It is convenient to enter such data directly from a drawn schematic by means of a digitizing pad or plotter, or from CAD (computer assisted design) files that have already been established for mine mapping. Alternatively, the schematic may be developed or modified directly via the monitor screen. To edit an established Coordinate Data File it is often quicker to enter numerical values for the amended or additional x,y,z coordinates.

7.4.3 Operating system for a VNET package

When running a ventilation network analysis package, the user wishes to focus his/her attention on ventilation planning and not to be diverted by matters relating to the transfer of data within the machine. Keyboard entries are necessary for control of the computer operations. However, these should be kept sufficiently simple that they allow a near automatic response from the experienced user. Messages on the screen should provide a continuous guide on operations in progress or alternative choices for the next operation. For these reasons, a simulation package intended for industrial use must include a management or **executive program** that controls all internal data transfers.

The user is conscious of the executive program only through the appearance of a hierarchy of toolbars, menus and windows on the screen. Each menu lists a series of next steps from which

the user may choose. These include progression to other toolbars, menus or windows. Hence, with few keyboard entries, and with very little conscious effort, the trained user may progress flexibly and rapidly through the network exercise.

Figure 7.7 illustrates the executive level (master menu) of one ventilation network package. Choosing the "execute ventilation simulation" option will initiate operation of the VNET program (Figure 7.6) using data currently held in the Network Input File. The "exit" option simply terminates operation of the network simulator. Each of the other four options leads to other menus and submenus for detailed manipulation of the operating system.

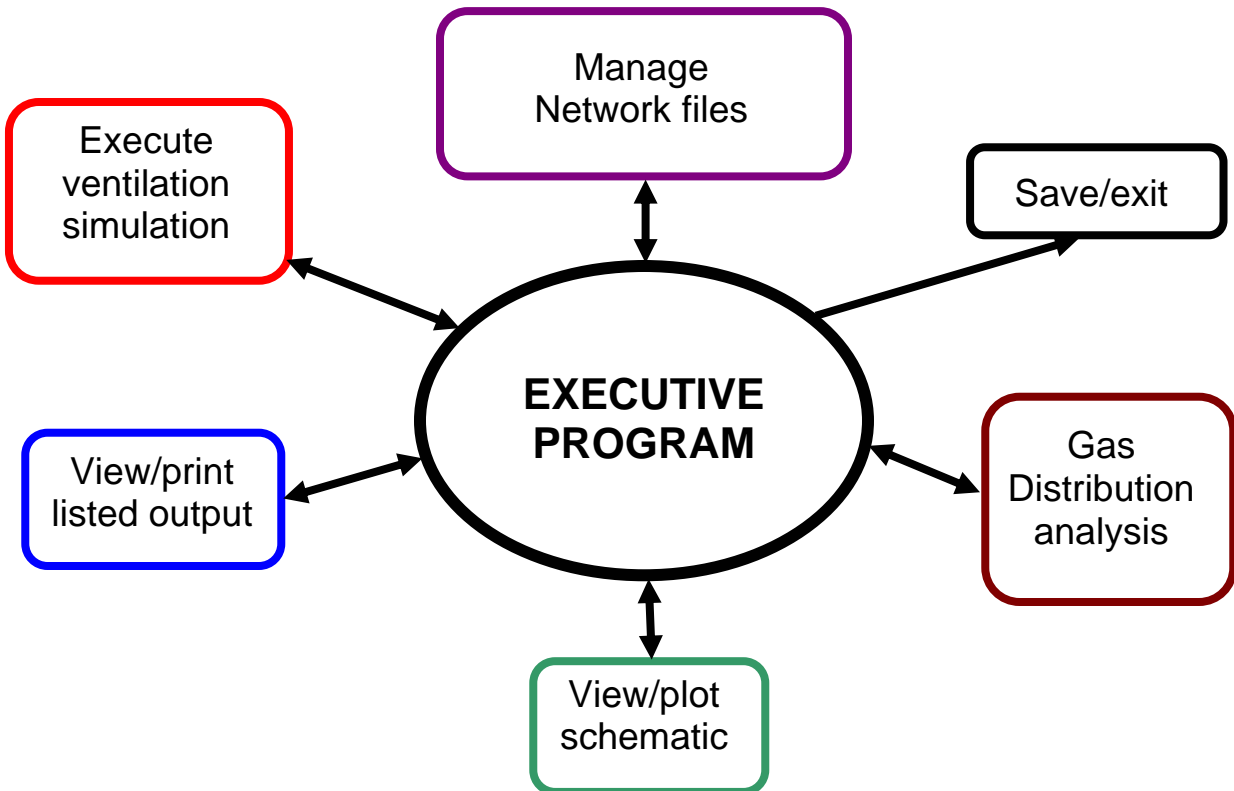


Figure 7.7. Structure of an internal management system for a ventilation network software package.

7.4.4 Incorporation of air quality into a network simulation package

The primary purpose of a ventilation network analysis package is to predict the airflows and pressure differentials throughout the network. However, the **quality** of the air with respect to gaseous or particulate pollutants, or its psychrometric condition also depend upon the distribution of airflow. Separate programs designed to predict individual aspects of air quality may, therefore, be incorporated into a more general ventilation package. Branch airflows and/or other data produced as output from the network analysis program may then be utilized as input to air quality simulators.

As an example, the operating system depicted by Figure 7.7 incorporates a **Gas Distribution Analysis**. This requests the user to identify the emitting locations and rates of production of any

gas, smoke or fumes. It then retrieves the airflow distribution contained in the Network Output File or any named output data file (Figure 7.6) in order to compute the distribution and concentrations of that pollutant throughout the network.

It is important that users be cognizant of the limitations of such adjunct programs. For instance, computer simulated gas distributions assume a steady state mixing of the pollutant into the airflow and, hence, that the pollutant is removed from the system at the same rate as it is emitted. This is acceptable for normal ventilation planning but will give misleading results if the airflow in any area is so low, or the rate of emission so high that local accumulations (e.g. gas layering) would occur in the real system. Such conditions might exist, for example, where ventilation controls have been disrupted by a mine explosion.

7.4.5 Obtaining a ventilation simulation package

The first step in establishing a ventilation network analysis package at any mine or other site is to review the availability of both hardware and software. There are several ventilation network packages available for personal computers. The potential user should consider the following factors:

Hardware requirements and size of network

The internal memory requirements of the computer will depend upon the scope of the software package and the largest network it is capable of handling. With modern personal computers, memory should seldom be a limiting factor. In addition to the microprocessor, keyboard and screen monitor, the type of package described in Section 7.4.2 and 7.4.3 will require a printer capable of handling graphical output. Again, most modern printers have this facility. For greater flexibility, an x,y plotter is useful and is normally available in mine surveying offices. Exporting network results to CAD/CAM systems allows results to be configured on mine maps.

Cost of software

This can vary very considerably depending upon the sophistication of the system and whether it was developed by a commercial company or in the more public domain of a university or national agency.

Speed

The speed of running a network depends upon the type of microprocessor, operating electrical frequency, and the size and configuration of the network. Typical run times should be sought from software developers for a specified configuration of hardware. For the majority of mine networks, computing speed is unlikely to be a limiting factor with current or future generations of personal computers.

Scope and ease of use

When reviewing simulation packages it is important that the user chooses a system that will provide all of the features that he/she will require in the foreseeable future. However, there is little point in expending money on features that are unlikely to be used. Furthermore, it is usually the case that the more sophisticated packages demand a greater degree of user expertise. Demonstration versions may be available to indicate the scope and ease of use of a program package. Other users may be approached for opinions on any given system. Software developers should be requested to give the names of several current users of their packages.

User's manual and back-up assistance

It is vital that any simulation package should be accompanied by a comprehensive user's manual for installation and operation of the system. A user-friendly help facility should be part of the software package. Additionally, the producer of the software must be willing and anxious to provide backup assistance to all users on request. This can vary from troubleshooting on the telephone or internet to updating the complete software system.

7.4.6 Example of a computed network

The ventilation networks of actual mines or other subsurface facilities may contain several hundred branches, even after compounding relevant airways into equivalent resistances (Section 7.3.1.1). However, in the interests of brevity and clarity, this example is restricted to the simple two-level schematic shown on Figure 7.8(a). The software employed is VNETPC, a commercially available ventilation network package.

In response to screen prompts, the user keys in each item of data shown in Table 7.2. This table is, in fact, a printout of the User Input File (Section 7.4.2). The pressure/volume coordinates for the fan are either read manually from the appropriate fan characteristic or copied over from a characteristic that has been entered previously into a fan data bank. Figure 7.8(b) shows the fan characteristic curve and corresponding pQ points entered into the computer for this example. The branch data section of the User Input File illustrates that airway resistances may be entered directly, from survey (p, Q) observations or from airway geometry and friction factor. The software package employed for this example requires shock losses to be entered as equivalent lengths (Section 5.4.5).

A request by the user to execute the simulation causes the User Input File to be translated to the Network Input File (Figure 7.6) and the computed results to be deposited in the Network Output File. These may be inspected on the screen or listed on a printer as shown on Tables 7.3, 7.4 and 7.5.

In order to produce plotted results, the x, y, z coordinates of each junction must be specified. This is usually accomplished by transferring the coordinates from a computer aided design (CAD) file. Alternatively, the coordinates can be entered manually or by placing a mine map or schematic on a digitizing tablet or plotter and a sight-glass positioned over each junction in turn as directed by screen prompts. The resulting Coordinate Data File is then combined with the computed results, on request by the user, to produce the graphical outputs shown on Figures 7.9, 7.10 and 7.11.* Similar plots may be generated for frictional pressure drops, resistance, airpower loss, and operating cost. Some programs allow the user to select band widths for **colour coding** of the plots. Similar plots may be generated for air quality parameters such as gas concentrations.

Following the relatively time consuming process of entering the initial data for a new network, and having inspected the corresponding output, amendments can be made to the user-interactive files or directly to schematics shown on the computer monitor, and the network re-run rapidly. In this way, errors in data entry can be corrected and further network exercises pursued with only a few keystrokes. It is this efficiency, rapidity and ease of testing many alternatives that has revolutionized the business of ventilation system design. Indeed, it is the skill of the engineer in interrogating computer output and deciding upon the next exercise that governs the speed of ventilation planning rather than the mathematical mechanics of older methods of network analysis.

INPUT DATA

VnetPC Model Data and Summary

TITLE: Textbook Example.

SETTINGS (chosen by the User):

Avg. Air Density: 1.20 kg/m³

Avg. Fan Efficiency: 65.0 %

Cost of Power: 8.00 c/kWh

Reference Junction: 1 - (Using junction 1 for a point on the mine surface is a common convention)

Units: SI (The User may choose between SI and British Imperial units)

* The graphical outputs given directly by the VNETPC package show fine detail and clarity. The translations necessary for incorporating into this textbook have resulted in greatly reduced quality.

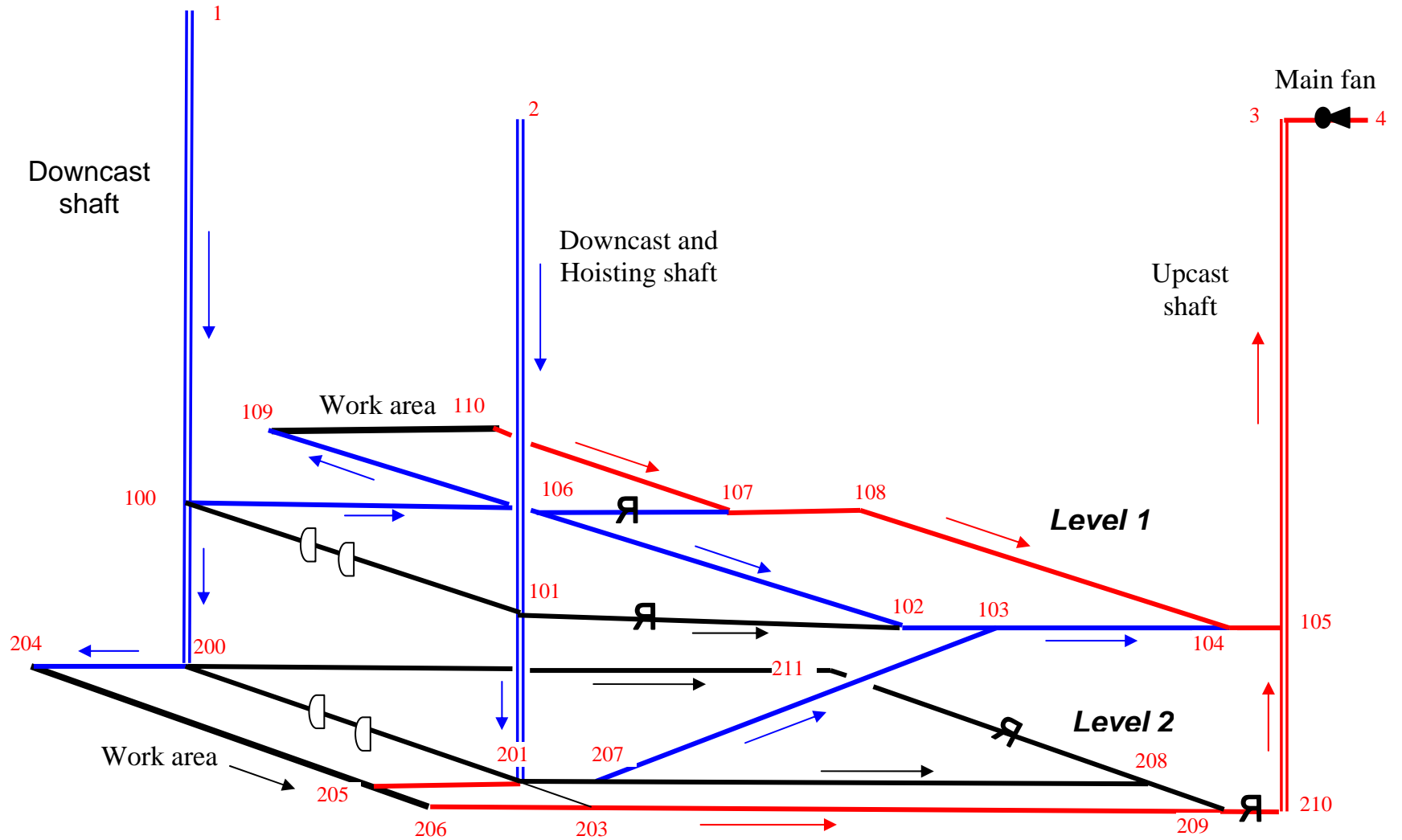


Figure 7.8(a) Layout of the example network. Junction numbers are shown in red.

Table 7.2 Branch input data for the example network (two pages). This input table illustrates alternative ways of entering airway resistance, R : (a) directly, (b) by friction [k] factor and airway geometry, or (c) by measured airflow and corresponding frictional pressure drop.

Junctions		Q (fixed)	Surface	Mode of		Measured	Measured	k factor	Resistance
From	To	F (fan)	connections	setting	Resistance	airflow Q	press. drop		per km
		I (inject/ reject)		resistance	Ns^2/m^8	m^3/s	Pa	kg/m^3	Ns^2/m per km
1	100		Surf. Intake	k Factor	0.00844			0.004	
100	200		Neither	k Factor	0.0031			0.004	
2	101		Surf. Intake	k Factor	0.03797			0.0075	
101	201		Neither	k Factor	0.01044			0.0075	
210	105		Neither	k Factor	0.0016			0.0035	
105	3		Neither	k Factor	0.00544			0.0035	
100	101		Neither	R	50				
100	106		Neither	p/Q	0.0608	100	608		
106	107	Q	Neither	R	0				
107	108		Neither	p/Q	0.08333	60	300		
108	104		Neither	k Factor	0.07504			0.008	
101	102	Q	Neither	R	0				
102	103		Neither	k Factor	0.08478			0.008	
103	104		Neither	k Factor	0.13688			0.008	
104	105		Neither	k Factor	0.00591			0.012	
106	102		Neither	k Factor	0.51852			0.016	
106	109		Neither	k Factor	0.36667			0.016	
109	110		Neither	R	0.9				
110	107		Neither	k Factor	0.43981			0.019	
200	201		Neither	R	200				
200	204		Neither	k Factor	0.084			0.012	
204	205		Neither	R	1.2				
205	206		Neither	k Factor	0.06455			0.017	
206	203		Neither	k Factor	0.16406			0.014	
203	209		Neither	k Factor	0.66445			0.014	
209	210	Q	Neither	R	0				
201	203		Neither	R	0.023				
201	207		Neither	k Factor	0.0336			0.012	
207	208		Neither	R/L	1.49994				0.8333
208	209		Neither	k Factor	0.14954			0.019	
200	211		Neither	R/L	0.28				0.14
211	208	Q	Neither	k Factor	0.1696			0.018	
207	103		Neither	R	0.35				
205	201		Neither	R	0.164				
3	4	F	Surf. Exhaust	R	0.0001				

Spreadsheet continued on next page

Table 7.2 continued

Junctions		Length	Equivalent	Area	Perimeter	Fixed	Description	Colour	Symbol
From	To		length			Quantity		code	
		m	m	sq.m	m	cu.m/s			
1	100	600	0	15.9	14.14		Main Downcast Shaft	Intake	None
100	200	220	0	15.9	14.14		Main downcast shaft	Intake	None
2	101	600	200	12.57	12.57		Hoisting shaft	Intake	None
101	201	220	0	12.57	12.57		Hoisting shaft	Intake	None
210	105	220	0	19.64	15.71		Upcast shaft	Return	None
105	3	600	150	19.64	15.71		Upcast shaft	Return	None
100	101						doors	Default	DD
100	106						Level 1 intake	Intake	None
106	107					20	Level 1 regulator	Intake	None
107	108						Level 1 return	Return	None
108	104	670	0	10	14		Level 1 return	Return	None
101	102					20	Level 1 regulator	Default	None
102	103	707	50	10	14		Level 1 conveyor	Intake	None
103	104	710	20	8	12		Level 1 travel way	Intake	None
104	105	21	0	8	12		Level 1 travel way	Return	None
106	102	700	0	6	10		Level 1 conveyor	Intake	None
106	109	495	0	6	10		Level 1 loader road	Intake	None
109	110						Level 1 Work Area	Default	None
110	107	490	10	6	10		Level 1 return	Return	None
200	201						Level 2 shaft bottom	Default	DD
200	204	500	0	10	14		Level 2 intake	Intake	None
204	205						Level 2 work area	Default	None
205	206	150	12	8	12		Level 2 return	Default	None
206	203	500	0	8	12		Level 2 return	Return	None
203	209	2000	25	8	12		Level 2 return	Return	None
209	210					140	Level 2 Main regulator	Default	R
201	203						Level 2 cross-cut	Default	None
201	207	200	0	10	14		Level 2 conveyor	Default	None
207	208	1800	0				Level 2 travel way	Default	None
208	209	150	20	6	10		Level 2 cross-cut	Default	None
200	211	2000	0				Level 2 travel way	Default	None
211	208	640	33	10	14	15	Level 2 travel way	Default	None
207	103							Intake	None
205	201							Return	None
3	4							Return	None

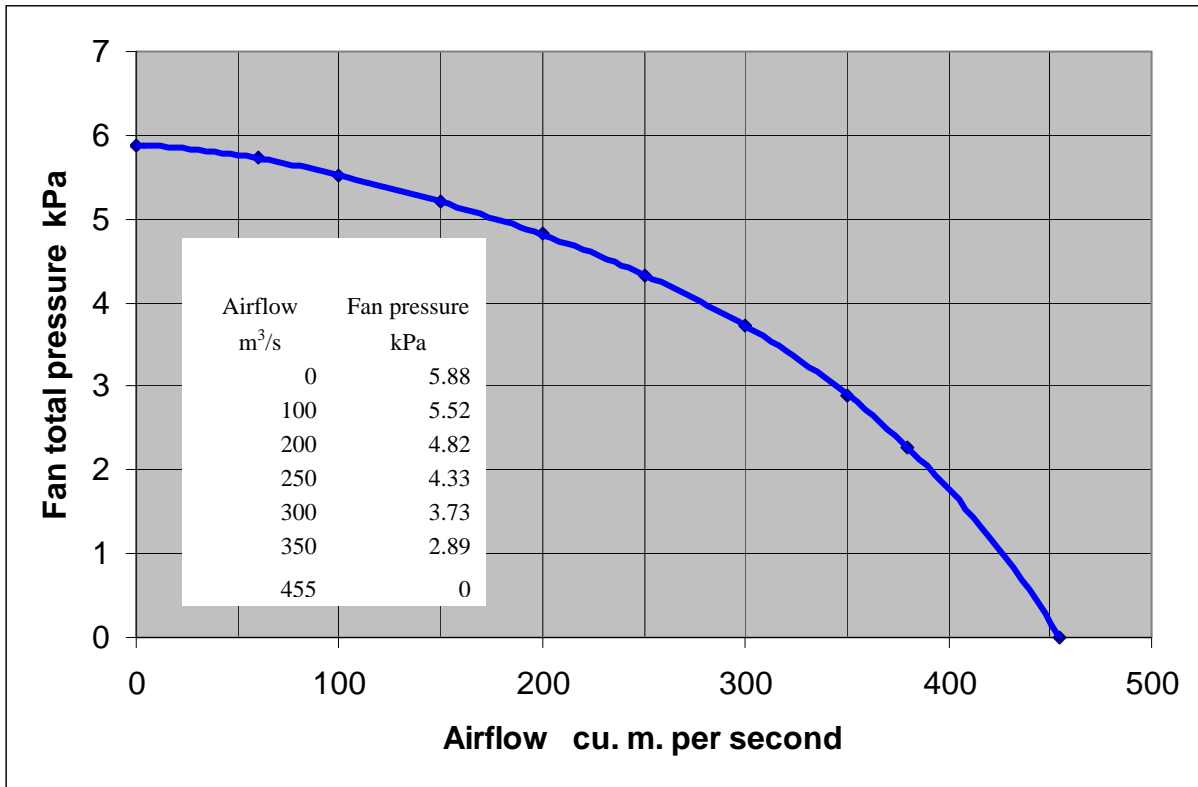


Figure 7.8(b) Fan characteristic curve for the example network. The tabulated coordinate points are entered into the computer. These should encompass the curve but need not be at even intervals of airflow.

Table 7.3 Output listing of branch results. Note that the computer has inserted regulators in three of the four branches that were specified as fixed quantity airflows in the input data. The computer has found it necessary to insert a booster fan (active regulation) in order to obtain the specified airflow in the other fixed quantity branch.

From	To	(R)egulator (B)ooster or (F)an	Total Resistance Ns ² /m ⁸	Airflow m ³ /s	Pressure drop Pa	Airpower loss kW	Operating cost \$/year	
1	100		0.00844	141.55	169.1	23.94	25807	Main Downcast Shaft
100	200		0.0031	43.37	5.8	0.25	271	Main downcast shaft
2	101		0.03797	151.88	875.9	133.03	143429	Hoisting shaft
101	201		0.01044	135.64	192.1	26.06	28093	Hoisting shaft
210	105		0.0016	140	31.4	4.4	4740	Upcast shaft
105	3		0.00544	293.43	468.4	137.44	148184	Upcast shaft
100	101		50	3.76	706.8	2.66	2865	doors
100	106		0.0608	94.41	542	51.17	55169	Level 1 intake
106	107	R	5.03444	20	2013.8	40.28	43424	Level 1 regulator
107	108		0.08333	54.35	246.2	13.38	14427	Level 1 return
108	104		0.07504	54.35	221.7	12.05	12991	Level 1 return
101	102	R	1.66824	20	667.3	13.35	14389	Level 1 regulator
102	103		0.08478	60.06	305.8	18.37	19802	Level 1 conveyor
103	104		0.13688	99.08	1343.7	133.13	143539	Level 1 travel way
104	105		0.00591	153.43	139.1	21.34	23010	Level 1 travel way
106	102		0.51852	40.06	832.2	33.34	35943	Level 1 conveyor
106	109		0.36667	34.35	432.7	14.86	16025	Level 1 loader road
109	110		0.9	34.35	1062.1	36.48	39334	Level 1 Work Area
110	107		0.43981	34.35	519	17.83	19221	Level 1 return
200	201		200	2.11	893.1	1.88	2032	Level 2 shaft bottom
200	204		0.084	26.26	57.9	1.52	1639	Level 2 intake
204	205		1.2	26.26	827.5	21.73	23428	Level 2 work area
205	206		0.06455	19.46	24.4	0.47	512	Level 2 return
206	203		0.16406	19.46	62.1	1.21	1303	Level 2 return
203	209		0.66445	78.06	4048.4	316.02	340716	Level 2 return
209	210	B	0	140	0	0	0	Level 2 Main regulator
201	203		0.023	58.6	79	4.63	4991	Level 2 cross-cut
201	207		0.0336	85.96	248.3	21.34	23012	Level 2 conveyor
207	208		1.49994	46.94	3305.4	155.16	167281	Level 2 travel way
208	209		0.14954	61.94	573.8	35.54	38319	Level 2 cross-cut
200	211		0.28	15	63	0.95	1019	Level 2 travel way
211	208	R	19.48297	15	4383.7	65.76	70895	Level 2 travel way
207	103		0.35	39.02	532.8	20.79	22415	Ramp
205	201		0.164	6.8	7.6	0.05	56	Level 2 cross-cut
3	4	F	0.0001	293.43	8.6	2.52	2721	Surface fan drift

Table 7.4 Output listing of fan operating (pQ) points, airpower generated and annual operating cost.

Fan No.	From	To	Fan Pressure	Fan Airflow	Fan curve	Fan configuration	Airpower kW	Operating Cost \$/year	Fan name
1	3	4	3.809	293.43	On	1 in Parallel	1117.68	1 205 027	Main Fan

Table 7.5 Output listing of fixed quantity branches.

From	To	Fixed quantity	Booster fan	Regulator	Branch	Total	Orifice	Branch
		m ³ /s	pressure	resistance	resistance	resistance	area	description
			Pa	Ns ² /m ⁸	Ns ² /m ⁸	Ns ² /m ⁸	m ²	
106	107	20		5.03444	0	5.03444	0.59	Level 1 regulator
101	102	20		1.66824	0	1.66824	1.02	Level 1 regulator
209	210	140	1895		0			Level 2 Main regulator
211	208	15		19.31337	0.1696	19.48297	0.3	Level 2 travel way

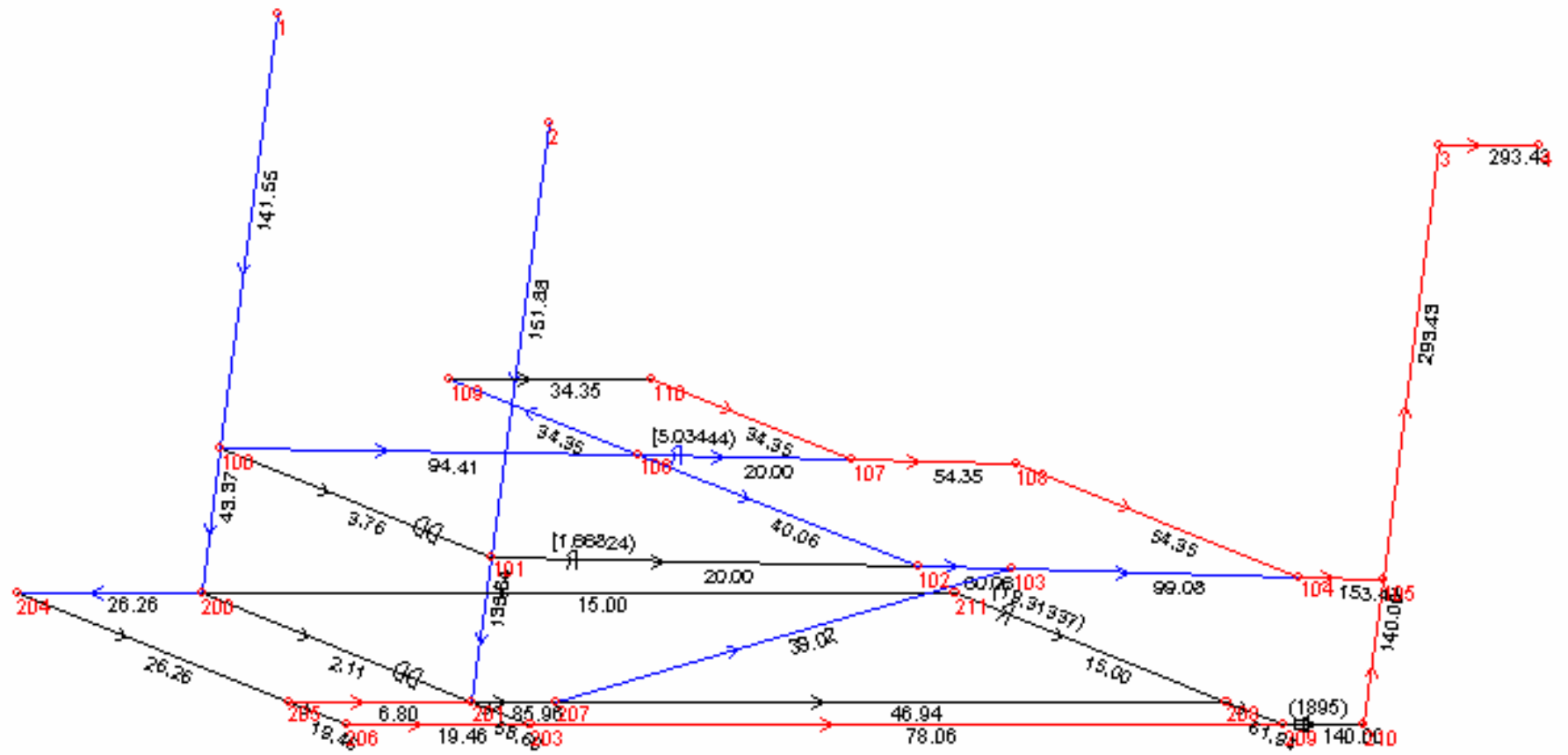


Figure 7.9. Three dimensional output schematic showing airflows (m^3/s). 3-D depictions can be rotated on the computer monitor – a particularly useful facility for metal mines.

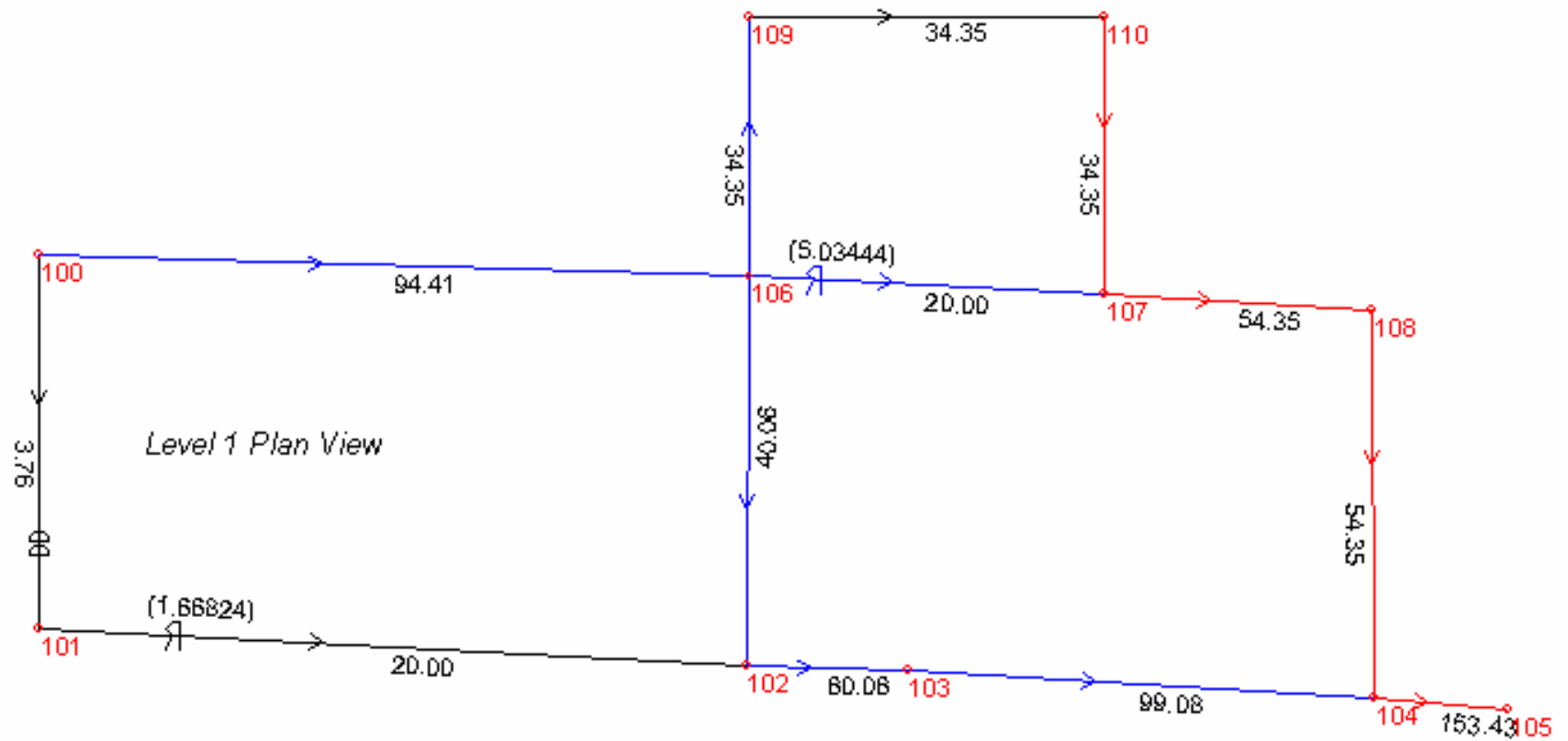


Figure 7.10 Output schematic showing airflows (m³/s) in Level 1

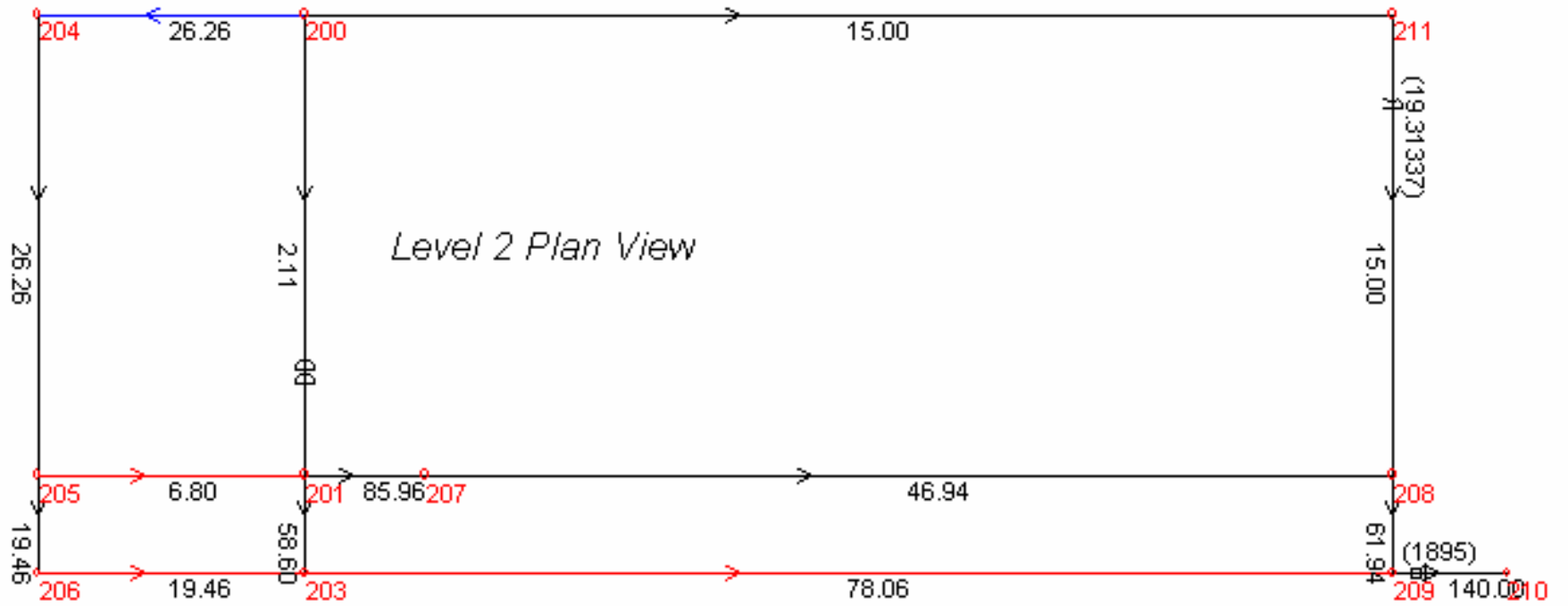


Figure 7.11 Output schematic showing airflows (m³/s) in Level 2.

References

Atkinson, J.J. (1854). On the Theory of the Ventilation of Mines. North of England Institute of Mining Engineers. No. 3, p.118.

Cross, H. (1936). Analysis of Flow in Networks of conduits or Conductors. Bull. Illinois University Eng. Exp. Station. No. 286.

Hartman, H.L. and Wang, Y.J. (1967). Computer Solution of Three Dimensional Mine Ventilation Networks with Multiple Fans and Natural Ventilation. Int. J. Rock Mech. Sc. Vol.4.

Maas, W. (1950). An Electrical Analogue for Mine Ventilation and Its Application to Ventilation Planning. Geologie en Mijnbouw, 12, April.

McElroy, G.W. (1954). A Network Analyzer for Solving Mine Ventilation Distribution Problems. U.S. Bureau of Mines Inf. Circ. 7704. 13 pp.

McPherson, M.J. (1964). Mine Ventilation Network Problems (Solution by Digital Computer). Colliery Guardian Aug. 21. pp.253-254.

McPherson, M.J. (1966). Ventilation Network Analysis by Digital Computer. The Mining Engineer. Vol. 126, No. 73. Oct. pp. 12-28.

McPherson, M.J. (1984). Mine Ventilation Planning in the 1980's. International Journal of Mining Engineering. Vol. 2. pp. 185-227.

Scott, D.R. and Hinsley, F.B. (1951/52). Ventilation Network Theory. Parts 1 to 5. Colliery Eng. Vol. 28, 1951; Vol. 29, 1952.

Scott, D.R., Hinsley, F.B., and Hudson, R.F. (1953). A Calculator for the Solution of Ventilation Network Problems. Trans. Inst. Mine. Eng. Vol. 112. p. 623.

Wang, Y.J. and Saperstein, L.W. (1970). Computer-aided Solution of Complex Ventilation Networks. Soc. Min. Engrs. A.I.M.E. Vol. 247.

Williams, R.W. (1964). A Direct Analogue Equipment for the Study of Water Distribution Networks. Industrial Electronics, Vol. 2. pp. 457-9.

Chapter 8. Mine Ventilation Thermodynamics

8.1. INTRODUCTION	1
8.2. COMPONENTS OF THE MINE CYCLE	2
8.2.1. Elements of the system	2
8.2.2. The downcast shaft	2
Example	8
8.2.3. Level workings	14
8.2.4. Upcast shaft	17
Example	17
8.3. THE COMPLETE MINE CYCLE	21
8.3.1. Natural ventilation	21
8.3.2. Combined fan and natural ventilation	26
8.3.3. Case Study	30
<i>General observations on the table of results</i>	32
<i>Polytropic indices</i>	32
<i>Fan performance</i>	33
<i>Natural ventilating energy, NVE</i>	33
<i>Natural ventilating pressure, NVP</i>	34
<i>Heat additions</i>	35
8.3.4. Inclined workings	36
Dip circuit	36
Rise Circuit	40
8.3.5. The effect of moisture	40
BIBLIOGRAPHY	41
APPENDIX A8.1	42
Survey data from the survey of the shafts used in the examples given in Sections 8.2.2 and 8.2.4	42
APPENDIX A8.2	44
A general steady flow analysis for airstreams that carry water vapour and liquid water droplets	44

8.1. INTRODUCTION

Many of the world's practising mine ventilation engineers - perhaps, even, the majority perform their duties very successfully on the basis of relationships that assume incompressible flow. Some of those engineers may question the need to concern themselves with the more detailed concepts and analyses of thermodynamics. There are, at least, two responses to that query.

First, if the ranges of temperature and pressure caused by variations in elevation and heat transfer produce changes in air density that are in excess of 5 per cent, then analyses that ignore those changes will produce consistent errors that impact significantly on the accuracy of planned ventilation systems. In practical terms, this means that for underground facilities extending more than 500 m below the highest surface connection, methods of analysis that ignore the compressibility of air may be incapable of producing results that lie within observational tolerances of accuracy.

However, there is a second and even more fundamental reason why all students of the subject, including practicing engineers, should have a knowledge of **mine ventilation thermodynamics**.

Although the incompressible flow relationships are simple to apply, they are necessarily based on an approximation. Air is, indeed, highly compressible. It follows, therefore, that if we are truly to comprehend the characteristics of subsurface ventilation systems, and if we are really to understand the behaviour of large-scale airflow systems then this can be accomplished only if we have a grasp of steady-flow thermodynamics.

In this chapter, thermodynamic analyses are carried out on a downcast shaft, underground airways and an upcast shaft. The three are then combined to produce a thermodynamic cycle for a complete mine, first, with natural ventilation only, then for the more usual situation of a combination of fans and natural ventilation. In all cases, the analyses utilize pressure-volume (PV) and temperature-entropy (Ts) diagrams. This chapter assumes familiarity with the basic concepts and relationships that are developed in Chapter 3. It is suggested that the reader study that chapter before proceeding with this one.

One further point - the temperatures and, to a lesser extent, pressures of the air are affected by variations of water vapour in the air. The final section of this chapter outlines the modifications that can be made while a more detailed treatment of moisture in air is given in Chapter 14. However, for the time being, we shall assume that the airways are dry and not affected by evaporative or condensation processes.

8.2. COMPONENTS OF THE MINE CYCLE

8.2.1. Elements of the system.

A subsurface ventilation system follows a closed cycle of thermodynamic processes and can be illustrated by visual representations of those processes on thermodynamic diagrams that are analogous to the indicator diagrams of heat engines. It was this resemblance that led **Baden Hinsley (1900-1988)** into the realization that a mine ventilation system is, indeed, a gigantic heat engine. Air enters the system and is compressed and heated by gravitational energy as it descends in downcasting shafts or slopes. More heat is added to the air from the strata, machines and other sources. Work is done by the air as it expands during its ascent through upcast shafts or slopes. Some of the added heat is converted temporarily to mechanical energy and assists in promoting airflow. In the great majority of mines, this "**natural ventilating energy**" is supplemented by input fan work.

When the exhaust air re-enters the pressure sink of the surface atmosphere, it cools to the original entry conditions, closing the cycle. Figure 8.1 illustrates the descending flow through a downcast shaft between stations 1 and 2, level workings 2 to 3, and returning to surface through an upcast shaft 3 to 4. We shall analyze each of the three processes separately before adding the isobaric (constant pressure) cooling in the surface atmosphere to complete the cycle.

8.2.2. The downcast shaft

Air enters a downcast shaft at the pressure and temperature of the atmosphere existing at the top of the shaft. As the air falls down the shaft, its pressure increases, just as the pressure on a diver increases as he descends into the ocean. The rise in pressure is caused by the increasing weight of the overlying column of fluid as we plunge deeper into the fluid. However, that simple observation belies the common belief that air always flows from a high pressure region to a connected lower pressure region. In a downcast shaft, exactly the opposite occurs showing how easily we can be misled by simplistic conceptions.

The process of **gravitational compression, or autocompression**, in the downcast shaft produces an increase in temperature of the air. This is independent of any frictional effects and will be superimposed upon the influence of any heat transfer with the surrounding strata that may occur across the shaft walls. The rate of that heat transfer depends upon the thermal properties of the rock and the difference between the rock temperature and air temperature at any given horizon.

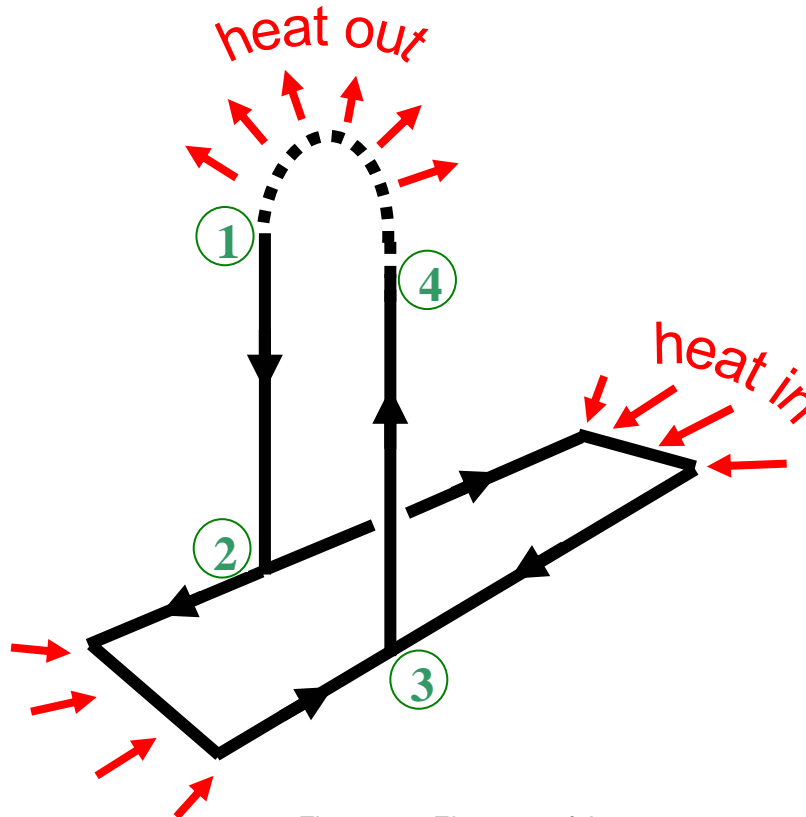


Figure 8.1. Elements of the system

Now, while the temperature of the mass of rock surrounding the shaft may change relatively slowly with time, the air temperature at the shaft entrance can change from hour to hour and, especially, between day and night. Because of these surface variations, it is common for the walls and rock surrounding a downcast shaft to absorb heat during the day and to emit heat during the night. The phenomenon continues along the intake airways and tends to dampen out the effects of surface temperature variation as we follow the air into a subsurface facility. This is sometimes called the "**thermal flywheel**". For the purposes of this chapter, we shall assume that any heat exchange that takes place in the downcast shaft is distributed equitably so that the process approximates closely to a polytropic law.

If we descend a downcast shaft, stopping every hundred metres or so to take measurements of pressure and temperature, we can plot the PV and Ts diagrams using equation (3.9):

$$V = \frac{RT}{P} \quad \frac{\text{m}^3}{\text{kg}}$$

(Chapter 14 shows how this relationship should be amended for the presence of water vapour). Equation (3.48) allows us to determine the variation of **entropy**

$$(s_b - s_a) = C_p \ln\left(\frac{T_b}{T_a}\right) - R \ln\left(\frac{P_b}{P_a}\right) \quad \frac{\text{J}}{\text{kgK}}$$

The starting point for the latter equation may be any defined temperature and pressure datum. It is differences in entropy rather than absolute values that are important.

The diagrams that emerge have the appearance of those given in Figure 8.2. In practice, there is often a scatter of points near the end extremities of the shaft due to high turbulence and uneven mixing of thermally stratified airstreams.

The first step in the analysis of the data is to conduct a curve fitting analysis to the points on the PV diagram. The form of the equation to be fitted is the **polytropic law**

$$P = \frac{C}{V^n}$$

where C is a constant and n the polytropic index. Least squares regression analyses are widely available for personal computers and hand calculators. The quality of the curve fit should be reviewed. It is sometimes apparent that some points, particularly at shaft ends, should be rejected or down-weighted.

If the value of the polytropic index is higher than the isentropic index, 1.4, for dry air, then the combined effect of added heat and internal friction is positive. If, however, the index is less than 1.4 then sensible heat is being lost from the air to the strata or through conversion into latent heat by evaporation of water. If the measurements have, unwisely, been taken shortly after a significant change in surface temperature, then a variation in n may become apparent by comparing the plotted points with the best-fit polytropic line.

In the majority of cases, satisfactory representation by a polytropic law can be obtained. Where significant deviation occurs then the flow work $\int_1^2 VdP$ can be obtained graphically as the area to the left of the curve on the PV diagram.

A thermodynamic analysis of a polytropic compression is given in section 3.5.3. The work done against friction, F_{12} , in the shaft is given by combining the steady flow energy equation (3.25) with the evaluation of the flow work term shown by equation (3.73). This gives

$$F_{12} = \frac{u_1^2 - u_2^2}{2} + (Z_1 - Z_2)g - R(T_2 - T_1) \frac{\ln\left(\frac{P_2/P_1}{T_2/T_1}\right)}{\ln\left(\frac{T_2/T_1}{P_2/P_1}\right)} \quad \frac{\text{J}}{\text{kg}} \quad (8.1)$$

or, alternatively

$$F_{12} = \frac{u_1^2 - u_2^2}{2} + (Z_1 - Z_2)g - \frac{n}{n-1} R(T_2 - T_1) \quad \frac{\text{J}}{\text{kg}} \text{ from equation (3.69)}$$

While most terms in these equations are measurable and, in principle, the values at the top (station 1) and the bottom (station 2) of the shaft can be used to determine F_{12} , there are some practical pointers that contribute greatly to the achievement of good results. First, it is often difficult to measure the mean velocity of air in a shaft. It may be preferable to measure the airflow(s) in underground airways and to carry out the necessary summations and corrections for air density to give u_1 and u_2 . Fortunately, the magnitude of the kinetic energy term is usually very small compared to the other factors.

The term $(Z_1 - Z_2)$ is simply the depth of the shaft connecting stations 1 and 2. The local value of gravitational acceleration, g , should be ascertained, taking into account mean elevation and latitude. For the pressures and temperatures P_1 , P_2 , T_1 and T_2 , **it is inadvisable to use the raw measurements made at the shaft extremities because of the unstable conditions that may exist at those locations.** It is preferable to construct separate plots of pressure and temperature against depth and to use best fit lines to establish representative pressures and temperatures at depths Z_1 and Z_2 .

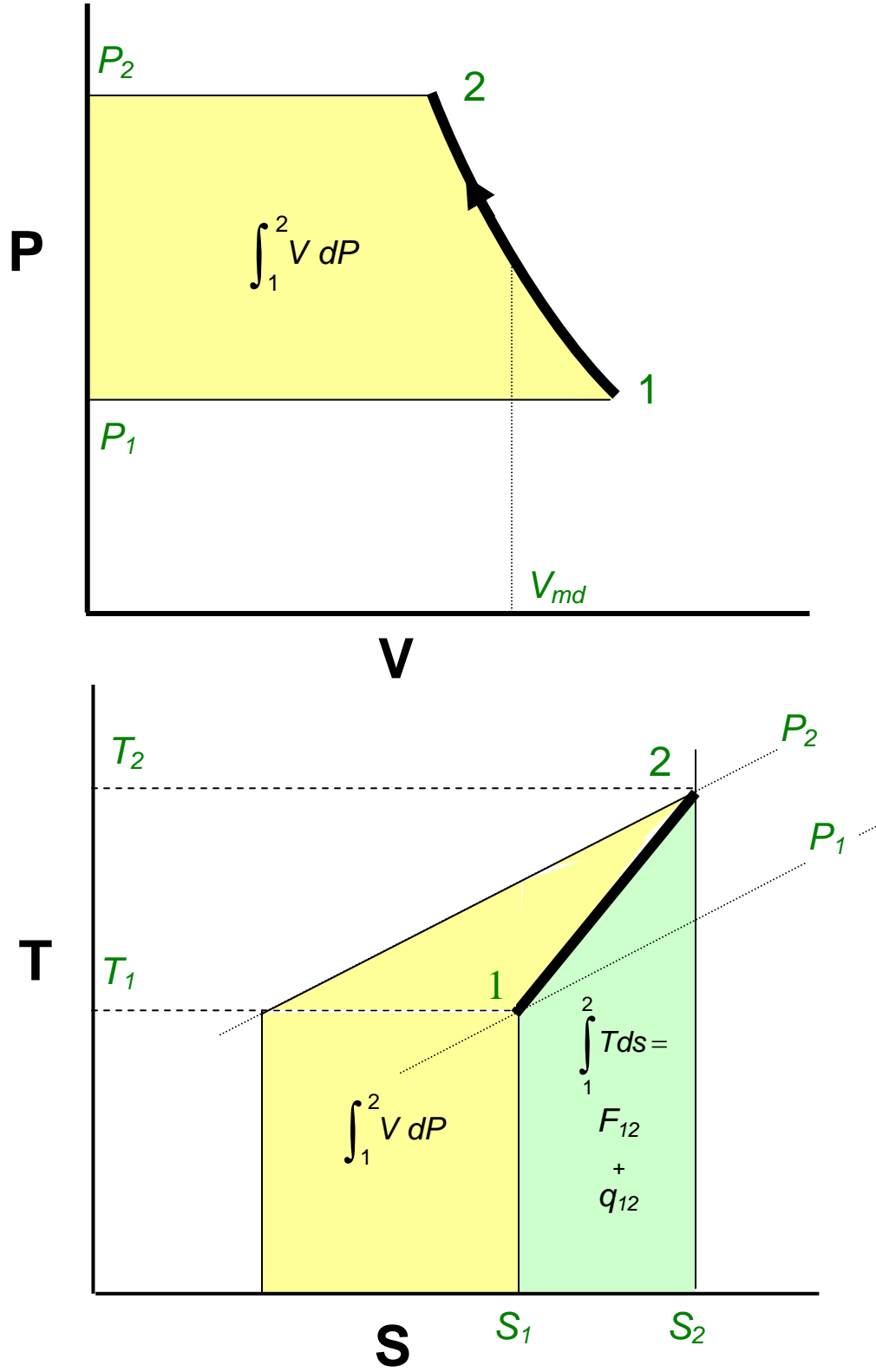


Figure 8.2. PV and Ts diagrams for a downcast shaft.

Equation (8.1) gives the amount of mechanical energy that is converted to heat through frictional processes within the shaft airflow. This can be employed to determine the Chezy Darcy coefficient of friction, f , for the shaft. From equation (2.46)

$$f = \frac{2d}{4Lu^2} F_{12} \quad (\text{dimensionless}) \quad (8.2)$$

where d = hydraulic mean diameter of the shaft (m)
 L = length of shaft (m) and
 u = mean air velocity (m/s)

Although the F term is the primary factor quantifying the work done against friction, it has one major drawback. It cannot be observed directly but must be computed from measurements including those of pressure and temperature. On the other hand, we know that the loss of mechanical energy by friction produces a frictional pressure drop, p , which *can* be measured directly (Chapter 6). It is, therefore, easier to conceptualize the notion of a frictional pressure drop, p , than the fundamental frictional work, F , which produces that pressure drop. Furthermore, recalling that ventilation planning for facilities of less than 500 m in depth can be conducted using the simpler relationships of incompressible flow, it is useful to remind ourselves of the relationship between p and F . This was introduced in Chapter 2.

$$p = \rho F \quad \text{Pa} \quad (8.3)$$

Hence, the work done against friction determined from equation (8.1) can be converted to a corresponding frictional pressure drop

$$p_{12} = \rho F_{12} \quad \text{Pa}$$

Now we have another problem. The density, ρ , varies throughout the shaft, so what value do we select? One option is to employ a mean value, ρ_{md} , where the subscript *md* denotes "mean downcast." For polytropic flow in a dry shaft the variations in both temperature and pressure are near linear with respect to depth. It follows that air density, $\rho = P/RT$, also increases in a near linear manner. Hence the arithmetic mean of densities measured at equal intervals throughout the shaft may be employed. Again, observers should be cognizant of the unrepresentative values that may be measured at shaft extremities. More generally,

$$\rho_{md} = \frac{\int_1^2 \rho dZ}{(Z_1 - Z_2)} \quad \frac{\text{kg}}{\text{m}^3} \quad (8.4)$$

Using the mean density, and ignoring the small kinetic energy term, the steady flow energy equation can be written as

$$(Z_1 - Z_2)g = V_{md}(P_2 - P_1) + F_{12}$$

where $V_{md} = 1/\rho_{md}$ (mean specific volume)
 or

$$p_{12} = F_{12} \rho_{md} = \rho_{md}(Z_1 - Z_2)g - (P_2 - P_1) \quad \text{Pa} \quad (8.5)$$

This is simply a form of **Bernoulli's equation** for incompressible flow. We have, however, taken account of compressibility by using a mean value of air density. Equation (8.5) is highlighted as we shall return to it later as a component in an approximation of natural ventilation pressure.

One further problem remains. If we wish to compare the frictional work done in a series of different airways then the F terms should be employed as these depend only upon the physical characteristics of the airway and the air velocity (equation (8.2)) - and are independent of the thermodynamic state of the air. On the other hand, if we compare frictional pressure drops, using equation (8.5), then these depend also upon the corresponding values of air density. As the latter may vary considerably around a mine circuit, frictional pressure drops are not a good basis for comparison. (This was the reason for consistent deviations that were noticed in the results of some pressure surveys prior to the development of mine ventilation thermodynamics). The problem can be met by choosing a "standard" value of air density, ρ_{st} , to relate ρ and F in equation (8.3). If the same value is used for all airways, then the comparison between airways becomes a constant multiple of F . The standard value of air density is normally taken as 1.2 kg/m^3 and the corresponding "frictional pressure drop", ρ_{st} , should then be identified as being 'standardized', or referred to standard density. It should be understood that **standardized pressure drops** have no direct physical significance other than the fact that they are a constant multiple of work done against friction.

Let us turn now to the Ts diagram on Figure 8.2. The area under the process line $\int_1^2 T ds$

represents the combination of added heat and the internal generation of friction heat $q_{12} + F_{12}$. Fortunately, the three-part steady flow energy equation (3.25) allows us to separate the two terms. Equation (8.1) gives F_{12} , and

$$q_{12} = (H_2 - H_1) - \frac{u_1^2 - u_2^2}{2} - (Z_1 - Z_2)g \quad \frac{\text{J}}{\text{kg}} \quad (8.6)$$

If the shaft is dry, then $(H_2 - H_1) = C_p (T_2 - T_1)$ and by ignoring the change in kinetic energy, we have

$$q_{12} = C_p (T_2 - T_1) - (Z_1 - Z_2)g \quad \frac{\text{J}}{\text{kg}} \quad (8.7)$$

In many shafts that have reached an effective equilibrium with respect to the temperature of the surrounding strata there is very little heat transfer, i.e. adiabatic conditions with $q_{12} = 0$. Equation (8.7) then gives

$$(T_2 - T_1) = \frac{(Z_1 - Z_2)}{C_p} \quad ^\circ\text{C} \quad (8.8)$$

This well known equation allows the increase in temperature with respect to depth to be calculated for a dry shaft in the absence of heat transfer. Inserting the constants 9.81 m/s^2 for g and 1020 J/kgK for C_p (value of specific heat of air with a moisture content of $0.0174 \text{ kg water vapour per kg dry air}$) gives

$$(T_2 - T_1) = 0.00962 (Z_1 - Z_2) \quad ^\circ\text{C} \quad (8.9)$$

This result is usually rounded off and quoted as a dry bulb temperature **adiabatic lapse rate** of 1°C per 100 m depth. The increase in temperature is a result of potential energy being converted to internal energy as the air falls through the shaft. The effect is also referred to as **autocompression**.

In practice, the change in temperature often varies considerably from $1^\circ\text{C}/100 \text{ m}$ due to both heat transfer and reductions in dry bulb temperature caused by evaporation of water.

In section 3.5.3, it was shown that in addition to areas on the Ts diagram illustrating heat, the same diagram may be used to indicate numerical equivalents of flow work. In particular, on the Ts diagram in Figure 8.2, the total area under the isobar P_2 between temperatures T_2 and T_1 represents the enthalpy change ($H_2 - H_1$).

However, the flow work is given by the steady flow energy equation as

$$\int_1^2 VdP = (H_2 - H_1) - (q_{12} + F_{12}) \quad \text{J/kg} \quad (8.10)$$

As the areas representing ($H_2 - H_1$) and ($q_{12} + F_{12}$) have already been identified on the Ts diagram, their difference gives a representation of the flow work.

Example.

This example is taken from an actual survey of an 1100 m deep downcast shaft of diameter 5.5m.¹ At the time of the survey, the mass flow of air was 353 kg/s. Figures 8.3 (a), (b) and (c) show the barometric pressures, wet and dry bulb temperatures and air density measured at approximately 100 m intervals throughout the shaft. The measurements taken at the extremities of the shaft have been omitted from these graphs as the turbulence at these points was not conducive to stable or precise readings. The raw data for the survey are tabulated in Appendix A8.1.

Variations in pressure, temperature and density.

The increase in pressure with respect to depth shown in Figure 8.3(a) is seen to be near linear with a slope of 1.22 kPa per 100m. The mean air density in the shaft was 1.26 kg/m³ illustrating the convenient rule of thumb that the rate of pressure increase in kPa/100m is approximately equal to the mean density (in SI units). This follows from

$$\Delta p = \rho gh = 981\rho \quad \text{Pa}$$

or $\Delta p = 0.981\rho \quad \text{kPa}$

where $g = 9.81 \text{ m/s}^2$ and $h = 100\text{m}$

The temperature plots shown in Figure 8.3(b) should, theoretically, also be linear with respect to depth for adiabatic conditions or where heat transfer is distributed uniformly throughout the length of the shaft. In this case, the actual variation in dry bulb temperature shows an interesting feature. The dry bulb temperature plot appears to be divided into discrete regions above and below 700m. Visual observation indicated the existence of free water in the shaft. The lower part passed through an aquifer. In this section tubing lining was employed and an increased water make produced falling droplets. The effects of enhanced evaporative cooling are shown clearly as a reduction in the slope of the dry bulb temperature-depth line in the lower part of the shaft. The mean dry bulb temperature lapse rate is 0.82 °C/100 m down to 700m and 0.67 °C/100 m at lower elevations, both less than the adiabatic lapse rate of 0.962 °C/100 m (equation (8.9)². This shows the important influence of water in the airway.

The wet bulb temperature observations exhibit slightly greater scatter but still follow a well defined linear relationship with respect to depth, irrespective of evaporation, and having a lapse rate of 0.44 °C/100 m. This is a little less than the wet bulb adiabatic lapse rate of 0.456 °C/100 m given by Figure 15.8 in Chapter 15. Hence, at the time of the survey there was a small heat loss from the air into the surrounding strata.

¹ Full details of the survey on which these examples were based are given in the paper listed in the Bibliography for this Chapter: *Barometric Survey of Shafts at Boulby Mine, Cleveland Potash, Ltd., Cleveland*, McPherson M.J. and Robinson, G.

² The mean moisture content in the shaft was 0.0108 kg/kg dry air. Inserting this value into equation (15.42) of Chapter 15 gives a corrected dry bulb adiabatic lapse rate of 0.967 °C per 100 m.

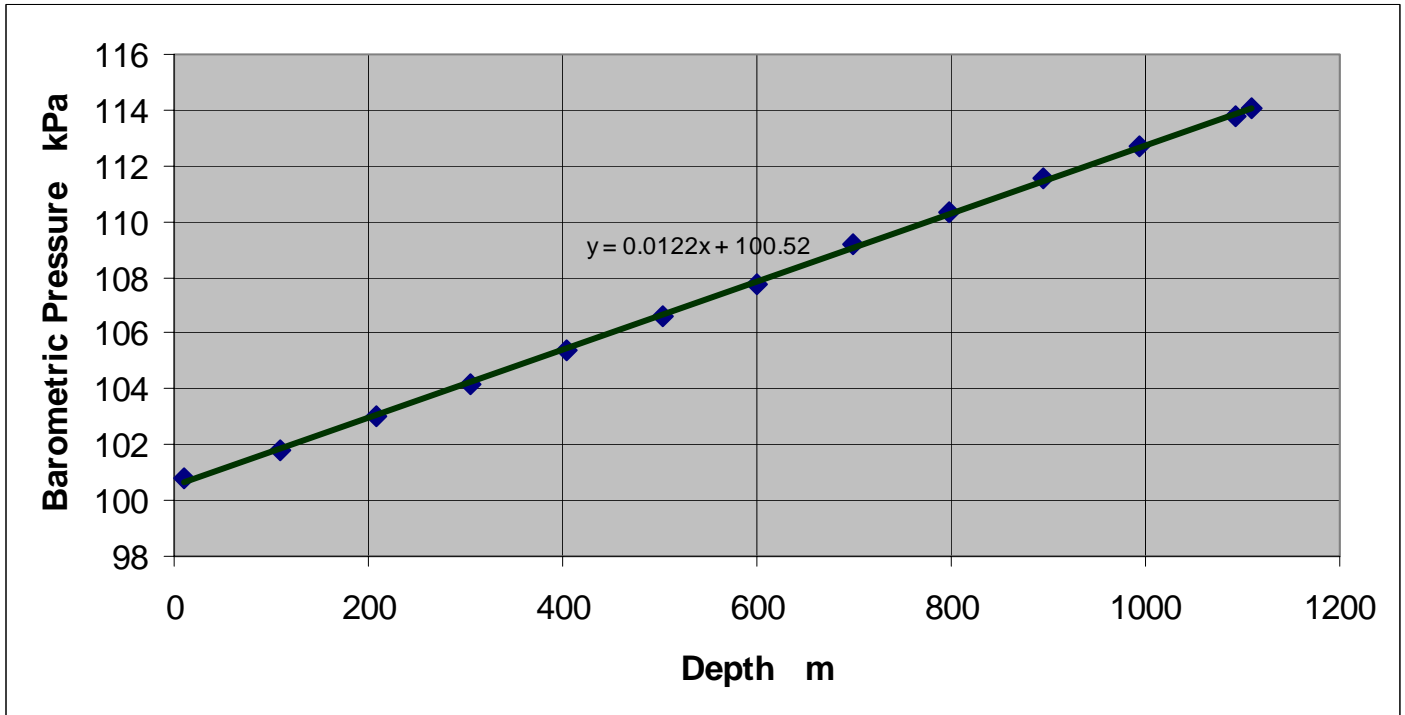


Figure 8.3(a). Measurements of barometric pressure in the downcast shaft with a best-fit straight line.

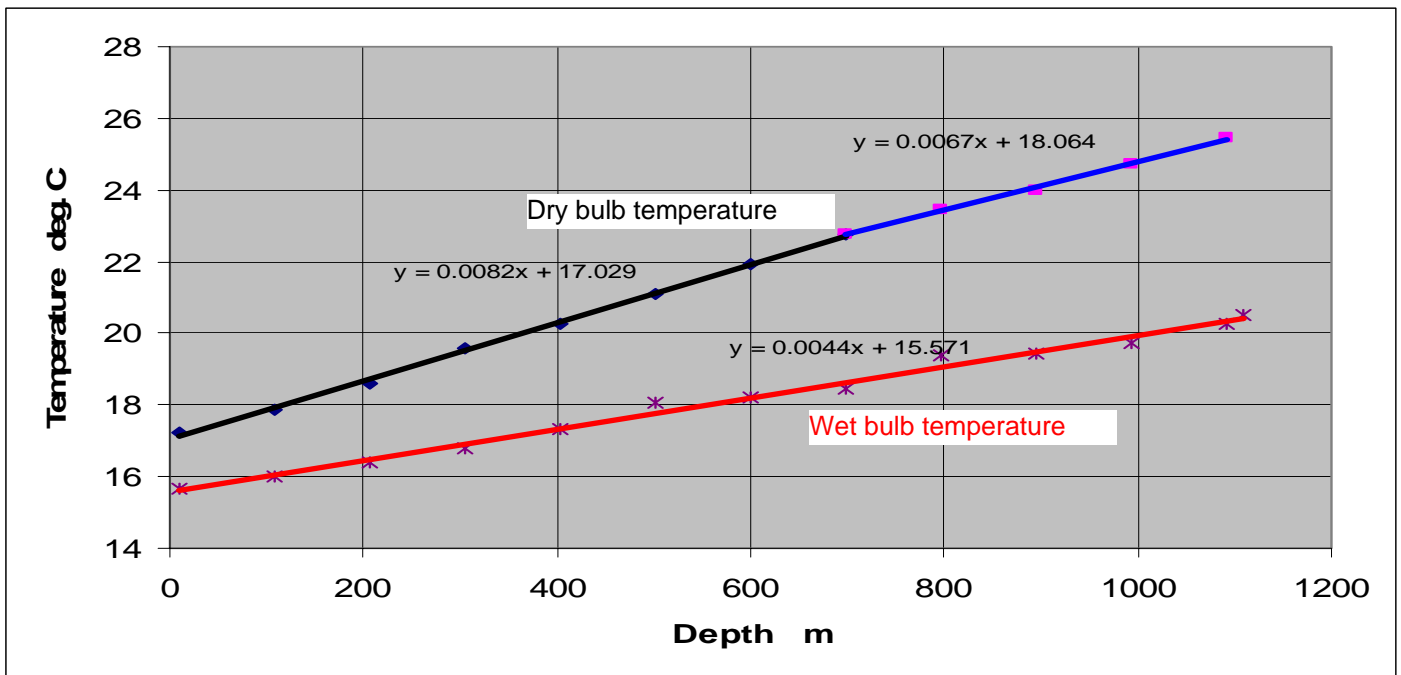


Figure 8.3(b). Increase in wet and dry bulb temperatures with respect to depth in the downcast shaft.

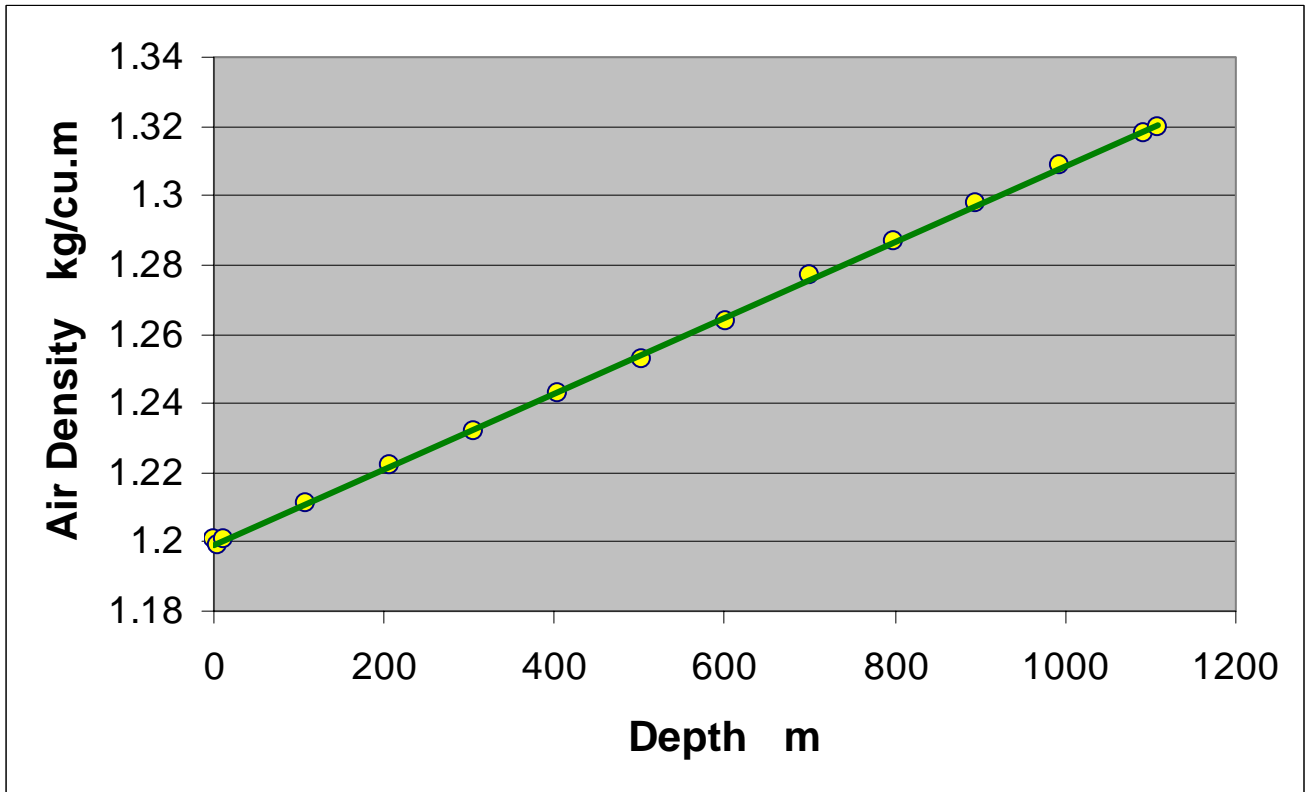


Figure 8.3(c). Increase in air density with respect to depth in the downcast shaft with a best-fit straight line.

Figure 8.3(c) illustrates that the air density increases linearly with depth.

PV diagram, work dissipated against friction and frictional pressure drop.

Figure 8.4 shows the *PV* diagram for the shaft. Despite the non-linearity of the temperature, a curve fitting exercise produced a good fit with the polytropic equation

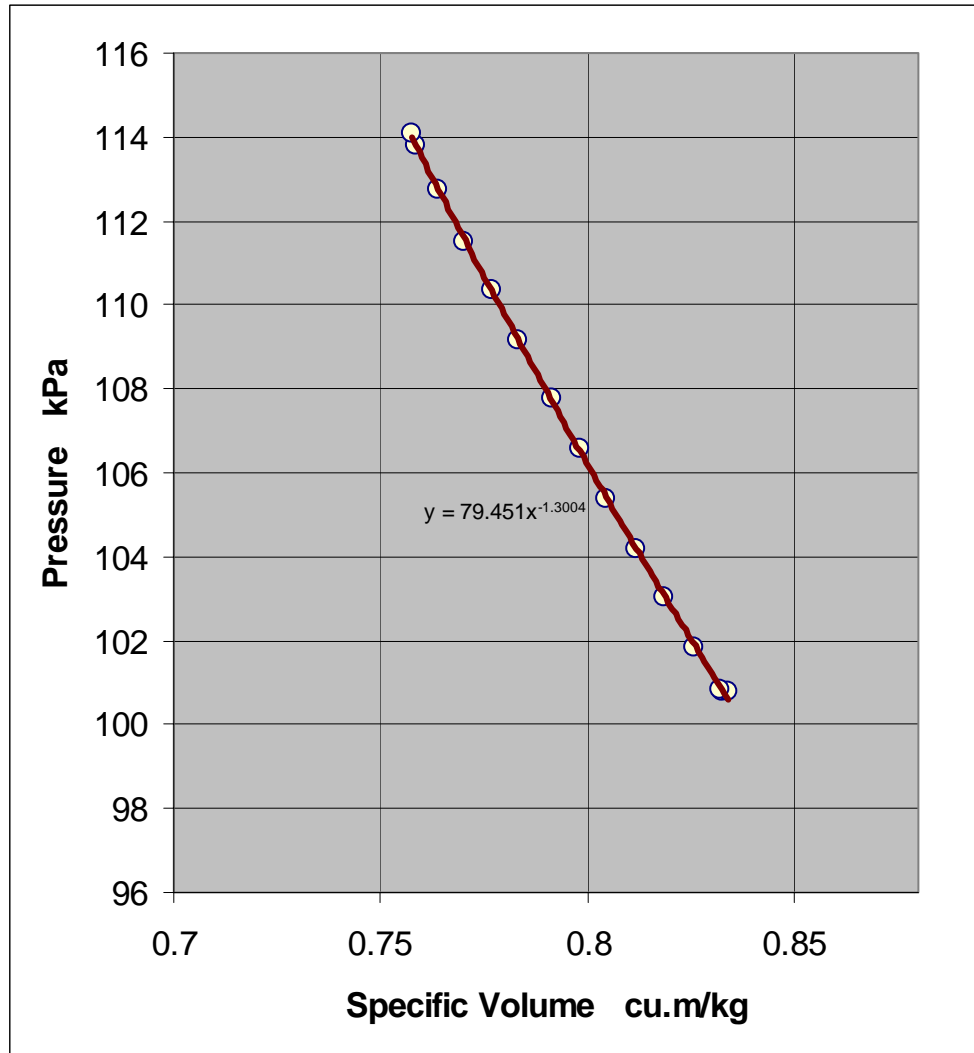
$$PV^{1.3004} = 79.451$$

Again, the non-representative points at the shaft ends were omitted for the curve fit. Figure 8.4 shows the curve of this equation superimposed upon the actual observations. The fact that the polytropic index was less than the isentropic 1.4 showed that sensible heat was being removed from the air - again, the combined effect of evaporative cooling and heat transfer.

The measurements may be used to determine the work done against friction within the airstream. Equation (8.1) gives:-

$$F_{12} = \frac{u_1^2 - u_2^2}{2} + (Z_1 - Z_2)g - R(T_2 - T_1) \frac{\ln\left(\frac{P_2}{P_1}\right)}{\ln\left(\frac{T_2}{T_1}\right)}$$

where subscripts 1 and 2 refer to the top and bottom of the shaft respectively.



Measured
 Curve fit
 $PV^{1.3004} = 79.45$
 where P is in kPa

Figure 8.4. PV diagram for the downcast shaft.

Independent measurements and corrections for density gave $u_1 = 12.78$ and $u_2 = 11.63$ m/s. The shaft depth, $(Z_1 - Z_2)$, was 1100 m and the value of g was 9.807 m/s². If the equation is to be used for the complete shaft then careful consideration must be given to the end values of pressure and temperature. The lack of uniform conditions at the shaft extremities indicates that single measurements of pressure and temperature at those locations are likely to produce erroneous results. The pressure and temperature plots should be examined carefully in order to select values of those parameters that are representative of an extrapolation of trends within the shaft. In this case, the values chosen from the relevant plots were:

$$P_1 = 100.79 \text{ kPa.} \quad \text{and} \quad P_2 = 113.90 \text{ kPa}$$

$$T_1 = 17.2 + 273.15 = 290.35 \text{ K} \quad \text{and} \quad T_2 = 25.5 + 273.15 = 298.65 \text{ K}$$

Equation (8.1) then gives

$$F_{12} = \frac{12.78^2 - 11.63^2}{2} + (1100 \times 9.807) - 287.04(25.5 - 17.2) \frac{\ln(113.9/100.79)}{\ln(298.65/290.35)}$$

$$= 14 + 10788 - 10336 \quad \text{J/kg}$$

$$= 466 \quad \text{J/kg}$$

This calculation illustrates that the kinetic energy term is, indeed, small compared with the other terms. More importantly, the potential energy and flow work terms are both large but similar numbers. Hence, small errors in the parameters that contribute to each of those terms can have a significant impact on the calculated value of F_{12} . For this reason, it is preferable to apply equation (8.1) for each increment of the shaft and sum the individual values of F rather than to use the complete shaft. This approach also accounts for variations in the polytropic index throughout the shaft. When this was done for the current example, the cumulative F_{12} was 493 J/kg.

The flow work may also be calculated from the alternative expression (equation (8.1))

$$\frac{n}{(n-1)} R(T_2 - T_1) = \frac{1.3004}{0.3004} 287.04(25.5 - 17.2) = 10313 \quad \text{J/kg}$$

giving

$$F_{12} = 14 + 10788 - 10313 = 489 \text{ J/kg}$$

We shall continue the analysis using the value of $F_{12} = 489 \text{ J/kg}$ obtained from this approach.

The frictional work can now be converted to a frictional pressure drop referred to any chosen air density. The mean density in the shaft was 1.260 kg/m^3 giving a corresponding frictional pressure drop of

$$\rho_{md} = \rho_{md} F_{12} \quad \text{Pa}$$

$$= 1.26 \times 489 = 616 \quad \text{Pa}$$

For comparison with other airways, the frictional pressure drop referred to standard air density, 1.2 kg/m^3 , becomes

$$\rho = \rho_{st} F_{12} \quad \text{Pa}$$

$$= 1.2 \times 489 = 587 \quad \text{Pa}$$

Coefficient of friction and airway resistance:

The Chezy Darcy coefficient of friction is given by equation (8.2)

$$f = \frac{2d}{4Lu^2} F_{12}$$

Using the mean air velocity of 12.20 m/s gives

$$f = \frac{2 \times 5.5}{4 \times 1100 \times (12.20)^2} \times 489$$

$$= 0.00821 \text{ (dimensionless)}$$

The Atkinson friction factor referred to standard density of 1.2 kg/m³ is

$$k = \frac{\rho_{st} f}{2} = \frac{1.2}{2} \times 0.00821 = 0.00493 \quad \text{kg/m}^3$$

(The values of f and k are mean values as the type of lining changed through the aquifer).

The rational resistance of the shaft is given from equation (2.51) as

$$R_t = \frac{f \text{ perimeter } L}{2 A^3} \quad \text{m}^{-4}$$

where perimeter = $\pi \times 5.5 = 17.28$ m
and area, $A = \pi (5.5)^2/4 = 23.76$ m²
giving

$$R_t = \frac{0.00821}{2} \times \frac{17.28}{(23.76)^3} \times 1100 = 0.00582 \quad \text{m}^{-4}$$

The Atkinson resistance referred to standard density becomes

$$R = \rho_{st} R_t$$

$$= 1.2 \times 0.00582 = 0.00698 \quad \text{Ns}^2/\text{m}^8$$

These resistance values refer to the 1100 m length of open shaft. The shock losses caused by conveyances, inlet and exist losses must be assessed separately and added to give the total shaft resistance.

Heat exchange.

The steady flow energy equation gives the heat transfer to the air as

$$q_{12} = (H_2 - H_1) - \frac{(u_1^2 - u_2^2)}{2} - (Z_1 - Z_2)g$$

The change in enthalpy, taking evaporation into account, may be determined from the methods given in Section 14.5.1. If no evaporation or condensation occurred then the change in enthalpy would be given by equation (3.33).

$$(H_2 - H_1) = C_p (T_2 - T_1)$$

The specific heat of the air, C_p , would be 1005 J/kgK if the air were perfectly dry. Again, Chapter 14 indicates how this can be corrected for the presence of water vapour. The actual value based on mean moisture content for this shaft was 1025 J/kgK.

If the shaft had been dry then

$$\begin{aligned}
 q_{12} &= 1025(25.5 - 17.2) - \frac{(12.78^2 - 11.63^2)}{2} - (1100 \times 9.807) \\
 &= 8507 - 14 - 10788 \\
 &= -2294 \quad \text{J/kg}
 \end{aligned}$$

The physical interpretation of this calculation is that for each kilogram of air:

- 14 J of heat accrue at the expense of kinetic energy as compression decelerates the air;
- 10 788 J of thermal energy arise from the loss of potential energy; but
- the total increase in thermal energy of the air is only 8 507 J.
- hence, 2 294 J of sensible heat must be transferred from the air.

We have conducted this latter calculation on the assumption of a dry shaft. This was not the situation in the actual case study. However, the result we have obtained does have a real meaning. The 2 294 J/kg heat loss reflects the reduction in the sensible heat of the air. Most of this was, in fact, utilized to evaporate water and, hence, was returned to the air as latent heat. Chapter 14 elaborates on the meanings of these terms.

In order to convert the heat exchange into kilowatts, we simply multiply by the mass flow of air

$$\frac{-2294}{1000} \times 353 = -810 \quad \frac{\text{kJ}}{\text{kg}} \times \frac{\text{kg}}{\text{s}} = \frac{\text{kJ}}{\text{s}} \text{ or kW}$$

8.2.3. Level workings

Figure 8.5 shows the *PV* and *Ts* diagrams for flow along level workings between stations 2 and 3. The diagrams reflect a decrease in pressure but increases in both specific volume and entropy, indicating heat additions to the air. In practice, a large part of the heat exchange with the strata takes place in the working areas where rock surfaces are freshly exposed.

Applying the steady flow energy equation to level workings gives

$$\frac{(u_2^2 - u_3^2)}{2} + (Z_2 - Z_3)g = \int_2^3 VdP + F_{23} = (H_3 - H_2) - q_{23} \quad \text{J/kg} \quad (8.11)$$

However, in this case $(Z_2 - Z_3) = 0$, giving

$$-\int_2^3 VdP = F_{23} - \frac{(u_2^2 - u_3^2)}{2} \quad \text{J/kg} \quad (8.12)$$

Remember that the flow work $\int VdP$ is the area to the left of the process curve on the *PV* diagram and, here, dP is negative (falling pressure). Hence, equation (8.12) shows that work is done by the air and, in level airways, is utilized entirely against friction and accelerating the air. Here again, the change in kinetic energy is usually negligible, leaving the simple relationship

$$-\int_2^3 VdP = F_{23} \quad \text{J/kg} \quad (8.13)$$

The heat flow into level workings or level airways may also be calculated by applying the condition $(Z_2 - Z_3) = 0$ to the steady flow energy equation.

$$\frac{(u_2^2 - u_3^2)}{2} + q_{23} = (H_3 - H_2) \quad \text{J/kg} \quad (8.14)$$

Again, changes in kinetic energy are normally negligible and, if we apply the condition of neither evaporation nor condensation, then

$$q_{23} = C_p (T_3 - T_2) \quad \text{J/kg} \quad (8.15)$$

An interesting situation often arises in well established return airways where equilibrium has effectively been established between the temperatures of the air and the surrounding rock. Heat transfer ceases giving adiabatic flow, $q_{23} = 0$. However, equation (8.15) shows that if q_{23} is zero then $T_3 = T_2$. The process becomes simultaneously adiabatic and isothermal. This is similar to a throttle in a gas stream, an example favoured by authors of textbooks on thermodynamics. In Section 3.4.1 it was shown analytically that the degree of friction has no influence on the temperature variation of the air. The adiabatic/ isothermal airway suggests a simple way of comprehending this phenomenon. An ideal adiabatic (isentropic) decompression would produce a fall in temperature. However, in a real (non-ideal) adiabatic decompression, frictional heat is generated within the airflow at exactly the correct rate to counteract that fall in temperature.

On the Ts diagram of Figure 8.5, the $\int_2^3 T ds$ heat area under the process line must be equal to the combined effects of added heat and internally generated friction, $q_{23} + F_{23}$. However, the area under the P_3 isobar between temperatures T_3 and T_2 is equal to the change in enthalpy $(H_3 - H_2)$ or $C_p(T_3 - T_2)$ for a dry airway. We have already shown that $q_{23} = C_p(T_3 - T_2)$. Hence, we can identify separate areas on the Ts diagram that represent F_{23} and q_{23} .

Unlike shafts of depths greater than 500m, most underground airflow paths involve relatively small changes in density. This is certainly the case for level workings or airways. While such airways play an important role in the mine thermodynamic cycle, the treatment of individual level airways is normally based on incompressible flow. The steady flow energy relationship then reduces to Bernoulli's equation with $(Z_2 - Z_3) = 0$

$$\frac{(u_2^2 - u_3^2)}{2} = \frac{(P_3 - P_2)}{\rho_{mw}} + F_{23} \quad \text{J/kg} \quad (8.16)$$

where the subscript mw denotes 'mean workings'. Neglecting the kinetic energy term, the frictional pressure drop referred to the mean density becomes simply

$$p_{23} = \rho_{mw} F_{23} = P_2 - P_3 \quad \text{Pa} \quad (8.17)$$

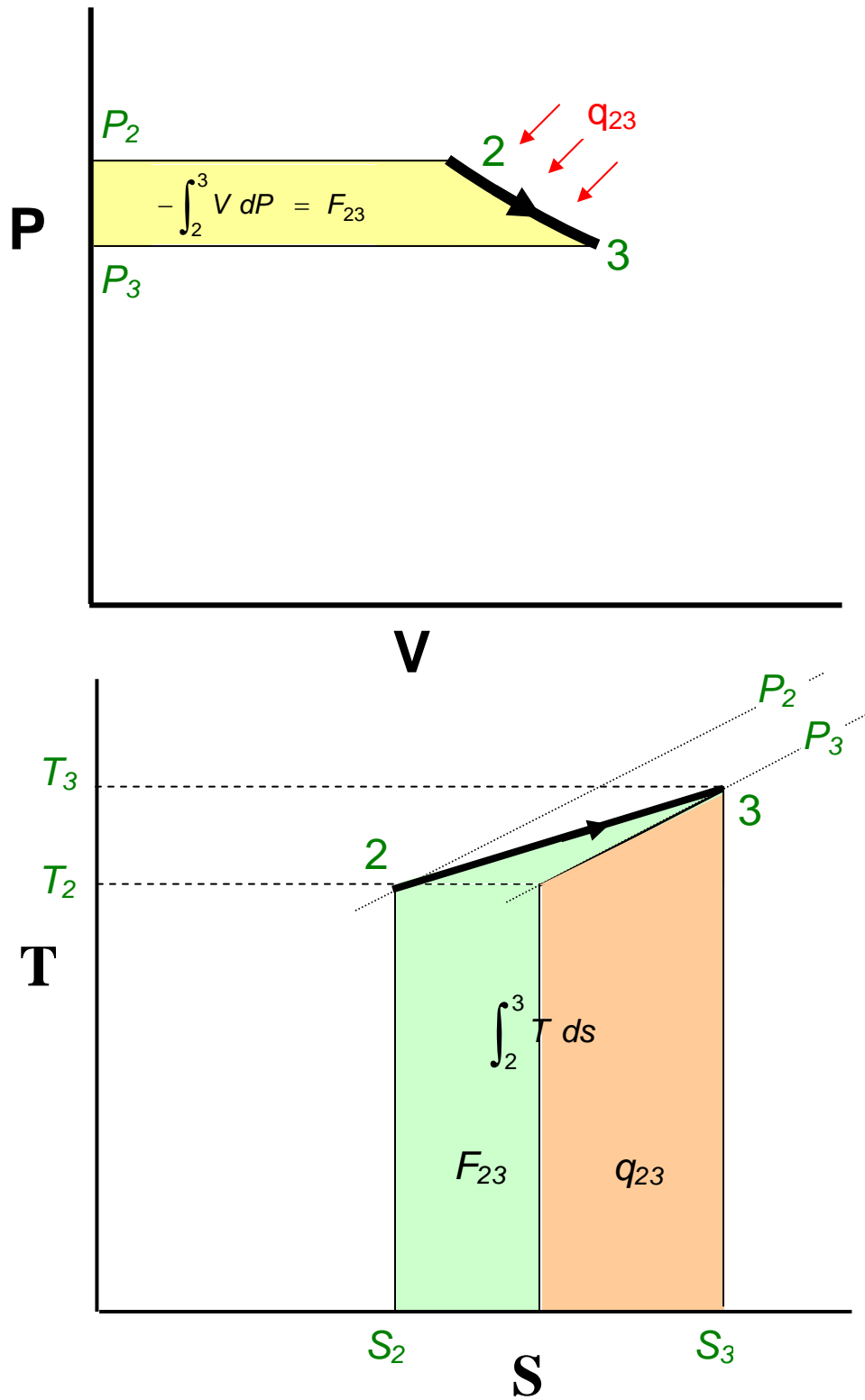


Figure 8.5. PV and Ts diagrams for level workings.

8.2.4. Upcast shaft.

Figure 8.6 shows the PV and Ts diagrams for an upcast shaft. As the air ascends the shaft, decompression results in an increase in specific volume despite a decrease in temperature. The latter is shown on the Ts diagram.

As the air returning from most underground facilities remains at a fairly constant temperature (the 'thermal flywheel'), upcast shafts are much less susceptible to variations in heat exchange than downcast shafts. It is common to find that an upcast shaft is operating at near adiabatic conditions. The path line 3 to 4 on the Ts diagram indicates a typical situation, descending from P_3, T_3 to P_4, T_4 and diverted to the right of an isentrope by the effects of friction.

A thermodynamic analysis of the downcast shaft was given in Section 8.2.2. The corresponding analysis for the upcast shaft follows the same logic and, indeed, the equations derived for the downcast shaft can also be used, with suitable changes of subscripts, for the upcast shaft. For that reason, details of the analysis will not be repeated. The reader may care to carry out a self test by attempting to derive the following results and to prove the annotation of areas shown on the Ts diagram.

For polytropic flow

$$F_{34} = \frac{u_3^2 - u_4^2}{2} - (Z_4 - Z_3)g + R(T_3 - T_4) \frac{\ln\left(\frac{P_3/P_4}{T_3/T_4}\right)}{\ln\left(\frac{T_3/T_4}{P_3/P_4}\right)} \quad \frac{\text{J}}{\text{kg}} \quad (8.18)$$

and

$$q_{34} = (Z_4 - Z_3)g - C_p(T_3 - T_4) \quad \frac{\text{J}}{\text{kg}} \quad (8.19)$$

Assuming constant (mean) density, ρ_{mu} ,

$$p_{34} = \rho_{mu}(Z_3 - Z_4) - (P_4 - P_3) \quad \text{Pa} \quad (8.20)$$

Example.

The earlier example dealt with the downcast shaft of an 1100 m deep mine. Figures 8.6 (a), (b) and (c) illustrate the conditions in the upcast shaft for the same mine and surveyed on the same day. The plots of pressure and temperature against depth show little scatter and stable conditions throughout the main length of the shaft. Again, measurements taken at the extremities of the shaft have been ignored in generating the graphs.

The dry bulb temperature increases at a rate of 0.97 °C/100 m indicating near adiabatic conditions with essentially no evaporation or condensation. This is a confirmation of the theoretical adiabatic lapse rate for dry bulb temperature in a dry shaft (ref. Section 15.3.1). The adiabatic conditions are further verified by the wet bulb temperature lapse rate of 0.42 °C/100 m (ref. Figure 15.8).

The PV diagram for the upcast shaft is shown on Figure 8.6(c). The polytropic curve fit gives the PV relationship to be $PV^{1.356} = \text{constant}$. The polytropic index of 1.356 is close to the isentropic value of 1.4 for dry air (ref. Section 3.4.3.). Comparing Figures 8.4 and 8.6(c) show that the barometric pressure at the base of the upcast shaft was greater than that at the base of the downcast shaft. This was because the main fans were sited underground at this mine in order to mitigate noise at the surface.

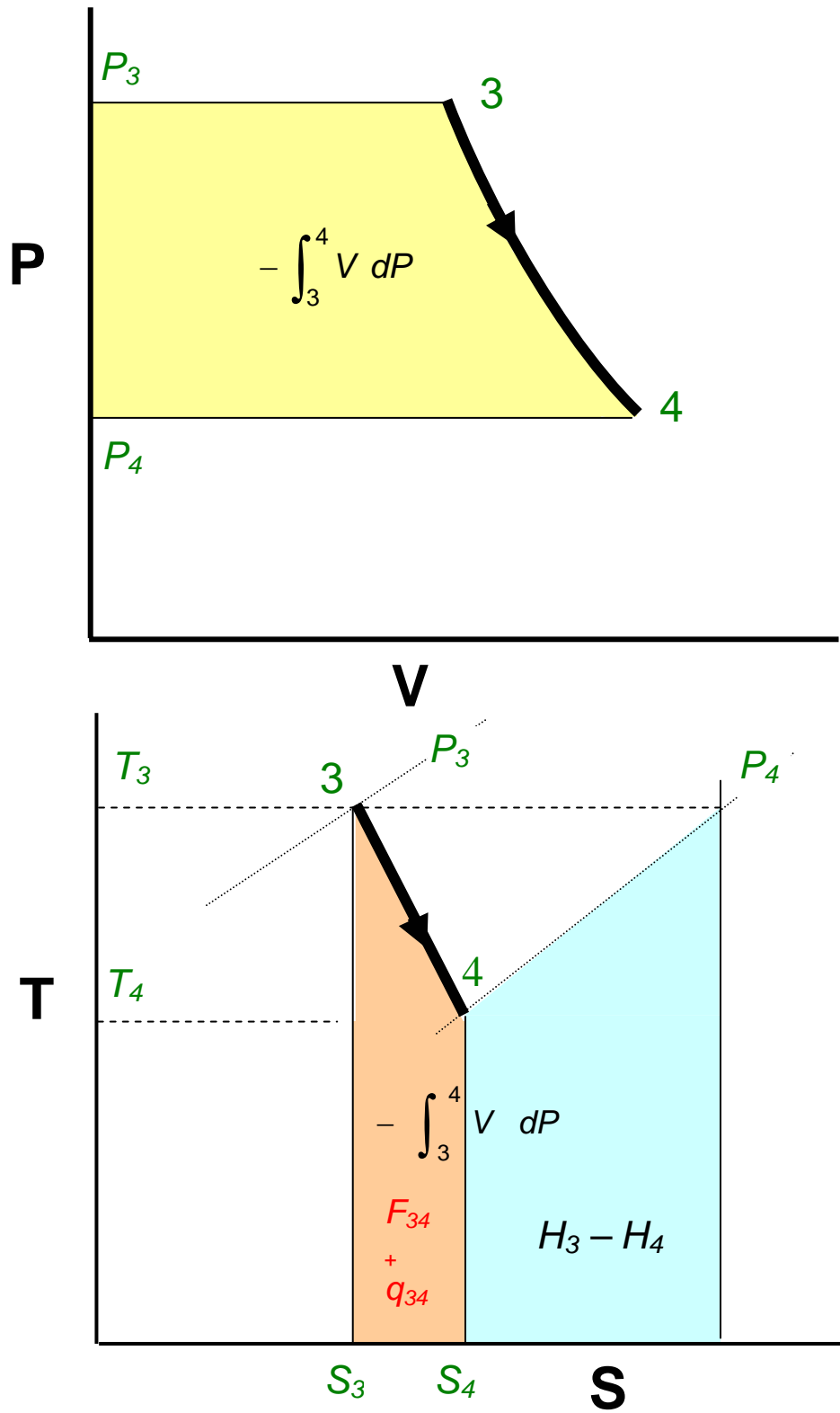


Figure 8.6. PV and Ts diagrams for an upcast shaft.

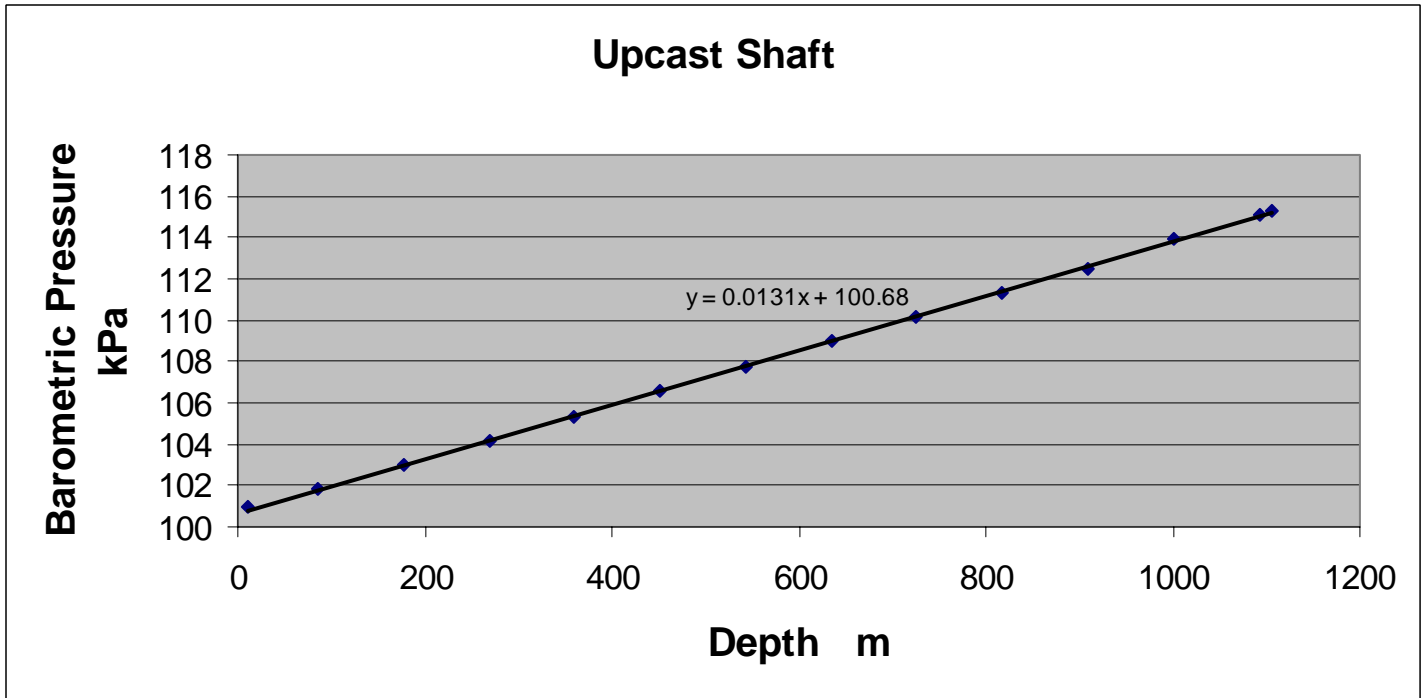


Figure 8.6(a) Measurements of barometric pressure in the upcast shaft with a best-fit straight line.

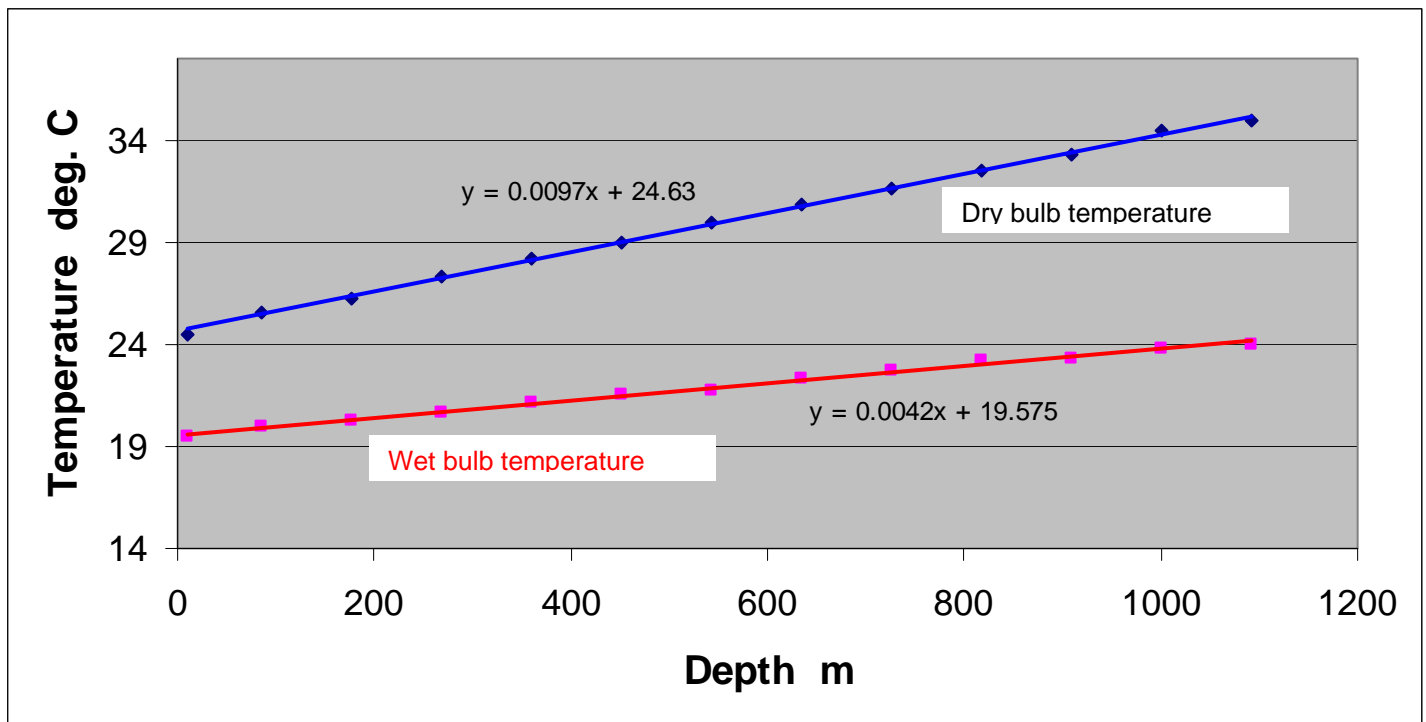
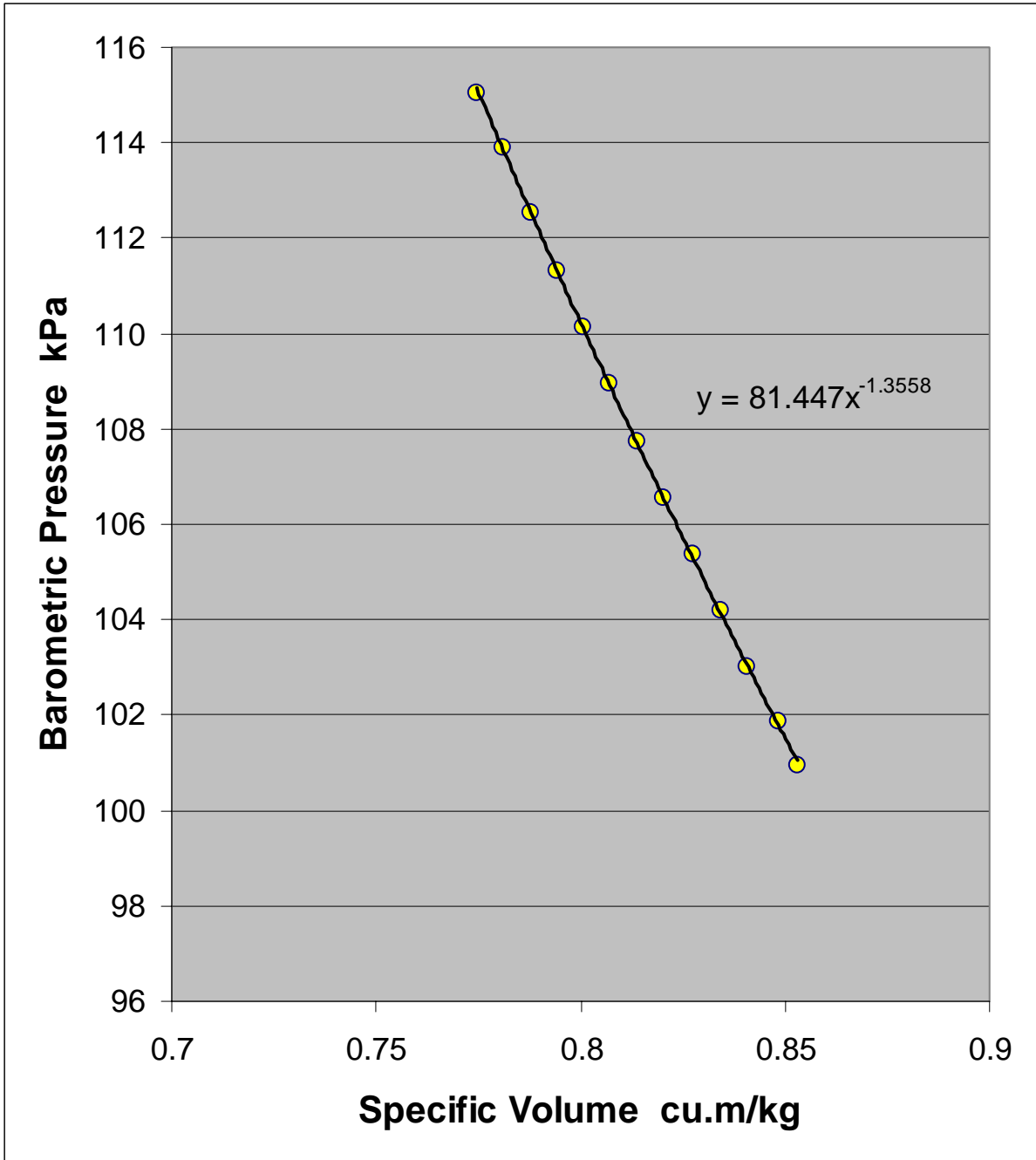


Figure 8.6(b). Increase in wet and dry bulb temperatures with respect to depth in the upcast shaft.



measured

Curve fit
 $PV^{1.3558} = 81.45$
 where P is in kPa

Figure 8.6(c). PV diagram for the upcast shaft.

8.3. THE COMPLETE MINE CYCLE

In the interests of clear explanation, it is convenient to investigate the phenomenon of natural ventilation first, before going on to the more usual situation of a combination of fan and natural ventilation.

8.3.1. Natural ventilation

Suppose that we have a vertical U tube with fluids of differing densities but the same height in the two limbs. This is an unstable situation. The heavier fluid will displace the lighter and the fluids will move. Motion will be maintained for as long as a difference exists between the mean densities of the fluids filling each limb of the U tube. It would be difficult to keep this experiment going with two completely different fluids. However, let us choose air as our fluid and apply heat at the base of the U tube. If any slight perturbation then caused a movement of air so that one limb contained warmer and, therefore, less dense air than the other, then the motion would accelerate until a state of dynamic equilibrium was reached, dependent upon the rate of heat addition. This is the process that causes natural ventilation in mines or any other flow system that involves heat transfer and differences in elevation. It is the same phenomenon that causes smoke to rise up a chimney or convective circulation in a closed cycle, and also explains the effectiveness of the old shaft bottom furnaces described in Chapter 1.

In most cases, heat is added to the air in underground facilities. The air in an upcast shaft is then warmer and less dense than in the downcast shaft. When the shaft bottoms are connected through workings, this constitutes an enormous out-of-balance U tube. Airflow is promoted and maintained at a rate that is governed by the difference between the mean densities of the air in the two shafts and the depths of those shafts.

If we take the simple case of two shafts of equal depth ($Z_1 - Z_2$), one a downcast containing air of mean density ρ_{md} , and the other an upcast of mean density ρ_{mu} , then the pressure at the base of the downcast due to the column of air in the shaft will be $\rho_{md} g(Z_1 - Z_2)$ (equation (2.8)) and the pressure at the base of the upcast due to its column of air will be $\rho_{mu} g(Z_1 - Z_2)$. Hence, the pressure difference across the shaft bottoms available for promoting airflow through the workings will be

$$NVP = \rho_{md} g(Z_1 - Z_2) - \rho_{mu} g(Z_1 - Z_2) = g(Z_1 - Z_2)(\rho_{md} - \rho_{mu}) \quad \text{Pa} \quad (8.21)$$

where NVP = Natural ventilating pressure (Pa)

This simple analysis provides the traditional expression for natural ventilating pressure. However, the following thermodynamic analysis indicates the limitations of equation (8.21) as well as providing a fuller understanding of the mechanisms of natural ventilating effects.

Natural ventilation will occur whenever heat transfer occurs in the subsurface. If the rock is cooler than the air then a natural ventilating pressure will apply in the reverse direction inhibiting the airflow. In the case of a geographical region where the diurnal or seasonal ranges of surface air temperature encompass the mean temperature of the strata in a naturally ventilated mine, then reversals of airflow can occur. Because of such instabilities, very few medium size or large mines are now ventilated purely by natural means.

The PV and Ts diagrams for a naturally ventilated mine are illustrated by combining Figures 8.2, 8.5 and 8.6 for the downcast shaft, level workings and upcast shaft respectively. The result is shown on Figure 8.7 with the slight curvature of each of the process lines ignored for simplicity.

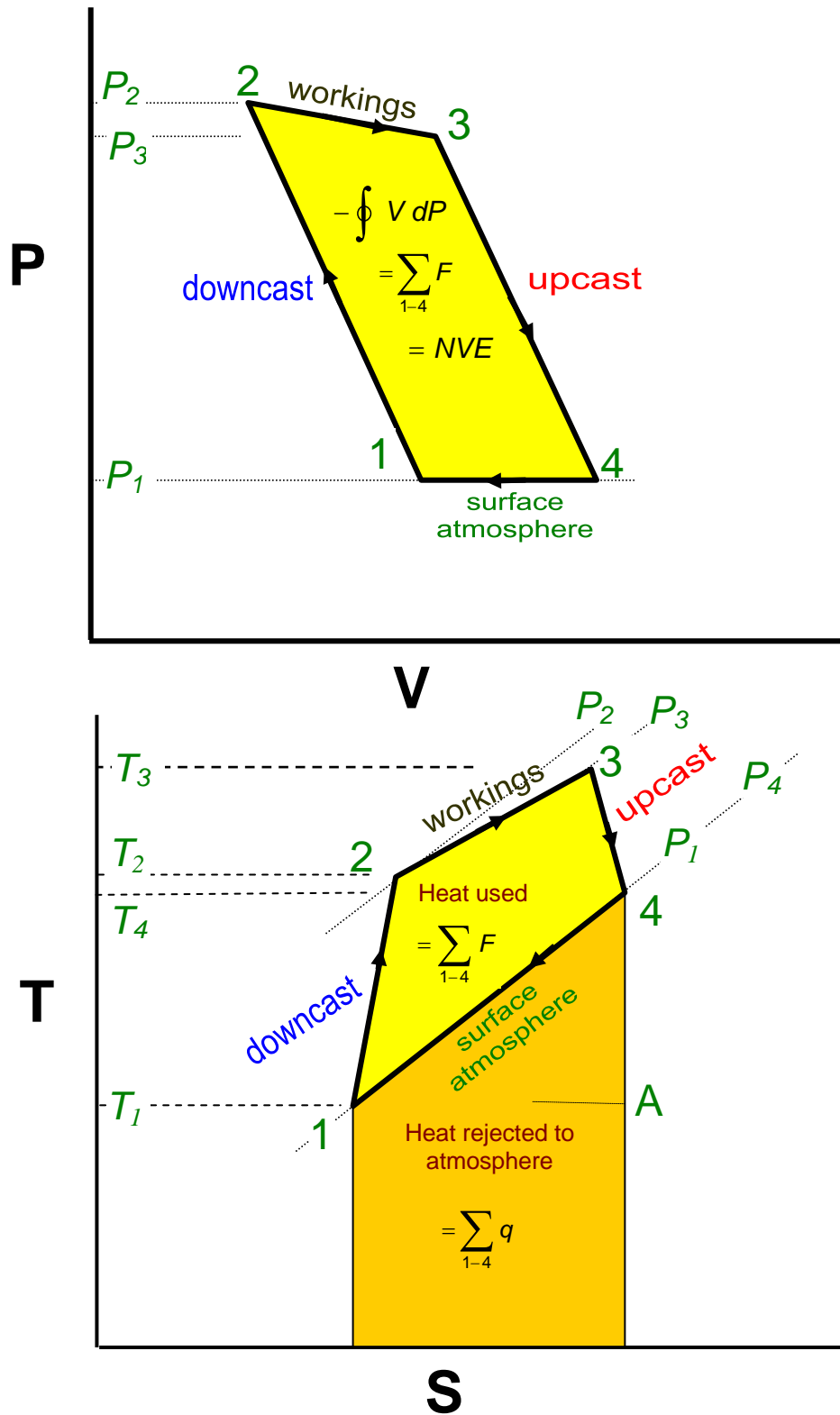


Figure 8.7. PV and Ts diagrams for a naturally ventilated mine.

In the absence of a main surface exhaust fan, the airflow is emitted from the top of the upcast shaft (station 4) at surface atmospheric pressure. We can now close the cycle back to station 1 (top of downcast shaft) by considering the process that takes place within the pressure sink of the surface atmosphere. The exhaust air is emitted from the top of the upcast shaft with some finite velocity. This causes turbulence within the atmosphere. In the majority of cases, the exhaust air is at a temperature higher than that of the surface atmosphere. It cools at constant pressure, rejecting heat to the atmosphere, contracts and follows the process lines 4 to 1 on both the PV and Ts diagrams of Figure 8.7.

Just as we have combined the separate processes into a closed cycle on the PV and Ts diagrams, so, also, can we combine the corresponding versions of the steady flow energy equation:

$$\text{Downcast: } \frac{u_1^2 - u_2^2}{2} + (Z_1 - Z_2)g = \int_1^2 VdP + F_{12} = (H_2 - H_1) - q_{12} \quad (8.22)$$

$$\text{Workings: } \frac{u_2^2 - u_3^2}{2} + (Z_2 - Z_3)g = \int_2^3 VdP + F_{23} = (H_3 - H_2) - q_{23} \quad (8.23)$$

$$\text{Upcast: } \frac{u_3^2 - u_4^2}{2} + (Z_3 - Z_4)g = \int_3^4 VdP + F_{34} = (H_4 - H_3) - q_{34} \quad (8.24)$$

$$\text{Atmosphere: } \frac{u_4^2 - u_1^2}{2} + (Z_4 - Z_1)g = \int_4^1 VdP + F_{41} = (H_1 - H_4) - q_{41} \quad (8.25)$$

$$\text{SUM: } \quad \quad \quad 0 \quad + \quad 0 \quad = \quad \oint VdP + \sum_{12341} F = \quad 0 \quad - \quad \sum_{12341} q \quad (8.26)$$

Note that when we sum the individual terms, the kinetic energy, potential energy and enthalpy all cancel out.

Let us examine some of the features of the summation equation (8.26). Recalling that each

individual $\int VdP$ term is represented by the area to the left of the curve on the relevant PV

diagram, when we sum those areas algebraically, the cyclic integral $\oint VdP$ for the complete loop

becomes the enclosed area, 1234, on the PV diagram of Figure 8.7. Furthermore, the

$\int VdP$ areas for the workings and upcast shaft are negative (falling pressures). Inspection of the PV diagram shows that the enclosed area is also negative, indicating that net flow work is done by the air. This is the mechanical energy that produces and maintains motion of the air. It has, as its source, an available part of the heat energy that is added to the air and is called the **Natural Ventilating Energy, NVE**.

Further examination of the PV diagram shows that the NVE area depends primarily upon two factors. First, the extent to which heat additions in the subsurface cause expansion of the specific volume between stations 2 and 3, and secondly, the difference in barometric pressures caused by the depths of the shafts, 1 to 2 and 3 to 4. The greater the heat additions or the depth of the mine then the greater will be the NVE.

Equation (8.26) for the complete cycle gives

$$-\oint VdP = \sum_{12341} F \quad \text{J/kg} \quad (8.27)$$

where the symbol $\sum_{12341} F$ denotes summation around the closed cycle. This shows that the natural flow work done by the air is utilized entirely against friction. The enclosed area, 1234, on the PV diagram also represents the work that is done against friction. Unlike a manufactured heat engine, a mine thermodynamic cycle produces no external work, although it would be perfectly possible to achieve this by introducing a high volume - low pressure turbine into the airstream. The mechanical energy thus produced would be at the expense of flow energy and the rate of airflow would then diminish.

Let us take a closer look at equation (8.25) for the isobaric cooling of the exhaust air. We can make three simplifications to this equation. First, if the tops of both shafts are at the same elevation then $Z_4 = Z_1$. Secondly, we can assume that the surface atmosphere is at rest, $u_1 = 0$

and, thirdly, as the free atmosphere is at constant pressure, $\int_4^1 VdP = 0$. Applying these

conditions gives

$$\frac{u_4^2}{2} = F_{41} \quad \text{J/kg} \quad (8.28)$$

This confirms that the kinetic energy of the air issuing from the top of the upcast shaft is utilized against the frictional effects of creating turbulence in the free atmosphere. Equation (8.25) also quantifies the heat that is rejected to the surface atmosphere:

$$-q_{41} = (H_4 - H_1) \quad \text{J/kg} \quad (8.29)$$

or, if no evaporation or condensation occurs during the isobaric cooling,

$$-q_{41} = C_p (T_4 - T_1) \quad \text{J/kg} \quad (8.30)$$

However, the summation equation (8.26) gives:

$$\sum_{12341} q = 0 \quad \text{J/kg} \quad (8.31)$$

It follows that the total heat added in the subsurface, $\sum_{1234} q = q_{12} + q_{23} + q_{34}$, is equal to the heat ultimately rejected to the surface atmosphere, $-q_{41}$, despite the fact that some of that added heat has, temporarily, been converted to mechanical (kinetic) energy in order to create movement of the air.

Turning to the Ts diagram, the heat area below each of the process lines 1-2, 2-3 and 3-4 represents the combination of added heat and frictional heat for the downcast shaft, workings and upcast shaft respectively. It follows that the total area under lines 1-2-3-4 represents

$\sum_{1234} F + \sum_{1234} q$ for the complete mine. However, the area under the isobar 4-1 represents the heat

rejected to the atmosphere, $-q_{41}$, which has already been shown to equal $\sum_{1234} q$. It follows that

the 1-4 enclosed area 1234 on the Ts diagram represents the work done against friction in the shafts and workings, $\sum_{1234} F$. As the frictional loss within the atmosphere does not appear on the

PV diagram, we have the revealing situation that areas 1234 on both diagrams represent frictional effects in the subsurface. The PV area represents the work done against friction while the Ts area shows that same work, now downgraded by friction, appearing as heat energy.

The area 41A on the Ts diagram lies above the atmospheric temperature line and, therefore, represents rejected heat that, theoretically, is available energy. It could be used, for example, to assist in the heating of surface facilities and can be significant in deep mines. However, that energy is contained in a large volume of air, often contaminated by solid, liquid and gaseous contaminants, and with a relatively small temperature differential with respect to the ambient atmosphere. For these reasons, very few mines attempt to take advantage of the available part of the **reject heat**.³

There are two main methods of quantifying the natural ventilating energy. First, if each of the subsurface processes approximates to a polytropic law then the work done against friction in each segment may be calculated from the form of equation (8.1).

$$F_{i,i+1} = \frac{u_i^2 - u_{i,i+1}^2}{2} + (Z_i - Z_{i,i+1})g - R(T_{i+1} - T_i) \frac{\ln\left(\frac{P_{i+1}}{P_i}\right)}{\ln\left(\frac{T_{i+1}}{T_i}\right)} \quad \frac{\text{J}}{\text{kg}}$$

where subscript i takes the relevant value 1, 2 or 3. The sum of the resulting F terms then gives the natural ventilation energy, NVE .

Secondly, if polytropic curve fitting shows significant deviations from observed data then each segment can be further subdivided, or the enclosed NVE area on the PV diagram can be determined graphically.

As most modern underground facilities are ventilated by a combination of fans and natural ventilation, it is useful to be able to compare the ventilating potential of each of them. The theoretically correct way of doing this is to express the mechanical work input from the fan in J/kg. This is then directly comparable with the NVE . The fan work can be determined from measurements of pressure, temperature and air velocity across the fan (Section 8.3.2.). However, the more usual convention in practice is to quote fan duties in terms of fan pressure and volume flow. A traditional and convenient device is to convert the natural ventilating energy, NVE , into a corresponding natural ventilating pressure, NVP . It should be remembered, however, that unlike a fan, an NVP is not located at a single location but is generated around a closed thermodynamic cycle.

$$NVP = NVE \times \rho \quad \text{Pa} \quad (8.32)$$

Here, again, we have the same difficulty of choosing a value of air density. If frictional pressure drops within individual branches have all been referred to standard density, 1.2 kg/m^3 , then it is appropriate also to refer both natural and fan ventilating pressures to the same standard density. This is, in effect, equivalent to comparing ventilating energies.

³ See section 18.4.2 for use of reject heat in cold climates.

Another method, although imprecise, is to sum equations (8.5, 8.17 and 8.20) that gave the frictional pressure drops for the downcast shaft, workings and upcast shaft, respectively, on the basis of the corresponding mean densities:

$$\begin{array}{llll} \text{Downcast:} & p_{12} & = & \rho_{md} (Z_1 - Z_2)g - (P_2 - P_1) & \text{Pa} & \text{see (8.5)} \\ \text{Workings:} & p_{23} & = & (P_2 - P_3) & \text{Pa} & \text{see (8.17)} \\ \text{Upcast:} & p_{34} & = & -\rho_{mu} (Z_4 - Z_3)g - (P_4 - P_3) & \text{Pa} & \text{see (8.20)} \end{array}$$

$$\text{SUM: } p_{12} + p_{23} + p_{34} = (Z_1 - Z_2)g(\rho_{md} - \rho_{mu}) \quad \text{Pa} \quad (8.33)$$

In arriving at this summation, we have assumed that the depths of the two shafts are equal, $(Z_1 - Z_2) = (Z_4 - Z_3)$, and that the atmospheric pressure at the tops of both shafts is the same, $P_1 = P_4$. This is identical to the equation that we arrived at earlier (equation (8.21)) from a consideration of the pressures at the bottoms of the two shafts and which were produced by their corresponding columns of air. Calculation of natural ventilation pressure as

$$NVP = p_{12} + p_{23} + p_{34} = (Z_1 - Z_2)g(\rho_{md} - \rho_{mu}) \quad \text{Pa} \quad (8.34)$$

is sometimes known as the mean density method. While equation (8.34) is simple to use and much quicker than the two methods of determining natural ventilating effects introduced earlier, it should not be regarded as an exact measure of the thermal energy that assists in the promotion of airflow. The difficulty is that the summation of pressure drops is not referred to a single defined value of air density. Each individual pressure drop is based on a different mean density. Their summation cannot, therefore, be justified as a definitive measure of natural ventilation but remains as a summation of measured frictional pressure drops. This can, in fact, be shown from the differential form of the steady flow energy equation and ignoring the kinetic energy and fan terms

$$-g dZ = VdP + dF \quad \text{J/kg (see equation (3.25))}$$

or, as $V = 1/\rho$

$$-g \rho dZ = dP + \rho dF \quad \text{J/m}^3 = \text{Nm/m}^3 = \text{N/m}^2 = \text{Pa}$$

Integrating around a closed cycle $\left(\oint dP = 0 \right)$ gives

$$-g \oint \rho dZ = \oint \rho dF \quad \text{J/m}^3 = \text{Pa}$$

The right side of this equation is the sum of the measured frictional pressure drops, $p = \rho F$, while the left side is the algebraic sum of the pressure heads exerted by the columns of air in the system. It is, therefore, an exact form of equations (8.21) and (8.33).

8.3.2. Combined fan and natural ventilation

Main ventilating fans might be placed at a number of strategic sites in a subsurface system, subject to any restrictions imposed by the governing legislation. However, to examine the combination of fan and natural ventilation, we shall use the most common situation - that of a main exhausting fan located at the top of the upcast shaft.

Figure 8.8 gives the corresponding PV and Ts diagrams. The difference between these and the corresponding diagrams for the purely naturally ventilated mine is that station 4, the top of the upcast shaft, is also the inlet to the fan and is at a sub-atmospheric pressure. On passing through the fan from station 4 to station 5, the air is compressed back to atmospheric pressure.

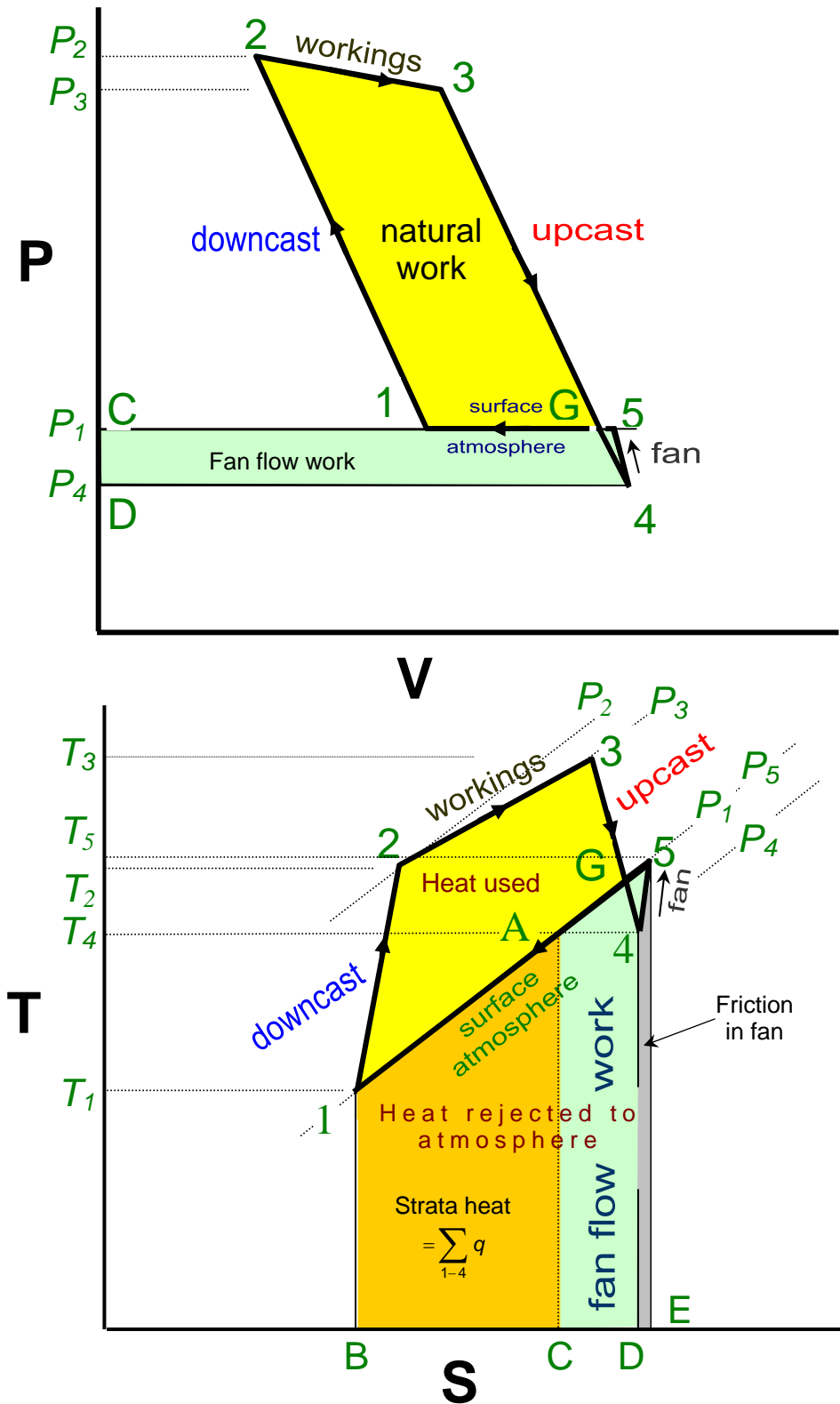


Figure 8.8. PV and Ts diagrams for a mine ventilated by both natural means and a main exhaust fan.

Concentrating, for the moment, on the segments of the PV diagram that represent the subsurface, the areas to the left of lines 1-2, 2-3 and 3-4 represent work done on or by the air as it progresses through the downcast shaft, workings and upcast shaft respectively. The algebraic summation of those work areas is the negative area 1234DC. This represents the net flow work done by the air between stations 1 and 4. The area to the left of the fan compression curve 4-5 represents the flow work done on the air by the fan. In practice, both the upcast shaft and fan processes are often near adiabatic, i.e. position 5 on the PV diagram is very close to position G. Hence, we can divide the total work done by the air into two identifiable zones; area 123G represents the natural ventilating energy and area C154D represents the fan work supplied to the air while compressing it back to surface atmospheric pressure. The combination of the two provides the total ventilating energy for the facility.

The process lines on the Ts diagram from station 1 to station 4 follow paths similar to those for the naturally ventilated mine except that station 4 is now at a sub-atmospheric pressure. The fan curve, 4 to 5 is angled slightly to the right of the ideal isentrope. Heat transfer is normally quite small across the fan casing in terms of J/kg because of the high airspeed. Hence, the fan process is essentially a frictional adiabatic. The derivation of the areas quantified on the Ts diagram representing the fan work and associated frictional heat is given in Section 3.5.3.

The quantitative analysis of the cycle commences, once again, by stating the component steady flow energy equations and summing them to determine the cycle equation.

$$\text{Downcast: } \frac{u_1^2 - u_2^2}{2} + (Z_1 - Z_2)g = \int_1^2 VdP + F_{12} = (H_2 - H_1) - q_{12} \quad (8.35)$$

$$\text{Workings: } \frac{u_2^2 - u_3^2}{2} + (Z_2 - Z_3)g = \int_2^3 VdP + F_{23} = (H_3 - H_2) - q_{23} \quad (8.36)$$

$$\text{Upcast: } \frac{u_3^2 - u_4^2}{2} + (Z_3 - Z_4)g = \int_3^4 VdP + F_{34} = (H_4 - H_3) - q_{34} \quad (8.37)$$

$$\text{Fan: } \frac{u_4^2 - u_5^2}{2} + (Z_4 - Z_5)g + W_{45} = \int_4^5 VdP + F_{45} = (H_5 - H_4) - q_{45} \quad (8.38)$$

$$\text{Atmosphere: } \frac{u_5^2 - u_1^2}{2} + (Z_5 - Z_1)g = \int_5^1 VdP + F_{51} = (H_1 - H_5) - q_{51} \quad (8.39)$$

$$\text{SUM: } \quad \quad \quad \frac{0}{2} + \frac{0}{2} + W_{45} = \oint VdP + \sum_{123451} F = 0 - \sum_{123451} q \quad (8.40)$$

Consideration of equations (8.35) to (8.40) reveals a number of significant points:

- (a) The work areas annotated on the PV diagram are confirmed by a rearrangement of equation (8.40)

$$\sum_{123451} F = W_{45} - \oint VdP \quad \text{J/kg} \quad (8.41)$$

Work done against friction = Work supplied by fan + Natural flow work done by air

Area 1234DC = Area 45CD + Area 123G

(b) The changes in kinetic energy and potential energy through the fan are both very small. Ignoring these terms simplifies equation (8.38) to

$$W_{45} = \int_4^5 VdP + F_{45} \quad \text{J/kg} \quad (8.42)$$

The fan input produces flow work and overcomes frictional losses within the fan unit. The fan flow work shows on the PV diagram. However, both flow work and the frictional losses appear on the Ts diagram.

(c) The equation for **isobaric cooling** ($dP = 0$) in the atmosphere (equation 8.39) gives

$$\frac{u_5^2}{2} = F_{51} \quad \text{J/kg} \quad (8.43)$$

assuming that the surface atmosphere is at rest ($u_1 = 0$). The kinetic energy of the air exhausting from the fan is dissipated against friction within the atmosphere. This is similar to the result obtained for the naturally ventilated mine (equation (8.28)). However, it now becomes more significant due to the higher velocity of the air issuing from the fan outlet, u_5 . The kinetic energy at outlet is a direct loss of available energy from the system. It is, therefore, advantageous to decelerate the airflow in order to reduce that loss. This is the reason that main fans are fitted with expanding evasees at outlet.

(d) Summing equations (8.35) to (8.38) for the subsurface and the fan, and taking $u_1 = 0$, gives

$$-\frac{u_5^2}{2} + W_{45} = (H_5 - H_1) - \sum_{12345} q$$

or

$$(H_5 - H_1) = W_{45} + \sum_{12345} q - \frac{u_5^2}{2} \quad \text{J/kg} \quad (8.44)$$

showing that the increase in enthalpy between the inlet and outlet airflows is equal to the total energy (work and heat) added, less the kinetic energy of discharge. However, if we inspect equation (8.39) for cooling in the atmosphere, we have

$$(H_5 - H_1) = -q_{51} - \frac{u_5^2}{2} \quad \text{J/kg} \quad (8.45)$$

where $-q_{51}$ is the heat rejected to the atmosphere.

Comparing equations (8.44) and (8.45) gives

$$-q_{51} = W_{45} + \sum_{12345} q \quad \text{J/kg} \quad (8.46)$$

This latter equation reveals the sad but unavoidable fact that all of the expensive power that we supply to the fans of a ventilation system, plus all of the heat energy that is added to the air, are ultimately **rejected as waste heat** to the surface atmosphere. It is possible to recover a little of the exhaust heat in cold climates (Section 18.4.2.).

8.3.3. Case Study

The mine described in this case study was ventilated primarily by a main exhausting fan connected to the top of the upcast shaft and passing an airflow of 127.4 m³/s at the fan inlet. Both the downcast and the upcast shafts were 1219 m deep. Measurements of temperature and pressure allowed Table 8.1 to be established. Throughout the analysis, it was assumed that the air remained dry.

		P	T	V	ρ	$\int VdP$	s	$\int Tds$
Location	Station No.	Pressure kPa	Temperature K	Sp. Vol. m ³ /kg (i)	Density kg/m ³	Flow work J/kg (ii)	Entropy J/kgK (iii)	$F+q$ J/kg (iv)
Top downcast	1	101.59	283.15	0.8000	1.250	11 356	31.61	614
Bottom downcast	2	116.49	295.06	0.7270	1.375	-1 923	33.73	29 842
Bottom upcast	3	113.99	322.84	0.8129	1.230	-12 621	130.39	651
Top upcast	4	99.22	310.93	0.8995	1.112	2 117	132.44	1018
Fan outlet	5	101.59	314.05	0.8873	1.127	0	135.70	-31 055
Top downcast	1	101.59	283.15	0.8000	1.250		31.61	

Table 8.1. Thermodynamic parameters based on representative values of pressure and temperature (i.e. taken far enough into the shafts to avoid end effects). In the compilation of the table, the following equations were used. The equation reference numbers indicate the location of their derivations.

$$(i) \quad V = \frac{RT}{P} \quad \text{and} \quad \rho = \frac{1}{V} \quad \text{where } R = 287.04 \quad \text{J/kg}$$

$$(ii) \quad \int_a^b VdP = R(T_b - T_a) \frac{\ln(P_b/P_a)}{\ln(T_b/T_a)} \quad \text{J/kg} \quad (3.73)$$

$$(iii) \quad s = s_a - s_o = C_p \ln(T_a/T_o) - R \ln(P_a/P_o) \quad \text{J/kg} \quad (3.48)$$

where $C_p = 1005 \text{ J/kgK}$

Subscript 'a' refers to the station number and subscript 'o' refers to the pressure and temperature datums of 100 kPa and 273.15 K respectively.

$$(iv) \quad \int_a^b Tds = (T_b - T_a) \left\{ C_p - R \frac{\ln(P_b/P_a)}{\ln(T_b/T_a)} \right\} \quad \text{J/kg} \quad (3.77)$$

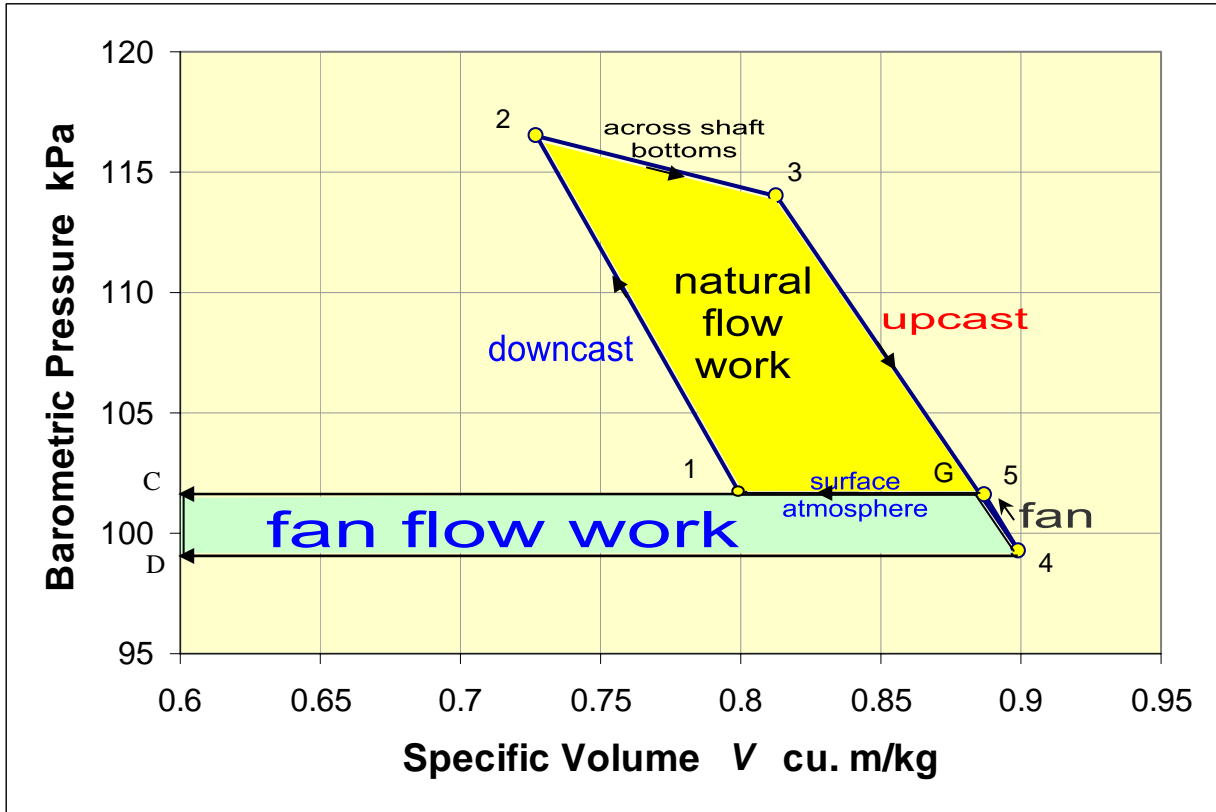


Figure 8.9(a) PV diagram for Case Study.

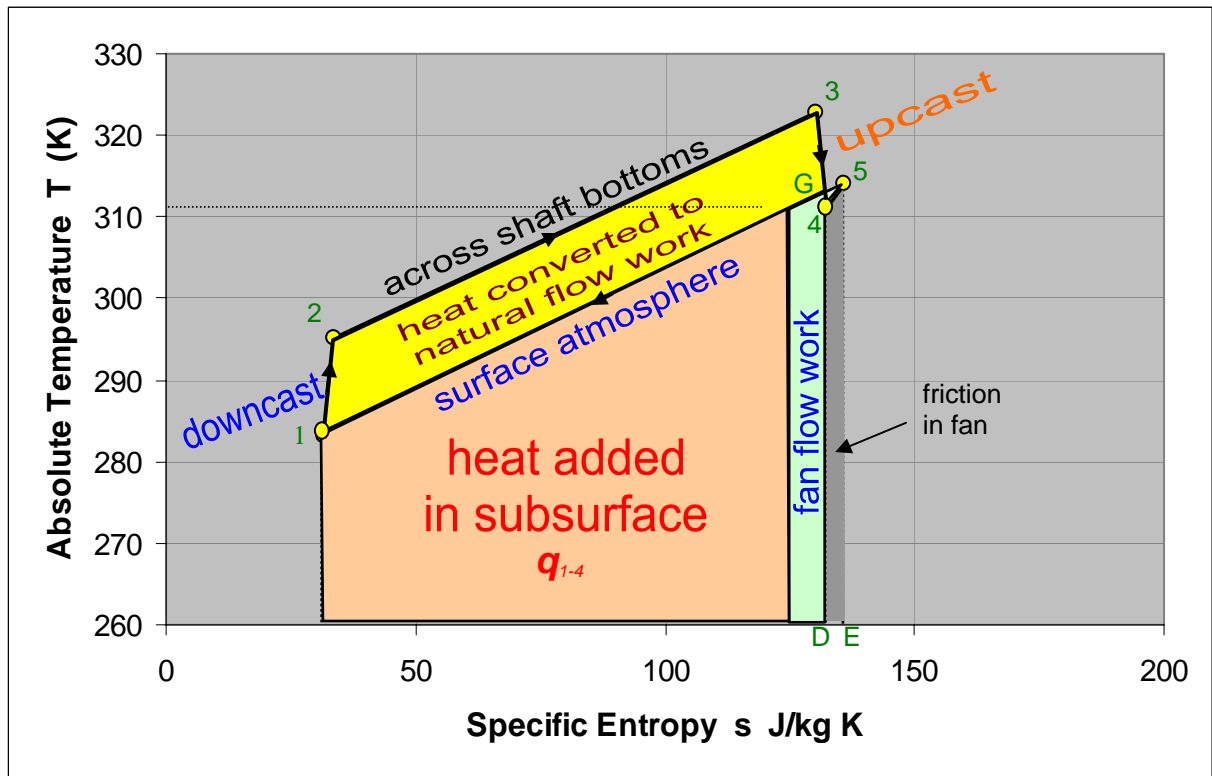


Figure 8.9(b). Ts diagram for Case Study

The PV and Ts diagrams were plotted as shown on Figures 8.9 (a) and (b) respectively. A great deal of information can be extracted from the table and visualized on the diagrams. It is useful to organize the analysis as follows:

General observations on the table of results

The $\int VdP$ column shows the large amount of flow work that is done *on* the air by gravity in the downcast shaft. However, this is more than offset by the work done *by* the air against gravity as it ascends the upcast shaft.

The addition of heat in the mine is concentrated in the workings, i.e. as the air progressed around the circuit from the downcast to the upcast shaft bottom. This is shown by both the $\int Tds$ and entropy columns. In this mine, the entropy increased continuously as the air passed through the shafts and workings. However, this is not always the case. In a mine where heat lost by cooling in any segment exceeds the heat generated by friction then that segment will exhibit a decrease in entropy.

It is interesting to observe that the difference in barometric pressure across the shaft bottoms,

$$116.49 - 113.99 = 2.50 \quad \text{kPa}$$

is greater than that across the main fan

$$101.59 - 99.22 = 2.37 \quad \text{kPa}$$

This occurs quite frequently in deep mines and has often caused observers some puzzlement. The phenomenon arises from natural ventilating effects in the shaft circuit.

Polytropic indices

For each segment of the circuit, a to b , the polytropic index, n , may be calculated from

$$\frac{n}{n-1} = \frac{\ln(P_b / P_a)}{\ln(T_b / T_a)} \quad \text{see (equation 3.72)}$$

Segment	Polytropic index n
Downcast shaft	1.4307
Workings	0.1943
Upcast shaft	1.3715
Fan	1.7330
Surface atmosphere	0

The effects of friction and added heat cause a PV curve to swing to the right, i.e. finish with a higher value of V than the corresponding isentropic process. This means that compression curves such as those for the downcast shaft and fan will become steeper and adapt an increased value of n , while decompression curves (workings and upcast shaft) will become shallower and take a lower value of n . The greatly reduced value of n for the workings is simply a reflection of the heat added in that segment. It should be noted, however, that the actual flow through the workings will occur through a network of airways, each with its own series of thermodynamic processes. The value of n calculated here for the workings is, therefore, a composite appraisal.

Fan performance

Table 8.1 shows that the fan produces 2 117 J/kg of useful flow work (area 45CD on the PV diagram) and also adds 1 018 J/kg of heat (area 45ED on the Ts diagram) to the air. Hence, by ignoring changes in kinetic energy and assuming no heat transfer across the fan casing, the energy input from the fan,

$$W_{45} = \int_4^5 VdP + \int_4^5 Tds = 2117 + 1018 = 3135 \quad \text{J/kg}$$

The same result is given by the change in enthalpy across the fan

$$W_{45} = C_p (T_5 - T_4) = 1005(314.05 - 310.93) = 3136 \quad \text{J/kg}$$

While the input from the fan impeller is mechanical energy, the $\int Tds$ part arises from the frictional losses incurred almost immediately by the generation of turbulence. The volume flow of $127.4 \text{ m}^3/\text{s}$ was measured at the fan inlet where the air density was 1.112 kg/m^3 , giving a mass flow of

$$M = 127.4 \times 1.112 = 141.6 \quad \text{kg/s}$$

$$\text{Then useful flow work} = \frac{2117}{1000} \times 141.6 = 300 \quad \frac{\text{kJ}}{\text{kg}} \frac{\text{kg}}{\text{s}} = \frac{\text{kJ}}{\text{s}} \text{ or kW}$$

$$\text{and fan frictional losses} = \frac{1018}{1000} \times 141.6 = 144 \quad \text{kW}$$

The polytropic efficiency of the fan may now be expressed as

$$\eta_{poly} = \frac{\int_4^5 VdP}{\int_4^5 VdP + \int_4^5 Tds} \quad (8.47)$$

or

$$\frac{300}{300 + 144} \times 100 = 67.6 \quad \text{per cent}$$

Natural ventilating energy, NVE

The net flow work done by the air against friction in the shafts and workings is the area 1234DC on the PV diagram. This is quantified by summing the tabulated $\int VdP$ values from station 1 to station 4.

$$\sum_{1234} F = \sum_{1234} \int VdP = (11356 - 1923 - 12621) = -3188 \quad \frac{\text{J}}{\text{kg}}$$

or

$$\frac{-3188}{1000} \times 141.6 = -451 \quad \text{kW}$$

However, the fan adds flow work to the air of only 2117 J/kg, or 300 kW. Hence, the balance is provided by natural ventilating energy,

$$NVE = -3188 + 2117 = -1071 \quad \text{J/kg}$$

(area 123G on both the PV and Ts diagrams)

$$\text{or} \quad -451 + 300 = -151 \quad \text{kW}$$

The negative signs show that this is work done *by* the air.

Natural ventilating pressure. NVP

The natural ventilating energy can be converted to a natural ventilating pressure by multiplying by a specified value of air density. Choosing the standard value of 1.2 kg/m gives

$$\begin{aligned} NVP &= NVE \times \rho \\ &= \frac{1071}{1000} \times 1.2 = 1.285 \quad \text{kPa} \end{aligned}$$

For comparison with the fan pressure, we must refer that also to standard density, ρ_{st}

$$\rho_{st} = \frac{\rho_i}{\rho_{st}} \rho_i$$

where subscript 'i' refers to fan inlet conditions, giving the standardized fan pressure as

$$\rho_{st} = \frac{1.112}{1.2} \times 2.37 = 2.196 \quad \text{kPa}$$

The mean density method (Section 8.3.1) gives a value of

$$NVP = (\rho_{md} - \rho_{mu})g(Z_1 - Z_2) \quad \text{Pa} \quad \text{see (equation 8.21)}$$

where

$$\rho_{md} = \frac{1.250 + 1.375}{2} = 1.3125 \quad \text{kg/m}^3$$

$$\rho_{mu} = \frac{1.230 + 1.112}{2} = 1.171 \quad \text{kg/m}^3$$

$$g = 9.81 \quad \text{m/s}^2$$

and

$$(Z_1 - Z_2) = 1219 \quad \text{m}$$

giving

$$\begin{aligned} NVP &= (1.3125 - 1.171)9.81 \times 1219 \\ &= 1692 \text{ Pa} \quad \text{or} \quad 1.692 \text{ kPa} \end{aligned}$$

This calculation illustrates that a natural ventilating pressure approximated by the mean density method is not the same as that determined through NVE or a summation of F terms (Section 8.3.1.).

Heat additions

The total energy addition to the air is given by $W_{45} + \sum_{12345} q$ and is equal to the increase in enthalpy across the system, $(H_5 - H_1) = C_p(T_5 - T_1)$. Hence the heat transferred to the air is

$$\begin{aligned} \sum_{12345} q &= C_p (T_5 - T_1) - W_{45} \\ &= 1005(314.05 - 283.15) - 3135 \\ &= 31055 - 3135 = 27920 \quad \text{J/kg} \end{aligned}$$

or

$$\frac{27920}{1000} \times 141.6 = 3953 \quad \text{kW}$$

The total heat rejected to the atmosphere is

$$\begin{aligned} q_{51} &= \sum_{12345} q + W_{45} = 27920 + 3135 \\ &= 31055 \quad \text{J/kg [also given directly by } C_p(T_5 - T_1) \text{]} \end{aligned}$$

or
$$\frac{31055}{1000} \times 141.6 = 4397 \quad \text{kW}$$

This agrees with the value in Table 8.1 for $\int Tds$ within the surface atmosphere.

The sum of the $\int Tds$ values from station 1 to station 4 (in Table 8.1) gives the combined effect of added heat and friction within the shafts and workings. The frictional component can be isolated as

$$\begin{aligned} \sum_{1234} F &= \int Tds - \sum_{1234} q \\ &= 31107 - 27920 = 3187 \quad \text{J/kg} \end{aligned}$$

or
$$\frac{3187}{1000} \times 141.6 = 451 \quad \text{kW}$$

This is in agreement with the value obtained earlier as $\sum_{1234} \int VdP$

Finally, the *NVE* may be checked by summing the complete $\int Tds$ column. This gives 1070 J/kg, also in agreement with the value determined earlier.

This case study has illustrated the power of thermodynamic analysis. From five pairs of specified temperatures and pressures, the following information has been elicited:

• Pressure across main fan	2.37 kPa (or 2.196 kPa at standard density)
• Pressure across shaft bottoms	2.50 kPa
• Fan flow work	300 kW
• Fan losses	144 kW
• Total energy input from fan (impeller work)	444 kW
• Fan polytropic efficiency	67.6 per cent
• Work done against friction in the shafts and workings:	451 kW
• Natural ventilating energy	151 kW
• Natural ventilating pressure at standard density	1.285 kPa
• Heat added to the air in shafts and workings	3953 kW
• Heat rejected to surface atmosphere	4397 kW

The case study also demonstrates the intrinsic coherence of the thermodynamic method; alternative procedures have been employed to cross-check several of the results. Students of the subject, having mastered the basic relationships, should be encouraged to experiment with the analyses and to develop their own procedures. Each exercise will provide new and intriguing insights into thermodynamic logic.

8.3.4. Inclined workings

So far, we have confined ourselves to a level connection between shaft bottoms and drawn a single line on the thermodynamic diagrams to represent that connection. However, the PV and TS diagrams take on a different appearance when the connecting workings between shaft bottoms or any two points on a main intake and main return, are inclined.

A steeply dipping circuit might be ventilated adequately with little or no ventilating pressure applied across it. During a visit underground, one mine manager was quite disconcerted when a ventilation survey team leader pointed out that opening an expensively constructed control door in an outby cross-cut made no difference to the airflow in an adjoining dip circuit. Just as natural ventilation plays a role in a shaft circuit, it also influences airflow in any other subsurface circuits that involve changes in elevation.

Dip circuit.

The PV and TS diagrams for a **dip circuit** are shown on Figure 8.10. As air flows down the descending intake airway(s) the pressure and temperature increase because of gravitational work done on the air. Expansion occurs through the workings and as the air ascends the rising return airways. If a survey team follows a route from station 1, an outby position in the main intake or downcast shaft bottom, to station 2, a corresponding outby position in the main return or upcast shaft bottom, then the resulting PV diagram will follow a loop from 1 to 2 whose shape is determined by the three dimensional geometry of the circuit and the degree of heat transfer.

Figure 8.10 (a) shows that the $\int_1^2 VdP$ flow work can be divided into two sections, the **applied ventilating energy (AVE)** generated by the pressure differential applied across the ends of the circuit, and the **natural ventilating energy (NVE)** generated by thermal effects within the district.

$$-\int_1^2 VdP = AVE + NVE = F_{12} \quad \text{J/kg} \quad (8.48)$$

On traversing around the circuit from station 1 to station 2, the elementary VdP strips to the left of the PV curve are dominant for falling pressure ($-dP$), giving a negative net value of $\int_1^2 VdP$.

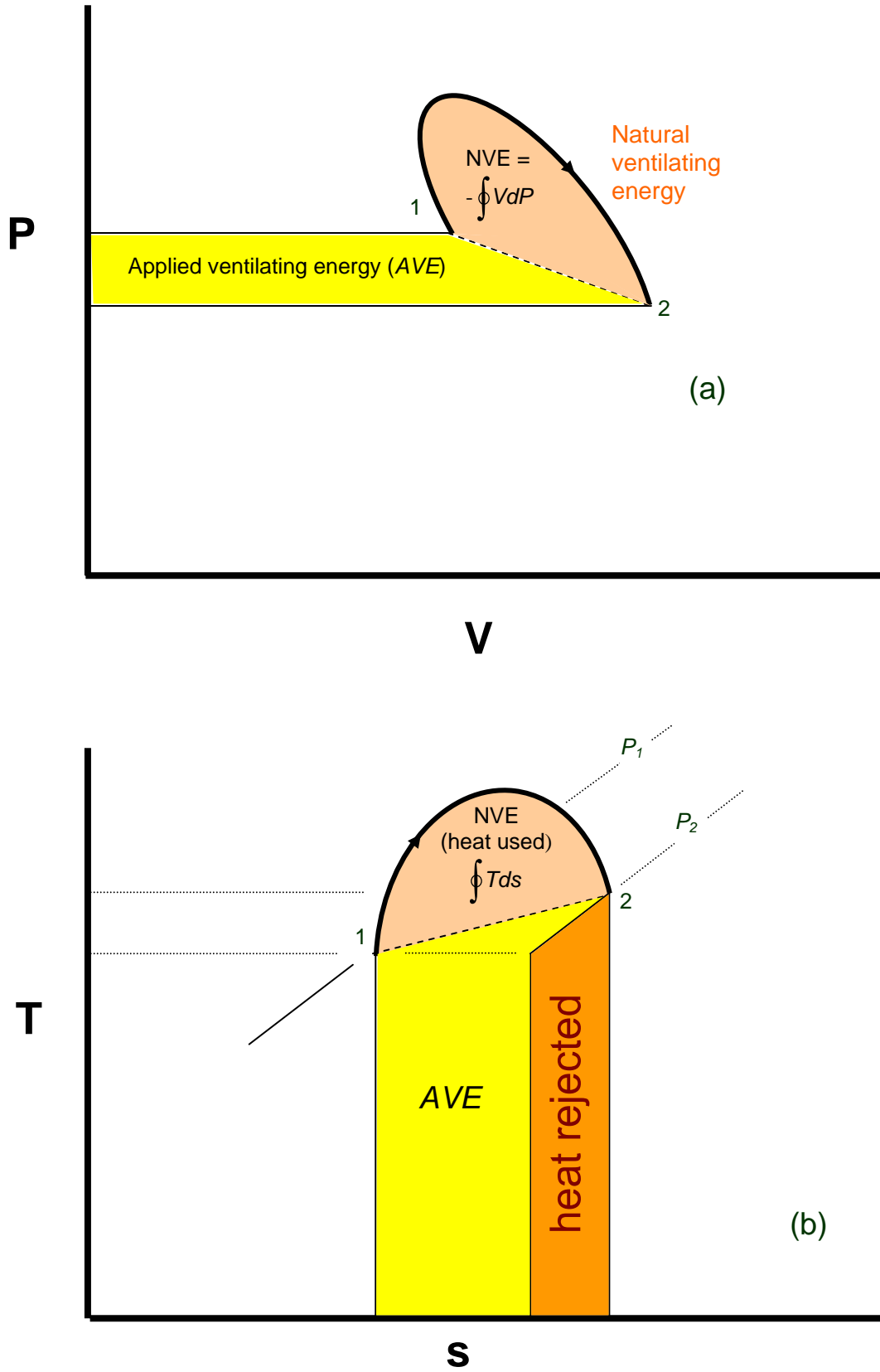


Figure 8.10. In dip workings, Natural Ventilating Energy (NVE) from added heat assists in producing ventilation.

The analysis can also be conducted in terms of frictional pressure drops. Suppose we divide the traverse route into a large number of small segments, then the frictional pressure drop along any one segment, ignoring the small changes in kinetic energy, is given as

$$dp = \rho dF = -\rho g dZ - dP \quad [\text{see equation (8.5)}]$$

In order to compare frictional pressure drops in differing segments, we refer the pressure drops to standard density ρ_{st}

$$dp_{st} = \frac{\rho_{st}}{\rho} dp = \rho_{st} dF = -\rho_{st} g dZ - \rho_{st} \frac{dP}{\rho}$$

Integrating around the traverse route gives

$$\int_1^2 dp_{st} = p_{st} = -\rho_{st} g \int_1^2 dZ - \rho_{st} \int_1^2 \frac{dP}{\rho}$$

But $V = 1/\rho$ and, if stations 1 and 2 are at the same level, $\int_1^2 dZ = 0$, giving

$$p_{st} = -\rho_{st} \int_1^2 V dP$$

Equation (8.48) then gives

$$p_{st} = \rho_{st} (AVE + NVE) \quad \text{Pa} \quad (8.49)$$

or

$$p_{st} = AVP + NVP \quad \text{Pa} \quad (8.50)$$

where AVP = Applied ventilating pressure across the circuit (Pa)
and NVP = natural ventilating pressure generated within the circuit, (Pa)
both being referred to standard density.

Equation (8.50) explains how a dip circuit may be ventilated by natural effects even when the applied ventilation pressure is zero.

The NVP for the circuit may be determined by measuring the NVE area on the PV diagram,

$$NVP = NVE \times \rho_{st} \quad (\text{see equation (8.32)})$$

or from the summation of frictional pressure drops, p_{st} , measured during a survey, each referred to standard density.

$$NVP = p_{st} - AVP \quad \text{Pa} \quad (8.51)$$

The total area under the traverse loop 1 to 2 on the Ts diagram of Figure 8.10 (b) represents the sum of frictional heat and added heat, $F_{12} + q_{12}$. However, provided the stations 1 and 2 are at the same level and ignoring changes in kinetic energy, the heat taken out of the district by the airstream is $(H_2 - H_1)$, or $C_p (T_2 - T_1)$ for dry conditions. This is identified as the heat rejected area on the Ts diagram.

The remaining areas represent

$$F_{12} = AVE + NVE \quad \text{J/kg} \quad (8.52)$$

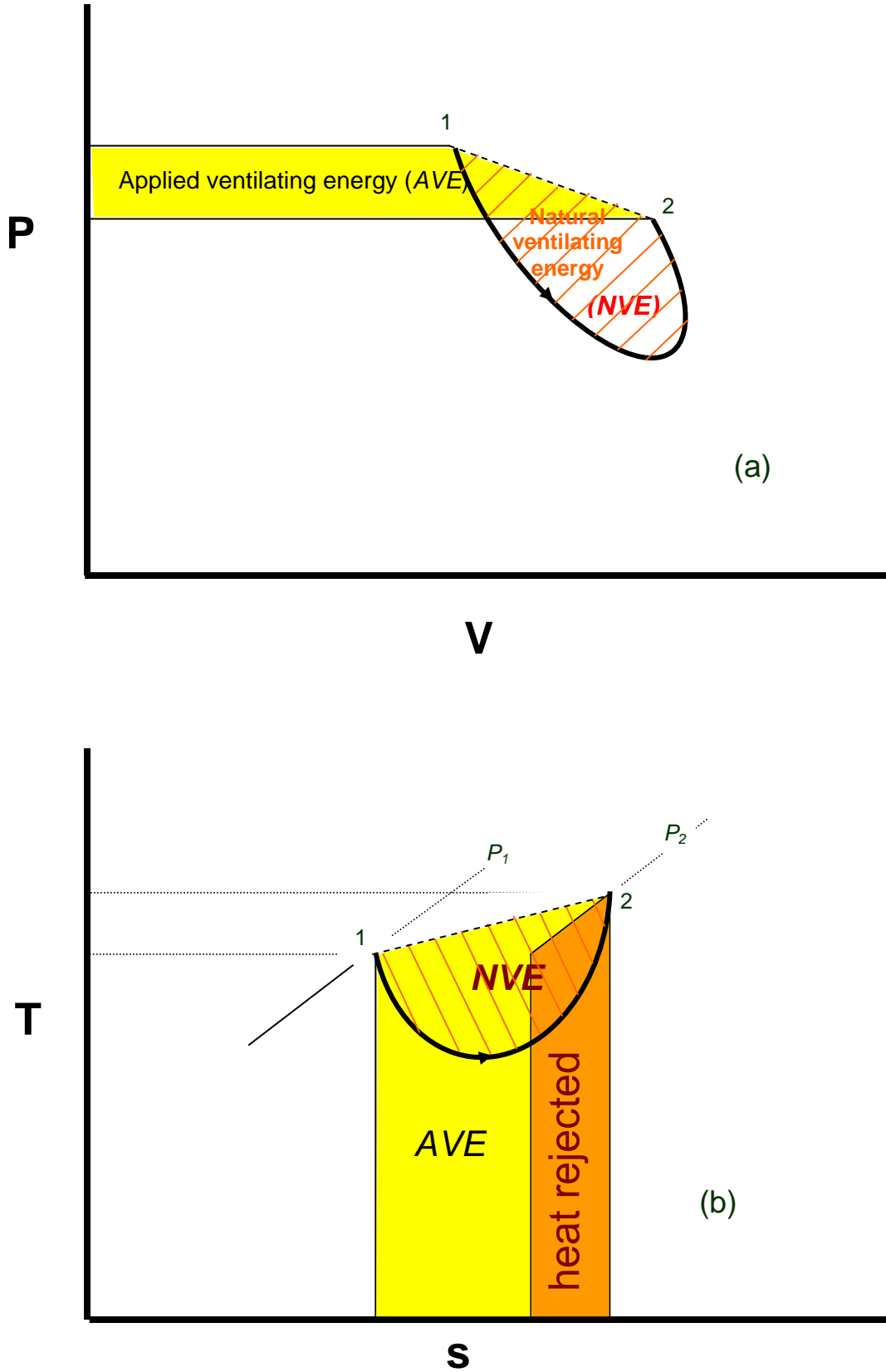


Figure 8.11. In rise workings, Natural Ventilating Energy (NVE) from added heat impedes ventilation.

Rise Circuit.

The PV and Ts diagrams for a **rise circuit** are illustrated on Figure 8.11. In this case the NVE has an opposite sign to the AVE . Hence natural ventilating effects oppose the applied ventilating energy. The analysis follows the same logic as for a dip circuit leading to the following results:

$$-\int_1^2 VdP = AVE - NVE = F_{12} \quad \text{J/kg} \quad (8.53)$$

$$\text{and } p_{st} = AVP - NVP \quad \text{Pa} \quad (8.54)$$

where, again, the applied and natural ventilating pressures are referred to standard density. These equations show that if the natural ventilating effects become sufficiently high then they will balance the applied ventilating energy or pressure. The flow work that can be done against friction, F_{12} , and the effective ventilating pressure, p_{st} , then both become zero and airflow ceases.

8.3.5. The effect of moisture

In order to highlight underlying principles, this chapter has concentrated on the flow of dry air throughout the system. This is seldom the case in practice. The air entering any facility from the free atmosphere invariably contains water vapour. If this is maintained throughout the system without further evaporation or condensation then the 'dry air' thermodynamic relationships developed in this chapter will continue to give satisfactory results. However, for more precise results or if free water exists in the subsurface, as it often does, then evaporation and condensation processes can have a major impact on the dry bulb temperature (see, for example, Figure 8.3(b)). In particular, the enthalpy change ($H_2 - H_1$) is no longer given simply by $C_p(T_2 - T_1)$. Equation (14.40), reproduced below, must be employed.

In order to take account of variations in moisture content the equations given below may be employed. These equations are derived in Chapter 14. The parameters that vary with respect to moisture content require to be redefined in terms of X kg of water vapour associated with each 1 kg of "dry" air, [i.e. in $(1 + X)$ kg of air/vapour mixture]. Subscript m is used to denote moist air.

$$\text{Gas constant:} \quad R_m = \frac{(287.04 + 461.5 X)}{(1 + X)} \quad \frac{\text{J}}{\text{kgK}} \quad [\text{see equation (14.14)}]$$

$$\text{Specific heat at constant pressure:} \quad C_{pm} = \frac{(1005 + 1884 X)}{(1 + X)} \quad \frac{\text{J}}{\text{kgK}} \quad [\text{see equation (14.16)}]$$

$$\text{Specific volume:} \quad V_m = \frac{(287.04 + 461.5 X) T}{(1 + X) P} \quad \text{m}^3/\text{kg of moist air} \quad [\text{see equation (14.18)}]$$

$$\text{Density:} \quad \rho_m = \frac{1}{V_m} \quad \text{kg moist air/m}^3 \quad [\text{see equation (14.21)}]$$

An apparent specific volume and density based on 1 kg of dry air are also useful:

$$V_m(\text{apparent}) = 461.5 \frac{T}{P} (0.622 + X) \quad \text{m}^3/\text{kg dry air}$$

$$\rho_m(\text{apparent}) = \frac{1}{V_m(\text{apparent})} \quad \text{kg dry air/m}^3$$

$$\text{Enthalpy} \quad H = 1005 t_d + X[4187 t_w + L + 1884(t_d - t_w)] \quad \text{J/kg dry air [see equation (14.40)]}$$

where t_w and t_d are wet and dry bulb temperatures respectively (degrees Celsius)

and $L =$ Latent heat of evaporation at wet bulb temperature

$$= (2502.5 - 2.386 t_w)1000 \quad \text{J/kg} \quad [\text{see equation (14.6)}]$$

The reference numbers of these equations indicate the location of their derivation in Chapter 14.

Appendix A8.2 gives a more general analysis of the effects of moisture on steady flow relationships.

Bibliography

Professor F. Baden Hinsley of Nottingham University, England, was the primary architect of the development of mine ventilation thermodynamics. He wrote many papers on the subject. Only the first of his major papers is listed here.

Hinsley, F.B. (1943). Airflow in Mines: A Thermodynamic Analysis. Proc. S. Wales Inst. of Engineers, Vol LIX, No. 2.

Hall, C.J. (1981). Mine Ventilation Engineering. Published by the Society of Mining Engineers of AIME.

Hemp, R. and Whillier A. (1982). Environmental Engineering in South African Mines. Chapters 2 and 16. Published by the Mine Ventilation Society of South Africa.

McPherson, M.J. (1967). Mine Ventilation Engineering. The Entropy approach. University of Nottingham Mining Magazine, Vol. 19.

McPherson, M.J. and Robinson, G. (1980). Barometric Survey of Shafts at Boulby Mine, Cleveland Potash, Ltd., Cleveland. Transactions of the Institution of Mining and Metallurgy, Volume 89, 1980, ppA18 – A28.

Appendix A8.1

Survey data from the survey of the shafts used in the examples given in Sections 8.2.2 and 8.2.4.

The examples given in Sections 8.2.2 and 8.2.4 of the text refer to the Boulby Potash Mine which has the deepest mine shafts in the United Kingdom. It is only rarely that detailed ventilation survey observations can be made throughout the lengths of major vertical shafts. The following tables give the observations and corresponding thermodynamic parameters obtained from that survey. They provide the basis for a useful case study by students and researchers in thermodynamic processes in mines.

Observations in Downcast Shaft

Depth m	Absolute Static pressure kPa	Temperature, °C		True specific volume m ³ /kg	Moisture content g/kg of dry air	Relative humidity %	Enthalpy kJ/kg	Sigma heat kJ /kg	True density kg/m ³	Comments
		Wet bulb	Dry bulb							
0	100.770	15.78	17.17	0.8326	10.7	86.9	44.3	43.6	1.201	Surface
4.0	100.797	15.78	17.78	0.8340	10.4	81.7	44.3	43.6	1.199	Above -30 level
10.7	100.831	15.67	17.22	0.8322	10.5	85.5	44.0	43.3	1.201	Below -30 level
109.0	101.819	16.00	17.89	0.8260	10.5	82.6	44.6	43.9	1.211	
207.4	103.016	16.39	18.61	0.8184	10.5	80.0	45.4	44.7	1.222	
305.7	104.193	16.78	19.56	0.8118	10.5	75.6	46.2	45.5	1.232	
404.1	105.391	17.33	20.28	0.8046	10.7	74.7	47.5	46.7	1.243	
502.4	106.575	18.06	21.11	0.7981	11.0	74.3	49.3	48.4	1.253	
600.8	107.769	18.22	21.94	0.7914	10.8	69.6	49.4	48.6	1.264	
699.1	109.179	18.44	22.78	0.7832	10.5	65.5	49.6	48.8	1.277	
797.5	110.349	19.39	23.44	0.7770	11.2	68.0	52.2	51.3	1.287	
895.8	111.523	19.44	24.00	0.7701	10.9	64.7	52.0	51.1	1.298	
994.2	112.727	19.72	24.72	0.7637	10.8	62.1	52.5	51.6	1.309	
1092.5	113.793	20.28	25.44	0.7585	11.1	61.5	53.9	52.9	1.318	
1108.5	114.070	20.50	25.83	0.7577	11.2	60.6	54.5	53.5	1.320	Manset

Observations in Upcast Shaft

Depth	Absolute Static pressure	Temperature, °C		True specific volume	Moisture content	Relative humidity	Enthalpy	Sigma heat	True density	Comments
		Wet bulb	Dry bulb							
m	kPa			m ³ /kg	g/kg of dry air	%	kJ/kg	kJ/kg	kg/m ³	
1110.6	115.321	24.17	32.89	0.7680	13.0	47.3	66.4	65.1	1.302	Manset
1105.5	115.281	24.17	33.89	0.7706	12.6	43.3	66.3	65.1	1.298	Below ventset
1092.2	115.055	24.00	35.00	0.7746	11.9	38.5	65.8	64.6	1.291	Above ventset
1000.7	113.901	23.78	34.44	0.7810	12.0	39.6	65.4	64.2	1.280	
909.2	112.521	23.33	33.33	0.7878	12.0	41.7	64.3	63.2	1.269	
817.7	111.331	23.22	32.50	0.7942	12.4	44.6	64.4	63.2	1.259	
726.2	110.147	22.72	31.67	0.8005	12.2	45.5	63.1	62.0	1.249	
634.7	108.970	22.33	30.83	0.8069	12.2	47.2	62.2	61.1	1.239	
543.2	107.718	21.78	30.00	0.8139	12.0	48.0	60.8	59.7	1.229	Passed cage
451.7	106.538	21.56	29.00	0.8204	12.3	51.5	60.5	59.4	1.219	
360.2	105.357	21.11	28.22	0.8274	12.2	52.8	59.4	58.3	1.209	
268.7	104.187	20.67	27.33	0.8342	12.1	54.7	58.3	57.3	1.199	
177.2	103.013	20.28	26.22	0.8406	12.2	58.3	57.5	56.4	1.190	
85.7	101.853	20.00	25.56	0.8483	12.3	60.2	57.0	55.9	1.179	
10.1	100.939	19.50	24.50	0.8529	12.2	63.1	55.7	54.7	1.172	Below -30 level
4.9	100.922	19.33	23.89	0.8514	12.2	65.6	55.1	54.1	1.175	Above -30 level
0	100.874	19.44	24.17	0.8526	12.3	64.7	55.5	54.5	1.173	Surface

Appendix A8.2

A general steady flow analysis for airstreams that carry water vapour and liquid water droplets.

The differential form of the steady flow energy equation (3.25) for 1 kg of air is:

$$-u du - g dZ + dW = VdP + dF = dH - dq \quad \text{J/kg} \quad (3.25)$$

Now consider an incremental length of airway within which every kg of air has associated with it X kg of water vapour and w kg of liquid water droplets, each of these increasing by dX and dw respectively through the increment. The vapour moves at the same velocity as the air, u . However, the droplets may move at a different velocity, u_w , and perhaps even in the opposite direction to the air in the case of an upcast shaft. The terms in the steady flow energy equation then become:-

Kinetic energy (J/kg dry air, i.e. Joules of energy associated with each kilogram of 'dry' air)

$u du$: 1 kg of dry air :

$X u du$: X kg of water vapour :

$w u_w du_w$: w kg of droplets

$\frac{u^2}{2} dX$: energy to accelerate dX of water vapour to u m/s :

$\frac{u_w^2}{2} dw$: energy to accelerate dw of liquid to u_w m/s

Potential energy (J/kg dry air)

$g dZ$: 1 kg of dry air

$X g dZ$: X kg of water vapour

$w g dZ$: w kg of liquid water

Fan energy (J/kg dry air)

The energy input terms are now based upon 1 kg of 'dry' air. The fan energy input, therefore, remains unchanged at dW but with redefined units of J/kg dry air.

Flow work (J/kg dry air)

Provided that the specific volume is the volume of the mixture that contains 1 kg dry air, V_m (apparent), then the flow work stays at $V dP$ J/kg dry air.

Work done against friction (J/kg dry air)

Again this remains simply as F but defined in units of J/kg dry air.

Enthalpy (J/kg dry air)

$$dH = C_p dT \quad : \text{1 kg of dry air}$$

$$X dH_x \quad : \text{X kg of water vapour of enthalpy } H_x$$

where $H_x = C_w t_w + L + C_{pv} (t_d - t_w)$
 C_w = specific heat of water
 C_{pv} = specific heat of water vapour

$$w dH_w \quad : \text{w kg of liquid water of enthalpy } H_w,$$

where $H_w = C_w t_w$, for droplets at wet bulb temperature

$$H_x dX \quad : \text{energy content of } dX \text{ kg of added vapour}$$

$$H_w dw \quad : \text{energy content of } dw \text{ kg of added droplets}$$

Added heat (J/kg dry air)

This term remains at q defined in terms of J/kg dry air.

All of these terms may be collated in the form of equation (3.25) i.e. a three part steady flow energy equation. In practice, the kinetic energy terms are normally very small and may be neglected. The steady flow energy equation for airflow of varying moisture content then becomes

$$-[g dZ + Xg dZ + wg dZ] + dW = VdP + dF = [dH + X dH_x + w dH_w + H_x dx + H_w dw] - dq$$

J/kg dry air (8.55)

This equation is cumbersome for manual use. However, it provides a basis for computer programs developed to simulate airflow processes involving phase changes of water. The enthalpy terms encompass the energy content of the air, water vapour, liquid water and any additions of vapour and liquid.

If we apply the mechanical energy terms around a closed cycle ($\oint dZ = 0$) then we obtain

$$W - \oint VdP = \sum_{total} F + g \left\{ \oint X dZ + \oint w dZ \right\} \quad \frac{J}{kg} \quad (8.56)$$

Comparing this to the corresponding equation for dry conditions (equation 8.41), we see that the fan and natural ventilating energies are now responsible not only for providing the necessary work against friction but also for removing water vapour and airborne water droplets from the mine.

Chapter 9. Ventilation Planning

9.1. SYSTEMS ANALYSIS OF THE PLANNING PROCEDURE	1
9.2. ESTABLISHMENT OF THE BASIC NETWORK.....	3
9.2.1. New mines or other subsurface facilities	3
9.2.2. Existing mines.....	3
9.2.3. Correlation study.....	5
9.3. AIRFLOW REQUIREMENTS.....	6
9.3.1. Strata gas.....	7
9.3.2. Diesel exhaust fumes.....	7
9.3.3. Dust.....	8
9.3.4. Heat.....	9
9.3.5. Workshops and other ancillary areas	12
9.3.6. Air velocity limits	13
9.4. PLANNING EXERCISES AND TIME PHASES.....	13
9.4.1. Network planning exercises	13
9.4.2. Time phases	14
9.4.3. Selection of main fans.....	15
9.4.4. Optimization of airflow systems	15
9.4.5. Short term planning and updating the basic network	15
9.5. VENTILATION ECONOMICS AND AIRWAY SIZING.....	16
9.5.1. Interest payments	16
9.5.2. Time value of money, present value.....	18
9.5.2.1. Present value of a lump sum.....	18
9.5.2.2. Present value of regular payments.	19
9.5.3. Equivalent annual cost.....	21
9.5.4. Ventilation operating costs.....	22
9.5.5. Optimum size of airway.....	23
9.5.5.1. Capital cost function	23
9.5.5.2. Operating cost function	24
9.5.5.3. Case Study	25
<i>Task 1: Establish the capital cost function:</i>	25
<i>Task 2: Establish the operating cost function:</i>	26
<i>Task 3: Establish the total cost function:</i>	26
<i>Task 4: Determine the optimum diameter:</i>	26
9.5.6. Incorporation of shaft design into network planning exercises.....	27
9.6. TRADITIONAL METHOD OF VENTILATION PLANNING	29
Bibliography	30

9.1. SYSTEMS ANALYSIS OF THE PLANNING PROCEDURE

In Section 1.3.3, we emphasized the importance of integrating ventilation planning with production objectives and overall mine design during the early stages of planning a new mine or other subsurface facility. The team approach should continue for ongoing forward planning throughout the active life of the mine. Compromises or alternatives should be sought which satisfy conflicting demands. For example, the ventilation planner may require a major airway that is too large from the viewpoint of the rock mechanics engineer. An alternative might be to drive two smaller airways but large enough for any equipment that is to move through them. Regular

liaison between engineering departments and exchanges during inter-disciplinary planning meetings can avoid the need for expensive re-designs and should promote an optimized layout.

Figure 9.1 illustrates an organized system of ventilation planning for an underground mine. The procedure assumes the availability of computer assistance including ventilation simulation software, and eliminates most of the manual techniques and intuitive estimates of older planning methodologies (Section 9.6). The initial step is to establish a data base in a **Basic Network File**. For an existing facility this requires information gained from ventilation surveys. The latter are described in detail in Chapter 6. For a completely new mine, initial layouts should be discussed at the cross-disciplinary planning meetings. It is usual, in this case, that several alternative layouts are required to be investigated by the ventilation design team. The data base for a new mine is established from initial estimates of required airway geometry, mining method, roughness of airway surfaces and network layout. Such data will be revised and refined as the design progresses.

In this chapter, we shall discuss the major facets of the planning procedure illustrated on Figure 9.1.

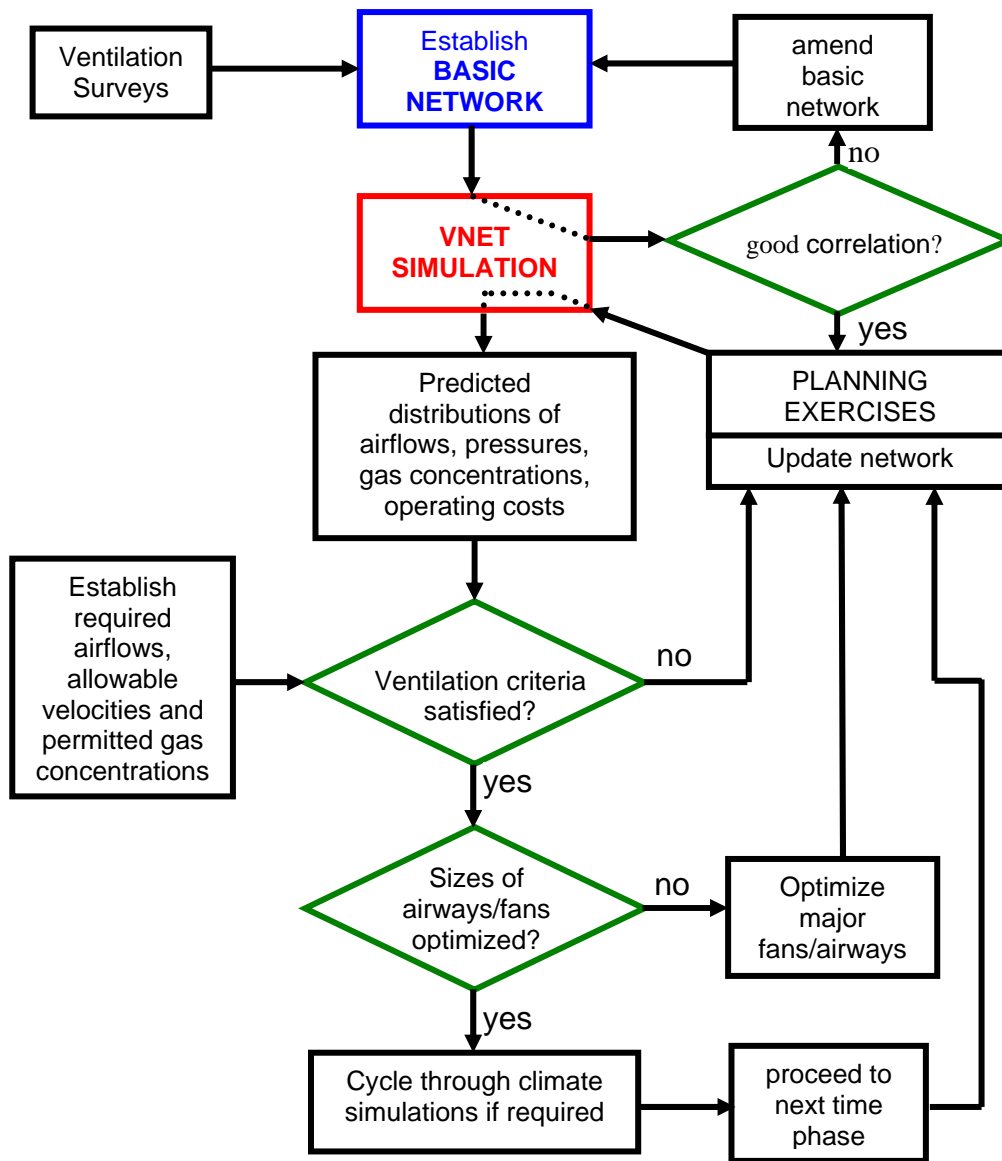


Figure 9.1. Systems analysis of subsurface ventilation planning.

9.2. ESTABLISHMENT OF THE BASIC NETWORK

9.2.1. New mines or other subsurface facilities

It will be recalled from Chapter 7 that a ventilation network consists of a line schematic, each branch representing one or more airways or leakage paths. In general, branches must be of known resistance or designated to pass a specified airflow. For a planned but yet unconstructed facility there are, of course, no airways or ventilation infrastructure that can be surveyed in order to establish actual values of resistance. Recourse must then be made to the methods of estimating airway resistance described in Section 5.4, incorporating airway geometry, types of lining (friction factors) and shock losses. Experience and data from other mines that utilize comparable layouts and methods of airway drivage, and operating in similar geological conditions can be most helpful.

A variety of alternative plans will often require investigation during the initial design of a new mine. Ventilation network analyses should be carried out in order to determine the efficiency and effectiveness of each layout. The results of those analyses may then be considered, together with the other aspects of mine design, at the general planning meetings.

9.2.2. Existing mines

The routes of surveys in the main ventilation infrastructure of an existing mine provide a skeleton network, often referred to as a **ventilation schematic**. Additional branches can then be added or incorporated as equivalent resistances to represent airways or leakage paths that were not included in the primary surveys. As illustrated in the computed network example of Section 7.4.6, branch resistances may be input to a network simulation program in several ways. This allows considerable flexibility in assembling a representative basic network, commencing from surveyed routes. Essentially, four methods are used to indicate resistance values in the first compilation of a basic network file or to update a basic network that has previously been established:

1. For surveyed airways, the measured values of frictional pressure drop, p (Pa), and corresponding airflow, Q (m^3/s), may be input to the basic network file. The computer can then calculate the resistance from the square law.

$$R = \frac{p}{Q^2} \quad \frac{\text{Ns}^2}{\text{m}^8}$$

2. There are situations in which it is difficult or impossible to determine resistance values for existing airways. If, for example, the airflow in an unrestricted branch is low at the time of measurement then so, also, will be the frictional pressure drop. Low frictional pressure drops will also occur in airways of large cross-sectional area even at substantial airflows. While any pressure difference shown by the gauge should be logged, those lower than 5 Pa may yield resistances of doubtful accuracy. Modern diaphragm gauges will indicate to within ± 0.5 Pa. At 5 Pa, the corresponding error is 0.1 or 10 per cent. Airflow measurements taken by approved methods (Chapter 6) will normally be accurate to within 5%. Compounding these possible errors gives a maximum corresponding error in airway resistance of

$$\frac{dR}{R} = \pm \frac{dp}{p} \pm 2 \frac{dQ}{Q} \quad (9.1)$$

(differentiation of the square law $R = p/Q^2$)

giving $dR/R = \pm 0.1 \pm (2 \times 0.05)$
 $= \pm 0.2$ or 20 per cent for the accuracy of the resistance of an airway that has a frictional pressure drop of 5 Pa.

If, because of low values, the airflow and/or pressure drop cannot be measured to the required accuracies, the airway resistance should be calculated from the Atkinson equation

$$R = kL \frac{per}{A^3} \frac{\rho}{1.2} \quad \text{Ns}^2/\text{m}^8 \quad (\text{see equation (5.9)})$$

where k = Atkinson friction factor at standard density (kg/m^3)
 L = length of airway (m)
 per = perimeter (m)
 A = cross sectional area (m^2)
 and ρ = air density (kg/m^3)

Representative values of friction factor, k , should, preferentially, be determined from similar airways that have been surveyed in that same mine. The density correction, $\rho/1.2$ is then often ignored. Otherwise, values of k may be estimated using one of the methods discussed in Section 5.3. In all cases, care should be taken to allow for shock losses and unrepresentative obstructions (Appendix A5, Chapter 5).

In many situations within a given mine, groups of airways are driven to the same dimensions and with a similar friction factor. Typical values of resistance per metre length can be established from measurements taken in, say, intakes, returns and conveyor routes. This facilitates the addition of new or unsurveyed branches to the network. However, here again care should be taken not to overlook obstructions or any other cause of shock losses.

- It is often difficult to measure the resistances of doors, stoppings or seals directly, either because of low airflows or inaccessibility (Kissell, 1978). In practice, the resistances of doors or stoppings in mines vary from several thousand to, literally, 1 or 2 Ns^2/m^8 . The reason for this wide range is the highly non-linear relationship between area available for flow and resistance

$$R \propto 1/d^5 \quad (\text{see equation (5.15)})$$

where d = hydraulic mean diameter of opening ($4A/per$).

Hence, the appearance of fractures or apertures in, or around, a previously tight stopping will result in dramatic reductions in its resistance.

The following ranges are suggested for planning purposes and for cross-sectional areas up to 25 m^2 .

Single doors	10 to 50 Ns^2/m^8 (typical value, 25 Ns^2/m^8)
Stoppings	50 to 2000 Ns^2/m^8 (typical value 500 Ns^2/m^8)
Seals	1000 to 5000 Ns^2/m^8

- The resistances of leakage paths including worked out areas and caved zones are the most difficult to assess for a network schematic. Leakage airflows can often be measured or estimated from survey results. These may be entered as "fixed quantity" leakage airflows, leaving the computer to evaluate the corresponding resistances. This 'inversion' method remains valid while the number of fixed quantity branches is sufficiently small for unique values of resistance to be calculated. A network that is over-restricted by too many fixed quantity branches will produce a warning message from the VNET simulation package (Section 7.4.6). Care should be taken to remove "fixed quantity" airways and to replace them with branches set at the corresponding computed resistances prior to progressing with planning exercises.

9.2.3. Correlation study

Figure 9.1 shows the data pertaining to the initial network schematic stored in the **Basic Network File** within computer memory. In order to ensure that the basic network is a true representation of the mine as it stood at the time of the survey, and before that basic network is used to launch planning exercises, it is important that it is subjected to verification through a correlation study. This involves running a ventilation network simulation package (Section 7.4) on the data contained in the basic network file and comparing the computed airflows with those that were measured during the surveys. If all airways had been surveyed instantaneously with perfect observers and perfect instruments, and if no errors had been made in compiling the basic network, then the computed and measured airflows would show perfect agreement. This utopian situation is never attained in practice. Despite the internal consistency checks on airflow and pressure drop measurements made during a survey (Section 6.4.3) there will, inevitably, remain some residual errors from observational and instrumental sources.

A larger potential source of difference between computed and measured airflows is the fact that a VNET airflow distribution is mathematically balanced to a close tolerance throughout the network and represents a steady-state 'snapshot' of the ventilation system. On the other hand, the surveys may have taken several weeks or even months to complete. In a large active mine, updating survey data should be a routine and continuous activity of the mine ventilation department. During the time taken for a survey the airflow distribution may have changed due to variations in natural ventilating pressures or the resistances offered by the ever-changing work areas.

Lastly, errors made in transcribing survey data into the basic network or in key-punching the information into the basic network file will, again, result in disagreement between computed and measured airflows.

The correlation itself is normally carried out by a subsidiary program that lists the computed and observed airflows together with their actual and percentage differences. **Leakage airflows** of less than 3 m³/s may be ignored in this comparison as large percentage errors in such low airflows will usually have little influence on the overall accuracy of the network.

The **overall network correlation** is quantified as

$$\frac{\sum \text{Absolute value of (differences between computed and actual airflows for surveyed branches)}}{\sum \text{Absolute values of (measured airflows for surveyed branches)}} \times 100 \quad (9.3)$$

A correlation is accepted as being satisfactory provided that:

- (i) no significant airflow branch shows a difference of more than 10 per cent between computed and measured airflows; and
- (ii) the overall correlation is also within 10 per cent.¹

However, because of the highly variable conditions that exist along mine traverses, the survey team will often be able to weight certain measurements as being more, or less, reliable than others. Such pragmatic considerations may be taken into account during the correlation study.

If the initial results of a correlation study indicate unacceptable deviations between computed and measured airflows then the basic network must be improved before it can be used as a basis for future planning exercises. The transcription of survey data into the basic network file should be checked. In the case of computed airflows being consistently higher or lower than the corresponding measurements then it is possible that an error has been made in the pressure

¹ Experienced teams can often achieve overall correlation within 5 percent.

ascribed to a main fan or may indicate that the resistances of primary airways such as shafts should be verified. Additional or **check measurements** of surveyed loops may be required.

It is fairly common that disagreements will occur in localized areas of the network. Again, this may indicate that the extent of the surveys had been insufficient to give an adequate representation of the mine network and that further measurements are necessary. More often, however, the problem can be resolved by adjustment of the estimated resistances or fixed airflows allocated to unsurveyed flowpaths. Provided that the main infrastructure of the surveyed network is sound then amendments to those estimated values will direct the simulated network towards an improved correlation. However, if measurements made in the surveyed loops are significantly out of balance then no amount of adjustment to subsidiary airways will produce a well-correlated basic network.

9.3. AIRFLOW REQUIREMENTS

The estimation of airflows required within the work areas of a mine ventilation network is the most empirical aspect of modern ventilation planning. The majority of such assessments remains based on local experience of gas emissions, dust, or heat load and is still often quoted in the somewhat irrational terms of m^3/s per ton of mineral output, particularly for non-coal mines. Corrections can be applied for variations in the age of the mine, the extent of old workings, distances from shaft bottoms, depth and rates of production. However, as in all empirical techniques, the method remains valid only whilst the proposed mining methods, machinery, and geological conditions remain similar to those from which the empirical data were evolved. Attempts to extrapolate beyond those circumstances may lead to serious errors in determining required airflows. Fortunately, simulation techniques are available to assist in assessing airflow requirements for both gassy and hot mines.

The characteristics of strata gas emissions, heat flow and dust production are discussed in Chapters 12, 15 and 20, respectively. In this section, we shall confine ourselves to an examination of the methods used to determine the airflows required to deal with given emission rates of airborne pollutants.

The overall necessity is that in all places where personnel are required to work or travel, airflows must be provided in such quantities that will safeguard safety and health, comply with statutory requirements, and that will also furnish reasonable comfort (Section 1.3.1).

The quantity of air required for the purposes of respiration of personnel is governed primarily by the concentration of exhaled carbon dioxide that can be allowed in the mine atmosphere rather than the consumption of oxygen. For vigorous manual work, this demands about $0.01 \text{ m}^3/\text{s}$ of air for each person and is negligible compared with the quantities of air needed to dilute the other gases, dust, heat and humidity that are emitted into the subsurface atmosphere.

It is a legal requirement that air volume flows must meet the governing state or national mining laws. Such legislation will normally define minimum airflows that should be provided at specified times and places in addition to threshold limit values for airborne pollutants or the psychrometric condition of the air. The ventilation planner must be familiar with the relevant legislation. In countries where mining law is absent or does not cover the particular circumstances of the project then it is prudent to follow well established regulations of a major mining country.

9.3.1. Strata gas

The various methods used to predict the emission rates of methane are described in Chapter 12. Whichever technique is employed, the final calculation of airflow requirement is

$$Q = \frac{100 E_g}{C_g} \quad \text{m}^3/\text{s} \quad (9.4)$$

where Q = required airflow (m^3/s)
 E_g = gas emission rate (m^3/s)
 C_g = general body concentration to which gas is to be diluted (percentage by volume).

The value of C_g is often taken to be one half of the concentration at which the law requires action to be taken.

Example

It has been predicted that during a 7 hour working shift, 2500 m^3 of methane will be emitted into a working face in a coal mine. If electrical power must be switched off at a methane concentration of 1 per cent, determine a recommended airflow for the face.

Solution

The average rate of gas emission during the working shift is

$$E_g = \frac{2500}{7 \times 60 \times 60} = 0.0992 \quad \text{m}^3/\text{s}$$

Let us take the allowable concentration for design purposes to be one half the legal limit. Then $C_g = 0.5$ per cent.

Equation (9.4) gives the required airflow as

$$Q = \frac{100 \times 0.0992}{0.5} = 19.84 \quad \text{say } 20 \text{ m}^3/\text{s}.$$

9.3.2. Diesel exhaust fumes

There are wide variations in the manner in which different countries calculate the ventilation requirements of mines in which diesels are used. The basic stipulation is that there should be sufficient ventilation to dilute exhaust gases and particulates to below each of their respective threshold limit values. One technique, based on engine tests, is to calculate the airflow required to dilute the mass emission of each pollutant to one half the corresponding TLV (threshold limit value). The maximum of those calculated airflows is then deemed to be the required air quantity. Some countries require analyses of the raw exhaust gases in addition to general body air sampling downstream from diesel equipment. Distinctions may be drawn between short-term exposure and time-weighted averages over an 8 hour shift (Section 11.2.1.).

In addition to exhaust gases, national enforcement agencies may require that other factors be taken into account in the determination of airflow requirements for diesel equipment. These include rated engine power (kW or bhp), number of personnel in the mine or area of the mine, rate of mineral production, engine tests, number of vehicles in the ventilation split and forced dilution of the exhaust gases before emission into the general airstream.

There is, as yet, no method of determining airflow requirements for diesels that will guarantee compliance with legislation in all countries. Here again, regulations pertinent to the location of the project must be perused for specific installations.

The generic criterion that is used most widely for initial estimates of required airflow is based on rated output power of the diesel equipment. For design purposes, many ventilation planners employ 6 to 8 m³/s of airflow over the machine for each 100 kW of rated diesel power, all equipment being cumulative in any one air split. However, it should be borne in mind that the actual magnitude and toxicity of exhaust gases depend upon the type of engine, conditions of operation and quality of maintenance in addition to rated mechanical power. It is for this reason that mining law refers to gas concentrations rather than power of the diesel equipment. Some manufacturers and government agencies give recommended airflows for specific diesel engines. In hot mines, it may be the heat produced by diesel equipment that sets a limit on its use.

9.3.3. Dust

Pneumoconiosis has been one of the greatest problems of occupational health in the mining industries of the world. Concentrated and long-term research efforts have led to greatly improved understanding of the physiological effects of dusts, methods of sampling and analysis, mandatory standards and dust control measures (Chapters 19 and 20).

There are many techniques of reducing dust concentrations in mines, ranging from water infusion of the solid mineral through to dust suppression by water sprays and air filtration systems. Nevertheless, with current mining methods, it is inevitable that dust particles will be dispersed into the air at all places wherever rock fragmentation or comminution occurs - at the rock-winning workplace and throughout the mineral transportation route. Dilution of airborne particles by ventilation remains the primary means of controlling dust concentrations in underground mines.

Dispersed dust particles in the respirable range (less than 5 µm diameter) will settle out at a negligible rate. For the determination of dilution by airflow, respirable dust may be treated as a gas. However, in this case it is realistic to estimate dust makes at working faces in terms of grams (or milligrams) per tonne of mineral mined. This will, of course, depend upon the method of working and means of rock fragmentation.

The required airflow is given as

$$Q = \frac{E_d}{C_d} \times \frac{P}{3600} \quad \text{m}^3/\text{s} \quad (9.5)$$

where

$$\begin{aligned} E_d &= \text{the emission rate of respirable dust (mg/tonne)} \\ P &= \text{rate of mineral production (tonnes/h) and} \\ C_d &= \text{allowable increase in the concentration of respirable dust (mg/m}^3\text{)}. \end{aligned}$$

Example.

The intake air entering a working area of a mine carries a mass concentration of 0.5 mg/m³ respirable dust. Face operations produce 1000 tonnes of mineral over an 8 hour shift and add respirable dust particles to the airflow at a rate of 1300 mg per tonne of mineral mined. If the concentration of respirable dust in the return air is not to exceed 2 mg/m³, determine the required airflow.

Solution.

$$\text{Average rate of mineral production} = \frac{1000}{8 \times 3600} = 0.0347 \quad \text{t/s}$$

$$\text{Average rate of emission of respirable dust} = 0.0347 \times 1300 \frac{\text{t mg}}{\text{s t}} = 45.14 \text{ mg/s}$$

$$\text{Dust removal capacity of air, } C_d = (\text{allowable dust concentration} - \text{intake dust concentration}) \\ = (2 - 0.5) = 1.5 \text{ mg/m}^3.$$

$$\text{Required airflow} = \frac{45.14}{1.5} \frac{\text{mg m}^3}{\text{s mg}} = 30.1 \text{ m}^3/\text{s}$$

For larger particles of dust, the treatment is rather different. In this case, it is primarily the velocity rather than the quantity of the airflow that is important. In any airway the distance over which dust particles are carried by the airstream depends upon the air velocity and the settling rate of the individual dust particles. The latter depends, in turn, upon the density, size and shape of the particle as well as the psychrometric condition of the air. The heavier and more spherical particles will settle more rapidly while the particles that are smaller or of greater aspect ratio will tend to remain airborne for a longer period of time.

An effect of non-uniform dispersal characteristics is that the **mineralogical composition** of the airborne and settled dust is likely to vary with distance downstream from the source. The sorting effect of airflow on dust particles explains the abnormally high quartz content of dust that may be found in the return airways of some coal mines (Section 20.3.8.).

The larger particles will not be diluted proportionally by increased airflow and, hence, higher velocities. As the airspeed increases, these particles will remain airborne for longer distances before settling out. Furthermore, as the air velocity continues to rise, previously settled particles may be entrained by turbulent eddies into the airstream. The dust concentration will increase.

The effects of these mechanisms are illustrated on Fig. 9.2. A minimum total dust concentration is obtained at a velocity of a little over 2 m/s. Fortunately, the total dust concentration passes through a fairly broad based curve and air velocities in the range 1 to 4 are acceptable. Above 4 m/s the problem is not so much a health hazard as it is the physical discomfort of large particles striking the skin. In addition to the question of ventilation economics, this limits the volume flow that can be passed through any workplace for cooling or the dilution of other pollutants.

9.3.4. Heat

Most of the pollutants that affect the quality of air in an underground environment enter the ventilating airstreams as gaseous or particulate matter and, hence, may be diluted by an adequate supply of air. The problem of heat is quite different, involving changes in the molecular behaviour of the air itself and its thermodynamic and psychrometric properties. Furthermore, it is normally the case that air entering mine workings from the base of downcast shafts, slopes or intake adits is relatively free of gaseous or particulate pollutants. On the other hand, the condition of the intake air with regard to temperature and humidity depends upon the surface climate, and the depth of the workings. Whilst the removal of heat by ventilation remains the dominant method of maintaining acceptable temperatures in the majority of the world's mines, quantifying the effects of varying airflow is by no means as straightforward as for gases or dust.

The complication is that air velocity and, by implication, airflow is only one of several variables that affect the ability of a ventilating airstream to produce a physiologically acceptable mine climate. Calculations of the climatic effect of variations in airflow are necessarily more involved than for gases or particulates.

The heat energy content of air, defined in terms of kilojoules of heat associated with each kilogram of dry air, is known as **Sigma Heat, S**. This concept is discussed fully in Section 14.5.3. Sigma heat depends only upon the wet bulb temperature of the air for any given barometric pressure.

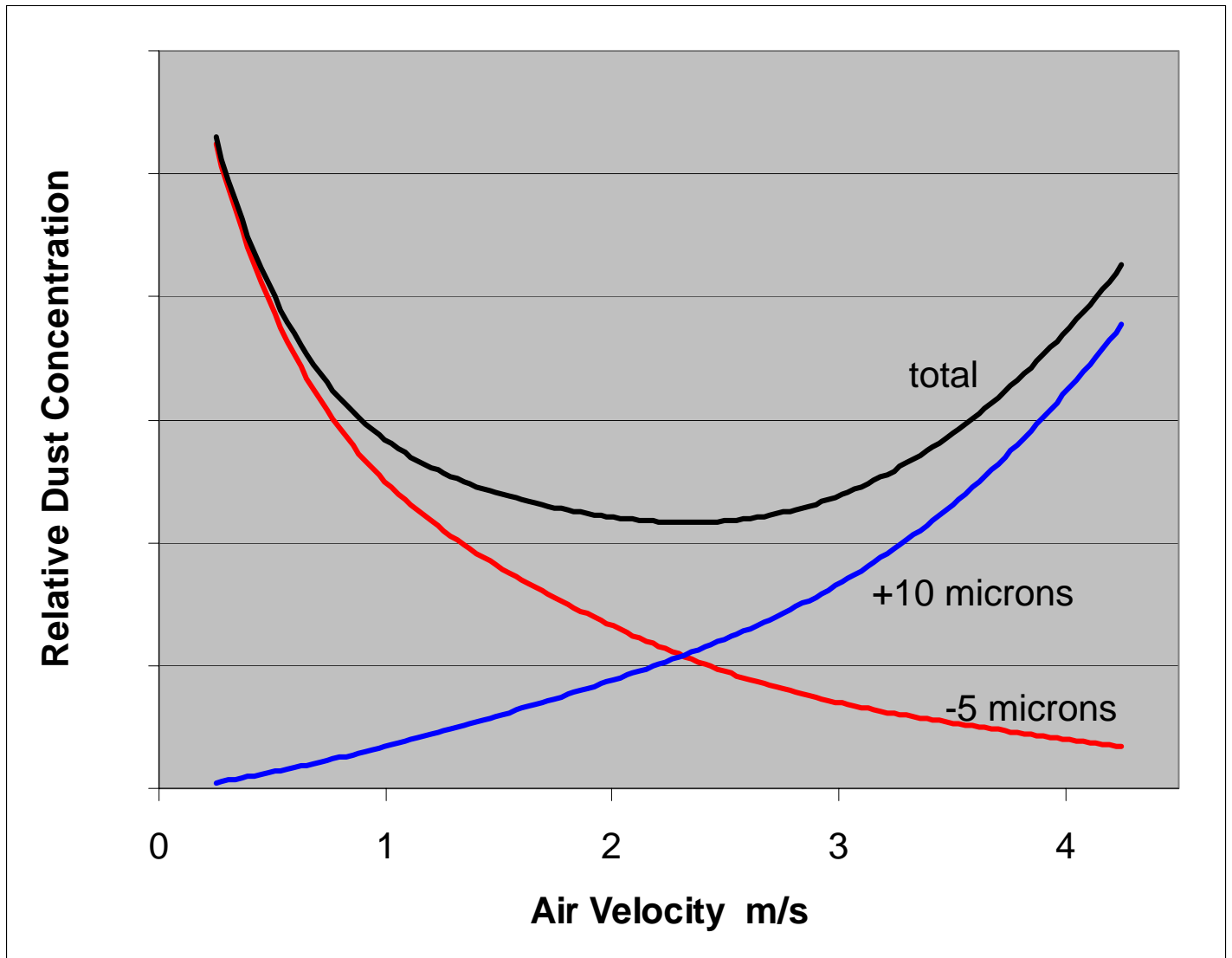


Figure 9.2 Variation of dust concentration with respect to air velocity.

The stages of determining the airflow required to remove heat from a mine or section of a mine are as follows:

- (a) Evaluate the sigma heat of the air at inlet, S_1 , using equations (14.44) to (14.47).
- (b) Evaluate the highest value of sigma heat, S_2 , that can be accepted in the air leaving the mine or section of the mine. This threshold limit value may be specified in terms of one of the indices of heat stress (Chapter 17) or simply as a maximum acceptable (cut-off) value of wet bulb temperature.
- (c) Estimate the total heat flux, q_{12} (kW), into the air from all sources between inlet and outlet (Chapter 15). This may involve simulation studies for additions of strata heat.

(d) The required airflow, Q , is then given as

$$Q = \frac{q_{12}}{\rho(S_2 - S_1)} \quad \frac{\text{m}^3}{\text{s}} \quad (9.6)$$

where ρ = mean density of the air (kg/m^3)

The factor $Q\rho(S_2 - S_1)$ is sometimes known as the Heat Removal Capacity (HRC) of a given airflow, Q .

It should be noted that as S_1 approaches S_2 , or for high values of added heat, q_{12} , the required airflow may become excessive. In this case, either q_{12} must be reduced or air cooling plant installed (Chapter 18).

Example.

Air enters a section of a mine at a wet bulb temperature, t_w of 20°C and a density, ρ , of $1.276 \text{ kg}/\text{m}^3$. The mean barometric pressure is 110 kPa . It has been determined that 2 MW of heat are added to the air in the section. If the wet bulb temperature of the air leaving the section is not to exceed 28°C and no air coolers are to be used, determine the required airflow.

Solution.

From equations (14.44 to 14.47, Chapter 14 on Psychrometry) sigma heat is given as

$$S = \frac{0.622 e_{sw}}{(P - e_{sw})} (2502.5 - 2.386 t_w) + 1.005 t_w \quad \frac{\text{kJ}}{\text{kg}} \quad (9.7)$$

where saturation vapour pressure at wet bulb temperature is calculated as

$$e_{sw} = 0.6106 \exp\left\{\frac{17.27 t_w}{237.3 + t_w}\right\} \quad \text{kPa}$$

At intake $t_w = 20^\circ\text{C}$, giving

$$e_{sw1} = 0.6106 \exp\left\{\frac{17.27 \times 20}{237.3 + 20}\right\} = 2.3375 \quad \text{kPa}$$

and

$$S_1 = \frac{0.622 \times 2.3375}{(110 - 2.3375)} (2502.5 - 2.386 \times 20) + (1.005 \times 20) = 53.25 \quad \frac{\text{kJ}}{\text{kg}}$$

At return Using the same equations with t_w set at the cut-off value of 28°C gives

$$S_2 = 82.03 \quad \text{kJ/kg.}$$

The required airflow at the intake density is given by equation (9.6)

$$\begin{aligned} Q_1 &= \frac{q_{12}}{\rho(S_2 - S_1)} = \frac{2000}{1.276(82.03 - 53.25)} \quad \frac{\text{kJ}}{\text{s}} \frac{\text{m}^3}{\text{kg}} \frac{\text{kg}}{\text{kJ}} \\ &= 54.5 \quad \text{m}^3 / \text{s} \end{aligned}$$

In this section, we have assumed that the heat added to the air can be determined. Although this may be straightforward for machine heat and other controlled sources (Section 15.3), it is more difficult to quantify heat emitted from the strata. For deep mines, the design of combined ventilation and air conditioning systems has been facilitated by the development of climatic simulation programs. These may be incorporated into the planning procedure as shown at the bottom of Figure 9.1. A more detailed discussion of the interaction between ventilation network and climatic simulation programs is given in Section 16.3.5.

9.3.5. Workshops and other ancillary areas

In addition to areas of rock fragmentation, there are many additional locations in mines or other subsurface facilities that require the environment to be controlled. These include workshops, stationary equipment such as pumps or electrical gear, battery charging and fuel stations, or storage areas. For long term storage of some materials in repository rooms, it may not be necessary or even desirable to maintain a respirable environment. However, temperatures and humidities will often require control.

In mines, it is usual for workshops and similar areas to be supplied with fresh intake air and to regulate the exit flow into a return airway either directly or through a duct.

The airflow requirement should, initially, be determined on the basis of pollution from gases, dust and heat as described in Sections 9.3.1 to 9.3.4. However, in the case of large excavations, this may give rise to excessively low velocities with zones of internal and uncontrolled recirculation. In this situation, it is preferable to employ the technique of specifying a number of **air changes per hour**.

Example

An underground workshop is 40m long, 15m wide and 15m high. Estimate the airflow required (a) to dilute exhaust fumes from diesel engines of 200 kW mechanical output and (b) on the basis of 10 air changes per hour.

Solution

(a) Employing an estimated airflow requirement of 8 m³/s per 100 kW of rated diesel power (Section 9.3.2) gives

$$\frac{200}{100} \times 8 = 16 \quad \text{m}^3/\text{s}$$

(b) Volume of room = 40 x 15 x 15 = 9000 m³
At 10 air changes per hour,

$$\text{Airflow} = \frac{9000 \times 10}{60 \times 60} = 25 \quad \text{m}^3/\text{s}$$

Hence, the larger value of 25 m³/s should be employed.

9.3.6. Air velocity limits

The primary consideration in the dilution of most pollutants is the volume flow of air. However, as indicated on Figure 9.1, the velocity of the air (flowrate/cross-sectional area) should also be determined. Excessive velocities not only exacerbate problems of dust but may also cause additional discomfort to personnel and result in unacceptable ventilation operating costs.

Legislation may mandate both maximum and minimum limits on air velocities in prescribed airways. A common lower threshold limit value for airways where personnel work or travel is 0.3 m/s. At this velocity, movement of the air is barely perceptible. A more typical value for mineral-winning faces is 1 to 3 m/s. Discomfort will be experienced by face personnel at velocities in excess of 4 m/s (Section 9.3.3) because of impact by large dust particles and, particularly, in cool conditions. Table 9.1 gives a guide to upper threshold limit values recommended for air velocity.

Area	Velocity (m/s)
Working faces	4
Conveyor drifts	5
Main haulage routes	6
Smooth lined main airways	8
Hoisting shafts	10
Ventilation shafts	20

Table 9.1 Recommended maximum air velocities

In wet upcast shafts where condensation or water emissions result in airborne droplets, the air velocity should not lie between 7 to 12 m/s. Water blanketing may occur in this range of velocities. The resulting variations in shaft resistance cause an oscillating load on main fans and can produce large intermittent cascades of water falling to the shaft bottom.

9.4. PLANNING EXERCISES AND TIME PHASES

The dynamic nature of a mine or any other evolving network of subsurface airways requires that the infrastructure of the ventilation system be designed such that it can accommodate major changes during the life of the undertaking. For a completely new mine, the early ventilation arrangements will provide for the sinking of shafts, drifts or adits, together with the initial development of the primary underground access routes. When the procedures illustrated on Figure 9.1 are first applied to an existing mine, the establishment and correlation of a basic network file will often reveal weaknesses and inefficiencies in the prevailing ventilation system. The **initial planning exercises** should then be directed towards correcting those deficiencies while, at the same time, considering the future development of the mine.

Following the establishment of a new or revised ventilation design, further planning investigations should be carried out for selected stages of future development. Although this is commonly termed "**time phasing**", it might more accurately be regarded as representing phases of physical development rather than definitive periods of time. Schedules have a habit of slipping or are subject to considerable revision during the course of mining.

9.4.1. Network planning exercises

Referring once again to Figure 9.1, the first step in a ventilation network planning exercise is to establish the airflows required in all places of work, travel or plant location (Section 9.3). Air velocity limits should also be set for the main ventilation flowpaths (Section 9.3.6). Additional

constraints on the direction and magnitudes of pressure differentials across doors, bulkheads or stoppings, or between adjoining areas of the facility, may also be imposed. This is of particular importance in **nuclear waste repositories**.

The ventilation engineers should review the existing network (correlated basic network or previous time phase) and agree upon a series of alternative designs that will satisfy revised airflow objectives and meet constraints on velocity and pressure differentials. The network schematic should then be modified to represent each of those alternative designs in turn. The **network modifications** may include

- sealing worked-out areas and opening up new districts
- adding main airways and lengthening existing airways
- adding and/or removing air crossings, doors and stoppings
- adding, removing or amending fixed quantity branches
- adding or sealing shafts and other surface connections
- adding, removing or relocating main or booster fans, or changing to different fan characteristic curves in order to represent adjustments to fan speed or vane settings
- amending natural ventilation pressures.

It is worth reminding ourselves, at this stage, that current network simulation programs do not perform any creative design work. They simply predict the airflow and pressure distributions for layouts that are specified by the ventilation planner. While computed output will usually suggest further or alternative amendments, it is left to the engineer to interpret the results, ensure that design objectives and constraints are met, compare the efficiency and cost effectiveness of each alternative design and to weigh the practicality and legality of each proposed scheme.

Each alternative layout chosen by the design engineers should be subjected to a series of VNET simulations and network amendments until either all the prescribed criteria are met or it becomes clear that the system envisaged is impractical. Tables, histograms and spreadsheets should be prepared in order to compare fan duties (pressures and air quantities), operating costs, capital costs and the practical advantages/disadvantages of the alternative layouts.

9.4.2. Time phases

During the operating life of an underground mine, repository or other subsurface facility, there will occur periods when substantial changes to the ventilation system must be undertaken. This will occur, for example, when:

- a major new area of the mine is to be opened up or an old one sealed
- workings become sufficiently remote from surface connections that the existing fans or network infrastructure are incapable of providing the required face airflows at an acceptable operating cost
- two main areas of the mine (or two adjoining mines) are to be interconnected.

"**Time phase**" studies should be carried out on alternative schematics to represent stages before and after each of these changes. Additional scenarios may be chosen at time intervals between major changes or to represent transitional stages. The latter often impose particularly heavy duties on the ventilation system.

Time phase exercises should be conducted to cover the life of the mine or as far into the future as can reasonably be predicted, assuming a continued market for the mined product.

It is, perhaps, intuitive to conduct time phase exercises in an order that emulates the actual planned chronological sequence. This may not always be the most sensible order for the network

exercises. For example, if it appears inevitable that a new shaft will be required at some time in the future, it may be prudent to first investigate the time phase when that shaft has become necessary and then to examine earlier time phases. This assists the planners in deciding whether it would be advantageous to sink the new shaft at a prior time rather than to wait until it becomes absolutely necessary.

The time phase exercises will produce a series of quantified ventilation networks for each time period investigated. These should be reviewed from the viewpoint of continuity between time phases and to ensure that major additions to the ventilation infrastructure have an acceptable and cost-effective life. Indeed, the need for such continuity should remain in the minds of the planners throughout the complete investigation, although not to the extent of stifling viable alternative designs at later stages of the time phase exercises.

The result of such a review should be a series of selected layouts that represent the continuous development of the ventilation system throughout the projected life of the mine. Again, tables and histograms should be drawn up to show the variations of fan duties and costs, this time with respect to chronological order.

9.4.3. Selection of main fans

Care should be taken that any main fan purchased should be capable of producing the range of pressure-volume duties necessary throughout its projected life. The variation in required fan duties resulting from time phase exercises should be considered, particularly where a fan is to be relocated at some time during its life.

For a new purchase, fan manufacturer's catalogues should be perused and, if necessary, discussions held with those manufacturers, in order to ensure that the fan selected is capable of providing the required range of duties. Fortunately, the availability of variable pitch axial fans and inlet vane control on centrifugal fans allows a single fan to provide a wide range of duties with a fixed speed motor. A more detailed discussion of fan specifications is given in Section 10.6.2.

9.4.4. Optimization of airflow systems

The network exercises carried out for any one time phase should incorporate a degree of optimization concerning the layout of airways, and the locations and duties of new shafts and fans. For a single major flowpath such as a proposed new shaft, a detailed optimization study can be carried out (Section 9.5.5). However, the larger questions that can arise involve a balance between capital and operating costs and might include a choice between additional airways and fans of greater power, or the minimization of total power costs incurred by alternative combinations of main and booster fans. Special purpose optimization programs have been written to assist in the resolution of such questions. (Calizaya et al, 1988)

9.4.5. Short term planning and updating the basic network

This chapter is concerned primarily with the major planning of a subsurface ventilation system. The time phases are chosen to encompass periods of significant change in the ventilation layout. However, much of the daily work of mine ventilation engineers involves planning on a much shorter time scale.

As working districts advance or retreat, the lengths of the airways that serve them change. Also, strata stresses can result in reductions of the cross-sectional areas of those airways. Additional roof support may be required resulting in increased friction factors. Stoppings, regulators, doors and air-crossings may deteriorate and allow greater leakage. All of these matters cause changes in the resistances of individual airways and, hence, of the complete network. Additionally, wear of

fan impellers can result in variations in the corresponding pressure - volume characteristic curves. For these reasons, a basic network file that correlated well with survey data at the start of any given time phase may become less representative of the changing real system.

In addition to regular maintenance of all ventilation plant and controls, further surveys should be carried out on a routine basis and, in particular, whenever measured airflows begin to deviate significantly from those predicted for that time phase. Visual inspections and frequent liaison with shift supervisors are also invaluable for the early identification of causes of deviation from planned airflows. Relationships with production personnel will remain more congenial if the latter are kept well advised of the practical consequences of blocking main airflow routes with supplies, equipment or waste material.

As new survey data become available, the basic network file should be updated accordingly. If the basic network file is maintained as a good representation of the current mine then it will prove invaluable in the case of any emergency that involves the ventilation system.

In the event that such updates indicate permanent and significant impact on the longer term plans then the network investigations for the future time phases should be re-run and the plans amended accordingly. In the majority of cases this may become necessary because of changes in mine production plans rather than from any unpredicted difficulties with ventilation.

9 .5. VENTILATION ECONOMICS AND AIRWAY SIZING

The subsurface ventilation engineer must be capable of dealing with two types of costs:

- (a) Capital costs that require substantial funds at a moment in time or distributed over a short time period. A main fan installation or sinking a new shaft comes into this category.
- (b) Working or operating costs, these representing the expenditure of funds on an ongoing basis in order to keep a system operating. Although consumable items, maintenance and even small items of equipment may be regarded as working costs, ventilation system designers often confine the term 'operating costs' to the price of providing electrical power to the fans.

The problem that typically arises concerns the combination of capital and operating costs that will minimize the real total cost to the company or mining organization; for example, whether to purchase an expensive but efficient fan to give low operating costs or, alternatively, a less expensive fan that will necessitate higher operating costs. Another question may be whether the money saved initially by sinking a small diameter ventilation shaft is worth the higher ongoing costs of passing a required airflow through that shaft. These are examples of the types of questions that we shall address in this section.

In the following examples and illustrations, we shall employ the dollar (\$) sign to indicate a unit of money. However, in all cases, this may be replaced by any other national unit of currency.

9.5.1. Interest payments

Money can be regarded as a commodity that may be circulated to purchase goods or services. If we borrow money to buy a certain item then we are, in effect, renting the use of that money. We must expect, therefore, that in addition to returning the borrowed sum, we must also pay a rental fee. The latter is termed the interest payment. Hence, if we borrow \$100 for a year at an annual interest rate of 9 per cent, then we must repay \$109 one year from now. Even if we owned the money and did not have to borrow, spending the \$100 now would mean that we are prevented from earning interest on that sum by investing or lending it to an individual, company, bank or other financial institution. Using money always involves an interest penalty.

If we borrow an amount of money, P (principal) at a fractional interest rate i (e.g. at 9 per cent, $i = 0.09$) then we will owe the sum S where

Now	$S = P$	
after 1 year	$S = P(1+i)$	
after 2 years	$S = P(1+i)(1+i) = P(1+i)^2$	
after 3 years	$S = P(1+i)^3$	
after n years	$S = P(1+i)^n$	(9.8)

Figure 9.3 gives a visual indication of the effects of compounding interest each year.

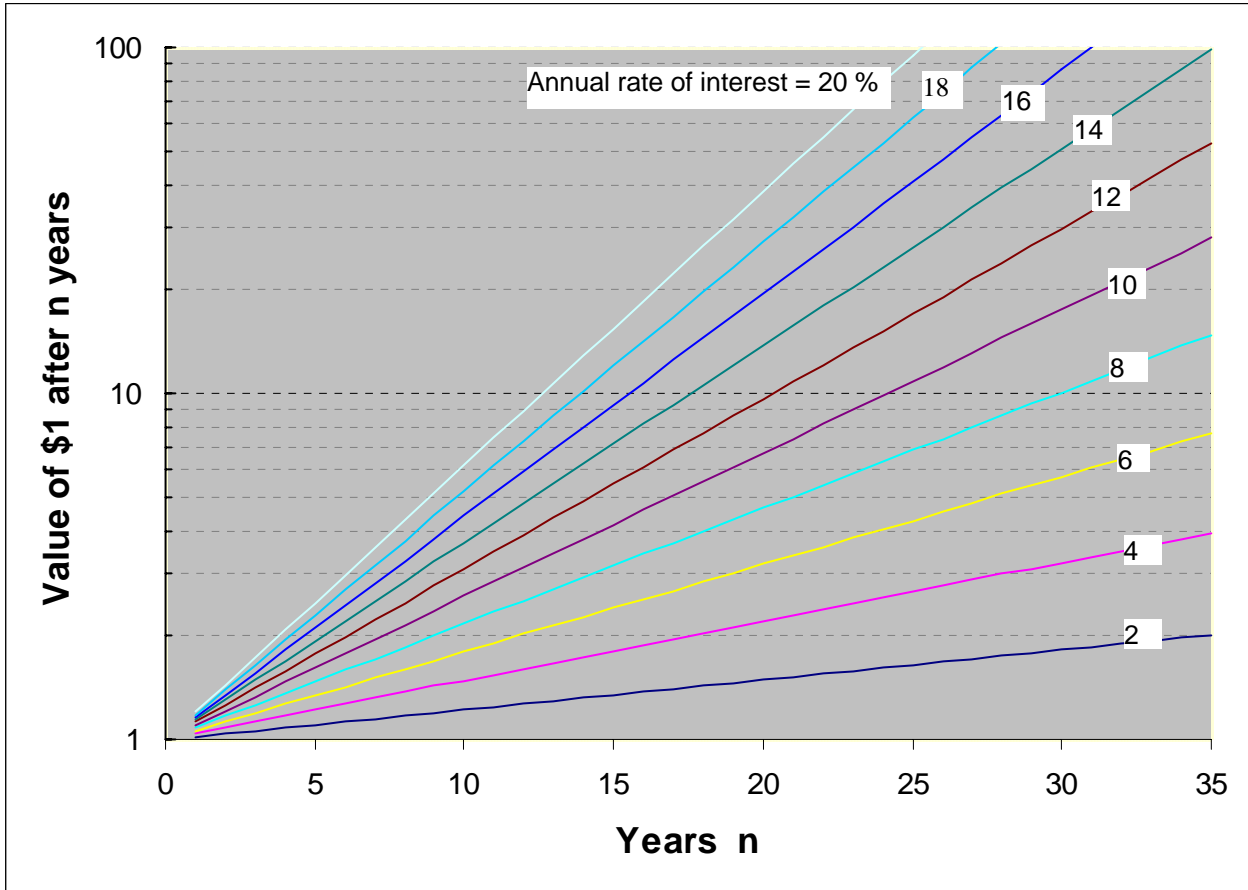


Figure 9.3 Effect of compounding interest.

Example 1

\$250 000 is borrowed for 8 years at an annual interest rate of 10 per cent. Determine the total sum that must be repaid at the end of the period, assuming that no intervening payments have been made.

Solution

$$S = 250\,000 (1 + 0.1)^8 = \$535\,897$$

Example 2

How long does it take for an investment to double in dollar value at an annual interest rate of 12 per cent?

Solution

In this example, the final sum is twice the principal, $S = 2P$. Hence, equation (9.8) becomes

$$2P = P(1 + 0.12)^n$$

giving

$$n = \frac{\ln(2)}{\ln(1.12)} = 6.12 \quad \text{years}$$

9.5.2. Time value of money, present value

It is clear from a consideration of interest that the value of a set sum of money will vary with time. At 9 per cent interest, \$100 now is worth \$109 in one year and \$118.81 two years from now. The effect of national inflation will, of course, partially erode growth in the value of capital. To determine real purchasing power, rates of interest should be corrected for inflation. In this section we are assuming that this has been done and quoted interest rates have taken projected inflation into account.

9.5.2.1. Present value of a lump sum.

The time variation of the value of money makes it inequitable to compare two sums that are borrowed or spent at different times. We need a common basis on which both sums can be fairly evaluated. One method of doing this is to determine what principal or capital, P , we need to invest now in order that it will grow to a desired sum, S , in a specified number of years. This is given by a simple transposition of equation (9.8)

$$P = \frac{S}{(1+i)^n} \quad (9.9)$$

When determined in this way, the value of P is known as the **present value** of the future sum S . If all future investments or expenditures are reduced to present values then they can correctly be compared.

Example

Three fans are to be installed; one immediately at a price of \$260 000, one in 5 years at an estimated cost of \$310 000 and the third 8 years from now at \$480 000. Determine the total expenditure as a present value if the annual interest rate is 10 per cent.

Solution

From equation (9.9), $P = \frac{S}{(1.1)^n}$

Fan	Time n	Purchase price S	Present value P
1	now	\$ 260 000	\$260 000
2	5 years	\$ 310 000	\$ 192 486
3	8 years	\$ 480 000	\$ 223 924
Total			\$ 676 410

In this example, the first fan is actually the most expensive.

9.5.2.2. Present value of regular payments.

In the case of operating costs, payments must be made each year. Such future payments may also be expressed as present values in order to compare and compound them with other expenditures.

We assume operating costs, S_o , to be constant and paid at the end of each year. Then at the end of the first year ($n = 1$), equation (9.9) gives

$$P_{o,1} = \frac{S_o}{(1+i)}$$

where $P_{o,1}$ = present value of the first year's annual operating cost S_o ; at an interest rate of i .

Similarly, the present value of the same operating cost, S_o , in the second year ($n = 2$) is

$$P_{o,2} = \frac{S_o}{(1+i)^2}$$

It follows that the total present value, P_o , of operating costs, S_o paid at each year-end for n years becomes

$$P_o = S_o \left[\frac{1}{(1+i)} + \frac{1}{(1+i)^2} + \frac{1}{(1+i)^3} + \dots + \frac{1}{(1+i)^n} \right] \tag{9.10}$$

The bracketed term is a geometric progression which can be summed to give

$$P_o = \frac{S_o}{i} \left[1 - \frac{1}{(1+i)^n} \right] \tag{9.11}$$

Figure 9.4 gives a graphical representation of this equation for $S_o = \$1$

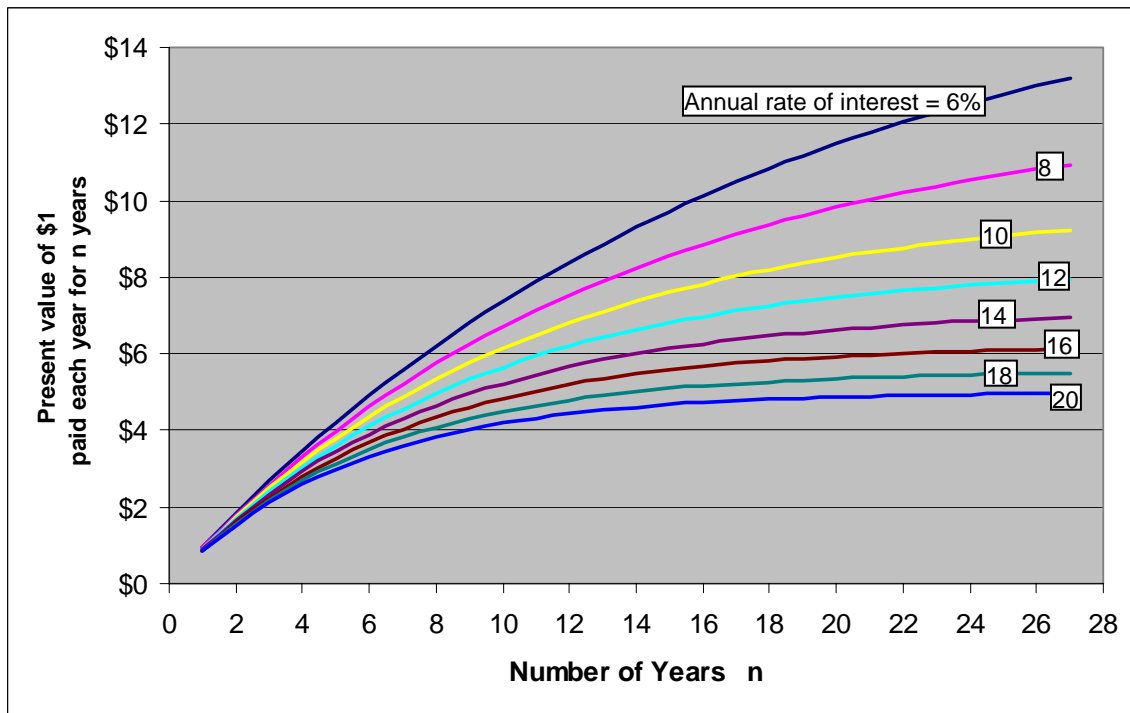


Figure 9.4 Present value of annual operating costs.

Example 1

Electrical power costs at a mine are estimated to be \$850 000 in each of the next 12 years. Determine the present value of this expenditure at 11 per cent interest.

Solution

With $S_o = \$850\,000$, $i = 0.11$ and $n = 12$ years, equation (9.11) gives

$$P_o = \frac{850\,000}{0.11} \left[1 - \frac{1}{(1 + 0.11)^{12}} \right] = \$5\,518\,503$$

Example 2

Tenders received from manufacturers indicate that a fan priced at \$170 000 will cost \$220 000 per year to run, while a fan with a purchase price of \$265 000 will require \$190 000 per year in operating costs. If the costing period is 5 years at an annual interest of 7 per cent, determine which fan is most economical.

Solution

Using equation (9.11) with $n = 5$ years, $i = 0.07$ and S_o set at \$220 000 and \$190 000 respectively allows the present value of the operating costs to be determined.

Fan	Current purchase price (\$)	Annual operating cost(\$/year)	Present values		
			Purchase price (\$)	Operating cost over 5 yr (\$)	Total (\$)
1	170 000	220 000	170 000	902 043	1 072 043
2	265 000	190 000	265 000	779 038	1 044 038

In this example, fan 2 is shown to be the more economic choice.

During the analysis of time phase exercises (Section 9.4.2) it may be necessary to establish the present value of operating costs for periods that do not commence at the present time. By applying equation (9.11) to periods of m years and n years respectively, and taking the difference, the present value of operating costs for the future period n to m years becomes

$$P_{o,nm} = \frac{S_o}{i} \left[\frac{1}{(1+i)^n} - \frac{1}{(1+i)^m} \right] \quad (9.12)$$

Example

This example shows an excerpt from a spreadsheet used to calculate the present values of capital and operating expenditures. Present values are calculated from equation (9.9) for capital (lump sum) expenditures and equation (9.12) for operating costs. The annual rate of interest is 10 per cent.

Period	Capital expenditure(\$)	Operating cost (\$/year)	Present value(\$)
1. now	500 000		500 000
2. now to end of 4 years. ($n = 0, m = 4$)		620 000	1 965 317
3. at end of 4 yrs	235 000		160 508
4. end of 4 yrs to end of 10 yrs ($n = 4, m = 10$)		680 000	2 022 797
Total present value=			\$4 648 622

Spreadsheets of this type can be set up on a personal computer to give a rapid means of costing the results of alternative network exercises.

9.5.3. Equivalent annual cost

When capital is borrowed, it is often more convenient to repay it, including interest, in equal installments each year, rather than as a lump sum paid at the end of the complete time period. This is a common method for domestic purchases such as a house (mortgage payments) or an automobile. In industry, this **equivalent annual cost** facilitates budgetary planning and enables major items of capital expenditure, such as a new shaft, to be spread evenly over a number of years. The method of equivalent annual cost allows capital expenditures to be compared with operating costs on a year by year basis and, for producing mines, also enables those capital expenditures to be expressed in terms of cost per tonne of mineral.

The equivalent annual cost is given by a re-interpretation of equation (9.11). P is the capital that must be invested now (present value) in order to be able to make a regular payment, S , each year. The statement may also be made in reverse, i.e. **S is the regular payment, or annual equivalent cost, to be met each year in order to pay off the capital and interest on a borrowed amount, P .**

Transposing equation (9.11) gives the equivalent annual cost, EAC, as

$$\text{EAC } (=S) = \frac{P i}{[1 - 1/(1+i)^n]} \quad (9.13)$$

Example

A mine shaft is to be sunk at a cost of \$5.6 million. The life of the shaft is estimated to be 15 years during which time the average planned rate of mineral production is 1.6 million tonnes per year. If the annual interest rate is 8.75 per cent, determine (a) the equivalent annual cost of the shaft in \$ per year and (b) corresponding production cost in \$ per tonne mined.

Solution

(a) Using equation (9.13) with $P = \$5.6$ million, $i = 0.0875$ and $n = 15$ years, gives the equivalent annual cost as

$$EAC = \frac{5\,600\,000 \times 0.0875}{[1 - 1/(1.0875)^{15}]} = \$684\,509$$

(b) The corresponding production cost is

$$\frac{684\,509}{1\,600\,000} = \$0.428 \text{ per tonne}$$

9.5.4. Ventilation operating costs

A fan unit, comprising an electric motor, transmission and impeller converts electrical energy into air power. The latter is reflected as kinetic energy of the air and a rise in total pressure across the fan. Air power delivered by a fan was quantified in Chapter 5 as

$$p_{ft} \times Q \quad \text{W} \quad (\text{from equation (5.6)})$$

where p_{ft} = rise in total pressure across the fan (Pa) and
 Q = airflow (m^3/s)

(See, also, Chapter 10 for the effects of compressibility).

However, the electrical power taken by the fan motor will be greater than this as losses occur inevitably in the motor, transmission and impeller. If the overall fractional efficiency of the unit is η , then the electrical input power to the motor will be

$$\frac{p_{ft} \times Q}{\eta} \quad \text{W}$$

Electrical power charges are normally quoted in cost per kilowatt-hour. Hence, the cost of operating a fan for 24 hours per day over the 365 days in a year is

$$S_o = \frac{p_{ft} Q}{1000 \eta} e \times 24 \times 365 \quad \$/\text{year} \quad (9.14)$$

where e is the cost of power (\$ per kwh).

In practice, the fan pressure, p_{ft} is often quoted in kPa, obviating the need for the 1000.

Equation (9.14) also applies for the annual cost of ventilating an individual airway. In this case, p_{ft} simply becomes the frictional pressure drop across the airway, p , at the corresponding airflow, Q , and η the overall efficiency of the fan primarily responsible for ventilating that airway. In cases of multiple fans, a weighted mean average of fan efficiency may be employed.

Example

An underground airway is driven at a capital cost of \$1.15 million dollars. During its life of 8 years, it is planned to pass an airflow, Q , of $120 \text{ m}^3/\text{s}$ at a frictional pressure drop, p , of 720 Pa. The main fans operate at an overall efficiency, η , of 72 per cent. If the annual rate of interest is 9.5 per cent and the average cost of electrical power is \$0.06 per kWh, determine the annual total cost of owning and ventilating the airway.

Solution

The equivalent annual cost of owning the airway is given by equation (9.13) with $P = \$1.15$ million, $i = 0.095$ and $n = 8$ years

$$\text{EAC} = \frac{1150\,000 \times 0.095}{[1 - 1/(1.095)^8]} = \$211\,652 \text{ per year}$$

The annual operating cost is given by equation (9.14) with $p_{ft} = 720 \text{ Pa}$, $Q = 120 \text{ m}^3/\text{s}$, $\eta = 0.72$ and $e = \$0.06$ per kWh

$$S_o = \frac{720 \times 120}{1000 \times 0.72} \times 0.06 \times 24 \times 365 = \$63\,072 \text{ per year}$$

The total yearly cost is given by adding the cost of owning the airway and the annual operating cost of ventilation:

$$\text{total annual cost } C = \text{EAC} + S_o = 211\,652 + 63\,072 = \$274\,724 \text{ per year}$$

9.5.5. Optimum size of airway

There are several factors that influence the optimum size of a subsurface airway, including

- the airflow to be passed through it
- the cost of excavation
- limitations on air velocity (Section 9.3.5)
- the span that can be supported adequately and
- the size of equipment required to travel through the airway.

This section considers the first two of these matters. However, the size of a planned new shaft or airway must satisfy the other constraints.

As the size of an airway is increased then its resistance and, hence, ventilation operating costs will decrease for any given airflow (Section 5.4.1). However, the capital cost of excavating the airway increases with size. The combination of capital and operating costs will be the total cost of owning and ventilating the airway. **The most economic or optimum size of the airway occurs when that total cost is a minimum.** The costs may be expressed either as present values or in terms of annual (equivalent) costs.

In order to quantify the optimum size, it is necessary to establish cost functions for both capital and operating costs that relate those expenditures to airway size.

9.5.5.1. Capital cost function

The business of arriving at a cost for excavating a mine shaft or major airway often involves protracted negotiations between a mining company and a contractor. Even when the task is to be undertaken in-house, the costing exercise may still be extensive.

There are, essentially, two components - fixed costs and variable costs. The fixed costs may include setting up and removal of equipment such as temporary headgear, hoisting facilities or a shaft drilling rig. Other items such as pipe ranges, electrical conduits, air ducts and track lines are usually independent of airway size but are a function of airway length.

The variable costs are those that can be expressed as functions of the length and cross-sectional area or diameter of the shaft or airway. These include the actual cost of excavation and supports.

The capital cost, P_c , may then be expressed as the cost function

$$P_c = C_f + f(A, L) \quad \$ \quad (9.15)$$

where C_f = fixed costs

and $f(A, L)$ = function of cross-sectional area, A and length, L .

In a simple case, the capital cost function may take the form

$$P_c = C_f + aV + bL \quad \$ \quad (9.16)$$

where V = volume excavated, $A \times L$ (m^3)
 a and b are constants.

For mechanized excavations, there may be discontinuities in the capital cost function due to step increases in the size and sophistication of the equipment for differing sizes of airway.

9.5.5.2. Operating cost function

Equation (9.14) gave the annual ventilation cost of an airway to be

$$S_o = \rho Q \frac{e}{1000 \eta} \times 24 \times 365 \quad \$/\text{year} \quad (9.17)$$

However, from equation (2.50),

$$\rho = R_t \rho Q^2$$

where R_t = rational resistance of the airway (m^{-4})

and ρ = air density (kg/m^3)

giving

$$S_o = R_t \rho Q^3 \frac{e}{\eta} \times \frac{24 \times 365}{1000}$$

This demonstrates that the operating cost varies with airway resistance, R_t , air density, ρ , and the cube of the airflow, Q .

Substituting for R_t from equation (2.51) gives

$$S_o = \frac{f L \text{ per}}{2 A^3} \rho Q^3 \times \frac{e}{\eta} \times \frac{24 \times 365}{1000} \quad \$/\text{year} \quad (9.18)$$

where f = coefficient of friction (dimensionless)

L = length of airway (m)

per = perimeter (m)

and A = cross-sectional area (m^2)

In order to achieve the corresponding result with the Atkinson friction factor, $k_{1,2}$, substituting for p from equation (5.8) allows the operating cost function of equation (9.17) to be written as

$$S_o = k_{1,2} \frac{L \text{ per } A^3}{1.2} \frac{\rho}{Q^3} \times \frac{e}{\eta} \times \frac{24 \times 365}{1000} \quad \$/\text{year} \quad (9.19)$$

9.5.5.3. Case Study

During the design of a proposed circular shaft, the following data were generated:

Shaft sinking:

- Equipment set up and decommissioning costs = \$650 000
- Excavation cost = \$290/m³
- Fittings and lining = \$460/m

Physical data:

- Depth of shaft, L = 700 m
- Effective coefficient of friction, f = 0.01
- (friction factor $k_{1,2} = 0.6f = 0.006 \text{ kg/m}^3$)
- Mean air density, ρ = 1.12 kg/m³
- Airflow, Q = 285 m³/s
- Fan efficiency, η = 0.65
- Life of shaft, n = 15 years

Additional financial data:

- Annual rate of interest, i = 10 per cent
- Average cost of electrical power e = \$0 .075 per kWh

Determine the optimum diameter of the shaft.

Solution

Task 1: Establish the capital cost function:

From the data given, the capital cost function can be expressed in the form of equation (9.16)

$$P_c = 650\,000 + 290 V + 460 L$$

where $V = AL = \frac{\pi D^2}{4} \times 700 \text{ (m}^3\text{)}$

and $D = \text{shaft diameter (m)}$

giving

$$P_c = 650\,000 + \left[290 \times 700 \times \frac{\pi D^2}{4} \right] + (460 \times 700)$$

The capital cost function then simplifies to

$$P_c = 972\,000 + 159\,436 D^2 \quad \$ \quad (9.20)$$

This is the present value of the capital cost of sinking the shaft. The complete analysis may be carried out either in terms of present values or in annual (equivalent) costs. The latter method is employed for this case study. Hence, the capital cost of shaft sinking must be spread over the 15 year life using equation (9.13) with $i = 0.1$ and $n = 15$.

Equivalent annual cost of shaft sinking:

$$\begin{aligned} \text{EAC} &= \frac{(972\,000 + 159\,436 D^2) \times 0.1}{[1 - 1/(1.1)^{15}]} \quad \text{from equation (9.13)} \\ &= 127\,793 + 20\,962 D^2 \quad \$/\text{year} \end{aligned} \quad (9.21)$$

Task 2: Establish the operating cost function:

This is accomplished by substituting the given data into equations (9.18) or (9.19)

Annual operating cost

$$\begin{aligned} S_o &= \frac{0.01 \times 700 \times \pi D}{2(\pi D^2 / 4)^3} \times 1.12 \times 285^3 \times \frac{0.075}{0.65} \times \frac{24 \times 365}{1000} \quad \$/\text{year} \\ &= 594.775 \times 10^6 / D^5 \quad \$/\text{year} \end{aligned} \quad (9.22)$$

Task 3: Establish the total cost function:

Addition of the capital and operating cost functions from equations (9.21) and (9.22) respectively gives the total annual cost function as

$$C = 127\,793 + 20\,962 D^2 + \frac{594.775 \times 10^6}{D^5} \quad \$/\text{year} \quad (9.23)$$

Task 4: Determine the optimum diameter:

This can be accomplished in either of two ways.

(a) By graphical means.

The three cost functions have been plotted on Figure 9.5. The minimum point on the total annual cost curve occurs at an optimum diameter of approximately 4.9m.

An advantage of constructing the cost curves is that it gives a visual indication of the behaviour of the cost functions. In particular, the operating and total costs rise rapidly when the airway diameter is reduced significantly below the optimum point. However, the total cost curve remains fairly shallow above the optimum point. This is a typical result and illustrates that the shaft size may be escalated to a standard diameter above the optimum to facilitate shaft sinking. Indeed, experience has shown the wisdom of sizing a shaft above the optimum. This allows subsequent flexibility for modifications to the airflow or mine production.

(b) By analytical means.

If the total cost function, C , has been expressed as a convenient function of cross-sectional area, A , or diameter, D , then it can be differentiated to find the optimum location when the slope dC/dA or dC/dD becomes zero.

In this case study, differentiation of equation (9.23) gives

$$\frac{dC}{dD} = 2 \times 20\,962 D - \frac{5 \times 594.775 \times 10^6}{D^6}$$

At $dC/dD = 0$

$$41924 D^7 = 2973.875 \times 10^6 \quad \text{from which} \quad D = 4.93 \text{ m.}$$

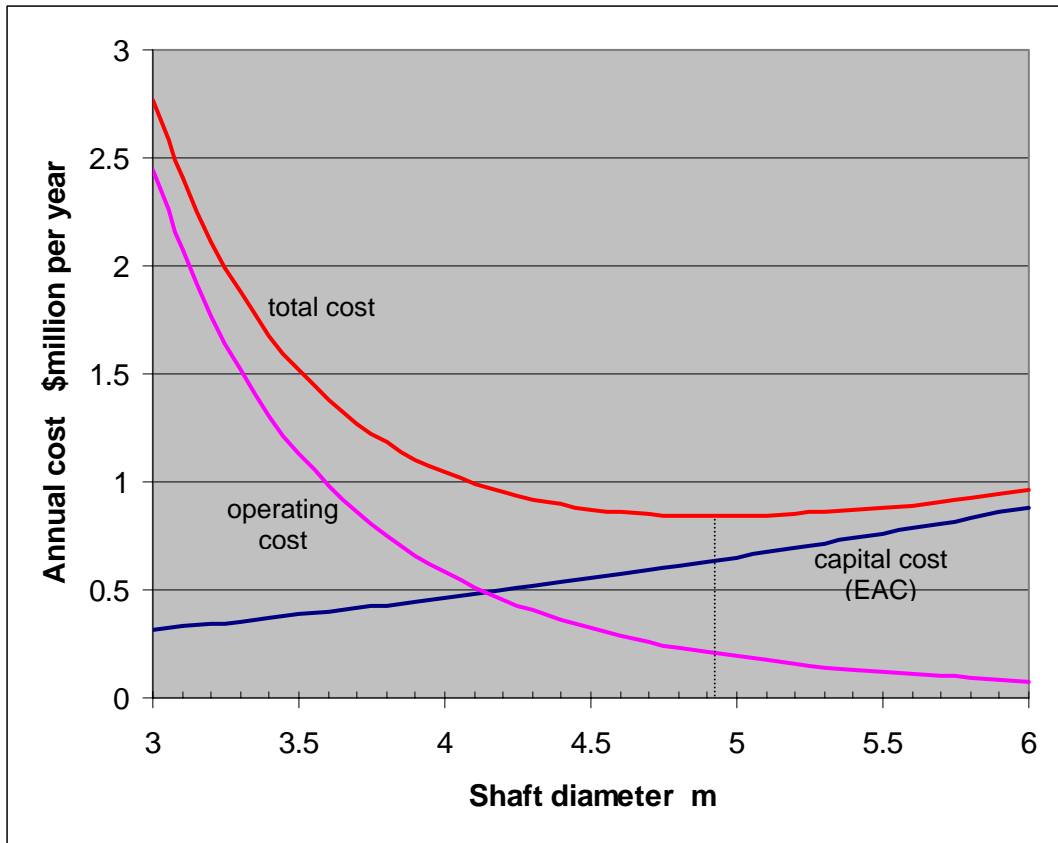


Figure 9.5 Annual cost functions for the circular shaft used in the Case Study

This is an accurate value of the optimum diameter previously read from Figure 9.5 as the approximation 4.9m. In practice, the recommended diameter would be rounded up to at least 5m.

The corresponding total annual equivalent cost can be estimated from Figure 9.5 or calculated by substituting $D = 9.3$ into equation (9.23):

$$\begin{aligned}
 C &= 127793 + 20962 \times 4.93^2 + \frac{594.775 \times 10^6}{4.93^5} \\
 &= \$ 841\,502 \text{ per year}
 \end{aligned}$$

9.5.6. Incorporation of shaft design into network planning exercises.

Figure 9.1 shows the optimization of major airways and fans to be a part of the ventilation planning process. However, it may be impractical to carry out such optimization for every investigatory cycle of a ventilation network exercise. The sizing of a shaft is normally conducted only after network analysis has established a satisfactory distribution of airflows underground and can be combined with the shaft design procedures described in Section 5.4.6.

The demands made upon a mine shaft may include access for personnel and equipment, the hoisting of planned tonnages of rock and the passing of specified airflows. We can now define a set of guidelines to assist in the management of a combined network analysis and shaft design exercise.

1. Assess the duties required for rock hoisting (tonnes per hour), number of personnel to be transported, time allowed at shift changes and the size, weight and frequency of hoisting materials and equipment.
2. Determine alternative combinations of conveyance sizes and hoisting speeds.
3. Conduct ventilation network investigations, initially on the basis of an estimated shaft resistance until a satisfactory distribution of airflow is achieved. This will establish the required airflow in the shaft.
4. Assess the dimensions of proposed shaft fittings including pipes, cables, guides and buntons.
5. Conduct an optimization exercise to find the size of shaft that will pass the required airflow at the minimum combination of operating costs and the capital expense of shaft construction (Section 9.5.5.).
6. Check the free area air velocity. If this exceeds 10 m/s in a hoisting shaft or 20 m/s in a shaft used only for ventilation then the cost of enlarging the shaft should be reviewed. It will be recalled that the total cost vs. diameter curve is usually fairly flat above its minimum point (Section 9.5.5.3).
7. Determine the **coefficient of fill**, C_F , for the largest of the proposed conveyances (Section 5.4.6.3). If this exceeds 30 per cent for two or more conveyances, or 50 per cent for a single conveyance shaft, then the dimensions of the skip or cage should be reviewed or the size of the shaft, again, be re-examined.
8. Calculate the maximum relative velocity between the airflow and the largest conveyance, $(u_a + u_c)/(1 - C_F)$ (See section 5.4.6.3 for nomenclature.)
If this exceeds 30 m/s then additional precautions should be taken to ensure aerodynamic stability of the moving conveyances. In any event, the relative velocity should not exceed 50 m/s.
9. Assess the air velocities at all loading/unloading stations and, if necessary, redesign the excavations to include air bypasses or enlarged shaft stations.
10. Determine the total resistance of the shaft using the methods described in Section 5.4.6. Examine all feasible means of reducing the resistance including the streamlining of buntons and the aerodynamic design of intersections. For shafts of major importance, construct and test physical or CFD² models of representative lengths of the shaft and main intersections.
11. Rerun ventilation network analyses with the established value(s) of shaft resistance in order to determine the final fan pressures required.

It is clear that there is a considerable amount of work involved in the design, sizing and costing of a proposed mine shaft or major airway. Fortunately, microcomputer program packages are available that reduce the effort to little more than assembling the essential data. These are particularly valuable for carrying out sensitivity studies in order to assess the effects of changes in design or financial constraints.

² Computational Fluid Dynamics

9.6. TRADITIONAL METHOD OF VENTILATION PLANNING

The methods of subsurface ventilation planning described in the previous sections of this chapter rely upon the availability of computers and appropriate software. A question that may arise is how such planning can be carried out without high speed computational aid. For this, we may revert back to the traditional methodology that was well developed prior to the computer revolution. Although the older techniques cannot begin to match the speed, versatility and detail of computer assisted planning, they do retain a role in estimating generic values for airflows, fan pressures and air quality at the early conceptual design stage of a proposed new mine or extension to an existing facility.

The traditional approach proceeds along the following sequence:

1. Determine air volume flows required in working areas. This can employ the methods discussed in Section 9.3. However, at a preliminary stage of planning, empirical values of airflow based on rate of tonnage might be used. In this case, care must be taken to ensure that the basis of the empirical guidelines is compatible with the intended mining method and geology.
2. Assess the airflow requirements for development areas, mechanical or electrical plant and workshops, and estimate the volume flows that pass through abandoned workings, stoppings and other leakage paths. The estimation of leakage flows relies strongly upon the experience and intuition of the ventilation engineer. Unfortunately, in many mines the volumetric efficiency (Section 4.2.3) is fairly low. Inaccuracies in the estimates of airflow through individual leakage paths, while perhaps of little consequence when considered individually, will accumulate into major errors in the main ventilation routes. The square law, $p = RQ^2$, then produces twice the corresponding percentage error in the frictional pressure drop. The treatment of leakage flows is probably the single greatest cause of imprecision in the traditional method of ventilation planning.
3. Indicate the estimated airflows on a mine plan and compound them to show air flowrates, Q , through every major airway.
4. Using the given airflows and proposed sizes of airways, determine the corresponding air velocities. If these exceed limiting values (Section 9.3.6), the need for larger or additional airways is indicated.
5. Assess the resistance, R , of each branch along the main ventilation routes, either from estimated friction factors and airway geometries or on the basis of local empirical data.
6. Using the square law, $p = RQ^2$, determine the frictional pressure drop, p , for each main branch and indicate these on the mine plan.
7. Starting at the entrance of a downcasting surface connection, trace a path along intake airways to the most distant workings, through those workings, and back to the surface via return airways. Sum the frictional pressure drops around the complete traverse. This exercise is repeated for a number of such traverses to incorporate various working areas. The loop showing the greatest summation of frictional pressure drops then gives an approximation of the main fan pressure required to ventilate the mine. Subsidiary circuits may be controlled by regulators or upgraded by booster fans³. **Pressure gradient diagrams** can be employed to give a visual indication of the cumulative pressure drops.

The traditional approach is similar, in principle, to that used for the design of duct systems in buildings. It is simple in concept and requires little computational aid. Unfortunately, it suffers from some severe drawbacks:

1. It relies strongly upon the experience of the engineer and his/her empirical knowledge of the airflow distribution patterns. A mine is very different to a duct system in a building, not

³ where booster fans are permitted by the governing legislation.

- only in scale but also because of the dynamic nature of mining operations, and the tremendous variability in the geometry of airflow paths with respect to time as well as location.
2. The highly interactive and nonlinear relationships that exist between ventilation parameters are largely ignored. Leakage airflows through caved strata, old workings or across stoppings, doors and air crossings are dependent upon the geometry of the flow paths, the pressure differential and the degree of turbulence. Ascribing fixed values or even fixed proportions of available airflow to leakage can do no more than achieve rough approximations. In many mines, the majority of total airflow passes through leakage paths. Errors in estimated leakages will accumulate and be reflected in the corresponding main airflow routes and, because of the nonlinearity of the laws of airflow, can result in large errors in the cumulative pressure drops.
 3. There is a basic lack of reality in a procedure that estimates an airflow pattern and then backtracks to find a fan pressure that will produce airflows capable of being manipulated into the required distribution. In practice, when a fan is switched on, a complex configuration of interdependent pressure drops and airflows is set up throughout the network, the ventilating pressures producing airflows and the airflows, in turn, producing frictional pressure drops. In effect, the airflows shown by the traditional method are simply the initial estimates based on desired airflows in the workplaces and assumed leakages. No attempt is made to simulate the actual airflow distribution that will occur when the fans are switched on.
 4. There is very little opportunity to study alternative options in order to optimize the effectiveness and operating economics of the ventilation system.
 5. Assuming the airflow distribution allows little flexibility in investigating the effects of fan duty/position, or the adjustment or re-siting of regulators, doors and booster fans.

Bibliography

- Aldridge, M.D. and Nutter, R.S. (1980).** An experimental ventilation control system. 2nd. Int. Mine Ventilation Congress, Reno, NV. pp.230-238.
- Calizaya, F. et al. (1989)** Guidelines for implementation of a booster fan monitoring and control system in coal mines. 4th U.S. Mine Ventilation Symposium. Berkeley, Ca pp 382-391
- Calizaya, F et al. (1988)** A computer program for selecting the optimum combination of fans and regulators in underground mines. Trans. 4th Int. Mine Ventilation Congress. Brisbane, Australia, pp 141-150.
- Dunmore, R. (1980)** Towards a method of prediction of firedamp emission for British coal mines. Proc. 2nd Int. Mine Ventilation Congress, Reno, Nevada, USA (AIME publication) pp 351-64.
- Kissell, F.N. (1978)** Some new developments in mine ventilation from the U.S. Bureau of Mines. July, Mine Ventilation Soc. of S. Africa. Vol 31. pp 85-89.
- Lambrechts, J. de V. and Howe, M.J. (1982)** Mine Ventilation Economics. Chapter 33. Environmental Engineering in South African Mines. Mine Ventilation Soc. of S. Africa.
- Mahdi, A. and McPherson, M.J. (1971).** An introduction to automatic control of mine ventilation systems. Mining Technology. May.
- McPherson, M.J. (1988)** An analysis of the resistance and airflow characteristics of mine shafts. 4th International Mine Ventilation Congress. July, Brisbane, Australia
- McPherson, M.J. (1984)** Mine ventilation planning in the 1980's. International Journal of Mining Engineering. Vol. 2 pp 185-227.
- Rustan, A. and Stockel, I. (1980).** Review of developments in monitoring and control of mine ventilation systems. 2nd Int. Mine Ventilation Congress. Reno, NV. pp. 223-229.

CHAPTER 10 FANS

10.1. INTRODUCTION	2
10.2. FAN PRESSURES.....	2
10.3. IMPELLER THEORY AND FAN CHARACTERISTIC CURVES	5
10.3.1. The centrifugal impeller.....	5
10.3.1.1. Theoretical pressure developed by a centrifugal impeller.....	6
10.3.1.2. Theoretical characteristic curves for a centrifugal impeller.....	9
10.3.1.3. Actual characteristic curves for a centrifugal impeller.....	11
10.3.2. The axial impeller.....	14
10.3.2.1. Aerofoils	14
10.3.2.2. Theoretical pressure developed by an axial fan	15
10.3.2.3. Actual characteristic curves for an axial fan.....	20
10.4 FAN LAWS.....	22
10.4.1. Derivation of the fan laws.....	22
10.4.2. Summary of fan laws	24
10.5. FANS IN COMBINATION.....	25
10.5.1. Fan in series	26
10.5.2. Fans in parallel.....	27
10.6. FAN PERFORMANCE	28
10.6.1. Compressibility, fan efficiency, and fan testing.....	29
10.6.1.1. The pressure-volume method	30
10.6.1.2. The thermometric method	34
10.6.2. Purchasing a main fan.	39
10.7. BOOSTER FANS.....	40
10.7.1. The application of booster fans.....	40
10.7.2. Initial planning and location	40
<i>Practical constraints on booster fan location.....</i>	<i>41</i>
<i>Leakage and recirculation.....</i>	<i>41</i>
<i>Steady state effects of stopping the booster fan</i>	<i>42</i>
<i>Economic considerations.....</i>	<i>42</i>
10.7.3. Monitoring and other safety features	42
10.7.4. Booster fan control policy.....	43
Bibliography	45
APPENDIX A10.1	46
Comparisons of exhausting and forcing fan pressures to use in pressure surveys....	46
APPENDIX A10.2	49
Derivation of the isentropic temperature-pressure relationship for a mixture of air, water vapour and liquid water droplets.	49

10.1. INTRODUCTION

A fan is a device that utilizes the mechanical energy of a rotating impeller to produce both movement of the air and an increase in its total pressure. The great majority of fans used in mining are driven by electric motors, although internal combustion engines may be employed, particularly as a standby on surface fans. Compressed air or water turbines may be used to drive small fans in abnormally gassy or hot conditions, or where an electrical power supply is unavailable.

In Chapter 4, mine fans were classified in terms of their location, main fans handling all of the air passing through the system, booster fans assisting the through-flow of air in discrete areas of the mine and auxiliary fans to overcome the resistance of ducts in blind headings. Fans may also be classified into two major types with reference to their mechanical design.

A centrifugal fan resembles a paddle wheel. Air enters near the centre of the wheel, turns through a right angle and moves radially outward by centrifugal action between the blades of the rotating impeller. Those blades may be straight or curved either backwards or forwards with respect to the direction of rotation. Each of these designs produces a distinctive performance characteristic. Inlet and/or outlet guide vanes may be fitted to vary the performance of a centrifugal fan.

An axial fan relies on the same principle as an aircraft propeller, although usually with many more blades for mine applications. Air passes through the fan along flowpaths that are essentially aligned with the axis of rotation of the impeller and without changing their macro-direction. However, later in the chapter we shall see that significant vortex action may be imparted to the air. The particular characteristics of an axial fan depend largely on the aerodynamic design and number of the impeller blades together with the angle they present to the approaching airstream. Some designs of axial impellers allow the angle of the blades to be adjusted either while stationary or in motion. This enables a single speed axial fan to be capable of a wide range of duties. Axial fan impellers rotate at a higher blade tip speed than a centrifugal fan of similar performance and, hence, tend to be noisier. They also suffer from a pronounced stall characteristic at high resistance. However, they are more compact, can easily be combined into series and parallel configurations and can produce reversal of the airflow by changing the direction of impeller rotation, although at greatly reduced performance. Both types of fan are used as main fans for mine ventilation systems while the axial type is favoured for underground locations.

In this chapter, we shall define fan pressures and examine some of the basic theory of fan design, the results of combining fans in series and parallel configurations, the theory of fan testing and booster fan installations.

10.2. FAN PRESSURES

A matter that has often led to confusion is the way in which fan pressures are defined. In Section 2.3.2. we discussed the concepts of total, static and velocity pressures as applied to a moving fluid. That section should be revised, if necessary, before reading on. While we use those concepts in the definitions of fan pressures, the relationships between the two are not immediately obvious. The following definitions should be studied with reference to Figure 10.1(a) until they are clearly understood.

- Fan total pressure, FTP , is the increase in total pressure, p_t , (measured by facing pitot tubes) across the fan,

$$FTP = p_{t2} - p_{t1} \quad (10.1)$$

- Fan velocity pressure, FVP , is the average velocity pressure at the fan outlet only,

$$p_{v2} = p_{t2} - p_{s2}$$

- Fan static pressure, FSP , is the difference between the fan total pressure and fan velocity pressure, or

$$FSP = FTP - FVP \quad (10.2)$$

$$= p_{t2} - p_{t1} - (p_{t2} - p_{s2}) = p_{s2} - p_{t1} \quad (10.3)$$

The reason for defining fan velocity pressure in this way is that the kinetic energy imparted by the fan and represented by the velocity pressure at outlet has, traditionally, been assumed to be a loss of useful energy. For a fan discharging directly to atmosphere this is, indeed, the case. As the fan total pressure, FTP , reflects the full increase in mechanical energy imparted by the fan, the difference between the two, i.e. fan static pressure has been regarded as representative of the useful mechanical energy applied to the system.

The interpretations of fan pressures that are most convenient for network planning are further illustrated on Figure 10.1. In the case of a fan located within an airway or ducted at both inlet and outlet (Figure 10.1(a)), the fan static pressure, FSP , can be measured directly between a total (facing) tube at inlet and a static (side) tapping at outlet. A study of the diagram and equation (10.3) reveals that this is, indeed, the difference between FTP and FVP .

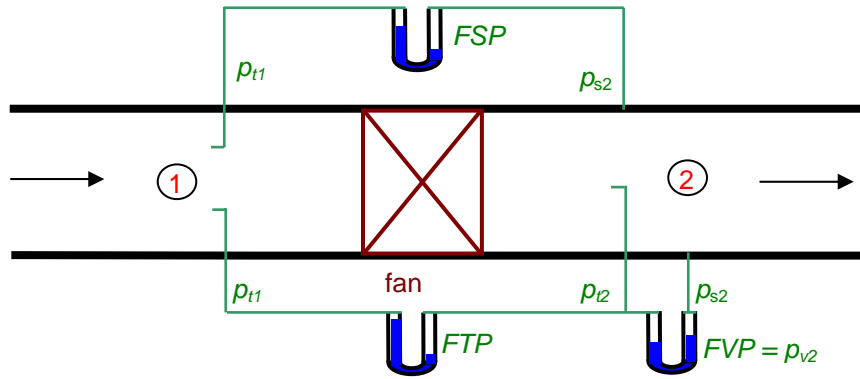
Figure 10.1 (b) shows the situation of a forcing fan drawing air from atmosphere into the system. A question that arises is where to locate station 1, i.e. the fan inlet. It may be considered to be

- (i) immediately in front of the fan
- (ii) at the entrance to the inlet cone, or
- (iii) in the still external atmosphere

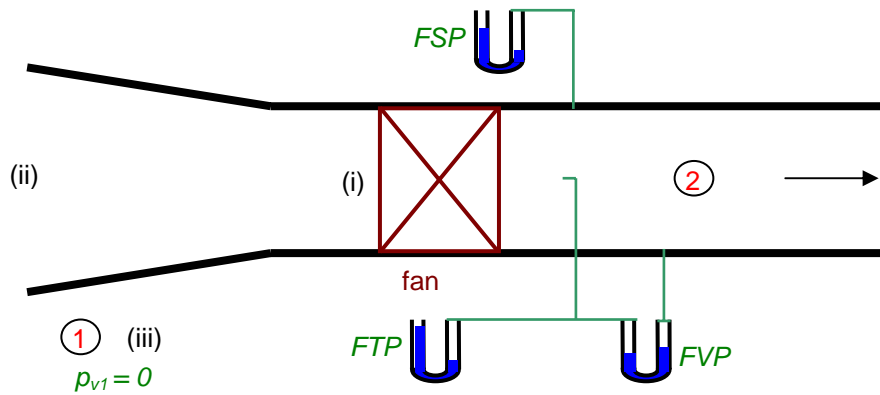
These three positions are labelled on Figure 10.1 (b). If location(i) is chosen then the frictional and shock losses incurred as the air enters and passes through the cone must be assessed separately. At location (ii) the fan and inlet cone are considered as a unit and only the shock loss at entry requires additional treatment. However, if location (iii) is selected then the fan, inlet cone and inlet shock losses are all taken into account. It is for this reason that location (iii) is preferred for the purposes of ventilation planning. Figure 10.1 (b) shows the connection of gauges to indicate the fan pressures in this configuration.

The same arguments apply for a fan that exhausts to atmosphere (Figure 10.1 (c)). If the outlet station is taken to be in the still external atmosphere then the fan velocity pressure is zero and the fan total and fan static pressures become equal. In this configuration the fan total (or static) pressure takes into account the net effects of the fan, frictional losses in the outlet cone and the kinetic energy loss at exit.

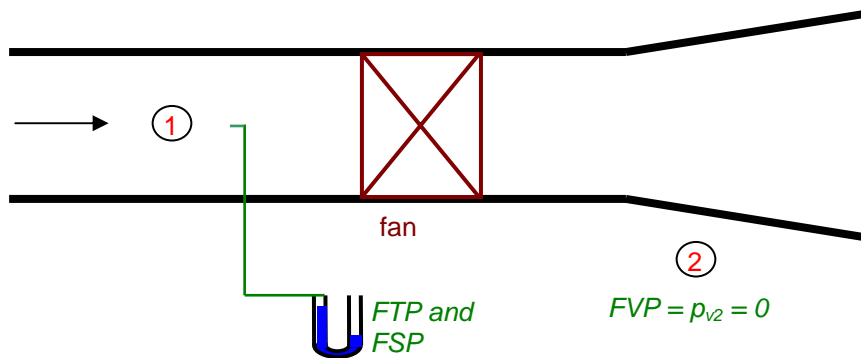
During practical measurements, it is often found that turbulence causes excessive fluctuations on the pressure gauge when total pressures are measured directly using a facing pitot tube. In such cases, it is preferable to measure static pressure from side tappings and to add, *algebraically*, the velocity pressure in order to obtain the total pressure. The mean velocity can be obtained as flowrate divided by the appropriate cross-sectional area. Particular care should be taken with regard to sign. In the case of an exhausting fan, (Figure 10.1 (c)) the static and velocity pressures at the fan inlet have opposite signs.



(a) Fan with inlet and outlet ducts



(b) Fan and inlet unit in a forcing system



(c) Fan and outlet unit in an exhausting system

Figure 10.1 Illustrations of fan pressures.

Fan manufacturers usually publish characteristic curves in terms of fan static pressure rather than the fan total pressure. In addition to being more useful for ventilation planning, this is understandable as manufacturers may have no control over the types of inlet and outlet duct fittings or the conditions at entry or exit to inlet/outlet cones. Where fan velocity pressures are quoted then they are normally referred to a specific outlet location, usually either at the fan hub or at the mouth of an evasee.

The question remains on which fan pressure should be used when a fan is included in the route of a pressure survey. The simple answer is that for main surface fans it is fan static pressure (*FSP*) that should be employed. For a main forcing fan the *FSP* is given by the gauge static pressure at the inby side of the fan (Figure 10.1(b)). But for a main exhausting fan the *FSP* is given by the gauge total pressure at the inby side of the fan (Figure 10.1(c)). This apparent anomaly arises from the way in which fan pressures are defined and is further explained in Appendix A10.1.

10.3. IMPELLER THEORY AND FAN CHARACTERISTIC CURVES

An important aspect of subsurface ventilation planning is the specification of pressure-volume duties required of proposed main or booster fans. The actual choice of particular fans is usually made through a process of perusing manufacturer's catalogues of fan characteristic curves, negotiation of prices and costing exercises (Section 9.5). The theory of impeller design that underlies the characteristic behaviour of differing fan types is seldom of direct practical consequence to the underground ventilation planner. However, a knowledge of the basics of that theory is particularly helpful in discussions with fan manufacturers and in comprehending why fans behave in the way that they do.

This section of the book requires an elementary understanding of vector diagrams. Initially, we shall assume incompressible flow but will take compressibility of the air into account in the later section on fan performance (Section 10.6.1).

10.3.1. The centrifugal impeller

Figure 10.2 illustrates a rotating backward bladed centrifugal impeller. The fluid enters at the centre of the wheel, turns through a right angle and, as it moves outwards radially, is subjected to centrifugal force resulting in an increase in its static pressure. The dotted lines represent flowpaths of the fluid relative to the moving blades. Rotational and radial components of velocity are imparted to the fluid. The corresponding outlet velocity pressure may then be partially converted into static pressure within the surrounding volute or fan casing.

At any point on a flowpath, the velocity may be represented by vector components with respect to either the moving impeller or to the fan casing. The **vector diagram** on Figure 10.2 is for a particle of fluid leaving the outlet tip of an impeller blade. The velocity of the fluid relative to the blade is W and has a vector direction that is tangential to the blade at its tip. The fluid velocity also has a vector component in the direction of rotation. This is equal to the tip (peripheral) velocity and is shown as u . The vector addition of the two, C , is the actual or absolute velocity. The radial (or meridional) component of velocity, C_m is also shown on the vector diagram.

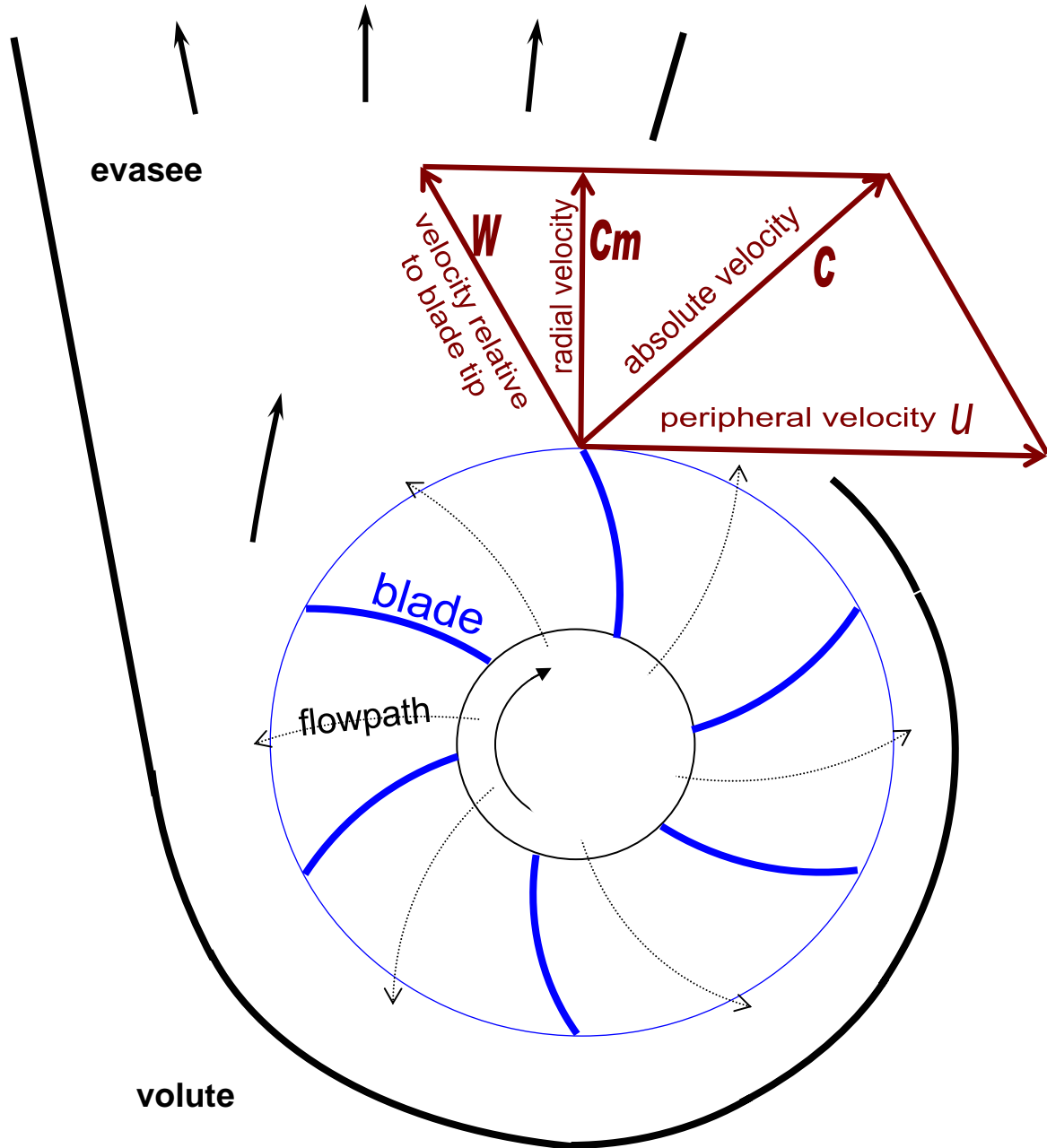
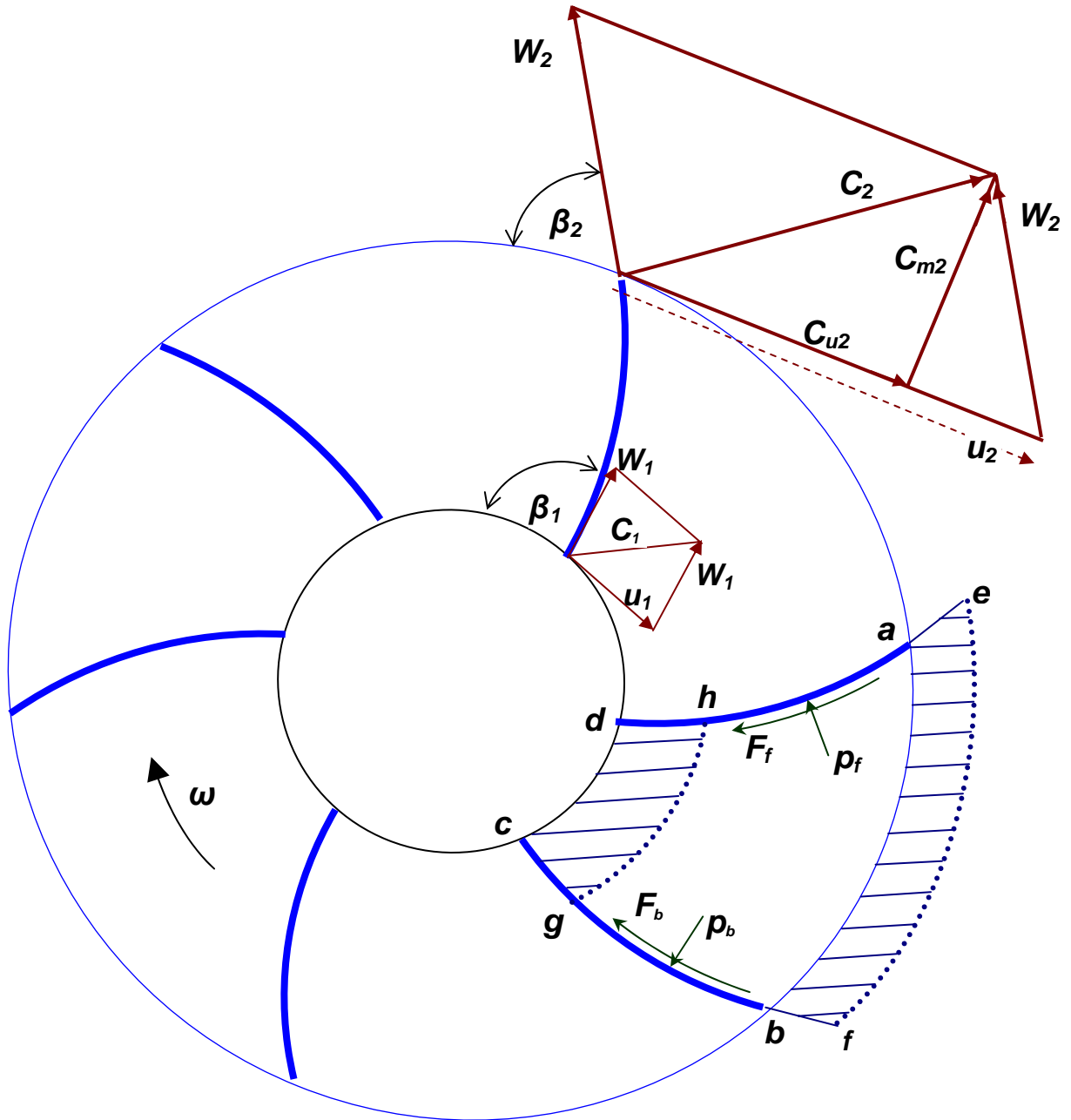


Figure 10.2 Idealized flow through a backward bladed centrifugal impeller.

10.3.1.1. Theoretical pressure developed by a centrifugal impeller.

A more detailed depiction of the inlet and outlet vector diagrams for a centrifugal impeller is given on Figure 10.3. It is suggested that the reader spend a few moments examining the key on Figure 10.3 and identifying corresponding elements on the diagram.



Subscript 1: Inlet

- ω : Angular velocity (radians/s)
- u : Peripheral speed of blade tip (m/s)
- C_m : Radial component of fluid velocity (m/s)
- β : Vane angle
- p_f : Pressure on front of vane (Pa)
- F_f : Shear resistance on front of vane (N/m^2)

Subscript 2: Outlet

- C : Absolute fluid velocity (m/s)
- W : Fluid velocity relative to vane (m/s)
- C_u : Peripheral component of fluid velocity (m/s)
- p_b : Pressure on back of vane (Pa)
- F_b : Shear resistance on back of vane (N/m^2)

Figure 10.3 Velocities and forces on a centrifugal impeller.

In order to develop an expression for the theoretical pressure developed by the impeller, we apply the principle of angular momentum to the mass of fluid moving through it.

If a mass, m , rotates about an axis at a radius, r , and at a tangential velocity, v , then it has an **angular momentum** of $mr v$. Furthermore, if the mass is a fluid that is continuously being replaced then it becomes a mass flow, dm/dt , and a **torque**, T , must be maintained that is equal to the corresponding continuous rate of change of momentum

$$T = \frac{dm}{dt} (rv) \quad \text{Nm or J} \quad (10.4)$$

In the case of the centrifugal impeller depicted in Figure 10.3, the peripheral component of fluid velocity is C_u . Hence the torque becomes

$$T = \frac{dm}{dt} (r C_u) \quad \text{Nm or J} \quad (10.5)$$

Consider the mass of fluid filling the space between two vanes and represented as $abcd$ on Figure 10.3. At a moment, dt , later it has moved to position $efgh$. The element $abfe$ leaving the impeller has mass dm and is equal to the mass of the element $cdhg$ entering the impeller during the same time. The volume represented by $abgh$ has effectively remained in the same position and has not, therefore, changed its angular momentum. The increase in angular momentum is that due to the elements $abfe$ and $cdhg$. Then, from equation (10.5) applied across the inlet and outlet locations,

$$T = \frac{dm}{dt} [r_2 C_{u2} - r_1 C_{u1}] \quad \text{J} \quad (10.6)$$

Extending the flow to the whole impeller instead of merely between two vanes gives dm/dt as the total mass flow, or

$$\frac{dm}{dt} = Q \rho \quad \frac{\text{kg}}{\text{s}}$$

where Q = volume flow (m^3/s)
and ρ = fluid density (kg/m^3)

giving

$$T = Q\rho [r_2 C_{u2} - r_1 C_{u1}] \quad \text{J} \quad (10.7)$$

Now the power consumed by the impeller, P_{ow} is equal to the rate of doing mechanical work,

$$P_{ow} = T\omega \quad \text{W} \quad (10.8)$$

where ω = speed of rotation (radians/s)

$$\text{giving } P_{ow} = Q\rho\omega [r_2 C_{u2} - r_1 C_{u1}] \quad \text{W} \quad (10.9)$$

But $\omega r_2 = u_2 =$ tangential velocity at outlet
and $\omega r_1 = u_1 =$ tangential velocity at inlet.

$$\text{Hence } P_{ow} = Q\rho [u_2 C_{u2} - u_1 C_{u1}] \quad \text{W} \quad (10.10)$$

The power imparted by a fan impeller to the air was given by equation (5.56) as $p_{ft} Q$

where p_{ft} = rise in total pressure across the fan.

In the absence of frictional or shock losses, $p_{ft} Q$ must equal the power consumed by the impeller, P_{ow} . Hence

$$p_{ft} = \rho(u_2 C_{u2} - u_1 C_{u1}) \quad \text{Pa} \quad (10.11)$$

This relationship gives the theoretical fan total pressure and is known as **Euler's equation**.

The inlet flow is often assumed to be radial for an ideal centrifugal impeller, i.e. $C_{u1} = 0$, giving

$$p_{ft} = \rho u_2 C_{u2} \quad \text{Pa} \quad (10.12)$$

Euler's equation can be re-expressed in a manner that is more amenable to physical interpretation. From the outlet vector diagram

$$\begin{aligned} W_2^2 &= C_{m2}^2 + (u_2 - C_{u2})^2 \\ &= C_{m2}^2 + u_2^2 - 2u_2 C_{u2} + C_{u2}^2 \end{aligned}$$

or

$$\begin{aligned} 2u_2 C_{u2} &= u_2^2 - W_2^2 + (C_{m2}^2 + C_{u2}^2) \\ &= u_2^2 - W_2^2 + C_2^2 \quad (\text{Pythagorus}) \end{aligned}$$

Similarly for the inlet,

$$2u_1 C_{u1} = u_1^2 - W_1^2 + C_1^2$$

Euler's equation (10.11) then becomes

$$p_{ft} = \rho \left\{ \frac{u_2^2 - u_1^2}{2} - \frac{W_2^2 - W_1^2}{2} + \frac{C_2^2 - C_1^2}{2} \right\} \text{Pa} \quad (10.13)$$

centrifugal effect
effect of relative velocity
change in kinetic energy

Gain in static pressure
Gain in velocity pressure

10.3.1.2. Theoretical characteristic curves for a centrifugal impeller

Euler's equation may be employed to develop pressure-volume relationships for a centrifugal impeller. Again, we must first eliminate the C_u term. From the outlet vector diagram on Figure 10.3,

$$\tan \beta_2 = \frac{C_{m2}}{u_2 - C_{u2}}$$

$$\text{giving } C_{u2} = u_2 - \frac{C_{m2}}{\tan \beta_2}$$

For radial inlet conditions, Euler's equation (10.12) then gives

$$p_{fi} = \rho u_2 C_{u2} = \rho u_2 \left\{ u_2 - \frac{C_{m2}}{\tan \beta_2} \right\} \quad \text{Pa} \quad (10.14)$$

$$\text{But } C_{m2} = \frac{Q}{a_2} = \frac{\text{volume flowrate}}{\text{flow area at impeller outlet}}$$

Equation (10.14) becomes

$$p_{fi} = \rho u_2^2 - \frac{\rho u_2 Q}{\tan \beta_2 a_2} \quad \text{Pa} \quad (10.15)$$

For a given impeller rotating at a fixed speed and passing a fluid of known density, ρ , u , a and β are all constant, giving

$$p_{fi} = A - BQ \quad \text{Pa} \quad (10.16)$$

$$\text{where constants } A = \rho u_2^2$$

$$\text{and } B = \frac{\rho u_2}{a_2 \tan \beta_2}$$

The flowrate, Q , and, hence, the pressure developed vary with the resistance against which the fan acts. Equation (10.16) shows that if frictional and shock losses are ignored, then fan pressure varies linearly with respect to the airflow.

We may apply this relationship to the three types of centrifugal impeller:

Radial bladed

$$\beta_2 = 90^\circ \text{ and } \tan \beta_2 = \text{infinity}$$

$$\text{giving } B = 0$$

Then

$$p_{fi} = \text{constant } A = \rho u_2^2$$

i.e. theoretically, the pressure remains constant at all flows [Figure 10.4 (a)]

Backward bladed

$$\beta_2 < 90^\circ, \quad \tan \beta_2 > 0$$

$$p_{fi} = A - BQ$$

i.e. theoretically, the pressure falls with increasing flow.

Forward bladed

$$\beta_2 > 90^\circ, \quad \tan \beta_2 < 0$$

$$p_{fi} = A + BQ$$

i.e. theoretically, pressure rises linearly with increasing flow.

The latter and rather surprising result occurs because the absolute velocity, C_2 is greater than the impeller peripheral velocity, u_2 , in a forward bladed impeller. This gives an impulse to the fluid which increases with greater flowrates. (In an actual impeller, friction and shock losses more than counteract the effect.).

The theoretical pressure-volume characteristic curves are shown on Figure 10.4 (a).

The theoretical relationship between impeller power and airflow may also be gained from equation (10.16).

$$P_{ow} = p_{it} Q = AQ - BQ^2 \quad W \quad (10.17)$$

The three power-volume relationships then become:

Radial bladed

$$B = 0 \quad \text{and} \quad P_{ow} = AQ \text{ (linear)}$$

Backward bladed

$$B > 0 \quad \text{and} \quad P_{ow} = AQ - BQ^2 \text{ (falling parabola)}$$

Forward bladed

$$B < 0 \quad \text{and} \quad P_{ow} = AQ + BQ^2 \text{ (rising parabola).}$$

The theoretical power-volume curves are shown on Figure 10.4 (b). Forward bladed fans are capable of delivering high flowrates at fairly low running speeds. However, their high power demand leads to reduced efficiencies. Conversely, the relatively low power requirement and high efficiencies of backward bladed impellers make these the preferred type for large centrifugal fans.

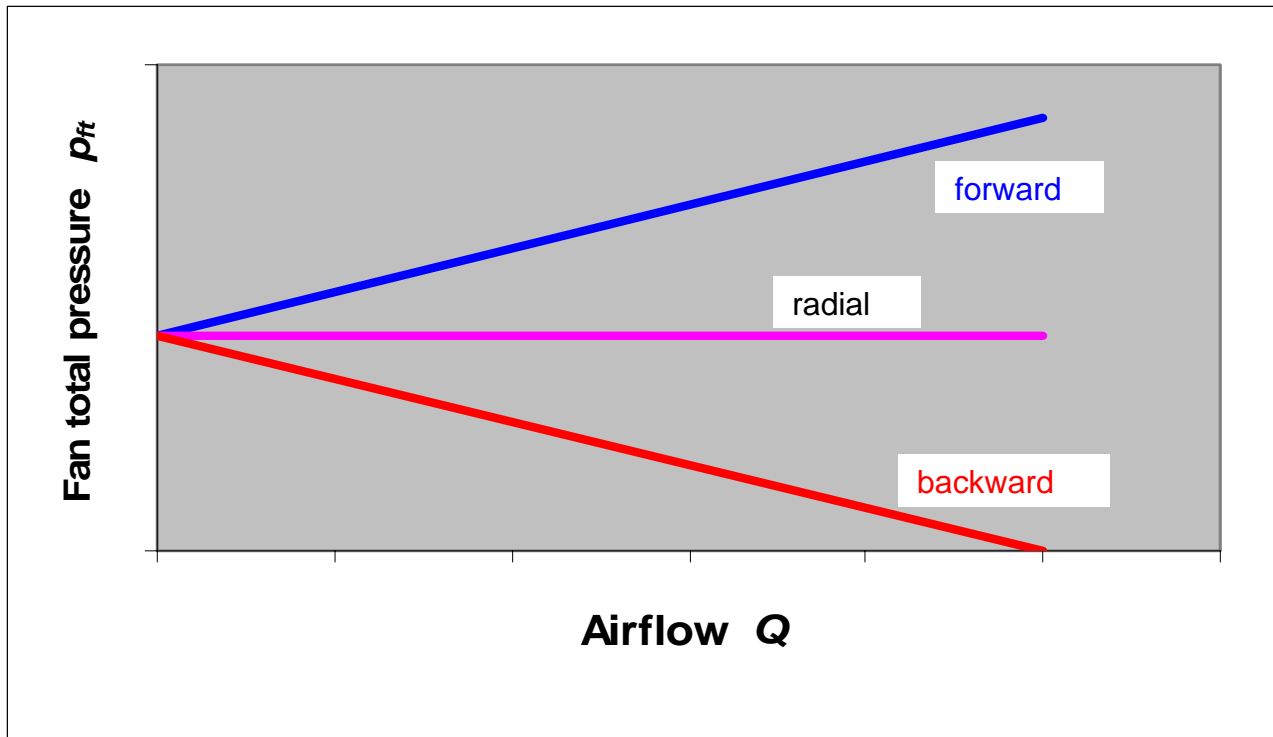
10.3.1.3. Actual characteristic curves for a centrifugal impeller

The theoretical treatment of the preceding subsections lead to linear pressure-volume relationships for radial, backward and forward bladed centrifugal impellers. In an actual fan, there are, inevitably, losses which result in the real pressure-volume curves lying below their theoretical counterparts. In all cases, friction and shock losses produce pressure-volume curves that tend toward zero pressure when the fan runs on open circuit, that is, with no external resistance.

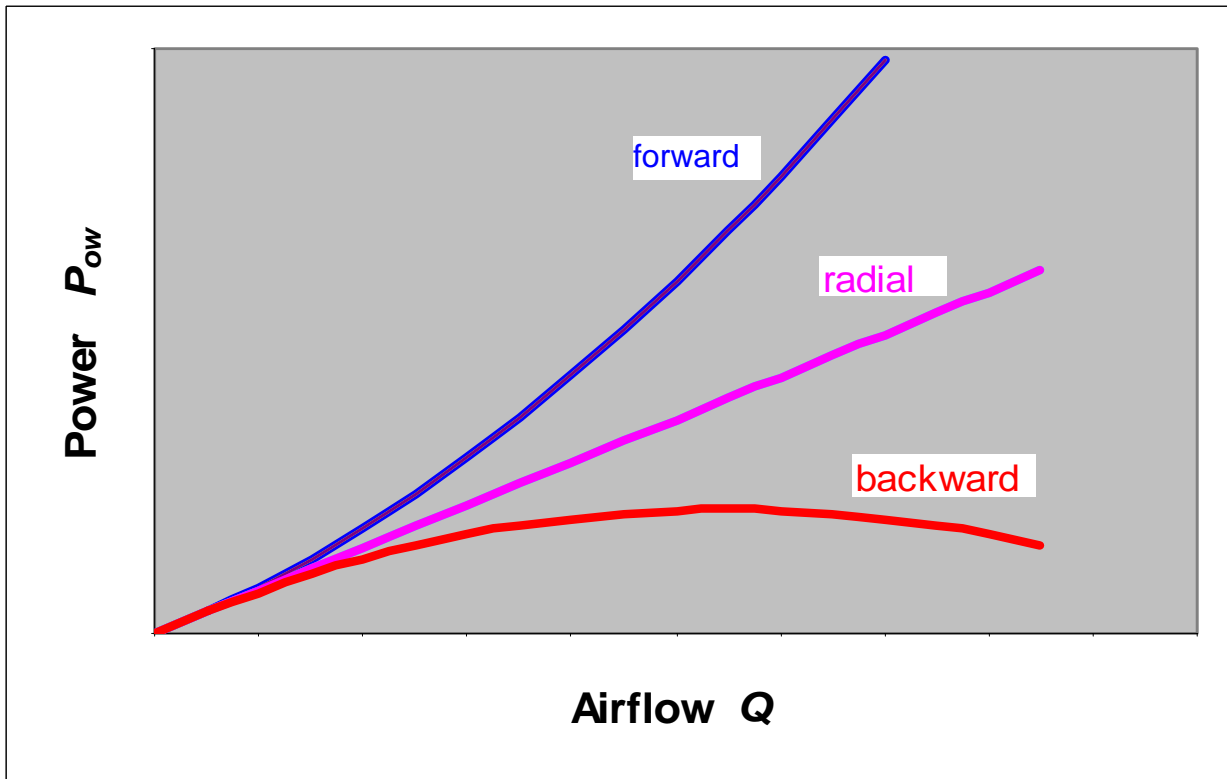
Figure 10.5 shows a typical pressure-volume characteristic curve for a backward bladed centrifugal fan. **Frictional losses** occur due to the viscous drag of the fluid on the faces of the vanes. These are denoted as F_f and F_b on Figure 10.3. A **diffuser effect** occurs in the diverging area available for flow as the fluid moves through the impeller. This results in a further loss of available energy. In order to transmit mechanical work, the pressure on the front face of a vane, p_f is necessarily greater than that on the back, p_b . A result of this is that the fluid velocity close to the trailing face is higher than that near the front face. These effects result in an asymmetric distribution of fluid velocity between two successive vanes at any given radius and produce an **eddy loss**. It may also be noted that at the outlet tip, the two pressures p_f and p_b must become equal. Hence, although the tip is most important in its influence on the outlet vector diagram, it does not actually contribute to the transfer of mechanical energy. The transmission of power is not uniform along the length of the blade.

The **shock** (or separation) losses occur particularly at inlet and reflect the sudden turn of near 90° as the fluid enters the eye of the impeller. In practice, wall effects impart a vortex to the fluid as it approaches the inlet. By a suitable choice of inlet blade angle, β_1 , (Figure 10.3) the shock losses may be small at the optimum design flow. An inlet cone at the eye of the impeller or fixed inlet and outlet guide vanes can be fitted to reduce shock losses.

In the development of the theoretical pressure and power characteristics, we assumed radial inlet conditions. When the fluid has some degree of pre-rotation, the flow is no longer radial at the inlet to the impeller. The second term in Euler's equation (10.11) takes a finite value and, again, results in a reduced fan pressure at any given speed of rotation.



(a) Pressure-volume theoretical characteristics



(b) Power-volume theoretical characteristics

Figure 10.4 Theoretical characteristic curves for a centrifugal fan

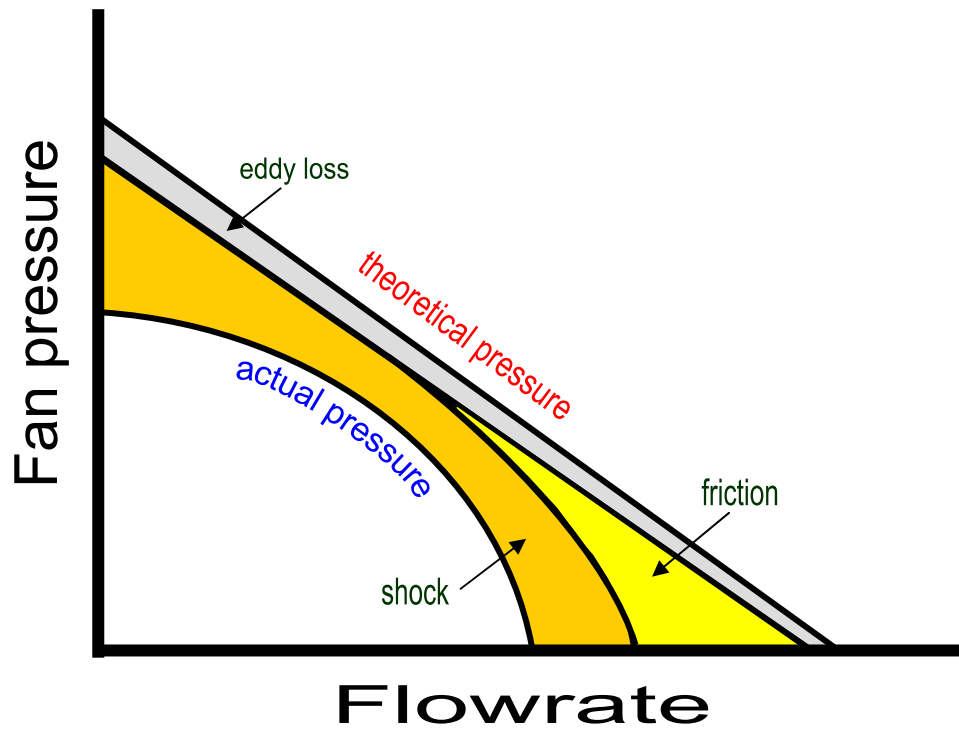


Figure 10.5 Effect of losses on the pressure-volume characteristic of a backward bladed centrifugal fan.

The combined effect of these losses on the three types of centrifugal impeller is to produce the characteristic curves shown on Figure 10.6. The non-overloading power characteristic, together with the steepness of the pressure curve at the higher flows, are major factors in preferring the backward impeller for large installations.

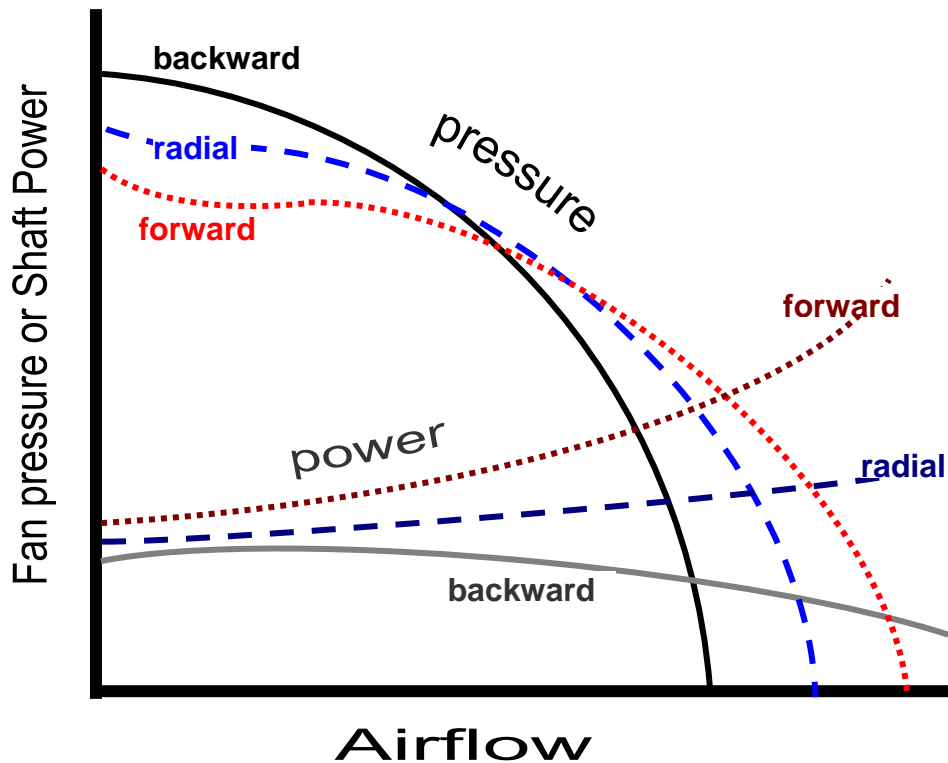


Figure 10.6 Actual pressure and shaft power characteristics for centrifugal impellers.

10.3.2. The axial impeller

Axial fans of acceptable performance did not appear until the 1930's. This was because of a lack of understanding of the behaviour of airflow over axial fan blades. The early axial fans had simple flat angled blades and produced very poor efficiencies. The growth of the aircraft industry led to intensive studies of aerofoils for the wings of aeroplanes. In this section, we shall discuss briefly the characteristics of aerofoils. This facilitates our comprehension of the behaviour of axial fans. The theoretical treatment of axial impellers may be undertaken from the viewpoint of a series of aerofoils or by employing either vortex or momentum theory. We shall use the latter in order to remain consistent with our earlier analysis of centrifugal impeller although aerofoil theory is normally also applied in the detailed design of axial impellers.

10.3.2.1. Aerofoils

When a flat stationary plate is immersed in a moving fluid such that it lies parallel with the direction of flow then it will be subjected to a small **drag force** in the direction of flow. If it is then inclined upward at a small angle, α , to the direction of flow then that drag force will increase. However, the deflection of streamlines will cause an increase in pressure on the underside and a decrease in pressure on the top surface. This pressure differential results in a lifting force. On an aircraft wing and in an axial fan impeller, it is required to achieve a high **lift**, L , without unduly increasing the **drag**, D . The dimensionless **coefficients of lift**, C_L , and **drag**, C_D , for any given section are defined in terms of velocity heads

$$L = \rho \frac{C^2}{2} AC_L \quad \text{N} \quad (10.18)$$

$$D = \rho \frac{C^2}{2} AC_D \quad \text{N} \quad (10.19)$$

where C = fluid velocity (m/s) and

A = a characteristic area usually taken as the underside of the plate or aerofoil (m^2)

The ratio of C_L/C_D is considerably enhanced if the flat plate is replaced by an aerofoil. Figure 10.7 illustrates an aerofoil section. Selective evolution in the world of nature suggests that it is no

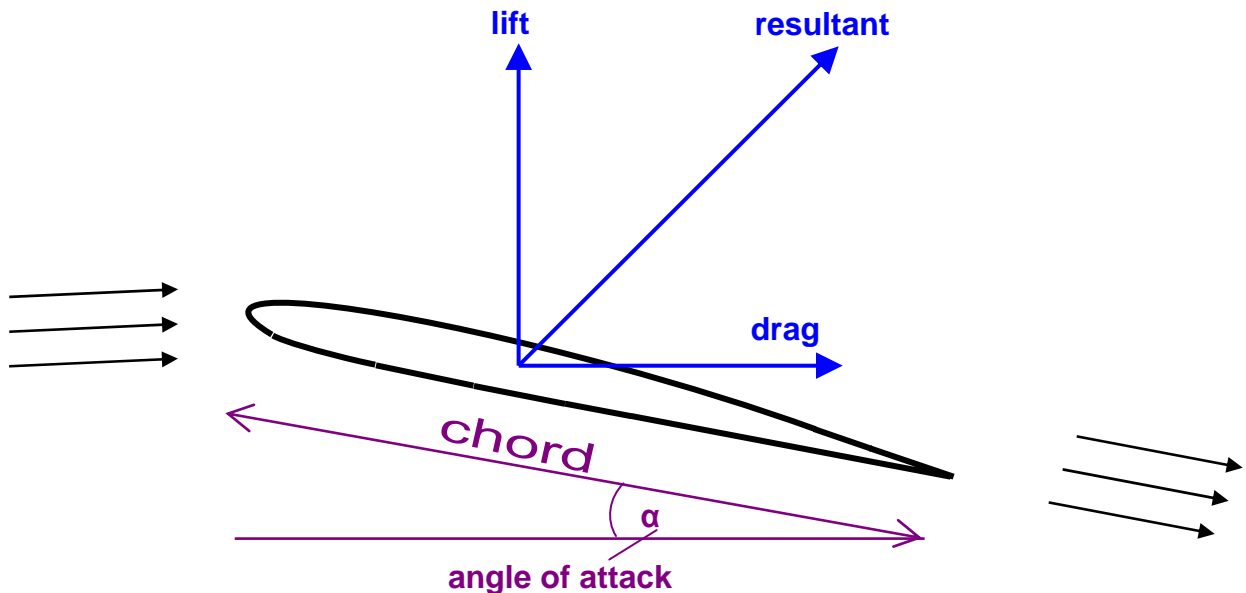


Figure 10.7 An aerofoil section.

coincidence that the aerofoil shape is decidedly fish-like. The line joining the facing and trailing edges is known as the chord while the **angle of attack**, α , is defined as that angle between the chord and the direction of the approaching fluid.

A typical behaviour of the coefficients of lift and drag for an aerofoil with respect to angle of attack is illustrated on Figure 10.8. Note that the aerofoil produces lift and a high C_L/C_D ratio at zero angle of attack. The coefficient of lift increases in a near-linear manner. However, at an angle of attack usually between 12 and 18°, breakaway of the boundary layer occurs on the upper surface. This causes a sudden loss of lift and an increase in drag. In this **stall condition**, the formation and propagation of turbulent vortices causes the fan to vibrate excessively and to produce additional low frequency noise. A fan should never be allowed to run continuously in this condition as it can cause failure of the blades and excessive wear in bearings and other transmission components.

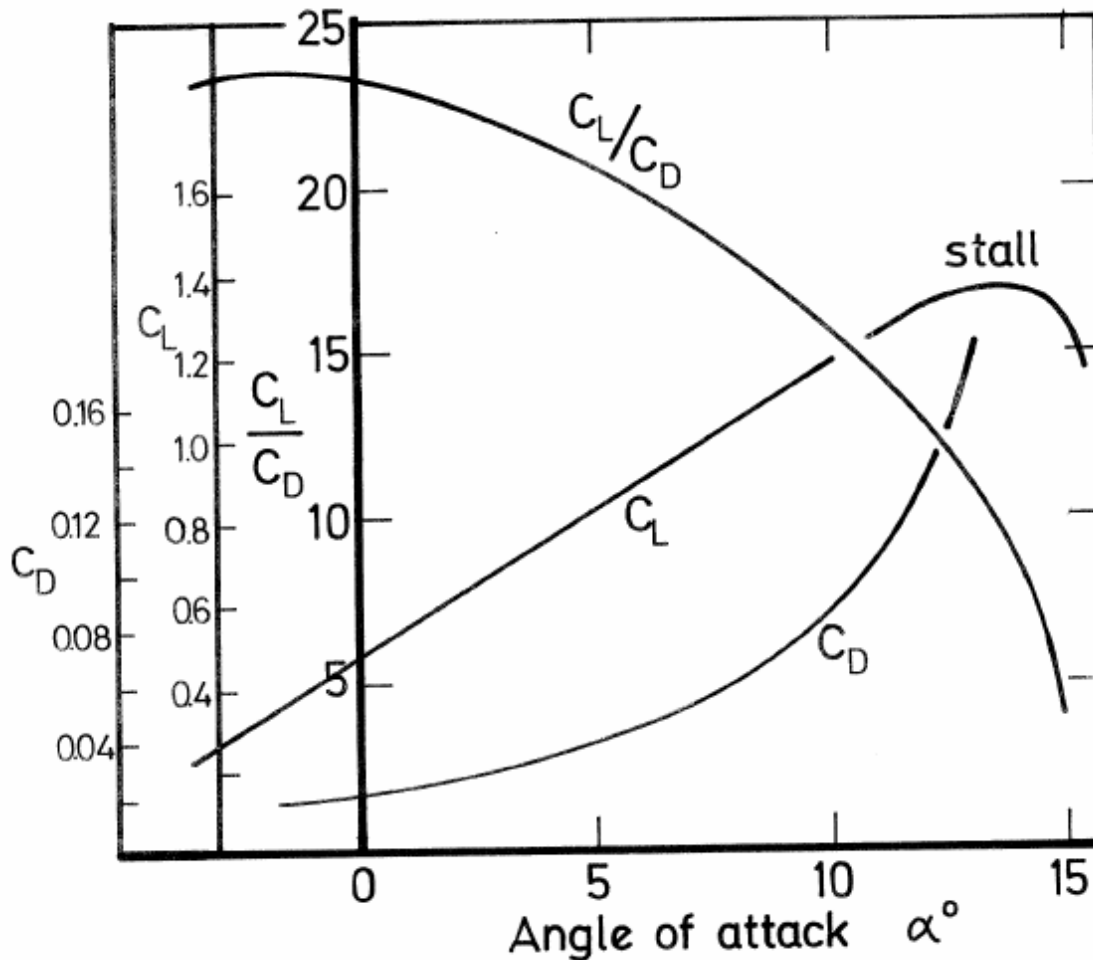
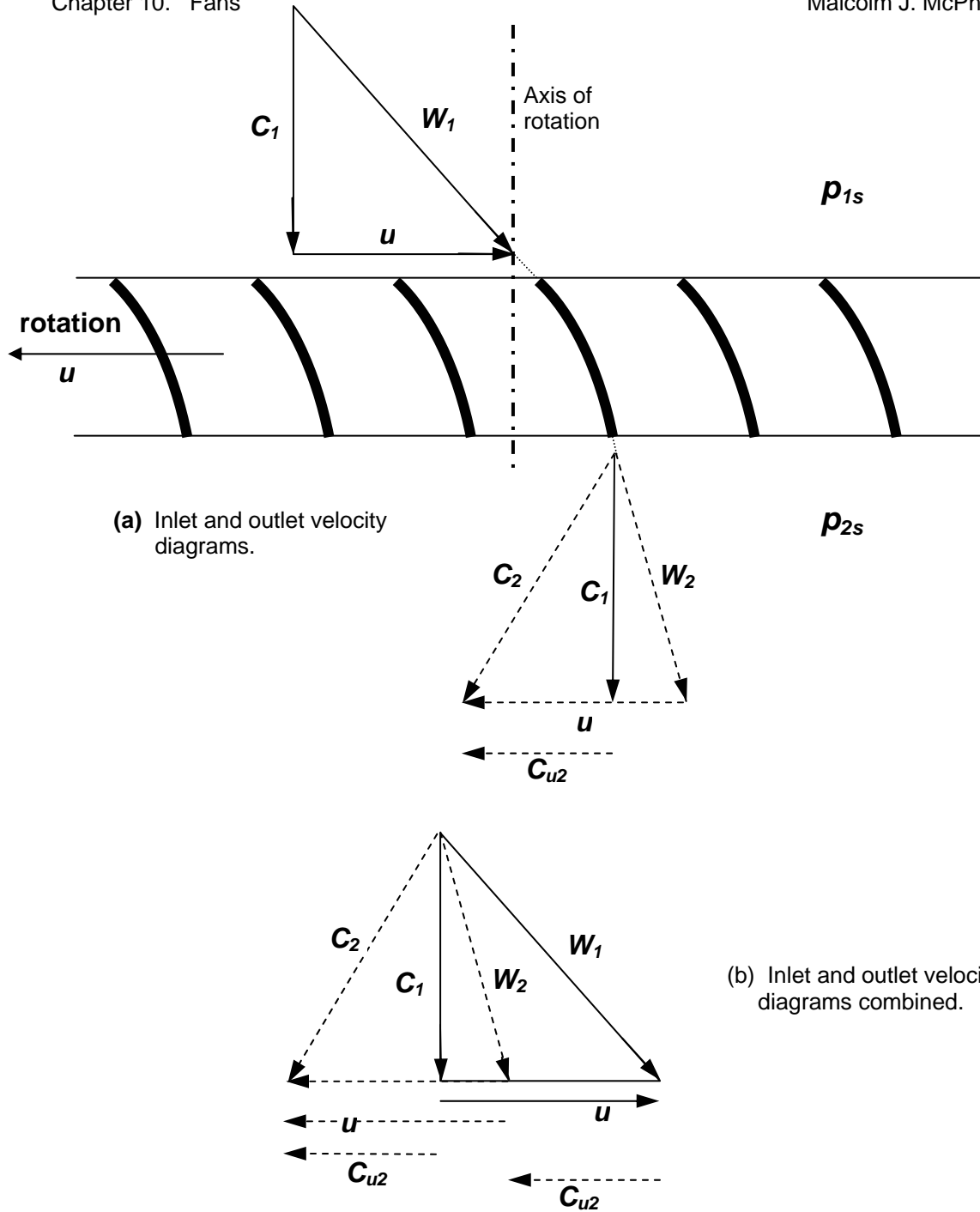


Figure 10.8 Typical behaviour of lift and drag coefficients for an aerofoil.

10.3.2.2. Theoretical pressure developed by an axial fan

Consider an imaginary cylinder coaxial with the drive shaft and cutting through the impeller blades at a constant radius. Depicting an impression of the cut blades on two dimensional paper produces a drawing similar to that of Figure 10.9 (a). For simplicity each blade is shown simply as a curved vane rather than an aerofoil section.



(a) Inlet and outlet velocity diagrams.

(b) Inlet and outlet velocity diagrams combined.

Figure 10.9 Velocity diagrams for an axial impeller without guide vanes.

The air approaches the moving impeller axially at a velocity, C_1 . At the optimum design point, the C_1 vector combines with the blade velocity vector, u , to produce a velocity relative to the blade W_1 , and which is tangential to the leading edge of the blade. At the trailing edge, the air leaves at a relative velocity W_2 , which also combines with the blade velocity to produce the outlet absolute velocity, C_2 . This has a rotational component, C_{u2} , imparted by the rotation of the impeller. The initial axial velocity, C_1 , has remained unchanged as the impeller has no component of axial velocity in an axial fan.

Figure 10.9 (b) shows how the inlet and outlet velocity diagrams can be combined. As W_1 and W_2 are both related to the same common blade velocity, u , the vector difference between the two, $W_1 - W_2$, must be equal to the final rotational component C_{u2} .

As the axial velocity, C_1 is the same at outlet as inlet, it follows that the increase in total pressure across the impeller is equal to the rise in static pressure.

$$p_{ft} = p_{2s} - p_{1s}$$

Now let us consider again the relative velocities, W_1 and W_2 . Imagine for a moment that the impeller is standing still. It would impart no energy and Bernoulli's equation (2.16) tells us that the increase in static pressure must equal the decrease in velocity pressure (in the absence of frictional losses). Hence

$$p_{ft} = p_{2s} - p_{1s} = \rho \left[\frac{W_1^2}{2} - \frac{W_2^2}{2} \right] \quad \text{Pa} \quad (10.20)$$

Applying Pythagoras' Theorem to Figure 10.9 (b) gives

$$W_1^2 = C_1^2 + u^2$$

and $W_2^2 = C_1^2 + (u - C_{u2})^2$

giving $p_{ft} = \frac{\rho}{2} [2C_{u2}u - C_{u2}^2]$

i.e. $p_{ft} = \rho u C_{u2} - \rho \frac{C_{u2}^2}{2} \quad (10.21)$

Comparison with equation (10.12) shows that this is the pressure given by Euler's equation, less the velocity head due to the final rotational velocity.

The vector diagram for an axial impeller with **inlet guide vanes** is given on Figure 10.10. In order to retain subscripts 1 and 2 for the inlet and outlet sides of the moving impeller, subscript 0 is employed for the air entering the inlet guide vanes. At the optimum design point the absolute velocities, C_0 and C_2 should be equal and axial, i.e. there should be no rotational components of velocity at either inlet or outlet of the guide vane/impeller combination. This means that any vortex action imparted by the guide vanes must be removed by an equal but opposite vortex action imparted by the impeller.

We can follow the process on the vector diagram on Figure 10.10 using the labelled points a, b, c, d, and e.

(a) The air arrives at the entrance to the guide vanes with an axial velocity, C_0 , and no rotational component (point a)

(b) The turn on the inlet guide vanes gives a rotational component, C_{u1} to the air. The axial component remains at C_0 . Hence, the vector addition of the two results in the absolute velocity shown as C_1 (point b).

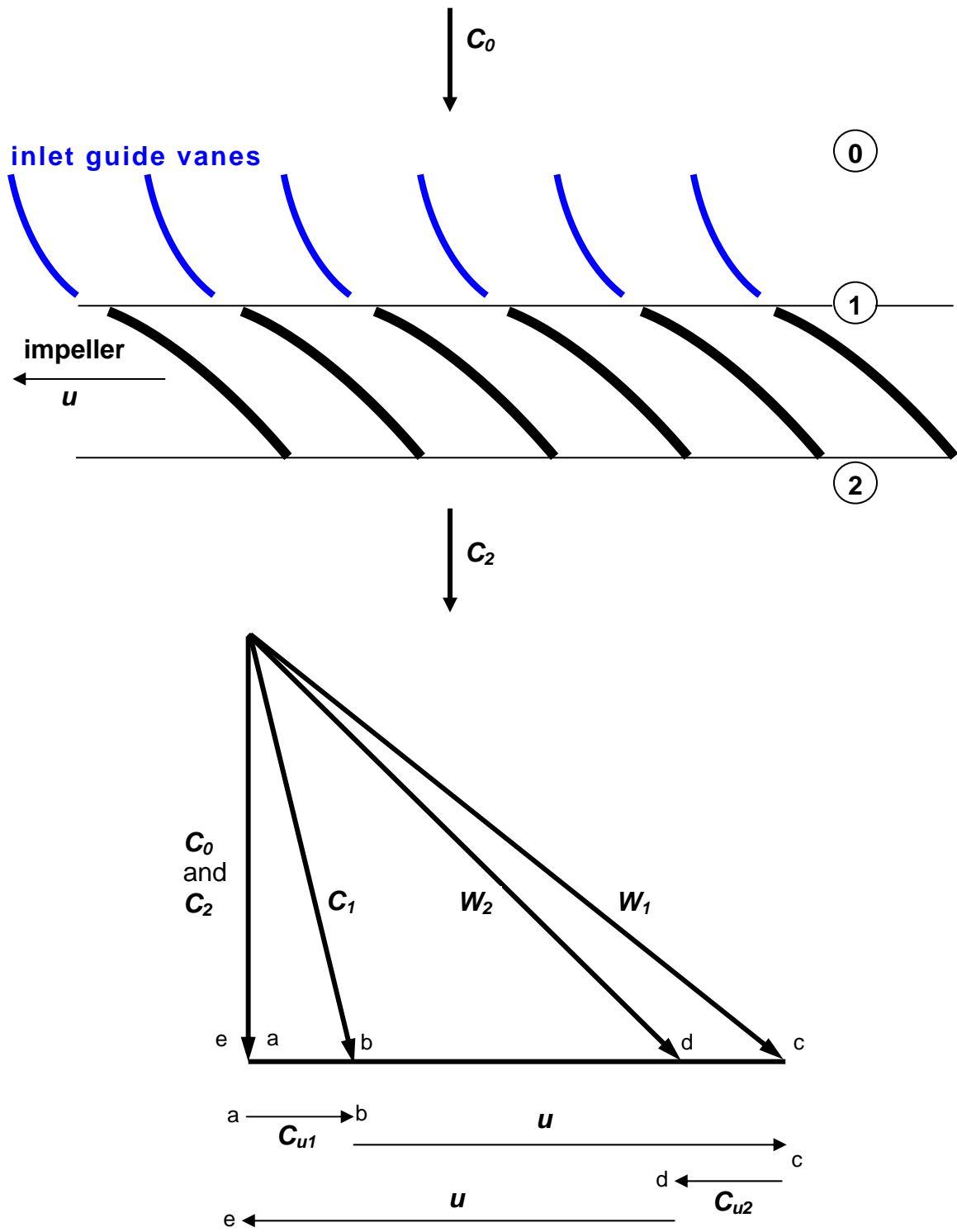


Figure 10.10 Velocity diagrams for an axial impeller with inlet guide vanes.

(c) In order to determine the velocity of the air relative to the moving impeller at location (1), we must subtract the velocity vector of the impeller, u . This brings us to position c on the vector diagram and an air velocity of W_1 relative to the impeller.

(d) The turn on the impeller imparts a rotational component C_{u2} to the air. The velocity of the air relative to the impeller is thus reduced to W_2 and we arrive at point d.

(e) In order to determine the final absolute velocity of the air, we must add the impeller velocity, u . This will take us to point e on the vector diagram (coinciding with point a), with no remaining rotational component **provided that $C_{u1} = C_{u2}$** .

It follows that the absolute velocities at inlet and outlet, C_o and C_2 , must be both axial and equal.

To determine the total theoretical pressure developed by the system, consider first the stationary inlet guide vanes (subscript g). From Bernoulli's equation with no potential energy term

$$p_g = \rho \left[\frac{C_o^2 - C_1^2}{2} \right]$$

Applying Pythagoras' theorem to the vector diagram of Figure 10.10 gives this to be

$$p_g = -\rho \frac{C_{u1}^2}{2} \quad (10.22)$$

and represents a pressure loss caused by rotational acceleration across the guide vanes.

The gain in total pressure across the impeller (subscript i) is given as

$$p_i = \frac{\rho}{2} (W_1^2 - W_2^2) \quad (10.23)$$

(see, also, equation (10.20))

Using Pythagoras on Figure 10.10 again, gives this to be

$$\begin{aligned} p_i &= \frac{\rho}{2} (C_o^2 + (u + C_{u2})^2 - (C_o^2 + u^2)) \\ &= \frac{\rho}{2} (C_{u2}^2 + 2C_{u2}u) \end{aligned}$$

But, as $C_{u1} = C_{u2}$, this can also be written as

$$p_i = \frac{\rho}{2} (C_{u1}^2 + 2C_{u2}u) \quad \text{Pa} \quad (10.24)$$

Now the total theoretical pressure developed by the system, p_{ft} must be the combination $p_g + p_i$.

Equations (10.22) and (10.24) give

$$p_{ft} = p_g + p_i = \rho C_{u2}u \quad \text{Pa} \quad (10.25)$$

Once again, we have found that the theoretical pressure developed by a fan is given by **Euler's equation** (10.12). Furthermore, comparison with equation (10.21) shows that elimination of the **residual** rotational component of velocity at outlet (by balancing C_{u1} and C_{u2}) results in an increased fan pressure when guide vanes are employed.

The reader might wish to repeat the analysis for outlet guide vanes and for a combination of inlet and outlet guide vanes. In these cases, Euler's equation is also found to remain true. Hence, wherever the guide vanes are located, the total pressure developed by an axial fan operating at its design point depends only upon the rotational component imparted by the impeller, C_{u2} , and the peripheral velocity of the impeller, u .

It is obvious that the value of u will increase along the length of the blade from root to tip. In order to maintain a uniform pressure rise and to inhibit undesirable cross flows, the value of C_{u2} in equation (10.25) must balance the variation in u . This is the reason for the "twist" that can be observed along the blades of a well-designed axial impeller.

10.3.2.3. Actual characteristic curves for an axial fan

The losses in an axial fan may be divided into **recoverable** and **non-recoverable** groups. The recoverable losses include the vortices or rotational components of velocity that exist in the airflow leaving the fan. We have seen that these losses can be recovered when operating at the design point by the use of guide vanes. However, as we depart from the design point, swirling of the outlet air will build up.

The non-recoverable losses include friction at the bearings and drag on the fan casing, the hub of the impeller, supporting beams and the fan blades themselves. These losses result in a transfer from mechanical energy to heat which is irretrievably lost in its capacity for doing useful work.

Figure 10.11 is an example of the actual characteristic curves for an axial fan. The **design point**, C, coincides with the maximum efficiency. At this point the losses are at a minimum. In practice, the region A to B on the pressure curve would be acceptable. Operating at low resistance, i.e. to the right of point B, would not draw excessive power from the motor as the shaft power curve shows a non-overloading characteristic. However, the efficiency decreases rapidly in this region.

The disadvantage of operating at too high a resistance, i.e. to the left of point A is, again, a decreasing efficiency but, more importantly, the danger of approaching the stall point, D. There is a definite discontinuity in the pressure curve at the stall point although this is often displayed as a smoothed curve. Indeed, manufacturers' catalogues usually show characteristic curves to the right of point A only. In the region E to D, the flow is severely restricted. Boundary layer breakaway takes place on the blades (Section 10.3.2.1) and centrifugal action occurs producing recirculation around the blades.

A fixed bladed axial fan of constant speed has a rather limited useful range and will maintain good efficiency only when the system resistance remains sensibly constant.. This can seldom be guaranteed over the full life of a main mine fan. Fortunately, there are a number of ways in which the range of an axial fan can be extended:-

- (a) The **angle of the blades** may be varied. Many modern axial fans allow blade angles to be changed, either when the rotor is stationary or while in motion. The latter is useful if the fan is to be incorporated into an automatic ventilation control system. Figure 10.12 gives an example of the characteristic curves for an axial fan of variable blade angle. The versatility of such fans gives them considerable advantage over centrifugal fans.

- (b) The **angle of the inlet and/or outlet guide vanes** may also be varied, with or without modification to the impeller blade angle. The effect is similar to that illustrated by Figure 10.12.
- (c) The **pitch of the impeller** may be changed by adding or removing blades. The impeller must, of course, remain dynamically balanced. This technique can result in substantial savings in power during time periods of relatively light load.
- (d) The **speed of the impeller** may be changed either by employing a variable speed motor or by changing the gearing between the motor and the fan shaft. The majority of fans are driven by A.C. induction motors at a fixed speed. Variable speed motors are more expensive although they may produce substantial savings in operating costs. Axial fans may be connected to the motor via flexible couplings which allow a limited degree of angular or linear misalignment. Speed control may be achieved by hydraulic couplings, or, in the case of smaller fans, by V-belt drives with a range of pulley sizes.

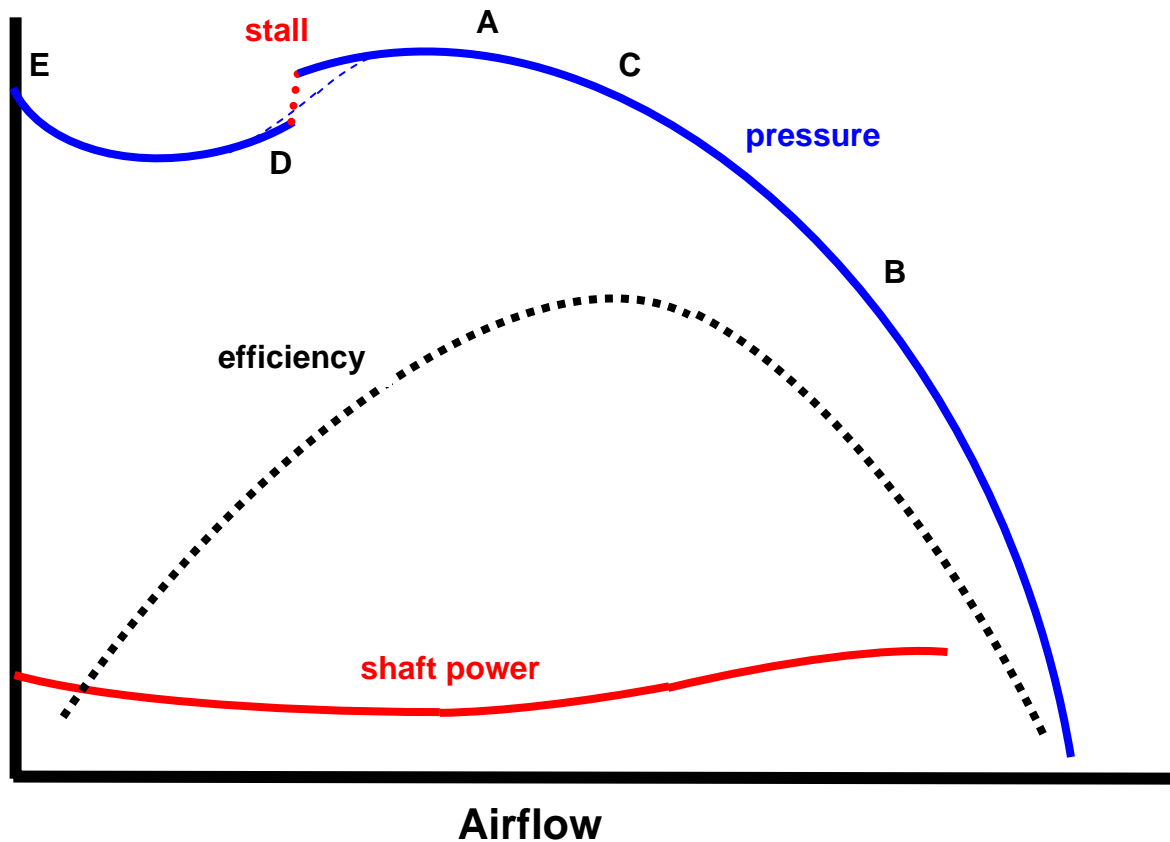


Figure 10.11 Typical characteristic curves for an axial fan.

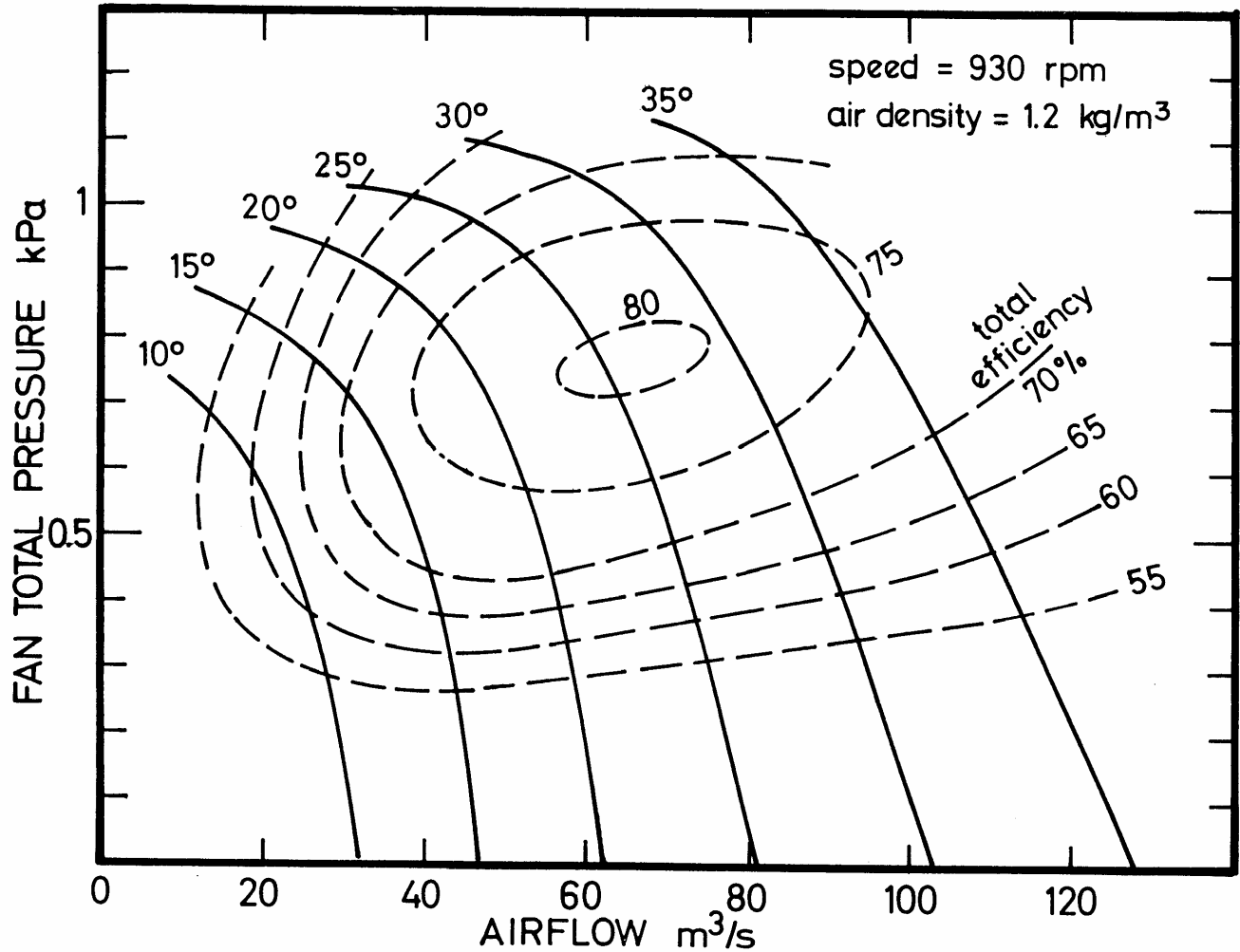


Figure 10.12 Example of a set of characteristic curves for an axial fan with variable blade angle.

10.4 FAN LAWS

The performance of fans is normally specified as a series of pressure, efficiency and shaft power characteristic curves plotted against airflow for specified values of rotational speed, air density and fan dimensions. It is, however, convenient to be able to determine the operating characteristic of the fan at other speeds and air densities. It is also useful to be able to use test results gained from smaller prototypes to predict the performance of larger fans that are geometrically similar.

Euler's equation and other relationships introduced in Section 10.3 can be employed to establish a useful set of proportionalities known as the fan laws.

10.4.1. Derivation of the fan laws

Fan pressure

From Euler's equation (10.12 and 10.25)

$$p_{ft} = \rho u C_{u2}$$

However, both the peripheral speed, u , and the rotational component of outlet velocity, C_{u2} (Figures 10.3 and 10.10) vary with the rotational speed, n , and the impeller diameter, d . Hence,

$$p_{fi} \propto \rho(nd)(nd)$$

or

$$p_{fi} \propto \rho n^2 d^2 \quad (10.26)$$

where \propto means 'proportional to.'

Airflow

For a centrifugal fan, the radial flow at the impeller outlet is given as

$$\begin{aligned} Q &= \text{area of flow at impeller outlet} \times C_{m2} \\ &= \pi d \times \text{impeller width} \times C_{m2} \end{aligned}$$

where d = diameter of impeller
and C_{m2} = radial velocity at outlet (Figure 10.3)

However, for geometric similarity between any two fans

$$\begin{aligned} &\text{impeller width} \propto d \\ \text{giving} & \quad Q \propto d^2 C_{m2} \end{aligned}$$

Again, for geometric similarity, all vectors are proportional to each other. Hence

$$\begin{aligned} &C_{m2} \propto u \propto nd \\ \text{giving} & \quad Q \propto nd^3 \quad (10.27) \end{aligned}$$

A similar argument applies to the axial impeller (Figure 10.10). At outlet,

$$Q = \frac{\pi d^2}{4} \times C_2$$

where C_2 = axial velocity

As before, vectors are proportional to each other for geometric similarity,

$$\begin{aligned} &C_2 \propto u \propto nd \\ \text{giving, once again,} & \end{aligned}$$

$$Q \propto nd^3$$

Density

From Euler's equation (10.12 or 10.25) it is clear that fan pressure varies directly with air density

$$p_{fi} \propto \rho \quad (10.28)$$

However, we normally accept volume flow, Q , rather than mass flow as the basis of flow measurement in fans. In other words, if the density changes we still compare operating points at corresponding values of volume flow.

Air Power

For incompressible flow, the mechanical power transmitted from the impeller to the air is given as

$$P_{ow} = p_{ft} Q \quad (\text{see equation (5.56)})$$

Employing proportionalities (10.26) and (10.27) gives

$$P_{ow} \propto \rho n^3 d^5 \quad (10.29)$$

10.4.2. Summary of fan laws

In the practical utilization or design of fans, we are normally interested in varying only one of the independent variables (speed, air density, impeller diameter) at any given time while keeping the other two constant. The fan laws may then be summarized as follows:

Variable speed (n)	Variable diameter (d)	Variable air density (ρ)
$p \propto n^2$	$p \propto d^2$	$p \propto \rho$
$Q \propto n$	$Q \propto d^3$	Q fixed
$P_{ow} \propto n^3$	$P_{ow} \propto d^5$	$P_{ow} \propto \rho$

These laws can be applied to compare the performance of a given fan at changed speeds or air densities, or to compare the performance of different sized fans provided that those two fans are geometrically similar.

If the two sets of operating conditions, or the two geometrically similar fans are identified by subscripts a and b, then the fan laws may be written, more generally, as the following equations

$$\frac{p_{ft,a}}{p_{ft,b}} = \frac{n_a^2}{n_b^2} \frac{d_a^2}{d_b^2} \frac{\rho_a}{\rho_b} \quad (10.30)$$

$$\frac{Q_a}{Q_b} = \frac{n_a}{n_b} \frac{d_a^3}{d_b^3} \quad (10.31)$$

$$\frac{P_{ow,a}}{P_{ow,b}} = \frac{n_a^3}{n_b^3} \frac{d_a^5}{d_b^5} \frac{\rho_a}{\rho_b} \quad (10.32)$$

where p_{ft} = fan pressure (applies for both total and static pressure)
 Q = airflow
 P_{ow} = airpower
 n = rotational speed
 d = impeller diameter
 and ρ = air density

Example.

Characteristic curves are available for a fan running at 850 rpm and passing air of inlet density 1.2 kg/m^3 . Readings from the curves indicate that at an airflow of $150 \text{ m}^3/\text{s}$, the fan pressure is 2.2 kPa and the shaft power is 440 kW . Assuming that the efficiency remains unchanged, calculate the corresponding points if the fan is run at 1100 rpm in air of density 1.1 kg/m^3 .

Solution.

As it is the same fan that is to be used in differing conditions, there is no change in impeller diameter or overall geometry.

Equation (10.30) gives the new pressure to be

$$p_f = 2.2 \left(\frac{1100}{850} \right)^2 \frac{1.1}{1.2} = 3.377 \quad \text{kPa}$$

From equation (10.31), the new volume flow is

$$Q = 150 \times \frac{1100}{850} = 194.1 \quad \text{m}^3/\text{s}$$

Equation (10.32) refers to the airpower rather than the shaft delivered to the impeller. However, if we assume that the impeller efficiency remains the same at corresponding points on the characteristic curves then we may also use that equation for shaft power.

$$P_{ow} = 440 \times \left(\frac{1100}{850} \right)^3 \times \frac{1.1}{1.2} = 874 \text{ kW}$$

By treating a series of points from the original curves in this way, a second set of characteristic curves can be produced that is applicable to the new conditions.

10.5. FANS IN COMBINATION

Many mines or other subsurface facilities have main and, perhaps, booster fans sited at differing locations; for example, there may be two or more upcast shafts, each with its own surface exhausting fan. With the advent of simulation programs for ventilation network analysis (Chapters 7 and 9), the relevant pressure-volume characteristic data may be entered separately for each fan unit. The system resistance offered to each of those fans becomes a function not only of the network geometry but also the location and operating characteristics of other fans in the system. That resistance is sometimes termed the **effective resistance** 'seen' by the fan.

There are situations in which it is advantageous to combine fans either in series or in parallel at a single location. Such combinations enable a wide spectrum of pressure-volume duties to be attained with only a limited range of fan sizes. In general, fans may be connected in series in order to pass a given airflow against an increased resistance, while a parallel combination allows the flow to be increased for any given resistance. Although ventilation network programs can allow each fan to be entered separately, it is sometimes more convenient to produce a pressure-volume characteristic curve that represents the combined unit.

10.5.1. Fans in series

Figure 10.13 shows two fans, **a** and **b**, located in series within a single duct or airway. The corresponding pressure-volume characteristics and the effective resistance curve are also shown. The characteristic curve for the combination is obtained simply by adding the individual fan pressures for each value of airflow.

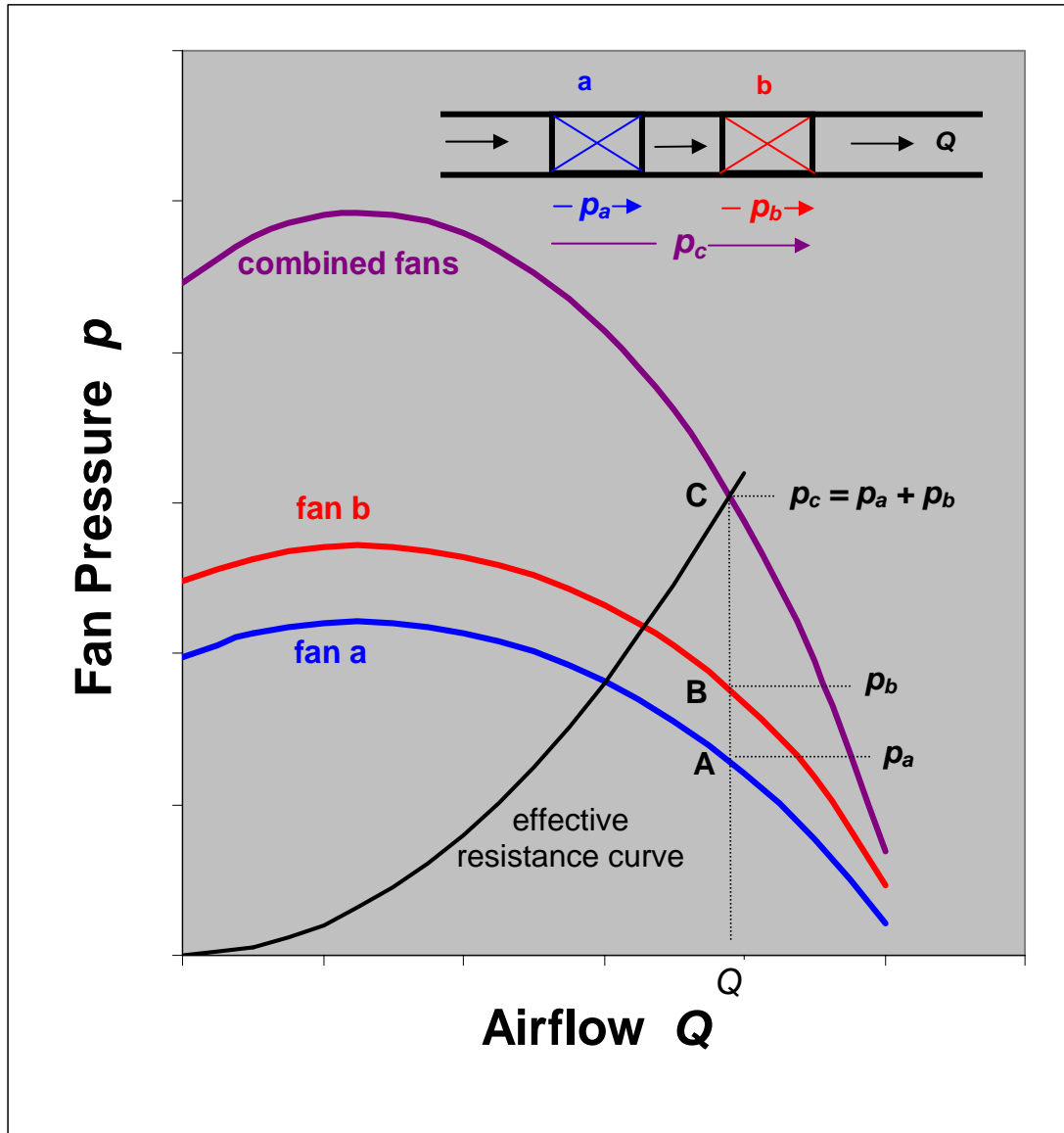


Figure 10.13 Characteristic curves for two fans connected in series.

The effective operating point is located at C, where the resistance curve intersects the combined characteristic. Fans **a** and **b** both pass the same airflow, Q , but develop pressures p_a and p_b respectively. The individual operating points are shown as A and B. For three or more fans, the process of adding fan pressures remains the same. However, if the change in density through the

combination becomes significant then the fan laws (Section 10.4.2) should be employed to correct the individual characteristic curves.

As shown in Figure 10.13, the individual fans need not have identical characteristic curves. However, if one fan is considerably more powerful than the other, or if the system resistance falls to a low level, then the impeller of the weaker unit may be driven in turbine fashion by its stronger companion. The weaker fan then becomes an additional resistance on the system. It is usual to employ identical fans in combination.

10.5.2. Fans in parallel

For fans that are combined in parallel, the airflows are added for any given fan pressure in order to obtain the combined characteristic curve. As shown in Figure 10.14, fans **a** and **b** pass airflows Q_a and Q_b , respectively, but at the same common pressure, p .

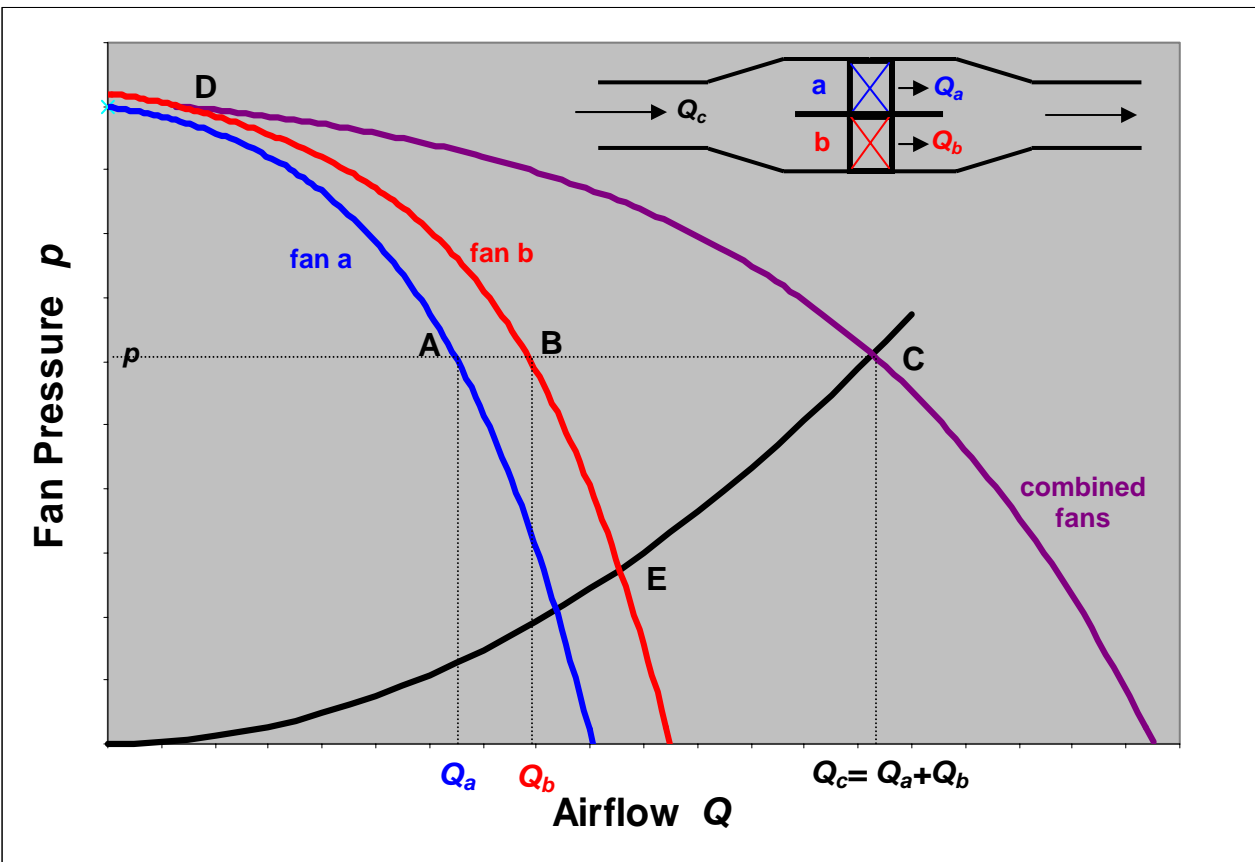


Figure 10.14 Characteristic curves for two fans connected in parallel.

The operating point for the complete unit occurs at C with the individual operating points for fans **a** and **b** at A and B respectively. Here again, the fans need not necessarily be identical. However, care must be taken to ensure that the operating points A and B do not move too far up their respective curves. This is particularly important in the case of axial fans because of their pronounced stall characteristic. In practice, before this condition is reached, the fans may exhibit

a noticeable "hunting" effect. For these reasons, the maximum variation in system resistance that is likely to occur should be investigated before installing fans in parallel.

Three or more fans may be combined in parallel, adding airflows to obtain the combined characteristic curve. Although Figure 10.14 shows two fans with differing characteristics, it is prudent to employ identical fans when connected in parallel. This will reduce the tendency for one of them to approach stall conditions before the other. However, variations in the immediate surroundings of ductwork or airway geometry often results in the fans operating against slightly different effective resistances. Hence, even when identical fans are employed, it is usual for measurements to indicate that they are producing slightly different pressure-volume duties. In the case of fans located in separate ducts or airways that are connected in parallel, the resistance of those ducts or airways may be taken into account by subtracting the frictional pressure losses in each branch from the corresponding fan pressures. In these circumstances, a better approach is to consider the fans as separate units for the purposes of network analysis.

An advantage of employing fans in parallel is that if one of them fails then the remaining fan(s) continue to supply a significant proportion of the original flow. In the example shown on Figure 10.14, if fan **a** ceases to operate then the operating point for fan **b** will fall to position E, giving some 70 per cent of the original airflow. The latter value depends upon the number of fans employed, the shape of their pressure-volume characteristic curves and the provision of non-return baffles at the fan outlets.

Fans may be connected in any **series/parallel configuration**, adding pressures and airflows respectively to obtain the combined characteristic curve. This is particularly useful for booster fan locations. A mine may maintain an inventory of standard fans, combining them in series/parallel combinations to achieve any desired operating characteristic.

10.6. FAN PERFORMANCE

Power is delivered to the drive shaft of a fan impeller from a motor (usually electric) and via a transmission assembly. Losses occur in both the motor and transmission. For a properly maintained electrical motor and transmission, some 95 per cent of the input electrical power may be expected to appear as mechanical energy in the impeller drive shaft. The impeller, in turn, converts most of that energy into useful airpower to produce both movement of the air and an increase in pressure. The remainder is consumed by irreversible losses across the impeller and in the fan casing (Sections 10.3.1.3 and 10.3.2.3) producing an additional increase in the temperature of the air.

Impeller efficiency may be defined as

$$\frac{\text{Airpower}}{\text{Shaft power}} \quad (10.33)$$

while the **overall efficiency** of the complete motor/transmission/impeller unit is given as

$$\frac{\text{Airpower}}{\text{Motor input power}} \quad (10.34)$$

In the following subsection, we shall define other measures of fan efficiency. As there are several different forms of fan efficiency it is prudent, when perusing manufacturers' literature, to ascertain the basis of any quoted values of efficiencies. It is also important to use the same measure of efficiency when comparing one fan with another. However, the one parameter that really matters is the input power required to achieve the specified pressure-volume duty, as this is the factor that dictates the operating cost of the fan.

10.6.1. Compressibility, fan efficiency, and fan testing

In our previous analyses, we have defined **airpower** as the product pQ on the basis of incompressible flow. That simplification will give an error of less than one percent when testing fans that develop pressures up to 2.8 kPa. Unfortunately, fan operating costs at many large mines are such that one per cent may represent a significant expenditure. Furthermore, mine fan pressures exceeding 6 kPa are not uncommon. For these reasons, we should take air compressibility into account when measuring fan performance.

Applying the steady-flow energy equation (3.25) to a fan gives

$$\frac{u_1^2 - u_2^2}{2} + (Z_1 - Z_2)g + W = \int_1^2 VdP + F_{12} = (H_2 - H_1) - q_{12} \quad \frac{\text{J}}{\text{kg}} \quad (10.35)$$

where subscripts 1 and 2 refer to the fan inlet and outlet respectively

W	=	Impeller shaft work (J/kg of air)
V	=	Specific volume of air (m^3/kg)
P	=	Absolute (barometric) pressure (Pa)
F_{12}	=	Frictional losses (J/kg)
H	=	Enthalpy (J/kg) and
q_{12}	=	Heat added through fan casing (J/kg)

For the purposes of this analysis we shall assume that the change in elevation through the fan is negligible, $Z_1 - Z_2 = 0$. Furthermore, we shall assume that the change in air velocity across the fan is also negligible compared to other terms, $u_1 = u_2$. This latter assumption implies that the fan total pressure, referred to here simply as p_f , is equal to the increase in barometric pressure across the fan, $P_2 - P_1$. Then

$$W = \int_1^2 VdP + F_{12} = (H_2 - H_1) - q_{12} \quad \frac{\text{J}}{\text{kg}} \quad (10.36)$$

It is also reasonable to assume that the heat transferred from the surroundings through the fan casing is small compared to the shaft work. The steady-flow energy equation then simplifies to the adiabatic equation

$$W = \int_1^2 VdP + F_{12} = (H_2 - H_1) \quad \frac{\text{J}}{\text{kg}} \quad (10.37)$$

In order to define a thermodynamic efficiency for the fan impeller, we must first designate a "perfect" fan against which we can compare the performance of the real fan. In the perfect fan, there are no losses, $F_{12} = 0$. As we now have a frictionless adiabatic, i.e. an isentropic compression we can write:

$$W_{isen} = \int_1^2 VdP = (H_{2,isen} - H_1) \quad \frac{\text{J}}{\text{kg}} \quad (10.38)$$

where the subscript *isen* denotes isentropic conditions.

10.6.1.1. The pressure-volume method

There are two methods of determining the efficiency of a fan. The technique that is accepted as standard by most authorities relies upon measurement of the fan pressure, airflow and shaft power, and is known as the pressure-volume method.

The first step is to evaluate the integral $\int_1^2 V dP$. Here, we have a choice. We can use the isentropic relationship

$$PV^\gamma = \text{Constant } C \quad (10.39)$$

where γ = the isentropic index (i.e. the ratio of specific heats $C_p/C_v=1.4$ for dry air). This will lead to the **isentropic efficiency** of the fan.

Alternatively, we could employ the actual polytrope produced by the fan

$$PV^n = \text{Constant}$$

and assume that it is a reversible (ideal) process. This will lead to the **polytropic efficiency** of the fan. Both measures of efficiency are acceptable provided that the choice is stated clearly. While the polytropic efficiency is closer to a true measure of output/input, and takes any heat transfer, q_{12} , into account, the isentropic efficiency has the advantage that the index γ is defined for any given gas. For this reason, we shall continue the analysis on the basis of isentropic compression within the ideal fan. In practice, polytropic and isentropic efficiencies are near equal for most fan installations.

Substituting $V = (C/P)^{1/\gamma}$ into equation (10.38) gives

$$W_{isen} = \int_1^2 \frac{C^{1/\gamma}}{P^{1/\gamma}} dP = C^{1/\gamma} \frac{\left[P^{1-1/\gamma} \right]_1^2}{1-1/\gamma}$$

but as $C^{1/\gamma} = P^{1/\gamma} V$

$$W_{isen} = \frac{\gamma}{\gamma-1} [P_2 V_2 - P_1 V_1] = \frac{\gamma}{\gamma-1} P_1 V_1 \left[\frac{P_2}{P_1} \frac{V_2}{V_1} - 1 \right]$$

Now $\frac{V_2}{V_1} = \left[\frac{P_1}{P_2} \right]^{1/\gamma}$ from equation (10.39)

* Fan efficiencies can be defined in terms of areas on the Ts diagram of Figure 3.7:

$$\eta_{isen} = \frac{\text{Area ACBXY}}{\text{Area DBXZ}} \quad \eta_{poly} = \frac{\text{Area ADBXY}}{\text{Area DBXZ}}$$

$$\text{giving } W_{isen} = \frac{\gamma}{\gamma-1} P_1 V_1 \left\{ \left[\frac{P_2}{P_1} \right]^{1-\frac{1}{\gamma}} - 1 \right\} \frac{\text{J}}{\text{kg}}$$

In order to convert the shaft work from J/kg to shaft power, P_{ow} , (J/s or Watts), we must multiply by the mass flow of air

$$M = Q_1 \rho_1 = \frac{Q_1}{V_1} \quad \text{kg/s}$$

where ρ = air density (kg/m³)

$$\text{Then } P_{ow,isen} = \frac{\gamma}{\gamma-1} P_1 Q_1 \left\{ \left[\frac{P_2}{P_1} \right]^{1-\frac{1}{\gamma}} - 1 \right\} \frac{\text{J}}{\text{kg}} \quad \text{W} \quad (10.40)$$

Now let us multiply both the numerator and denominator by fan pressure, p_f .

$$P_{ow,isen} = p_f Q_1 \frac{\gamma}{\gamma-1} \frac{P_1}{p_f} \left\{ \left[\frac{P_2}{P_1} \right]^{1-\frac{1}{\gamma}} - 1 \right\} \quad \text{W}$$

We can rewrite this equation as

$$P_{ow,isen} = p_f Q_1 K_p \quad (10.41)$$

$$\text{where } K_p = \frac{\gamma}{\gamma-1} \frac{P_1}{p_f} \left\{ \left[\frac{P_2}{P_1} \right]^{1-\frac{1}{\gamma}} - 1 \right\} \quad (10.42)$$

and is known as the **Compressibility Coefficient**. By substituting $p_f = (P_2 - P_1)$ we obtain

$$K_p = \frac{\gamma}{\gamma-1} \left[\frac{\left(\frac{P_2}{P_1} \right)^{\frac{(\gamma-1)}{\gamma}} - 1}{\frac{P_2}{P_1} - 1} \right] \quad (10.43)$$

We can now see that our earlier assumption of incompressible flow ($P_{ow} = p_f Q$) involved an error represented by the deviation of K_p from unity. Figure 10.15 shows the variation in compressibility coefficient with respect to the pressure ratio P_2/P_1 . For unsaturated air the value $\gamma = 1.4$ may be used.

The isentropic efficiency of the fan can now be defined as

$$\eta_{isen} = \frac{P_{ow,isen}}{\text{Shaft power}} = \frac{p_f Q_1 K_p}{\text{Shaft power}} \quad (10.44)$$

Employment of this equation is a standard technique of determining fan efficiency and is known commonly as the **pressure-volume method**.

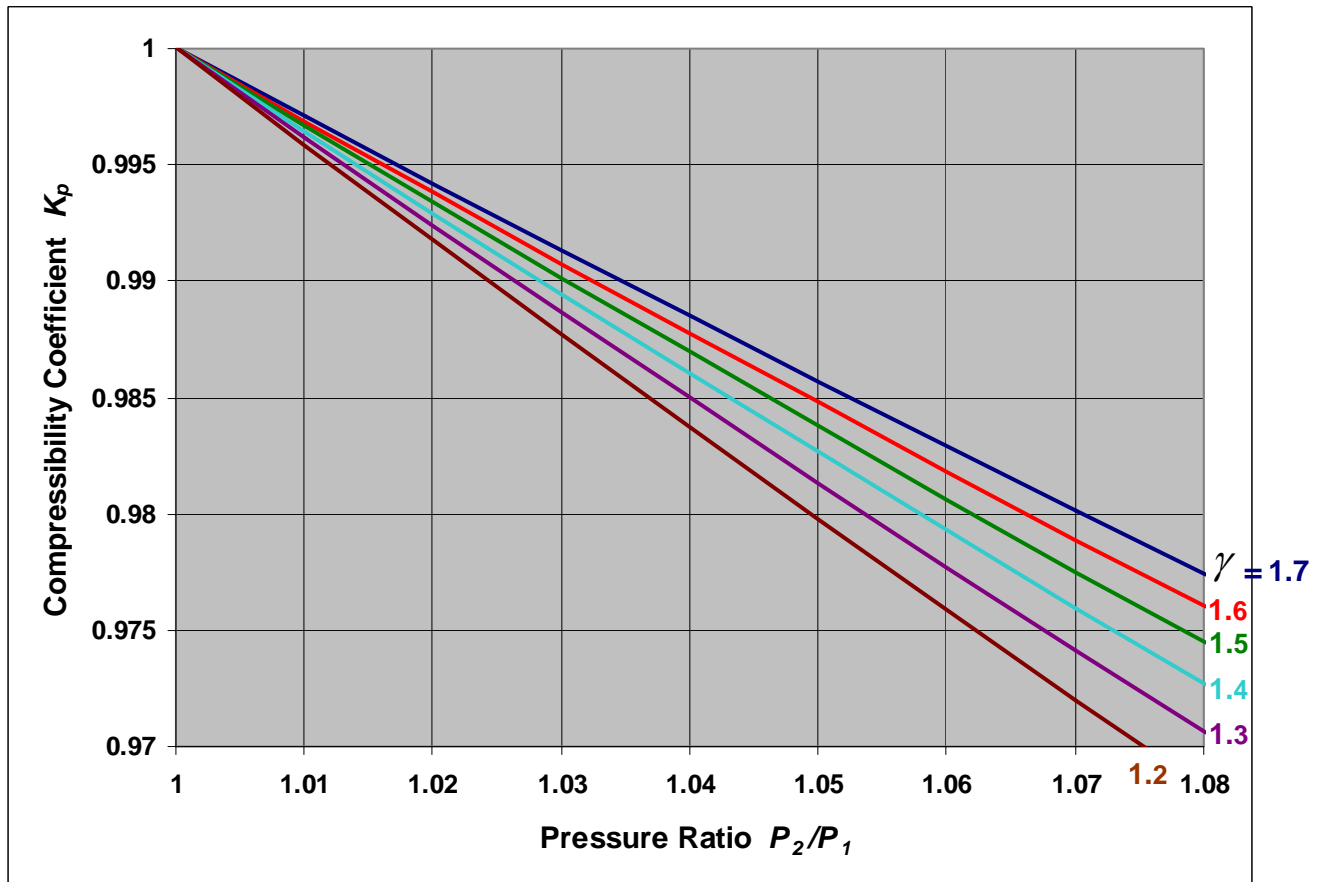


Figure 10.15 Variation of Compressibility Coefficient with respect to pressure ratio.
($\gamma=1.4$ for dry air.)

Two other terms used frequently in the literature are **static efficiency** and **total efficiency**. These are obtained simply by using fan static pressure and fan total pressure, respectively, for p_f in equation (10.44).

All of these measures of efficiency are matters of definition rather than precision. However, care should be taken to ensure that the same measure is employed when comparing fan performances.

Equation (10.44) indicates that the pressure-volume method of fan testing requires the measurement of pressures, air volume flow and the impeller shaft power. It is frequently the case that a large fan installed at a mine site does not meet the specifications indicated by factory tests. Part of the problem may be the less than ideal inlet or outlet conditions that often exist in field installations. In particular, uneven distribution of airflow approaching the fan can produce a diminished performance and may even result in premature blade failure.

Another problem is that turbulence and an asymmetric velocity profile may make it difficult to obtain good accuracy in the measurement of airflow (Section 6.2). Water droplets in the airstream can also result in erroneous readings from both anemometers and pitot tubes.

Impeller shaft power can be obtained accurately in the laboratory or factory test rig by means of torque meters or, in the case of smaller fans, swinging carcass (dynamometer) motors. However, for in-situ tests, it may be necessary to resort to the measurement of input electrical power and to rely upon manufacturer's data for the efficiencies of the motor and transmission.

Despite these difficulties, it is always advisable to conduct an in-situ test on a new main fan in order to verify, or modify, the fan characteristic data that are to be used for subsequent ventilation network exercises.

Example.

A fan passes an airflow of $300 \text{ m}^3/\text{s}$ at the inlet, and develops a pressure of 2.5 kPa. The barometric pressure at the fan inlet is 97 kPa. The motor consumes an electrical power of 1100 kW. Assuming a combined motor/transmission efficiency of 95 per cent, determine the isentropic efficiency of the impeller and, also, of the total unit.

Solution.

$$P_1 = 97 \text{ kPa}, \quad P_2 = 97 + 2.5 = 99.5 \text{ kPa}$$

Using a value of $\gamma = 1.4$ for air, equation (10.40) gives the air power (or isentropic shaft power) as

$$\begin{aligned} P_{ow,isen} &= \frac{\gamma}{\gamma-1} P_1 Q_1 \left\{ \left[\frac{P_2}{P_1} \right]^{1-\frac{1}{\gamma}} - 1 \right\} \frac{\text{J}}{\text{kg}} \\ &= 3.5 \times 97000 \times 300 \left\{ \left[\frac{99.5}{97} \right]^{0.286} - 1 \right\} \\ &= 743.9 \times 10^3 \text{ W} \quad \text{or} \quad 743.9 \text{ kW} \end{aligned}$$

Actual shaft power,

$$P_{ow} = 1100 \times 0.95 = 1045 \text{ kW}$$

Isentropic efficiency of impeller

$$\eta_{isen} = \frac{P_{ow,isen}}{P_{ow}} = \frac{743.9}{1045} = 0.712 \text{ or } 71.2 \text{ per cent}$$

The overall isentropic efficiency of the unit is

$$\eta_{isen} \text{ (overall)} = \frac{743.9}{1100} = 0.676 \text{ or } 67.3 \text{ per cent}$$

Note that if compressibility had been ignored, the isentropic shaft power would have been

$$P_{ow,isen} = p_f Q = 2.5 \times 300 = 750 \text{ kW}$$

involving an error of 0.8 per cent from the true value of 743.9 kW.

10.6.1.2. The thermometric method

Unsaturated Conditions

The problems associated with in-situ pressure-volume tests on mine fans have led researchers to seek another method that did not require the measurement of either airflow or shaft power. The earliest such work appears to have been carried out on the 1920's (Whitaker) although later work was required to make it a practical proposition (McPherson 1971, Drummond 1972).

The thermometric method of fan testing is based on the enthalpy terms in the steady flow energy equation. The shaft work for the ideal isentropic fan is given by equation (10.38)

$$W_{isen} = (H_{2,isen} - H_1)$$

If we assume that the air contains no free water droplets and that neither evaporation nor condensation occurs within the fan then equation (3.33) gives

$$W_{isen} = (H_{2,isen} - H_1) = C_p (T_{2,isen} - T_1) \quad \text{J/kg} \quad (10.45)$$

where C_p = Specific heat at constant pressure of the air (1005 J/kgK for dry air).

Similarly, for the real fan (no secondary subscript)

$$W = C_p (T_2 - T_1) \quad \text{J/kg} \quad (10.46)$$

The **isentropic efficiency** is then given as the ratio of the shaft work for the isentropic fan to that for the actual fan

$$\eta_{isen} = \frac{W_{isen}}{W} = \frac{(T_{2,isen} - T_1)}{(T_2 - T_1)} \quad (10.47)$$

$$\text{or} \quad \eta_{isen} = \frac{\Delta T_{isen}}{\Delta T} \quad (10.48)$$

where $\Delta T_{isen} = (T_{2,isen} - T_1) \text{ } ^\circ\text{C}$ and $\Delta T = (T_2 - T_1) \text{ } ^\circ\text{C}$

ΔT_{isen} is, therefore, the increase in dry bulb temperature that would occur as air passes through an isentropic fan, while ΔT is the temperature rise that actually occurs in the real fan. These two parameters are illustrated on the Ts diagram of Figure 3.7.

As ΔT can be measured, it remains to find an expression for the **isentropic temperature rise**. This was derived in Chapter 3 as equation (3.53)

$$\frac{T_{2,isen}}{T_1} = \left[\frac{P_2}{P_1} \right]^{(\gamma-1)/\gamma} \quad (10.49)$$

where γ = Ratio of specific heats, C_p/C_v (1.4 for dry air).

Then

$$\Delta T_{isen} = (T_{2,isen} - T_1) = T_1 \left\{ \left[\frac{P_2}{P_1} \right]^{(\gamma-1)/\gamma} - 1 \right\} \quad ^\circ\text{C} \quad (10.50)$$

$$\text{giving } \eta_{isen} = \frac{\Delta T_{isen}}{\Delta T} = \frac{T_1}{\Delta T} \left\{ \left[\frac{P_2}{P_1} \right]^{(\gamma-1)/\gamma} - 1 \right\} \quad (10.51)$$

This equation may be employed directly as all of its variables are measurable. It can, however, be simplified by employing the compressibility coefficient, K_p , from equation (10.42)

$$\left\{ \left[\frac{P_2}{P_1} \right]^{(\gamma-1)/\gamma} - 1 \right\} = K_p \frac{\rho_f}{P_1} \frac{(\gamma-1)}{\gamma}$$

Substituting in equation (10.51) gives

$$\eta_{isen} = \frac{(\gamma-1)}{\gamma} \frac{\rho_f}{P_1} \frac{T_1}{\Delta T} K_p \quad (10.52)$$

Using the value of $\gamma = 1.4$ for dry air gives

$$\eta_{isen} = 0.286 \frac{\rho_f}{P_1} \frac{T_1}{\Delta T} K_p \quad (10.53)$$

Furthermore, for fan pressures not exceeding 2.8 kPa, the compressibility coefficient may be ignored for one per cent accuracy, leaving the simple equation:

$$\eta_{isen} = 0.286 \frac{\rho_f}{P_1} \frac{T_1}{\Delta T} \quad (10.54)$$

This analysis has assumed that the airflow contains no liquid droplets of water. The presence of water vapour has very little effect on the accuracy of equations (10.53 or 10.54) provided that the air remains unsaturated. (See equations A10.15 and A10.16 in Appendix A10.2 following this chapter.)

Saturated Conditions

In many deep and hot mines, the reduction in temperature as the return air ascends an upcast shaft may cause condensation. Exhaust fans operating at the surface will then pass fogged air - a mixture of air, water vapour and droplets of liquid water. Equation (10.53) no longer holds due to the cooling effect of evaporation within the fan. A more complex analysis, taking into account the air, water vapour, liquid droplets, and the phase change of evaporation produces the following differential equation which quantifies the temperature-pressure relationship for the isentropic behaviour of fogged air:

$$\frac{dT}{dP} = \frac{\left[(R + R_v X_s) \frac{T}{P} + \frac{L X_s}{(P - e_s)} \right]}{\left[C_p + X C_w - B X_s + \frac{L^2 P}{(P - e_s)} \frac{X_s}{R_v T^2} \right]} \quad \text{°C/Pa} \quad (10.55)$$

A derivation of equation (10.55) and the full definition of the symbols are given in Appendix A10.2 at the end of this chapter.

Inserting the values of the constants gives

$$\frac{dT}{dP} = \frac{0.286 \left[(1 + 1.6078 X_s) \frac{T}{P} + \frac{L X_s}{287.04 (P - e_s)} \right]}{\left[1 + 4.1662 X - 2.3741 X_s + \frac{L^2 P X_s}{463.81 \times 10^3 (P - e_s) T^2} \right]} \quad \text{°C/Pa} \quad (10.56)$$

where T = Absolute temperature (K)
 P = Absolute pressure (Pa)
 L = Latent heat of evaporation (J/kg)
 X = Total moisture content (kg/kg dry air)
 X_s = Water vapour content at saturation (kg/kg dry air) and
 e_s = Saturation vapour pressure at temperature T (Pa).

This equation can be programmed into a calculator or microprocessor for the rapid evaluation of dT/dP .

For the relatively small pressures and temperatures developed by a fan, we can write to a good approximation

$$\Delta T_{isen} = p_f \frac{dT}{dP} \quad (10.57)$$

To improve accuracy, the values used for T and P should be the mean temperature and pressure of the air as it passes through the fan.

Although the thermometric method eliminates the need for airflow and shaft power in the determination of fan efficiency, it does introduce other practical difficulties. The temperature of the air may vary with both time and position over the measurement cross-sections due to vortex action and thermal stratification. The method of measuring the temperature rise across the fan must give an instantaneous reading of the difference between the mean temperatures at inlet and outlet measuring stations. This may be accomplished by thermocouples, connected in series, with the hot and cold junctions distributed over supporting grids at the outlet and inlet measuring stations respectively (Drummond).

Poorly designed evasees on exhausting centrifugal fans may suffer from a re-entry down-draught of external air on one side. A test should be made for this condition before positioning the exit thermocouple heads.

Although the thermometric technique does not require an airflow in order to calculate efficiency, the airflow is nevertheless still needed if that efficiency is to be compared with a manufacturer's characteristic curve. If the site conditions are such that greater confidence can be placed in a determination of shaft power than airflow, then the latter may be computed as

$$Q = \frac{\text{Shaft power}}{\rho_1 (H_2 - H_1)} \quad \frac{\text{m}^3}{\text{s}} \quad (10.58)$$

where the shaft power is in Watts,
 ρ_1 = air density at inlet (kg/m^3)
 and H = enthalpy (J/kg)

If the air is unsaturated then

$$(H_2 - H_1) = C_p (T_2 - T_1)$$

In the case of fogged air, the enthalpies must be determined from equation (A10.3) in Appendix A10.2 in order to account for water vapour and liquid droplets..

Example 1.

A temperature rise of 5.96 °C is measured across a fan developing an increase in barometric pressure of 5 kPa and passing unsaturated air. The inlet temperature and pressure are 25.20 °C and 101.2 kPa respectively. Determine the isentropic temperature rise and, hence, the isentropic efficiency of the impeller.

Solution.

From equation (10.50)

$$\Delta T_{isen} = (273.15 + 25.2) \left\{ \left[\frac{101.2 + 5}{101.2} \right]^{0.286} - 1 \right\} = 4.143 \quad ^\circ\text{C}$$

$$\text{Then } \eta_{isen} = \frac{\Delta T_{isen}}{\Delta T} = \frac{4.143}{5.96} = 0.695 \quad \text{or } 69.5 \text{ per cent}$$

Ignoring the effects of compressibility allows equation (10.54) to be applied, giving

$$\eta_{isen} = 0.286 \times \frac{5}{101.2} \times \frac{(273.15 + 25.2)}{5.96} = 0.707 \quad \text{or } 70.7 \text{ per cent}$$

Hence, in this example, ignoring compressibility causes the percentage fan efficiency to be overestimated by 1.2.

Example 2.

A surface exhausting fan passes fogged air of total moisture content $X = 0.025$ kg/kg dry air. The pressure and temperature at the fan inlet are 98.606 kPa and 18.80 °C respectively. If the temperature rise across the fan is 2.84 °C when the increase in pressure is 5.8 kPa, calculate the isentropic efficiency of the impeller.

Solution.

The mean barometric pressure in the fan is

$$P = 98.606 + 5.8/2 = 101.506 \text{ kPa}$$

$$\text{At inlet, } T_1 = 273.15 + 18.8 = 291.95 \text{ K}$$

$$\text{and at outlet, } T_2 = 291.95 + 2.84 = 294.79 \text{ K}$$

Hence, the mean temperature is

$$T = 293.37 \text{ K or } t = 20.22 \text{ °C}$$

The psychrometric equations in Section 14.6 allow the following parameters to be calculated. For saturation conditions, the wet and dry bulb temperatures are, of course, equal.

Saturation vapour pressure:

$$\begin{aligned} e_s &= 610.6 \exp \left[\frac{17.27 t}{237.3 + t} \right] \\ &= 610.6 \exp \left[\frac{17.27 \times 20.22}{237.3 + 20.22} \right] = 2369.5 \text{ Pa} \end{aligned}$$

Saturation vapour content:

$$\begin{aligned} X_s &= 0.622 \frac{e_s}{(P - e_s)} \\ &= 0.622 \times \frac{2369.5}{(101506 - 2369.5)} = 0.01487 \text{ kg/kg} \end{aligned}$$

Latent heat of evaporation:

$$\begin{aligned} L &= (2502.5 - 2.386 t) 1000 \\ &= (2502.5 - 2.386 \times 20.22) 1000 = 2454.26 \times 10^3 \text{ J/kg} \end{aligned}$$

Substituting the known values into equation (10.56) gives

$$\frac{dT}{dP} = \frac{0.286 [0.002959 + 0.001282]}{[1 + 0.10416 - 0.03530 + 2.29693]} = 3.604 \times 10^{-4} \text{ °C per Pa}$$

This example shows that the term involving the total moisture content, X , is relatively weak (0.10416). Hence, no stringent efforts need be made to measure this factor with high accuracy.

$$\begin{aligned} \text{Then } \Delta T_{isen} &= p_f \frac{dT}{dP} \quad (\text{equation (10.57)}) \\ &= 5800 \times 3.604 \times 10^{-4} = 2.09 \text{ °C} \end{aligned}$$

The isentropic efficiency is

$$\eta_{isen} = \frac{\Delta T_{isen}}{\Delta T} = \frac{2.09}{2.84} = 0.736 \quad \text{or } 73.6 \text{ per cent}$$

10.6.2. Purchasing a main fan.

The results of ventilation network planning exercises will produce a range of pressure-volume duties required of any new major fan that is to be installed. The process of finding and ordering the fan often commences with the ventilation engineer perusing the catalogues of fan characteristics produced by **fan manufacturers**. Several of those companies should be invited to submit **tenders** for the manufacture and, if required, installation of the fan. However, in order for those tenders to be complete, information in addition to the required pressure-volume range should be provided by the purchasing organization.

- (a) The mean temperature, barometric pressure, humidity and, hence, air density at the fan inlet should be given. This allows data based on standard density to be corrected to the psychrometric conditions expected in the field.
- (b) In many cases of both surface and underground fans, noise restrictions need to be applied. These restrictions should be quantified in terms of noise level and, if necessary, with respect to direction.
- (c) A plan and sections of the site should be provided showing the proposed fan location and, in particular, highlighting any restrictions on space.
- (d) The request for a tender must identify and, wherever possible, quantify the concentrations and types of pollutants to be handled by the fan. These include dusts, gases, water vapour and liquid water droplets. In particular, any given agents of a corrosive nature should be stressed. The purchaser should further indicate any preference for the materials to be used in the manufacture of the fan impeller and casing. Specifications on paints or other protective coatings might also be necessary.
- (e) Any preference for the type of fan should be indicated. Otherwise, the manufacturer should be specifically invited to propose one or more fans that will meet the other specifications.
- (f) The scope of the required tender should be clearly defined. If the contractor is to be responsible for providing, installing and commissioning the new fan, the individual items should be specified for separate costing.
- (g) The motor, transmission, electrical switchgear and monitoring devices may be acquired and installed either by the provider of the fan or separately. In either case, the voltage and any restrictions on power availability should be stated.
- (h) Areas of responsibility for site preparation and the provision and installation of ducting should be identified.

10.7. BOOSTER FANS

10.7.1. The application of booster fans

In deep mines or where workings have become distant from surface connections the pressures required to be developed by main fans may be very high in order to maintain acceptable face airflows. This leads to practical difficulties at airlocks and during the transportation of personnel, mined mineral and materials. More serious, however, is the fact that higher pressures at main fans inevitably cause greater leakage throughout the entire system. Any required fractional increase in face airflows will necessitate the same fractional increase in main fan volume flows for any given system resistance. Hence, as both fan operating power and costs are proportional to the product of fan pressure and airflow, those costs can rapidly become excessive as a large mine continues to expand. In such circumstances, the employment of booster fans provides an attractive alternative to the capital penalties of driving new airways, enlarging existing ones, or providing additional surface connections. Legislation should be checked for any national or state restrictions on the use of booster fans.

Unlike the main fans which, in combination, handle all of the mine air, a booster fan installation deals with the airflow for a localized area of the mine only. The primary objectives of a booster fan are

- to enhance or maintain adequate airflow in areas of the mine that are difficult or uneconomic to ventilate by main fans, and
- to redistribute the pressure pattern such that air leakage is minimized.

A modern booster fan installation, properly located, monitored and maintained creates considerable improvements in environmental conditions at the workplace, and can allow the extraction of minerals from areas that would otherwise be uneconomic to mine. It has frequently been the case that the installation of underground booster fans has resulted in improved ventilation of a mine while, at the same time, producing significant reductions in total fan operating costs. However, these benefits depend upon skilled system design and planning. An inappropriate use of booster fans can actually raise operating costs if, for example, fans act in partial opposition to each other. Furthermore, if booster fans are improperly located or sized then they may result in undesired recirculation.

This section is directed towards the planning, monitoring and control of a booster fan installation.

10.7.2. Initial planning and location

An initial step in planning the incorporation of a booster fan into an existing subsurface system is to obtain or update data by conducting ventilation surveys throughout the network (Chapter 6) and to establish a correlated basic network (Section 9.2). Two sets of network exercises should then be carried out.

First, a case must be established for adding a booster fan to the system. Network exercises should investigate thoroughly all viable alternatives. These may include

- adding or upgrading main fans
- enlarging existing airways and/or driving new ones including shafts or other surface connections
- redesigning the underground layout to reduce leakage and system resistance - for example, changing from a U-tube to a through-flow system (Section 4.3), and
- reducing face resistance by a redesign of the face ventilation system or the replacement of line brattices with auxiliary ducts and fans.

If it is decided to progress with the planning of a booster fan installation then a second series of network exercises should be carried out to study the preferred location and corresponding duty of the proposed booster fan. Conventional VNET programs can be used for this purpose. Each of the alternative feasible locations is simulated in a series of computer runs in order to compare flow patterns and operating costs¹. Flow patterns predicted by the simulations should be checked against the constraints of required face airflows and velocity limits as for any other network exercise (Figure 9.1). Additionally, there are several other checks that should be carried out for a booster fan investigation:-

Practical constraints on booster fan location

Although there may be a considerable number of branches in the network within which a booster fan may, theoretically, be sited in order to achieve the required flow enhancement, the majority of those might be eliminated by practical considerations.

Booster fans should, wherever possible, avoid locations where airlocks would interfere with the free movement of minerals, materials or personnel. Furthermore the availability of dedicated electrical power and monitoring circuitry, or the cost of providing such facilities to each potential site should be considered. If a booster fan is located remotely from frequently travelled airways, then particular vigilance must be maintained to ensure that it receives regular visual inspections in addition to continuous electronic surveillance (Section 10.7.3).

Leakage and recirculation

For any given pressure developed by a booster fan in a specified circuit, there exists a fan position where the summation of leakages inby and outby the fan is a minimum without causing undesired recirculation. In a U-tube circuit (Figure 4.4), this location occurs where the operation of the fan achieves zero pressure differential between intake and return airways at the inlet or outlet of the fan. (See, also Figure 21.7.) Conventional wisdom is to locate the booster fan at this "neutral point." In practice, there are some difficulties. The neutral point is liable to move about quite considerably because of

- variations in resistance due to face operations and advance/ retreat of workings
- changes in the pressures developed by the booster fan or any other fan(s) in the system
- variations in the system resistance due to movement of vehicles or longer term changes in airway resistances.

It is preferable to examine the complete leakage pattern predicted by ventilation network analysis for each proposed booster fan location.

The question of **recirculation** must be examined most carefully. If the purpose of the booster fan is to induce a system of controlled partial recirculation (Section 4.5), then the predicted airflow pattern must conform to the design value of percentage recirculation. However, undesired or uncontrolled recirculation must be avoided. At all times, legislative constraints must be observed.

Installing a booster fan in one area of a mine will normally cause a reduction in the airflows within other districts of the mine. In extreme cases, reversals of airflow and unexpected recirculations can occur. While examining network predictions involving booster fans, care should be taken to check airflows in all parts of the network and not simply in the section affected most directly by the booster fan.

In addition to modifying airflow patterns, booster fans are also a very effective means of managing the pressure distribution within a network. It is this feature that enables booster fans to influence the leakage characteristics of a subsurface ventilation system. A properly located and

¹ Optimization programs have been developed (e.g. Calizaya, 1988) that determine the optimum combination of main and booster fan duties, based on the minimization of total operating costs for each booster fan location investigated by the engineers.

sized booster fan can be far more effective in controlling leakage across worked out areas than sealants used on airway sides or stoppings. Conversely, a badly positioned booster fan can exacerbate leakage problems. These matters are of particular consequence in mines liable to spontaneous combustion (Section 21.4.5). Hence, the pressure differences predicted across old workings or relaxed strata should be checked carefully.

Steady state effects of stopping the booster fan

For each proposed location for a booster fan, network simulations should be run to investigate the effect of stopping that fan. In general, the result will be that the airflow will fall in that area of the mine and increase in others. (A cross-cut recirculation booster fan can cause the opposite effect as discussed in Section 4.5.3). In all cases, the ventilation must remain sufficient, without the booster fan, to ensure that all persons can evacuate the mine safely and without undue haste. The implication is that main fans alone must always be able to provide sufficient airflows for safe travel within the mine, and that booster fans merely provide additional airflow to working faces for dilution of the pollutants caused by breaking and transporting rock. It is good practice to employ two or more fans in parallel for a booster fan installation. This allows the majority of the airflow to be maintained if one fan should fail (Section 10.5.2). Further, considerations regarding the transient effects of stopping or starting fans are discussed in Section 10.7.3.

Economic considerations

The cost-benefits of a proposed booster fan should be analysed with respect to time. A major booster fan installation should be assured of a reasonable life; otherwise it may be preferable to tolerate short-lived higher operating costs. On the other hand, a cluster of standard axial fans connected in a series/parallel configuration (Section 10.5) can provide an inexpensive booster fan solution to a short term problem. The financial implications of such questions can be quantified by combining total fan operating costs and the capital costs of purchasing and installing the booster fans, using the methods described in Section 9.5.

10.7.3. Monitoring and other safety features

When a booster fan is installed in a subsurface ventilation system, it becomes an important component in governing the behaviour of that system. However, unlike other components such as stoppings, regulators or air crossings, the booster fan is actively powered and has a high speed rotating impeller. Furthermore, it is usually less accessible than a surface fan in case of an emergency condition. For these reasons a subsurface booster fan should be subjected to continuous surveillance. The traditional way of doing this was to post a person at the booster fan location at all times when it was running. This was one of life's more tedious jobs. Some installations reverted to the use of television cameras. A bank of display monitors covering a number of sites could be observed by a single observer at a central location. The problems associated with such methods were that they depended upon the vigilance of human beings and were limited to visual observations. The task may now be undertaken much more reliably and efficiently by **electronic surveillance**, employing transducers to sense a variety of parameters. These transducers transmit information in a near continuous manner to a central control station, usually located on surface, where the signals are analysed by computer for display, recording and audio-visual alarms when set limits are exceeded. Alarms and, if required, displays may be located both at the control station and also at the fan site.

The monitors used at a booster fan may form part of a mine-wide environmental monitoring system which can, itself, be integrated into a general communication network for monitoring and controlling the condition and activities of conveyors, roof supports, excavation machinery and other equipment. However, sufficient redundancy should be built into the booster fan surveillance such that it remains operational in the event of failures in other parts of the mine monitoring system.

The parameters to be monitored at, or near, a booster fan installation include:

- gas concentrations (e.g. methane) in the air approaching the fan
- carbon monoxide and/or smoke both before and after the fan
- pressure difference across the fan measured, preferably, at the adjoining airlock
- an indication of airflow in the fan inlet or outlet
- bearing temperatures and vibration on both the motor and the fan impeller and
- positions of the airlock and anti-reversal doors.

All monitors should be fail-safe, i.e. the failure of any transducer should be detected by interrogative signals initiated by the computer, resulting in automatic transfer to a companion transducer, display of a warning message and printing of an accompanying hardcopy report. It follows that all transducers must be provided with at least one level of back-up devices.

The monitoring function is particularly important where controlled partial recirculation is practiced or at times of rapid transient change in the ventilation system. The latter may occur by an imprudent operation of doors in other areas of the mine or at a time when either the booster fan itself or other fans in the system are switched on or off. Any **sudden reduction in air pressure** caused by such activities can cause gases held in old workings or relaxed strata to expand into the ventilating airstream (Section 4.2.2).

A booster fan should be provided with electrical power that is independent of the main supply system to the mine. However, **electrical interlocks** should be provided according to a predetermined control policy (Section 10.7.4). This policy might include:

- automatic stoppage of the booster fan if the main fan(s) cease to operate
- stoppage of the booster fan if all of the local airlock doors are opened simultaneously
- isolation of electrical power in by if the booster fan ceases to operate.

The second item on this list may also be required in reverse. Hence, for example, the booster fan could not be started if the local airlock doors were all open. However, those doors should open automatically when the booster fan stops, in order to re-establish conventional ventilation by the main fans. The question of interlocks may be addressed by legislation and might also be influenced by existing electrical systems. All electrical equipment should be subject to the legislation pertaining to that mine.

If the fan is to operate in a return airway, then the design will be improved if the motor is located out of the main airstream and ventilated by a split of fresh air taken from an intake airway. In this regard, it is also sensible to ensure that there are no flammable components within the transmission train.

Anti-reversal doors, flaps or louvres should be fitted to a booster fan in order to prevent reversal of the airflow through the fan when it stops.

All materials used in the fan, fan site and within some 50m of the fan should be non-flammable. Furthermore, no flammable materials should be used in the construction of the local airlock, stoppings or air crossings. Finally an **automatic fire suppression system** should be provided at the fan station.

10.7.4. Booster fan control policy

Continuous electronic monitoring systems provide a tremendous amount of data. During the normal routine conditions that occur for the vast majority of the time, all that is required is that the monitoring system responds to any manual requests to display monitored parameters, and to

record information on electronic or magnetic media. However, the ability to generate and transmit control signals raises the question of how best to respond to unusual deviations in the values of monitored parameters.

The vision of complete **automatic control** of the mine environment produced a flurry of research activity in the 1960's and '70's (Mahdi, Rustan, Aldridge). This work resulted in significant advances in the development of transducers and data transmission systems suitable for underground use. However, a completely closed loop form of environmental control has seldom been implemented for practical use in producing mines. The difficulty is that there are a number of variables which, although of vital importance in an emergency condition, may not be amenable to direct measurement. These include the locations of personnel and any local actions those personnel might have taken in an attempt to ameliorate the emergency situation.

If an automatic control policy is to be implemented for a booster fan, careful consideration should be given to the action initiated by the system in response to deviations from normal conditions. The **control policy** that is established should then be incorporated into the computer software (Calizaya, 1989).

The simplest control policy is to activate audio-visual alarms and to allow control signals to be generated manually. Manual over-ride of the system must be possible at all times. In order to examine additional automatic responses, unusual deviations in each of the **monitored parameters** listed in the previous subsection are considered here:

(a) Methane (or other gas of concern)

Four concentration levels may be chosen or mandated by law

- (i) concentration at which personnel are to be withdrawn
- (ii) concentration at which power inby the fan is to be cut off
- (iii) concentration at which power to the booster fan should be cut
- (iv) concentration below which no action is to be initiated.

Levels (i) and (ii) are usually fixed by law. Electrical power inby the fan should be isolated automatically when level (ii) is reached. If the fan is powered by an electric motor which is located within the airstream then the power to the fan should also be cut when level (ii) is reached. However, this may cause even more dangerous conditions for any personnel that are located inby. Having the motor located in a fresh air split allows greater flexibility. At the present time, it is suggested that when level (iii) is exceeded manual control should be established.

Level (iv) is relevant only for those systems where control of the volume flow of air passing through the fan is possible. This may be achieved by automatic adjustment of impeller blade angle, guide vanes or motorized regulators. Level (iv) may be set at one half the concentration at which power inby the fan must be cut. Variations in the monitored gas concentration that occur below level (iv) are to be considered as normal and no action is taken. Variations between levels (iv) and (iii) may result in a PID (proportional/integral/differential) response. This means that control signals will be transmitted to increase the airflow to an extent defined by the level of the monitored concentration, how long that level has existed and the rate at which it is increasing. The objective is to prevent the gas concentration reaching level (iii). The maximum increase in airflow must have been predetermined by network analysis such that the ventilation of the rest of the mine is maintained at an acceptable level.

(b) Smoke or carbon monoxide

The system should be capable of distinguishing hazardous levels of smoke or carbon monoxide from short-lived peaks caused by blasting or nearby diesel equipment. A monitoring system that initiates alarms frequently and without good cause will rapidly lose its effectiveness on human operators. There is no single answer to the response to be initiated if these alarms indicate an actual fire. Similar alarms arising from detectors in other parts of the mine may allow the probable

location of the fire to be determined. Permitting the booster fan to continue running may accelerate the spread of the fire and products of combustion. On the other hand, stopping the fan might allow toxic gases to spread into areas where personnel could have gathered, particularly if damage to the integrity of air crossings or stoppings is suspected. The only realistic action in these circumstances is to revert to manual control.

(c) Pressure differential and airflow

An increase in the pressure developed by the fan will usually indicate an increase in resistance inby. This might be caused by normal face operations, partial blockage of an airway by a vehicle or other means, or obstruction of the fan inlet grill. No action is required other than a warning display and activation of an alarm if the fan pressure approaches stall conditions. A rapid fall in fan pressure accompanied by an increase in airflow is indicative of a short circuit and local recirculation. A warning display should be initiated together with checks on the positions of air lock doors followed, if necessary, by a manual inspection of the area. A simultaneous rapid fall in pressure and airflow suggests a problem with the fan itself. The power supply should be checked and, again, the fan should be inspected manually. Such circumstances will usually be accompanied by indications of the source of the difficulty from other transducers.

(d) Bearing temperatures, vibration

Indications of excessive (or rising) values of bearing temperatures or vibration at either the motor or the fan impeller should result in isolation of power to the fan and all electrical equipment inby the fan.

(e) Positions of airlock doors

An airlock door which is held open for more than a pre-determined time interval should initiate a warning display and, if uncorrected, should warrant a manual inspection.

Bibliography

Aldridge, M.D. and Nutter, R.S. (1980). An experimental ventilation control system. 2nd. Int. Mine Ventilation Congress, Reno, NV. pp.230-238.

ASHRAE (1985). Laboratory methods of testing fans for ratings. ANSI/AMCA. Atlanta, Georgia, USA.

British Standard 848 (1963). Methods of testing fans for general purposes, Part 1. HMSO. London.

De La Harpe J.H. (1982). Basic fan engineering. Chapter 7. Environmental Engineering in South African Mines. Mine Ventilation Society of South Africa.

Drummond, J.A. (1972). Fan efficiency investigations on mines of Union Corp. Ltd. J. Mine Ventilation Society of South Africa. Vol. 25, pp.180-195.

Mahdi, A. and McPherson, M.J. (1971). An introduction to automatic control of mine ventilation systems. Mining Technology. May.

McFarlane, D. (1966). Ventilation Engineering. Davidson & Co. Ltd, Belfast, N. Ireland.

McPherson, M.J. (1971). The isentropic compression of moist air in fans. J. Mine Ventilation Society of South Africa, Vol. 24, pp.74-89.

Rustan, A. and Stockel, I. (1980). Review of developments in monitoring and control of mine ventilation systems. 2nd Int. Mine Ventilation Congress. Reno, NV. pp. 223-229.

Stepanoff, A.J. (1955). Turboblenders. Wiley & Sons Ltd.

Whitaker, J.W. (1926, 1928). The efficiency of a fan. Trans. Inst. of Mining Engineers. Vol. 72, p.43. Vol. 74, p.93.

APPENDIX A10.1

Comparisons of exhausting and forcing fan pressures to use in pressure surveys.

As stated in Section 10.2 of this chapter, it is fan static pressures that should be employed when a main surface fan is included in the route of a pressure survey. It is not immediately obvious why this should be so when total pressures are used at all other survey measuring points. The apparent anomaly arises from the way in which fan pressures are defined.

In this Appendix, we will consider an identical main fan at a mine surface in each of three configurations. In each case the fan operates at the same speed and passes the same airflow against a constant mine resistance. In such circumstances the fan will deliver the same air power and, hence, produce the same rise in total (facing tube) pressure. In this illustrative example we will take the increase in total pressure across the fan to be $\Delta p_t = 4000$ Pa while the air velocity at the fan measuring station produces a velocity pressure $p_v = 500$ Pa.

Configuration 1.

Mine Resistance

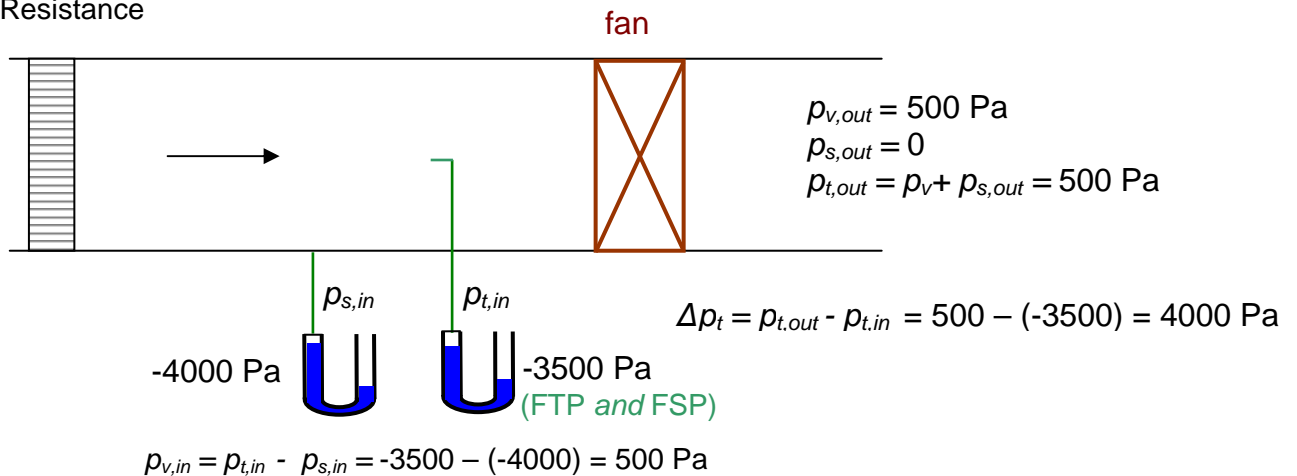


Figure A10.1 Main surface exhaust fan with no outlet cone.

Figure A10.1 shows the fan operating in an exhausting configuration with the same inlet and exhaust cross sectional areas and no outlet cone. At the point of exit to the outside atmosphere the velocity pressure remains at 500 Pa but the gauge static pressure is $p_{s,out} = 0$, giving the total pressure at this location to be

$$p_{t,out} = p_{v,out} + p_{s,out} = 500 + 0 = 500 \text{ Pa}$$

But as $\Delta p_t = p_{t,out} - p_{t,in} = 4000$ Pa, it follows that the total pressure shown by a facing tube at the fan inlet must be

$$p_{t,in} = p_{t,out} - \Delta p_t = 500 - 4000 = -3500 \text{ Pa (negative with respect to the external atmospheric pressure)}$$

and the corresponding static pressure is $p_{s,in} = p_{t,in} - p_{v,in} = (-3500) - 500 = -4000$ Pa

As the kinetic energy of the outlet air is dissipated entirely within the external atmosphere, it does not contribute to the ventilating pressure applied to the mine. Hence, that effective ventilating pressure becomes 3500 Pa rather than 4000 Pa and is indicated by the reading on the facing tube gauge, i.e. $p_{t,in}$. Note, however that because of the way in which fan pressures are defined, the total pressure at the fan inlet in a surface exhausting fan is equal to the Fan Static Pressure, FSP (Figure 10.1(c)).

Configuration 2.

Mine Resistance

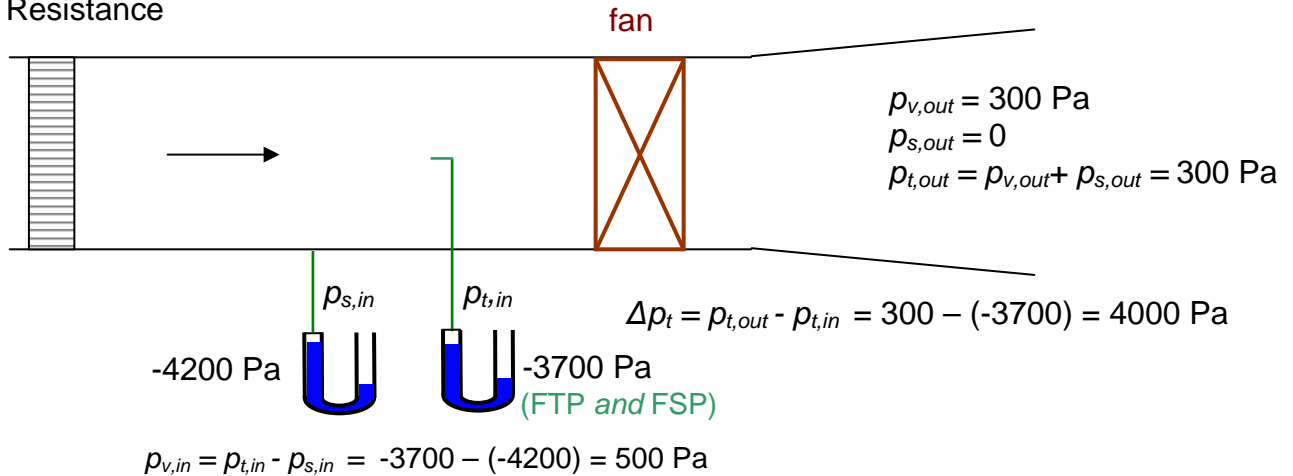


Figure A10.2 Exhausting fan with an outlet cone, slowing discharge air and reducing exit velocity pressure to 300 Pa.

Figure A10.2 illustrates the effect of adding an outlet cone to the previous example of a surface exhausting fan. The mine resistance, airflow and fan power remain unchanged. Hence the increase in total pressure across the fan remains at 4000 Pa. However, as shown in the figure, the exit total pressure is now 300 Pa. Hence the gauge inlet total pressure becomes

$$p_{t,in} = 300 - 4000 = -3700 \quad \text{Pa}$$

Furthermore, as the inlet velocity pressure has remained unchanged at 500 Pa, the inlet static pressure is now

$$p_{s,in} = p_{t,in} - p_{v,in} = -3700 - 500 = -4200 \quad \text{Pa}$$

As in Configuration 1, the kinetic energy of the outlet air is dissipated entirely in the external atmosphere and does not contribute to the ventilating pressure applied to the mine. However, the corresponding exit velocity pressure has now been reduced from 500 Pa to 300 Pa, increasing the effective ventilation pressure applied to the mine from the previous 3500 Pa to 3700 Pa, measured as the total pressure at the fan inlet.

This example further illustrates the advantage of adding an outlet cone to an exhausting fan. Note, however, that losses due to excessive turbulence and/or wall friction can more than counteract this advantage if the cone is too long or diverges too rapidly.²

² Angles of divergence (i.e. between opposite sides) are normally in the range 7 to 15° for mine fans.

Configuration 3

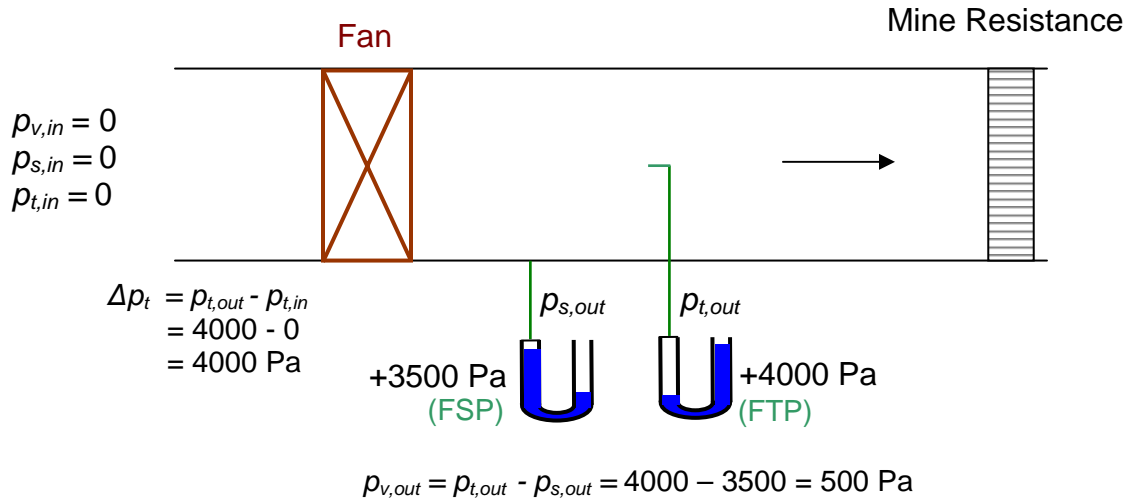


Figure A10.3 Forcing fan.

Figure A10.3 shows the same fan in a forcing mode with all other parameters as in the previous two configurations. In this case we take the external station to be outside the duct entrance as part of the fan power must be used to accelerate the air from zero to a velocity pressure of 500 Pa^3 .

As the total pressure at the external station, $p_{t,in}$, is zero and the increase in total pressure across the fan remains at 4000 Pa , it follows that the total pressure at the fan outlet, $p_{t,out}$, must be 4000 Pa and the corresponding static pressure becomes

$$p_{s,out} = p_{t,out} - p_{v,out} = 4000 - 500 = 3500 \text{ Pa}$$

This is the effective pressure that remains to ventilate the mine and, hence, the pressure to be used if the forcing fan is included in a pressure survey. Once again, because of the way in which fan pressures are defined, this is also the pressure designated as the Fan Static Pressure, FSP, for a forcing fan (Figure 10.1(b)).

³ It is also the case that part of the airpower developed by an exhausting fan is utilized in accelerating the air at the intake portals of the mine. However, in that case it is normally measured separately as shock losses at those portals.

APPENDIX A10.2**Derivation of the isentropic temperature-pressure relationship for a mixture of air, water vapour and liquid water droplets.**

It is suggested that the reader delays working on this appendix until Chapter 14 (Psychrometry) has been studied.

During a flow process, the work done by expansion or compression of the air is given by VdP . In the case of fogged air containing X kg of water (vapour plus liquid) per kg of dry air, this becomes $V_s dP$ where the specific volume of the $(1 + X_s)$ kg of the air/vapour mixture is

$$V_s = (R + R_v X_s) \frac{T}{P} \quad (\text{see equation (14.14)})$$

where

P	=	barometric pressure (Pa)
R	=	gas constant for dry air (287.04 J/kg K)
R_v	=	gas constant for water vapour (461.5 J/kg K)
T	=	Absolute temperature (K)
and X_s	=	mass of water vapour associated with each 1 kg of "dry" air in the saturated space (kg/kg dry air)

The volume of the $(X - X_s)$ kg of liquid water is negligible compared to that of the gases. In a fogged airstream, the wet and dry bulb temperatures are equal.

The steady flow energy equation (10.35) for an isentropic process ($dF = dq = 0$) then becomes

$$V_s dP = (R + R_v X_s) \frac{T}{P} dP = dH \frac{J}{kg} \quad (\text{A10.1})$$

The enthalpy of the $(1 + X)$ kg of air/vapour/liquid mix, based on a datum of 0 °C, is the combination of

$C_p t$: heat required to raise 1 kg of dry air through t °C
$X C_w t$: heat required to raise X kg of liquid water through t °C
and $L X_s$: heat required to evaporate X_s kg of water at t °C

where C_p	=	Specific heat of dry air (1005 J/kgK)	
C_w	=	Specific heat of liquid water (4187 J/kgK)	
L	=	Latent heat of liquid water at temperature t °C	
	=	$(2502.5 - 2.386 t)1000$ J/kg	(A10.2)
		(see equation (14.6))	

$$\text{Then } H = C_p t + X C_w t + L X_s \quad \frac{J}{kg} \quad (\text{A10.3})$$

Differentiating,

$$dH = (C_p + X C_w) dt + X_s dL + L dX_s \quad \frac{J}{kg} \quad (\text{A10.4})$$

It is assumed that no water is added or removed during the process. Hence, X remains constant. We must now seek to formulate this expression in terms of temperature and pressure. First, we evaluate dL and dX_s as functions of temperature and pressure

(a) Change of latent heat of evaporation, dL

From equation (A10.2),

$$dL = -B dt \quad \text{where } B = 2386 \quad (\text{A10.5})$$

(b) Change of vapour content, dX_s

From equation (14.4) for saturation conditions

$$X_s = G \frac{e_s}{(P - e_s)} \quad (\text{A10.6})$$

where $G = 0.622$
 $e_s =$ saturation vapour pressure (Pa) at t °C
 and $P =$ absolute (barometric) pressure (Pa).

By partial differentiation,

$$dX_s = \frac{\partial X_s}{\partial e_s} de_s + \frac{\partial X_s}{\partial P} dP \quad (\text{A10.7})$$

From equation (A10.6)

$$\frac{\partial X_s}{\partial e_s} = G \left[\frac{1}{(P - e_s)} + \frac{e_s}{(P - e_s)^2} \right] = \frac{GP}{(P - e_s)^2} \quad (\text{A10.8})$$

and

$$\frac{\partial X_s}{\partial P} = \frac{-G e_s}{(P - e_s)^2} \quad (\text{A10.9})$$

Furthermore, the Clausius-Clapeyron equation (14.5) gives

$$de_s = \frac{L e_s}{R_v T^2} dt \quad \text{Pa} \quad (\text{A10.10})$$

where $R_v =$ gas constant for water vapour (461.5 J/kg K)
 and $T = (273.15 + t)$ (K)
 giving $dt = dT$

Substituting from equations (A10.8, A10.9, and A10.10) into equation (A10.7) gives

$$dX_s = \frac{GP}{(P - e_s)^2} \frac{L e_s}{R_v T^2} dT - \frac{G e_s}{(P - e_s)^2} dP \quad (\text{A10.11})$$

But as $X_s = \frac{G e_s}{(P - e_s)}$ from equation (A10.6),

equation (A10.11) becomes

$$dX_s = \frac{X_s P}{(P - e_s)} \frac{L}{R_v T^2} dT - \frac{X_s}{(P - e_s)} dP \quad (\text{A10.12})$$

Having evaluated dL (equation (A10.5)) and dX_s (equation (A10.12)), we can substitute these expressions into equation (A10.4) and, hence, (A10.1)

$$dH = (C_p + X C_w) dt - B X_s dt + \frac{X_s P}{(P - e_s)} \frac{L^2}{R_v T^2} dt - \frac{L X_s}{(P - e_s)} dP = (R + R_v X_s) \frac{T}{P} dP$$

Collecting the dt and dP terms, and replacing dt by dT for consistency (the two are identical),

$$\frac{dT}{dP} = \frac{\left[(R + R_v X_s) \frac{T}{P} + \frac{L X_s}{(P - e_s)} \right]}{\left[C_p + X C_w - B X_s + \frac{L^2 P}{(P - e_s)} \frac{X_s}{R_v T^2} \right]} \quad \frac{^\circ\text{C}}{\text{Pa}} \quad (\text{A10.13})$$

This is a general isentropic relationship describing the rate of change of temperature with respect to pressure for a saturated mixture of air, water vapour and liquid water. All of the variables X_s , L , and e_s depend only upon T and P .

For unsaturated air involving no liquid water, X_s becomes X and there is no change of phase. Hence, the terms that include L become zero. Then

$$\frac{dT}{dP} = \frac{(R + R_v X) T}{C_p + (C_w - B) X} \frac{T}{P} \quad \frac{^\circ\text{C}}{\text{Pa}} \quad (\text{see footnote}^*) \quad (\text{A10.14})$$

Inserting values for the constants gives

$$\frac{dT}{dP} = \frac{R (1 + 1.6078 X) T}{C_p (1 + 1.7920 X) P}$$

Expansion of $(1 + 1.7920 X)^{-1}$ and ignoring terms of X^2 and smaller leads to the approximation

$$\frac{dT}{dP} = \frac{R}{C_p} (1 - 0.2 X) \frac{T}{P} = 0.286 (1 - 0.2 X) \frac{T}{P} \quad (\text{A10.15})$$

* By considering an isothermal-isobaric change of phase, it can be shown that $C_w - B = C_{pv}$, where C_{pv} = specific heat at constant pressure of water vapour. This gives a value for C_{pv} to be $4187 - 2386 = 1801$ J/kgK. The 4.4 per cent deviation from the normally accepted value of 1884 J/kgK indicates the uncertainty of C_{pv} within the atmospheric range of temperatures.

For dry air, $X = 0$ leaving

$$\frac{dT}{dP} = 0.286 \frac{T}{P} \quad (\text{A10.16})$$

(This correlates with equation (10.54) when $dT = \Delta T$, $dP = p_f$ and $\eta_{isen} = 1$).

Equation (A10.15) shows that if moist but unsaturated air is assumed to be dry then the fractional error involved is approximately $0.2X$. Hence, for an error of one per cent

$$\begin{array}{l} 0.2 X = 0.01 \\ \text{or } X = 0.05 \text{ kg/kg dry air} \end{array}$$

This vapour content represents fully saturated conditions at 40 °C and 100 kPa. It is unlikely that such moisture content will exist in mining circumstances without liquid water being present. Thus, for unsaturated air in the normal atmospheric range, assuming dry air will give an accuracy of within one per cent for the temperature/pressure gradient.

PART 3

CHAPTER 11 GASES IN SUBSURFACE OPENINGS

11.1. INTRODUCTION	2
11.2. CLASSIFICATION OF SUBSURFACE GASES.....	2
11.2.1. Threshold limit values (TLV)	2
11.2.2. Oxygen, O ₂	5
11.2.3. Nitrogen, N ₂	6
11.2.4. Methane, CH ₄	6
11.2.5. Carbon dioxide, CO ₂	9
11.2.6. Carbon monoxide, CO	9
11.2.7. Sulphur dioxide, SO ₂	12
11.2.8. Oxides of nitrogen, NO _x	12
11.2.9. Hydrogen sulphide, H ₂ S.....	13
11.2.10. Hydrogen, H ₂	14
11.2.11. Radon, Rn	14
11.3. GAS MIXTURES.....	15
11.3.1. Threshold limit values for gas mixtures	15
11.3.2. Diesel emissions	17
11.3.3. Fires	18
11.3.4. Explosives	19
11.3.5. Welding	19
11.4. GAS DETECTION AND MONITORING	20
11.4.1. Objectives and overview	20
11.4.2. Principles of gas detection	20
11.4.2.1. Filament and catalytic oxidation (pellistor) detectors	20
11.4.2.2. Flame safety lamps	22
11.4.2.3. Thermal conductivity and acoustic gas detectors	23
11.4.2.4. Optical methods	23
11.4.2.5. Electrochemical methods	24
11.4.2.6. Mass spectrometers	25
11.4.2.7. Paramagnetic analysers.....	25
11.4.2.8. Gas chromatography.....	25
11.4.2.9. Semiconductor detectors	25
11.4.2.10. Stain tubes	25
11.4.3. Methods of sampling.....	26
11.4.3.1. Manual methods.....	26
11.4.3.2. Automatic and remote monitors	26
References	27

11.1. INTRODUCTION

When air enters any mine or other subsurface structure, it has a volume composition of approximately 78 percent nitrogen, 21 percent oxygen and 1 percent other gases on a moisture free basis. A more precise analysis is given in Table 14.1. However, as the air progresses through the network of underground openings, that composition changes. There are two primary reasons for this. First, the mining of subsurface structures allows any gases that exist in the surrounding strata to escape into the ventilating airstream. Such **strata gases** have been produced over geological time and remain trapped within the pores and fracture networks of the rock. Methane and carbon dioxide are commonly occurring strata gases.

Secondly, a large number of chemical reactions may cause changes in the composition of mine air. Oxidation reduces the percentage of oxygen and often causes the evolution of carbon dioxide or sulphur dioxide. The action of acid mine water on sulphide minerals may produce the characteristic odour of hydrogen sulphide while the burning of fuels or the use of explosives produce a range of gaseous pollutants. Most of the fatalities resulting from mine fires and explosions have been caused by the toxic gases that are produced rapidly in such circumstances.

Several of the gases that appear in subsurface facilities are highly toxic and some are dangerously flammable when mixed with air. Their rate of production is seldom constant. Furthermore, their propagation through the multiple airways and often convoluted leakage paths of a subsurface ventilation system is further modified by the effects of gas density differences, diffusion and turbulent dispersion. These matters all influence the variations in concentrations of mine gases that may be found at any time and location in an underground mine.

A primary requirement of a mine ventilation system is to dilute and remove airborne pollutants (Section 1.3.1.). It is, therefore, necessary that the subsurface environmental engineer should be familiar with the physical and chemical properties of mine gases, their physiological effects, how they may be detected and preferred methods of control. In this chapter we shall classify and discuss those gases that may appear in subsurface ventilation systems.

11.2. CLASSIFICATION OF SUBSURFACE GASES

Table 11.1 lists the gases that are most commonly encountered in underground openings. Each of those gases is discussed in further detail within this section.

11.2.1. Threshold limit values (TLV)

Threshold limit values of airborne substances refer to those concentrations within which personnel may be exposed without known adverse effects to their health or safety. The guideline TLVs given on Table 11.1 have been arrived at through a combination of industrial experience and from both animal and human studies. They are based primarily on recommendations of the American Conference of Governmental Industrial Hygienists (ACGIH) and the U. S. National Institute for Occupational Safety and Health (NIOSH). The values quoted should be regarded as **guidelines** rather than clear demarcations between safe and dangerous concentrations. There are two reasons for this. First, wide variations in personal response to given substances occur between individuals, depending upon one's state of health, exposure history and personal habits (e. g. smoking and use of alcohol). Secondly, TLVs are necessarily based on current scientific knowledge and are subject to revision as new evidence becomes available.

To ensure compliance with statutory requirements, ventilation/environmental engineers and industrial hygienists should familiarize themselves with any mandatory TLVs that have been established within their particular country or state.

Table 11.1 Classification of gases most commonly found in subsurface openings

Name	Symbol	Molecular Weight (based on C ¹²)	Density at 20°C and 100 kPa kg/m ³	Density relative to dry air	Gas Constant J/kg °C	Primary sources in mines	Smell, colour, taste	Hazards	Guideline TLVs	Methods of detection*	Flammability limits in air per cent
dry air		28.966	1.1884	1	287.04		none				
oxygen	O ₂	31.999	1.3129	1.1047	259.83	air	none	oxygen deficiency; may cause explosive mixtures with reactive gases	>19.5	electro-chemical, paramagnetic, flame lamp	
nitrogen	N ₂	28.015	1.1493	0.9671	296.80	air, strata	none	inert		by difference	
methane	CH ₄	16.04	0.6581	0.554	518.35	strata	none	explosive; layering	1%:isolate electricity 2%:remove personnel	catalytic oxidation, thermal conductivity, optical, acoustic, flame lamp	5 to 15
carbon dioxide	CO ₂	44.00	1.805	1.519	188.96	oxidation of carbon, fires, explosions, IC engines, blasting, respiration	slight acid taste and smell	promotes increased rate of respiration	TWA=0.5% STEL=3.0%	optical, infra-red	
carbon monoxide	CO	28.01	1.149	0.967	296.8	fires, explosions, IC engines, blasting, spontaneous or incomplete combustion of carbon compounds	none	highly toxic; explosive	TWA= 0.005% STEL=0.04%	electro-chemical, catalytic oxidation, semi-conductor, infra-red	12.5 to 74.2
sulphur dioxide	SO ₂	64.06	2.628	2.212	129.8	oxidation of sulphides, acid water on sulphide ores, IC engines	acid taste, suffocating smell	very toxic; irritant to eyes throat and lungs	TWA=2ppm STEL=5ppm	electro-chemical, infra-red	

Name	Symbol	Molecular Weight (based on C ¹²)	Density at 20°C and 100 kPa kg/m ³	Density relative to dry air	Gas Constant J/kg °C	Primary sources in mines	Smell, colour, taste	Hazards	Guideline TLVs	Methods of detection*	Flammability limits in air Per cent
nitric oxide	NO	30.01	1.231	1.036	277.1	IC engines, blasting, welding	irritant to eyes, nose and throat	oxidizes rapidly to NO ₂	TWA=25ppm	electro-chemical, infra-red	
nitrous oxide	N ₂ O	44.01	1.806	1.519	188.9		sweet smell	narcotic (laughing gas)	TWA=50ppm	electro-chemical	
nitrogen dioxide	NO ₂	46.01	1.888	1.588	180.7		reddish brown, acidic smell and taste	very toxic; throat and lung irritant; pulmonary infections	TWA=3ppm ceiling: 5ppm	electro-chemical, infra red	
hydrogen sulphide	H ₂ S	34.08	1.398	1.177	244.0	acid water on sulphides, stagnant water, strata, decomposition of organic materials	odour of bad eggs	highly toxic; irritant to eyes and respiratory tracts; explosive	TWA=10ppm STEL=15ppm	electro-chemical, semi-conductor	4.3 to 45.5
hydrogen	H ₂	2.016	0.0827	0.0696	4124.6	battery charging, strata, water on incandescent materials, explosions	none	highly explosive		catalytic oxidation	4 to 74.2
radon	Rn	≈ 222	9.108	7.66	37.45	uranium minerals in strata	none	radioactive; decays to radioactive particles	1 WL and 4 WL-months per year	radiation detectors	
water vapour	H ₂ O	18.016	0.739	0.622	461.5	evaporation of water, IC engines, respiration, spon.com. and other fires	none	affects climatic environment		psychrometers, dielectric effects	

*In addition to the methods listed, most of these gases can be detected by gas chromatography and stain tubes

Three types of threshold limit values are expressed in Table 11.1. The **Time-Weighted Average (TWA)** is the average concentration to which nearly all workers may be exposed over an 8 hour shift and a 40 hour work week without known adverse effects. However, many substances are sufficiently toxic that short-term exposures at higher concentrations may prove harmful or even fatal. The **Short-Term Exposure Limit (STEL)** is a time-weighted average concentration occurring over a period of not more than 15 minutes. That is, concentrations above the TWA and up to the STEL should not last for longer than 15 minutes. It is also recommended that such circumstances should not occur more than four times per day nor at intervening intervals of less than one hour.

The **Ceiling Limit** is the concentration that should not be exceeded at any time. This is relevant for the most toxic substances or those that produce an immediate irritant effect.

11.2.2. Oxygen, O₂

Human beings and, indeed, the vast majority of the animal kingdom are completely dependent upon the oxygen that comprises some 21 percent of fresh atmospheric air. Oxygen diffuses through the walls of the alveoli in the lungs to form **oxyhaemoglobin** in the bloodstream. This unstable substance breaks down quite readily to release the oxygen where required throughout the body.

As muscular activity increases, so also does the rate of respiration and the volume of air exchanged at each breath. However, the percentage of oxygen that is utilized decreases at heavier **rates of breathing**. For low levels of physical activity, exhaled air contains approximately 16 percent oxygen, 79 percent nitrogen and 5 percent carbon dioxide. Table 11.2 indicates typical rates of oxygen consumption and production of carbon dioxide. This table is helpful in estimating the effects of respiration on the gas concentrations in a confined area.

Activity	Breaths/min	Inhalation rate litres/s	Oxygen consumption litres/s	Carbon dioxide produced litres/s
At rest	12-18	0.08 - 0.2	≈ 0.005	≈ 0.004
Moderate work	30	0.8 - 1.0	≈ 0.03	≈ 0.027
Vigorous work	40	≈ 1.6	≈ 0.05	≈ 0.05

Table 11.2. Gas exchange during respiration (based on work by Forbes and Grove (1954)).

Example

Air is supplied at a rate of 5m³/s to ten persons working at a moderate rate in a mine heading. The intake air contains 20.6 percent oxygen and 0.1 percent carbon dioxide. Determine the changes in concentrations of these gases caused by respiration.

Solution

For a moderate rate of activity, Table 11.2 indicates an individual consumption rate of some 0.03 litres/s for oxygen and a production rate of about 0.027 litres/s for carbon dioxide. Hence, for ten persons:

$$\begin{aligned} \text{oxygen depletion} &= 10 \times 0.03 \times 10^{-3} = 0.0003 \text{ m}^3/\text{s} \\ \text{carbon dioxide added} &= 10 \times 0.027 \times 10^{-3} = 0.00027 \text{ m}^3/\text{s} \end{aligned}$$

In the intake air:

$$\begin{aligned} \text{oxygen flow} &= 5 \times 0.206 = 1.03 \text{ m}^3/\text{s} \\ \text{carbon dioxide flow} &= 5 \times 0.001 = 0.005 \text{ m}^3/\text{s} \end{aligned}$$

Therefore, in the exit air:

$$\begin{aligned} \text{oxygen flow} &= 1.03 - 0.0003 = 1.0297 \text{ m}^3/\text{s} \\ \text{carbon dioxide flow} &= 0.005 + 0.00027 = 0.00527 \text{ m}^3/\text{s} \\ \text{oxygen concentration} &= \frac{1.0297}{5} \times 100 = 20.594 \text{ percent} \\ \text{carbon dioxide concentration} &= \frac{0.00527}{5} \times 100 = 0.1054 \text{ percent} \end{aligned}$$

This example illustrates the very limited effect of respiration on the concentrations of oxygen and carbon dioxide in a mine ventilation system. Indeed, the ventilating air necessary for breathing is negligible compared with other airflow requirements in the subsurface (Section 9.3.).

As air flows through an underground facility, it is probable that its oxygen content will decrease. This occurs not only because of respiration but, more importantly, from the oxidation of minerals (particularly coal and sulphide ores) and imported materials. The burning of fuels within internal combustion engines and open fires also consume oxygen. The primary danger of this gas is, therefore, that it may be depleted below a level that is necessary for the well being of the workforce. In Table 11.1, oxygen is the only gas whose concentration should be maintained above its recommended threshold limit value. The effects of **oxygen depletion** are as follows:

Percent oxygen in air	Effects
19.0	Flame height on a flame safety lamp reduced by 50 percent.
17	Noticeable increase in rate and depth of breathing - this effect will be further enhanced by an increased concentration of carbon dioxide.
16	Flame lamp extinguished.
15	Dizziness, increased heartbeat.
13 to 9	Disorientation, fainting, nausea, headache, blue lips, coma.
7	Coma, convulsions and probable death.
below 6	Fatal.

Oxygen deficiency implies an increased concentration of one or more other gases. Hence, although not listed explicitly in Table 11.1, even non-toxic gases will endanger life by asphyxiation if they are present in sufficient concentration to cause a significant oxygen deficiency.

11.2.3. Nitrogen, N₂

Nitrogen constitutes approximately 78 percent of air and is, therefore, the most abundant gas in a ventilated system. It is fairly inert and occurs occasionally as a strata gas, usually mixed with other gases such as methane and carbon dioxide.

11.2.4. Methane, CH₄

Methane is produced by bacterial and chemical action on organic material. It is evolved during the formation of both coal and petroleum, and is one of the most common strata gases. Methane is

not toxic but is particularly dangerous because it is flammable and can form an explosive mixture with air. This has resulted in the deaths of many thousands of miners. A methane: air mixture is sometimes referred to as **fire damp**.

Although methane is especially associated with coal mines, it is often found in other types of subsurface openings that are underlain or overlain with carbonaceous or oil-bearing strata. The methane is retained within fractures, voids and pores in the rock either as a compressed gas or adsorbed on mineral (particularly carbon) surfaces. When the strata is pierced by boreholes or mined openings, then the gas pressure gradient that is created induces migration of the methane towards those openings through natural or mining-induced fracture patterns. The phenomena of methane retention within the rock and the mechanisms of its release are discussed in Chapter 12.

Methane itself has no odour but is often accompanied by traces of heavier hydrocarbon gases in the paraffin series that do have a characteristic oily smell. As indicated in Table 11.1, methane has a density that is a little over half that of air. This gives rise to a dangerous behaviour pattern - **methane can form pools or layers along the roofs of underground openings**. Any ignition of the gas can then propagate along those layers to emission sources (Section 12.4.2). The buoyancy of methane can also create problems in inclined workings.

Methane burns in air with a pale blue flame. This can be observed over the lowered flame of a safety lamp at concentrations as small as 1¼ percent. In an abundant supply of air, the gas burns to produce water vapour and carbon dioxide.



Unfortunately, within the confines of mined openings and during fires or explosions, there may be insufficient oxygen to sustain full combustion, leading to formation of the highly poisonous carbon monoxide.



The explosible range for methane in air is normally quoted as 5 to 15 percent¹ by volume, with the most explosive (stochastic) mixture occurring at about 9.8 percent. While the lower limit remains fairly constant, the upper explosive limit reduces as the oxygen content of the air falls. The flame will propagate through the mixture while it remains within the flammable range. Figure 11.1 illustrates a well known diagram first produced by **H. F. Coward** in 1928. This can be used to track the flammability of air:methane mixtures as the composition varies. In zone A, the mixture is not flammable but is likely to become so if further methane is added or that part of the mine is sealed off. In zone B, the mixture is explosive and has a minimum nose value at 12.2 percent oxygen. Zones C and D illustrate mixtures that may exist in sealed areas. A mixture in zone C will become explosive if the seals are breached and the gases intermingle with incoming air. However, dilution of mixtures in zone D can be accomplished without passing through an explosive range.

¹ The flammability limits (and particularly the UEL) for any flammable gas or vapour are not absolute constants but vary with the conditions under which the ignition occurs. The UEL values of 14% and 15% that are often quoted for methane encompass the range that has been observed for most tests involving upward propagation of the flame. The type and energy of the igniting source (e.g. open flame or temperature and area of heated surface also affect the results). Although 'ignition temperatures' of sources are often quoted, it is the temperature to which the flammable mixture is raised that really matters. The pressure of the mixture has only a small effect. Values of explosibility limits, quoted without specifying the test conditions, should be regarded as average values. It is prudent to assume the wider measured limits of flammability for regulatory purposes and in guidelines for practice.

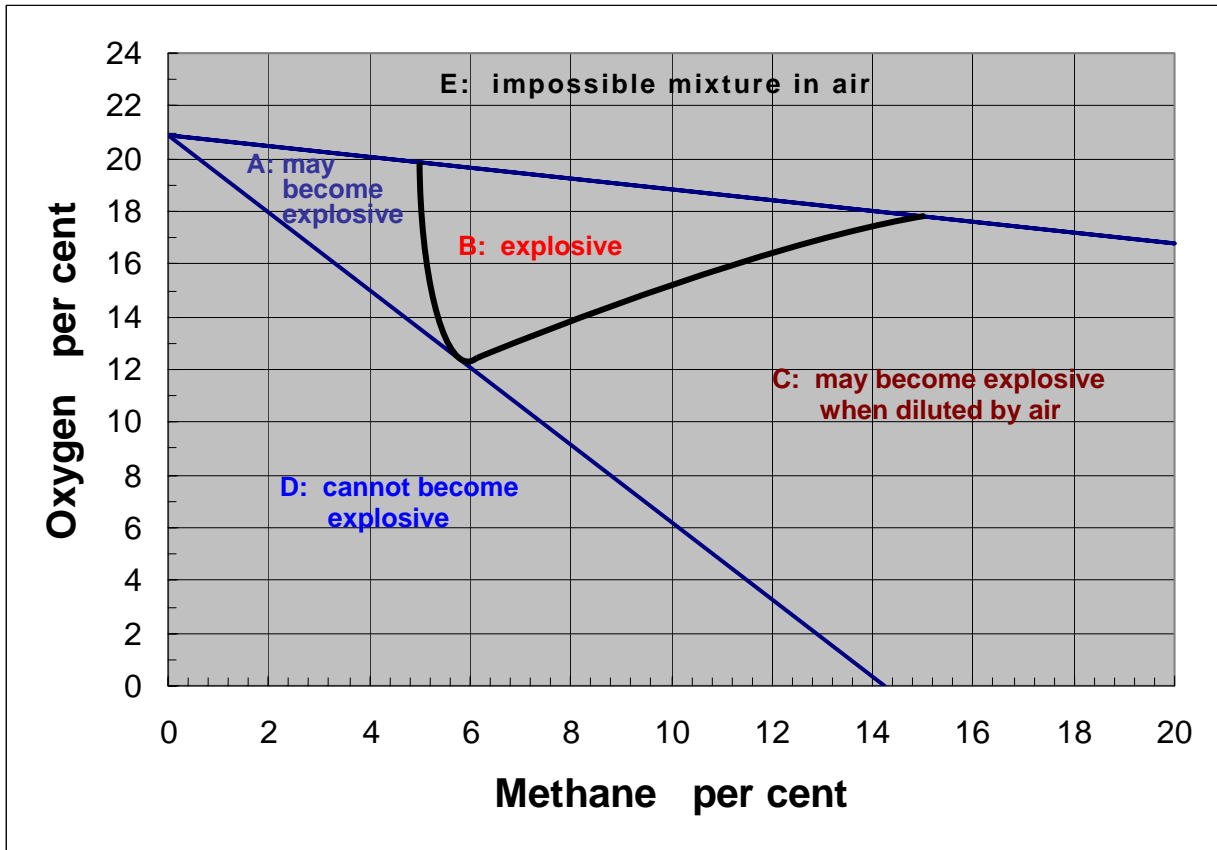


Figure 11.1 The Coward diagram for methane in air.

Mining law specifies actions that must be taken when certain fractions of the lower flammable limit have been reached. For example, legislation may require that electrical power must be switched off when the methane concentration exceeds 1 or 1¼ percent. Personnel other than those concerned with the improvement of ventilation should leave any area when the methane concentration exceeds 2 or 2½ percent. The legislation of the relevant country or state must be consulted for the precise values of limiting concentrations and required actions. Other regulations specify the frequency at which measurements of methane concentration must be taken and threshold limit values to be applied in specified locations.

In many countries, underground mines are classified as either **gassy** or **non-gassy**. These legal terms relate to the potential for methane to be emitted into the workings. It is prudent that all underground coal mines be designated as gassy. Any other mine may become legally gassy if

- methane emissions from the roof, floor or sides of openings have been observed or the surrounding strata are deemed capable of producing such emissions,
- a methane ignition has occurred in the past, or
- the mine is connected underground to another mine that has already been classified as gassy.

Imposing a gassy designation on a mine can result in a significant increase in capital and operating costs as all equipment and operating procedures must then be designed and maintained to minimize the risk of igniting a methane:air mixture.

11.2.5. Carbon dioxide, CO₂

Carbon dioxide appears in subsurface openings from a variety of sources including strata emissions, oxidation of carbonaceous materials, internal combustion engines, blasting, fires, explosions and respiration. Stagnant mixtures of air in sealed off areas often have an increased concentration of carbon dioxide and decreased oxygen content. Such mixtures are sometimes called **blackdamp**.

Table 11.1 indicates that carbon dioxide is more than fifty percent heavier than air and will, therefore, tend to collect on the floors of mine workings. This was the reason for the small animals depicted in some of Agricola's woodcuts of sixteenth century mine workings. It is common to find emanations of blackdamp from the bottoms of seals behind which are abandoned workings, particularly during a period of falling barometric pressure. Particular care must be taken when holing through into a mined area that has not been ventilated for some time.

In addition to diluting oxygen in the air, carbon dioxide acts as a stimulant to the respiratory and central nervous systems. The solubility of carbon dioxide is about twenty times that of oxygen. Diffusion of the gas into the bloodstream is rapid and the effects on rate and depth of breathing are soon noticed. Cylinders of oxygen used for resuscitation often contain some 4 percent of carbon dioxide to act as a respiratory stimulant (**carbogen gas**).

The physiological effects of carbon dioxide have been listed by Strang and MacKenzie-Wood (1985) as follows:

Percent carbon dioxide in air	Effects
0.037 – 0.038 ²	None, normal concentration of carbon dioxide in air.
0.5	Lung ventilation increased by 5 percent
2.0	Lung ventilation increased by 50 percent.
3.0	Lung ventilation doubled, panting on exertion.
5 to 10	Violent panting leading to fatigue from exhaustion, headache.
10 to 15	Intolerable panting, severe headache, rapid exhaustion and collapse.

Fortunately, the administration of oxygen accompanied by warmth and an avoidance of exertion will usually lead to recovery with no known long term effects.

11.2.6. Carbon monoxide, CO

The high toxicity of carbon monoxide coupled with its lack of smell, taste or colour make this one of the most dangerous and insidious of mine gases. It has a density very close to that of air and mixes readily into an airstream unless it has been heated by involvement in a fire, in which case it may layer with smoke along the roof.

Carbon monoxide is a product of the incomplete combustion of carbonaceous material. Although colourless, it has the traditional name of **whitedamp**. The great majority of fires and explosions in

² The percentage of carbon dioxide in air has been increasing over the past century, currently at a rate of some 1.5 parts per million (0.00015 percent) each year. The rise is superimposed on an annual cyclic variation of about 5 ppm (0.0005 percent) caused by seasonal reactions of plant life.

mines produce carbon monoxide. Indeed, most fatalities that have occurred during such incidents have been a result of carbon monoxide poisoning. The mixture of gases, including carbon monoxide, resulting from a mine explosion, is often referred to as **afterdamp**. Carbon monoxide is also formed by internal combustion engines, blasting and spontaneous combustion in coal mines. It can be generated as a component of **water gas** (carbon monoxide and hydrogen) when water is applied to the base of incandescent coal during firefighting operations.

Carbon monoxide burns with a blue flame and is highly flammable, having a wide range of flammability, 12.5 to 74.2 percent in air, with the maximum explosibility at 29 percent.

In order to understand the physiological effects of carbon monoxide, let us recall from Section 11.2.2. that oxygen passes through the walls of alveoli in the lungs and is absorbed by haemoglobin (red cells) in the blood to form the fairly unstable **oxyhaemoglobin**. Unfortunately, haemoglobin has an affinity for carbon monoxide that is about three hundred times greater than that for oxygen. To compound the problem, the new substance formed in the bloodstream, **carboxyhaemoglobin** (CO.Hb), is relatively stable and does not readily decompose. The consequences are that very small concentrations of carbon monoxide cause the formation of carboxyhaemoglobin which accumulates within the bloodstream. This leaves a reduced number of red cells to carry oxygen molecules throughout the body. The physiological symptoms of carbon monoxide arise because of oxygen starvation to vital organs, particularly the brain and heart.

Physiological reactions to carbon monoxide depend upon the concentration of the gas, the time of exposure and the rate of lung ventilation, the latter being governed primarily by physical activity. In order to relate the symptoms of carbon monoxide poisoning to a single parameter, the degree of saturation of the blood by carboxyhaemoglobin is employed. Although variations exist between individuals, the following list provides a guideline of the progressive symptoms.

Blood saturation percent CO.Hb	Symptoms
5-10	Possible slight loss of concentration
10-20	Sensation of tightness across forehead, slight headache
20-30	Throbbing headache, judgment impaired.
30-40	Severe headache, dizziness, disorientation, dimmed vision, nausea, possible collapse.
40-60	Increased probability of collapse, rise in rates of pulse and respiration, convulsions
60-70	Coma, depressed pulse and respiration, possible death.
70-80	Fatal.

Figure 11.2 gives a more practical guide of physiological reactions to carbon monoxide and takes the level of physical activity and exposure time into account.

Due to the bright red colour of carboxyhaemoglobin, a victim of carbon monoxide poisoning may have a flushed appearance, even after death. At high blood saturation levels, deterioration of the body is often retarded after death due to the absence of internal oxygen.

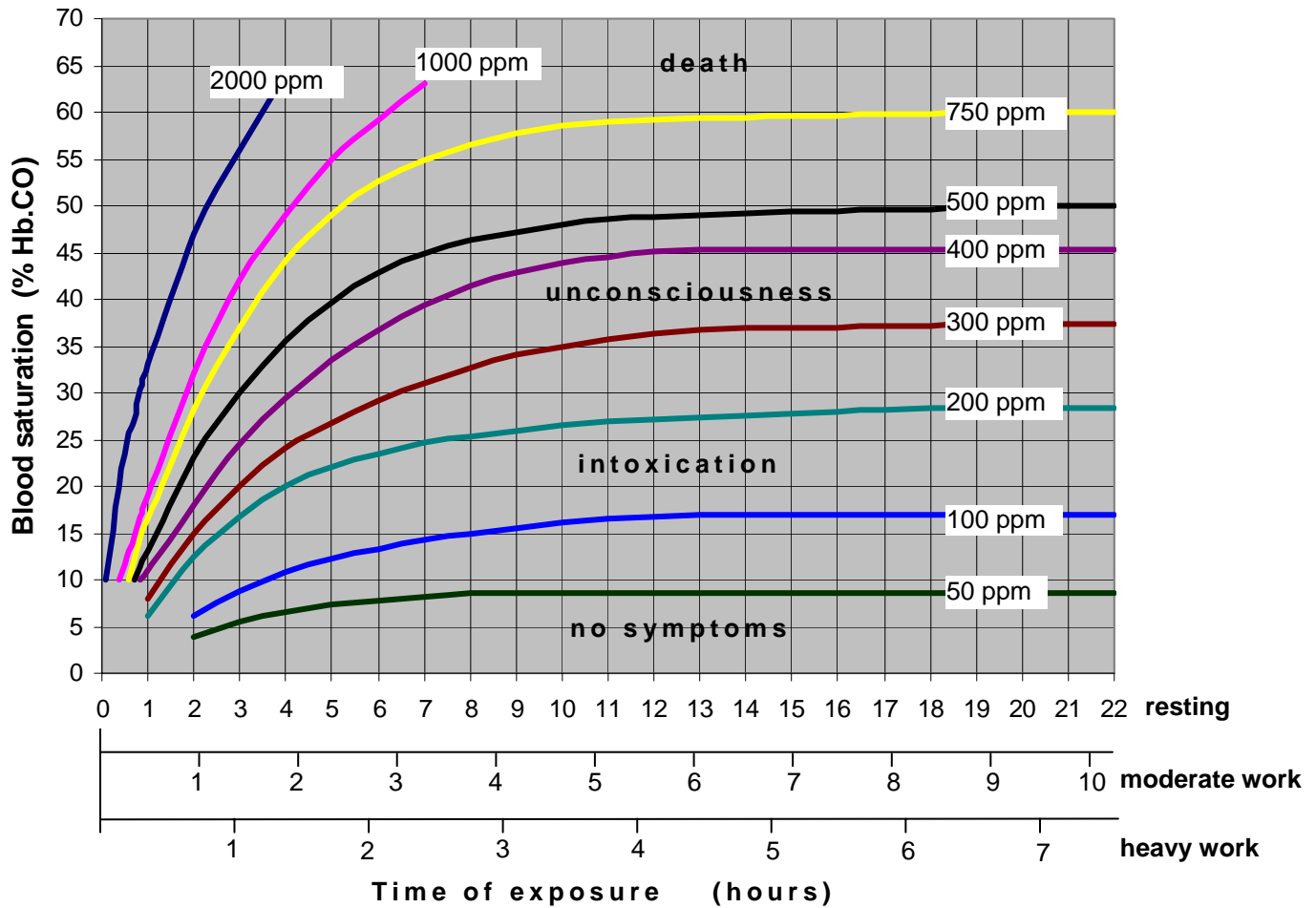


Figure 11.2 Physiological effects of carbon monoxide (developed from Strang and Wood, 1985).
[The three horizontal axes represent hours of exposure for each of three levels of activity.]

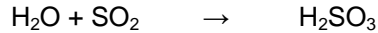
Persons suffering from carbon monoxide poisoning should be kept warm and removed from the polluted atmosphere, preferably, on a stretcher. It may take more than twenty four hours for blood saturation levels to return to normal. During this time, severe headaches may be experienced. However, the return to normal blood saturation levels can be accelerated significantly by the administration of pure oxygen. The rapidity with which carbon monoxide is absorbed into the bloodstream and the slowness of its expurgation can result in dangerous blood saturation levels occurring in firefighters who make short repeated expeditions into a polluted area.

In addition to the physical symptoms that have been listed for carbon monoxide poisoning, experience of personnel involved in mine fires has indicated significant psychological reactions that have had grave repercussions. Low levels of blood saturation can give an appearance of intoxication including impairment of judgment and an unsteady gait preceding collapse. Victims may become silent and morose, and may resist or fail to comprehend instructions that will lead them to safety. The sense of time may be affected, a particularly significant symptom when self-rescuer devices are being worn. However, all of these reactions vary considerably between individuals. In particular, total collapse will occur rapidly in high concentrations of carbon monoxide.

A small degree of acclimatization has been observed in persons who are repeatedly exposed to low levels of carbon monoxide as experienced, for example, by habitual smokers. This is thought to occur because of an increase in the number of red cells within the bloodstream.

11.2.7. Sulphur dioxide, SO₂

This is another highly toxic gas but one which, fortunately, can be detected at very low concentrations both by its acidic taste and the intense burning sensation it causes to the eyes and respiratory tracts. The latter is a result of the high solubility of the gas in water to form sulphurous acid.



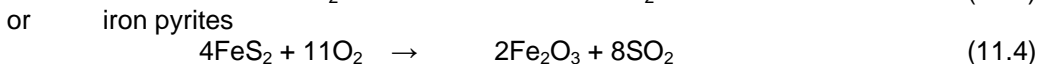
This, in turn, can oxidize to sulphuric acid, H₂SO₄.

When discussing very small concentrations, it is convenient to refer to parts per million (ppm) rather than percentages. The conversion between the two is accomplished simply by moving the decimal point four places in the appropriate direction. The following list of physiological reactions to sulphur dioxide employs parts per million.

Concentration of sulphur dioxide ppm	Effects
1	Acidic taste
3	Detectable by odour.
20	Irritation of eyes and respiratory system.
50	Severe burning sensation in eyes, nose and throat.
400	Immediately dangerous to life.

First aid for sulphur dioxide poisoning includes the administration of oxygen, immobility and warmth. The longer term treatment is for acid corrosion of the eyes and respiratory system.

Sulphur dioxide is formed in internal combustion engines and by the oxidation of sulphide ores, for example:



These and other similar reactions can occur when sulphide ores are heated in a fire or by spontaneous combustion. Although sulphur dioxide is colourless, white fumes may be seen due to condensation of acidic water vapours or traces of sulphur trioxide, SO₃.

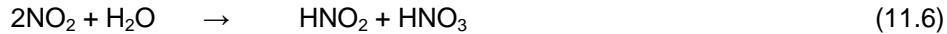
11.2.8. Oxides of nitrogen, NO_x

Three oxides of nitrogen are listed on Table 11.1. Nitric oxide, NO, nitrous oxide, N₂O, and nitrogen dioxide, NO₂, are formed in internal combustion engines and by blasting. The proportion of nitrous oxide is likely to be small. Furthermore, nitric oxide converts rapidly to nitrogen dioxide in the presence of air and water vapour.



As nitrogen dioxide is the most toxic of these oxides of nitrogen, it is sensible to concentrate upon the physiological effects of this gas.

At the temperatures found in underground openings, it is probable that nitrogen dioxide will be mixed with a companion gas, nitrogen tetroxide, N_2O_4 , having similar physiological effects. The brown fumes of nitrogen dioxide dissolve readily in water to form both nitrous (HNO_2) and nitric (HNO_3) acids.



These acids cause irritation and, at higher concentrations, corrosive effects on the eyes and respiratory system. The progressive symptoms are as follows:

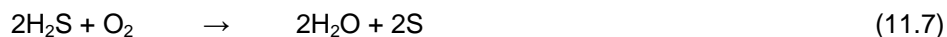
Concentration of nitrogen dioxide ppm	Effects
40	May be detected by smell.
60	Minor throat irritation
100	Coughing may commence.
150	Severe discomfort, may cause pneumonia later.
200	Likely to be fatal

The immediate treatment for nitrogen dioxide poisoning is similar to that for sulphur dioxide, namely, the administration of oxygen, immobility and warmth. An insidious effect of nitrogen dioxide poisoning is that an apparent early recovery can be followed, soon afterwards, by the development of acute bronchopneumonia.

11.2.9. Hydrogen sulphide, H_2S

The presence of this highly toxic gas is readily detected by its characteristic smell of bad eggs. This has given rise to the colloquial name **stinkdamp**. Unfortunately, hydrogen sulphide has a narcotic effect on the nervous system including paralysis of the olfactory nerves. Hence, after a short exposure, the sense of smell can no longer be relied upon.

Hydrogen sulphide is produced by acidic action or the effects of heating on sulphide ores. It is formed naturally by bacterial or chemical decomposition of organic compounds and may often be detected close to stagnant pools of water in underground mines. Hydrogen sulphide may occur in natural gas or petroleum reserves and migrate through the strata in a weakly acidic water solution. It can also be generated in gob fires. In such cases, free sulphur may be deposited by partial oxidation of the gas.



This can sometimes be seen as a yellow deposit in burned areas. However, in a plentiful supply of air, hydrogen sulphide will burn with a bright blue flame to produce sulphur dioxide.



The physiological effects of hydrogen sulphide may be listed as follows:

Concentration of hydrogen sulphide ppm	Effects
0.1 to 1	Detectable by smell.
5	Beginning of toxicity
50 to 100	Slight irritation to eyes and respiratory tract, headache, loss of odour after 15 minutes.
200	Intensified irritation of nose and throat.
500	Serious inflammation of eyes, nasal secretions, coughing, palpitations, fainting.
600	Chest pains due to corrosion of respiratory system, may be fatal.
700	Depression, coma, probable death.
1000	Paralysis of respiratory system, very rapid death.

A victim who recovers from hydrogen sulphide poisoning may be left with longer term conjunctivitis and bronchitis.

11.2.10. Hydrogen, H₂

Although non-toxic, hydrogen is the most explosive of all the mine gases. It burns with a blue flame and has the wide flammable range of 4 to 74.2 percent in air. Hydrogen can be ignited at a temperature as low as 580 °C, and with an ignition energy about half of that required by methane.

Hydrogen occasionally appears as a strata gas and may be present in afterdamp at about the same concentrations as carbon monoxide. The action of water on hot coals can produce hydrogen as a constituent of water gas (Section 11.2.6.). Dangerous accumulations of hydrogen may occur at locations where battery charging is in progress. Hydrogen has a density only some 0.07 that of air. It will, therefore, tend to rise to the roof. Battery charging stations should be located in intake air with a duct or opening at roof level that connects into a return airway.

11.2.11. Radon, Rn

This chemically inert gas is one of the elements formed during radioactive disintegration of the uranium series. Although its presence is most serious in uranium mines, it may be found in many other types of underground openings. Indeed, seepages of radon from the ground into the basements of surface buildings have been known to create a serious health hazard.

Radon emanates from the rock matrix or from ground water that has passed over radioactive minerals. It has a half life of 3.825 days and emits alpha radiation. The immediate products of the radioactive decay of radon are minute solid particles known as the radon daughters. These adhere to the surfaces of dust particles and emit alpha, beta and some gamma radiation.

Radon and the problems of radiation in mines are discussed further in Chapter 13.

11.3. GAS MIXTURES

Although the gases that occur most commonly underground have been discussed separately in Section 11.2., it is more usual that several gaseous pollutants appear together as gas mixtures. Furthermore, the importation of an ever-widening range of materials into subsurface facilities also introduces the risk of additional gases being emitted into the mine environment.

11.3.1. Threshold limit values for gas mixtures

In order to widen the applicability of this section, the recommended threshold limit values of a number of other gases and vapours are given in Table 11.3 and grouped in terms of probable sources. Again, we are reminded that these TLVs are simply guidelines and that national or state mandated limits should be consulted to ensure compliance with the relevant laws.

In any given atmosphere, if there are two or more airborne pollutants (gaseous or particulate) that have adverse effects on the same part of the body, then the threshold limit value should be assessed on the basis of their combined effect. This is calculated as the dimensionless sum.

$$\frac{C_1}{T_1} + \frac{C_2}{T_2} + \dots + \frac{C_n}{T_n} \quad (11.9)$$

where C = measured concentration
and T = corresponding threshold limit value.

If the sum of the series exceeds unity, then the threshold limit value of the mixture is deemed to be exceeded. (ACGIH, 1989)

Example

An analysis of air samples taken in a return airway indicates the following gas concentrations:

carbon dioxide: 0.2 percent, carbon monoxide: 10 ppm
hydrogen sulphide: 2 ppm, sulphur dioxide: 1 ppm

Determine the threshold limit values, TWA and STEL for the mixture.

Solution

Sulphur dioxide and hydrogen sulphide are both irritants to the eyes and respiratory system. Furthermore, carbon dioxide is a stimulant to breathing, increasing the rate of ventilation of the lungs. Hence, it may be regarded as being synergistic with the sulphur dioxide and hydrogen sulphide. Carbon monoxide, however, affects the oxygen carrying capacity of the bloodstream and need not be combined with the other gases in determining the threshold limit values for the mixture.

From Table 11.1, the following time weighted averages (TWA) and short term exposure limits (STEL) are determined:

Component	Threshold limit values	
	TWA	STEL
carbon dioxide	0.5 percent	3.0 percent
hydrogen sulphide	10 ppm	15 ppm
sulphur dioxide	2 ppm	5 ppm
carbon monoxide	50 ppm	400 ppm

Table 11.3 Threshold limit values for other gases and vapours that may be present underground

Substance	Guideline time weighted average limit (ppm unless otherwise stated)
Cleaners and solvents	
acetone	750 (STEL = 1000)
ammonia	25 (STEL = 35)
toluene)	100 (STEL = 150)
turpentine	100 (STEL= 150)
Refrigerants	
ammonia	25 (STEL = 35)
R11	1000 (ceiling)
R12	1000
R22	1000
R112	500
Fuels	
butane	800
gasoline vapour	300 (STEL = 500)
liquid petroleum gas	1000
naphtha (coal tar))	100
pentane	600 (STEL = 750)
propane	1000
Welding and soldering	
general welding fumes	5 mg/m ³
iron oxide fumes	5 mg/m ³
lead fumes	0.15 mg/m ³
ozone (arc welding)	0.1 ppm ceiling
fluorides (fluxes)	2.5 mg/m ³
Heated plastics	
carbon dioxide	0.5% (STEL = 3.0%)
carbon monoxide	50 (STEL = 400)
hydrogen chloride fumes	5 ppm ceiling
hydrogen cyanide	10
hydrogen fluoride	3 ppm ceiling
phenol (absorbed by skin)	5
Explosives	
carbon dioxide	0.5% (STEL = 3.0%)
carbon monoxide	50 (STEL = 400)
oxides of nitrogen	25
ammonia	25 (STEL = 35)
sulphur dioxide	2 (STEL = 5)
nitrous acid fumes	
nitric acid fumes	2 (STEL = 4)
Others	
chlorine (biocides)	0.5 (STEL = 1)
cresol (wood preservative)	5
mercury vapour	0.05 mg/m ³
oil mist (mineral): vapour free	5 mg/m ³
oil mist (vegetable): vapour free	10 mg/m ³
sulphuric acid fumes (batteries)	1 mg/m ³

The carbon monoxide concentration measured at 10 ppm and treated separately is shown to be less than the TWA of 50 ppm.

The equivalent threshold limit value of the remainder of the mixture is assessed from equation (11.9) as:

$$\text{TWA: } \frac{0.2}{0.5} + \frac{2}{10} + \frac{1}{2} = 1.1$$

carbon dioxide	hydrogen sulphide	sulphur dioxide
-------------------	----------------------	--------------------

$$\text{STEL: } \frac{0.2}{3} + \frac{2}{15} + \frac{1}{5} = 0.4$$

The dimensionless TWA is greater than 1. Hence, the time weighted average limit is exceeded. However, the short term exposure limit is less than unity. The implication is that personnel may spend time periods not exceeding 15 minutes in this atmosphere, but not a complete 8 hour shift.

In some cases of gas mixtures, it may be practicable to monitor quantitatively for one pollutant only, even though it is known that other gases or particulates are present. In such circumstances, a pragmatic approach is to reduce the threshold limit value of the measured substance by a factor that is assessed from the number, toxicity and estimated concentrations of other contaminants known to be present.

11.3.2. Diesel emissions

The flexibility and reliability of diesel engines have resulted in a proliferation in their use for all types of underground mines. This is, however, tempered by the emissions of exhaust gases, heat and humidity that result from the employment of diesels. Guidance on the airflow requirements for diesel equipment is given in Section 9.3.2.

The substances that are emitted from diesel exhausts include:

- nitrogen
- carbon monoxide
- carbon dioxide
- oxides of nitrogen
- sulphur dioxide
- diesel particulate matter
- water vapour (Sections 15.3.2.2. and 16.2.3.)

The actual magnitude and composition of diesel exhausts are governed by the engine design, quality of maintenance, exhaust treatment units, rating for altitude and skill of the operator.

Catalytic converters cause the exhaust gases to filter through granulated oxidizing agents. These can successfully convert up to 90 percent of the carbon monoxide and 50 percent of unburned fuel to carbon dioxide and water vapour. Sulphur dioxide may be partially converted to sulphur trioxide and appear as vapour of sulphuric acid.

Water scrubbers give an improved removal of sulphur dioxide and particulate matter but do little for carbon monoxide. Engine gas recirculation (EGR) systems help to reduce the oxides of nitrogen.

The **diesel particulate matter** is a combination of soot, unburned fuel and aldehydes, and is regarded as being the component of diesel exhaust that is most hazardous to health. There are two reasons for this. First, the particles are typically less than one micron in diameter. They are inhaled deeply into the lungs and have a high probability of being retained within the walls of the alveoli. Secondly, the porous or fibrous nature of the soot particles enables them to adsorb a range of polynuclear and aromatic hydrocarbons, giving diesel smoke its characteristic greasy feel. There is evidence that these have carcinogenic properties (Waytulonis, 1988) although the relationship between exposure to diesel exhaust emissions and the incidence of cancer remains unclear (French, 1984). Exhaust filters assist greatly in the removal of particulate matter.

The operating advantages of diesel equipment are in direct conflict with the potentially hazardous nature of exhaust emissions. This has resulted in a considerable research effort into the use of diesels in mining during the 1980's (e. g. World Mining, 1982; Daniel, 1989; Haney, 1989; Gunderson, 1990).

11.3.3. Fires

The predominant cause of loss of life associated with underground fires has been the gaseous products of combustion. The particular gases depend upon the type of fire and the materials that are being burned. Although carbon monoxide has resulted in the majority of such fatalities, the importation of a widening variety of manufactured materials into mines has produced the potential for other toxic gases to be emitted during a mine fire.

Coal mine fires that involve burning of the coal itself are likely to produce an atmosphere that is deficient in oxygen and may contain

- carbon dioxide
- carbon monoxide
- methane
- water vapour

and smaller amounts of sulphur dioxide, hydrogen sulphide and hydrogen. Fires involving **timber** emit the same gases. The actual concentration of each gas depends primarily upon the oxygen content of the air within the fire zone (Chapter 21).

Metal mine fires arising from the spontaneous combustion of sulphide ores will emit products of combustion that are rich in sulphur dioxide and, possibly, sulphuric acid vapour.

Fires involving **diesel equipment** will produce gases from burning diesel oil and also from any plastic or rubber components that may become heated. The burning oil itself will emit

- | | |
|-------------------|----------------------|
| ● carbon monoxide | ● carbon dioxide |
| ● sulphur dioxide | ● oxides of nitrogen |
| ● hydrogen | ● hydrogen sulphide |

Plastic materials are employed for an increasing variety of purposes in underground workings, including brattice cloths, machine components, electrical cables and fittings, thermal insulation on pipes or airway linings, the pipes themselves, instrumentation, containers and meshing. Some plastic polymers will begin to disintegrate at about 250°C and before actual combustion

commences. However, the evolution of gases increases rapidly when the material burns. While all heated plastics give off

- carbon monoxide and
- carbon dioxide

the most dangerous are the polyurethanes, nylon and polyvinyl chloride (PVC) which may also produce

- hydrogen cyanide
- hydrofluoric acid fumes
- hydrochloric acid fumes

The **phenolic plastics** evolve the same gases but require a higher temperature for pyrolysis. Rubber based materials may also emit hydrogen sulphide when heated. Local or national regulations may prohibit the use of certain plastics.

In addition to gases, fires will normally also produce copious amounts of the respirable particulates that appear as visible smoke. These particles themselves may be toxic and are irritating to the eyes and respiratory tracts.

11.3.4. Explosives

The gases that may be produced by blasting are listed in Table 11.3. The concentrations of gases depend upon the type, quality and weight of explosive used, the means of detonation and the psychrometric condition of the air. The degree of confinement also affects the concentrations and time distribution of the gas emission - firing "on the solid" produces a sharper and higher peak of blasting fumes than if a free face were available. Some of the gases and fumes may be adsorbed onto mineral faces within the fragmented rock and be emitted over a longer time period (Rossi, 1971).

The oxides of nitrogen are formed mainly as nitric oxide during the detonation. The rate at which this oxidizes to nitrogen dioxide depends upon the degree to which the blasting fumes are diluted by a ventilating air current. Fumes that are purged from a mine during a re-entry period following blasting may still contain a significant proportion of nitric oxide when the pulse of fumes exits the mine.

11.3.5. Welding

The constituents of welding fumes can vary widely dependent upon the metals or alloys involved, the welding process employed and any fluxes that may be used. The fumes contain particles of amorphous slags and oxides of the metals being welded.

Arc welding in a local inert atmosphere such as argon will inhibit the formation of welding fumes but can produce ozone. On the other hand, arc welding within the air can produce copious fumes and carbon monoxide. Where stainless steel is involved, compounds of chromium and nickel can appear as constituents of the welding fumes. The employment of welding fluxes may also result in fluorides as well as a range of oxides being generated.

If no toxic compounds are present in the metals, welding rods or metal coatings, and the conditions do not favour the formation of toxic gases, then the threshold limit of 5 mg/m^3 given for general welding fumes in Table 11.3 may be used as a guideline.

11.4. GAS DETECTION AND MONITORING

11.4.1. Objectives and overview

The primary purpose of monitoring the concentrations of airborne pollutants in a mine is to ensure that the atmosphere provides a safe environment free from levels of toxicants that would create a hazard to health. There are essentially three matters to consider. The first is the threshold limit values deemed to be acceptable for each pollutant. Second is the choice of instrumentation best suited for the detection and measurement of particular gases. Third, the question of where and how frequently measurements are required must be addressed. Having discussed threshold limit values in Sections 11.2.1. and 11.3.1., we now turn our attention to the operating principles of instruments used to measure gas concentrations and methods of sampling.

11.4.2. Principles of gas detection

Advances in the fields of electronics, electrochemistry and micro-manufacturing have resulted in significant improvements in the accuracy and reliability of equipment for the detection and measurement of gas concentrations. Instruments now available are capable of measuring concentrations of more than one gas and indicating fractions of a part per million for some toxic gases. The same principles of detection method may be applied to more than one gas. Hence, in this section we shall concentrate on those principles rather than discussing each gas in turn. The methods of gas detection and monitoring used most frequently for subsurface gases are listed in Table 11.1.

11.4.2.1. Filament and catalytic oxidation (pellistor) detectors

These devices are used primarily for the measurement of methane and other gases that will burn in air such as carbon monoxide, hydrogen or the higher gaseous hydrocarbons. If an electrical filament is heated to a sufficiently high temperature, then a **combustible gas** in the surrounding air will burn and, hence, elevate the temperature of the filament even further. This will change the electrical resistance of the filament. By arranging for the filament to act as one arm of a Wheatstone bridge circuit, its change of resistance can be sensed as a change in voltage drop or current that is proportional to the concentration of combustible gas. A second filament of the Wheatstone bridge is also exposed to the air but inhibits oxidation of the gas either by a lower operating temperature or catalytic poisoning. This acts as a balancing control against variations in the temperature, moisture content and barometric pressure of the ambient air. The device is, essentially, a resistance thermometer sensing the temperature of the active filament. Filament detectors have been available since at least the 1950's.

Platinum has been used as the filament coil material as it has good resistance-temperature characteristics at the 900 to 1000°C temperatures required to promote the oxidation process in a stable manner. There are, however, severe drawbacks to platinum filament detectors. First, the response of the instrument is very sensitive to the geometry of the coil. Slight variations in the pitch of the coil caused during manufacture or due to mechanical shock produce significant deviations in the electrical output. Secondly, at the required high operating temperature, evaporation of the metal causes the cross sectional area of the wire to be reduced and, hence, increases its resistance. This is reflected by a slow but significant increase in bridge output for any given gas concentration and a zero drift in fresh air.

During the 1960's, research was carried out in a number of countries to overcome the difficulties inherent in filament methanometers. The platinum filament was reduced to less than 1 mm in length and encased in a tiny bead of refractory material, such as alumina. The outside of the bead was coated by a thin layer of catalytic material that produces stable oxidation of methane at

temperatures of some 500°C. The catalysts are, typically, metal-salt combinations of palladium and thorium or platinum and rhodium. These beads are called **pellistors** or **pelements** (Baker, 1969; Richards, 1970) and overcome most of the problems of the earlier filament detectors. First, the encapsulation of the coil makes it almost immune to mechanical damage. Indeed, further developments of electronic materials have enabled the coil to be eliminated. Secondly, there is no evaporation of the coil and, hence, near elimination of zero drift. Furthermore, the life of the unit is greatly increased while the reduced operating temperature requires less battery power and improves the safety of the instrument. The balancing or reference pellistors to compensate for air temperature, humidity and pressure are identical units except that the catalyst is poisoned by dipping it in a hot solution of potassium hydroxide. The first commercial methanometers to utilize pellistors appear to have been produced by Mine Safety Appliances (MSA).

Modern pellistor methanometers have a high degree of reliability, and operate satisfactorily and continuously on mining machines within conditions of high humidity, dust and vibration. The bridge output signals may be used to indicate on a dial or digital register, activate audio/visual alarms, isolate electrical power to a machine, drive a recorder or transmit to distant devices through a telemetering system. However, they still retain some disadvantages.

First, pellistors rely upon the oxidation process and, hence, the availability of oxygen. A good quality, heavy duty, pellistor will indicate increasing concentrations of methane up to 9 or 10 percent. Beyond that, the decreasing concentration of oxygen will diminish the rate and temperature of catalytic oxidation giving a reduced and false reading. Pellistor methanometers are, in the main, manufactured for the range 0 to 5 percent. However, use in an oxygen-deficient and methane-rich atmosphere could, again, give a false reading - apparently within the 0 to 5 percent scale. In some modern instruments, this promotes a warning signal or is combined with another mode of detection for high concentrations of combustible gas. Another possible consequence of repeated exposures to high concentrations of combustible gases is that "cracking" of a hydrocarbon gas can deposit carbon within the catalytic layer resulting in scaling and eventual destruction of the pellistor. The catalyst should contain an inhibitor to minimize the effects of cracking. The choice of refractory material that forms the bead also influences the degree of cracking.

A second disadvantage of pellistors is that they are subject to poisoning by some other gases and vapours. Vaporized products of silicon compounds (greases, electrical components) or phosphate esters (fluid couplings) will produce permanent poisoning of pellistors while halogens from refrigerants or heated plastics can give a temporary reduction of the instrument output. The readings of pellistor methanometers should be treated with caution when such instruments are used downstream from a mine fire. Most of these instruments allow the ambient air to reach the pellistor heads by diffusing through a layer of absorbent material such as activated charcoal. This removes most potential poisons and also permits the instrument to be near independent of the air velocities generally encountered underground.

A third feature of pellistor transducers is that they react to any combination of combustible gases that pass through the absorbent filter. The instruments used in mines are primarily calibrated for methane as this is the most common of the combustible gases found in the subsurface. However, hydrogen, carbon monoxide and ethane will also pass through simple activated filters and produce a response from the instrument. At 1 percent concentration of each gas, a catalytic combustion methanometer will indicate the readings shown on Table 11.4. The readings remain proportional to those given by methane up to the lower explosive limit of each gas.

Gas	Methanometer reading percent
methane	1.00
carbon monoxide	0.39
hydrogen	1.24
ethane	1.61
propane	1.96

Table 11.4. Approximate readings on a catalytic combustion methanometer given by a 1 percent concentration of each gas.

Fortunately, a pellistor methanometer is unlikely to be used in concentrations of carbon monoxide that would be indicated on the instrument. Furthermore, hydrogen, ethane and propane all give a reading above that for methane. Hence, the error is on the side of safety.

Example

A methanometer used in a mixture of air and ethane gives a reading of 3.4 percent. What is the actual concentration of ethane? Assume that there are no other combustible gases present.

Solution

From Table 11.4, the correction factor for ethane is 1.61. Hence,

$$\text{actual concentration of ethane} = \frac{3.4}{1.61} = 2.1 \text{ per cent}$$

A useful feature of oxidation methanometers is that any given reading indicates approximately the same fraction of the lower flammable limit of the combustible gas being monitored. Hence, a pellistor methanometer would indicate 5 per cent (approximately) if any one gas from Table 11.4 were present in a concentration equal to its lower flammable limit. The same is true of mixtures of the gases, enabling a pellistor methanometer to be used as an indicator of how close a gaseous mixture is to its lower flammable limit.

11.4.2.2. Flame safety lamps

These lamps were introduced early in the nineteenth century for the purposes of providing illumination from an oil flame without igniting a methane-air mixture (Section 1.2). Their use for illumination disappeared with the development of electric battery lamps. However, the devices were retained for the purposes of testing for methane and oxygen deficiency.

A blue halo of burning gas over the lowered flame of the lamp becomes visible at about 1¼ percent methane. The size of the halo increases with methane concentration. At 2½ percent, it forms a very clear equilateral triangle. At 5 percent the flame spirals upwards into the bonnet of the lamp and either continues burning or self extinguishes in a small contained explosion. In both cases, the flame is prevented from propagating into the surrounding atmosphere by the tightly woven wire gauzes (Section 1.2). The use of the flame safety lamp for methane testing has now largely been replaced by pellistor methanometers as these are more accurate, reliable and safer.

Some coal mining industries have retained the flame safety lamp for its ability to indicate oxygen deficiency (Section 11.2.2.). The height of the flame reduces progressively with oxygen content and is extinguished at 16 percent oxygen. However, in a methane-rich atmosphere, the flame may remain lit down to an oxygen concentration of 13 percent.

Various attempts were made to convert modified flame lamps into alarm and recording devices (for example, Pritchard, 1961). However, some ignitions of methane have been attributed to flame safety lamps that have been damaged or inadequately maintained (Strang, 1985). The flame safety lamp has an honourable place in the history of mine ventilation but its role is almost over.

11.4.2.3. Thermal conductivity and acoustic gas detectors

At 20°C and at normal atmospheric pressures, the thermal conductivity of methane is 0.0328 W/m °C compared with 0.0257 W/m °C for air. This difference is utilized in some high range methanometers. Two heated sensors are employed, one exposed to the gas sample and the other retained as a reference within a sealed air-filled chamber. A sample of the ambient air is drawn through the instrument at a constant rate. The sample sensor cools at a greater rate due to the higher thermal conductivity of the methane. The change in resistance of the sample sensor is detected within an electrical bridge to give a deflection on the meter. Typical ranges for a thermal conductivity methanometer are 2 or 5 percent to 100 percent. The principle is sometimes used in conjunction with pellistors to provide a dual range instrument or to over-ride the falsely low readings that may be given by catalytic combustion detectors at high concentration (Section 11.4.2.1.). To reduce interference from other gases, suitable filters should be employed. In particular, carbon dioxide gives about half the response of methane but in a negative direction. For use in mining, a soda lime filter is, therefore, advisable.

Acoustic gas detectors rely upon changes in the velocity of sound as the composition of a sample varies. It is used, primarily, for high concentrations and has been employed in methane drainage systems.

11.4.2.4. Optical methods

These subdivide into three groups. **Interferometers** utilize the refraction of light that occurs when a parallel beam is split, one half passing through the sample and the other through a sealed chamber containing pure air. The two beams are recombined and deflected through a mirror or glass prism arrangement for viewing through a telescope. The optical interference between the two beams causes a striped fringe pattern to appear in the field of view. This typically takes the form of two black lines in the centre with red and green lines on both sides. The fringe moves along a scale in proportion to the amount of gas present. Rotational adjustments of one of the deflecting prisms can be read on a vernier and added to the optical scale in order to widen the range of the instrument. Interferometers are sensitive to the presence of other gases and appropriate filters should be used when necessary. Hydrogen gives a negative response with respect to methane. At equal concentrations of the two gases, the reading is near zero. Carbon dioxide and methane give similar responses. For air containing both carbon dioxide and methane two readings are taken, one with a soda lime filter to remove the carbon dioxide and gives the methane concentration only, and the second without that filter. The difference between the two readings is an indication of the carbon dioxide concentration. The effects of other gases render the interferometer unsuitable for situations where the composition of the sample is dramatically different from that of normal air, for example, afterdamp, downstream from fires or samples taken from behind seals.

The nondispersive **infra-red gas analyser** is one form of absorption spectrometer that is frequently used for mine gas analysis. Identical beams of slowly pulsating infra-red radiation pass through two parallel chambers, one containing a gas that does not absorb infra-red (typically nitrogen) and the other fed by a stream of the sample. The pulsations of 3 to 4 Hertz may be achieved electronically or by a rotating chopper arrangement. Beyond the sample and reference chambers is a two-compartment sealed container (detector unit) filled with a pure specimen of that particular gas which is to be detected. Detector units can be interchanged to determine the concentrations of different gases. The two compartments of the detector unit are at

the same nominal pressure and are separated by a flexible diaphragm. The pulses of infra-red radiation are directed sequentially into the two sides of the detector unit, heat the contained gas and, hence, raise its pressure. However, the beam that has passed through the sample chamber has already been partially absorbed at the relevant wavelength by molecules of the sought gas. Hence, the pulses of pressure induced in that corresponding side of the detector unit are weakened. The amplitude of the vibrating diaphragm is sensed by an electrical capacitor and translated electronically to an output signal. Infra-red gas analysers are employed primarily at fixed monitoring stations or laboratories. However, portable versions are available.

Laser spectroscopy is another means of air analysis that has considerable potential for subsurface application. There are two systems that can be employed. One is the differential absorption unit (DIAL system) in which two similar lasers are used, one tuned to the absorption wavelength of the gas to be detected, and the other to a slightly different wavelength. The two laser beams pass through the sample gas stream and are reflected back to a single receiver unit. The difference in the two signals is processed to indicate the concentration of the gas being monitored. The employment of a reference beam eliminates the effects of dust, humidity or other gases. (Holmes and Byers, 1990).

The second laser technique for gas analysis is the light detection and ranging (LIDAR) method which depends upon the **Raman effect**. When a gas is excited by monochromatic radiation from a laser, a secondary scattered radiation is produced. The spectrum of this scattered radiation can be analysed to indicate the concentrations of the gases that caused it.

The attraction of laser techniques for mine air sampling is that the laser beams may be directed across or along subsurface openings to give continuous mean analyses for large volumes of air. Furthermore, the lasers can also be used to monitor air velocity.

11.4.2.5. Electrochemical methods

Very small concentrations of many gases can be detected by their influence on the output from an electrochemical cell. There are two primary types, both based upon oxidation or reduction of the gas within a galvanic cell. The cell has at least two electrodes and an intervening electrolyte. In the polarographic or voltametric analyser, a voltage from an external battery is applied across the electrodes in order to induce further polarization (or retardation) of the electrodes. The gas sample is supplied to the interface between the electrolyte and one of the electrodes (the "sensing electrode"). This may be accomplished by diffusion of the sample gas through a hollowed and permeable sensing electrode. The electrochemical reaction at the electrode/electrolyte interface changes the rate at which free electrons are released to flow through the electrolyte and be collected by the "receiving electrode". For example, in a sulphur dioxide electrochemical analyser, the oxidation is as follows:



The resulting change in electrical current is proportional to the concentration of sulphur dioxide in the sample.

In amperometric cells, the gas reacts directly with the electrolyte and, hence, enhances or reduces the current produced. Both types of cell are subject to interference by other gases. This is minimized by appropriate selection of the materials employed for the electrodes and electrolyte, the polarizing voltage applied to the polarographic cells and a suitable choice of filters.

Electrochemical cells may indicate the partial pressure rather than the concentration of a gas. These require the zero to be reset when taken through a significant change in barometric pressure - as will occur when travelling to different levels in a mine. Another disadvantage of electrochemical analysers is that they can become temporarily saturated when exposed to high concentrations of gas. The recovery period may be several minutes.

11.4.2.6. Mass spectrometers

In these instruments, the gas sample passes through a field of free electrons emitted from a filament or other source. Collision of the electrons with the gas molecules produces ions, each with a mass/charge ratio specific to that gas. The ions are accelerated by electromagnets and then pass through a magnetic deflection field which separates them into discrete beams according to their mass/charge ratios. The complete mass spectrum can be scanned and displayed on an oscilloscope or the signals transmitted to recorders.

11.4.2.7. Paramagnetic analysers

Oxygen is one of the very few gases that are paramagnetic, i.e. it aligns itself as a magnetic dipole in the presence of an applied magnetic field and, hence, creates a local anomaly within that field. This property is utilized in a paramagnetic oxygen analyser. A weak permanent dumb-bell magnet is suspended against a light applied torque within a non-uniform magnetic field. One end of the dumb-bell is encapsulated within a bulb of nitrogen while the other end is exposed to the gas sample. A rotation of the magnet is induced as the oxygen content of the sample varies. The movement is amplified optically or electrically for display or recording.

11.4.2.8. Gas chromatography

Gas chromatographs are used widely for the laboratory analysis of sampled mixtures of gases. Portable units are also manufactured. An inert carrier gas is pumped continuously through one or more columns (or coils) which contain gas adsorbents. The latter may be granulated solids or liquids. A small pulse of the sample gas mixture is injected into the line upstream from the columns. The constituent gases are initially adsorbed by the column materials. However, the continued flow of the carrier gas causes subsequent desorption of each gas at a time and rate dependent upon its particular adsorption characteristics. The result is that the gases leave the adsorbent columns as discrete and separated pulses. Their identification and measurement of concentration is carried out further downstream by one or more of the detection techniques described in this section.

11.4.2.9. Semiconductor detectors

One of the more recent techniques introduced for gas detection involves passing the sample over the surface of a semi conducting material which is maintained at a constant temperature. Adsorption of gas molecules on to the surface of the semiconductor modifies its electrical conductance. Selectivity of the gas to be detected may be achieved by the choice of semiconductor and the operating temperature. However, filters may be necessary to avoid interference or poisoning from other airborne pollutants. Coupled with the development of thin film technology, the semiconductor technique holds promise for increased future utilization.

11.4.2.10. Stain tubes

Stain tubes are used widely for a large variety of gases. They are simply glass phials containing a chemical compound that changes colour in the presence of a specified gas. The phials are sealed at both ends. To carry out a test, the ends are snipped open and a metered volume of sample air pulled through at a constant rate, usually by means of a simple hand pump. The concentration of gas is estimated either from the length of the stain or by comparing the colour of the stain with a chart. Despite the lack of precision, stain tubes are used extensively in practice because of their simplicity, portability and low cost.

11.4.3. Methods of sampling

The methods of sampling for subsurface gases vary from judicious positioning of the human nose to sophisticated telemetering systems. The techniques most commonly applied can be divided into two classes: (a) manual and (b) automatic or remote.

11.4.3.1. Manual methods

The locations and times at which hand-held equipment should be employed to measure methane concentrations in gassy mines are normally mandated by the governing legislation. These include pre-shift inspections by qualified persons prior to entry of the work force, and at intervals of some twenty minutes throughout the shift on a working face.

The instruments that are most widely used for manual detection and measurement are catalytic oxidation methanometers, oxygen deficiency meters and stain tubes. Multiple gas instruments are commonly employed. Light gases, including methane, are most likely to collect at roof level while carbon dioxide will tend to pool in low lying areas. Hence, measurements should be taken in those locations in addition to within the general body of air. Extension probes provide a means of drawing a sample from a location that is unsafe or out of reach.

Grab samples are volumes of air or gas mixtures that are collected in sample containers underground for subsequent laboratory analysis. Typically, the sample is drawn into a metal or plastic container by means of a hand-operated pump or by water displacement. This is usually the method employed for retrieving samples from behind seals or stoppings. The sample pipe should extend far enough beyond the seal to prevent contamination by air that has “breathed” through the seal during preceding periods of rising barometric pressure. Sufficient gas should be drawn from the pipe prior to sampling in order to ensure that the captured gas is representative of the atmosphere beyond the seal. Care should be taken to prevent loss or pollution of the sample caused by pressure changes as the container transported to the surface. The gas seals on the containers should be well maintained and samples should be sent to a laboratory for expeditious analysis.

Personal samplers are devices that are worn continuously by personnel while at work. The simplest are badges that change colour in the presence of selected gases or radiation. More sophisticated samplers for dust or gases draw power from either an internal battery or a cap lamp battery. Personal gas samplers may emit audio-visual alarm signals when a preselected concentration of gas is exceeded.

11.4.3.2. Automatic and remote monitors

Permanent environmental monitors may be sited at strategic locations throughout a subsurface ventilation system. The gases most frequently subject to this type of monitoring are methane, carbon monoxide and carbon dioxide. Other gases may be monitored in workshops, storage repositories and for special applications such as hydrogen at the roofs of battery charging stations. Environmental monitors in an underground repository for nuclear waste must also be provided to detect airborne radionuclides.

Permanent monitors should be mounted at strategic locations chosen on a site-specific basis. However, it is prudent to site transducers at the intake and return ends of working areas and at intervals along return routes. Carbon monoxide sensors mounted at intervals along conveyor roads provide an earlier warning of fire than temperature-sensitive devices.

In addition to providing local audio-visual alarms, an environmental monitoring system operates most effectively when it is integrated into a **telemetry network**. The signals from gas, airflow, pressure and temperature transducers are transmitted to a remote computer and control station, usually on surface, where those signals are analysed for trends, recorded on magnetic media, operate alarms when appropriate and, possibly, generate feedback control signals to fans, doors or motorized regulators. (See, also, Sections 9.6.3 and 9.6.4.) Monitors at critical locations such as booster fans should be installed as dual or, even, triple units to safeguard against instrument failure. Rechargeable batteries can provide backup in the event of a cut in electrical power. A system of planned maintenance should be implemented in order to ensure continuous and reliable operation. A computer-controlled telemetry system should be capable of detecting and identifying failed monitors.

Machine mounted gas monitors should be provided on rock breaking equipment to test for methane in coal and other gassy mines. These devices must be particularly rugged in order to remain operational when subjected to dust, water sprays, vibration and impact. Machine-mounted methanometers should not only provide audio-visual warnings but also be connected such that the electrical power supply to the machine is isolated when the methane concentration reaches one percent (or other concentration as required by the relevant mining legislation). Here again, machine-mounted monitors may be integrated into a mine telemetry system.

Tube bundle systems are a slower alternative means of remote sampling. Air is drawn through plastic tubing from chosen locations in the mine to monitoring stations which may be located either underground or on surface. At a monitoring station, automatic valves on the tubes are operated in a cyclic manner in order to draw samples from the tubes sequentially, and to pass those samples into gas detection units. The latter are often infra-red analysers (Section 11.4.2.4.) connected in series to monitor the concentrations of each of the required gases. A gas pump on each tube maintains continuous flow. However, the main disadvantage of the tube bundle system is the travel time of the gas between entering a tube and analysis. It is recommended that this should not exceed one hour. While surface monitoring stations are preferred, workings distant from shaft bottoms may necessitate local underground stations. Tube bundle systems are not suitable for emergency situations that occur quickly such as an equipment fire. However, they have proved valuable for the identification of longer term trends including incipient spontaneous combustion.

The tubes should be fitted with dust filters and water traps. Variations of temperature and pressure may cause condensation as the air passes through the tubes. Care must be taken during the installation of a tube bundle system, particularly at joints, as leaks are difficult to detect and locate. An important advantage of the system is that it requires no electrical power in by the monitoring station. Hence, it remains operational when sampling from behind seals or when no electrical supply is available.

References

ACGIH (1989). Threshold limit values and biological exposure indices for 1989-1990. American Conference of Governmental Industrial Hygienists, Cincinnati, Ohio, USA.

Baker, A. R. (1969). A review of methanometry. *The Mining Engineer*, Vol. 128, No. 107, Aug., pp 643-653.

Baker, A. R. and Firth, J. G. (1969). The estimation of firedamp: Applications and limitations of the pellistor. *The Mining Engineer*, Vol. 128, No. 100, Jan., pp 237-244.

Coward, H. F. and Jones, G. W. (1952). Limits of flammability of gases and vapours. *Bull. US Bureau of Mines*, No. 503.

- Coward, H. F. (1928).** Explosibility of atmospheres behind stoppings. Trans. Inst. Mining Engineers, Vol. 77, p 94.
- Daniel, J. H. (1989).** Diesels - backbone of a changing mining industry. 4th U. S. Mine Ventilation Symposium, Berkeley, California USA, pp 561-568.
- Forbes, J. J. and Grove, G. W. (1954).** Mine gases and methods for detecting them. US Bureau of Mines, M. C., No. 33.
- French, I. W. and Assoc. Ltd. (1984).** Health implications of exposure of underground mine workers to diesel exhaust emissions - an update. Dept. of Energy, Mines and Resources, Ottawa, Canada, p 607.
- Gunderson, R. E. (1990).** The advantages of electrically powered equipment for deep hot mines. Journal of the Mine Ventilation Society of S. Africa, Vol. 43, No. 6, June, pp 102-111.
- Haney, R. A. and Stolz, R. T. (1989).** Evaluation of personal diesel particulate samplers. 4th US Mine Ventilation Symposium, Berkeley, California, pp 579-587.
- Holmes, J. M. and Byers, C. H. (1990).** Countermeasures to airborne hazardous chemicals. Published by Noyes Data Corp., New Jersey USA.
- NIOSH (1987).** Pocket guide to chemical hazards. National Institute for Occupational Safety and Health; US Dept. of Health and Human Services, Washington, D. C. USA.
- Pritchard, F. W. and Phelps, B. A. (1961).** A recorder of atmospheric methane concentration based on a butane flame lamp. Colliery Engineering, 120, Feb. 9th, pp 163-166.
- Richards, G. O. and Jones, K. (1970).** Some recent work on the detection and determination of firedamp. The Mining Engineer, Vol. 130, No. 121, Oct., pp 31-40.
- Rossi, B. D. (1971).** Control of noxious gases in blasting work and new methods of testing industrial explosives (translated from Russian). NTIS, Tech. translation no. TT70-50163.
- Strang, J. and MacKenzie-Wood, P. (1985).** A manual on mines rescue and gas detection. Published by Weston and Co., Kiama, Australia.
- US Bureau of Mines (1987).** Diesels in underground mines. Proceedings of technology transfer seminar, pp 1-165.
- Waytulonis, R. W. (1988).** Bureau of Mines diesel research high lights. 4th Int. Mine Ventilation Congress, Brisbane, Australia, pp 627-633.
- World Mining/World Coal (1982).** Diesels in Mining. Special issue, Nov., pp 6-54

CHAPTER 12 METHANE

12.1. OVERVIEW AND ADDITIONAL PROPERTIES OF METHANE	2
12.2. THE RETENTION AND RELEASE OF METHANE IN COAL	3
12.2.1. Gas retention in coal	3
12.2.2. The release of methane from coal	7
12.2.2.1. Diffusion and Darcy flow.	7
12.2.2.2. Desorption kinetics	8
12.2.3. Determination of gas content.....	11
12.2.3.1. Indirect method (adsorption isotherms).....	11
12.2.3.2. Direct measurement method.....	12
12.3. MIGRATION OF METHANE	13
12.3.1. Fluid Flow through a permeable medium.	14
12.3.1.1. Incompressible flow	14
12.3.1.2. Compressible flow	16
12.3.1.3. Radial flow of gas	17
12.3.1.4. Transient radial flow	18
12.3.2. The permeability of coal.....	19
12.3.2.1. Effect of mechanical stress	19
12.3.2.2. Effect of gas pressure	21
12.3.2.3. Two phase flow	22
12.4. EMISSION PATTERNS INTO MINE WORKINGS	23
12.4.1. Sources of methane in coal mines.....	23
12.4.2. Methane layering	25
12.4.3. Gas outbursts.....	28
12.4.3.1. In-seam outbursts.....	28
12.4.3.2. Outbursts from roof and floor	29
12.4.4 Prediction of methane emissions into the ventilation system	31
12.5. METHANE DRAINAGE	32
12.5.1. In-seam drainage	32
12.5.2. Gob drainage by surface boreholes.....	35
12.5.3. Cross-measures methane drainage	36
12.5.4. Drainage from worked-out areas	37
12.5.5. Components of a methane drainage system	38
12.5.5.1. Pipe ranges	38
12.5.5.2. Monitors.....	39
12.5.5.3. Controls and safety devices	40
12.5.5.4. Extractor Pumps.....	41
12.5.6. Planning a methane drainage system	42
12.5.6.1. Data collection and estimation of gas capture	42
12.5.6.2. Design of the drainage network	43
12.5.7. Utilization of drained gas	46
References	47

12.1. OVERVIEW AND ADDITIONAL PROPERTIES OF METHANE

The major properties and behavioural characteristics of methane were outlined in Section 11.2.4. That Section should be reviewed as an introduction to the more detailed treatment given in this chapter.

There are three primary reasons for giving particular attention to methane. First, it is the naturally occurring gas that most commonly appears in mined underground openings. Secondly, it has resulted in more explosions and related loss of life than any other cause throughout the recorded history of mining. The flammability characteristics of this gas have been studied since, at least, the time of Agricola in the 16th Century. The number and severity of coal dust explosions initiated by methane ignitions declined after the development of electric cap lamps and the replacement of shaft bottom furnaces with fans (Section 1.2.). However, the intensity and wider deployment of mechanized rock-breaking equipment resulted in a renewed incidence of frictional ignitions of methane following the 1960's (Richmond et al, 1983). Fortunately, modern standards of ventilation and dust control prevent most of these from developing into the larger dust explosions and disastrous loss of life.

The third reason for giving special attention to methane concerns the continued development of methane drainage technology. Although the primary reason for extracting methane at high concentration from the strata around mines continues to be the reduction of methane emissions into these mines, a growing incentive has been the drainage of methane to provide a fuel source in its own right. Methane drainage may now be undertaken for this purpose from strata where there is no known intention of subsequent mining.

In this chapter we shall consider four broad areas; first, the manner in which methane is retained within the strata and the mechanisms of its release when the rock is disturbed by mine workings or boreholes. We shall also outline means of determining the gas content of carbonaceous strata. Secondly, we shall examine the migration of the gas from its geologic sources towards workings or boreholes. This will encompass an analysis of strata permeability and flow through fracture networks. The third consideration is the dynamic pattern of methane emission into active mine workings, varying from normal cyclic variations, through gas layering phenomena, to outburst activities.

Finally, we shall classify the major techniques of methane drainage. No one of these has universal application and the selection of drainage method must be made with great care according to the geology of the area, the methods and layout of mining (if any) and the natural or induced physical properties of the rocks.

First, however, let us list some further properties of methane in addition to those given in Table 11.1. The data are referred, wherever applicable, to standard temperature and pressure of 0°C and 101.3 kPa.

molecular structure :	$ \begin{array}{c} \text{H} \\ \\ \text{H} - \text{C} - \text{H} \\ \\ \text{H} \end{array} $
melting point :	90.5 K
boiling point :	111.3 K
critical temperature and pressure :	190.5 K and 4.63 MPa
latent heat of vaporization (at 111.3K) :	508.2 kJ/kg

latent heat of fusion (at 90.5 K) :	58.8 kJ/kg
specific heat C_p :	2184 J/(kg K)
specific heat C_v :	1680 J/(kg K)
isentropic index :	1.300
solubility in water :	55.6 litres per m ³ of water (33.1 litres/m ³ at 20°C)
upper calorific value :	55.67 MJ/kg
lower calorific value :	50.17 MJ/kg
thermal conductivity :	0.0306 W/(m °C) [0.0328 W/(m °C) at 20°C]
dynamic viscosity :	(10.26 + 0.0305t) x 10 ⁻⁶ Ns/m ² (temperature t = 0 to 100°C)

12.2. THE RETENTION AND RELEASE OF METHANE IN COAL

In order to understand the manner in which methane is retained within coal and the mechanisms of its release, it is first necessary to comprehend the internal structures of coal. The existence of a large number of exceptionally small pores and the corresponding high internal surface area of coal has been recognized for many years and numerous conceptual models have been suggested. However, electron microscopy has revealed the actual structures that exist.

Coal is not a single material but a complex mix of fossilised organic compounds and minerals. The composition and structure depend upon the nature of the original vegetation from which a given coal seam formed, the timing and turbidity of the water flows involved in the sedimentary processes of deposition and the metamorphic effects of pressure, temperature and tectonic stressing over geological time. Electron micrographs have, indeed, confirmed the existence of pores, many of which may not be interconnected. An example is shown on Plate 2. However, other areas may indicate amorphous, granular, sponge-like or fibrous structures, even within the same seam. Furthermore, the coal substance is intersected by a fracture network with apertures varying from those that are comparable to pore diameters through to some large enough to be seen with the naked eye.

In this Section we shall concentrate on the manner in which methane is held within the coal, the kinetics of its release when the geological equilibrium is disturbed by mining or drilling, and how the gas content of a seam may be determined.

12.2.1. Gas retention in coal

Methane exists within coal in two distinct forms, generally referred to as **free gas** and **adsorbed gas**. The free gas comprises molecules that are, indeed, free to move within the pores and fracture network. Porosities of coals have been reported from 1 to over 20 percent. However, those values depend upon the chosen definition of porosity and the manner in which it is measured. **Absolute (or total) porosity** is the total internal voidage divided by the bulk volume of a sample and may be difficult to measure accurately. **Effective (or macroscopic) porosity** is the ratio of interconnected void space to the bulk volume. The latter definition is more useful in the determination of recoverable gas from a seam. Unfortunately, the usual procedures of measuring porosity depend upon saturating the internal voidage with some permeating fluid. The probability of a gas molecule entering any pore or interconnection rises as its molecular diameter decreases or its mean free path increases. (The mean free path is the statistical average distance between collisions of the gaseous molecules.) Furthermore, any adsorptive bonding between the fluid and the solid may obstruct the narrower interconnections. The measured effective porosity is, therefore, dependent upon the permeating fluid. In order to handle the extremely small pores that exist in coal, the maximum value of effective porosity is obtained by using helium as the permeating fluid. Helium has a small molecular diameter (some 0.27×10^{-9} m), a relatively large mean free path (about 270×10^{-9} m at 20°C and atmospheric pressure) and is non-adsorptive with respect to coal. For comparison, pore diameters of eastern U.S. coals vary from over 30×10^{-9} m to less than 1×10^{-9} m (Gan, 1972).

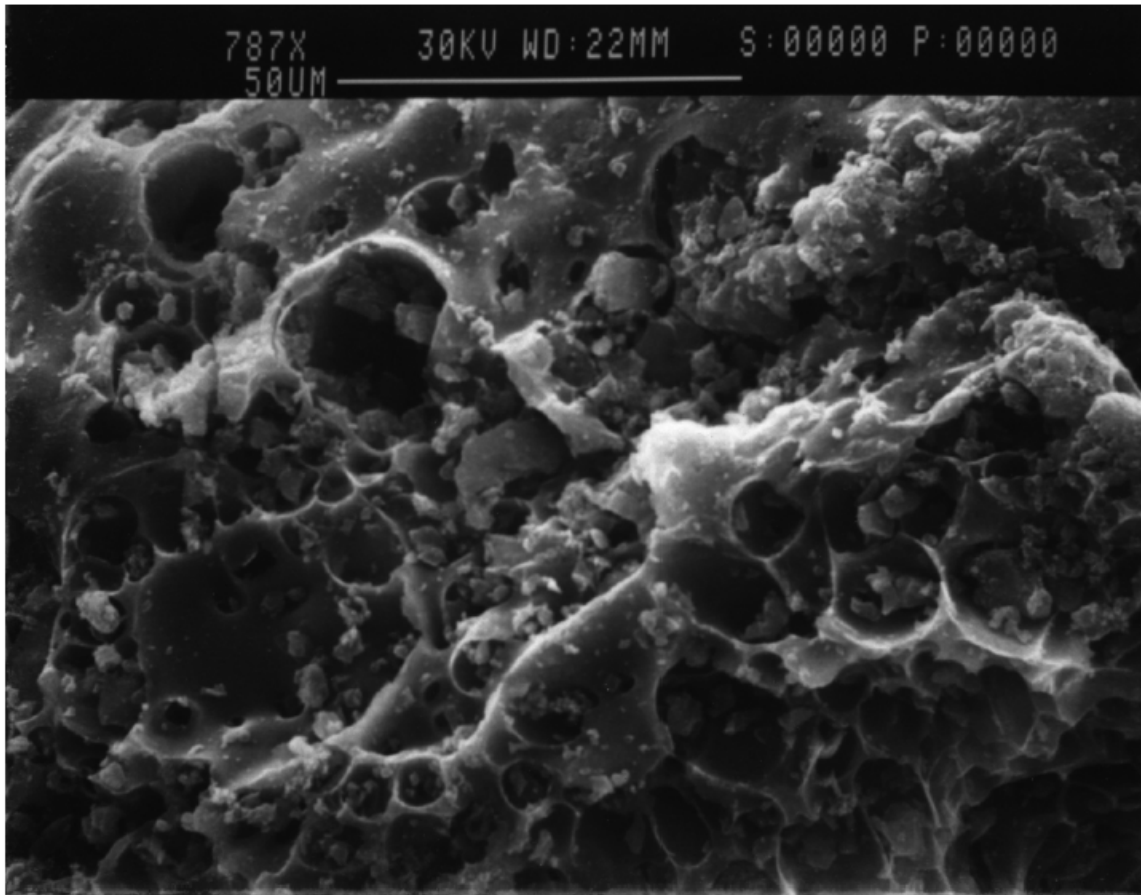


Plate 2. Electron micrograph of a bituminous coal (after Harpalani).

An attractive force exists between the surfaces of some solids and a variety of gases. Coal surfaces attract molecules of methane, carbon dioxide, nitrogen, water vapour and several other gases. Those molecules adhere or are adsorbed onto the coal surface. When the adsorptive bond exceeds the short-distance repulsive force between gas molecules (Section 2.1.1.), then the adsorbed molecules will become packed together as a monomolecular layer on the surface. At very high gas pressures, a second layer will form with a weaker adsorptive bond (Jolly, 1968).

Figure 12.1 illustrates the variation of both total and adsorbed methane with respect to gas pressure and at constant temperature. The curve illustrating adsorbed methane is known as the adsorption isotherm. Some 95 percent of the total gas will, typically, be in the adsorbed form, explaining the vast reserves of methane that are contained within many coal seams.

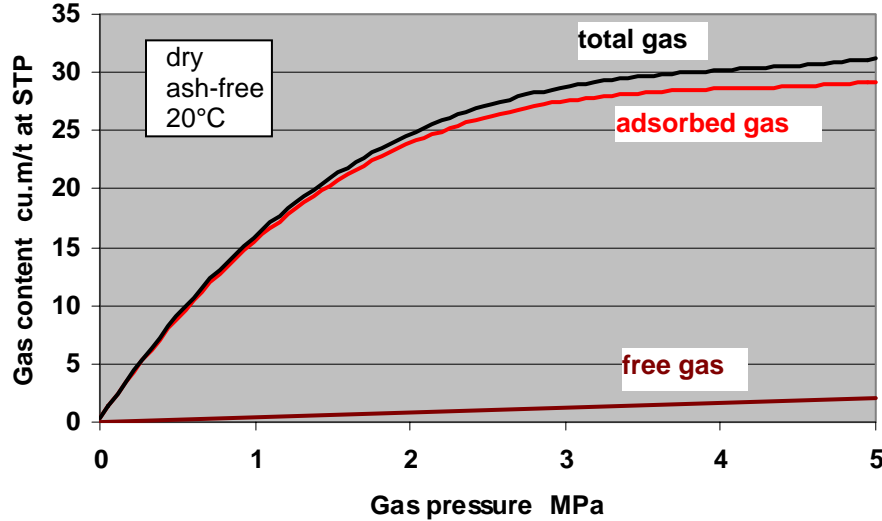


Figure 12.1 Examples of adsorbed, free and total gas isotherms for methane in coal.

The most widely used mathematical relationship to describe adsorption isotherms was developed by I. Langmuir (1916 and 1918) for a monomolecular layer. This may be expressed as

$$\frac{q}{q_{\max}} = \frac{bP}{1 + bP} \quad (12.1)$$

where q = volume of gas adsorbed at any given pressure (m^3/t at NTP)
 q_{\max} = the maximum amount of gas that can be adsorbed as a monomolecular layer at the prevailing temperature (m^3/t at NTP)
 P = gas pressure (usually expressed in MPa)
 b = Langmuir's "constant" (MPa^{-1}), a function of the adsorptive bond between the gas and the surface ($1/b$ is the pressure at which $q/q_{\max} = 1/2$)

The values of Langmuir's constant depend upon the carbon, moisture and ash contents of the coal as well as the type of gas and prevailing temperature. Boxho et al (1980) reports values of b decreasing from 1.2 MPa^{-1} at a volatile content of 5 percent to 0.5 MPa^{-1} at a volatile content of 40 percent. Figure 12.2(a) indicates the increased adsorptive capacities of the higher rank coals, these having greater values of carbon content. Values of q_{\max} are shown to vary from about 14 to over $30 \text{ m}^3/\text{t}$. The effect of the type of gas is illustrated on Figure 12.2(b).

Adsorption isotherms are normally quoted on a dry, ash-free basis. The amount of methane adsorbed decreases markedly at small initial increases in moisture content of the coal. Most of this natural moisture is adsorbed on to the coal surfaces. However, adsorptive saturation of water molecules occurs at about 5 percent moisture above which there is little further decrease in methane content. A widely used approximation is given by Ettinger (1958):

$$\frac{q_{\text{moist}}}{q_{\text{dry}}} = \frac{1}{1 + 0.31h} \quad (12.2)$$

where q_{moist} = gas content of moist coal (m^3/t)
 q_{dry} = gas content of dried coal (m^3/t)
 h = moisture content (percent) in the range 0 to 5 percent.
 (Assume 5 percent for greater moisture contents)

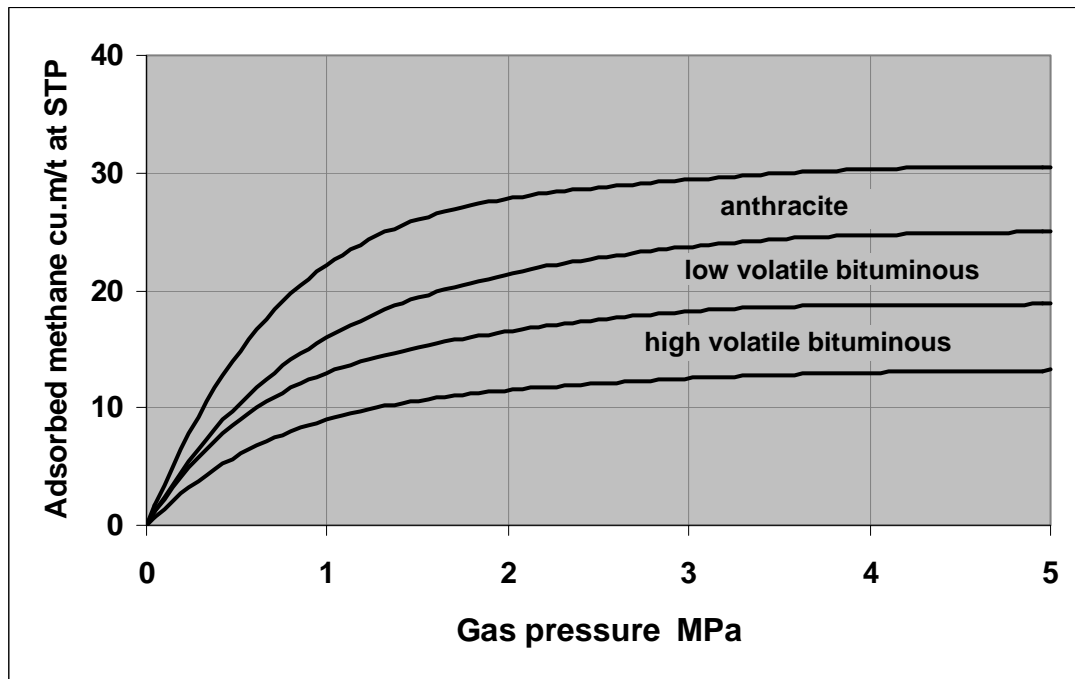


Figure 12.2(a) Examples of adsorption isotherms for methane in coal. The amount of gas adsorbed increases with the carbon content of the coal.

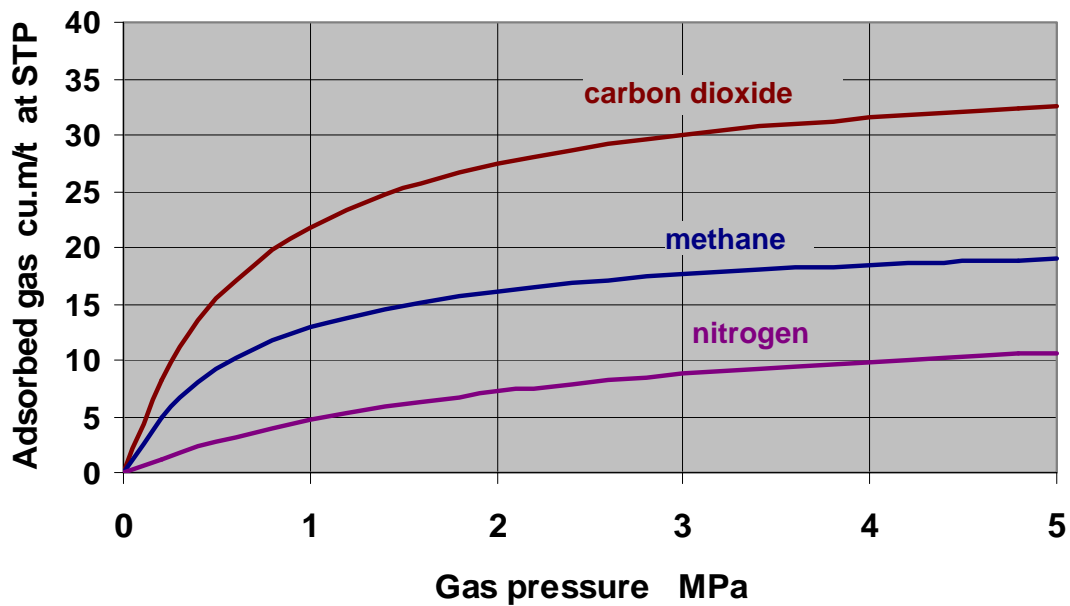


Figure 12.2(b) Adsorption isotherms for carbon dioxide, methane and nitrogen in a bituminous coal at 25°C.

The mineral matter that comprises the ash constituent of coal is essentially non-adsorbing. Hence the methane content decreases as the percentage of ash rises (Barker-Read, 1989). In order to express gas content on an ash-free basis, a simple correction may be applied.

$$q_{actual} = q_{ash-free} (1 - 0.01a) \quad (12.3)$$

where a = ash content (percent)

12.2.2. The release of methane from coal

In the undisturbed state, equilibrium exists between free gas and adsorbed gas in the pores and fracture networks of coal. If, however, the coal seam is intersected by a borehole, or disturbed by mining, then the gas pressure gradient that is created will result in flow through natural or stress-induced fractures. The resulting reduced gas pressure in the pores will promote desorption. The process will move from right to left along the appropriate adsorption isotherm. A glance at Figures 12.1 or 12.2 indicates that the rate of desorption with respect to gas pressure increases as the pressure falls. The migration of methane from its original location is retarded by narrow and tortuous interconnections between pores and microfractures, obstruction by adsorbed molecules and the resistance offered by the fracture network.

12.2.2.1. Diffusion and Darcy flow.

Current thinking is that two types of flow take place. Within the micropore structure, diffusion flow occurs while, in the fractures, laminar flow dominates. Let us first discuss diffusion flow. This occurs whenever a difference in concentration of molecules of a given gas occurs. The simplest means of quantifying diffusion flow is by Fick's Law:

$$u_x = -D \frac{\partial C}{\partial x} \quad \text{m/s} \quad (12.4)$$

where u_x = velocity of diffusion in the x direction (m/s)
 D = coefficient of diffusion (m^2/s but often quoted in cm^2/s)
 C = concentration of the specific gas (m^3/m^3 of coal)

(The negative sign is necessary as movement occurs in the direction of decreasing concentration.)

Bulk diffusion is the normal gas-to-gas diffusion that occurs because of a concentration gradient in free space (see Appendix A15.4). However, within the confines of a micropore structure, two other forms of diffusion may become effective. **Surface diffusion** arises from lateral movement of the adsorbed layer of gas on the coal surfaces while Knudson diffusion occurs due to transient molecular interactions between the gas and the solid.

Laminar flow in the fracture network follows **Darcy's Law** (1856) for permeable media.

$$u = \frac{k}{\mu} \frac{\partial P}{\partial x} \quad \text{m/s} \quad (12.5)$$

where u = gas velocity (m/s)
 k = permeability (m^2)
 μ = dynamic viscosity (Ns/m^2)
 $\partial P/\partial x$ = pressure gradient (Pa/m).

(Note the analogy between Darcy's Law and Fourier's Law of heat conduction, equation (15.4).) Darcy's Law is essentially empirical and assumes that the gas velocity at the surface is zero (Section 2.3.3). For narrow passages, slippage at the walls (surface diffusion) may become significant and can be taken into account by adjusting the value of permeability (Klinkenberg effect, Section 12.3.2.2.).

Controversy has existed on whether diffusion flow or Darcy flow predominates in coal. Disagreements in the findings of differing researchers are probably a consequence of the wide variations that exist in coal structure. It would appear that diffusion flow governs the rate of degassing coals of low permeability while Darcy flow in the fracture network is the dominant effect in high permeability coals.

12.2.2.2. Desorption kinetics

A newly exposed coal surface will emit methane at a rate that decays with time. Figure 12.3(a) illustrates a desorption curve. This behaviour is analogous to the emission of heat (Section 15.2.2.). A number of equations have been suggested depending, primarily, on the conceptual model adopted for the structure of coal. For a spherical and porous particle with single sized and non-connecting capillaries, work by Wheeler (1951) and Carslaw (1959) leads to the series

$$\frac{q(t)}{q_{\max}} = 1 - \frac{6}{\pi^2} \sum_{n=1}^{\infty} \frac{1}{n^2} \exp\left(-\frac{4 D n^2 \pi^2 t}{d^2}\right) \quad (12.6)$$

where

$$\begin{aligned} q(t) &= \text{volume of gas (m}^3\text{) emitted after time } t \text{ (s)} \\ q_{\max} &= \text{total volume of gas in particle} \\ D &= \text{coefficient of diffusion (m}^2\text{/s)} \\ d &= \text{equivalent diameter (m) of particle (= 6 x volume/surface area)} \end{aligned}$$

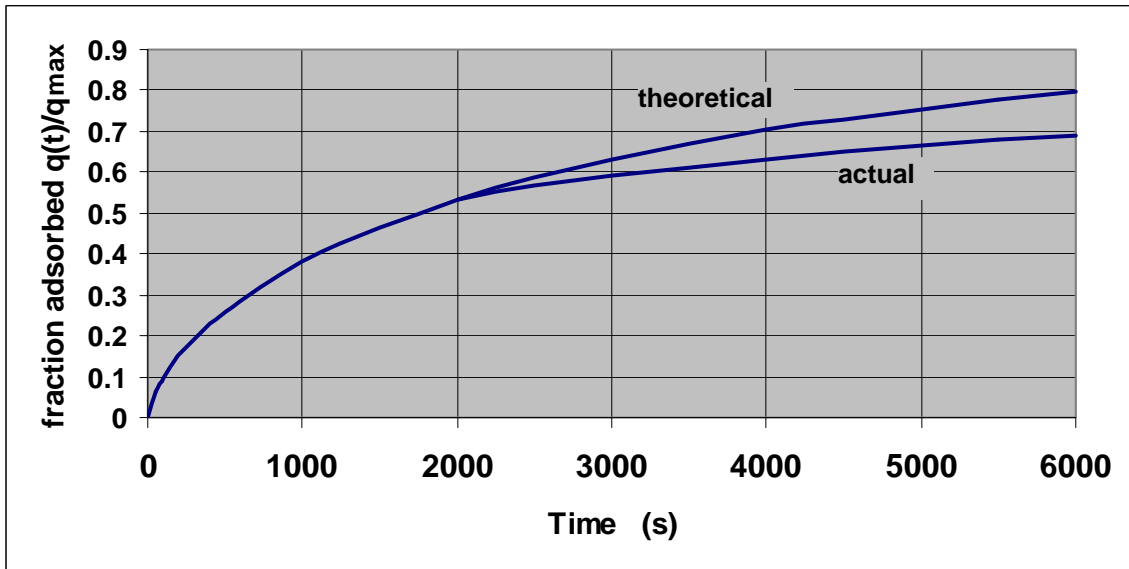


Figure 12.3(a) Example of a methane desorption curve plotted against time.

A more practicable approximation is given by Boxho et al (1980) as follows:

$$\frac{q(t)}{q_{\max}} \approx \sqrt{1 - \exp\left(\frac{-4 \pi^2 D t}{d^2}\right)}. \quad (12.7)$$

Both of these equations approximate to:

$$\frac{q(t)}{q_{\max}} \approx \frac{12}{d} \sqrt{\frac{Dt}{\pi}} - \frac{12Dt}{d^2} \quad (12.8)$$

while for $q(t)/q_{\max} < 0.25$, the relationship can be simplified further to

$$\frac{q(t)}{q_{\max}} \approx \frac{12}{d} \sqrt{\frac{Dt}{\pi}} \quad (12.9)$$

This latter equation implies that during the early stages of desorption the emission rate is proportional to \sqrt{t} . This is illustrated on Figure 12.3(b). Furthermore, plotting the initial emission rate against \sqrt{t} allows the corresponding value of the **coefficient of diffusion**, D , to be determined.

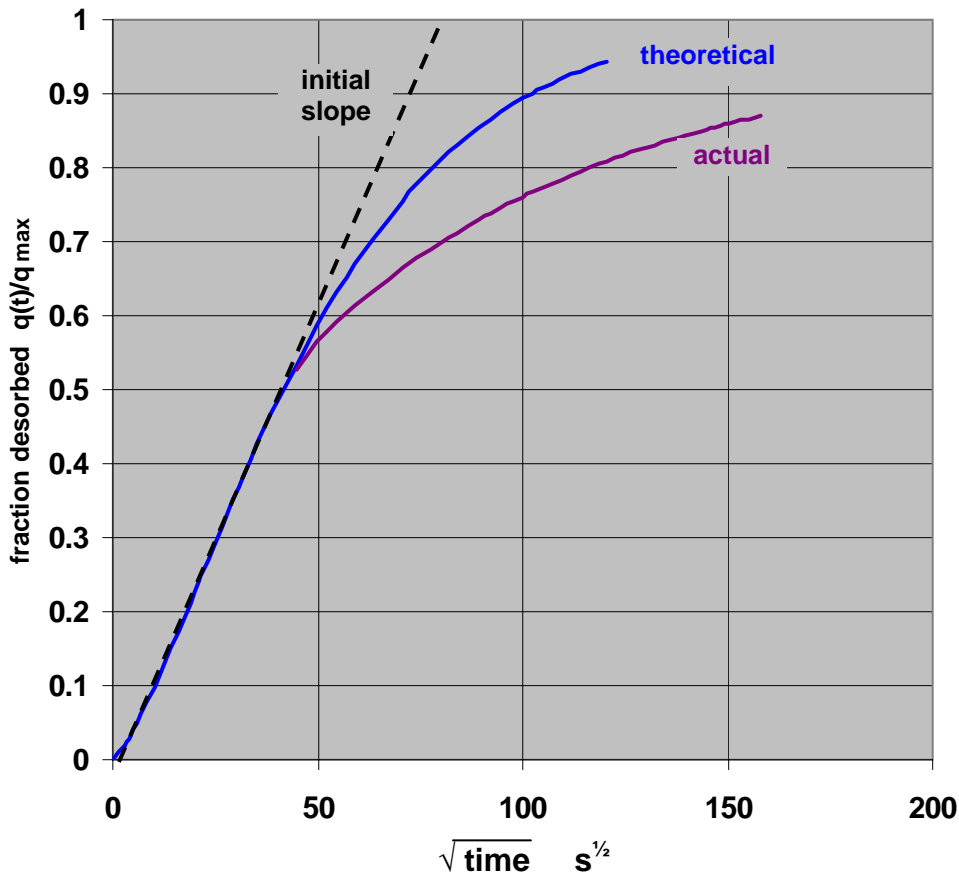


Figure 12.3(b) A methane desorption curve plotted against the square root of time.

Unfortunately, there is a major problem associated with all of these equations. The coefficient of diffusion, D , is not a constant for any given sample. It is dependent upon

- the size range of individual particles
- the distribution of pore sizes
- the number, sizes and tortuosity of fractures (this, in turn, depending upon the stress history of the sample)
- temperature
- pressure and current gas content.

The latter factors are particularly troublesome as these, and hence D , will vary as the degassing proceeds. Lama (1987) has suggested the relationship

$$D = D_o \frac{P}{P_o} \quad \frac{\text{m}^2}{\text{s}} \quad (12.10)$$

where P = current value of pressure (Pa) and
 D_o = coefficient of diffusion at some original (seam) pressure, P_o (m^2/s)

The variations in D contribute to the changes in apparent permeability of a coal sample when subjected to mechanical stress or variations in mean gas pressure (Section 12.3.2.). Considering the sensitivity of D to a significant number of variables, it is not altogether surprising that a wide range of values have been reported, from 1×10^{-8} to 1×10^{-14} m^2/s . In order to take the particle size into account, it has become common to express the diffusivity as the ratio D/a^2 (s^{-1}) where a = particle radius (m).

A further weakness is that the fundamental equation (12.6) is based on uniformly sized capillaries. This leads to significant deviations between predicted and observed desorption rates at the longer times ($q(t)/q_{max} > 0.6$) as indicated on Figure 12.4 (Smith and Williams, 1984).

The difficulties encountered in the derivation and general applicability of analytical desorption equations led E. M. Airey (1968) to propose an empirical relationship:

$$\frac{q(t)}{q_{max}} = 1 - \exp\left[-\left(\frac{t}{t_0}\right)^n\right] \quad (12.11)$$

where t_0 = 'time constant' = time for 63 percent of the gas to desorb (s) and
 n = an index that varies from some 1/3 for bituminous coals to 1/2 for anthracites and dependent, also, upon the degree of fracturing.

Both t_0 and n are influenced by the range and magnitude of particle sizes and, hence, should be quoted with reference to a specific size spectrum. For example, values of t_0 for Welsh anthracite lie, typically, between 1500 and 2100 seconds for the size range 0.05 to 0.30 mm at 25 °C (Barker-Read, 1989). Smaller particles will give reduced values of both t_0 and n .

An improved desorption time parameter, τ , that is independent of the gas capacity of a sample has been proposed by Radchenko (1981) and Ettinger et al (1986) (see, also, Barker-Read and Radchenko (1989) and may be related to Airey's constants:

$$\tau = 60 \left[1 - \exp\left\{-\left(\frac{t_0}{60}\right)^{-n}\right\}\right]^{-2} \quad \text{sec} \quad (12.12)$$

It can also be shown that

$$\tau = \frac{\pi a^2}{36D} \quad \text{sec} \quad (12.13)$$

where a = radius of the particle (m)

The value of τ can be gained from the desorbed fraction v $\sqrt{\text{time}}$ curve (e. g. Figure 12.3(b)):

$$\tau = 1/(\text{initial slope})^2 \quad \text{sec} \quad (12.14)$$

Equations (12.13 and 12.14) provide a ready means of determining D/a^2 from a desorption test.

12.2.3. Determination of gas content

There are two reasons for measuring the methane contents of coal seams and associated strata. First, such data are required in the assessment of methane emissions into mine workings and, hence, the airflows required to dilute those emissions to concentrations that are safe and within mandatory threshold limit values (Sections 9.3.1. and 11.2.1.). Secondly, the gas content of the strata is a required input for computer models or other computational procedures to determine the gas flows that may be obtained from methane drainage systems.

There are also two distinct approaches to the evaluation of gas content, the **indirect method** which employs adsorption isotherms and the **direct measurement method** which relies upon observations of gas release from newly obtained samples. Let us consider each of these in turn.

12.2.3.1. Indirect method (adsorption isotherms)

In this technique, representative chippings are obtained from the full thickness of the seam, mixed and ground to a powder of known particle size range. The sample is dried at a temperature of not more than 80°C and evacuated to remove the gases that remain in the pore structure. Unfortunately, the process of evacuation may alter the internal configuration of the pore structure due to the liquefaction of tars (Harpalani, 1984). The phenomenon can be overcome by evacuating at low temperature – submerging the sample container into liquid nitrogen (-150°C) prior to and during the evacuation.

After returning to the desired ambient temperature, methane is admitted in stages and the gas pressure within the sample container recorded at each increment. The volume of gas admitted may be monitored at inlet (volumetric method) or by measuring the increase in weight of the sample and container (gravimetric method). After correcting for free space in the sample container, a plot of cumulative methane admitted against pressure provides the total gas isotherm. If the porosity of the sample has been determined separately (Section 12.2.1.), then the results can be divided into free gas and adsorbed gas as illustrated on Figure 12.1. The isotherms should, ideally, be determined at, or close to, the virgin rock temperature of the actual strata. If necessary, the curves can be corrected to seam temperature. At any given pressure, the quantity of gas adsorbed falls as the temperature increases. Starting at 26°C, the gas adsorbed decreases by some 0.8 percent per °C for bituminous coal and 0.6 percent per °C for anthracite (Boxho et al, 1980). The curves should also be corrected to the actual moisture content of the seam using Ettinger's formula, equation (12.2).

In order to utilize the corrected gas isotherm, a borehole is drilled into the seam, either from the surface or from an underground location. In the latter case, the hole must be sufficiently long (10 to 20 m) in order to penetrate beyond the zone of degassing into the mine openings. Seals are

emplaced in the borehole to encapsulate a representative length within the seam. A tube from the encapsulated length of borehole is attached to a pressure gauge and the rise in pressure is monitored. The rate of pressure rise will be greater for coals of higher permeability. The initial rate of pressure rise may be used in conjunction with open hole flowrates to determine in-situ permeability. However, for the purposes of assessing seam gas content, it is the maximum (or equilibrium) pressure that is required. Using this pressure, the gas content of the seam can be read from the corrected isotherm curve.

An advantage of the indirect method is that it gives the total gas content of the seam. However, this is not indicative of the actual gas that may be emitted into mine workings or recoverable by methane drainage. Furthermore, the measured in-situ gas pressure will be influenced not only by methane but also by other gases that may be present and, particularly, by the presence of water.

12.2.3.2. Direct measurement method.

This technique involves taking a sample of the seam from a borehole and placing it immediately into a hermetically sealed container. The gas is bled off to atmosphere in stages and its volume measured. The process is continued until further gas emissions are negligible.

An early method of direct measurement of gas content was developed in France (Bertrand et al, 1970). This utilized samples of small chippings from the borehole. Further research carried out by the U. S. Bureau of Mines during the 1970's led to a procedure that used complete cores (Diamond, 1981). Although developed primarily for surface boreholes, the technique is applicable also to horizontal holes drilled from mine workings. The sampling personnel must be present at the time the hole is drilled into the seam. A stopwatch is used to maintain an accurate record of the elapsed times between which the sample length of strata is penetrated, start of core retrieval, arrival of the sample at the mouth of the borehole and confinement within the sealed container.

Each container should be capable of holding about 2 kg of core and some 35 to 40 cm in length. Longer cores should be subdivided as a precaution against major loss of data should one container suffer from leakage. The seals on containers must be capable of holding a gas pressure of 350 kPa without leaking. A pressure gauge should be fitted to each container.

Gas is bled off from the container at intervals of time commencing at 15 minutes (or less if a rapid rise in container pressure is observed). The volume of gas emitted at each stage is measured, usually by water displacement, in a burette. The time intervals are increased progressively and the process allowed to continue until an average of not more than 10 cubic cm per day has been maintained for one week.

There is, inevitably, some gas lost from the core between the time of seam penetration and its confinement in a sample container. The volume of lost gas may be assessed by plotting the cumulative gas emitted from the container against $\sqrt{\text{time}}$. The initial straight line may be extrapolated backwards through the recorded elapsed time of core retrieval in order to quantify the lost gas. The retrieval time can be minimized by using wireline drilling. The technique is illustrated on Figure 12.4. The analytical background to the procedure is embodied in equation (12.9). [Should subsequent tests show that the rate of desorption follows a t^n law where n deviates significantly from 0.5 (Equation (12.11)), then the appropriate plot may be constructed as gas evolved $v t^n$ in order to determine the lost gas.]

Another method of estimating the lost gas, developed by Smith and Williams (1984) makes separate allowance for the elapsed times of drilling through the coal, core retrieval and period spent at the mouth of the borehole before containment. This more sophisticated technique is based on an analysis that takes account of the lack of uniformity in pore sizes (Smith and Williams (1984a), Close and Erwin, (1989).

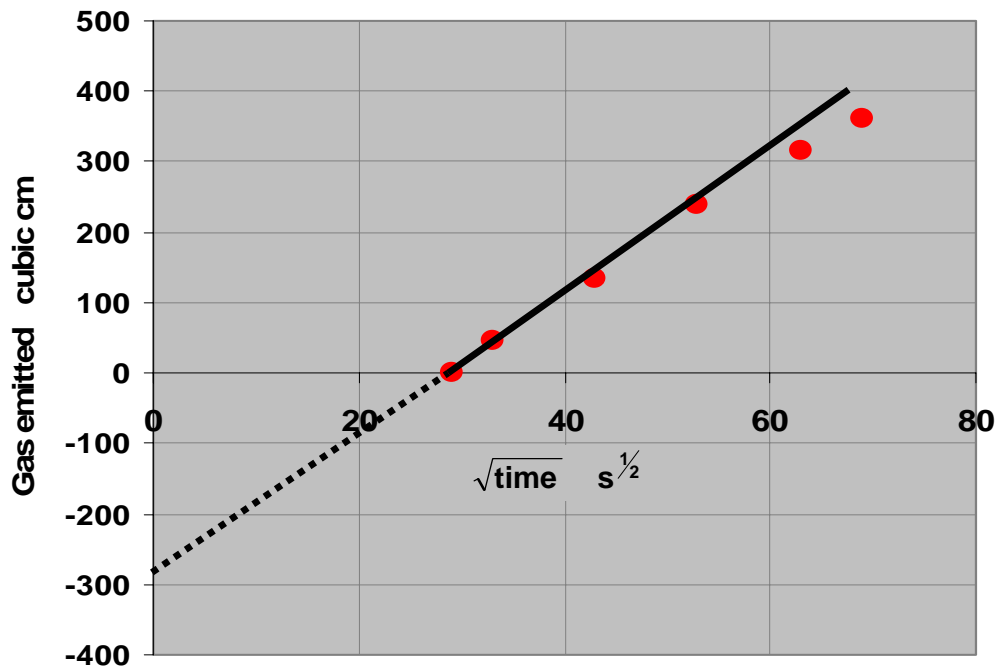


Figure 12.4 Assessment of gas lost during core retrieval. In this example, elapsed time before containment, $t = 840$ seconds (i.e. $\sqrt{t} = 29 \text{ s}^{1/2}$). Backward extrapolation of the initial straight line gives the gas lost as 285 cm^3 .

The combination of measured gas and lost gas gives an estimate of the maximum amount of gas that may be emitted into mine workings or captured by methane drainage. (It may be much less than this.) However, following the termination of gas evolution measurements, the core will still contain some **residual gas**. This can be quantified, if required, by crushing the coal and continuing to measure the additional gas that is then liberated. The crushing process may take place in a separate sealed ball mill within a nitrogen atmosphere. However, steel balls in the sample container allow the crushing to take place without removing the sample from the container. Another method is to activate a steel hammer by electromagnetic means within the container in order to crush the sample through a fixed grid. In either case, the sample and evolved gas should be cooled to the original ambient temperature before the gas is bled off.

A variation of the direct measurement method of gas content is the “desorbmeter” (Hucka, 1983) in which desorbing methane from coal chippings in a sample vessel pushes a small plug of fluid along a transparent spiral tube. An electronic version employing the same principle has been developed in Germany (Janas, 1980).

12.3. MIGRATION OF METHANE

Following release from its long term geologic home, methane will migrate through rock under the influence, primarily, of a gas pressure gradient. That movement will occur through the coal seam and if the gas pressure gradient is transverse to the seam, also through adjoining fractured or permeable strata. We assume that the flow paths and velocities are sufficiently small that laminar flow exists. Hence, Darcy’s Law applies. This was introduced in its simplest form as equation (12.5). In this Section, we shall consider the further ramifications of Darcy’s Law.

12.3.1. Fluid Flow through a permeable medium.

12.3.1.1. Incompressible flow

Let us consider, first, an incompressible fluid (liquid) passing through a permeable medium in the direction x as illustrated on Figure 12.5. An elemental volume of the fluid within the medium has a thickness, dx , and an orthogonal area A . Two forces act upon the element.

First, a force in the direction of flow is exerted because of the pressure differential, dP , across its two faces. Let us call this F_p , where.

$$F_p = -A dP \quad \text{N} \quad (12.15)$$

(negative because P decreases in the x direction).

Secondly, a vertical downward force, F_v , exists due to gravitational pull:

$$F_v = m g$$

where the mass of the element (density ρ , x volume $A dx$)

$$m = \rho A dx$$

giving

$$F_v = \rho g A dx$$

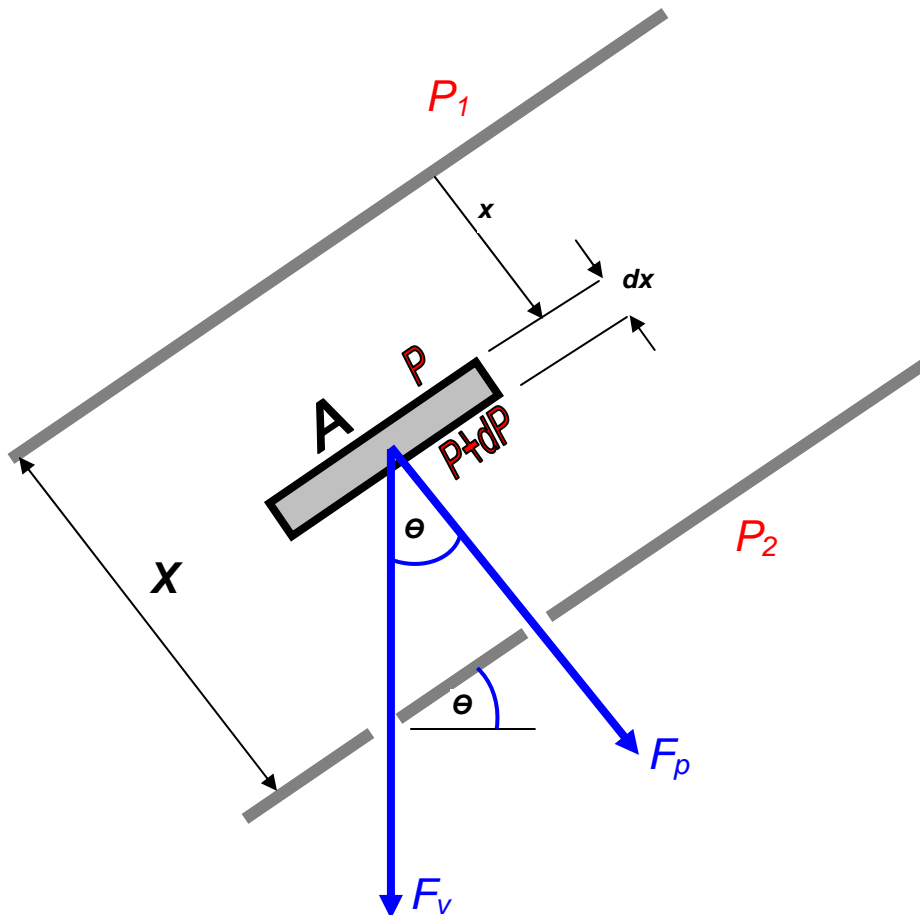


Figure 12.5 Forces on an elemental volume of fluid, $A dx$, within a permeable medium.
Total force in the x direction, $F_t = F_p + F_v \cos \theta$.

If the direction of flow is at an angle Θ to the vertical then the component of F_v in the x direction is

$$F_v \cos \Theta = \rho g A \cos \Theta dx \quad \text{N} \quad (12.16)$$

(Note that Θ is also the inclination of the permeable medium to the horizontal.)

The total force on the element in the direction of flow is then

$$F_t = F_p + F_v \cos \Theta = -AdP + \rho g A \cos \Theta dx \quad \text{N} \quad (12.17)$$

This can be expressed as force per unit volume

$$\frac{F_t}{Adx} = -\frac{dP}{dx} + \rho g \cos \theta \quad \frac{\text{N}}{\text{m}^3} \quad (12.18)$$

This is a fuller version of the pressure gradient $-\partial P / \partial x$ in Darcy's Law, equation (12.5).

Hence, we can rewrite Darcy's Law for an incompressible fluid in a non-horizontal flow field as

$$u_x = -\frac{k}{\mu} \left\{ \frac{dP}{dx} - \rho g \cos \theta \right\} \quad \frac{\text{m}}{\text{s}} \quad (12.19)$$

where u_x = fluid velocity in the x direction (m/s)

k = permeability of medium (m^2)

μ = dynamic viscosity of fluid (Ns/m^2)

and dP is negative in the x direction.

In the case of horizontal flow ($\cos \Theta = 0$) or where the fluid density is small, then equation (12.19) reverts to the simple form of Darcy's Law.

$$u = -\frac{k}{\mu} \frac{dP}{dx} \quad \text{m/s} \quad (12.20)$$

As the fluid is incompressible, then u remains constant and we can integrate directly between the bounding walls shown on Figure 12.5, giving

$$u = -\frac{k}{\mu} \frac{(P_2 - P_1)}{X} = \frac{k}{\mu} \frac{(P_1 - P_2)}{X} \quad \text{m/s} \quad (12.21)$$

or, flowrate, Q , across a given orthogonal area, A becomes

$$Q = uA = \frac{k}{\mu} A \frac{(P_1 - P_2)}{X} \quad \frac{\text{m}^3}{\text{s}} \quad (12.22)$$

12.3.1.2. Compressible flow

For gases the fluid density is, indeed, low and the gravitational term may be neglected even for non-horizontal flow. However, the gas will expand as it progresses along the flowpaths due to the reduction in pressure. Hence the flowrate, Q , and gas velocity, u , will both increase.

$$Q = uA = \frac{k}{\mu} A \frac{dP}{dx} \quad \frac{\text{m}^3}{\text{s}} \quad (12.23)$$

where A = given orthogonal area across which the flow occurs (m^2)

As Q is a variable, we can no longer integrate directly. However, if we write the equation in terms of a steady-state (constant) mass flow, M (kg/s), then

$$M = Q\rho = -\frac{k}{\mu} A \rho \frac{dP}{dx} \quad \frac{\text{kg}}{\text{s}} \quad (12.24)$$

But density $\rho = \frac{P}{RT} \frac{\text{kg}}{\text{m}^3}$ (General Gas Law, equation 3.11)

where R = gas constant (J/(kg K)) and T = absolute temperature (K)

$$\text{giving } M = -\frac{k}{\mu} \frac{A}{RT} \frac{P dP}{dx} \quad \frac{\text{kg}}{\text{s}} \quad (12.25)$$

As M is constant, we can integrate across the full thickness of the medium (Figure 12.5) to give

$$M = \frac{k}{\mu} \frac{A}{RT} \frac{(P_1^2 - P_2^2)}{2X} \quad \frac{\text{kg}}{\text{s}} \quad (12.26)$$

This can be converted to a volume flow, Q , at any given density. In particular, at the density, ρ_m , corresponding to the arithmetic mean pressure, the flow becomes

$$Q_m = \frac{M}{\rho_m} \quad \frac{\text{m}^3}{\text{s}} \quad (12.27)$$

However, equation (12.26) can be written as

$$M = \frac{k}{\mu} \frac{A}{RT} \frac{(P_1 + P_2)}{2} \frac{(P_1 - P_2)}{X} \quad \frac{\text{kg}}{\text{s}} \quad (12.28)$$

$$= \frac{k}{\mu} A \frac{P_m}{RT} \frac{(P_1 - P_2)}{X} \quad \frac{\text{kg}}{\text{s}}$$

$$= \frac{k}{\mu} A \rho_m \frac{(P_1 - P_2)}{X} \quad \frac{\text{kg}}{\text{s}} \quad (12.29)$$

Combining equations (12.27 and 12.29) gives

$$Q_m = \frac{k}{\mu} A \frac{(P_1 - P_2)}{X} \quad \frac{\text{kg}}{\text{s}} \quad (12.30)$$

Comparing this with equation (12.22) shows that the volume flow of a gas at the position of mean pressure is given by the same expression as for an incompressible fluid.

At any other density, ρ , the volume flowrate, Q , is given by

$$Q = Q_m \frac{\rho_m}{\rho} \quad \frac{\text{m}^3}{\text{s}} \quad (12.31)$$

If the flow is isothermal (constant temperature) then this correction can be expressed in terms of pressure

$$Q = Q_m \frac{P_m}{P} \quad \frac{\text{m}^3}{\text{s}} \quad (12.32)$$

$$= Q_m \frac{(P_1 + P_2)}{2P} \quad \frac{\text{m}^3}{\text{s}} \quad (12.33)$$

12.3.1.3. Radial flow of gas

Figure 12.6 illustrates a borehole of radius r_b intersecting a gas bearing horizon of thickness h . The gas pressure in the borehole at the seam is P_b while, at some greater radius r_s into the seam, the gas pressure is P_s .

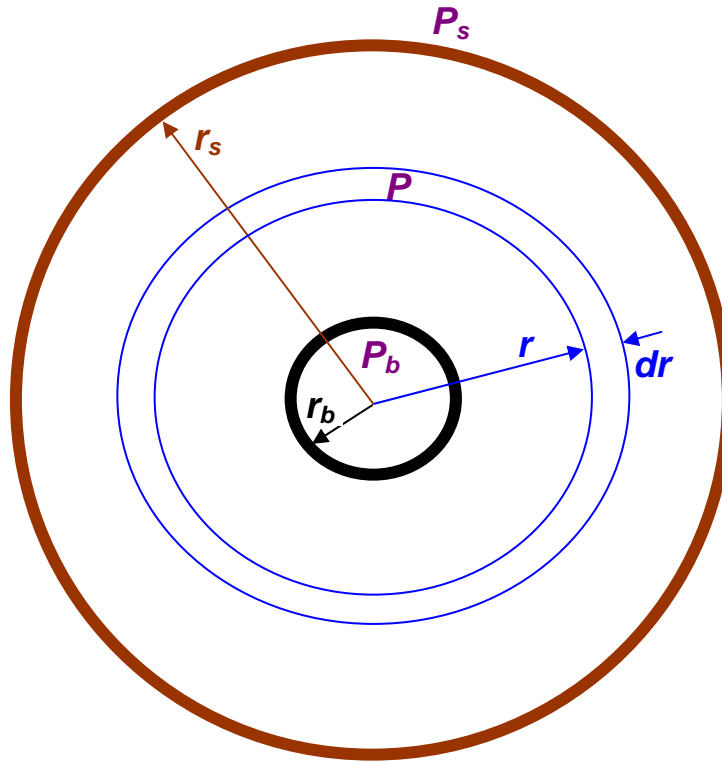


Figure 12.6 Radial flow into a borehole.

Consider the elemental cylinder of radius r and thickness dr , at which the gas pressure is P . Then, from equation (12.25)

$$M = -\frac{k}{\mu} \frac{A}{RT} P \frac{dP}{dr} \quad \frac{\text{kg}}{\text{s}}$$

where $A = 2\pi r h \quad \text{m}^2$

giving $M = -\frac{k}{\mu} \frac{2\pi h}{RT} P dP \frac{r}{dr} \quad \frac{\text{kg}}{\text{s}}$

or

$$M \frac{dr}{r} = -\frac{k}{\mu} \frac{2\pi h}{RT} P dP \quad \frac{\text{kg}}{\text{s}} \quad (12.34)$$

Integrating between r_s and r_b gives

$$M \ln\left(\frac{r_s}{r_b}\right) = \frac{k}{\mu} \frac{2\pi h}{RT} \frac{(P_s^2 - P_b^2)}{2} \quad \frac{\text{kg}}{\text{s}}$$

or $M = \frac{k}{\mu} \frac{2\pi h}{RT} \frac{(P_s + P_b)}{2} \frac{(P_s - P_b)}{\ln\left(\frac{r_s}{r_b}\right)} \quad \frac{\text{kg}}{\text{s}} \quad (12.35)$

But as $\frac{(P_s + P_b)}{2RT} = \frac{P_m}{RT} = \rho_m$

$$Q_m = \frac{M}{\rho_m} = \frac{k}{\mu} 2\pi h \frac{(P_s - P_b)}{\ln\left(\frac{r_s}{r_b}\right)} \quad \frac{\text{m}^3}{\text{s}} \quad (12.36)$$

Equations (12.31 and 12.33) can again be used to give the flowrate at any other density or pressure.

12.3.1.4. Transient radial flow

The previous Section assumed a steady-state distribution in gas pressure throughout the medium. This is not, of course, the real situation in practice. As a given source bed is drained, the gas pressure will decline with time. An analysis analogous to that given for heat flow (Section 15.2.5.) leads to the time transient equation for a non-adsorbing medium:

$$\frac{k}{\mu} \frac{P}{\phi} \left\{ \frac{\partial^2 P}{\partial r^2} + \frac{1}{r} \frac{\partial P}{\partial r} \right\} = \frac{\partial P}{\partial t} \quad \frac{\text{Pa}}{\text{s}} \quad (12.37)$$

where $\phi =$ rock porosity (dimensionless)
and $t =$ time (s)

For methane in coal, gas will be generated by desorption as the gas pressure falls (Figure 12.1) and, hence, retard the rate of pressure decline very significantly. The gas desorption equations of Section 12.2.2.2. must be coupled with equation (12.37) to track the combined effects of drainage and desorption.

12.3.2. The permeability of coal

In the previous section, it was assumed that the permeability, k , of the rock remained constant. Unfortunately, in some cases including coal, this no longer holds. The anisotropy of the material causes the natural permeability to vary with direction. Furthermore, the permeability changes with respect to mechanical stress, gas pressure and the presence of liquids. We shall examine each of these three effects in turn. First, however, let us clarify the concept of permeability and its dimensions in the SI system of units.

Permeability, k , may be construed as the conductance of a given porous medium to a fluid of known viscosity, μ . That conductance must depend only upon the geometry of the internal flowpaths. In a rational system of units, the permeability must, therefore, be expressed in terms of the length dimension. This can be illustrated by re-expressing Darcy's Law, equation (12.5) as

$$k = -u \mu \frac{\partial x}{\partial P} \quad \frac{\text{m}}{\text{s}} \frac{\text{Ns}}{\text{m}^2} \text{m} \frac{\text{m}^2}{\text{s}} = \text{m}^2$$

The units of permeability in the SI system are, therefore, m^2 . However, the older units of Darcys (or millidarcies, md) remain in common use. The Darcy was defined as "the permeability of a medium that passes a single-phase fluid of dynamic viscosity 1 centipoise (0.01 Ns/m^2) in laminar flow at a rate of $1 \text{ cm}^3/\text{s}$ through each cm^2 of cross-sectional area and under a pressure gradient of 1 atmosphere ($101\,324 \text{ Pa}$) per cm ". Such definitions make us grateful for the simplicity of the SI system. The conversion between the unit systems is given as

$$1 \text{ md} = 0.98693 \times 10^{-15} \quad \text{m}^2 \quad (12.38).$$

12.3.2.1. Effect of mechanical stress

Many researchers have reported tests on the response of coal permeability to applied loading (e.g. Somerton, 1974; Gawuga, 1979; Harpalani, 1984). Such tests consist of delicate machining of coal into sample cylinders of 30 to 50 mm in diameter and a length/diameter ratio of about 2 (Obert, 1967), then placing a sample into a triaxial permeameter. This device allows a liquid or gas to be passed while the sample is subjected to axial loading (by a stiff compression machine) and radial stressing (by oil pressure exerted on a synthetic rubber sleeve around the sample).

Such tests on coal have revealed the following phenomena during non-destructive loading.

- Permeability reduces during loading and recovers during unloading. However, there may be a significant hysteresis effect with lower permeabilities during unloading, particularly when the axial and radial stresses are unequal.
- Samples left under a constant applied stress exhibit a creep effect. The permeability reduces with time down to a limiting value.
- Following a loading test, a sample may not recover its initial permeability. Furthermore, repeated loading tests will give progressively reduced permeabilities.

These observations suggest that coals exhibit a combination of elasticity and non-recoverable strain. The latter is thought to be caused by permanent damage to the weaker bridges between pores.

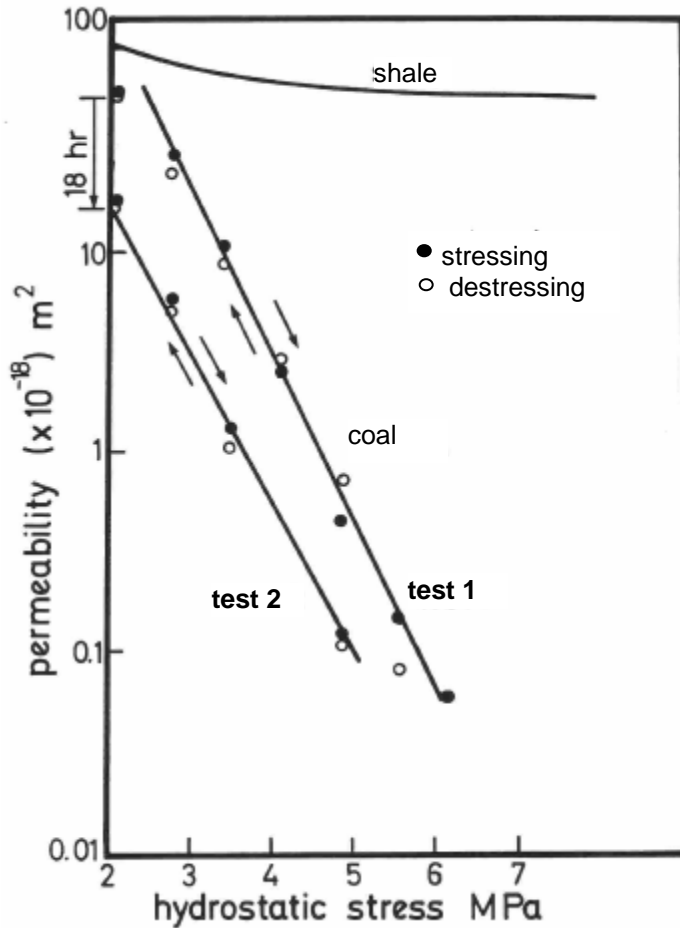


Figure 12.7 The variation of permeability with hydrostatic stress for two load/unload tests of a bituminous coal, After the completion of test 1 the sample was left lightly loaded for 18 hours before commencing test 2.

Figure 12.7 shows the results of hydrostatic loading (axial and radial stresses remaining equal) on the permeability of a bituminous coal. Hydrostatic stressing appears to minimize the hysteresis effect. Two load/unload cycles are shown. After completion of the first test, the sample was left for 18 hours in the triaxial cell at a holding stress of slightly more than 2 MPa. The creep reduction in permeability before commencement of the second test shows clearly.

It appears from such tests that the indicated permeability of a coal sample measured during a laboratory test depends upon the stress history of the sample. That is, the cycles of loading and unloading caused by mining close to the original location of the sample, and the method of recovering that sample. However, for any given laboratory test, the coal permeability falls logarithmically with respect to applied hydrostatic stress, i. e. the relationship is of the form

$$k = A \exp(B\sigma) \quad \text{m}^2 \quad (12.39)$$

where σ = effective stress (MPa) = applied hydrostatic stress - pore (mean gas) pressure
 A = constant (m^2)
 B = constant ($1/\text{MPa}$).

The value of A is the theoretical permeability at zero stress and depends not only upon the coal structure but also the stress history of the sample. Values of B from -1.5 to -2.5 ($1/\text{MPa}$) have been reported for bituminous coal.

For comparison, Figure 12.7 includes a similar test on shale. The reduction in permeability with applied stress is much less marked than that for coal.

12.3.2.2. Effect of gas pressure

For most rocks, the permeability increases as the pore pressure exerted by a saturating gas decreases. The effect was investigated by **Klinkenberg** (1941) who proposed the relationship

$$k = k_{liq} \left[1 + \frac{a}{P} \right] \quad m^2 \quad (12.40)$$

where k_{liq} = permeability of the medium to a single phase liquid, or permeability at a very high gas pressure (m^2)

and a = constant depending upon the gas (Pa)

The values of k_{liq} and a may be determined by plotting experimentally determined values of k against $1/P$.

It is thought that the **Klinkenberg effect** is caused by surface diffusion, i. e. slippage of gas molecules along the internal surfaces of the medium (Section 12.2.2.1.). However, in the case of coal, a straight line relationship is not found when measured values of k are plotted against $1/P$. Hence, there is no longer any advantage in plotting the variables in that way.

Researchers have reported both rising and falling permeabilities with respect to mean gas pressure during laboratory tests on coal. Figure 12.8 illustrates a typical set of results and shows the effects of gas pressure and applied hydrostatic stress. Curve fitting exercises show that such curves take the form

$$k = C_1 + \frac{C_2}{P} + \exp(C_3 P - C_4) \quad m^2 \quad (12.41)$$

Klinkenberg effect + dilation of flowpaths

where C_1 , C_2 , C_3 and C_4 are constants for the curve.

It will be observed that $(C_1 + C_2/P)$ has the form of the Klinkenberg effect and is dominant at low

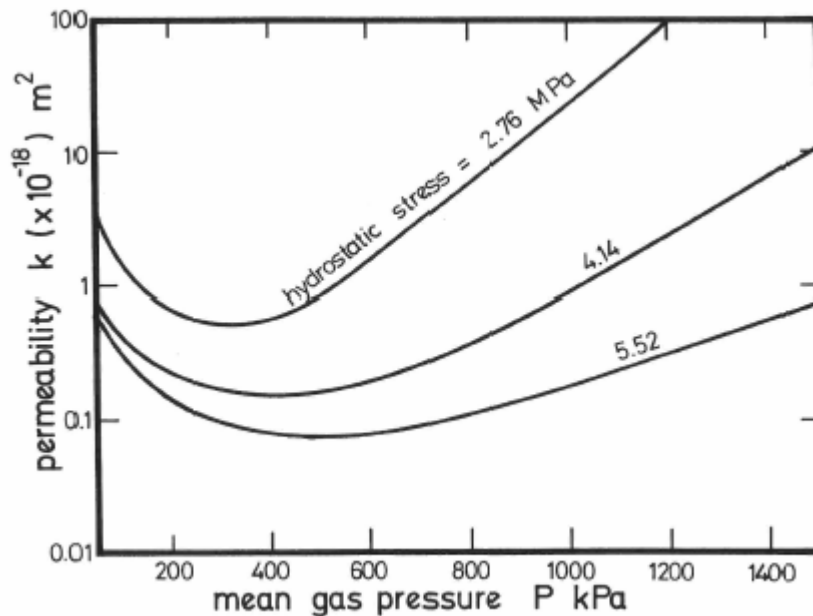


Figure 12.8 In addition to the effects of mechanical stress, the permeability of coal is also a function of the internal gas pressure.

gas pressures. As the gas pressure rises through this phase, surface diffusion reduces and, adsorbed molecules begin to obstruct the flowpaths. Hence, the permeability falls. However, with further increases in gas pressure, the exponential term in equation (12.41) becomes dominant causing the permeability to rise again. One hypothesis is that a sufficiently high pore pressure results in compression of the coal substance and unconnected pores while the flowpaths become dilated.

12.3.2.3. Two phase flow

The pores and fracture networks of strata are often occupied by a mixture of fluids. In petroleum reservoirs, three phase flow may occur with oil, gas and water as the occupying fluids. In most other cases, including coal, two phase flow takes place as a mixture of gases and water.

The presence of water greatly inhibits the flow of gas and vice versa and, hence, reduces the permeability of the rock to both phases. The effect is described quantitatively in terms of the relative permeabilities $k_{r,g}$ and $k_{r,w}$ for gas and water respectively:

$$k_{r,g} = \frac{k_g}{k_{sg}} \quad (\text{dimensionless}) \quad (12.42)$$

and
$$k_{r,w} = \frac{k_w}{k_{sw}} \quad (\text{dimensionless}) \quad (12.43)$$

where k_g and k_w are the effective permeabilities of the rock to gas and water respectively, m^2 (dependent on degree of saturation)

k_{sg} = permeability of the rock to gas when saturated by gas, m^2 (no water present)
and k_{sw} = permeability of the rock to water when saturated by water, m^2 (no gas present)

In the petroleum industry, it is often assumed that $k_{sg} = k_{sw}$ for the sandstones and limestones that are typical of petroleum reservoir rocks. However, the effects of adsorption and gas pressure indicate that this may not hold for coal.

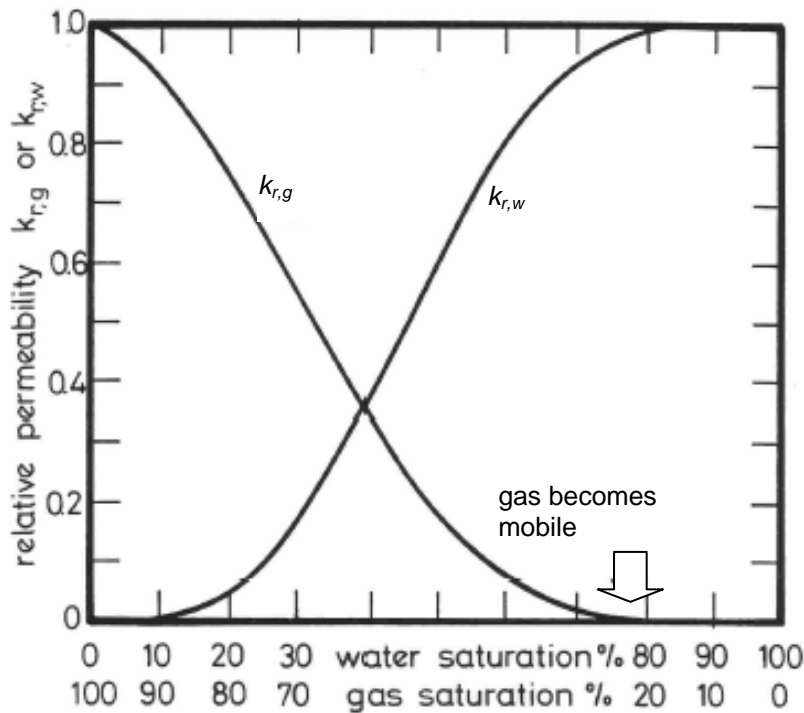


Figure 12.9 The relative permeabilities to gas, $k_{r,g}$, and water $k_{r,w}$ depend upon the degree of rock saturation by the two fluids.

Figure 12.9 illustrates a typical behaviour of relative permeabilities with respect to saturations of water and gas. The actual loci of the relative permeability curves depend upon whether the coal substance is wetted preferentially by the water or the gas. This, in turn, varies with the proportion of coal constituents, vitrain and clarain tending to prefer the gas while durain and fusain are more easily wetted by water.

The curves on Figure 12.9 suggest a net hydrophobic coal, i.e. the gas is the preferred wetting phase. The water will, therefore, tend to reside in the larger openings within the matrix and inhibit

migration of the gas which exists in the smaller interstices. Hence, as indicated on Figure 12.9, the gas will not become mobile until the water saturation has fallen significantly below 100 percent. This explains why considerable volumes of water may be produced from a borehole before gas flows appear.

12.4. EMISSION PATTERNS INTO MINE WORKINGS

The rates at which methane are emitted into mine workings vary from near steady-state, through cycles that mimic rates of mineral production, to the dangerous phenomena of gas outbursts or "sudden large emissions". In general, the rate of gas emission into the mine ventilation system depends upon:

- initial gas content of the coal
- degree of prior degassing by methane drainage or mine workings
- method of mining
- thickness of the worked seam and proximity of other seams
- coal production rate
- panel width (of longwalls) and depth below surface
- conveyor speeds
- the natural permeability of the strata and, in particular, the dynamic variations in permeability caused by mining
- comminution of the coal.

12.4.1. Sources of methane in coal mines

Variations in methane emissions into mines are influenced strongly by the dominant sources of the gas. In room and pillar workings, gas will be produced from faces, ribsides and the pillars of the seam being worked. While exposed pillars may be degassed fairly quickly (dependent upon the coal permeability), ribside gas may continue to be troublesome for considerable periods of time. In such cases, it is preferable for ribsides that border on virgin coal to be ventilated by return air (Figure 4.7a). Peaks of gas emission will, in general, occur at the faces of the rooms due to the high rate of comminution caused by mechanized coal winning. This will be moderated by the degree of earlier degassing, either by methane drainage or by gas migration towards the workings. The latter is enhanced by high coal permeability and a low rate of advance.

In addition to ribsides, the major sources of methane in longwall mines are the working faces and roof and floor strata. **Ribside gas** tends to be a slow and near constant source. It is convenient to classify the other sources of methane in a longwall mine into **face (or coal front) gas and gob gas**. Peak emissions occur at coal-winning machines due to rapid fragmentation of the coal. It is this emission that gives rise to frictional ignitions at the pick point (Section 12.1). The peak emission moves along a longwall face with the machine. However, the freshly exposed coal front will also emit methane - rapidly at first and decaying with time until the machine passes that point again. Coal front gas is an immediate and direct load on the district ventilation system. Figure 12.10 is an example of a smoothed record of methane concentration in air returning from a longwall face. In this example, coal was produced on two out of three shifts for five days per week. The correlation of methane make with face activity shows clearly, decaying down to a background level over the weekend.

The gas flow into the gob area behind a longwall face originates from any roof or floor coal that has not been mined from the worked seam, but more particularly from source beds within the roof or floor strata. Any coal seams or carbonaceous bands within a range of some 200 m above to 100 m below the working horizon are liable to release methane that will migrate through the relaxed strata into the gob area. If methane drainage is not practiced, then that methane will subsequently be emitted into the mine ventilation system. Figure 12.11 illustrates the variations in stress-induced permeability of roof and floor strata that create enhanced migration paths for the gas.

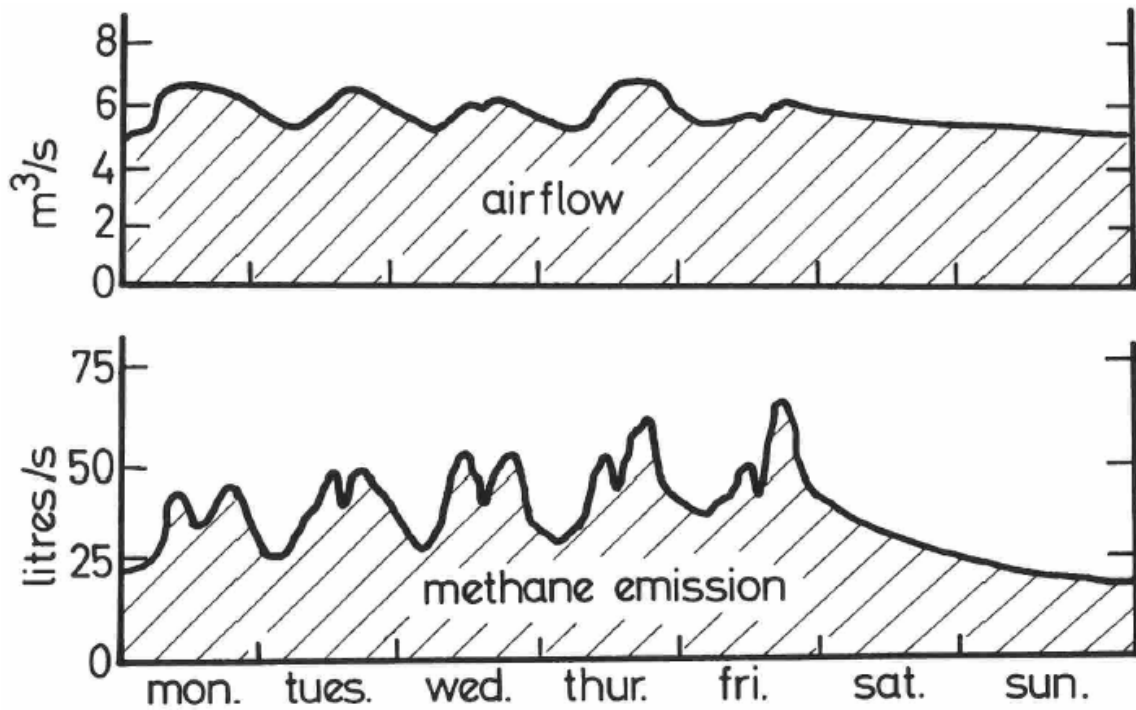


Figure 12.10 Recordings of airflow and methane flow in an airway returning from a longwall face.

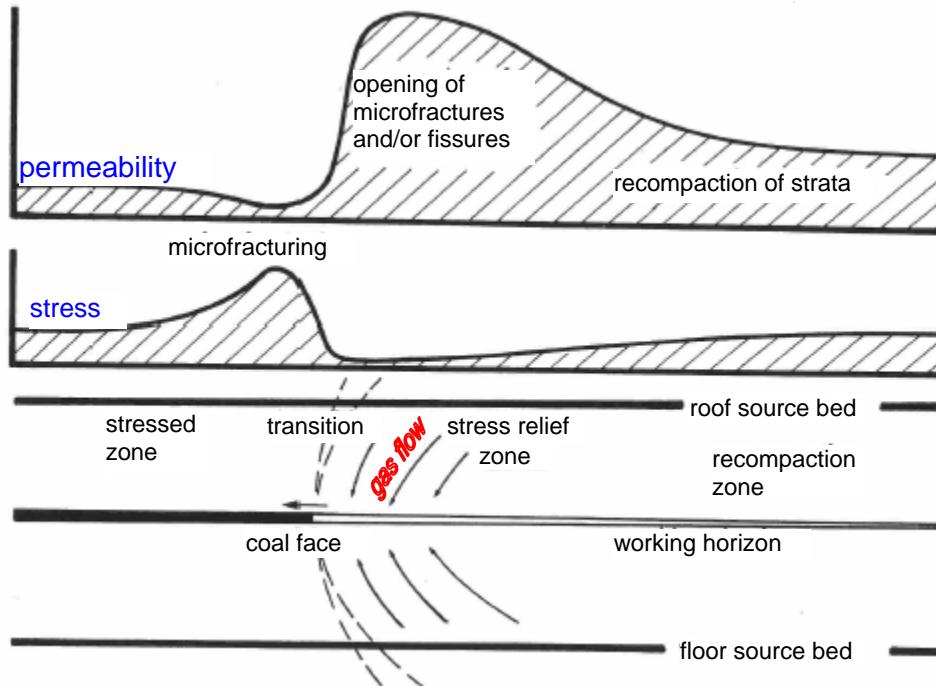


Figure 12.11 The migration of gas from roof and flow source beds toward the working horizon occurs because of the large increase in permeability of adjacent strata in the stress relief zone immediately behind a longwall face.

As fragmented coal is transported out of the mine, it will continue to emit methane. The gas make depends upon the degree of fragmentation, gas content of the cut coal on leaving the face, the tonnage and the time spent during transportation. The desorption equations given in Section 12.2.2.2. allow estimates of the transport gas to be made. Precautions should continue to be taken against accumulations of methane after the coal has left the mine. Gas explosions have occurred in surface hoppers and in the holds of coal transport ships.

12.4.2. Methane layering

Methane emitted from the strata into a mine opening will often be at concentrations in excess of 90 percent. While being diluted down to safe general body concentrations, the methane will, inevitably, pass through the 5 to 15 percent range during which time it is explosive. It is, therefore, important that the time and space in which the explosive mixture exists are kept as small as possible. This can be achieved by good mixing of the methane and air at the points of emission. Unfortunately, the buoyancy of methane with respect to air (specific gravity 0.554) produces a tendency for concentrated methane to collect in roof cavities and to layer along the roofs of airways or working faces.

In level and ascensionally ventilated airways with inadequate airflow, the layer will stream along the roof in the direction of airflow, increasing in thickness and decreasing in concentration as it proceeds (Figure 12.12(a)). Multiple feeders of gas will, of course, tend to maintain the concentration at a high level close to the roof.

There are two main hazards associated with methane layers. First, they extend greatly the zones within which ignitions of the gas can occur. Secondly, when such an ignition has taken place, a methane layer acts very effectively as a fuse along which the flame can propagate -perhaps leading to much larger accumulations in roof cavities or gob areas.

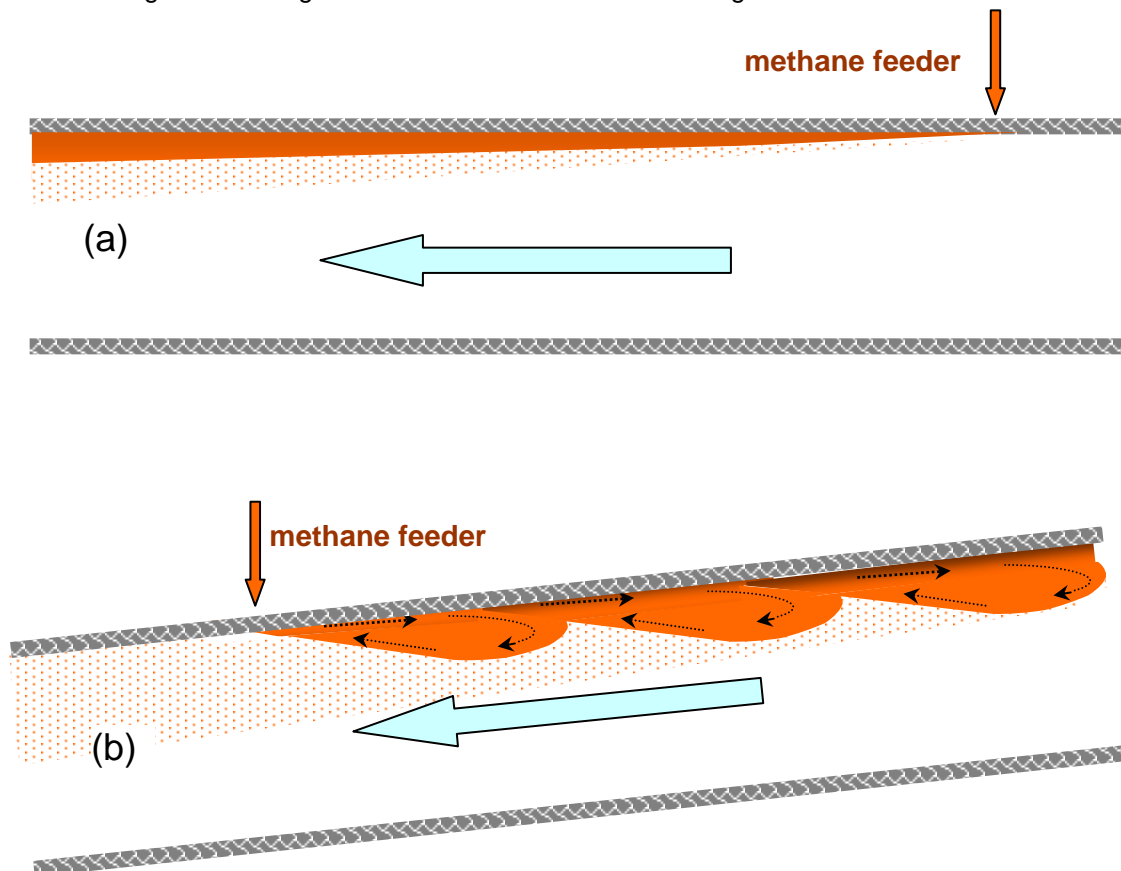


Figure 12.12 Methane layering in (a) a level airway
(b) a descensionally ventilated airway.

Figure 12.12(b) indicates that in a descentally ventilated airway, the buoyant methane layer may stream uphill close to the roof and against the direction of the airflow. However, at the fringe between gas and air, viscous drag and eddy action will cause the gas/air mixture to turn in the same direction as the airflow. The result is that explosive mixtures may be drawn down into the airway upstream from points of emission.

Although the layering phenomenon of methane in mines was all too obvious during the Industrial Revolution (Section 1.2), systematic research on the topic seems not to have been well organized until the 1930's (Coward, 1937). A combination of analytical and experimental work at the Safety in Mines Research Establishment, England in the early 'sixties led to a quantification of the important parameters (Bakke and Leach, 1962). These were

- velocity of the ventilating airstream, u (m/s)
- rate of gas emission, Q_g (m^3/s)
- width of airway W (m)
- inclination of airway
- relative densities of the air and gas
- roughness of the roof above the layer.

Although a rough lining will promote better mixing than a smooth one (except for free-streaming layers), the effect of roughness is fairly weak (Raine, 1960). Bakke and Leach found that the characteristic behaviour of a gas layer was proportional to the dimensionless group

$$\frac{u}{\left\{g \frac{\Delta\rho}{\rho} \frac{Q_g}{W}\right\}^{1/3}} \quad (12.44)$$

where $\Delta\rho/\rho$ is the difference in relative densities of the two gases. ($1 - 0.554 = 0.446$ for air and methane)

Using a value of $g = 9.81 \text{ m/s}^2$ gives the dimensionless number for methane layers in air to be

$$L = \frac{u}{(9.81 \times 0.446 \times Q_g / W)^{1/3}} \quad \text{or} \quad L = \frac{u}{1.64} \left\{ \frac{W}{Q_g} \right\}^{1/3} \quad (12.45)$$

The dimensionless group, L , is known as the Layering Number and is of fundamental significance in the behaviour of methane layers. Examination of equation (12.45) indicates that the air velocity is the most sensitive parameter in governing the Layering Number and, hence, the length and mixing characteristics of the layer. Although u is, theoretically, the air velocity immediately under the layer, the mean value in the upper third of the airway may be used. For non-rectangular airways, W may be taken as some three quarters of the roadway width. The power of 1/3 in equation (12.45) reduces the effects of errors in estimated values of W and Q_g .

Experimental data from Bakke and Leach have been employed to produce Figure 12.13 for level airways. For any given gas make and roadway width, the horizontal axis may be scaled in terms of air velocity. It can be seen from this graph that at low Layering Numbers (and, hence, low velocity) the layer is affected very little by small additional increases in velocity. Indeed, in an ascensional airway, the layer will actually lengthen as the airspeed increases from zero to the free-streaming velocity of the methane. The mixing process is primarily due to turbulent eddies.

The efficiency of mixing increases as the relative velocity between the methane and air rises. However, as the air velocity continues to increase giving Layering Numbers of over 1.5 the layer shortens rapidly. On the basis of such results, it can be recommended that Layering Numbers should be not less than 5 in level airways.

Similar experiments in inclined airways have led to the recommended minimum layering numbers shown in Table 12.1 in order to inhibit the formation of methane layers.

Angle to horizontal (deg.)	0	5	10	15	20	25	30	35	40	45
<i>Ascentional</i>	5	5.7	6.2	6.6	6.9	7.2	7.4	7.6	7.7	7.8
<i>Descentional</i>		3.3	3.7	4.1	4.3	4.5	4.6	4.7	4.8	4.9

Table 12.1. Recommended minimum Layering Numbers at various roadway inclinations.

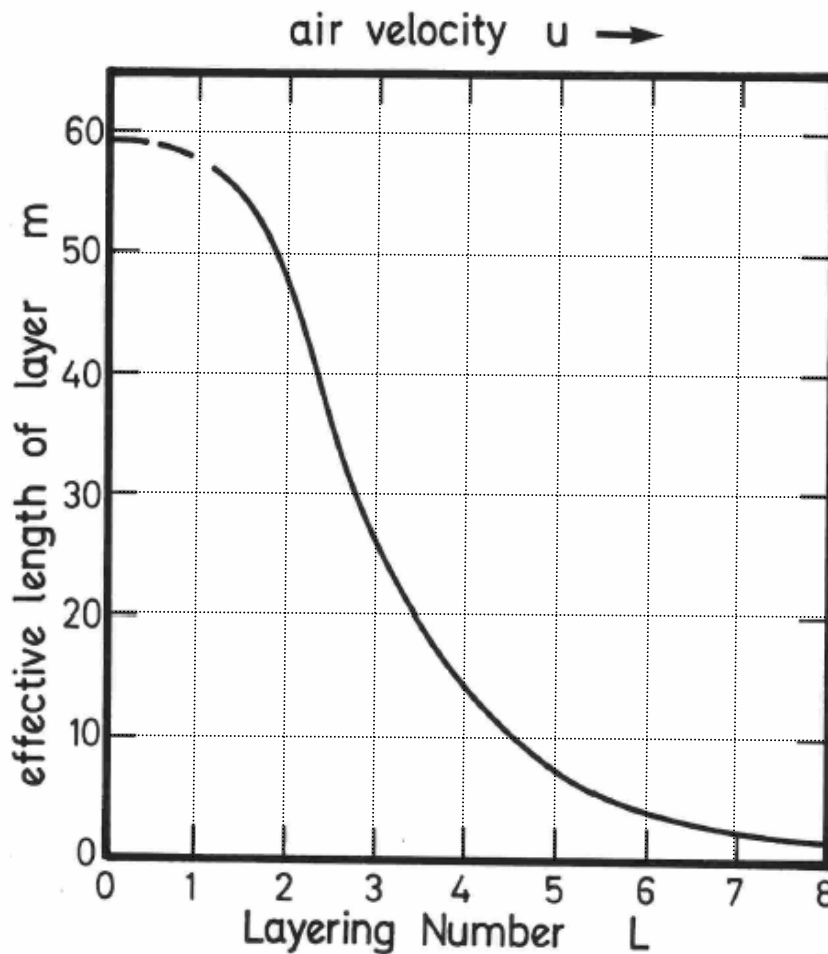


Figure 12.13 Variation of layer length with Layering Number for level airways.

Methane layers can be detected by taking methanometer readings or siting monitors at roof level. The most probable locations are in bleeder airways or return roadways close to a longwall face. On detecting a methane layer, an immediate temporary remedy is to erect a **hurdle cloth**, that is, a brattice cloth attached to the sides and floor but leaving a gap at the top. The size of the opening should be such that the increased air velocity near the roof disperses the layer. The hurdle cloth may need to extend some three quarters of the height of the airway. However,

anemometer readings should be taken to ensure that the overall volume flow of air through the area is not reduced significantly. Compressed air venturis or other forms of **air movers** can be used to disperse methane layers provided that they are earthed against electrostatic sparking.

The longer term solutions are to (a) increase the airflow and, hence, the air velocities through the affected panel; (b) reduce the rate of methane emission, or a combination of the two. Ventilation network analyses should be employed to investigate means of increasing the airflow (Chapter 7). These may include adjusting the settings of regulators or fans, and controlled partial recirculation (Section 4.5.). The methane emissions can most effectively be reduced by installing a system of methane drainage (Section 12.5.).

While methane layering was once a common occurrence in gassy coal mines, well designed systems of ventilation and gas drainage are capable of eliminating this hazard from modern mines. However, if stoppings or other ventilation controls are disrupted by any incidents in gassy mines the reduction in airflows can result in the formation of methane layers and the possibility of gas explosions.

12.4.3. Gas outbursts

The most dramatic mode of gas emission into mine workings is the release of an abnormally large volume of gas from the strata in a short period of time. Such incidents have caused considerable loss of life. In many cases, the rate of emission has been explosive in its violence, fracturing the strata and ejecting large quantities of solid material into the workings. Gas outbursts are quite different from rock bursts that are caused by high strata loadings. However, the probability of a disruptive gas release from adjacent strata is enhanced in areas of abnormally high stress such as a pillar edge in overlying or underlying workings.

There are two distinct types of gas outbursts, in-seam bursts and sudden large emissions from roof and floor. Each of these will be discussed in turn.

12.4.3.1. In-seam outbursts

As the name implies, these are outbursts of gas and solids from the seam that is currently being mined. They have occurred in many countries, particularly in coal and salt (or potash) mines. The geologic conditions that lead to in-seam outbursts appear to be quite varied. The one common feature is the existence of mechanically weakened pockets of mineral within the seam and which also contain gas at high pressure. Methane, carbon dioxide and mixtures of the two have been reported from in-seam outbursts in coal mines while nitrogen may be the major component in potash mines (Robinson et al, 1981).

The genesis and mechanisms of in-seam gas outbursts have been a matter of some controversy. A current hypothesis is that the structure of the material within outburst pockets has been altered by tectonic stressing over geological time. Seam outbursts in coal mines have been known to eject up to 5000 t of dust, much of it comprised of particles less than 10 μm in diameter (Evans and Brown, 1973). This can be accompanied by several hundred thousand cubic metres of gas (Campoli, 1985). It is thought that pulverization of the coal has been caused by very high shear forces. Laboratory tests have shown that a sample of normal anthracite can be reduced to the fragile "outburst" anthracite by such means. Coal mines located in areas that have been subject to thrust faulting are more prone to in-seam outbursts. A sample of "outburst" coal is, typically, severely slickensided and friable to the extent that it may crumble to dust particles by squeezing it in the hand. The seam is often heavily contorted in the vicinity of the outburst pocket - again, evidence of the excessive tectonic stressing to which it has been subjected.

If the overlying caprock had maintained a low permeability during and since the pulverization of the coal, then the entrained methane will remain within the zone. However, the small size of the particles ensures that desorption of the gas can occur very quickly if the pressure is relieved (equation (12.9)).

When a heading or face approaches an outburst zone that contains highly compressed coal dust and gas, stress increases on the narrowing barrier of normal coal that lies between the free face and the hidden outburst pocket (Sheng and Otuonye, 1988). At some critical stage, the barrier will begin to fracture. This causes audible noise that has been variously described as "cracking, popping" or "like a two-stroke engine". When the force exerted by gas pressure in the outburst pocket exceeds the resistance of the failing barrier, the coal front bursts outwards explosively. The blast of expanding gas may initiate shock waves throughout the ventilation system of the mine. A wave of decompression also passes back through the pulverized coal. The expansion of the gas, reinforced by rapid desorption of large volumes of methane expels the mass of dust into the airway. Although the outburst may last only a few seconds, the desorbing gas causes the dust to behave as a fluidized bed. This can flow along the airway, almost filling it and engulfing equipment and personnel for a distance that can exceed 100 m (Williams and Morris, 1972). The cavities that remain in the seam following an outburst may, themselves, indicate slickensides. Several cavities that are interconnected can contribute to a single outburst. The volume of dust subsequently removed from the airway or face has often appeared too large for the cavity from which it was apparently expelled.

The dangers associated with gas outbursts in mines are, first, the asphyxiation of miners by both gas and dust. Compressed air 'lifelines' may be maintained on, or close to, faces that are prone to in-seam outbursts. These are racks of flexible tubes connected to a compressed air pipe, and with valves that open automatically when picked up. Such devices can save the lives of miners who become engulfed in outburst dust. A second hazard is that the violence of the outburst may damage equipment and cause sparking that can ignite the highly flammable gas/dust/air mixture. Spontaneous ignitions of methane during outbursts in a salt mine have also been reported (Schatzel and Dunsbier, 1989). Thirdly, the sudden expansion of a large volume of gas can cause disruption of the ventilation system of a mine.

Precautionary measures against in-seam gas outbursts include forward drilling of exploratory boreholes. However, pre-drainage of outburst pockets has met with limited success due to rapid blockage of the boreholes. Similarly, testing samples of coal for strength or structure is uncertain as normal coal may exist very close to an outburst pocket. Monitoring for unusual micro-seismic activity is a preferred warning technique (Campoli, 1985). When it is suspected that a face or heading is approaching an outburst pocket, then machine mining should be replaced by drill and blast methods (volley firing), clearing the mine of personnel before each blast. This should be continued until an outburst is induced or the dangerous area has been mined through.

12.4.3.2. Outbursts from roof and floor

These are most likely to occur in longwall mines. As discussed in Section 12.4.1. and illustrated on Figure 12.11, methane will migrate from higher or lower source beds towards the working horizon behind the working face. Strata in the stress relief zone normally exhibit a substantial increase in permeability due to relaxation of the fracture network. The migration of gas then proceeds through the overlying and underlying strata at a rate that follows cyclic face operations and, under normal conditions, is quite controlled. However, a band of strong and low permeability rock (**caprock**) existing in the strata sequence between the source beds and the working horizon may inhibit the passage of gas. This can result in a **reservoir of pressurized gas** accumulating beyond the caprock. Any sudden failure of this retention band will then produce a large and rapid inundation of gas into the working horizon (Wolstenholme et al, 1969).

Figure 12.14 illustrates the development of a potential outburst from the floor. In Figure 12.14(a), relaxation of the strata allows gas to be evolved from the source bed and migrate upwards. A strong intervening bed of sufficiently high natural permeability or which contains induced fractures allows the gas to pass through.

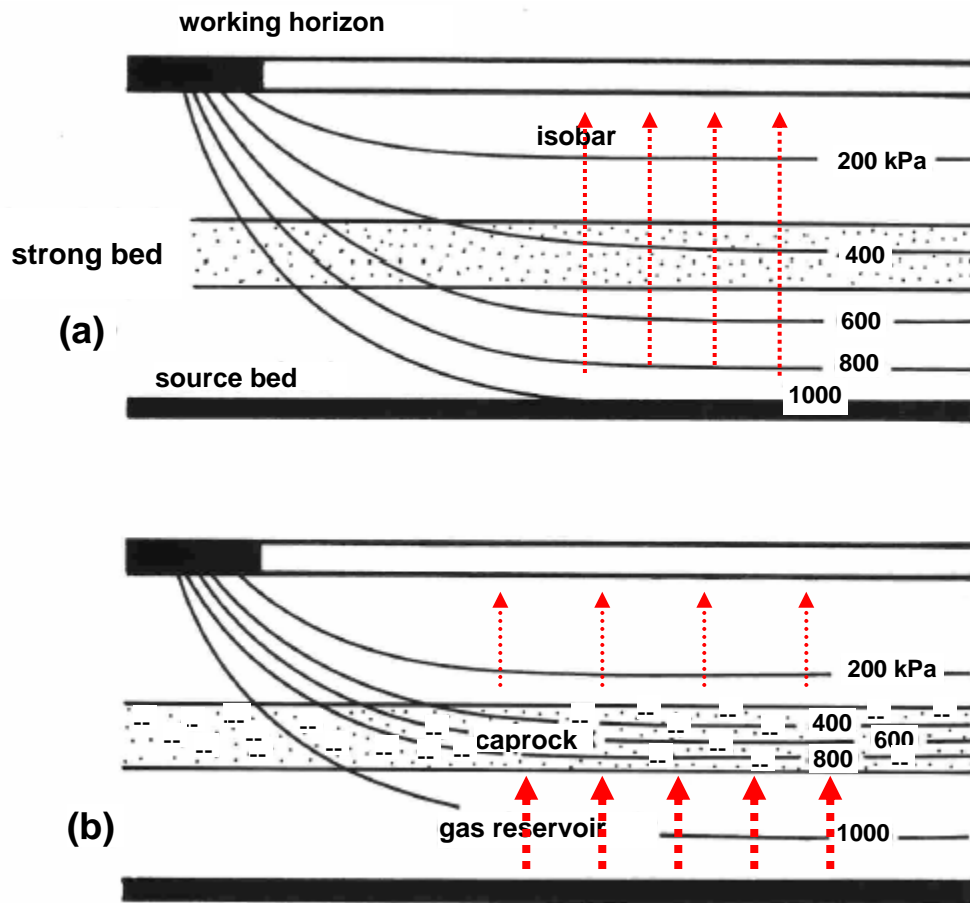


Figure 12.14 Development of a gas outburst condition under a longwall panel.

- (a) Safe condition: Isobars distributed; strong bed sufficiently permeable (or fractured) allowing gas to migrate through in a controlled manner.
- (b) Potential outburst condition: reduced permeability of the strong bed resulting in an increased pressure gradient across this bed and high pressure gas accumulations under it.

However, Figure 12.14(b) illustrates a condition in which a strong low permeability bed has failed to fracture. Gas accumulates under this bed which is then subjected to an intensified gas pressure gradient. This is the potential outburst situation. The rate at which gas accumulates in the reservoir rock depends upon the relative rates of gas make from the source seam and gas leakage through the caprock. Either an increase in the gas make from the source seam or a decrease in flow through the caprock can produce the potential outburst condition.

Resistance to gas flow through the fracture network of the caprock may occur by increases in its strength or thickness. Furthermore, a porous bed such as a fine-grained sandstone may suffer a large decrease in relative permeability to gas if it becomes partially saturated by water (Figure 12.9).

There are considerable differences between the sudden large emissions that occur from roof and floor strata. Strata above the worked seam are subjected to larger vertical movement due to subsidence of the rock mass. This creates greater voidage in which gas can accumulate. Bed

separation also promotes flowpaths parallel to the strata. Very large gas reservoirs may, therefore, develop in the overlying rocks. However, fracturing of low permeability beds is more probable and high pressures are less likely to develop in the gas reservoir rocks. For these reasons, sudden emissions from the roof have usually been characterized by large flows that may last from a few hours to several months (Morris, 1974). However, the initiation of the emission is unlikely to be accompanied by violent dislocation of the immediate roof strata.

In contrast, gas outbursts from the floor are usually of shorter duration but more violent - even to the extent of rupturing the floor strata upwards with ejection of solid material. The reduced deformation in the floor sequence enables a caprock to resist induced enlargement of fractures. This leads to high pressure accumulations of gas. However, the extent of the gas reservoir is likely to be much less than one in roof strata. Morris (1974) reported methane emissions as large as $140\,000\text{ m}^3$ from floor outbursts, but over $8 \times 10^6\text{ m}^3$ from sudden roof emissions.

Gas outbursts from roof or floor are often preceded by smaller increases in general body gas concentrations, often intermittent in nature, during the hours before the major flow occurs. This is probably caused by increasing strain within the caprocks and interconnection of bed separation voidages before the main failure. Continuous gas monitors can detect such warnings. Immediately before the burst, severe weighting on the roof supports and caving in the gob may occur. Roof and floor outbursts are more likely to occur along planes of maximum shear stress in the strata, i.e. in bleeders or airways bordering gob areas, or on the longwall face itself. Roof outbursts may occur due to the initial failure of an overlying caprock within some two face lengths of the initial starting-off line of the longwall. Similarly, passing under or over old pillar edges in other seams can promote sudden failure of caprocks. However, previous workings may have caused partially degassing of source beds. Most floor outbursts have occurred when no previous mining has taken place at a lower level.

The most effective means of preventing roof and floor outbursts is regular drilling of methane drainage holes wherever any potential caprock may exist. The holes should be angled over or under the caved area and should penetrate beyond the caprock to the source bed(s). The spacing between holes should be dictated by local conditions but may be as little as 10 m. It is particularly important that the drilling pattern be maintained close up to the face. All holes should be connected into a methane drainage system (Section 12.5.5.). In outburst prone areas, it is essential that drilling takes place through a stuffing box in order that the flow can be diverted immediately into the pipe range should a high pressure accumulation be penetrated.

It is often the case that routine floor boreholes produce very little gas. However, in areas liable to floor outbursts, these holes should continue to be drilled as a precautionary measure. Tests should be made of open-hole flow rates and rate of pressure build-up on the closed hole. When both of these tests show higher than normal values, then it is probable that an outburst condition is developing (Oldroyd et al, 1971). In the event of any indication that a gas reservoir is accumulating in roof or floor strata, then additional methane drainage holes should be drilled immediately to relieve that pressure and to capture the gas into the drainage pipe system.

12.4.4 Prediction of methane emissions into the ventilation system

As indicated earlier in Section 12.4 a considerable number of variables affect the rate at which methane is emitted into the ventilation systems of coal mines or captured by methane drainage. The non-linear interaction of the variables renders it difficult to apply analytical means to the problem of predicting methane emissions. For this reason numerous numerical and empirical models have been developed and utilized in several countries (e.g. Durucan et al (1992)).

Older empirical methods of predicting gas emissions into coal mines varied from curve fitting procedures to pocket calculators (e.g. Creedy et al (1988); CEC (1988)). The continued enhancement of computing power on desk and portable machines has promoted the utilization of

sophisticated data processing software. This has resulted in improved reliability of predicting methane emissions from data that are often difficult to correlate (e.g. Lunarzewski (1998). One such procedure utilizes artificial neural networks (Karacan (2007)). This technique seeks patterns and relationships between groups of input data that have appear to have obscure inter-relationships from conventional mathematical or statistical methodologies.

A feature of artificial neural network software is that it can “learn” as more data is added, so increasing its accuracy of prediction. Nevertheless, we are reminded that the reliability of all empirical models is dependent on the range, quality and detail of the measurements on which the model is based. Hence, it is the responsibility of the user to ascertain that any given model is applicable to the mine under consideration.

12.5. METHANE DRAINAGE

The organized extraction of methane from carboniferous strata may be practiced in order to (a) produce a gaseous fuel, (b) reduce methane emissions into mine workings or (c) a combination of the two. If the intent is to provide a fuel for sale or local consumption, then it is important that the drained gas remain within prescribed ranges of purity and flowrates.

There is no single preferred technique of methane drainage. The major parameters that influence the choice of method include

- the natural or induced permeability of the source seam(s) and associated strata
- the reason for draining the gas
- the method of mining (if any).

In this Section, we shall outline methods of methane drainage, the infrastructure of pipe ranges and ancillary equipment, methods of predicting gas flows and conclude with a summary of the procedure for planning a methane drainage system.

12.5.1. In-seam drainage

Drainage of methane by means of boreholes drilled into a coal seam is successful only if the coal has a sufficiently high natural permeability or where a fracture network is induced in the seam by artificial methods. Hence, for example, while in-seam drainage can be practiced in some North American coalfields, it has met with very limited success in the low permeability coals of the United Kingdom or Western Europe. A knowledge of coalbed permeability is necessary before in-seam drainage can be contemplated (Section 12.3.2).

Advances in drilling technology have increased the performance potential of in-seam gas drainage (Schwoebel, 1987). Using down-the-hole motors and steering mechanisms, boreholes may be drilled to lengths exceeding 1600 m within the seam (Brunner (2006). Provided that the coal permeability is sufficiently high, methane flows into mine workings can be reduced very significantly by pre-draining the seam to be worked. Gas capture efficiencies up to 50 percent are not uncommon, where

$$\text{Gas capture efficiency} = \frac{\text{Gas captured by methane drainage}}{\text{Gas captured} + \text{gas emitted into ventilation}} \times 100 \quad (12.46)$$

In gassy and permeable seams, ribsides bordering on solid coal are prolific sources of gas. Figure 12.15 illustrates flanking boreholes used to drain gas from the coal ahead of headings that are advancing into a virgin area. On the other hand, previously driven headings or workings may have degassed the area to a very considerable extent.

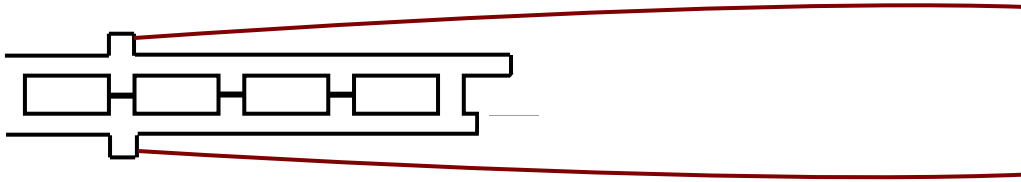


Figure 12.15 In-seam drainage boreholes to reduce methane flow into advancing headings, applicable only where the coal is sufficiently permeable.

In-seam gas drainage can also be effective in permeable seams that are worked by the retreating longwall system (Mills and Stevenson, 1989; Ely and Bethard, 1989). Figure 12.16 illustrates the layout. Boreholes are drilled into the seam from a return airway and connect into the methane drainage pipe system. The preferred spacing of the holes depends upon the permeability of the seam and may vary from 10 to over 80 m. The distance from the end of each borehole and the opposite airway should be about half the spacing between holes. The application of suction on the boreholes is often unnecessary but may be required for coals of marginal permeability or to increase the zone of influence of each borehole.

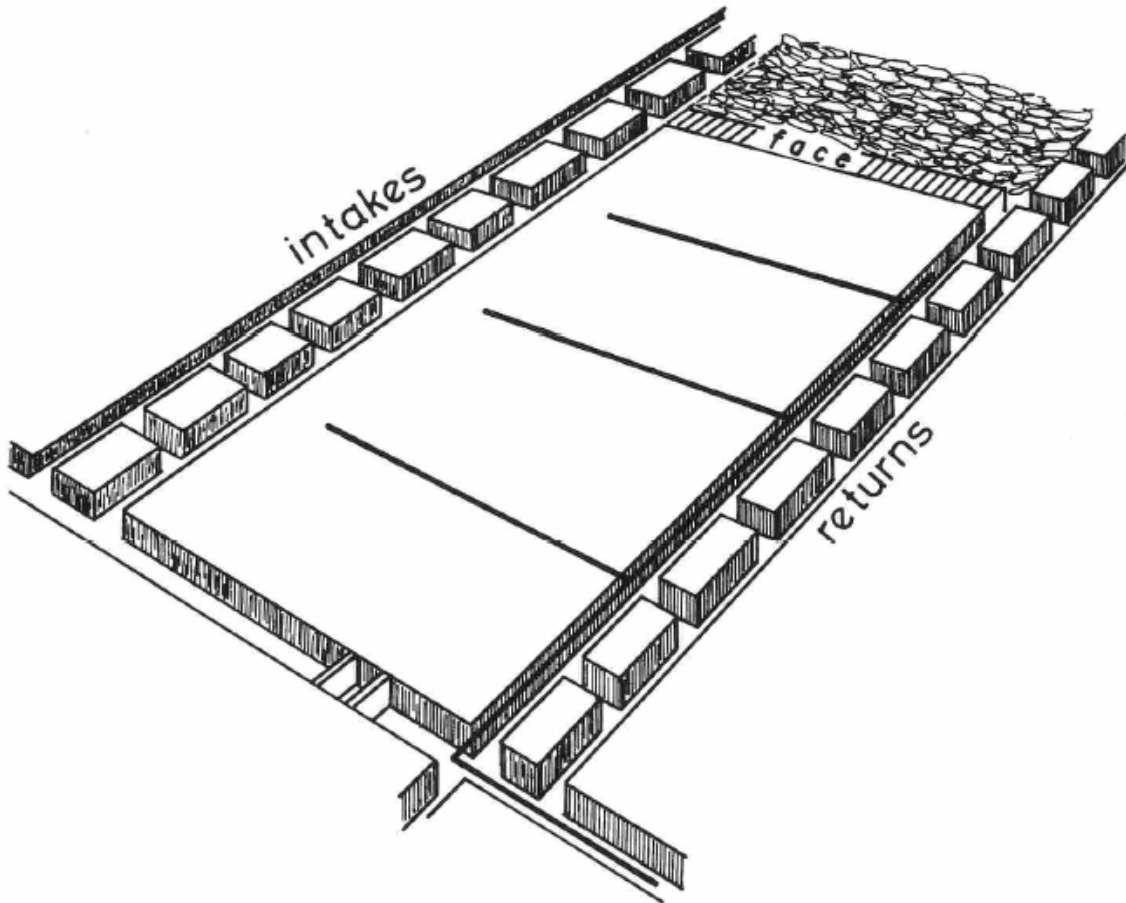


Figure 12.16. In-seam boreholes draining methane from a coal seam in a two-entry retreating longwall.

The time allowed for drainage should be at least six months and, preferably, over one year. Hence, the holes should be drilled during the development of what will become the tailgate of the longwall.

Spalling of coal into the borehole can be a problem, especially in the more friable coals. This may be reduced by employing smooth drill rods. Drill chippings can be removed by means of a continuous water flush. Additionally, augers may be used to remove spalled coal from the boreholes. The internal diameter of some sections of finished borehole may be considerably larger than the drill bit. Perforated plastic liners can be inserted in order to maintain the holes open, subject to the governing legislation. The first 5 to 10 m of each borehole are typically drilled at 100 mm diameter. A standpipe is cemented into place and connected through a stuffing box into the methane drainage pipeline (Section 12.5.5.1.). The remainder of the hole is drilled through the standpipe at a diameter of some 75 mm.

The flowrate of gas from a gas drainage borehole will vary with time. Figure 12.17 illustrates a typical life cycle for an in-seam borehole. A high initial flow occurs from the expansion and desorption of gas in the immediate vicinity of the hole. This may diminish fairly rapidly but then increase again as the zone of influence is dewatered, hence, increasing the relative permeability of the coal to gas (Figure 12.9). This, in turn, is followed by a decay as the zone of influence is depleted of gas.

In-seam boreholes drilled into outcrops or from surface mines may produce little methane. The gas content of coal seams tends to increase with depth. It is probable that seams near the surface have lost most of their mobile gas. However, multiple boreholes drilled with directional control from a surface drill rig can be guided to follow a coal seam for distances that produce acceptable flowrates.

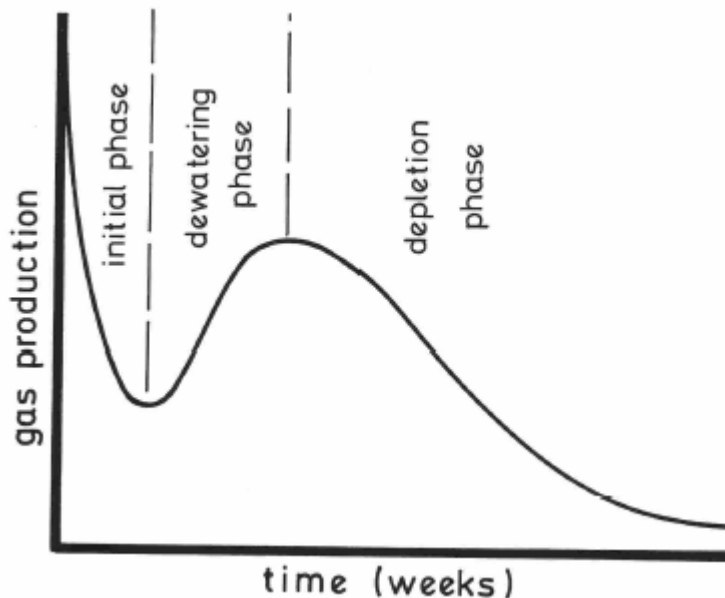


Figure 12.17 Typical life cycle of a gas drainage borehole in coal.

Vertical holes drilled from the surface to intersect coal seams are likely to produce very little gas because of the short length of hole exposed to any given seam. However, **hydraulic stimulation** or **hydrofracturing** can be used to enhance the flowrates. This involves injecting water or foam containing sand particles into the seam. Other sections of the borehole are cased. The objective is to dilate the fracture network of the seam by hydraulic pressure. The sand particles are intended to maintain the flowpaths open when injection ceases. The success of hydrofracturing depends upon the natural fracture network that exists within the seam and the absence of clays that

swell when wetted. Friable coals are more likely to respond well to hydrofracturing. On the other hand, in stronger coals, induced fractures may be concentrated along discrete bedding planes

and give a poor recovery of gas. In the majority of cases, water must be pumped from surface boreholes before gas flows can be attained.

Another means of in-seam gas drainage is to sink a small diameter shaft to intersect the coal bed (U. S. Bureau of Mines, 1980). Long multiple boreholes are drilled radially outwards from the shaft into the seam and connected into a methane drainage line that rises to the surface. This method may be considered when a shaft is to be sunk at a later date at that location for mine ventilation or service access. This enables degassing of an area for several years prior to mining.

12.5.2. Gob drainage by surface boreholes

The relaxation of strata above and below the caved zone in a longwall panel creates voidage within which methane can accumulate at high concentration, particularly when other coal beds exist within those strata. If this gas is not removed, then it will migrate towards the working horizon and become a load on the ventilation system of the mine (Figure 12.11). Capture of this "gob gas" may be accomplished either underground by cross-measures drainage (Section 12.5.3.) or by drilling boreholes from the surface.

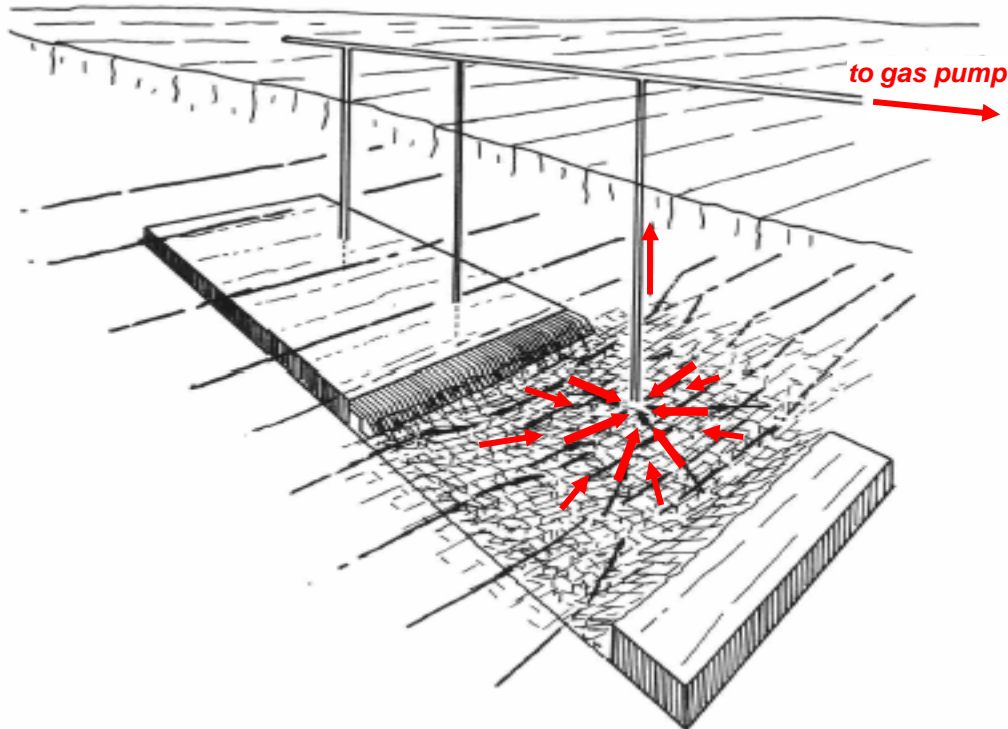


Figure 12.18 Gob drainage of a longwall panel. Each hole becomes productive after passage of the faceline.

Figure 12.18 depicts methane drainage from the gob of a longwall panel by surface boreholes. This is a method that is favoured in the United States. Typically, three or four holes are drilled from surface rigs at intervals of 500 to 600 m along the centreline of the panel and ahead of the coal face. The holes may be 200 to 250 mm in diameter and drilled to within some 8 to 10 m of the top of the coal seam (Mills and Stevenson, 1989). The holes should be cased from the surface to a depth that is dictated by the local geology and, in particular, to extend below any beds that are likely to act as bridging caprocks. A perforated liner can be employed in the rest of the hole to inhibit closure from lateral shear.

The initial gas made from the surface holes is likely to be small. However, as the face passes under each borehole, the methane that accumulates in the caved area will be drawn towards that borehole. Bed separation assists drainage from across the complete gob area. The first borehole should be located far enough from the face start line (typically about 150 m) to ensure that it connects into the caved zone. When a hole becomes active, the rate of gas production increases sharply and may yield over 50 000 m³/day of commercial quality methane for a period of several months, depending upon the rate of mining. The more gradual decay is a result of reconsolidation of the caved strata. Gas drainage pumps located on surface ensure that the gas flow remains in the correct direction and may be employed to control both the rate of flow and gas purity. If the applied suction is too great, then ventilating air will be drawn into the gob and may cause excessive dilution of the drained methane.

In addition to longwall panels, gob drainage by surface boreholes can be utilized in pillar extraction areas. In both cases, the technique can result in very significant reductions in emissions of methane into mine workings.

12.5.3. Cross-measures methane drainage

Where the depth of coal workings precludes the drilling of methane drainage holes from surface, the extraction of methane from relaxed strata can be accomplished by drilling from underground airways. The principle of cross-measures drainage is illustrated on Figure 12.19. Capture efficiencies in the range 20 to 70 percent have been reported for this technique, depending upon the design and control of the system. Boreholes are drilled into the roof and, if necessary, also the floor strata. The holes are normally drilled parallel to the plane of the coal face but inclined over or under the waste. This is the dominant method of methane drainage in Europe and is particularly applicable to advancing longwall panels. However, the technique can also be employed for multiple-entry retreat systems.

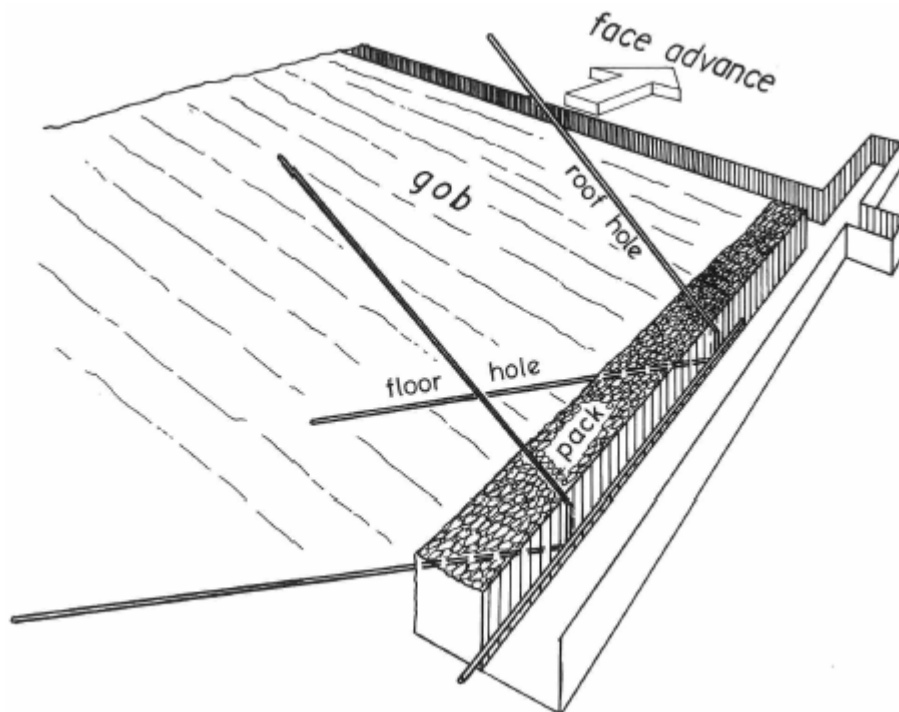


Figure 12.19 Cross-measures methane drainage in an advancing longwall panel.

The angle, length and spacing of boreholes must be decided on a site-specific basis. In general, the holes should intersect the major gas emitting horizons. The spacing between holes should be such that their zones of influence overlap slightly. Significant increases in general body methane concentration along the airway is indicative of too great a distance between boreholes. Conversely, if closing a borehole causes a rapid increase in the flowrate from neighbouring holes, then the boreholes may be too close together. The hardness of the strata or other difficulties of drilling will also influence the spacing. Typical spacings lie in the range 10 to 25 m between boreholes.

Computer modelling procedures have been developed to assist in planning an optimum layout of cross-measures boreholes (e. g. O'Shaughnessy, 1980). However, a practical study of the local geology followed by a period of experimentation remains the most pragmatic means of establishing a successful drilling pattern.

The boreholes are normally drilled from a return airway. However, in particularly gassy situations, boreholes may be required on both sides of the panel. Although cross-measures methane drainage is usually carried out from the current working horizon, a variation is to drill from airways that exist in either overlying or underlying strata. Dewatering is facilitated by upward holes.

Routine underground drilling may require boreholes of smaller diameter than surface holes. Cross-measures drainage holes are normally in the range 50 to 100 mm diameter. However, it is necessary to employ standpipes in order to prevent excessive amounts of air being drawn into the system. For any given degree of suction applied to a borehole, the purity of the extracted gas will vary with the length of the standpipe. Hence, to ensure a high concentration, the standpipe may need to be extended to within a few metres of the main gas-producing horizon. Standpipes may be grouted into place with cement or resin, while rubber and sealing compounds have also been used (Boxho et al, 1980).

The suction applied to gob drainage holes, whether drilled from the surface or underground, is a sensitive means of controlling both the flowrate and the purity of the drained gas. The suction to be applied on each individual borehole is a function of the gas pump duties, the geometry of the network of pipes and settings of borehole valves. In general, increasing the suction applied to an active borehole will increase the flow but decrease the purity. Borehole tests may be employed to determine the optimum suction when the mass flow of methane attains a maximum value.

If the suction is too high, then the concentration of methane in the pipelines may fall below 15 percent when it becomes explosive. It is prudent to decrease the suction automatically when the concentration falls to 30 percent. Much higher cut-off concentrations may be imposed by local regulations or where the gas is utilized as a fuel. If the applied suction is too low, then excessive emissions of methane can occur into the mine ventilation system. The optimum suction required increases with respect to the rate of gas make from the source beds. A pragmatic approach is to ensure that the interface between the air and methane remains in the strata above the level of the airways. Although a borehole suction of some 10 kPa is fairly typical of cross-measures drainage systems, large variations occur in practice. Indeed, as indicated in Section 12.4.3.2., gas may exit the borehole at a positive pressure.

12.5.4. Drainage from worked-out areas

Although the rate of gas emission from any given source decays with time, an abandoned area of a coal mine is likely to be surrounded by a large envelope of fragmented and relaxed strata. The total make of gas may be considerable and continue for an extended period. In cases where fragmentation has occurred across coal beds and between multiple seam workings, such emissions of gas may go on for several years. In order to reduce pollution of a current ventilation system, methane drainage pipes can be inserted through stoppings and gas drained from the old workings. The pipes should extend beyond the stoppings to a point that is not affected by air penetration during a period of rising barometer. The objective is to extract the gas at

approximately the same rate as it is produced. However, additional suction may be applied when the barometer is falling. Pressure balance chambers assist in reducing leakage across stoppings (Section 21.5.5.).

Gas drainage can also be practiced when a gassy mine is abandoned. Again, pipes are left in the seals on shafts or adits. This type of drainage may prevent seepages of methane escaping to the surface and, possibly, creating a hazard in the basements of buildings. Drainage pipes that are vented to the surface atmosphere should be elevated above ground level, well fenced against unauthorised approach and provided with notices giving warning of inflammable gas. However, as methane is a “greenhouse gas” discharging it to the surface atmosphere should be discouraged.

12.5.5. Components of a methane drainage system

The methane that is produced from drainage boreholes must be transported safely to the required point of delivery at surface level. The infrastructure that is necessary comprises five sets of components:

- . pipe ranges
- . monitors
- . safety devices
- . controls
- . extractor pumps (if required)

12.5.5.1. Pipe ranges

The standpipe of each borehole connects into a branch pipe via a flexible hose, a valve and a water trap. In the case of methane drainage in an underground mine, the branch pipes from each district or section connect into main or trunk gas lines. Each main leads to a surface-connecting pipe. Devices for monitoring, safety and control are located at strategic positions throughout the system.

Both steel and high density polyethylene have been used as materials for methane drainage pipes. Steel has the advantage of mechanical strength. However, it must be galvanized or otherwise protected against corrosion on both the inner and outer surfaces. Where permitted by legislation, heavy duty plastic piping may be preferred because of its lighter weight and ease of installation (Thakur and Dahl, 1982). Polyethylene tubing up to some 75 mm in diameter may be brought into the mine on reels, eliminating most of the joints that are required every five or six metres with steel pipes. Pipes are sized according to the gas flows expected and vary from 75 mm to 600 mm in diameter. All pipes should be colour coded for easy recognition and in correspondence with the relevant mine plan.

Pipes that are installed in underground airways should be suspended from the roof to reduce the impact of falling objects. Where steel pipes are employed the joints should be capable of flexing in order to accommodate airway convergence or other strata movements. Methane drainage pipes should not be located in any airway where electrical sparking might occur such as a trolley locomotive road. In any event, pipes should be earthed against a build-up of electrostatic charges. Following the installation of a new length of pipe, it should be pressure tested either by suction or by compressed air at a pressure of some 5000 kPa. All pipework should be inspected regularly for corrosion and damage.

Pipes should be installed with a uniform gradient and water traps installed at unavoidable low points including the base of a vertical or inclined surface connecting branch. Steel is preferred for the main pipe. This may be located within an existing shaft. It is prudent to choose an upcast shaft and this may, indeed, be enforced by law. Shaft pipes should be fitted with telescopic joints to accommodate expansion and contraction. However, an alternative is to position a vertical pipe in a dedicated surface connecting borehole. This method is attractive for the shallower mines and

is the common technique within the United States. If necessary, surface pipes should be protected against frost damage, either by thermal insulation or heated cladding.

12.5.5.2. Monitors

There are, essentially, three types of parameters that should be monitored in a gas drainage system; pressure, flow and gas concentration. Pressure measurements are made at the mouths of boreholes, across orifice plates to indicate flow and at strategic locations within the pipe network. For boreholes that penetrate relaxed strata (Sections 12.5.2. and 12.5.3.) there may be a sensitive relationship between borehole pressure, gas flowrate and concentration of the drained gas, particularly where extractor pumps are used to maintain a negative gauge pressure at the mouth of each borehole. Pressure differential indicators may vary from simple U tubes (Section 2.2.4.2.) containing water or mercury to sophisticated capsule or diaphragm gauges (Boxho et al, 1980). The latter may be capable of transmitting signals to remote recorders, alarms or control centres. A simpler arrangement employs mechanical regulators to maintain set pressures at each chosen location.

A variety of devices are used to indicate the rate of flow in gas pipes, including both swinging vane or rotating vane anemometers and pitot tubes. However, the most popular method is to monitor the pressure drop across an orifice plate (Figure A5.8). The gas flowrate, Q (m^3/s at pipe pressure) and the pressure drop across the orifice, p , are related as shown by equation (2.50), i.e.

$$p = R_t \rho Q^2 \quad (\text{Pa})$$

where R_t = rational turbulent resistance of the orifice (m^{-4}) and
 ρ = density of the gas (kg/m^3).

Furthermore, the rational turbulent resistance is given by equation (5.18) as

$$R_t = \frac{X}{2A^2}$$

where X = shock loss factor for the orifice (dimensionless) and
 A = cross-sectional area of the pipe (m^2).

Combining these two equations gives

$$Q = \frac{A}{\sqrt{X}} \sqrt{\frac{2p}{\rho}} \quad \text{m}^3/\text{s} \quad (12.47)$$

where the pressure drop, p , is measured in Pascals.

An estimate for the value of X may be made from Figure A5.8 (Appendix to Chapter 5) for a clean sharp-edged orifice plate, or from the corresponding equations:

$$X = \frac{1}{C_c^2} \left\{ \left(\frac{D}{d} \right)^4 - 1 \right\} \quad (12.48)$$

where D = diameter of pipe
 d = diameter of orifice
 and the orifice coefficient C_c is given by

$$C_c = 0.48(d/D)^{4.25} + 0.6 \quad (12.49)$$

For greater precision, further multiplying factors may be incorporated into equation (12.47) to account for variations in Reynolds Number, gas viscosity and, in particular, the roughness of the edge of the orifice.

Spot measurements of gas concentrations in methane drainage networks may be made by inserting probes through ports into the gas line and using high-range methanometers. Permanent transducers are used to transmit signals of methane concentration at fixed locations to a remote monitoring or control centre.

While the majority of methanometers described in Section 11.4.2 are intended for measurements made in the subsurface airflow system, those employed in methane drainage pipes must be capable of indicating gas concentrations up to 100 percent. The most popular instruments used for this purpose are based on the variation of thermal conductivity with respect to gas concentration (Section 11.4.2.3.). Interferometers and acoustic methanometers are also employed while infrared gas analyzers may be used at permanent monitoring stations (Section 11.4.2.4.).

12.5.5.3. Controls and safety devices

The primary means of controlling an installed methane drainage system is by valves located in all main and branch lines as well as at the mouth of each borehole. Manually operated isolating valves are usually of the gate type in order to minimize pressure losses when fully open. These are employed to facilitate extension of the system and pressure tests on specific lengths of pipeline.

Diaphragm or other types of activated valves may be employed to react to control or alarm signals. These might be used to vary the gas pressure at the mouth of each borehole in response to changes in pipeline gas concentration. Abnormally high (or rapidly increasing) signals from a general body methane monitor located in an airway that carries a gas pipeline may be used to cut off gas flow into that branch. A simple but effective technique that is popular in the United States is to attach a length of mechanically weak plastic tubing along the upper surface of each gas pipe. The tubing is pressurized by compressed air or nitrogen which also holds open one or more mechanically activated valves. Any fall of roof or other incident that damages the pipe is likely also to fracture the monitoring tube. The resulting loss of air or nitrogen pressure causes immediate closure of the corresponding valves.

The gas mixture that flows through methane drainage pipes is usually saturated with water vapour. Liquid water is introduced into the system from the strata, by condensation and, perhaps, following the connection of a borehole that has been drilled using a water flush. In order not to impede the flow of gas, it is necessary to locate a water trap in the connection between each borehole and the branch pipe, and also at all low points throughout the network. Water traps vary from simple U-tube arrangements to automated devices. The latter consist essentially of a compressed air or electric pump, activated by a float within a water reservoir. The size of the reservoir and the settings of the high and low water levels are chosen according to the make of water expected.

It is prudent to locate a lightning conductor close to any surface point of gas discharge. Furthermore, **flame traps** should be inserted into the surface pipeline to prevent any ignition from propagating into the subsurface system. Flame traps are devices that allow rapid absorption or dissipation of heat without introducing an unacceptable pressure drop. Alternative designs include closely spaced parallel plates, corrugated metal sheets or a series of wire gauze discs. A device that is popular in Germany consists of a vessel containing glass spheres (Boxho et al.1980). Flame traps are liable to be affected by dust deposits and should be designed for easy inspection and maintenance. It is useful to locate a pressure differential transducer across the flame trap to monitor for an unduly high resistance. If burning continues for any length of time at one end of a flame trap, then the device can lose its effectiveness. **Flame extinguishers** may be used in

conjunction with flame traps. These are pressurized containers that pulse an extinguishing powder into the pipeline when activated by a temperature sensor.

The methane drainage network of a mine can be incorporated into an **electronic environmental surveillance** and control system (Section 9.6.3.). This has a number of significant advantages. The characteristic behaviour of the system can be investigated very readily from a control centre by varying valve openings at chosen boreholes and observing the effect on gas flow and concentration. Optimum settings can be determined and site-specific control policies established for automatic control under the supervision of a computer. A fully monitored system also allows the rapid detection and location of problem areas such as blockages, abnormal flows, fractured pipes or faulty components.

12.5.5.4. Extractor Pumps

If in-seam gas drainage is practiced (Section 12.5.1.) and the coal bed has a high natural permeability, then a satisfactory degree of degassification of the coal may be attained from the in-situ gas pressure and without the use of extractor pumps. However, for gob or cross-measures drainage (Sections 12.5.2. and 12.5.3.), it is usually necessary to apply controlled suction at the boreholes in order to achieve a satisfactory balance between flowrate, gas concentration and methane emissions into the mine.

There are two major types of gas extractor pumps used in methane drainage systems. Water seal extractors take the form of a curved, forward bladed centrifugal impeller located either eccentrically within a circular casing or centrally within an elliptical casing. In both cases, one or two zones occur around the impeller where the casing approaches closely, but does not touch, the impeller. In the remaining zones the casing widens away from the impeller. During rotation, the water is thrown radially outwards by centrifugal action in the wide zones, drawing in a pocket of gas from a central inlet port; then, as the impeller continues to turn, the water is forced inwards by the converging casing, causing the pocket of trapped gas to be discharged into a conveniently located central discharge port. Figure 12.20 illustrates a typical pressure volume characteristic curve for a water seal extractor.

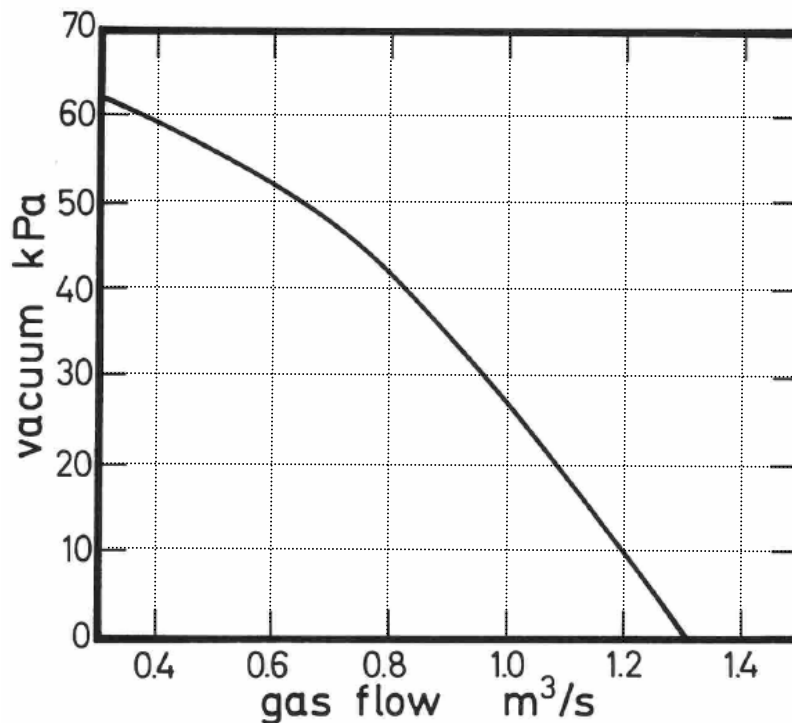


Figure 12.20 A typical pressure-volume characteristic curve for a wet-seal extractor pump.

The major advantage of water seal extractors is that a gas seal is maintained without any contact between moving and stationary components. Hence, there is little risk of igniting the gas or propagating a flame. Water seal extractors have proved to be reliable and robust in practice, and may be employed in banks of parallel machines to increase capacity. The temperature rise across each unit is small, enabling the machines to be used in continuous or automatic operation. However, periodic maintenance is required to remove any scaling or to guard against corrosive action of the water.

The second family of gas pumps is the dry extractor. These may be reciprocating machines or take the form of two lemniscate (dumb bell) shaped cams that rotate against each other within an elliptical casing. This action encapsulates pockets of gas from the inlet port and transports them across to the discharge port. Dry extractors are compact and, for any given speed, produce a flowrate that is near independent of pressure differential. However, these devices are subject to wear, create a substantial temperature rise in the gas and may produce considerable noise.

In the majority of cases, extractor pumps are located on the surface of a mine and, indeed, this may be mandated by legislation. In some situations where the amount of drained gas is small, it may be possible to site the extractor pumps underground and to release the gas into a well ventilated return airway (if permitted by law or special exemption). A section of the airway around the point of emission should be caged in and free from equipment to ensure that the gas has been diluted to permissible limits before it enters any areas of activity.

12.5.6. Planning a methane drainage system

The detailed design and planning of a methane drainage system consists of two major phases. First, a variety of data must be collated and analysed in order to estimate the gas flows that will pass through the network of pipes. These flows provide the necessary input for the second phase, the design of the actual network itself, including the dimensions of pipes and the duties and locations of all ancillary components.

12.5.6.1. Data collection and estimation of gas capture

The data requirements and corresponding analyses for in-seam methane drainage (Section 12.5.1.) differ from those involved in gob drainage or cross-measures systems (Sections 12.5.2. and 12.5.3.). However, a common first requirement is to obtain samples of coal from all source beds and to determine the corresponding gas contents (Section 12.2.3.).

If particularly heavy emissions of methane occur from the worked horizon in headings, faces and ribsides in virgin areas, then in-seam drainage may be practicable. In this case, it is vital that permeability tests be carried out. Laboratory investigations are helpful in tracking the variations in permeability with respect to stress, gas pressure and two phase flow (Section 12.3.2.). However, in-situ tests provide the most reliable estimates of the actual permeabilities that will be encountered. These involve one or more boreholes fitted with packers that encapsulate a length within the seam of interest. **Pressure build-up and draw-down tests** indicate the transient increase in pressure when the hole is shut in and the subsequent flow behaviour when it is re-opened. Analysis of that time transient data allows the in-situ permeability to be determined (Section 12.3.1.4.). A simpler method that can be employed in beds of higher permeability is the slug test (GRT, 1988). In this technique, a surface borehole is drilled to intersect the coal bed. A packer is inserted above the seam through which passes a column into which is introduced a head of water. A pressure transducer monitors the time transient variation in pressure and, hence, water flowrate as the water enters the seam and the level in the column falls. Again, the transient radial flow equation given in Section 12.3.1.4. is used as the basis of a computer algorithm to indicate in-situ permeability.

The coal samples should also be used to conduct adsorption and desorption tests (Sections 12.2.3.1. and 12.2.2.2.). The adsorption isotherm (Figure 12.1) can be employed to determine the volume of gas that will be produced from a given area of coal reserves as the seam gas pressure declines from its initial value to an estimated final state. The desorption tests provide data on the variation of diffusion characteristics with respect to gas pressure and particle size.

Computer simulation programs have been developed that accept these various items of data and model the flow of methane through coal beds towards boreholes or mine workings (e.g. Mavor and Schwoebel, (1991); Patton et al (1994)). The models are based on interactions between the relationships for gas release and migration given in Sections 12.2 and 12.3. Such programs can most helpful in estimating the amount of gas that may be captured with differing sizes and locations of in-seam boreholes.

Where a methane drainage system is to be designed for an existing mine, the emission patterns into the mine workings should be established for all working areas, bleeder airways, development headings and old workings. This is particularly important where the method is to be gob or cross-measures drainage. Let us now turn to data collection and estimation of gas capture that are pertinent to these systems.

Historical records of monitored data are very helpful but should be related to the corresponding stratigraphy, mining layout and methods of working. The gas captured by gob and cross-measures methane drainage is released primarily because of the stress relaxation and fragmentation of source beds above and below the working horizon (Figures 12.11, 12.18 and 12.19). The natural permeability of those seams prior to mining may, therefore, have little relevance to the subsequent rates of gas emission. However, the permeability-stress tests described in Section 12.3.2.1. give an indication of the increased permeabilities induced by stress relaxation. These, coupled with gas content data, desorption kinetics and the gas migration relationships allow predictions to be made of future gas makes. Here again, computer models have been developed to assist in such analyses (King and Ertekin, 1988). Several methods have also been produced that allow hand calculations of predicted methane emissions from relaxed roof and floor source beds (Dunmore, 1980).

In predicting gas production from future workings, it is important to take into account any changes in the mine layout and the method and rate of coal extraction. In multi-seam areas, degassification by earlier workings within some 200 m above or below the current horizon is likely to result in a significant decrease in the gas available for drainage. Strata sequences should also be examined for gas outburst potential (Section 12.4.3.).

12.5.6.2. Design of the drainage network

The first task in designing the hardware configuration of a methane drainage system is to draw a line schematic of the layout. The network should be shown at its future maximum extent. The locations of boreholes at that time and the corresponding predicted flowrates should be indicated for all branches of the pipe network.

First estimates of pipe diameters can be made at this time (Section 12.5.5.1.). Gas velocities in the range 8 to 12 m/s are suggested but, in any event, should not be greater than 15 m/s. Pipes that are undersized for a future enhanced system will reduce the amount of gas that can be drained or necessitate higher duties of the extractor pumps.

A number of methods are available for assessing the pressure distribution throughout the network. Slide rules to assist in pipe network design are helpful (Boxho, 1980). A number of computer programs have been produced for this purpose varying from single branch assessment to full network analysis employing compressible flow relationships (Section 7.2.2.). These programs can also be used for compressed air networks and allow the consequences of changing pipe sizes, network layout or other design parameters to be assessed very rapidly.

Significant changes in pressure and, hence, density occur as gas proceeds through the pipes of a methane drainage system. It is, indeed, necessary to employ compressible flow relationships for all but the simplest systems in order to determine frictional pressure drops. A methodology for hand calculations can be derived from equations (2.50) and (2.51)

$$p = r_t \rho Q^2 \quad \text{Pa} \quad \text{from equation (2.50)}$$

where p = frictional pressure drop (Pa)
 ρ = gas density (kg/m^3)
 Q = flowrate (m^3/s)
 and r_t = rational turbulent resistance of the pipe (m^{-4})
 (We are using lower case r_t for rational resistance here to avoid confusion with gas constants).

Now from equation (2.51)

$$r_t = \frac{f L \rho v}{2 A^3} = \frac{f L \pi d}{2 (\pi d^2 / 4)^3} = \frac{64 f L}{2 \pi^2 d^5} \quad \text{m}^{-4} \quad (12.50)$$

where f = coefficient of friction (dimensionless)
 L = length (m)
 and d = diameter of pipe.

In order to take compressibility into account, let us replace volume flow, Q , (m^3/s) by mass flow $M = Q \rho$ (kg/s) in equation (2.50) giving

$$p = r_t \frac{M^2}{\rho} \quad \text{Pa} \quad (12.51)$$

But

$$\rho = \frac{P}{RT} \quad \text{kg/m}^3 \quad (12.52)$$

where P = absolute pressure (Pa)
 R = gas constant (J/kg K)
 and T = absolute temperature (K) of the gas

$$\text{giving } P p = r_t M^2 RT \quad (\text{Pa})^2 \quad (12.53)$$

If we consider a very short length of horizontal pipe, dL , having a resistance (dr_t) and pressure drop dp , then equation (12.53) becomes

$$P dp = M^2 RT (dr_t) \quad (\text{Pa})^2 \quad (12.54)$$

However, for a horizontal pipe, $dp = -dP$, and we may rewrite equation (12.54) as

$$-P dP = M^2 RT (dr_t) \quad (\text{Pa})^2 \quad (12.55)$$

Integrating over the complete length of pipe (stations 1 and 2) and assuming isothermal conditions ($T = \text{constant}$), gives

$$\frac{P_1^2 - P_2^2}{2} = M^2 RT r_t \quad (\text{Pa})^2 \quad (12.56)$$

Substituting for r_t from equation (12.50),

$$P_1^2 - P_2^2 = \frac{64 f L}{\pi^2 d^5} M^2 RT \quad (\text{Pa})^2 \quad (12.57)$$

Hence, if the pressure at one end of the pipe is known, then the pressure at the other end can be determined.

Example

A methane/air mixture containing 45 percent methane enters an extractor pump at a pressure of $P_2 = 50$ kPa. The connecting pipe is 1000 m long, 300 mm in diameter and has a coefficient of friction, $f = 0.004$. If the volume flowrate is $1 \text{ m}^3/\text{s}$ at standard atmospheric pressure and temperature while the actual mean temperature of the gas is 25°C , determine the gas pressure, P_1 , entering the pipe.

Solution

First, let us establish the values of the parameters required by equation (12.57)

$$P_2 = 50\,000 \text{ Pa}; \quad f = 0.004; \quad d = 0.3 \text{ m}; \quad L = 1000 \text{ m}; \quad T = 273 + 25 = 298 \text{ K}$$

To establish the gas constant and mass flow of the mixture, we utilize the fractional components of 0.45 (methane) and 0.55 (air)

$$\text{For methane: } R_m = 518.35 \text{ J/(kg K)} \text{ (Table 11.1);}$$

$$\text{for air: } R_a = 287.04 \text{ J/(kg K)}$$

$$\text{and for the mixture: } R = (0.45 \times 518.35) + (0.55 \times 287.04) = 391.13 \text{ J/(kg K)}.$$

The flowrate is given as $Q = 1 \text{ m}^3/\text{s}$ at standard conditions. As the density of air at those same conditions is 1.2 kg/m^3 and the relative density of methane is 0.554 (dimensionless, Table 11.1) then the corresponding density of the mixture is:

$$\rho = (0.45 \times 0.554 + 0.55 \times 1) 1.2 = 0.959 \text{ kg/m}^3.$$

$$\text{giving mass flow } M = \rho Q = 1 \times 0.959 = 0.959 \text{ kg/s}$$

Substituting for the known values in equation (12.57) gives

$$P_1^2 - (50\,000)^2 = \frac{64}{\pi^2} \times \frac{0.004}{(0.3)^5} \times 1000 \times (0.959)^2 \times 391.13 \times 298$$

$$\text{giving } P_1 = 60\,368 \text{ Pa or } 60.37 \text{ kPa}$$

This technique can be used, branch by branch, to determine the effective pressures (producing flow) throughout the network. If an extractor pump is used, then the starting point will be the absolute pressure at the pump inlet. On the other hand, the analysis may commence from a given borehole pressure and proceed through the network in the direction of flow. This indicates the suction pressure required to generate any desired flowrate. Iterative exercises can be carried out to determine optimum pipe sizes. Allowance must be made for the pressure drops that occur at all bends, valves, monitors and other fittings. Such assessments can normally be made from tables or charts, provided by manufacturers.

The buoyancy pressure, p_{buoy} , that assists gas flow in vertical pipes may be estimated simply as

$$p_{buoy} = (\rho_a - \rho_g) g \Delta Z \quad \text{Pa} \quad (12.58)$$

where ρ_a = mean density of air in shafts (kg/m^3)
 ρ_g = mean density of gas mixture in the vertical pipe (kg/m^3)
 g = gravitational acceleration (m/s^2) and
 ΔZ = length of vertical pipe (m)

Where extractor pumps are employed, the buoyancy pressure is often ignored for design purposes. However, if no pumps are used, it becomes a significant factor affecting gas flowrate.

The selection of the network monitoring system, transducers and safety devices should be considered most carefully. Such choices must be made in accord with any national or state legislation appertaining to gas pipelines.

Finally, a colour coded mine plan should be prepared showing the positions, dimensions and other specifications of all pipes, control points, monitors, safety devices and extractor pumps. This plan should be kept up to date as the system is extended.

12.5.7. Utilization of drained gas

Much of the methane produced from mines is passed into the surface atmosphere either via the mine ventilation system or by venting the gas directly to the atmosphere from methane drainage systems. Not only is this a waste of a valuable fuel resource but may have long-term global environmental repercussions.

Where coalbed methane drainage is practiced, the production of gas of a consistent quantity and quality may enable it to be employed in gas distribution facilities for sale to industrial or domestic users. For other methods of methane drainage, variations in purity are likely to restrict utilization of the gas to more local purposes. The simplest use of drained gas is for heating. Gas-fired boilers or furnaces can provide hot water, steam or heated air for low cost district heating schemes. Surface buildings on the mine and local communities can benefit from such systems. Mineral processing plants may utilize the heat for drying purposes or to facilitate chemical reactions. Variations in the purity of the gas fed to burners can be monitored continuously and automatic adjustment of air: fuel ratios employed to maintain the required heat output.

Gas-fired turbines can be employed to produce electricity. Units are available that will develop mine site electrical power from drained gas (Boxho et al, 1980, Owen and Esbeck, 1988). These turbines can act as excellent co-generators producing not only several megawatts of electrical power but also useful heat from the exhaust gases. Gas is normally delivered to the site of the engines at relatively low pressure but is compressed to a pressure of 1000 to 1400 kPa before injection into the combustion chambers. A supply of some $0.7 \text{ m}^3/\text{s}$ (standard pressure and temperature) at 50 percent methane and 50 percent air can produce up to 4 MW of electrical power and 9 MW of useable heat from a mine site gas turbine. Dual units may accept either methane or fuel oil.

Other uses that have been found for drained methane include the firing of furnaces in local metallurgical plants, kilns, coke ovens and for the synthesis of chemicals. In very gassy mines, the methane concentration in the ventilating air returned to surface may be as high as 0.8 percent. Where furnaces are used on the mine site, then fuel savings may be achieved by feeding those furnaces with return air.

References

- Airey, E. M. (1968).** Gas emission from broken coal: An experimental and theoretical investigation. *Int. J. Rock Mechanics and Min. Eng. Sc.*, Vol. 5, pp 475-494.
- Bakke, P. and Leach, S. J. (1962).** Principles of formation and dispersion of methane roof layers and some remedial measures. *The Mining Engineer*. Vol. 121, No. 22, pp 645-658.
- Barker-Read, G. R. and Radchenko, S. A. (1989).** Methane emission from coal and associated strata samples. *Int. Journ. of Mining and Geological Engineering*, Vol. 7, No. 2, pp 101- 126.
- Bertrard, C., Bruyet, B. and Gunther, J. (1970).** Determination of desorbable gas concentration of coal (direct method). *Int. Jnl. of Rock Mechanics and Mining Sc.*, Vol. 7, pp 43-65.
- Boxho, J. et al (1980).** Firedamp drainage handbook. Published by the Coal Directorate of the Commission of the European Communities, pp. 1-415.
- Brunner, D.J., Schwoebel, J.J. and Brinton, J.S. (2006).** Modern CMM strategies. 11th North American Mine Ventilation Symp., Editors Mutmansky and Ramani, Penn State University.
- Campoli, A. A. et al (1985).** An overview of coal and gas outbursts. 2nd U. S. Mine Ventilation Symp. Reno, NV, pp. 345-351.
- CEC (1988).** Investigation of firedamp and its emissions in coal seams. Final Report on ECSC Contract 7220-AC/819, Report EUR 1147, Commission of the European Communities.
- Close, J. C. and Erwin, T. M. (1989).** Significance and determination of gas content data as related to coalbed methane reservoir evaluation and production implications. *Proc. of the 1989 Coalbed Methane Symp.*, Univ. of Alabama, Tuscaloosa, 19 pp.
- Creedy, D.P. and Kershaw S. (1988).** Firedamp prediction – a pocket calculator solution. *The Mining Engineer*. Inst of Mining Engineers, Vol. 147, No. 317, Feb., pp.377-379.
- Coward, H. L. (1937).** Movement of firedamp in air. *Trans. Inst. of Mining Engrs.*, Vol. 94, p. 446.
- Darcy, Henri (1856).** *Les fontaines publique de la ville de Dijon*, Dalmant. Paris.
- Diamond, W. P. and Levine, J. R. (1981).** Direct method determination of the gas content of coal: Procedures and results. U. S. Bureau of Mines Report No. 8515, pp. 1-36.
- Dunmore, R. (1980).** Towards a method of prediction of firedamp emission for British coal mines. 2nd Int. Mine Ventilation Congress. Reno, Nevada, pp 351-364.
- Durucan, S., Creedy, D.P. and Edwards, J.S. (1992).** Geological and geotechnical factors controlling the occurrence and flow of methane in coal seams. *Symp. on coalbed methane research and devevelopment in Australia*, Townsville, Australia.
- Ely, K. W. and Bethard, R. C. (1989).** Controlling coal mine methane safety hazards through vertical and horizontal degasification operations. *Proc. 4th U. S. Mine Ventilation Symp.*, Berkeley, CA, pp. 500-506.
- Ettinger, I. L. et al (1986).** Specification of gas dynamics in coal seams with the application of methane diffusion in pieces, in "Urgent problems of mine aerogas dynamics." *Izd-vo IPKON AN SSSR*, Academy of Sciences, Moscow, pp. 88-93.

Ettinger, I. L. et al (1958). Systematic handbook for the determination of the methane content of coal seams from the seam pressure of the gas and the methane capacity of the coal. Inst. of Mining Academy, Moscow. NCB translation A1606/S.E.H.

Evans, H. and Brown, K. M. (1973). Coal structures in outbursts of coal and firedamp conditions. *The Mining Engineer*. Vol. 173, No. 148, pp. 171-179.

Gan, H., Nandi, S. P. and Walker, P. L. (1972). Nature of the porosity in American coals. *Fuel*. Vol. 51, pp. 272-277.

Gawuga, J. (1979). Flow of gas through stressed carboniferous strata. Ph.D. thesis. Univ. of Nottingham, U. K.

GRI (1988). Technology Profile, Gas Research Institute, Chicago, Ill.

Harpalani, S. (1984). Gas flow through stressed coal. Ph. D. thesis. Univ. of California, Berkeley.

Harpalani, S. and McPherson, M. J. (1984). The effect of gas evacuation on coal permeability test specimens. *Int. Jnl. of Rock Mechanics and Mining Sc.*, Vol. 21, No. 3, pp. 161-164.

Hucka, V. J. and Lisner, U. W. (1983). In-situ determination of methane gas in Utah coal mines (a case history). SME-AIME meeting, Atlanta, Georgia, USA, pp. 1-9.

James, T. E. and Purdy, J. L. (1962). Experiments with methane layers in a mine roadway. *The Mining Engineer*. Vol. 121, No. 21, pp. 561-569.

Janas, H. (1980). Bestimmungen des desorbierbaren methaninhaltes an kohlenproben aus explorationsbohrungen. Unpublished report.

Jolly, D. C., Morris, L. H. and Hinsley, F. B. (1968). An investigation into the relationship between the methane sorption capacity of coal and gas pressure. *The Mining Engineer*. Vol. 127, No. 94, pp. 539-548.

Karacan, C.Ö (2007). Modeling and prediction of ventilation methane emissions of U.S. longwall mines using supervised artificial neural networks. *International Journal of Coal Geology*, doi:10.1016/j.coal.2007.09.003.

King, G. R. and Ertekin, T. (1988). Comparative evaluation of vertical and horizontal drainage wells for the degasification of coal seams. *SPE Reservoir Engineering*. May, pp 720-734.

King, G. R. and Ertekin, T. (1989). State of the art in modeling of unconventional gas recovery. SPE (18947) Symposium. Denver, Colorado.

Klinkenberg, L. J. (1941). The permeability of porous media to liquids and gases. *API Drill Prod. Pract.*, pp. 200-213.

Lama, R. D. and Nguyen, V. U. (1987). A model for determination of methane flow parameters in coal from desorption tests. APCOM '87. Proc. 20th Int. Symp. on the appl. of computers and mathematics in the Minerals Ind. Johannesburg, pp. 275-282.

Langmuir, I. (1916). The constitution and fundamental properties of solids and liquids. *J. Amer. Chem. Soc.*, Vol. 38, pp. 2221-2295.

Langmuir, I. (1918). The adsorption of gases on plane surfaces of glass, mica and platinum. *J. Amer. Chem. Soc.*, Vol. 40, pp. 1361-1403.

- Lunarzewski, L. (1998).** Gas emission prediction and recovery in underground coal mines. *International Journal of Coal Geology* 35, pp. 117-145.
- Mavor, M. J. and Schwoebel, J. J. (1991).** Simulation based selection of underground coal mine degasification methods. 5th U. S. Mine Ventilation Symposium, West Virginia, pp. 144-155.
- Mills, R. A. and Stevenson, J. W. (1989).** Improved mine safety and productivity through a methane drainage system. Proc. 4th U. S. Mine Ventilation Symp., Berkeley, CA, pp. 477-483.
- Morris, I. H. (1974).** Substantial spontaneous firedamp emissions. *The Mining Engineer*. Vol. 133, No. 163, pp. 407-421.
- Obert, L. and Duvall, W. I. (1967).** Rock mechanics and design of structures in rock. Wiley and Sons, New York, p. 333.
- Oldroyd, G. C. et al (1971).** Investigations into sudden abnormal emissions of firedamp from the floor strata of the Silkstone Seam at Cortonwood Colliery. *The Mining Engineer*. Vol. 130, No. 129, pp. 577-591.
- O'Shaughnessy, S. M. (1980).** The computer simulation of methane flow through strata adjacent to a working longwall coalface. Ph.D. Thesis, Univ. of Nottingham, U. K.
- Owen, W. L. and Esbeck, D. W. (1988).** Industrial gas turbine systems for gob gas to energy projects. Solar Turbines Inc., San Diego, CA, pp. 1-14..
- Patton S. B., Fan H., Novak T., Johnson P. W. and Sanford R L (1994),** Simulator for degasification, methane emission prediction and mine ventilation, *Mining Engineering* (Littleton, Colorado), April. Vol 46, part 4, pp. 341 – 345.
- Radchenko, S. A. (1981).** The time of diffusion relaxation as the characteristics of coal disturbance, in "The main questions of the complex development of the deposits of solid mineral resources." *Izd-vo IPKON AN SSSR, Academy of Sciences, Moscow*, pp. 43-118.
- Raine, E. J. (1960).** Layering of firedamp in longwall workings. *The Mining Engineer*. Vol. 119, No. 10, pp. 579-591.
- Richmond, J. K. et al (1983).** Historical summary of coal mine explosions in the United States, 1959-81. U. S. Bureau of Mines Information Circular No. 8909, pp. 1-51.
- Robinson, G. et al (1981).** Underground environmental planning at Boulby Mine, Cleveland Potash, Ltd., England. *Trans. Inst. of Min. Met.*, July. Also published in *Jnl. Mine Ventilation Soc. of S. Africa*. Vol. 35, No. 9, Sept. 1982, pp. 73-88.
- Schatzel, S. J. and Dunsbier, M. S. (1989).** Roof outbursting at a Canadian bedded salt mine. 4th U. S. Mine Ventilation Symp., Berkeley, CA, pp. 491-499.
- Schwoebel, J. J. (1987).** Coalbed methane: Conversion of a liability to an asset. *Mining Engineering*, April, pp. 270-274.
- Sheng, J. and Otuonye, F. (1988).** A model of gas flow during outbursts. 4th Int. Mine Ventilation Congress, Brisbane, Australia, pp. 191-197.
- Smith, D. M. and Williams, F. L. (1984a).** Diffusional effects in the recovery of methane from coalbeds. *Jnl. of Soc. of Petroleum Engrs*. Vol. 24, No. 5, Oct., pp. 529-535.

- Smith, D. M. and Williams, F. L. (1984b).** Diffusion models for gas production from coal - application to methane content determination. *Fuel*, Vol. 63, pp. 251-255.
- Somerton, W. et al (1974).** Effect of stress on permeability of coal, Berkeley, CA. U. S. Bureau of Mines Contract H0122027.
- Thakur, P. C. and Dahl, H. D. (1982).** Mine Ventilation and Air Conditioning (ed. H. L. Hartman), Chapter 4, "Methane Drainage", pp. 69-83.
- U. S. Bureau of Mines (1980).** Creating a safer environment in U. S. coal mines. The Bureau of Mines Methane Control Program. U. S. Govt. Printing Office, Washington, D. C.
- Williams R. and Morris, I. H. (1972).** Emissions and outbursts in coal mining. Proc. Symp. Environmental Eng. in Coal Mining. Inst. of Mining Engrs. Harrogate, U. K., pp. 101- 116.
- Wolstenholme, E. F. et al (1969).** Movement of firedamp within the floor strata of a coal seam liable to outbursts. *The Mining Engineer*. Vol. 128, No. 105, pp. 525-539.

CHAPTER 13. RADIATION AND RADON GAS

13.1. INTRODUCTION	1
13.2. THE URANIUM SERIES AND RADIOACTIVE DECAY	2
13.2.1. Atomic structure; alpha, beta and gamma radiation	2
13.2.2. Radioactive decay and half-life	4
13.3. RADON AND ITS DAUGHTERS	7
13.3.1. Emanation of radon.....	8
13.3.2. Growth of radon daughters	11
13.3.3. Threshold limit values	12
13.4. PREDICTION OF LEVELS OF RADIATION	14
13.4.1. Emanation rate.....	14
13.4.2. Changes in working levels of radon daughters.....	14
13.5. METHODS OF MONITORING FOR RADIATION	18
13.5.1. Measurement of radon daughters.....	19
13.5.2. Measurement of radon concentration	20
13.5.3. Personal dosimeters	20
13.6. CONTROL OF RADIATION IN SUBSURFACE OPENINGS	21
13.6.1. Ventilation systems for uranium mines	21
13.6.2. Dilution and mixing processes	21
13.6.3. Radiation surveys	23
13.6.4. Mining methods, mineral clearance and backfill.....	24
13.6.5. Contamination from abandoned workings	26
13.6.6. The influence of water.....	26
13.6.7. Air filters and rock surface liners.....	27
13.6.8. Education and training	28
References	28

13.1. INTRODUCTION

The element uranium is widely distributed within the crust and oceans of the earth. It has been estimated that crustal rocks contain an average of some 4 grams of uranium per tonne. The structure of the uranium atom is unstable. Emission of subatomic particles from the nucleus causes uranium to change or decay into a new element, thorium. The process of radioactive decay continues down through a series of elements until it reaches a stable form of lead. This process has existed on earth from before the crust was formed. All forms of life on earth have evolved and exist within a constant bombardment of natural radiation including that from the uranium series of elements.

Although most of the uranium series of elements are solids, one known as **radon**, Rn, is a gas. This facilitates escape, or **emanation** of radon from mineral crystals into the pore structure of the rock from where it may migrate via a fracture network or interconnected interstices towards the free atmosphere. However, the liberated radon itself decays into microscopic solid particles known as **radon daughters** which may adhere to dust or other aerosol particulates, or remain suspended as free ions in the air. If the rate of radon emanation into mine workings is high or the

space inadequately ventilated, then the radioactivity caused by continued decay of radon and its daughters will reach levels that are hazardous to health. This is likely to occur within closed environments in close proximity to rocks that contain traces of uranium ores. Radon is a potential problem in any mine and tests for its presence should be carried out early in the development of a new mineral deposit. The hazard can also exist in the basements of surface buildings.

As would be expected, the problem of radon is greatest in uranium mines and particular precautions have to be taken in order to protect personnel from the development of lung cancers caused by the inhalation and possible alveolar retention of radon daughters.

In this chapter, we shall outline the uranium decay series and quantify the mechanisms of radon emanation and the growth of radon daughters within the atmospheres of subsurface openings. Methods of measurement will be discussed while the final section is devoted to pragmatic guidelines to be followed in designing a ventilation system for a mine with high radon emanations.

Readers who are interested only in the control of radiation in subsurface openings should turn directly to Section 13.6.

13.2. THE URANIUM SERIES AND RADIOACTIVE DECAY

13.2.1. Atomic structure; alpha, beta and gamma radiation

The current concept of the structure of an atom is that of a nucleus consisting of protons of net positive electric charge and neutrons of net zero charge, orbited by negatively charged electrons. The electrical charge on the nucleus may be expressed in terms of the unit charge of an electron. The **atomic number** of any given element indicates the level of net positive charge on the nucleus. Figure 13.1 gives the atomic numbers of the elements in the uranium series. The **atomic mass** is the nearest integer to the actual mass of the atom expressed relative to the mass of an individual proton or neutron (atomic mass unit).

There are many classes of ionizing radiation. However, three are particularly relevant to decay through the uranium series. An alpha (α) particle has a positive charge of 2 units and a mass of 4 (helium nucleus). Hence, when an alpha particle is emitted from the nucleus, the atomic number of that element reduces by 2 and the atomic mass reduces by 4. The next element in the decay series is formed. A glance at Figure 13.1 will reveal the stages at which alpha particles are emitted in the uranium decay chain. Alpha particles have relatively low energy levels. They travel no more than a few centimeters in normal atmospheres and are halted by human skin. However, if alpha particles are emitted within the lung, they can cause cellular alteration within the alveolar walls, leading to possible lung cancer.

A **beta β particle** has a negative charge of 1 and a negligible mass (electron). When this is emitted, the atomic mass of the element remains effectively unchanged but the net positive charge on the nucleus (atomic number) increases by one. This can be observed by movement from left to right at atomic masses of 234, 214 and 210 on Figure 13.1. Beta particles not only cause damage to the lung but can also penetrate human skin and may produce alteration of cell tissue.

Both alpha and beta radiation involve the emission of subatomic particulates. **Gamma (γ) radiation**, however, is a very high frequency electromagnetic wave form (like x-rays) and is deeply penetrating with respect to the human body.

A T O M I C N U M B E R

A T O M I C M A S S

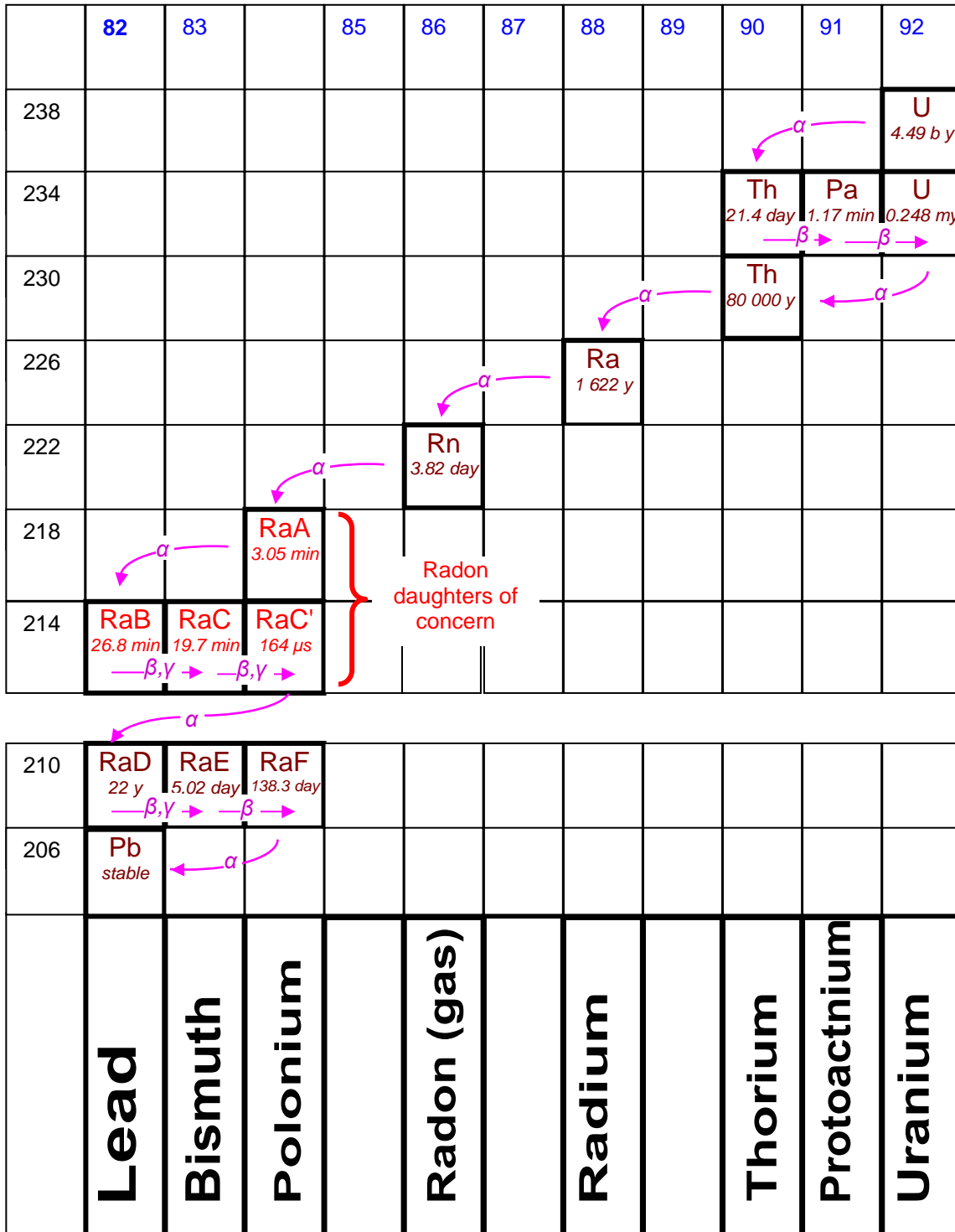


Figure 13.1 The uranium decay series and corresponding half lives. Radon gas, disintegrating through the radon daughters RaA, RaB, RaC and RaC' give rise to *alpha*, *beta* and *gamma* radiation.

13.2.2. Radioactive decay and half-life

The rate at which atoms disintegrate, I , is known as the **radioactivity** and depends upon the number of unaltered atoms and the probability of disintegration.

$$I = \lambda N \quad \text{dis/s} \quad (13.1)$$

where

λ = the decay constant (s^{-1}) for that material and is a measure of the probability of disintegration of any one atom.

For radon, $\lambda = 2.1 \times 10^{-6}$ disintegrations (dis) per second.

and N = number of unaltered atoms remaining

The activity may also be expressed as

$$I = -\frac{dN}{dt} \quad \text{dis/s} \quad (13.2)$$

If we commence with a fresh sample of a radioactive substance, then all of the atoms are capable of disintegrating to the next lower element in the chain. However, as this process continues, there are progressively fewer atoms remaining of the original substance. Hence, the rate of decay of that substance will decline exponentially. This may be expressed in terms of the reducing number of atoms that remain unaltered.

$$N = N_0 \exp(-\lambda t) \quad (13.3)$$

where N_0 = original number of atoms
 t = time (s)

or, from equations (13.2) and (13.3),

$$I = -\frac{d}{dt} \{ N_0 \exp(-\lambda t) \} = \lambda N_0 \exp(-\lambda t)$$

But the initial activity $I_0 = \lambda N_0$ from equation (13.1).

Hence,

$$I = I_0 \exp(-\lambda t) \quad \text{dis/s} \quad (13.4)$$

showing that the radioactivity also decays exponentially with time. Figure 13.2 illustrates a decay curve. By measuring the activity given by a radioactive substance while removing the decay products, the corresponding curve can be plotted and the value of λ determined.

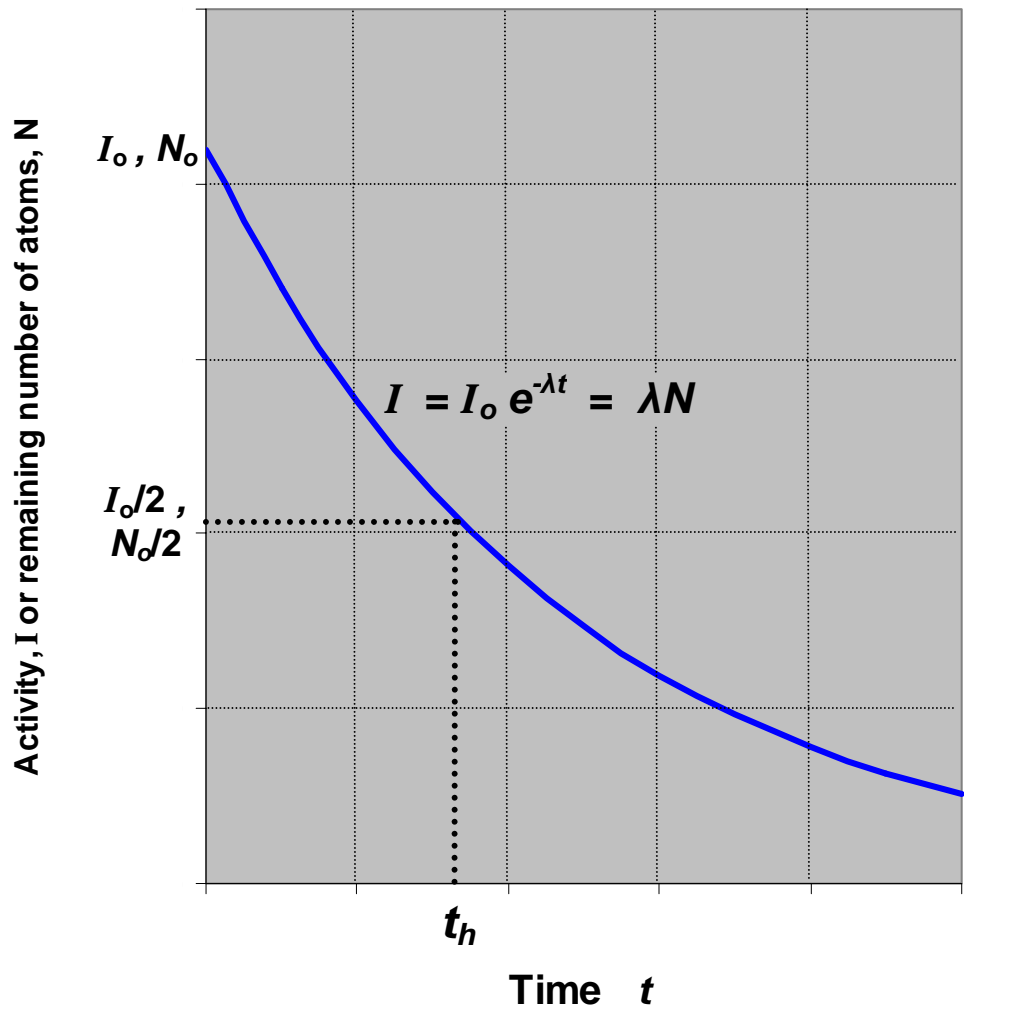


Figure 13.2 The activity, I , and number of atoms, N , of the original substance both decay exponentially with time. The half life, t_h , occurs when I and N are each half of their original values.

The decay curve approaches zero activity exponentially; hence, the theoretical full lifespan of a radioactive element is infinite. A more useful indicator of the aging process is the **half-life** of the element. This is defined as the time taken for half of the original atoms to decay. As $I = \lambda N$, the activity also reduces to half its original value at this same time. A simple relationship exists between the half-life, t_h , and the decay constant, λ :

Initially,

$$I = I_0 \quad \text{and at the half-life} \quad I = I_0/2 = I_0 \exp(-\lambda t_h)$$

Hence,

$$\exp(-\lambda t_h) = \frac{1}{2} \quad \text{or} \quad -\lambda t_h = \ln\left(\frac{1}{2}\right) = -0.6931$$

giving

$$t_h = \frac{0.6931}{\lambda} \quad \text{seconds} \quad (13.5)$$

For radon, $\lambda = 2.1 \times 10^{-6}$ dis/s, giving

$$t_h (\text{radon}) = \frac{0.6931}{2.1 \times 10^{-6}} = 0.33 \times 10^6 \text{ seconds or } 3.82 \text{ days.}$$

The half-lives of the other elements in the uranium decay series are given in Figure 13.1 and vary from U^{238} (4.49 billion years) to RaC' (164 microseconds).

The problems of radon in mines occur not only because it is a gas and can be emitted into the ventilating airstream, but also from a consideration of half-lives. Radon gas is the decay product of radium, Ra^{226} . This has a half-life of 1622 years, i.e. extremely long relative to the time taken for a ventilating airstream to traverse through a mine. Hence, the source of radon is effectively infinite. With a half-life of only 3.82 days, some of the radon will decay before it leaves the mine. More importantly, the short half-lives of the radon daughters, RaA, RaB, RaC and RaC', indicate that they will disintegrate readily, emitting alpha, beta and gamma radiation. These observations have an important bearing on the design of ventilation systems for uranium mines.

13.2.3. Units of radioactivity

In the previous section we referred to the level of radioactivity in terms of atomic disintegrations per second, dis/s. This unit is sometimes called the **Becquerel** (Bq) after the French physicist who found in 1896 that uranium salts are radioactive.

$$1 \text{ Bq} = 1 \text{ dis/s} \quad (13.6)$$

A less rational but widely used unit of radioactivity is the **Curie** named after Marie (1867-1934) and Pierre (1859-1906) Curie, who, in France, first separated and identified radium and a number of other radioactive elements.

One Curie, Ci, approximates to the activity of 1 gram of radium or, more precisely, a source that is disintegrating at a rate of 3.700×10^{10} atoms per second. Owing to the magnitude of this latter value, sub-multiples of the unit are normally employed.

$$\begin{aligned} 1 \text{ microcurie} &= 1 \mu\text{Ci} = 10^{-6} \text{ Ci} = 37000 \text{ dis/s} \\ 1 \text{ picocurie} &= 1 \text{ pCi} = 10^{-12} \text{ Ci} = 0.037 \text{ dis/s} \end{aligned} \quad (13.7)$$

$$\text{Hence,} \quad 1 \text{ pCi} = 0.037 \text{ Bq} \quad (13.8)$$

$$\text{or} \quad 1 \text{ Bq} = 27 \text{ pCi} \quad (13.9)$$

Analyses on radioactivity may be conducted in terms of either Becquerels or Curies.

Prior to the establishment of current knowledge on the effects of radioactivity on the human body, it was thought that an average level of 100 pCi/litre from radon daughters was safe. This has since been reduced to a third of that value. However, 100 pCi/litre became known as an acceptable working level. The term was truncated to **Working Level, WL**, and is now used widely with respect to radon daughters¹.

¹ The term Working Level is also defined as that concentration of short-lived radon daughters which represents 1.3×10^5 MeV of potential α particle energy while decaying to the stable Pb^{210} .

Ionizing electromagnetic radiation produced by **gamma emissions** is measured in Röntgens (after Wilhelm Röntgen of Germany who discovered x-rays in 1895). The Röntgen is defined formally as the level of x or gamma radiation that produces 1 electrostatic unit of charge² per 0.001293 g of air (1 cc at 101.324 kPa and 0°C). In order to apply this in terms of the effect on human bodies, the Rem (Röntgen equivalent man) is employed. This is the amount of ionizing radiation that will cause the same biological effect as 1 Röntgen of x or gamma rays. **Dose rates** are quoted in mRem/hour. Hence, a dose rate of 50 mRem/hour would produce a dose equivalent of 25 mRem after half an hour.

The Röntgen and the Rem are the most commonly used units for ionizing radiation and biological dosage. They are not, however, SI units. The rational SI equivalents are:

$$\begin{aligned} 1 \text{ C/kg (Coulomb per kilogram)} &= 3876 \text{ Roentgens} \\ 1 \text{ Sv (Sievert)} &= 1 \text{ J/kg} = 100 \text{ Rems} \end{aligned}$$

As a Sievert is a very large unit, radiation doses are quoted in milli-Sieverts (mSv). One chest x-ray is equivalent to about 0.2 mSv.

13.3. RADON AND ITS DAUGHTERS

Radon gas emanates from the crystalline structure of minerals into the pores and fracture networks of rocks. It migrates through the strata by a combination of diffusion and pressure gradient towards mine openings. Radioactive decay produces the solid particulates of the radon daughters as given in Figure 13.1, namely

half life

polonium,	Po ²¹⁸ or radium A,	RaA	3.05 min
lead,	Pb ²¹⁴ or radium B,	RaB	26.8 min
bismuth,	Bi ²¹⁴ or radium C,	RaC	19.7 min
polonium,	Po ²¹⁴ or radium C',	RaC'	164 μ s
and lead	Pb ²¹⁰ or radium D,	RaD	22 years

As the half-life of RaD is 22 years, we need concern ourselves only with the radon series down to RaC'. Furthermore, RaC' has the extremely short half-life of 164 microseconds. Hence, the effect of its decay is normally coupled with that of RaC.

The solid particulates of radon daughters that form during migration of the gas through strata are likely to plate on to the mineral surfaces and be retained within the rock. However, the remaining radon will continue to decay after it has been emitted into a mine opening. The radon daughters will then adhere to aerosol particles or remain as free ions within the airstream.

In this Section, we shall examine the migration of radon through the rock and the growth of radon daughters within a ventilating airflow.

² 1 electrostatic unit of charge is equivalent to 2.083×10^9 ion pairs.

13.3.1. Emanation of radon

When an alpha particle is projected from an atom of radium, the resulting atom of radon recoils through a distance of some 3×10^{-8} m in minerals and 6×10^{-5} m in air (Thompkins, 1982). Furthermore, the **diffusion coefficient** for radon within mineral crystals is very small. Hence, although movements of radon atoms will occur within the crystals, the distances of individual motion are small in comparison to most mineral grain sizes; the probability of any one radon atom escaping into a pore is, therefore, also small. Nevertheless, a sufficient number do escape to give rise to radon problems in uranium mines.

The migration of radon through the pore and fracture network of the strata may be analysed on the basis of Fick's laws of diffusion modified for radon production and decay (Bates and Edwards, 1980). This leads to an approximate equation that describes the radon concentration, C , within the pores with respect to distance into the rock

$$C = C_{\infty} \left\{ 1 - \exp \left[-x \sqrt{\frac{\lambda \phi}{D}} \right] \right\} \quad \text{pCi/m}^3 \text{ of space} \quad (13.10)$$

where

$$\begin{aligned} C_{\infty} &= \text{radon concentration at infinite distance into rock (pCi/m}^3\text{)} \\ x &= \text{distance into rock from free surface (m)} \\ \lambda &= \text{radon decay constant (} 2.1 \times 10^{-6} \text{ Bq)} \\ \phi &= \text{rock porosity (fraction)} \\ \text{and } D &= \text{diffusion coefficient for rock (m}^2\text{/s)} \end{aligned}$$

The units of radon concentration require a little explanation. The normal volumetric concentration commonly used for other gases would give excessively low values for radon. It is more convenient to express radon concentration in terms of the level of radioactivity (pCi or Bq) emitted by each m^3 of the radon:air (or radon:water) mixture.

Equation (13.10) is based on an assumed radon concentration of zero at the open rock surface. The actual **emanation at the rock surface** can be measured directly or calculated as

$$J = C_{\infty} \sqrt{\lambda D \phi} \quad \frac{\text{pCi}}{\text{m}^2 \text{s}} \quad (\text{Bates and Edwards, 1980}) \quad (13.11)$$

The maximum value of radon concentration in the rock, C_{∞} may be determined from

$$C_{\infty} = \frac{B}{\lambda \phi} \quad \frac{\text{pCi}}{\text{m}^3} \quad (13.12)$$

where B is the rate of **emanation from unit volume of rock** ($\text{pCi/m}^3\text{s}$) (sometimes known as emanating power) and can be measured from samples of the rock. Values of both B and J for differing rocks vary by several orders of magnitude.

To reiterate, J indicates the radon emanation from a solid rock surface while B refers to radon emanation from fragmented rock.

Combining equations (13.11 and 13.12) gives

$$J = B \sqrt{\frac{D}{\lambda \phi}} \quad \frac{\text{pCi}}{\text{m}^2 \text{s}} \quad (13.13)$$

A guide to coefficients of diffusion for radon in a range of materials is given in Table 13.2. Figure 13.3 may be used as a guideline to estimate a coefficient of diffusion for radon in rocks of known porosity. However, it should be noted that the coefficient of diffusion varies widely with the type and condition of pore fluid.

Medium	Coefficient of diffusion D m ² /s
Rocks:	
dense rock	0.05×10^{-6}
porosity 6.2 percent	0.2×10^{-6}
porosity 7.4 percent	0.27×10^{-6}
porosity 12.5 percent	0.5×10^{-6}
porosity 25 percent	3×10^{-6}
Air	$(10 \text{ to } 12) \times 10^{-6}$
Water	0.0113×10^{-6}
Alluvial soil	$(3.6 \text{ to } 4.5) \times 10^{-6}$
Concrete	$(0.0017 \text{ to } 0.003) \times 10^{-6}$

Table 13.2. Coefficients of diffusion, D , for radon in various porous media (after Thompkins, 1985).

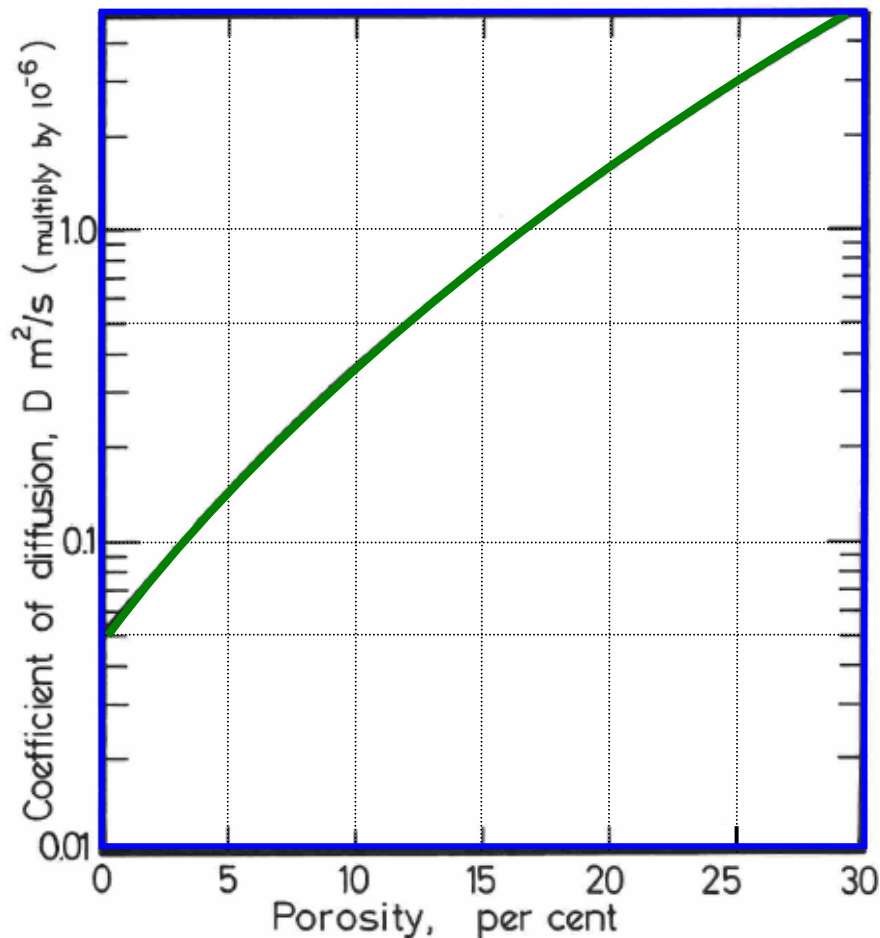
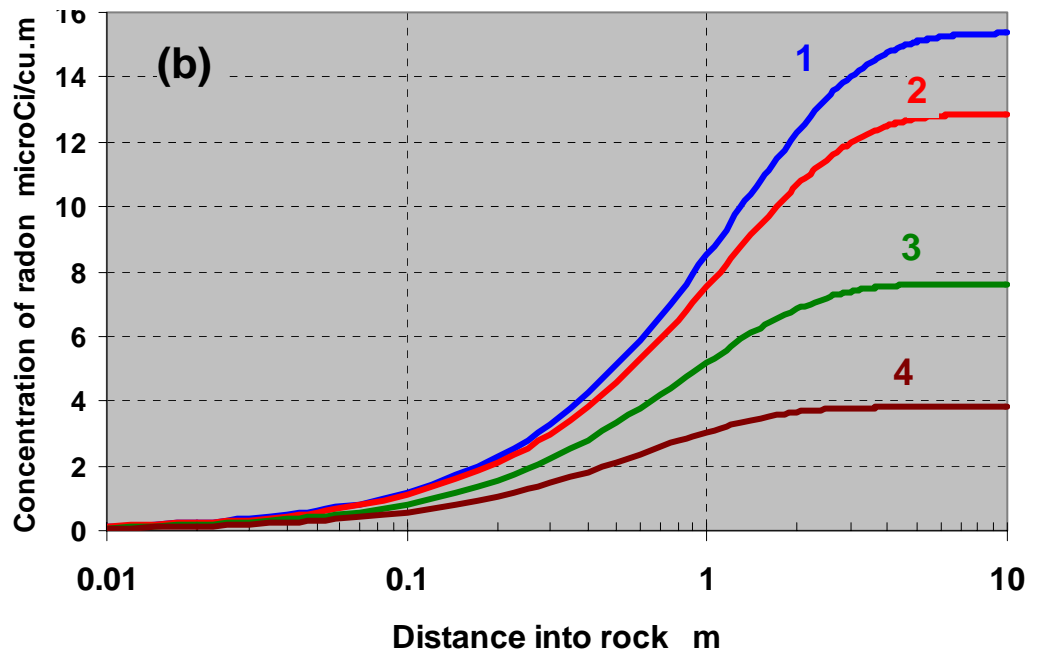
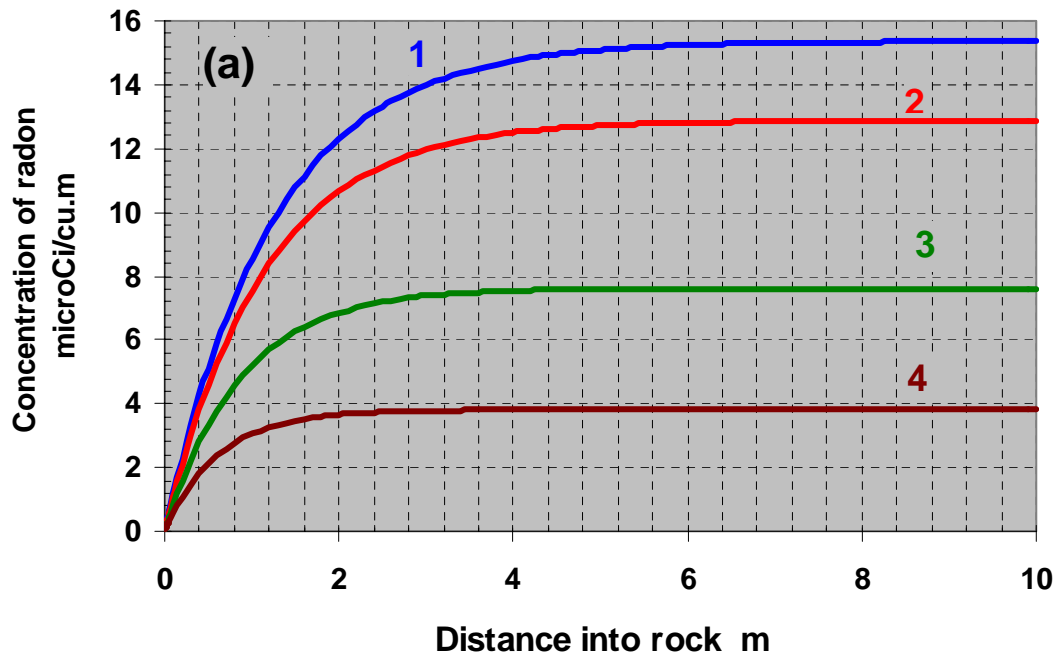


Figure 13.3 Guideline to the approximate coefficient of diffusion, D , for radon in rocks of known porosity. Note that actual coefficients of diffusion depend upon the type and state of pore fluids.



Curve	Porosity ϕ per cent	Coefficient of Diffusion D m^2/s
1	6.2	0.2×10^{-6}
2	7.4	0.27×10^{-6}
3	12.5	0.5×10^{-6}
4	25	3.0×10^{-6}

Figure 13.4 (a) Examples of variation of radon concentration with distance into rock, constructed from equations (13.10) and (13.12) with $B = 2 \text{ pCi/m}^3\text{s}$ and $\lambda = 2.1 \times 10^{-6}$ becquerels. (b) The same curves plotted on a log scale for distance shows better accuracy at shorter distances.

Figure 13.4 illustrates the variation of radon concentration within the pores for the four rocks of specified porosities and corresponding coefficients of diffusion given in Table 13.2. These curves indicate that peak emanations of radon are likely to occur when rock is broken from the orebody and reduced to fragments of about 10 cm in size. However, below that dimension there is relatively little change in radon concentration within the pores, particularly for the higher porosity rocks.

13.3.2. Growth of radon daughters

Radon is emitted into mine openings not only directly from the surrounding rock surfaces but also from old workings and other zones of voidage. Hence, the total emanations will consist of a mixture of the gas and its particulate daughters. In order to analyse the growth of the daughters, consider an imaginary experiment. We commence with one litre of filtered air that contains a radon concentration of 100 pCi/litre. The radon will immediately begin to suffer disintegration into RaA. This has a half-life of only 3.05 minutes. Hence, the second radon daughter, RaB soon appears. However, this has a half-life of 26.8 minutes and concentrations of the RaC (and RaC') do not become significant until some 20 minutes from the start of the experiment. We now have a situation in which the initial amount of radon gas is diminishing slowly (half-life of 3.82 days) but each of the daughters is simultaneously being generated and decaying on a shorter time scale. With its relatively small half-life, the concentration of RaA reaches a state of dynamic equilibrium within a few minutes. Figure 13.5 illustrates the growth of the radon daughters from an initial radon concentration of 100 pCi/litre, i.e. 1 Working Level.

Full (secular) equilibrium is reached in some 30 hours when the air is said to have fully "aged". However, 80 percent of the aging occurs within 90 minutes (5400 seconds). The concept of the "age" of the air is most important in understanding the radioactive decay of radon. At secular equilibrium, the number of atoms in each radon daughter is proportional to its half-life. The age of the air can be estimated from the growth curve of Figure 13.5 for a given working level of radon daughters and having corrected for the actual concentration of radon gas present. The latter may be eliminated by using Figure 13.9 which gives the growth in total radon daughters for a range of initial radon gas concentrations.

With a half-life of 3.82 days, the radioactivity caused by the decay of radon during the short time it spends within the human lung is very limited. However, the shorter half-lives of the radon daughters cause them to be much more prolific emitters within the respiratory system. Furthermore, as they are particulates, they may adhere to mucous membranes and be retained within the lung tissue. It is, therefore, the daughters of radon rather than the gas itself that are dangerous to health.

As it is the decay of the radon daughters that causes the health hazard, it is clear from Figure 13.5 that airflows should be sufficiently vigorous to remove radon from mine workings as rapidly as possible and before significant aging has occurred. It is also clear that near stagnant air in old workings will be fully aged, i.e. contain the maximum concentrations of radon daughters and may cause serious escalations in working levels if leakage occurs from those old workings into active airways.

Although Figure 13.5 illustrates the growth of each radon daughter, it will be recalled that each daughter is simultaneously suffering disintegration. Hence, a mirror image of Figure 13.5 would indicate the corresponding decay curves. At full secular equilibrium, the growth and decay curves for each radon daughter would be horizontal lines, equal in magnitude but opposite in sign. For clarity, the decay curve for total radon daughters only is shown on Figure 13.5.

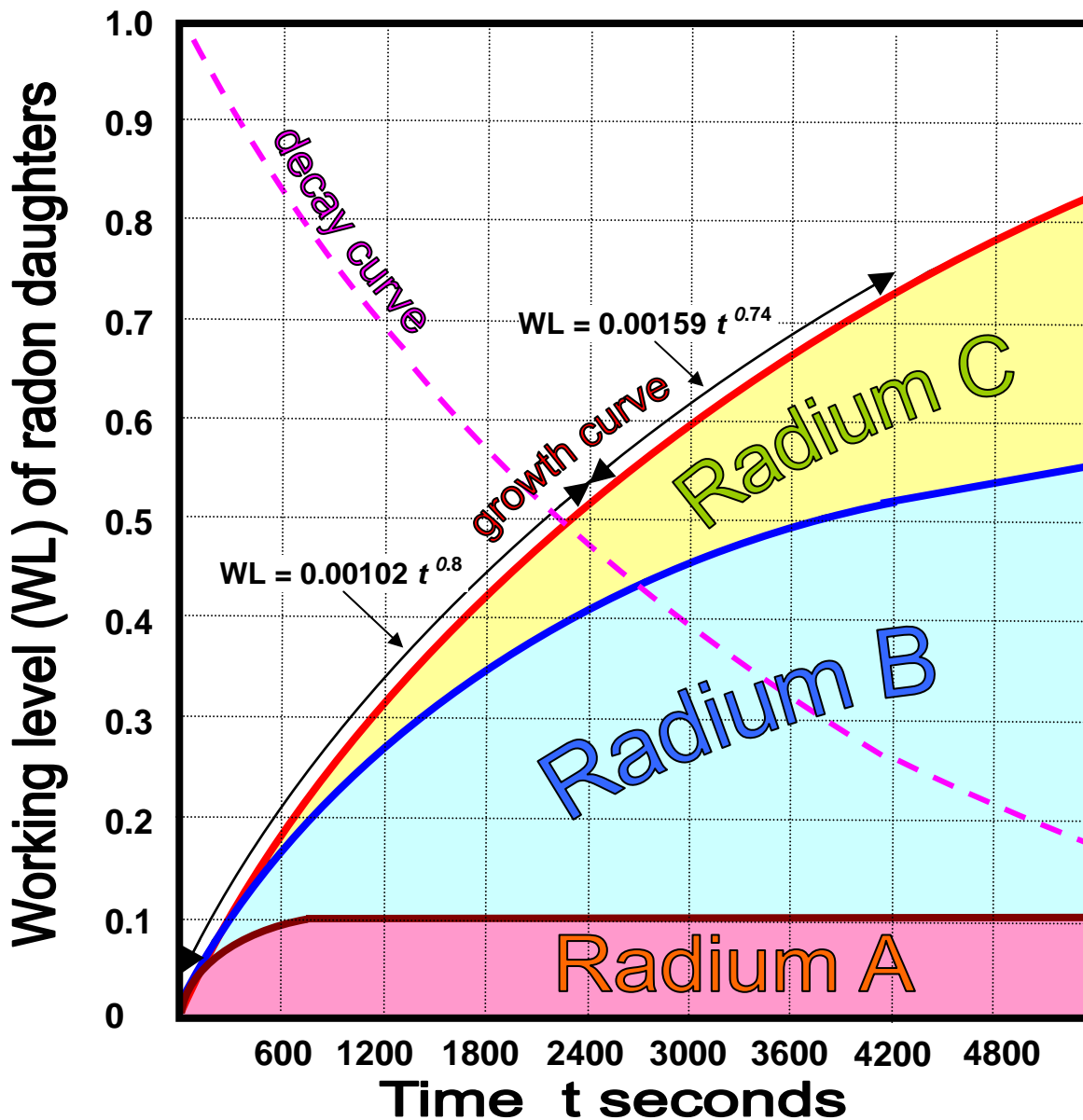


Figure 13.5 The growth curve shows the development of radon daughters from an initial radon concentration of 100 pCi/litre and with no replenishing radon. The decay curve shows the fall in total working level due to radon and radon daughters and is a mirror image of the growth curve.

13.3.3. Threshold limit values

Lung cancers occur throughout the general population but are exacerbated by the inhalation of some types of dust particles and products of combustion. However, the higher incidence of lung cancer in uranium mine workers is attributed to radon daughters. The current method of dosage assessment is based on cumulative exposure. Any unit of time may be employed. However, the most widespread measure of cumulative exposure is the Working Level Month, WLM, defined as an exposure of 1 WL for a period of 1 month.

Assuming that an average of 170 hours are spent in the workplace each month, the cumulative exposure of any individual may be calculated as

$$\frac{\sum(WL \times \text{hours of exposure})}{170} \quad \text{WLM}$$

Example

During the 40 hours a miner spends underground during a week, radiological monitoring indicates the following levels and periods of exposure to radon daughters:

20 hours at 0.1 WL

15 hours at 0.2 WL

5 hours at 0.4 WL

Determine the cumulative exposure in WLM for that week.

Solution

$$\text{Cumulative exposure} = \frac{(20 \times 0.1) + (15 \times 0.2) + (5 \times 0.4)}{170} = 0.041 \quad \text{WLM}$$

The most commonly accepted TLV (threshold limit value) for mine workers is that no person should be subjected to a cumulative exposure exceeding 4 WLM in one year. Legislation may also require that there should be an upper limit of 2 WLM in any consecutive three months and an instantaneous ceiling limit level of 1.0 WL.

The TLV of 4 WLM per year implies an average of $4/12 = 0.33$ WLM per month, i.e. an average radiation level of 0.33 WL. Legislation may require mandatory reporting and increased rates of sampling at higher levels. However, the aim should be for lower actual levels in the active work areas of a mine as leakage from old workings can cause rapid escalation of working levels in return airways. [National or state legislation may also mandate notification to inspection agencies at very low levels of radiation (Howes, 1990).]

There remains considerable doubt on the long term effects of exposure to low levels of radioactivity. It should be expected that threshold limit values will be decreased yet further. In the meantime, the International Commission on Radiological Protection has recommended that in addition to remaining within specified threshold limit values, radiation levels should be maintained "as low as reasonably achievable". This is often termed the **ALARA principle**. The practical application of this rather vague phrase may involve mine management being required to notify the inspectorate when a specified fraction of the exposure TLV is exceeded for any worker; and, furthermore, to demonstrate that all reasonable steps have been taken to alleviate the problem.

The threshold limit values for gamma (ionizing) radiation are, typically, 5 Rems per year. Where average gamma radiation measurements are in excess of 2 milli-Röntgens per hour, personal gamma radiation dosimeters may be mandated for all personnel and records of cumulative exposure maintained for each individual (e.g. Title 30 US Code of Federal Regulations, paragraph 57.5047).

13.4. PREDICTION OF LEVELS OF RADIATION

13.4.1. Emanation rate

In order to predict the levels of radiation to be expected in any active area of a mine, the emanation rates, J (pCi/m²s), from exposed surfaces and/or emanating powers, B (pCi/m³s), from drill cores or other samples must first be measured. The relationship between the two is given by equation (13.13). Surface emanation rates can be measured in-situ by attaching steel collection receptacles tightly to a rock face (Archibald, et al, 1980) or by excavating chambers into the rock. Multiple measurements made on a variety of ores and waste rock allow tables of surface emanation rates, J , and emanating powers, B , to be assembled for a given mine or rock type.

In order to determine the total rate of emanation in a specified zone, the surface area of all exposed rock faces, A (m²), and the volumes of broken ore, V (m³), must be assessed and multiplied by the relevant values of J and B respectively.

Example

In the walls of a given stope, 350 m² of ore and 300 m² of waste rock surface are exposed. The stope contains 320 t of fragmented ore. If the density of the ore is 2000 kg/m³, determine the rate of emanation into the stope given that

$$\begin{array}{l} \text{and} \quad J(\text{ore}) = 500 \text{ pCi/m}^2\text{s}; \quad B(\text{ore}) = 600 \text{ pCi/m}^3\text{s} \\ \quad \quad J(\text{waste}) = 100 \text{ pCi/m}^2\text{s} \end{array}$$

Solution

$$\begin{array}{l} \text{Radon from:} \quad \text{Ore wall surface} = 350 \times 500 = 175\,000 \text{ pCi/s} \\ \quad \quad \quad \text{Waste wall surface} = 300 \times 100 = 30\,000 \\ \quad \quad \quad \text{Total wall surface} = \quad \quad \quad 205\,000 \text{ pCi/s} \end{array}$$

$$\text{Volume of ore fragments} = \frac{320\,000}{2000} \frac{\text{kg m}^3}{\text{kg}} = 160 \text{ m}^3$$

$$\text{Radon from fragmented ore} = 160 \times 600 = 96\,000 \text{ pCi/s}$$

$$\text{Total emanation of radon} = 205\,000 + 96\,000 = 301\,000 \text{ pCi/s}$$

13.4.2. Changes in working levels of radon daughters

A commonly accepted method of calculating the variation in natural radioactivity due to radon daughters along an airway was developed by Schroeder and Evans at the Massachusetts Institute of Technology in 1969. Consider the length of airway shown in Figure 13.6. The working level of radon daughters at the exit from the airway, distance x (m) from the entrance, arises from three factors

- (i) decay of the radon gas already in the air at the entry point,
- (ii) decay of the radon that emanates from the walls or fragmented rock within the airway itself, and
- (iii) continued aging of radon daughters that already exist in the airway at the entry point.

Each of these three behaves independently of the others. They may, therefore, be determined separately and summed to give the working level of radon daughters at exit. Let us consider each component in turn.

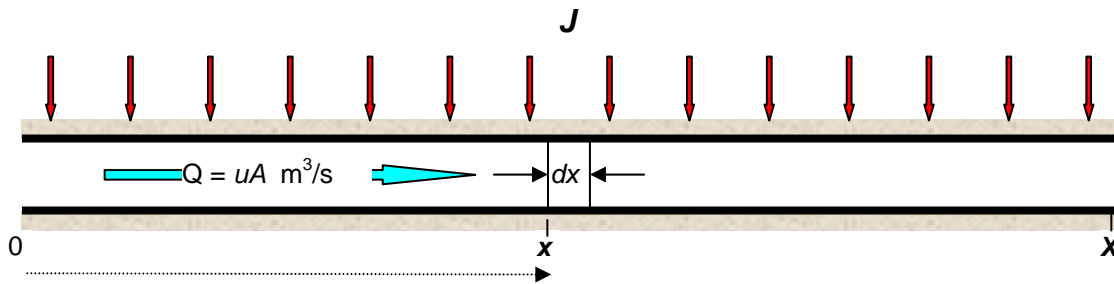


Figure 13.6 Radon emanates from rock surfaces at a rate of J pCi/m²s.

(i) *Decay of radon existing at entry*

This can be determined from Figure 13.5. Curve fitting to the total working level (growth) curve on this Figure gives

$$WL = 102 \times 10^{-5} t^{0.8} \text{ Working Levels for } t < 2400 \text{ s (40 minutes)} \quad (13.14)$$

where WL = Working level due to decay of 100 pCi/litre of initial radon
and t = travel time for air to traverse the airway (s)

(the coarser equation: $WL = 159 \times 10^{-5} t^{0.74}$ may be used for $t < 4200$ s or 70 minutes).

For other concentrations of radon, C (pCi/litre), equation (13.14) becomes

$$WL_1 = \frac{C}{100} \times 102 \times 10^{-5} t^{0.8} \quad (13.15)$$

This equation is the basis of Figure 13.9.

Example 1

An airflow of 24 m³/s with a radon concentration of 20 pCi/litre enters an 800 m long rectangular airway of dimensions 4m by 3m. Calculate the working level of radon daughters at exit caused by the initial radon.

Solution 1

$$\text{Cross-sectional area, } A = 4 \times 3 = 12 \text{ m}^2$$

$$\text{Mean velocity} = \frac{\text{Airflow}}{A} = \frac{24}{12} = 2 \text{ m/s}$$

$$\text{Residence time, } t_r = \frac{\text{distance}}{\text{velocity}} = \frac{800}{2} = 400 \text{ seconds}$$

Then equation (13.15) gives

$$WL_1 = \frac{20}{100} \times 102 \times 10^{-5} (400)^{0.8} = 0.025 \text{ Working Levels}$$

This result may also be read directly from Figure 13.9.

The example will be continued for the remaining sources of radon daughters.

(ii) *Decay of radon emanated from rock surfaces into the airway*

To facilitate the analysis, it is assumed that radon emanates at a uniform rate of J pCi/m²s from all solid surfaces around the opening. Consider the airway shown in Figure 13.6. The air enters at position 0 and leaves after traversing a distance of X (m). Over the short length dx , the wall area is $per \times dx$ (m²), where per = perimeter (m).

The radon emitted over this increment is, therefore,

$$J \text{ per } dx \quad \text{pCi/s.}$$

If the airflow is $Q = uA$ m³/s

where u = mean velocity (m/s) and A = cross sectional area (m²)

then the radon emanation may be expressed in terms of cubic meters of air, i. e. an increase in concentration:

$$\text{Concentration from radon emitted in increment } dx = \frac{J \text{ per } dx}{Q} = \frac{J \text{ per } dx}{uA} \quad \frac{\text{pCi}}{\text{m}^3} \quad (13.16)$$

The time taken for the air to travel from x to X is

$$t = \frac{(X - x)}{u} \quad \text{seconds}$$

Equation (13.14) states that from a radon concentration of 1 Working Level, i.e. 100 pCi/litre (or 100 000 pCi/m³) the working level of radon daughters that will develop in this time is

$$102 \times 10^{-5} \frac{(X - x)^{0.8}}{u^{0.8}} \quad \text{WL}$$

Hence, from a radon concentration of

$$\frac{J \text{ per } dx}{uA} \left(\frac{\text{pCi}}{\text{m}^3} \right) \quad \text{or} \quad \frac{J \text{ per } dx}{100\,000 \, uA} = \text{Working Levels}$$

the working level of radon daughters will grow to

$$\frac{J \text{ per } dx}{100\,000 \, uA} 102 \times 10^{-5} \frac{(X - x)^{0.8}}{u^{0.8}} \quad \text{WL at exit from the airway.}$$

To find the working level of radon daughters at exit due to radon emanations throughout the complete length of airway, WL_2 , we must integrate from 0 to X :

$$WL_2 = 102 \times 10^{-10} \frac{J \text{ per}}{Au^{1.8}} \int_0^X (X-x)^{0.8} dx$$

The integration is accomplished by substitution to give

$$WL_2 = 102 \times 10^{-10} \frac{J \text{ per}}{Au^{1.8}} \frac{X^{1.8}}{1.8}$$

But the total residence time is $t_r = X/u$, giving

$$WL_2 = 56.7 \times 10^{-10} \frac{J \text{ per}}{A} t_r^{1.8} \quad (13.17)$$

Example 2

Continuing from Example 1, the known values are

$$u = 2 \text{ m/s} \quad t_r = 400 \text{ seconds} \quad \text{per} = 14 \text{ m}$$

Determine the activity of radon daughters at exit due to radon being emitted from the airway surfaces at a rate of $J = 250 \text{ pCi}/(\text{m}^2\text{s})$.

Solution 2

Equation (13.17) gives

$$WL_2 = 56.7 \times 10^{-10} \frac{250 \times 14}{12} (400)^{1.8} = 0.080 \text{ WL}$$

(iii) Continued aging of radon daughters that existed in the air at the entry point

In general, the air that enters at location 0 on Figure 13.6 will already contain radon daughters. These will continue to age and, hence, decay to a reduced working level by the time they reach the exit. The fact that the daughters are continuously being replenished from the decay of radon can be ignored as those effects have been considered separately in (i) and (ii).

The reduction in working levels may be read from the decay curve on Figure 13.5 and adjusted for the initial working level, WL_{in} or, as the decay curve is a mirror image of the growth curve, calculated as

$$WL_3 = WL_{in} (1 - 102 \times 10^{-5} t_r^{0.8}) \quad \text{WL}$$

Example 3

If the activity of radon daughters at entry into the airway of Example 2 is 0.05 WL, then after the residence time of 400 s, this will have decayed to

$$WL_3 = 0.05 \{1 - 102 \times 10^{-5} (400)^{0.8}\} = 0.0438 \quad \text{WL}$$

There is, however, a weakness in this technique. It assumes that the radon daughters are in equilibrium with each other and with their parent radon gas. This is not usually the situation in

ventilated areas underground. Further analysis of a suggestion made by Schroeder and Evans (1969) leads to an improved estimate:

$$WL_3 = WL_{in} \left\{ \frac{(t_{in} + t_r)^{0.8} - (t_r)^{0.8}}{(t_{in})^{0.8}} \right\} \quad (13.18)$$

where t_{in} = the "age" of the air at entry.

Let us repeat this previous example using the Schroeder and Evans technique, given that the radon concentration at entry is $C = 20$ pCi/litre.

An estimate of the age of the air at entry, t_{in} , is given by an inversion of equation (13.15).

$$t_{in} = \left\{ WL_{in} \frac{100}{C} \frac{1}{102 \times 10^{-5}} \right\}^{0.8} \quad (s) \quad (13.19)$$

$$= \left\{ 0.05 \times \frac{100}{20} \frac{1}{102 \times 10^{-5}} \right\}^{0.8} = 970 \text{ seconds}$$

(This result can be estimated from Figure 13.9 at $WL = 0.05$ and radon concentration = 20 pCi/litre.)

Equation (13.18) then gives

$$WL_3 = 0.05 \left\{ \frac{(970 + 400)^{0.8} - (400)^{0.8}}{(970)^{0.8}} \right\} = 0.0413 \quad WL$$

To complete the series of examples given in this Section, the total working level of radon daughters exiting the airway is

$$WL_{out} = WL_1 + WL_2 + WL_3 = 0.025 + 0.080 + 0.041 = 0.146 \text{ WL}$$

13.5. METHODS OF MONITORING FOR RADIATION

When radioactive emissions strike the atoms of other substances, they produce effects that may include increases in temperature or secondary radiation. These effects can be measured and are a function of the level of the primary emission. In general, there are two types of radiation instrumentation, the thermal and photosensitive detectors.

In thermal detectors, the radiation is directed on to the hot junctions of a series of thermocouples (thermopile) or a resistance thermometer within an evacuated chamber. The increase in temperature of these sensors produces an electrical output that is representative of the level of radiation. Another type employs a sensitive gas thermometer. Thermal detectors tend to be fragile and are less suitable for portable instruments.

The most widely used principle of radiation detection in subsurface openings is photosensitivity. The radiation is aimed at a material that emits photons (quanta of light) when irradiated. Zinc

sulphide is commonly employed. The photons are directed towards a photomultiplier tube (PMT) where the light is amplified and converted to electrical pulses for counting and display.

13.5.1. Measurement of radon daughters

A number of instruments have been devised to measure the working levels of radon daughters (Williamson, 1988). In the Kusnetz (1956) method, the air is pumped for 5 minutes at a steady rate of 2 to 10 litres/minute through a filter of pore size less than 0.8 microns. The radon daughters collected on the filter are allowed to age for a further 40 to 90 minutes and are then exposed to a photomultiplier tube. The pulses of output energy are counted over a period that depends upon the level of activity but should be small compared with the delay period, typically 1 to 2 minutes (Calizaya, 1991). The concentration of radon daughters in working levels is then given as

$$WL = \frac{C \times CE}{TF \times V} \quad (13.20)$$

where C = measured count rate (counts/min)
 CE = counter efficiency (instrument factor)
 TF = time factor corresponding to the 40 to 90 minute delay (Figure 13.7) between the end of sampling and the midpoint of the counting interval
 and V = sample volume (litres)

A disadvantage of the Kusnetz and similar methods is the delay between sampling and measurement. This limits the number of samples that can be taken in any one shift. "Instant" radiation meters reduce the sampling and measurement cycle to a few minutes but may suffer from reduced accuracy, particularly at low levels of activity (Williamson, 1988). These instruments also involve the collection of radon daughters on filters and employ photomultiplier tubes and display units to indicate count rates. The Instant Working Level Meter (IWLM) gives gamma radiation in mRem/h as well as separate counts for alpha and beta radiation.

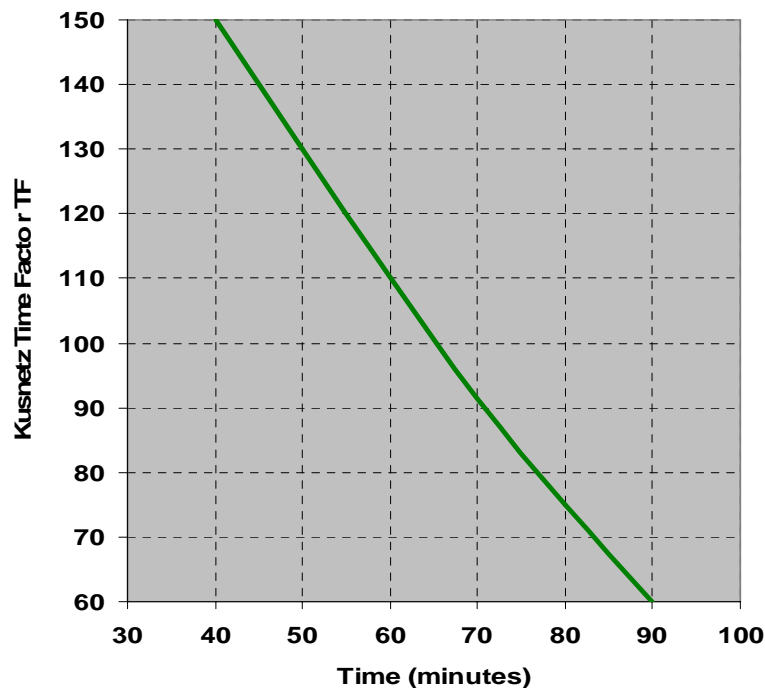


Figure 13.7 Time factors for the Kusnetz method.

13.5.2. Measurement of radon concentration

An early grab sample technique for measuring radon concentration is the **Lucas flask**. This is a lucite container whose sides and top are coated with zinc sulphide. To measure radon concentration the flask is first evacuated by a vacuum pump. Sample air is then admitted via a valve and filtered to remove radon daughters. The sample is allowed to age for about 3 hours in order to achieve secular equilibrium. A flash of light (photon emission) occurs when an alpha particle strikes the wall of the container. A window at the bottom of the flask is attached to a photomultiplier unit and a reading taken of the output count rate.

The radon concentration is given as

$$\frac{(C - b) TF}{FE \times 2.22 \times 3 \times CE \times V} \quad \frac{\text{pCi}}{\text{litre}} \quad (13.21)$$

where C = counts per minute
 b = counts per minute due to background radiation from the ambient surroundings
 TF = time factor (varies from 0.9762 at 2.5 hours to 1.0051 at 3.5 hours of elapsed time)
 FE = flask efficiency (given by flask manufacturer)
 2.2 = conversion of counts per minute to pCi (60×0.037 from equation (13.8))
 CE = counter efficiency (instrument factor)
 and V = volume of flask (litres)

The remaining constant of 3 arises from the fact that alpha emission occurs at three levels during decay from radon to RaD. This is shown on Figure 13.1. At secular equilibrium, the alpha emissions at each level are equal. As the instrument detects total alpha activity the result must be divided by 3 to give the concentration of radon alone (Calizaya, 1985).

Further developments have produced instruments suitable for continuous and integrating sampling over longer periods. These are useful in establishing variations and average values of radon concentrations at fixed locations.

13.5.3. Personal dosimeters

Radiation badges or personal dosimeters are designed to be attached to the clothing and provide a measure of the cumulative radiation dosage to which the wearer has been subjected. Thermoluminescent dosimeters (TLD) consist of four luminescent phosphors. At periods of one to three months each badge is processed by heating it to a given temperature. The amount of light emitted from each phosphor indicates the average levels and types of radiation to which the badge has been exposed. Another type of radon detector employs an element consisting of poly-allyl diglycol carbonate (PADC detector). A difficulty with personal detectors is that they may be incapable of distinguishing between the radon daughters which are the main radiation hazard in mines and other less harmful forms of radiation including the radon gas itself (Howes, 1990). They are also susceptible to changes in atmospheric pressure, temperature and humidity that are characteristic of subsurface environments.

Miniature versions of the pump and filtration units may prove to be more reliable than current radiation badges. However, these are likely to be cumbersome as well as expensive for routine use. Electronic dosimeters have also been developed for personal use (Bartlett, 1993). To this time, personal dosimeters have not found widespread use in subsurface workings.

13.6. CONTROL OF RADIATION IN SUBSURFACE OPENINGS

The control of radon and its daughters in underground mines should be addressed during the design of the mine layout, choice of mining method and in selecting mineral transportation routes as well as in planning the ventilation system. In this Section, we shall discuss the measures that may be taken to reduce the hazard of radiation in mines. The guidelines that are suggested have been established through a combination of practical observations and theoretical analyses. Although these guidelines can be followed without regard to theoretical background, their success is better assured if the ventilation engineer is familiar with the earlier sections in this chapter. The concepts of **aging** and **residence time** are particularly important. It follows that the need for rapid removal of radon and its daughters results in higher airflow requirements in uranium mines than for most other subsurface openings. The high operating costs that can ensue make it particularly important to design the ventilation system with a view to high efficiency and to employ the techniques of computer-assisted network analysis (Chapter 7). A further prerequisite is to obtain data on the geology of the area, rock surface emanation (*J*) rates and emanating powers of fragmented ore (*B*) (Section 13.3.1.).

13.6.1. Ventilation systems for uranium mines

Particular regard should be paid to the locations and dimensions of intake airways in uranium mines. The purpose is to deliver the intake air to stoping areas as free as practicable from radon or its daughters. There are three methods of achieving this objective. First, the intakes should be driven in the native rock and, as far as possible, not within the orebody. Such airways will be less subject to emanations of radon from the rock surfaces.

Secondly, the residence times of air in intake airways should be kept to a minimum. Air velocity limits normally accepted for the purposes of economics and dust control (Section 9.3.6.) are frequently exceeded in the intakes of uranium mines. Ventilation requirements for uranium mines are usually much higher than for other mines. Thirdly, where long intake airways are unavoidable, then even higher velocities may be necessary and consideration may be given to the use of airway liners. These are discussed further in Section 13.6.7.

Within the stoping areas, emphasis should, again, be placed on rapid air changes. Series ventilation should be avoided and when booster fans are used, particular care should be taken in the choice of their locations and duties in order to minimize recirculation. Uranium mines are a case in which systems of controlled partial recirculation should not be employed.

Pressure differentials across sealed old workings should be in a direction such that any leakage will pass into return airways and not into intakes. The "dirty pipe" principle may be used to advantage in the design of ventilation systems for uranium mines (Section 18.3.1.). The number of personnel required to work or travel in the return airways of uranium mines should be kept to a minimum.

In order to provide "young" air to the faces of headings in uranium mines, it is preferable to employ forcing systems of auxiliary ventilation. An exhaust overlap duct and filter may be added to deal with dust problems (Section 4.4.2.).

13.6.2. Dilution and mixing processes

At a constant rate of emission, the rise in concentration of non-radioactive gases is inversely proportional to the rate of through flow of fresh air (Section 9.3.1.). This is not the case for radon daughters because of the ongoing effects of radioactive decay. Equation (13.17) indicates that if an airway or stope is supplied with uncontaminated air and the rate of radon emanation remains

constant, then the exit working level of radon daughters is proportional to the residence time raised to the power 1.8, i. e.,

$$WL \propto (t_r)^{1.8} \quad (13.22)$$

where \propto means 'proportional to'.

This shows that if the airflow is halved and, hence, the residence time doubled, then the exit working level of radon daughters will increase by a factor of $2^{1.8} = 3.48$.

A more general relationship is gained by substituting

$$Q \propto \frac{1}{t_r} \text{ for a given airway geometry, where } Q = \text{airflow (m}^3/\text{s)}$$

giving

$$WL \propto \frac{1}{Q^{1.8}} \quad (13.23)$$

Then

$$\frac{WL_1}{WL_2} = \left(\frac{Q_2}{Q_1} \right)^{1.8} \quad (13.24)$$

Example 1

A mine opening is ventilated by an airflow of $10 \text{ m}^3/\text{s}$. The exit concentration of radon daughters is 0.9 WL . If this is to be reduced to 0.33 WL , determine the required airflow.

Solution

From equation (13.24)

$$Q_2 = Q_1 \left(\frac{WL_1}{WL_2} \right)^{\frac{1}{1.8}} = 10 \left(\frac{0.9}{0.33} \right)^{\frac{1}{1.8}} = 17.46 \text{ m}^3/\text{s}$$

Example 2

The radon daughter concentration leaving a mine section is 0.3 WL when the airflow is $15 \text{ m}^3/\text{s}$. A temporary obstruction caused by stocked materials reduces the airflow to $5 \text{ m}^3/\text{s}$. Determine the effect on the radon daughter concentration.

Solution

Equation (13.24) gives

$$WL_2 = WL_1 \left(\frac{Q_1}{Q_2} \right)^{1.8} = 0.3 \left(\frac{15}{5} \right)^{1.8} = 2.17 \text{ WL}$$

This is a dangerous concentration of radon daughters and illustrates the importance of maintaining adequate airflows at all times in a uranium mine.

It should be recalled that equation (13.24), upon which this method of estimating the effects of airflow is based, assumes that the air at entry to the opening is uncontaminated. This may not be the situation in practice and, indeed, experience has shown that the formula often underestimates the amount of air required (Rock and Walker, 1970).

When two airstreams of differing concentrations of radon daughters are mixed, then the resulting concentration is given simply as the weighted mean:

$$WL_{\text{mixture}} = \frac{\Sigma(Q \times WL)}{\Sigma Q} \quad (13.25)$$

Example 3

An airflow of 10 m³/s and radon daughter concentrations of 0.25 WL passes a seal from which issues a leakage flow of 0.3 m³/s at 150 WL. (Near stagnant air in sealed areas can reach very high concentrations of radon and its daughters.) Determine the radon daughter concentration in the downstream airflow.

Solution

From equation (13.25)

$$WL_{\text{mixture}} = \frac{(10 \times 0.25) + (0.3 \times 150)}{10.3} = 4.61 \quad \text{WL}$$

This example illustrates the dangerous levels of radiation that can arise from small leakages through abandoned areas.

13.6.3. Radiation surveys

The preceding section makes it clear that modifications to the airflow distribution and small leakages from old workings can have very significant effects on levels of radioactivity in mines subject to radon emanations. In order to ensure the continuity of acceptable conditions and to locate sources of contamination, it is useful to conduct radiation surveys. These involve taking measurements of radon and radon daughters, commencing at points of fresh air entry and tracing the primary ventilation routes through to mine exits. Figure 13.8 illustrates the type of results produced by a radiation survey.

Sampling Control stations may be selected at strategic locations in order to establish time-transient trends or to correlate radiation levels with mining activities. Permanent monitoring stations with recording and alarm facilities provide an even greater degree of Control (Bates and Franklin, 1977).

The degree of equilibrium between the measured concentrations of radon and radon daughters enables the "age" of the air to be established (Figures 13.5, 13.9 or equation (13.19)). High equilibrium levels ("old" air) measured along the airflow paths are indicative of inadequate ventilation, recirculation or leakage from old workings. Low equilibrium levels ("young" air) but with elevated concentrations of radon and radon daughters imply that high rates of radon emanation are occurring.

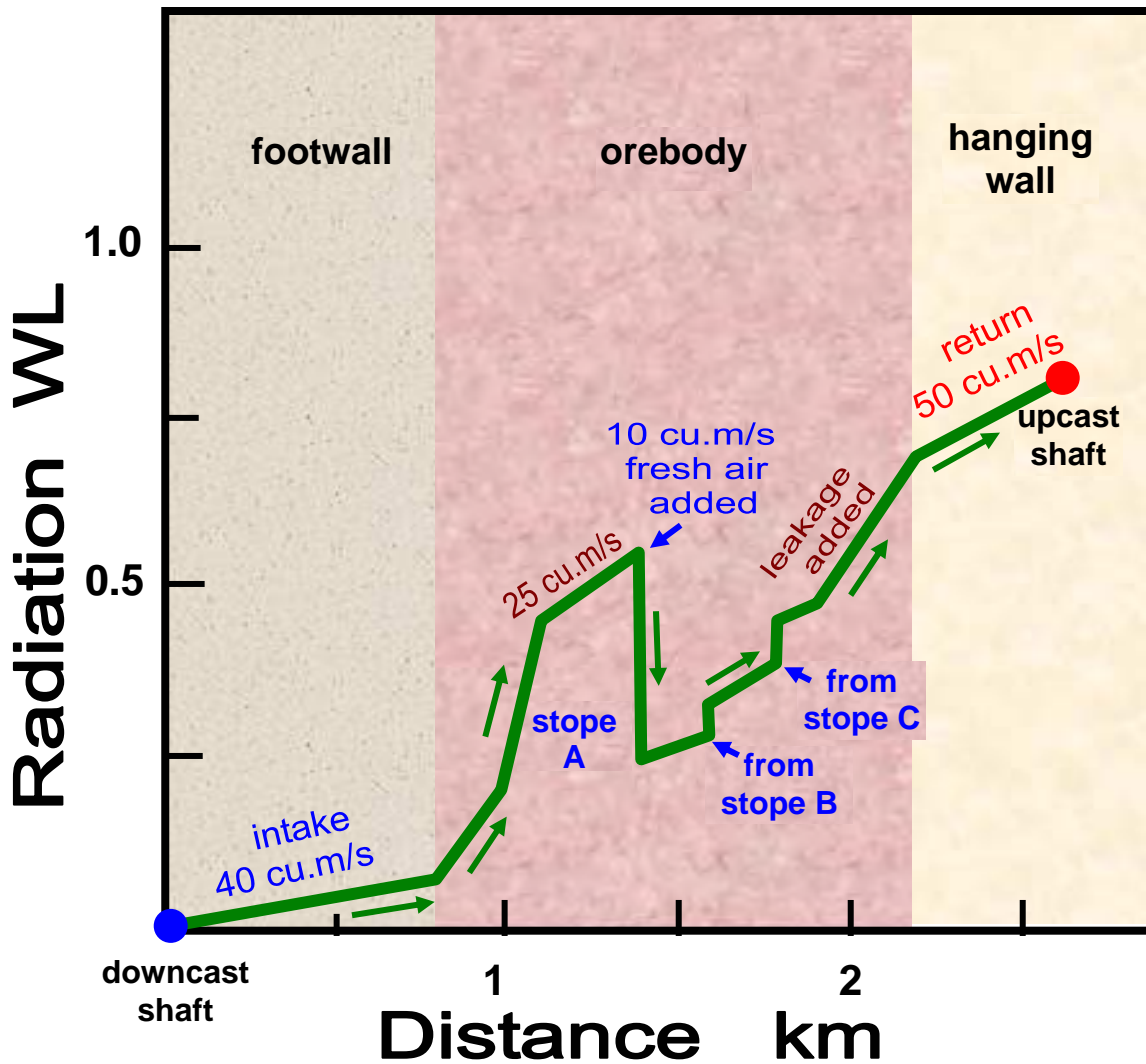


Figure 13.8 Example of a radiation profile produced from a radiation survey along a main ventilation route in a uranium mine. (Airways adding or subtracting air from the main route are not shown.)

13.6.4. Mining methods, mineral clearance and backfill

The choices of mine planning, stoping methods and operational procedures have a large influence on the severity of a mine radiation problem that must, subsequently, be handled by the ventilation system. In planning the extraction sequence, stoping areas should progress from the main exhaust airways towards the trunk intake zones. This strategy of retreat mining ensures that worked out areas and zones of fragmentation and voidage do not contribute towards the radioactive contamination of current workings. Leakages from abandoned areas pass directly into return airways.

Stoping methods should avoid systems that involve large areas of exposed ore, sluggish ventilation or high tonnages of fragmented rock. Hence, open or shrinkage stoping and caving techniques are not advisable in uranium mines. Peak emanations of radon occur during and after blasting. It is particularly important that adequate re-entry periods are employed for the clearance of blasting fumes and the associated radon daughters before personnel are allowed to return to the workings.

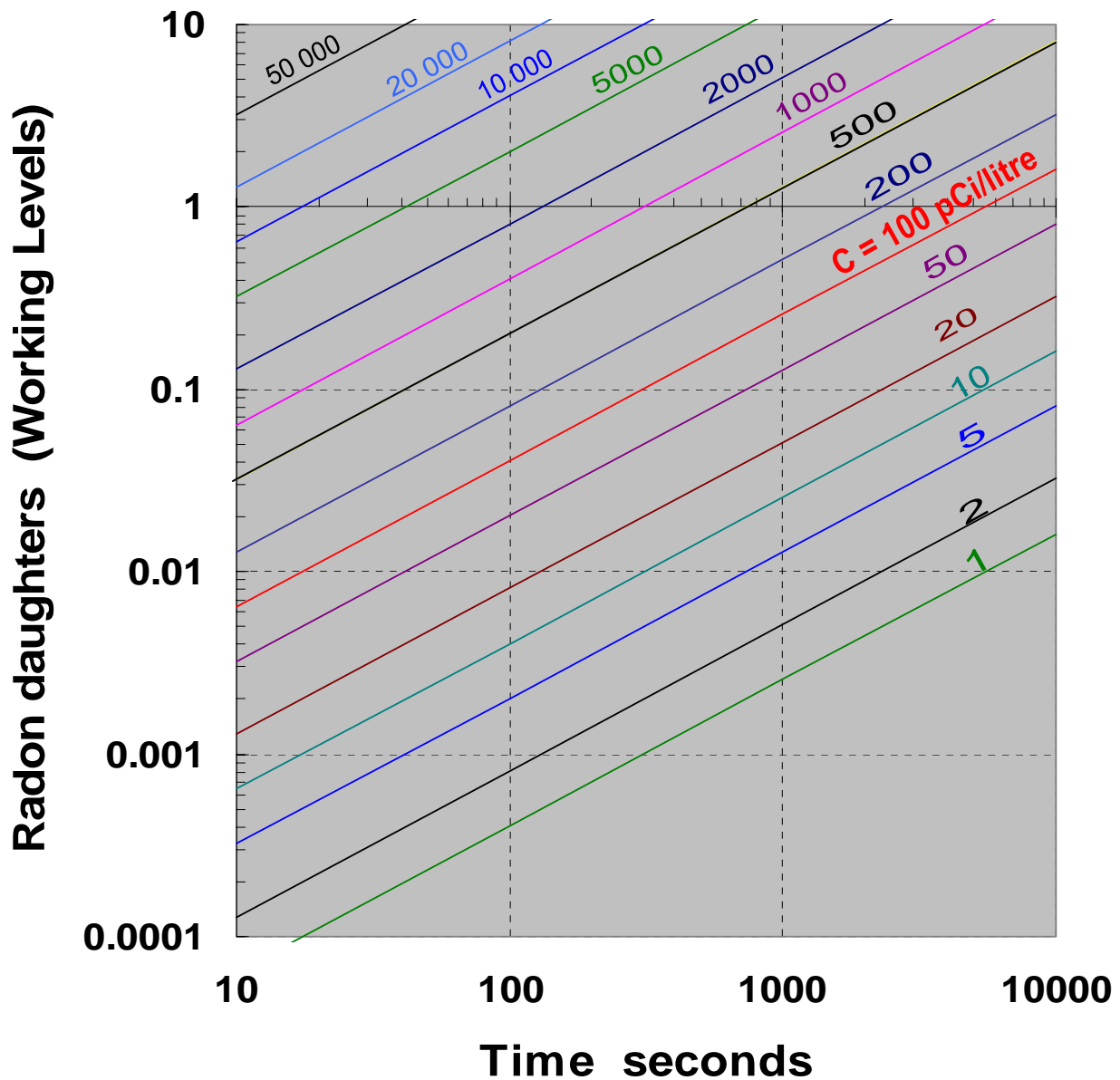


Figure 13.9 Growth of radon daughters as a function of time and radon concentration.

Piles of fragmented ore may produce high radiation levels, especially when they are disturbed by mucking operations. This can result in very large variations in radon daughter concentrations during a mining cycle. The broken ore should be transported from the mine as rapidly as practicable. Where some aeration of fragmented ore is unavoidable such as in orepasses or at transfer points, then consideration should be given to the use of exhaust hoods or air bypasses to route the contaminated air directly into a return airway. The number of ore handling operations within the mine should be kept as low as possible and out of main intake airways.

Haulage airways should be well maintained in order to avoid unnecessary comminution of the ore or spillage during transportation. Furthermore, the production of dust particles from uranium-bearing rocks will cause increased levels of radiation (Bigu and Grenier, 1985). The settlement of

such dust particles within subsurface airways produces an escalating source of radon. Dust suppression by water sprays or filters is particularly important in uranium mines (but refer to Section 13.6.6 for the effects of water vapour on emanating surfaces).

Localized peaks of radon emanation may occur during drilling operations either for blasting or for orebody exploration. Consideration should be given to the location of machine operators. Long exploration holes should be sealed. Blasting patterns for developments should be selected to minimize the overbreak envelope of fractured rock around the opening. The induced fracture network within this envelope produces additional surface area for radon emanation as well as enhancing the inflow of radon-contaminated groundwater. Good strata control techniques including rock bolting and other support methods will help to minimize radon emanations.

In addition to controlling ground movement, the employment of backfill material will reduce leakage flows through old workings. Both of these features are particularly important in uranium mines. However, tests should be carried out on the radon emanation characteristics of the fill material itself, particularly when it contains mill tailings. Freshly placed wet fill may emanate radon gas at about twice the rate of the consolidated fill (Bates and Franklin, 1977; Thompkins, 1982). The addition of cement to the fill material can result in a reduction of the radon emanation rate. If backfilling operations produce a significant amount of radon, then care should be taken to ensure that the contaminated air is exhausted into return airways.

13.6.5. Contamination from abandoned workings

Example 3 in Section 13.6.2. illustrates the high level of radioactive contamination that can occur in uranium mine ventilation systems when slight leakage occurs from abandoned areas or unventilated blind headings. The near stagnant air in such zones achieves a high concentration of radon at secular equilibrium with the radon daughters (fully aged). Radon concentrations of many thousands of pCi/litre may occur behind seals in uranium mines. It becomes particularly important that barrier seals in uranium mines should be constructed and maintained to a high standard. The faces of stoppings and adjoining rock walls may be coated with additional sealant material (Section 13.6.7.). However, minor transients in atmospheric pressure can cause "breathing" through seals and stoppings, resulting in peak emanations of radon and radon daughters during periods of falling barometric pressure (Section 4.2.2.).

Such effects occur not only from sealed areas of the mine but also from fracture networks and other voidages within the strata. Attempts have been made to modify mine atmospheric pressures by fan control in uranium mines such that air pressures are elevated during working shifts and depressed when few or no persons are underground (Schroeder et al, 1966; Bates and Franklin, 1977). Leakages from sealed areas can be controlled by pressure balance chambers (Section 21.5.5.) which maintain pressure differentials across seals at near zero. Another technique is to employ a bleed pipe that connects the sealed area to a main return airway or through a vertical borehole to surface. The sealed zone can be maintained at sub-atmospheric pressure by employing a low capacity extractor pump or fan within the bleed pipe. Leakage into the sealed area then remains safely in an inward direction. In the absence of these pressure control techniques, a small pressure differential should be maintained across the sealed area such that any leakage that occurs will be into return airways.

13.6.6. The influence of water

The emanation of radon from mineral crystals into the pores of a rock will be essentially the same whether the interstices are filled with air or water. However, any migration of the groundwater can provide a transport mechanism for the dissolved radon that is more efficient than diffusion of the gas through a dry rock. When the water reaches a mine opening it will yield up its dissolved radon very readily, particularly if the water is aerated by spraying or dripping into the airway. It is

prudent to capture such water into pipes as soon as possible in uranium mines and minimize its exposure to the air.

In permeable wet strata, the emanation of radon can be reduced significantly by pre-draining the area. This may be achieved by pumping from a ring of drainage boreholes. Better results can be obtained by driving drainage levels below the stopping areas prior to mining. The effectiveness of this technique can be further enhanced by boreholes drilled into the strata from the drainage levels. In severe cases, the flow of water into development headings can be reduced by grouting.

Radioactive decay of the radon occurs whether it is contained within air or water. Hence, the concentration of radon in groundwater depends upon the elapsed time since the gas was emitted from mineral crystals into the water-filled interstices. Mine water that contains dissolved radon should not be used for dust suppression sprays. However, if it is first brought to the mine surface and aerated, then the radon content may be diminished to a level that renders the water suitable for dust suppression.

Experimental observations indicate that commencing with dry rock, radon emanations can increase dramatically as the moisture content of the rock increases (Bates and Franklin, 1977). A similar effect occurs from raising the moisture content of the air that is in proximity to rock surfaces. However, as the rock or air approaches saturation, the effect diminishes and radon emanations fall when liquid water appears on the rock surface. The mechanisms that produce these phenomena appear not to be clearly understood. It is thought that displacement of adsorbed radon by water molecules on mineral surfaces may explain the initial increase in emanation rates, while the later inhibition of radon release may be due to the interstices near the surface becoming filled with liquid water.

13.6.7. Air filters and rock surface liners

As radon daughters are particulates, a large proportion of them can be removed by passing the air through high efficiency dust filters. These should be capable of removing at least 95 percent of particles 0.3 microns in size. As such filters are relatively expensive and can rapidly become blocked in mining conditions, fibreglass prefilters may be used to remove the coarser particles and, hence, improve the life of the high efficiency filters (Rock and Walker, 1970). The latter are also affected adversely by humid conditions. The pressure drop across filters can be monitored to indicate when renewal or cleaning has become necessary.

The major drawback to filters is that they do not remove the radon gas that continues to replenish radon daughters. The filtered air must be supplied quickly to the personnel who are to be protected. Figure 13.9 or equation (13.15) show that even if perfect filtration of particulates is achieved, a radon concentration of 100 pCi/litre will generate 0.3 WL of radon daughters in 1218 seconds (20.3 minutes). However, if the radon concentration is 500 pCi/litre, then 0.3 WL of radon daughters will appear in only 163 seconds (2.7 minutes) after filtration. Filters for radon daughters are perhaps most effective for forcing duct systems supplying rejuvenated air to headings.

Activated charcoal can remove radon gas from air. At the present time, large scale applications appear to be impractical. However, gas masks with activated charcoal filters can be used to protect personnel who are required to venture into high radon and radon daughter concentrations for a short time.

A number of trials have been carried out into the use of sprayed coatings and film membranes to reduce radon emanations into mine openings. These are unlikely to replace good ventilation as the primary means of combatting the radon problem. However, they can have an application in long intakes driven in high grade ore or permanent work places such as workshops. Liquid sprays are suitable for application on rock surfaces while membranes may be attached to the faces of

stoppings. Grouting of the rock envelope with or without rock bolting can also be effective in reducing inflows of both radon and water.

Tests conducted by the U. S. Bureau of Mines investigated the ability of a range of polymer sealants to resist the passage of radon (Bates and Franklin, 1977). The permeability of a material with respect to air has little bearing on its resistance to radon gas. The latter is a monatomic gas that will diffuse through most substances. Furthermore, any lining material intended for use in mines should have low toxicity and flammability both during application and after curing has been completed. Additionally, it should be convenient to apply, inexpensive and not productive of smoke or toxic fumes when heated. These stringent requirements limit the use of radon barriers in practice.

The U. S. Bureau of Mines tests indicated that water-based epoxies were suitable for application to rock surfaces. However, two spray applications are recommended, the first with a low viscosity liquid to penetrate surface interstices, and the second with a thicker fluid to seal visible fractures. Using differing colours for the two applications assists in achieving full coverage.

Further tests in Canada indicated that a polysulphide copolymer spray and aluminized mylar sheeting were both capable of reducing radon diffusion through a bulkhead by more than 95 percent (Archibald and Hackwood, 1985). Additional data on the permeability of membranes to radon is given by Jha et al (1982).

13.6.8. Education and training

Radon gas and radon daughters are a particularly insidious hazard. They are invisible, odourless and can be detected only by specialized instruments. Furthermore, they have no short term observable effects on the human body. It becomes particularly important that all workers in affected environments should be made aware of the health hazards associated with radon and the steps that can be taken to alleviate the problem. Booklets, videotapes and classroom teach-ins are particularly effective. These should emphasize the importance of a brisk throughflow of air and the hidden dangers that may arise from recirculation, damaged stoppings or ventilation doors left open.

References

Archibald, J.F. et al (1980). Determination of radiation levels to be encountered in underground and open-pit uranium mines. 2nd Int. Congress on Mine Ventilation. Reno, Nevada pp 399-404.

Archibald, J. F. and Hackwood, H. J. (1985). Membrane barriers for radon gas flow restriction, 2nd U. S. Mine Ventilation Symposium, Reno, Nevada, pp. 251-257

Bartlett, D.T. (1993). Electronic Dosemeters: Use in personal dosimetry. Radiation protection Dosimetry, Vol. 47, No. 1, pp 335-339. Oxford University Press.

Bates, R. C. and Edwards, J. C. (1980). Mathematical modeling of time dependent radon flux problems, 2nd Int. Congress on Mine Ventilation, Reno, Nevada, pp 412-419.

Bates, R. C. and Franklin, J. C. (1977). U.S. Bureau of Mines Radiation Control Research, Conf. on Uranium Mining Technology, Reno, Nevada.

Bigu, J. and Grenier, M. G. (1985). Characterization of radioactive dust in Canadian underground uranium mines, 2nd U. S. Mine Ventilation Symp., Reno, Nevada, pp 269-277.

Calizaya, F. (1991). Private communication.

Calizaya, F. (1985). Control study of the evolution of radon and its decay products in radioactive mine environments, Ph. D. thesis, Colorado School of Mines.

CFR. (1990) US Code of Federal Regulations, Vol. 30 (Mineral Resources), Part 57, Metallic and non-metallic underground mines, US Govt. Printing Office, Washington, D. C.

Howes, M. J. (1990). Exposure to radon daughters in Cornish tin mines, Trans. Inst. of Mining & Metallurgy, U. K., Vol. 99, pp A85-A90.

Jha, G. et al (1982). Radon permeability of some membranes. Health Physics, Vol. 42, 5, pp 723-725.

Kusnetz, H. L. (1956). Radon daughters in mine atmospheres -a field method for determining concentrations, Ind. Hygiene Quart., March, pp 85-88.

Rock, R. L. and Walker, D. K. (1970). Controlling employee exposure to alpha radiation in underground uranium mines, U. S. Bureau of Mines, U. S. Government Printing Office, Washington, D. C.

Schroeder, G. L. and Evans, R. D. (1969). Some basic concepts in uranium mine ventilation, Trans. AIME, Vol. 244, pp 301-307.

Schroeder, D. L. et al (1966). Effect of applied pressure on the radon characteristic of an underground mine environment, Trans. AIME, Vol. 235, pp 91-98.

Thompkins, R. W. (1985). The safe design of a uranium mine, 2nd US Mine Ventilation Symp., Reno, Nevada, pp 289-294.

Thompkins, R. W. (1982). Radiation in uranium mines, CIM Bulletin, Vol. 75, Nos. 845, 846, 847.

Williamson, M. J. (1988). The exposure of mining personnel to ionizing radiations in Cornish tin mines, 4th Inst. Mine Ventilation Congress, Brisbane, Australia, pp 585-592.

Part 4

Heat and Humidity

CHAPTER 14. PSYCHROMETRY: THE STUDY OF MOISTURE IN AIR

14.1. INTRODUCTION	2
14.2. BASIC RELATIONSHIPS.....	3
14.2.1. Basis of measurement	3
14.2.2. Moisture content (specific humidity) of air	4
14.2.3. Saturation vapour pressure	5
14.2.4. Gas constant and specific heat (thermal capacity) of unsaturated air.....	7
14.2.5. Specific volume and density of unsaturated air	8
14.2.6. Relative humidity and percentage humidity	9
14.3 THE MEASUREMENT OF WATER VAPOUR IN AIR	11
14.3.1. Chemical methods	11
14.3.2. Electrical methods (electronic psychrometers or humidity meters)	11
14.3.3. Hair hygrometers	11
14.3.4. Dew point hygrometers	12
14.3.5. Wet and dry bulb hygrometers (psychrometers)	12
14.4. THEORY OF THE WET BULB THERMOMETER.....	13
14.4.1. Heat balance on a wet bulb	14
14.4.2. Determination of moisture content and vapour pressure from psychrometer readings	15
14.5. FURTHER PSYCHROMETRIC RELATIONSHIPS	17
14.5.1. Enthalpy of moist air	17
14.5.2. The adiabatic saturation process	19
14.5.3. Sigma Heat, S	20
14.6. SUMMARY OF PSYCHROMETRIC EQUATIONS	21
14.7. DEVIATIONS FROM CLASSICAL THEORY	22
14.7.1. Fogged air	22
14.7.2. Imperfect gas behaviour	23
14.8. PSYCHROMETRIC CHARTS.....	24
References	28
APPENDIX A14	29
Derivation of the Clausius-Clapeyron equation.....	29

14.1. INTRODUCTION

Around the surface of the earth, air that is not affected by any local source of pollution has a composition that is remarkably constant. Air analyses are usually carried out on samples from which all traces of water vapour have been removed. The moisture-free composition of air is given on both a volume and mass basis in Table 14.1. Argon forms the largest fraction, by far, of the monatomic gases. The value of the molecular weight given is, in fact, that for argon.

Gas	Volume per cent	Mass per cent	Molecular weight
Nitrogen	78.03	75.46	28.015
Oxygen	20.99	23.19	32.000
Carbon Dioxide	0.038 ¹	0.05	44.003
Hydrogen	0.01	0.0007	2.016
Monatomic gases	0.94	1.30	39.943
Equivalent molecular weight of dry air			28.966

Table 14.1 Composition of dry air

However, there is another gas present in the free atmosphere, water vapour, that is rather different to the others in that its concentration varies widely from place to place and with time. This is because the pressures and temperatures that exist within the blanket of air that shrouds our planet also encompass the ranges over which water may exist in the gaseous, liquid or solid forms - hence the appearance of clouds, rain, snow and ice. Evaporation of water, mainly from the oceans, coupled with wind action, produce and transport water vapour through the atmosphere. Increases in pressure or, more effectively, decreases in temperature may result in condensation of the water vapour to form clouds which, in turn, can produce droplets large enough to be precipitated as rain, snow or hail.

On other planets with very different atmospheres and gravitational fields, similar phase changes occur in other gases. Because of its variable concentration within the earth's atmosphere, airborne water has become the subject of a special study, psychrometry.

Changes of phase are particularly important within the confines of closed environments, including subsurface ventilation systems. Ice to liquid and ice to vapour phase changes occur in mines located in cold climates and, particularly, if situated in permafrost. However, the vast majority of humidity variations that occur in underground airflows are caused by the evaporation of liquid water or the condensation of water vapour. This chapter concentrates on the phase changes between liquid water and water vapour. Virtually all mines produce water from the strata and/or dust suppression techniques. Even with the hygroscopic minerals of evaporite mines, the water vapour content in return airways is normally higher than that in the intakes.

Subsurface environmental engineers have a particular interest in psychrometry for two reasons. First, if we are to comprehend fully the thermodynamic processes that occur in ventilation circuits then variations in humidity must be taken into account. For example, strata heat may be emitted into a wet airway without there being a corresponding increase in air temperature. This could occur if all the added heat were utilized in exciting some of the water molecules until their kinetic energy exceeded the attractive forces of other molecules in the liquid water. They would then escape through the liquid/air surface and become airborne as a gas. The process of evaporation

¹ The concentration of atmospheric carbon dioxide varies with both location and time. At the time of writing, the average global concentration is increasing at about 0.00016 percent per year

increases the energy content of the air/vapour mixture. This may be termed a **latent** (or hidden) rise in the heat content of the air as there is no commensurate increase in temperature and, hence, no indication on an ordinary thermometer.

Alternatively, if there were no liquid water present, then the strata heat would be directed immediately to the airstream, causing a temperature rise of the air that would be sensed by a thermometer. This is an increase in the **sensible heat** of the air.

These examples illustrate that if we are to predict quantitatively the climatic effects of strata heat, water inflows, machines or air coolers, then we need to have methods of analysis that take humidity into account.

The second reason for the study of psychrometry is the effect of heat and humidity on the human body. This is examined in detail in Chapter 18. However, for the time being, we will concentrate on developing means of quantifying the psychrometric relationships that enable predictions to be made of temperature and other climatic variables in the environment.

14.2. BASIC RELATIONSHIPS

Most of the psychrometric equations that are used in practice are based on the premise that air is a mixture of perfect gases and that the air itself behaves as a perfect gas. Within the ranges of temperatures and pressures that are reasonable for human tolerance, this assumption gives rise to acceptable accuracy. The majority of this chapter assumes perfect gas laws. However, in certain areas of some underground facilities, (including possible future mining scenarios) the atmosphere will require control, but not necessarily within physiologically acceptable ranges. For this reason, more accurate relationships are included that take some account of deviations from the perfect gas laws.

14.2.1. Basis of measurement

A question that should be settled before embarking on a quest for psychrometric relationships is how best to express the quantity of water vapour contained within a given airstream. As we saw in Chapter 3, it is preferable to conduct our analyses on a mass (kg) basis rather than volume (m^3), as variations in pressure and temperature cause the volume of the air to change as it progresses through a ventilation system. That choice relied upon the assumption that the mass flow of air remained constant along a single airway. Now we are faced with a different situation. The addition of water vapour to an airstream through evaporative processes, or its removal by condensation, result in the mass flow of the air/vapour mixture no longer remaining constant.

Within the mixture, molecules of water vapour coexist with, and occupy the same volume, as the nitrogen, oxygen and other gases that comprise the air. We can assume, however, that in the absence of chemical reactions or the addition of other gases, it is only the concentration of water vapour that varies, due to evaporation and condensation. The mass flow of the rest of the air remains constant.

It is a convenient, although somewhat artificial, device to consider the air to be divided into a fixed mass of "dry air" and an associated but variable mass of water vapour. For most purposes, we can then refer to the moisture content in terms of grams or kilograms of water vapour per kilogram of "dry air". Occasionally, we may use the alternative measure of grams or kilograms of vapour per kilogram of the real mixture of air and vapour. Throughout this chapter we shall use the term "air" to mean the actual mixture of air and water vapour, and "dry air" for that fraction which does not include the water vapour. Hence, a moisture content of 0.02 kg/kg dry air means that in each 1.02 kilograms of air, 0.02 kilograms are water vapour and 1 kilogram is "dry air".

14.2.2. Moisture content (specific humidity) of air

In order to quantify the mass of water vapour associated with each kilogram of "dry air", let us conduct an imaginary experiment.

Suppose we have a closed vessel of volume $V \text{ m}^3$ containing 1 kg of perfectly dry air at a pressure P_a Pascals and temperature T degrees Kelvin. If we inject X kg of water vapour at the same temperature, the pressure within the vessel will increase to:

$$P = P_a + e \quad \text{Pa}$$

where e is the partial pressure exerted by the water vapour (Dalton's law of partial pressures for perfect gases). Both the air and the water vapour occupy the same volume, V , and are at the same temperature, T .

The problem is to determine the mass of water vapour, X , if we can measure nothing more than the initial and final pressures, P_a and P .

From the general gas law:

(i) for the X kg of water vapour:

$$eV = X R_v T \quad \text{Joules (J)} \quad (14.1)$$

where $R_v =$ gas constant for water vapour (461.50 J/kg K), and

(ii) for the original 1 kg of dry air,

$$P_a V = 1 \times R_a T \quad \text{J} \quad (14.2)$$

where $R_a =$ gas constant for dry air (287.04 J/kg K)

Dividing equation (14.1) by (14.2) gives

$$\frac{e}{P_a} = \frac{R_v}{R_a} X$$

However, the absolute (barometric) pressure in the vessel is

$$P = P_a + e$$

Hence,

$$X = \frac{R_a}{R_v} \frac{e}{(P - e)} \quad (14.3)$$

Inserting the values of the gas constants gives

$$X = 0.622 \frac{e}{(P - e)} \quad \frac{\text{kg}}{\text{kg dry air}} \quad (14.4)$$

This gives the moisture content of the vessel in kg per kg of dry air, provided that the partial pressure of the water vapour, e , can be evaluated. This is, of course, simply the difference between the initial and final absolute pressures. However, e can be determined independently, as we shall see a little later in the chapter.

14.2.3. Saturation vapour pressure

Returning to our experiment, suppose we continue to inject water vapour. The partial pressure of water vapour (and, hence, the absolute pressure in the vessel) will continue to rise - but only to a certain limiting value. The partial pressure of the dry air fraction, P_a , will remain constant. If we insist upon forcing yet more vapour into the system while keeping the temperature constant, then the excess will condense and collect as liquid water on the sides and bottom of the vessel. (It is, in fact, possible to achieve a condition of supersaturation in the laboratory but that will not occur in natural atmospheres and is not considered here).

When the system refuses to accept any more water vapour then we say, rather loosely, that the air has become saturated. In fact, it is not the air but the space that has become saturated. If we were to repeat the experiment starting with the vessel evacuated and containing no air then exactly the same amount of vapour could be injected before condensation commenced, provided that the temperature remained the same.

The pressure, e_s , exerted by the water vapour at saturation conditions depends only upon temperature and not upon the presence of any other gases. The relationship between saturation vapour pressure and temperature for water has been determined not only experimentally but also through thermodynamic reasoning by a number of authorities. The tables of **Goff and Gratch** produced in 1945 are still regarded as a standard. The simplest analytical equation is known as the **Clausius-Clapeyron equation**.

$$\frac{1}{e_s} \frac{de_s}{dT} = \frac{L}{R_v T^2} \quad \text{K}^{-1} \quad (14.5)$$

where the **latent heat of evaporation**, L (J/kg) is the heat required to evaporate 1 kg of water.

The derivation of the **Clausius-Clapeyron equation** is given in the Appendix A14 at the end of the chapter. This equation is based on the perfect gas laws and must, therefore, be regarded as an approximation. Furthermore, the latent heat of evaporation, L , is not constant. The higher the initial temperature of the liquid water then the less will be the additional heat required to evaporate it. The relationship between latent heat of evaporation and temperature is near linear.

The equation

$$L = (2502.5 - 2.386 t) 1000 \quad \text{J/kg} \quad (14.6)$$

(where temperature, t , is in degrees Centigrade)

is accurate to within 0.02 per cent over the range 0 to 60 °C.

The equation may also be written as

$$L = (3154.2 - 2.386 T) 1000 \quad \text{J/kg} \quad (14.7)$$

where the temperature T is in degrees Kelvin.

The Clausius Clapeyron equation can be integrated over any given interval

$$\int_1^2 \frac{de_s}{e_s} = \frac{1}{R_v} \int_1^2 \frac{(a - bT)}{T^2} dT$$

where $a = 3\,154\,200$ J/kg and $b = 2386$ J/kg K from equation (14.7).

Integrating gives

$$\ln\left(\frac{e_{s2}}{e_{s1}}\right) = \frac{1}{R_v} \left\{ a \left[\frac{1}{T_1} - \frac{1}{T_2} \right] + b \ln\left(\frac{T_1}{T_2}\right) \right\}$$

giving

$$e_{s2} = e_{s1} \exp \left[\frac{1}{R_v} \left\{ a \frac{(T_2 - T_1)}{T_1 T_2} + b \ln\left(\frac{T_1}{T_2}\right) \right\} + \right] \quad \text{Pa} \quad (14.8)$$

If the saturation vapour pressure, e_{s1} , at any given temperature, T_1 , is known, then equation (14.8) allows the saturation vapour pressure, e_{s2} , at any other temperature, T_2 , to be calculated. At 100°C, the saturation vapour pressure is one standard atmosphere (101.324 kPa) by definition (Section 2.2.3). Hence, this may be used as a starting point for the integration.

There are two problems with equation (14.8). First, it is cumbersome for rapid calculation and, secondly, the assumption of perfect gas behaviour in its derivation introduces some uncertainty. The latter is not serious. Integrating down from a vapour pressure of 19.925 kPa at 60 °C and using equation (14.8) gives a maximum error of only 0.52 per cent over the range of 0 to 60 °C. Nevertheless, we can do much better and simplify the format of the relationship at the same time.

Let us take temperature T_1 to be the freezing point of water, 273.15 K or 0°C. Then temperature T_2 may be expressed in degrees Centigrade as

$$t = (T_2 - 273.15) \quad \text{°C}$$

$$\text{or} \quad T_2 = (t + 273.15) \quad \text{K}$$

Furthermore, the logarithmic term in equation (14.8) can be rewritten as

$$\ln\left[\frac{T_1}{T_2}\right] = \ln\left[1 + \frac{(T_1 - T_2)}{T_2}\right] = \ln\left[1 - \frac{t}{T_2}\right]$$

Expanding from the logarithmic series for the condition where t is much less than T_2 gives the term as approximately $(-t/T_2)$.

Substituting into equation (14.8), simplifying and gathering constants together gives the form

$$e_{s2} = A \exp\left[\frac{Bt}{C + t}\right] \quad \text{Pa} \quad (14.9)$$

where A, B and C are constants.

Curve fitting from the standard tables of Goff and Gratch over the range 0 to 60°C gives the widely used equation:

$$e_{s2} = 610.6 \exp\left[\frac{17.27t}{237.3 + t}\right] \quad \text{Pa} \quad (14.10)$$

This is accurate to within 0.06 percent over the given range.

For the more usual mining range of 10 to 40°C the curve fitting procedure gives

$$e_{s2} = 610.162 \exp\left[\frac{17.291t}{237.481 + t}\right] \quad \text{Pa} \quad (14.11)$$

having an excellent accuracy of within 0.01 per cent for that range.

Example

Find the saturation vapour pressure at a temperature of 30°C.

Solution

(i) Inserting $t = 30$ °C into equation (4.10) gives $e_s = 4241.7$ Pa or 4.2417 kPa

This is in error by 0.026 percent when compared with the value of 4.2428 kPa given by the Goff and Gratch tables.

(ii) Using equation (4.11) gives $e_s = 4.2431$ kPa, having an error of only 0.007 percent.

14.2.4. Gas constant and specific heat (thermal capacity) of unsaturated air

From the gas laws for 1 kg of dry air and X kg of associated water vapour, we have

$$\begin{aligned} P_a V &= 1 R_a T \\ \text{and } e V &= X R_v T \end{aligned}$$

Adding these two equations gives

$$(P_a + e) V = (R_a + X R_v) T$$

$$\text{or } PV = (R_a + X R_v) T \quad \text{J/kg} \quad (14.12)$$

Alternatively, we can treat the $(1 + X)$ kg of air/vapour mixture as a perfect gas having an equivalent gas constant of R_m . Then

$$PV = (1 + X) R_m T \quad \text{J/kg} \quad (14.13)$$

Equating (14.12) and (14.13) gives

$$R_m = \frac{(R_a + X R_v)}{(1 + X)} \quad \text{J/(kg K)} \quad (14.14)$$

Hence, we have shown that the gas constant for the moist air is given simply by adding the gas constants for dry air, R_a , and water vapour, R_v , in proportion to the relative masses of the two components.

The equivalent gas constant for moist air can also be expressed in terms of pressures by substituting for X from equation (14.4), leading to

$$R_m = 287.04 \frac{P}{(P - 0.378e)} \quad \text{J/(kg K)} \quad (14.15)$$

Similarly, the equivalent specific heat (thermal capacity) of moist unsaturated air can be found by adding the specific heats of the two components in proportion to their masses. The specific heat at constant pressure becomes

$$C_{pm} = \frac{(C_{pa} + XC_{pv})}{(1 + X)} \quad \text{J/(kg K)} \quad (14.16)$$

where C_{pa} = Specific heat of dry air at constant pressure (1005 J/kg K)
and C_{pv} = Specific heat at constant pressure for water vapour (1884 J/kg K).

Also, the specific heat of moist air at constant volume is given as

$$C_{vm} = \frac{(C_{va} + XC_{vv})}{(1 + X)} \quad \text{J/(kg K)} \quad (14.17)$$

where C_{va} = Specific heat of dry air at constant volume (718 J/(kg K))
and C_{vv} = Specific heat of water vapour at constant volume (1422 J/(kg K)).

14.2.5. Specific volume and density of unsaturated air

The actual specific volume of moist unsaturated air, V_m , can be calculated from the general gas law for 1 kg of the air/vapour mixture:

$$V_m = R_m \frac{T}{P}$$

Substituting for R_m from equations (14.14) and (14.15) gives

$$V_m = \frac{(R_a + XR_v) T}{(1 + X) P} \quad \text{m}^3/\text{kg of moist air} \quad (14.18)$$

$$\text{and } V_m = 287.04 \frac{T}{(P - 0.378e)} \quad \text{m}^3/\text{kg of moist air} \quad (14.19)$$

In these equations, T is in degrees Kelvin and P in Pascals.

As we saw in section 14.2.1 it is more convenient, for most purposes, to conduct our analyses on the basis of 1 kg of “dry air” rather than a kilogram of the true mixture. The **apparent specific volume**, based on 1 kg of dry air is simply

$$V_m (\text{apparent}) = 287.04 \frac{T}{(P - e)} \quad \text{m}^3/\text{kg of dry air} \quad (14.20)$$

The actual density of the moist air, ρ_m , is the reciprocal of the actual specific volume

$$\rho_m = \frac{(1 + X) P}{(R_a + XR_v) T} \quad \text{kg moist air/m}^3 \quad (14.21)$$

$$\text{or } \rho_m = \frac{(P - 0.378e)}{287.04T} \quad \text{kg moist air/m}^3 \quad (14.22)$$

A useful approximate formula to calculate the effect of moisture on air density can be derived from equation (14.21) giving

$$\rho_m = \frac{P}{R_a T} (1 - 0.608 X) \quad \text{kg moist air/m}^3 \quad (14.23)$$

This equation makes clear that the density of air decreases as its moisture content rises.

The **apparent density**, based on 1 kg of dry air, is the reciprocal of equation (14.20).

$$\rho_m (\text{apparent}) = \frac{(P - e)}{287.04T} \quad \text{kg of dry air/ m}^3 \quad (14.24)$$

14.2.6. Relative humidity and percentage humidity

Relative humidity is widely used by heating and ventilating engineers as an important factor governing comfort of personnel in surface buildings. In open surface areas or in through-flow subsurface facilities, its use as a physiological parameter is very limited and can be misleading, owing to the wider range of air temperatures that may be encountered (see, also, Chapter 18). On the other hand, the concept of relative humidity, rh , is a convenient way of expressing the degree of saturation of a space. It is defined as

$$rh = \frac{e}{e_{sd}} \times 100 \quad \text{percent} \quad (14.25)$$

where e_{sd} = saturation vapour pressure at the air (dry bulb) temperature.

This definition indicates that relative humidity is the ratio of the prevailing vapour pressure to that which would exist if the space were saturated at the same temperature. A similar concept is that of **percentage humidity**, ph , defined as

$$ph = \frac{X}{X_{sd}} \times 100 \quad \text{percent} \quad (14.26)$$

where X_{sd} is the moisture content (kg/kg dry air) that would exist if the space were saturated at the same dry bulb temperature.

Percentage humidity is approximately equal to relative humidity over the normal atmospheric range. Substituting from equation (14.4) gives

$$\begin{aligned} ph &= \frac{X}{X_{sd}} = \frac{e}{(P - e)} \frac{(P - e_{sd})}{e_{sd}} \times 100 \\ &= rh \times \frac{(P - e_{sd})}{(P - e)} \end{aligned}$$

As P is much larger than e or e_{sd} over the normal atmospheric range, the bracketed terms are near equal.

Example

An airstream of temperature 20°C and barometric pressure 100 kPa is found to have an actual vapour pressure of 1.5 kPa.

Determine (i) the moisture content of the air, X
(ii) the gas constant, R_m
(iii) the specific heat, C_{pm}
(iv) the actual and apparent specific volumes
(v) the actual and apparent densities
(vi) the relative humidity, rh
and (vii) the percentage humidity, ph

Solution

(i) *moisture content, X :*

$$X = 0.622 \frac{1.5}{(100 - 1.5)}$$

$$= 0.009472 \quad \text{kg vapour/kg dry air} \quad \text{or} \quad 9.472 \text{ g/kg dry air.}$$

(ii) *gas constant:*

From equation (14.15) $R_m = \frac{287.04 \times 100}{100 - (0.378 \times 1.5)} = 288.68 \text{ J/kg K}$

(iii) *specific heat, C_{pm}*

From equation (14.16)

$$C_{pm} = \frac{(1005 + 0.009472 \times 1884)}{(1 + 0.009472)} = 1013 \text{ J/kg K}$$

(iv) *specific volumes:*

From equation (14.19), Actual specific volume:

$$V_m = \frac{287.04(273.15 + 20)}{1000(100 - 0.378 \times 1.5)} = 0.8463 \text{ m}^3/\text{kg moist air}$$

(the 1000 in the denominator is necessary to convert the pressures from kPa to Pa)

Apparent specific volume:

From equation (14.20)

$$V_m \text{ (apparent)} = \frac{287.04(273.15 + 20)}{1000(100 - 1.5)} = 0.8543 \text{ m}^3/\text{kg dry air}$$

(v) *air densities:*

Actual density is given by equation (14.22) or the reciprocal of actual specific volume

$$\rho_m = \frac{1}{V_m} = \frac{1}{0.8463} = 1.1816 \text{ kg moist air/m}^3$$

Similarly, the apparent density is given as

$$\rho_m \text{ (apparent)} = \frac{1}{V_m \text{ (apparent)}} = \frac{1}{0.8543} = 1.1705 \text{ kg dry air/m}^3$$

(vi) *relative humidity, rh:*

From equation (14.10), the saturation vapour pressure at a temperature of 20°C is

$$e_{sd} = 610.6 \exp \left[\frac{17.27 \times 20}{(237.3 + 20)} \right] = 2337.5 \text{ Pa or } 2.3375 \text{ kPa}$$

Then, from equation (14.25)

$$rh = \frac{e}{e_{sd}} \times 100 = \frac{1.5}{2.3375} \times 100 = 64.17 \text{ percent}$$

(vii) *percentage humidity, ph*

If the space were saturated at 20°C, then the saturation vapour pressure would be 2.3375 kPa.

Equation (14.4) gives the corresponding saturation moisture content to be

$$X_{sd} = 0.622 \frac{2.3375}{(100 - 2.3375)} = 0.014887 \text{ kg/kg dry air}$$

and equation (14.26) gives

$$ph = \frac{X}{X_{sd}} \times 100 = \frac{0.009472}{0.014887} \times 100 = 63.62 \text{ percent}$$

14.3 THE MEASUREMENT OF WATER VAPOUR IN AIR

There are a number of methods of measuring the humidity of air. Numerous instruments are available commercially. These may be divided into five types.

14.3.1. Chemical methods

This involves passing a metered volume of air through a hygroscopic compound such as calcium chloride, silica gel or sulphuric acid and observing the increase in weight. The method is slow and somewhat cumbersome. However, it gives a direct measure of the total moisture content of an airstream and, with care, will give results of high accuracy.

14.3.2. Electrical methods (electronic psychrometers or humidity meters)

The changes in the electrical properties (resistivity, dielectric constants) of some compounds in the presence of water vapour are used in a variety of instruments to give a rapid indication of humidity. Such equipment needs to be compensated against the effect of variations in ambient temperature. Modern devices of this type may employ semi-conductors and electronic micro processors to improve the versatility, reliability and stability of the instrument. Nevertheless, for accurate work, it is advisable to check the calibrations of electronic psychrometers against a more direct method.

14.3.3. Hair hygrometers

Many organic compounds such as bone, hair or other fibrous materials exhibit changes in their volume and elasticity when exposed to water vapour. An example is the opening and closing of fir cones as the weather changes. Human hair is particularly reactive.

Most inexpensive humidity meters sold for domestic display incorporate strands of hair maintained under spring tension. Variations in humidity cause small changes in the length of the

hair. These are amplified mechanically through a lever arrangement. Recording instruments of this type are used to move a pen across a revolving paper chart.

14.3.4. Dew point hygrometers

If an air/vapour mixture is cooled at constant barometric pressure then the actual vapour pressure remains unchanged (see equation (14.4)). However, the falling temperature will cause the corresponding saturation vapour pressure to decrease (equation (14.10)). At some point, the saturation vapour pressure will become equal to the actual vapour pressure. According to classical theory, condensation will then commence. (See also Figure 14.4).

The temperature at which saturation conditions are attained is known as the dew point temperature. An inversion of equation (14.10) gives

$$t \text{ (dew point)} = \frac{237.3 \ln\left(\frac{e}{610.6}\right)}{17.27 - \ln\left(\frac{e}{610.6}\right)} \quad ^\circ\text{C} \quad (14.27)$$

In a dew point hygrometer, a sample of air is drawn over a mirrored surface. The rear of the mirror is cooled, often by evaporation of a volatile liquid. A thermometer attached to the mirror gives the temperature of its surface. This is read at the moment when misting first appears on the mirror to find the dew point temperature. While dew point apparatus gives a good demonstration of the effect of condensation by cooling, the visual detection of the initial film of condensate on the mirror is somewhat subjective. Such instruments are used little in practice.

14.3.5. Wet and dry bulb hygrometers (psychrometers)

These are the most widely used type of hygrometers in subsurface ventilation engineering. They give reliable results when employed by competent personnel and are simple to use. Because of their widespread employment, the theory of the wet bulb thermometer is developed in Section (14.4).

A wet and dry bulb hygrometer is simply a pair of balanced thermometers, one of which has its bulb shrouded in a water-saturated muslin jacket. Air passing over the two bulbs will cause the dry bulb thermometer to register the ordinary temperature of the air. However, the cooling effect of evaporation will result in the wet bulb thermometer registering a lower temperature. Knowledge of the wet and dry bulb temperatures, together with the barometric pressure, allow all other psychrometric parameters to be calculated.

Instruments vary in (a) the precision of the thermometers, (b) the manner in which water is supplied to the wet bulb and (c) the means of providing the required airflow over the thermometer bulbs. The term "psychrometer", rather than "hygrometer", tends to be used for the more accurate instruments.

The accuracy of the thermometers depends upon the quality of their manufacture and calibration, and also upon their length. The better psychrometers can be read to the nearest 0.1°C. Variations considerably greater than this may occur over the cross section of an airway, particularly near shaft stations. In order to maintain the instrument at a portable size, some models achieve accuracy at the expense of range. The approximate extremes of temperature should be known prior to conducting an important psychrometric survey, and an appropriate instrument selected. Replacement thermometers should be purchased as balanced pairs. The difference between the wet and dry bulb temperatures is more important than the absolute temperature. Significant errors in both the wet and dry bulb temperature readings may occur by

radiation from surrounding surfaces or between the bulbs. This can be reduced by increasing the air velocity over the thermometer bulbs. However, for precise results a polished radiation shield should be provided separately around each of the bulbs.

Many hygrometers are fitted with a small reservoir of water into which dips one end of the muslin wick. Capillary action draws water through the muslin to feed the wet bulb. In such devices, it is important that the water reaching the wet bulb is already at wet bulb temperature. The water within the reservoir will be at dry bulb temperature and, if supplied to the wet bulb at too liberal a rate, will give a falsely elevated wet bulb temperature. Conversely, if the water supply is insufficient then drying out of the wick will occur and, again, the wet bulb thermometer will read too high. Because of these difficulties, the more precise psychrometers have no integrated water reservoir and must have their wet bulbs wetted manually with distilled water.

If a wet bulb thermometer is located in a wind tunnel and air of fixed psychrometric condition passed over it at increasing velocity, the indicated wet bulb temperature will decrease initially, then level off. The reason for this phenomenon is that the envelope of saturated air surrounding the wet bulb must be removed efficiently to maintain the evaporative process. The steady state reading observed is essentially identical to the true thermodynamic wet bulb temperature attained during an adiabatic saturation process (see section 14.5.2). The minimum air velocity which gives the true wet bulb temperature is a function of the size and shape of the wet bulb, and its orientation with respect to the direction of the airflow. For most commercially available instruments, an air velocity of at least 3 m/s over the bulbs is suggested.

The static hygrometer (sometimes known as the **Mason hygrometer**) has no intrinsic means of creating the required air velocity and relies on being hung in a location where the thermometer bulbs are exposed to an external air velocity. The "whirling" or "**sling**" **psychrometer** has its thermometers and water reservoir mounted on a frame which may be rotated manually about its handle. Whirling the instrument at about 200 rpm will give the required air velocity over the bulbs. After 30 seconds of rotation, the whirling should be terminated (but not by clamping one's hands around the bulbs), the instrument held such that the observer is not breathing on it, and the wet bulb temperature read immediately. The process of whirling should be repeated until the reading becomes constant.

Aspirated psychrometers have small fans driven by clockwork or batteries. Air is drawn through the radiation shield surrounding each bulb. Again, the wet bulb temperature should be observed until it becomes constant. While the whirling hygrometers are, by far, the most widely used instruments for routine measurements, aspirated psychrometers are recommended for important surveys.

14.4. THEORY OF THE WET BULB THERMOMETER

The wet bulb temperature is a most important parameter in hot climatic conditions for two separate but inter-related purposes. The first lies in its vital importance in evaluating the ability of the air to remove metabolic heat from personnel. The second is the use of the wet bulb temperature in quantifying the humidity of the air.

14.4.1. Heat balance on a wet bulb

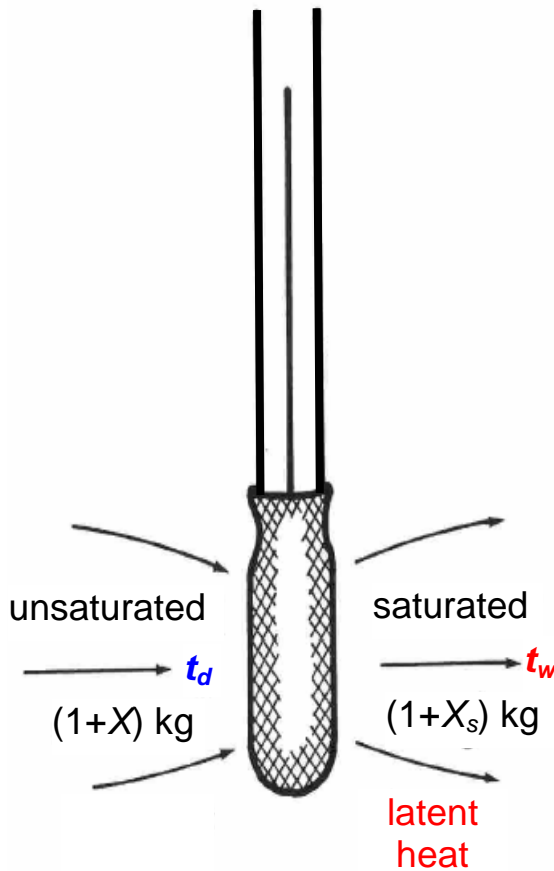


Figure 14.1 Heat balance on a wet bulb.

Figure 14.1 illustrates $(1 + X)$ kg of moist unsaturated air approaching and flowing closely over the surface of a wet bulb. On leaving the wet surface, the 1 kg of air remains the same but the mass of associated water vapour has increased from X kg to X_s kg and the air has become saturated. Thus a mass of $(X_s - X)$ kg of water has evaporated from the wet surface for each kilogram of "dry" air passing. The reason for employing 1 kg of dry air as the basis of measurement is, again, apparent - this remains constant, while the mass of water vapour varies.

As the molecules of water leave the wet surface they take energy with them. This "latent heat" energy is transferred to the air, leaving the wet bulb at a reduced energy level. This is reflected by a drop in temperature (the evaporative cooling effect) and the wet bulb thermometer gives a reading depressed below that of the dry bulb. The greater the rate of evaporation, the greater the wet bulb depression.

As there is now a difference between the air temperature and the cooler wet surface, a transfer of sensible heat will occur by convection from the air to the wet bulb. A dynamic equilibrium will be established at which the heat loss from the wet bulb by evaporation is balanced by the convective sensible heat gain:

$$\text{Latent heat loss from wet bulb} = \text{Sensible heat gain by wet bulb} \quad (14.28)$$

Each of these terms can be quantified. Latent heat transfer from the wet bulb to the air

$$q = L (X_s - X) \quad \text{J per kg dry air} \quad (14.29)$$

where L = latent heat of evaporation (J/kg evaporated) at wet bulb temperature.

The air/vapour mixture approaches the wet surface at dry bulb temperature, t_d , and leaves at wet bulb temperature, t_w . The sensible heat transfer from the air to the wet bulb is then

$$\begin{aligned} q &= \text{mass} \times \text{specific heat} \times \text{change in temperature} \\ &= (1 + X) \times C_{pm} \times (t_d - t_w) \quad \text{J/kg dry air} \quad (14.30) \end{aligned}$$

At equilibrium, latent heat transfer equals sensible heat transfer. Equations (14.29) and (14.30) quantify the heat balance that exists on the wet bulb

$$L (X_s - X) = (1 + X) C_{pm} (t_d - t_w) \quad \text{J/kg dry air} \quad (14.31)$$

14.4.2. Determination of moisture content and vapour pressure from psychrometer readings

If the barometric pressure, P , and the wet and dry bulb temperatures, t_w and t_d , are known then the moisture content and, indeed, all other psychrometric parameters can be determined.

Commencing from the heat balance for the wet bulb, and using the shorthand notation Δt for the wet bulb depression, $t_d - t_w$, we have

$$L (X_s - X) = (1 + X) C_{pm} \Delta t$$

But

$$C_{pm} = \frac{C_{pa} + X C_{pv}}{(1 + X)} \quad \text{from equation (14.16)}$$

$$\text{then } LX_s = (C_{pa} + X C_{pv}) \Delta t + LX = C_{pa} \Delta t + X (C_{pv} \Delta t + L)$$

giving the moisture content, X , as

$$X = \frac{LX_s - C_{pa} \Delta t}{C_{pv} \Delta t + L} \quad \text{kg/kg dry air} \quad (14.32)$$

All variables on the right side of this equation are known, or can be calculated easily for the given P , t_d and t_w . Hence, the moisture content, X , is defined.

The actual vapour pressure then follows from a transposition of equation (14.4)

$$e = \frac{PX}{0.622 + X} \quad \text{Pa} \quad (14.33)$$

Example

Determine the moisture content and vapour pressure for a barometric pressure of 100 kPa and wet and dry bulb temperatures of 20 and 30°C respectively.

Solution

At the wet bulb temperature, the variables required by equation (14.32) are calculated as follows:

$$\begin{aligned} L &= (2502.5 - 2.386 \times 20) 1000 \quad \text{from equation (14.6)} \\ &= 2454.78 \times 10^3 \quad \text{J/kg or 2454.78 kJ/kg} \end{aligned}$$

$$e_{sw} = 610.6 \exp \left[\frac{17.27 \times 20}{237.3 + 20} \right] \quad (\text{equation (14.10)}) = 2.3375 \quad \text{kPa}$$

$$X_s = 0.622 \frac{2.3375}{(100 - 2.3375)} \quad (\text{equation (14.4)})$$

$$= 0.014887 \quad \text{kg/kg dry air}$$

Then equation (14.32) gives

$$X = \frac{2454.78 \times 10^3 \times 0.014887 - 1005(30 - 20)}{1884(30 - 20) + 2454.78 \times 10^3} = \frac{36544 - 10050}{18840 + 2454780}$$

$$= 0.01071 \quad \text{kg/kg dry air}$$

The actual vapour pressure is then given by equation (14.33)

$$e = \frac{100 \times 0.01071}{0.622 + 0.01071} = 1.6927 \text{ kPa}$$

This example illustrates that the term involving C_{pv} (1884 J/kg K) in equation (14.32) is very small compared with L . A more traditional equation for actual vapour pressure follows from ignoring the smaller term. Then equation (14.32) simplifies to

$$X = X_s - \frac{C_{pa}\Delta t}{L}$$

Substituting for X and X_s from equation (14.4) gives

$$0.622 \frac{e}{(P - e)} = 0.622 \frac{e_{sw}}{(P - e_{sw})} - \frac{C_{pa}\Delta t}{L}$$

$$\text{or} \quad e = e_{sw} \frac{(P - e)}{(P - e_{sw})} - \frac{C_{pa}\Delta t}{0.622L}(P - e)$$

If we now assume that e and e_{sw} are small compared with P , the equation simplifies further to

$$e = e_{sw} - \frac{C_{pa}}{0.622L} P \Delta t \quad \text{Pa} \quad (14.34)$$

or

$$e = e_{sw} - A P \Delta t \quad \text{Pa} \quad (14.35)$$

The parameter A is known as the **psychrometric "constant"**. However, because of the simplifications made in the derivation, it is not a true constant; neither is it given precisely as $C_{pa} / (0.622L)$ but varies non-linearly with temperature and pressure between 0.00058 and 0.000648 $^{\circ}\text{C}^{-1}$ over the atmospheric range. This variation of the psychrometric "constant" is a weakness in the relationship. However, a value of 0.000644 $^{\circ}\text{C}^{-1}$ gives acceptable results for most practical purposes.

Example

Determine the actual vapour pressure from equation (14.35) for $P = 100 \text{ kPa}$, $t_w = 20 \text{ }^{\circ}\text{C}$ and $t_d = 30 \text{ }^{\circ}\text{C}$.

Solution

These are the same conditions as specified in the previous example. This gave

$$e_{sw} = 2.3375 \quad \text{kPa}$$

Then equation (14.35) gives

$$e = 2.3375 - 0.000644 \times 100 \times (30 - 20) = 1.6935 \text{ kPa}$$

(a difference of less than 0.05 per cent from the earlier solution).

14.5. FURTHER PSYCHROMETRIC RELATIONSHIPS

14.5.1. Enthalpy of moist air

In Chapter 3, the steady flow energy equation was derived as

$$\frac{u_1^2 - u_2^2}{2} + (Z_1 - Z_2)g + W_{in} = \int_2^1 VdP + F_{12} = (H_2 - H_1) - q_{in} \quad \text{J/kg} \quad (14.36)$$

where	u	=	air velocity, m/s
	Z	=	height above datum, m
	g	=	gravitational acceleration, m/s ²
	W_{in}	=	mechanical (fan) work input, J/kg
	V	=	specific volume, m ³ /kg
	F	=	frictional conversion of mechanical to heat energy, J/kg
	H	=	enthalpy, J/kg
And	q_{in}	=	heat input from external sources, J/kg

In its application to mine ventilation thermodynamics, (Chapter 8) the change in enthalpy between end stations 1 and 2 was earlier assumed to be

$$H_2 - H_1 = C_{pa} (t_2 - t_1) \quad \text{J/kg} \quad (14.37)$$

where t_1 and t_2 were the dry bulb temperatures. This assumption was based on the premise that the airway was dry - neither evaporation nor condensation was considered. For moist, but unsaturated air, the specific heat term may be replaced by C_{pm} for the actual air/vapour mixture. However, if evaporation or condensation does take place then the exchange of latent heat will have a large additional effect on the dry bulb temperature. Equation (14.37) no longer applies. As this is the situation in most underground airways, we must seek a method of evaluating enthalpy that takes the moisture content of the air into consideration.

Let us carry out another imaginary experiment. Suppose we have 1 kg of dry air at 0°C and, in a separate container, a small amount, X kg, of liquid water. Now let us heat the air until it reaches a dry bulb temperature of t_d . Similarly, we add heat to the water until it vaporizes and continue heating until the vapour also reaches a dry bulb temperature of t_d . Finally, we mix the two components to obtain $(1 + X)$ kg of moist unsaturated air at a dry bulb temperature of t_d and some lower value of wet bulb temperature, t_w .

The total amount of heat that we have added to the air and water during this experiment represents the increase in enthalpy of the system over its starting condition at 0°C. If we choose 0°C as our enthalpy datum, that same added heat represents the enthalpy level of the final $(1 + X)$ kg of mixture.

In order to quantify the added heat, consider the air and water separately:

- (i) The heat required to raise the temperature of 1 kg of dry air from 0°C to t_d is simply

mass x specific heat x change in temperature

i.e.

$$q_{air} = 1 \times C_{pa} \times t_d \quad \text{J}$$

(ii) We can convert the water at 0°C to vapour at t_d in any of three ways, depending upon the pressure that we maintain in the vessel:

(a) We could consider evaporating the X kg of water at 0°C then raising the temperature of the vapour to t_d .

$$q_{water} = L(0) X + X C_{pv} t_d \quad \text{J}$$

where $L(0) =$ Latent heat of evaporation at 0°C.

(b) Alternatively, we might raise the temperature of the liquid water to t_d then evaporate at that temperature.

$$q_{water} = X C_w t_d + L(t_d) X \quad \text{J}$$

where $C_w =$ specific heat of liquid water (4187 J/kg K)
and $L(t_d) =$ Latent heat of evaporation at t_d °C

or

(c) We could raise the temperature of the liquid to any intermediate value, t , evaporate at that temperature, then continue to superheat the vapour until it reaches the required temperature, t_d .

$$q_{water} = X C_w t + L(t) X + X C_{pv} (t_d - t) \quad \text{J} \quad (14.38)$$

where $L(t) =$ Latent heat of evaporation at t °C

In fact, as the two end conditions are precisely defined, it does not matter which method is used. They all give the same result provided that account is taken of the variations of latent heat and specific heat with respect to temperature.

For a reason that will become apparent later, let us choose method (c) with the intermediate value of temperature chosen to be t_w , the eventual wet bulb temperature of the air/vapour mixture.

We have now found the total amount of heat added to the system and, hence, its enthalpy relative to a 0°C datum

$$\begin{aligned} H &= q_{air} + q_{water} \\ &= C_{pa} t_d + X [C_w t_w + L + C_{pv} (t_d - t_w)] \quad \text{J per kg dry air} \quad (14.39) \end{aligned}$$

Here, the symbol L has reverted to its earlier meaning of latent heat of evaporation at wet bulb temperature.

All of the parameters on the right side of the equation can either be measured, are constant or can be calculated from equations (14.6) and (14.32). Hence, the enthalpy of an air/vapour mixture can be determined from psychrometric measurements of air pressure and wet and dry bulb temperatures. If such values of enthalpy are employed in the steady-flow energy equation (14.36) then that equation may continue to be used for airways that involve evaporation or condensation processes.

14.5.2. The adiabatic saturation process

Consider a long level airway with no heat additions from any source and free standing water covering the floor (Figure 14.2). Unsaturated air enters at one end and moves sufficiently slowly to allow full saturation to occur. The air exits at saturation conditions.

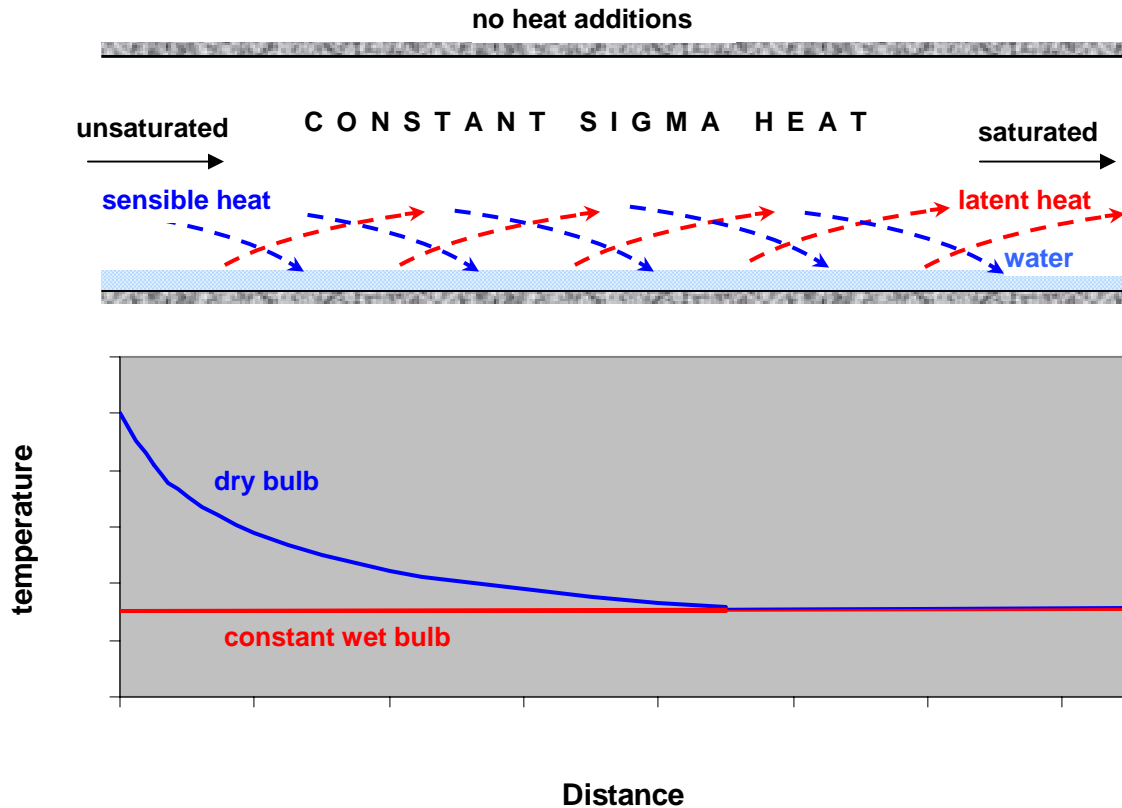


Figure 14.2 An adiabatic saturation process.

The surface of the liquid water reacts in the same way as that of a wet bulb thermometer (Section 14.4.1) and, indeed, will be at wet bulb temperature. At inlet, the dry bulb temperature will be at a higher value. Hence, sensible heat transfer will occur from the air to the water resulting in a reduction in dry bulb temperature. Simultaneously, heat and mass transfer from the water to the air will take place as water molecules escape from the liquid surface - a latent heat gain by the air. These exchanges will continue until saturation when wet bulb, dry bulb and water temperature all become equal (thermodynamic wet bulb temperature).

This is known as an **adiabatic saturation process**. The sensible heat lost by the air is balanced by the latent heat gained by the air and the process involves no net addition or loss of heat. This latter statement is true for the combination of air and water, but not quite true for the air alone. Mass has been added to the airstream in the form of water molecules, and those molecules already contained sensible heat before they were evaporated. Hence, the enthalpy of the air does not quite remain constant. However, if we were to move along the airway taking psychrometric readings, calculating enthalpy from equation (14.40) but omitting the term for the sensible heat of liquid water, $X C_w t_w$ that has evaporated then the result would be a property value that remained truly constant throughout the adiabatic saturation process. The significance of this property seems first to have been recognized by Carrier and was named Sigma Heat, S , to distinguish it from its near neighbor, enthalpy.

14.5.3. Sigma Heat, S

Sigma heat is much more than simply an interesting property of an adiabatic saturation process. Indeed, it features in the majority of analyses concerning subsurface climatic changes.

Ignoring the sensible heat of the liquid water in equation (14.40) gives

$$S = H - X C_w t_w \quad \text{J/kg dry air} \quad (14.40)$$

and

$$S = C_{pa} t_d + X[L + C_{pv}(t_d - t_w)] \quad \text{J/kg dry air} \quad (14.41)$$

But from equation (14.32), and replacing Δt with $(t_d - t_w)$

$$X[L + C_{pv}(t_d - t_w)] = LX_s - C_{pa}(t_d - t_w)$$

Notice that the left side of this relationship appears in equation (14.42). Substituting for

$$X[L + C_{pv}(t_d - t_w)] \text{ in that equation}$$

gives

$$S = C_{pa} t_d + LX_s - C_{pa}(t_d - t_w)$$

or

$$S = LX_s + C_{pa} t_w \quad \text{J/kg dry air} \quad (14.42)$$

The t_d term cancels to produce a really neat equation for sigma heat. Now we are about to discover a phenomenon of major significance in psychrometric processes. Recalling that X_s is the saturation moisture content dependent only on wet bulb temperature and pressure (equations (14.4) and (14.10)), and that L is the latent heat of evaporation, also at wet bulb temperature, it follows that for any given barometric pressure, sigma heat, S , is a function of wet bulb temperature only. Furthermore, as sigma heat remains constant during an adiabatic saturation process so must also the wet bulb temperature remain constant. This is why the wet bulb temperature appears as a horizontal line in Figure 14.2.

Using the concept of sigma heat, thermal additions or losses from an airstream can readily be quantified from psychrometric observations. Furthermore, the behaviour of the wet bulb temperature, a directly measurable parameter, is an immediate indication of heat transfer from the strata, machines, coolers, potential energy or any other source. Contrasting this with dry bulb temperature which varies during evaporation or condensation, we see the fundamental importance of the wet bulb temperature in psychrometric processes.

14.6. SUMMARY OF PSYCHROMETRIC EQUATIONS

This is a convenient point to make a reference list of the more important equations that have been derived in the previous sections, and to re-order them in the sequence that they are required for most psychrometric calculations where P , t_w and t_d are the measured variables. All temperatures are expressed in degrees Centigrade and pressures in Pascals.

$$e_{sw} = 610.6 \exp\left[\frac{17.27 t_w}{237.3 + t_w}\right] \quad \text{Pa} \quad (14.43)$$

$$X_s = 0.622 \frac{e_{sw}}{(P - e_{sw})} \quad \text{kg/kg dry air} \quad (14.44)$$

$$L_w = (2502.5 - 2.386 t_w) 1000 \quad \text{J/kg} \quad (14.45)$$

$$S = L_w X_s + 1005 t_w \quad \text{J/kg dry air} \quad (14.46)$$

$$X = \frac{S - 1005 t_d}{[L_w + 1884(t_d - t_w)]} \quad \text{kg/kg dry air} \quad (14.47)$$

or

$$X = \frac{L_w X_s - 1005(t_d - t_w)}{[L_w + 1884(t_d - t_w)]} \quad \text{kg/kg dry air} \quad (14.48)$$

$$e = \frac{PX}{(0.622 + X)} \quad \text{Pa (when } P \text{ is in Pascals)} \quad (14.49)$$

$$\rho_m \text{ (apparent)} = \frac{(P - e)}{[287.04(t_d + 273.15)]} \quad \text{kg dry air/m}^3 \quad (14.50)$$

$$\rho_m \text{ (actual)} = \frac{(P - 0.378e)}{[287.04(t_d + 273.15)]} \quad \text{kg moist air/m}^3 \quad (14.51)$$

$$H = S + (4187 t_w X) \quad \text{J/kg dry air} \quad (14.52)$$

$$(rh) = \frac{e}{e_{sd}} \times 100 \quad \text{percent} \quad (14.53)$$

(Equation (14.44) is used for e_{sd} with t_w replaced by t_d). Note that in this list of important relationships, the need for the old troublesome psychrometric "constant" (Equation (14.35)) has been entirely eliminated. **This summary of equations can be programmed into spreadsheet software or a programmable calculator to provide a rapid and accurate means of determining values of psychrometric parameters from given barometric pressure and wet and dry bulb temperatures.**

Example

At entry to a level continuous underground airway of constant cross-section, psychrometer readings give $P_1 = 110.130$ kPa, $t_{w1} = 23$ °C and $t_{d1} = 28$ °C. The corresponding readings at exit are $P_2 = 109.850$ kPa, $t_{w2} = 26$ °C and $t_{d2} = 32$ °C. If the volume flow of air at inlet is $25 \text{ m}^3/\text{s}$, calculate the heat and moisture added to the airstream during its passage through the airway.

Solution

The following table was produced in a few seconds from a spreadsheet programmed with the psychrometric equations:

Equation	Parameter	Inlet	Outlet	Units
measured	P	110.13	109.85	kPa
measured	t_w	23	26	°C
measured	t_d	28	32	°C
(14.43)	e_{sw}	2808.5	3360.3	Pa
(14.10) using t_d	e_{sd}	3778.7	4753.2	Pa
(14.44)	X_s	0.016277	0.019628	kg/kg dry air
(14.45)	L_w	2447.6×10^3	2440.5×10^3	J/kg water
(14.46)	S	62.955×10^3	74.032×10^3	J/kg dry air
(14.47)	X	0.01417	0.017078	kg/kg dry air
(14.49)	e	2453.0	2935.0	Pa
(14.50)	$\rho(app)$	1.2457	1.2206	kg dry air/m ³
(14.51)	$\rho(act)$	1.2633	1.2415	kg moist air/m ³
(14.52)	H	64 320.1	75 889.43	J/kg dry air
(14.53)	rh	64.91599	61.8	percent

As the airflow was measured as 25 m³/s at inlet conditions, the mass flow of dry air

$$\begin{aligned}
 M &= Q \rho \text{ (inlet, apparent)} \\
 &= 25 \times 1.2457 \frac{\text{m}^3 \text{ kg dry air}}{\text{s m}^3} = 31.14 \text{ kg dry air/s}
 \end{aligned}$$

Increase in sigma heat along airway

$$S_2 - S_1 = 74.032 - 62.955 = 11.077 \text{ kJ/kg dry air}$$

Heat added

$$\begin{aligned}
 q_{in} &= M(S_2 - S_1) \\
 &= 31.14 \times 11.077 \frac{\text{kg dry air}}{\text{s}} \frac{\text{kJ}}{\text{kg dry air}} \\
 &= 344.9 \text{ kJ/s or kW}
 \end{aligned}$$

Increase in moisture content along airway

$$X_2 - X_1 = 0.017078 - 0.01417 = 0.002908 \text{ kg/kg dry air}$$

Rate of evaporation = $M(X_2 - X_1)$

$$= 31.14 \times 0.002908 = 0.0906 \text{ kg/s or litres/s}$$

14.7. DEVIATIONS FROM CLASSICAL THEORY

14.7.1. Fogged air

The classical theory of condensation makes the premise that condensation cannot commence until saturation conditions are reached. This is not quite in agreement with observable phenomena. The formation of fog is likely to commence before 100 per cent relative humidity is reached although the process of condensation accelerates rapidly as saturation is approached.

Smoke fogs (smogs) may occur over cities at relative humidities of less than 90 per cent.

The physical mechanism of condensation is complex. Condensation can occur only in the presence of hygroscopic and microscopic nuclei on which the process can commence. It has been estimated (Brunt) that there are between 2 000 and 50 000 hygroscopic nuclei in each cubic centimeter of the atmosphere, having radii of 10^{-6} to 10^{-5} cm. The most productive sources of these hygroscopic particles are the oceans and sulphurous smokes from burning hydrocarbon fuels.

The natural formation of fog would appear to be a continuous process of condensation commencing at comparatively low relative humidities when the more strongly hygroscopic nuclei begin to attract water. This can often result in a noticeable haze in the atmosphere. As the relative humidity approaches 100 per cent, the rate of condensation on all hygroscopic nuclei increases; the droplets of water so formed increase rapidly in size and the haze develops into fog.

Fogging in subsurface ventilation systems occurs in two situations. First, when the strata are cooler than the dew point temperature of the incoming air and, secondly, due to decompressive cooling of humid return air. Hence, fogging in ascending return airways and, especially, upcast shafts is not uncommon.

The formation of fogs in underground structures is undesirable for a number of reasons. The reduction in visibility may produce a safety hazard, particularly where moving vehicles are involved. High humidity can result in physical and chemical reactions between the airborne water and **hygroscopic minerals** within the strata, and may produce falls of roof and spalling of the sides of airways. Such problems can reach serious proportions in certain shales and evaporite mines. Another difficulty that may arise in salt mines is absorbance of water vapour by the mined rock. If the air is humid then the material may become "sticky" and difficult to handle. The problem may be alleviated by transporting the ore in the return airways. One further problem of fogging in upcast shafts is that it creates very wet conditions throughout the shaft, headgear and/or exhaust fans.

If the air velocity in an upcast shaft lies within the range 7 to 12 m/s then droplets will tend to remain in suspension, encouraging **water blankets** to form. The resulting increase in shaft resistance causes a fluctuating load to be imposed on main fans, even to the extent of stalling them. The resulting sudden reduction in airflow results in water cascading to the bottom of the shaft and the whole process will be repeated in a cyclic manner. In extreme cases this may lead to failure of the fan blades.

If it becomes necessary to dehumidify the air because of any of these problems then there are two possibilities. The less expensive option, where it can be used, is to divert the air through old stopes or workings that contain water-absorbent minerals in the broken strata. Alternatively the air temperature may be reduced to below dew point in air coolers and the condensed water removed from the system. All, or part of the reject heat produced by the refrigeration plant may be returned to the downstream airflow to control its temperature. Chemical dehumidification is seldom practicable in mining circumstances because of the large volumes of air involved.

14.7.2. Imperfect gas behaviour

The equations given for saturation vapour pressure ((14.10) and (14.11)) took deviations from perfect gas behaviour into account. However, the other relationships derived in this chapter assume that dry air, water vapour, and air/vapour mixtures all obey the perfect gas laws. These laws assume that the molecules of the air are perfectly elastic spheres of zero volume and that they exhibit no attractive or repulsive forces.

For the ranges of pressures and temperatures encountered in atmospheric psychrometrics, assumption of the perfect gas laws gives results of acceptable accuracy. Where additional

precision is required, Hemp (1982) has suggested the following two corrections based on the earlier work of Goff and Gratch.

Equation (14.3) for moisture content

$$X = \frac{R_a}{R_v} \frac{e}{(P - e)} \text{ becomes } X = \frac{R_a}{R_v} \frac{1.0048e}{(P - 1.0048e)} \quad \text{kg/kg dry air} \quad (14.55)$$

and gas constants, R , are corrected for pressure and temperature as follows:

$$R(\text{corrected}) = R \{1 - [(5.307 \times 10^{-9} P + 9.49 \times 10^{-6}) - (8.115 \times 10^{-11} P + 2.794 \times 10^{-6}) t_d]\} \quad (14.56)$$

where P is in Pa and t_d in °C.

This gives a maximum change in R of 0.06 percent over the ranges 80 to 120 kPa and 0 to 60°C. At the mid range value of 100 kPa and 30°C, the difference is 0.02 percent.

14.8. PSYCHROMETRIC CHARTS

Prior to the advent of electronic computation, employment of psychrometric equations was an onerous process. In order to minimize the calculations, graphical depictions of psychrometric processes were devised. These are known as **Psychrometric Charts**. Although the use of such charts has largely been supplanted by programming psychrometric equations into spreadsheet software and programmable calculators they still provide a powerful means of visualizing psychrometric processes.

Most psychrometric charts show a representation of the psychrometric parameters for a fixed barometric pressure. Figure 14.3 gives an example of a 100 kPa chart. This is one of a series of such charts ranging from 80 to 130 kPa at intervals of 2.5 kPa produced by **A.W.T, Barenbrug** (1974). As pressure is the least sensitive of the independent variables, interpolation between charts is unnecessary for most practicable purposes. More sophisticated types of chart have been produced that allow for pressure variations (Whillier, 1971). However, these seem not to have found widespread use.

Returning to Figure 14.3 it is clear that knowledge of any two of the variables will fix a location on the chart, indicating the climatic condition of the air, and enabling other psychrometric variables to be read directly or determined with a minimum of calculation. The usual situation is one in which the wet and dry bulb temperatures are known and can be plotted on the relevant chart. Engineers who are adept at using psychrometric charts are better able to visualize variations in climatic conditions.

Figure 14.4 illustrates the ease with which processes can be followed. Movement along a constant wet bulb line (i.e. constant sigma heat) indicates adiabatic conditions. Any movement to a higher or lower wet bulb temperature indicates that the air has been heated or cooled respectively. A path to a higher moisture content (labelled as apparent specific humidity on Figure 14.3) indicates evaporation while movement along a constant moisture line denotes sensible heating or cooling. Similarly, pure latent heating or cooling is indicated by a constant dry bulb temperature.

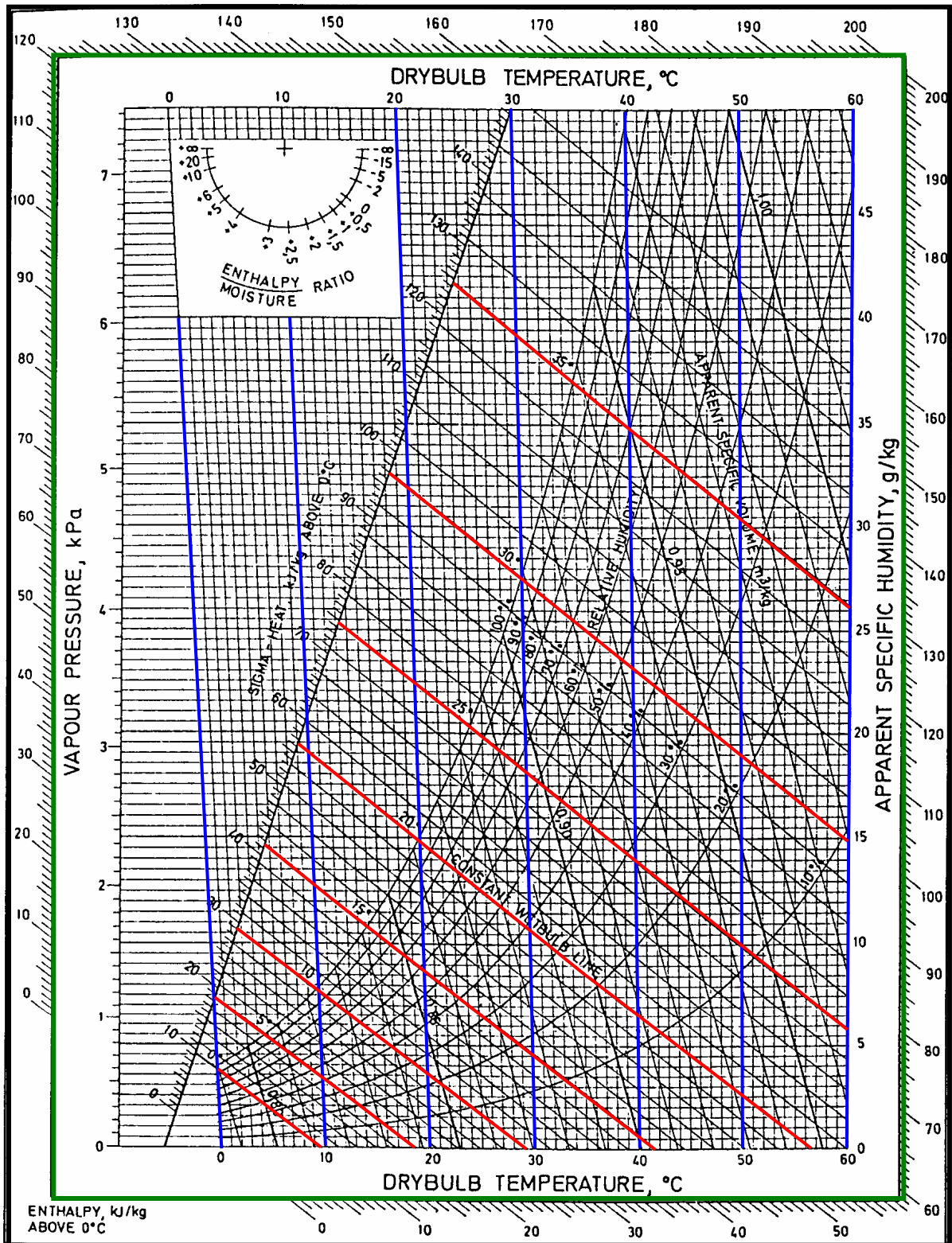


Figure 14.3. Example of a psychrometric chart, at 100kPa.
 (after Barenburg A.W.T. "Psychrometry and Psychrometric Charts"(1))
 Reproduced by courtesy of the Chamber of Mines of South Africa

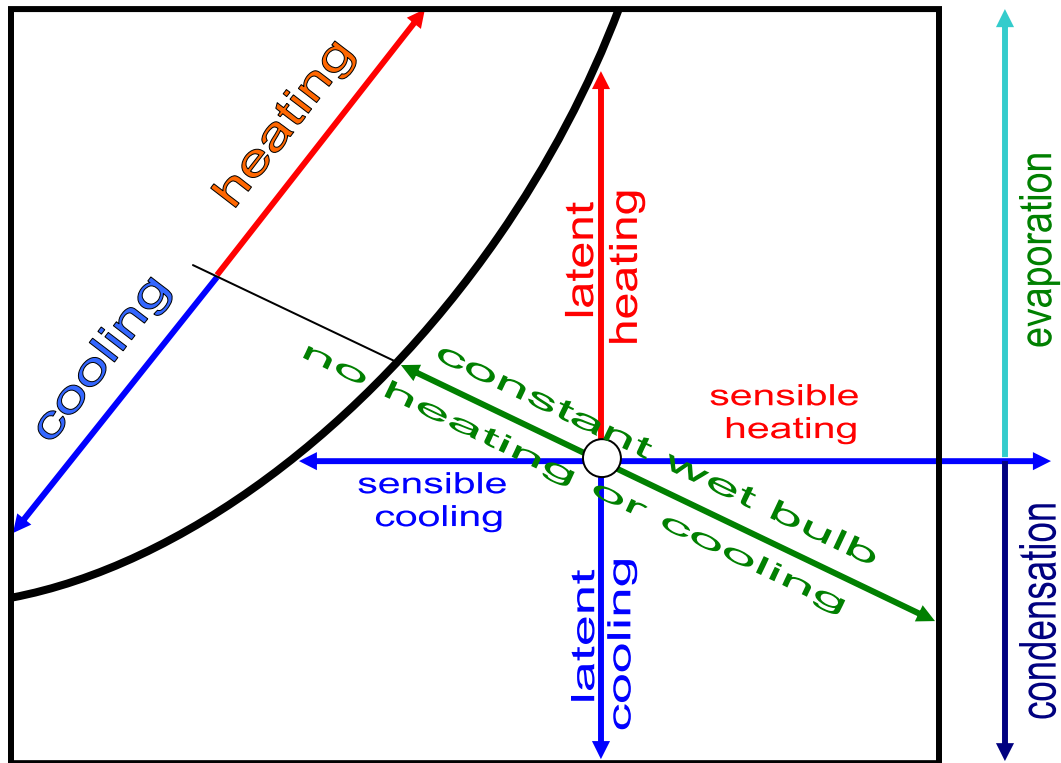


Figure 14.4 Process lines on a psychrometric chart

Example

Air passes through a cooler at a mean pressure of 100 kPa. It enters at wet and dry bulb temperatures of 30 and 40 °C respectively, and exits at 25 °C saturated. If the volume flow at inlet, Q , is 20 m³/s, use the psychrometric chart to determine the rates of heat exchange and production of condensate.

Solution

On the 100 kPa psychrometric chart, plot the two points 30/40 °C and 25/25 °C (Figure 14.5). The latter lies on the saturation line (100 per cent relative humidity). It is immediately obvious that during the flow of air from inlet to outlet both the moisture content (specific humidity) and sigma heat have decreased. The following values are read from the chart. The corresponding values calculated from the equations in section 14.6 are given in parentheses for comparison).

	Inlet	Outlet
t_w/t_d °C	30/40 °C	25/25 °C
X g/kg dry air	23.2 (23.24)	20.3 (20.34)
S kJ/kg dry air	97.0 (97.1)	74.7 (74.8)
V (app) m ³ /kg dry air	0.932 (0.9324)	0.884 (0.8838)
e_{act} kPa	3.6 (3.601)	3.16 (3.167)

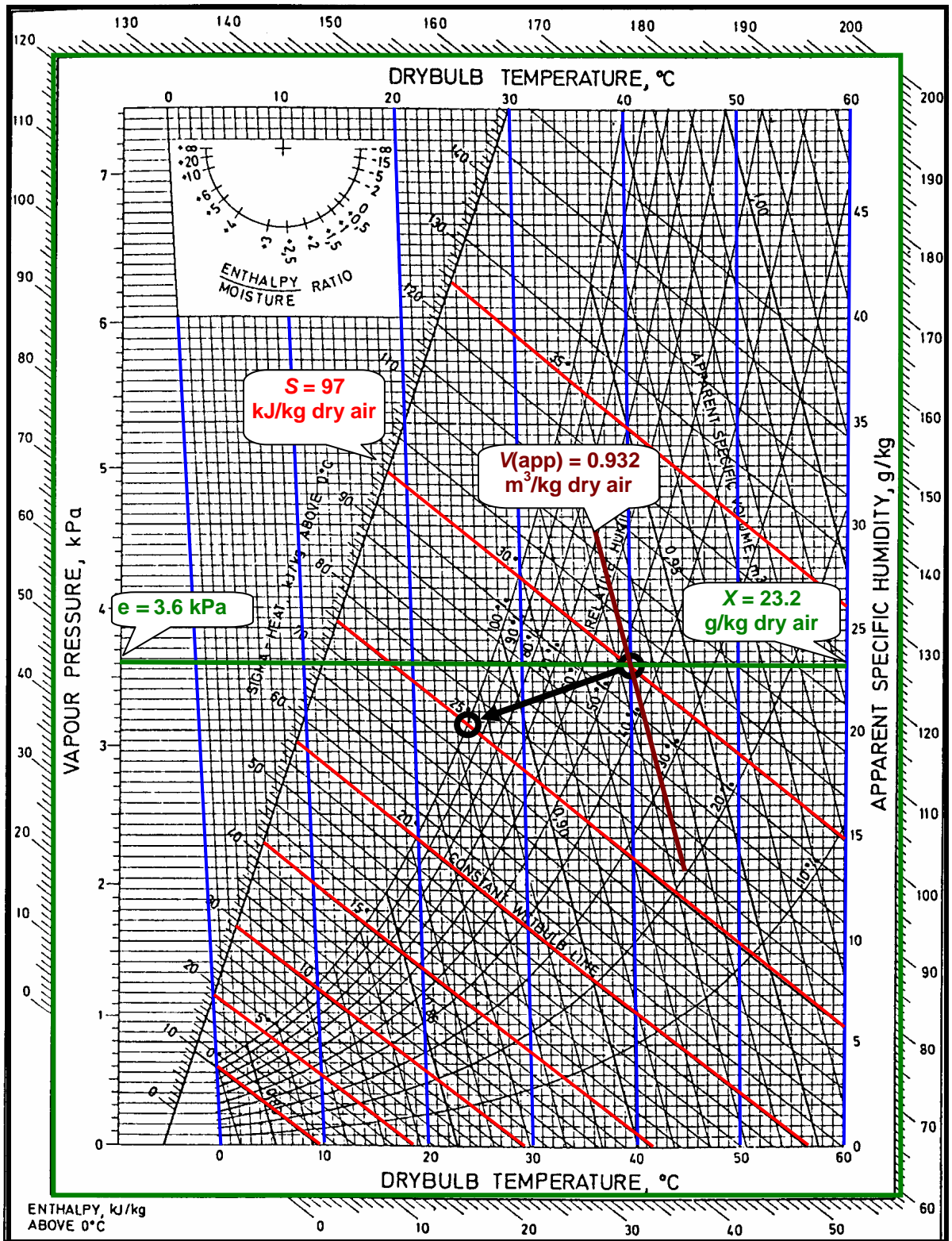


Figure 14.5 Process line for the example. Wet and dry bulb temperatures at inlet and outlet are plotted. The inlet point is used to illustrate how to read other psychrometric parameters.

$$\text{Mass flow of dry air, } M = Q \rho (\text{app}) = 20 \times \frac{1}{0.932} = 21.5 \text{ kg dry air/s}$$

$$\text{Heat exchange} = (S_1 - S_2) M = (97 - 74.7) 21.5 \frac{\text{kJ kg}}{\text{kg s}} = 479.5 \text{ kW}$$

$$\begin{aligned} \text{Rate of condensation} &= (X_1 - X_2) M = (0.0232 - 0.0203) 21.5 \\ &= 0.0623 \text{ kg water/s or } 0.0623 \times 60 = 3.74 \text{ litres per minute.} \end{aligned}$$

References

Barenbrug, A. W. T. (1974). Psychrometry and Psychrometric Charts 3rd Edition, Chamber of Mines of South Africa.

Brunt, D. (1939). Physical and Dynamical Meteorology. Cambridge Press.

Goff, J. A. and Gratch, S. (1945). Thermodynamic Properties of Moist Air. ASHVE Trans. Vol. 51, pp. 125-158.

Hemp, R. (1982). Psychrometry. Chapter 18. Environmental Engineering in South African Mines. Mine Ventilation Society of South Africa pp. 435-463.

Van der Walt, N. T. and Hemp, R. (1982). Thermometry and Temperature Measurements. Chapter 17. Environmental Engineering in South African Mines. Mine Ventilation Society of South Africa, pp. 413-433.

Whillier, A. (1971). Psychrometric charts for all barometric pressures. J. Mine Ventilation Society of South Africa, Vol. 24, pp. 138-143.

APPENDIX A14

Derivation of the Clausius-Clapeyron equation

When the enthalpy, or overall energy, of a system is increased by doing mechanical work on it, then this work represents available energy all of which can theoretically be utilized. On the other hand, if the enthalpy increase is brought about by the addition of heat then the Second Law of Thermodynamics insists that only a part of this heat is available energy. The unavailable fraction is utilized in increasing the internal energy of the system. Thus if we have 1 kg of liquid water of volume V , internal energy U and pressure e_s and add an increment of heat energy the corresponding increase in enthalpy will be

$$dH = dU + e_s dV \quad (\text{ref. equation (3.19)}) \quad (14.A1)$$

Now a change of phase (evaporation from liquid to vapour) occurs at constant temperature and constant pressure. During such a process the enthalpy change is also related to the increase in entropy of the system

$$dH = Tds \quad (\text{see equation (3.46) with } dP = 0) \quad (14.A2)$$

where s = entropy

Hence (14.A1) and (14.A2) give

$$dH = dU + e_s dV = Tds \quad (14.A3)$$

If the 1 kg of water is completely evaporated, then the total heat added to accomplish this is the latent heat of evaporation, L .

Equation (14.A3) can be integrated over the change of phase from liquid water (subscript L) to vapour (subscript s)

$$L = H_s - H_L = U_s - U_L + e_s (V_s - V_L) = T(s_s - s_L) \quad (14.A4)$$

or

$$U_s + e_s V_s - Ts_s = U_L + e_s V_L - Ts_L \quad (14.A5)$$

This relationship defines a function of state, $d\phi$, known as the thermodynamic potential which remains constant during any isobaric - isothermal change of phase:

$$\phi = U + e_s V - Ts \quad (14.A6)$$

Now consider the situation at a slightly different temperature $T+dT$ and pressure e_s+de_s . The thermodynamic potential that will apply under these conditions will be $\phi+d\phi$. Differentiating equation (14.A6) to find $d\phi$ gives

$$d\phi = dU + e_s dV + V de_s - T ds - s dT \quad (14.A7)$$

but from equation (14.A3)

$$dU + e_s dV - T ds = 0$$

Hence

$$d\phi = V de_s - s dT \quad (14.A8)$$

As $d\phi$ is constant during evaporation at conditions T and e_s , and $d\phi + d\phi$, remains constant during evaporation at conditions $T + dT$ and $e_s + de_s$, it follows that $d\phi$ remains constant as T approaches $T + dT$ and e_s approaches $e_s + de_s$. Therefore from equation (14.A8)

$$V_L de_s - s_L dT = V_s de_s - s_s dT \quad (14.A9)$$

or

$$\frac{de_s}{dT} = \frac{s_L - s_s}{V_L - V_s} \quad (14.A10)$$

This equation was first derived by Clapeyron in 1832.

The volume of liquid water, V_L , is negligible compared with that of the vapour, V_s , (At normal atmospheric conditions V_s/V_L is of the order of 2500). Furthermore, from equation (14.A4)

$$-(s_L - s_s) = \frac{L}{T}$$

and (14.A10) becomes

$$\frac{de_s}{dT} = \frac{L}{T} \frac{1}{V_s} \quad (14.A11)$$

but from the general gas law for 1 kg of water vapour

$$V_s = \frac{R_v T}{e_s}$$

Hence,

$$\frac{1}{e_s} \frac{de_s}{dT} = \frac{L}{R_v T^2} \quad \text{the Clausius-Clapeyron equation} \quad (14.A12)$$

CHAPTER 15 HEAT FLOW INTO SUBSURFACE OPENINGS

15.1. INTRODUCTION	2
15.2. STRATA HEAT	2
15.2.1. Methods of determining strata heat load	2
15.2.2. Qualitative observations.....	4
15.2.3. Fourier's law of heat conduction	5
15.2.4. Geothermic gradient, geothermal step and thermal conductivity	6
15.2.5. An analysis of three dimensional heat conduction.	7
15.2.6. Solution of the radial heat conduction equation.....	12
15.2.7. Heat transfer coefficient for airways	14
15.2.7.1. Convective heat transfer	15
15.2.7.2. Radiative heat transfer	16
15.2.8. Summary of procedure for calculating heat flux at dry surfaces.....	19
15.2.9. Heat transfer at wet surfaces	22
15.2.10. In-situ measurement of rock thermal conductivity	27
15.3. OTHER SOURCES OF HEAT	29
15.3.1. Autocompression	29
15.3.2. Mechanized equipment.....	32
15.3.2.1. Electrical equipment.....	34
15.3.2.2. Diesel equipment.....	35
15.3.2.3. Compressed air	36
15.3.3. Fissure water and channel flow	38
15.3.4. Oxidation	41
15.3.5. Explosives	42
15.3.6. Falling rock.....	42
15.3.7. Fragmented rock.....	43
15.3.8. Metabolic heat.....	44
BIBLIOGRAPHY	45
APPENDIX A15.1	46
<i>Analytical solution of the three dimensional transient heat conduction equation (15.13) as obtained by Carslaw and Jaeger (1956).....</i>	46
APPENDIX A15.2	46
<i>Gibson's algorithm for the determination of dimensionless temperature gradient, G.</i>	46
APPENDIX A15.3.	47
<i>Background to equations for the heat transfer coefficient, h.</i>	47
APPENDIX A15.4	53
<i>Derivation of the equation for latent heat of evaporation at a wet surface.</i>	53

15.1. INTRODUCTION

Heat is emitted into subsurface ventilation systems from a variety of sources. In the majority of the world's coal mines, the airstream itself is sufficient to remove the heat that is produced. In deep metal mines, heat is usually the dominant environmental problem and may necessitate the use of large-scale refrigeration plant (Chapter 18). Conversely, in cold climates, the intake air may require artificial heating in order to create conditions that are tolerable for both personnel and equipment.

In Section 9.3.4, quantification of the heat emitted into a mine or section of a mine was required in order to assess the airflow needed to remove that heat. Hence, a sensible place to commence the study of heat flow into mine openings is to classify, analyze and attempt to quantify the various sources of heat. The three major heat sources in mines are the conversion of potential energy to thermal energy as air falls through downcasting shafts or slopes (autocompression), machinery and geothermal heat from the strata. The latter is, by far, the most complex to analyze in a quantitative manner. We shall deal with this separately in Section 15.2, then quantify other sources of heat in Section 15.3.

15.2. STRATA HEAT

15.2.1. Methods of determining strata heat load

In reviewing the literature for means of determining the amount of heat that will be emitted from the strata, the ventilation engineer is faced with a bewildering array of methods varying from the completely empirical, through analytical and numerical, to computer simulation techniques. The basic difficulty is the large number of variables, often interacting with each other, which govern the flow of strata heat into mine airways. These include:

- the length and geometry of the opening
- depth below surface and inclination of the airway
- method of mining
- wetness of the airway surfaces
- roughness of the airway surfaces
- rate of mineral production or rock breaking
- time elapsed since the airway was driven
- volume flow of air
- barometric pressure, and wet and dry bulb temperatures
- virgin (natural) rock temperature
- distance of the workings from downcast shafts or slopes
- geothermic step or geothermic gradient
- thermal properties of the rock
- other sources of heating or cooling such as machines and cooling plant.

With such a variety of parameters, it is hardly surprising that traditional methods of predicting strata heat loads have been **empirical**. Perhaps the simplest and most common of these has been to quote strata heat flux in terms of **heat load per unit rate of mineral production**; for example, **kW per tonne per day**. This can provide a useful and rapid guideline provided that all conditions are similar to those on which the value was based. However, as rate of production is only one of the several variables listed above, it is obvious that this technique can lead to gross errors if it is applied where the value of any one of those variables is significantly different from the original sets of measurements used to establish the kW/tonne/day value.

The more sophisticated empirical techniques extend their range of application by incorporating estimated corrections for depth, distance, age, inlet conditions or, indeed, any of the listed variables considered to be of local importance.

The purely analytical methods of quantifying heat flow from the strata are somewhat limited for direct practical application because of the complexity of the equations that describe three-dimensional, time-transient heat conduction. Indeed, they can be downright frightening. However, the theory that has evolved from analytical research has provided the basis for numerical modelling which, in turn, has resulted in the development of pragmatic computer simulation packages for detailed prediction of variations in the mine climate.

A **hybrid method** has grown out of experience in running climatic simulation packages. It is often the case that, for particular conditions, some of the input variables have a very limited effect on the results. By ignoring those weaker parameters it is then sometimes possible to develop simple equations that give an approximation of the heat flow.

In view of these alternative methodologies, what is the mine environmental engineer to do when faced with the practical problems of system design? Experience gained from major planning projects has indicated the following recommended guidelines:

1. If the objective is to plan the further development of an existing mine, or if there are neighbouring mines working similar deposits at equivalent depths and employing the same methods of working, then the **empirical approach** (kW per tonne per day) may be adopted for the overall strata heat load on the whole mine or major sections of the mine. This presupposes the existence of data that allow acceptable empirical relationships to be established and verified.

Employing past and relevant experience in this way provides a valuable and simple means of arriving at an approximate heat load which, when combined with the methodology of Section 9.3.4, will give an indication whether the heat can be removed by the airflow alone, or if refrigeration is required.

However, **let the user beware**. If the proposed mine project deviates in any significant manner from the conditions in which the empirical data were compiled (check the list of variables at the beginning of this section), then the results may be misleading. In particular, great caution should be exercised when employing empirical relationships established in other geographical regions. A phrase commonly heard at mine ventilation conferences is "what works there, doesn't work here."

2. The hybrid equations are very useful for rapid approximations of heat flow into specified types of openings. **Dr. Austin Whillier** of the Chamber of Mines of South Africa produced many hybrid equations for easy manual application, including:

(a) *Radial heat flow into established tunnels*

$$q = 3.35 L k^{0.854} (VRT - \theta_d) \quad \text{W} \quad (15.1)$$

where

- q = heat flux from strata (W)
- L = length of tunnel (m)
- k = thermal conductivity of rock (W/m°C)
- VRT = virgin (natural) rock temperature (°C)
- θ_d = mean dry bulb temperature (°C)

Throughout this chapter we shall use the symbol k for thermal conductivity and θ for temperature.

(b) *Advancing end of a heading*

$$q = 6k(L + 4DFA)(VRT - \theta_d) \quad W$$

where

L = length of the advancing end of the heading (m). This should be not greater than the length advanced in the last month. Equation (15.1) may be used for the older sections of the heading. .

DFA = daily face advance (m).

(c) *One dimensional heat flow towards planar surfaces*

Assuming good convective or evaporative cooling of the surfaces,

$$q = \frac{A(k\rho C)^{0.5}(VRT - \theta_d)}{t^{0.5}} \quad W \quad (15.3)$$

where

A = area of surface (m²)

ρ = rock density (kg/m³)

C = specific heat of rock (J/(kg°C))and

t = time since the surface was exposed (s)

A weakness of these equations is that they each contain the mean dry bulb temperature, θ_d . As this is initially unknown, it must be estimated. If, when the resulting value of q is used to determine the temperature rise, the initial estimate of θ_d is found to have been significantly in error then the process may be repeated. However, as the hybrid equations promise nothing more than rough approximations there may be little point in progressing beyond a single iteration.

- For accurate and detailed planning, a mine climate simulation package should be employed. These are computer programs that have been developed to take all of the relevant variables into account. They may be used for single airways or combined into a total underground layout. Climate simulation programs go beyond the calculation of heat load by predicting the effects of that heat on the psychrometric conditions in the mine. The principles of a climate simulation program are outlined in Chapter 16.

For major projects, estimates of heat loads may be based on empirical and hybrid methodologies for initial conceptual layouts, progressing to simulation techniques for detailed planning.

15.2.2. Qualitative observations

Before embarking upon a quantitative analysis of strata heat flow, it will be useful to introduce some of the observable phenomena in a purely qualitative manner.

First, when cool air passes through a level airway, its temperature usually increases. This is caused by natural geothermal heat being conducted through the rock towards the airway, then passing through the boundary layers that exist in the air close to the rock surface. In working areas, the newly exposed rock surfaces are often perceptibly warmer than the air. However, those surfaces cool with time until they may be only a fraction of a degree C higher than the temperature of the air.

If the airway is wet then the increase in dry bulb temperature is less noticeable. Indeed, that temperature may even fall. This is a result of the cooling effect of evaporation. Heat may still emanate from the strata but all, or much of it, is utilized in exciting water molecules to the extent

that they leave the liquid phase and form water vapour. The heat content and wet bulb temperature of the air/vapour mixture then rise because of the internal energy of the added water vapour.

Another observation that can be made in practice is that although the air temperature in main intake arteries rises and falls in sympathy with the surface climate, the temperatures in main returns remain remarkably constant throughout the year. This is because cool air will encourage heat to flow from the rock. However, as the temperature of the air approaches the natural temperature of the rock such heat transfer will diminish. It can, of course, work in reverse. For example, the temperature of the air leaving an intensively mechanized working area may be greater than the local strata temperature. In that case, heat will pass from the air to the rock. The air will cool and, again, approach equilibrium when its temperature equals that of the strata. A mine is an excellent thermostat.

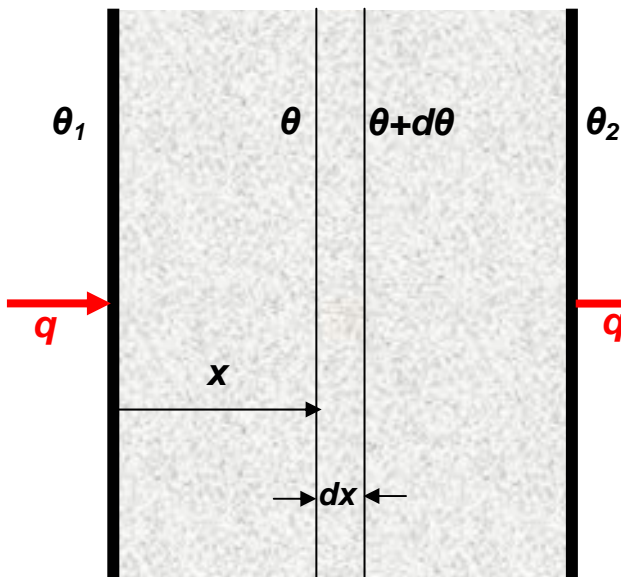
The envelope of rock immediately surrounding a newly driven airway will cool fairly rapidly at first. There will, accordingly, be a relatively high rate of initial heat release into the air. This will decline with time. A well-established return airway may have reached near thermal equilibrium with the surrounding strata. However, the linings and envelope of rock around downcast shafts or main intakes will emit heat during the night when the incoming air is cool and, conversely, absorb heat during the day if the air temperature becomes greater than that of the surrounding envelope of rock. This cyclic phenomenon, sometimes known as the "thermal flywheel" (Stroh, 1979) is superimposed upon longer term cooling of the larger mass of rock around the opening.

The boundary layers that exist within the airflow close to the rock surface act as insulating layers and, hence, tend to inhibit heat transfer between the rock and the main airstream. It follows that any thinning or disturbance of those boundary layers will increase the rate at which heat transfer takes place. This can occur either through a rise in air velocity or because of a greater degree of roughness on the surface (Section 2.3.6).

Finally, although there may be significant rises in the air temperature along intake airways, the most noticeable increase usually occurs in the mineral winning areas. This is because, first, the newly exposed and warm surfaces of both the solid and broken rock give up their heat readily and, secondly, the mechanized equipment that may be concentrated in stopes or working faces.

Having introduced these concepts in a purely subjective manner, we now have a better intuitive understanding from which to progress into a quantified and analytical approach.

15.2.3. Fourier's law of heat conduction



When a steady heat flux, q , passes through a slab of homogeneous material, the temperature will fall from θ_1 at entry to θ_2 at exit (Figure 15.1). Planes of constant temperature, or isotherms, will exist within the material. Figure 15.1 also shows two isotherms at a short distance, dx , apart and with temperatures θ and $\theta + d\theta$.

The heat flux, q , is proportional to both the orthogonal area, A , through which the heat travels and the temperature difference, $d\theta$, between isotherms. It is also inversely proportional to the distance, dx , between those isotherms.

Figure 15.1 Linear heat flow.

Hence,

$$q \text{ is proportional to } -A \frac{d\theta}{dx}$$

where q = heat flux (W)
 A = area through which q passes (m^2),
 θ = temperature ($^{\circ}\text{C}$) and
 x = distance (m)

The negative sign is necessary since θ reduces in the direction of heat flow, i.e. $d\theta$ is negative. To convert this relationship into an equation, a constant of proportionality, k , is introduced, giving

$$q = -k A \frac{d\theta}{dx} \quad \text{W} \quad (\text{Fourier's Law}) \quad (15.4)$$

k is termed the **thermal conductivity** of the material and has units of $\text{W}/(\text{m}^{\circ}\text{C})$.

To be precise, k is a slowly changing function of temperature. It may also vary with the mechanical stress applied to the material. In the strata around mine openings, the **effective thermal conductivity** of the strata can be significantly different from those given by samples of the rock when measured in a laboratory test (Section 15.2.10). The reasons for such differences include natural or induced fractures in the strata, variations in mineralogy that may be direction dependent, movements of groundwater, radioactive decay and local geothermal anomalies.

15.2.4. Geothermic gradient, geothermal step and thermal conductivity

The crustal plates upon which the continents drift over geological time are relatively thin compared to the diameter of the earth. Furthermore, it is only in the upper skin of those plates that mining takes place at the present time. The geothermal flow of heat emanating from the earth's core and passing through that skin has an average value of 0.05 to $0.06 \text{ W}/\text{m}^2$. It can, of course, be much higher in regions of anomalous geothermal activity

In Fourier's law, equation (15.4), if we use the value of 0.06 W for each square metre of land surface to give the variation of temperature, θ , with respect to depth D ($= -x$), then

$$\frac{d\theta}{dD} = \frac{0.06}{k} \quad \frac{^{\circ}\text{C}}{\text{m}} \quad (15.5)$$

The increase of strata temperature with respect to depth is known as the **geothermic gradient**. In practical utilization, it is often inverted to give integer values and is then referred to as the

$$\text{Geothermal step} = dD/d\theta \quad \text{m}/^{\circ}\text{C} \quad (15.6)$$

It is clear from equations (15.5) and (15.6) that as we progress downwards through a succession of strata, the geothermal gradient and geothermal step will vary according to the thermal conductivity of the local material.

Table 15.1 has been assembled from several sources as a guide to the thermal conductivities and corresponding geothermal steps that may be expected for a range of rock types. However, it should be remembered that these parameters are subject to significant local variations. Site specific values should be obtained, preferably from in-situ tests, for any important planning work.

Rock type	Thermal conductivity W/(m°C)	Geothermal step m/°C
Copper orebody (Montana)	0.8 to 1.1	13 to 18
Copper orebody (Arizona)	1.3	22
Carboniferous	1.2 to 3.0	20 to 50
Clays	1.8	30
Limestone	3.3	55
Sandstone	2.0 to 3.6	30 to 60
Dolerite	2.0	33
Quartzite	4.0 to 7.0	65 to 120
Potash (low grade)	3.5 to 5.0	60 to 80
(high grade)	5.0 to 7.0	80 to 120
Halite (low grade)	1.5 to 4.0	25 to 70
(high grade)	4.0 to 6.0	70 to 100

Table 15.1. Typical values of thermal conductivity and geothermal step for a range of rock types.

For air and water in the range 0 to 60°C (Hemp, 1985)

$$k_a = 2.2438 \times 10^{-4} T^{0.8353} \quad \text{W/(m}^\circ\text{C)}$$

$$k_w = 0.2083 + 1.335 \times 10^{-3} T \quad \text{W/(m}^\circ\text{C)}$$

where T = Absolute temperature (K)

15.2.5. An analysis of three dimensional heat conduction.

During the practical application of empirical, hybrid or simulation techniques of assessing strata heat loads (Section 15.2.1) the mine environmental engineer need give little conscious thought to the theory of heat conduction or the derivations given in this Section. **These analyses are included here because they provide the essential relationships for the development and internal operation of numerical models and, hence, mine climate simulation packages. Readers who are not concerned with the analytical treatment should skip directly to Section 15.3.**

Within the envelope of rock that surrounds an underground airway, the temperature varies with both position and time. Our first task is to derive a general relationship that defines the temperature of the rock as a function of location and time. For simplicity, we shall assume that the thermal properties of the rock remain constant with respect to both position and time.

The general equations for heat conduction are readily derived in Cartesian co-ordinates. However, for mine airways, it is more practical to work in cylindrical polar co-ordinates. Figure 15.2 represents a mass of strata surrounding an underground airway. The z axis represents an airway simply as a line. The position of any point in the strata can be defined by co-ordinates z , r and θ where r is the radial distance from the centreline and θ is the angle from the horizontal measured in radians.

Consider a small trapezoidal element lying in a thin annulus of rock at a distance r from the centre line. The length of the element is dz , and its radial height is dr . The inner width is $r d\theta$ increasing to $(r + dr)d\theta$ at its outer limit.

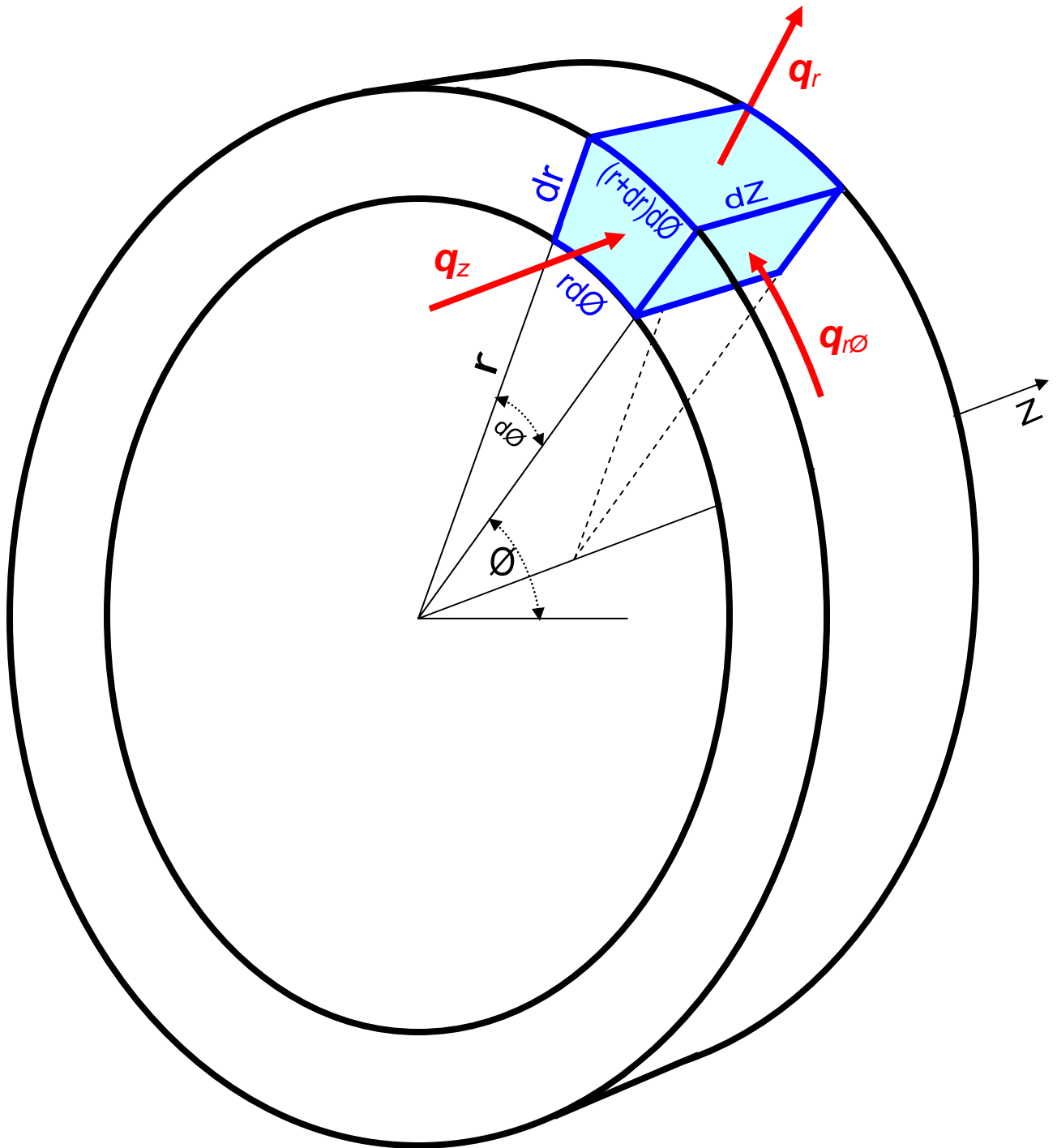


Figure 15.2 Three dimensional heat flow.

We shall analyse the heat flux passing through the element shown shaded. This can be accomplished by examining, in turn, the partial heat flows in the directions of increasing r , θ and z , and in that order.

1. The base of the element has an area $r d\phi dz$, the curvature being negligible over such short distances. The flux passing through this face is given by Fourier's Equation (15.4)

$$dq_{1,r} = -k r d\phi dz \frac{\partial \theta}{\partial r} \quad \text{W}$$

The opposite face has an area of $(r + dr) d\phi dz$ and passes a heat flow of

$$dq_{2,r} = -k(r + dr) d\phi dz \frac{\partial}{\partial r} \left(\theta + \frac{\partial \theta}{\partial r} dr \right) \quad \text{W}$$

Heat retained by the element in the r direction is

$$dq_{1,r} - dq_{2,r} = k r d\phi dz \frac{\partial^2 \theta}{\partial r^2} dr + k dr d\phi dz \left\{ \frac{\partial \theta}{\partial r} + \frac{\partial^2 \theta}{\partial r^2} dr \right\} = k dr d\phi dz \left\{ \frac{r \partial^2 \theta}{\partial r^2} + \frac{\partial \theta}{\partial r} \right\} \quad (15.7)$$

as the term involving $(dr)^2$ is insignificant.

2. The heat flux in the direction of increasing ϕ passes through opposite faces, each of area $dr dz$. The direction is actually $r\phi$. Hence, Fourier's equation for heat entering the element is

$$dq_{1,\phi} = -k dr dz \frac{\partial \theta}{\partial(r\phi)} = -k dr dz \frac{\partial \theta}{r \partial \phi} \quad \text{W}$$

while the heat leaving the element is

$$dq_{2,\phi} = -k dr dz \frac{\partial}{r \partial \phi} \left\{ \theta + \frac{\partial \theta}{r \partial \phi} r d\phi \right\} = -k dr dz \left\{ \frac{\partial \theta}{r \partial \phi} + \frac{\partial^2 \theta}{r \partial \phi^2} d\phi \right\} \quad \text{W}$$

Heat gain in the $r\phi$ direction is

$$dq_{1,\phi} - dq_{2,\phi} = k dr dz d\phi \frac{\partial^2 \theta}{r \partial \phi^2} \quad \text{W} \quad (15.8)$$

3. Repeating the exercise for the z direction, the opposite faces are trapeziums of height dr and opposite edges of length $r d\phi$ and $(r + dr)d\phi$, the curvature of the lines being insignificant over such small distances. The latter have an average length of

$$\frac{r d\phi + (r + dr) d\phi}{2} \quad \text{m}$$

The product of the differentials $dr d\phi$ is negligible compared with $r d\phi$, giving the width to be $r d\phi$ and face area of $r d\phi dr$.

The heat entering the element in the z direction is

$$dq_{1,z} = -k r d\phi dr \frac{\partial \theta}{\partial z} \quad \text{W}$$

and leaving the opposite face,

$$dq_{2,z} = -k r d\phi dr \frac{\partial}{\partial z} \left(\theta + \frac{\partial \theta}{\partial z} dz \right) \quad \text{W}$$

Then the rate of heat accumulated in the z direction is

$$dq_{1,z} - dq_{2,z} = k r d\phi dr dz \frac{\partial^2 \theta}{\partial z^2} \quad \text{W} \quad (15.9)$$

The total rate of heat gain by the element, dq , is given by summing equations (15.7, 15.8 and 15.9)

$$dq = k dr d\phi dz \left\{ r \frac{\partial^2 \theta}{\partial r^2} + \frac{\partial \theta}{\partial r} + \frac{1}{r} \frac{\partial^2 \theta}{\partial \phi^2} + r \frac{\partial^2 \theta}{\partial z^2} \right\} \quad \text{W} \quad (15.10)$$

The heat gain by the element in time ∂t (where t = time in seconds) can also be expressed as

$$dq = mC \frac{\partial \theta}{\partial t} \quad \text{W}$$

where m = mass of element and C = specific heat of the material.

But m = volume x density (ρ) = $dr dz rd\phi \rho$

Then

$$dq = dr dz rd\phi \rho C \frac{d\theta}{\partial t} \quad \text{W} \quad (15.11)$$

Hence, from Equations (15.10 and 15.11)

$$k \left\{ r \frac{\partial^2 \theta}{\partial r^2} + \frac{\partial \theta}{\partial r} + \frac{1}{r} \frac{\partial^2 \theta}{\partial \phi^2} + r \frac{\partial^2 \theta}{\partial z^2} \right\} = r \rho C \frac{\partial \theta}{\partial t} \quad \frac{\text{W}}{\text{m}^2} \quad (15.12)$$

or

$$\frac{k}{\rho C} \left\{ \frac{\partial^2 \theta}{\partial r^2} + \frac{1}{r} \frac{\partial \theta}{\partial r} + \frac{1}{r^2} \frac{\partial^2 \theta}{\partial \phi^2} + \frac{\partial^2 \theta}{\partial z^2} \right\} = \frac{\partial \theta}{\partial t} \quad \frac{^\circ\text{C}}{\text{s}}$$

This fundamental relationship is the general three-dimensional equation for unsteady heat conduction expressed in cylindrical polar co-ordinates.

For most purposes in strata heat conduction towards airways, we can assume that

$$\frac{\partial \theta}{\partial z} = \frac{\partial^2 \theta}{\partial z^2} = 0$$

and that

$$\frac{\partial \theta}{\partial \phi} = \frac{\partial^2 \theta}{\partial \phi^2} = 0$$

These simplifications are based on the premise that the natural geothermic gradient is small compared to the radial variation in temperature around the incremental length of airway, and that the heat conduction is radial along the full length.

Then

$$\frac{k}{\rho C} \left\{ \frac{\partial^2 \theta}{\partial r^2} + \frac{1}{r} \frac{\partial \theta}{\partial r} \right\} = \frac{\partial \theta}{\partial t} \quad \frac{^\circ\text{C}}{\text{s}}$$

The term $k/\rho C$ is a constant for the material and is called the **thermal diffusivity**, α (m^2/s) giving

$$\alpha \left\{ \frac{\partial^2 \theta}{\partial r^2} + \frac{1}{r} \frac{\partial \theta}{\partial r} \right\} = \frac{\partial \theta}{\partial t} \quad \frac{^\circ\text{C}}{\text{s}} \quad (15.13)$$

This is the form of the equation normally quoted for **radial heat conduction** and is the basis on which strata heat flow is determined in mine climate simulation programs. Figure 15.3 gives a graphical illustration of the time transient heat conduction equation.

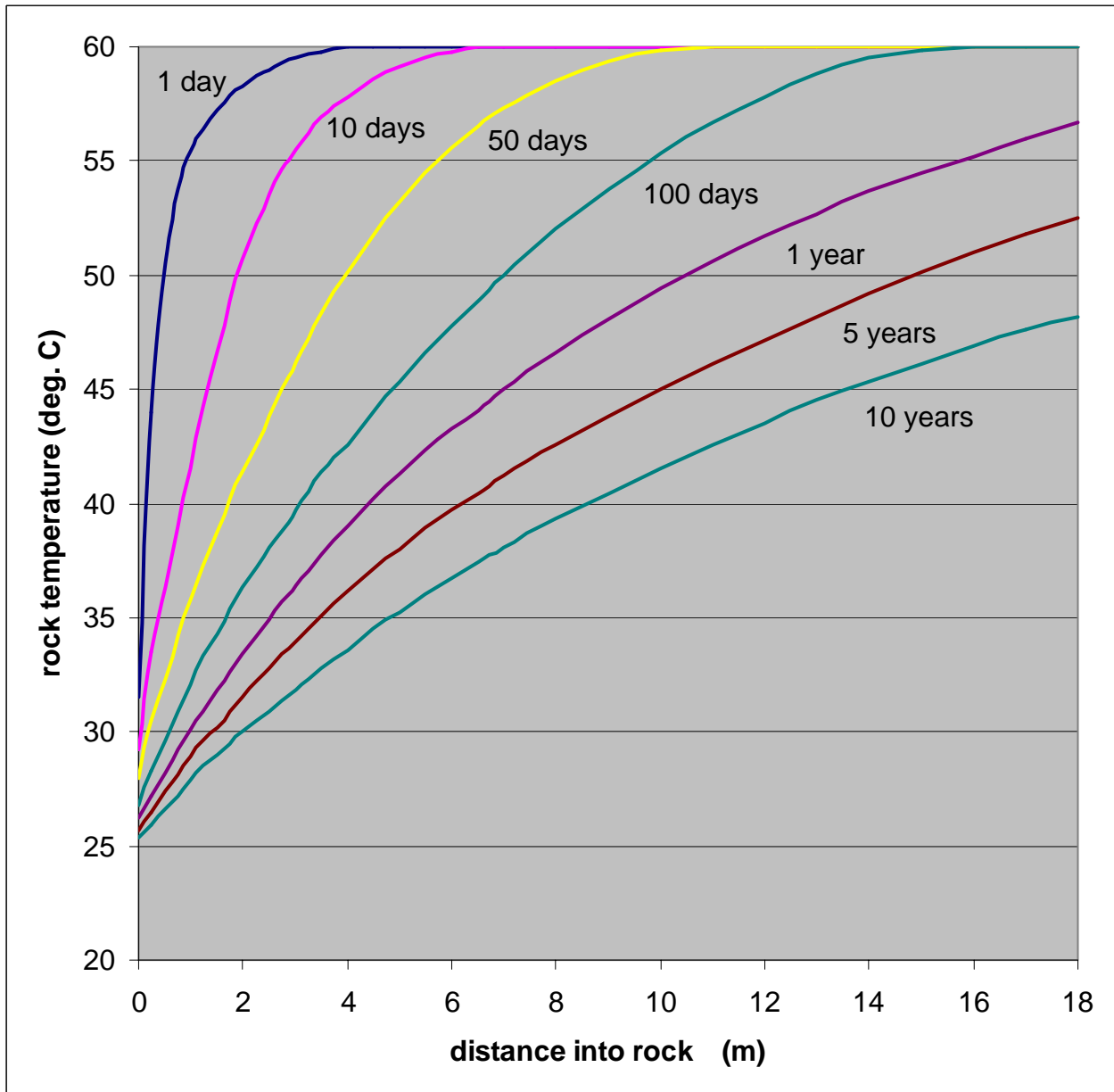


Figure 15.3 An illustration of the variation of rock temperature with respect to time and distance into the rock.

15.2.6. Solution of the radial heat conduction equation

Having derived equation (15.13) for the time-space variation in temperature around an underground airway, we must now attempt to transform it into a practical procedure to determine strata heat emission into the airway.

In order to facilitate further analysis and generality, it is convenient to express radial distances and time as dimensionless numbers.

$$\text{Dimensionless radius } r_d = \frac{r}{r_a}$$

where r_a = effective radius of the airway (= perimeter / 2π)

The actual shape of the cross section has little effect on the influx of strata heat into airways.

$$\text{Dimensionless time } F_o = \frac{\alpha t}{r_a^2} \quad (\text{this is called the Fourier number})$$

Equation (15.13) then becomes

$$\frac{\partial^2 \theta}{\partial (r_d r_a)^2} + \frac{1}{r_d r_a} \frac{\partial \theta}{\partial (r_d r_a)} = \frac{1}{\alpha} \frac{\partial \theta}{\partial (F_o r_a^2 / \alpha)}$$

As r_a and α are constants

$$\frac{\partial^2 \theta}{r_a^2 \partial (r_d)^2} + \frac{1}{r_d r_a^2} \frac{\partial \theta}{\partial (r_d)} = \frac{1}{\alpha r_a^2 / \alpha} \frac{\partial \theta}{\partial (F_o)}$$

The r_a^2 and α terms cancel, giving the radial heat conduction equation as

$$\frac{\partial^2 \theta}{\partial (r_d)^2} + \frac{1}{r_d} \frac{\partial \theta}{\partial (r_d)} = \frac{\partial \theta}{\partial (F_o)} \quad (15.14)$$

The determination of heat flux into the airway commences by applying Fourier's law (equation (15.4)) to each square metre of rock surface :

$$q = k \left(\frac{\partial \theta}{\partial r} \right)_s \quad \frac{W}{m^2} \quad (15.15)$$

where $\left(\frac{\partial \theta}{\partial r} \right)_s$ is the temperature gradient in the rock but at the rock/air interface (subscript s for surface).

This same heat flux, q , passes from each square metre of surface through the boundary layers into the main airstream. However, for any given type of surface and flow conditions, the heat transferred through the boundary layers is proportional to the temperature difference across those layers,

$$\text{i.e. } q = h(\theta_s - \theta_d) \quad W/m^2 \quad (15.16)$$

where θ_s = temperature of the rock surface ($^{\circ}\text{C}$)
 θ_d = dry bulb temperature in the main airstream ($^{\circ}\text{C}$) and
 h = a **heat transfer coefficient** ($\text{W}/(\text{m}^2\text{C})$) that is a function mainly of the air velocity and the characteristics of the rock surface.

We shall discuss the heat transfer coefficient further in Section 15.2.7. However, for the moment let us accept it simply as a constant of proportionality between q and $(\theta_s - \theta_d)$.

Assuming that we know the values of h and θ_d , then we only need the rock surface temperature, θ_s , for equation (15.16) to give us the required heat flux, q . The problem turns to one of finding θ_s .

As the heat flux from the strata must be the same as that passing through the rock/air interface, we can combine equations (15.15) and (15.16) to give

$$q = k \left(\frac{\partial \theta}{\partial r} \right)_s = h(\theta_s - \theta_d) \quad \frac{\text{W}}{\text{m}^2} \quad (15.17)$$

Again, for generality, **the temperature gradient at the surface** may be expressed in dimensionless form, G , where

$$G = \frac{r_a}{(\text{VRT} - \theta_d)} \left(\frac{\partial \theta}{\partial r} \right)_s \quad (15.18)$$

where VRT = virgin (natural) rock temperature ($^{\circ}\text{C}$)

Combining with equation (15.17) gives

$$G(\text{VRT} - \theta_d) = \frac{h r_a}{k} (\theta_s - \theta_d) \quad ^{\circ}\text{C} \quad (15.19)$$

The group $h r_a/k$ is known as the **Biot Number, B** , or dimensionless heat transfer coefficient.

Then $G(\text{VRT} - \theta_d) = B(\theta_s - \theta_d) \quad ^{\circ}\text{C}$
 or

$$\theta_s = \frac{G}{B}(\text{VRT} - \theta_d) + \theta_d \quad ^{\circ}\text{C} \quad (15.20)$$

We have now found an expression for θ_s . However, it contains the dimensionless but yet unknown temperature gradient G . This may be obtained from a solution of the general radial heat conduction equation (15.13) using Laplace transforms. The mathematics of the solution process can be found in Carslaw and Jaeger (1956). The result involves a series of Bessel functions and is reproduced in Appendix A15.1 at the end of this chapter. Unfortunately, the solution appears even more disconcerting for practical use than the original differential equation (15.13). However, it is now more amenable to numerical integration. The results are shown on Figure 15.4 as a series of curves from which the dimensionless temperature gradient, G , can be read for given ranges of Fourier Number, F_o , and Biot number, B .

An algorithm produced by Gibson (1975) allows G to be determined much more easily than the full numerical integration of the Carslaw and Jaeger solution. Gibson's algorithm (Appendix A15.2) is suitable for programming into a personal computer and gives an accuracy of within 2 per cent over the majority of the ranges covered in Figure 15.4.

Older solutions to the general equation (15.13) (Carrier, 1940; Goch and Patterson, 1940) assumed that the rock surface temperature was equal to the dry bulb temperature of the air. This ignored the insulating effect of the boundary layers or, put another way, inferred an infinite heat transfer coefficient and, hence, an infinite Biot Number. The uppermost curve on Figure 15.4 represents this bounding condition and gives the same results as the tables produced by Carrier, and Goch and Patterson.

Having established a value of G , equations (15.17) and (15.20) then combine to give the required heat flux:

$$q = h \frac{G}{B} (VRT - \theta_d) \quad \frac{W}{m^2} \quad (15.21)$$

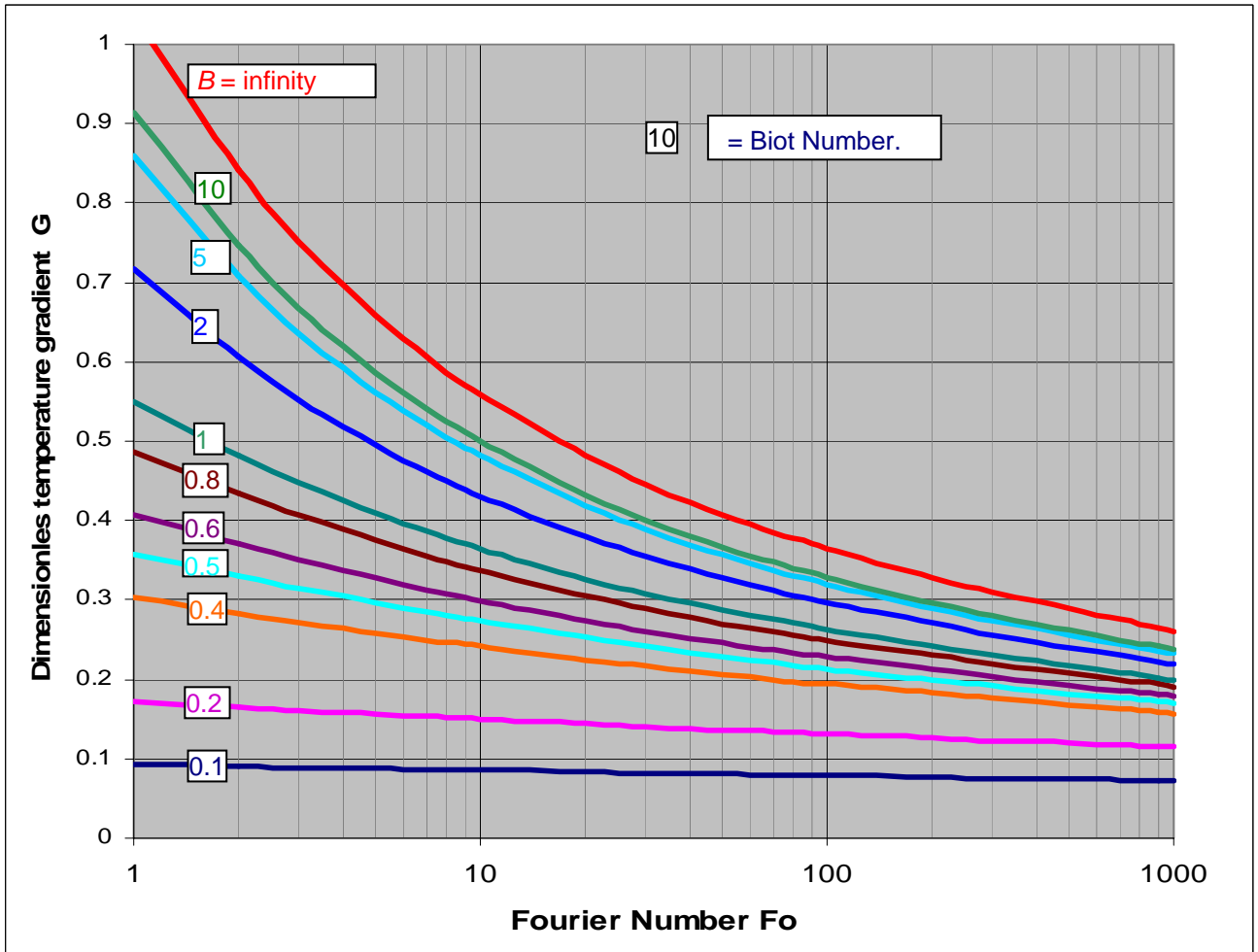


Figure 15.4 These curves enable the dimensionless temperature gradient, G , in the rock at its surface to be estimated for known Fourier and Biot Numbers.

15.2.7. Heat transfer coefficient for airways

In section 15.2.6, we introduced the heat transfer coefficient, h , for the rock surface as the 'constant' of proportionality between heat flux across a boundary layer and the corresponding temperature difference between the rock surface and the general airstream:

$$q = h(\theta_s - \theta_d) \quad \frac{W}{m^2} \quad (15.16)$$

It is clear from this equation that for a well established airway where the rock surface temperature, θ_s , is very close to the air dry bulb temperature, θ_d , the strata heat flux q will be small. The value of the heat transfer coefficient will then have little effect on climatic variations in the airway. Conversely, for newly exposed surfaces $(\theta_s - \theta_d)$ will be relatively high and the heat transfer coefficient will be a significant factor in controlling the flow of heat from the strata.

It can be seen from Figure 15.4 that for Biot Numbers ($B = hr_a/k$) of 10 or more, errors in the heat transfer coefficient and, hence, Biot Number will have little effect on the dimensionless temperature gradient, G , which in turn controls heat flux into the airway. For typical sizes of modern mine airways, the Biot Number is generally in excess of 5 where its accuracy (and, hence, the accuracy of the heat transfer coefficient) remains of limited consequence. It is, nevertheless, prudent to establish relationships that will allow us to evaluate the heat transfer coefficient.

The heat transfer coefficient is a constant only within the confines of equation (15.16). The overall heat transfer coefficient, h , for mine airways is made up of two parts, the convective heat transfer coefficient, h_c , and a component of the radiative heat transfer coefficient, h_r .

15.2.7.1. Convective heat transfer

In practice the convective heat transfer coefficient changes with those factors that cause variations in the thickness of the boundary layers, i.e. the air velocity and roughness on the surface that produce near-wall turbulence. Hence, the convective heat transfer coefficient depends upon the coefficient of friction, f , (or Atkinson friction factor) and the Reynolds Number, Re . These parameters were introduced in Section 2.3 as factors that influence airway resistance and losses of mechanical energy.

A rise in near-wall turbulence causes not only increased cross-flow momentum transfer close to the laminar sublayer but also helps transport heat across the turbulent boundary layer into the mainstream. There is a close analogy between heat and momentum transfer across boundary layers. This has engaged the attention of researchers since the time of Osborne Reynolds and many equations relating heat transfer coefficients to fluid properties and flow regimes have been proposed for both hydraulically smooth and rough surfaces.

A relationship that has shown itself to agree with practical observations both underground (Mousset-Jones et al, 1987; Danko et al, 1988) and in scale models (Deen, 1988) is based on earlier work by Nunner (1956). For application in mine ventilation, it may be stated as

$$N_u = \frac{0.35 f Re}{1 + 1.592 (15.217 f Re^{0.2} - 1) / Re^{0.125}} \quad \text{dimensionless} \quad (15.22)$$

The **convective heat transfer coefficient**, h_c , is then given as

$$h_c = \frac{N_u k_a}{d} \quad \text{W/(m}^2\text{C)} \quad (15.23)$$

where

k_a = thermal conductivity of air ($2.2348 \times 10^{-4} T^{0.8353}$ W/(m°C)), T being the absolute temperature in degrees Kelvin

and d = hydraulic mean diameter (m)

The **Nusselt Number** ($N_u = h_c d / k_a$) is simply a means of expressing the heat transfer coefficient as a dimensionless number in order to extend the generality of equation (15.22). It is analogous to the Biot Number but is referred to the air and the characteristics of the airway rather than the rock.

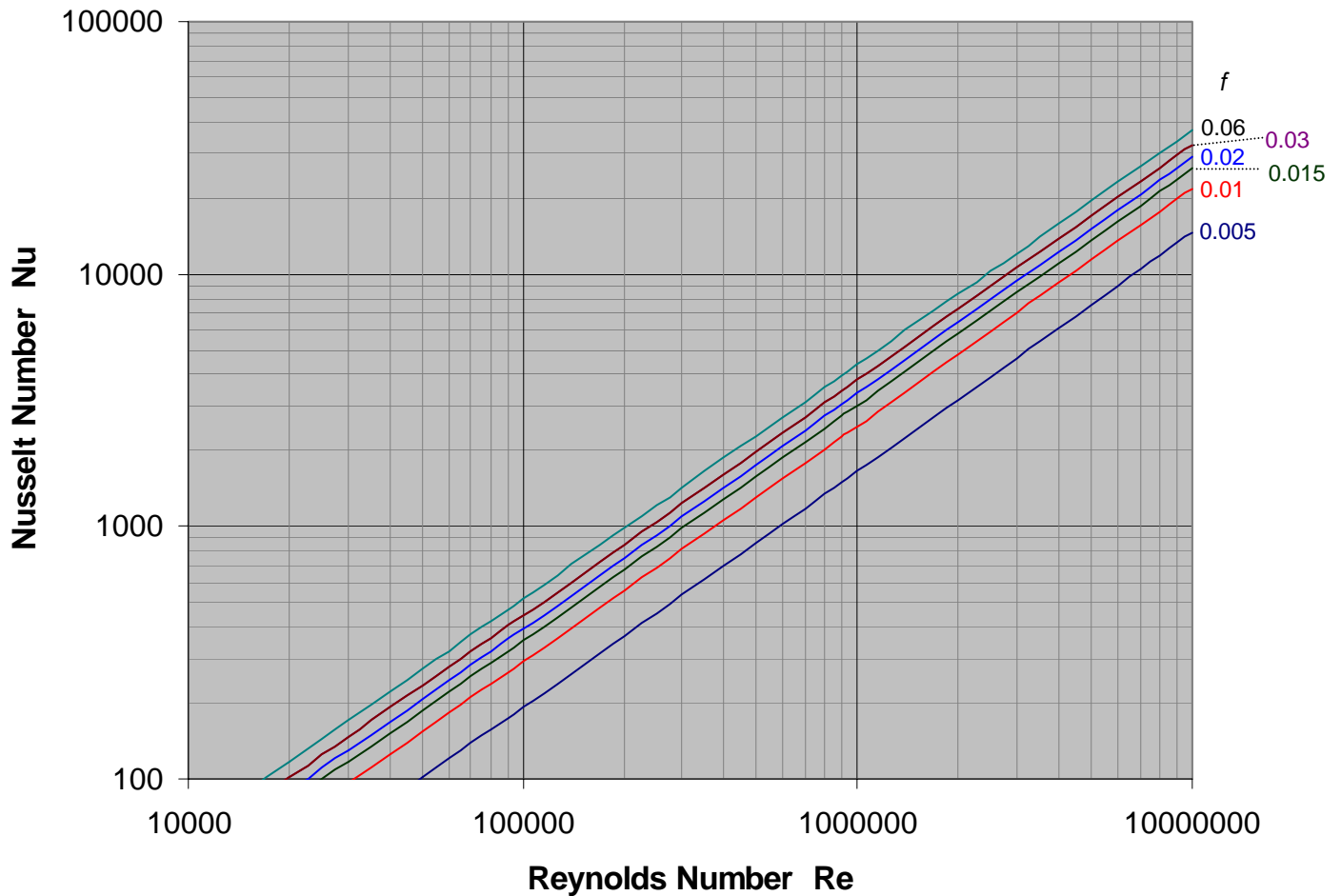


Figure 15.5 Variation of Nusselt Number, Nu , with coefficient of friction, f , and Reynolds Number, Re . (Based on air at 20 °C)

Here again, equations (15.22) and (15.23) may be programmed into a calculator or personal computer for a rapid determination of the convective heat transfer coefficient. For manual estimation, the Nusselt Number may be read directly from Figure 15.5 for any given values of f and Re . The background to equation (15.22) is given in Appendix A15.3.

A further phenomenon that has been observed experimentally and subjected to theoretical analyses is a tendency for the convective heat transfer coefficient to decrease as the wall temperature rises for any given value of Reynolds Number. This is caused by a thickening of the temperature or thermal boundary layer and, hence, giving an enhanced insulating effect against heat transfer between the wall and the main airstream. However, the actual heat transfer will normally increase because of the greater value of $(\theta_s - \theta_d)$ in equation (15.16).

15.2.7.2. Radiative heat transfer

In addition to convective effects, heat may be lost from a rock surface by **radiation**. Oscillations in atomic energy levels at the surface produce electromagnetic radiation. This propagates through space until it reaches another solid surface where some of it is reflected, the remainder returning

to thermal energy by excitation of atoms on the receiving surface. Additionally, some gases, including water vapour and carbon dioxide, will absorb a fraction of the thermal radiation causing a rise in temperature of the gas. Elemental gases such as oxygen and nitrogen, the major constituents of air, are not affected in this way.

According to the **Stefan-Boltzmann equation**, the net heat transfer by radiation from a hotter to a cooler surface is given as

$$q_r = 5.67 \times 10^{-8} (T_1^4 - T_2^4) A \times F_{ev} \quad \text{W} \quad (15.24)$$

where T_1 and T_2 are the absolute temperatures of the hotter and cooler surfaces respectively (K)
 A = the smaller of the two surfaces (m)

and 5.67×10^{-8} = the Stefan-Boltzmann constant. ($\text{Wm}^{-2} \text{K}^{-4}$) (15.25)

The parameter F_{ev} , combines the thermal emissivity of the surfaces and the view factor which quantifies the degree to which the surfaces can “see” each other (Whillier, 1982).

In subsurface environmental engineering, a more practical relationship for radiant heat transfer (in Watts per square meter) from airway surfaces is

$$q_r = h_r (\theta_s - \theta_d) F_{ev} \quad \text{W/m}^2 \quad (15.26)$$

where h_r = **radiative heat transfer coefficient** [$\text{W}/(\text{m}^2\text{C})$]

The emissivity of polished metal surfaces is fairly low. However, for rough natural surfaces it is usually more than 0.95. Furthermore, the view factor of each unit area of surface to water vapour in the passing airstream, or to much of the nearby rock surface, also approaches unity. Hence, we may approximate F_{ev} to 1.

The radiative heat transfer coefficient varies from 5 to 7 $\text{W}/(\text{m}^2\text{C})$ in the range of surface temperatures 10 to 40 °C. More precisely, it may be estimated as

$$h_r = 4 \times 5.67 \times 10^{-8} \times T_{av}^3 \quad \text{W}/(\text{m}^2\text{C}) \quad (15.27)$$

where T_{av} = Average absolute temperature of the two surfaces (K). In practice, this may be taken as the dry bulb temperature of the air.

For a dry airway, the temperature of the rock surface will remain the same around any given perimeter. Hence, $T_1 = T_2$ in equation (15.24) and there will be no net transfer of radiant heat between rock surfaces. If part of the surface is wet, however, radiant heat will pass from the dry areas to the cooler wet surface. This will cause a slight increase in strata heat transfer from dry areas. However, the small rise in temperature of the wet surfaces will result in a slightly diminished flow of strata heat to those surfaces. Although the two may not balance, the net effect is small. Radiative heat transfer between rock surfaces is usually ignored.

The amount of thermal radiation absorbed by water vapour in the air varies exponentially with the product of the vapour content and the distance travelled by the radiation through the air/vapour mixture. At a vapour content of 0.019 kg/kg dry air, 22 per cent of the radiant heat will be absorbed within 3 metres and 47 per cent within 30 metres. The remaining radiation that is not absorbed will be received on other rock surfaces and, again, will have little impact on the mine climate.

The radiative heat transfer coefficient, h_r , is usually considerably lower than the convective heat transfer coefficient, h_c , in mine airways and may, indeed, be of the same order as the uncertainty

in h_c . An estimate of the fraction a_b of thermal radiation absorbed by water vapour in the air may be obtained from

$$a_b = 0.104 \ln(147 X L) \quad (15.28)$$

where \ln = natural logarithm

X = water vapour content of air (kg/kg dry air) (Section 14.2.2.)

and L = distance travelled by the radiation through the air (path length, m)

This equation is based on curve fitting to empirical data.

The mean path of the electromagnetic waves propagating from a given point on a rock surface and before they strike another rock surface will depend upon the geometry of the mine opening. For a mine airway a typical mean path length may be of the order of three times the hydraulic mean diameter.

The effective radiant heat transfer coefficient for thermal radiation between the rock and the air becomes $a_b h_r$.

The overall heat transfer coefficient is then

$$h = h_c + a_b h_r \quad \text{W/(m}^2 \text{ }^\circ\text{C)}$$

Analyses can also be carried out for the absorption of thermal radiation by carbon dioxide and dust particles. However, under normal conditions the corresponding rates of thermal absorption are very small.

Example.

The dry bulb temperature of the air in a 4m by 3m underground opening is 26 °C. The corresponding moisture content is 0.015 kg/kg dry air. Estimate the effective radiant heat transfer coefficient.

Solution.

$$\text{Hydraulic mean diameter, } d_h = \frac{4 \times \text{Area}}{\text{perimeter}} = \frac{4 \times 12}{14} = 3.43 \text{ m}$$

Assume the mean path length of the radiation to be

$$3 d_h = 3 \times 3.43 = 10.3 \text{ m}$$

Fraction of radiation absorbed (from equation (15.28))

$$a_b = 0.104 \ln(147 \times 0.015 \times 10.3) = 0.32$$

From equation (15.27)

$$h_r = 4 \times 5.67 \times 10^{-8} (273.15 + 26)^3 = 6.1 \quad \text{W/(m}^2 \text{ }^\circ\text{C)}$$

Then the effective radiant heat transfer coefficient is

$$a_b h_r = 0.32 \times 6.1 = 1.95 \quad \text{W/(m}^2 \text{ }^\circ\text{C)}$$

15.2.8. Summary of procedure for calculating heat flux at dry surfaces

Sections 15.2.5 to 15.2.7 have detailed the derivation of relationships that describe the radial flow of strata heat through the rock towards a mine opening and across a dry surface into the main airstream. As often occurs in engineering, the application of those relationships is straightforward compared with the theoretical analyses that have produced them.

Before moving on to consider heat exchange at wet surfaces, it is convenient to summarize the procedure for calculating the emission of strata heat across a dry surface and to illustrate that procedure by a case study.

Calculation procedure for dry surface

1. Assemble the data:

- airway dimensions (m) .
- coefficient of friction, f (= Atkinson friction factor/0.6)
- age of airway, t (seconds) .
- airflow Q (m³/s) .
- mean dry bulb temperature of air, θ_d (°C)
wet bulb temperature, θ_w (°C)
barometric pressure, P (Pa) .
- rock thermal properties
thermal conductivity, k_r (W/m°C)
density, ρ_r (kg/m³)
specific heat, C_r (J/kg °C)
diffusivity, $\alpha_r = \frac{k_r}{\rho_r C_r}$ (m²/s)
virgin rock temperature, VRT (°C)

2. Determine derived parameters:

- cross sectional area, A (m²)
- perimeter of airway, per (m)
- hydraulic mean diameter, $d_h = 4A/per$ (m)
- effective radius, $r_a = per/(2\pi)$ (m)
- Reynolds' Number, Re . For the purposes of this procedure, Re may be calculated from the approximation $Re = 268\,000 Q/per$
- moisture content of air, X (kg/kg dry air) (from Section 14.6)
- mean radiation path length, L (m)

3. Determine the Nusselt Number, N_u , either from Figure 15.5 or from equation (15.22): i.e.

$$N_u = \frac{0.35 f Re}{1 + 1.592 \left(\frac{15.217 f Re^{0.2} - 1}{Re^{0.125}} \right)}$$

4. Determine the overall heat transfer coefficient, h :

- (a) Convective heat transfer coefficient, h_c

$$h_c = 0.026 \frac{N_u}{d_h} \quad \text{W/(m}^2\text{°C)}$$

where 0.026 W/(m°C) = thermal conductivity of air

- (b) Effective radiative heat transfer coefficient,
- $a_b h_r$

$$h_r = 22.68 \times 10^{-8} (273.15 + \theta_d)^3 \quad \text{W/(m}^2\text{°C)}$$

$$\text{Absorption fraction } a_b = 0.104 \ln(147 \times L)$$

$$\text{Effective radiative heat transfer coefficient} = a_b h_r$$

- (c) Overall heat transfer coefficient,

$$h = h_c + a_b h_r \quad (\text{W/m}^2\text{°C})$$

5 Calculate Biot Number, B :

$$B = \frac{h r_a}{k_r} \quad (\text{dimensionless})$$

6 . Calculate Fourier Number, F_o :

$$F_o = \frac{\alpha_r t}{r_a^2} \quad (\text{dimensionless})$$

7. Determine dimensionless temperature gradient in the rock but at the surface, G , either from Figure 15.4 or from Gibson's algorithm (Appendix A15.2).8 Determine heat flux, q :

$$q = h \frac{G}{B} (\text{VRT} - \theta_d) \quad (\text{W/m}^2)$$

9 . Calculate heat emission into airway:

$$\frac{q \times \text{per} \times \text{length of airway}}{1000} \quad (\text{kW})$$

Case Study

This case study illustrates not only the calculation procedure but also typical magnitudes of the variables. The purpose of the exercise is to determine the strata heat that will flow into an incremental length of dry airway. The stages of calculation are numbered to coincide with the steps of the procedure given above.

1. Given data:

- airway dimensions
width = 3.5 m, height = 2.5 m, length = 20 m
- Atkinson friction factor (at $\rho_a = 1.2 \text{ kg/m}^3$) = 0.014 kg/m^3
i.e. coefficient of friction, $f = 0.014/0.6 = 0.0233$ (dimensionless) .
- airway age = 3 months
 $t = \frac{365}{4} \times 24 \times 3600 = 7.884 \times 10^6$ seconds
- airflow, $Q = 30 \text{ m}^3/\text{s}$.
- dry bulb temperature in airway, $\theta_d = 25 \text{ °C}$
- from psychrometric data, the moisture content of the air has been determined to be
 $X = 0.01 \text{ kg/kg dry air}$.

- rock thermal properties:

conductivity, $k_r = 4.5 \text{ (W/m}^\circ\text{C)}$

density, $\rho_r = 2200 \text{ kg/m}^3$

specific heat, $C_r = 950 \text{ J/(kg}^\circ\text{C)}$

diffusivity, $\alpha_r = \frac{4.5}{2200 \times 950} = 2.153 \times 10^{-6} \text{ m}^2/\text{s}$

virgin rock temperature, VRT = 42 °C

- Further derived parameters:

- cross-sectional area, $A = 3.5 \times 2.5 = 8.75 \text{ m}^2$

- perimeter, $per = 2(3.5 + 2.5) = 12 \text{ m}$

- hydraulic mean diameter, $d_h = \frac{4A}{per} = \frac{4 \times 8.75}{12} = 2.917 \text{ m}$

- effective radius, $r_a = \frac{per}{2\pi} = \frac{12}{2\pi} = 1.910 \text{ m}$

- Reynolds' Number, $Re = 268000 \times \frac{30}{12} = 670000$

- mean radiation path length, L , is taken as $3 d_h = 3 \times 2.917 = 8.751 \text{ m}$

- The Nusselt Number, N_u , at $Re = 670000$ and $f = 0.0223$ is estimated from Figure 13.5 to be 2400. Alternatively, it may be calculated as

$$N_u = \frac{0.35 \times 0.0233 \times 670000}{1 + 1.592 \left(\frac{15.217 \times 0.0233 \times 670000^{0.2} - 1}{670000^{0.125}} \right)} = 2433 \text{ (dimensionless)}$$

- Overall heat transfer coefficient, h

- convective heat transfer coefficient, h_c ,

$$h_c = 0.026 \frac{N_u}{d_h} = 0.026 \times \frac{2433}{2.917} = 21.69 \frac{\text{W}}{\text{m}^2 \text{ }^\circ\text{C}}$$

- effective radiative heat transfer coefficient, $a_b h_r$

$$h_r = 22.68 \times 10^{-8} (273.15 + 25)^3 = 6.01 \text{ W}/(\text{m}^2 \text{ }^\circ\text{C})$$

absorption fraction

$$a_b = 0.104 \ln(147 \times 0.01 \times 8.751) = 0.266$$

$$a_b h_r = 0.266 \times 6.01 = 1.60$$

- overall heat transfer coefficient,

$$h = h_c + a_b h_r = 21.69 + 1.60 = 23.29 \text{ W}/(\text{m}^2 \text{ }^\circ\text{C})$$

This result illustrates the limited effect of thermal radiation.

- Biot Number, B

$$B = \frac{h r_a}{k_r} = \frac{23.29 \times 1.91}{4.5} = 9.885 \text{ (dimensionless)}$$

- Fourier Number, F_o

$$F_o = \frac{\alpha_r t}{r_a^2} = \frac{2.153 \times 10^{-6} \times 7.884 \times 10^6}{(1.91)^2} = 4.653 \text{ (dimensionless)}$$

7. Dimensionless rock temperature at the surface, G , for $B = 9.885$ and $F_o = 4.653$. This may be read from Figure 15.4 or computed from Gibson's algorithm (Appendix A15.2) as 0.60. It is clear from the graphical method that non-excessive errors in B (and, hence, heat transfer coefficient) will have a very limited effect on G for the conditions cited in this case study.

8. Heat flux

$$q = h \frac{G}{B} (VRT - \theta_d) = 23.29 \times \frac{0.60}{9.885} (42 - 25) = 24 \quad \frac{W}{m^2}$$

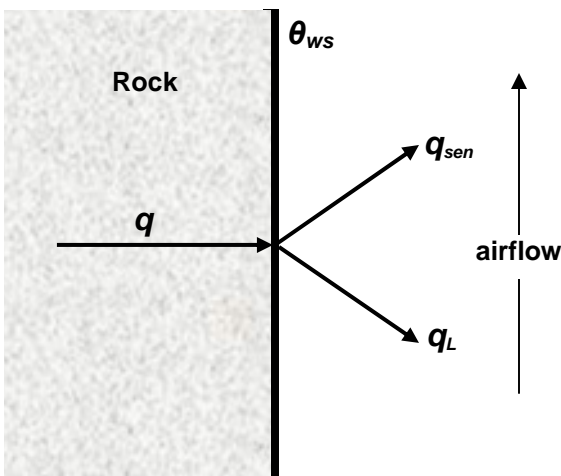
9. Heat emission into the 20m length of airway
= $q \times$ rock surface area W

or
$$\frac{24.0 \times 12 \times 20}{1000} = 5.76 \text{ kW}$$

15.2.9. Heat transfer at wet surfaces

The majority of underground openings have some degree of water evaporation or condensation occurring on rock surfaces even if no liquid water is visible. The cooling effect of evaporation or the heating effect of condensation on the rock surface will then result in a reduction or increase, respectively, of the wall surface temperature. This, in turn, will modify the strata heat flow toward that surface.

Figure 15.6 shows the heat balance that must exist for thermal equilibrium at the rock/air interface.



$$q = q_L + q_{sen} \text{ W/m}^2 \quad (15.29)$$

where

$$q = \text{strata heat flux} \quad (\text{W/m}^2)$$

$$q_L = \text{latent heat transfer} \quad (\text{W/m}^2)$$

$$q_{sen} = \text{sensible heat transfer} \quad (\text{W/m}^2)$$

In practice, any of these heat flows may be positive or negative. Indeed, a common situation occurs when the wet surface temperature, θ_{ws} , is less than the dry bulb temperature of the air, θ_d . In this case, sensible heat will pass from the air to water on the rock surface; q_L must then accommodate the combined values of q and q_{sen} .

In order to prevent unnecessary repetition, we shall assume evaporation in the following analysis. The same logic applies for condensation except that q_L is negative.

Figure 15.6 The heat balance at a wet surface.

Much of the theory pertaining to heat transfer at dry surfaces applies, also, to wet surfaces. In particular, let us re-examine equation (15.21) which was derived for a dry surface.

$$q = h_c \frac{G}{B} (VRT - \theta_d) \quad \frac{W}{m^2} \quad \text{ref (15.21)}$$

(We shall ignore the small effect of radiative heat transfer. Hence, the overall heat transfer coefficient, h , becomes the convective heat transfer coefficient, h_c).

Consider the functional dependence of each parameter in this equation in turn:

h_c depends upon f , Re , k_a and d (equations (15.22 and 15.23))

B depends upon h_c , r_a and k_r (equation (15.19))

G depends upon the Fourier Number, $F_o = \frac{\alpha_r t}{r_a^2}$ and the Biot Number, B

and VRT , the virgin rock temperature, is constant for any fixed location.

(Subscript r refers to the rock and a to the air or airway).

Notice that none of these parameters depends upon time transient temperatures within the rock nor whether the surface is wet or dry. They have exactly the same values for both wet and dry surface conditions. It is particularly significant that the dimensionless temperature gradient in the rock at the surface, G , is independent of the surface temperature - another illustration of the value of dimensionless numbers. Hence, the relationships derived earlier for h_c , B and G for a dry surface apply equally well for a wet surface. However, the evaporative cooling at a wet surface has not been taken into account and this must cause the strata heat flux, q , to increase.

In order to compensate for evaporation while continuing to use equation (15.21) we could select a value of θ_d reduced sufficiently such that the value of q given by equation (15.21) becomes equal to the heat flux actually passing through the wet surface. Let us name that reduced temperature the **effective dry bulb temperature**, θ_{ef} .

Then for the wet surface:

$$q = h_c \frac{G}{B} (VRT - \theta_{ef}) \quad \frac{W}{m^2} \quad (15.30)$$

Provided that we replace θ_d by θ_{ef} then the equations for heat transfer at a dry surface become applicable also for a wet surface. The problem now is to find the value of θ_{ef} .

In order to evaluate q_L and q_{sen} , we shall require the wet surface temperature, θ_{ws} . The form of equation (15.20) gives a relationship between θ_{ws} and θ_{ef} .

$$\theta_{ws} = \frac{G}{B} (VRT - \theta_{ef}) + \theta_{ef} \quad ^\circ\text{C} \quad (15.31)$$

This transposes to

$$\theta_{ef} = \left\{ \theta_{ws} - \frac{G}{B} VRT \right\} \frac{B}{B - G} \quad ^\circ\text{C} \quad (15.32)$$

Substituting for θ_{ef} in equation (15.30) and simplifying gives

$$q = h_c \frac{G}{(B - G)} (VRT - \theta_{ws}) \quad \frac{W}{m^2} \quad (15.33)$$

We now have an equation for the **strata heat flux** where everything is known except the wet surface temperature, θ_{ws} . Let us establish similar equations for q_L and q_{sen} , the other two terms in the heat balance of equation (15.29).

The **sensible heat** is given simply as

$$q_{sen} = h_c (\theta_{ws} - \theta_d) \quad W/m^2 \quad (\text{see equation (15.16)}) \quad (15.34)$$

The **latent heat** term, q_L , is given by

$$q_L = 0.0007 h_c L_{ws} \frac{(e_{ws} - e)}{P}, \quad W/m^2 \quad (15.35)$$

where L_{ws} = latent heat of evaporation at the wet surface temperature (J/kg)
 e_{ws} = saturated vapour pressure at the wet surface temperature (Pa)
 e = actual vapour pressure in the mainstream (Pa) and
 P = barometric pressure (Pa)

The derivation of equation (15.35) is given in Appendix A15.4. Values of L_{ws} , e_{ws} and e may be determined from the relationships given in Section 14.6. In particular L_{ws} and e_{ws} are functions of θ_{ws} only while e depends upon the wet and dry bulb temperatures of the mainstream, θ_w and θ_d , and the barometric pressure, P .

Equations (15.33, 15.34, and 15.35) allow q , q_{sen} and q_L to be determined on the basis of known mainstream conditions and an assumed wet surface temperature, θ_{ws} . If the assumed value of θ_{ws} were correct, then the heat balance

$$q = q_{sen} + q_L \quad (\text{from equation (15.29)})$$

would hold. However, an error in θ_{ws} will cause a corresponding error E in the heat balance:

$$E = q - (q_{sen} + q_L) \quad (15.36)$$

The wet surface temperature, θ_{ws} , may now be corrected according to the value of E and the process repeated iteratively until E becomes negligible. All heat flows are then defined.

Case Study

In order to illustrate the effect of water on heat flow across a rock surface, we shall use the same data given for the case study in Section 15.2.8 but now assuming that the surface is fully wetted.

To recap on the data:

1. Constants:

$$\begin{aligned} \text{Fourier Number, } F_o &= 4.653 \quad (\text{dimensionless}) \\ \text{Convective heat transfer coefficient, } h_c &= 21.69 \quad (W/m^2\text{ }^\circ\text{C}) \\ \text{Biot Number, } B = h_c \times \frac{r_a}{k_r} &= 21.69 \times \frac{1.91}{4.5} = 9.207 \quad (\text{dimensionless}) \end{aligned}$$

The value of B has changed by some 7 percent as we are now ignoring radiative effects i.e. using h_c instead of the overall heat transfer coefficient, h . However, when we employ F_o and the modified B on Figure 15.4 or in Gibson's algorithm (Appendix A15.2), the value of dimensionless temperature gradient G is not significantly different from the 0.6 obtained previously.

2 Psychrometric Data

The psychrometric relationships used here are listed in Section 14.6. In addition to the dry bulb temperature of 25°C, we shall also require the wet bulb temperature, θ_{wb} , and the barometric pressure, P , of the mainstream. For this case study we shall take these to be 17.9°C and 100 kPa respectively. Additionally, we need to assume a value for the temperature of the wet surface. As a first estimate, let us assume θ_{ws} to be the mean of the wet and dry bulb temperatures in the airstream, i.e. $\theta_{ws} = (25.0 + 17.9)/2 = 21.45$ °C.

(a) For the main airstream:

$$\text{Saturated vapour pressure, } e_{sat,air} = 610.6 \exp\left(\frac{17.27 \times 17.9}{237.3 + 17.9}\right) = 2050.4 \text{ Pa}$$

$$\text{Saturated moisture content, } X_{sat,air} = \frac{0.622 \times 2050.4}{100\,000 - 2050.4} = 0.01302 \text{ kg/kg dry air}$$

$$\begin{aligned} \text{Latent heat of evaporation at wet bulb temperature, } L_{w,air} &= (2502.5 - 2.386 \times 17.9)10^3 \\ &= 2459.79 \times 10^3 \text{ J/kg} \end{aligned}$$

$$\text{Sigma heat, } S_{air} = (2459.79 \times 10^3 \times 0.01302) + (1005 \times 17.9) = 50016 \text{ J/kg}$$

$$\text{Actual moisture content } X_{air} = \frac{50016 - (1005 \times 25)}{2459.79 \times 10^3 + 1884(25 - 17.9)} = 0.01006 \text{ kg/kg dry air}$$

$$\text{Actual vapour pressure, } e = \frac{100\,000 \times 0.01006}{(0.622 + 0.01006)} = 1592 \text{ Pa}$$

(b) For the wet surface (at temperature θ_{ws})

$$\text{Saturated vapour pressure, } e_{ws} = 610.6 \exp\left(\frac{17.27 \times 21.45}{237.3 + 21.45}\right) = 2556 \text{ Pa}$$

$$\text{Latent heat of evaporation, } L_{ws} = (2502.5 - 2.386 \times 21.45)10^3 = 2451.3 \times 10^3 \text{ J/kg}$$

3 Heat flows:

$$\text{Strata heat, } q = \frac{h_c G}{B - G} (VRT - \theta_{ws}) = \frac{21.69 \times 0.6}{(9.207 - 0.6)} (42 - 21.45) = 31.1 \text{ W/m}^2$$

$$\text{Sensible heat, } q_{sen} = h_c (\theta_{ws} - \theta_d) = 21.69(21.45 - 25) = -77.0 \text{ W/m}^2$$

Latent heat,
$$q_L = 0.0007 h_c L_{ws} (e_{ws} - e) / P$$

$$= 0.0007 \times 21.69 \times 2451.3 \times 10^3 \frac{(2556 - 1592)}{100000} = 358.8 \text{ W/m}^2$$

4 Correction of θ_{ws} :

The error in the heat balance is

$$E = q - (q_{sen} + q_L) = 31.1 - (-77.0 + 358.8) = -251 \text{ W/m}^2$$

$$\text{Corrected value of } \theta_{ws} = 21.45 + (-251) \times 0.01 = 18.94 \text{ }^\circ\text{C}$$

The correction function used here is 0.01 E. The constant 0.01 is chosen to give a reasonable rate of convergence. While mathematical techniques are available to find optimum correction functions for given iterative procedures, a more pragmatic approach (assuming computer availability) is simply to experiment with a set of typical data until satisfactory convergence is achieved.

The procedure from steps 2b to 4 is repeated iteratively until the absolute value of E becomes less than 0.01 W/m². This is clearly a task for a personal computer or programmable calculator. Programming the equations and logic into an algorithm is a useful student exercise. The results of running such an algorithm on this particular example are shown on Table 15.2. Balance was achieved to within 0.01 W/m² after nine iterations. The first line of the table gives values that are in sensible agreement with the hand calculations given above.

Iteration	Wet surface temperature θ_{ws} °C	Strata heat q W/m ²	Latent heat q_L W/m ²	Sensible heat q_{sen} W/m ²	Error E W/m ²
1	21.45	31.1	358.6	-77.0	-250.49
2	18.95	34.9	222.7	-131.4	-56.43
3	18.38	35.8	194.5	-143.6	-15.11
4	18.23	36.0	187.1	-146.9	-4.19
5	18.19	36.1	185.0	-147.8	-1.17
6	18.18	36.1	184.4	-148.0	-0.33
7	18.17	36.1	184.3	-148.1	-0.09
8	18.17	36.1	184.2	-148.1	-0.03
9	18.17	36.1	184.2	-148.1	-0.01

Table 15.2. Successive values computed during the iterative process for a wet surface.

At balance, 36.1 W of strata heat arrive at each square metre of wet surface. Simultaneously, 148.1 W of sensible heat pass from the air to the wet surface (q_{sen} is negative). Hence, the sum of the two, 184.2 W/m² is emitted as latent heat to the air. The temperature of the wet surface is 18.17 °C.

The effect of water on the surface has now been quantified. The net heat emission of 36.1 W/m² compares with 24.0 W/m² for the corresponding (dry) surface of the earlier case study. For the 20 m

length of airway at a perimeter of 12 m, this translates into a heat load of $\frac{36.1 \times 20 \times 12}{1000} = 8.66$ kW

compared with 5.76 kW when the surface was dry. However, whereas the 5.76 kW of heat from the formerly dry surface was sensible heat, the net 8.66 kW emitted from the wet surface now takes the form of latent heat. This results in significant increases in the sigma heat, wet bulb temperature and moisture content of the air.

This Case Study has illustrated that the determination of heat flux from a wet airway surface involves lengthy calculations including an iterative procedure. The integrity of those calculations can be checked through the effective dry bulb temperature, θ_{ef} , which was introduced as a device to assist in the analysis. Equation (15.32) gave:

$$\theta_{ef} = \left\{ \theta_{ws} - \frac{G}{B} VRT \right\} \frac{B}{B - G}$$

Using the value of wet surface temperature $\theta_{ws} = 18.17^\circ\text{C}$, determined through the iterative procedure this becomes

$$\theta_{ef} = \left\{ 18.17 - \frac{0.6}{9.207} \times 42 \right\} \frac{9.207}{9.207 - 0.6} = 16.51^\circ\text{C}$$

Recall that θ_{ef} is what the value of the dry bulb temperature in a completely dry airway would have to be in order to give the same value of heat flux as the actual wet airway. Equation (15.30) or (15.21) for this hypothetical dry airway give a heat flux of

$$q = h_c \frac{G}{B} (VRT - \theta_{ef}) = 21.69 \times \frac{0.6}{9.207} (42 - 16.51) = 36 \frac{\text{W}}{\text{m}^2}$$

and is in good agreement with the 36.1 W/m² obtained for the actual wet airway.

It is clear from these case studies that the analytical determination of strata heat flux into subsurface openings does not lend itself to manual calculation. Chapter 16 discusses simulation programs which can readily be employed for rapid and detailed predictions of the underground climate. However, the engineer who uses such programs is utilizing the theory and procedures that have been described in this Section.

15.2.10. In-situ measurement of rock thermal conductivity

The experimental determination of the thermal conductivity of solids depends essentially upon Fourier's law (equation (15.4)). A source of heat is applied to one side of a sample. The heat flux across a known area and the corresponding temperature difference across the sample are measured leaving the thermal conductivity as the only unknown.

A number of laboratory test rigs have been developed for the determination of the thermal conductivities of rock samples. However, for subsurface environmental engineering, it is preferable to measure rock thermal conductivity in-situ. The reason for this is the significant difference that may be found between an in-situ value and the mean of numerous samples measured in the laboratory. If the rock is homogeneous and unfractured around mine openings, and if workings are above the water table then good correlation may be achieved between laboratory tests and in-situ determinations. However, in the more usual situation of mining induced fractures in addition to the existence of natural fracture patterns, and particularly in the presence of groundwater migration, the effective thermal conductivity may be more than double that indicated by small and unfractured laboratory samples (Mousset-Jones, 1984).

Water has a thermal conductivity of 0.62 W/(m°C) which is considerably lower than that of most rocks. Hence, the presence of still connate water in fissured or porous media will tend to inhibit

heat flow. Unfortunately, water in the strata surrounding subsurface openings is seldom stationary and, dependent upon the rate of water migration, the transmission of heat by moving water may be far greater than that resulting from conduction through the rock (see, also, section 15.3.3.). This can result in considerable increases in the effective thermal conductivity of the strata.

The simplest method of determining rock thermal conductivity in-situ is to use natural geothermal energy as the heat source. If possible, an airway should be found that is fairly well established, but sufficiently long to give a readily measured rise in wet bulb temperature of the air over its length. A thermocouple circuit to indicate the rise in wet bulb temperature over the selected length of airway will give better accuracy than mercury in glass thermometers. From a cross section within the chosen length, four boreholes should be drilled radially outward to a depth of at least 10 m. These should each be fitted with strings of thermocouples or other type of temperature transducers, positioned to indicate the variation in temperature along the hole. Precautions should be taken to ensure good thermal contact between the transducers and the side of the borehole, and to prevent convection currents of air or water within the hole.

Returning to Figure 15.2, consider an elongated annulus of rock at radius r and length Y . The heat flux, q , passes radially through the annulus which has an orthogonal area $2\pi r Y$ and thickness dr . Fourier's law (equation (15.4)) gives

$$q = -k_r 2\pi r Y \frac{(d\theta)}{(-dr)}$$

(dr is negative as r is measured outward from the airway while q is usually directed toward the airway).

$$\text{Then } \frac{dr}{r} = \frac{2\pi k_r Y}{q} d\theta$$

If we assume steady state conditions, q is constant for all values of r . We can then integrate to give

$$\ln(r) = \frac{2\pi k_r Y}{q} \theta + \text{constant} \quad (15.37)$$

From the measurements taken in a borehole, θ can be plotted against $\ln(r)$ to give a straight line of slope

$$q/(2\pi k_r Y) \quad (15.38)$$

Now, values of wet and dry bulb temperature, together with barometric pressures measured at the two ends **a** and **b** of the airway allow the corresponding values of sigma heat, S , to be established (Section 14.6). Furthermore, anemometer traverses give the airflow, Q , (Section 6.2) and, hence, the mass flow of air, M

$$M = Q \rho \quad \text{kg/s}$$

where ρ = actual density of air (kg/m^3)

Then

$$q = M(S_b - S_a) \quad \text{W} \quad (15.39)$$

Substituting for q in the expression for the measured slope of the θ v $\ln(r)$ graph (15.38) allows k_r to be determined. An average value of rock thermal conductivity will be given by the data obtained from several boreholes.

Although simple in principle, this in-situ method of measuring effective thermal conductivity of strata may involve several difficulties. First, the airflow in the airway and the psychrometric conditions at the inlet should, ideally, remain constant. Accuracy will be improved if all

measurements are made electronically and data logged every few minutes for several days. The plots of θ against $\ln(r)$ are not always straight lines. A sudden change in slope along a given set of borehole data indicates that the borehole has intersected a change in rock type. A more gradual curvature suggests that the strata temperatures have not reached equilibrium. Deviations towards the mouth of the hole indicate non-steady conditions in the airway. In such situations, the slope of the line at the rock surface should be used in the determination of k_r . Differences in the slopes of the lines are often found between boreholes drilled in different directions from the same cross-section of the airway. Such deviations may indicate differences in rock type or, often, the effect of water distribution within the strata.

A major advantage of this method is that it gives the effective thermal conductivity of the complete envelope of rock around the chosen cross-section. Other techniques have been developed that produce an artificial source of heat within a borehole with instrumentation to monitor the resulting temperature field at other locations along the borehole (Danko, 1987). Such equipment can produce results within a few hours for more limited representative volumes of rock.

15.3. OTHER SOURCES OF HEAT

15.3.1. Autocompression

When air or any other fluid flows downward, some of its potential energy is converted to enthalpy ($H = PV + U$, equation (3.19)) producing increases in pressure, internal energy and, hence, temperature. Actual examples are shown on Figure 8.3.

The rise in temperature as air falls through a downcast shaft or other descentional airway is independent of any frictional effects (Section 3.4.1). Ignoring the small change in kinetic energy, the steady flow energy equation (3.22) gives

$$(H_2 - H_1) = (Z_1 - Z_2)g + q_{12} \quad (15.40)$$

where H = enthalpy J/kg
 Z = height above datum (m)
 g = gravitational acceleration (m/s^2) and
 q = heat added from surroundings (J/kg)

(subscripts 1 and 2 refer to the inlet and outlet ends of the airway respectively).

This equation shows that the increase in enthalpy is, in fact, due to two components,

- (a) the heat actually added, q_{12} , and
- (b) the conversion of potential energy $(Z_1 - Z_2)g$.

The heat added, q_{12} , may be positive, negative or zero but the increase in temperature due to depth alone is definitive for any given dry shaft and moisture content of the air.

The effects of autocompression are virtually independent of airflow. In deep mines, the intake air leaving the bottoms of downcast shafts may already be at a temperature that necessitates air cooling. This is the inevitable result of autocompression.

The reverse effect, auto-decompression, occurs in upcast shafts or ascensional airways. This is usually of less concern as upcast air will have no effect on conditions in the workings. However, the reduction in temperature due to auto-decompression in upcast shafts can result in condensation and fogging (Section 9.3.6). The mixture of air and water droplets may then reduce the life of the impellers of exhaust fans sited at the shaft top.

The increase in temperature due to depth is sometimes known as the **adiabatic lapse rate**. For completely dry airways, the change in enthalpy is given by equation (3.33)

$$H_2 - H_1 = C_{pm} (T_2 - T_1) \quad \text{J/kg}$$

where T = dry bulb temperature ($^{\circ}\text{C}$ or K)
and C_{pm} = specific heat of the actual(moist) air ($\text{J/kg}^{\circ}\text{C}$).

(We are reverting to the symbol T for temperature in this section in order that we may use it to denote absolute temperatures). Hence, equation (15.40) gives the adiabatic ($q_{12} = 0$) rise in dry bulb temperature to be

$$(T_2 - T_1) = \frac{(Z_1 - Z_2)g}{C_{pm}} \quad ^{\circ}\text{C} \quad (15.41)$$

Substituting for C_{pm} from equation (14.16) gives

$$(T_2 - T_1) = \frac{(1 + X)}{(1005 + 1884 X)} (Z_1 - Z_2)g \quad ^{\circ}\text{C} \quad (15.42)$$

where X = mass of water vapour (kg/kg dry air).

For a completely dry shaft or slope and at a value of $g = 9.81 \text{ m/s}^2$, this gives a **dry bulb adiabatic temperature lapse** rate varying from $0.976 \text{ }^{\circ}\text{C}$ per 100 m depth for dry air to $0.952 \text{ }^{\circ}\text{C}$ per 100 m depth at a water vapour content of 0.03 kg/kg dry air.

However, in the majority of cases, the shaft or airway surfaces are not completely dry and the rate of increase in dry bulb temperature is eroded by the cooling effect of evaporation. If the increase in vapour content of the air due to evaporation is $\Delta X \text{ kg/kg}$ dry air, then this will result in a conversion of sensible heat to latent heat, $L \Delta X \text{ (J/kg)}$ where L = latent heat of evaporation. Equation (15.41) then becomes

$$(T_2 - T_1) = \frac{(Z_1 - Z_2)g - L \Delta X}{C_{pm}} \quad ^{\circ}\text{C} \quad (15.43)$$

Using mid-range values of $C_{pm} = 1010 \text{ J/kgK}$ and $L = 2453 \times 10^3 \text{ J/kg}$ gives the approximation

$$(T_2 - T_1) = 0.00971(Z_1 - Z_2) - 2428.7 \Delta X \quad ^{\circ}\text{C} \quad (15.44)$$

This equation is shown graphically in Figure 15.7 and is useful only if the increase in vapour content is known. In practical design exercises, ΔX is normally unknown but an estimate may be made of the wetness of the shafts. Recourse must then be made to computer simulation techniques (Chapter 16). It must be emphasized that equations (15.41 to 15.44) refer to the dry bulb temperature only and while the air remains unsaturated. Should saturation occur then the dry bulb temperature will follow the wet bulb temperature adiabatic lapse rate.

The behaviour of the wet bulb temperature due to adiabatic compression is more predictable than dry bulb temperature. The enthalpy (and sigma heat) of the air increase linearly with depth in the absence of any heat transfer with the surroundings. Furthermore, the increase in air pressure is also near linear with respect to depth. Hence, as wet bulb temperature varies only with sigma heat and pressure, **the wet bulb adiabatic lapse rate in a shaft will be near constant irrespective of shaft wetness**. Any significant deviation in the wet bulb temperature can be due only to heat transfer with the walls or shaft fittings.

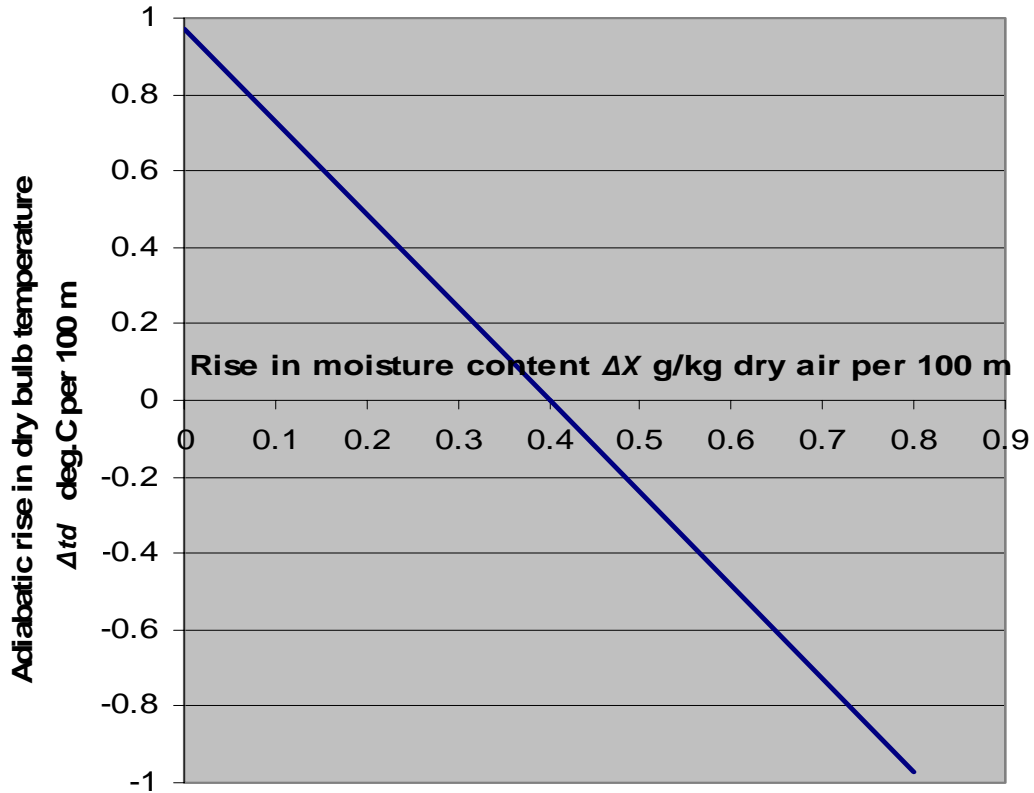


Figure 15.7 The dry bulb adiabatic lapse rate (variation of air temperature with depth) depends upon the rate at which water is evaporated.

Unfortunately, calculation of the wet bulb adiabatic lapse rate is somewhat more involved than for the dry bulb.

We can write the variation in wet bulb temperature, T_w , with respect to depth, Z , as

$$\frac{dT_w}{dZ} = \frac{dT_w}{dP} \frac{dP}{dZ} \quad \text{°C} \quad (15.45)$$

From the steady flow energy equation for isentropic conditions ($F = q = 0$) and negligible change in kinetic energy (equation (3.25)),

$$-g dZ = V dP \quad \text{or} \quad \frac{dP}{dZ} = -\frac{g}{V} \quad \text{N/m}^3 \quad \text{or} \quad \text{Pa/m} \quad (15.46)$$

where $V =$ specific volume (m^3/kg) = $287.04 T_w / (P - 0.378 e_s)$ for saturation conditions (equation (14.19))

Furthermore, we have already derived the isentropic pressure/temperature relationship for an air/vapour/liquid water mixture for fans as equation (10.56). The same equation applies to any other isentropic airflow process involving air/vapour/liquid water mixtures. In order to track the adiabatic wet bulb temperature lapse rate, we apply the constraint that critical saturation is maintained throughout the shaft, i.e. $X = X_s$. Equation (10.56) then becomes

$$\frac{dT_w}{dP} = \frac{0.286 \left[(1 + 1.6078 X_s) \frac{T_w}{P} + \frac{L_w X_s}{287.04 (P - e_s)} \right]}{\left[1 + 1.7921 X_s + \frac{L_w^2 P X_s}{463.81 \times 10^3 (P - e_s) T_w^2} \right]} \quad \text{°C/Pa} \quad (15.47)$$

In this equation T_w is the absolute wet bulb temperature (K) and barometric pressure, P , is in Pa.

Equations (15.45 to 15.47) allow the wet bulb lapse rate, dT_w/dZ to be determined for any given P and T_w as X_s and e_s are functions of pressure and temperature only (Section 14.6). Tracking the behaviour of dT_w/dZ for a downcast shaft from equation (15.47) and commencing from known shaft top pressure and wet bulb temperature shows that the adiabatic lapse rate for wet bulb temperature is not exactly constant but decreases slowly with depth. For manual application, Figure 15.8 has been constructed from values calculated for a depth of 500 m below the shaft top. This gives an accuracy within 4 per cent for a 1000m shaft over the ranges of pressure and starting temperatures shown¹.

It should be recalled that the equations derived for autocompression effects give the changes in temperature due to depth only. Actual measurements will reflect, also, heat transfer with the shaft walls or other sources. These are likely to be most noticeable in downcast shafts due to transients in the surface conditions.

15.3.2. Mechanized equipment

The operation of all mechanized equipment results in one, or both, of two effects; work is done against gravity and/or heat is produced. A conveyor transporting material up an incline, a shaft hoist and a pump are examples of equipment that work, primarily, against gravity. Vehicles operating in level airways, rock breaking machinery, transformers, lights and fans are all devices that convert an input power, via a useful effect, into heat.

With the exceptions of compressed air motors and devices such as liquid nitrogen engines, all other forms of power including electricity and chemical fuels produce thermal pollution that must be removed by the environmental control system.

Increasing utilization and power of mechanization in mines and other subsurface facilities has resulted in such equipment joining geothermal effects and autocompression as a major source of heat. With machines consuming about 2 MW of electrical power on some highly mechanized longwall faces, a number of coal mines in the United Kingdom and Europe had to resort to refrigeration equipment at depths below surface where it was not previously required. The calculation of equipment heat is straightforward compared to that for strata heat.

¹ The error depends primarily on the starting wet bulb temperature and is approximately 4 per cent at an initial wet bulb temperature of 0°C. At a starting wet bulb temperature of 20°C the error is about 2 per cent.

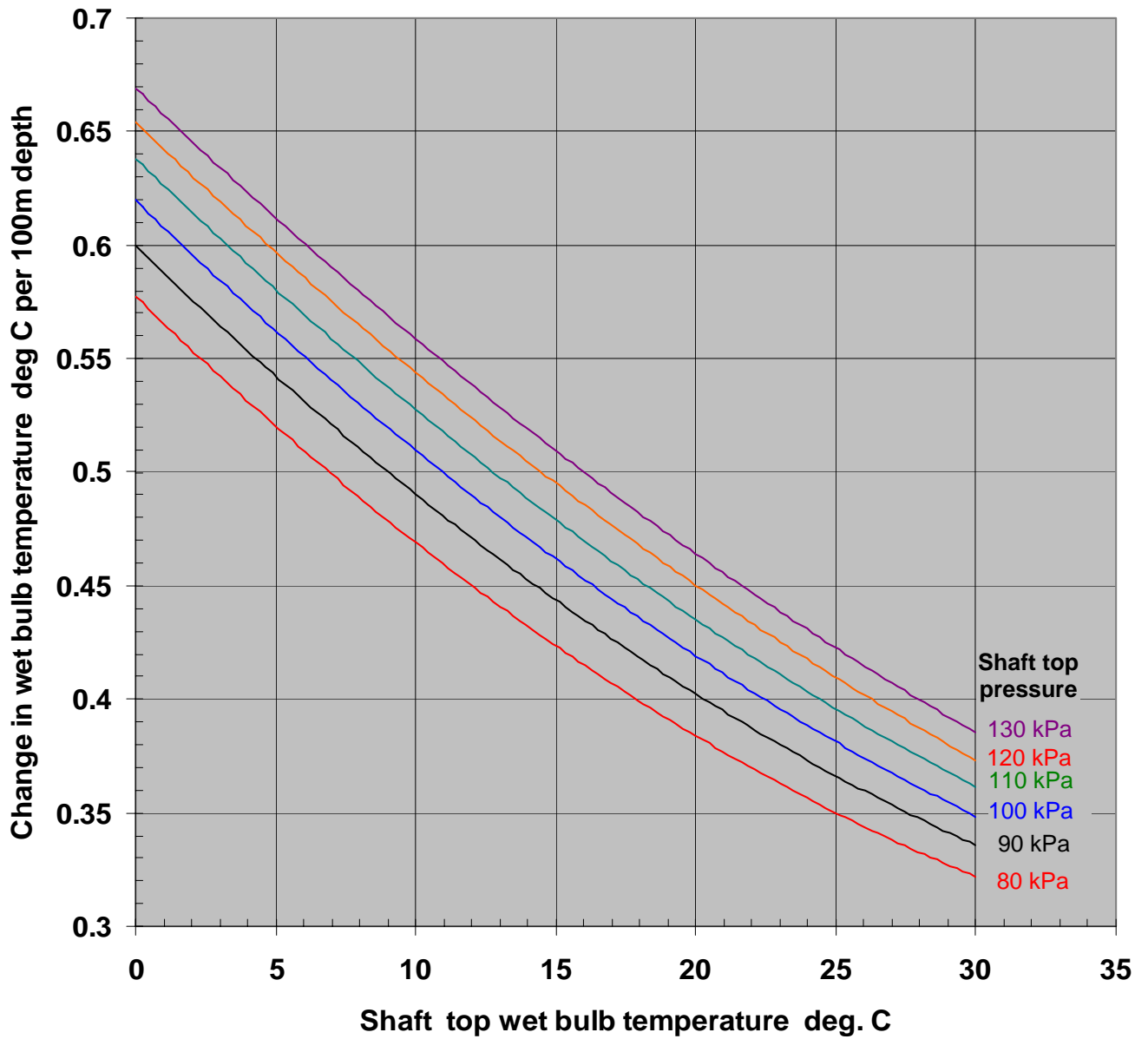


Figure 15.8 The wet bulb adiabatic lapse rate depends upon the initial pressure and wet bulb temperature but is independent of evaporation within the shaft.

The following algorithm gives a good approximation to these curves:

Enter shaft top wet bulb temperature (tw) °C
 Enter shaft top barometric pressure (P) kPa
 $a = -7.6286E-07 \cdot P + 1.7593E-04$
 $b = -1.2554E-07 \cdot P^2 + 2.238E-05 \cdot P + 1.1012E-02$
 $c = -9.4107E-06 \cdot P^2 + 3.8054E-03 \cdot P + 0.33327$
 Wet bulb temp. adiabatic lapse rate = $a \cdot tw^2 - b \cdot tw + c$

15.3.2.1. Electrical equipment

Figure 15.9 illustrates the manner in which the power taken by an electrical machine is utilized. The machine efficiency is relevant, within this context, in two ways. First, the total amount of heat produced can be reduced only if the machine is replaced by another of greater efficiency to give the same mechanical power output at lower power consumption. For any given machine, the total heat produced is simply the rate at which power is supplied, less any work done against gravity. Secondly, the efficiency of the machine determines the distribution of the heat produced. The higher the efficiency, the lower the heat produced at the motor and transmission, and the greater is the percentage of heat produced at the pick-point, conveyor rollers, along the machine run or by any other frictional effects caused by the operation of the device.

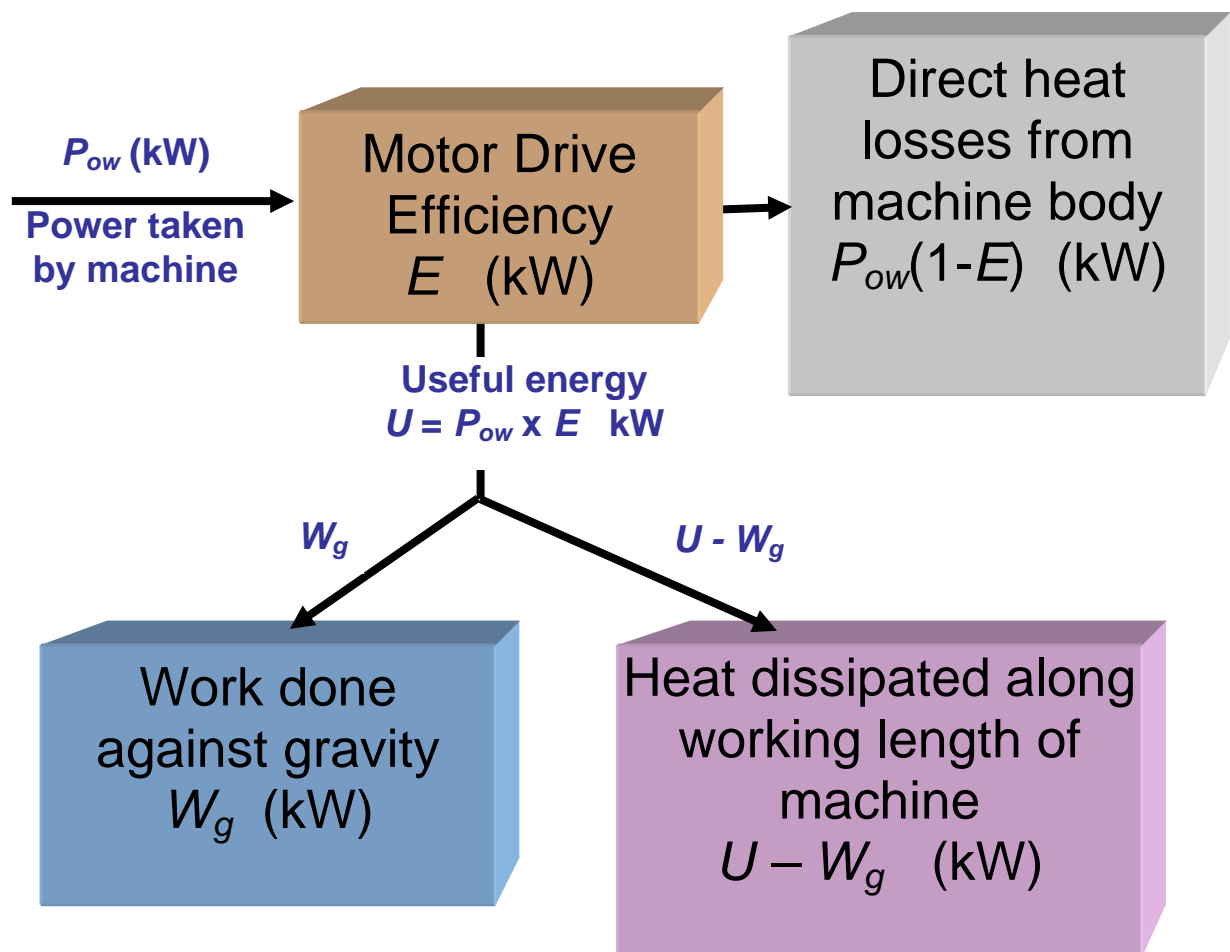


Figure 15.9 Heat produced by electrical machines.

Example.

A 2000 m long conveyor transports 500 t/hr through a vertical lift of 200 m. If the conveyor motor consumes 1000 kW at a combined motor/transmission efficiency of 90%, calculate the heat emitted

- (1) at the gearhead and
- (2) along the length of the conveyor.

Solution.

Work done against gravity = mass flow × g × vertical lift

$$= \frac{500 \times 1000}{60 \times 60} \times 9.81 \times 200 = 272.5 \times 10^3 \text{ W or } 272.5 \text{ kW}$$

$$\frac{\text{kg}}{\text{s}} \quad \frac{\text{m}}{\text{s}^2} \quad \text{m}$$

- 1 . Heat generated at gearhead = (100 - 90)% of 1000 kW = 100 kW
- 2 . Heat generated along length of conveyor = 1000 - 272.5 - 100 = 627.5 kW

15.3.2.2. Diesel equipment

The internal combustion engines of diesel equipment have an overall efficiency only about one third of that achieved by electrical units. Hence, diesels will produce approximately three times as much heat as electrical equipment for the same mechanical work output. This can be demonstrated by taking a typical rate of fuel consumption to be 0.3 litres per rated kW per hour. At a calorific value of 34 000 kJ/litre for the diesel fuel, the heat produced is

$$\frac{0.3}{60 \times 60} \frac{\text{(litres)}}{\text{(kW output. second)}} \times 34000 \frac{\text{(kJ heat)}}{\text{(litre)}}$$

= 2.83 kJ/s (or kilowatts) of heat emitted for each kilowatt of mechanical output.

This heat appears in three ways each of which may be of roughly the same magnitude. One third appears as heat from the radiator and machine body, one third as heat in the exhaust gases and the remaining third as useful shaft power which is then converted to heat (less work done against gravity) by frictional processes as the machine performs its task.

As with other types of heat emitting equipment there is little need, in most cases, to consider peak loads. It is sufficient to base design calculations on an average rate of machine utilization. The most accurate method of predicting the heat load is on the basis of average fuel consumption during a shift. However, in many mines, records of fuel consumption by individual machines or, even, in separate sections of the mine, seem not to be maintained. The ventilation planner often must resort to the type of calculation shown above and using an estimated value for machine utilization. The latter is defined as the fraction of full load which, if maintained continuously, would use the same amount of fuel as the actual intermittent load on the machine. (Section 16.2.3)

A difference between diesel and electrical equipment is that the former produces part of its heat output in the form of latent heat. Each litre of diesel fuel that is consumed produces approximately 1.1 litres of water (liquid equivalent) in the exhaust gases (Kibble, 1978). This may be multiplied several times over by the evaporation of water from engine cooling systems, some emission control units and enhanced evaporation from airway surfaces. In-situ tests have shown that the factor can vary from 3 to 10 litres of water per litre of fuel (McPherson, 1986) depending upon the power and design of the engine, exhaust treatment system and the proficiency of maintenance.

Example.

Two load-haul-dump vehicles consume 600 litres of diesel fuel in an 8 hour shift. Tests have shown that water vapour is produced at a rate of 5 litres (liquid equivalent) per litre of fuel. If the combustion efficiency is 95 per cent and the total calorific value of the fuel is 34 000 kJ/litre, calculate the sensible and latent heat loads on the stope ventilation system.

Solution.

Total amount of heat produced from burning 600 x 0.95 litres of fuel

$$\begin{aligned}
 &= 600 \times 0.95 \times 34\,000 \\
 &= 19.38 \times 10^6 \text{ kJ in 8 hours} \\
 &= \frac{19.38 \times 10^6}{8 \times 60 \times 60} = 673 \text{ kW}
 \end{aligned}$$

(This is equivalent to the continuous running of diesel machinery of rated output = $673/2.83 = 238$ kW)

Amount of water produced as vapour

$$= 600 \times 0.95 \times 5 = 2\,850 \text{ litres (liquid equivalent)}$$

i.e. 2 850 kg of water

Latent heat emitted in 8 hours

$$= 2450 \times 2850 = 6.982 \times 10^6 \text{ kJ}$$

where 2450 kJ/kg is an average value for the latent heat of evaporation of water.

$$\text{i.e. } \frac{6.982 \times 10^6}{8 \times 3600} = 242 \text{ kJ/s or kW}$$

Then, sensible heat produced = total heat - latent heat

$$= 673 - 242 = 431 \text{ kW}$$

In summary, operation of the diesels results in heat emissions at an average rate of

431 kW sensible heat

242 kW latent heat

673 kW total heat

In addition to the particulate and gaseous pollutants emitted in diesel exhausts, the heat produced by these machines mitigates against their use in hot mines. Nevertheless, the flexibility and reliability of diesel units has tended to perpetuate their continued widespread employment underground.

15.3.2.3. Compressed air

When **compressed air** is used for drilling or any other purpose then there are two opposing effects that govern the heat load. First, the work output of the machine will result in frictional heat at the pick point or other places as the machine performs its task. Second, the removal of energy from the compressed air will result in a reduction of the temperature of that air at the exhaust ports of the machine.

If we assume that the change in potential energy of the air is negligible and that there is no significant heat transfer across the machine casing then the steady flow energy for the compressed air motor is

$$\frac{u_1^2 - u_2^2}{2} + W = C_p (\theta_2 - \theta_1) \quad \text{J/kg} \quad (15.49)$$

where u_1 and u_2 are the velocities of the air in the supply pipe and the exhaust ports, respectively, W is the mechanical work done on the air (this is numerically negative as mechanical energy is leaving the system; J/kg), C_p is the specific heat of air, (1005 J/kg°C) for dry air, θ_1 is the temperature of the supply air (°C) and θ_2 is the temperature of air at the outlet ports (°C).

In the majority of cases the temperature of the compressed air supplied to the motor is equal to the ambient dry bulb temperature, θ_{amb} . Furthermore, the velocity of the compressed air in the supply pipe, u_1 , is small compared with that at the exhaust ports, u_2 .

$$\text{Hence, } \frac{-u_2^2}{2} + W = C_p (\theta_2 - \theta_{amb}) \quad \text{J/kg} \quad (15.50)$$

Now consider the subsequent process during which the cold exhaust air mixes with the ambient air, increasing in temperature, extracting heat from the general ventilating airstream and, hence, cooling that airstream. Again, the velocity of the ambient airstream will be small compared with that at the outlet ports, u_2 . The steady flow energy equation for this process becomes

$$\frac{u_2^2}{2} = C_p (\theta_{amb} - \theta_2) - q \quad \text{J/kg} \quad (15.51)$$

where q is the heat added to the machine exhaust from the ambient air.

The overall effect may be quantified by adding equations (15.50 and 15.51) giving

$$W = -q \quad \text{J/kg}$$

Hence, the mechanical work output of the machine (which is subsequently transferred by friction into heat) is balanced precisely by the cooling effect on the ventilating airstream. If the moisture content of the compressed air is similar to that of the ambient airstream, then there is no net heating or cooling arising from the expansion of the air through the compressed air motor.

Despite this analysis, a cooling effect is certainly noticeable when standing immediately downstream from a compressed air motor. There are two reasons for this. First, the cooling of the ambient airstream, q , by a motor exhausting at sub-zero temperatures is immediate and direct, whilst part of the balancing heat produced by friction may be stored temporarily within the body of the machine, in the solid or broken rock, and distributed over the working length of the machine. Secondly, the compressed air supply will normally be drier and have a much lower sigma heat than the ventilating air. The increase in sigma heat of the exhaust air will then exceed the numerical equivalent of the work output and, hence, result in a true net cooling of the ambient air. This will be of consequence only if the mass flow of compressed air is significant compared with the mass flow of the ventilating airstream. The dryness of compressed air, coupled with a very local kinetic energy effect [$u^2/2 = C_p(\theta_2 - \theta_1)$] also explains why air issuing from a leaky compressed air pipe appears cool even though no energy has been extracted from it.

In calculating the heat load for a complete airway, district or mine, it errs on the side of safety to assume that there is no net cooling effect from compressed air motors. Only if a detailed analysis in the immediate vicinity of compressed air devices is required need the local cooling effects be considered.

Air compressors are large sources of heat. Indeed, the local cooling effect at the outlet ports of the compressed air motors are reflected by an equivalent amount of heat produced at the compressors, even if the latter are 100 % efficient. This need be of little import if the compressors are sited on surface and the compressed air is cooled before entering the shaft pipes. If, however, compressors are sited in intake airways close to hot workings, then it is beneficial to investigate the circulation of hot water from the compressor coolers through heat exchangers in return airways.

15.3.3. Fissure water and channel flow

Groundwater migrating through strata toward a subsurface opening can add very considerably to the transfer of geothermal heat through the rock (Section 15.2.10). Such water may continue to add heat to the ventilating airstream after it has entered the mined opening.

Fissure water is often emitted at a temperature close to the virgin rock temperature (*VRT*). In circumstances of local geothermal activity or radioactive decay, it may even be higher. The total heat load on the mine environment can be calculated from the flowrate and the drop in temperature of the water between the points of emission and effective exit from the mine ventilation system.

Example.

A mine produces 5 million litres of water per day, emitted at an average temperature of 42 °C. When the water is delivered into the shaft sump for pumping to the surface, the water temperature is 32 °C. Determine the heat load from the water on the mine ventilation system.

Solution.

$$\begin{aligned} \text{Heat load} &= \text{Mass flow} \times \text{specific heat} \times \text{drop in temperature} \\ &= \frac{5\,000\,000}{24 \times 60 \times 60} \times \frac{4187}{1000} \times (42 - 32) = 2\,423 \text{ kW} \\ &\quad \frac{\text{kg}}{\text{s}} \quad \frac{\text{kJ}}{\text{kg}^\circ\text{C}} \quad ^\circ\text{C} \end{aligned}$$

The rate at which heat is emitted into the airstream depends upon the difference between the temperature of the air and the water, and whether the water is piped or in open channels. In the latter case, cooling by evaporation will be the major mode of heat transfer and will continue while the temperature of the water exceeds the wet bulb temperature of the air. **Hot fissure water should be allowed no more than minimum direct contact with intake air.** The most effective means of dealing with this problem are

- (a) to transport the water in closed pipes and
- (b) to restrict water flow routes to return airways.

A less effective but expedient measure close to the points of water emission is to restrict air/water contact by covering drainage channels by boarding or other materials.

Where chilled service water is employed, condensate run-off may be at a temperature below that of the local wet bulb temperature. While this continues, the condensate will continue to absorb both sensible and latent heat, thus providing a cooling effect on the airflow.

In, or close to the working areas of many mines, it is often inevitable that open drainage channels will be used. Similarly, the footwalls or floors may have areas that are covered with standing or slowly moving water.

The transfer of sensible and latent heat between the surface of the water and the air may be determined from equations (15.34 and 15.35).

$$\text{i.e. } q_{sen} = h_c (\theta_{ws} - \theta_d) \quad \text{W/m}^2$$

$$\text{and } q_L = 0.0007 h_c L_{ws} \frac{(e_{ws} - e)}{P} \quad \text{W/m}^2$$

where subscript *ws* means water surface and *d* means dry bulb.

The heat transfer coefficient for the water surface, h_c , is the least certain of the variables, depending upon the geometry of the airway, the condition of the airflow (in particular, the local air velocity) and the degree of turbulence existing in the flowing water. An approximation may be obtained from equations (15.22 and 15.23) using the Reynolds' Number for the airway and a value of coefficient of friction, f , that represents the degree of water turbulence on the liquid surface. This may vary from 0.002 for a calm flat surface to 0.02 for a highly turbulent surface.

Example.

Water flows at a rate of 60 litres per second along an open drainage channel that is 0.5 m wide and 0.25 m deep. The channel is located in an airway of cross-sectional area 12 m² and perimeter 14 m, and which passes an airflow of 50 m³/s. Over a 10 m length of channel, the following mean values are given:

water temperature,	θ_{ws}	=	32 °C
air dry bulb temperature,	θ_d	=	30 °C
air wet bulb temperature,	θ_w	=	25 °C
barometric pressure,	P	=	112 kPa

Determine the sensible and latent heat emitted from the water to the air and the corresponding drop in water temperature over the 10 m length. Assume that no heat is added to the water from the strata.

Solution.

(a) Determine the heat transfer coefficient for the water surface.

$$\text{Volume flow of water} = \frac{60}{1000} = 0.06 \text{ m}^3/\text{s}$$

$$\text{Velocity of water} = \frac{0.06}{0.5 \times 0.25} = 0.48 \text{ m/s}$$

At this velocity, it is estimated that ripples on the water surface will have an equivalent coefficient of friction, $f = 0.008$.

The Reynolds' Number for the airway

$$Re = 268\,000 \frac{Q}{per} = 268\,000 \times \frac{50}{14} = 957\,140$$

Equation (15.22) gives the Nusselt Number to be $N_u = 2127$ (this can be estimated directly from Figure 15.5)

Hydraulic mean diameter of the airway,

$$d = \frac{4A}{per} = \frac{4 \times 12}{14} = 3.429 \text{ m}$$

The convective heat transfer coefficient is then given by equation (15.23).
Using $k_a = 0.026 \text{ W/(m}^2\text{C)}$ (reference Table 15.1),

$$h_c = \frac{2127 \times 0.026}{3.429} = 16.1 \text{ W/(m}^2\text{C)}$$

(b) Determine the psychrometric conditions.

Using the psychrometric relationships given in Section 14.6, the following values are determined:

for the water surface at 32 °C

$$\begin{aligned} L_{ws} &= 2426 \times 10^3 \text{ J/kg} \\ \text{and } e_{ws} &= 4753 \text{ Pa} \end{aligned}$$

$$\begin{aligned} \text{for the air at } \theta_w &= 25 \text{ °C, } \theta_d = 30 \text{ °C and } P = 112 \text{ kPa,} \\ e &= 2805 \text{ Pa} \end{aligned}$$

[The advantages of keeping the psychrometric equations of Section 14.6 programmed into a pocket calculator should be very obvious by now.]

(c) Determine the heat transfers from the water to the air:

$$\text{Sensible heat, } q_{sen} = h_c (\theta_{ws} - \theta_d) = 16.1 (32 - 30) = 32.2 \text{ W/m}^2$$

$$\text{Latent heat, } q_L = 0.0007 h_c L_{ws} \frac{(e_{ws} - e)}{P} = 0.0007 \times 16.1 \times 2426 \times 10^3 \times \frac{(4753 - 2805)}{112000} = 475.5 \text{ W/m}^2$$

As the width of the drainage channel in the 10 m length is 0.5 m, the heat flows may be stated as:

$$\text{Sensible heat } \frac{32.2 \times 10 \times 0.5}{1000} = 0.161 \text{ kW}$$

$$\text{Latent heat } \frac{475.5 \times 10 \times 0.5}{1000} = 2.378 \text{ kW}$$

These values illustrate the dominant effect of latent heat transfer and why it is important to prevent direct contact between the air and the water.

The total heat gained by the air from the water is the sum of the sensible and latent heat transfers,

$$q = 2.378 + 0.161 = 2.539 \text{ kW.}$$

(d) Determine the drop in temperature of the water.

As 1 litre of water has a mass of 1 kg, the mass flow of water, $m = 60 \text{ kg/s}$. The total heat lost by the water, then becomes

$$q = m \Delta\theta C_w$$

where

$$\begin{aligned} \Delta\theta &= \text{change in water temperature (°C)} \\ \text{and } C_w &= \text{specific heat of water (4187 J/(kg°C))} \end{aligned}$$

$$\text{giving } \Delta\theta = \frac{q}{m C_w} = \frac{2.539 \times 10^3}{60 \times 4187} = 0.0101 \text{ °C in the 10 m length.}$$

15.3.4. Oxidation

Coal and sulphide ore mines are particularly liable to suffer from a heat load arising from oxidation of fractured rock. An estimate of the heat produced can be determined from the rate of oxygen depletion.

Assuming complete combustion of carbon and using the atomic weights of the elements,



Each 1 kg of oxygen consumed oxidizes 12/32 kg of carbon. Taking the calorific value of carbon as 33 800 kJ/kg gives a corresponding heat production of $(12/32) \times 33\,800 = 12\,675$ kJ of heat per kg of oxygen used.

Similarly, for complete oxidation of sulphur:



Each 1 kg of oxygen consumed will oxidize 1 kg of sulphur (calorific value 9304 kJ/kg) to produce 9304 kJ of heat.

Example.

10 m³/s of air enters a working district in a coal mine at an oxygen content of 21% by volume, and leaves at 20.8%. Calculate the heat generated by oxidation assuming complete combustion.

Solution.

The equivalent volume flow of oxygen at entry = $0.21 \times 10 = 2.1$ m³/s

The equivalent volume flow of oxygen at exit = $0.208 \times 10 = 2.08$ m³/s

Taking the density of oxygen to be 1.3 kg/m³ gives the oxygen depletion rate to be

$$(2.1 - 2.08) \times 1.3 = 0.026 \text{ kg/s}$$

$$\text{Heat produced} = 0.026 \times 12\,675 = 330 \text{ kW}$$

The type of calculation illustrated by this example is useful in determining the heat produced by oxidation in an existing mine or section of a mine where air samples can be taken for analysis in intake and return airways. The extent to which oxidation takes place depends upon the mineralogical content of the material being oxidized, the psychrometric condition of the air and the surface area exposed. These factors make it difficult to predict heat loads from oxidation by other than empirical means.

In the case of open surfaces in operating airways and working places, the heat of oxidation will be an immediate and direct load on the mine ventilation system. On the other hand the heat that is produced by oxidation in waste areas, old workings, orepasses or in caved stopes will initially be removed only partially by leakage air. The remainder will be retained causing a rise in the temperature of the rock. This, in turn, enhances the rate of heat transfer to the leakage air and, in most cases, an equilibrium is reached when the heat removed by the air balances the heat of oxidation. However, in minerals liable to spontaneous combustion the increased temperature of the rock will accelerate the oxidation process to an extent that the heat removed may not reach equilibrium with the heat produced. In such cases the temperature will continue to rise until the rock becomes incandescent resulting in a spontaneous fire (Section 21.4).

15.3.5. Explosives

The heat that is produced during blasting varies with the type and amount of explosives used (charge density). The amount of heat released by most explosives employed in mining falls within the range of 3700 kJ/kg for ANFO² to 5800 kJ/kg for nitro-glycerine (Whillier, 1981). This heat is dispersed in two ways. First, a fraction of it will appear in the blasting fumes and cause a peak heat load on the ventilation system following blasting. In mines where a re-entry period is enforced this peak load should have cleared prior to personnel being readmitted to the area.

Secondly, the remainder of the heat will be stored in the broken rock. The magnitude of this will depend upon the mining method. If the rock is blasted into a free space through which the ventilating airstream passes, such as an open stope or on a longwall face, and the fragmentation is high, then as much as 40 - 50 % of the heat produced by the explosive may be removed rapidly as a peak load with the blasting fumes. On the other hand, if the blast occurs within a region through which there is little or no ventilation such as in sublevel or forced caving techniques, or if the fragmentation is poor, then a much larger proportion of the heat will be retained in the rock.

Example.

In a 2000 tonne blast, the charge density of ANFO is 0.8 kg/t. It is estimated that 20% of the blast heat will be removed within 1 h with the blasting fumes.

- (1) Calculate the mean value of the rate of heat removed by the airflow during this hour.
- (2) If the specific heat of the rock is 950 J/kg °C determine the average increase in temperature of the rock due to blasting.

Solution:

$$\begin{aligned} 1. \text{ Mass of explosive used} &= 2000 \times 0.8 = 1\,600 \text{ kg ANFO} \\ \text{Heat produced by ANFO} &= 3700 \times 1600 = 5\,920\,000 \text{ kJ} \end{aligned}$$

Twenty per cent of this heat is removed in the blasting fumes over 1 hour.

Average rate of heat removal with blasting fumes

$$= \frac{5\,920\,000}{3600} \times 0.2 \frac{\text{kJ}}{\text{s}} = 329 \text{ kW}$$

$$2. \text{ Heat retained in rock} = 5\,920\,000 \times 0.8 = 4\,736\,000 \text{ kJ}$$

$$\begin{aligned} \text{Rise in rock temperature} &= \frac{\text{Heat retained}}{\text{Mass} \times \text{Specific heat}} = \frac{4\,736\,000}{2000 \times 1000 \times 0.950} \frac{\text{kJ kg}^{-1} \text{ } ^\circ\text{C}}{\text{kg kJ}} \\ &= 2.49 \text{ } ^\circ\text{C} \end{aligned}$$

15.3.6. Falling rock

When strata or fractured rock moves downward under gravitational effects, the loss of potential energy will ultimately produce an increase in temperature through fragmentation, impact, braking, or other frictional effects. The fraction of the resulting heat that produces a load on the ventilation system again depends upon the exposure of the broken rock to a ventilating airstream. Hence, for example, a large amount of heat is produced by the mass of superincumbent strata subsiding through to the surface over a period of time. Fortunately, the vast majority of this is retained within the rock mass, raising its temperature very slightly, and little enters the mine ventilation system.

² Ammonium nitrate, fuel oil mixture.

On the other hand, mineral descending through an ore pass or vertical bunker may immediately, or subsequently, be exposed to a ventilating airstream. The loss of potential energy of the rock will then appear as a heat load on the ventilation system. This can be significant.

Assuming that there is negligible heat transfer between the fragmented material and the surrounding strata, the rise in temperature of falling rock, $\Delta\theta_r$, is given by the expression

$$\Delta\theta_r = \frac{\Delta z g}{C} \quad ^\circ\text{C} \quad (15.54)$$

where Δz is the distance fallen (m),
 g is the gravitational acceleration (9.81 m/s^2),
 C is the specific heat of rock ($\text{J/kg}^\circ\text{C}$)

or

$$\Delta\theta_r = 981/C \quad ^\circ\text{C per 100 m fall} \quad (15.55)$$

15.3.7. Fragmented rock

When fragmented rock is exposed to a ventilating airstream and there is a temperature difference between the rock and the air, then heat transfer will take place. This will occur on working faces, drawpoints, conveyors and along other elements of a mineral transportation system.

The heat load from broken rock is given by

$$mC(\theta_1 - \theta_2) \quad \text{kW} \quad (15.56)$$

where

m is the mass flow of rock (kg/s),
 C is the specific heat of rock ($\text{kJ/kg}^\circ\text{C}$),
 θ_1 is the temperature of the broken rock immediately after fragmentation ($^\circ\text{C}$) and
 θ_2 is the temperature of the rock at exit from the ventilation system ($^\circ\text{C}$).

In most mining methods the temperature of the solid rock immediately prior to fragmentation will be less than the virgin rock temperature (VRT) due to cooling of the rock surface. On the other hand, the process of fragmentation, whether by blasting or mechanized techniques, will raise the temperature of the broken rock. As shown in earlier sections, estimates may be made of these effects. However, in practice, the procedure may be simplified by assuming that the temperature of the newly broken rock, θ_1 , is equal to VRT.

The mean temperature of the broken rock at exit from the system, θ_2 , will depend upon the degree of fragmentation, the exposure of rock surfaces to the airstream, and the velocity and psychrometric condition of the air. Mineral transported along a conveyor system will cool to a much greater extent than in a locomotive system. Furthermore, wetted material will yield up its heat more readily due to evaporative cooling. Although the rate of heat transfer from a given particle size of rock to a known quantity and quality of airflow can be calculated, the many variables in any actual transportation system enforce the use of empirical measurements of temperature along the mineral transportation system. Such measurements are facilitated by the use of infra-red thermometry.

Example.

Fragmented ore of specific heat $900 \text{ J}/(\text{kg}^\circ\text{C})$ enters the top of an ore pass at a temperature of 35°C and at a rate of 500 tonnes per hour. At an elevation 200 m below, the ore is discharged onto a conveyor and reaches the shaft bottom at a temperature of 32°C . Calculate the heat transferred from the broken ore to the ventilation system over the length of the conveyor.

Solution.

From equation (15.54), temperature rise of the rock in the ore pass

$$= \frac{200 \times 9.81}{900} = 2.18^\circ\text{C} \quad (\text{assuming no heat transfer between the fragmented ore and the surrounding strata})$$

Temperature of rock at bottom of ore pass = $35 + 2.18 = 37.18^\circ\text{C}$

$$\text{Mass flow of ore, } m = \frac{500 \times 1000}{3600} = 138.9 \text{ kg/s}$$

Heat transfer to the airflow from ore on the conveyor (see equation (15.56))

$$mC(\theta_1 - \theta_2) = 138.9 \times 0.900 \times (37.18 - 32) = 647 \text{ kW}$$

15.3.8. Metabolic heat

The rate at which the human body produces metabolic heat depends upon a number of factors including rate of manual work, physical fitness and level of mental stress. The question of heat transfer between the human body and the surrounding environment is of great importance in ascertaining the risk of heat stress in mine workers (Chapter 17). However, metabolic heat makes only a small contribution to mine heat load. It may, nevertheless, become significant where labour intensive activities take place in a location of limited throughflow ventilation such as a poorly ventilated heading or a barricaded refuge chamber.

Like other heat engines, the human body emits heat by three mechanisms. The most significant of these in physiological processes is heat loss from the body surface. Secondly, the large, wet surface area of the lungs provides an effective heat exchanger and 'exhaust' heat is emitted through respiration. Third, any mechanical work done by the individual on the external surroundings will produce frictional heat, unless that work is done against gravity. As the human body is an inefficient heat engine, this latter mechanism is the least significant and is often omitted in calculations of physiological heat transfer.

The metabolic heat produced by a fit worker who is acclimatized to the environment varies from about 100 W for sedentary work, through 400 W for a medium level of activity such as walking, to over 600 W during intermittent periods of strenuous manual work. (See Table 17.1)

BIBLIOGRAPHY

- ASHRAE (1985).** American Society of Heating, Ventilating and Air Conditioning Engineers. Fundamentals Handbook in SI units. Chapters 3 and 5.
- Bluhm, S.J. (1987).** Chamber of Mines of South Africa. Private communication.
- Chilton, T.H. and Colburn, A.P. (1934).** Mass transfer (absorption) coefficients - prediction from data on heat transfer and fluid friction. Industrial and Engineering Chemistry, Nov. p. 1183.
- Carrier, W.H. (1940).** Air cooling in the gold mines on the Rand. Trans. AIME, Vol. 141. pp. 176-287.
- Carslaw, H. and Jaeger, J.C. (1956).** Conduction of heat in solids. Oxford University Press.
- Danko, G. et al (1987).** Development of an improved method to measure in-situ thermal rock properties in a single drill hole. Proc. 3rd U.S. Mine Ventilation Symposium. Penn State. pp. 33-52.
- Danko, G. et al (1988).** Heat, mass and impulse transport for underground airways. Trans. 4th Int. Mine Ventilation Congress. Brisbane, Australia, pp 237-247.
- Deen J.B. (1988).** Laboratory verification of heat transfer analogies. M.S. Dissertation. University of California, Berkeley.
- Gibson, K.L. (1976).** The computer simulation of climatic conditions in underground mines. Ph.D. Thesis, University of Nottingham.
- Goch., D.C. and Patterson, H.S. (1940).** Heat flow into tunnels. Jnl. Chem., Metal., and Mining Soc. of S. Africa. Vol. 41. pp. 117-28.
- Hartman, H.L. (1982).** Mine Ventilation and Air Conditioning, Ch. 20. Wiley.
- Hemp, R. (1965).** Air temperature increases in airways. Journal of the Mine Ventilation Society of S. Africa. Vol. 38, No. 2, Jan, Feb.
- Hemp, R. (1982).** Environmental Engineering in South African Mines. Ch. 22. Mine Vent. Soc. of S. Africa.
- Kibble, J.D. (1978).** Some notes on mining diesels. Mining Technology. October, pp. 393-400.
- McPherson, M.J. (1976).** Refrigeration in South African Gold Mines. Mining Engineer (Feb.) pp 245-258.
- McPherson, M.J. (1986).** The analysis and simulation of heat flow into underground airways. International Journal of Mining and Geological Engineering, Vol. 4. pp.165-196.
- Moussset-Jones, P. and McPherson, M.J. (1984).** Measurement of in-situ thermal parameters in an underground mine. Proc. 2nd Annual Workshop, Generic Mineral Technology Center (Mine System Design and Ground Control) USA. pp.113-131.
- Moussset-Jones, P. et al (1987).** Heat transfer in mine airways with natural roughness. 3rd US Mine Ventilation Symposium. Penn State. pp. 42-52.
- Nunner, W. (1956).** Z ver. Deut. Forschungshaft, 455.

Robinson, G. et al (1981). Underground environmental planning at Boulby Mine, Cleveland Potash Ltd. Trans. Inst. of Mining and Met. London, July.

Stewart, J. (1982). Environmental Engineering in South African mines. Ch. 20. Fundamentals of heat stress. pp. 495-533.

Stroh, R. (1979). A note on the downcast shaft as a thermal flywheel. Jnl. of the Mine Vent. Soc. of S. Africa, 32. pp. 77-80.

Verma, Y.K. (1981). Studies in virgin strata temperatures, with special reference to the NCB'S Western Area Mines. The Mining Engineer Vol. 140. No. 234 (March). pp. 655-663.

Whillier, A. (1981). Predicting cooling requirements for caving and sublevel stoping in hot rock. Int. Conf. on Caving and Sublevel Stopping. AIME Denver.

Whillier, A. (1982). Environmental Engineering in South African Mines Ch. 19.

APPENDIX A15.1

Analytical solution of the three dimensional transient heat conduction equation (15.13) as obtained by Carslaw and Jaeger (1956).

$$G = \frac{4}{\pi^2} \int_0^{\infty} \frac{e^{-V^2\tau}}{[I_0(V) + V/DI_1(V)]^2 + [Y_0(V) + V/DY_1(V)]^2 V} dV$$

where I_0 , I_1 , Y_0 and Y_1 are Bessel functions and V is the variable of integration.

APPENDIX A15.2

Gibson's algorithm for the numeric determination of dimensionless temperature gradient, G .

Enter α (rock diffusivity, m^2/s)
 t (age of airway, seconds)
 r_a (effective radius of airway = perimeter/(2π), metres)
 k (thermal conductivity of rock, $W/(m^{\circ}C)$).

Then

$$F = at / r_a^2 \text{ (Fourier Number)}$$

$$B = hr_a / k \text{ (Biot Number)}$$

$$x = \log_{10}(F)$$

$$y = \log_{10}(B)$$

$$c = x(0.000104x + 0.000997) - 0.001419$$

$$c = - \{x[x(xc - 0.046223) + 0.315553] + 0.006003\}$$

$$d = y - (x(4x - 34) - 5) / 120$$

$$d = 0.949 + 0.1 \exp(-2.69035 d^2)$$

$$m = \text{sq}r \left[(y - c)^2 + \frac{(216 + 5x)}{70} \left\{ 0.0725 + 0.01 \tan^{-1} \left(\frac{x}{0.7048} \right) \right\} \right]$$

$$n = (y + c - m) / 2$$

$$G = 10^n / d$$

APPENDIX A15.3.

Background to equations for the heat transfer coefficient, h .

Consider the transfer of heat, q (W/m^2) across the boundary layers shown on Figure A15.1. In the laminar sublayer, there are no cross velocities and Fourier's law of heat conduction applies:

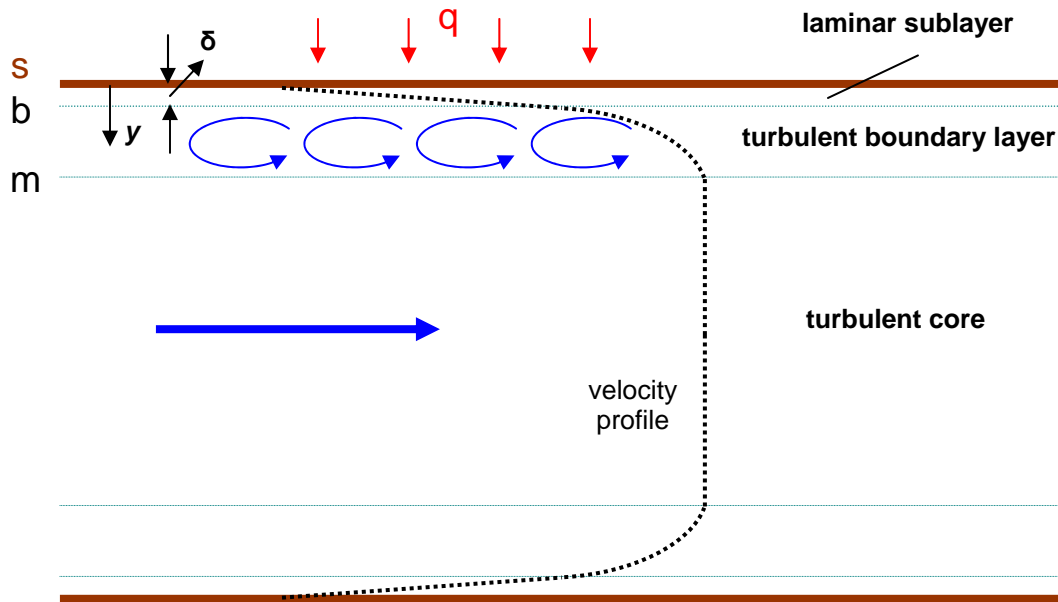


Figure A15.1 Heat is transported by conduction and molecular diffusion across the laminar sublayers, and by eddy diffusion across the turbulent boundary layers.

$$q = -k_a \frac{d\theta}{dy} \quad \text{W}/\text{m}^2 \quad (\text{A15.1})$$

where k_a = thermal conductivity of air $\text{W}/(\text{m}^\circ\text{C})$
 θ = fluid temperature ($^\circ\text{C}$) and
 y = distance from the wall (m)

In the turbulent boundary layer (and within the mainstream), heat transfer is assisted by eddy action and the equation becomes:

$$q = -(k_a + \rho_a C_p E_h) \frac{d\theta}{dy} \quad \text{W}/\text{m}^2 \quad (\text{A15.2})$$

where ρ_a = air density (kg/m^3)
 C_p = specific heat ($1005 \text{ J}/\text{kg}^\circ\text{C}$ for dry air) and
 E_h = eddy diffusivity of heat (m^2/s)

The term $\rho_a C_p$ ($\text{J}/\text{m}^3^\circ\text{C}$) is the amount of heat transported in each m^3 for each Centigrade degree of temperature difference while E_h (m^2/s) represents the rate at which this heat is transported by eddy action. The product $\rho_a C_p E_h$ is much larger than k_a .

Equation (A15.2) can be re-written as

$$\begin{aligned}\frac{q}{\rho_a C_p} &= - \left\{ \frac{k_a}{\rho_a C_p} + E_h \right\} \frac{d\theta}{dy} && \frac{\text{m}^\circ\text{C}}{\text{s}} \\ &= - \{ \alpha + E_h \} \frac{d\theta}{dy} && \text{(A15.2a)}\end{aligned}$$

as $\alpha = \frac{k_a}{\rho_a C_p} = \text{thermal diffusivity of still air (m}^2/\text{s)}$

Figure A15.1 illustrates two boundary layers only. In fact, a third transitional or buffer layer exists between the laminar and turbulent layers, within which both conduction and eddy diffusion are significant. This is similar to the transitional region between laminar flow and fully developed turbulence shown on Figure 2.6 for pipes.

Let us now consider the transfer of momentum across the boundary layers. For the laminar sublayer where the flow is viscous, Newton's equation (2.22) applies:

$$\tau = \mu \frac{du}{dy} \quad \text{N/m}^2 \quad \text{(A15.3)}$$

where τ = shear stress transmitted across each lamina of fluid (N/m² or Pa)

μ = coefficient of dynamic viscosity Ns/m²

u = fluid velocity (m/s)

Note that the units of shear stress may be written also as Ns/(m²s)

Therefore, as Ns are the units of momentum, τ also represents the transfer of momentum across each square metre per second.

For the turbulent boundary layer, the equation becomes

$$\tau = (\mu + \rho_a E_m) \frac{du}{dy} \quad \text{N/m}^2 \quad \text{(A15.4)}$$

where E_m = eddy diffusivity of momentum (m²/s) and

$\rho_a E_m$ = momentum transfer across each m² by eddy action (Ns/m²)

Again, $\rho_a E_m$ is much larger than μ .

$$\begin{aligned}\text{Then } \frac{\tau}{\rho_a} &= \left\{ \frac{\mu}{\rho_a} + E_m \right\} \frac{du}{dy} \\ &= (\nu + E_m) \frac{du}{dy} && \frac{\text{J}}{\text{kg}}\end{aligned} \quad \text{(A15.5)}$$

where $\nu = \frac{\mu}{\rho_a} = \text{kinematic viscosity or momentum diffusivity (m}^2/\text{s)}$

In order to combine heat transfer and momentum transfer, Reynolds divided equations (A15.2a) and (A15.5), giving,

$$\frac{q}{\rho_a C_p \tau} \frac{\rho_a}{\tau} = - \frac{(\alpha + E_h)}{(\nu + E_m)} \frac{d\theta}{dy} \frac{dy}{du}$$

or

$$\frac{q}{C_p \tau} = - \frac{(\alpha + E_h)}{(\nu + E_m)} \frac{d\theta}{du} \quad (\text{A15.5a})$$

Reynolds argued that as the eddy components predominate and the eddy diffusivity for heat, E_h , must be closely allied to the eddy diffusivity for momentum, E_m , we may equate those terms, leaving

$$\frac{q}{C_p \tau} = - \frac{d\theta}{du} \quad (\text{A15.6})$$

Reynolds integrated this equation directly, making the approximation that u remained linear with respect to y across the composite boundary layers (see the velocity profile on Figure A15.1). However, both Taylor and Prandtl, working independently, later realized that the integration had to be carried out separately for the laminar sublayer and the turbulent boundary layer.

Laminar sublayer

From equation (A15.1)

$$\begin{aligned} q \int_0^{\delta} dy &= -k_a \int_{\theta_s}^{\theta_b} d\theta \\ q \delta &= k_a (\theta_s - \theta_b) \end{aligned} \quad (\text{A15.7})$$

where

$$\begin{aligned} \delta &= \text{thickness of laminar sublayer (m)} \\ \theta_s &= \text{temperature at the surface (}^\circ\text{C)} \\ \text{and } \theta_b &= \text{temperature at the edge of the laminar sublayer (}^\circ\text{C)} \end{aligned}$$

Similarly, integrating equation (A15.3) from zero velocity at the wall to u_b at the edge of the laminar sublayer

$$\tau = \mu \frac{u_b}{\delta} \quad (\text{A15.8})$$

Dividing (A15.7) by (A15.8) gives

$$\frac{q}{\tau} = \frac{k_a}{\mu} \frac{(\theta_s - \theta_b)}{u_b} \quad (\text{A15.9})$$

Turbulent boundary layer

Here we employ equation (A15.6)

$$\frac{q}{C_p \tau} du = - d\theta$$

and integrate from the edge of the laminar sublayer (subscript b) to the mainstream (subscript m) (see Figure A15.1):

$$\frac{q}{C_p \tau} \int_{u_b}^{u_m} du = - \int_{\theta_b}^{\theta_m} d\theta$$

giving $\frac{q}{C_p \tau} = \frac{(\theta_b - \theta_m)}{(u_m - u_b)}$ (A15.10)

A difficulty here is that neither θ_b nor u_b are amenable to accurate location or measurement. We can eliminate θ_b by rewriting (A15.9) as

$$\theta_b = \theta_s - \frac{q \mu}{\tau k_a} u_b \quad (A15.11)$$

Substituting for θ_b in equation (A15.10) and engaging in some algebraic manipulation leads to

$$\frac{q}{C_p \tau} = \frac{(\theta_s - \theta_m)}{u_m} \frac{1}{\left\{ 1 + \frac{u_b}{u_m} \left(\frac{\mu C_p}{k_a} - 1 \right) \right\}}$$

Now the combination $\mu C_p/k_a$ is another dimensionless number known as the **Prandtl Number** P_r

$$\frac{q}{C_p \tau} = \frac{(\theta_s - \theta_m)}{u_m} \frac{1}{\left\{ 1 + \frac{u_b}{u_m} (P_r - 1) \right\}} \quad (A15.12)$$

Furthermore, the shear stress, τ , is related to the coefficient of friction, f , and the mainstream velocity, u_m , by equation (2.41)

$$\tau = f \rho_a \frac{u_m^2}{2}$$

Also,

$$q = h(\theta_s - \theta_m) \text{ from equation (15.16) where } \theta_m = \theta_d = \text{dry bulb temperature of the mainstream}$$

Substituting for τ and q in equation (A15.12),

$$\frac{h(\theta_s - \theta_m)}{C_p \frac{f}{2} \rho_a u_m^2} = \frac{(\theta_s - \theta_m)}{u_m} \frac{1}{[1 + (P_r - 1)u_b / u_m]}$$

$$\frac{h}{C_p \rho_a u_m} = \frac{f}{2} \frac{1}{[1 + (P_r - 1)u_b / u_m]}$$

The left hand side of this equation can be separated into three dimensionless groups

$$\frac{hd}{k_a} \quad \frac{\mu}{\rho_a u_m d} \quad \frac{k_a}{C_p \mu} = \frac{N_u}{R_e P_r}$$

Nusselt No. N_u $\frac{1}{\text{Reynolds No. (Re)}}$ $\frac{1}{\text{Prandtl No. (} P_r \text{)}}$

Hence

$$N_u = \frac{f}{2} \text{Re } P_r \frac{1}{[1 + (P_r - 1)u_b / u_m]} \quad (\text{A15.13})$$

This is sometimes known as the **Taylor** or **Taylor-Prandtl** equation and is the basic relationship that has been used by numerous other workers. These varied in the manner in which they treated the u_b/u_m ratio as u_b remains elusive to measure. Taylor himself used an empirical value of $u_b/u_m = 0.56$. Several other relationships are listed in Table A15.1. A more comprehensive listing is given by Danko (1988)

Authority	Value of u_b/u_m
Taylor	0.56
Von Kármán	$9.77 \sqrt{f/2}$
Rogers and Mayhew	$1.99 \text{Re}^{-0.125}$

Table A15.1 Some reported values of the u_b/u_m ratio

A comprehensive theoretical and experimental study of flow over rough surfaces by Nunner (1956) produced a more sophisticated equation

$$N_u = \frac{f}{2} \text{Re } P_r \frac{1}{\left[1 + \frac{1.5}{\text{Re}^{1/8} P_r^{1/6}} \left(P_r \frac{f}{f_0} - 1\right)\right]} \quad (\text{A15.14})$$

where

f_0 = friction coefficient for a smooth tube at the same value of Reynolds' Number.

This is known as **Nunner's equation**.

An analysis of hydraulically smooth pipes by Colburn gave

$$N_u = 0.023 \text{Re}^{0.8} P_r^{0.4} \quad (\text{A15.15})$$

For air in the atmospheric range, the Prandtl Number is near constant. Using the values at 20°C,

$$\mu = (17 + 0.045 \times 20) \times 10^{-6} = 17.9 \times 10^{-6} \quad \text{Ns/m}^2 \quad (\text{Section 2.3.3})$$

$$k_a = 2.2348 \times 10^{-4} (273.15 + 20)^{0.8353} = 0.0257 \quad \text{W/(m}^\circ\text{C)} \quad (\text{Table 15.1})$$

$$C_p = 1005 \quad \text{J/(kg}^\circ\text{C)}$$

gives

$$P_r = \frac{C_p \mu}{k_a} = \frac{1005 \times 17.9 \times 10^{-6}}{0.0257} = 0.700 \quad (\text{A15.16})$$

In order to illustrate the differences between the relationships quoted, Figure A15.2 has been produced for values of $P_r = 0.7$ and $f = 0.02$. There is reasonable agreement within the Von Kármán, Taylor and Rogers equations. The Nunner relationship produces Nusselt Numbers a little less than one half those given by the other authorities. As might be expected, the Colburn smooth tube equation gives much lower Nusselt Numbers and, hence, heat transfer coefficients.

Experimental evidence in mine airways (Mousset-Jones et al, 1987 and Danko et al, 1988) and also in scale models under controlled conditions (Deen, 1988) has indicated a better correlation with the Nunner equation than the others. Hence, this is the relationship suggested for use in underground openings at the present time. Ongoing research will no doubt produce further equations or algorithms for N_u .

One further problem remains with equation (A15.14), the evaluation of f_0 , the coefficient of friction for a hydraulically smooth tube at the same Reynolds Number. However, the approximation given in Section 2.3.6.3 gives acceptable results for the range of Reynolds' Numbers common in mine airways:

$$f_0 = 0.046 \text{ Re}^{-0.2} \quad (\text{A15.17})$$

Substituting for f_0 in the Nunner equation and using $P_r = 0.7$ gives

$$N_u = \frac{0.35 f \text{ Re}}{\left[1 + \frac{1.592}{\text{Re}^{0.125}} (15.217 f \text{ Re}^{0.2} - 1) \right]} \quad (\text{A15.18})$$

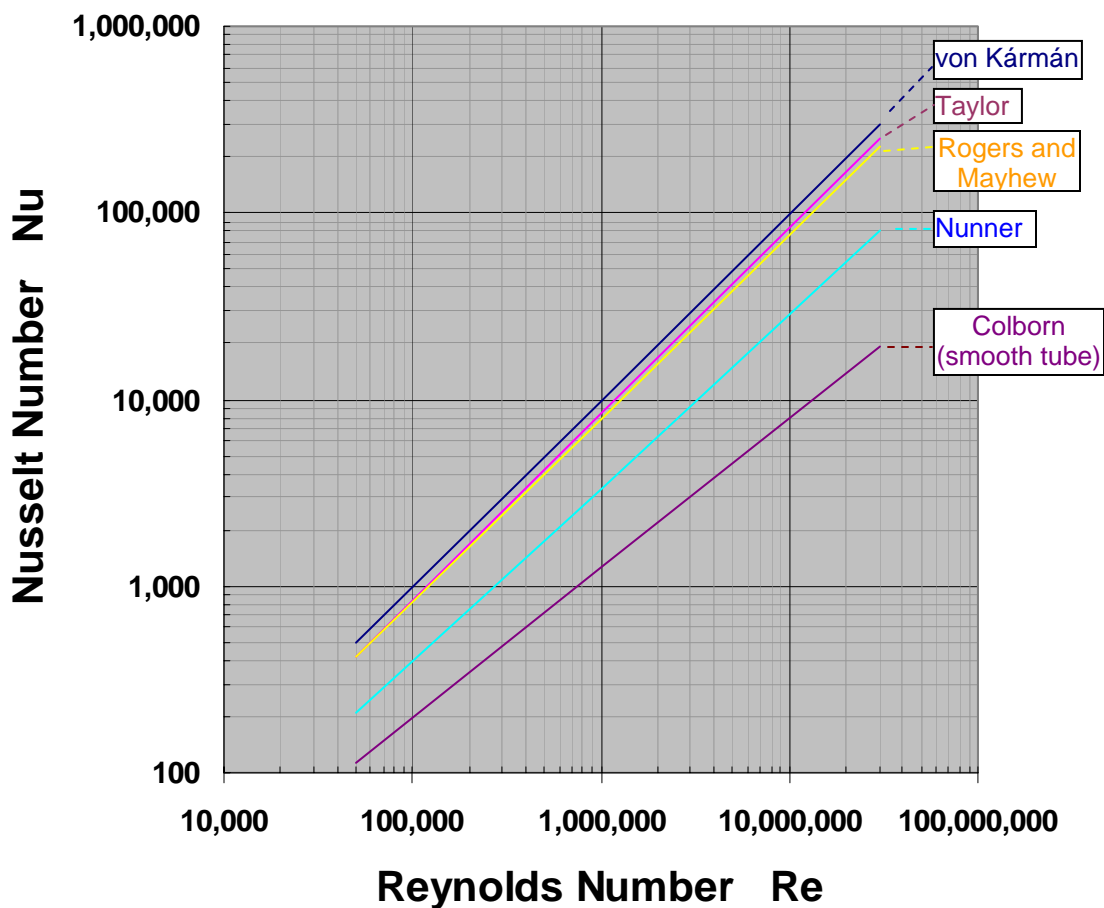


Figure A15.2 Relationships between Nusselt Number and Reynolds Number proposed by various authorities for $P_r = 0.7$ and $f = 0.02$.

APPENDIX A15.4

Derivation of the equation for latent heat of evaporation at a wet surface.

When any two gases, **a** and **b**, are brought into contact then molecules of each gas will diffuse into the other at the interface. The fundamental law governing the rate of diffusion is

$$m = D_v \frac{\partial \rho_a}{\partial x} \quad \frac{\text{kg}}{\text{m}^2 \text{s}} \quad (\text{A15.19})$$

where

m = rate of diffusion across unit area of gas **a** into gas **b** ($\text{kg}/(\text{m}^2 \text{s})$)
 ρ_a = density of gas **a** (kg/m^3)
 x = distance beyond the interface (m) and
 D_v = diffusion coefficient of gas **a** into gas **b** (m^2/s)
(experimental results give this as $25.5 \times 10^{-6} \text{ m}^2/\text{s}$ for the diffusion of water vapour into air (ASHRAE, 1985))

This is known as Fick's Law and is analogous to Fourier's law for heat conduction:

$$q = -k \frac{\partial \theta}{\partial x} \quad \text{W}/\text{m}^2$$

At a wet surface with unsaturated air flowing over it, water vapour is produced continuously by evaporation and will be transported by molecular diffusion through the laminar sublayer then, additionally, by eddy action through the transitional (buffer) and turbulent layers. The transfer of heat, momentum and mass are all affected in the same way by eddies at any given surface. Hence, the governing equations have the same form for all three. Just as we had

$$q = h(\theta_s - \theta_d) \quad \text{W}/\text{m}^2 \quad (\text{see equation (15.6)})$$

for heat flow across the boundary layers, so we can write an analogous equation for the migration of water molecules:

$$m = h_m (\rho_{vws} - \rho_v) \quad \text{kg}/(\text{m}^2 \text{s}) \quad (\text{A15.20})$$

where

m = mass of water vapour migrating from each square metre per second ($\text{kg}/(\text{m}^2 \text{s})$)
 h_m = mass transfer coefficient (m/s)
 ρ_{vws} = density of water vapour at the wet surface (kg/m^3)
 ρ_v = density of water vapour in the mainstream (kg/m^3)

The density difference ($\rho_{vws} - \rho_v$) provides the potential or driving mechanism for the diffusion of mass.

Now from the general gas law

$$e = \rho_v R_v T \quad \text{Pa} \quad (\text{see equation (3.11)})$$

where

e = partial pressure of water vapour (Pa)
 R_v = gas constant for water vapour (461.5 J/kg K) and
 T = absolute temperature (K)

Hence, equation (A15.20) becomes

$$m = h_m \frac{1}{R_v T} (e_{ws} - e) \quad \frac{\text{kg}}{\text{m}^2 \text{s}} \quad (\text{A15.21})$$

e is the vapour pressure within the main airstream and e_{ws} the vapour pressure at the wet surface. It is reasonable to assume that immediately adjacent to the liquid surface, the space will be saturated. e_{ws} is then also the saturated vapour pressure at the wet surface temperature, θ_{ws} .

Now, the general gas law for a mixture of air and water vapour gives

$$\rho_m = \frac{P}{R_m T} \quad \text{Pa}$$

where

$$\begin{aligned} \rho_m &= \text{density of moist air (kg/m}^3\text{)} \\ P &= \text{barometric pressure (Pa) and} \\ R_m &= \text{gas constant for moist air (J/(kg K))} \end{aligned}$$

However, for the atmospheric range in mines, R_m differs only slightly from the gas constant for dry air, $R_a = 287.04 \text{ J/(kg K)}$ [Section 14.2.4]. Hence, we can express equation (A15.21) as

$$\begin{aligned} m &= h_m \frac{\rho_m}{R_v T} \frac{1}{\rho_m} (e_{ws} - e) \\ &= h_m \frac{\rho_m}{R_v T} \frac{R_a T}{P} (e_{ws} - e) \\ &= h_m \rho_m 0.622 \frac{(e_{ws} - e)}{P} \quad \frac{\text{kg}}{\text{m}^2\text{s}} \end{aligned} \quad (\text{A15.22})$$

as

$$\frac{R_a}{R_v} = \frac{287.04}{461.5} = 0.622$$

Now let us turn our attention to the mass transfer coefficient, h_m . In 1934, Chilton and Colburn, investigating the analogy between heat transfer and mass diffusion, produced a relationship between the convective heat transfer coefficient, h_c , and the mass transfer coefficient, h_m . In its most compact form (ASHRAE, 1985), this can be expressed as

$$h_m = \frac{h_c}{C_p \rho_m} \left[\frac{P_r}{S_c} \right]^{2/3} \quad \text{m/s} \quad (\text{A15.23})$$

where

C_p = specific heat of air (J/kg K)

$P_r = \frac{\mu_a C_p}{k_a}$ is the Prandtl Number for air (Appendix A15.3)

μ_a = dynamic viscosity of air (Ns/m²)
 k_a = thermal conductivity of air (W/(m°C))

and S_c is yet another dimensionless number (**Schmidt Number**) = $\frac{\mu_a}{\rho_a D_v}$

Both the Prandtl and Schmidt dimensionless numbers remain reasonably constant over the range of air pressures and temperatures found in subsurface facilities.

Using the values for air at 20°C,

$$\begin{aligned} \mu_a &= 17.9 \times 10^{-6} \text{ Ns/m}^2; & k_a &= 0.0257 \text{ W/(m}^\circ\text{C)} \\ C_p &= 1010 \text{ J/(kgK)} \text{ (mid-range value for moist air):} \\ \rho_a &= 1.2 \text{ kg/m}^3 \text{ (standard air density) and} \\ D_v &= 25.5 \times 10^{-6} \text{ m}^2\text{/s for the diffusion of water vapour into air,} \end{aligned}$$

gives $P_r = 0.703$
and $S_c = 0.585$

Combining equations (A15.22 and A15.23) gives

$$m = \frac{h_c}{C_p \rho_m} \left[\frac{P_r}{S_c} \right]^{2/3} \rho_m 0.622 \frac{(e_{ws} - e)}{P}$$

and, inserting the numerical values for P_r and S_c ,

$$m = h_c 1.130 \times \frac{0.622}{C_p} \frac{(e_{ws} - e)}{P} \quad \frac{\text{kg}}{\text{m}^2 \text{s}} \quad (\text{A15.24})$$

Now the latent heat emitted in the vapour when m kg of surface water is evaporated is

$$q_L = m L_{ws} \quad \frac{\text{kg}}{\text{m}^2 \text{s}} \frac{\text{J}}{\text{kg}} = \text{W/m}^2 \quad (\text{A15.25})$$

where

$$\begin{aligned} L_{ws} &= \text{latent heat of evaporation at the temperature of the wet surface (see equation (14.6))} \\ &= (2502.5 - 2.386 \theta_{ws}) 10^3 \quad \text{J/kg} \end{aligned}$$

Substituting for m from equation (A15.24) gives

$$q_L = h_c 1.130 \times \frac{0.622 L_{ws}}{C_p} \frac{(e_{ws} - e)}{P} \quad \frac{\text{W}}{\text{m}^2} \quad (\text{A15.26})$$

or, using the value $C_p = 1010$ J/kgK for moist air,

$$q_L = 0.0007 h_c L_{ws} \frac{(e_{ws} - e)}{P} \quad \frac{\text{W}}{\text{m}^2} \quad (\text{A15.27})$$

Equation (A15.27) may also be written as

$$q_L = h_e (e_{ws} - e) \quad \frac{\text{W}}{\text{m}^2} \quad (\text{A15.28})$$

where the evaporative heat transfer coefficient, h_e , is given as

$$h_e = 0.0007 h_c \frac{L_{ws}}{P} \quad \frac{\text{W}}{\text{m}^2 \text{ Pa}} \quad (\text{A15.29})$$

The ratio h_e/h_c is known as the **Lewis Ratio** (LR) .

Using the latent heat of evaporation of water at 20°C (2455×10^3 J/kg) and a barometric pressure of 100×10^3 Pa gives

$$\text{LR} = \frac{h_e}{h_c} = 0.017 \quad \frac{^\circ\text{C}}{\text{Pa}} \quad (\text{A15.30})$$

The Lewis ratio changes slowly through the atmospheric range of pressures and temperatures.

A correlation with psychrometric relationships occurs in equation (A15.26). The group $0.622 L_{ws}/C_p$ is the reciprocal of the psychrometric "constant" introduced in Section (14.4.2).

CHAPTER 16. SIMULATION OF CLIMATIC CONDITIONS IN THE SUBSURFACE

16.1. BACKGROUND	1
16.2. ELEMENTS OF A MINE CLIMATE SIMULATION PROGRAM.....	2
16.2.1. Organization of the programs	2
16.2.2. Incrementation of airway length.....	2
16.2.3. Heat additions	2
<i>Strata heat</i>	2
<i>Machines and other sources of heat</i>	3
16.2.4. Change in moisture content.....	5
16.2.5. Change in dry bulb temperature and autocompression.....	5
16.2.6. Change in barometric pressure	7
16.2.7. Change in wet bulb temperature.....	7
16.2.8. Relative humidity and saturation conditions	8
16.2.9 Indices of heat stress	8
16.3. USING A MINE CLIMATE SIMULATOR	9
16.3.1. Data preparation	9
16.3.1.1. Physical description of airway	9
16.3.1.2. Condition of airflow at inlet.....	10
16.3.1.3. Thermal parameters and other heat sources	10
16.3.1.4. Physiological parameters (Worker data)	11
16.3.2. Correlation tests.....	11
16.3.3. Case Study	12
16.3.4. Organization of mine climate simulation exercises.....	18
16.3.5. Interaction with Ventilation Network Analysis packages.....	18
Bibliography	20

16.1. BACKGROUND

The complexities of the relationships that govern heat flow from the strata into ventilated underground openings are illustrated by the analyses given in Section 15.2. Indeed, the routine use of those relationships became practical only through the availability of computer assistance. The first computer programs to simulate heat flow into mine workings were developed in South Africa (Starfield, 1966). The early programs estimated strata heat flow from the **Goch and Patterson** tables (Section 15.2.6.), either by interpolation or from regression fitted equations that approximated those tables. Since that time, simulation programs of increasing sophistication have been developed in a number of countries. Current programs recognize the influence of boundary layers close to the rock/air interface, allow for heat sources other than the strata (Section 15.3) and predict the psychrometric effects of heat and moisture additions on the mine climate and physiological effects on workers.

A common feature of mine climate simulation models is that they are based on solutions of the fundamental equation for heat conduction (equation (15.13)), and on utilization of the dimensionless Fourier and Biot Numbers. However, the programs may vary in the manner in which they determine rock surfaces temperatures, heat transfer coefficients, and in the characterization and treatment of wet surfaces (Mousset-Jones, 1988).

Individual programs may be constrained to particular geometries of stopes or working faces, while others have been written for airways or headings. Some involve empirical relationships that are applicable only to specified layouts or methods of working. Again, some program packages allow

combinations of airways, headings and working faces within a network structure while others are essentially "single airway" simulators that must either be run separately for each branch or used in conjunction with a ventilation network analysis package (Section 16.3.5).

This chapter is divided into two main sections. Section 16.2 outlines the logical operations of the CLIMSIM (climatic simulation) program package and is written for researchers involved in further program development or those who seek an understanding of the numerical procedures used in the simulation. **Readers who are interested only in the practical utilization of a mine climate simulation package should turn directly to Section 16.3.**

16.2. ELEMENTS OF A MINE CLIMATE SIMULATION PROGRAM

16.2.1. Organization of the programs

All mine climate simulations commence with the initial psychrometric condition of the air at the inlet end of the airway (or face) being defined by the user. This is normally accomplished by specifying the inlet wet bulb temperature, dry bulb temperature and barometric pressure. Under user control, the program divides the airway into incremental lengths, each of which is sufficiently short that wet and dry bulb temperatures may be assumed to be constant within the increment for the calculation of strata heat flows.

Each increment is traversed in the direction of airflow and the following parameters are calculated:

- sensible and latent heat flows from the strata and other sources
- change in moisture content of the air
- change in dry bulb temperature
- conversions between potential and thermal energies for shafts or inclined openings (autocompression)
- change in barometric pressure
- change in wet bulb temperature
- other psychrometric parameters and indices of heat stress at the exit end of the increment

The conditions for the start of the next successive increment are then defined. Each incremental length is treated in this way until the complete airway has been traversed. The following subsections outline the computational procedures involved in each of the steps listed.

16.2.2. Incrementation of airway length

The length of airway increment, Y_i , over which changes in temperature have no significant impact on strata heat flux will vary according to the magnitude of heat additions, the airflow and inclination of the airway. The value of Y_i may be (i) fixed at some small value (say 2 to 20 m) within the program, (ii) a fixed fraction of the total length or (iii) chosen by the user.

16.2.3. Heat additions

In any incremental length of airway there will, in general, be transfers of both sensible and latent heat from one or more sources. In order to determine the corresponding psychrometric changes in the airflow, the sensible and latent heat components are each accumulated separately.

Strata heat

Let us consider the rock surface to be divided into wet and dry areas. We can then define a **wetness fraction**, w , as that fraction of total surface area that is covered or coated with liquid water. The concept of wetness fraction is discussed further in Section 16.3.1.1.

The area of wet surface within the incremental length Y_i now becomes

$$A_w = 2\pi r_a Y_i w \quad \text{m}^2 \quad (16.1)$$

where r_a = the effective radius of the airway (perimeter/ 2π)

The remaining dry surface area is

$$A_d = 2\pi r_a Y_i (1-w) \quad \text{m}^2 \quad (16.2)$$

Sensible heat transfer will take place on both the dry and wet surfaces while latent heat transfer occurs at the wet surface only. The normalized strata heat flows (per square metre) may be calculated using the methods described in Sections 15.2.8 and 15.2.9.

Let us denote these heat flows as follows:

- sensible heat from dry surface: $q_{sen,d}$ (W/m^2)
- sensible heat from wet surface: $q_{sen,w}$ (W/m^2)
- latent heat from wet surface: $q_{L,w}$ (W/m^2)

The strata heat flowing into the increment, Y_i , is then the combination of:

- dry surface: $q_{sen,d} A_d = 2\pi r_a q_{sen,d} Y_i (1-w) \quad \text{W} \quad (16.3)$

- wet surface: $q_{sen,w} A_w = 2\pi r_a q_{sen,w} Y_i w \quad \text{W} \quad (16.4)$

- wet surface: $q_{L,w} A_w = 2\pi r_a q_{L,w} Y_i w \quad \text{W} \quad (16.5)$

where A = surface area (m²)

and subscripts w and d refer to wet and dry areas respectively.

Machines and other sources of heat

Here again, heat additions from operating equipment must be separated into components of sensible and latent heat. In the case of **electrical plant**, all of the power supplied may be considered as a sensible heat addition to the airflow, excepting any work that is done against gravity (Section 15.3.2.1). The user must supply two values representing

- (a) the full power rating (kW) of the motor or device, FPR , reduced, if necessary, by the rate of work done against gravity, and
- (b) the machine utilization factor, MUF , defined as that fraction of time over which, if the machine were running at full load, would consume the same amount of energy as the actual intermittent operation of the device. Hence, the machine utilization factor for a motor running continuously at full load would be 1.0.

The value of sensible heat produced by the electrical device is then given as

$$FPR \times MUF \quad \text{W} \quad (16.6)$$

Diesel engines produce both sensible and latent heat (Section 15.3.2.2.). Here again, the user must supply a full power rating, FPR and a machine utilization factor, MUF , for each piece of diesel equipment. The average machine load, given as the product $FPR \times MUF$ (kW), is then converted to fuel consumption (litres/hour) using a mean empirical value (typically 0.3 litres of fuel per kW engine rating per hour). The total heat produced is then simply the fuel consumption multiplied by the calorific value of the fuel (typical value 34 000 kJ/litre).

Using the values quoted, the fuel consumed, FC , becomes

$$FC = FPR \times MUF \times \frac{0.3}{3600} \quad \text{litres/s} \quad (16.7)$$

$$\text{and the total heat produced} = FC \times 34\,000 \times 10^3 \quad \text{W} \quad (16.8)$$

The user may, of course, specify the rate of fuel consumption directly rather than through the factors on the right side of equation (16.7). However, practical experience has indicated that most mine ventilation engineers find it more convenient to assess machine rating and utilization data than to acquire fuel consumption for individual diesel units.

In order to separate out the amount of water vapour produced by the diesel engine, the user must supply a third item of data, namely, the water/fuel ratio, WFR , defined as the litres of water (liquid equivalent) produced for each litre of fuel consumed. The combustion of one litre of diesel fuel will produce between 1.1 and 1.5 litres of water. However, this may be multiplied several times by engine cooling systems and exhaust scrubbers in addition to enhanced evaporation from rock surfaces in the immediate vicinity of the machine. Values as high as 9 litres of water per litre of fuel have been reported (Mousset-Jones, 1987).

Water vapour is then added to the airstream at a rate of

$$FC \times WFR \quad \frac{\text{litres of fuel}}{\text{s}} \quad \frac{\text{litres of water}}{\text{litre of fuel}} \quad (16.9)$$

i.e. kg of water vapour per second

The equivalent value of latent heat is given as

$$FC \times WFR \times L \quad \text{W} \quad (16.10)$$

where L = latent heat of evaporation of water in J/kg
while the sensible heat produced by the diesel becomes (total diesel heat - latent diesel heat) from equations (16.8 and 16.10) respectively.

Compressed air equipment adds no overall heat to a ventilating airstream and, indeed, can produce a small net cooling effect (Section 15.3.2.3). Such equipment is usually ignored in mine climate simulations.

Other sources of heat (Sections 15.3.3 to 15.3.8) may be specified by the user. In the general purpose climate simulators, it is left to the user to select the sensible and latent heat components. However, special purpose programs have been developed to handle cases such as ducts, pipes, cables, water channels or spray chambers located within the airway. Air coolers may be specified simply as negative heat sources.

A climate simulation program will compute the components of strata heat for each incremental length of airway. In the case of machines or other sources of heat, the user must identify the locations of those machines or other sources. This can be accomplished by specifying either (a) a spot source, or (b) a distributed source.

A spot source will produce its heat at a fixed location and, hence, will appear in a single element of airway length. This is the type of heat source chosen for stationary pieces of equipment such as transformers, conveyor gearheads or mobile devices that move over short distances only. A distributed source, as the term implies, will spread its heat load over a distance specified by the user (e.g. length of a conveyor, hot or cold pipes, drainage channels). In a simple case, the heat will be

distributed linearly over the selected distance. A more sophisticated program may allow the heat to be distributed according to a function specified by the user.

For each increment of airway length, the simulation program will determine and sum both the sensible and latent heat components from all sources relevant to that increment. We can now refer to the corresponding summations as Σq_{sen} and Σq_L , respectively, for each increment.

16.2.4. Change in moisture content

The apparent density, ρ_{app} , of the air at inlet to the airway is calculated from the psychrometric condition of the air specified by the user for that starting location

$$\rho_{app} = \frac{(P - e)}{287.04(\theta_d + 273.15)} \quad \frac{\text{kg of dry air}}{\text{m}^3 \text{ of air}} \quad (\text{see equation (14.51)})$$

where P = barometric pressure (Pa)
 e = actual vapour pressure (Pa) and
 θ_d = dry bulb temperature ($^{\circ}\text{C}$)

The mass flow, M , of the 'dry air' component of the air/vapour mixture is then given as

$$M = Q \rho_{app} \quad \frac{\text{kg dry air}}{\text{s}} \quad (16.11)$$

where Q is the known rate of airflow at inlet (m^3/s)

The value of M remains constant along any given airway.

The rate at which water vapour is added to an increment of airway length is simply

$$\frac{\Sigma q_L}{L} \quad \frac{\text{J kg}}{\text{s J}} = \frac{\text{kg}}{\text{s}} \quad \text{where } L = \text{latent heat of evaporation (J/kg)}$$

The increase in moisture content of the air becomes

$$\Delta X = \frac{\Sigma q_L}{LM} \quad \text{kg/kg dry air} \quad (16.12)$$

Hence, if we denote subscripts 1 and 2 for entry and exit from the incremental length, then

$$X_2 = X_1 + \Delta X \quad \text{kg/kg dry air} \quad (16.13)$$

16.2.5. Change in dry bulb temperature and autocompression

In the absence of any fan work the steady flow energy equation (3.25) gives

$$(H_2 - H_1) - q_{12} = \frac{u_1^2 - u_2^2}{2} + (Z_1 - Z_2)g \quad \frac{\text{J}}{\text{kg}} \quad (16.14)$$

where H = enthalpy (J/kg)
 q_{12} = heat added (J/kg)
 u = air velocity (m/s) and
 Z = height above datum (m)

However, equation (14.40) shows that the enthalpy term comprises a sensible heat component, $C_{pa}\theta_d$, and a latent heat component, just as q_{12} involves both sensible and latent heat. As it is only the sensible heat component that affects the dry bulb temperature we can subtract the latent heat component from both the H and q terms. Then equation (16.14) can be re-written as

$$(C_{pa}(\theta_{d,2} - \theta_{d,1}) - q_{12,sen}) = \frac{u_1^2 - u_2^2}{2} + (Z_1 - Z_2)g \quad \text{J/kg} \quad (\text{see equation (3.33)})$$

where C_{pa} = specific heat for dry air (1005 J/kg °C)

We must remember that $q_{12,sen}$ is the sensible heat addition in J/kg while our earlier sensible heat summation for the increment, $\sum q_{sen}$, was in Watts.

$$\text{Hence, } q_{12,sen} = \frac{\sum q_{sen}}{M} \quad \frac{\text{J}}{\text{kg dry air}} \quad (16.15)$$

The increase in dry bulb temperature then becomes

$$\Delta\theta_d = (\theta_{d,2} - \theta_{d,1}) = \left[\frac{u_1^2 - u_2^2}{2} + (Z_1 - Z_2)g + \frac{\sum q_{sen}}{M} \right] \frac{1}{C_{pa}} \quad ^\circ\text{C} \quad (16.16)$$

All terms on the right hand side of equation (16.16) are known except the change in kinetic energy. This is caused only by the change in density in an airway of fixed cross-sectional area and, hence, is very small. However, it can be estimated as follows:

$$\frac{u_1^2 - u_2^2}{2} = \frac{1}{2} \frac{(Q_1^2 - Q_2^2)}{A^2}$$

where Q = volume flowrate (m³/s) and
 A = cross-sectional area (m²)

From equation (16.11), $Q = M/\rho_{app}$
giving

$$\frac{u_1^2 - u_2^2}{2} = \frac{1}{2} \frac{M^2}{A^2} \left[\frac{1}{\rho_{1,app}^2} - \frac{1}{\rho_{2,app}^2} \right] \quad \frac{\text{J}}{\text{kg}} \quad (16.17)$$

A difficulty arises here in that $\rho_{2,app}$ requires a knowledge of the psychrometric conditions at the exit end of the increment. These are still unknown. However, as the change in kinetic energy is a very weak parameter, satisfactory results are obtained by using the change in air density established for the previous increment in equation (16.17). For the first increment in the airway, the kinetic energy correction may be ignored without significant loss of accuracy.

Equation (16.16) then enables the change in dry bulb temperature, θ_d , to be determined, having taken into account both the sensible heat added and the change in elevation. The dry bulb temperature of the air leaving the increment is simply

$$\theta_{d,2} = \theta_{d,1} + \Delta\theta_d \quad ^\circ\text{C} \quad (16.18)$$

16.2.6. Change in barometric pressure

In the absence of a fan the variation in absolute pressure of the air, P , is caused by (a) the conversion of mechanical energy into heat causing a frictional pressure drop, p , and (b) changes in elevation ($Z_1 - Z_2$).

The effect of changes in moisture content on barometric pressure through any single element remains small provided that the incremental length is not excessive.

The frictional pressure drop is given by Atkinson's equation (5.2)

$$p = k Y_i \frac{\text{per}}{A} u^2 \quad \text{Pa} \quad (16.19)$$

where k = Atkinson's friction factor ($(\rho f)/2$ kg/m³) and
per = airway perimeter (m)

This can be converted into the work done against friction

$$F_{12} = p / \rho_m \quad \text{J/kg} \quad (16.20)$$

where ρ_m = mean air density in the increment (kg/m³). Here again, ρ_1 may be used for the first increment then, subsequently, ρ_m extrapolated from the previous increment.

Assuming polytropic flow through the incremental length of the airway, the steady flow energy equation written in the form of equation (8.1) gives

$$R_m (T_2 - T_1) \frac{\ln(P_2 / P_1)}{\ln(T_2 / T_1)} = \frac{u_1^2 - u_2^2}{2} + (Z_1 - Z_2)g - F_{12} \quad \text{J/kg} \quad (16.21)$$

The gas constant is given as

$$R_m = \frac{287.04 + 461.5 X}{1 + X} \quad \text{J/kg K} \quad [\text{see equation (14.14)}]$$

where T = absolute dry bulb temperature ($\theta_d + 273.15$ K)
and X and θ_d are the mean values for the increment.

The outlet pressure, P_2 , remains the only unknown in equation (16.21) and, hence, may be calculated.

16.2.7. Change in wet bulb temperature

The psychrometric condition of air is completely defined if any three of its psychrometric properties are specified. At the exit from the incremental length of airway, the moisture content, X_2 , the dry bulb temperature, $\theta_{d,2}$, and the barometric pressure, P_2 , have now all been determined. All other psychrometric parameters can then be calculated from the equations given in Section 14.6.

In particular, the wet bulb temperature, $\theta_{w,2}$, may be found from the following equations.

$$X_2 = \frac{S_2 - 1005 \theta_{d,2}}{[L_{w,2} + 1884(\theta_{d,2} - \theta_{w,2})]} \quad \frac{\text{kg}}{\text{kg dry air}}$$

$$\text{where } S = L_{w,2} X_{s,2} + 1005 \theta_{w,2} \quad \text{J/kg dry air}$$

$$L_{w,2} = (2502.5 - 2.386 \theta_{w,2}) 1000 \quad \text{J/kg}$$

$$X_{s,2} = 0.622 \frac{e_{sw,2}}{(P - e_{sw,2})} \quad \frac{\text{kg}}{\text{kg dry air}}$$

$$\text{and } e_{sw,2} = 610.6 \exp \left[\frac{17.27 \theta_{w,2}}{237.3 + \theta_{w,2}} \right] \quad \text{Pa}$$

In this sequence of equations, $\theta_{w,2}$ is the only unknown independent parameter. Hence, by assuming an initial value, the equations may be cycled iteratively until a value of $\theta_{w,2}$ is found that satisfies all the equations simultaneously.

16.2.8. Relative humidity and saturation conditions

One of the psychrometric variables that may be calculated for each incremental length of airway is the relative humidity, defined as

$$rh = \frac{e}{e_{sd}} \quad (\text{see equation (14.54)})$$

where e = actual vapour pressure (Pa) and
 e_{sd} = saturated vapour pressure at dry bulb temperature (Pa)

If the result of this calculation is a value exceeding unity (supersaturation) then this indicates that condensation will take place. Such condensation will occur on all surfaces with a temperature less than that of the air wet bulb temperature and also as a fog within the airstream. Indeed, the former will occur even if the relative humidity is less than 1.0. If the computed psychrometric variables indicate supersaturation, then the heat of condensation released causes the dry bulb temperature to rise until saturation is attained at the same level of enthalpy as the original supersaturation condition. This is approximated closely by setting the revised dry bulb temperature equal to the current value of wet bulb temperature.

16.2.9 Indices of heat stress

Some mine climate simulators go beyond predicting variations in psychrometric conditions to include one or more of the indices of heat stress. These fall into two main groups:

- (a) indices that can be determined from measured or predicted climatic parameters (e.g. effective temperature, ET, or wet bulb globe temperature, WBGT). These are sometimes referred to as 'empirical indices'.
- (b) indices that are based on physiological responses of the healthy human body to an actual or predicted environment for a specified work rate and type of clothing (e.g. Mean Skin Temperature, MST, sweat rate, or Air Cooling Power, ACP). These are often called 'rational indices'.

The methods used within mine climate simulators to determine most of these indices are described in Section 17.4.

16.3. USING A MINE CLIMATE SIMULATOR

The first stage of commissioning a mine climate simulation system is to obtain a program package that provides the required features. The pointers given in Section 7.4.5 for network simulation packages apply equally well here. Secondly, for any given airway or network of airways, the data must be assembled. There is a much greater variety of information required for the prediction of psychrometric conditions along each airway than for the ventilation network analyses described in Chapter 7. Furthermore, some of those data may, initially, be of uncertain precision. Hence, the correlation exercises that must precede employment of a climate simulator for long term planning will often involve modifications of the initial data.

This section deals with data preparation, correlation trials, the procedures involved in running a mine climate simulator, and design exercises that can be carried out with the assistance of such program packages.

6.3.1. Data preparation

The parameters that influence heat flow into a subsurface airway were introduced in Section 15.2.1. The following subsections deal more specifically with the data that must be quantified for each airway in preparation for a mine climate simulation.

16.3.1.1. Physical description of airway

Geometry. The parameters required are airway length, cross-sectional area, perimeter, and levels below a surface datum of both the inlet and exit ends of the airway. It is normally assumed that the cross-sectional area, perimeter and gradient each remain constant throughout the length of the airway. Should there be significant deviations in any of these parameters then the airway should be divided into two or more sub-lengths for simulation.

Friction factor. The roughness of the airway lining is normally quantified as the Atkinson friction factor (Section 5.2).

Age. The program package may allow the age of each end of the airway to be specified separately. The age of each simulated increment of airway length is then computed assuming a uniform rate of drive. This feature takes into account the time taken to develop the airway and is particularly useful for advancing headings.

Wetness fraction. This parameter was introduced in Section 16.2.3 as the fraction of airway surface that is covered or coated with liquid water. However, we have not yet discussed the actual distribution of water over the surface. Furthermore, although the strata heat flow analyses of Section 15.2 considered both dry and wet surfaces, the solution of the basic equation for heat conduction assumed radial heat flow. In a simple case of a square airway with a completely wetted floor but dry sides and roof, the wetness fraction would be 0.25. However, the heat flow through the rock would no longer be radially symmetric.

The concept of wetness fraction as originally introduced by Starfield in 1966, envisaged the wetness to be spread uniformly over the surface. With a surface that is damp but not completely covered in water, asperities on the rough surface may be dry on their peaks but with liquid water in the troughs. This water may be emitted through capillaries in the rock matrix or from discrete fractures before spreading out by a combination of surface capillarity and gravitational forces. The temperature of this type of surface will then take a value lying between those of the completely dry and completely wet surfaces analyzed in Section 15.2 and, hence, be dependent upon the degree of wetting.

In practice, the wetting of airway surfaces is usually far from uniform. Within a single airway there may be surface areas varying from completely wetted to visually dry. Mack and Starfield (1983) proposed an "equivalent wetness factor" for such circumstances, this being defined as the wetness

fraction over a uniformly wetted surface that would give the same rates of heat and moisture transfer as the actual surface of non-uniform wetness.

Values of wetness fraction can be established for existing airways through correlation exercises (Section 16.3.2). Furthermore, ventilation engineers who are experienced in running a climate simulation package become adept at estimating wetness fractions by visual inspection of airways in much the same way that they can estimate friction factors from the appearance of surface roughnesses. Wetness fractions seldom fall below 0.04, even in airways that appear quite dry.

For planned but yet unconstructed airways, the wetness fraction may be estimated from previous experience of mining within that same geologic formation and at similar depths. If no such data are available then hydrologic studies and the projected use of service water can provide an indication of the potential average wetness of future workings. For particularly important projects including underground repositories for hazardous wastes, test drivages within the relevant horizon(s) will provide invaluable data regarding the migration of moisture from the strata.

16.3.1.2. Condition of airflow at inlet

Most mine climate simulators assume that the airflow and psychrometric condition of the air at inlet have remained constant since the airway was driven. In the majority of cases this gives acceptable results because of the thermal flywheel effect (Section 15.2.2). Variations in the surface climate are usually well damped by the time the air reaches the working areas. If the transients that occur along intake airways are of concern then methods that employ the principles of superposition are available for such analyses (Hemp, 1982).

The inlet data required for conventional non-transient simulators are simply airflow, barometric pressure, and wet and dry bulb temperatures. Satisfactory results for hot mines can be obtained by assuming mean summer (not extremes) atmospheric conditions on surface.

16.3.1.3. Thermal parameters and other heat sources

The data in this category comprise:

Rock thermal conductivity:

It is the effective thermal conductivity of the strata that should be specified. It is preferable that this parameter should have been established through in-situ tests as described in Section 15.2.10. If values are available from laboratory samples only, then corrections may be necessary to obtain the effective thermal conductivity that actually pertains underground (Mousset-Jones, 1988). Here again, correlation trials with a climate simulator are valuable in establishing values of effective thermal conductivity.

Rock thermal diffusivity:

This can be measured directly in-situ as well as by laboratory methods. However, it is normally satisfactory to determine thermal diffusivity indirectly as

$$\alpha = \frac{k_r}{\rho_r C_r} \quad \text{m}^2/\text{s} \quad (\text{see equation (15.13)})$$

where k_r = effective thermal conductivity W/(m°C)
 ρ_r = rock density kg/m³ and
 C_r = specific heat of the rock J/(kg°C)

Virgin rock temperature and geothermic step (Section 15.2.4):

The combination of VRT at the inlet of the airway and the rate at which rock temperature increases with depth allows the VRT to be determined for each increment of length along a non-horizontal

airway. These parameters may be determined from temperature logs taken from boreholes. In the case of a downcast shaft, the inlet VRT should actually be the rock temperature sufficiently far below the surface to be unaffected by variations in the surface climate. This is usually between 10 and 20 m.

Heat sources other than the strata:

The location of every machine or other source of heating or cooling and the distance over which it extends must be specified. The magnitudes of both the sensible and latent heat components should be quantified either directly or indirectly by identifying a machine type (Section 16.2.3).

16.3.1.4. Physiological parameters (Worker data)

For mine climate simulators that predict a physiological index of heat stress (see Section 16.2.9), two more sets of data are requested. One of these includes the metabolic work rate in Watts per square meter of body surface and the typical posture (body view factor) of a worker. The second set of physiological factors involves the thermal resistance of the clothing ensemble and the increase in body surface area associated with that ensemble. Fortunately, all of these parameters can be entered in a user-friendly fashion simply by choosing from lists of work activities and types of clothing (see Table 16.1).

16.3.2. Correlation tests

All simulation packages should be subject to correlation tests in order to verify that they do, indeed, simulate the real system to the required accuracy prior to their being employed for planning purposes. The accuracy of data must also be verified by site-specific correlation trials. This is true for ventilation network analysis (Section 9.2.3) and is also the case for mine climate simulation studies.

Due to the uncertainty that may be associated with some of the data, correlation trials of mine climate simulators should include sensitivity runs involving those input parameters of uncertain accuracy. Experience has shown that such correlations conducted for a few airways in any mine can not only highlight previously unidentified sources of heat and humidity but also provide a range of typical data values that may be tested against other airways until sufficient confidence has been established to embark upon planning studies.

There is a definite procedure to follow in conducting sensitivity studies and correlations of climatic simulation output with actual conditions in a mine. The airways chosen for initial correlation should each be well established and continuous with no intermediate additions or losses of airflow. Any gradient from horizontal to vertical is acceptable provided that it remains uniform along the length of the airway. The primary trials should seek to provide correlation between computed results and the effects of strata heat and, perhaps, autocompression. Additional sources of heat that can be quantified easily, such as metered electrical equipment, may also be included. However, the initial trials should avoid airways that contain diesel equipment or open drainage channels. Such sources of heat should be subject to secondary correlation runs.

Careful measurements of airflow, barometric pressure, and wet and dry bulb temperatures should be made at the intake end of the correlation airway. Additional wet and dry bulb temperatures should also be taken at about 100 m intervals along the airway. All of the other parameters required as input (Section 16.3.1) should be ascertained or ascribed initial estimated values.

In comparing the computed output with observed temperatures, attention should be focused first on the wet bulb temperatures. If there is a consistent divergent trend between the computed and measured values then it is probable that a continuous heat source has been over or underestimated, or perhaps even omitted entirely. A check should be carried out on the depths of the airway ends and their corresponding ages (if less than two years). Sensitivity runs should also be made to test the effect of thermal conductivity.

If the observed wet bulb temperatures do not show a smooth trend then the reasons for discontinuities should be investigated. There may be occurrences such as leakage of air or other fluids from old workings, machine heat, or increased inflow of fissure water. Correlation exercises provide a valuable educational experience in tracing sources of heat in the mine.

When reasonable correlation ($\pm 1\text{ }^{\circ}\text{C}$) has been obtained for the wet bulb temperature, attention should be turned to the dry bulb temperature. Any remaining deviations of this parameter will almost certainly be due to the evaporation or condensation of water. If the deviation shows a consistent trend then it is likely that the wetness factor has been wrongly assessed. Sensitivity runs on wetness factor will test for such a condition. More localised deviations may be caused by inaccurate assessment of the water vapour produced by diesel equipment, or the effects of dust suppression sprays.

Having followed this correlation procedure over a series of airways, the ventilation engineer will have built up a store of information on the values and dispersion of heat sources in his mine. He will also have determined a range of in situ values for thermal conductivities, wetness factors and contributions of heat and humidity from mechanized equipment. At that stage, forward planning studies may be initiated with confidence levels that have been established through the correlation procedures. Climatic simulations then provide an invaluable tool of unprecedented detail in planning environmental control for hot underground facilities.

16.3.3. Case Study

For clarity of explanation, this case study involves a single airway rather than a sequence of branches. Figure 16.1 illustrates a 500 m inclined airway descending from 450 to 530 m below a surface datum. The airway contains a diesel unit of output rating 175 kW working at a mean rate of 60 per cent full load, an air cooler of 200 kW cooling capacity and a conveyor expending 230 kW along its length from the midpoint to the exit of the airway. The complete data for the airway have been assembled under the categories given in Section 16.3.1 and are shown in Table 16.1. The order and format of the input data depend upon the particular software package being used.

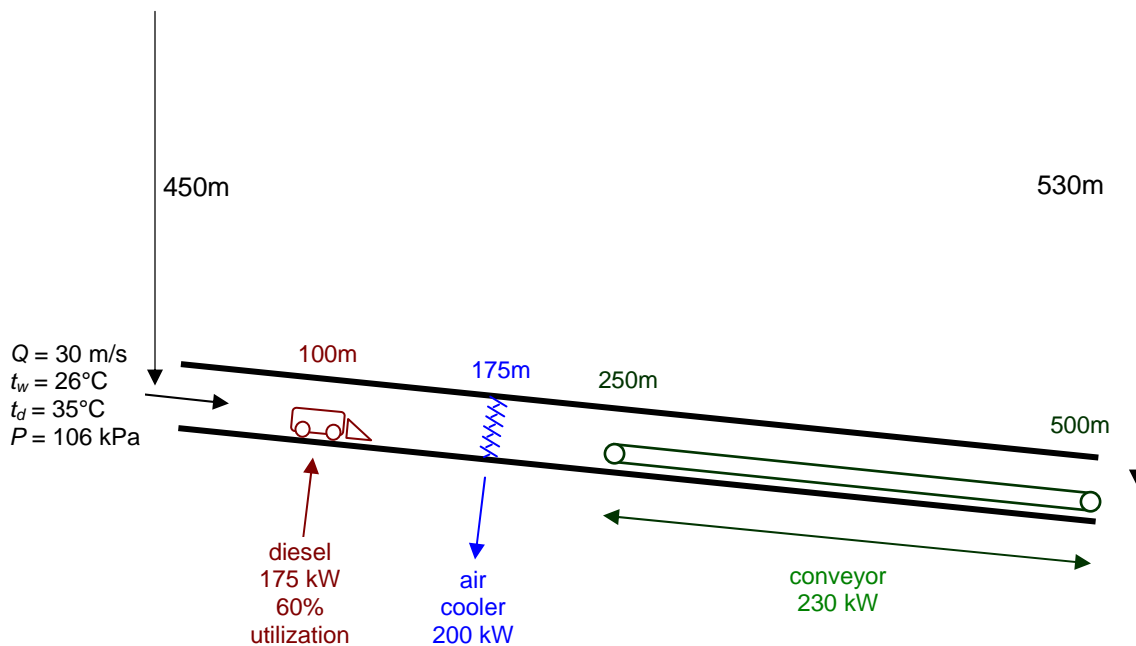


Figure 16.1 Ramp used in case study of mine climate simulation.

Airway and Rock data

Branch	Name	Dry bulb at inlet	Wet bulb at inlet	Pressure at inlet	Airflow	Length	Depth in	Depth out	c-s Area	Perimeter
		°C	°C	kPa	m ³ /s	m	m	m	m ²	m
1	Textbook	30	24	106	30	500	450	530	8.75	12

Friction factor	Wetness factor	Age in	Age out	VRT in	Geothermal step	Rock conductivity	Rock diffusivity	Print interval	Description
kg/m ³		days	days	°C	m/°C	W/(m°C)	m ² /sx10 ⁻⁶	m	
0.014	0.2	350	70	42	40	4.5	2.153	2	conveyor slope

Branch heat sources

Spot source	Location (m)		Sensible heat (kW)	Latent heat (kW)	Description
1	175		-200	0	Cooler

Diesel	Location (m)	Rated Power (kW)	Utilization (%)	Water output to fuel ratio	Description
1	100	175	60	7.0	Diesel No.1

Linear	Start Location (m)	Length (m)	Sensible heat (kW)	Latent heat (kW)	Description
1	250	250	230	0	Conveyor

Worker data

Clothing	Thin trousers, short-sleeved shirt
Type of work	Light to moderate manual work

Table 16.1 Input data for the case study as requested by the CLIMSIM mine climate simulator. The shaded boxes are screen prompts. The values are entered by the user.

The tabulated results of the simulation are shown in Table 16.2. Here again, the form of the output depends upon the program employed. The CLIMSIM package used for this case study allows any of the computed variables to be produced in graphical form. Figures 16.2 and 16.3 are computer plots of the variations in air temperature and relative humidity respectively. The effects of the diesel unit, cooler and conveyor are shown clearly. Despite the influence of autocompression and strata heat, evaporation in this rather wet airway results in an initial decrease of dry bulb temperature.

Figures 16.4 and 16.5 show the variation in mean skin temperature of the workforce and the wet bulb globe temperature respectively. The mean skin temperature is seen to exceed the limit (for the prevailing climatic conditions) at which workers may begin exhibiting the effects of heat stress. This occurs at about 440 m from the beginning of the airway. An interesting feature of the mean skin temperature graph is the increase in its slope at 368 m from the entrance, even though there are no additional heat sources at or after this location. This is the point at which the average healthy worker becomes fully covered in perspiration. As his body can no longer increase its cooling by further wetting of body surface area it attempts to maintain thermal equilibrium by additional increases in skin temperature (ref. Section 17.3 and Figure 17.6). This effect is not reflected by empirical indices of heat stress such as wet bulb globe temperature or effective temperature as these are determined solely by the condition of the airflow and do not indicate physiological response.

The actual reaction of workers on approaching the onset of heat stress or a full coating of perspiration will be behavioural, i.e. reducing the work rate via less strenuous activity or more frequent rest periods, and/or discarding clothing. Figures 16.6 and 16.7 show that the mean skin temperature can be maintained below the relevant limit throughout the airway either by reducing the metabolic work rate from 200 to 185 W/m² or by wearing shorts rather than thin trousers.

Distance	dry bulb	wet bulb	air	moisture	air	relative	enthalpy	sigma	dry wall	virgin rock	mean skin	effective	wet bulb	Strata heat to air	heat	
	temp.	temp.	pressure	content	density	humidity		heat	temp.	temp.	temp.	temp.	globe	latent	sensible	transfer
													temp.			coef.
m	°C	°C	kPA	g/kg	kg/m ³	%	kJ/kg	kJ/kg	°C	°C	°C	°C	°C	kW	kW	W/(m ² °C)
0	30.00	24.00	106.000	15.41	1.207	60.42	69.55	68.01	30.5	42.0	34.04	21.03	25.80	0	0	23.619
20	29.91	24.04	106.033	15.50	1.208	61.07	69.69	68.13	30.5	42.1	34.04	20.97	25.80	0.76	-0.42	23.602
40	29.83	24.07	106.067	15.58	1.208	61.71	69.83	68.26	30.4	42.2	34.03	20.92	25.80	0.75	-0.40	23.591
60	29.76	24.11	106.100	15.67	1.209	62.32	69.97	68.39	30.3	42.2	34.03	20.86	25.81	0.73	-0.38	23.581
80	29.69	24.15	106.134	15.75	1.210	62.92	70.11	68.51	30.3	42.3	34.03	20.81	25.81	0.72	-0.36	23.572
100	29.62	24.19	106.167	15.83	1.210	63.50	70.25	68.65	30.2	42.4	34.02	20.77	25.82	0.71	-0.35	23.562
120	33.48	26.36	106.200	17.66	1.194	56.76	78.90	76.95	33.9	42.5	34.78	24.96	28.49	0.92	-0.64	24.112
140	33.34	26.39	106.233	17.76	1.195	57.55	79.03	77.06	33.8	42.6	34.79	24.88	28.47	0.90	-0.62	24.096
160	33.21	26.42	106.266	17.86	1.196	58.32	79.15	77.18	33.6	42.6	34.79	24.80	28.45	0.88	-0.59	24.081
180	27.71	25.02	106.299	17.95	1.218	80.24	73.68	71.80	28.4	42.7	33.93	19.13	25.83	0.39	0.03	23.478
200	27.75	25.07	106.333	18.00	1.218	80.27	73.83	71.94	28.5	42.8	33.94	19.19	25.87	0.39	0.04	23.477
220	27.80	25.11	106.366	18.04	1.218	80.30	73.99	72.09	28.5	42.9	33.95	19.25	25.91	0.39	0.04	23.476
240	27.84	25.15	106.400	18.09	1.218	80.31	74.15	72.24	28.6	43.0	33.96	19.32	25.96	0.39	0.05	23.475
260	28.13	25.26	106.434	18.13	1.218	79.18	74.57	72.65	28.9	43.0	33.99	19.69	26.12	0.41	0.03	23.502
280	28.66	25.44	106.467	18.18	1.216	77.02	75.24	73.30	29.4	43.1	34.06	20.34	26.40	0.45	-0.02	23.554
300	29.17	25.61	106.501	18.23	1.214	75.00	75.92	73.96	29.9	43.2	34.12	20.95	26.68	0.49	-0.06	23.606
320	29.68	25.79	106.535	18.29	1.212	73.11	76.59	74.61	30.4	43.3	34.18	21.53	26.95	0.53	-0.11	23.657
340	30.17	25.96	106.568	18.36	1.211	71.33	77.26	75.27	30.9	43.4	34.23	22.08	27.22	0.57	-0.15	23.707
360	30.65	26.13	106.601	18.43	1.209	69.68	77.94	75.92	31.3	43.4	34.29	22.61	27.48	0.61	-0.19	23.756
380	31.12	26.30	106.635	18.50	1.208	68.12	78.61	76.57	31.8	43.5	34.44	23.11	27.74	0.65	-0.23	23.804
400	31.58	26.47	106.668	18.58	1.206	66.66	79.28	77.22	32.2	43.6	34.62	23.58	28.00	0.69	-0.27	23.851
420	32.02	26.63	106.701	18.66	1.205	65.29	79.96	77.88	32.7	43.7	34.80	24.04	28.25	0.72	-0.31	23.898
440	32.46	26.80	106.735	18.74	1.203	63.99	80.63	78.53	33.1	43.8	34.97	24.48	28.50	0.76	-0.34	23.943
460	32.89	26.96	106.768	18.83	1.202	62.78	81.31	79.18	33.5	43.8	35.14	24.90	28.74	0.79	-0.38	23.989
480	33.31	27.13	106.801	18.92	1.201	61.63	81.98	79.83	34.0	43.9	35.32	25.30	28.98	0.83	-0.41	24.033
500	33.72	27.29	106.834	19.02	1.199	60.54	82.66	80.49	34.4	44.0	35.49	25.69	29.22	0.86	-0.44	24.077

Diesel heat source at 100 m, sensible heat = 147.41 kW, latent heat = 149.74 kW

Spot heat source at 175 m, sensible heat = -200.00 kW, latent heat = 0.00 kW

Linear heat source starts at 250 m, length = 250 m, sensible heat = 230.00 kW, latent heat = 0.00 kW

Strata heat totals: sensible heat = -68.03 kW, latent heat = 164.87 kW

Other heat totals: sensible heat = 177.41 kW, latent heat = 149.74 kW

Metabolic rate = 200 W/m², Skin temperature limit value = 34.98 °C

Table 16.2 Tabulated CLIMSIM output for the case study. This is shown at 20m intervals for conciseness but is computed at 2m intervals as requested in the input data.

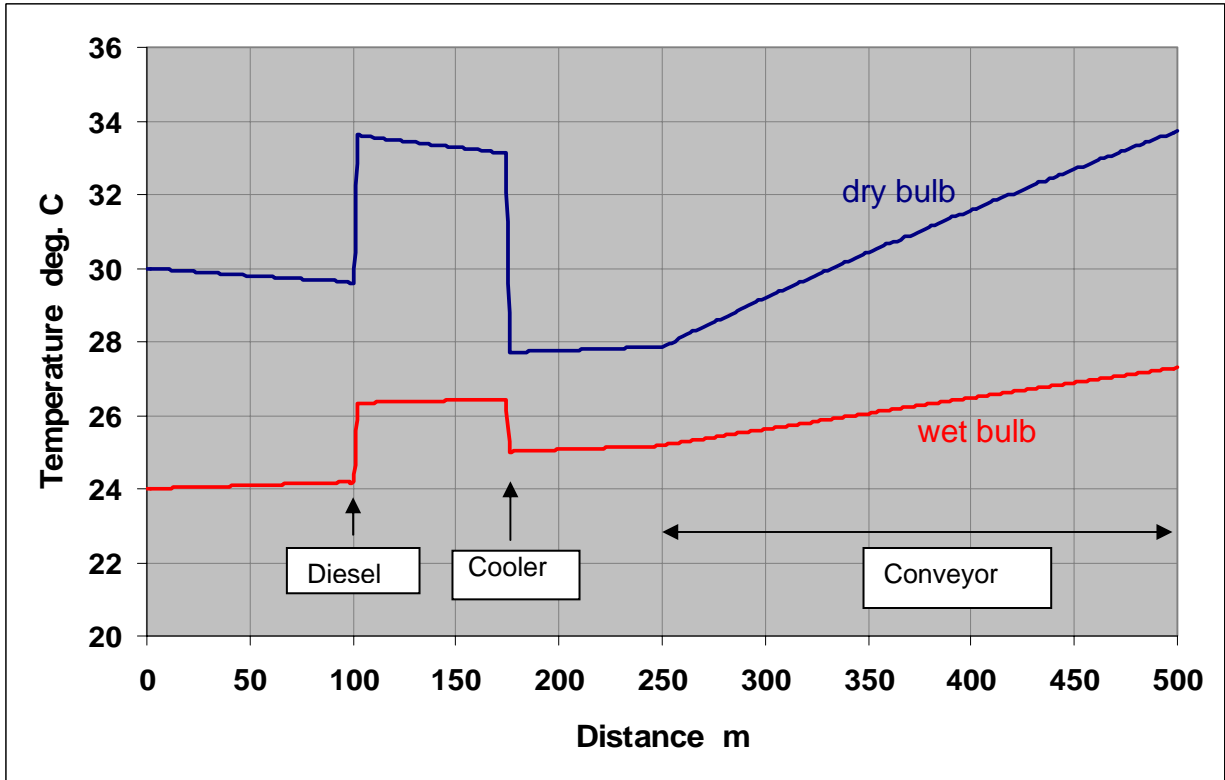


Figure 16.2 Graphical output for wet and dry bulb temperatures along the airway.

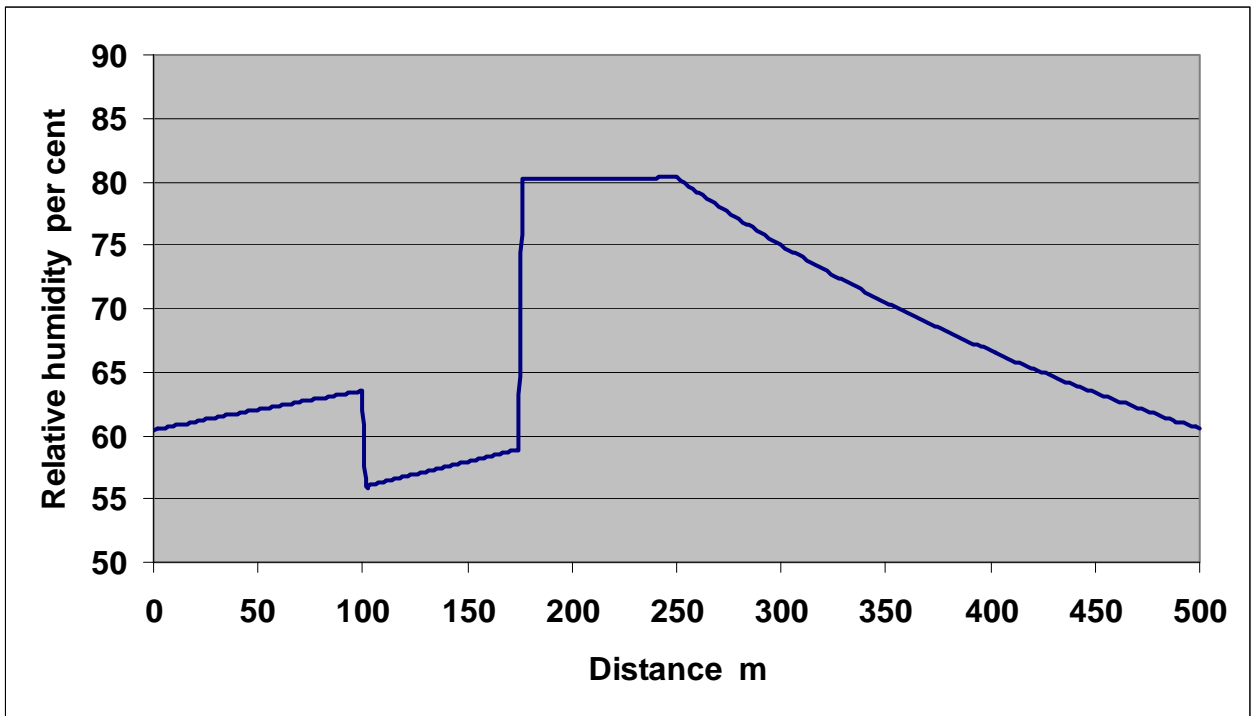


Figure 16.3 Graphical output for relative humidity along the airway.

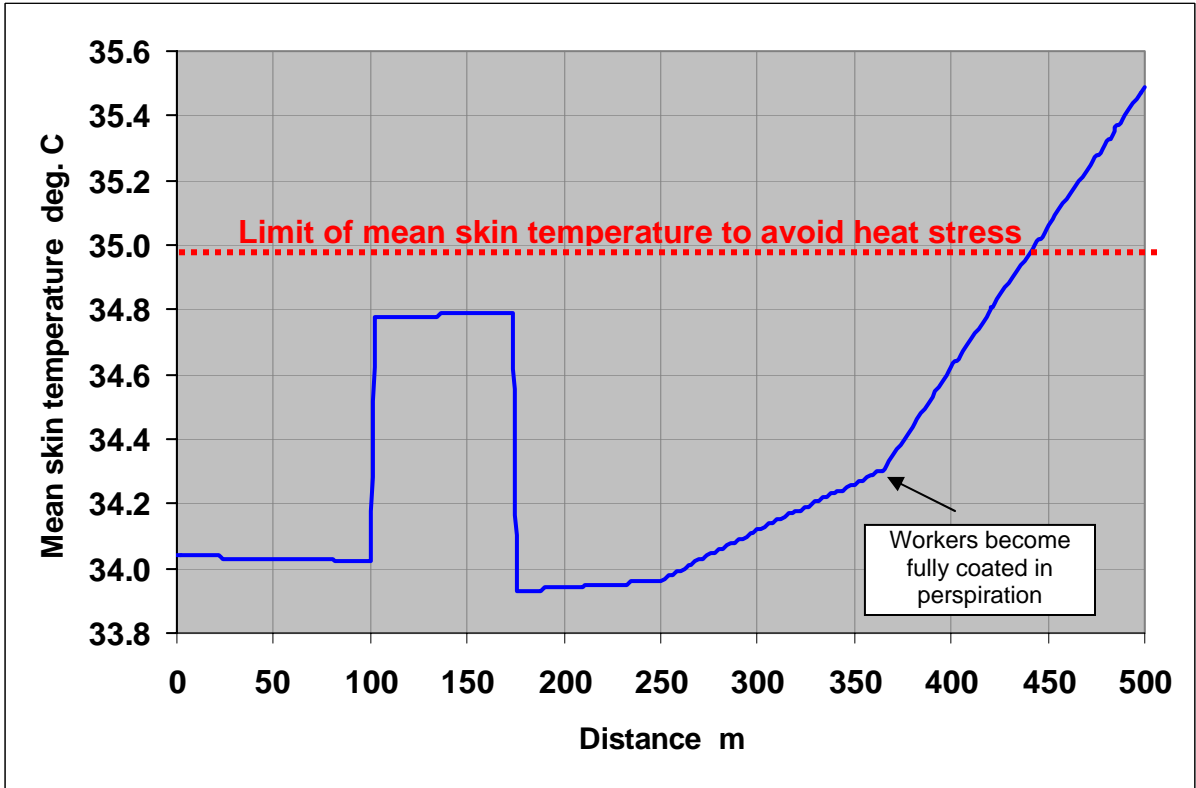


Figure 16.4 Graphical output for average mean skin temperature of workers along the airway.

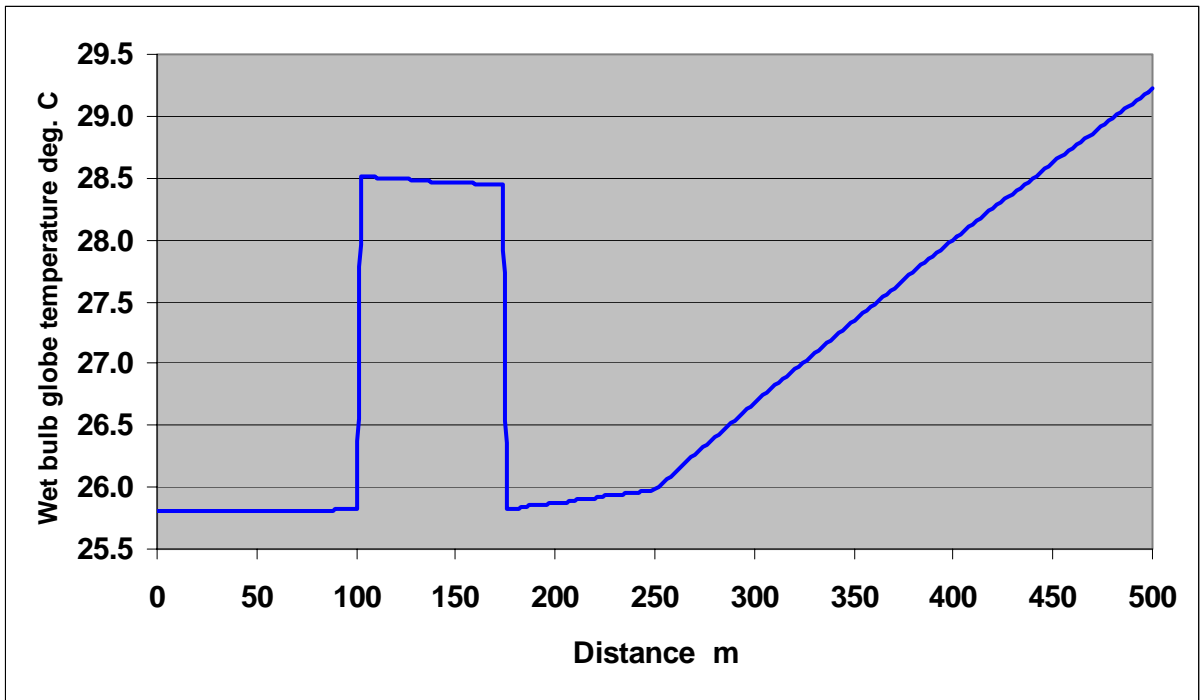


Figure 16.5 Graphical output for Wet Bulb Globe Temperature along the airway.

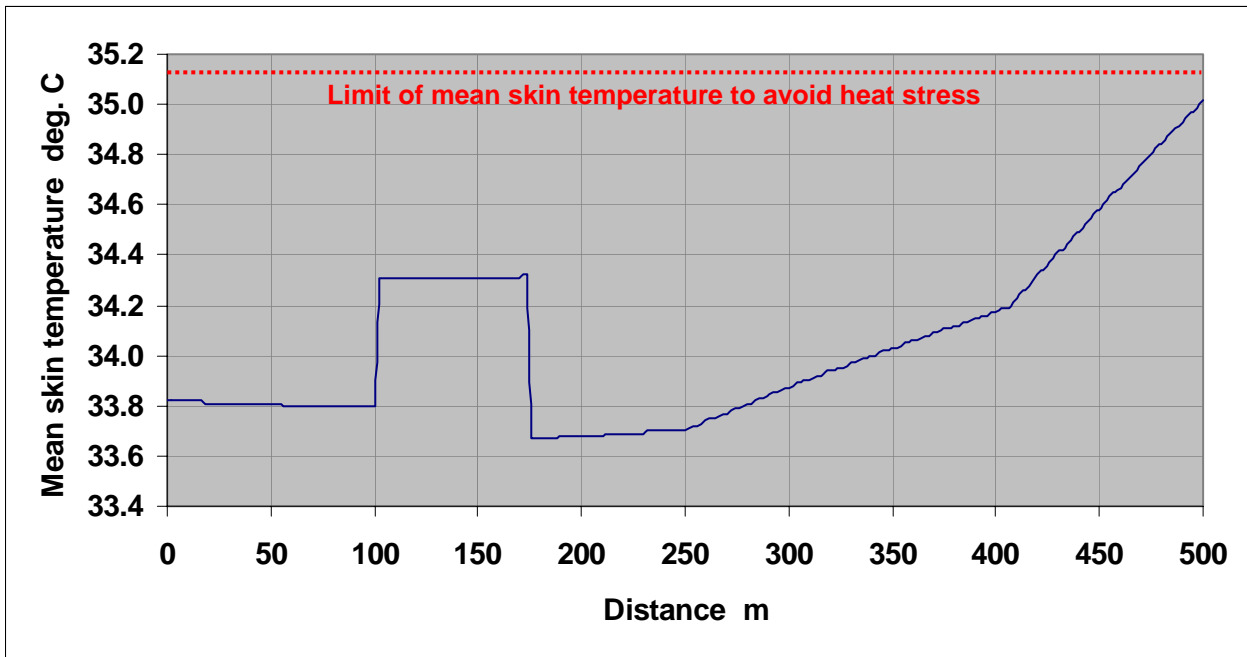


Figure 16.6 Mean skin temperature with metabolic work rate reduced to 185 W/m².

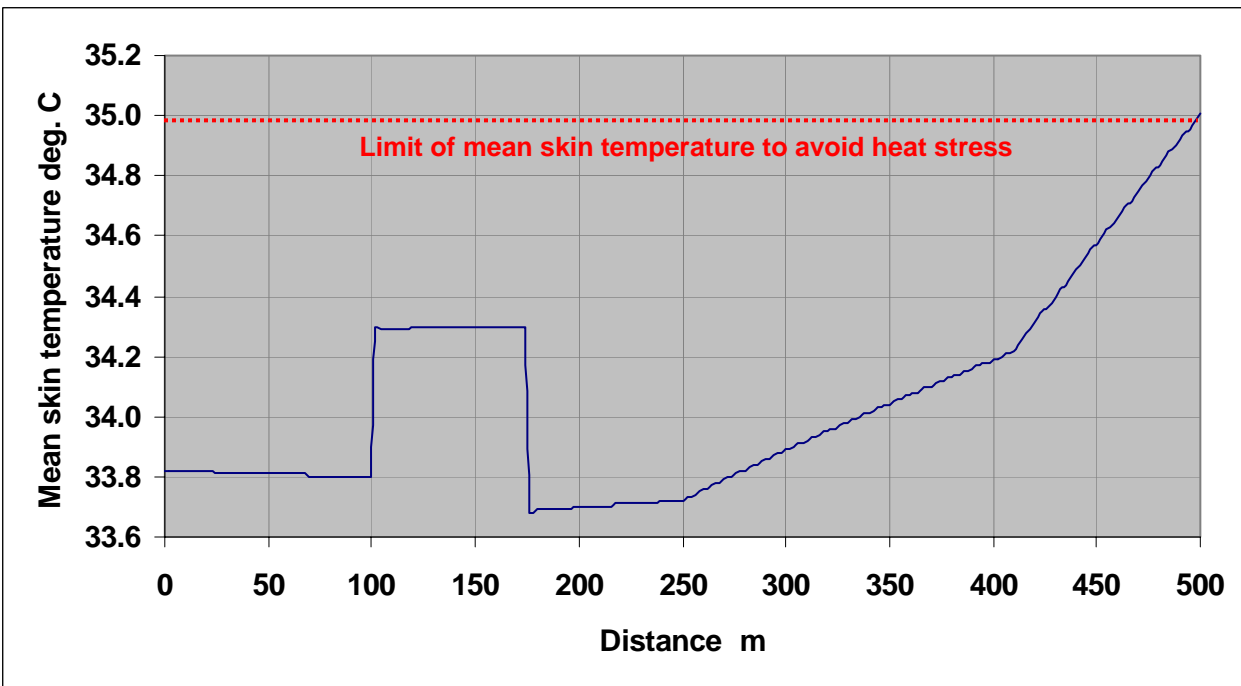


Figure 16.7 Mean skin temperature with workers wearing shorts and short-sleeved shirt.

16.3.4. Organization of mine climate simulation exercises

The flow chart given on Figure 16.8 illustrates the procedure for investigating variations in the air temperatures, humidities and indices of heat stress throughout a ventilation network. From the results of a ventilation network analysis, one or more routes should be selected through the system. These may commence at an air intake point on surface, proceed through shafts, intake airways, work areas and return passages back to surface. Routes should be chosen that may be expected to produce the severest psychrometric conditions. Climatic simulations may then be conducted along successive branches throughout the selected routes.

The input shown on Figure 16.8 may be supplied by manual interaction with the climate simulation package as illustrated in the case study of Section 16.3.3. Alternatively, the input may be drawn from data files that have been assembled over a period of time, again, either manually or as a result of previous simulations. Such files may also be used or amended by other program packages. For example, the airflow for each individual branch may have been determined from a ventilation network analysis package (Sections 7.4 and 9.1). Similarly, branch inlet temperatures and pressures will have been produced by climate simulations on upstream airways.

Figure 16.8 indicates that the computed results from a mine climate simulation should be reviewed with respect to the selected heat stress indices (Chapter 17) or other climatic criteria relevant to the particular study. Should these criteria not be met then the program should be rerun successively in order to investigate means of reaching the desired standards. Parameters that may typically be amended are airflow, airway size or lining, reduction in machine power (for example, replacing diesels by electrical equipment), the installation, siting and cooling capacities of heat exchangers or the attire and workrate of personnel. Sensitivity studies should also be run to test the influence of any input parameters that may be of questionable accuracy.

The convenient editing features of modern climate simulators allow individual items of input data to be updated with very few keystrokes and the program re-run within a matter of seconds.

There will usually be several ways of meeting the climatic criteria. Again, the procedure may be cycled successively to investigate alternative arrangements. This sometimes necessitates going back to re-evaluate an upstream airway.

16.3.5. Interaction with Ventilation Network Analysis packages

Figure 9.1, introduced in Chapter 9 to illustrate the systems analysis of subsurface ventilation planning, shows the relationships of climate simulations to ventilation network exercises. While the initial airflows used in climate simulations may have been produced by VNET exercises, it might have been necessary to amend those airflows during the climate investigations in order to meet set criteria. The sizes and linings of some airways may also have been altered, affecting their resistances. In those cases, it becomes necessary to re-run the network analysis package in order to revise fan duties and other consequential effects throughout the ventilation system.

Where the installation of cooling plant has proved to be necessary during the climate simulation exercises, the airflow requirements should be reviewed most carefully in order to approach an optimized combination of ventilating and cooling costs while, at the same time, providing airflows capable of diluting other airborne contaminants (Section 9.3) (Anderson, 1986).

Programs have been developed that combine the functions of ventilation network analysis and climate simulation. However the volume and variety of both data and output can become daunting to the user. Practical experience of ventilation engineers leads to a preference for separate program packages for network analysis and climate simulation while, at the same time,

maintaining the efficiencies of rapid transfer of information between data files. This also allows manual modification of those files whenever required and establishes firmer control over the design process by the planning engineers.

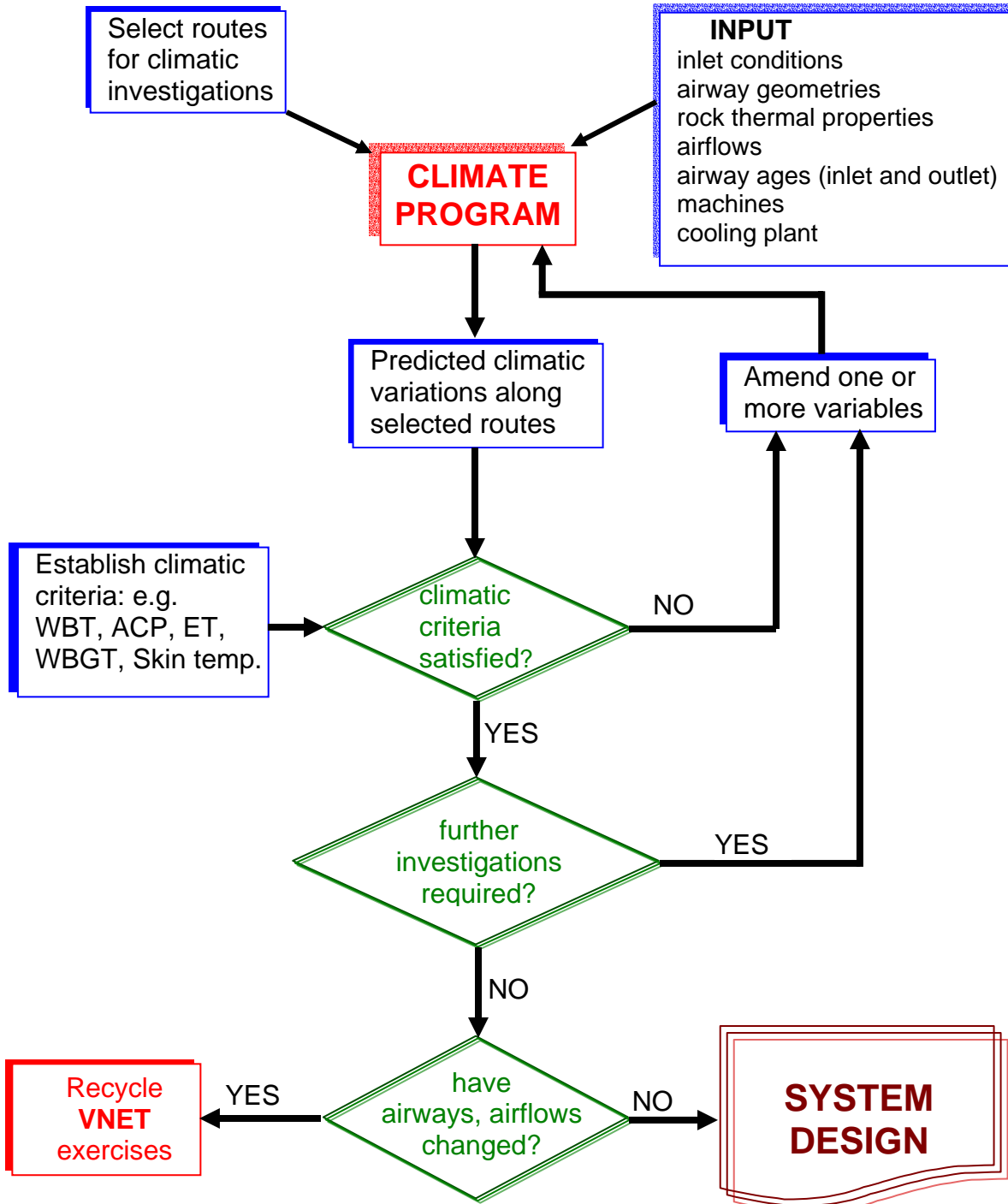


Figure 16.8 Climatic planning procedure.

Bibliography

- Amano, K. et al (1980).** Variation of temperature and humidity of air current passing through a partially wetted airway. *Journal Min. Metall, Inst. Japan.* Vol.96 pp. 13-17
- Anderson, J. and Longson, I. (1986).** The optimisation of ventilation and refrigeration in British coal mines. *The Mining Engineer (U.K.).* No.146 pp. 115-120
- Banerjee, S.P. and Chernyak, V.P. (1985).** A simplified method for prediction of temperature and moisture content changes of air during its passage in a mine airway. *Int. Bureau of Mining Thermophysics, U.K. May Vol.1*
- Boldizsar, T. (1960).** Geothermal investigations concerning the heating of air in deep and hot mines. *Mine and Quarry Eng.* June pp. 253-258
- Cifka, I. and Eszto, M. (1978).** Investigation of the method of determining in-situ characteristics of underground climatic conditions and the thermal properties of rocks. Report No. 16-5/78.K. Mining Research Inst. Budapest, Hungary
- Gibson, K.L. (1977).** The computer simulation of climatic conditions in mines. 15th APCOM Symp. Brisbane, Australia, pp. 349-354
- Hall, A.E. (1975).** Computer techniques for calculating temperature increases in stopes and mine airways. *Journal Mine Vent. Soc. of S. Africa.* Vol.28. No.4. pp. 55-59
- Hall, A.E. (1976).** The design and analysis of ventilation systems in deep metal and non-metal mines. MSHA Contract No. SO231095
- Hemp, R. (1982).** Sources of heat in mines. Chapter 22 of *Environmental engineering in South African mines.* Mine Vent. Soc. of S. Africa.
- Hemp, R. (1985).** Air temperature increases in airways. *Jour. Mine Vent. Soc. of S. Africa.*
- Lambrechts, J de V. (1967).** Prediction of wet bulb temperature gradients in mine airways. *Journal Mine Vent. Soc. of S. Africa.* Vol.67. pp. 595-610
- Longson, I. and Tuck, M.A. (1985).** The computer simulation of mine climate on a longwall coal face. 2nd U.S. Mine Vent. Symp., Reno, Nevada. pp. 439-448
- Mack, M.G. and Starfield, A.M. (1985).** The computation of heat loads in mine airways using the concept of equivalent wetness. 2nd U.S. Mine Vent. Symp. Reno, Nevada pp. 421-428
- McPherson, M.J. (1975).** The simulation of airflow and temperature in the stopes of S. African gold mines. Proc. 1st Int. Mine Vent. Congress. Johannesburg pp. 35-51
- McPherson, M.J. (1986).** The analysis and simulation of heat flow into underground airways. *Int. Journal of Mining and Geological Eng.* Vol.4. pp. 165-196.
- Mine Ventilation Services. (2006).** CLIMSIM for Windows 1.2. Climatic simulation program user's manual..
- Moussset-Jones, P. (1988).** Determination of in-situ rock thermal properties and the improved simulation of the underground climate. Ph.D thesis. Royal School of Mines. University of London, pp. 553

Starfield, A.M. (1966). The flow of heat into the advancing stope. Journal Mine Ventilation Soc. of South Africa. Vol.19 pp. 13-28.

Starfield, A.M. (1966). The computation of air temperature increases in advancing stopes. Journal Mine Vent. Soc. of South Africa. Vol.19. pp. 189-199

Voss, J. (1975). Control of the mine climate in deep coal mines. Proc. 1st Int. Mine Ventilation Congress. Johannesburg, p. 331

Vost. K.R. (1982). The prediction of air temperatures in intake haulages in mines. Journal Mine Vent. Soc. of S. Africa. Nov. pp. 316-328

Whillier, A. and Thorpe, S.A. (1971). Air temperature increases in development ends. Research Report 18/71. Chamber of Mines of S. Africa.

CHAPTER 17. PHYSIOLOGICAL REACTIONS TO CLIMATIC CONDITIONS

17.1 INTRODUCTION	2
17.2 THERMOREGULATION OF THE HUMAN BODY	2
17.3 PHYSIOLOGICAL HEAT TRANSFER	4
17.3.1 The metabolic heat balance	4
17.3.2 Respiratory heat transfer	7
17.3.3 Convective heat transfer	8
17.3.3.1 The convective heat transfer equation	8
17.3.3.2 Clothing factors	9
17.3.3.3 Convective heat transfer coefficient, h_c	9
17.3.3.4 Mean skin temperature, t_{sk}	10
17.3.4 Radiant heat transfer	13
17.3.5 Evaporative heat transfer	14
17.3.5.1 Evaporation from unclothed and clothed bodies	14
17.3.5.2 Skin wetness fraction	15
17.3.6 A thermoregulation model	18
17.4 INDICES OF HEAT STRESS	22
17.4.1 Purpose and types of heat stress indices	22
17.4.2 Single measurements	23
17.4.3 Empirical methods	23
17.4.3.1 Effective temperature, ET	23
17.4.3.2 Wet Kata thermometer	24
17.4.3.3 Wet bulb globe temperature and wet globe temperature	25
17.4.4 Rational indices	27
17.4.4.1 Air Cooling Power (M scale), ACPM	27
17.4.4.2 Specific Cooling Power (A scale), ACPA	29
17.4.5 Choice of heat stress index	30
17.5 HEAT ILLNESSES	30
17.5.1 Heat fainting	31
17.5.2 Heat exhaustion	31
17.5.3 Heat cramps	31
17.5.4 Heat rash	31
17.5.5 Heat stroke	32
17.5.6 Precautions against heat illnesses	32
17.6 COLD ENVIRONMENTS	33
17.6.1 Physiological reactions to cold environments	33
17.6.2 Protection against cold environments	34
17.6.3 Indices of cold stress	35
17.7 HEAT TOLERANCE AND ACCLIMATIZATION	36
17.7.1 Physiological tests	36
17.7.1.1 Initial screening	36
17.7.1.2 Heat Tolerance Screening	37
17.7.2 Acclimatization	38
17.7.2.1 In-situ acclimatization	38
17.7.2.2 Physiological changes during acclimatization	38
17.8 EFFECT OF MINE CLIMATE ON PRODUCTIVITY	39
References	41
APPENDIX A17.1	43
Listing of the thermoregulation model developed in Section 17.3.6	43
APPENDIX A17.2	46
Acclimatization of workers in South African gold mines prior to 1990	46

17.1 INTRODUCTION

In conventional mining operations, the need to control air temperatures and humidities arises primarily because of the relatively narrow range of climatic conditions within which the unprotected human body can operate efficiently. In some areas of underground repositories or where remotely controlled equipment is in use, a different spectrum of atmospheric criteria may be allowed or even required. However, in this chapter, we shall concentrate on the effects of climatic variations on the human body, and alternative means of quantifying the ability of a given environment to maintain an acceptable balance between metabolic heat generation and body cooling.

Section 17.3 on Physiological Heat Transfer is fairly comprehensive as this provides the basis of computer models that predict the physiological reactions of the average acclimatized worker in hot environments. Readers are encouraged to consult the chapter contents in order to select the topics of his/her particular interest.

17.2 THERMOREGULATION OF THE HUMAN BODY

Within the human body, chemical and biological processes act upon consumed nutrients to produce **metabolic energy**. A little of this is in the form of mechanical energy expended against external forces. However, the majority of metabolic energy results in the internal generation of heat. If the body is to remain in thermal equilibrium then this **metabolic heat** must be transferred to the ambient surroundings at a rate equal to that at which it is produced. Section 17.3 analyses and attempts to quantify the various elements of physiological heat exchange, namely, by respiration, convection, radiation and evaporation, whose net sum must equal the rate of metabolic heat generation for thermal equilibrium to exist. First, however, let us discuss in general terms the mechanisms employed by the human body in adjusting to variations in climatic conditions.

A conceptual model that is commonly envisioned is one in which the body is made up of a **central core** of average temperature, t_c , surrounded by an outer layer of tissue that has an average temperature t_{sk} . The latter is referred to simply as the **mean skin temperature** or MST. Contrary to popular belief, the core temperature is not constant but varies normally between 36 and 38°C with respect to both location within the body and muscular activity for a healthy individual experiencing no heat strain. The skin temperature is even more variable depending upon position on the body surface, clothing, temperature and velocity of the ambient air, rate of perspiration and, to a lesser extent, metabolic activity. The average temperature and wettedness of the skin are parameters of major importance in physiological heat exchange. For a resting person located within an environment that gives no sensation of either heat or cold, mean skin temperature approximates to 34°C. This may be termed the **neutral skin temperature**.

When the surrounding environment removes heat from the human body at a rate that is not equal to the metabolic heat generation then one or both of two types of response will occur. A **behavioural response** consists of conscious steps taken to alleviate the situation. These might consist of shedding or donning clothing, and by decreasing or increasing physical activity. The second type of response comprises the involuntary actions taken by the body to re-establish a stable heat balance with the surroundings. This is known as **body thermoregulation**.

Temperature sensitive receptors exist throughout both the core and skin elements of the body. These react to departures of t_c and t_{sk} away from their neutral values. The predominant mode of heat conductance from the core to skin tissues is by the flow of blood. A 'high' signal from the core receptors will produce **vasodilation**, the relevant blood vessels expand to allow a greater flow of blood and, hence, heat from the core to the skin. Further increases in the "high" signals from

core receptors will result in perspiration and evaporative cooling, the most powerful mode of surface heat transfer from the body.

When the skin temperature exceeds its neutral value of some 34°C the skin receptors react to excite the sweat glands into additional activity. However, some areas are more efficient at producing perspiration than others to the extent that unevaporated run-off may occur in those zones before other areas are fully wetted. There is also considerable variation in sweat rates between individuals.

“Low” signals from the skin receptors (cold conditions) cause **vasoconstriction**. The blood vessels that supply skin tissues contract. The vital organs in the core of the body continue to be supplied by warm blood and are thus protected preferentially while the skin is allowed to cool. This can cause extremities such as fingers, toes or ears to suffer tissue damage by **frostbite** in very cold conditions. Reduced skin temperature may also produce the involuntary muscular movement of **shivering** in an attempt to generate additional metabolic heat.

In order to follow the thermoregulatory reactions of the human body to hot conditions, let us conduct an imaginary experiment in which a volunteer undertakes physical work at a steady but unhurried rate within an environment that is initially fairly cool, say at 10°C. In this situation, heat loss from the body will occur, mainly, by convection with lesser amounts of cooling by respiration and radiation. The sweat glands are effectively inactive and evaporation of water by direct diffusion through the skin contributes only a little evaporative cooling. The procedure of the experiment is to increase the air temperature in increments, maintaining all other parameters constant, including the rate of work and, hence, metabolic heat generation. The incremental changes in air temperature are made sufficiently slowly to allow the body to maintain itself in or near thermal equilibrium. The purpose of the experiment is to observe the changes that take place in the modes of heat transfer.

As the air temperature rises from its initial low value, the skin temperature, t_{sk} , also increases in an attempt to retain the differential between t_{sk} and the temperature of the surrounding environment and, hence, to maintain convective and radiant cooling. However, the influence of respiratory cooling decreases because the heat content of the expired air rises at a lesser rate than that of the inspired air.

At some point, as the air temperature continues to climb and depending upon the rate of work, signals from the core receptors cause sweating to commence, resulting in partial wetting of the body surface. This initiates some significant changes in the heat transfer processes. First, throughout the period of increased sweating and until full surface wetness occurs, evaporative cooling moderates the rate at which skin temperature continues to rise with respect to ambient temperature. Also, throughout this stage, the combined effects of convective and radiative cooling are progressively replaced by evaporative heat transfer. When the skin temperature approaches and exceeds some 34°C, the skin receptors react to produce further enhanced sweating. The increased area that is coated in perspiration and the corresponding effectiveness of evaporative cooling both grow rapidly. However, when the skin becomes fully wetted, further cooling can be gained only by additional rises in skin temperature. Hence, the skin temperature resumes a higher rate of increase (see Figure 17.6).

If the dry bulb temperature of the surroundings exceeds skin temperature then the convective and radiant heat transfers will reverse. Evaporative cooling must then balance the heat gain from convection and radiation in addition to metabolic heat.

When mean skin temperature exceeds about 36°C the subject is likely to begin exhibiting the effects of heat strain (Section 17.5) unless he has been well acclimatized to hot working environments. At mean skin temperatures above 37°C the person is in danger of excessive and, perhaps, even fatal core temperatures. This might be a good time to terminate the experiment.

17.3 PHYSIOLOGICAL HEAT TRANSFER

A great deal of research has been devoted to quantification of the various modes of heat exchange associated with the human body and the corresponding physiological reactions. Such work has involved laboratory and field experiments, analytical studies and numerical simulations. The development of a numerical thermoregulation model utilizes a combination of relationships that approximate the modes of heat transfer between the human body and the surrounding environment. The purpose of such a model is to predict one or more of the parameters that are deemed to represent physiological reaction such as mean skin temperature, core temperature or sweat rate. One such model is described in Section 17.3.6. First, however, we must develop relationships that quantify the individual modes of physiological heat transfer.

17.3.1 The metabolic heat balance

In common with many other living organisms, the human body is a biological heat engine of low mechanical efficiency. Fuel is consumed in the form of nutrients and combines with oxygen to produce

- metabolic heat
- mechanical work and
- changes in mass (body growth)

The rate of body growth is negligible compared to other physiological changes and can be ignored for the purposes of this analysis. The mechanical work output, shown as W on Figure 17.1, is seldom more than 20 per cent of the total metabolic energy even for strenuous efforts by trained athletes and is usually very much less than this. It is considered only when the work involves significant lifting or lowering of a mass, including the human body itself.

Metabolic energy = metabolic heat + work done against gravity (W)
[proportional to oxygen consumption]

For example, a person of mass 70 kg walking up an incline of 4 in 100 at a speed of 2 m/s would do work against gravity at a rate of

$$70 \times 9.81 \times 2 \times \frac{4}{100} = 55 \quad \text{kg} \frac{\text{m}}{\text{s}^2} \frac{\text{m}}{\text{s}} = \text{N} \frac{\text{m}}{\text{s}} = W$$

The metabolic energy produced by the person should be reduced by this amount to give the corresponding metabolic heat generation. However, in walking uphill, the rate of oxygen consumption and, hence, metabolic energy is itself increased. In practice, it is usual to ignore mechanical work in analyses of physiological response to climatic conditions.

At equilibrium, the generation of metabolic heat, M , is balanced by heat transfer from the body to the surroundings. However, a fraction of the metabolic heat, A_c , may be accumulated within the body resulting in a transient rise in core temperature, Δt_c , and (usually) also skin temperature. By assuming that 80 per cent of the body mass is at core temperature, t_c , and 20 per cent at skin temperature, t_{sk} , the rate of heat accumulation may be approximated as

$$A_c = \frac{m_b C_b (0.8 \Delta t_c + 0.2 \Delta t_{sk})}{\text{time (seconds)}} \quad W \quad (17.1)$$

where m_b = mass of body (kg)

and C_b = average **specific heat of the body** (3470 J/(kgK)) (Stewart, 1982)

For sedentary persons at thermal equilibrium with the surroundings, average oral temperature is approximately 36.9°C. Skin temperature varies over the body surface and with the ambient air temperature but has an average value of 34°C for non-stressed personnel experiencing a sensation of thermal comfort. The effect of heat storage, Ac , is to increase core temperature, t_c , and, hence, skin temperature. This normally results in enhanced body cooling in order to attain a new equilibrium at which the rate of heat accumulation declines to zero.

Figure 17.1 shows that heat loss from the body occurs through a combination of heat transfer processes:

- respiratory heat exchange (breathing), Br .
- convection, Con .
- radiation, Rad , and
- evaporation, $Evap$

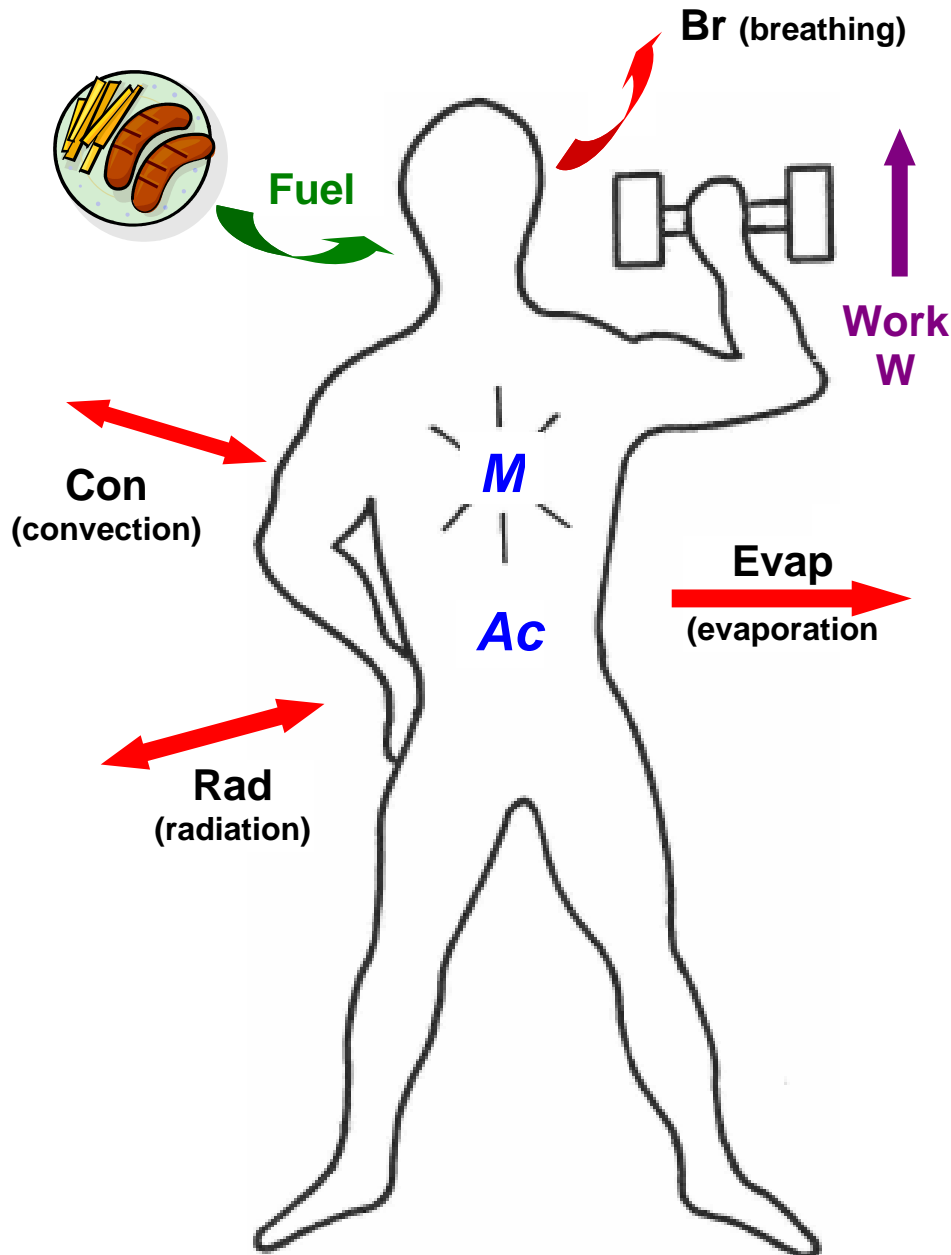


Figure 17.1 The human body is a biological heat engine producing both work and metabolic heat, M :

$$M = Con + Rad + Evap + Br + Ac$$

Conductive heat transfer may also take place at any areas of contact with solid surroundings. Here again, this is usually small and is neglected in the following sections. In this analysis we will also ignore any heating or cooling caused by the ingestion of food or drink. We can now state the metabolic heat generation, M , to be

$$M = Br + Rad + Con + Evap + Ac \quad (17.2)$$

At thermal equilibrium, the rate of heat accumulation, Ac , is zero.

Then

$$M = Br + Rad + Con + Evap \quad (17.3)$$

This equation is known as the **metabolic heat balance**. Each of the terms Br , Rad , Con , and $Evap$ may, theoretically, be negative. However, their net sum must be equal to the rate of internal heat generation, M , if equilibrium is to be maintained. In this condition, evaporative and respiratory heat transfer from the body must remain positive while both Rad and Con may be negative.

Physiological heat exchange and metabolic heat generation are usually quoted in terms of Watts per square meter of body surface (W/m^2) where the skin area, A_{sk} , may be estimated from the DuBois relationship

$$A_{sk} = 0.202 m_b^{0.425} h_b^{0.725} \quad m^2 \quad (17.4)$$

where h_b = height of body (m)
and m_b = body mass (kg)

For an average sized man of mass 70 kg and height 1.73 m, $A_{sk} = 1.83 m^2$.

Metabolic heat generation depends primarily upon muscular activity but also varies with respect to the condition of individual health, physical fitness and emotional state. Table 17.1 gives average metabolic rates for a series of activities both in terms of total energy production (W) and normalized (W/m^2) on the basis of $A_{sk} = 1.83 m^2$. From this point on we shall refer to the modes of heat transfer in terms of W/m^2 .

Table 17.1 Metabolic rates for various activities

Activity	Metabolic heat production	
	W	W/m^2 (M)
Sleeping	73	40
Seated	107	58.5*
Standing but relaxed	128	70
Walking on the level at:		
1 m/s	238	130
1.4 m/s	320	175
1.8 m/s	403	220
Manual work:		
very light	174	95
light	265	145
moderate	448	245
heavy	622	340

* 1 met = $58.5 W/m^2$ and is sometimes used as a unit of metabolic rate

17.3.2 Respiratory heat transfer

The large internal area and wetness of human lungs give a good efficiency of heat exchange. The actual degree of respiratory cooling depends upon the rate of breathing and the wet bulb temperature of the ambient air.

$$\text{Br} = \frac{m_{resp} (S_{out} - S_{in})}{A_{sk}} \quad \text{W/m}^2 \quad (17.5)$$

where m_{resp} = mass rate of breathing (kg air/s)
 S_{out} = sigma heat of exhaled air (J/kg)
 S_{in} = sigma heat of inhaled (ambient) air (J/kg)

Experimental evidence (Fanger, 1970) has indicated that the rate of respiration, m_{resp} is proportional to the total metabolic energy production

$$m_{resp} = 1.7 \times 10^{-6} \times \text{metabolic energy} = 1.7 \times 10^{-6} \times M \times A_{sk} \quad \text{kg/s} \quad (17.6)$$

Hence, equation (17.5) becomes

$$\text{Br} = 1.7 \times 10^{-6} M (S_{out} - S_{in}) \quad \text{W/m}^2 \quad (17.7)$$

where the metabolic rate, M (W/m^2) may be estimated from Table 17.1.

The sigma heat terms S_{out} and S_{in} are calculated from the equations given in Section 14.6 at the corresponding wet bulb temperatures for exhaled air, t_{ex} , and ambient inhaled air, t_w , respectively. The latter can be measured directly. The wet bulb temperature of the near-saturated exhaled air depends upon body temperature and the psychrometric condition of the ambient air. Again, empirical data (Fanger, 1970) have produced the relationship

$$t_{ex} = 32.6 + 0.066 t_d + 0.0002 e \quad ^\circ\text{C} \quad (17.8)$$

where t_d = ambient dry bulb temperature ($^\circ\text{C}$)
and e = actual vapour pressure of the ambient air (Pa)

Example

Estimate the rate of respiratory cooling for a man of average size ($A_{sk} = 1.83 \text{ m}^2$) walking at 1.8 m/s in an atmosphere of wet bulb temperature, $t_w = 18^\circ\text{C}$, dry bulb temperature, $t_d = 25^\circ\text{C}$ and barometric pressure, $P = 110 \text{ kPa}$.

Solution

From Table 17.1 the metabolic rate, M , is selected as 220 W/m^2 . Applying the given climatic conditions to the psychrometric equations of Section 14.6 leads to:

Sigma heat, $S_{in} = 47\,334 \text{ J/kg}$
and actual vapour pressure, $e = 1566 \text{ Pa}$.

Then, temperature of exhaled air (equation (17.8))

$$t_{ex} = 32.6 + (0.066 \times 25) + (0.0002 \times 1566) = 34.563^\circ\text{C}$$

Applying this temperature of saturated air to the same equations of Section 14.6 gives the sigma heat of the expired air to be

$$S_{out} = 113\,756 \text{ J/kg}$$

Equation (17.7) then gives the heat removed by respiration as

$$Br = 1.7 \times 10^{-6} \times 220 (113\,756 - 47\,334) = 24.8 \quad \text{W/m}^2$$

This represents some 11 per cent of the metabolic rate of 220 W/m^2 . We shall continue with this example later as we introduce the other modes of heat transfer.

The influence of respiratory cooling decreases as the ambient wet bulb temperature rises towards that of the expired air. At ambient wet bulb temperatures in excess of t_{ex} , condensation will occur within the lungs and respiratory tracts, accompanied by a rapid onset of heat strain.

17.3.3 Convective heat transfer

17.3.3.1 The convective heat transfer equation

The convective, radiative and evaporative modes of heat transfer from the human body are all affected by the degree of covering and the thermal properties of clothing. In the case of an unclothed body, the convective heat transfer is given by equation (15.16)

$$\text{Con} = h_c (t_{sk} - t_d) \quad \text{W/m}^2 \quad (17.8)$$

where h_c = convective heat transfer coefficient ($\text{W}/(\text{m}^2 \text{ } ^\circ\text{C})$)
and t_{sk} = skin temperature ($^\circ\text{C}$)

To take the effect of clothing into account, let us consider the heat transfer in two parts:

- (i) from the skin at temperature t_{sk} to the outside of the clothing at temperature t_{cl} , and
- (ii) from the clothing to the surrounding air of dry bulb temperature t_d .

For each square metre of skin surface, we can write

$$\text{Con} = h_{cl} (t_{sk} - t_{cl}) \quad \text{W/m}^2 \quad (17.9)$$

where h_{cl} = effective heat transfer coefficient through the clothing ($\text{W}/(\text{m}^2 \text{ } ^\circ\text{C})$)
and $\text{Con} = h_c f_{cl} (t_{cl} - t_d) \quad \text{W/m}^2 \quad (17.10)$

h_c remains the surface convective heat transfer coefficient from the (now clothed) body to the surroundings ($\text{W}/(\text{m}^2 \text{ } ^\circ\text{C})$) while

$$f_{cl} = \frac{\text{surface area of clothed body}}{\text{surface area of unclothed body}} \quad (17.10A)$$

The latter factor accounts for the increase in overall surface area caused by clothing.

At equilibrium, equations (17.9) and (17.10) represent the same value of Con.

As t_{cl} is particularly difficult to establish independently, we can eliminate it by re-writing equation (17.9) as

$$t_{cl} = t_{sk} - \frac{\text{Con}}{h_{cl}} \quad ^\circ\text{C} \quad (17.11)$$

For practical application, $1/h_{cl}$ may be expressed as

$$R_{cl} = 1/h_{cl} \quad \text{m}^2 \text{C/W} \quad (17.12)$$

and is known as the **thermal resistance of the clothing**. Substituting for t_{cl} in equation (17.10) and re-arranging gives

$$\text{Con} = \frac{(t_{sk} - t_d)}{R_{cl} + 1/(f_{cl} h_c)} \quad \text{W/m}^2 \quad (17.13)$$

Note that for an unclothed body, $R_{cl} = 0$ and $f_{cl} = 1$. The relationship then simplifies to equation (17.8).

The only variable in equation (17.13) that is amenable to direct measurement is the ambient dry bulb temperature. The remaining parameters may be estimated from the following empirical data and relationships.

17.3.3.2 Clothing factors

The effective **thermal resistances, R_{cl} , of clothing ensembles** commonly worn in underground workings are given in Table 17.2 together with typical corresponding area factors, f_{cl} . This table has been derived from data reported in the ASHRAE Fundamentals Handbook (1985).

Ensemble*	Thermal resistance [†] R_{cl} $^{\circ}\text{C m}^2/\text{W}$	Area factor f_{cl}	$h_{cl} = 1/R_{cl}$ $\text{W}/(\text{m}^2\text{C})$
Unclothed	0	1.00	infinite
Walking shorts	0.051	1.05	19.6
Shorts & short sleeved shirt	0.076	1.11	13.2
Thin trousers & short sleeved shirt	0.085	1.14	11.8
Thick trousers & long sleeved shirt	0.110	1.28	9.1
Long sleeved coveralls & long sleeved shirt	0.143	1.28	7.0

*All ensembles include hardhat, boots and stockings

[†]Thermal resistance of clothing is sometimes stated in units of clo, where 1 clo = 0.155 $^{\circ}\text{C m}^2/\text{W}$

Table 17.2 Clothing factors for ensembles commonly worn in mining.

The insulation provided by clothing is primarily due to the small pockets of air trapped within it. If the clothing is fully wetted then heat transfer through it may be estimated as for conduction through still water in a porous medium. The heat transfer coefficient may then be the order of some 50 $\text{W}/(\text{m}^2 \text{ } ^{\circ}\text{C})$ and R_{cl} of 0.02 ($\text{m}^2\text{C})/\text{W}$.

17.3.3.3 Convective heat transfer coefficient, h_c

A number of authorities have reported experimental data and proposed empirical relationships for the convective heat transfer coefficient applicable to the human body (Stewart, 1982; ASHRAE, 1989). This parameter depends upon the psychrometric condition of the air, the localized (**microclimate**) relative velocity, and the size and shape of the body. A simplified relationship that gives acceptable agreement with experimental data for the velocity range 0.2 to 5 m/s is

$$h_c = 0.00878 P^{0.6} u^{0.5} \quad \text{W/(m}^2\text{ }^\circ\text{C)} \quad (17.14)$$

where P = barometric pressure (Pa)
and u = local (effective) relative velocity (m/s)

The local (effective) relative velocity is not the same as the difference between the velocities of the body and the general airstream. Migration of heat and water vapour creates an envelope around the body within which the velocity and psychrometric properties of the air differ from those in the general airstream. This envelope is known as the **body microclimate**. The velocity within the microclimate is affected by the corresponding temperature gradient and body movements as well as the mainstream air velocity. However, a practical approximation may be obtained for the range 0 to 3 m/s as

$$u = 0.8 u_r + 0.6 \quad \text{m/s} \quad (17.15)$$

where u_r = relative velocity between the main airstream and the general motion of the body.

For values of u_r in excess of 3 m/s, the correction becomes negligible and we may then accept that $u = u_r$.

17.3.3.4 Mean skin temperature, t_{sk}

The only parameter in equation (17.13) that remains to be investigated is the mean skin temperature. This is a factor of prime importance, controlling convective, radiant and evaporative modes of heat transfer. While neutral skin temperature is of the order of 34°C (Section 17.2) it may rise to 36°C in hot conditions without the subject necessarily suffering from heat strain. Well acclimatized individuals may be able to tolerate skin temperatures of up to 37°C without harm. However, the probability of progressive symptoms of heat strain increases rapidly after skin temperatures have reached 36°C. Skin temperatures of more than 37°C are likely to be indicative of dangerously high core temperatures. A close correlation has been observed between mean skin temperature and heat strain. Hence, mean skin temperature is one of the physiological response parameters that may be used as an indicator of heat strain.

Skin temperature may vary considerably over the surface of the body depending upon the temperature and velocity of the ambient airstream, orientation of the body, the degree of covering and thermal resistance of clothing, and wetness of the skin.

Figure 17.2 shows an experimental curve obtained by Gagge et al (1969) for unclothed subjects within an airflow of 40 per cent relative humidity and low velocity. Fanger (1970) and other authorities have reported some indication that skin temperature reduces as metabolic rate increases. However, those experiments were related to the measurement of thermal "comfort" in surface buildings rather than for hot industrial conditions.

The relationship obtained by regression analysis on the curve shown on Figure 17.2 is

$$t_{sk} = 24.85 + 0.322 t_d - 0.00165 t_d^2 \quad ^\circ\text{C} \quad (17.16)$$

where t_d = dry bulb temperature of the ambient air (°C).

The value given by this curve or equation has been known as a *Base Skin Temperature*¹.

¹ Base skin temperature is included here as background interest. It is not, however, a required parameter in the development of a human thermoregulation model (Section 17.3.6).

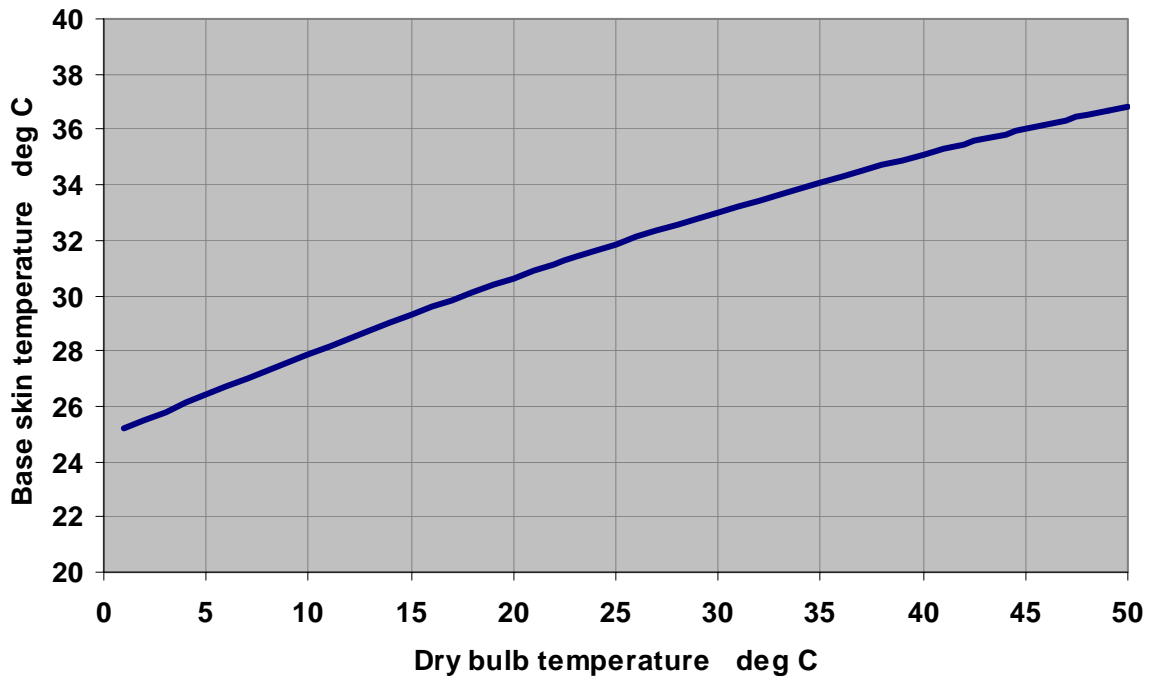


Figure 17.2 Mean skin temperature for unclothed subjects as a function of dry bulb temperature in air of low velocity and relative humidity of 40 per cent (after Gagge, 1969).

$$t_{sk} = 24.85 + 0.322 t_d - 0.00165 t_d^2$$

The reducing slope of this curve as t_d and t_{sk} increase indicates the moderating effect of evaporative cooling.

The average skin temperature obtained from equation (17.16) should be corrected for air velocity and the effects of clothing. As the velocity increases the base skin temperature will, in general, fall provided that the air temperature is less than that of the skin. The effect is mitigated by the presence of clothing. It is assumed here that heavy clothing having a thermal resistance, R_{cl} , of $0.15 \text{ (}^\circ\text{C m}^2/\text{W)}$ will provide full protection against the effect of air velocity on skin temperature. The correction to be applied to the "low velocity" skin temperature, t_{ski} of equation (17.16) is

$$\Delta t_{sk,vel} = -0.009 h_c (t_{sk} - t_d) \frac{(0.15 - R_{cl})}{0.15} \quad ^\circ\text{C} \quad (17.17)$$

The heat transfer coefficient, h_c , is calculated as a function of air velocity from equation (17.14). The constant 0.009 has been determined by curve fitting to results reported for unclothed and fully wetted personnel (Stewart, 1982).

The base skin temperature should be increased beyond the values given on Figure 17.2 because of the insulation provided by clothing. Gagge (1969) estimated that the skin temperature for fully clothed bodies was approximately 1°C higher than for unclothed subjects. In order to take account of the degree of thermal insulation, the clothing correction to base skin temperature may be approximated as

$$\Delta t_{sk,cl} = + \frac{R_{cl}}{0.15} \quad ^\circ\text{C} \quad (17.18)$$

Despite the corrections for air velocity and clothing, the skin temperature obtained in this way remains based upon measurements that were made in a low air velocity and a relative humidity of 40 per cent. This is the reason it is called an initial or base skin temperature that will subsequently be amended to reflect the response of the human thermoregulation system to the actual conditions.

Example

In the previous example, a man walking at a speed of 1.8 m/s was found to produce respiratory cooling of 24.8 W/m². Let us continue that example to determine the convective heat transfer, Con.

The psychrometric condition of the air given in the earlier example was:

$$t_w = 18^\circ\text{C}, \quad t_d = 25^\circ\text{C}, \quad P = 110 \text{ kPa}$$

The additional data now supplied are:

(i) The man is clothed in thick trousers, long sleeved shirt and boots. From Table 17.2, the corresponding values are obtained for

$$R_{cl} = 0.110 \text{ }^\circ\text{C m}^2/\text{W} \quad \text{and} \quad f_{cl} = 1.28$$

(ii) The ambient air velocity is 0.5 m/s and the man is walking at 1.8 m/s in the same direction as the airflow. The relative velocity between the two is, therefore, $u_r = 1.3 \text{ m/s}$.

Solution

The microclimate velocity is given by equation (17.15)

$$u = (0.8 \times 1.3) + 0.6 = 1.64 \text{ m/s}$$

Equation (17.14) then gives the convective heat transfer coefficient to be

$$h_c = 0.00878(110\,000)^{0.6} (1.64)^{0.5} = 11.91 \text{ W}/(\text{m}^2 \text{ }^\circ\text{C})$$

In the absence of any skin wetness data (for the moment), we use equation (17.16) to determine a base skin temperature, i.e. for an unclothed subject in a low velocity air stream

$$t_{sk} = 24.85 + (0.322 \times 25) - (0.00165 \times 25^2) = 31.869 \text{ }^\circ\text{C}$$

Equation (17.17) gives the correction for air velocity to be

$$\Delta t_{sk,vel} = -0.009 \times 11.91 (31.87 - 25) \frac{(0.15 - 0.11)}{0.15} = -0.196 \text{ }^\circ\text{C}$$

The clothing correction is given by equation (17.18) as

$$\Delta t_{sk,cl} = \frac{0.11}{0.15} = 0.733 \text{ }^\circ\text{C}$$

The corrected base skin temperature now becomes

$$t_{sk} = 31.869 - 0.196 + 0.733 = 32.406 \text{ } ^\circ\text{C}$$

The convective cooling is then given by equation (17.13)

$$\text{Con} = \frac{(32.406 - 25)}{(0.11 + 1/(1.28 \times 11.91))} = 42.2 \quad \text{W/m}^2$$

17.3.4 Radiant heat transfer

The exchange of radiant heat takes place between the outer surface of the body or clothing and any surrounding surfaces or ambient water vapour. The temperature of the outer surface of clothing is given by equations (17.11 and 17.12) as:

$$t_{cl} = t_{sk} - \text{Con} \times R_{cl} \quad ^\circ\text{C} \quad (17.19)$$

This reduces to t_{sk} if the body is unclothed, i.e. $R_{cl} = 0$. If the radiant temperature of the surroundings is t_r then the absolute average radiant temperature becomes

$$T_{av} = \frac{(t_{cl} + t_r)}{2} + 273.15 \quad \text{K} \quad (17.20)$$

The **Stefan Boltzman** relationship (equation (15.27)) then gives the radiant heat transfer coefficient to be:

$$h_r = 4 \times 5.67 \times 10^{-8} T_{av}^3 \quad \text{W/(m}^2 \text{ } ^\circ\text{C)} \quad (17.21)$$

For most mining circumstances, h_r lies within the range 5 to 7 W/(m² °C). The radiant heat transfer equation (15.26) gives

$$\text{Rad} = h_r f_r (t_{cl} - t_r) \quad \text{W/m}^2 \quad (17.22)$$

The emissivity of the body may be taken as unity unless especially reflective clothing is worn.

The **view (or posture) factor**, f_r , has been reported in the range 0.7 to 0.75 for seated, standing or crouching personnel (ASHRAE, 1989; Stewart, 1982).

Example

Continuing again with the previous example, the man is walking along an airway where the temperature of the rock walls is 26°C. Calculate the radiant heat exchange.

Solution

From equation (17.19) the temperature of the outer surface of the clothing is

$$t_{cl} = 32.406 - 42.2 \times 0.11 = 27.76 \text{ } ^\circ\text{C}$$

As $t_r = 26^\circ\text{C}$, the absolute average radiant temperature (equation (17.20)) is

$$T_{av} = \frac{(27.76 + 26)}{2} + 273.15 = 300.03 \quad \text{K}$$

Equation (17.21) then gives the radiant heat transfer coefficient to be

$$h_r = 4 \times 5.67 \times 10^{-8} (300.03)^3 = 6.13 \quad \text{W/(m}^2\text{°C)}$$

Taking the posture factor, f_r , to be 0.73 for a walking person, equation (17.22) gives the radiant cooling as

$$\text{Rad} = 6.13 \times 0.73 \times (27.76 - 26) = 7.9 \text{ W/m}^2$$

17.3.5 Evaporative heat transfer

17.3.5.1 Evaporation from unclothed and clothed bodies

An analysis of the heat and mass transfers at a wet surface was given in Appendix A15.4 following Chapter 15. Equation (A15.28) gave the evaporative or latent heat transfer to be

$$\text{Evap} = q_L = h_e (e_{ws} - e) \quad \text{W/m}^2 \quad (17.23)$$

where h_e = evaporative heat transfer coefficient at the outer surface

$$= 0.0007 h_c \frac{L_{sk}}{P} \quad \frac{\text{W}}{\text{m}^2 \text{ Pa}} \quad (17.24)$$

e_{ws} = saturated vapour pressure at the wet surface temperature (Pa)

e = actual vapour pressure in the main airstream (Pa)

and L_{sk} = latent heat of evaporation of water at wet surface temperature (J/kg)

The ratio h_e/h_c (known as the **Lewis Ratio**) is then

$$\frac{h_e}{h_c} = 0.0007 \frac{L_{sk}}{P} \quad \text{°C /Pa} \quad (17.25)$$

Employing mid-range values of $L_{sk} = 2455 \times 10^3 \text{ J/kg}$ and $P = 100\,000 \text{ Pa}$ gives a Lewis Ratio of 0.017 °C/Pa .

In the case of physiological heat transfer, e_{ws} becomes e_{sk} , the saturated vapour pressure at the wet skin temperature. Furthermore, if the skin is only partially wetted then equation (17.23) becomes

$$\text{Evap} = w h_e (e_{sk} - e) \quad \text{W/m}^2 \quad (17.26)$$

where w = fraction of the surface that is wet (see, also, **Wetness fraction**, Section 16.3.1.1)

In order to take the effect of clothing into account, we employ the analogy between heat and mass transfers by expanding equation (17.26) to the same form as equation (17.13)

$$\text{i.e.} \quad \text{Evap} = \frac{w(e_{sk} - e)}{R_{e,cl} + 1/(f_{cl} h_e)} \quad \text{W/m}^2 \quad (17.27)$$

where $R_{e,cl}$ = the resistance to **latent heat transfer through the clothing**, ($\text{m}^2 \text{ Pa/W}$), and is analogous to the thermal resistance, R_{cl}

and f_{cl} = the clothing area ratio [Equation (17.10A)].

In order to evaluate $R_{e,cl}$, let us recall from equation (17.12) that $R_{cl} = 1/h_{cl}$. We might expect, therefore, that the heat and mass transfer analogy would give $R_{e,cl} = 1/h_{e,cl}$ where $h_{e,cl}$ is the evaporative heat transfer coefficient through the clothing. Practical observations on sweating mannikins have determined that $R_{e,cl}$ is proportional but not equal to $1/h_{e,cl}$ for any given clothing ensemble. We can write

$$R_{e,cl} = \frac{1}{i_{cl} h_{e,cl}} \quad \text{m}^2 \text{ Pa/W} \quad (17.28)$$

where i_{cl} may be called the vapour permeation efficiency of the clothing. This varies from 0 for a completely vapour proof garment to 1.0 for an unclothed person. Oohori (1984) reported that most indoor clothing ensembles have i_{cl} values of approximately 0.45. Direct experimentation with sweating mannikins or other means have been employed to determine i_{cl} values for a range of clothing types. Most of the i_{cl} values published by ASHRAE (1993) are in the range 0.35 to 0.41.

The evaporative heat transfer coefficient for the outer surface of the body or clothing was given by equation (17.24). By replacing the coefficients h_e and h_c by their counterparts for evaporative heat transfer through the clothing, we obtain

$$h_{e,cl} = 0.0007 h_{cl} \frac{L_{sk}}{P} \quad \text{W/(m}^2 \text{ Pa)} \quad (17.29)$$

Hence, as $h_{cl} = \frac{1}{R_{cl}}$ and $h_{e,cl} = \frac{1}{R_{e,cl} i_{cl}}$

$$R_{e,cl} = \frac{R_{cl} P}{0.0007 L_{sk} i_{cl}}$$

$$\text{or} \quad R_{e,cl} = \frac{h_c R_{cl}}{h_e i_{cl}} \quad \frac{\text{m}^2 \text{ Pa}}{\text{W}} \quad (17.30)$$

Substituting into equation 17.27 (from equation (17.30)) in order to eliminate $R_{e,cl}$ gives

$$\text{Evap} = \frac{w h_e (e_{sk} - e)}{\left(h_c \frac{R_{cl}}{i_{cl}} \right) + \left(\frac{1}{f_{cl}} \right)} \quad \text{W/m}^2 \quad (17.31)$$

17.3.5.2 Skin wetness fraction

The skin wetness fraction, w , or "sweat fraction" is a measure of the proportion of skin surface area from which evaporation of sweat takes place. Diffusion of water vapour through the skin occurs at a rate normally equivalent to about $w = 0.06$ and this may be taken as a base value. (Individuals who are dehydrated or who are acclimatized to living in arid regions may reduce this base value to about 0.03).

Signals from temperature receptors within the body activate sweat glands in order to increase the size of the wetted area. The sweat rate is closely related to the core temperature and mean skin temperature. Each of these three may be employed as an indicator of potential heat strain. Furthermore, as core temperature is affected strongly by metabolic energy, M , it follows that sweat rate must also be influenced by the metabolic rate.

An analysis of the effective limits of evaporative cooling given in the ASHRAE Handbook on Fundamentals (1985) leads to the estimated curves shown on Figure 17.3. These provide a **base wetness fraction** for any given metabolic heat generation and ambient wet bulb temperature.

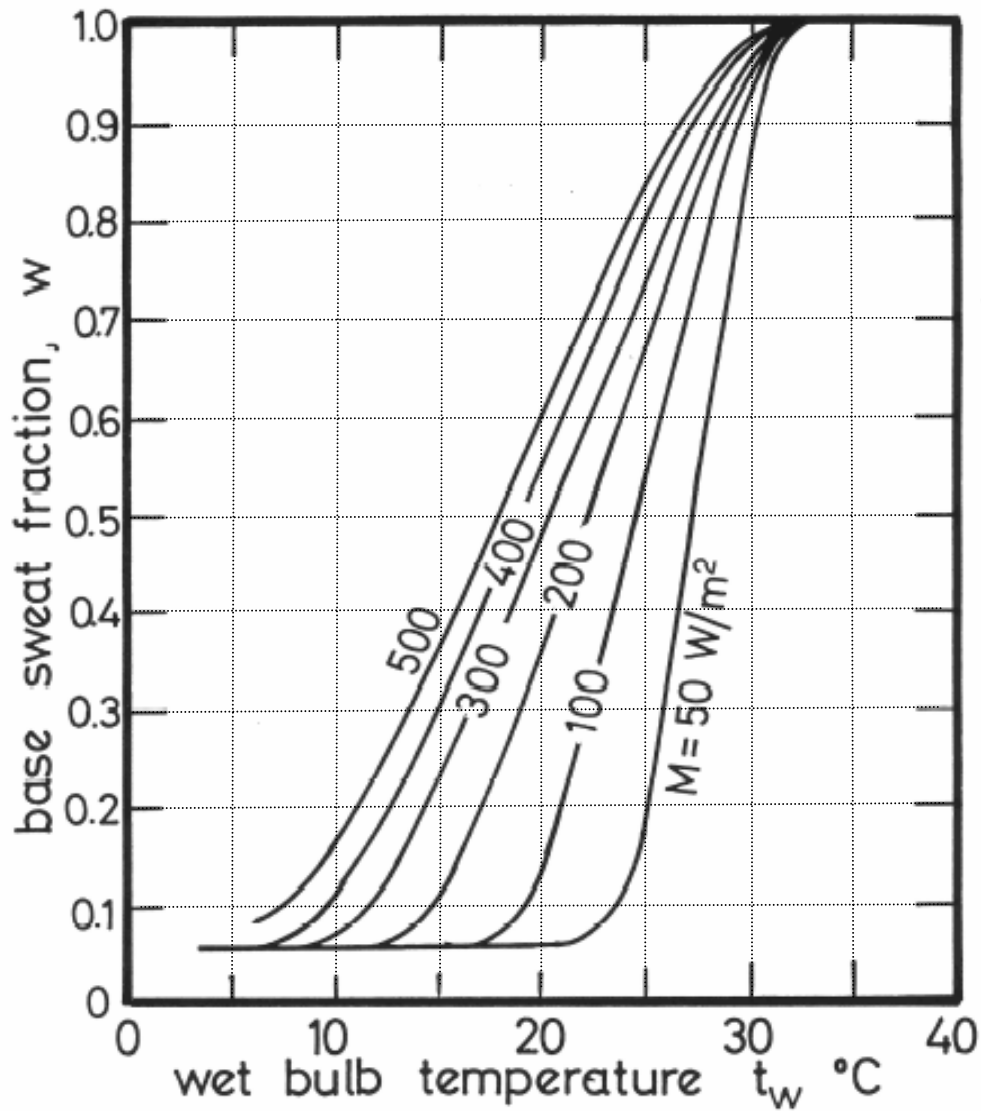


Figure 17.3 Base wetness fraction as a function of ambient wet bulb temperature and metabolic rate.

The curves converge to give a fully wetted body surface ($w = 1$) at a wet bulb temperature of 33°C, irrespective of the metabolic heat production. The curves are described numerically by the algorithm contained within the Sweat Fraction subroutine of the computer program listed in Appendix A17.1 at the end of this chapter.

There is, however, an additional effect when the temperature receptors indicate a high skin temperature. Figure 17.4 illustrates the value to be added to the base wetness fraction when skin temperature exceeds 32.5°C. This curve has been obtained from a consideration of sweat production as a function of the thermoregulatory signals generated by body temperature receptors. The curve is represented adequately by the equation

$$\Delta w_{sk} = \frac{\sin((31.85 t_{sk} - 762) \times 0.01745)}{2} + 0.5 \quad (17.32)$$

(where the sine function is computed in radians) for skin temperatures between 32.5 and 39.0°C.

The actual value of skin wetness fraction is then calculated as

$$w = \text{base wetness fraction} + \Delta w_{sk} \quad (17.33)$$

with the maximum value set at $w = 1$

There is considerable variation in sweat rate between individuals and according to the degree of acclimatization. Furthermore, the production of perspiration is by no means constant over the body surface. A run-off of sweat may occur in some zones before others are fully wetted. Light absorbent clothing may assist in holding and distributing perspiration that might otherwise be lost as run-off, so improving the evaporative cooling process. This can result in a distinct chilling effect on wetted skin during rest periods or when entering a cooler or drier atmosphere.

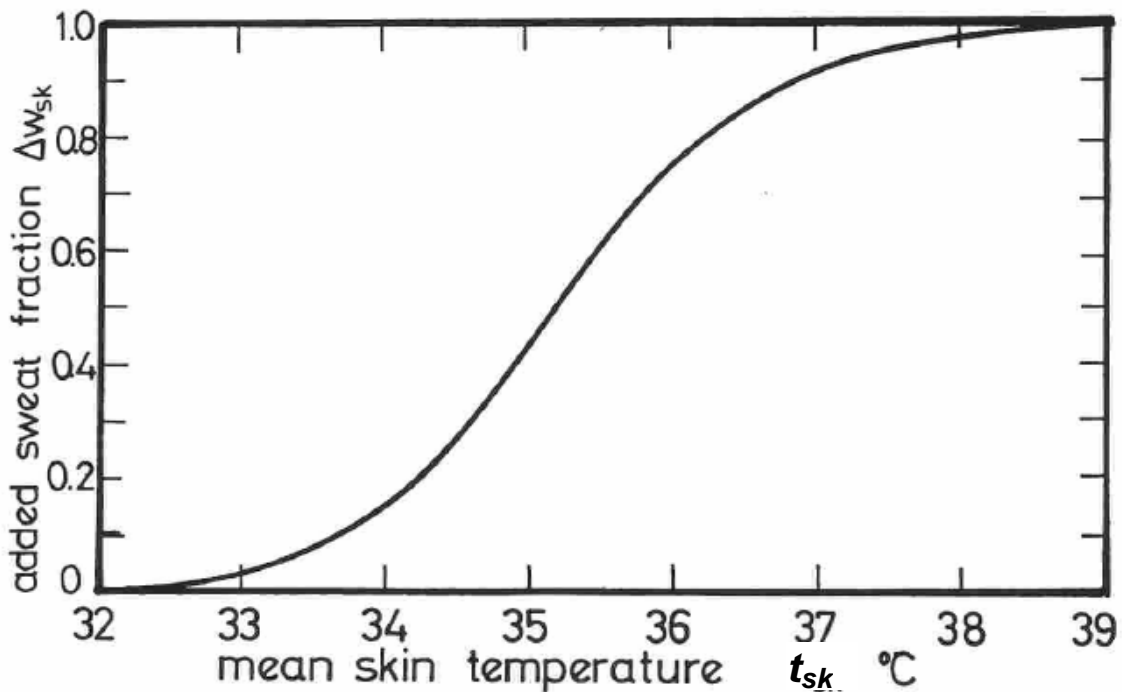


Figure 17.4 Additional wetness (sweat) fraction caused by high skin temperature.

Example

Let us continue once again with the earlier example to find the evaporative heat transfer. As a reminder,

metabolic heat generation,	M	=	220	W/m^2
base skin temperature,	t_{sk}	=	32.406	$^{\circ}\text{C}$
ambient wet bulb temperature,	t_w	=	18	$^{\circ}\text{C}$
ambient dry bulb temperature,	t_d	=	25	$^{\circ}\text{C}$
barometric pressure,	P	=	110 000	Pa
convective heat transfer coefficient,	h_c	=	11.91	$\text{W}/(\text{m}^2 \text{ } ^{\circ}\text{C})$
thermal resistance of the clothing,	R_{cl}	=	0.11	$^{\circ}\text{C m}^2/\text{W}$
and clothing area factor,	f_{cl}	=	1.28	

The only additional item of information that we now require is the vapour permeation efficiency of the clothing, i_{cl} . This is taken as 0.45.

Solution

The evaporative heat transfer is given by equation (17.31), i.e.

$$\text{Evap} = \frac{w h_e (e_{sk} - e)}{\left(h_c \frac{R_{cl}}{i_{cl}} \right) + \left(\frac{1}{f_{cl}} \right)}$$

We must determine the values of those parameters in this equation that are not already known.

From the psychrometric equations given in Section 14.6 the saturation vapour pressure at a skin temperature of 32.406°C is calculated as

$$e_{sk} = 4863 \text{ Pa}$$

with a corresponding latent heat of evaporation

$$L_{sk} = 2425.2 \times 10^3 \text{ J/kg}$$

The actual vapour pressure in the ambient atmosphere has already been calculated (in the respirable cooling example) as

$$e = 1566 \text{ Pa}$$

Equation (17.24) gives the evaporative heat transfer coefficient to be

$$h_e = 0.0007 \times 11.91 \times \frac{2425.2 \times 10^3}{110000} = 0.1838 \quad \text{W/(m}^2 \text{ Pa)}$$

The base wetness fraction, w , at a metabolic rate of $M = 220 \text{ W/m}^2$ and a wet bulb temperature $t_w = 18^\circ\text{C}$ may be estimated from Figure 17.3 or computed from the Sweat Factor subroutine given within the program listed in Appendix 17.1 as $w = 0.268$. Had the base skin temperature been greater than 32.5°C then an addition to the wetness fraction would have been required from Figure 17.4.

Equation (17.31) then gives

$$\text{Evap} = \frac{0.268 \times 0.1838 (4863 - 1566)}{(11.91 \times 0.11/0.45) + (1/1.28)} = 44.0 \quad \text{W/m}^2$$

17.3.6 A thermoregulation model

The analyses in the previous subsections have produced a set of equations that describe the heat transfers from a human body. A numerical model of the human thermoregulation system involves organizing those equations into a logical sequence: then, after comparing the net heat transfer with a known metabolic heat generation, adjust one or more of the physiological parameters in a manner that simulates the thermoregulatory response of an average, healthy person. The process is repeated iteratively until either thermal equilibrium is reached (when net heat transfer equals metabolic heat) or the model indicates untenable conditions of heat strain.

It must be appreciated that considerable variation occurs between individuals in their reaction to climatic variations. Empirical data gained from physiological tests represent average response. Combined with the approximations that are inherent in the analyses of surface heat and mass transfer theory, this indicates that the results of any thermoregulation model provide guidelines to average reaction rather than precise predictions for individual workers.

The thermoregulation model developed here employs mean skin temperature as the physiological indicator of heat strain. The model calculates an initial or base skin temperature on the basis of ambient dry bulb temperature from Gagge's equation (17.16) or from Figure 17.2.² The heat transfer from respiration, Br, convection, Con, radiation, Rad, and evaporation, Evap, are calculated from equations (17.7, 17.13, 17.22 and 17.31) respectively. The difference between net heat transfer and metabolic heat then indicates the heat accumulated, Ac (see equation (17.2)).

$$Ac = M - (Br + Con + Rad + Evap) \quad \text{W/m}^2 \quad (17.34)$$

If Ac is positive then heat is temporarily accumulated within the body. The reaction of an actual person may be to rest, reduce the rate of work, or discard clothing (the behavioural response). However, the simulation model assumes that the metabolic rate, M, is maintained. The skin temperature, t_{sk} , and, consequently, wetness fraction are increased as a function of Ac. In the thermoregulation model given as a program listing in Appendix A17.1, the correction to t_{sk} may be taken as 0.01 Ac or 0.02 Ac.

The heat transfer equations are re-evaluated iteratively until Ac is within 1 W/m² of zero. If the final equilibrium skin temperature is over 36°C then the worker may exhibit the progressive symptoms of heat strain, while skin temperatures in excess of 37°C should be considered to be dangerous.

Example

The example that was built up sequentially through Sections 17.3.2 to 17.3.5 is continued here to illustrate the reaction of the model and iterative convergence towards thermal equilibrium. Recalling the results of the earlier calculations, the initial or base skin temperature² was calculated to be 32.406°C and the heat transfers associated with this skin temperature were calculated to be

Respiration, Br,	=	24.8	W/m ²	
Convection, Con,	=	42.2	W/m ²	
Radiation, Rad,	=	7.9	W/m ²	and
Evaporation, Evap,	=	44.0	W/m ²	
Total (net cooling)	=	118.9	W/m ²	

The metabolic rate was, however, 220 W/m². Hence, the initial rate of heat accumulation is

$$Ac = 220 - 118.9 = 101.1 \text{ W/m}^2$$

This causes the simulated skin temperature to increase to

$$32.406 + (0.02 \times 101.1) = 34.428^\circ\text{C}.$$

The heat transfer equations are then re-evaluated iteratively until Ac approaches zero.

Table 17.3 illustrates the convergence of the model (listed in Appendix A17.1) towards equilibrium when net cooling equals metabolic rate.

² Alternatively, the initial skin temperature may simply be assumed to be the neutral value of 34°C

	Skin Temperature °C	Respiration Br W/m ²	Convection Con W/m ²	Radiant Rad W/m ²	Evaporation Evap W/m ²	Wetness fraction	Net Cooling W/m ²	Heat accumulated Ac W/m ²
1	32.41	25	42	8	44	0.27	119	101
2	34.43	25	54	11	106	0.55	196	24
3	34.90	25	56	12	135	0.68	229	-8
4	34.73	25	55	12	124	0.63	216	4
5	34.80	25	56	12	129	0.65	221	-2

Table 17.3. Convergence of the thermoregulation model towards thermal equilibrium.

These results show that the person will be perspiring at a medium rate ($w = 0.65$) and will attain an equilibrium skin temperature of 34.8°C if he maintains his work rate at 220 W/m². This skin temperature indicates acceptable conditions with negligible risk of heat strain.

By running the thermoregulation model listed in Appendix A17.1, the equilibrium skin temperature for any given combination of psychrometric conditions, air velocity, type of clothing and metabolic rate can be computed. This may then be used as a measure of potential heat strain. As indicated earlier, the probability of unacceptable heat strain is small for skin temperatures up to 36°C in acclimatized workers. However, for even greater stringency, Figure 17.5 has been developed from the work of Stewart (1982) and Wyndham (1974). This gives maximum allowable values of **equilibrium skin temperature** for fully wetted and acclimatized persons after four hours of continuous work if there is to be a probability of no more than 10⁻⁶ of dangerous core temperatures.

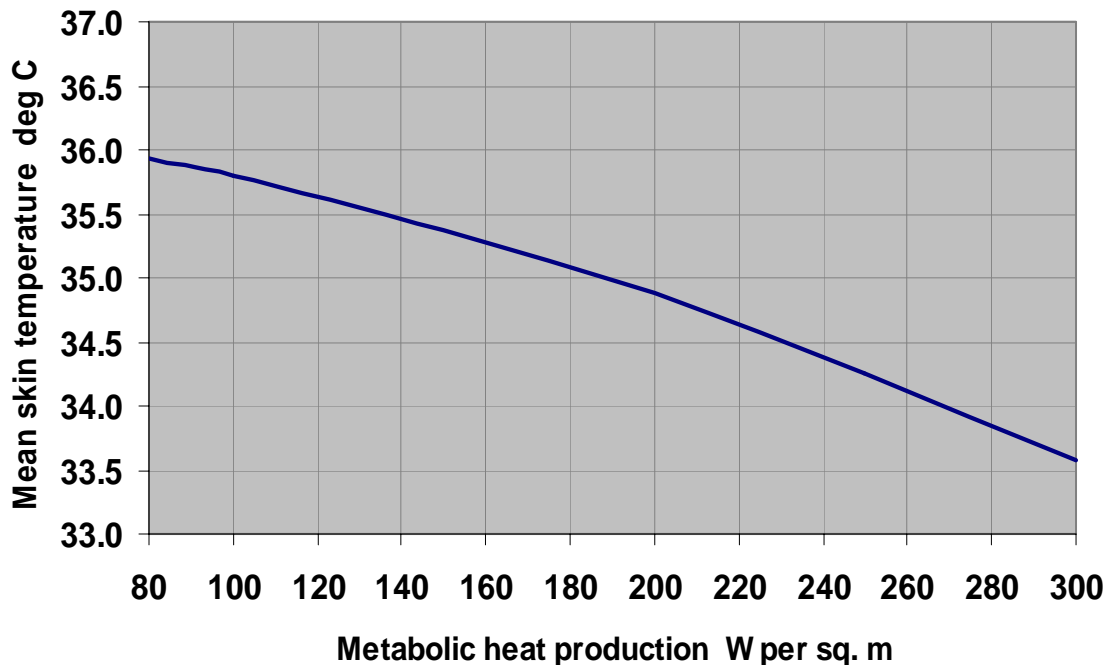


Figure 17.5 Limiting values of mean skin temperature corresponding to a one in a million risk of core temperature rising above 40°C in fully wetted acclimatized men after four hours of continuous work.

For the purposes of illustrating the behaviour of equilibrium skin temperature, cyclic runs of the thermoregulation model produced the results that are depicted on Figures 17.6 (a, b, c) for three degrees of clothing. In these runs the barometric pressure was maintained at 100 kPa, metabolic

rate at 100 W/m^2 , and the dry bulb temperature and radiant temperature both set at 5°C above the wet bulb temperature. For those specific conditions, the equilibrium skin temperature can be read from Figure 17.6 for given values of wet bulb temperature, air velocity, and type of clothing.

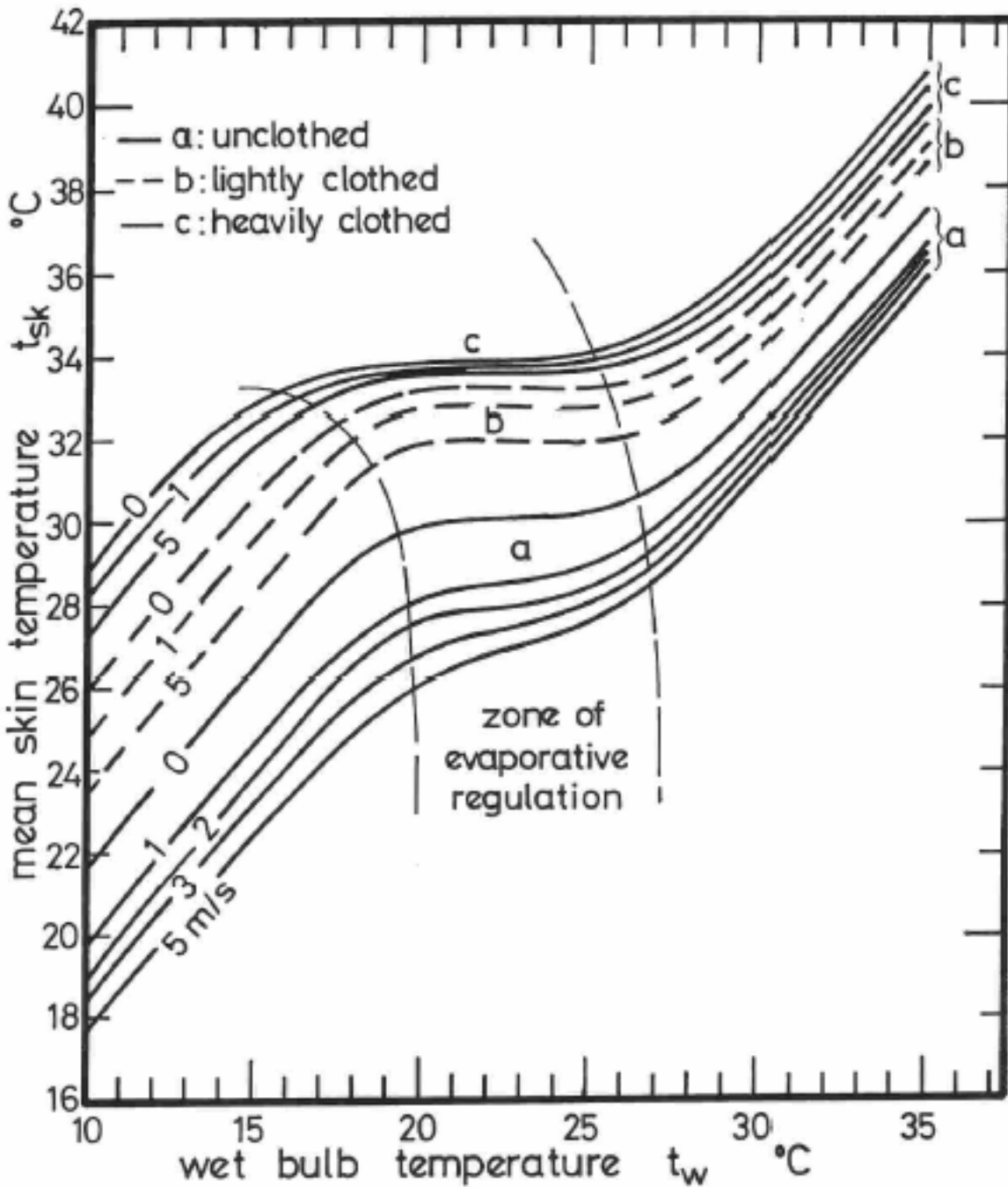


Figure 17.6

For the specific values $M = 100 \text{ W/m}^2$, $t_d = t_r = t_w + 5^\circ\text{C}$ and $P = 100 \text{ kPa}$, this figure illustrates the variation of mean skin temperature with ambient wet bulb temperature on

(a) unclothed, (b) lightly clothed (c) heavily clothed personnel

These sets of curves show clearly:

- the increases in skin temperature both below and above the zone of evaporative regulation
- the levelling of skin temperatures during evaporative regulation (when body wetness is increasing)
- the increased skin temperatures caused by clothing, and
- the reduced influence of air velocity as clothing is added.

17.4 INDICES OF HEAT STRESS

17.4.1 Purpose and types of heat stress indices.

It is clear from the preceding sections that the reaction of the human body to climatic variations involves a complex mix of psychrometric parameters and physiological responses. It is due to such complexity that heat stress indices rely, directly or indirectly, on data gained from experimental tests on volunteer human subjects undergoing monitored work rates in a range of environmental conditions. For more detailed and wider investigations, the availability of high speed computing allows a thermoregulation model such as that described in Section 17.3.6 to be employed. This requires a specification of all relevant data pertaining to work rate, clothing and psychrometric condition of the air.

For less rigorous applications such as routine checking of the cooling power of an existing environment or for initial conceptual designs, it is convenient to employ some measure of air cooling power or physiological reaction that can be quoted as a single number or **index of heat stress**. For manual use, such an index should be capable of direct measurement, or calculated easily from only a few types of observation. Over ninety indices of heat stress were developed during the twentieth century (Hanoff, 1970). This reflects the large number of variables involved, the complexity of the human thermoregulation system and the range of climatic conditions under which human beings may be required to work.

Even with similar climatic conditions, work rates and clothing ensembles, differing indices of heat stress can exhibit substantial variations in their predicted limits of environmental acceptability (Brake and Bates, 2002). The further reasons for such differences include the variety of treatments, assumptions and numerical values used by researchers with respect to clothing and physiological responses. It should also be borne in mind that most research into heat stress in non-sedentary workers is based on young, healthy and acclimatized personnel. In practice, there are significant variations between individuals within any given workforce. It is for this reason that initial screening and heat tolerance tests are advisable for recruits or returnees who will work in hot conditions (ref. Section 17.7).

We may classify heat stress indices into three types:

- single measurements
- empirical methods (dependent on measurements of temperature and air velocity)
- rational indices (based on the metabolic heat balance [equation 17.2] and physiological thermoregulation models).

Indices within each of these groups that have been recommended for subsurface ventilation systems are introduced in the following subsections.

17.4.2 Single measurements

No single psychrometric parameter is, by itself, a reliable indicator of physiological reaction. In hot and humid environments where the predominant mode of metabolic heat transfer is evaporation, the wet bulb temperature of the ambient air is the most powerful variable affecting body cooling. Indeed, some mines retain the wet bulb temperature as a sole indicator of climatic acceptability. A **psychrometric (aspirated) wet bulb temperature** of 27 to 28°C may be employed as a proximate criterion above which work rates or shift hours should be reduced, while in former years 32°C has been regarded as an upper limit of acceptability for very hot mines.

The second most important variable in hot conditions is the air velocity. Although air velocity, by itself, gives little indication of climatic acceptability, it can easily be combined with wet bulb temperature. This may be achieved by measuring the **natural wet bulb temperature**, that is, the temperature indicated by a non-aspirated wet bulb thermometer held stationary within the prevailing airstream.

Dry bulb temperature alone has a very limited role on climatic acceptability in hot mine environments. However, dry bulb temperatures in excess of 45°C can give a burning sensation on exposed skin facing the airstream. Hot dry environments may also result in skin ailments (Section 17.5.4). Heating and ventilating engineers concerned with comfort conditions in surface buildings often employ a combination of dry bulb temperature and relative humidity. Unfortunately, workers in underground mines or involved in the development of other subsurface facilities must often have to contend with much wider ranges of climatic acceptability.

For cold conditions where convection and radiation are the primary modes of heat exchange, dry bulb temperature and air velocity become the dominant factors. These may be combined into a wind chill index (Section 17.6).

17.4.3 Empirical methods

These techniques produce indices of heat stress that have either evolved from a statistical treatment of observations made on volunteers working in a controlled climate or are based on simplified relationships that utilize measurable parameters but have not been derived through a rational or theoretical analysis.

17.4.3.1 Effective temperature, ET

Effective temperature is one of the older indices of heat stress. In the mid 1920's, F.C. Houghton and C.P. Yaglou of the then American Society of Heating and Ventilating Engineers (ASHVE) conducted a series of experiments in which three volunteers were asked to pass between two adjoining rooms. One room was maintained at saturated conditions and negligible air velocity during any given experiment while the wet bulb temperature, dry bulb temperature and air velocity were varied in the second room. The instantaneous and subjective thermal sensation of each volunteer on passing between rooms was recorded simply as "hotter, cooler or the same". The experiments were conducted first on men stripped to the waist then repeated with the same subjects wearing lightweight suits.

The **effective temperature** was defined as the temperature of still saturated air that would give the same instantaneous thermal sensation as the actual environment under consideration. Charts were produced that allowed the effective temperature to be read for given wet bulb temperature, dry bulb temperature and air velocity. An example is shown on Figure 17.7.

The concept of effective temperature has been employed widely both as a comfort index for office workers and also as a heat stress index for industrial and military occupations. The effect of

radiant heat exchange may be taken into account in the Corrected Effective Temperature in which the dry bulb temperature is replaced by the **globe temperature** measured at the centre of a blackened 150 mm diameter hollow copper sphere.

The use of effective temperature for the prediction of physiological strain has been shown to have several shortcomings (Wyndham, 1974) and most mining industries have abandoned it. Where effective temperature remains in use, it is recommended that periods of continuous work should be reduced at effective temperatures in excess of 28°C and work should be terminated if it rises above 32°C.

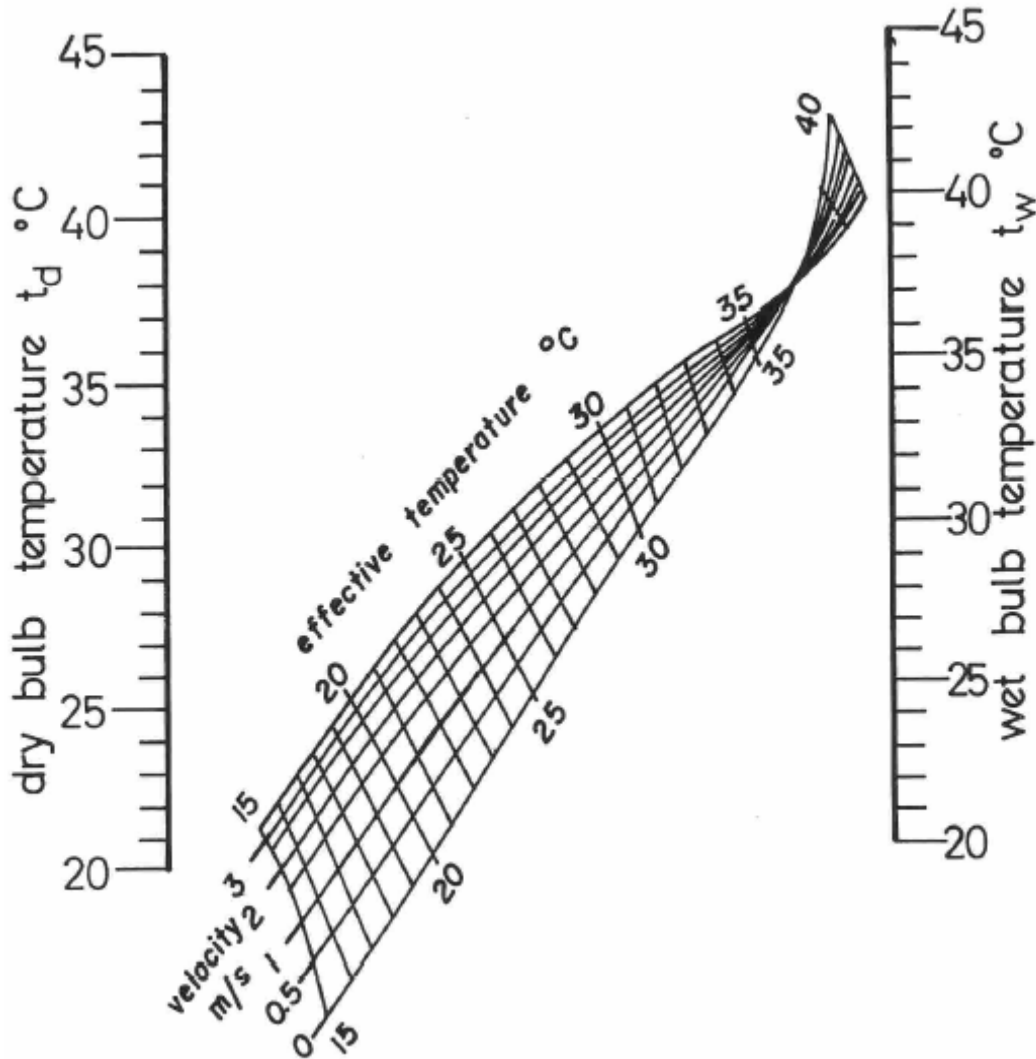


Figure 17.7 Effective temperature chart (normal scale) for lightly clothed personnel.

17.4.3.2 Wet Kata thermometer

The Kata thermometer appears to have been introduced by **Dr. L. Hill** in 1916. It consists of an alcohol thermometer with an enlarged bulb at the base and a smaller bulb at the top of the stem. In use, the enlarged bulb is submerged in warm water until the alcohol partially fills the upper reservoir. The instrument is then hung freely in the prevailing airstream and a stopwatch employed to determine the time taken for the alcohol level to fall between two marks inscribed on

the stem. This is combined with an instrument factor given with each individual thermometer to produce a measure of the cooling power of the air in $\text{mcal}/(\text{cm}^2\text{s})$.

When the main reservoir of the Kata thermometer is covered in wet muslin, the instrument gives cooling powers that are representative of a 20 mm wetted bulb at 36.5°C . These have been found to correlate reasonably well with core temperatures of unclothed and acclimatized workers subjected to hot and humid conditions (Stewart, 1982). Wet Kata readings may be approximated from measurements of air velocity, u , and wet bulb temperature, t_w ,

$$\text{Wet Kata cooling power} = (0.7 + u^{0.5})(36.5 - t_w) \quad \text{mcal}/(\text{cm}^2\text{s}) \quad (17.35)$$

(South African Chamber of Mines, 1972)

The use of Wet Kata readings as an index of heat stress is limited to hot and humid environments. Only the South African gold mining industry has utilized the Wet Kata reading in mines as a heat stress index on a routine basis.

17.4.3.3 Wet bulb globe temperature and wet globe temperature

The **wet bulb globe temperature** (WBGT) relies upon two measurements only. The first is the reading indicated by a wet bulb thermometer held stationary in the prevailing airstream. This is sometimes termed the natural wet bulb temperature, t_{nw} , and, at air velocities of less than about 3 m/s, will indicate a temperature greater than that of the normal psychrometric (aspirated) wet bulb thermometer, t_w (Section 14.3.5). Secondly, the temperature at the centre of a matte black hollow sphere or globe temperature, t_g , is measured. The two are combined to give

$$\text{WBGT} = 0.7 t_{nw} + 0.3 t_g \quad ^\circ\text{C} \quad (17.36)$$

When a significant source of radiant heat is visible then

$$\text{WBGT} = 0.7 t_{nw} + 0.2 t_g + 0.1 t_d$$

where t_d = dry bulb temperature $^\circ\text{C}$ (17.37)

This latter form of the equation is normally employed only in sunlight.

The wet bulb globe temperature is a function of the major climatic parameters that affect physiological reaction, i.e. wet and dry bulb temperatures, air velocity and radiant temperature. However, it has the advantage that it does not require a separate measurement of air velocity. The National Institute of Occupational Safety and Health of the United States (NIOSH, 1986) has employed WBGT as a heat stress standard and recommended the exposure limits shown on Figure 17.8. Heat stress levels based on the WBGT have also been subject to an International Standard (ISO, 1982).

A simplified version of the wet bulb globe temperature was developed by J.H. Botsford in 1971 and is known as the **wet globe temperature** (WGT). The instrument, now called a Botsball, consists of a 6 cm diameter blackened copper sphere covered by a wetted black fabric. A dial thermometer indicates the temperature at the middle of the hollow sphere.

Regression equations may be employed to relate WGT to WBGT (Ciriello, 1977) for known psychrometric conditions. For the particular range of dry bulb temperatures 20 to 35°C , relative humidities greater than 30 per cent and air velocities less than 7 m/s, Onkaram (1980) has suggested the experimentally derived equation

$$\text{WBGT} = 1.044 \text{WGT} - 0.187 \quad ^\circ\text{C} \quad (17.38)$$

where WGT is measured in $^\circ\text{C}$.

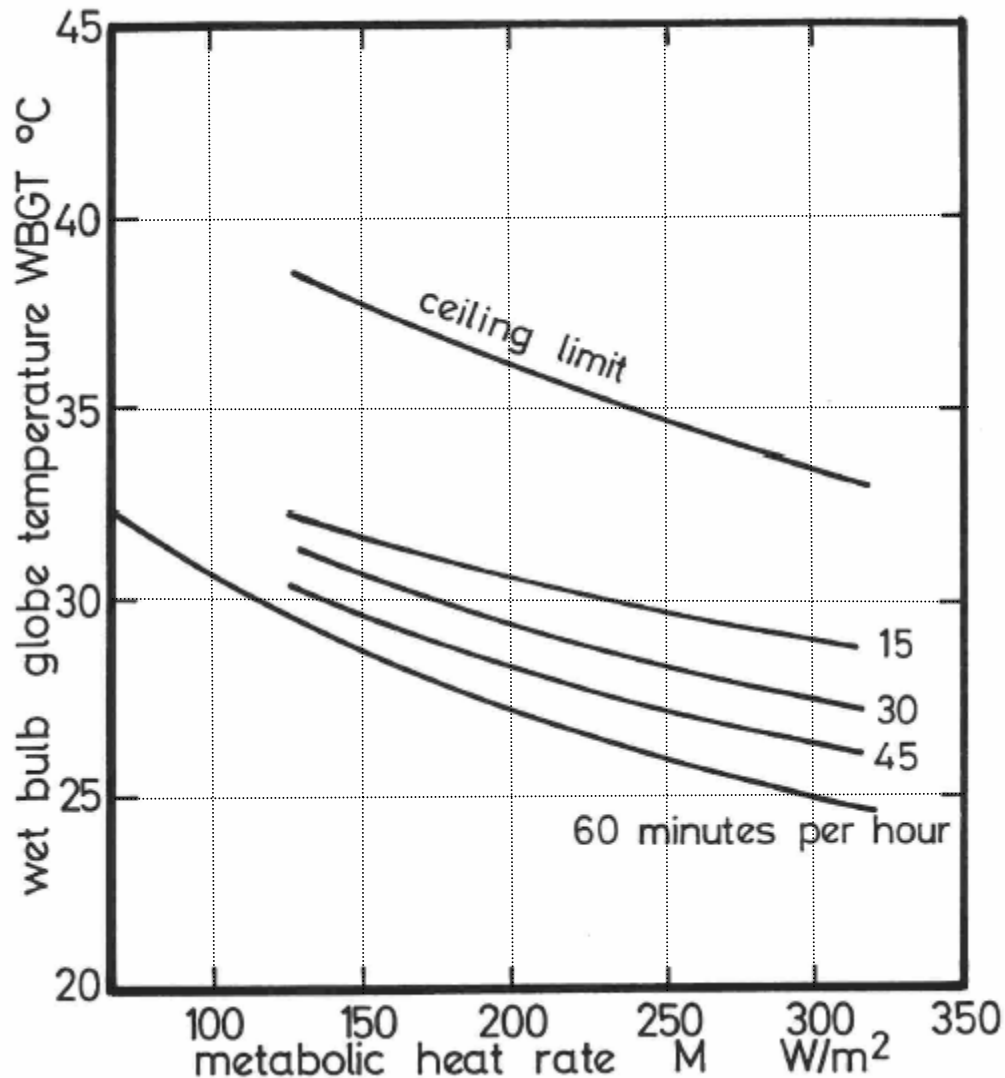


Figure 17.8 Wet bulb globe temperature exposure for acclimatized workers at varying working time per hour (recommended by the U.S. National Institute of Occupational Safety and Health, Pub. 86-113).

The WBGT and its simplified companion, WGT are both well suited to the rapid assessment of climatic conditions in existing locations where instrumentation may be located. They are, at present, less useful for the prediction of air cooling power in underground openings that have not yet been constructed, as neither natural wet bulb temperature nor wet or dry globe temperatures are included as output in current subsurface climate simulators.

Improvements in instrumentation, microelectronics and computer software have resulted in the development of hand-held devices that give an in-situ indication of air cooling power (e.g. Wu and Gillies, 1997).

17.4.4 Rational indices

A rational index of heat stress is one that has been established on the basis of the physiological heat balance equation (17.3) and that conforms to heat transfer relationships such as those developed in Section 17.3. A thermoregulation model (Section 17.3.6) may be used for detailed investigations of existing or proposed facilities. The establishment of such a model on a mine office microcomputer enables it to be employed for day to day routine assessments. However, for rapid manual assessment or where predictions of average cooling power for a work area are required, a thermoregulation model can be simplified into charts or tables by establishing specific values for the weaker parameters, or defining fixed relationships between those parameters and the more dominant variables.

A choice must be made on the physiological response that is to be used as an indicator of climatic acceptability. This is usually one of the linked parameters, core temperature, mean skin temperature or sweat rate. In the thermoregulation model output illustrated in Figure 17.6, mean skin temperature is employed in association with the limit values of Figure 17.5 as the indicator of acceptability.

17.4.4.1 Air Cooling Power (M scale), ACPM

The illustrative example shown on Figure 17.6 (a) gives a series of curves relating equilibrium skin temperature to wet bulb temperature and air velocity for unclothed personnel producing 100 W/m² of metabolic heat, and for specified values of

$$P = 100 \text{ kPa} \quad \text{and} \quad t_d = t_r = t_w + 5^\circ\text{C} \quad (17.39)$$

Figure 17.5 indicates that at $M = 100 \text{ W/m}^2$ an equilibrium skin temperature of 35.8°C is associated with a probability of no more than one in a million that core temperature will exceed 40°C, i.e. a negligible risk of unacceptable heat strain. Scanning across the $t_{sk} = 35.8^\circ\text{C}$ line on Figure 17.6 (a) allows us to read the corresponding limiting wet bulb temperatures for air velocities 0 to 5 m/s.

If the procedure were repeated with a sufficiently large and detailed number of charts of the type illustrated on Figure 17.6 then tables relating metabolic heat, wet bulb temperature and air velocity could be compiled for each clothing ensemble. This exercise has been carried out, not by a graphical construction of charts, but by cyclic operation of the thermoregulation model described in Section 17.3.6. The results are shown on Figure 17.9.

The lines on this chart have been established from equilibrium conditions when the ambient environment removes metabolic heat at the same rate as it is generated. Hence, they may be regarded as limit lines of climatic acceptability. For this reason, the vertical axis has been renamed Air Cooling Power (M scale) as a reminder that the lines represent equilibrium with metabolic heat, M , and to distinguish it from earlier versions of Air Cooling Power.

In order to use the chart as a rapid means of assessing climatic acceptability of any given environment, the psychrometric wet bulb temperature, t_w , and metabolic heat generation, M , are plotted as a coordinate point. If this point lies above the relevant air velocity line for the chosen clothing ensemble then the average cooling power of the air is greater than metabolic heat generation and personnel will be able to attain thermal equilibrium with the environment at that same rate of work. However, if the air cooling power is less than the relevant limit curve then the workers will discard clothing, reduce their work rate or risk the onset of heat strain.

In addition to the specified relationships of $t_d = t_r = t_w + 5^\circ\text{C}$ and $P = 100 \text{ kPa}$, the ACPM chart is based on a body posture factor of $f_r = 0.75$ and the following specifications for clothing:

	Unclothed	Light Clothing	Heavy Clothing
thermal resistance R_{cl} ($^{\circ}\text{Cm}^2/\text{W}$)	0	0.085	0.143
area factor, f_{cl}	1	1.14	1.28
vapour permeation efficiency	1	0.45	0.45

It will be recalled, also, that the air velocity is the relative velocity between the worker's body and the main airstream.

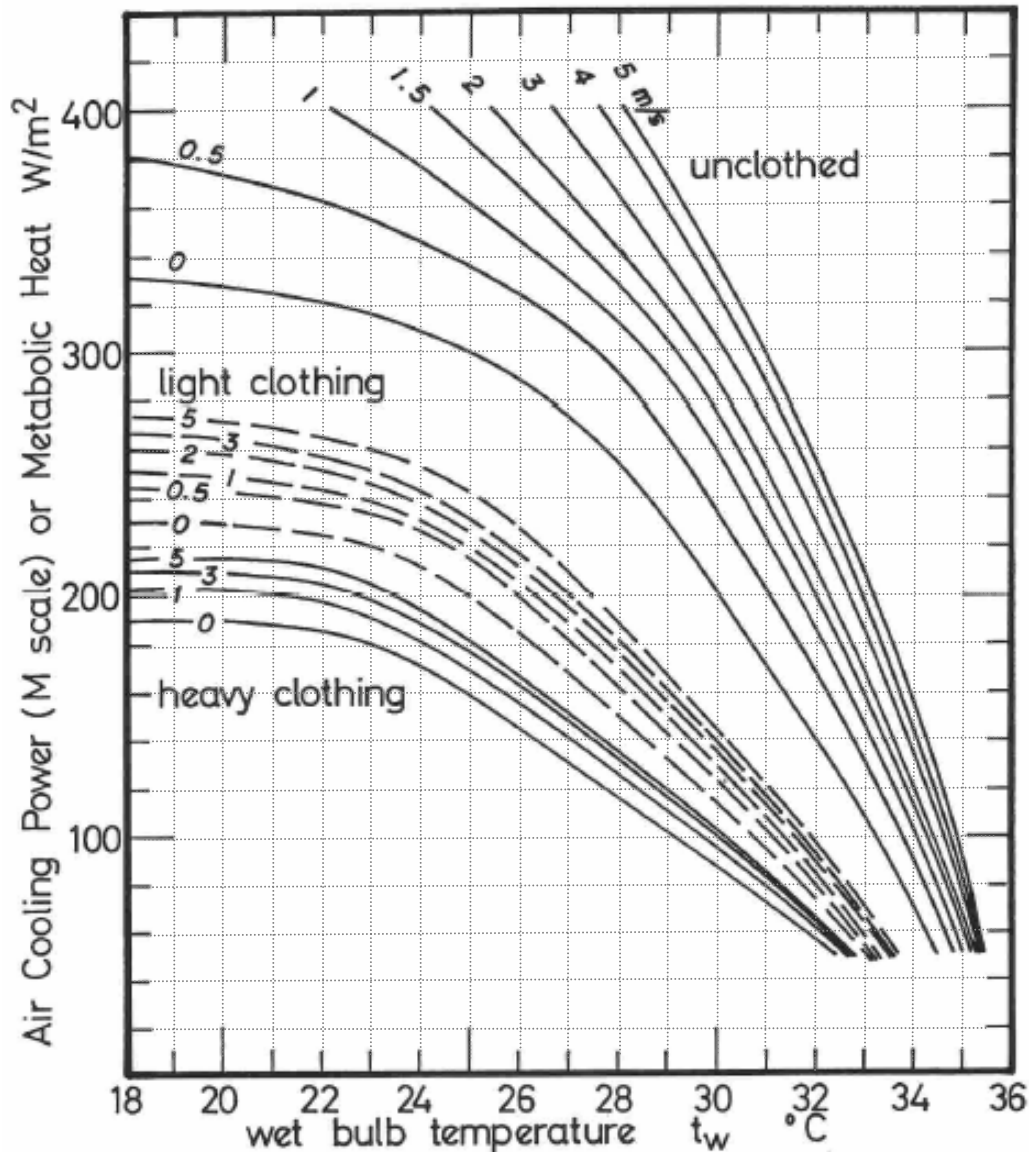


Figure 17.9 Air Cooling Power (M scale) or ACPM chart.
[Based on $t_d = t_r = t_w + 5^{\circ}\text{C}$ and $P = 100 \text{ kPa}$]

As the effects of dry bulb temperature, radiant temperature and barometric pressure are relatively weak in underground environments, the ACPM chart may be used without undue error for wet bulb depressions from 2 to 8 $^{\circ}\text{C}$ and for the range of atmospheric pressures that normally exist in

mine workings. The computer model listed in Appendix A17.1 can be used to develop similar charts for any other specified conditions. Air cooling charts have the advantage that they are based on a thermoregulation model and can also be used to assess the acceptability of existing workplace conditions.

Example 1

In a mine working, the wet bulb temperature is 28°C and the air velocity is 1 m/s. Estimate the limiting rates of continuous work for unclothed, lightly clothed and heavily clothed personnel.

Solution

From Figure 17.9 the three values of air cooling power at $t_w = 28^\circ\text{C}$ and $u = 1$ m/s are estimated at:

unclothed: 313 W/m² lightly clothed: 168 W/m² heavily clothed: 127 W/m²

Table 17.1 may be used to relate these cooling powers to types of work activity.

Example 2

It is predicted that in a future subsurface development the air velocity will be 2 m/s. If personnel are to sustain a metabolic rate of 220 W/m² while lightly clothed, estimate the upper limit of psychrometric wet bulb temperature.

Solution

From the light clothing curves on Figure 17.9, at an air velocity of 2 m/s and an air cooling power of 220 W/m², the limiting wet bulb temperature is estimated at 25.6°C.

Example 3

Acclimatized mine employees are required to work in a location where the wet bulb temperature is 29 °C. The workrate will be moderate with occasional extra effort. Recommend the type of clothing and the minimum air velocity to minimize the probability of unacceptable heat stress.

Solution

From Table 17.1 an average metabolic heat production rate is estimated at 260 W/m². Plotting a point at $M = 260$ W/m² and $t_w = 29^\circ\text{C}$ on the Air Cooling Power (M scale) chart of Figure 17.9 shows that it lies close to an air velocity of 0.5 m/s in the unclothed region. Hence, the recommendation is that these workers should wear no more than brief shorts, boots and hardhats, and that the air velocity should not be less than 0.5 m/s.

17.4.4.2 Specific Cooling Power (A scale), ACPA

The original concept of air cooling power as employed in this chapter arose from pioneering work conducted by the Chamber of Mines Research Organization of South Africa (Mitchell and Whillier, 1972; Wyndham, 1974; Stewart and Whillier, 1979; Stewart, 1982). This involved detailed analytical investigations as well as some thousands of tests in a large environmentally controlled and monitored wind tunnel. A thermoregulation model was developed on the basis of the physiological heat transfer equation (17.3). That model was restricted to the hot and humid conditions prevalent in the stopes of deep South African gold mines. In those conditions the influence of respiratory cooling is relatively small and was ignored. The model was further confined to fully wetted and unclothed personnel. An air cooling power chart was produced for the specific conditions of $t_{cl} = t_r = t_w + 2^\circ\text{C}$ and $P = 100$ kPa and for wet bulb temperatures in the range 25 to 35°C (Stewart, 1982). This was termed the Specific Cooling Power (A Scale) chart and yielded curves that are comparable to those given for unclothed personnel on Figure 17.9 within that range of wet bulb temperature.

17.4.5 Choice of heat stress index.

With such a variety of heat stress indices the question arises on when to employ an empirical or rational index. It would be impractical to conduct measurements of physiological response (e.g. body core temperature, sweat rate or mean skin temperature during normal mining operations. Hence, for routine manual monitoring of the workplace empirical indices are usually preferred by supervisors (Section 17.4.3)³. The values obtained for the preferred empirical index can then be compared with limits of acceptability that have been estimated from controlled experiments on volunteers (e.g. Figures 17.7 and 17.8).

As the reliability and costs of handheld cooling power instruments continue to improve we may see these being more widely used for routine workplace monitoring. Similar devices might also be incorporated into minewide monitoring systems for hot mines.

Where computer simulation programs are employed to predict climatic conditions in planned future workings a wider choice is available. Provided that the relevant variables of environmental temperatures and air velocities are produced by the simulation package then one or more of the empirical indices of heat stress can again be shown. However, a thermoregulation model may also be included in the simulation package in order to predict one or more of the physiological responses. The latter can be used as a direct and more precise indicator of the level of heat stress experienced by workers for specified types of clothing and rates of physical work. For example, in the CLIMSIM package (Chapter 16) the empirical indices produced are effective temperature and wet bulb globe temperature. Additionally, the thermoregulation model listed in Appendix A17.1 is incorporated within CLIMSIM in order to predict mean skin temperature as an indication of physiological reaction and to give warnings of impending heat stress (see Case Study, Section 16.3.3).

17.5 HEAT ILLNESSES

The human thermoregulation system depends upon the efficient operation of the core and skin temperature receptors, the flow of blood throughout the body but particularly between the core and skin tissues, and the production of perspiration. If any of these mechanisms loses its effectiveness then the body will progressively exhibit the symptoms of one or more of a series of disorders known collectively as the heat illnesses. These may arise as separate and recognizable ailments with identifiable causes. However, for workers in hot and humid environments they can occur in combination.

A common initial symptom is a loss of interest in the task and difficulty in remaining alert. In any adverse environment, the desire to seek more comfortable surroundings is a psychological reaction that is just as much a part of the body's defence mechanism as thermoregulatory effects. Suppression of such predilection may result in irritability or displays of anger. This may be observed even in persons who are cognizant of the effect. The physical symptoms often reveal themselves first as a loss of coordination and dexterity.

It follows, even from these initial symptoms of heat strain, that both manual and mental work productivity will suffer, morale is likely to be low, absenteeism high and standards of safety will decline in environments that are unduly hot. This is true for either a labour intensive method of working or one that is heavily mechanized.

³ However, Air Cooling Power Charts (e.g. Figure 17.9) are also directly applicable to existing workplaces.

Heat illnesses are introduced in the following subsections and in order of increasing seriousness. However, it should be remembered that symptoms may overlap and, in cases of doubt, it should be assumed that the patient is a victim of heat stroke.

17.5.1 Heat fainting

This occurs most frequently when a person stands still for an extended period in a warm environment. Blood tends to pool in the lower parts of the body causing a temporary reduction in blood supply to the brain and, hence, a short term loss of consciousness. A common example arises when soldiers in heavy uniform are required to remain motionless for long periods of time during ceremonial parades.

The treatment is simply to restore an adequate supply of blood to the brain by allowing the patient to lie flat in a cooler area and to loosen or remove clothing. Recovery is normally rapid and complete. The probability of heat fainting is reduced by intermittent body movements.

17.5.2 Heat exhaustion

Conductance of heat within the body is facilitated primarily by the flow of blood. If the volume of blood is insufficient then heat exhaustion may ensue. A decrease in blood volume may result from dehydration caused either by an inadequate intake of fluids or by a salt deficient diet. Alternatively, a combination of environmental heat stress and metabolic rate may cause the heartbeat to exceed some 180 bpm. The inadequate time interval between contractions of heart muscles may then be insufficient to maintain an adequate supply to the heart chambers - the rate of blood flow drops. A significant increase in total volume of blood occurs during periods of heat acclimatization.

The additional symptoms of heat exhaustion are

- tiredness, thirst, dizziness
- numbness or tingling in fingers and toes
- breathlessness, palpitations, low blood pressure
- blurred vision, headache, nausea and fainting
- clammy skin that may be either pale or flushed.

On the spot treatment should include removal to a cool area and administration of moderate amounts of drinking water. If the patient is unconscious then heat stroke should be assumed. In any case, a medical examination should be carried out before the victim is allowed to return to work.

17.5.3 Heat cramps

If the electrolytic balance of body fluids is sufficiently perturbed then painful muscular contractions occur in the arms, legs and abdomen. This may occur by salt deficiency or drinking large amounts of water following dehydration. Medical opinion no longer favours salt tablets but recommends a diet that provides a more natural supply of salt. However, immediate treatment may include the administration of fluid containing no more than 0.1 per cent salt.

17.5.4 Heat rash

This is sometimes known as **prickly heat** by residents of equatorial regions. It is caused by unrelieved periods of constant perspiration. The continuous presence of unevaporated sweat produces inflammation and blockage of the sweat ducts. The typical appearance of the ailment is

areas of tiny red blisters causing irritation and soreness. Although not serious in itself, heat rash may lead to secondary infections of the skin and, if sweat rates are sufficiently inhibited, may produce an increased susceptibility to heat stroke. Heat rash can be prevented by frequent bathing and the provision of cool living quarters.

Skin irritations can also occur in the hot, dry environments of some evaporite mines, especially at areas of skin contact with hat bands or protective devices.

17.5.5 Heat stroke

The most serious of the heat illnesses, heat stroke, may occur when the body core temperature rises above 41°C. Co-ordination of the involuntary nervous system, including body thermoregulation, is achieved by means of proteins controlled by the hypothalamus, part of the brainstem. At temperatures in excess of 41°C, damage to those proteins results in the transmission of confused signals to the muscles and organs that control involuntary reactions. Furthermore, irreversible injury may be caused to the brain, kidneys and liver. Heat stroke carries a high risk of fatality.

The initial symptoms of impending heat stroke are similar to those of the less serious heat illnesses, i.e. headaches, dizziness, nausea, fatigue, thirst, breathlessness and palpitations. If the patient loses consciousness, then heat stroke should be assumed. The additional symptoms arise from disruption of the thermoregulatory and other nervous systems of the body:

- perspiration ceases, the skin remains hot but is dry and may adopt a blotchy or bluish colouration.
- disorientation may become severe involving dilated pupils, a glassy stare and irrational or aggressive behaviour.
- shivering and other uncontrolled muscular contractions may occur.
- there may be a loss of control of bodily functions.

Although treatment should commence as soon as possible, current medical opinion is that the patient should not be moved until core temperature has been brought under control. The administration of first aid should include:

- Cooling by air movement and the application of water to the skin. The water temperature should be not less than 15°C in order to avoid vasoconstriction of the skin blood capillaries. Massaging the skin also assists in promoting blood flow through the surface tissues.
- The application of CPR (cardiopulmonary resuscitation) in cases where perceptible heart beat or respiration are absent. This includes chest massage and mouth-to-mouth breathing.
- Frequent sips of water if the patient is conscious.

Medical assistance should be sought and treatment continued until the core temperature falls below 38.5°C. The patient should then be covered by a single blanket and transported by stretcher to hospital. Unfortunately, death or permanent disability may still occur if irreversible damage has occurred in vital organs. Even after physical recovery, the heat tolerance of the victim may be impaired, perhaps permanently.

17.5.6 Precautions against heat illnesses

There is a great deal that can be done to protect a workforce against unacceptable heat strain. First, the design and engineering control of the ventilation and air quality systems of the mine or facility should be directed toward providing a safe climatic environment within all places where

personnel work or travel routinely. If threshold limit values for climatic parameters have not been set by legislative action, then they should be chosen and enforced by self-imposed action of the mine or industry. Cool and potable **drinking water** should be available to workers in hot mines.

Clothing that is appropriate for the work environment and level of activity should be worn by personnel. In hot environments, this may mean very little clothing or lightweight garments that are loosely weaved, porous and absorbent. For unusual circumstances such as rescue operations where personnel are occasionally required to enter hot areas that do not meet the criteria of climatic acceptability, **microclimate protective garments** may be used as a short-term and temporary measure. Such devices typically take the form of specialized jackets that contain distributed pockets to hold solid carbon dioxide (dry ice), cooled gels or water ice. The microclimate garments are worn over underclothing in order to avoid ice burns. Outer clothing reduces direct heat transfer from the surroundings. It is important that this type of microclimate jacket is changed before the cooling medium is exhausted, as the garment may then become an effective insulator. More sophisticated microclimate suits, incorporating temperature controlled fluids circulating through capillary tubing, have also been manufactured. However, these are expensive and less applicable to mining environments.

A workforce that is required to work in hot environments should be trained to recognize the initial symptoms of heat strain and to adopt sensible work habits. The latter include appropriate, but not excessive, rest periods and adequate consumption of cool drinking water. A good dietary balance should be sought that includes sufficient but, again, not excessive salt. Vitamin C supplementation is also regarded as improving heat tolerance (Visagie, 1974).

Finally, workers should have been subjected to a process of natural or induced acclimatization prior to being employed in particularly hot conditions (Section 17.7).

17.6 COLD ENVIRONMENTS

This chapter is concerned primarily with physiological reactions to heat. However, personnel at mines or other facilities that are located in cold climates or at high altitudes may be subjected to low temperatures for at least part of the year. Even in the more temperate zones, workers in main intake airways may suffer from cold discomfort during winter seasons. It is, therefore, appropriate that we include the effects of cold environments on the human body.

17.6.1 Physiological reactions to cold environments

Heat loss from the clothed body in cold surroundings is mainly by convection with lesser amounts by radiation and respiration. The most important climatic parameters in these circumstances are ambient (dry bulb) temperature and air velocity. These may be combined into an equivalent wind chill temperature (Section 17.6.3).

As heat loss occurs, the initial behavioural response is to don additional clothing and to increase metabolic heat production by conscious muscular activity. Involuntary physiological reaction is initiated by reductions in either the body core temperature or mean skin temperature and consists of an increase in muscular tension. In skin tissues, this causes the familiar "gooseflesh" and progresses into **shivering** within localized muscle groups. This may result in metabolic heat generation being raised by up to 120 W/m^2 . With further cooling, the degree of shivering increases to encompass the whole body, producing as much as 300 W/m^2 of metabolic heat and effectively incapacitating the person.

If the core temperature falls below 35°C, the body thermoregulation system will be affected. Core temperatures of less than 28°C can prove fatal, although successful recovery of individuals has been achieved from core temperatures of less than 20°C. The subjective feeling of comfort depends upon the mean skin temperature and also the surface temperature of the extremities. Commencing from the neutral mean skin temperature of 34°C, this table shows subjective reactions that have been reported for sedentary persons. However, the increased blood flow caused by a medium or hard work rate may enable reduced values of mean skin temperature to be tolerated.

Mean skin temperature °C	Subjective response
31	uncomfortably cold
30	shivering
29	extremely cold
25	limit of tolerance without numbing

The large surface to volume ratio of fingers, toes, and ears maximizes heat loss while the influence of **vasoconstriction** is particularly effective in reducing blood flow to those areas. The latter is a natural reaction to protect, preferentially, the vital organs within the body core. However, it can give rise to severe discomfort and tissue (frost) damage to the extremities. The following reactions to **hand surface temperatures** have been reported:

20°C	uncomfortably cold
16°C	limit of finger dexterity
15°C	extremely cold
5°C	painful

Skin surface temperatures some 1.5 to 2.0°C higher produce similar reactions at the feet.

17.6.2 Protection against cold environments

Human beings have been described as “tropical animals” inasmuch as our thermoregulation is much more effective in warm environments. In cold conditions we rely more on the behavioural response of donning extra clothing and/or engaging in additional muscular activity.

The first line of defence against any potentially adverse environment in the subsurface is the initial design and subsequent control of the ventilation and air conditioning systems. Methods of heating mine air are discussed in Section 18.4. These are subject to economic limitations and can lead to problems of strata control if the mine is within permafrost. It may, therefore, be necessary to provide means of personal protection against a cold working environment.

Personnel should be instructed on physiological reactions to cold ambient surroundings and, particularly, on the use of protective clothing. The **thermal insulating properties of garments** depend upon the entrapment of air rather than the fibres of the material. The incorporation of radiation reflective layers can also be helpful. A compromise must be sought between the body movements required to perform the work and the restraint offered by bulky insulated clothing. An ambient temperature of -35°C appears to be the practical limit for many activities while, at -50°C only short term exposure should be permitted. Protection to the hands and feet is particularly important but does, of course, affect dexterity. Auxiliary heating of some 10W to each hand and foot allows activity to continue at even lower temperatures provided that the rest of the body is well insulated.

Facial tissues do not suffer unduly from vasoconstriction. Hence, face masks are usually unnecessary. However, the effects of wind chill can result in freezing of exposed skin. Fur-lined hoods should be used to avoid direct wind on the face at low ambient temperatures. Pre-heating inspired air is not required for healthy individuals for air temperatures down to -45°C.

A limited degree of cold acclimatization can occur in personnel who have been subjected to frequent exposure. An improved blood flow to skin tissues gives increased circulation to the

extremities and reduces the risk of frostbite. Additional heat is also generated by the metabolism of body reserves of adipose (fatty) tissue.

17.6.3 Indices of cold stress

A series of experiments were carried out by Siple and Passel (1945) in Antarctica involving rates of cooling by convection and radiation from a plastic cylinder of 5.7 cm diameter whose surface temperature was 33°C. This led to an empirical formulation known as the **Wind Chill Index**, WCI, which described the rate of heat loss from the cylinder. When expressed in SI units, this becomes

$$\text{WCI} = 1.163(10.45 + 10\sqrt{u} - u)(33 - t_d) \quad \text{W/m}^2 \quad (17.40)$$

where u = air velocity (m/s) and t_d = dry bulb temperature (°C)

Although the Wind Chill Index is open to criticism arising from the differences in heat transfer phenomena between a small plastic cylinder and a human body, it has been used as a basis for the more commonly employed **Equivalent Wind Chill Temperature**, t_{eq} . This is defined as the ambient temperature in an airstream moving at 1.79 m/s (4 mph) that gives the same WCI (rate of cooling) as the actual combination of air temperature and velocity. That definition leads to the equation

$$t_{eq} = 33 - \frac{(10.45 + 10\sqrt{u} - u)(33 - t_d)}{22} \quad \text{°C} \quad (17.41)$$

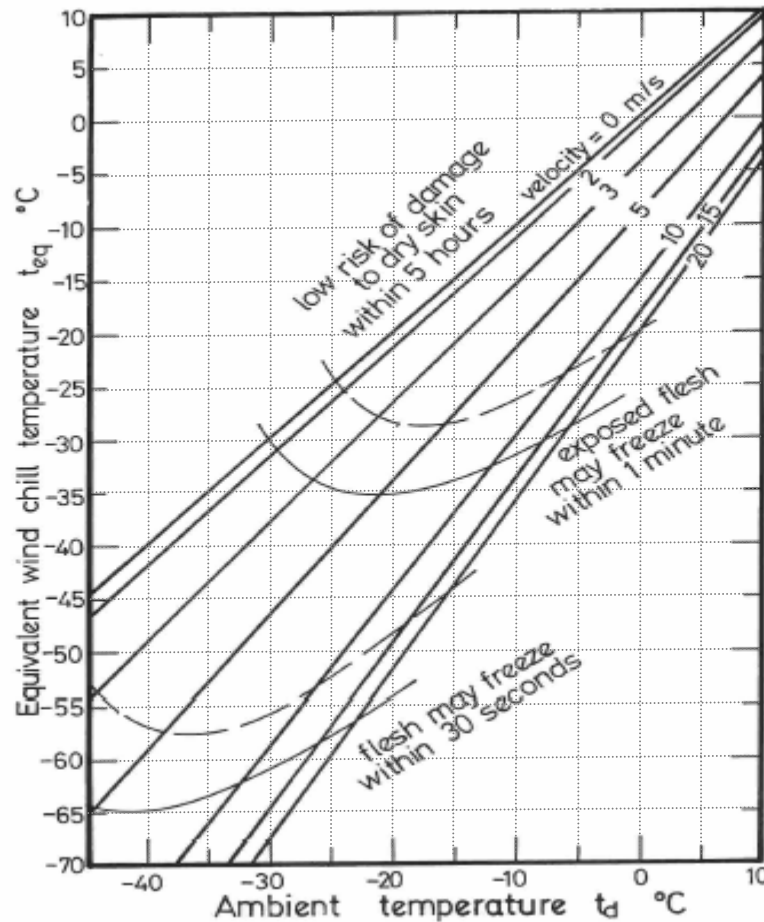


Figure 17.10 Equivalent wind chill temperature (developed from data reported by the U.S. Army Research Institute of Environmental Medicine).

This relationship may be employed for air velocities not less than 2 m/s. Figure 17.10 gives a graphical depiction of equivalent wind chill temperature. It is important to remember that t_{eq} is indicative of a rate of cooling rather than a physical temperature. The ambient temperature, t_d , controls the limit to which any body can cool and is independent of air velocity.

17.7 HEAT TOLERANCE AND ACCLIMATIZATION

In any mine or other subsurface facility where the wet bulb temperature exceeds 25°C, it is advisable to consider means of combatting potential heat strain within the workforce. The return on such efforts is shown not only by a decreased risk of heat illnesses but also improvements in safety statistics and productivity. This section considers procedures of physiological testing and the acclimatization procedures that may be conducted on personnel prior to their employment in hot conditions.

Much of the research and development on heat stress and acclimatization procedures for hot mines has been carried out for the gold mining industry of South Africa. Most of the information given in this Section originates from that work (e.g. South African Department of Minerals and Energy, 2002; Bluhm and von Glehn, 2006; Burrows, 1989; Stewart, 1982).

Prior to 1990, the primary objective of heat stress procedures practiced in South Africa was to reduce the incidence of heat stroke for persons who worked in deep gold mines. It was not uncommon for wet bulb temperatures to reach 32 °C in stoping areas. Following initial screening and work/heat tolerance tests to identify the heat intolerant, new and returning mine recruits underwent acclimatization procedures over several days in surface-located climatic chambers. For historical interest those former procedures are outlined in Appendix A17.2.

Since the early 1990s the approach has changed. First, a determined effort was undertaken to reduce wet bulb temperatures to not more than 28 °C in active mining zones. Secondly, the primary objective of reducing heatstroke has given way to a more general form of risk assessment through an approach known as **Heat Stress Management**. This also includes revised procedures of initial screening and heat tolerance tests but is followed by a natural progression of supervised on-the-job heat acclimatization. The combination of reduced wet bulb temperatures and the more holistic approach of Heat Stress Management has enabled the elimination of several days spent in surface acclimatization chambers.

17.7.1 Physiological tests

17.7.1.1 Initial screening

The initial screening of new or returning recruits who will work in hot conditions in South Africa's gold mines consists of two parts. First, a general medical examination is carried out on each candidate. In addition to health checks this examination includes the medical, occupational and heat disorder history of each recruit being recorded within a database.

Secondly, a separate physical evaluation is carried out to identify features that would indicate unsuitability for physical work in hot environments. These factors include:

Age

Tolerance to heat declines with age, a trend which accelerates rapidly over the age of 40 years. A general recommendation is that persons of 50 years or more should not normally undertake strenuous activities in hot environments.

Body dimensions.

Both body mass and Body Mass Index (BMI) should be recorded during the physical examination. The latter is defined as:

$$\text{BMI} = \frac{\text{body mass}}{\text{height}^2} \quad \frac{\text{kg}}{\text{m}^2} \quad (17.42)$$

Table 17.4 gives recommendations of the Department of Minerals and Energy, Mine Health and Safety Inspectorate of South Africa, 2002.

Employee status	Criterion/Standard	Recommendation
New or returning recruit	Body mass < 50 kg	Unsuitable: reject
	Body mass 50 to 55 kg	Suitable but not for strenuous work
	BMI: 15 to 29	Suitable
	BMI: 30 to 35	Suitable if no medical concerns
	BMI > 35	Unsuitable: reject
Existing worker	Body mass < 45 kg	Unsuitable: reject
	Body mass 45 to 50 kg	Suitable if no medical concerns or history of heat disorders
	Body mass 45 to 55 kg	No allocation to strenuous work (i.e. $M > 160 \text{ W/m}^2$)
	BMI < 15	Unsuitable
	BMI: 15 to 19	Suitable if no medical concerns or history of heat disorders
	BMI: 20 to 29	Suitable
	BMI: 30 to 35	Suitable if no medical concerns or history of heat disorders
	BMI > 35	Unsuitable

Table 17.4. Body mass and Body Mass Index criteria for physical work in hot environments.

Source: Department of Minerals and Energy, Mine Health and Safety Inspectorate of South Africa, 2002.

http://www.dme.gov.za/pdfs/mhs/guidelines/thermal_stress.pdf

17.7.1.2 Heat Tolerance Screening

The aim of heat tolerance screening is to identify persons who are likely to suffer from heat stress while working in hot environments. It is also indicative of the physical fitness of the individual.

The procedure commences with a rest period of 30 minutes in an environment that feels comfortable to men wearing shorts only. Candidates who have oral temperatures greater than 37 °C at the end of the rest period are excused from the heat tolerance screening and referred for further medical evaluation.

The heat tolerance screening itself consists of a 30 minute period during which the test subjects undertake a bench-stepping procedure at a rate of 24 steps per minute to a bench height of 30.5 cm. This approximates to a work rate of 80 W. One step consists of raising the upright body such that both feet are placed on the bench then back to the floor. The climate should be maintained at a dry bulb temperature of 29.5 °C and a wet bulb temperature of 28 ± 0.3 °C while the air velocity is maintained within the range 0.3 to 0.5 m/s.

Individuals whose oral temperature at the end of the test does not exceed 37.6 °C are deemed to be able to acclimatize successfully under supervision in the mine environment. Those with oral temperatures higher than 37.6 °C are recognized as heat intolerant and will not be required to work in hot areas of the mine.

17.7.2 Acclimatization

17.7.2.1 In-situ acclimatization

For candidates who have successfully passed the medical, physical and heat tolerance screenings, full acclimatization can be expected within some 12 successive work shifts in hot conditions. During this time physiological changes take place which reduce susceptibility to heat stress. Formal supervision must be provided during the period of acclimatization. Supervisors should be capable of measuring wet and dry bulb temperatures, recognizing signs of ill health and heat stress, ensuring that potable water is available and trained in emergency treatments.

Workers in hot conditions should be trained to recognize symptoms of heat stress, not only in themselves but also in fellow workers. The training should also encompass good work practices such as self-pacing of physical work and the use of rest periods. The latter may be imposed by management.

It is important to remember that acclimatization does not provide immunity against heat illnesses, including heat stroke, if good work practices are not maintained on a permanent basis. A loss of full acclimatization can occur after missing only a few days of work in hot conditions. Similarly, if exposure to those conditions occurs only intermittently full acclimatization will neither occur nor be maintained. Hence, visits by persons such as senior officials or visitors should take place only while accompanied by acclimatized supervisors.

17.7.2.2 Physiological changes during acclimatization

During the process of acclimatization, several significant physiological changes take place that enhance the effectiveness of the body thermoregulation system. These are accompanied by a noticeable psychological improvement. Acclimatization produces a dramatic increase in blood volume, averaging about 25 per cent. This, in turn, results in several beneficial reactions. First, there is an improvement in the response of blood flow conductance to increased metabolic heat production or greater heat stress. Coupled with an enhanced elasticity in the walls of blood vessels, this allows a greater flow of blood both to internal organs and to skin tissues. As a consequence, both core temperature and heartbeat decrease for any given workrate and level of environmental heat stress.

There is also a dramatic increase in sweat rate for any given core temperature during acclimatization. Perspiration commences at a lower core temperature, increasing the range and efficiency of evaporative cooling. The improved ability to produce sweat appears also to be associated with the increased blood volume as well as enhanced performance of the sweat glands.

Finally, acclimatization raises the mechanical efficiency of the human body, i.e. any given task is achieved with a lower production of metabolic heat. This, again, results in a lower core temperature and reduced thermal strain.

The combined effect of the changes obtained through acclimatization is that the worker can perform appropriate tasks in hot conditions more efficiently, with a greatly reduced risk of heat illness, and in a more stable psychological state.

17.8 EFFECT OF MINE CLIMATE ON PRODUCTIVITY

From a consideration of the psychological as well as physiological effects of hot working conditions, it can be expected that as the cooling power of the ambient airstream decreases below some 300 W/m^2 , personnel will become substantially less effective. There will be a deterioration in the rate and quality of individual work performance. Unduly hot conditions may result in poor morale and are likely to produce increased accident rates and problems of absenteeism.

However, the same difficulties can arise from other causes including standards of supervision, management style and labour relations, geological conditions and legislative requirements. For this reason, few studies have been reported that give quantified relationships between mine environmental conditions and those factors that contribute to overall mine productivity. It is, however, relatively easy to demonstrate the debilitating influence of heat on individual work performance. Figure 17.11(a) summarizes results obtained from monitoring the effectiveness of acclimatized men engaged in manual work in a heading (Poulton, 1970). The work consisted of shovelling fragmented rock into ore cars. The temperature of the near saturated air and the air velocity at the workplace were varied to give the range of effective temperatures (Section 17.4.3.1) shown on the figure. The work performance at an effective temperature of 22°C was taken to represent 100 per cent. The results show that work efficiency begins to suffer at an effective temperature of about 27°C and declines rapidly when the effective temperature exceeds 30°C . The latter approximates to an air cooling power of some 270 W/m^2 for unclothed personnel.

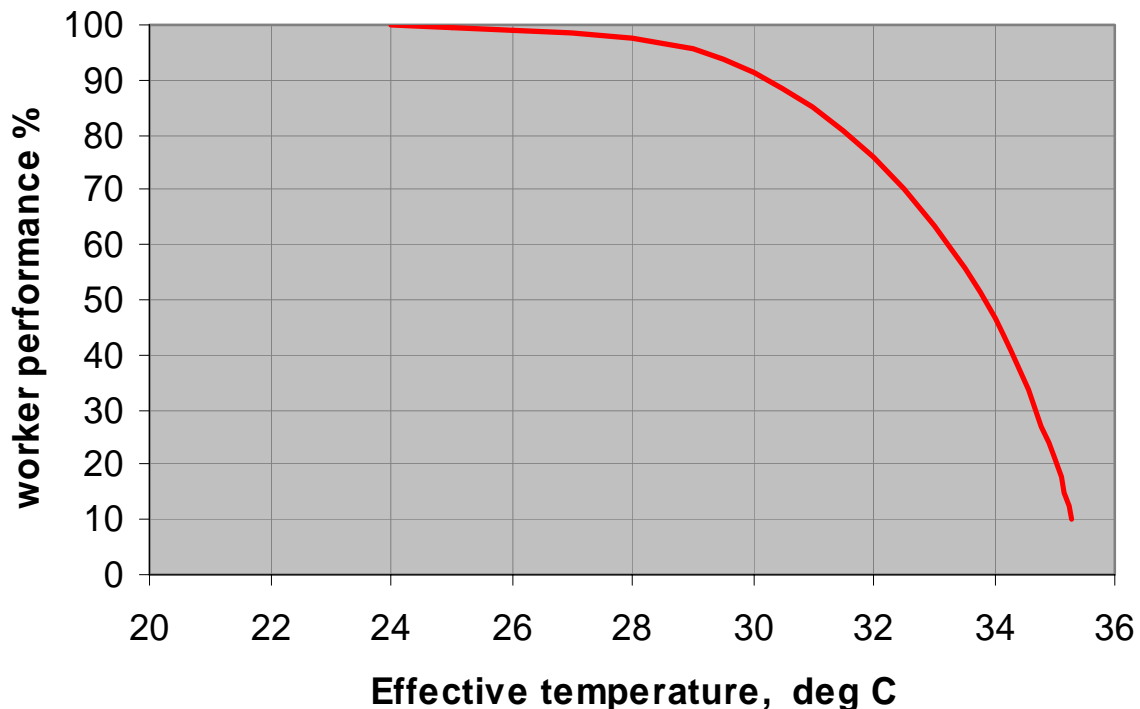


Figure 17.11(a) Influence of Effective Temperature on worker performance(after Poulton). Performance is expressed as a percentage of the largest value reported.

Figure 17.11 (b) depicts results reported in a comprehensive study by Howes (1978) using statistics collated by the Chamber of Mines for gold mines in South Africa. The air cooling power used in this figure was an early version of the ACP (A scale).

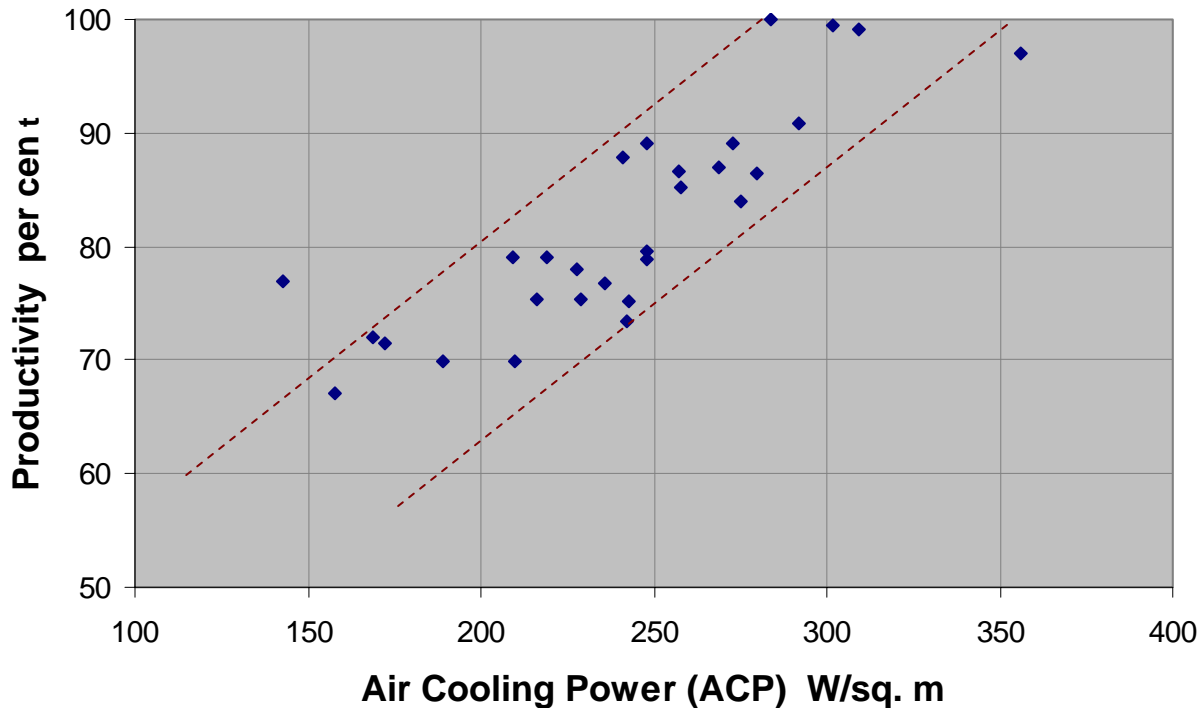


Figure 17.11(b) Effect of Air Cooling Power on mine productivity (after Howes).
Productivity is expressed as a percentage of the largest value reported.

The correlation between Figures 17.11 (a) and (b) is clear for a labour intensive operation. However, any environment that causes physical discomfort will involve a decline in standards of care and attention. The potential for accidents and loss of production is greater in a mechanized operation where an error made by a single person can have serious repercussions. Low morale and the irritability that often appear as an early symptom of heat strain can easily lead to strained industrial relations. This can have disastrous effects on overall mine profitability. Furthermore, the costs of the additional personnel that are required to compensate for absenteeism in hot mines can be high in an expensive labour market.

Failure to create a reasonably comfortable working environment underground not only puts the health and safety of the workforce at risk, it also results in lower productivity and profitability.

References

- ASHRAE (1985, 1989 and 1993).** American Society of Heating, Refrigerating and Air Conditioning Engineers. Fundamentals Handbooks.
- Bluhm, S. and von Glehn, F (2006).** Private communication.
- Botsford, J.H. (1971).** A wet globe thermometer for environmental heat measurement. American Industrial Hygiene Assoc. Journal: 38, 264
- Brake, R. and Bates, G, (2002).** A valid method for comparing and rational and empirical heat stress indices. Ann. Occupational Hygiene, Vol. 46, No.2. pp. 165-174. Published by Oxford University Press.
- Burrows, J.H. (1989).** Private communication.
- Chamber of Mines of South Africa (1972).** Routine mine ventilation measurements. Johannesburg.
- Ciriello, V.M. and S.H. Snook, 1977.** The prediction of WBGT from the Botsball. American Industrial Hygiene Association Journal, 38(June): p. 264-271.
- Dreosti, A.O. (1935).** Problems arising out of temperature and humidity in deep mines of the Witwatersrand. J. Chem, Metall, Min. Soc. of S. Africa, Vol. 36, pp 102-129.
- duBois, D. and duBois, E.F. (1916).** A formula to estimate approximate surface area if height and weight are known. Archives of Internal Medicine. 17: pp. 863-871.
- Fanger, P.O. (1970).** Thermal comfort. Danish Technical Press. Copenhagen.
- Gagge, J. et al (1969).** The prediction of thermal comfort when thermal equilibrium is maintained by sweating. ASHRAE Trans. Vol. 75 Part 2 p.108.
- Hanoff, J.S.T. (1970).** Investigation of the limit of tolerable stresses to men subjected to climatic and working conditions in coal mines. Glückauf-Forschung. Vol. 31 (4). pp. 182-195.
- Hill, L. Griffith, O.W. and Flack, M. (1916).** The measurement of the rate of heat loss on body temperature by convection, radiation and evaporation. Phil. Trans. Royal Soc., Section B (London) Vol. 207 pp 183-220.
- Houghton, F.C. and Yaglou, C.P. (1923).** Determining lines of equal comfort. ASHVE Trans. Vol. 29 pp.163-176 and 361-384.
- Howes, M.J. (1978).** The development of a functional relationship between productivity and the thermal environment. J. Mine Vent. Soc. of S. Africa, Vol. 31, pp 21-38.
- International Organisation for Standardization (1982).** Hot environments - Estimation of the heat stress on working man, based on the WBGT (wet bulb globe temperature). ISO Standard 7243 (See also Standard 7730, 1984).
- Mitchell, D. And Whillier, A. (1972).** The cooling power of underground environments. Journ. Mine Ventilation Soc. of S.Africa. Vol 25, pp 140-151.

NIOSH (1986). Criteria for a recommended standard – Occupational exposure to hot environments, revised criteria. U.S. Dept. of Health and Human Services, USDHHS (NIOSH) publication 86-113.

Onkaram, B. et al (1980). Three instruments for assessment of WBGT and a comparison with WGT (Botsball). American Industrial Hygiene Assoc. 41: pp. 634-641.

Oohori, T. et al (1984). Comparison of current two-parameter indices of vapor permeation of clothing as factors governing thermal equilibrium and human comfort. ASHRAE Trans. Vol. 90 (2).

Poulton, E.C. (1970). Environment and human efficiency. C.C. Thomas, Springfield, Illinois, U.S.A.

Siple, P.A. and Passel, C.F. (1945). Measurements of dry atmospheric cooling in subfreezing temperatures. Proc. Americ. Philosophical Soc., Vol. 89, p.177.

South African Department of Minerals and Energy, Mine Health and Safety Inspectorate (2002). Guideline for the compilation of a Mandatory Code of Practice for an Occupational Health Programme on Thermal Stress. 78pp.

http://www.dme.gov.za/pdfs/mhs/guidelines/thermal_stress.pdf

Stewart, J.M. (1982). Environmental engineering in South African mines, Chapters 20 and 21. Mine Ventilation Soc. of S. Africa.

Stewart, J.M. and Whillier, A. (1979). A guide to the measurement and assessment of heat stress in gold mines. Journ. Mine Ventilation Soc. of S.A. Vol. 32, No. 9. pp. 169-178.

Visagie, M.E. et al (1974). Changes in vitamin A and C levels in black mine workers. S. African Med. Journ. Vol. 48, pp. 2502-2506.

Windham, C.H. (1974). The physiological and psychological effects of heat. Chapter 7 The Ventilation of South African Gold Mines. Mine Vent. Soc. of S. Africa. pp 93-137.

Wu, H.W. and Gillies, A.D.S. (1997). The development of a personal response heat stress meter calibrated to the range of physiology of the range of employees within the mine workplace. Proc. 6th International Mine Ventilation Congress, Pennsylvania, U.S. pp. 255-261. Published by the Society of Mining Engineers.

Yaglou, C.P. and Miller, W.F. (1925). Effective temperatures with clothing. ASHVE Trans. Vol. 31 pp. 89-99.

APPENDIX A17.1**Listing of the thermoregulation model developed in Section 17.3.6**

The program is listed in the original BASIC language in which it was developed and can be translated into any other preferred language suitable for running on a personal computer. Alpha characters are printed in upper case for clarity.

The data required are indicated in lines 20 to 100 and the computed parameters identified in lines 560 to 790. The program cycles iteratively, varying the mean skin temperature and other dependent variables until the Air Cooling Power (M scale) equals the input metabolic rate. Mean skin temperatures in excess of 36°C generate a warning message.

```

10 OPEN "LPT1" FOR OUTPUT AS #1
20 INPUT "TW,TD (deg C),P(kPa) ",TW,TD,P
30 INPUT "RAD TEMP OF SURROUNDINGS (deg C) ",TR
40 P=1000*P
50 INPUT "RELATIVE AIR VELOCITY (m/s) ",UR
60 INPUT "CLOTHING RESISTANCE, RCL (degC m^2/W) ",RCL
70 INPUT "CLOTHING AREA RATIO,Fcl ",FCL
80 INPUT "CLOTH VAPOUR PERMEABILITY EFFICIENCY, Icl ",ICL
90 INPUT "METABOLIC RATE (W/m^2) ",M
100 INPUT "BODY VIEW FACTOR,Fr ",FR
110 IF UR<3 THEN 140
120 U=UR
130 GOTO 150
140 U=0.8*UR+0.6
150 T=TW
160 HC=.00878*P^.6*SQR(U)
170 GOSUB 930
180 SINT=S
190 GOSUB 1010
200 GOSUB 1050
210 TEX=32.6+(.066*TD)+(0.0002*E)
220 EA=E
230 GOSUB 1080
240 REM
250 REM RESPIRATORY HEAT, BR
260 T=TEX
270 GOSUB 930
280 SEX=S
290 BR=.0000017*M*(SEX-SINT)
300 REM
310 REM CONVECTIVE HEAT, C
320 CNV=(TSK-TD)/(RCL+1/(FCL*HC))
330 TCL=TSK-CNV*RCL
340 REM RADIATIVE HEAT, R
350 TCL=TSK-CNV*RCL
360 TAV=(TCL+TR)/2+273.15
370 HR=4*5.67E-08*(TAV)^3
380 R=HR*FR*(TCL-TR)
390 REM
400 REM EVAPORATIVE HEAT, EV
410 GOSUB 1190
420 IF TSK>32.5 THEN GOSUB 1410

```



```

430 T=TSK
440 GOSUB 850
450 HE=.0007*HC*L/P
460 GOSUB 810
470 RECL=RCL*P/(.0007*L*ICL)
480 EV=W*(ES-EA)/(RECL+1/(FCL*HE))
490 ACPM=BR+CNV+R+EV
500 PRINT TSK
510 IF ABS(ACPM-M)<1 THEN 560
520 TSK=TSK-.01*(ACPM-M)
530 W=W1
540 IF TSK>32.5 THEN GOSUB 1410
550 GOT0 310
560 PRINT #1,"ACPM = ",:PRINT #1,USING "####";ACPM;:PRINT #1," W/m^2"
570 PRINT #1,"TCLOTH = ",:PRINT #1,USING "###.##";TCL;:PRINT #1," C  ",
580 PRINT #1,"SKIN TEMP = ",:PRINT #1,USING "###.##";TSK;:PRINT #1," C"
590 IF TSK>=36 AND TSK<37 THEN PRINT #1,"***ONSET OF HEAT STRAIN***":GOTO 610
600 IF TSK>=37 THEN PRINT #1,"*** DANGEROUS SKIN TEMPERATURE ***"
610 PRINT #1,"TEXHAUST = ",:PRINT #1,USING "###.##";TEX;:PRINT #1," C  "
620 PRINT #1,"SWEAT = ",:PRINT #1,USING "###.##";W
630 PRINT #1,"HC = ",:PRINT #1,USING "###.##";HC;:PRINT #1," W/m^2 C",
640 PRINT #1,"HR = ",:PRINT #1,USING "###.##";HR;:PRINT #1," W/m^2 C",
650 PRINT #1,"HE = ",:PRINT #1,USING "###.##";HE;:PRINT #1," W/m^2 Pa",
660 PRINT #1,"FCL = ",FCL
670 PRINT #1,"RECL = ",:PRINT #1,USING "###.###";RECL;:PRINT #1," m^2 Pa/W",
680 PRINT #1,"RCL = ",RCL
690 PRINT #1,"RESP = ",:PRINT #1,USING "###.##";BR;:PRINT #1," W/m^2  ",
700 PRINT #1,"CONV = ",:PRINT #1,USING "###.##";CNV;:PRINT #1," W/m^2"
710 PRINT #1,"RAD = ",:PRINT #1,USING "###.##";R;:PRINT #1," W/m^2  ",
720 PRINT #1,"EVAP = ",:PRINT #1,USING "###.##";EV;:PRINT #1," W/m^2"
730 PRINT #1,"SINT = ",:PRINT #1,USING "###.##";SINT*.001;:PRINT #1," kJ/kg  ",
740 PRINT #1,"SEX = ",:PRINT #1,USING "###.##";SEX*.001;:PRINT #1," kJ/kg"
750 PRINT #1,"LSK = ",:PRINT #1,USING "###.##";L*.001;:PRINT #1," kJ/kg  ",
760 PRINT #1,"EAIR = ",:PRINT #1,USING "###.##";EA*.001;:PRINT #1," kPa"
770 PRINT #1,"ESK = ",:PRINT #1,USING "###.##";ES*.001;:PRINT #1," kPa  ",
780 PRINT #1,"X = ",:PRINT #1,USING "###.###";X;:PRINT #1," kg/kg dry  "
790 PRINT #1,"MICRO VELOCITY = ",:PRINT #1,USING "###.##";U;:PRINT #1," m/s"
800 END
810 REM SAT VAP PRESS
820 ES=610.6*EXP(17.27*T/(237.3+T))
830 RETURN
840 REM
850 REM LATENT HEAT
860 L=(2502.5-2.386*T)*1000
870 RETURN
880 REM
890 REM MOISTURE CONTENT
900 X=.622*E/(P-E)
910 RETURN
920 REM
930 REM SIGMA HEAT
940 GOSUB 850
950 GOSUB 810
960 E=ES
970 GOSUB 890
980 S=L*X+1005*T

```

```

990 RETURN
1000 REM
1010 REM ACT. MOISTURE CONTENT
1020 X=(S-1005*TD)/(L+1884*(TD-TW))
1030 RETURN
1040 REM
1050 REM ACT VAP PRESS
1060 E=P*X/(.622+X)
1070 RETURN
1080 REM SKIN TEMP
1090 REM REF GAGGE, 1969
1100 TSK=24.85+.322*TD-.00165*TD*TD
1110 IF W<.9 THEN 1130
1120 TSK=24.49+.249*TD
1130 REM VELOCITY (HC) CORRECTION
1140 DTSK=8.999999E-03*HC*(TSK-TD)*(.15-RCL)/0.15
1150 TSK=TSK-DTSK
1160 REM CLOTHING CORRECTION
1170 TSK=TSK+(RCL/.15)
1180 RETURN
1190 REM SWEAT FRACTION
1200 IF TW> 27.194*EXP(-.004*M) THEN 1230
1210 W=0.06
1220 GOT0 1390
1230 IF TW<33 THEN GOT0 1260
1240 W=1
1250 GOT0 1390
1260 IF M>=200 THEN GOT0 1320
1270 A=-(.1781265E-04-2.544E-07*M+8.557743/M^2.218731)
1280 B=.012095-1.79735E-05*M+1063.187/M^2.31927
1290 C=-.194294-3.279531E-04*M+46903/M^2.44229)
1300 D=.998117-1.816454E-03*M+924321/M^2.651246
1310 GOT0 1360
1320 A=-(.397379E-05+7.075456E-08*M+17.880231/M^2.218441)
1330 B=2.369825E-03+3.359426E-06*M+2211.1688/M^2.316119
1340 C=-(-5.682282E-03+5.86905E-05*M+95583.18/M^2.437565)
1350 D=-.321605+7.958265E-04*M+1875636/M^2.645912
1360 W=D+TW*(C+TW*(B+TW*A))
1370 IF W<.06 THEN W=.06
1380 IF W>1 THEN W=1
1390 W1=W
1400 RETURN
1410 REM INCREASE W FOR TSK>32.5
1420 IF TSK<38 THEN 1450
1430 W=1
1440 GOT0 1480
1450 DW=SIN((31.85*TSK-762)*.01745)*.5+.5
1460 W=W1+DW
1470 IF W>1 THEN W=1
1480 RETURN

```

APPENDIX A17.2

Acclimatization of workers in South African gold mines prior to 1990.

This appendix is included for historical interest and is taken from the earlier printed version of this textbook. It reflects the philosophy and procedures of the South African gold mining industry relating to heat stress in underground workers before 1990. The updated procedures at the time of this current writing are outlined in Section 17.7 of the main text.

Physiological tests

Initial screening

An initial screening of recruits for work in wet bulb temperatures of more than 25°C should investigate both body mass and age. Any person with a body mass of less than 50kg is unlikely to have a skin surface area that is sufficient to ensure efficient body cooling. Conversely, individuals with a mass exceeding 100kg have a high and constant metabolic burden in supporting their own weight. No persons in either of these groups should be asked to work in hot environments. After the age of 40 years, the probability of heat stroke increases significantly. Although considerable variation exists between individuals, it is prudent to relocate persons of more than 45 years of age to zones of reduced heat stress.

Work capacity tests

A simple test of work capacity consists of a ten minute period of constant and controlled activity that requires an oxygen consumption rate of 1.25 litres per minute. At the conclusion of the period, the heartbeat provides an indication of maximum rate of oxygen consumption and, hence, work capacity. Persons with test heartbeats of over 140 bpm should be prohibited from tasks requiring hard manual exertion or from working in conditions of heat stress. If the test results indicate a heartbeat of less than 120 bpm then that individual should be capable of strenuous work. If the wet bulb temperature in the workings does not exceed 27.5°C the initial screening and the work capacity tests are all that are required.

Heat tolerance test

This more rigorous test may be carried out on persons who have passed both the initial screening and the work capacity tests, and who may be required to work in wet bulb temperatures in excess of 27.5°C. The test consists of requiring the participants to engage in a controlled activity corresponding to an oxygen consumption of 1.25 litres/minute for a period of four hours in a climatic chamber. The wet bulb temperature should be at least equal to the highest value that will be encountered within work areas in the mine.

Oral temperatures are taken at intervals of not more than 30 minutes throughout the test and the following criteria applied:

If oral temperature –

remains below 37.5°C:	person eligible immediately for work in hot mine environment
varies between 37.5 and 38.6°C:	eligible for short-term or micro-climate acclimatization
varies between 38.6 and 40.0°C:	eligible for full acclimatization
exceeds 40.0°C:	test terminated and person classified as heat intolerant

If it is suspected that heat intolerance is caused by a temporary illness or body disorder then the test may be repeated after treatment and recovery.

Heat acclimatization

The organized process of heat acclimatization may take place over a period of several days during which the participants are subjected to gradually increasing work rates and/or levels of heat stress. During this time, definite physiological changes occur that enable the human body to better resist the adverse effects of a hot environment.

The first attempts at organized acclimatization for work in hot mines appear to have been carried out in 1926 within the South African gold mining industry (Dreosti). Considerable effort was devoted to the improvement of acclimatization procedures and South Africa seems to have been the only country that provided formal acclimatization for the majority of recruits into deep and hot mines. However, advances in the design of ventilating and air conditioning systems have led to significant improvements in climatic conditions within those mines. The modern philosophy is to promote working environments that do not necessitate full acclimatization procedures.

Methods of acclimatization

There are essentially three methods of acclimatization for workers in hot environments. The first and, perhaps, most natural is for the individual to spend the first two weeks of underground work in tasks of increasing physical effort (or less frequent rest periods) within the actual mine environment. This may be combined with commencing in relatively cool areas of the mine and progressively moving the participants to locations of increased heat stress through the two week period.

Although such "on-the-job" acclimatization appears to be convenient, it does have significant drawbacks. If successful acclimatization is to be achieved, then the process must be monitored and controlled by well-trained supervisors. Work rates, body temperatures and psychrometric conditions must be logged and, if necessary, modifications made to the place or rate of work. Individuals who exhibit signs of heat intolerance must be identified before they suffer unduly from heat strain. Drinking water must be administered at frequent intervals. The difficulty is that such procedures do not blend readily into the production-oriented activities of a working stope or face. It is for this reason that "on-the-job" acclimatization has, in general, been less successful than the more easily controlled procedures.

For individuals whose oral temperature does not exceed 38.6°C during a heat tolerance test a shorter period of acclimatization may provide the required degree of protection. The use of micro-climate jackets during acclimatization may be deemed acceptable for candidates who are familiar with underground operations. For the first week in hot conditions, the worker performs his expected rate of work while wearing a micro-climate jacket. This allows the individual to be fully productive during the acclimatization period while, at the same time, offering protection against heat illness.

The use of surface or underground climatic chambers designed specifically for fully controlled acclimatization procedures was developed for the South African gold mining industry (Stewart, 1982). The success of those procedures in reducing the incidence of heat stroke and improving productivity led to the widespread use of the technique within that country. The environment within the climatic chamber is maintained at a wet bulb temperature of about 31.7°C and an air velocity of 0.5 m/s. The work consists of stepping on and off a bench at a rate indicated by an audible and visual metronome. The height of the bench is adjusted according to each man's body weight such that every person works at the same rate. This correlates with an oxygen consumption of some 1.4 litres/minute and, hence, is equivalent to hard manual work. The task is carried out for four continuous hours per day over a period of several days. Measurements are made of body temperature, and drinking water is administered every thirty minutes. During the first day of acclimatization, the stepping task is conducted at only half the normal pace for most of the four hours. The time spent on full work rate (oxygen consumption of 1.4 litres/minute) is increased gradually until the final day is entirely at the full rate.

The period of acclimatization within a climatic chamber originally encompassed eight days. However, the improvement of conditions underground, coupled with heat tolerance testing have resulted in the acclimatization period being reduced to four days with far fewer men required to undergo it. The ultimate objective is to reduce the wet bulb temperature to less than 27.5°C in all mines at which time acclimatization will no longer be required (Burrows, 1989).

CHAPTER 18. REFRIGERATION PLANT AND MINE AIR CONDITIONING SYSTEMS

18.1. INTRODUCTION 2

18.2. THE VAPOUR COMPRESSION CYCLE 2

18.2.1. Basic principles 2

18.2.2. Refrigerant fluids 4

18.2.3. Basic components of the vapour compression cycle 5

18.2.4. Performance of a refrigeration cycle 6

 18.2.4.1 The Carnot cycle 6

Coefficient of Performance, COP, 8

 18.2.4.2. The actual cycle 8

18.3. COMPONENTS AND DESIGN OF MINE COOLING SYSTEMS..... 15

18.3.1. Overview of mine cooling systems 15

18.3.2. Heat exchangers 20

 18.3.2.1. Indirect heat exchangers 22

 18.3.2.2. Performance calculations for indirect heat exchangers 22

 18.3.2.3. Direct heat exchangers 26

Chilled water spray chambers 28

 18.3.2.4. Performance calculations for direct heat exchangers 31

 18.3.2.5. Heat exchange across the walls of pipes and ducts 41

Air inside a duct 42

Water inside a pipe 42

Air outside a pipe 43

Radiative heat transfer coefficient 43

18.3.3. Water distribution systems 45

 18.3.3.1. Pipe sizing 46

 18.3.3.2. Pipe insulation 47

Table 18.3. Thermal conductivities of pipe materials. 48

 18.3.3.3. Energy and temperature changes within water systems 48

18.3.4. Energy recovery devices 53

 18.3.4.1. Water turbines 54

 18.3.4.2. Hydrolift systems 55

18.3.5. Design of mine cooling systems 56

 18.3.5.1. Location of main plant 56

Surface plant 57

Underground plant 57

Combinations of surface and underground plant 59

 18.3.5.2. Service water cooling 61

 18.3.5.3. Hydropower 62

 18.3.5.4. Ice systems 62

Manufacture of ice 64

Transportation of ice 65

Incorporation into the mine cooling system 66

Economics of ice systems 67

 18.3.6. Summary of design process 67

18.4. AIR HEATING 68

18.4.1. Utilization of waste heat 69

18.4.2. Heat recovery from exhaust air 69

18.4.3. Direct heating 71

Table 18.4. Gross calorific values of gases 71

18.4.4. Indirect heating 72

18.4.5. Ice stopes 73

18.4.6. Geothermal and cycled storage heat 74

References 76

18.1. INTRODUCTION

One of the earliest methods of temperature control in underground mines was the importation of naturally produced ice from the surface. Blocks of ice were transported in ore cars to cool miners in the **Comstock Lode** under Virginia City in Nevada, USA, during the 1860's. The vapour compression refrigeration cycle, currently the most widespread method of artificial cooling, appears to have first been used in mining during the 1920's. Examples included the famous **Morro Velho** Mine in Brazil (1923) and experimental work in British coal mines (Hancock, 1926). Air cooling techniques in mining gained further recognition in the 1930's including their utilization in the gold mines of **South Africa** and in the **Kolar Goldfields** of India. However, it was the 1960's that saw the start of a real escalation of installed mine cooling capacity.

Large centralized refrigeration plant, located underground, became popular in the South African gold mines. Limitations on the heat rejection capacity of return air, combined with the development of energy recovery devices for water pipelines in shafts and improved "coolth" distribution systems led to a renewed preference for surface plant. (The term "coolth" is a decidedly unscientific but descriptive word sometimes used in association with chilled fluid distribution systems.)

Although the traditional role of mine cooling has been to combat geothermal heat and the effects of autocompression in deep metal mines, an additional influence has been the escalating amount of mechanized power employed underground, particularly in longwall coal mines. This resulted in smaller scale and more localized use of air cooling units in such mines at depths where, prior to intensive mechanization, heat had not been a limiting environmental problem. Examples of these installations appeared in the United Kingdom and Germany.

In this chapter, we shall examine the essential theory of the vapour compression refrigeration cycle in addition to discussing the design of mine cooling systems and some of the methods of distributing "coolth" to the working areas of a subsurface facility. The chapter concludes with a section on the opposite problem, that of increasing the temperature of the intake air for mines in cold climates.

18.2. THE VAPOUR COMPRESSION CYCLE

There are many transient phenomena that are known to produce a cooling effect, varying from endothermic chemical reactions to the sublimation of solid carbon dioxide (dry ice). Where a continuous cooling effect is required, then a means must be employed by which a supply of mechanical, electrical or thermal energy is utilized to remove heat from some source, and to transport it to a thermal sink where it can be rejected. If the primary objective is to cool the source, then the device is known as a **refrigerator**. If, however, the desired effect is to heat the sink, then it is called a **heat pump**. In fact, both effects occur simultaneously. Hence, a domestic refrigerator cools the interior of the container but heats the air in the kitchen.

Of the several devices that have been developed to achieve a continuous refrigeration or heat pump effect, the most common is based on the vapour compression cycle. This may be used on small units such as air conditioning equipment fitted to automobiles or for very large scale cooling of mine workings where many megawatts of heat require to be transferred. In this section, we shall examine the basic principles of the vapour compression cycle, how rates of heat exchange may be calculated, and the essential components of a refrigeration plant.

18.2.1. Basic principles

When a liquid boils, it does so at constant temperature provided that the applied pressure remains fixed. The heat added is utilized in increasing the internal kinetic energy of the molecules until they

can no longer remain in the liquid phase but burst free to form a vapour or gas (Section 2.1.1). If, however, the applied pressure is raised to a higher value, then additional heat is required to vaporize the liquid. The boiling temperature will increase. The relationship between pressure and boiling point for any given liquid may be defined as the **vapour pressure line** on a pressure-temperature diagram such as that shown on Figure 18.1. The fluid is a liquid on the left of the curve and a vapour (gas) on the right of the curve. The liquid may be vaporized either by increasing the temperature or decreasing the pressure. Similarly, condensation from vapour to liquid may occur either by decreasing the temperature or increasing the pressure.

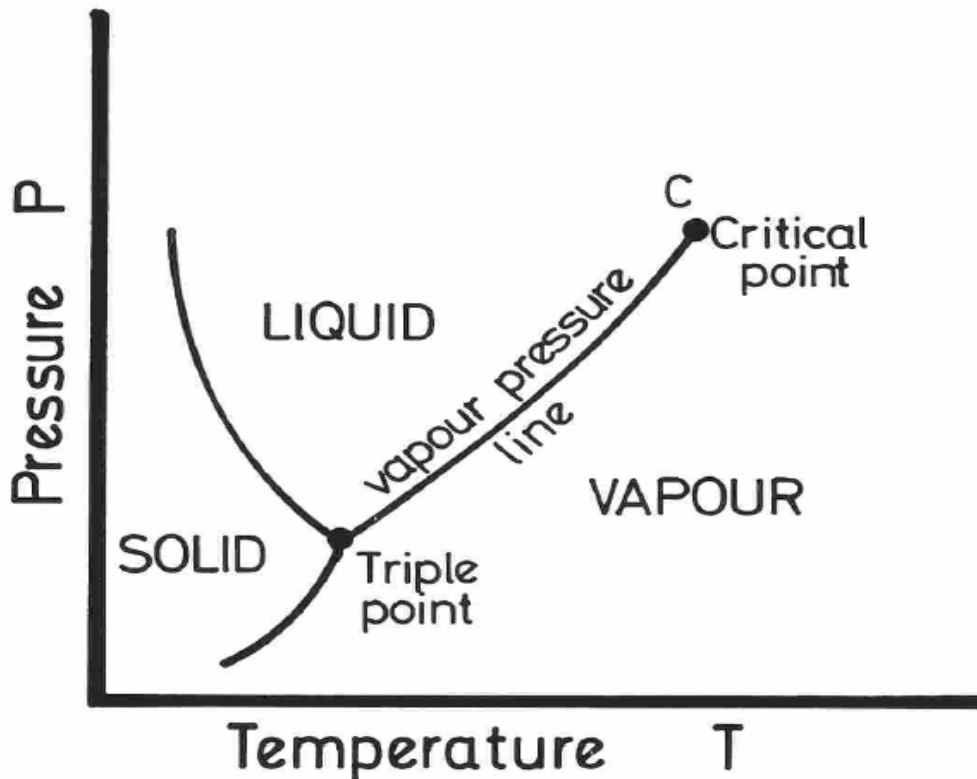


Figure 18.1 A pressure-temperature diagram showing limits of phase change.

The change in physical appearance of a fluid on crossing the vapour pressure line is quite distinct, liquid to gas or vice versa. However, there is a critical pressure-temperature coordinate beyond which the change of phase is gradual rather than sudden and there is no clearly defined moment of evaporation or condensation. This is known as the **critical point**.

Although the vapour pressure curve appears as a single line on the pressure-temperature diagram, it takes a finite amount of time and energy exchange to cross that line. During this time, part of the fluid will be liquid and the remainder will be vapour. This is the situation that exists inside a boiling kettle. The region within which the two phases coexist is more clearly shown on the PV (pressure against specific volume) diagram of Figure 18.2(a). The corresponding temperature-entropy (Ts) and pressure-enthalpy (PH) diagrams are shown on Figures 18.2(b) and (c) respectively. The latter two diagrams are particularly useful in analyzing and quantifying both the work and heat transfer processes in the vapour compression cycle.

In all three diagrams of Figure 18.2, a horizontal line within the two phase region indicates that the pressure and temperature both remain constant during any given isobaric phase change. However, the volume, entropy and enthalpy all increase significantly during vaporization. Different horizontal lines on anyone of these diagrams will indicate different values of pressure and corresponding boiling (or condensation) temperature (Figure 18.1). When a liquid boils at a given value of applied pressure it will extract heat from the surroundings or other available medium. If the vapour thus produced is then transported to a new location and compressed to a higher pressure, then it can be condensed at a correspondingly higher temperature, yielding up its heat of condensation to the new surroundings or any cooling medium that may be supplied. This is the basic principle underlying the vapour compression refrigeration cycle.

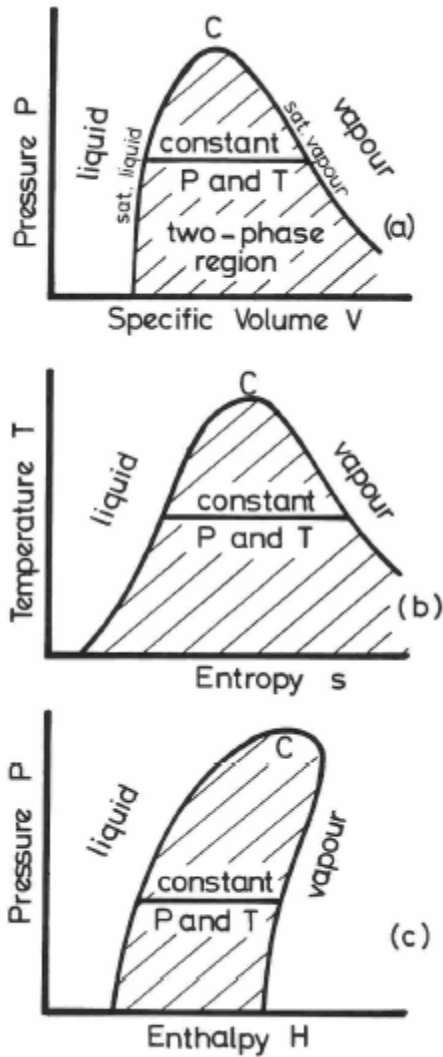


Figure 18.2 PV, Ts and PH diagrams for change of phase.

18.2.2. Refrigerant fluids

The differing pressure-temperature relationships of various fluids allow each of those fluids to act as a refrigerant over specified temperature ranges. Carbon dioxide and even water have been used as refrigerants. For the ranges of pressures and temperatures acceptable in refrigeration plant for air conditioning, **ammonia** is a particularly efficient refrigerant although its toxicity limits its use. The ideal refrigerant for mining use is one that gives a high efficiency of heat transfer, is non-corrosive to metal, non-toxic and has a boiling temperature close to 0°C at a positive pressure with respect to the ambient atmosphere. **Fluorinated hydrocarbons** have been widely employed in many types of industrial plant as well as domestic refrigeration equipment. Although non-toxic, fluorinated hydrocarbons react adversely with atmospheric ozone and are being replaced by alternative refrigerants.

Refrigerant fluids are commonly referred to, not by their chemical names, but by R (refrigerant) number. Table 18.1 indicates some of those designations.

Refrigerant No.	Chemical name	Refrigerant No	Chemical Name
R11	trichlorofluoromethane	R122	trichlorodifluoroethane
R12	dichlorodifluoromethane	R170	ethane
R22	chlorodifluoromethane	R290	propane
R23	trifluoromethane	R600	butane
R30	dichloromethane	R717	ammonia
R50	methane	R718	water
R110	hexachloroethane	R744	carbon dioxide
R113	trichlorotrifluoroethane	R1150	ethylene
R120	pentachloroethane	R1270	propylene

Table 18.1 Refrigerant numbers of selected fluids.

18.2.3. Basic components of the vapour compression cycle

Figure 18.3 shows that there are four essential components of hardware in a vapour compression refrigeration unit. The evaporator is a heat exchanger, typically of the shell-and-tube configuration in mining refrigeration plant. In the larger units, the refrigerant liquid is on the outside of the tubes while the medium to be cooled (for example, water, brine or glycol) passes through the tubes. Smaller units employed for direct cooling of an airstream are sometimes called "direct evaporators" and contain the refrigerant within the tubes while the air passes over their outer surface.

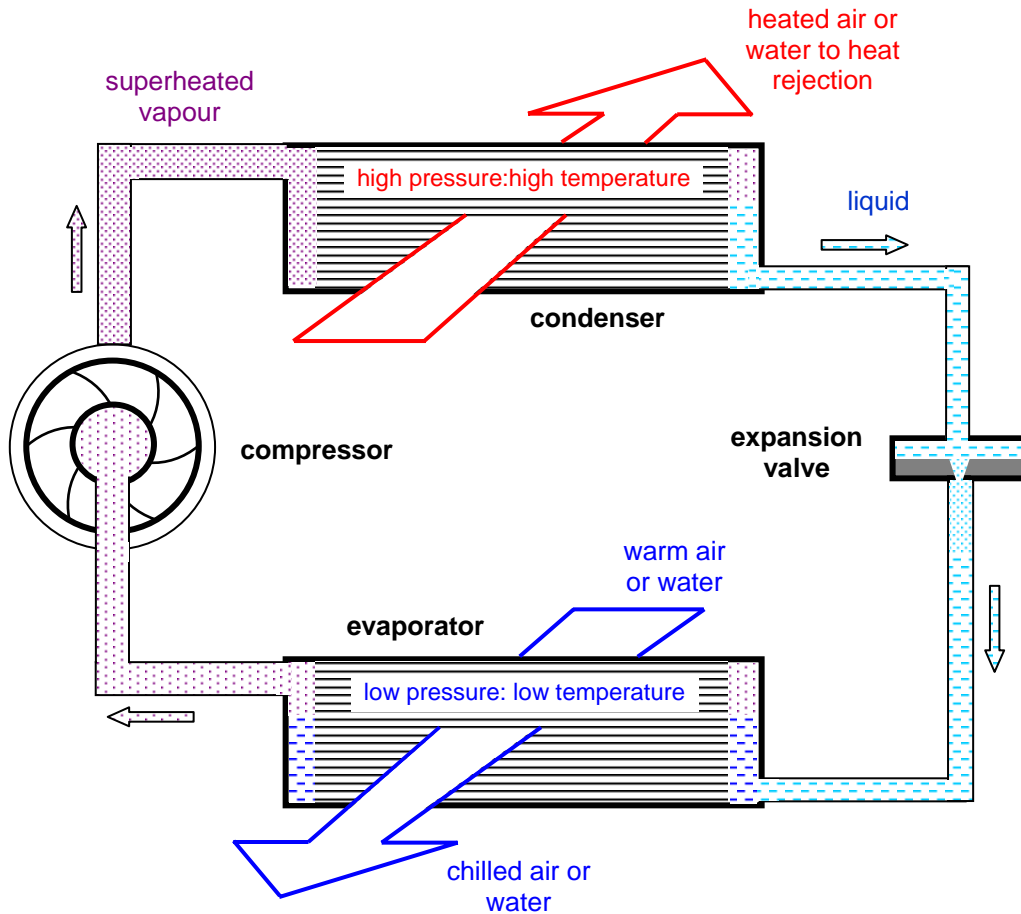


Figure 18.3 Major components of a vapour compression cycle.

Within the evaporator, the refrigerant pressure is maintained at a relatively low level and boils at a correspondingly low temperature. For example, refrigerant R12 will boil at 4°C if the pressure is 351 kPa (approximately 3.5 atmospheres). The heat required to maintain the boiling is extracted from the gas or liquid passing on the other side of the tube walls. Hence, that gas or liquid is cooled. The refrigerant, now vaporized, collects at the top of the evaporator and is allowed to gain a few degrees of superheat to ensure full vaporization before it passes on the compressor. Except for direct evaporators, it may be necessary to insulate the external surface of the evaporator in order to prevent excessive heat gain from the ambient atmosphere.

The compressor is the device where mechanical work is input to the system. Reciprocating, screw or centrifugal compressors are all employed. The latter are favoured for the larger units and where the required pressure ratio remains constant. However, the development of large diameter screw compressors allows a good efficiency to be maintained under conditions of variable cooling load. (Baker-Duly, 1989). Multi-stage compressors are employed to give high differentials of pressure and, hence, large temperature differences between the evaporator and condenser. Electric motors are normally employed to drive the compressors on mine refrigeration units although internal combustion engines may be used on surface or as standby units. The duty of a refrigeration plant can be modified by changing the speed of the compressor. The flow of vapour through the compressor and, hence, rate of heat transfer can also be controlled by inlet guide vanes.

The refrigerant vapour leaves the compressor and passes into the condenser at a relatively high pressure and temperature. The condenser itself may be of similar construction to the evaporator, that is, a shell-and-tube heat exchanger. Heat is removed from the refrigerant by air, water or some other fluid medium to the extent that the refrigerant cools and condenses back to a liquid. As the pressure is high, this occurs at a relatively high temperature. At a pressure of 1217 kPa, refrigerant R12 will condense at 50°C. The latent heat of condensation is removed by the cooling fluid for subsequent rejection in a cooling tower or other type of separate heat exchanger. As the vapour compression cycle is a closed system (ignoring heat losses or gains from the surrounding atmosphere), the rate at which heat is removed from the refrigerant in the condenser must equal the combined rates of heat addition in the evaporator and work provided by the compressor.

The condensed refrigerant passes from the condenser to the fourth and final component of the cycle. This is the expansion valve whose purpose is simply to reduce the pressure of the refrigerant back to evaporator conditions. An expansion valve may be a simple orifice plate or can be controlled by a float valve. At the exit from the expansion valve, the liquid is at low pressure and has a correspondingly low boiling temperature. Provided that the pipework is insulated, the latent heat for boiling can come only from the liquid refrigerant itself. Hence, the temperature of the refrigerant drops rapidly as it passes from the expansion valve to the evaporator where it enters as a mixture of liquid and vapour, thus closing the cycle.

18.2.4. Performance of a refrigeration cycle

18.2.4.1 The Carnot cycle

Electrical motors or heat engines are devices that convert one form of energy into another. Their efficiency may, therefore, be defined as an energy output/input ratio. However, in the case of refrigerators or heat pumps, the purpose is to remove heat from a given source and to reject it at a higher temperature to a receiving sink. A different measure of performance is required.

Figure 18.4 shows the temperature-entropy diagram for the ideal (frictionless) Carnot cycle to which an actual vapour compression cycle can aspire but never attain. We may follow the ideal cycle by commencing at position 1, the entry of refrigerant vapour to the compressor.

The ideal compression process is isentropic (Section 10.6). The compressed refrigerant vapour enters the condenser at position 2 and, in the ideal condenser, passes through to position 3 with neither a pressure drop nor a fall in temperature. This assumes frictionless flow and perfect heat transfer. The ideal expansion valve allows an isentropic fall in pressure and temperature to station 4, the entrance to the evaporator. The cycle closes via frictionless flow and perfect heat transfer in the evaporator.

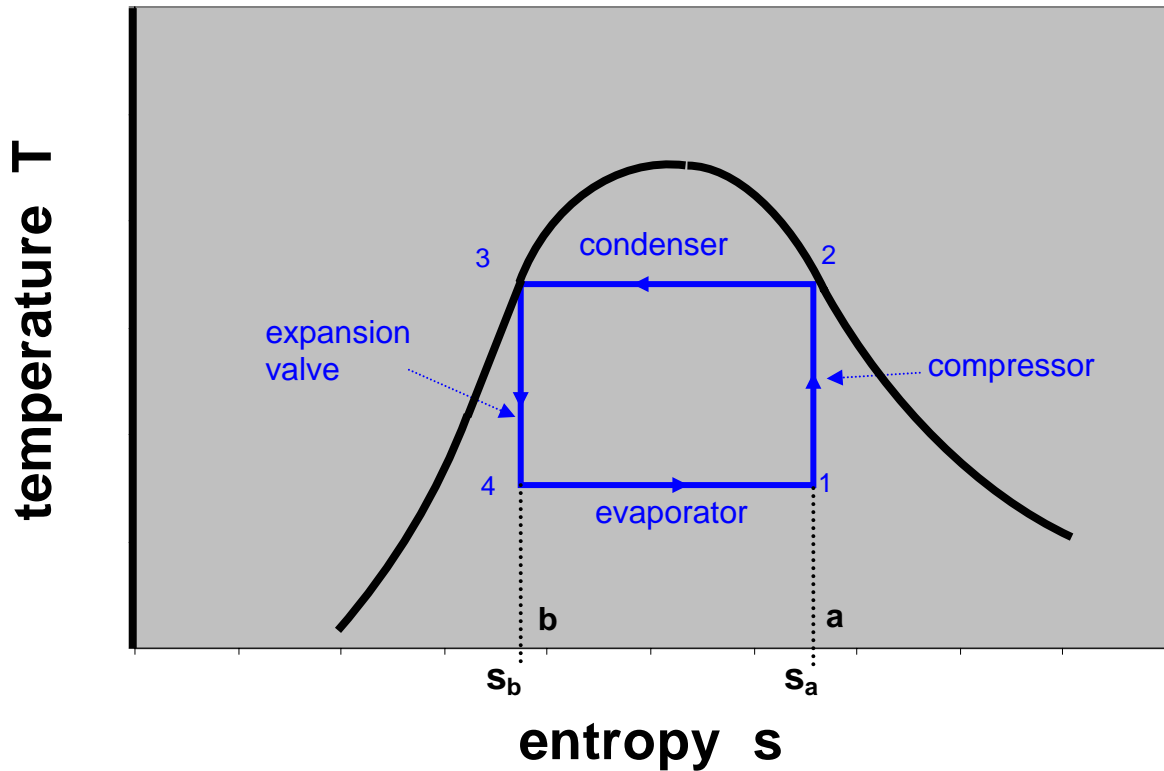


Figure 18.4 Temperature-entropy diagram for an ideal vapour compression cycle (Carnot cycle)

In order to quantify the ideal Carnot cycle, we apply the steady-flow energy equation (3.25). The kinetic and potential energy terms are small and, in any event, cancel out in a closed cycle. Using the numbered station points from Figure 18.4, the steady-flow energy equation gives:

$$\text{compressor:} \quad W_{12} = H_2 - H_1 \text{ J/kg} \quad (18.1)$$

$$\text{condenser:} \quad q_{23} = H_3 - H_2 \text{ J/kg} \quad (18.2)$$

$$\text{expansion valve:} \quad 0 = H_4 - H_3 \text{ J/kg} \quad (18.3)$$

$$\text{evaporator:} \quad q_{41} = H_1 - H_4 \text{ J/kg} \quad (18.4)$$

$$\text{cycle summation:} \quad \underline{W_{12} + q_{23} + q_{41}} = \underline{0} \text{ J/kg} \quad (18.5)$$

where:

W_{12} = mechanical energy added by the compressor

q_{23} = heat exchange in the condenser (this is numerically negative as heat is leaving the refrigerant)

q_{41} = heat added to the refrigerant in the evaporator

H = enthalpy

We can rewrite equation (18.5) as

$$W_{12} + q_{41} = -q_{23} \text{ J/kg} \quad (18.6)$$

thus confirming our earlier statement that the heat rejected in the condenser is numerically equal to the sum of the compressor work and the heat added to the refrigerant in the evaporator.

The measure of performance of a refrigeration cycle is known as the **Coefficient of Performance, COP**, and is defined as

$$COP = \frac{\text{Useful cooling effect (evaporator heat transfer)}}{\text{Work input from the compressor}} = \frac{q_{41}}{W_{12}} \quad (18.7)$$

Using equation (18.5) once again, this may be rewritten as

$$COP = \frac{q_{41}}{-q_{23} - q_{41}} \quad (18.8)$$

Recalling that the area under a process line on a Ts diagram represents heat (Section 3.5), the terms in equation (18.8) may be related to Figure 18.4 for the Carnot cycle:

$$\begin{aligned} q_{41} &= \text{Area } 41ab \\ -q_{23} &= \text{Area } 23ba \\ \text{and } -q_{23} - q_{41} &= \text{Area } 1234 \text{ (remember that } q_{23} \text{ is numerically negative)} \end{aligned}$$

Hence, $W_{12} = \text{Area } 1234$ and equation (18.8) becomes

$$\begin{aligned} \text{Carnot } COP &= \frac{\text{Area } 41ab}{\text{Area } 1234} = \frac{T_1(s_a - s_b)}{(T_2 - T_1)(s_a - s_b)} \\ &= \frac{T_1}{(T_2 - T_1)} \text{ or } \frac{T_4}{(T_3 - T_4)} \end{aligned} \quad (18.9)$$

$$\text{as } T_1 = T_4 \text{ and } T_2 = T_3$$

Hence, the ideal or Carnot coefficient of performance is given as the ratio:

$$\text{Carnot } COP = \frac{\text{Evaporator temperature (absolute)}}{\text{Condenser temperature} - \text{Evaporator temperature}} \quad (18.10)$$

Example

The evaporator and condenser of a refrigeration unit have temperatures of 4 and 50°C respectively. Determine the maximum possible coefficient of performance of this unit.

Solution

The Carnot or ideal coefficient of performance is given by equation (18.10)

$$\text{Carnot } COP = \frac{(273.15 + 4)}{(50 - 4)} = 6.025$$

18.2.4.2. The actual cycle

A real vapour compression cycle has a coefficient of performance that is necessarily lower than the corresponding Carnot COP. There are two reasons for this. First, in actual compressors and expansion valves, there are, inevitably, increases in entropy. Furthermore, as the refrigerant passes through real condensers and evaporators there will be slight changes in pressure and temperature. In

a well designed unit, the latter are small compared with the differences in pressure or temperature between the condenser and evaporator.

Secondly, it would be impractical to design a refrigeration unit that attempted to follow the Carnot cycle. Referring again to Figure 18.4, it can be seen that station 1 (entry to the compressor) lies within the two-phase region. The presence of liquid droplets would cause severe erosion of the compressor impeller. It is for this reason that a few degrees of superheat are imparted to the vapour before it leaves a real evaporator.

Figure 18.5 illustrates the temperature-entropy and pressure-enthalpy diagrams for a practical vapour compression cycle. The major difference between Figure 18.5(a) and the Carnot cycle shown on Figure 18.4 is that the compression commences slightly beyond the saturated vapour line (station 1) and involves an increase in entropy to station 2. On entering the condenser, the superheated vapour undergoes a near isobaric cooling process (stations 2 to 2'), losing sensible heat to the cooling medium until condensing temperature is reached at station 2'.

Although the process through the expansion valve is no longer isentropic, the fluid remains at constant enthalpy (no heat exchange takes place) and, hence, appears on the pressure-enthalpy diagram as a vertical line 3 to 4.

Equations (18.1 to 18.4) arose from those parts of the steady-flow energy equation that do not involve the friction term. They apply equally well to both the real and the ideal cases. Furthermore, the definition of coefficient of performance given in equation (18.7) remains applicable. Substituting for W_{12} and q_{41} from equations (18.1) and (18.4) respectively gives

$$\text{Actual COP} = \frac{q_{41}}{W_{12}} = \frac{H_1 - H_4}{H_2 - H_1} \quad (18.11)$$

The reason for introducing the pressure-enthalpy diagram now emerges. The coordinate points for real vapour compression cycles can be plotted on pressure-enthalpy-temperature charts that have been derived through tests on many refrigerant fluids. An example is given for refrigerant R12 on Figure 18.6. The values of enthalpy may be read from the relevant chart enabling the actual coefficient of performance and other parameters to be determined. For more precise work, tables of the thermodynamic behaviour of refrigerants are available. The values of enthalpy and entropy on the charts and tables are based on a specified datum temperature. This is usually either absolute zero (-273.15°C) or -40°C. The datum employed has little import as it is differences in values that are used in practical calculations.

A measure of efficiency of the refrigeration unit may now be defined by comparing the actual COP with the ideal Carnot COP.

$$\text{Cycle efficiency} = \frac{\text{Actual COP}}{\text{Carnot COP}} \quad (18.12)$$

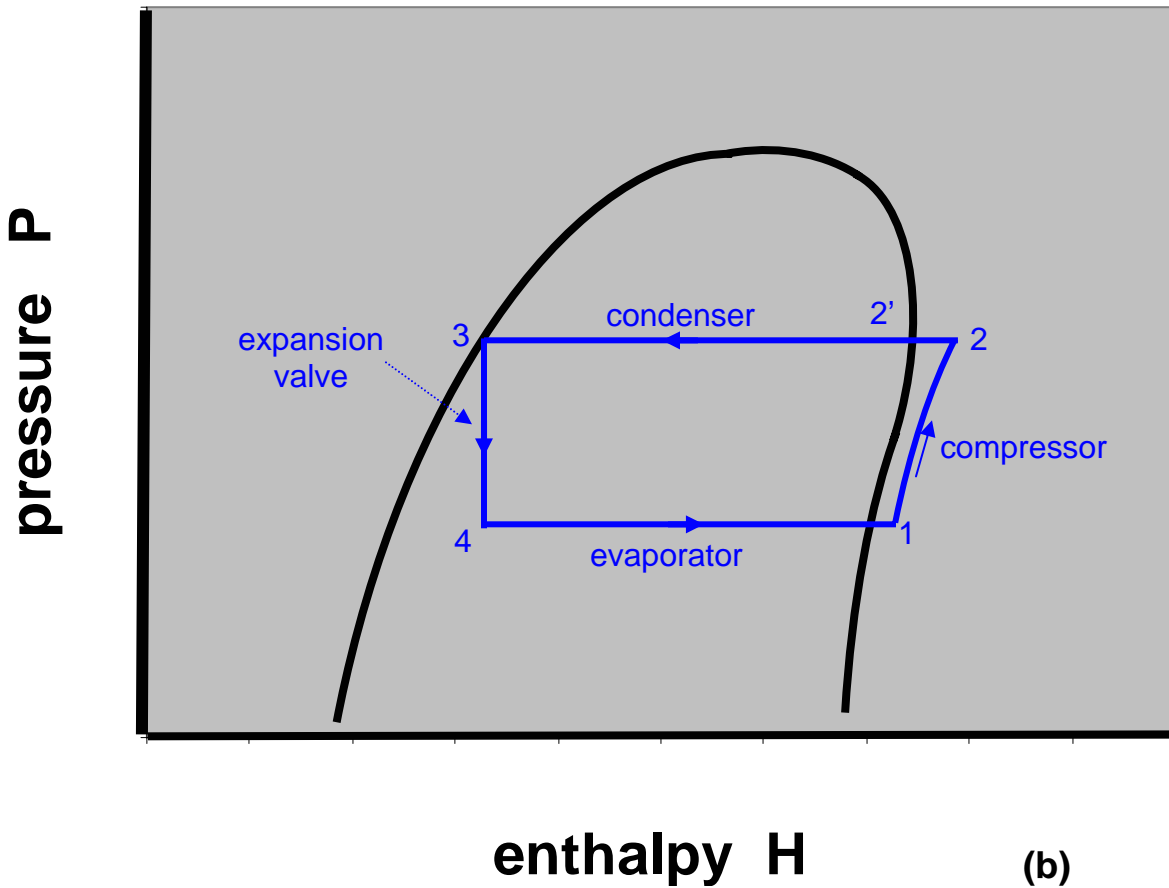
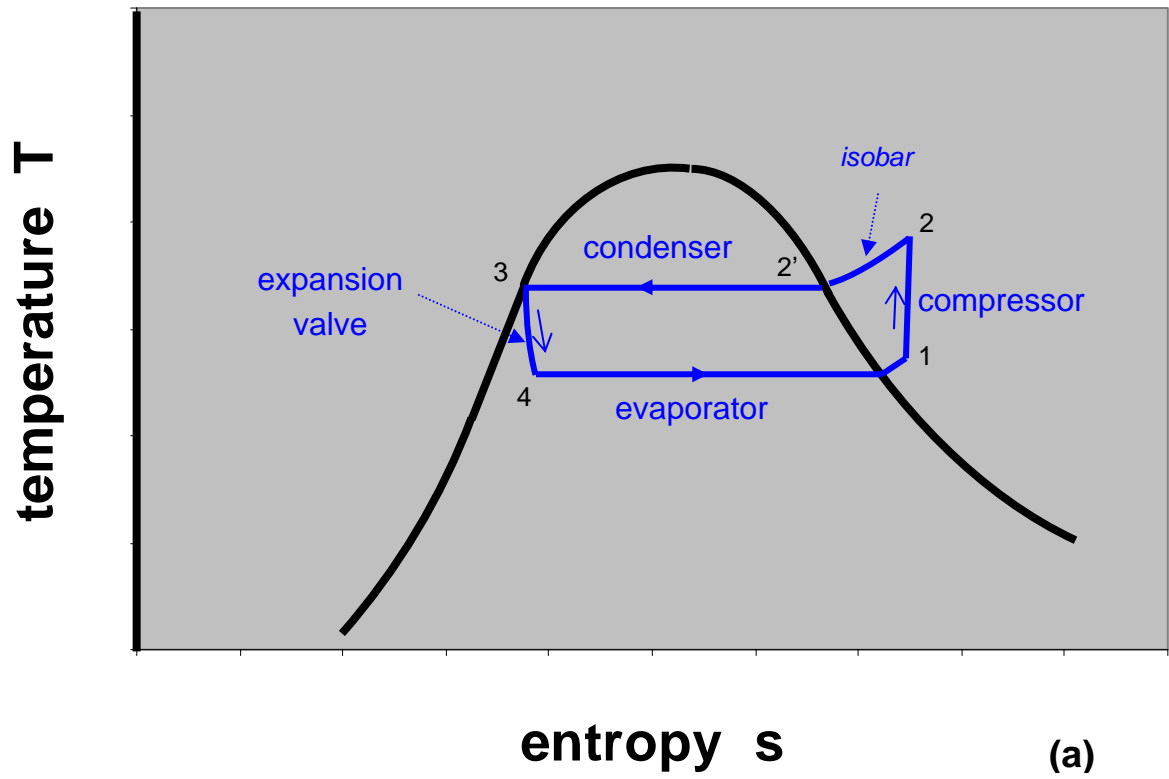


Figure 18.5 Temperature-entropy and pressure-enthalpy diagrams for an actual vapour compression cycle

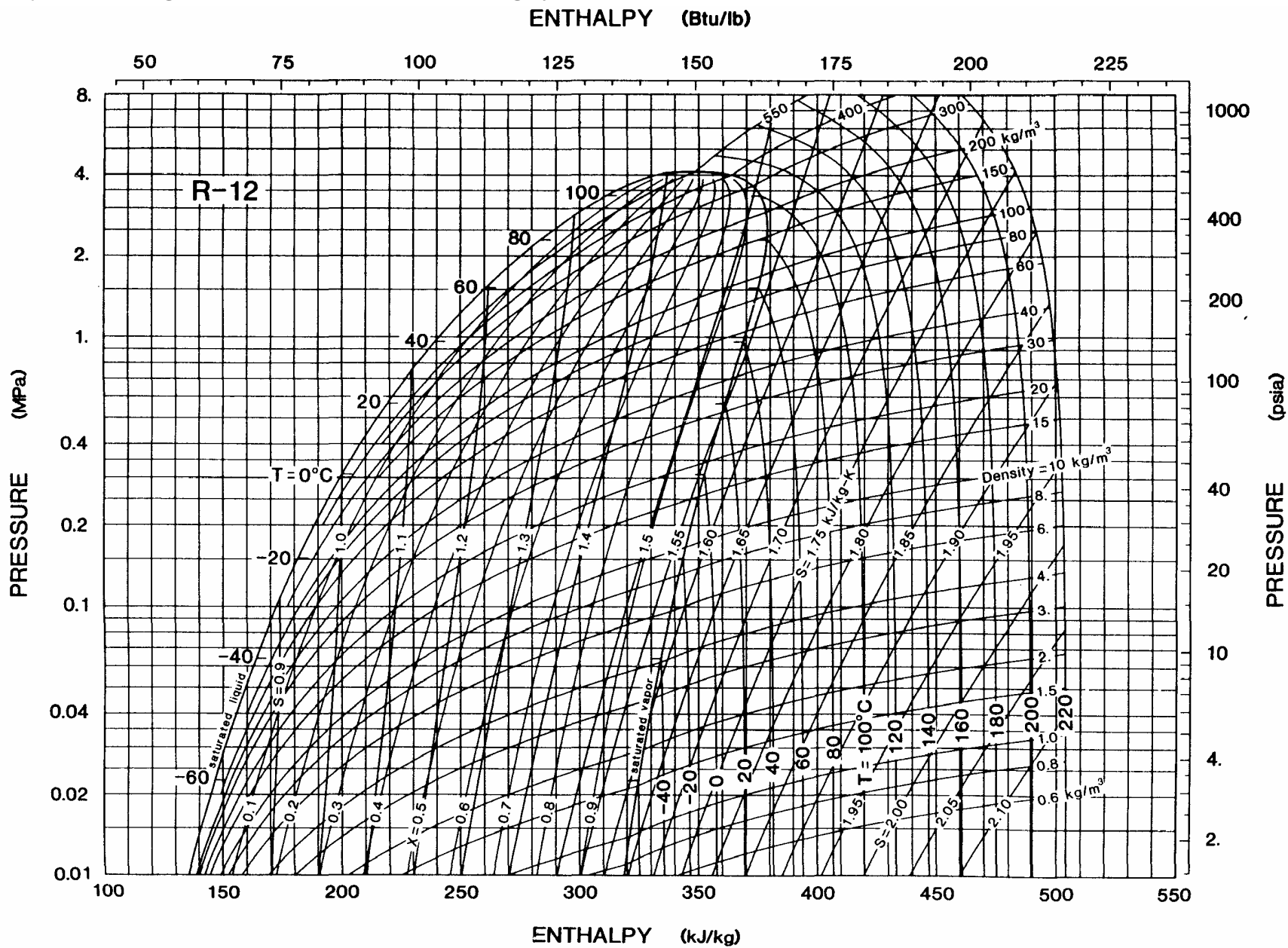


Figure 18.6 Pressure-enthalpy diagram for refrigerant R12 (based on zero degrees Kelvin).
 Reprinted by permission from the 1985 ASHRAE Handbook – Fundamentals.

Example

A plant employing refrigerant R12 is used to chill water for a mine distribution system. Water is also used to remove heat from the condenser. The following measurements are made:

Evaporator:

Water flowrate:	50 litres/s
Water inlet temperature:	20°C
Water outlet temperature:	10°C
Refrigerant pressure:	363 kPa

Condenser:

Water flowrate:	140 litres/s
Refrigerant pressure:	1083 kPa

Compressor:

Refrigerant inlet temperature:	7°C
Refrigerant outlet temperature:	65°C

Using the pressure-enthalpy chart for R12, analyze the performance characteristics of the unit.

Solution

Step 1: On the pressure-enthalpy diagram, draw horizontal lines to represent the pressures in the evaporator (363 kPa) and condenser (1083 kPa). For clarity, the relevant area of the R12 pressure-enthalpy chart has been enlarged and reproduced as Figure 18.7. The corresponding temperatures may be estimated directly from the chart.

$$t_{evap} = t_4 = 5^\circ\text{C}$$

$$t_{cond} = t_3 = 45^\circ\text{C}$$

These temperatures can, of course, be verified by direct measurement.

Step 2: Establish the nodal points on the pressure-enthalpy chart and read the corresponding values of enthalpy.

The temperature of the refrigerant entering the compressor (station 1) is given as 7°C. This represents 7 - 5 = 2° of superheat. Station 1 is, therefore, established on the evaporator pressure line at a temperature of 7°C. Note that the lines of constant temperature change from horizontal to near vertical on passing the saturated vapour line. We have ignored the small pressure drop between the evaporator and the compressor inlet.

Station 2 is established in a similar manner, i.e. at the measured compressor outlet temperature of 65°C and lying on the condenser pressure line.

Station 3, representing the refrigerant leaving the condenser, lies on the junction of the evaporator pressure line and the saturated liquid curve.

The expansion process is represented by a vertical line dropped from station 3 until it intersects the evaporator pressure line at station 4.

The four critical enthalpies may now be estimated from the chart:

compressor inlet	$H_1 = 356 \text{ kJ/kg}$
compressor outlet/condenser inlet	$H_2 = 386 \text{ kJ/kg}$
condenser outlet	$H_3 = 244 \text{ kJ/kg}$
evaporator inlet	$H_4 = 244 \text{ kJ/kg}$

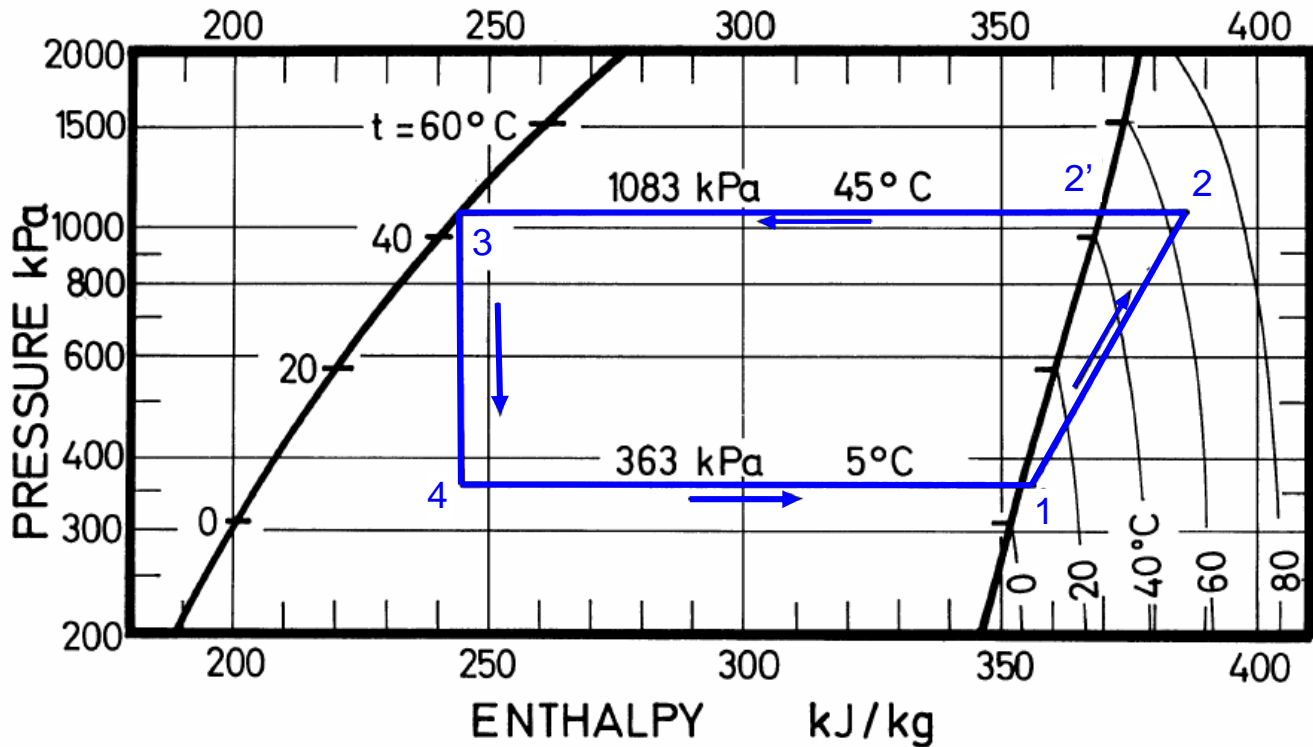


Figure 18.7 Example vapour compression cycle on the Pressure-enthalpy chart.

Step 3: Establish the coefficients of performance and cycle efficiency:

$$\text{Carnot COP} = \frac{T_4}{(t_3 - t_4)} = \frac{(273.15 + 5)}{(45 - 5)} = 6.954 \text{ equations (18.9 or 18.10)}$$

$$\text{Actual COP} = \frac{(H_1 - H_4)}{(H_2 - H_1)} = \frac{356 - 244}{386 - 356} = 3.733 \text{ equation (18.11)}$$

$$\text{Cycle efficiency} = \frac{\text{Actual COP}}{\text{Carnot COP}} = \frac{3.733}{6.954} \times 1000 = 53.7 \text{ per cent equation (18.12)}$$

Step 4: Determine the useful cooling effect, or evaporator duty, q_{evap} . This can be established from the known flowrate and temperature drop of the water being cooled as it passes through the evaporator:

$$q_{evap} = m_{w, evap} C_w \Delta T_{w, evap} \quad \text{kW} \quad (18.13)$$

where: water mass flowrate $m_{w, evap}$ = 50 litres/s = 50 kg/s
 specific heat of water, C_w = 4.187 kJ/kg°C
 temperature drop of water $\Delta T_{w, evap}$ = 20 - 10 = 10°C

$$\text{giving } q_{evap} = 50 \times 4.187 \times 10 \text{ kJ/s or kW} = 2093.5 \text{ kW}$$

Step 5: Determine the mass flowrate of refrigerant, m_r , around the system. The evaporator duty, already found to be 2093.5 kW, can also be expressed as

$$q_{evap} = m_r (H_1 - H_4) \quad \text{kW} \quad (18.14)$$

Hence,

$$m_r = \frac{2093.5}{(356 - 244)} = 18.69 \quad \text{kg/s}$$

Step 6: Determine the compressor duty. The work input from the compressor to the refrigerant, W_{12} , can be established in two ways. First,

$$W_{12} = m_r (H_2 - H_1) = 18.69(386 - 356) = 560.7 \quad \text{kW} \quad (18.15)$$

and, secondly, from the definition of coefficient of performance given in equation (18.7),

$$W_{12} = \frac{q_{evap}}{\text{Actual COP}} = \frac{2093.5}{3.733} = 560.8 \quad \text{kW}$$

The slight difference arises from rounding errors.

Step 7: Evaluate the condenser duty. The heat transferred from the refrigerant in the condenser is simply

$$-q_{cond} = q_{evap} + W_{12} = 2093.5 + 560.7 = 2654.2 \quad \text{kW} \quad (\text{equation (18.6)})$$

As the cooling water flowrate through the condenser is known to be $m_{w,cond} = 140$ kg/s, the temperature rise of this water, $\Delta T_{w,cond}$, may be determined from

$$-q_{cond} = m_{w,cond} C_w \Delta T_{w,cond}$$

$$\text{giving} \quad \Delta T_{w,cond} = \frac{2654.2}{140 \times 4.187} = 4.53 \quad ^\circ\text{C}$$

The performance of a refrigeration unit may be enhanced beyond that illustrated in the example. For large units, it may be necessary to employ two or more stages of compression in order to achieve the desired difference in temperature between evaporator and condenser. In that case, it is usual to employ the same number of expansion valves as stages of compression. A fraction of the refrigerant is vaporized on passing through an expansion valve. That fraction can be read from the corresponding point on the pressure-enthalpy diagram or calculated from the isobaric enthalpies at the saturated liquid and saturated vapour curves. This "flash gas" may be separated out and piped to the corresponding intermediate point between compressor stages. This is known as **interstage cooling** or, simply, **intercooling** and reduces the total mass of refrigerant that passes through all stages of compression. The result is to reduce the required compressor power and/or increase the useful refrigerating effect.

In some units, the hot liquid refrigerant leaving the condenser is partially cooled by a secondary cooling circuit. This **subcooling** reduces the fraction of flash gas produced at the downstream side of expansion valves and gives a small increase in the performance of the plant.

The coefficient of performance as defined by equation (18.7) takes into account the isentropic efficiency of the compressor. However, it does not cater for the efficiency of the motor or other device that drives the compressor. Hence, the W_{12} in equation (18.7) may be replaced by the power fed to the compressor drive unit to give a more practical coefficient of performance. Furthermore, the compressor is not the only device that consumes energy in a refrigeration unit. There will also be water pumps or fans to promote the flow of the cooled medium at the evaporator and the cooling medium at the condenser. An overall coefficient of performance may be defined as:

$$\text{Overall COP} = \frac{\text{Heat transfer in the evaporator}}{\text{Total energy consumption of the refrigeration unit}} \quad (18.16)$$

Care should, therefore, be taken that any quoted values of *COP* are interpreted in the correct manner.

18.3. COMPONENTS AND DESIGN OF MINE COOLING SYSTEMS

18.3.1. Overview of mine cooling systems

In the majority of large scale mine cooling systems, there are usually three sets of heat transfer involved:

- transfer of heat from the work areas to the evaporators of the refrigeration units
- transfer of heat from the evaporators to the condensers in the refrigeration units (the vapour compression cycle)
- transfer of heat from the condensers to the free atmosphere on surface.

There exist tremendous variations in the duty, complexity and efficiency of the hardware involved in these three phases, dependent upon the severity and dispersion of the heat problem in the mine. In this section we shall discuss a range of systems varying from a simple spot cooler for very localized applications to large integrated systems that may be required for deep and hot mines. This will serve both as an overview and an introduction to a more detailed examination of individual components and overall system design.

Figure 18.8 shows a simple application of a **direct evaporator** or "**spot cooler**" to a specific working area in a mine. The evaporator of the refrigeration unit takes the form of copper or cupronickel tubular coils located within an air duct. The refrigerant passes through the inside of the evaporator tubes and cools the air flowing along the duct. The heat from the condenser is rejected directly to the return air. This system has the advantage that the cooling effect produced by the refrigeration unit is utilized directly and immediately at the place where cooling is required. There is no loss of efficiency introduced by an intervening water reticulation system between the evaporator and working area. Similarly, heat rejection from the condenser is direct and immediate. The spot cooler is merely an industrial version of a domestic air conditioning unit where heat is rejected directly to the outside atmosphere.

Unfortunately, the spot cooler has a major disadvantage that limits its application in subsurface ventilation systems. Glancing, again, at the blind heading illustrated in Figure 18.8, it is clear that the air emerging from the end of the duct will be at a reduced temperature when the refrigeration unit is operating. Although this is the desired effect, a consequence will be that the flow of strata heat into the heading will increase due to the lowered air temperature, a phenomenon that is examined in Chapter 15. Yet more heat is added as the air returns over the condenser. The net effect is that the return air leaving the area has a greater enthalpy (and, usually, temperature and humidity) than would

be the case if the refrigeration unit were not operating. The increase in enthalpy is the sum of the additional strata heat and the energy taken by the compressor. The use of spot coolers is restricted by the availability of return air and the debilitating effect on psychrometric conditions within local return airways.

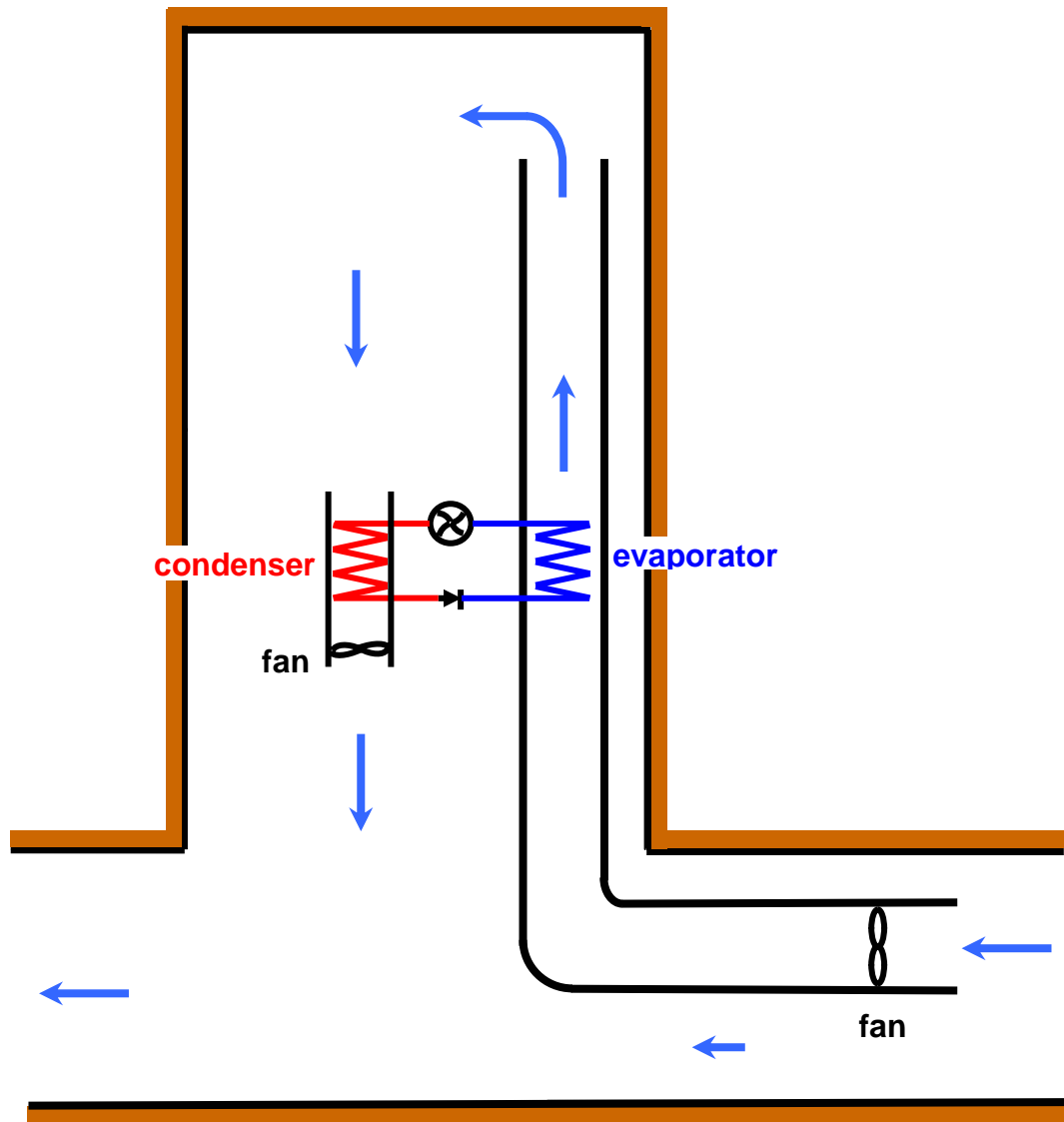


Figure 18.8 The simplest application of a direct evaporator or spot cooler with local heat rejection in a mine heading.

There are three ways of alleviating the situation. First, the condenser could take the form of a shell and tube heat exchanger and be cooled by a water circuit (Figure 18.3). The hot water can then be piped away and recirculated through a heat exchanger in a main return airway. Secondly, the refrigeration unit itself may be located away from the working area and water that has been chilled by the evaporator piped to a heat exchanger in the workings. Thirdly, the first two arrangements may be combined, resulting in the system illustrated in Figure 18.9. Here, the refrigeration plant of, perhaps, 2 MW cooling duty, is sited in a stable location and provides chilled water for a number of work areas. The chilled water flows through thermally insulated pipes to heat exchangers in the faces, stopes or headings and returns to the plant via uninsulated pipes. Some of the chilled water may be used for

dust suppression purposes in which case additional make-up water must be supplied to the plant. Hot water from the condenser is recirculated through heat exchangers that are located in a main return airway. If that return airway is to remain open for persons to travel, either for routine purposes or as an emergency escapeway, then the psychrometric conditions must remain physiologically acceptable (Chapter 17). Again, this provides a limit on the degree of heat rejection and, hence, size of refrigeration plant that can be utilized as a district cooler. If, however, a return route can be dedicated fully to heat rejection, then physiological acceptability limits may be exceeded. In this case, the dedicated return or "dirty pipe", as it is sometimes called, must be made inaccessible to inadvertent entry by personnel. Inspection or maintenance can be carried out either when the plant is shut down or by persons wearing protective clothing (Section 17.5.6). It may be necessary to seek exemption from national or state legislation in order to utilize a "dirty pipe" arrangement.

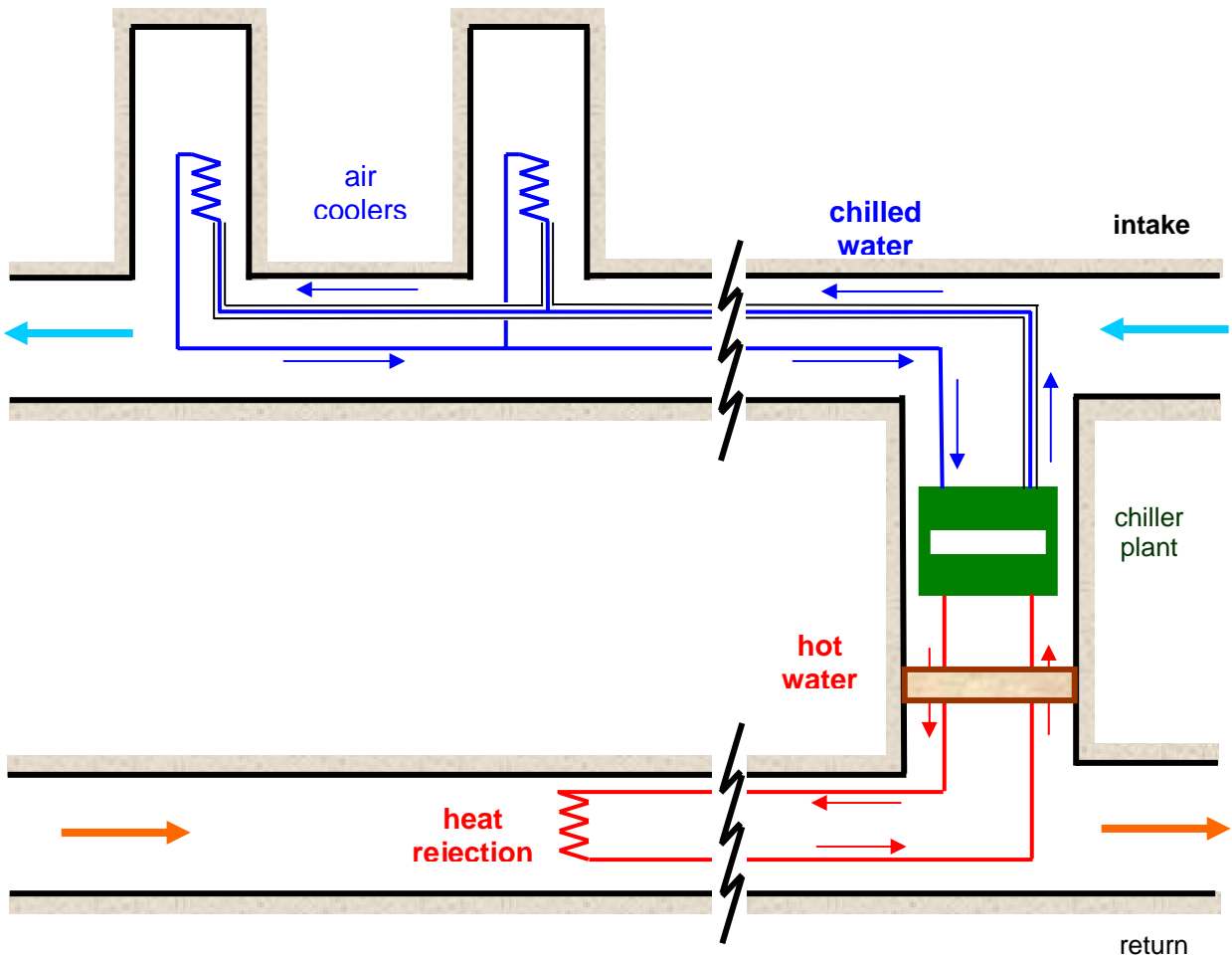


Figure 18.9 A district chiller supplying cold water to air coolers in headings, stopes or faces and rejecting heat into a return airway.

For mines that have a widespread heat problem, the economies of scale and the need for flexibility indicate a requirement for large centralized cooling facilities. Banks of individual refrigeration units, each producing a typical 3.5 MW of cooling capacity, may be assembled to give a total duty which might exceed 100 MW for a large and deep metal mine. The "coolth" is normally distributed via chilled water lines to provide any required combination of bulk air cooling, face or stope air cooling and chilled service water.

Until the mid-nineteen seventies, centralized plant tended to be located underground in excavated refrigeration chambers close to shaft bottoms. All of the mine return air could then be utilized for heat rejection. In South Africa, it was common for large cooling towers to be situated in, or adjacent to, the upcast shaft bottoms. Chilled water from the centralized underground plant could be transmitted to other levels. However, at elevations greater than some 500 m below the plant, water pressures in the pipe ranges become excessive. This can be counteracted either by **pressure reducing valves** (adjustable orifices) or by employing **water to water heat exchangers** and secondary, low pressure, cold water circuits. Unfortunately, there are difficulties associated with both of these types of device. Pressure reducing valves necessitate the employment of high duty pumps to raise the heated water back to the plant elevation. Maintaining the high pressure water in a closed circuit by means of water to water heat exchangers balances the pressure heads in the supply and return shaft ranges. However, the intermediate water to water heat exchangers produce an additional loss of heat transfer efficiency between the work areas and the refrigeration plant. Furthermore, they are a further source of potential corrosion and fouling of internal tubes.

In the mid 'seventies a number of factors coincided to promote a trend towards the location of **centralized refrigeration plant** at the surface of deep and/or hot mines. First, there was a significant drop in the wet bulb temperatures at which mining workforces would be expected to work. **Cut-off wet bulb temperatures** have been reduced from 32°C to 28°C with an expectation of further improvements to 27°C or less. Secondly, the combination of greater depths of workings and more intensive mechanization produced higher heat loads to be handled by the mine environmental control system. These factors combined to give very significant increases in the required cooling capacities of mine refrigeration plant, to the extent that untenable and uneconomic quantities of return air would be required for heat rejection. There was no choice but to locate the larger new plant on surface where heat rejection is relatively straightforward. Thirdly, the problem of high pressures developing in the shaft pipes was combatted by the development of energy recovery devices including water turbines (Section 18.3.4).

A simplified schematic of one arrangement involving surface refrigeration plant is indicated on Figure 18.10. The figure illustrates water being cooled by a surface refrigeration plant and collected temporarily in a cold water dam. The hot water from the condensers is cycled around the condenser cooling tower for heat rejection to the atmosphere. If a natural supply of sufficiently cool water is available from a stream or river, then there may be no need for the capital and operating expense of refrigeration plant. Alternatively, in dry climates, a modest required degree of cooling may be achievable simply by spraying the water supply through a surface cooling tower. Furthermore, it may be necessary to operate the refrigeration plant during the summer months only.

The water passes from the surface cold water dam to an insulated shaft pipe through which it falls to the working levels. The water may then be passed through a turbine at one or more subsurface levels before being stored temporarily in underground cold water dams. The turbine(s) achieve three beneficial results. First, the pressure of the water is reduced to that of the mine atmosphere at the corresponding level. Hence, no extensive high pressure water systems need exist in the workings. Secondly, the mechanical output power produced by the turbines may be employed directly to assist in driving the pumps that raise the return hot water to surface. However, because the demand for cold water may be out of phase with the availability of hot return water, it is preferable to use the turbines to drive generators for the production of electrical power. Third, the removal of energy from the water by the turbines results in a reduced temperature rise of that water, improving the cooling efficiency of the system.

From the underground cold water dams, the chilled water may be utilized for a variety of purposes including water to air heat exchangers for cooling the air at the entrance to a stope or face, or for recooling at intermediate points along the stope or face. Water to water heat exchangers may be employed to cool secondary water circuits such as a supply of potable drinking water or dust suppression service water. However, the modern trend is to supply chilled service water directly from the cold water dam.

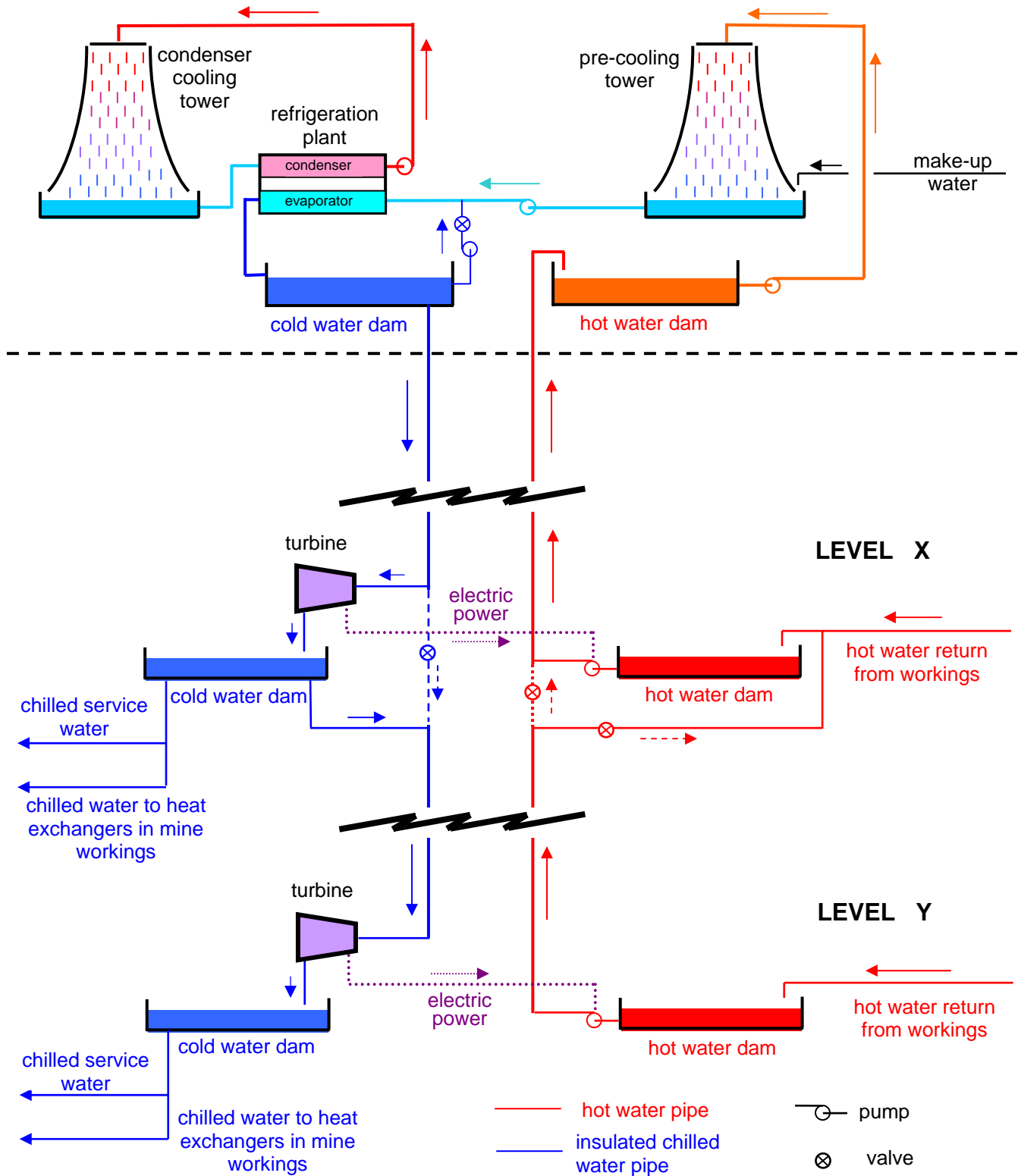


Figure 18.10 Schematic of centralized plant on surface supplying chilled water for underground heat exchangers and mine service water.

Warm water returning from the heat exchangers or via drainage channels is directed into hot water dams adjacent to a shaft. The pumps that return this water to surface may be powered partly by the energy recovered by the turbines. Where surface refrigeration plant is in use, the hot water from the mine may be sprayed through pre-cooling towers prior to its return to the plant evaporators. This gives an additional low cost supplement to the cooling capacity of the system. Any required make-up water and anti-corrosion chemicals are added at this stage.

The purpose of the dams on both the cold and hot water sides of the layout is to provide capacitance to the system. This permits short term fluctuations in demand for chilled water while using smaller refrigeration plant than would otherwise be necessary. At times of low demand, the temperature of the water in the surface dams can be further reduced by recycling that stored water through the plant. This smoothes the variations in cooling load required of the refrigeration units.

Having introduced the broad concepts of subsurface cooling systems, we are now in a better position to examine the component parts in greater detail.

18.3.2. Heat exchangers

In general, a heat exchanger may be defined as a device that facilitates the transfer of thermal energy from one solid or fluid system to another. In subsurface air conditioning systems, there are two classifications of heat exchanger in common use, both involving heat transfer between fluids.

An **indirect heat exchanger** promotes heat transfer across a solid medium that separates the two fluids. There is no direct contact between the fluids. Examples include:

- the shell and tube evaporators and condensers of refrigeration units (Figure 18.3)
- shell and tube water to water heat exchangers employed to transfer heat between water systems of differing pressure and/or water quality (Figure 18.11)
- tubular coil heat exchangers to transfer heat from air to water (Figure 18.12).

As the term implies, **direct heat exchangers** involve direct contact between the two fluids. Cooling towers and other types of spray chambers fall into this category. The objective may be to reject heat from the water to the air as in a conventional cooling tower. Conversely, a spray chamber supplied with chilled water provides a means of cooling an airstream.

The higher efficiency of heat transfer associated with direct heat exchangers caused a distinct trend away from tube coil air coolers during the nineteen eighties. Good performance of large horizontal spray chambers for bulk air cooling promoted the further development of compact and enclosed spray chambers for more localized use.

In this section we shall examine the essential structure and operating principles of both indirect and direct forms of heat exchanger.

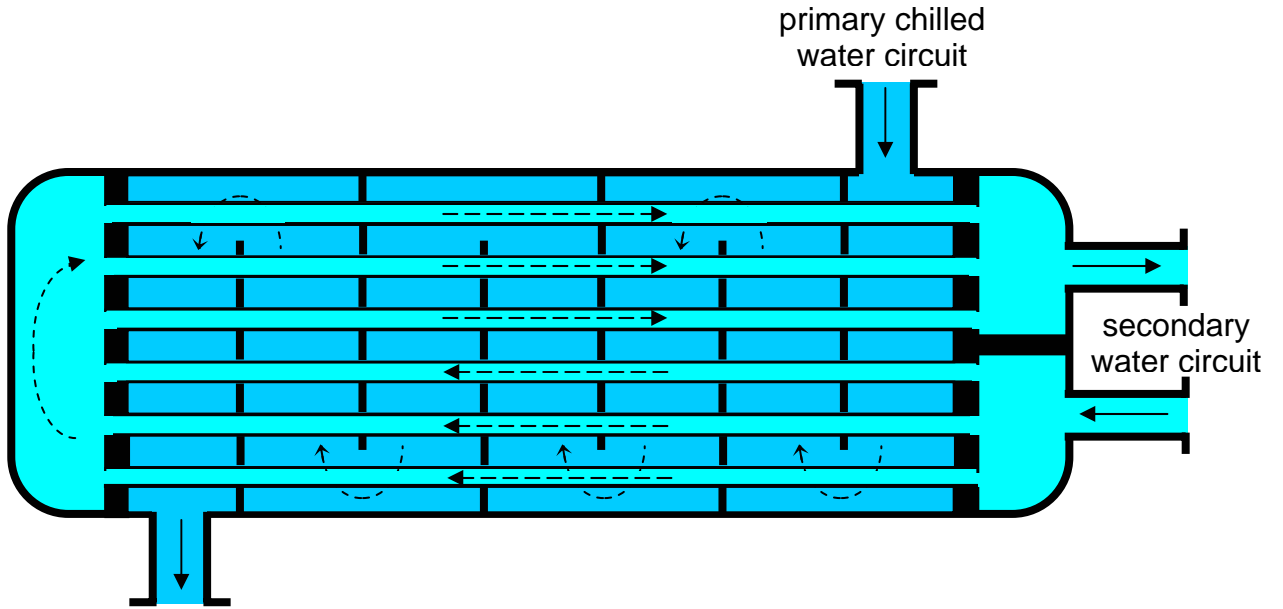


Figure 18.11 A water-to-water heat exchanger

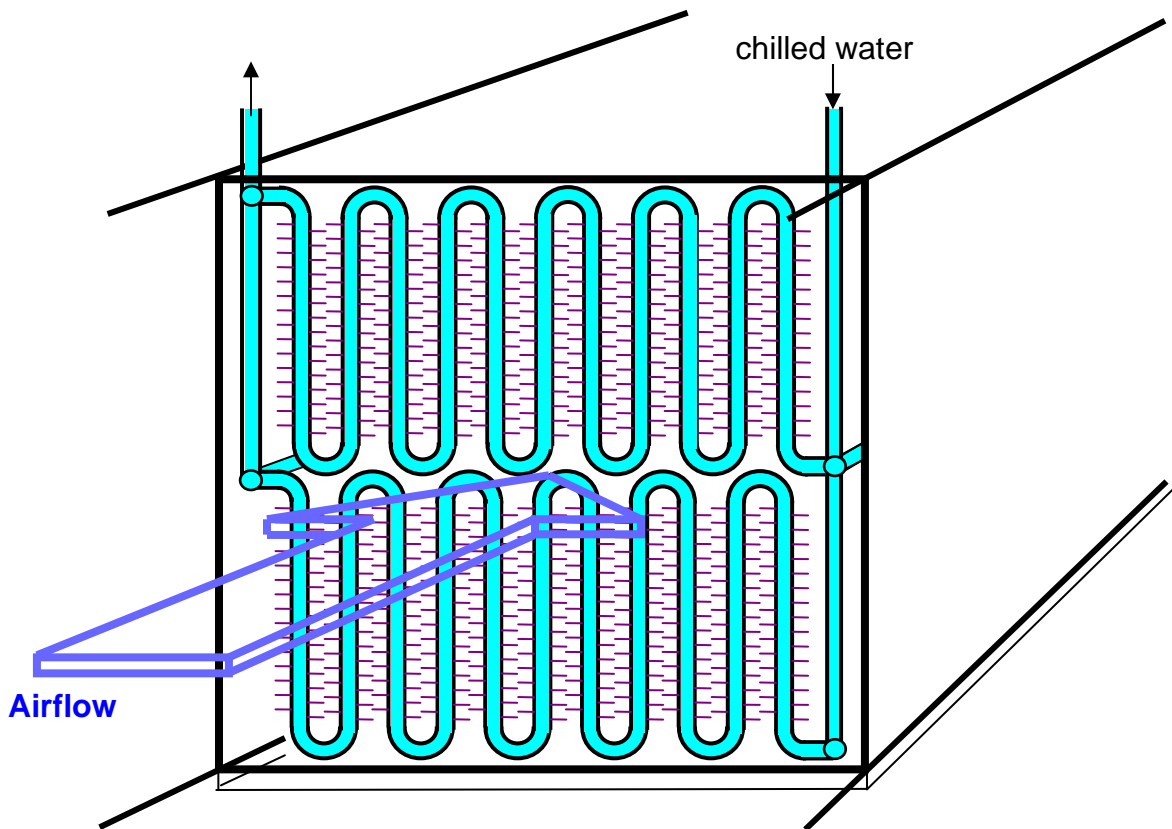


Figure 18.12 An air-to-water heat exchanger showing one layer of tubes.

18.3.2.1. Indirect heat exchangers

A **shell and tube heat exchanger** may contain over 200 tubes. In a counter-flow heat exchanger, the fluids inside and outside the tubes move in opposite directions, maximizing the total heat transfer. However, the water to water heat exchanger illustrated in Figure 18.11 shows that this may be sacrificed in the interest of compactness.

In an air to water indirect heat exchanger, a bank of tubes carrying chilled water is located within an air duct. Figure 18.12 shows one layer in a bank of tubes. The tubes are often inclined to the direction of airflow to improve the efficiency of the unit and to control the movement of condensate.

The two important features of a heat exchanger are that a good efficiency of heat transfer is obtained and that the pressure drops suffered by both fluid streams should remain within acceptable limits. Heat transfer is facilitated by choosing a tube material that has a high thermal conductivity and is also resistant to corrosion and the build-up of scale deposits within the tubes. Chemical additives can be used to control such fouling of the tubes. Copper tubes are commonly employed for air to water heat exchangers. For water to water heat exchangers and in the evaporator and condensers of refrigeration units, cupronickel and stainless steel are more resistant to corrosion. Even titanium may be used within evaporators and condensers.

If tubes are not maintained in a clean condition then the efficiency of the unit can fall dramatically. Periodic manual brushing of the tubes is time-consuming and may be replaced by a variety of automatic tube cleaning devices including reverse flushing with brush inserts or ultrasonic vibration. Air to water tube coils, as illustrated on Figure 18.12, are subject to caking by dust deposits in mine atmospheres. This may be handled by periodic cleaning with a high pressure water jet. Alternatively, sprays may be located permanently upstream from the coils. In humid atmospheres, the coils may be made self-cleaning by arranging them into horizontal banks with air passing upwards over the tubes. The droplets of condensate fall back through the coils giving a continuous and oscillating cleaning action on the outer surfaces of the tubes.

A second major factor that controls the duty of a heat exchanger is the effective area available for thermal transfer. Spiral fins welded to the tubes, as illustrated on Figure 18.12, may be used. Metal plates welded between consecutive and partially flattened tubes have also been used (Mücke, 1984; Weuthen, 1975). It is important that such means of area enlargement should have good thermal contact with the tubes and that they are oriented such that they present minimum resistance to flow over the tubes. In evaporators and condensers, the tube surfaces may be knurled or sintered. In addition to enhancing the surface area, this assists in the promotion of boiling or condensation.

18.3.2.2. Performance calculations for indirect heat exchangers

At equilibrium, the heat gained by one fluid in a heat exchanger must equal the heat lost by the other fluid. Hence, taking the example of an air to water heat exchanger, we can express the rate of heat transfer to be

$$q = m_w C_w \Delta t_w = m_a \Delta S \quad \text{W} \quad (18.17)$$

where m_w = mass flow of water (kg/s)
 C_w = specific heat of water (4187 J/(kg °C))
 Δt_w = rise in temperature of the water (°C)
 m_a = mass flow of air (kg/s)
 ΔS = fall in sigma heat of the air (J/kg) (ref. section 14.6).

As each of the factors in equation (18.17) can be calculated easily from measured temperatures and flowrates, either the water or the air may be used to determine the rate of heat transfer, q . As measurements on the water circuit can normally be made more accurately than those on the airflow, the former are preferred for a determination of heat transfer. If condensation occurs on the outside of the coils then the third part of equation 18.17 is slightly in error as it does not take into account the heat removed from the system by the condensate. However, this is usually small and may be neglected.

Another way of expressing the heat transfer is in terms of an **overall heat transfer coefficient**, U , ($\text{W}/\text{m}^2\text{°C}$) for the coils and adjacent fluid boundary layers, and the difference between the mean temperatures of the air and the water, ($t_{ma} - t_{mw}$), giving

$$q = UA (t_{ma} - t_{mw}) \quad \text{W} \quad (18.18)$$

where A = area available for heat transfer. (This is analogous to equation (15.16) for a rock surface.)

As the temperatures of both the air and water streams are likely to vary in a logarithmic rather than a linear fashion through the heat exchanger, it is more accurate to employ **logarithmic mean temperature difference** in equation (18.18), giving

$$q = \frac{UA (\Delta t_1 - \Delta t_2)}{\ln (\Delta t_1 - \Delta t_2)} \quad \text{W} \quad (18.19)$$

where \ln indicates natural logarithm and Δt_1 and Δt_2 are the temperature differences between the fluids at each end of the heat exchanger.

The **UA product** is usually quoted as a measure of the **effectiveness** of an indirect heat exchanger.

A performance check should be carried out at monthly or three monthly intervals in order to determine any deterioration in the UA caused by corrosion, scaling, or other forms of deposition on the tube surfaces.

Example

Measurements made on a counterflow air to water cooling coil give the following results.

Air: Inlet wet bulb/dry bulb temperature = 28/34°C
 Outlet wet bulb/dry bulb temperature = 22.7/22.7°C
 Mass flowrate = 5.1 kg/s
 Barometric pressure = 105 kPa

Water: Inlet temperature = 17 °C
 Outlet temperature = 23 °C
 Mass flowrate = 4 kg/s

Determine the operating duty of the coil and the UA value.

Solution

From the psychrometric equations given in section 14.6, the sigma heats of the air at inlet and outlet conditions of 28/34 and 22.7/22.7°C, respectively, are found to be

$$S_{in} = 84\,696 \text{ J/kg}$$

and

$$S_{out} = 63\,893 \text{ J/kg}$$

From equation (18.17) the heat lost from the air is:

$$q_a = m_a (S_{in} - S_{out}) = 5.1 (84\,696 - 63\,893) = 106.1 \times 10^3 \text{ W or } 106.1 \text{ kW.}$$

Also, from equation (18.17), the heat gained by the water is:

$$q_w = m_w C_w \Delta t_w = 4 \times 4187 \times (23-17) = 100.5 \times 10^3 \text{ W or } 100.5 \text{ kW.}$$

At equilibrium, q_a and q_w must be equal, showing that the errors in measurements have caused a deviation of some 5.5 percent. Much larger discrepancies often occur due mainly to difficulties in making measurements in highly turbulent and, often, saturated airflows. We shall continue the calculation using the rate of heat transfer given by the water circuit, 100.5 kW.

In order to calculate the UA value from equation (18.19), we must first evaluate the temperature differences between the water and air at the air inlet and air outlet ends (subscripts 1 and 2, respectively).

$$\Delta t_1 = t_{a,in} - t_{w,out} = 34 - 23 = 11 \quad ^\circ\text{C}$$

$$\Delta t_2 = t_{a,out} - t_{w,in} = 22.7 - 17 = 5.7 \quad ^\circ\text{C}$$

Notice that we use the dry bulb temperature at the air inlet and before saturation conditions are attained for the determination of Δt_1 . This is equivalent to taking the latent heat of condensation as a factor contributing towards the UA value of the heat exchanger.

Equation (18.19) now gives

$$UA = q_w \frac{\ln(\Delta t_1 / \Delta t_2)}{(\Delta t_1 - \Delta t_2)} = 100.5 \frac{\ln(11/5.7)}{(11 - 5.7)} = 12.47 \text{ kW}/^\circ\text{C}$$

The UA of a clean coil may lie between 10 and 25 kW/ $^\circ\text{C}$ depending upon the design of the heat exchanger and the configuration of fluid flows. Records should be kept of the periodic performance tests on each heat exchanger. Significant reductions in UA values indicate the need for cleaning or replacement of the tubes.

Although UA values are normally determined by measurement as illustrated in the example, they may also be defined by the following equation:

$$\frac{1}{UA} = \frac{1}{h_i A_i} + \frac{1}{h_{fi} A_i} + \frac{x}{k_t A_m} + \frac{1}{h_o A_o} + \frac{1}{h_{fo} A_o} \quad ^\circ\text{C} \quad (18.20)$$

where h = heat transfer coefficients (W/(m²°C))
 A = area available for heat transfer (m²)
 x = thickness of tube walls (m)
 k_t = thermal conductivity of tube material (W/(m°C))

and subscripts

i = inside surface of tubes
 o = outside surface of tubes
 m = mean of inner and outer surfaces.

h_{fi} and h_{fo} are the heat transfer coefficients associated with fouling (deposits) on the inside and outside surfaces of the tubes respectively. On a clean tube there are no such deposits; h_{fi} and h_{fo} are both then infinite.

Radiation terms have been left out of equation (18.20) as these are normally small in a heat exchanger. They may, however, become significant in situations such as an uninsulated pipe suspended in an airway.

Equation (18.20) can be further simplified for practical application. First, the term $x/(k_t A_m)$ is very small compared with the others. Secondly, the terms involving fouling of the tubes are often combined and attributed to the inside surface only, giving

$$\frac{1}{UA} = \frac{1}{h_i A_i} + \frac{1}{h_o A_o} + \frac{1}{h_f A_i} \quad ^\circ\text{C/W} \quad (18.21)$$

As fouling of the tubes occurs, h_f will decrease causing the UA value also to fall. Whillier (1982) quotes a typical value of some 3000 W/(m²°C) for h_f in a mine refrigeration plant. For turbulent flow inside smooth tubes, the **heat transfer coefficient** can be determined from equation (15.23) and the **Colburn equation** (A15.15)

$$h_i = 0.023 \frac{k}{d} \text{Re}^{0.8} \text{Pr}^{0.4} \quad \text{W/(m}^2 \text{ } ^\circ\text{C)} \quad (18.22)$$

where k = thermal conductivity of fluid (W/(m°C))

d = internal diameter of tube (m)

Re = Reynolds number = $\rho u d / \mu$ (dimensionless)

ρ = fluid density (kg/m³)

u = fluid velocity (m/s)

μ = dynamic viscosity (Ns/m²)

Pr = Prandtl number = $C_p \mu / k$ (dimensionless, may be taken as 0.7 for air)

and C_p = Specific heat at constant pressure (J/(kg°C))

For air and water, the values of viscosity and thermal conductivity within the temperature range 0 to 60°C are given in sections 2.3.3 and 15.2.4 respectively. Other expressions for the heat transfer coefficient at rough surfaces are given in Table A15.1.

The values of h_o for the outer surfaces of the tubes vary widely according to geometry and the configuration of tubes. For turbulent cross flow of air over tubular surfaces, **McAdams** (1954) gives:

for a single tube:

$$h_o = 0.24 \frac{k_a}{d} \text{Re}^{0.6} \quad \frac{\text{W}}{\text{m}^2 \text{ } ^\circ\text{C}} \quad (18.23)$$

and for a bank of staggered tubes:

$$h_o = 0.29 \frac{k_a}{d} \text{Re}^{0.6} \quad \frac{\text{W}}{\text{m}^2 \text{ } ^\circ\text{C}} \quad (18.24)$$

In these relationships, d is the outer diameter of the tubes and Reynolds' Numbers are determined on the basis of the maximum velocity of the air as it flows between the tubes. The selection of cooling coils is facilitated greatly by tables and graphs provided by manufacturers.

18.3.2.3. Direct heat exchangers

In direct heat exchangers, air is brought into contact with water surfaces. The purpose may be to cool water from the condensers of a refrigeration plant. In this case the hot water is sprayed into a **cooling tower** and descends as a shower of droplets through an ascending airstream. Heat is transferred from the water droplets to the air by a combination of convection (sensible heat) and evaporation (latent heat). The cooled water that collects at the base of the cooling tower is then returned to the condenser (see the condenser cooling tower on Figure 18.10).

Alternatively, the objective may be to cool the air. In this case, chilled water is sprayed into a vertical or horizontal **spray chamber**. Provided that the airflow enters with a wet bulb temperature that is higher than the temperature of the water, then heat will be transferred from the air to the water by a combination of convection and condensation.

Although there are significant differences between the designs of cooling towers and spray coolers, there are several common factors that influence the amount and efficiency of heat exchange:

- water mass flowrate
- supply temperature of water
- air mass flowrate
- psychrometric condition of the air at inlet
- duration and intimacy of contact between the air and the water droplets.

This latter factor depends upon the physical design of the heat exchanger. In particular,

- (i) the relative velocity between the air and water droplets
- and
- (ii) the size and concentration of water droplets - governed by the flow and pressure of the supply water, the type and configuration of spray nozzles, and the presence of packing within the heat exchanger.

The traditional use of direct heat exchangers in mine air conditioning systems has been for cooling towers either underground or on surface. Tube coil heat exchangers with closed circuit water systems have been used extensively for air cooling in or close to mine workings. However, the greater efficiency of direct heat exchangers led to the development of large permanent spray chambers for bulk air cooling. Furthermore, through the nineteen eighties, smaller portable spray chambers began to be employed for local cooling.

Cooling Towers

First, let us examine the essential features of cooling towers. Figure 18.13 illustrates a vertical forced draught cooling tower of the type that may be used on the surface of a mine. Hot water from refrigeration plant condensers is sprayed into the cooling tower and moves downward in counterflow to the rising air current. The purpose of the packing is to distribute the water and airflow uniformly over the cross section and to maximize both the time and total area of contact between the air and water surfaces. The packing may take the form of simple splash bars or ruffles arranged in staggered rows, egg-crate geometries or wavy (film-type) surfaces located in vertical configurations. The materials used for packing may be treated fir or redwood timber, galvanized steel, metals with plastic coatings and injection molded PVC or polypropylene. Concrete is used primarily for casings, structural reinforcements and water sumps or dams. Air velocities through counterflow packed cooling towers lie typically in the range 1.5 to 3.6 m/s.

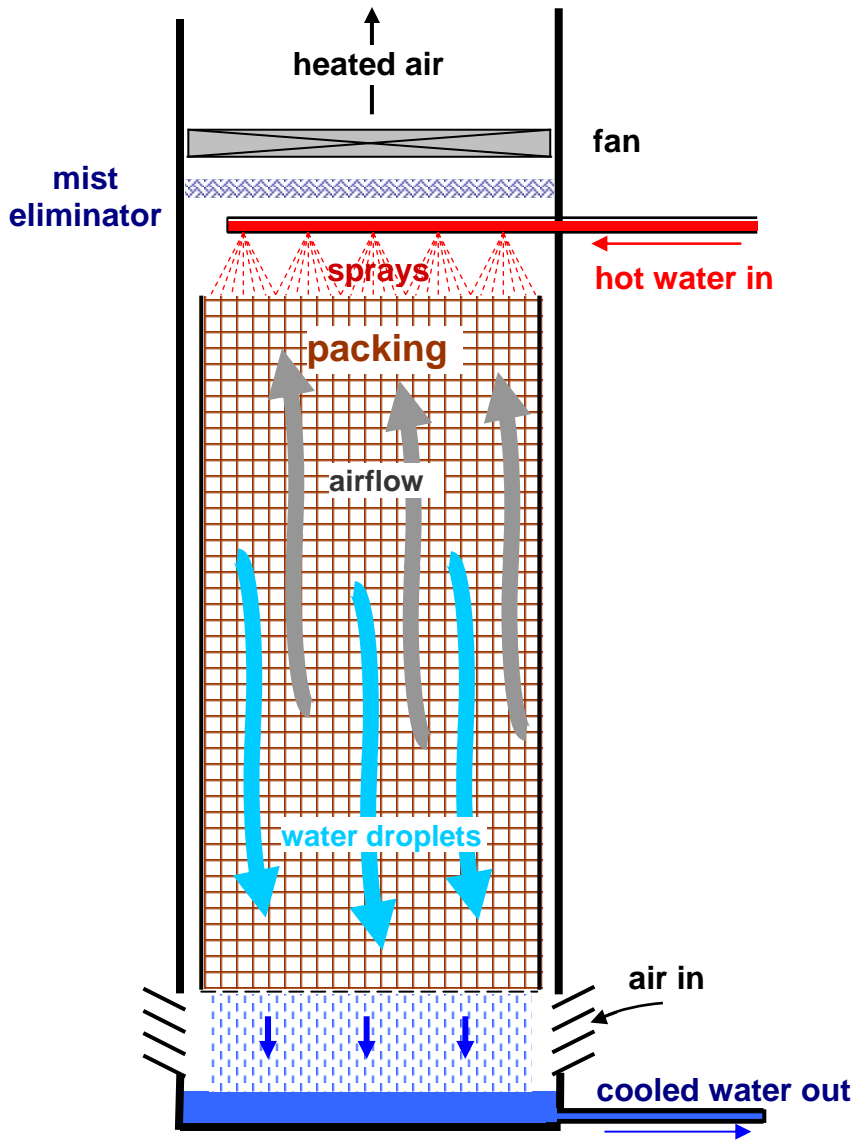


Figure 18.13 Counterflow cooling tower. (The same configuration may be used to cool air by supplying the tower with chilled water.)

In underground cooling towers, the packing is often eliminated completely or takes the form of one or two screens arranged horizontally across the tower. Such heat exchangers are essentially vertical spray chambers. Other means of maximizing contact time are then employed. These include designs that introduce a swirl into the air at entry, and directing the sprays upward rather than downward. Again, in underground installations, airflow is induced through the cooling towers by the mine ventilating pressure or by booster fans in return airways rather than by fans connected directly to the tower. The pressure drop through underground cooling towers may be further reduced by replacing the mist eliminator screens with an enlarged cross-sectional area; the lower air velocity in this zone decreases the carry-over of water droplets. The optimum air velocity in open spray towers lies in the range 4 to 6 m/s with a maximum of some 8 m/s. Water loadings should not be greater than 16 litres/s per square metre of cross-sectional area (Stroh, 1982).

Cooling towers of the type used for mine air conditioning are typically 10 to 20 m in height and some 3 to 8 m in diameter, depending upon the rate at which heat is to be exchanged. Heat loads may be as high as 30 MW.

Natural draught cooling towers do not have fans but rely upon air flow induction by the action of the sprays, or by density difference between the outside atmosphere and the hot moist air within the tower. The hyperbola shaped cooling towers employed commonly for the high heat loads of power stations are of this type and may be over 150 m high in order to accentuate the chimney effect.

The air leaving a cooling tower is usually saturated. This often results in the formation of a fog plume in the surface atmosphere. The environmental effects of such a plume should be considered carefully and may influence the siting of a surface cooling tower. In large installations with unacceptable fog plumes, part of the hot condenser water may be cooled within a finned tube indirect heat exchanger. This involves sensible heat exchange only and reduces the humidity of the air leaving the cooling tower. However, such an arrangement detracts from the overall efficiency of heat transfer.

In a direct exchange cooling tower, some water is lost continuously from the circuit both by evaporation and by **drift** (or **carry-over**) of small droplets. The evaporation loss approximates some one percent for each 7°C of water cooling and drift loss is usually less than 0.2 percent of the water circulation rate (ASHRAE, 1988). However, evaporation can result in a rapid escalation in the concentration of dissolved solids and other impurities leading to scaling, corrosion and sedimentation within the system. In order to limit the buildup of such impurities, some water is continuously removed from the system (**bleedoff** or blowdown). The bleedoff rate is controlled by monitoring the quality of the water but may be of the order of one percent of the circulation rate. The combined losses from evaporation, drift and bleedoff are made up by adding clean water to the circuit.

Further protection of metal components and, particularly the tubes of condensers is obtained by administering **anticorrosion compounds**. These generally take the form of chromates, phosphates or polyphosphonates of zinc, and promote the formation of a protective film on metal surfaces. Some of these compounds are toxic and precautions may be necessary against accidental release into natural drainage systems. **Biocides** such as chlorine are also added on a periodic basis to control the growth of algae and other organic slimes.

Chilled water spray chambers

If the water supplied to a direct contact heat exchanger is at a temperature below that of the wet bulb temperature of the air, then cooling and dehumidification of the air is achieved. Chilled water spray chambers fall into two categories with respect to size. First, the larger installations are constructed at fixed sites for bulk cooling of main airflows. Secondly, portable spray chambers for localized use within working areas have many advantages over the more traditional tube coil (indirect) stoop or face coolers. We shall consider each of these two applications in turn.

For **bulk air cooling**, spray chambers may be designed in vertical or horizontal configuration. Indeed, if the cooling tower shown on Figure 18.13 were supplied with chilled water, then it would act equally well as a vertical spray air cooler. Such designs may be employed either on surface or underground for bulk cooling of intake air and may have heat transfer duties up to 20 MW.

Horizontal spray chambers have more limited maximum capacities of some 3.5 MW. They are, however, more convenient for underground use in that existing airways may be utilized without additional excavation. Figure 18.14 illustrates a single stage horizontal spray chamber. The sprays may be directed against or across the airflow. The nozzles can be distributed over the cross section as shown in the sketch or, alternatively, located at the sides or near the base of the chamber. Although the position of the nozzles appears not to be critical, it is important that both the sprays and the airflow are distributed uniformly over the cross section. The **spray density** should lie within the range 2 to 5 litres/second for each square metre of cross sectional area (Bluhm, 1983).

The area of liquid/air interface and efficiency of heat exchange increase for smaller **sizes of droplets**. However, very small droplets result in excessive carry-over or necessitate highly constrictive mist eliminators. Furthermore, higher water pressures and, therefore, pumping costs are required to produce fine sprays. In practice, droplet diameters of some 0.5 mm and water pressures in the range 150 to 300 kPa give satisfactory results in horizontal spray chambers (Reuther, 1988).

At positions fairly close to the nozzles, the relative directions of the air and water droplets may be counterflow or crossflow, dependent upon the orientation of the nozzles. However, aerodynamic drag rapidly converts the spray to parallel flow, particularly for the smaller droplets. In order to regain the higher efficiency of counterflow heat exchange, the spray chamber may be divided into two or three stages so that the air leaves the chamber at the position of the coldest sprays. Chilled water should be supplied at as low a temperature as practicable but, in any event, not higher than 12°C.

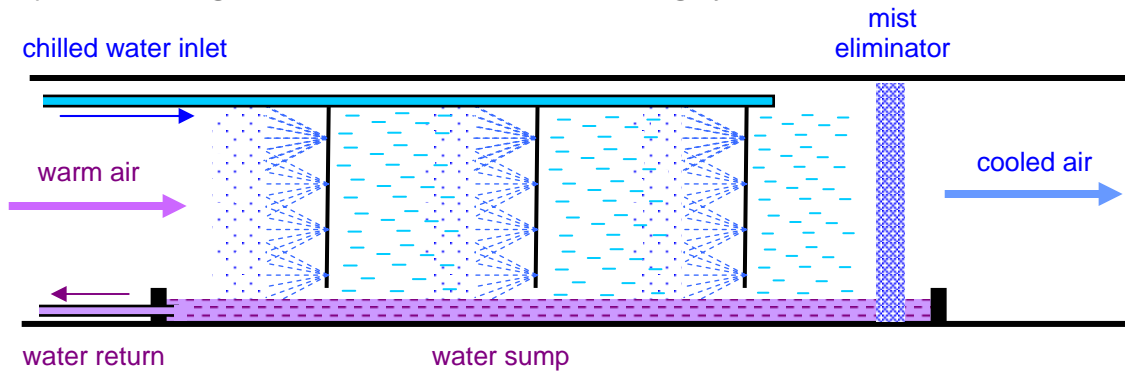


Figure 18.14 A single stage , horizontal spray chamber.

Figure 18.15 illustrates a two stage spray chamber. An additional sump at each end assists in balancing the pumping duties.

If the surrounding strata are unfractured and unaffected by water, then the spray chamber may utilize the full cross section of a bypass airway. If, however, the rock must be protected against the effects of water, then concrete lining or prefabricated sections may be employed to contain the spray chamber. In cases where the strata is very sensitive to water (such as evaporite strata) then it is advisable to protect the rock surfaces for 50 to 100 m downstream from the spray chamber.

The cross-sectional area of the spray chamber should be chosen to give a preferred air velocity of some 4 to 6 m/s, but not more than 7 m/s. Higher air velocities will reduce the efficiency of heat exchange and can result in excessive pressure drops in the airflow.

In addition to cooling and dehumidifying the air, spray coolers can also reduce dust concentrations. However, the buildup of dust particles in the recirculating water system may cause fouling of the pipes and other heat exchangers. This may require filters or sedimentation zones to be included in the design.

Internal packing can also be employed to improve the efficiency of horizontal spray chambers (Stroh, 1980). This can increase the air frictional pressure drop across the cooler. However, the water supply pressure (gauge) may be as low as 30 kPa since the spray nozzles can be replaced by low resistance dribbler bars.

In order to extend the applicability of direct spray coolers, enclosed and portable units have been developed (Thimons, 1980; Ramsden, 1984; Reuther, 1988). These may be mounted on wheels or sleds and are often referred to as **spray mesh coolers**. Figure 18.16 illustrates the principle of operation. In order to maintain the design to acceptable dimensions for portable application, the water loading may be much higher than open spray chambers and it becomes even more important to maximize the area and time of contact between the air and water. This occurs in three stages. First, the air passes through the lower mesh of plastic or knitted stainless steel. Secondly, the airflow is directed through the upward pointing and finely divided sprays. The final stage of cooling occurs within the upper mesh which also acts as a demister. The distribution of droplets of water falling from the upper to the lower mesh may be assisted by installing drip fins. These also help to prevent water running down the walls (Heller, 1982). Between the two meshes, heat exchange occurs by a combination of counterflow, crossflow and parallel flow. Another type of portable spray cooler employs film packing and crossflow heat exchange (Reuther, 1988).

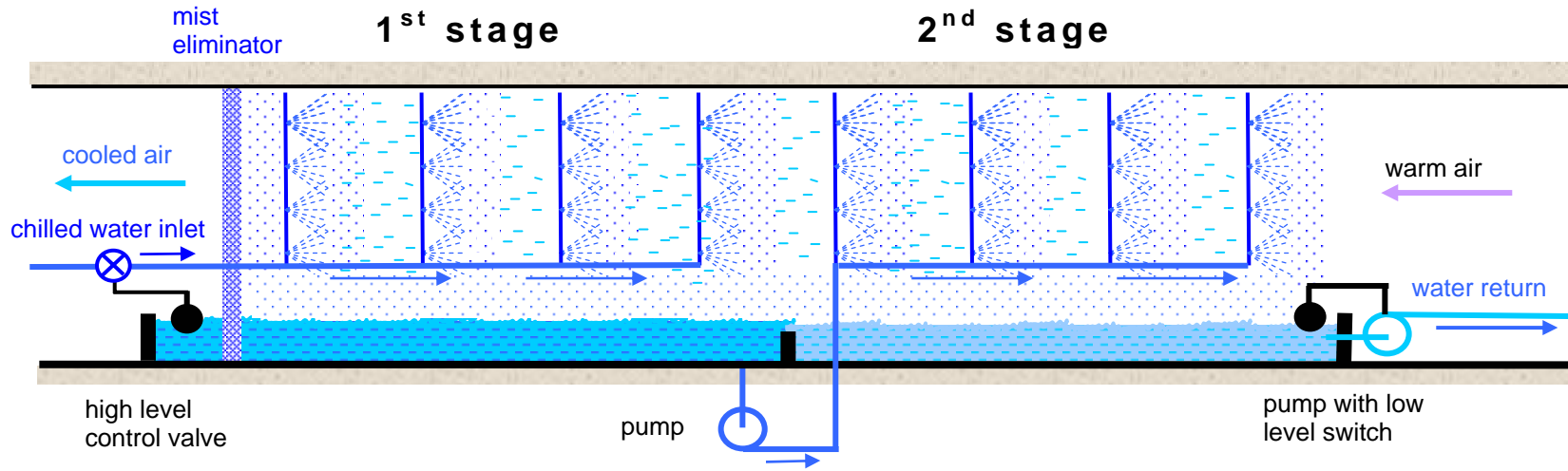


Figure 18.15 A two-stage horizontal spray chamber

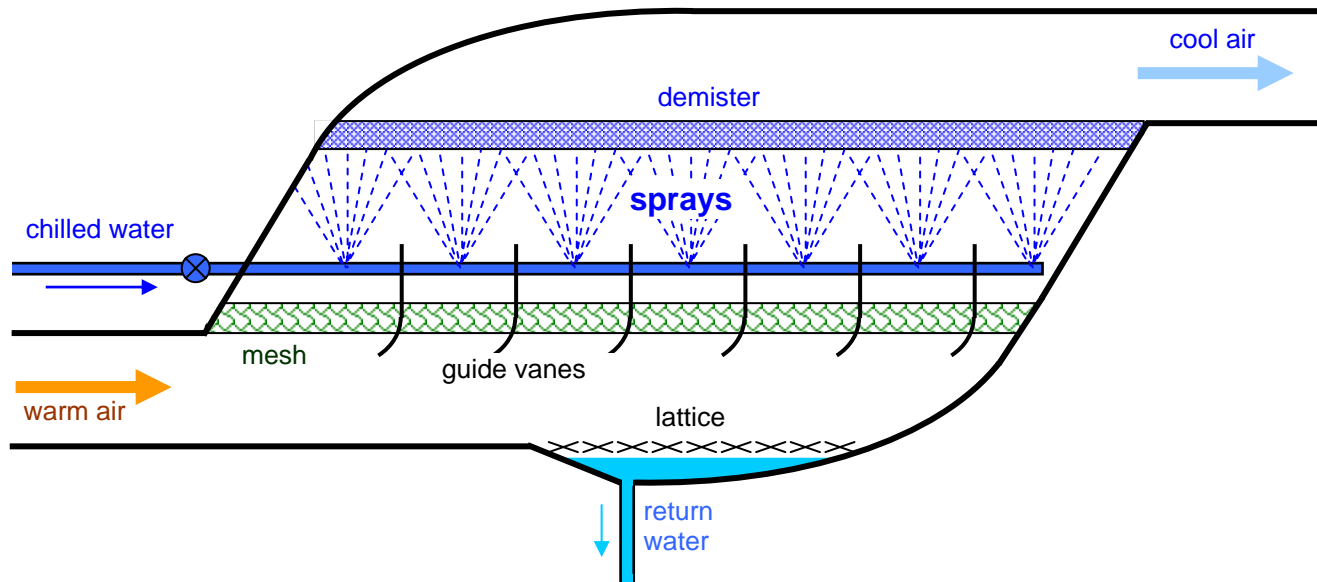


Figure 18.16 A section through a portable mesh cooler.

The dry bulb temperature of air can be reduced by passing it through a spray chamber supplied with unchilled water. The device is then known as an **evaporative cooler**. No heat is removed from the air. Hence, if the water is supplied at wet bulb temperature, then the exhaust air may attain that same wet bulb temperature while the moisture content will have increased. Evaporative coolers have an application for surface structures in hot dry climates but are seldom used in underground mines. They have been employed for very localized effects in hot evaporite mines. However, the reduced dry bulb temperature encourages enhanced heat flow from the strata (Section 15.2.2) which, when combined with the raised moisture content, reduces the cooling power of the air downstream from the cooled area.

18.3.2.4. Performance calculations for direct heat exchangers.

A common theoretical analysis may be applied to direct heat exchangers irrespective of the direction of heat transfer. The results of such analyses apply equally well to cooling towers and chilled water spray chambers. In order to avoid unnecessary repetition, we will conduct the following analysis on the assumption of a cooling tower (Figure 18.13). Water recycles continuously through the condenser of a refrigeration plant (where it gains heat) and the cooling tower where it rejects that heat to the atmosphere.

The first observation is that if we ignore the small heat losses from interconnecting pipes and the equally small effects of make-up water, then, at steady state, the heat rejected in the cooling tower must be equal to the heat gained in the condenser. This leads to the initially surprising statement that the rate of heat rejection in the cooling tower depends only upon the heat load imposed by the condenser and not at all upon the design of the cooling tower. However, if the cooling tower is inefficient in transferring heat from the water to the air, then the temperature of the water throughout the complete circuit will rise until balance is attained between heat gain in the condenser and heat rejection in the cooling tower. This would be unfortunate as the coefficient of performance of the refrigeration plant deteriorates as the condenser temperature increases (Section 18.2.4).

Figure 18.17 illustrates the decrease in temperature of the water as it falls through the cooling tower and the corresponding increase in the wet bulb temperature of the ascending air.

Figure 18.17 also defines the meaning of two terms that are commonly employed:

The **range** is the change in temperature of the water

$$\text{range} = t_{w,in} - t_{w,out} \quad ^\circ\text{C} \quad (18.25)$$

while the **approach** is the difference between the temperatures of the water outflow and the wet bulb temperature of the air inflow:

$$\text{approach} = t_{w,out} - t_{a,in} \quad ^\circ\text{C} \quad (18.26)$$

where t = temperature, $^\circ\text{C}$
 and subscripts w = liquid water
 a = air (wet bulb)
 in = inflow
 and out = outflow

Manufacturers will usually accept requests for approach values down to 2°C .

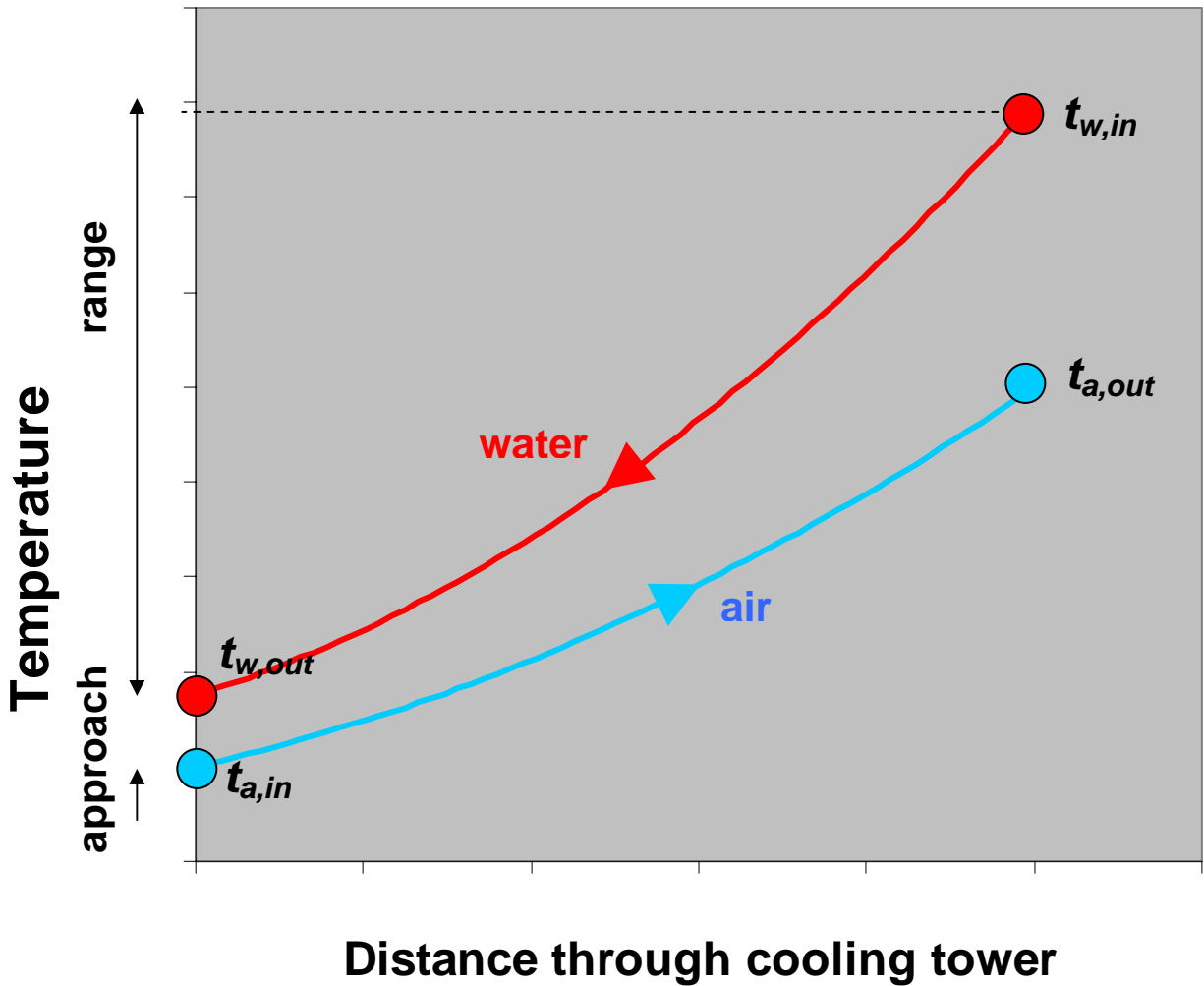


Figure 18.17 Variation of water temperature, t_w , and wet bulb temperature of the air, t_a , through a cooling tower.

The quantitative analysis of the cooling tower commences by writing down the balance that must exist between rates of heat gained by the air and heat lost from the water:

$$m_a (S_{out} - S_{in}) = m_w C_w (t_{w,in} - t_{w,out}) \quad W \quad (18.27)$$

where m = mass flow, kg/s
 S = sigma heat of air, J/kg
 and C_w = specific heat of water (4187 J/kg °C)

This is, in fact, an approximation as evaporation changes the value of m_w within the tower. However, the error does not normally exceed 4 percent and may be neglected for practical purposes.

As in so many cases of assessing performance, it is useful to imagine the unattainable perfect cooling tower. In such a device, the two curves on Figure 18.17 would coincide and, in particular, the water would leave at inlet air wet bulb temperature while the air would leave at the temperature of the incoming water, that is:

$$t_{w,out} = t_{a,in} \quad (18.28)$$

$$\text{and } t_{a,out} = t_{w,in} \quad (18.29)$$

The concept of a perfect cooling tower allows us to devise efficiencies of heat transfer for both the water and the air streams:

water efficiency

$$\begin{aligned} \eta_w &= \frac{\text{actual heat lost from the water}}{\text{theoretical maximum heat that could be lost from the water}} \\ &= \frac{m_w C_w (t_{w,in} - t_{w,out})}{m_w C_w (t_{w,in} - t_{a,in})} = \frac{(t_{w,in} - t_{w,out})}{(t_{w,in} - t_{a,in})} = \frac{\text{range}}{\text{range} + \text{approach}} \end{aligned} \quad (18.30) \text{ (See Figure 18.17)}$$

Similarly, air efficiency

$$\begin{aligned} \eta_a &= \frac{\text{actual heat gained by the air}}{\text{theoretical maximum heat that could be gained by the air}} \\ &= \frac{m_a (S_{out} - S_{in})}{m_a (S_{w,in} - S_{in})} = \frac{(S_{out} - S_{in})}{(S_{w,in} - S_{in})} \end{aligned} \quad (18.31)$$

where $S_{w,in}$ = sigma heat of saturated air at a temperature equal to that of the inlet water, J/kg.

[The term "thermal capacity" is sometimes employed where we have used "theoretical maximum heat".]

Although the water and air efficiencies are useful indicators of the efficacy of heat transfer for each of the two fluids, neither gives any clue to the overall quality of design for the complete cooling tower. For example, if the water flow were low giving relatively few small droplets falling through a large airflow, then the water efficiency would be very high. However, the air would be used to only a small fraction of its thermal capacity and, hence, the air efficiency and overall heat transfer would be low.

To examine this problem let us consider, again, perfect heat transfer in a cooling tower. Then,

$$\text{maximum thermal capacity of water} = m_w C_w (t_{w,in} - t_{a,in}) \text{ J}$$

$$\text{and maximum thermal capacity of airstream} = m_a (S_{w,in} - S_{in}) \text{ J}$$

The ratio of these maximum thermal capacities defines the **tower capacity factor**, R

$$R = \frac{m_w C_w (t_{w,in} - t_{a,in})}{m_a (S_{w,in} - S_{in})} \quad (\text{dimensionless}) \quad (18.32)$$

The liquid to gas ratio, m_w/m_a normally lies within the range 0.4 to 2.0.

The theoretical concept of tower capacity factor ignores the practical reality that in a real cooling tower the rate of heat loss from the water must equal the rate of heat gain by the air. It may be defined in words as follows:

'If both of the given fluid streams were used to their maximum thermal capacity, then R would be the number of Watts lost by the water for each Watt gained by the air.'

An important observation here is that R depends only upon the flowrates and the inlet conditions of the water and air. It is completely independent of the construction of the cooling tower. Notice also that we have been quite arbitrary in choosing to define R as the ratio of water thermal capacity divided by air thermal capacity, rather than the other way round. The values of tower capacity factor vary from 0.5 to 2.

The tower capacity factor is also related to the ratio of air and water efficiencies. From equations (18.30 and 18.31)

$$\frac{\eta_a}{\eta_w} = \frac{(S_{out} - S_{in}) (t_{w,in} - t_{a,in})}{(S_{w,in} - S_{in}) (t_{w,in} - t_{w,out})}$$

and substituting for

$$(S_{out} - S_{in}) = \frac{m_w}{m_a} C_w (t_{w,in} - t_{w,out}) \quad \text{from equation (18.27) gives}$$

$$\frac{\eta_a}{\eta_w} = \frac{m_w}{m_a} C_w \frac{(t_{w,in} - t_{a,in})}{(S_{w,in} - S_{in})} \quad (18.33)$$

As this is identical to equation (18.32), then tower capacity factor

$$R = \frac{\eta_a}{\eta_w} \quad (18.34)$$

indicating that the ratio of air and water efficiencies is also independent of the design of the cooling tower or spray chamber.

The overall effectiveness of heat transfer within the cooling tower must be dependent on the fluid having the smaller thermal capacity, i.e. the fluid having the larger efficiency. To quantify this concept, we can say that the Effectiveness, E , is the larger of the values of η_a and η_w . Another way of expressing this, using equation (18.34), is:

$$\begin{aligned} E &= \eta_a \quad \text{if } R \geq 1 \\ \text{and} \\ E &= \eta_w \quad \text{if } R \leq 1 \end{aligned} \quad (18.35)$$

η_a and η_w are, of course, equal when $R = 1$.

Prior to 1977, there seems to have been no one single parameter that could be used to describe the quality of design for any given cooling tower. The rate of heat transfer, air and water efficiencies, and the tower capacity factor are all dependent on inlet temperatures. It is, therefore, somewhat misleading to quote a single value of cooling duty to characterize a heat exchanger.

In the mid 1970's, Whillier of the South African Chamber of Mines conducted an analysis on results published earlier by Hemp (1967 and 1972) relating to a series of tests during which a spray tower was successively supplied with a range of inlet water temperatures. Whillier (1977) noticed that two distinct curves were produced when (a) water efficiency and (b) air efficiency were plotted against tower capacity factor. Furthermore, these two curves appeared to be mirror images of each other. In a moment of inspiration he recalled that the order of the ratio that we choose to define R is quite arbitrary (equation (18.32)). Whillier took the values of tower effectiveness, E , as defined by equations (18.35) and plotted them against R^* , where

$$R^* = R \text{ when } R < 1$$

and

$$(18.36)$$

$$R^* = 1/R \text{ when } R > 1$$

(i.e. inverting the ratio when R exceeds unity).

To his delight, all the points for the spray tower then lay on a single curve within an acceptable experimental scatter, and no matter whether the tower was used to cool water or air. The shape of that curve is illustrated on Figure 18.18. The fact that all test results lay on a single curve held promise that an equation or characteristic number for that curve could be used as a means of quantifying the overall merit of the design and construction of the cooling tower or spray chamber, and independent of the inlet temperatures or flowrates of the air and water. Whillier attempted several curve fitting exercises on his results and found that a reasonable correlation was obtained by the exponential relationship

$$E = F^{R^*} \tag{18.37}$$

where F was a constant for that particular spray tower. Different values of F in the range 0 to 1 would be obtained for other cooling towers or spray chambers. Whillier termed this parameter the **Factor of Merit** for the cooling tower. A means had been found by which the performance characteristic of a direct heat exchanger could be quantified in a single number. A factor of merit of 1.0 would indicate a perfect counterflow direct-contact heat exchanger. Practical values lie within the range 0.3 to 0.8.

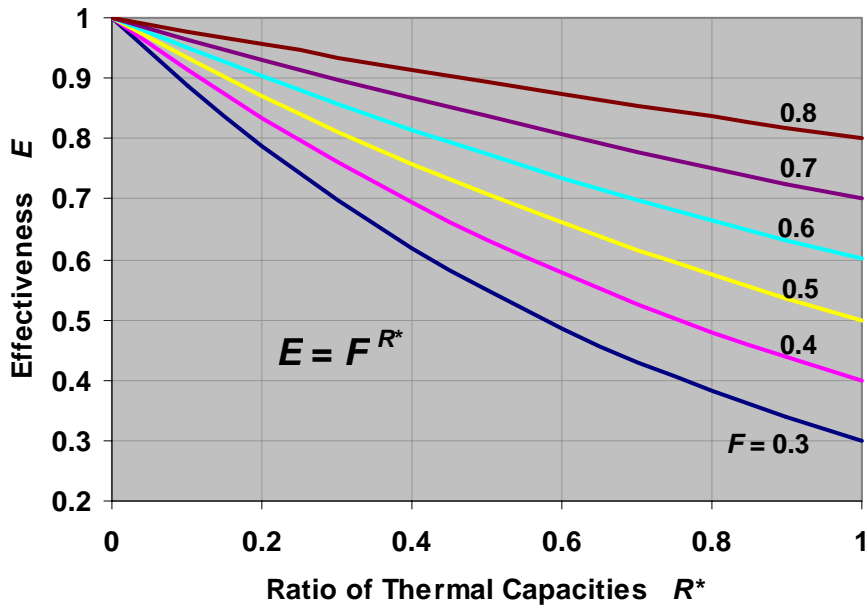


Figure 18.18 Variation of E with respect to R^* over a range of Factors of Merit, F , for a direct heat exchanger.

Further work by Bluhm (1980, 1984) investigated the factor of merit for multi-stage spray chambers, and produced an improved algorithm for spray coolers:

$$\eta_w = \frac{1 - \exp(-N(1-R))}{1 - R \exp(-N(1-R))} \quad (18.38)$$

$$\text{where } N = \frac{F}{R^{0.4}(1-F)} \quad (18.39)$$

It is recommended that this algorithm is used for factors of merit below 0.4 or above 0.7.

Typical factors of merit suggested by Whillier (1977) and Bluhm (1980) are shown on Table 18.2. Once the factor of merit has been established for any direct-contact heat exchanger, either by testing or by estimation from Table 18.2, then the performance of the unit can be established for any given flow rates and inlet conditions of the air and water streams.

Type of unit	Typical Values of Factor of Merit, F
Vertical spray filled towers	
No packing:	
high water loading	0.5 to 0.6
low water loading	0.6 to 0.7
With packing:	
high water loading	0.55 to 0.65
low water loading	0.65 to 0.75
Industrial packed tower	0.7 to 0.8
Horizontal spray chambers	
single-stage	0.4 to 0.5
two-stage	0.58 to 0.68
three-stage	0.65 to 0.75
Packed air coolers	
crossflow	0.55 to 0.65
counterflow	0.68 to 0.78
Mesh coolers	0.55 to 0.65

Table 18.2. Typical factors of merit for direct contact heat exchangers.

Example 1

A cooling tower operates at a barometric pressure of 95 kPa. The following temperature measurements were obtained:

air inlet wet bulb temperature,	$t_{a,in}$	= 18.0 °C
air outlet wet bulb temperature,	$t_{a,out}$	= 28.0 °C
water inlet,	$t_{w,in}$	= 32.0 °C
water outlet,	$t_{w,out}$	= 22.5 °C

Determine the factor of merit for the cooling tower.

Solution

Using the psychrometric equations given in section 14.6 (or from a 95 kPa psychrometric chart), sigma heats may be determined to be:

$$\begin{aligned} \text{at air inlet (18.0 }^\circ\text{C)} & \quad S_{in} = 52.05 \text{ kJ/kg} \\ \text{at air outlet (28.0 }^\circ\text{C),} & \quad S_{out} = 90.90 \text{ kJ/kg} \\ \text{at water inlet temperature (32.0 }^\circ\text{C),} & \quad S_{w, in} = 111.64 \text{ kJ/kg} \end{aligned}$$

Air efficiency (from equation (18.31))

$$\eta_a = \frac{(S_{out} - S_{in})}{(S_{w, in} - S_{in})} = \frac{(90.90 - 52.05)}{(111.64 - 52.05)} = 0.652$$

Water efficiency (from equation (18.30))

$$\eta_w = \frac{(t_{w, in} - t_{w, out})}{(t_{w, in} - t_{a, in})} = \frac{(32.0 - 22.5)}{(32.0 - 18.0)} = 0.679$$

Tower capacity factor (from equation (18.34))

$$R = \frac{\eta_a}{\eta_w} = \frac{0.652}{0.679} = 0.961$$

Tower effectiveness(from equations (18.35))

As $R < 1$ then $E = \eta_w = 0.679$.

Also, from equations (18.36)

$$R^* = R = 0.961$$

Factor of merit (from equation (18.37))

$$E = F^{R^*}$$

$$\ln(E) = R^* \ln(F)$$

or

$$F = \exp\left[\frac{\ln(E)}{R^*}\right] = \exp\left[\frac{\ln(0.679)}{0.961}\right] = 0.668$$

Note that we have been able to calculate the factor of merit using measured temperatures and the barometric pressure only. We have not required any fluid flowrates.

Bluhm's equations (18.38 and 18.39) give the factor of merit to be 0.659, a difference of some 1.3 percent in this example.

Example 2

Suppose the cooling tower of the previous example were to be converted into a vertical spray cooler by supplying it with chilled water. Calculate the operating characteristics of the cooler given that:

$$\begin{aligned} \text{water inlet temperature,} & \quad t_{w, in} = 5^\circ\text{C} \\ \text{air inlet wet bulb temperature,} & \quad t_{a, in} = 18^\circ\text{C} \\ \text{water flowrate,} & \quad m_w = 100 \text{ litres/s or kg/s} \\ \text{air flowrate} & \quad = 120 \text{ m}^3\text{/s (at an air density of } 1.1 \text{ kg/m}^3\text{),} \\ & \quad \text{or } m_a = 120 \times 1.1 = 132 \text{ kg/s} \\ \text{barometric pressure,} & \quad P = 95 \text{ kPa} \end{aligned}$$

Solution

The wet bulb temperature of the inlet air is the same as in the previous example. Hence, the corresponding sigma heat remains at

$$S_{in} = 52.05 \text{ kJ/kg}$$

However, at the new inlet water temperature of 5°C, the psychrometric equations of Section 14.6 give $S_{w,in} = 19.38 \text{ kJ/kg}$.

Tower capacity factor (from equation (18.32))

$$R = \frac{m_w}{m_a} C_w \frac{(t_{w,in} - t_{a,in})}{(S_{w,in} - S_{in})} = \frac{100}{132} \times 4187 \frac{(5 - 18)}{(19.38 - 52.05)1000} = 1.262$$

Tower effectiveness

As $R > 1$ then $R^* = 1/R$ (equation (18.36))

$$R^* = \frac{1}{1.262} = 0.7923$$

Now the factor of merit for the tower, F , was calculated in the previous example as 0.668. This remains the same despite the new inlet conditions. Equation (18.37) gives

$$E = F^{R^*} = 0.668^{0.7923} = 0.7264$$

Fluid efficiencies

As $R > 1$, $E = \eta_a$ (equation (18.35))

Hence $\eta_a = 0.7264$ and from equation (18.34)

$$\eta_w = \frac{\eta_a}{R} = \frac{0.7264}{1.262} = 0.5755$$

Now, equation (18.30) gives

$$\eta_w = \frac{(t_{w,in} - t_{w,out})}{(t_{w,in} - t_{a,in})}$$

or

$$t_{w,out} = t_{w,in} - \eta_w (t_{w,in} - t_{a,in}) = 5 - 0.5755(5 - 18) = 12.48 \text{ } ^\circ\text{C}$$

and equation (18.31) gives

$$\eta_a = \frac{(S_{out} - S_{in})}{(S_{w,in} - S_{in})}$$

from which

$$\begin{aligned} S_{out} &= \eta_a (S_{w,in} - S_{in}) + S_{in} \\ &= 0.7264(19380 - 52050) + 52050 = 28319 \text{ J/kg or } 28.3 \text{ kJ/kg} \end{aligned}$$

The air wet bulb temperature giving this sigma heat may be read from the 95 kPa psychrometric chart or calculated by iterating equations (14.44 to 14.47), giving $t_{a,out} = 9.18^\circ\text{C}$.

Rate of heat transfer, q
Using the water circuit,

$$\begin{aligned} q &= m_w C_w (t_{w,out} - t_{w,in}) = 100 \times 4187 (12.48 - 5) \\ &= 3.132 \times 10^6 \text{ or } 3.132 \text{ MW} \end{aligned}$$

As a cross-check, we may use the air circuit to give

$$\begin{aligned} q &= m_a (S_{out} - S_{in}) = 132 (28319 - 52050) \\ &= -3.132 \times 10^6 \text{ W or } -3.132 \text{ MW} \end{aligned}$$

The heat gained by the water is shown to balance the heat lost by the air.¹

Example 3

A mesh spray cooler is to be supplied with water at a temperature of 10°C . The unit is required to cool 12 kg/s of air from a wet bulb temperature of 29°C to 23°C and at a barometric pressure of 100 kPa. Determine the rate of water flow that must be sprayed through the cooler, the temperature of the return water and the cooling duty of the unit.

Solution

In the absence of further data concerning the device, we take a mean value of 0.6 as the factor of merit for a mesh cooler (from Table 18.2).

The data may then be summarized as follows:

$$\begin{array}{lll} t_{a,in} = 29^\circ\text{C} & t_{a,out} = 23^\circ\text{C} & m_a = 12 \text{ kg/s} \\ t_{w,in} = 10^\circ\text{C} & t_{w,out} = \text{unknown,} & m_w = \text{unknown} \\ F = 0.6 & & \end{array}$$

The sigma heats can be calculated from the psychrometric equations given in section 14.6 or approximated from the 100 kPa psychrometric chart:

$$\begin{array}{ll} S_{in} \text{ (at } 29^\circ\text{C wet bulb temperature)} &= 92.28 \text{ kJ/kg} \\ S_{out} \text{ (at } 23^\circ\text{C)} &= 67.11 \text{ kJ/kg} \\ S_{w,in} \text{ (at } 10^\circ\text{C)} &= 29.21 \text{ kJ/kg} \end{array}$$

Air efficiency (from equation (18.31))

$$\eta_a = \frac{(S_{out} - S_{in})}{(S_{w,in} - S_{in})} = \frac{(67.11 - 92.28)}{(29.21 - 92.28)} = 0.3991$$

Water efficiency (from equation (18.30))

$$\eta_w = \frac{(t_{w,in} - t_{w,out})}{(t_{w,in} - t_{a,in})} = \frac{(10 - t_{w,out})}{(10 - 29)} = \frac{(t_{w,out} - 10)}{19} \quad (18.40)$$

¹ Note that because of measurement uncertainties, good agreement may not be obtained in actual operating conditions.

Capacity factor (from equation (18.34))

$$R = \frac{\eta_a}{\eta_w} = \frac{0.3991 \times 19}{(t_{w,out} - 10)} = \frac{7.583}{(t_{w,out} - 10)} \quad (18.41)$$

We now have a decision to make - whether to assume that R is greater or less than unity, allowing us to ascribe values for E and R^* . Let us assume that $R > 1$ (we shall see in a moment that this was the wrong decision). Using equations (18.35 and 18.36), if $R > 1$, then $E = \eta_a$ and $R^* = 1/R$. Equation (18.37) gives

$$E = F^{R^*}$$

or

$$0.3991 = 0.6 \left\{ \frac{(t_{w,out} - 10)}{7.583} \right\}$$

giving

$$(t_{w,out} - 10) = 7.583 \frac{\ln(0.3991)}{\ln(0.6)} = 13.64$$

or

$$t_{w,out} = 23.64^\circ\text{C}.$$

In order to check the consistency of the value of R , we can return to equation (18.41):

$$R = \frac{7.583}{(23.64 - 10)} = 0.56$$

showing that our assumption of $R > 1$ was incorrect.

Let us, therefore, repeat the analysis assuming that $R < 1$. Then equations (18.35 and 18.36) give $E = \eta_w$ and $R^* = R$. Equation (18.37) gives

$$E = F^{R^*}$$

or, using $\eta_w = (t_{w,out} - 10)/19$ from equation (18.40) and $R = 7.583/(t_{w,out} - 10)$ from equation (18.41)

$$\frac{(t_{w,out} - 10)}{19} = 0.6^{\{7.583/(t_{w,out} - 10)\}}$$

To simplify the algebra, we may substitute

$$(t_{w,out} - 10) = a$$

giving

$$a = 19 \times 0.6^{(7.583/a)}$$

This can easily be solved iteratively on a pocket calculator to give

$$a = 14.56$$

and

$$t_{w,out} = 24.56^\circ\text{C}$$

Using equation (18.41), again, to check the value of R gives

$$R = 7.583/14.56 = 0.521$$

In this case, our assumption that $R < 1$ is shown to be consistent.

Water flowrate (from equation (18.32))

$$m_w = R \frac{m_a (S_{w,in} - S_{in})}{C_w (t_{w,in} - t_{a,in})} = 0.521 \times \frac{12(29210 - 92280)}{4187(10 - 29)} = 4.955 \text{ kg/s}$$

Cooling duty

This can be calculated directly from the air data:

$$q = m_a (S_{out} - S_{in}) = 12(67.11 - 92.28) = -302 \text{ kW}$$

To check the heat balance, the heat gain by the water is given as

$$q = m_w C_w (t_{w,out} - t_{w,in}) = 4.955 \times 4.187 \times (24.56 - 10) = 302 \text{ kW}$$

18.3.2.5. Heat exchange across the walls of pipes and ducts

When a fluid flowing through a pipe or duct is at a temperature different to that of the ambient air, then heat exchange will occur across the walls of the pipe and any insulating material that surrounds it. The analysis of indirect heat exchangers given in Section 18.3.2.2 applies equally well for pipes and ducts.

Consider the insulated pipe shown on Figure 18.19 carrying a fluid of temperature t_{in} when the temperature of the outside air is t_{out} .

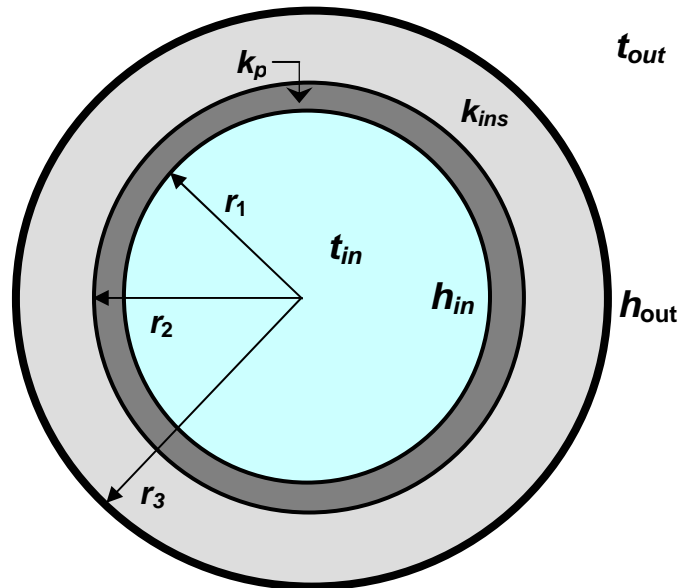


Figure 18.19 Heat transfer across an insulated pipe or duct.

The rate of heat transfer from a short length of pipe over which neither t_{in} nor t_{out} change significantly is given as:

$$q = UA(t_{in} - t_{out}) \quad \text{W (see equation (18.18))}$$

The UA value is given by

$$\frac{1}{UA} = \frac{1}{h_{in} A_{in}} + \frac{r_2 - r_1}{k_p A_{12}} + \frac{r_3 - r_2}{k_{ins} A_{23}} + \frac{1}{(h_{out} + 0.95 h_r) A_{out}} \quad \text{°C/W} \quad (18.42)$$

where h_{in} = heat transfer coefficient at the inner surface (W/(m² °C))
 h_{out} = heat transfer coefficient at the outer surface (W/(m² °C))
 h_r = radiative heat transfer coefficient at the outer surface (W/(m² °C))
 r = radii (m)
 k_p = thermal conductivity of pipe (W/(m °C))
 k_{ins} = thermal conductivity of insulation (W/(m °C))
 A = area (or mean area) across which heat transfer occurs (m)
 0.95 = assumed value for the product of emissivity and view factor, (Whillier, 1982)

Values of thermal conductivity for pipe materials can be obtained from Table 18.3.

The heat transfer coefficients may be estimated from the following relationships which take into account the variations of fluid viscosity and thermal conductivity with respect to temperature.

Air inside a duct

The Colburn equation (18.22) gives the heat transfer coefficient for turbulent flow inside smooth tubes. For air, the Prandtl Number, Pr, remains essentially constant at 0.7 over a wide range of temperatures and pressures (Appendix A15.3). Further analysis of the Colburn equation gives the approximation

$$h_{in}(\text{air}) = 3.169 \frac{(\rho_a u_a)^{0.8}}{d^{0.2}} \left(1 + 9.4 \times 10^{-4} t_{in} - 6.49 \times 10^{-6} t_{in}^2 \right) \quad \text{W/(m}^2 \text{ °C)} \quad (18.43)$$

where ρ_a = air density (kg/m³)
 u_a = air velocity in duct (m/s)
 d = internal diameter of duct (m)

The effect of temperature is fairly small over the range of 0 to 60°C. Hence, taking a value of 20°C gives the simpler approximation

$$h_{in}(\text{air}) = 3.22 \frac{(\rho_a u_a)^{0.8}}{d^{0.2}} \quad \text{W/(m}^2 \text{ °C)} \quad (18.44)$$

The incorporation of air density allows this relationship to be employed for compressed air pipes as well as ventilation ducts.

Water inside a pipe

A similar analysis for water inside a pipe leads to the approximation

$$h_{in}(\text{water}) = (1430 + 20.9 t_{in}) \frac{u_w^{0.8}}{d^{0.2}} \quad \text{W/(m}^2 \text{ °C)} \quad (18.45)$$

where u_w = water velocity (m/s)

In this case, the near constant value of water density allows it to be eliminated as a variable. However, the viscosity of water varies significantly in the range 0 to 60°C. Hence, the effect of temperature should not be ignored in equation (18.45).

Air outside a pipe

This time, the relationship given by McAdams for the outside of a single tube (equation (18.23)) provides the basis for further analysis. This leads to an approximation that may be used for both longitudinal flow and cross flow in subsurface airways.

$$h_{out} \text{ (air)} = 4.24 \frac{(\rho_a U_a)^{0.6}}{d^{0.4}} (1 + 0.0015 t_{out}) \quad \text{W/(m}^2 \text{ }^\circ\text{C)} \quad (18.46)$$

Radiative heat transfer coefficient

This can be calculated from the Stefan-Boltzman equation (15.27) using the dry bulb temperature of the surrounding air, giving

$$h_r = 22.68 \times 10^{-8} (273.15 + t_{out})^3 \quad \text{W/(m}^2 \text{ }^\circ\text{C)} \quad (18.47)$$

However, an adequate accuracy for most purposes is obtained simply by assuming a value of $h_r = 6 \text{ W/(m}^2 \text{ }^\circ\text{C)}$.

Over long lengths of pipe or ducting the inner and outer temperatures, t_{in} and t_{out} , are each likely to change in a nonlinear manner. In this case the **log. mean temperature difference** should be employed giving

$$q = UA \frac{(\Delta t_1 - \Delta t_2)}{\ln(\Delta t_1 / \Delta t_2)} \quad \text{W} \quad (18.48)$$

where Δt_1 and Δt_2 are the values of the temperature difference ($t_{in} - t_{out}$) at the two ends of the pipe
and $\ln =$ natural logarithm

Example

A chilled water pipeline is 1000 m long and comprises a 200 mm internal diameter steel pipe of thickness 4 mm, inside a 30 mm sheath of phenol formaldehyde insulation. The water has a velocity of 2 m/s and a mean temperature of 8°C while the surrounding air has a velocity of 4 m/s, a mean dry bulb temperature of 25.5°C and a density of 1.12 kg/m³.

Determine

- (a) the UA value per metre length of pipeline,
 - (b) the actual heat gain and temperature rise of the water
- and (c) the temperature of the outer surface of the insulation.

Solution

(a) Let us first collate the data required by equation (18.42)

Thermal conductivities (from Table 18.3)

steel: $k_p = 45 \text{ W/(m }^\circ\text{C)}$

phenol formaldehyde: $k_{ins} = 0.032 \text{ W/(m }^\circ\text{C)}$

Radii (with reference to Figure 18.19)

$r_1 = 0.1\text{m}; \quad r_2 = 0.104\text{m}; \quad r_3 = 0.134 \text{ m}$

Areas of heat transfer (per metre length)

$$A_{in} = 2\pi r_1 = 2\pi \times 0.1 = 0.6283 \text{ m}^2$$

$$A_{out} = 2\pi r_3 = 2\pi \times 0.134 = 0.8419 \text{ m}^2$$

$$A_{12} = 2\pi \frac{(r_1 + r_2)}{2} = 2\pi \frac{(0.1 + 0.104)}{2} = 0.6409 \text{ m}^2$$

$$A_{23} = 2\pi \frac{(r_2 + r_3)}{2} = 2\pi \frac{(0.104 + 0.134)}{2} = 0.7477 \text{ m}^2$$

Heat transfer coefficients

For water in the pipe (from equation (18.45)):

$$h_{in} \text{ (water)} = (1430 + 20.9 t_{in}) \frac{u_w^{0.8}}{d_1^{0.2}} \quad \text{W/(m}^2 \text{ }^\circ\text{C)}$$

$$= (1430 + 20.9 \times 8) \frac{2^{0.8}}{(0.2)^{0.2}} = 3837 \text{ W/(m}^2 \text{ }^\circ\text{C)}$$

For air outside the pipe (from equation (18.46)):

$$h_{out} \text{ (air)} = 4.24 \frac{(\rho_a u_a)^{0.6}}{d_3^{0.4}} (1 + 0.0015 t_{out})$$

$$= 4.24 \frac{(1.12 \times 4)^{0.6}}{0.268^{0.4}} (1 + 0.0015 \times 25.5) = 18.33 \frac{\text{W}}{\text{m}^2 \text{ }^\circ\text{C}}$$

For radiative heat transfer at outside of pipe (from equation (18.47))

$$h_r = 22.68 \times 10^{-8} (273.15 + 25.5)^3 = 6.04 \text{ W/(m}^2 \text{ }^\circ\text{C)}$$

The large value of h_{in} (water) shows the relative ease with which heat is transferred from the water to the steel pipe.

The UA value per metre length can now be calculated from equation (18.42). Inserting the numerical value gives:

$$\frac{1}{UA} = \frac{1}{3837 \times 0.6283} + \frac{0.004}{45 \times 0.6409} + \frac{0.03}{0.032 \times 0.7477} + \frac{1}{(18.33 + 0.95 \times 6.04) 0.8419}$$

$$= 0.00041 + 0.00014 + 1.2538 + 0.0493$$

$$= 1.3037 \quad \text{ }^\circ\text{C/W}$$

$$\text{or } UA = 1/1.3037 = 0.7670 \quad \text{W/}^\circ\text{C}$$

The dominant effect of the insulation is shown here. Indeed, the terms involving the water inside the pipe and the steel pipe itself may be neglected without significant loss of accuracy.

(b) The average heat loss per metre length of pipe is then simply

$$q = UA (t_{in} - t_{out}) = 0.7670 (8 - 25.2) = -13.42 \text{ W per metre}$$

(negative as heat is transferred from the air to the water).

Over the 1000 m pipeline, the total heat transferred to the water is then

$$q_{tot} = 13.42 \times 1000 = 13\,420 \text{ W}$$

In order to determine the actual increase in temperature of the water, Δt_w , it is first necessary to calculate the mass flow of water

$$m_w = \rho_w \times u_w \times \text{area of flow} = 1000 \times 2 \times \frac{\pi \times 0.2^2}{4} = 62.83 \text{ kg/s}$$

where ρ_w = density of water (1000 kg/m³)

$$\text{Then } \Delta t_w = \frac{q_{tot}}{C_w m_w}$$

where C_w = specific heat of water (4187 J/(kg°C) giving

$$\Delta t_w = \frac{13\,420}{4187 \times 62.83} = 0.051 \text{ °C}$$

This small rise in temperature justifies the assumption of a "constant" water temperature at a mean value. In practice, the actual temperature rise may be significantly greater because of damaged or imperfectly applied insulation, particularly at flange points.

- (c) The heat flux remains the same at each surface boundary of the pipe and insulation. This allows the temperatures at those boundaries to be determined. In particular, at the outer surface of the insulation,

$$q = h_{out} A_{out} (t_{surf} - t_{out}) \quad \text{where } t_{surf} = \text{surface temperature of the insulation.}$$

Inserting the known values gives

$$t_{surf} = \frac{-13.42}{18.33 \times 0.8419} + 25.5 = -0.87 + 25.5 = 24.63\text{°C}$$

No condensation will occur on the outside of the insulation provided that the wet bulb temperature of the air remains below 24.63°C. However, any imperfections in the insulation may allow the ingress of water vapour and condensation on the steel tube. This can result in problems of corrosion.

The techniques described in this section can be incorporated into mine climate simulation programs (Chapter 16) in order to take into account heat transfers between pipes or ducts and the surrounding airflow. If the fluid inside the pipe moves in the same direction as the ventilating airstream, then the heat transfers and corresponding temperature changes can be computed sequentially along each incremental length of simulated airway (Section 16.2.2.). In the case of the piped fluid and the ventilating airstream moving in opposite directions, then an iterative procedure becomes necessary to compute the equilibrium condition.

18.3.3. Water distribution systems

A significant item in the design and economic analysis of mine air conditioning systems is the choice of piping that carries water between the refrigeration plant and heat exchangers or mining equipment.

There are, essentially, two matters of importance. First, the size of the pipe should be selected carefully. If it is too small for the given flowrate, then the frictional pressure drops and pumping costs will be high. On the other hand, if too large a pipe is chosen the costs of purchase and insulation will be high while the larger surface area and low velocity will exacerbate unwanted heat transfer with the surroundings.

This brings us to the second consideration, the thermal properties of the pipe material and the need for additional insulation. We shall discuss each of these matters in turn.

18.3.3.1. Pipe sizing

The first step in determining the diameters of the various pipes that comprise a water network is to assess the flowrates that are to be carried in each branch. The cooling duty, q , of a heat exchanger is given as

$$q = m_w C_w (t_{w,out} - t_{w,in}) \quad W \quad (18.49)$$

where m_w = water flowrate through the heat exchanger (litres/s or kg/s)
 C_w = specific heat of liquid water (4187 J/kg °C)
 $t_{w,in}$ = inlet water temperature (°C)
 and $t_{w,out}$ = outlet water temperature (°C)

The heat transferred is dependent equally upon the water flowrate and the temperature rise of the water through the unit. The latter, in turn, is governed by the construction of the heat exchanger and the supply temperature of the water. Calculations of the type included in Section 18.3.2 allow flowrates to be assessed. For service water lines, the flowrates must also satisfy the machine requirements for dust suppression or hydraulic power.

Having established the water flowrate, the actual sizing of a pipe becomes a combination of simple analysis and practical considerations. Taking into account capital, operating and installation costs, [van Vuuren](#) (1975) suggested optimum water velocities of 1.8 to 2.0 m/s for 4000 kPa pipes and 2.0 to 2.2 m/s for 7000 kPa pipes. A common rule of thumb is to employ 2 m/s for an initial exercise in pipe sizing. The size of pipe is then given as

$$\frac{\pi d^2}{4} = A = \frac{Q}{u} \quad m^2$$

or

$$d = \sqrt{\frac{4Q}{\pi u}} = 1.13 \sqrt{\frac{Q}{u}} \quad m$$

where d = pipe diameter (m)
 A = pipe cross sectional area (m²)
 Q = flowrate (m³/s)
 and u = velocity (m/s)

The frictional pressure drop, p , along the pipe may then be determined from the Chezy Darcy relationship (equation (2.45)):

$$p = \frac{4fL\rho_w u^2}{2d} \quad Pa \quad (18.51)$$

For practical calculations, water density, ρ_w , may be taken as constant at 1000 kg/m^3 . The length L is often set at unity to give the frictional pressure loss in Pa per metre.

New steel pipes will have a coefficient of friction, f , approximating 0.0039. However, the aging processes of corrosion and scaling may cause this to increase by 20 to 50 percent. Plastic pipes have a coefficient of friction averaging about 0.0032. Manufacturers usually provide charts for their pipes relating frictional pressure losses to pipe diameter and flowrate. The pressure loss that can be tolerated depends upon the pumping cost function which is proportional to the product pQ (ref. equation (9.17)), and the pressure required at the end of the pipeline. If the pumping costs are shown to be high, then consideration should be given to increasing the pipe diameter and reducing the velocity.

Pressure losses are also incurred at bends or pipe fittings. Again, manufacturer-specific data can be employed to determine such losses. However, for mine water systems, it is common to cater for bends and fittings by simply adding ten percent to the computed pressure drop.

Pipe diameters determined through this procedure should be rounded up to the next highest standard size. Consideration should be given to any increases in water flow that may be required in the future. Furthermore, pipe ranges that might be used for fire fighting should be sized to give adequate flow and pressure at the hydrants. The sizes of pipes that are to be installed within existing airways or shafts may also be constrained by the space available.

18.3.3.2. Pipe insulation

The performance of heat exchangers is dependent upon the temperature of the supply water. It is, therefore, important that heat gain along chilled water pipelines is minimized. This is normally accomplished by providing thermal insulation on those pipes. One exception is the special case where the pipeline is located within an intake airway which, itself, requires air cooling. In such circumstances, the insulation may be partially, or totally, omitted.

In addition to having a low thermal conductivity, the insulating materials for chilled water pipes in mines should conform to several other criteria:

- The insulation should provide a barrier against the ingress of water that condenses on the outer surfaces. A porous and permeable insulation that becomes waterlogged will be much more conductive to heat. Furthermore, water that reaches the surface of metal pipes will cause problems of corrosion. The required **vapour barrier** may be achieved either by covering the insulation with an impermeable sheath or by using an insulating material that is, itself, non-permeable. An example is cellular glass in which the small air pockets are isolated from each other.
- The insulation or outside sheath should have sufficient mechanical strength to withstand the rigours of transport and utilization in mine environments. Insulation on shaft pipelines must be able to withstand impact from falling objects.
- The flammability of insulating materials and the toxicity of gases that they may produce when heated in a mine fire is of great importance. Polyurethane foams have been employed widely in the past. However, they emit carbon monoxide and, perhaps, cyanide vapours at temperatures that may be reached in mine fires. Phenolic foams in which phenols are bound into a resin base are safer in that they have a higher ignition temperature, and a much lower rate of flame spread (Rose, 1989).
- The cost of purchase and ease of installation of insulating materials or pre-insulated piping should also be taken into account.

A common practice has been to apply insulating materials to pipes on the mine site - either on the surface or after the pipework has been installed in its underground location. The application of foam insulators may be carried out by injecting the foam within a PVC vapour barrier sheath that has been pulled over spacers on the outside of the pipe. Pre-cast semicircular sections of cellular glass or other rigid insulators may be bound on to the pipes with adhesives or an outer sealing material. Expanded polystyrene granules and fibreglass have also been used widely (Arkle, 1985; Ramsden, 1985). The thickness of applied insulators varies from 25 to 40 mm.

The continued development of **thermoplastics** has allowed the manufacture of pipes that combine mechanical strength with good thermal insulating properties. These may consist of concentric and impermeable cylinders with the annulus containing a cellular infill. Typical values of thermal conductivity are given in Table 18.3.

Material	Thermal conductivity
	W/(m °C)
Still air	0.028
Expanded polystyrene	0.038
Polyurethane and polystyrene	0.034
Polyisocyanurate	0.023
Phenol formaldehyde	0.032
Glass fibre	0.029
Unplasticised polyvinylchloride (UPVC)	0.14
Still water	0.62
Wood	0.17
Steel	45

Table 18.3. Thermal conductivities of pipe materials.

18.3.3.3. Energy and temperature changes within water systems

In Section 3.4.1 we saw that fluid frictional effects have no influence on temperature changes within a steady-state airflow. This is not the case for water or other near incompressible fluids. Furthermore, in Section 15.3.1, the auto-compression of air in a mine shaft was shown to produce an increase in air temperature that depended upon the depth of the shaft. Again, this is not true for water in a shaft pipe.

In order to reassess the situation for water, let us return to the steady flow energy equation (3.25).

$$\frac{u_1^2 - u_2^2}{2} + (Z_1 - Z_2)g + W_{12} = \int_1^2 V dP + F_{12} = (H_2 - H_1) - q_{12} \quad \frac{\text{J}}{\text{kg}} \quad (18.52)$$

where

u = velocity (m/s)

Z = height above datum (m)

g = gravitational acceleration (m/s^2)

W = work input (J/kg)

V = specific volume of fluid (m^3/kg) = $1/\rho$ where ρ = fluid density (kg/m^3)

F = work done against friction (J/kg)

H = enthalpy (J/kg).

and q = heat added from surroundings (J/kg).

In applying this equation to water, we recall the basic definition of enthalpy from equation (3.19):

$$H = PV + U \quad \text{J/kg} \quad (18.53)$$

where U = internal energy and by assuming the water to be incompressible, V = constant.

The right hand sides of equation (18.52) then give

$$V(P_2 - P_1) + F_{12} = P_2V - P_1V + U_2 - U_1 - q_{12}$$

or

$$F_{12} = U_2 - U_1 - q_{12} \quad (\text{J/kg}) \quad (18.54)$$

However, we may take a single value for the specific heat of water, $C_w = 4187 \text{ J/(kg } ^\circ\text{C)}$. Equation (3.28) then gives

$$(U_2 - U_1) = C_w(T_2 - T_1) \quad \text{J/kg} \quad (18.55)$$

Substituting in equation (18.54),

$$F_{12} = C_w(T_2 - T_1) - q_{12} \quad \text{J/kg} \quad (18.56)$$

Furthermore, the frictional pressure drop, p , is given by equation (2.46)

$$p = \rho_w F_{12} = \rho_w C_w(T_2 - T_1) - \rho_w q_{12} \quad \text{Pa} \quad (18.57)$$

where ρ_w = density of water (kg/m^3)

In the particular case of adiabatic flow ($q_{12} = 0$), the increase in water temperature along a pipeline becomes

$$(T_2 - T_1) = \frac{p}{\rho_w C_w} \quad ^\circ\text{C} \quad (18.58)$$

The term $1/\rho_w C_w$ is sometimes known as the Joule-Thompson coefficient and, for water, has a standard value of $1/(1000 \times 4187) = 2.39 \times 10^{-7} \text{ } ^\circ\text{C/Pa}$.

The adiabatic rise in temperature along a water pipe is shown by equation (18.58) to be directly proportional to the frictional pressure drop and is independent of changes in elevation. The frictional pressure drop, p , may occur by viscous or turbulent action within the length of the pipe or by shock loss across a valve or other obstruction.

For flow through a water pump or turbine, we can apply the left and right sides of equation (18.52). However, the change in kinetic energy and the difference in elevation across the device are both negligible, giving

$$\begin{aligned} W_{12} &= (H_2 - H_1) - q_{12} \\ &= V(P_2 - P_1) + (U_2 - U_1) - q_{12} \\ &= \frac{(P_2 - P_1)}{\rho_w} + C_w(T_2 - T_1) - q_{12} \quad \text{J/kg} \end{aligned} \quad (18.59)$$

If there is negligible heat exchange across the casing of the pump or turbine, then we may assume adiabatic flow ($q_{12} = 0$) giving the temperature rise as

$$(T_2 - T_1) = \frac{1}{C_w} \left\{ W_{12} - \frac{(P_2 - P_1)}{\rho_w} \right\} \quad ^\circ\text{C} \quad (18.60)$$

While W_{12} is the total work applied to a pump impeller, the term $(P_2 - P_1)/\rho_w$ represents the output of useful mechanical energy. The difference between the two indicates the degradation of some of the input power to thermal energy and produces a measurable temperature rise. In a turbine, it is the other way round with $(P_1 - P_2)/\rho_w$ representing the work input and $-W_{12}$ being the output work.

For a **pump**, we can also write that the actual work output is given by

$$W_{12} \eta = \frac{(P_2 - P_1)}{\rho_w} \quad \frac{\text{J}}{\text{kg}} \quad (18.61)$$

and, for a **turbine**, the actual work output is

$$W_{12} = \frac{(P_2 - P_1)\eta}{\rho_w} \quad \frac{\text{J}}{\text{kg}} \quad (18.62)$$

where η = efficiency of the device

Substituting for W_{12} in equation (18.60) gives the temperature rise

across a pump:

$$(T_2 - T_1) = \frac{(P_2 - P_1)}{C_w \rho_w} \left\{ \frac{1}{\eta} - 1 \right\} \quad ^\circ\text{C} \quad (18.63)$$

and across a water turbine

$$(T_2 - T_1) = \frac{(P_2 - P_1)}{C_w \rho_w} (\eta - 1) = \frac{(P_1 - P_2)}{C_w \rho_w} (1 - \eta) \quad ^\circ\text{C} \quad (18.64)$$

In these analyses, it has been assumed that water is incompressible. In fact, the slight compressibility of water does give it a small isentropic temperature change with respect to pressure (Whillier, 1967). This is given approximately as

$$\frac{\Delta t}{\Delta P} = (0.759 t - 0.2) \times 10^{-6} \quad ^\circ\text{C per kPa} \quad (18.65)$$

where t = initial temperature ($^\circ\text{C}$)

This effect may be neglected for most practical purposes. However, if equations (18.63) or (18.64) are transposed in order to determine the efficiency of the device from temperature observations, then the measured temperature rise should be corrected according to equation (18.65) (negatively for a pump and positively for a turbine).

Example 1

The barometric pressures at the top and bottom of a 1500 m deep shaft are 90 and 107 kPa respectively. Chilled water at 3°C and ambient atmospheric pressure enters the top of a 150 mm diameter steel pipe that is suspended in the shaft. A pressure reducing valve at the bottom of the pipe controls the water flowrate to 35 litres/s and reduces the water pressure to that of the ambient surroundings. Determine the pressures and temperatures of the water at the inlet and outlet of the pressure reducing valve. Assume that no heat exchange occurs across the pipe wall.

Solution

The frictional pressure drop in the pipe is given by equation (18.51)

$$p = \frac{4 f L \rho_w u^2}{2 d} \quad \text{Pa}$$

The known values are

$$L = 1500 \text{ m} \quad \rho_w = 1000 \text{ kg/m}^3 \quad d = 0.15 \text{ m}$$

$$\text{where } Q = \text{flowrate} = 35/1000 = 0.035 \text{ m}^3/\text{s} \text{ and } A = \text{c-s area} = \pi \times (0.15)^2/4 = 0.01767 \text{ m}^2$$

$$\text{giving } u = Q/A \quad u = 1.981 \text{ m/s}$$

Allowing for aging effects, we shall assume the coefficient of friction for the steel pipe to be $f = 0.005$. We shall also allow an additional pressure loss of 10 percent to allow for bends and fittings.

Then

$$p = \frac{4 \times 0.005 \times 1500 \times 1000 \times (1.981)^2}{2 \times 0.15} (1 + 0.1) = 431.68 \times 10^3 \quad \text{Pa}$$

$$\text{Water pressure at shaft top} = 90 \times 10^3 \text{ Pa}$$

Water pressure at shaft bottom (inlet to pressure reducing valve)

$$\begin{aligned} &= 90 + \rho_w g L - p \\ &= 90 \times 10^3 + (1000 \times 9.81 \times 1500) - 431.68 \times 10^3 \\ &= 14\,373 \times 10^3 \text{ Pa} \quad \text{or} \quad 14\,373 \text{ kPa} \end{aligned}$$

At outlet from the valve, the water pressure is reduced to the shaft bottom barometric pressure of 107 kPa.

Hence,

$$\begin{aligned} \text{pressure drop across the valve} &= \text{gauge pressure at valve inlet} \\ &= 14\,373 - 107 = 14\,266 \text{ kPa} \end{aligned}$$

The temperature rise in the shaft pipe is given by equation (18.58) as

$$\Delta t_{sh} = \frac{p}{\rho_w C_w} = \frac{431.68 \times 10^3}{1000 \times 4187} = 0.103 \quad ^\circ\text{C}$$

$$\text{Temperature at valve inlet} = \text{water temperature at shaft top} + 0.103 = 3.103 \text{ } ^\circ\text{C}$$

As no energy is added or extracted by the pressure reducing valve, the flow is purely frictional. Hence, equation (18.58) gives

$$\Delta t_{valve} = \frac{\text{Pressure loss across valve}}{\rho_w C_w} = \frac{14\,266 \times 10^3}{1000 \times 4187} = 3.407^\circ\text{C}$$

giving the water temperature at the valve outlet to be

$$3.103 + 3.407 = 6.510 \quad ^\circ\text{C}.$$

The same total increase in water temperature of 3.51°C from shaft top to outlet of the valve at the shaft bottom would occur whatever the cause of the restriction on flow - a valve, rougher lining of the pipe or a smaller diameter of pipe, provided that no energy of any kind is added or extracted from the water and that the water is emitted at the shaft bottom barometric pressure.

As a check, the overall temperature rise of the water between the shaft top and the outlet of the shaft bottom valve can be calculated directly. From the steady flow energy equation (18.52) with no work input ($W_{12} = 0$), for an incompressible fluid $V = 1/\rho = \text{constant}$, and ignoring changes in kinetic energy

$$(Z_1 - Z_2)g = V(P_2 - P_1) + F_{12}$$

or

$$\begin{aligned} p_{tot} &= \rho_w F_{12} = (Z_1 - Z_2)g \rho_w - (P_2 - P_1) \\ &= 1500 \times 9.81 \times 1000 - (107 - 90) 1000 \\ &= 14.715 \times 10^6 - 0.017 \times 10^6 \\ &= 14.698 \times 10^6 \text{ Pa} \end{aligned}$$

(The difference in barometric pressure is shown to have very little effect on p_{tot} .)

Then

$$\begin{aligned} \Delta t_{tot} &= \frac{p_{tot}}{\rho_w C_w} \quad (\text{equation (18.58)}) \\ &= \frac{14.698 \times 10^6}{1000 \times 4187} = 3.51 \text{ }^\circ\text{C} \end{aligned}$$

This check calculation illustrates that when the water is emitted from the pipe at the underground barometric pressure, the temperature rise is given approximately as

$$\frac{(Z_1 - Z_2)g}{4187} = 3.51 \text{ }^\circ\text{C} \text{ over the 1500m depth of the shaft, or } 2.34 \text{ }^\circ\text{C per 1000 m depth.}$$

In the past, this has mistakenly been referred to as an "autocompression temperature rise." The misconception arose because in the special case of a pipe open at the bottom, the frictional pressure drop in the pipe approximates the static pressure caused by a column of fluid in the shaft pipe.

Example 2

If, in Example 1, the pressure reducing valve at the shaft bottom were replaced by a water turbine of efficiency 75 percent, what would be the temperature of the water leaving the turbine? Calculate, also, the power produced by the turbine. Assume that all other parameters, including the flowrate of 35 litres/s, remain unchanged.

Solution

As the condition and flow of water in the pipe have not been altered, the increase in water temperature down the pipe remains at $\Delta t_{sh} = 0.103^\circ\text{C}$ and the water enters the turbine at a pressure of $P_{in} = 14\,373 \text{ kPa}$ and a temperature of 3.103°C .

At outlet from the turbine, the water pressure has fallen to the shaft bottom barometric pressure of $P_{out} = 107$ kPa. The temperature rise across the turbine is given by equation (18.64).

$$\Delta t_{turb} = \frac{(P_{in} - P_{out})}{C_w \rho_w} (1 - \eta) = \frac{(14373 - 107)10^3}{4187 \times 1000} (1 - 0.75) = 0.852 \text{ } ^\circ\text{C}$$

Then the temperature of the water leaving the turbine is

$$3.103 + 0.852 = 3.955 \text{ } ^\circ\text{C}.$$

Comparing this with the temperature of water leaving the pressure reducing valve of Example 1, i.e. $6.510 \text{ } ^\circ\text{C}$, shows that replacing the valve by a water turbine not only produces useful power but reduces the temperature of the chilled water leaving the shaft station by $6.510 - 3.955 = 2.555 \text{ } ^\circ\text{C}$.

This represents an equivalent refrigeration capacity of

$$m_w C_w \Delta t = 35 \times 4187 \times 2.555 = 374.5 \times 10^3 \text{ W or } 374.5 \text{ kW}$$

The output work from the turbine is given by equation (18.62)

$$W_{12} = \frac{(P_{out} - P_{in})\eta}{\rho_w} = \frac{(107 - 14373)10^3}{1000} \times 0.75 = -10700 \frac{\text{J}}{\text{kg}}$$

(negative, as work is leaving the water). To transform this to an output power, we simply multiply by the mass flowrate, i.e.

$$10700 \times 35 = 374.5 \times 10^3 \text{ W or } 374.5 \text{ kW}$$

We have, therefore, demonstrated that the power output from the turbine is equal to the equivalent refrigeration capacity that has been produced by the system. This suggests a rapid means of approximating the overall temperature rise of the water from the shaft top to the turbine outlet at shaft bottom barometric pressure:

$$\begin{aligned} \Delta t_{tot} &= \frac{(Z_1 - Z_2)g}{C_w} - \frac{\text{turbine output power}}{m_w C_w} \\ &= \frac{1500 \times 9.81}{4187} - \frac{374500}{35 \times 4187} = 3.514 - 2.555 = 0.959 \text{ } ^\circ\text{C} \end{aligned}$$

This method remains acceptable provided that the frictional pressure losses are small compared with the static pressure caused by the column of water.

18.3.4. Energy recovery devices

The trend towards siting main refrigeration plant on the surface of mines accelerated during the 1980's. This was caused in large part by the utilization of energy recovery devices, particularly water turbines. Prior to that time, the provision of chilled water at the surface had three major drawbacks. First, it caused high water pressures at shaft bottoms which necessitated a choice between high pressure heat exchangers and associated pipework or, alternatively, to pass the water through pressure reducing valves. The latter choice not only resulted in high operating costs of pumping to return the water to surface, but also converted the potential energy of the water to thermal energy, giving a rise in temperature and eroding the cooling capacity of the chilled water.

Energy recovery devices address each of these problems and divide into two major groups. First, water turbines or hydraulic motors employ the potential energy of shaft water lines to drive electrical generators or other devices. Secondly, hydrolift systems utilize the weight of descending chilled water to help raise heated return water back to surface. We shall discuss each of these systems in turn.

18.3.4.1. Water turbines

As illustrated by Example 2 in section 18.3.3.3, shaft bottom turbines provide:

- work output that may be used to drive pumps, generators or any other mechanical device; this work may provide part of the energy required to raise return water back to surface;
- reduced temperature of the subsurface supply of chilled water, and hence, savings in refrigeration costs;
- a low pressure water system underground.

Two types of turbines are in use. Figure 18.20 illustrates an impulse turbine, commonly known as a Pelton Wheel. In this device, the pressure of the supply water is used to produce kinetic energy by means of one or more nozzles. The high velocity jets are directed at cups attached to the periphery of a rotating wheel. Inside the casing of the device, the jets operate at the ambient atmospheric pressure. Hence, the water leaves at zero gauge pressure. Control of the mechanical output may be achieved by a needle valve in the nozzle which changes the water flowrate. Alternatively, if the flow is to be maintained, deflector plates may be used to direct part of the jets away from the cups.

The advantages of a Pelton Wheel are that it is simple and rugged in construction, reliable and may reach efficiencies of over 80 percent. The speed control is effective and no high pressure seals are required on the casing.

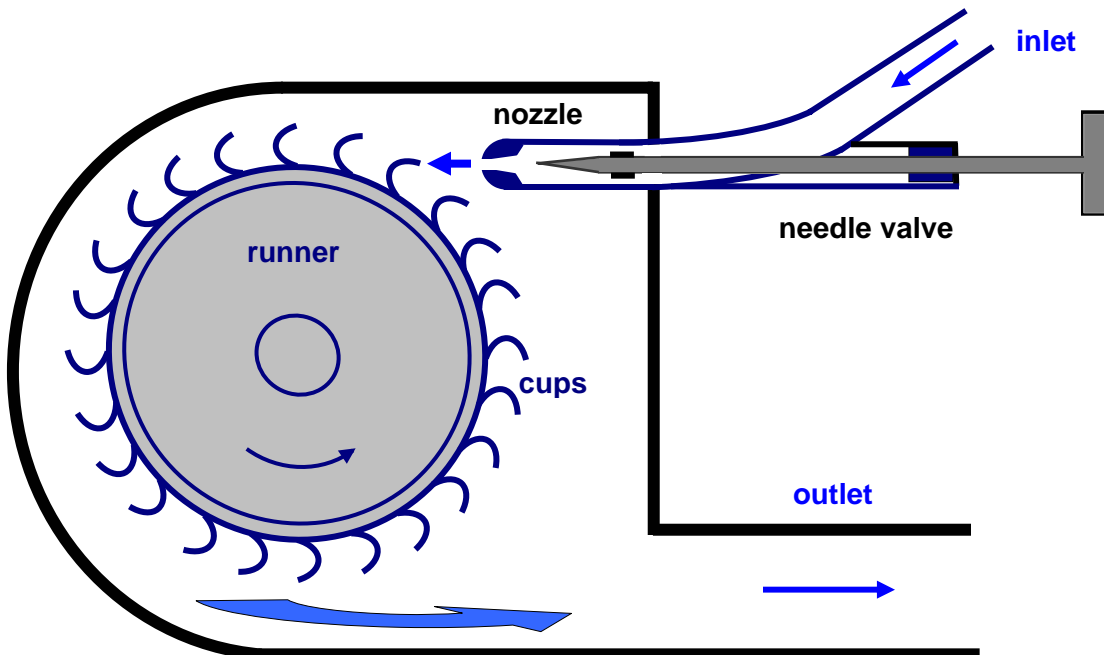


Figure 18.20 Diagrammatic representation of a Pelton Wheel.

The second type of water turbine is the reaction device and is often referred to as a Francis or Kaplan turbine. This is essentially a centrifugal runner (Figure 10.2) with the impeller designed to operate in reverse and incorporating guide vanes to minimize shock losses. Indeed, a reversed centrifugal pump may be used as a reaction turbine although at a considerably reduced efficiency. Control of the device is by valves located upstream and/or downstream. Unlike the Pelton Wheel, a reaction turbine operates in a "flooded" mode giving rise to its primary advantage, i.e. the water pressure at exit can be maintained above the ambient air pressure and, hence, may be utilized further downstream to overcome pipe losses, provide the required pressure at spray chambers or to activate further hydraulic devices. Pelton Wheels give better efficiencies at the higher duties, typically 2 MW. The Francis turbines are better suited for lower duties².

In addition to shaft bottom stations, water turbines may be used for more local applications. For example, if the water pressure available at a spray chamber exceeds that required at the spray nozzles, then a turbine can be sited in the water supply line and used to power local pumps or fans. This is particularly advantageous for multi-stage spray chambers (Ramsden, 1985).

18.3.4.2. Hydrolift systems

The principle of operation of a hydrolift system is illustrated on Figure 18.21. The device is sometimes also known as a hydrochamber or hydrotransformer. The chamber is excavated or constructed underground and is alternately filled from opposite ends with chilled water delivered from surface, then with hot water returned from the mine.

Let us assume that the chamber is initially filled with warm water. Both of the automated valves A are opened and valves B are closed. The pump at the surface cold water dam causes chilled water to flow down the shaft pipe and into the chamber. This, in turn, forces the hot water to exit the chamber and ascend the return shaft pipe. As the two columns of water are nearly balanced, the duty of the pump is simply to overcome pipe friction. When the chamber is filled with chilled water, valves A are closed and valves B are opened. The underground hot water dam pump then forces the hot return water into the chamber, expelling the chilled water to the underground cold water dam.

The cyclic nature of the system can be negated by having three hydrolift chambers with the sets of valves phased to give a continuous flow into and out of the water dams. The size of chambers and water dams should be determined on the basis of the cooling requirements of the mine. An inherent disadvantage of the hydrolift system is that the rate of chilled water flow must be equal to that of the heated return water. It is, therefore, advisable that the water dams should be sized to accommodate several hours supply.

A loss of efficiency occurs because of heat exchange with the walls of the chamber and due to mixing and thermal transfer at the hot and cold interface within the chamber. The latter may be minimized by inclining the chamber such that the hot water end is at a higher elevation.

² As a guide, if the pressure differential available across the turbine (in kPa) is less than $70 m_w^{0.67}$ (where m_w is the flowrate in litres/s), then a Francis turbine will give a better performance.

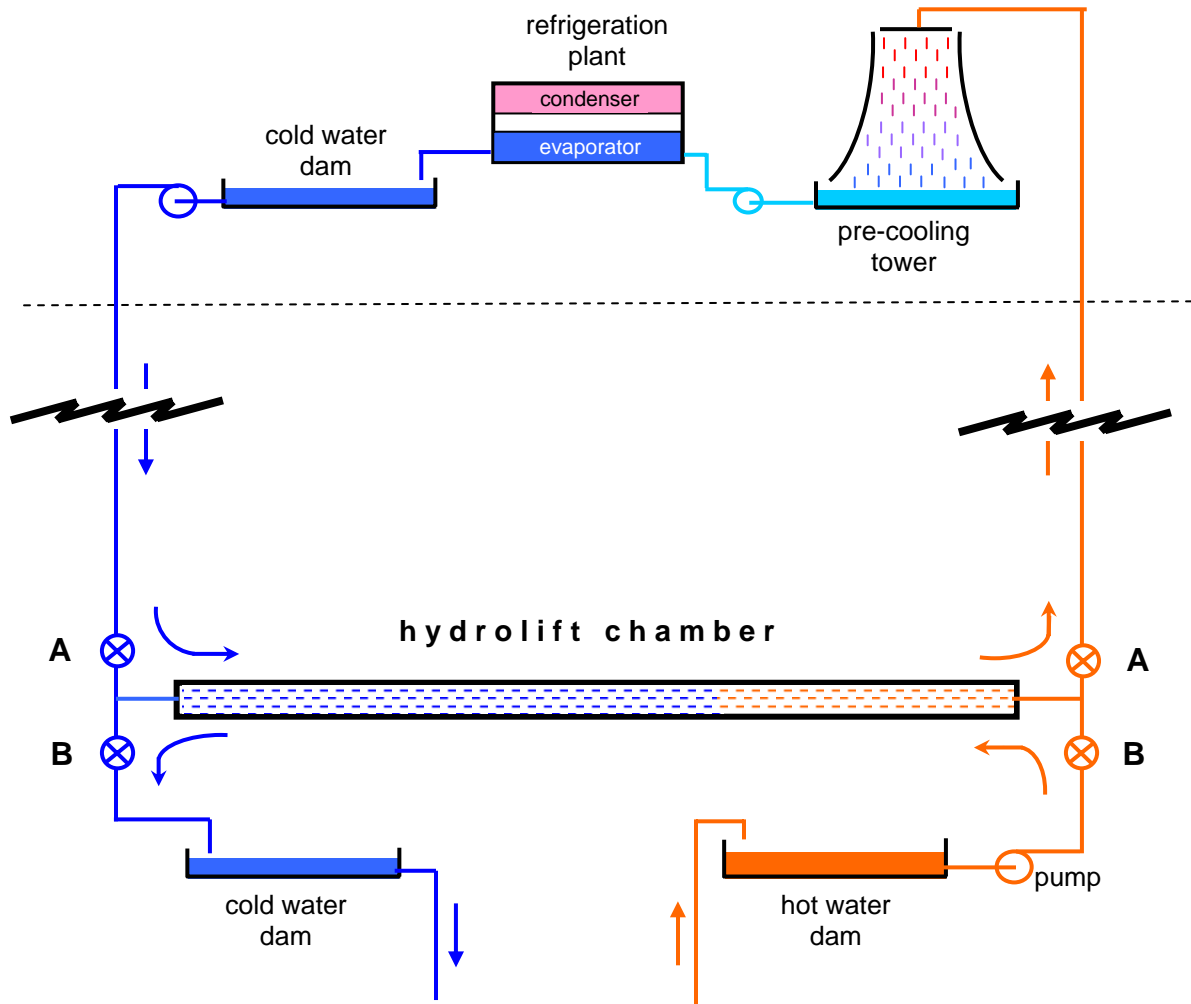


Figure 18.21 Operating principle of a hydrolift system.

18.3.5. Design of mine cooling systems

The demand on a subsurface cooling system is dictated by the magnitude and distribution of the heat load and the surface climate. The availability of cold natural water at the surface can result in large savings in cooling costs. Similarly, passing the water supply through a surface cooling tower either prior to or instead of a refrigeration plant can produce low-cost cooling.

Section 18.3.1 gave an overview of mine cooling systems and introduced spot coolers for isolated heat loads (Figure 18.8), water chiller plant for sections of a mine (Figure 18.9) and a large centralized system (Figure 18.10). In this Section, we shall concentrate on the latter and discuss the alternative arrangements by which the hardware components may be integrated into a unified mine cooling system.

18.3.5.1. Location of main plant

Figures 18.22 to 18.24 give examples of system configurations using main refrigeration plant located on surface, underground and a combination of the two. In these figures, the ancillary components of pumps, valves and retention dams are not shown.

Surface plant

The ease of maintenance, construction and heat rejection, coupled with the utilization of energy recovery devices have led to a preference for the main refrigeration units to be located on surface. Figure 18.22(a) illustrates the simplest system that employs surface plant. Chilled water from the refrigeration plant passes down an insulated pipe in the shaft to a high pressure water to water heat exchanger at one or more shaft stations. This heat exchanger is a source of potential loss of system efficiency and care should be taken with the design and choice of tube materials to minimize problems of corrosion, scaling and erosion. Figure 18.22(b) shows the water to water heat exchanger replaced by a turbine. This configuration requires the water flow in the shafts to approximate that cycling through the mine, with capacitance provided by water dams.

In both cases, the heated water ascending to surface may be sprayed through a pre-cooling tower in order to lower its temperature before returning to the refrigeration plant. This can be advantageous in reducing the required capacity and operating costs of the refrigeration plant. However, the effectiveness of a pre-cooling tower is dependent upon the difference between the temperature of the return water and the wet bulb temperature of the surface atmosphere. An "approach" (see Figure 18.18) of 2°C is typical. For this reason, a pre-cooling tower may be utilized only during the colder seasons.

Figure 18.22(b) also shows part of the chilled water being used for bulk cooling of the air before it enters the downcast shaft. The vertical packed spray chambers used for this purpose are normally of the induced-draught type with the fan located between the spray chamber and the shaft. This helps to prevent fogged air from entering the shaft. If the experience of any given mine is that a heat problem exists during the summer months only, then all that may be necessary is to install a surface bulk air cooling system and utilize it during the warm season. However, if the workings are distant from the shaft bottoms and the heat production is concentrated heavily within those working zones, then bulk air cooling on surface will have greatly reduced effectiveness.

Underground plant

Figure 18.23 illustrates the principle of the system favoured by the South African gold mines prior to the 1980's. The refrigeration plant is located entirely underground. Hot water from the condensers is cycled through open spray cooling towers situated at or near the base of upcast shafts and supplied by air returning from the mine. The advantages of this system are that it eliminates the need for surface-connecting pipe ranges and the associated pumping costs. It also avoids any environmental problems that may arise from surface plant. The major disadvantage of the system is that its duty is limited by the capacity of the return air to accept heat rejected in the underground cooling towers. Furthermore, saturated air subjected to decompression in the upcast shaft can cause problems of heavy fogging, water blanketing in the shaft (Section 9.3.6) and reduced life of main exhaust fans.

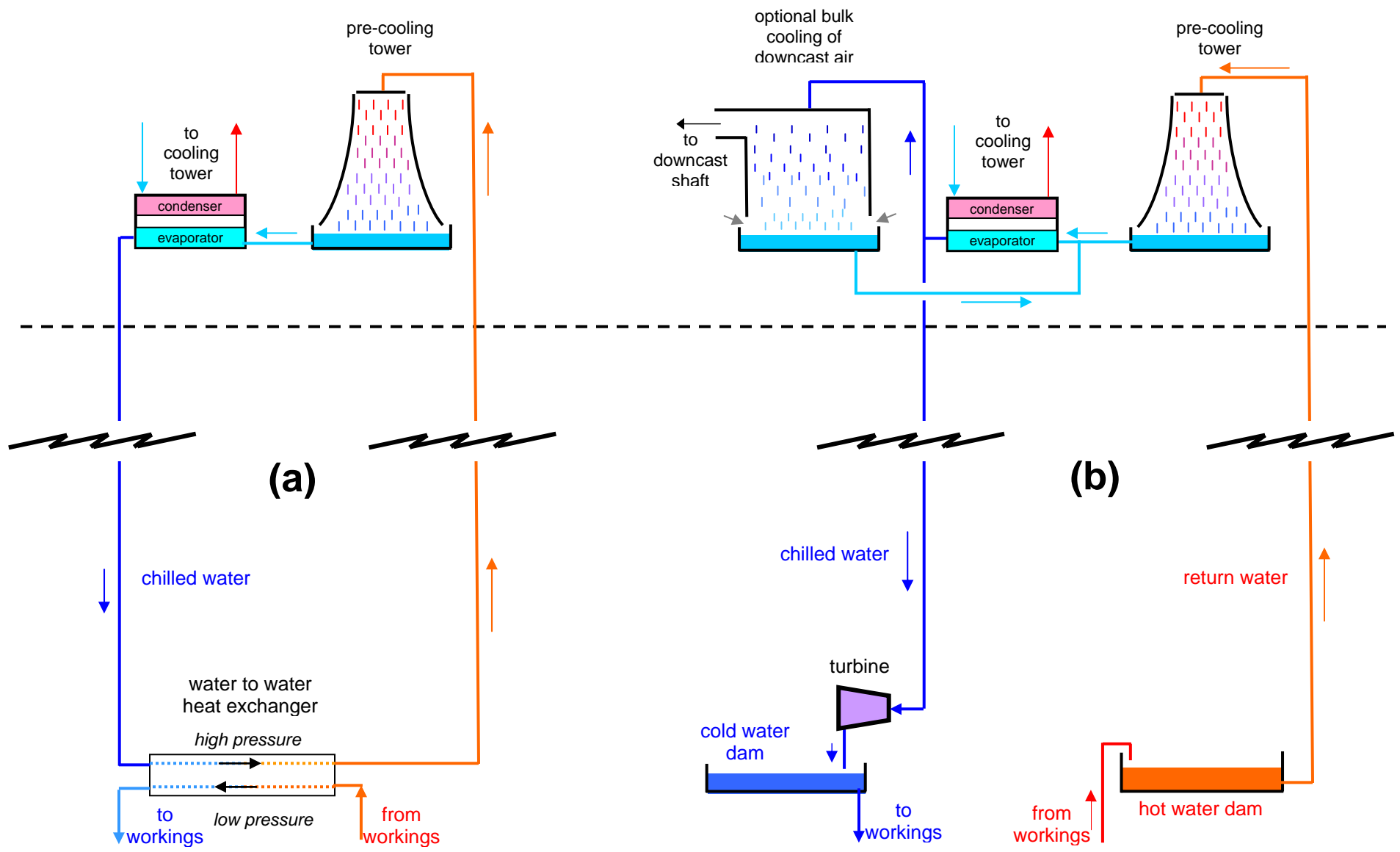


Figure 18.22 Examples of system configurations using surface refrigeration plant.

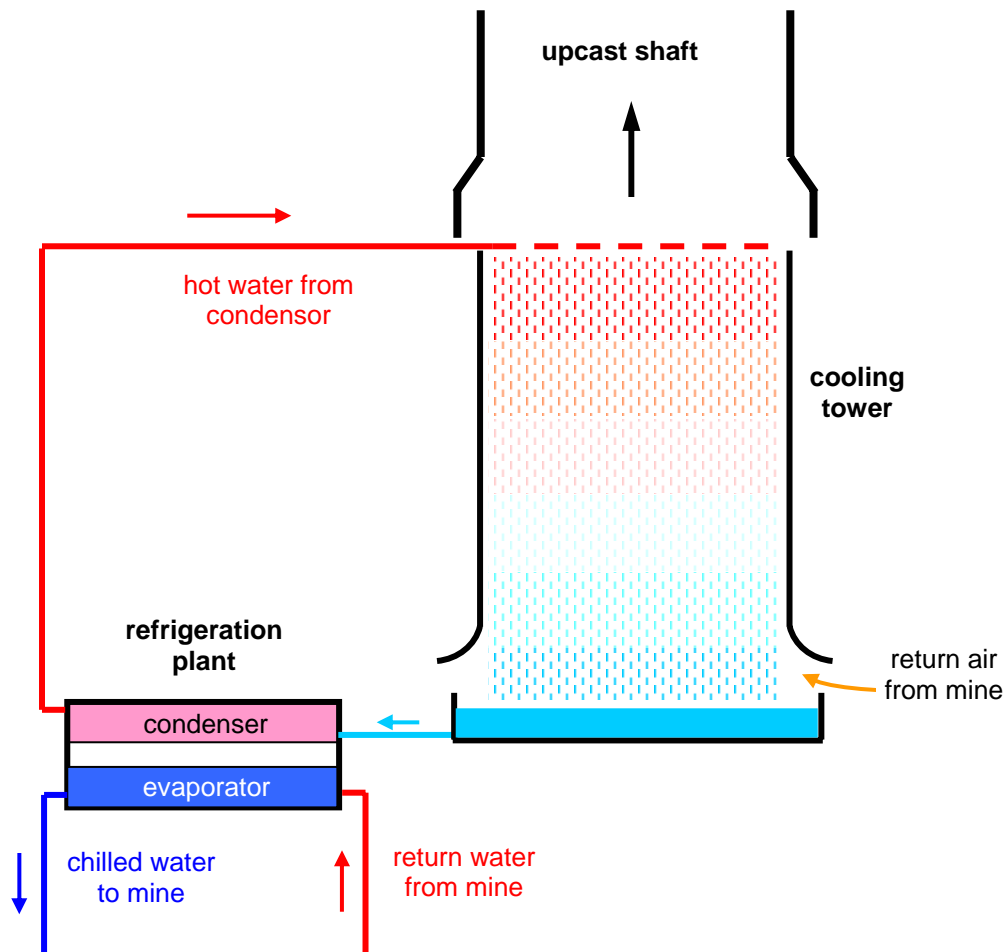


Figure 18.23 System configuration for underground plant.

Combinations of surface and underground plant

As the depth of mining increases, so also does the severity of geothermal and autocompressive heat problems. Unfortunately, increasing depth also exacerbates the costs of installing, maintaining and operating pipelines in shafts and, hence, eroding the advantages of a surface plant. Figures 18.24 (a, b and c) illustrate examples of alternative means of combining surface and underground refrigeration plant into an integrated system. In each of these configurations, the essential role of the underground plant is to concentrate the heat in the return mine water into a lower flow, higher temperature system for transmission to surface.

This enables smaller shaft pipes to be selected and also reduces the pumping costs. Furthermore, the increased temperature of the water returning to surface improves the effectiveness of the pre-cooling tower, allowing it to be utilized throughout the year. Another advantage of the combined system is that it adds considerably to the flexibility and future upgrading of the cooling duty. Surface plant alone is ultimately limited by the flow capacity of the shaft pipes. Similarly, underground plant alone is limited by the thermal capacity of the return air. However, with a combined system the cooling duty can be more easily upgraded by adding to the capacity of both surface and underground plant and, hence, increasing the temperature difference between the descending and ascending shaft pipes.

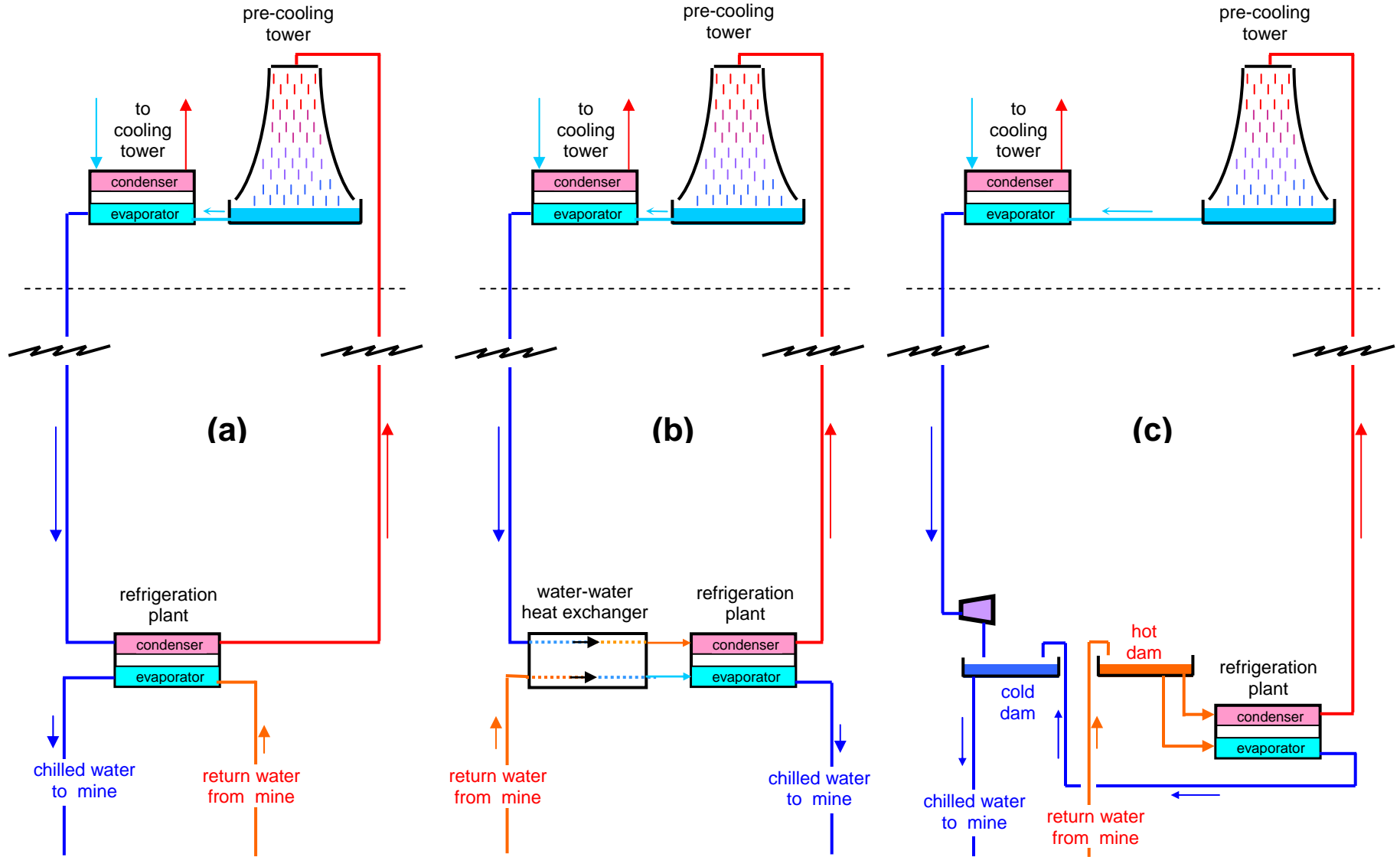


Figure 18.24 Examples of system configurations for combined surface and underground refrigeration plant.

The simplest combined system is shown on Figure 18.24(a) where the surface plant is used to cycle water through the shaft pipes and to remove heat from the subsurface condensers. Figure 18.24(b) shows a system of potentially improved efficiency in which the chilled water from surface first passes through a water-to-water heat exchanger before entering the condensers. The warm return water from the mine is pre-cooled in the water-to-water heat exchanger prior to passing through the evaporators.

Figure 18.24(c) shows the water-to-water heat exchanger replaced by a turbine. In this case, the chilled water emerging from the turbine passes on to the mine via a cold water dam. The return water in the hot water dam is split. Part of it removes heat from the condenser and returns to surface. The remainder is re-cooled through the subsurface evaporator and returned to the cold water dam.

In each of the three examples of combined plant shown on Figures 18.24 (a, b and c), some of the chilled water produced on surface may be used for bulk cooling the downcast air. Similarly, in all three cases, if mine return air is available for heat rejection, then some of the hot water from the underground condenser may be cycled through a subsurface cooling tower before returning to the hot water dam.

18.3.5.2. Service water cooling

Service water is supplied to mining equipment primarily for dust suppression purposes and perhaps, also, as a means of transmitting hydraulic power (Section 18.3.5.3). Heat and dust problems are generally greatest in the working areas and, particularly, where rock breaking equipment is in use. The heat emitted by the machines combines with that from the newly exposed strata to cause rapid increases in air temperature (Section 15.2.2). Uncooled water supplied at dry bulb temperature to dust suppression sprays exacerbates the problem by increasing the humidity of the air. However, if the service water is chilled, then it will both cool and dehumidify the air through which it is sprayed. This effect will continue until the effluent water running into drains or on rock surfaces attains the ambient wet bulb temperature.

The effect of chilled service water in a local workplace can be quite dramatic, depending upon the temperature and flowrate of both the water and the ventilating airstream. Indeed, it is recommended that the temperature of the service water should not be less than 12°C to prevent cold discomfort of personnel. A primary advantage of chilled service water is that it is applied where and when cooling is most needed, i.e. where and when rock breaking or rock transportation is taking place.

The cooling efficiency of chilled service water is greater than that normally obtained from heat exchangers because of the higher temperature of the return water. For example, water supplied to sprays at 12°C may eventually leave the district at the prevailing wet bulb temperature of, say, 27°C, giving a range of 15°C. For comparison, typical temperature ranges of water across local heat exchangers may be of the order of 6 to 10°C. It follows that for the same cooling duty, lower water flowrates can be used when the service water is chilled. This, in turn, reduces the required size of pipes and pumping costs. Furthermore, the increased temperatures of return water enhance the utilization of the low-cost pre-cooling towers on the mine surface.

The effectiveness of air cooling at the entrance to a stope or face is diminished by a large heat flux from newly exposed or fragmented strata. However, such heat can be partially counteracted by the use of chilled dust suppression water, enabling intake air cooling to be employed more effectively.

The benefits to be gained from chilled service water clearly depend upon how much water is required by the equipment, and any adverse effects on the strata or travelling conditions that may arise from too copious a supply of water. The practical approach is to determine the rate of water flow required for dust suppression or other machine purposes and the expected temperature range. The fraction of the total heat load removed by service water can then be estimated.

Example

Dust suppression water is supplied to a workplace at a rate of 100 litres per tonne of rock mined. If the water is supplied to the machine at 12°C and leaves the district at 26°C, determine the cooling provided by the service water at a mining rate of 5 tonnes per minute.

Solution

$$\text{Water flowrate, } m_w = \frac{100 \times 5}{60} = 8.333 \text{ litres or kg/s}$$

$$\begin{aligned} \text{Rate of heat removal} &= m_w C_w \Delta t \\ &= 8.333 \times 4187 \times (26 - 12) \\ &= 488.5 \times 10^3 \text{ W or } 488.5 \text{ kW} \end{aligned}$$

The amount of service water used may vary from 20 to 3000 litres per tonne depending upon the mining method and the mineralogical constituents of the dust particles. There is a corresponding large range in the rate of possible heat removal by dust suppression water. However, due to the high efficiency of the technique and the utilization of existing water lines, it may be regarded as the first approach to the supply of "coolth" to a rock breaking area.

The fraction of total heat load that can be removed by chilled service water is eroded at greater depths due to the increased effects of autocompression and geothermal heat, while the supply of service water remains constant for any given mining method.

18.3.5.3. Hydropower

In section 18.3.4, we discussed the utilization of potential energy made available in shaft water pipes. In addition to driving shaft station turbines or hydrolift systems, the water pressure available at spray chambers can also be used to activate fans and pumps at those locations. The concept of hydropower takes this idea further and combines it with service water cooling (Section 18.3.5.2).

The use of electrical or diesel power involves the production of heat. Expenditure is then incurred to remove this heat from the mine by ventilation and/or cooling systems. The utilization of machine power by such means involves both an environmental and an associated cost penalty. However, if the machine is activated by chilled water under pressure provided by the shaft column, then the hydraulic machine power and climatic control act in concert rather than in opposition. In a hot and deep mine, chilled hydropower provides, simultaneously, a means of machine power, cooling and dust suppression, all from a single system.

For relatively low powered units such as drills, hydraulic motors may be employed directly while, for larger machines, turbine-electric combinations may be more practical. Furthermore, differing combinations of water flow, pressure and temperature may be required for the demands of power, cooling and dust suppression. A hydropower system should be designed and balanced to satisfy those varying demands.

18.3.5.4. Ice systems

The limitations of heat rejection capability underground, together with the use of energy recovery devices, have promoted the trend away from subsurface refrigeration plant towards surface units. However, despite water turbines and hydrolift devices, pumping costs remain the factor which limits the mass flow of water that can be circulated through the shaft pipelines of deep mines. Recalling the

relationship $q = m_w C_w \Delta t$, heat removal from a mine can be enhanced by increasing the temperature differential, Δt , between supply and return water. This can be accomplished by combinations of surface and underground refrigeration plant (Section 18.3.5.1). Despite such advances in mine cooling technology, heat remains the primary limitation on the depth at which mining can take place.

In order to proceed beyond the physical restraints imposed by the circulation of fluids, other means of transmitting "coolth" have to be considered. One of these is to employ the latent heat of melting ice. Although the use of ice in mines is not new (Section 18.1), the first pilot plant employing an ice pipeline was constructed in 1982 at the East Rand Proprietary Mines in South Africa (Sheer, 1984). Further full scale applications followed soon afterwards (Hemp, 1988).

Ice has a specific heat varying from 2040 J/(kg °C) at 0°C to 1950 J/(kg °C) at -20°C. It has a latent heat of melting of 333.5 kJ/kg. The mass flow of water circulated around a mine for cooling purposes can be reduced by a factor of over 5 if it is supplied in the form of ice.

Example

A mine requires 10 MW of cooling. Calculate the mass flow of water involved

- (a) if the water is supplied at 3°C and returns at 20°C
- (b) if the water is supplied as ice at -5°C and returns at 20°C.

Solution

(a) for the water system:

$$q = m_w C_w \Delta t_w$$

$$\text{or } m_w = \frac{q}{C_w \Delta t_w} = \frac{10 \times 10^6}{4187 \times (20 - 3)} = 140.5 \text{ kg/s or litres/s}$$

(b) for the ice supply:

Heat absorbed as the temperature of m_i kg of ice increases from -5 to 0°C,

$$q_{ice} = m_i C_i \Delta t_i$$

Choosing the specific heat of ice as 2030 J/(kg °C) gives

$$q_{ice} = m_i \times 2030 \times 5 = 10\,150 m_i \quad \text{W}$$

Latent heat absorbed as m_i kg of ice melts at 0 °C

$$q_L = L_{ice} m_i = 333\,500 m_i$$

Heat absorbed as m_i kg of liquid water increases in temperature from 0 to 20°C:

$$q_w = m_i C_w \Delta t_w = m_i \times 4187 \times 20 = 83\,740 m_i \quad \text{W}$$

Then, total heat absorbed

$$q = q_{ice} + q_L + q_w = 10 \times 10^6 \quad \text{W}$$

$$m_i (10\,150 + 333\,500 + 83\,740) = 10 \times 10^6 \quad \text{W}$$

giving $m_i = 23.4 \text{ kg/s}$

Hence, in this example, the volume of cooling water is reduced by a factor of 6 when it is supplied as ice at -5°C . The calculation also illustrates the dominant amount of heat involved in the change of phase from ice to liquid, q_L .

There are four primary items to consider when investigating an ice system for mine cooling;

- the large scale manufacture of ice,
- the means of transporting it underground,
- how it is best incorporated into a mine cooling system, and
- the economics of the system.

Each of these factors will be considered in turn.

Manufacture of ice

The ice that is utilized in a mine cooling system may be supplied either as particulate ice at sub-zero temperature or as a slurry of ice crystals within liquid water or brine.

Particulate ice can be manufactured as cubes, cylinders or tubes of clear ice, or as ice flakes that can be compressed into pellets for transportation. Water is sprayed or caused to flow over the surfaces of plates, tubes, concentric cylinders or drums that are cooled on their opposite sides by a refrigerant fluid. The formation of ice creates an additional thermal resistance to heat transfer. This necessitates an evaporator temperature of some -15 to -30°C giving rise to coefficients of performance in the range 2.3 to 3.5, lower than might be expected from a well designed water chiller.

The ice is usually removed from the cold surfaces by mechanical scrapers or by periodic cycling of hot refrigerant through the freezer unit. In the production of flake ice, a thin film of ice is removed continuously from the surface of a rotating drum or metal belt. The particles of ice fall into a hopper that feeds into a screw or belt conveyor for removal from the unit.

As an example of large-scale particulate ice manufacture, a plant at East Rand Proprietary Mines (South Africa) produced 6000 tonnes of ice per day from six 1000 tonne/day units. Each tubular unit consisted of eighty double walled tubes with ice formation on both the inner (99 mm dia) and outer (508 mm diameter) surfaces of the 4.5 m long tubes. The refrigerant passed through the annulus of each tube. The 15 minute cycle consisted of 13.5 minutes of freezing and 1.5 minutes harvesting (Hemp, 1988). The refrigerant was ammonia and ice harvesting was achieved by passing hot ammonia liquid through the annuli in the icemaker tubes. This arrangement also improved the efficiency of the unit by subcooling the liquid refrigerant before it returned to the evaporators.

Slurry icemakers promote the formation of microcrystals of ice within a stream of water or brine and are at an earlier stage of development for mine cooling systems. Slurry ice has one significant advantage over particulate ice. All industrial and domestic supplies of water contain many impurities including dissolved salts of calcium, magnesium and sodium. The freezing process favours pure water. Hence, if the freezing occurs sufficiently slowly or if the ice/water interface is continuously washed with water, then the ice crystals will have a greater purity than the water in which they grow. The dissolved salts remain in the liquid and, hence, become more concentrated. In contrast, the formation of plate, tube or flake (particulate) ice occurs quickly and with a more limited washing action by the water, giving rise to the entrapment of salts within the ice matrix. If the microcrystals, usually of less than 1 mm in size, are removed from the ice slurry and washed, then they will be relatively free from impurities. This process is known as **freeze desalinization**. The provision of purified water to a mine cooling system assists greatly in minimizing corrosion and scaling within pipes and heat exchangers.

There are at least three methods that have the potential for large-scale manufacture of slurry ice (Shone, 1988). In the **indirect process**, water or brine is passed through tubes that are surrounded by cold refrigerant. Microcrystals of ice are formed within the moving stream of water. Careful control of the salinity, flowrate and temperature is required to prevent the formation of solid ice on the sides of the tube. Scraper devices can also be used to prevent ice from accumulating on the walls.

The **vacuum ice-making process** involves the evacuation of water vapour from a vessel that contains brine. The triple point of water is reached at 0.6 kPa and 0 °C when boiling and freezing occur simultaneously (ref. Figure 18.1). Ice, liquid water and vapour coexist at this point. The ice slurry that is formed is kept in motion by an agitator until it is pumped from the vessel. About 1 kg of water vapour must be removed for each 7.5 kg of nucleated ice. The vapour is compressed and condensed for recycling. In the vacuum ice-making process, the water acts as its own refrigerant fluid (Section 18.2.2).

An even less developed method is the **direct process** in which a mixture of brine and immiscible liquid refrigerant are sprayed through a nozzle into a receiving chamber. The evaporation of the refrigerant cools the mixture and promotes the nucleation of ice crystals within the brine. The ice slurry collects at the bottom of the vessel and is pumped out. The refrigerant vapour is evacuated from the top of the vessel for compression, condensing and recycling.

In all three processes, the salinity of the brine has an important influence on the manufacture of ice slurry. In general, a higher concentration of dissolved salts will give a smaller production of ice crystals but at greater purity. The freezing temperature will also be lower, resulting in a reduced coefficient of performance for the unit. For mine cooling systems, a salt concentration between 5 and 15 percent would appear to be appropriate. However, the optimum salinity for any given installation should be determined from tests on the actual water to be used.

Future employment of ice slurries in mine cooling systems may be combined with energy recovery devices. The duties of direct-contact heat exchangers are considerably enhanced when the sprays are supplied with ice slurry of up to 20 percent ice (Gebler, 1988). Droplets in the spray chamber remain at 0°C until the ice crystals are melted. Tests have indicated that with an ice fraction of only 40 percent, pipeline pressure drops are about three times those for water (Shone, 1988).

Transportation of ice

The mass of ice required for a mine cooling system is such that it must be supplied continuously rather than in a batch transportation system. While slurry ice can be pumped through pipes, particulate ice must be transported from the ice-making plant to the shaft by conveying systems or by a hydraulic or pneumatic pipeline. In the latter case, the supply air temperature should be not more than 8°C in order to prevent undue agglomeration of the ice particles.

The particulate ice falls through the shaft pipeline either as **dilute flow** in which the particles are separated and retain their individual identity or as **dense** or **slug flow**. In the latter case, the ice particles agglomerate into discrete slugs separated by air spaces. If the ratio of ice to air is too great, then **extrusion flow** will develop accompanied by a greatly increased risk of pipe blockage. The factors involved in the type of flow through an ice pipeline are the ice/air ratio, the shape, temperature and size of the particles, and the type and size of pipe. Unplasticised (U) PVC has been found to be a satisfactory pipe material for ice lines. However, changes in cross section or lips at expansion joints should be avoided. At shaft stations, radii of curvature of 3 m or more allow the pipelines to be extended horizontally for several hundred metres. To cite the East Rand Mines example again, four uninsulated UPVC pipes of inside diameter 270 mm and wall thickness 22.5 mm were employed (Hemp, 1988). The longest pipe extended through a vertical distance of approximately 2900 m. Each pipe was capable of carrying 200 tonnes per hour (55.6 kg/s) allowing for considerable future expansion of the mine cooling duty.

Incorporation into the mine cooling system

Figure 18.25 gives a simplified representation of one layout that utilizes particulate ice.

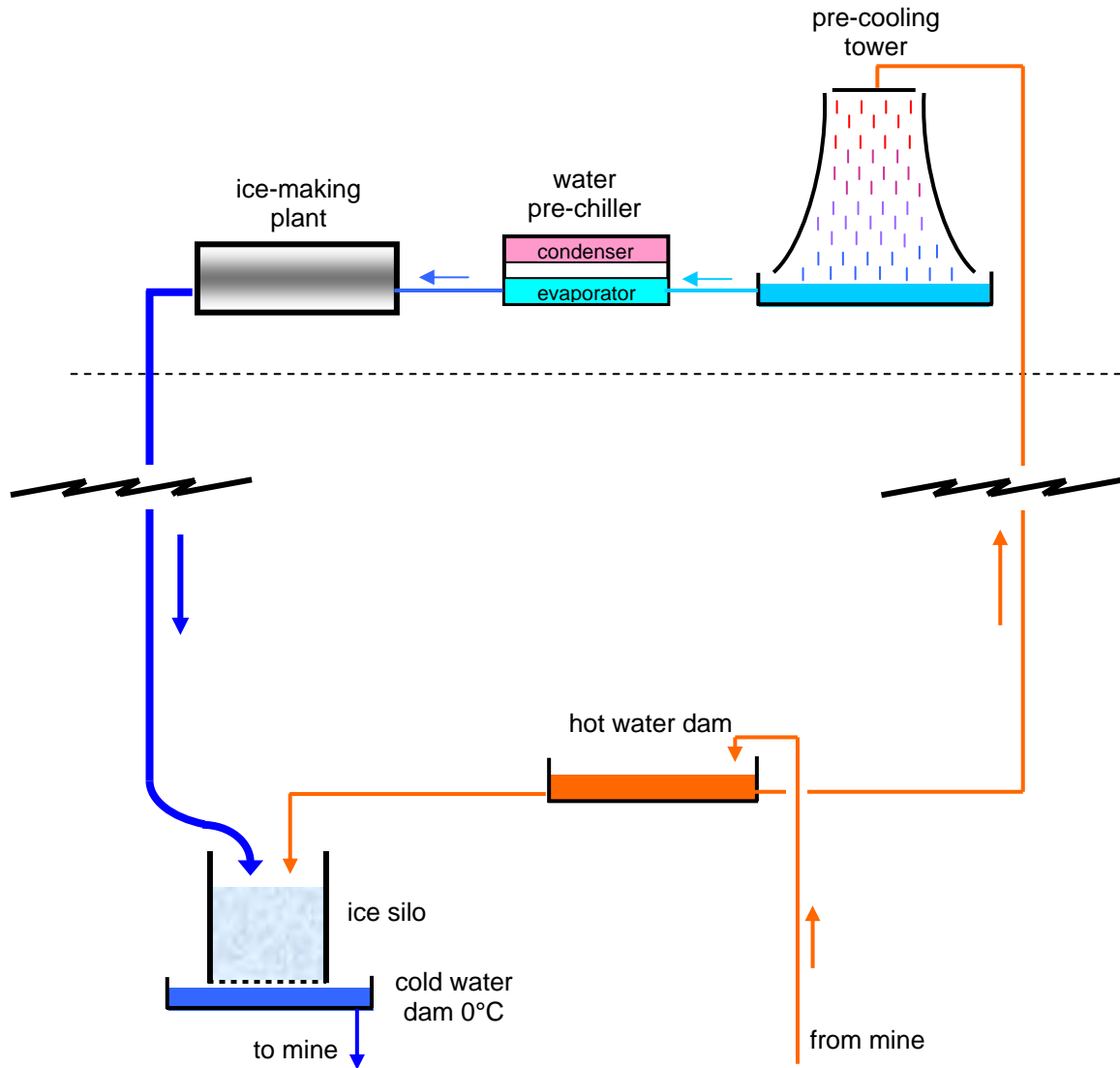


Figure 18.25 Layout of an ice system. Ice silos may be located on several levels.

Return water pumped from the mine passes through a surface pre-cooling tower and is further cooled in a water pre-chiller. This may be supplied by "coolth" from the ice-making refrigeration plant or, alternatively, be a separate water chiller package. The particulate ice falls through the shaft pipeline and is discharged into an ice/water mixing dam or a silo with a perforated base. Water from the hot water dam is also sprayed into the ice silo. The discharge from the silo enters the cold water dam at 0°C.

The bed of ice in the silo should be maintained at a thickness of 1 to 2 m. The supply of ice to each silo must be matched to the required cooling duty at that level. Position transducers can be used to monitor the ice level in each silo. The transmitted signals may be employed to control ice feed rates. It is advisable to provide sufficient ice bunkering to handle short term fluctuations in demand. Longer

term variations can be handled by activating an appropriate number of individual sets in the ice-making plant or by compressor control on the refrigeration units (Section 18.2.3).

Economics of ice systems

The benefits of ice as a medium of heat transfer in mines may be listed as follows:

- greatly reduced water flow in shaft pipelines; therefore - smaller pipes and lower pumping costs
- water is available at 0°C underground rather than the 3 to 6°C common with conventional chilled water systems; therefore there is less flow and reduced pumping costs in the subsurface (secondary) circuits, and improved performance of heat exchangers.
- "coolth" is stored in ice bunkers and silos to satisfy short term variations in demand
- the system is more easily capable of being uprated for future increases in cooling load
- the subsurface system is simpler having reduced or eliminated the need for turbines
- the quality of the water is improved by ice-making.

The major disadvantage of the system is the considerable increase in both capital and operating costs of the ice-making plant. As the depth of a mine increases and the heat load and associated pumping costs both rise, then, at some point, it becomes economically advantageous to convert from water chilling to an ice system. A study in South Africa showed that the crossover point occurs at a depth of approximately 3000 m (Sheer, 1984). However, this will be influenced not only by the cost of hardware but also power charges, surface climate, geothermic gradient, rock properties and heat from equipment or stored materials (in the case of subsurface repositories). It is, therefore, prudent to conduct a site-specific economic study on any proposed ice system.

18.3.6. Summary of design process

Although this chapter has concentrated on the hardware associated with mine air conditioning systems, it is pertinent to remind ourselves that the design of such systems cannot be separated from ventilation planning (Sections 9.1 and 16.3.5). In particular, the initial question is how much heat can, or should, be removed by ventilation and how much by cooling systems.

This leads us into the first stages of the design procedure for a mine cooling system.

1. Establish the expected heat load for the entire mine and for each identifiable district, level or zone in the mine. The techniques for doing this are discussed in Chapters 15 and 16.
2. Again, for the whole mine and each individual area, determine the airflows required to deal with dust and polluting gases, taking into account air velocity limits (Section 9.3). Ventilation network analyses should be conducted in order to establish airflow distribution and leakage patterns (Chapter 7).
3. Determine the heat removal capacities of the airflows (Section 9.3.4). If this is greater than the corresponding heat loads for individual sections of the mine, then the heat can be removed entirely by ventilation and there is no need to consider a cooling system.
4. Conduct exercises to determine the feasibility of removing the excess heat by increased airflows without exceeding velocity limits set by physiological, economic or legislative considerations

(Section 9.3.6). If the additional airflows are unacceptable, then the need for air conditioning is established and the design of the cooling system can proceed.

5. Determine the heat to be removed by cooling as the difference between the heat load and the heat removal capacity of the air (Section 9.3.4). Preferably, a climatic simulation program should be used in order to conduct a detailed analysis of the positions and duties of heat exchangers and application of chilled service water (Chapter 16).

Interactive studies should also be conducted to optimize between ventilation and air conditioning (Figures 9.1 and 16.4) (Anderson, 1986). These investigations will establish the required distribution of air cooling devices. If this is limited to a few localized areas, then the feasibility of employing spot or district coolers (Section 18.3.1) should be investigated. If, however, the heat problem is more widespread, then the study should be widened to examine centralized refrigeration plant.

6. Investigate the alternative locations of refrigerating plant (Section 18.3.5.1) and the feasibility of employing energy recovery devices (Section 18.3.4).
7. By summing heat exchanger capacities and allowing for line losses, establish the duty of the refrigeration plant.
8. Estimate evaporator and condenser temperatures on the basis of the desired temperature of the cooled medium and the heat rejection facilities respectively.
9. Determine the required flowrates of chilled water and, hence, the sizes of pipelines (Section 18.3.3.1) and pumping duties.
10. Invite tenders from manufacturers of refrigeration plant and ancillary equipment, including valves, pipelines, pumps, heat exchangers, instrumentation and controls.
11. Establish capital, installation and operating costs of the cooling system.

18.4. AIR HEATING

In the colder countries of the world, the temperature of intake air entering a mine may fall well below 0°C for a major part of the year. This can result in severe problems along intake routes, and particularly in surface connecting downcast shafts, slopes or adits. First, a build-up of ice on shaft walls and fittings can cause a significant increase in resistance to airflow. Furthermore, large pieces of ice dislodged by shaft operations or melting can present a hazard to personnel working in or near the shaft. Repeated cycles of freezing and thawing occurring on a daily or seasonal basis can result in severe damage to concrete linings in shafts or other intake airways, particularly when there is a seepage of ground water through the lining.

Secondly, sub-zero temperatures can have adverse effects on the operation and maintenance of equipment. This may result in poor productivity as well as a reduction in safety.

Thirdly, personnel who are inadequately protected against a cold environment will suffer the symptoms described in Section 17.6. Here again, this will lead to diminished levels of productivity and a deterioration in safety standards.

Winter temperatures can fall below -40°C at the surfaces of mines in cold climates (Hall, 1988; Moore, 1985). In these conditions, it becomes necessary to heat the intake air. This is the situation that obtains at many Canadian mines (Hall, 1989).

The methods of air heating suitable for mine applications may be listed as follows:

- utilization of waste heat produced from plant or processes on the mine surface
- heat recovery from warm return air
- direct heating
- indirect heating
- ice stopes
- geothermal or cycled storage heating.

Each of these techniques is examined in the following subsections. To choose the method most applicable for any given facility, it is necessary to consider technical feasibility, reliability, flexibility and economics. Because of the large airflows that are usually involved, the costs of heating may far exceed those of producing the ventilation (Hall, 1985). In very cold climates, it is often the aim simply to increase the intake air temperature to about 0°C and to allow autocompression, geothermal and other sources of heat to produce more comfortable temperatures in the main working areas.

In order to minimize operating costs, air heating systems might be employed only during main working shifts and when the surface temperature drops below a preset value. Furthermore, two or more of the systems listed above may be combined to minimize energy demand or to provide additional capacity for periods of abnormally low temperature.

There is, however, one situation in which air heating should be avoided or used with great caution. This occurs when the mine workings are in permafrost. Allowing air temperatures to exceed 0°C may cause partial melting of the permafrost and give rise to problems of ground control in the mine. Indeed, at the Polaris Mine, 1400 km from the North Pole, refrigeration techniques have been employed during the short summer in order to maintain the intake temperatures below the melting point of permafrost (Van der Walt, 1984).

18.4.1. Utilization of waste heat

The first matter to investigate for any proposed air heating project is whether heat is available from other plant or processes on the surface of the mine. Secondly, the costs and technical feasibility of using that thermal energy to raise the temperature of intake air should be studied. Common sources of waste heat are compressor stations, generators and mineral processing operations (de Ruiter, 1989). If the waste heat is in the form of hot water or steam, then it may be pumped directly through insulated pipes to heat exchanger coils located within all, or part, of the intake airstream. Ice accumulations on the heat exchanger can be avoided by using a single array of coils only.

In water systems, an automatic procedure should be incorporated in order to empty the coils and associated pipework during a shut-down period or if the water temperature approaches freezing point. A further safeguard against frost damage is to employ a glycol-water mixture. A 50 percent glycol mixture lowers the freezing point to -40°C.

If the available heat source provides relatively low temperature thermal energy, then it may be necessary to employ a heat pump (Section 18.2). Heat pumps may also allow the utilization of natural heat sources such as a large lake or the ocean, provided that these remain unfrozen through the winter months.

18.4.2. Heat recovery from exhaust air

This method may be considered if the downcast and upcast shafts are close to each other and there is a significant difference between the intake and return air temperatures. Figure 18.26 shows that during cold periods, the warm air returning from the mine is diverted through a direct contact spray chamber, transferring useful heat to the descending water droplets. Water from the sump is pumped

through a heat exchanger located within the intake airstream. Again, it is advisable to employ a single array of coils to minimize ice build-up, and to allow for automatic dumping of water from the heat exchanger and pipework when the flow ceases.

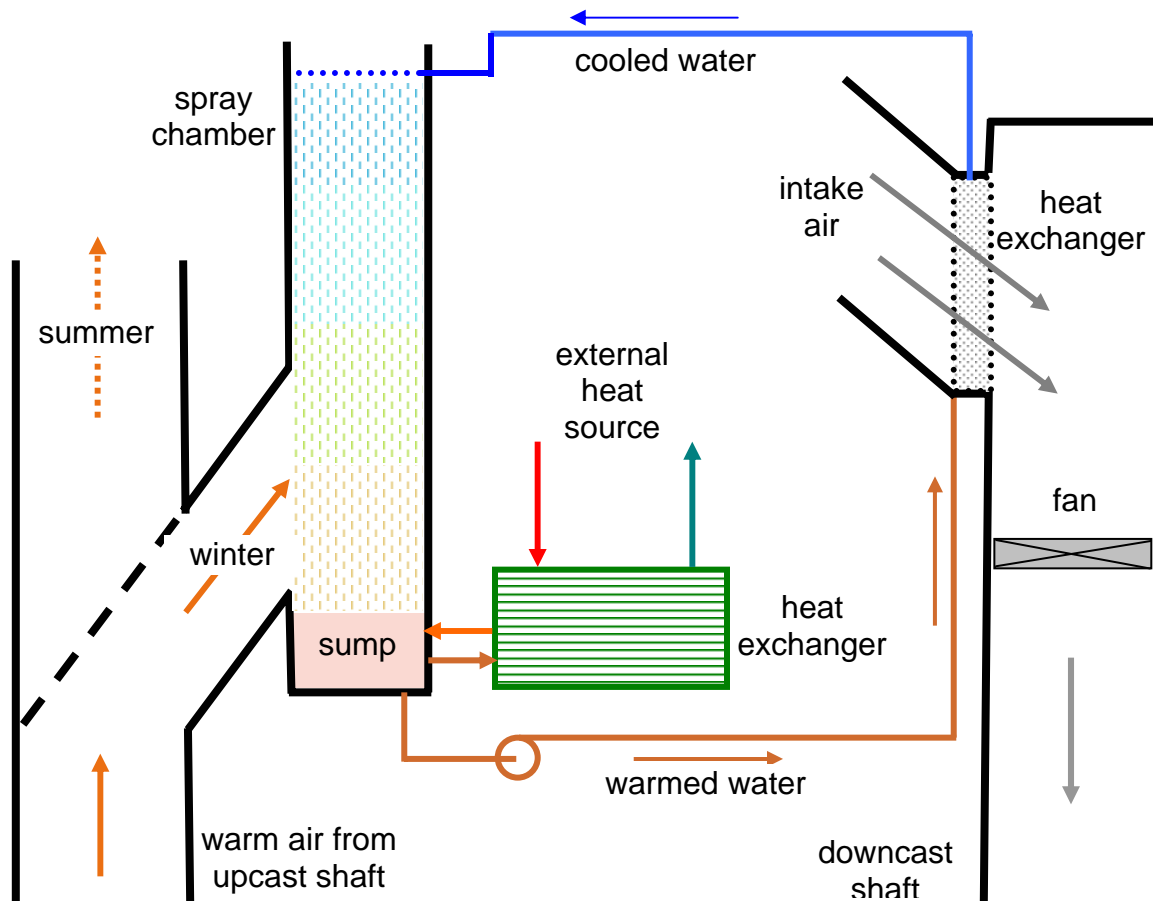


Figure 18.26 Heat recovery from return air augmented from an external heat source.

The spray chamber may be replaced by a tube coil heat exchanger. However, this reduces the overall heat transfer efficiency of the system and also introduces the dangers of ice accumulation and corrosion of the tubes, particularly if the return air is humid.

Heat exchange from upcast to downcast airflows is seldom practicable by itself. However, it may be employed in combination with an external source of heat as shown on Figure 18.26. If that source is waste heat from other plant, then it may be kept in continuous operation. However, if the external source of heat is gas, oil or electricity, then it may be used only during working shifts and when the surface air temperature falls below a set value.

A more direct means of recovering some of the heat from warm return air is by **controlled partial recirculation** (Hall, 1988, 1989). This technique gives one hundred percent efficiency of heat transfer from return to intake for that fraction of the air which is recirculated. This is limited by the rate at which gaseous and particulate pollutants are added to the mine air. The system should be capable of reverting to normal through-flow ventilation should monitors indicate a trend towards unacceptable concentrations of pollutants or following blasting operations. The volume of air that is recirculated may be controlled automatically by the pollutant concentrations in the return air or set at a fixed

fraction of the return airflow. The recirculating cross-cut should be located as close to the surface connection as practicable in order to take advantage of the pollutant dilution arising from air leakage.

If the level of contamination by airborne pollutants is sufficiently low to allow a reduction in the through-flow of fresh air, then the costs of heating the intake air will also be reduced. However, any proposed system of controlled partial recirculation must incorporate all of the safeguards and precautions discussed in Section 4.5.

18.4.3. Direct heating

The employment of electrically heated elements to raise the temperature of mine air is limited by high operating costs. It is practical only for very light duties or where electrical power is particularly cheap.

Natural gas, propane or other light hydrocarbon fuels may be injected through nozzles and burned in flame jets within the intake airstream. As no intermediate heat exchangers are involved, this is the most efficient way of using the fuel. The products of combustion, carbon dioxide and water vapour, are added to the airstream in relatively small amounts. However, the gas nozzles should be well maintained to prevent the formation of carbon monoxide through incomplete combustion. A prudent precaution is to locate a gas monitor downstream from the jets with alarms and automatic fuel cut-off at a predetermined concentration of carbon monoxide.

The rate of fuel consumption for any given heating duty may be calculated from the calorific value of the fuel. At the temperatures to which the products of combustion are cooled in mine air, the majority of water vapour will condense. Hence, it is the **gross calorific value** that should be used. Table 18.4 gives the gross calorific values of several gases. For natural gas and other mixtures, an approximate value may be obtained by summing the calorific values of the constituents weighted according to percentage composition.

Gas	Gross calorific value MJ/m ³
carbon monoxide	11.8
hydrogen	11.9
methane	37.1
ethylene	58.1
ethane	64.5
propylene	85.7
propane	93.9
butane	121.8
natural gas (depends upon composition)	26 to 56

Table 18.4. Gross calorific values of gases based on a temperature and pressure of 15°C and 101.3 kPa respectively. For petroleum fuel oils, gross calorific values vary from 42 to 47 MJ/kg.

Example

An airflow of 100 m³/s and density of 1.4 kg/m³ is to be heated from -20°C to 2°C by propane jets.

- Determine the rate of fuel consumption in m³ per hour.
- If the air is supplied at 21 percent oxygen and 0.03 percent carbon dioxide, determine the corresponding concentrations downstream from the jets.

Solution

$$\begin{aligned} \text{(a) Mass flow of air } m_a &= Q \rho \\ &= 100 \times 1.4 = 140 \text{ kg/s} \end{aligned}$$

$$\begin{aligned} \text{Heat required, } q_a &= m_a \times C_p \times \Delta t \\ &= 140 \times 1005 \times (2 - (-20)) \\ &= 3.095 \times 10^6 \text{ W} \\ \text{or} & \quad 3.095 \text{ MW.} \end{aligned}$$

[To be precise, we should take the presence of water vapour into account. However, the effect is very small at these low temperatures and may be neglected.]

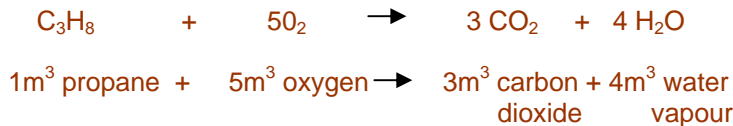
The gross calorific value of propane is selected from Table 18.4 as 93.9 MJ/m³. Hence, heat produced at the jets

$$q_p = 93.9 \times \text{propane flowrate} \quad \frac{\text{MJ m}^3}{\text{m}^3 \text{ s}} \quad \text{or MW}$$

As $q_p = q_a = 3.095 \text{ MW}$, the required propane flowrate = $3.095/93.9 = 0.0330 \text{ m}^3/\text{s}$

or $0.0330 \times 3600 = 118.7 \text{ m}^3$ per hour at standard temperature and pressure.

(b) The chemical balance for burning propane is



Therefore 0.0330 m³/s of propane will consume

$$\begin{aligned} 5 \times 0.0330 &= 0.165 \text{ m}^3/\text{s} \text{ oxygen to produce} \\ 3 \times 0.0330 &= 0.099 \text{ m}^3/\text{s} \text{ carbon dioxide} \end{aligned}$$

At entry, the airflow includes

$$100 \times 0.21 = 21 \text{ m}^3/\text{s} \text{ oxygen and } 100 \times 0.0003 = 0.03 \text{ m}^3/\text{s} \text{ carbon dioxide.}$$

Downstream from the jets,

$$\begin{aligned} \text{oxygen flowrate} &= 21 - 0.165 = 20.835 \text{ m}^3/\text{s} \text{ and} \\ \text{carbon dioxide flowrate} &= 0.03 + 0.099 = 0.129 \text{ m}^3/\text{s} \end{aligned}$$

As the airflow is 100 m³/s these same values give close approximations to the concentrations of the gases downstream from the jets.

18.4.4. Indirect heating

In order to prevent products of combustion from entering the mine ventilation system, fuels may be used in a separate burner to heat a glycol-water mixture. This is then recirculated through an indirect heat exchanger located within the intake air. Again, a single array of coils will minimize the risk of ice accumulation on the tubes. This technique of indirect or offline heating inevitably gives a lower thermal efficiency than open flame jets within the intake air. However, the flowrate of the glycol mixture provides an added measure of control and flexibility.

18.4.5. Ice stopes

Figure 18.27 illustrates a metal mining technique that allows air to be heated from sub-zero temperatures to approaching 0°C at very low cost. Water is sprayed into the top of an abandoned open stope. Cold air coming directly from the downcast shaft or slope enters near the top and circulates through the stope, freezing the water droplets, before exiting at the other end.

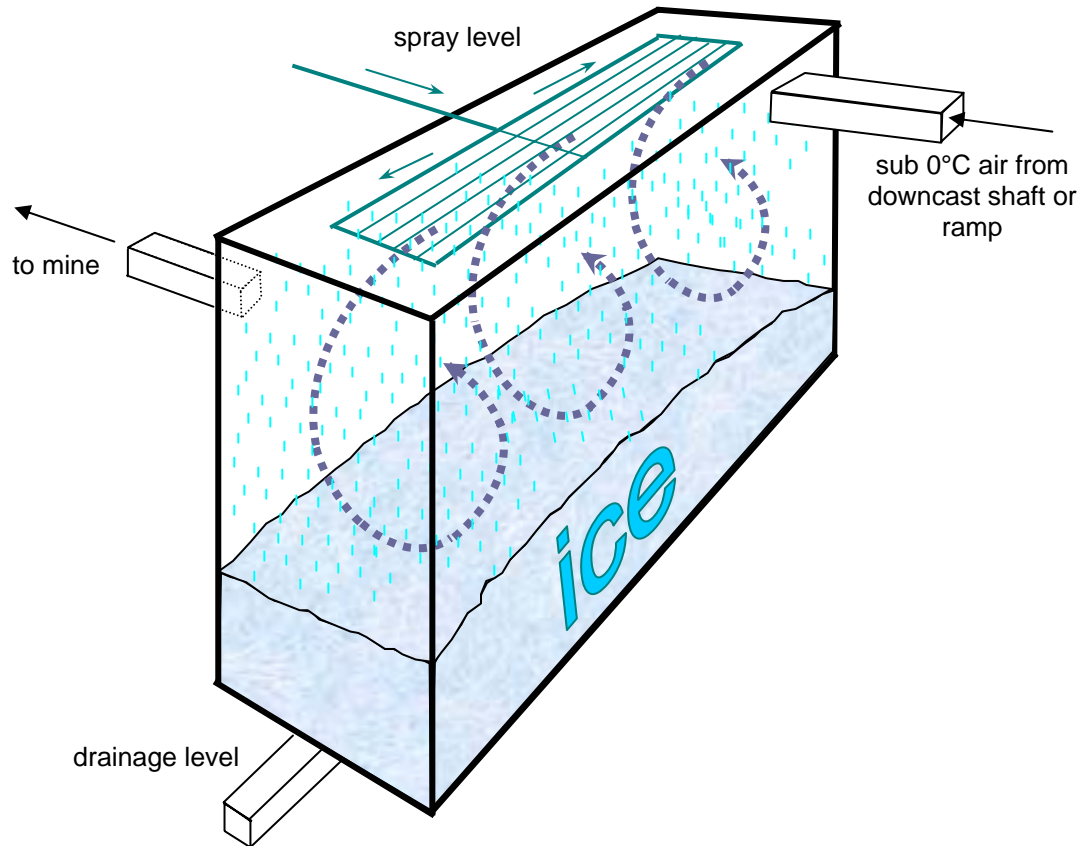


Figure 18.27 Depiction of an ice stope.

The air is heated by three mechanisms:

- (a) directly from the liquid water droplets,
- (b) by latent heat of fusion (333.5 k/Jkg) as the water freezes, and
- (c) by strata heat from the wall rock.

The ice particles fall and form an ice bed that gradually accumulates in the stope through the winter months.

In summer, warm intake air may be cooled by circulating it through the same stope and melting the ice. A drain level at the base of the stope carries water to a main sump. However, the air cooling may be enhanced by circulating the liquid melt back through the sprays.

The ice stope technique has been used very successfully at the **Stobie Mine** of Inco Ltd. in Canada (Stachulak, 1989). In this mine an airflow of 307 m³/s is heated in two ice stopes at a cost estimated at about one-ninth that for equivalent gas heating. In that installation, water is supplied to the nozzles

at a pressure of between 550 and 760 kPa. Compressed air is added to the line shortly before the nozzles. This provides a finely divided spray and prevents icing up of the jets. The compressed air is also used to clear water from the pipes when the system is to be shut down.

The disadvantages of the ice stope technique are that it requires the availability of large open excavations and also necessitates an increased pumping capacity for the mine drainage system.

Example

Water at 7°C is sprayed at a rate of 30 litres per second into an ice stope. Air enters the stope at -22 °C and is required to be heated to -2 °C. Calculate the maximum air flowrate through the stope that can attain this 20 C° increase in air temperature.

Solution

Mass flowrate of water, $m_w = 30$ kg/s

Heat released by water in cooling from 7°C to 0°C

$$q_w = m_w C_w \Delta t_w$$

$$= \frac{30 \times 4187 \times 7}{1000} = 879 \text{ kW}$$

Heat of fusion released by ice formation (latent heat of fusion, $L_f = 333.5$ kJ/kg)

$$q_i = L_f m_w = 333.5 \times 30 = 10\,005 \text{ kW}$$

Total heat transferred to air

$$q_a = q_w + q_i = 879 + 10\,005 = 10\,884 \text{ kW}$$

(This illustrates the dominant effect of the latent heat of ice formation.)

However, this is also equal to $m_a C_p \Delta t_{air}$

$$\text{giving } m_a = \frac{10\,884 \times 1000}{1005 \times 20} = 541 \text{ kg/s}$$

If the air density were 1.3 kg/m³, this would give an air volume flowrate of 541/1.3 = 417 m³/s.

18.4.6. Geothermal and cycled storage heat

Another low cost method of controlling the temperature and humidity of intake air is to course it through one or more sets of old workings or fragmented strata before admitting it to current work areas. This takes advantage of a combination of natural geothermal energy and the "thermal flywheel" effect of heat storage within the envelope of rock surrounding a mine opening (Section 15.2.2).

The flow of geothermal heat into a mine airway is greatest at the moment of excavation and reduces with time until near equilibrium is attained when temperatures in the surrounding envelope of rock no longer change significantly with respect to time (Figure 15.3). If, however, the inlet air is cycled between hot and cold, then the surrounding rock will act as a storage heater, absorbing heat during the hot periods and emitting it during the cold periods. This cyclic behaviour is superimposed upon the longer term flux of geothermal heat.

Let us assume a situation in which the virgin rock temperature (VRT) at a given level is higher than the mean annual dry bulb temperature of air entering that level from the downcast shaft or slope. In order to moderate the extremes of winter temperature, the air is passed through a set of old workings that we may refer to as the **control district**. Figure 18.28 illustrates the seasonal variation of air temperature at inlet and exit of a control district, and ignoring the shorter-term diurnal changes. The moderating effect of the control district is shown clearly. The inlet peaks and troughs of summer and winter temperatures are damped very considerably by the time the air reaches the exit.

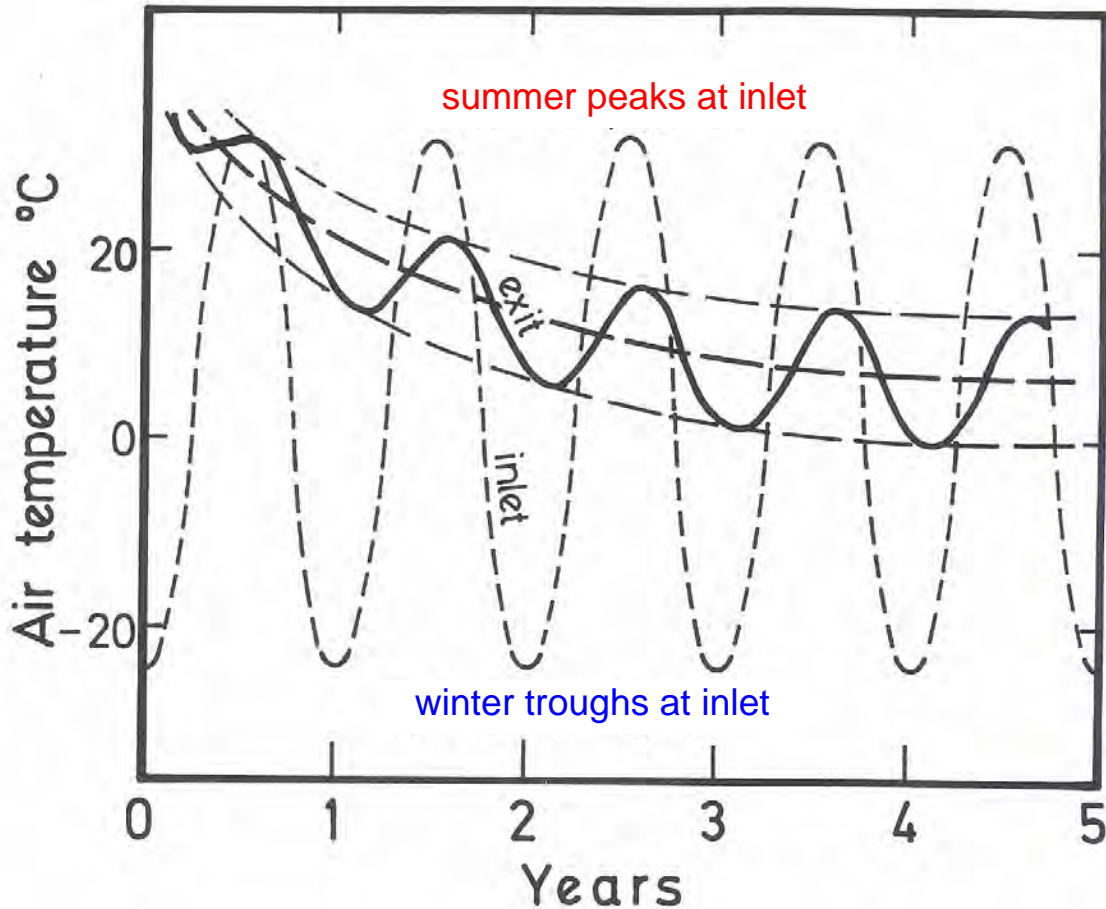


Figure 18.28 Example of the variation in air temperature at the inlet and exit of a climate control district

However, the figure also shows a longer term trend over which the average exit temperature falls until a repeated cyclic variation is attained. If the winter temperatures of the air leaving the control district are acceptable in this condition of dynamic equilibrium, then that district can be used indefinitely to moderate the extremes of seasonal variations. If, however, after a few years the winter exit temperatures fall below tolerable levels, then the intake air should be diverted through a younger control district.

Control districts that are no longer effective may be allowed to regenerate by sealing them off. The surrounding rock temperature will gradually tend towards the VRT. After a regeneration period which may be several years, the panel can again be opened up as a control district. If several old districts are available, then some of them may be used as control districts at any one time while others are regenerating (Moore, 1985).

The actual form of Figure 18.28 for any given mine depends upon the extremes of surface climate, the rate of airflow through the control district and the thermal properties of the surrounding strata. Simulation programs (Chapter 16) are most helpful in predicting the cyclic behaviour of the air temperatures (Moore, 1985; MVS, 1990). Manual methods of estimating the effects of varying inlet temperatures on strata heat flow have also been developed (Hemp, 1982) .

Although the use of a control district can yield a useful degree of air conditioning, it does have some disadvantages and limitations. First, the passage of air through old workings requires additional fan energy. This can be minimized by arranging for the air to move fairly slowly along multiple flow paths, requiring only a small applied pressure differential. Simulation tests coupled with site-specific measurements allow the optimum layout to be determined.

Secondly, old workings are liable to changes in resistance due to strata closure and falls of roof. Hence, in order to ensure continuity of ventilation, control districts should be capable of being bypassed at short notice. Neither should they be relied upon as emergency escapeways.

Thirdly, the conditioning of intake airflow through old workings is untenable where there is a danger of spontaneous combustion or significant emissions of strata gases.

In addition to moderating temperatures, control districts can also serve a useful purpose where variations in intake humidity cause roof control problems. This can occur in deposits of salt or some shales. The hygroscopic nature of these rocks results in absorption of water vapour and a loss of mechanical strength (Robinson et al, 1981).

Where caving techniques in a metal mine have left a fragmented and permeable rock mass that extends to the surface, then winter air may be heated and summer air cooled by drawing intake ventilation through the broken rock. This technique can combine the phenomena of storage heating and the latent heat of ice formation. One of the best known examples of this essentially free form of air conditioning is at the Creighton Mine in the Sudbury Basin of Canada (Stachulak, 1989). Intake air is drawn through a bed of broken rock that is approximately 244 m by 183 m in plan and 137 m high. Precipitation and seepage results in ice formation during the winter and melting in the summer. The air progresses through old drawpoints, slusher drifts and ore passes where it is regulated according to its temperature. This technique results in intake air of near constant temperature reaching the deeper current workings throughout the year.

References

Anderson, J. and Longson, I. (1986). The optimization of ventilation and refrigeration in British coal mines. *The Mining Engineer*. Vol. 146, pp 115-120.

Arkle, K. et al (1985). Use of thermal insulation materials in mines. *Jnl. Mine Ventilation Soc. of S. Africa*. Vol. 38, No.4, April, pp 43-45.

ASHRAE (1988). Handbook on Equipment. Ch. 20. Cooling towers. American Society of Heating, Refrigerating and Air Conditioning Engineers.

Baker-Duly, C. et al (1988). Design of a large flexible underground refrigeration installation. 4th Int. Mine Ventilation Congress, Brisbane, Australia, pp 443-449.

Bluhm, S.J. (1980). Predicting performance of spray chambers for cooling air. *Heating, Refrigeration and Air Conditioning*, S. Africa, pp 27-39.

Bluhm, S.J. (1981). Performance of direct contact heat exchangers. *Jnl. Mine Ventilation Society of S. Africa*. Vol. 34, Aug. and Sept., Nos. 8 and 9.

Bluhm, S.J. (1983). Spot cooling of air in direct contact heat exchangers. Report of Environmental Engineering Lab. Chamber of Mines Research organization, South Africa.

Burrows, J. (1982). Refrigeration - theory and operation. Environmental engineering in S. African mines. Chapter 23. Published by Cape and Transvaal Printers (Pty), Cape Town.

deRuiter, H. et al (1989). Geothermal heat recovery at Lac Minerals Ltd., Macassa Division. 91st CIMM Annual General Meeting. May, Quebec, Canada.

Gebler, W.F. et al (1988). The design and evaluation of a large direct-contact ice-air cooler for Vaal Reefs Gold Mine. 4th Int. Mine Ventilation Congress, Brisbane, Australia, pp 425-432.

Hall A.E. (1985). The use of controlled recirculation ventilation to conserve energy. 2nd U.S. Mine Ventilation Symposium, Reno, Nevada, pp. 207-215.

Hall, A.E. et al (1988). The use of controlled recirculation to reduce heating costs in Canada. 4th Int. Mine Ventilation Congress, Brisbane, Australia, pp 301-307.

Hall, A.E. et al (1989). Controlled recirculation investigation at Central Canada Potash Division of Noranda Minerals, Inc. 4th U.S. Mine Ventilation Symposium, Berkeley, CA, pp 226-233.

Hancock, W. (1926). Local air-conditioning underground by means of refrigeration. Trans. Inst. Mining Engrs., Vol. 72, pp 342-366.

Heller, K. et al (1982). Development of a high performance, low maintenance, in-line water spray cooler for mines. 1st US Mine Ventilation Symposium, Tuscaloosa, AL.

Hemp, R. (1967). The performance of a spray-filled counterflow cooling tower, Jnl. Mine Ventilation Soc. of S. Africa, Vol. 25, pp 159-173.

Hemp, R. (1972). Contribution to the design of underground cooling towers by **A. Whillier**. Jnl. Mine Ventilation Society of S. Africa, Vol. 25, No.6, June, pp 85-93.

Hemp, R. (1982). Environmental engineering in South African mines, Chapter 22. Sources of heat in mines, pp 569-612. Published by Cape and Transvaal Printers (Pty), Cape Town.

Hemp, R. (1988). A 29 MW ice system for mine cooling. 4th Int. Mine Ventilation Congress, Brisbane, Australia, pp 415-423.

McAdams, W.H. (1954). Heat transmission. McGraw-Hill, New York, 3rd. ed.

Moore, D.T. (1985). Geothermal air heating in a southwestern Wyoming trona mine. 2nd U.S. Mine Ventilation Symposium, Reno, Nevada, pp 561-570.

Mücke, G. and Uhlig, H. (1984). Performance of finned coil and water spray coolers. 3rd Int. Mine Ventilation Congress, Harrogate, England, pp 231-237.

MVS (1990). Investigation of geothermal air heating for General Chemical's Green River soda ash operations. Mine Ventilation Services, Inc. Report to General Chemical Corp., May, pp 1-33.

Ramsden, R. and Bluhm, S.J. (1984). Air cooling equipment used in South African gold mines. 3rd Int. Mine Ventilation Congress, Harrogate, England, pp 243-251.

Ramsden, R. and Bluhm, S. (1985). Energy recovery turbines for use with underground air coolers. 2nd U.S. Mine Ventilation Symposium, Reno, Nevada, pp 571-580.

Ramsden, R. (1985). Insulation used on chilled water pipes in South African gold mines. Jnl. Mine Ventilation Soc. of S. Africa, Vol. 38, No.5, May, pp 49-54.

Reuther, E.U. et al (1988). Optimization of spray coolers for cooling deep coal mines. 4th Int. Mine Ventilation Congress, Brisbane, pp 451-458.

Robinson, G., Weller, R.C and McPherson, M.J. (1981). Underground environmental planning at Boulby Mine, Cleveland Potash Ltd. Trans. Inst. of Mining and Metallurgy (U.K.), July. Reprinted in the Jnl. of S. African Mine Ventilation Soc., Vol. 35, No.9, Sept. 1982, pp 73-88.

Rose, H. (1989). Personality Profile. Jnl. Mine Ventilation Soc. of S. Africa, Vol. 42, No.6, June, pp 110-113.

Sheer, T.J. et al (1984). Research into the use of ice for cooling deep mines. 3rd Int. Mine Ventilation Congress, Harrogate, U.K., pp 277-282.

Shone, R.D.C. and Sheer, T.J. (1988). An overview of research into the use of ice for cooling deep mines. 4th Int. Mine Ventilation Congress, Brisbane, Australia, pp 407-413.

Stachulak, J. (1989). Ventilation Strategy and Unique Air Conditioning at Inco Limited. 4th U.S. Mine Ventilation Symposium, Berkeley, CA, pp 3-9.

Stroh, R.M. (1980). Refrigeration practice on Anglo American gold mines. Mine Ventilation Soc. of S. Africa Symposium on Refrigeration and Air Conditioning. Published by Cape and Transvaal Printers (Pty), Cape Town.

Stroh, R.M. (1982). Refrigeration practice, Chapter 24, and Chilled water reticulation, Chapter 25. Environmental engineering in S. African mines. Published by Cape and Transvaal Printers (Pty), Cape Town.

Thimons, E.D. et al (1980). Water spray vent. tube cooler for hot stopes. US Bureau of Mines Tech. Progress Report TPR 107.

Van der Walt, J. (1984). Cooling the world's coldest mine. Jnl. S. African Mine Ventilation Society. Vol. 37, No. 12, Dec., pp 138-141.

Van Vuuren, S.P.J. (1975). The optimization of pipe sizes in a refrigeration system. Jnl. Mine Ventilation Soc. of S. Africa, Vol. 28, No. 6, pp. 86-90.

Weuthen, P. (1975). Air coolers in mines with moist and warm climatic conditions. 1st Int. Mine Ventilation Congress, Johannesburg, S. Africa, pp 299-303.

Whillier, A. (1967). Pump efficiency determination from temperature measurements. South African Mechanical Engineer, Oct., pp 153-160.

Whillier, A. (1977). Predicting the performance of forced draught cooling towers. Jnl. Mine Ventilation Soc. of S. Africa, Vol. 30, No. 1, Jan., pp 2-25.

Whillier, A. (1982). Heat transfer: Environmental engineering in S. African mines, Chapter 19. Published by Cape and Transvaal Printers (Pty), Cape Town.

Part 5

Dust

CHAPTER 19. THE HAZARDOUS NATURE OF DUSTS

19.1. INTRODUCTION	1
19.2. CLASSIFICATIONS OF DUST	2
19.2.1. Size of aerosol particles.....	2
19.2.2. Physiological effects of dusts.....	3
19.3. DUST IN THE HUMAN BODY	4
19.3.1. The respiratory system	4
19.3.2. Mechanisms of dust deposition in the respiratory system	6
19.3.2.1. Impaction.....	6
19.3.2.2. Sedimentation	6
19.3.2.3. Diffusion	6
19.3.2.4. Interception.....	6
19.3.2.5. Electrostatic precipitation	7
19.3.3. Dust diseases	7
19.3.3.1. Fibrogenic effects	7
19.3.3.2. Coal workers' pneumoconiosis (black lung).....	7
19.3.3.3. Silicosis	7
19.3.3.4. Asbestosis	8
19.3.3.5. Precautions against dust diseases.....	8
19.3.4. Threshold limit values	9
19.4. THE ASSESSMENT OF AIRBORNE DUST CONCENTRATIONS	10
19.4.1. Background.....	10
19.4.2. Particle count methods	11
19.4.3. Gravimetric methods.....	12
19.4.4. Photometric (light-scattering) methods	13
19.4.5. Personal samplers	15
19.4.6. Other methods of airborne dust measurement.....	16
19.4.7. Discrimination of quartz particles.....	16
19.4.8. Sampling strategy	16
References	18

19.1. INTRODUCTION

The natural atmosphere that we breathe contains not only gaseous constituents but also large numbers of liquid and solid particles. These are known by the generic name **aerosols**. They arise from a combination of natural and industrial sources including condensation, smokes, volcanic activity, soils and sands, and microflora. Most of the particles are small enough to be invisible to the naked eye. *Dust* is the term we use in reference to the solid particles. The physiologies of air-breathing creatures have evolved to be able to deal efficiently with most of the aerosols that occur naturally. However, within closed industrial environments, concentrations of airborne particulates may reach levels that exceed the ability of the human respiratory system to expel them in a timely manner. In particular, mineral dusts are formed whenever rock is broken by impact, abrasion, crushing, cutting, grinding or explosives. The fragments that are formed are usually irregular in shape. The large total surface area of dust particles may render them more active physically, chemically and biologically than the parent material. This has an important bearing on the ability of certain dusts to produce lung diseases.

Respiratory problems caused by dust are among the oldest of industrial ailments. The first legislation for mine dust appears to have been formulated in 1912 when the Union of South Africa

introduced laws governing working conditions in the gold mines of the Witwatersrand. Other countries introduced similar legislation in the 1920's and '30's. However, those laws were concerned primarily with silicosis and required proof of employment in siliceous rock mining (Carver, 1975). The early legislation reflected medical opinion of the time, namely, that hardrock dust caused silicosis which led to tuberculosis and eventual death. At that time coal dust was not regarded as particularly harmful. However, the number of recognized cases of coal workers' pneumoconiosis (CWP) increased dramatically through the 1930's. The British Medical Research Council initiated an investigation into respirable disease within the anthracite workers of South Wales. In 1936, the need for protective legislation in the United States was acknowledged by a National Silicosis Conference. Both in Europe and the United States the hazards of coal dust were identified first in anthracite mines but by 1950 it was confirmed that workers in bituminous coal mines were also subject to coal workers' pneumoconiosis (known, also, in America as *black lung*).

It took many years for a quantitative and definitive link to be established between the "dustiness" of mine atmospheres and respiratory disfunction. In retrospect, there were three reasons for this. First, it may take several years of exposure before the victim becomes aware of breathing impairment. Secondly, the lung reactions to dust are often similar to those of naturally occurring ailments and, thirdly, the commonly used measure of dust concentration was the number of particles in a unit volume of air. Correlations between dust concentration measured in this way and the incidence of pneumoconiosis were not clear.

A turning point occurred in 1959 at the *International Pneumoconiosis Conference* held in Johannesburg, South Africa (Orenstein, 1959). Recommendations were made at that conference which resulted in a re-direction of pneumoconiosis studies, particularly with regard to the methods and strategies of dust sampling. It was recognized that those particles of equivalent diameter less than 5×10^{-6} m (5 microns) were the ones most likely to be retained within the lungs. These were named *respirable dust*. It was further established that the *mass concentration* of respirable dust in any given atmosphere was a much better measure of the potential health hazard than the earlier particle count methods. Instruments began to be developed that mimicked the dust retention selectivity of the human lung and, furthermore, could be used continuously to give the integrated effect over an 8 hour period.

In this chapter we shall concentrate on the effects of mineralogical dusts on the human respiratory system and the techniques that are now employed for the sampling and measurement of airborne dust.

19.2. CLASSIFICATIONS OF DUST

There are a number of ways to classify aerosol particles depending upon the purpose of any given study. Two such classifications are particularly relevant to the subsurface environmental engineer, first with regard to size distributions of the particulates and, secondly, in terms of physiological effects.

19.2.1. Size of aerosol particles

Mine dusts vary widely in shape, dependent largely upon the prevalent mineral constituents. The simplest method of quantifying the size of a non-spherical particle is the *projected area* or *equivalent geometric diameter*. This is the diameter of a sphere that has the same projected area as the actual particle. Other measures of equivalent diameter are defined in Chapter 20.

Typical size ranges of some common aerosols are given in Table 19.1. In general, the size distribution within each range follows a lognormal curve. Particles do not become visible to the naked eye until they are more than 10 microns equivalent diameter. It follows that the harmful

respirable dusts are invisible. Nevertheless, it must be assumed that heavy visible concentrations of dust in a mine atmosphere are accompanied by high levels of respirable dust (Section 20.3.1.). Another unfortunate aspect of the small sizes of respirable dusts is that they have a very low settling velocity and, indeed, can remain suspended in air indefinitely.

Type of aerosol	Size range in microns (10^{-6} m)	
	Lower	Upper
Respirable dust	-	7
Coal and other rock dusts	0.1	100
Normal atmospheric dusts	0.001	20
Diesel particulates	0.05	1
Viruses	0.003	0.05
Bacteria	0.15	30
Tobacco smoke	0.01	1
Pollens causing allergies	18	60
Fog	5	50
Mist	50	100
Light drizzle	100	400

Table 19.1. Size ranges of common aerosols.

19.2.2. Physiological effects of dusts

A classification of dusts with respect to potential hazard to the health and safety of industrial workers may be divided into five categories.

1. **Toxic dusts.** These can cause chemical reactions within the respiratory system or allow toxic compounds to be absorbed into the bloodstream through the alveolar walls. They are poisonous to body tissue or to specific organs. Some metalliferous ores fall into this category. The most hazardous include compounds of arsenic, lead, uranium and other radioactive minerals, mercury, cadmium, selenium, manganese, tungsten, silver and nickel (Walli, 1982).

2. **Carcinogenic (cancer causing) dusts.** The cell mutations that can be caused by alpha, beta and gamma radiation from decay of the uranium series make radon daughters the most hazardous of the carcinogenic particulates (Chapter 13). A combination of abrasion of lung tissue and surface chemical action can result in tumour formation from asbestos fibres and, to a lesser extent, freshly produced quartz particles. Exposure to arsenic dust can also cause cancers. Diesel exhaust particulates are a causative factor in lung and other types of cancer.

3. **Fibrogenic dusts** The scouring action of many dusts causes microscopic scarring of lung tissue. If continued over long periods this can produce a fibrous growth of tissue resulting in loss of lung elasticity and a greatly reduced area for gas exchange. The silica (quartz, chert) and some silicate (asbestos, mica, talc) dusts are the most hazardous of the fibrogenic dusts and may also produce toxic and carcinogenic reactions. Welding fumes and some metalliferous ores produce fibrogenic dusts. Long and excessive exposure to coal dusts also gives rise to fibrogenic effects.

4. **Explosive dusts.** These are a concern of safety rather than health. Many organic materials, including coals other than anthracite, become explosive when finely divided at high concentrations in air. Sulphide ores and many metallic dusts are also explosive. Hazards associated with the explosive nature of some dusts are discussed more fully in Chapter 21.

5. **Nuisance dusts.** Quite apart from adverse effects on the health of personnel, all dusts can be irritating to the eyes (Gibson and Vincent, 1980), nose and throat and when in sufficiently high concentration may cause reduced visibility. Some dusts have no well-defined effects on health but remain in the category of a nuisance dust. These include the evaporites (halite, potash, gypsum) and limestones. The soluble salts of halite (NaCl) and potash (KCl) can occasionally cause skin irritations, particularly around hatbands or tightly fitting dust masks.

19.3. DUST IN THE HUMAN BODY

The lungs are the organs where the oxygen necessary for metabolic activity is introduced into the body. Through repetitive inhalations and exhalations air is brought into very close proximity to flows of blood, the two being separated by a very thin membrane of about 0.5 microns in thickness. Oxygen diffuses across the membrane from the air to the blood while carbon dioxide diffuses in the other direction. The exchange is maintained by a difference in concentration across the membrane for each of the two gases.

The respiratory system is equipped with defence mechanisms against gaseous or aerosol pollutants that may exist in the inspired air. However, these mechanisms can be defeated by toxic or carcinogenic agents. Furthermore, after years of exposure to unnaturally high concentrations of dust, the defence system can simply become overloaded allowing the lungs to become much less efficient as gas exchangers and, also, more susceptible to bronchial infections and pulmonary illnesses.

In this Section, we shall outline the structure and normal operation of the human respiratory system, the mechanisms of dust deposition within that system, and the processes that lead towards those ailments known collectively as dust diseases.

19.3.1. The respiratory system

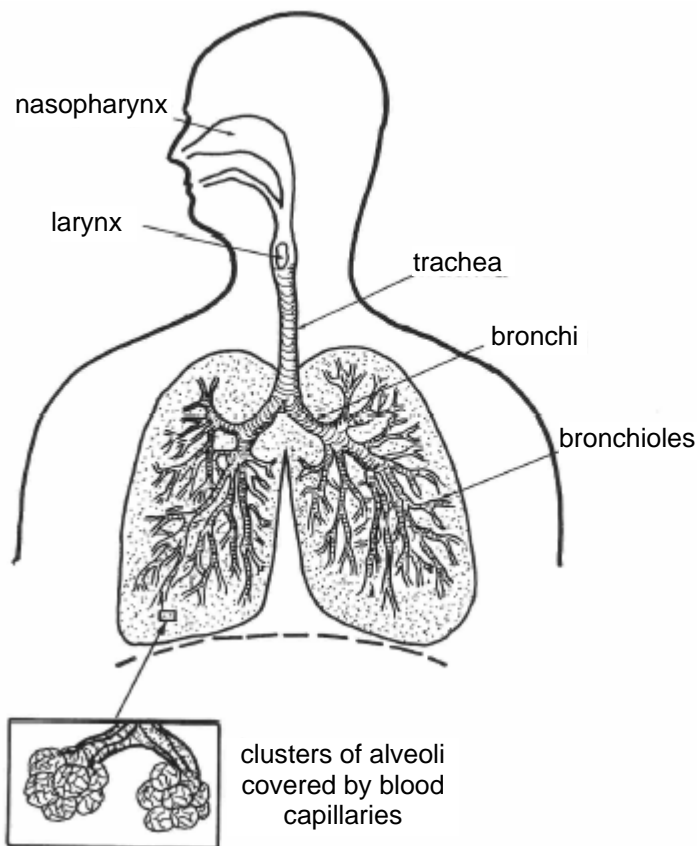


Figure 19.1 Diagrammatic representation of the human respiratory system.

Figure 19.1 is a simplified illustration of the human respiratory system. Air enters through the nostrils where it passes through a mat filter of hairs in order to enter the *nasopharynx*. This filter is the first line of defence and removes the larger dust particles. Those remain trapped until they are blown out or pass back through the *nasopharynx* to be swallowed. Within the larger volume of the *nasopharynx*, the air velocity is reduced. In this zone and, indeed, throughout all of the branched air passages leading to the alveoli, the walls are lined with ciliated and mucous-secreting cells. The hairlike *cilia* wave to and fro with a directional bias that promotes movement of the mucous towards the throat where it can be swallowed. Most dust particles greater than 10 microns in size are captured by the hair filter or mucous before inhaled air reaches the larynx. Air that is breathed through the mouth bypasses the protection offered by the nostrils and *nasopharynx*.

The air then progresses through the *trachea*, a tube some 20 mm in diameter, 120 mm long and comprised of a series of tough cartilage rings. This divides into the left and right *bronchi* averaging about 12 mm in diameter and 48 mm long. There are, of course, considerable variations in these dimensions between individuals. The air passages continue to subdivide repeatedly into the *bronchioles* in a manner that is analogous to the roots of a tree. After sixteen subdivisions the bronchiole diameter is about 0.6 mm. The total number of branched passages in human lungs may be over 80 million.

Although the diameter of individual air passages decreases with branching, their greatly increased number produces a significant rise in total cross sectional area available for flow. Hence, the air velocity decreases to the extent that airflow is completely laminar in the smaller bronchioles. All of these passages are coated with mucous which is continuously expelled upwards towards the trachea by the motions of cilia. The mucous secretions and any captured particulates are usually expelled by coughing or swallowing within one day. Mucous coatings within the air passages are normally quite thin. However, bronchial ailments can cause an increase in both the viscosity and thickness of mucous layers to the extent that they can restrict air movement significantly. The higher air velocities through constricted passages can lead to audible noise (wheezing).

The smallest bronchioles terminate in clusters of air sacs or *alveoli* some 0.2 to 0.6 mm in size. The walls of the alveoli provide the 0.5 micron thick membrane, or *epithelium*, across which gas exchange occurs. There are an estimated three to four hundred million alveoli in the average human lungs with a total area of some 75 m² available for gas exchange in a healthy adult. Involuntary muscular movements of the diaphragm and ribcage induce rhythmic changes of pressure differential between the alveoli and the external atmosphere giving rise to normal cycles of inhalation and exhalation. Breathing rates vary from 12 to 40 inhalations per minute depending upon the level of activity. Table 11.2 indicates corresponding gas exchange rates for oxygen and carbon dioxide.

Few dust particles of sizes greater than 3 microns reach the alveoli. Numerous models have been proposed to indicate the relationship between particle size and sites of deposition (e.g. Walli, 1982; Schröder, 1982; National Research Council, 1980). For very small captured particles, clearance from the alveoli may be slow or non-existent. Particles of 0.2 micron diameter have a 25 percent probability of retention while, for 0.02 micron particles, the retention rate rises to about 55 percent.

Mucous producing cells within the alveoli lubricate the surfaces and facilitate their freedom to dilate and contract. Removal of dust particles from the alveoli is undertaken by relatively large (10 to 50 micron) cells known as *macrophages* or *phagocytes*. These nomadic cells originate in some white blood cells, are free to move over the alveolar walls and are capable of engulfing particles up to 10 microns in diameter. A commonly accepted view is that the macrophages and any encapsulated dust particles migrate out of an alveolar cluster into the bronchioles where they can be expelled by ciliary motion. Another theory is that macrophages are transported from the alveoli through fluid filled capillaries that lead to lymphoids at bronchiole junctions (Brundelet, 1965).

The average life expectancy of a macrophage is about one month. However, these scavenger cells may die rapidly if they engulf toxic particles. The number of macrophages increases when the lungs are subjected to increased entry of dust particles. However, there remains considerable doubt about the relationship between respirable dust concentration and macrophage production. It appears to depend upon the mineralogical composition of the particles. Furthermore, dust loaded cells are cleared less rapidly than the normal turnover of dust-free cells (National Research Council, 1980).

Soluble particles dissolve in mucous. The resulting ions are either removed in the mucous or diffuse through the epithelium for elimination through the bloodstream.

19.3.2. Mechanisms of dust deposition in the respiratory system

Deposition of dust particles within the zones of the respiratory system varies with the size and aerodynamic characteristics of the particles, the geometry of the air passages and the patterns of airflow. The three most important mechanisms of deposition are impaction, sedimentation and diffusion, while interception and electrostatic precipitation can become significant for particular types of dust. These five modes of deposition are discussed in the following subsections.

19.3.2.1. Impaction

The density and, therefore, the momentum of dust particles are greater than that of a comparable volume of air. At each bend of the tortuous paths followed by air as it pulses in and out of the lungs, dust particles will tend to follow a straight line and impact into the mucous coated walls of the air passages.

The effectiveness of deposition by impaction increases with the acuteness of the bend and the velocity of the air. There appears to be considerable anatomical variation between individuals in the tortuosity of the branching bronchioles. Velocities are greater in the upper air passages. However, the latter also have a larger diameter and particles must travel further across the streamlines before impact occurs. During exertion, breathing rates and, hence, air velocities increase throughout the system. The subject takes air deeper into the lungs and, furthermore, the resistance of the nostrils and hair filter will promote breathing through the mouth. For all of these reasons, heavy physical labour will increase deposition by impaction in the respiratory system.

Constriction of air passages by thickening of the mucous layer, bronchial infections or lung damage will also result in higher air velocities and, hence, increased deposition by impaction.

19.3.2.2. Sedimentation

This term refers to the gravitational settlement of particles and is effective at low air velocities for dust particles greater than 0.5 microns. Smaller particles become subject to Brownian motion and diffusion effects. Sedimentation assists in the deposition of larger particles in the nasopharynx during the reversal points of the breathing cycle. More importantly, however, sedimentation is an effective mechanism of deposition in the low velocity laminar flows within the finer bronchioles and the alveoli.

Another factor is that the full capacity of the lungs is seldom used. During normal quiescent breathing the *tidal volume* may utilize some 65 to 75 percent of lung capacity. Sedimentation of dust particles will occur in the near stagnant air of the unused dead-space. A phase of heavy breathing followed by a quiescent period will first draw dust particles into the deeper recesses of the lung and then encourage deposition by sedimentation in the dead-space as breathing becomes more shallow.

19.3.2.3. Diffusion

Submicron particles are subject to random displacement by bombardment from gas molecules (Brownian motion). The effect increases as the size of the particles decreases and becomes significant for particle diameters of less than 0.5 microns. Although Brownian motion occurs throughout the respiratory system, it becomes an effective mode of dust deposition only when the mean displacement becomes comparable with the size of the air passage. Hence, it is particularly important in the alveoli and finer bronchioles.

19.3.2.4. Interception

Interception becomes significant for **fibrous particles**. A dust fibre is often defined as a particle where the length to diameter ratio exceeds 3. Such particles tend to align themselves with the direction of airflow and fibres 200 microns long can penetrate deeply into the lung. Nevertheless, the ends of fibres are likely to contact the walls of air passages, particularly at bends and bifurcations, and accumulations of fibres can occur at these locations. This is the mechanism of

interception. The effect is accentuated by curly fibres such as those of **chrysotile asbestos** while the straight fibres of **amphibole asbestos** have a greater probability of penetrating to the alveoli.

19.3.2.5. Electrostatic precipitation

Within the working areas of a mine, newly produced particles of mineral dust may carry a substantial electrostatic charge. The moving electromagnetic fields that surround such particles can induce charges of opposite sign on the walls of air passages in the respiratory system. This results in the electrostatic precipitation of particles on to the walls and capture by the film of mucous.

19.3.3. Dust diseases

Pneumoconiosis, now more usually shortened to pneumoconiosis, is a generic term for damage to cardio-respiratory organs caused by the inhalation of dust. More specific names have been given to illnesses caused by particular types of dust. Some of those are discussed in this Section and are often known as the dust diseases.

While the toxic and carcinogenic properties of some dusts cause specific physiological reactions (Section 19.2.2.), most dusts that occur in mines are not in themselves fatal. However, through progressive incapacitation of the lungs, they render the victim more susceptible to respiratory ailments such as colds or influenza as well as tuberculosis, chronic bronchitis and emphysema which may result in hastened death. Chronic bronchitis is an inflammation of the linings of the respiratory system and is accompanied by periodic or constant coughing. Emphysema involves the rupture of inter-alveolar walls caused by excessive pressure within the alveoli. This is often a result of constrictions in the bronchioles. The rupture frequently occurs during bouts of coughing. Adjacent alveoli break through into each other. This leads to progressive abnormal breathlessness, particularly on even light exertion. Respiratory difficulties may also cause excessive strain on the heart with resultant cardiac complications

19.3.3.1. Fibrogenic effects

The fibrogenic dusts introduced in Section 19.2.2. promote the abnormal development of fibrous tissue within the alveolar clusters. They may commence at discrete foci with fibrous tissue that may then radiate outwards to form fibroblasts. These, in turn, can merge into nodules and conglomerates. The permanent scarring and change in the alveolar structure can have severe secondary effects. Gas exchange across the alveolar walls is inhibited and the loss of natural elasticity can cause a significant reduction in tidal volume. Furthermore, the production of macrophages is reduced allowing uncontrolled accumulations of dust particles to occur in the alveoli. Large fibrous masses can also distort or damage blood vessels, causing functional impairment of the heart (National Academy of Sciences, 1976).

19.3.3.2. Coal workers' pneumoconiosis (black lung)

Many dusts, including coal, produce a low biological response. However, over sufficiently long periods of exposure a build-up of retained dust occurs in the form of soft plaques within the lung tissue. These can be observed as small black spots on chest x-rays. Similar early diagnoses can be made for other mineral dusts including ores of iron (siderosis), tin (stannosis) and aluminium (aluminosis). In the case of coal, such indication of coal workers' pneumoconiosis may not be revealed for some 10 to 15 years after initial employment in coal mines. Furthermore, the subjects may not be aware of any incapacitation during that time. In more advanced cases, the opacities grow in size and number until they coalesce. This is likely to be accompanied by fibrosis and all of the consequences described in the previous subsection.

19.3.3.3. Silicosis

This is one of the most dangerous of the dust diseases and is caused by particles of free crystalline silica (quartz, sandstones, flint) but not by the silicates in clays or fireclay. The hazard is greatest from freshly produced dust in operations involving mining or comminution of silica

bearing rocks, or from sandblasting. It is suspected that the more severe cases of coal workers' pneumoconiosis may be associated with quartz particles mixed with coal dust.

The early stages of the disease produce, again, local foci of dust accumulations that may be observed on x-ray films. However, there appears to be a level of silica accumulation above which progressive massive fibrosis occurs. A number of theories have been advanced to explain this behaviour (Schröder, 1982). It is probable that the initial accumulations cause simple microscopic abrasion from the hard cutting edges of the particles. The initiation of progressive fibrosis may be the result of a toxic reaction to silicic acid or electro-chemical surface energy on newly cut and charged particles. A further suggestion is that the breakdown of poisoned macrophages may invoke an auto-immune reaction that produces fibrous antibody structures.

19.3.3.4. Asbestosis

Asbestos is an inorganic mineral fibre comprised mainly of silicate chains. The two common forms of asbestos are **chrysotile** containing tough curly fibres, and **amphibole** with long, straight and brittle fibres. Asbestos fibres are captured in the respiratory system primarily by interception (Section 19.3.2.4.) and accumulations are most likely to occur at bends and bifurcations. However, the aerodynamic characteristics of fibres are determined by their diameter rather than length and long fibres may reach the alveoli.

Asbestosis is associated with fibrosis, but of a different type from that given by advanced cases of silicosis or coal workers' pneumoconiosis. The initial plaques are more brittle and contain sharp raised ridges that may become calcified. During further progression of the disease, fibrous bands radiate throughout the lungs and cause a significant loss of elasticity. This reduces the tidal volume and, together with the fibrotic loss of gas exchange area, leads to abnormal breathlessness. The reduction in oxygen transfer causes blood pressure in the pulmonary artery to rise putting the right ventricle of the heart under strain. Cardiac failure may follow.

Cancers of the bronchial system, lung tissue and abdominal organs have been linked with excessive exposure to asbestos fibres. However, it is considered that it is not the silicate chains themselves that cause these cancers but rather carcinogens that are adsorbed on the fibre surfaces prior to inhalation.

19.3.3.5. Precautions against dust diseases

The problems of dust diseases have probably attracted more research funding than any other environmental hazard in underground mining. Three distinct areas of research have been undertaken in countries with major mining industries, namely medical studies into the development, treatment and diagnosis of dust diseases, the techniques of sampling and measurement of airborne dust, and dust suppression and control in mines.

The primary precautions against dust diseases mirror those same three areas. Experience has shown that although highly skilled interpretation of x-ray films is required, this remains the most important tool in discovering the onset of a dust disease and in monitoring its progress. Personnel who are required to work in atmospheres that contain any of the toxic, carcinogenic or fibrogenic dusts should be given free access to chest x-ray examinations. An examination should be given before the commencement of employment in order to identify any existing condition. Further chest x-rays are recommended at intervals of not more than two years. Workers should be assured that early identification of coal workers' pneumoconiosis or silicosis does not necessarily imply physical impairment nor loss of employment but should be regarded as an indication that reassignment to work in less dusty conditions would be prudent. Legislation may guard against significant reductions in financial remuneration.

The second group of precautions concerns organized and routine procedures of dust sampling, preferably by means of instruments that measure mass concentration of respirable dust. This area is discussed further in Section 19.4. and is intended to test compliance with set threshold limit values. In most countries the latter are mandatory values enforced by law.

The most effective means of protecting mine personnel against dust diseases is control of the dust. This involves minimizing the production of dust, suppressing it at the source, removing airborne dust and separating workers from dusty areas. Great improvements have been made in these areas since the 1950's. The subject is handled in greater detail in Chapter 20.

19.3.4. Threshold limit values

National experience of mining systems, geological conditions, legislation, litigation, labour organizations, research and social consciousness in various countries has resulted in wider variations in recommended or mandated threshold limit values for dusts than for other airborne contaminants in mines. The threshold limit values given in Table 19.2 are based primarily on recommendations of the American Conference of Governmental Industrial Hygienists (ACGIH) and are *simply a guide* to airborne concentrations that are currently thought to produce no adverse effects from a daily working time exposure.

Aerosol	TLV (TWA) mg/m ³ unless otherwise stated*	Comments
Aluminium oxide	10	
Arsenic	0.01	carcinogen
Asbestos	0.1 fibres/ml	carcinogen, for fibres longer than 5 microns
Borates		
decahydrate	5	
others	1	
Calcium carbonate	10	marble, limestones
Calcium sulphate	10	gypsum
Carbon black	3.5	carcinogen
Coal	2 10/(% quartz) for >5% quartz)	respirable (<5% quartz)
Fibrous glass	10	
Fluorides	2.5	
Graphite (natural)	2	respirable fraction
Iron oxide fumes	5.0	(>1% quartz)
Kaolin	2	respirable, no asbestos, <1% silica
Magnesite (magnesium oxide)	10 (total), 5(respirable)	
Mica	3	respirable fraction
"Nuisance" dusts	10	non-hazardous materials
Oil mist		
mineral	5	excluding vapour
vegetable	10	
Perlite	10 (total), 3 (respirable)	
Portland cement	10(total), 5 (respirable)	
Radon daughters	4 WLM/year	see Section 13.3.3
Quartz	0.05	respirable fraction
Silicon Carbide	10	respirable, no asbestos, <1%silica
Soapstone	3	respirable fraction
Talc	2	respirable fraction
Welding fumes	5	

Table 19.2. *Guideline* threshold limit values for selected aerosols given in milligrams per cubic metre of air (based primarily on recommendations of the American Conference of Governmental Industrial Hygienists). Considerable variations occur in the laws of other countries.

See Section 11.2.1. for definitions of *Threshold Limit Value* and *Time Weighted Average*.

The comments made in Section 11.2.1. on threshold limit values for gases apply equally well here. In particular, subsurface ventilation engineers *must* become familiar with limiting concentrations mandated by their own national or state laws.

There is a further reservation that applies to the use of threshold limit values for dust concentrations. Despite the move from particle count to gravimetric methods of measurement, there remain considerable variations in the results given by differing instruments (e.g. Phillips, 1984). These arise from differences in the design of instruments, the particle size distribution curves they are intended to follow and the efficiency of dust capture. Even a single instrument can indicate a different result if the rate of sample airflow through the device is altered. For these reasons, individual countries or mining industries have tended to "adopt" a particular instrument as a standard and to employ empirical conversion factors in order to compare data obtained by other devices (Rogers, 1991). It follows that while such variations in instrument performance exist, the application of dust threshold limit values for purposes of legislation or enforcement should be referred to a particular instrument used according to a specified procedure.

Another factor should be borne in mind when comparing threshold limit values imposed by differing legislative authorities. Laws governing dust concentrations usually specify not only the limiting concentrations of respirable dust but also the sampling locations. Hence, a measurement required to be taken in a return airway should not be compared to one that is obtained at the position of a machine operator.

For coal mines, legislation may require reduced threshold limit values in certain areas. For example, the 2 mg/m³ TLV for respirable dust in American coal mines is reduced to 1 mg/m³ for intake airways within 61 m (200 ft) of a working face. Further restrictions are applied when quartz particles are present in the coal dust. One method is to reduce the TLV to 10 divided by the quartz percentage when the quartz content in the dust exceeds 5 percent. This is based on a quartz TLV of 0.1 mg/m³.

19.4. THE ASSESSMENT OF AIRBORNE DUST CONCENTRATIONS

19.4.1. Background

The accurate assessment of dust concentrations in relation to the health of personnel in mines is beset with difficulties. First, the fact that physiological consequences develop very slowly is compounded by dust concentrations varying across wide limits with respect to both time and place in a mine. Readings of dust concentrations measured over a short time interval have very little relevance to the long term health of the workforce. It was this difficulty that masked correlations between most particle count data and incidence of pneumoconiosis until the 1959 Johannesburg Conference. Secondly, as indicated in the previous Section, it is not only the concentration of particles that matters but also their size distribution and mineralogical composition. It is not surprising, therefore, that even modern instruments may vary quite significantly in the quality and type of data they produce.

In choosing dust instrumentation it is important to define the primary purpose of the intended measurements. These may be part of long term investigations with the aim of establishing environmental standards. Other research surveys may be aimed at the spatial and temporal variations of dust concentration to which specific groups of personnel are exposed, or to investigate the effects on airborne dust of particular mining equipment or dust suppression techniques. Routine measurements in a mine are made to protect the health of the workforce and to check or ensure compliance with mandatory standards.

The earliest attempts to measure airborne dust quantitatively are reported to have occurred in the eighteenth century using observations of dust deposition on a polished surface (Walli, 1982).

However, the major developments in this field have taken place since the introduction of the konimeter, a hand held jet-impact device invented by **Kotz**, a South African government mining engineer, in 1916. Modern versions of the konimeter remain in use in that country although its remaining life must be very limited.

Since the Johannesburg Conference of 1959, the vast majority of new instruments measure the mass concentration of respirable dust (<5 microns). Most of these instruments pass the dust in a continuous air sample through combinations of elutriators (settling chambers), cyclones, or jet-impactors and filters. Furthermore, in order to meet the need for longer term readings, most gravimetric instruments have been designed to operate over several hours. Such data are necessary from the viewpoint of health protection but mitigate against rapid readout, continuous monitoring and short term control. Alternative methods of dust assessment combined with modern electronic integrating circuitry allow short term and long term data collection to proceed simultaneously. Many such instruments have utilized the principle of light beam scattering by dust particles (the Tyndall effect).

A recognition of the differing objectives of health protection and more immediate concerns such as dust explosibility, visibility and nuisance effects have led to two distinct applications of dust monitors. First, lightweight personal samplers are increasingly being worn by underground workers. These give a record of the respirable dust concentrations to which the person has been exposed, on a shift by shift basis. Secondly, heavier and more sophisticated instruments may be set up to measure dust concentrations either for several hours or, on a more permanent basis, to allow continuous monitoring for local indication and recording or transmission to a central control station.

Modern trends in dust instrumentation are toward:

- an increase in the use of personal samplers,
- cascade devices or other means of selection to indicate mass concentrations in each of a number of particle size ranges,
- an immediate indication of mineral content (particularly quartz) in addition to mass concentration and
- an increase in light scattering methods for continuous monitoring.

In the following subsections, we shall introduce the main principles employed in instruments for the assessment of airborne dust. However, because of the rapid evolution and number of new devices, we shall not attempt detailed descriptions of individual monitors. For these, the reader is referred to trade journals and manufacturers' literature.

19.4.2. Particle count methods

Although particle count methods were used for many years and models were produced in a number of countries, they are now nearing obsolescence for use in mines. There were essentially two families of particle count instruments. One of these relied on the impact principle in which a short-lived but high velocity pulse of air was induced through a jet and directed at a receiving surface of treated glass, film or liquid. The most enduring of this type of instrument is the konimeter (Section 19.4.1.).

The second type of particle count instruments was the thermal precipitator. Molecular bombardment from a heated wire diverted dust particles from a moving sample stream on to an adjacent glass slide (Section 20.2.4.). The slides, films or liquids produced by particle count instruments were subjected to microscope analysis for counting the number of particles in each size range. For many years this was carried out manually and was somewhat subject to individual bias. Latterly, it has been conducted by "light assessors" that really measure surface area (Martinson, 1982). Computer controlled particle analyzers are now available that can perform such a task much more rapidly and efficiently.

19.4.3. Gravimetric methods

Figure 19.2 illustrates the operation of one of the earlier and very successful gravimetric samplers, the MRE, developed at the Mining Research Establishment of the then National Coal Board in the United Kingdom (Dunmore et al, 1964). This instrument continues to be a standard in several countries. Air passes through the instrument at a rate of 2.5 litres/min under the action of a diaphragm pump. The air velocity between the parallel plates of the elutriator drops to the extent that particles larger than 7 microns settle out. The remaining finer particles pass on to be collected on a 5 micron membrane filter. The filter is weighed before and after a sampling period which may, typically, be eight hours.

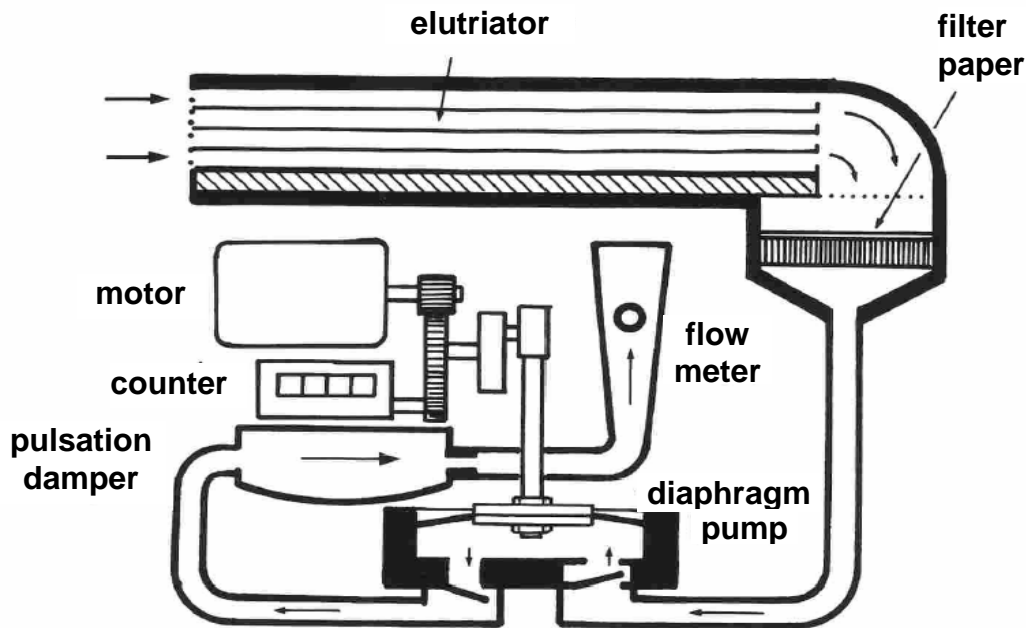


Figure 19.2 Schematic of an MRE Gravimetric Dust Sampler

The specifications of the elutriator are such that it gives a particle removal characteristic which resembles the BMRC curve on Figure 19.3. This curve was defined by the British Medical Research Council as representing the penetration rates of respirable dust to the alveoli of the human lungs. An alternative model adopted by the American Conference of Governmental Industrial Hygienists is illustrated for comparison on the same figure. The MRE instrument achieved the rare distinction of being specified, by name, as a standard in American mine legislation.

Many other gravimetric samplers have been produced since the 1960's. Some have replaced the elutriator with a nylon or metal cyclone as illustrated on Figure 19.4. The small dimensions and light weight of these cyclones make them particularly suitable for personal samplers.

Other types and sizes of filters are also employed. While the filter should be efficient in trapping respirable dust, it should not restrict the airflow to the extent that it inhibits the required constant airflow throughout the sampling period. Silver metal filters have been shown to be useful if the sample is subsequently to be heated in order to determine combustible content or if x-ray

diffraction is used to measure the amount of quartz present (Knight and Cochrane, 1975). The maximum period of sampling through any given filter is reduced because of premature blockage in the presence of diesel fumes or mists of water or oil (Gardiner, 1988).

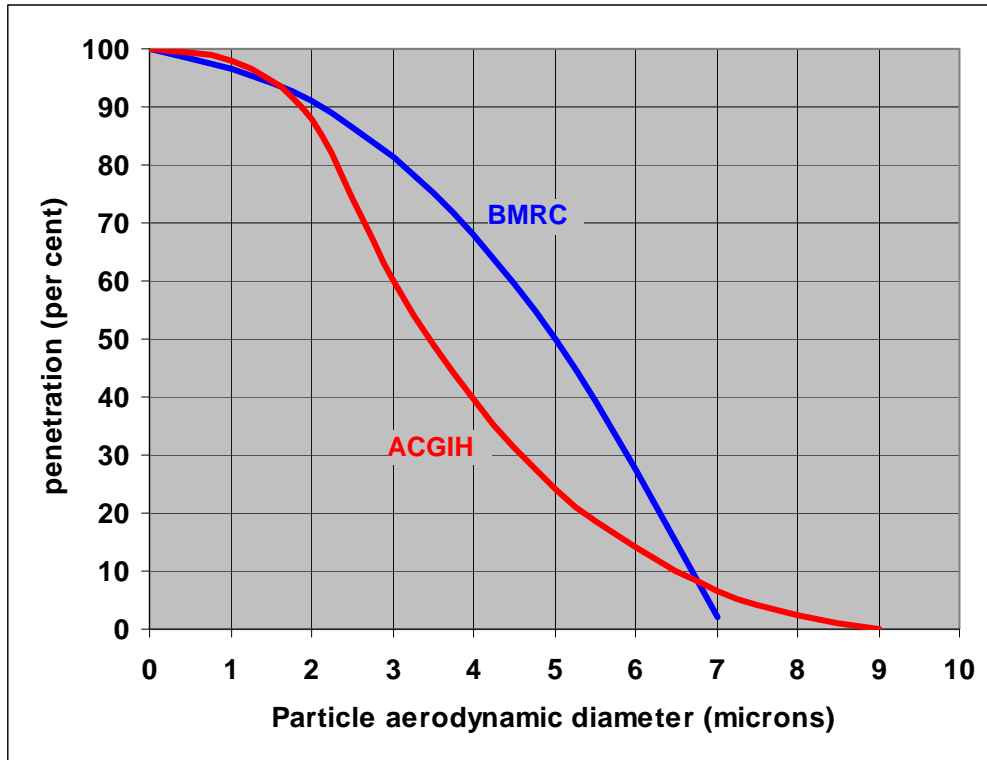


Figure 19.3 Lung penetration curves for respirable dust as defined by the British Medical Research Council (BMRC) and the American Conference of Governmental Industrial Hygienists (ACGIH).

19.4.4. Photometric (light-scattering) methods

It was the English physicist **John Tyndall** (1820-'93) who first explained the scattering of sunlight by dust particles in the atmosphere. The blue component of white light is scattered most which explains why the sky appears blue. The same effect is utilized in the photometric methods of measuring dust concentration. The corresponding instrumental techniques have been developed, particularly in Germany, although devices using the same principle are now also produced in the United Kingdom and the United States of America.

The early Tyndalloscope split the beam from a white light source. Half proceeded through polarizing filters to the eye-piece. The other half was diverted through a sample chamber where light reflected by the dust particles was collected and directed to the eyepiece. The filters were rotated until the two half beams that were visible simultaneously in the eyepiece appeared to have the same intensity. The angle of filter rotation was employed as an indication of the dust concentration. Modern Tyndallometers use **photosensors** to detect the deflected light and produce an electrical output for visual display, recording or transmission. Preferred angles of forward light scatter can be chosen to minimize the effects of particle shape or index of refraction.

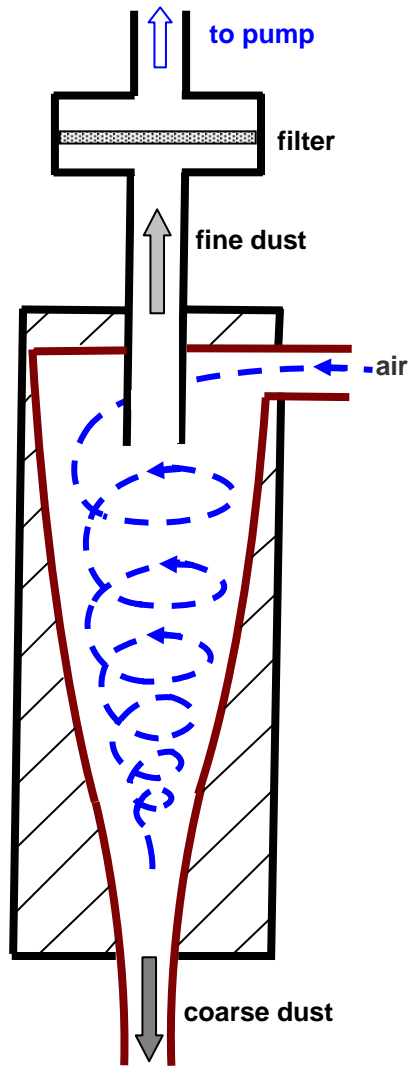


Figure 19.4 Cyclone head of a personal dust filter.

There are two techniques of particle size discrimination used in these devices. Some photometric dust instruments eliminate the non-respirable particles by passing the sample through a pre-classifier comprised of an elutriator or a cyclone. A number of cyclones in cascade can be used to give several size ranges. The other method of particle size discrimination is to use a laser or monochromatic light source. The choice of wavelength gives a means of discriminating in favour of the desired size range of particles. The angle between the light source and the photodetector is another method of selecting a preferred size range (Breuer et al, 1973; Thaer, 1975).

Although photometric dust instruments really respond to light reflected from particle surfaces, using them for selected size ranges enables the readings to be interpreted in terms of total volume of those particles and, hence, mass concentration (assuming constant density of the particle material). Figure 19.5 illustrates an instrument that combines a forward scattering laser unit with an 8 hour filtration system. This permits direct calibration of the light unit with respect to mass concentration of respirable dust.

The major advantage of modern light scattering instruments is that the addition of electronic circuitry permits a combination of immediate readout and integration over any chosen time interval. Hence, they can be employed for both short term and long term sampling. Coupled with cascade (sequential) interrogation of a sample stream they can indicate, record and transmit information for each of a series of particle size ranges (Breuer, 1975; Oberhalzer, 1987).

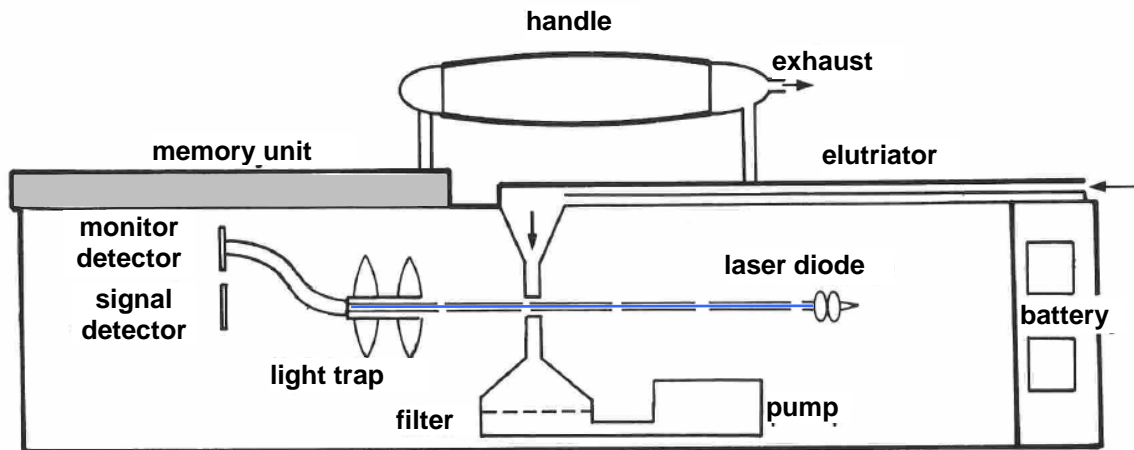


Figure 19.5 Schematic of a SIMSLIN II dust sampler.

19.4.5. Personal samplers

Stationary gravimetric dust monitors provide a means of sampling over an extended time period (typically an eight hour shift) and are useful for assessing average dust concentrations at specified locations. However, they do not measure the actual dust inhaled by individual workers. Neither are they capable of showing temporal variations of dust concentrations to which the worker is subjected. For many years attempts were made to develop practical and wearable dust monitors. Personal monitors should be unobtrusive to the worker and capable of giving reliable indications of dust level either instantaneously or over short time intervals. Furthermore, they should also be capable of recording full shift average dust concentrations for subsequent entry into a data log for the individual worker.

Early versions of personal dust monitors included a small lightweight cyclone (Figure 19.4) that was pinned to the lapel of the worker's clothing. The unit was powered by a battery worn on the belt. The position of the cyclone inlet could result in non-representative readings caused by dust from clothing. The device was also incapable of giving short-term readings.

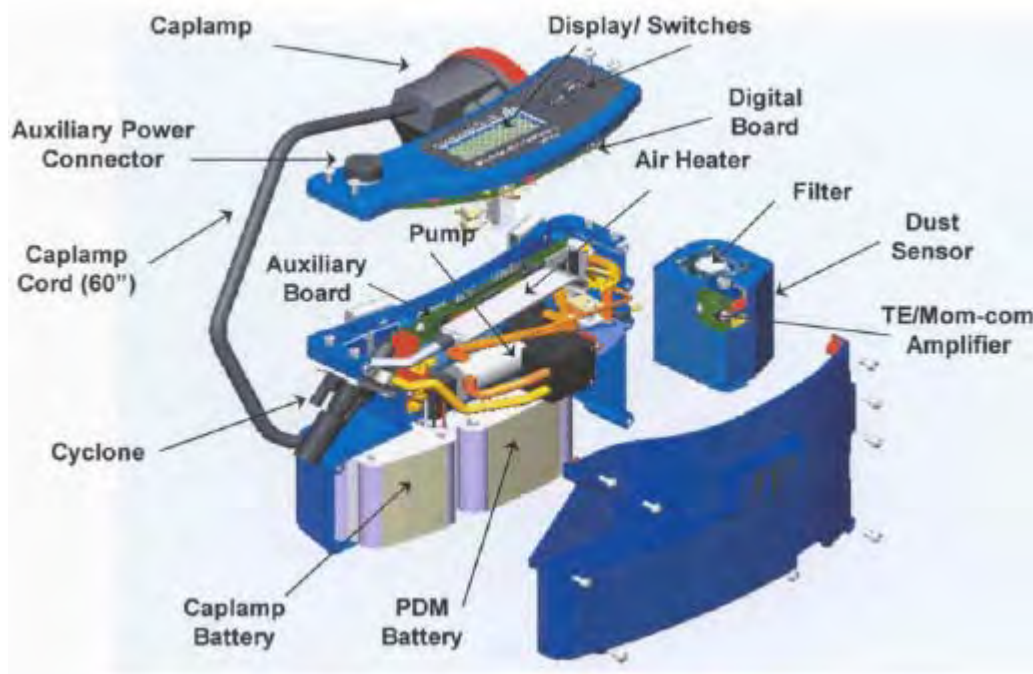


Figure 19.6. The NIOSH 2004 tapered-element oscillating microbalance personal dust sampler. *Reproduced from Volkwein, J.C. et al (2004). Performance of a new personal respirable dust monitor for mine use. Pittsburgh Research Laboratory, Report of Investigations 9663. NIOSH Publication No. 2004-151.*

A determined multi-year effort funded by the U.S. National Institute for Occupational Safety and Health (NIOSH)¹ produced a personal dust monitor that overcame many of the drawbacks of earlier models (Volkwein et al (2004), Volkwein et al (2005)). The heart of this monitor is a tapered-element oscillating microbalance. Air is drawn into the unit via an inlet located close to the lens of the wearer's caplamp, i.e. representative of the air being inhaled. A continuous sample passes through a 48mm diameter tube alongside the caplamp cord down to the sampler which is incorporated into a casing that also holds the caplamp battery (Figure 19.6).

¹ Development work was conducted by Rupprecht and Patashnick Co., Inc of Albany, New York.

Within the sampler the air passes through a cyclone to separate out the respirable fraction of dust. The latter passes along the hollow tapered element and through an exchangeable filter which is located on the narrow end of the element. Electronic components are employed to oscillate the element and filter at resonant frequency. As the mass of dust collected by the filter increases, the resonant frequency decreases. From that change the monitor evaluates the mass captured by the filter over a given time period. The readings given by a screen display on top of the belt worn unit include the average respirable dust concentration since the start of the shift and a running average over the past 15 or 30 minutes. Data from the sampler can be downloaded into a personal computer after the end of a shift.

19.4.6. Other methods of airborne dust measurement

In addition to the principles of dust measuring units outlined in the preceding subsections, there are several other types of devices that are available or under development. The impact principles employed in some of the old particle count devices still have a role as classifiers to remove non-respirable dust. This may further reduce the weight of personal samplers. A series of jet orifice sizes can be used to simulate a lung penetration curve (National Research Council, 1980).

Another type of device utilizes a carbon-14 radioactive source to pass beta rays through a mass of dust particles on a filter or impact collection plate. A detector measures the attenuation of the beta rays. In use, the device is run for a predetermined time. The difference between the flux of beta rays before and after sampling is processed by internal circuitry to indicate the mass of particles collected (National Research Council, 1980). A similar device developed in Poland employs strontium-90 as the radioactive source and measures reflected back-scatter of beta rays from the surface of the sample (Krzystolik et al, 1985).

A technique that may find further application is to measure the change in resonant frequency of a piezo-electric quartz crystal as a mass of sampled dust collects on it. Here again, such units arranged in cascade with interstage cyclones or impactors can be used to indicate a number of particle size ranges (Sem et al, 1977).

19.4.7. Discrimination of quartz particles

Mine dust is seldom composed of a single mineral. As quartz particles occur commonly and are particularly dangerous (Section 19.3.3.3.), efforts have been directed at quantifying the quartz content of dust samples. This is of concern not only in hardrock mines but also because of the increased use of mechanized extraction and roof bolting in coal mines.

The employment of x-ray diffraction gives well defined peaks for quartz on the output spectrum. This method has been used for a number of years as a means of mineralogical analysis of mine dust (Knight and Cochrane, 1975; Bradley, 1975). A further development is to incorporate the principle into dust monitoring equipment in order to display the quartz content concurrently with respirable dust concentration.

19.4.8. Sampling strategy

Throughout the history of organized dust measurements in mines, investigators have been faced with problems of large variations in the observed results. Furthermore, the significance of these results has often been subject to debate and interpretation. The very real variations in the concentration and mineralogical content of dusts that exist with respect to time and location in any mine are compounded by the differing efficiencies with which alternative instruments simulate the dust retention characteristics of the human lung. These difficulties have led to coining of the phrase of *sampling strategy* which really means the "why, where, when and how" dust samples are taken.

The "why", i.e. the objectives of dust sampling, were outlined in Section 19.4.1. It is, indeed, important to have a clearly defined purpose for any given set of dust measurements, particularly where the setting or checking of mandatory standards is involved. The objectives of a dust survey will then usually influence the "where, when and how."

When checking compliance with threshold limit values, the *locations* of area measuring points are normally dictated by law - for example at specific points in intake and return airways or with respect to the positions of machine operators. Research into dust minimization techniques in various countries has been greatly influenced by the wording of the relevant national law. For example, spray fan or other air diversion techniques can produce significant reductions in dust concentrations at the operator position of a continuous miner but may have little or no effect on respirable dust counts in the return airway. If, on the other hand, the purpose of a measurement is to check the dust production of a particular piece of equipment or operation, then the instruments should be located at specified distances upwind and downwind from that equipment or operation.

The *times and durations* of area sampling will, again, usually be specified by law, often at intervals of two or three months at each mandatory sampling point. The samples may be required to be submitted for analysis to specified laboratories operated or authorized by government agencies. Furthermore, check samples may be taken by government inspectors.

For short term sampling, it is all too easy to introduce conscious or inadvertent bias into dust measurements. The maximum dust make from a machine will be obtained when the equipment is running at full load. However, the measured concentration of non-toxic dust should not necessarily be interpreted as an epidemiological (health) hazard. It becomes so only if personnel are working in or downstream from the dust make and are exposed to concentrations that exceed the set standards on the basis of an 8 hour time weighted average.

The importance of adhering to agreed types of instruments and sampling procedures was emphasized in Section 19.3.4., particularly when checking compliance with statutory requirements. Indeed, the instruments and measurement procedures may be specified within the regulations. A factor that is often overlooked is the effect of air velocity on the sampling ports of the instrument. At the higher air velocities, dust particles can be diverted around the sampling ports (Baskhar and Ramani, 1987). Isokinetic devices can be fitted to the instrumentation in order to match the inlet port sampling velocity with that of the approaching airstream.

The variability of measured dust concentrations coupled with the intrinsic uncertainties of instrumentation and sampling procedures should dictate that those measurements be subjected to statistical analysis. In practice this is often relegated to a rejection of "unrepresentative or suspect" samples and the straight averaging of the remainder (National Academy of Sciences, 1976; Martinson, 1982). Such a procedure is clearly open to bias and is not to be recommended. Where any given sampling practice or location consistently yields a significant number of suspect samples, then an investigation should be carried out in order to determine whether the unexpected variations are, indeed, real and, if not, the weaknesses of the sampling technique. Statistical examinations can be carried out to test whether the number of samples is sufficiently large to be representative of the particular type of work, time or location. The data produced by wider use of personal samplers, together with computer based records and statistical analyses, facilitate such tasks.

This returns us to the utilization of personal samplers. The question of sampling strategy became of particular importance with the advent of 8 hour gravimetric sampling units and the relationship between the results given by these instruments and the earlier, short term, particle count units. Personal samplers have revolutionized the philosophy of dust sampling strategy. Provided that a correlation has been established between the results given by specified types of personal sampler and corresponding levels of epidemiological hazard, then there appears to be little

reason why those types of personal sampler should not be used for both individual exposure monitoring and compliance with appropriately worded regulations. This separates sampling for health reasons from those measurements that may be taken for purposes of control or planning.

The question arises on how many underground personnel should be asked to wear personal samplers. This would appear to depend upon the degree of perceived exposure to dust and the type of mining. In heavily mechanized workings, there may be relatively few persons within the more dusty areas. Furthermore, the mobility and differing occupations of some workers may subject them to wide variations of dust exposure. In such circumstances, it would be in the interests of those workers to wear personal samplers. The initiation of the practice should be accompanied by suitable explanations of the benefits of the devices, how they should be treated, and the manner in which the data will be used.

In labour intensive mines with much larger numbers of personnel, many of them engaged in similar occupations, it may be unnecessary to ask all persons to wear personal samplers. A minimum number that is deemed to be representative of each work group should be decided, including the more mobile supervisory staff (Quilliam, 1975). The actual persons wearing the samplers may be changed on a rota basis. However, after each shift the exposure record of each individual should be updated according to the relevant representative value for that group and location. Provided that the instruments are compatible, the data obtained can be used to compare dust indices for differing occupations, locations and mines (van Sittert, 1988).

The modern approach is to combine full-shift personal samplers with both long and short term dust monitoring that is incorporated into mine environmental electronic surveillance systems. The data obtained from such means will help to safeguard the health of workers and be valuable in the planning and design of future mining operations.

References

Baskhar, R. and Ramani, R.V. (1987). A comparison of the performance of impactors and gravimetric dust samplers in mine airflow conditions. 3rd U.S. Mine Ventilation Symposium, Penn State, pp 502-508.

Bradley, A.A. (1975). The determination of the quartz content of gravimetric mass samples of airborne dust by an x-ray technique. 1st Int. Mine Ventilation Congress, Johannesburg, South Africa, pp 455-458.

Breuer, H. (1975). TBF 50 and Tyndallometer TM digital - two instruments supplementing each other for the occupational hygienic and technical assessment of dust conditions. 1st Int. Mine Ventilation Congress, Johannesburg, South Africa, pp 445-452.

Breuer, H., Gebhart, J. and Robock, K. (1973). Photoelectric measuring apparatus for determination of the fine dust concentration. Staub Reinhaltung der Luft (in English), Vol 33.

Brundelet, P.J. (1965). Experimental study of the dust-clearance mechanism of the lung. Acta Pathol. Microbiol. Scand. Suppl. 175, pp 1-141.

Carver, J. (1975). Respirable dust regulations in the United Kingdom. 1st Int. Mine Ventilation Congress, Johannesburg, South Africa, pp 399-405.

Dunmore, J.H., Hamilton, R.J. and Smith, D.S.G. (1964). An instrument for the sampling of respirable dust for subsequent gravimetric assessment. Journ. Sc. Instruments, Vol. 41, pp 69-672.

- Gardiner, L.R. (1988).** Personal gravimetric dust sampling for the South African gold mining industry. 4th International Mine Ventilation Congress, Brisbane, Australia, pp 507-515.
- Gibson, H. and Vincent, J.H. (1980).** An investigation of "fly-dust" nuisance in mines. 2nd Int. Mine Ventilation Congress, Reno, USA, pp 620-622.
- Knight, G. and Cochrane, T.S. (1975).** Gravimetric dust sampling with quartz analysis and its use in metal and mineral mines. 1st Int. Mine Ventilation Congress, Johannesburg, S. Africa, pp 407-414.
- Krzystolik, P.A. et al (1985).** Portable coal dust/stone dust analyzer. 2nd U.S. Mine Ventilation Symposium, Reno, USA, pp 171-179.
- Martinson, M.J. (1982).** Sampling pathogenic airborne particulates. Chap. 14, Environmental engineering in South African mines. Mine Ventilation Society of South Africa, pp 357-378.
- National Academy of Sciences (1976).** Mineral resources and the environment: Coal workers' pneumoconiosis - medical considerations, some social implications. Washington, D.C.
- National Research Council (1980).** Measurement and control of respirable dust in mines. U.S. National Academy of Sciences, Washington, D.C., NMAB-363.
- Oberhalzer, J.W. (1987).** Assessment of colliery dust levels using a computerized dust measuring system. 3rd U.S. Mine Ventilation Symp. Penn State, pp 617-624.
- Orenstein, A.J. (editor) (1959).** Proc. of the International Pneumoconiosis Conference, Johannesburg, South Africa. Published by Churchill, London, 1960, pp 632.
- Phillips, H.R. (1984).** New methods and standards for respirable dust monitoring in the New South Wales coal industry. 3rd Int. Mine Ventilation Congress, Harrogate, U.K., pp 203-208.
- Quilliam, J.H. (1975).** A review of dust sampling techniques in South African gold mines. 1st Int. Mine Ventilation Congress, Johannesburg, S. Africa, pp 419-421.
- Rogers, W.G. (1991).** Silica; Crystalline quartz exposure standards... What is the most appropriate standard to use? Journ. of the Mine Ventilation Society of South Africa, March, pp 38-43.
- Schröder, H.H.E. (1982).** The properties and effects of dust. Chapter 12, Environmental Engineering in South African Mines, Mine Ventilation Soc. of S. Africa, pp 313-336.
- Sem, G.J., Tsurubayashi, K. and Homma, K. (1977).** Performance of the piezo-electric microbalance respirable aerosol monitor. Am. Ind. Hyg. Assoc. Jour., Vol. 38, p 580.
- Thaer, A. (1975).** The Leitz Tyndallometer TM digital as applied to the determination of fine dust concentration under the auspices of Occupational and Environmental Medicine. Presented at the Kungl Arbetarskyddsstyrelsen Seminar, Stockholm, April 23.
- Van Sittert, J.M.O. (1988).** An overview of the proposed guidelines to standardize the respirable dust sampling strategy for risk determination in collieries. 4th Int. Mine Ventilation Congress, Brisbane, Australia, pp 527-531.
- Volkwein, J.C. et al (2004).** Performance of a new personal respirable dust monitor for mine use. Pittsburgh Research Laboratory, Report of Investigations 9663. NIOSH Publication No. 2004-151.

Volkwein, J.C. et al (2005). Implementing a new personal dust monitor as an engineering tool. International Occupational Hygiene Association, 6th International Scientific Conference, Pilanesberg, South Africa.

Walli, R.A. (1982). Mine dusts. Mine ventilation and air conditioning (ed. Hartman), Chap. 5, pp 84-130.

CHAPTER 20. THE AERODYNAMICS, SOURCES AND CONTROL OF AIRBORNE DUST

20.1. INTRODUCTION	2
20.2. THE AERODYNAMIC BEHAVIOUR OF DUST PARTICLES.....	2
20.2.1. Gravitational settlement	2
20.2.1.1. Stokes' Law and terminal velocities.	3
20.2.1.2. Slip flow	5
20.2.2 Brownian motion	9
20.2.2.1. Brownian displacements	9
20.2.2.2. Brownian diffusivity	10
20.2.3. Eddy diffusion	11
20.2.4. Other forms of dust transportation	12
20.2.5. Coagulation.....	13
20.2.6. Impingement and re-entrainment.....	15
20.2.7. Computer models of dust transport	16
20.3. THE PRODUCTION OF DUST IN UNDERGROUND OPENINGS	16
20.3.1. The comminution process.....	16
20.3.2. Mechanised mining	19
20.3.3. Supports.....	20
20.3.4. Blasting	20
20.3.5. Loading operations	21
20.3.6. Transportation and crushing	21
20.3.7. Workshops	22
20.3.8. Quartz dust in coal mines	22
20.4. CONTROL OF DUST IN MINES.....	23
20.4.1. Dust suppression	23
20.4.1.1. Pick face flushing and jet-assisted cutting	23
20.4.1.2. Water infusion	24
20.4.1.3. Wetting agents, foams and roadway consolidation.....	25
20.4.2. Removal of dust from air.....	25
20.4.2.1. Water sprays	26
20.4.2.2. Wet scrubbers	30
20.4.2.3. Dry filters and separators.....	33
20.4.2.4. Personal respirators	37
20.4.3. Dilution and layout of the ventilation system	37
20.4.4. Separation of personnel and dust.....	38
References	38

20.1. INTRODUCTION

The physical characteristics of aerosols have been subjected to intensive study for the free surface atmosphere. This is an important area in meteorology and investigations of the behaviour of contaminant plumes in the atmosphere. Somewhat less attention has been paid to the aerodynamic characteristics of dust when the carrying airstream is confined within the boundaries of ducts or tunnels.

The first main section in this chapter outlines the several phenomena that govern the manner in which airborne dust is transported through the branches of a ventilation network and the deposition of dust particles on the roof, floor and sides of mine airways.

A prerequisite to the successful control of airborne dust in a mine is an understanding of the potential sources of the dust. These are discussed in the second main part of the chapter. While some sources are obvious such as a power loader or tunneling machine, others are less so including the crushing of immediate roof strata by modern powered roof supports. The final section outlines the methods of dust control in mining operations. These include prevention of the formation of dust, suppression and removal of dust particles from the air, isolating personnel from concentrations of dust and the diluting effects of airflow. The latter was introduced in Section 9.3.3.

Readers who are interested only in the practical aspects of the topic are advised to concentrate on Sections 20.3.2 to 20.4.1 and 20.4.2.2 to 20.4.4.

20.2. THE AERODYNAMIC BEHAVIOUR OF DUST PARTICLES

The very large size range of dust particles that exist in the ventilation system of an active mine results in a variety of differing phenomena influencing the behaviour of the particles. The smallest particles act almost as a gas and react to molecular forces while the larger particles are influenced primarily by inertial and gravitational effects. In this section we shall consider the influence of gravitational settlement, molecular diffusion, turbulent or eddy diffusion, coagulation, impingement, re-entrainment and computer simulations.

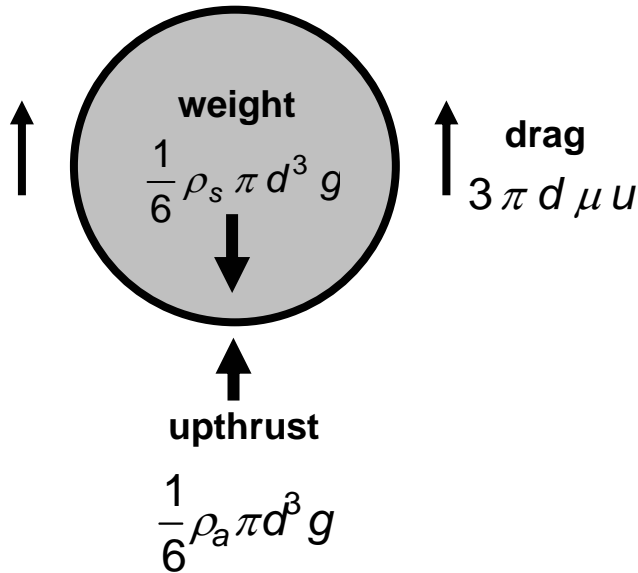
20.2.1. Gravitational settlement

The rate at which a particle falls through air under the action of gravity depends not only upon the size and density of the particle but also its shape. In Section 19.2.1., the concept of an **equivalent geometric diameter** based on projected area was introduced. This is *the diameter of a sphere that has the same projected area as the actual particle*.

The majority of analyses in this subject assume that each particle is a homogeneous sphere. In the study of particle aerodynamics this has given rise to further alternative definitions of equivalent diameter including:

- *Stokes' diameter:* *the diameter of a sphere that has same density as the actual particle and falls through air at the same rate*
- *aerodynamic diameter:* *the diameter of a sphere of density 1 g/cm^3 that falls through air at the same rate as the actual particle.*

Despite these additional definitions, the geometric diameter remains the one that is most commonly used in practice.



20.2.1.1. Stokes' Law and terminal velocities. When any body is suspended in a fluid, at least two forces act upon it (Figure 20.1). One is the weight of the body within the prevailing gravitational field. The volume of a sphere of diameter d is $\frac{1}{6} \pi d^3 \text{ m}^3$. If this has a density of $\rho_s \text{ (kg/m}^3\text{)}$ then its weight becomes

$$\frac{1}{6} \rho_s \pi d^3 g \quad \text{N} \quad (20.1)$$

where $g = \text{gravitational acceleration (m/s}^2\text{)}$

However, the sphere displaces its own volume of fluid and will experience an opposing upthrust equal to the weight of fluid displaced, i.e.

$$\frac{1}{6} \rho_a \pi d^3 g \quad \text{N} \quad (20.2)$$

where $\rho_a = \text{density of the fluid (kg/m}^3\text{)}$

Figure 20.1 Forces on a particle falling in air.

At equilibrium $\frac{1}{6} \pi d^3 g (\rho_s - \rho_a) = 3 \pi d \mu u$

The net force causing downward movement is the combination of the two:

$$\frac{1}{6} \pi d^3 g (\rho_s - \rho_a) \quad \text{N} \quad (20.3)$$

If the particle is moving relative to the fluid then it will experience a further resistance or drag because of viscous shear and conversion of some of its kinetic energy into turbulent eddies within the fluid. A general expression for drag was given in Section 5.4.6.2. as

$$\text{Drag} = C_D A_b \rho_a \frac{u^2}{2} \quad \text{N} \quad (20.4)$$

where $C_D = \text{coefficient of drag (dimensionless)}$
 $u = \text{relative velocity between the particle and the fluid, m/s}$
 and $A_b = \text{projected area (= } \pi d^2/4\text{), m}^2$

Many investigators have investigated relationships between C_D and Reynolds' Number, Re , for fully submerged bodies (e.g. Prandtl 1923). In the case of spheres, the diameter is used as the characteristic length in the calculation of Reynolds' Number. For the particular case of laminar flow around a particle, Sir George G. Stokes (1819-1903), the Cambridge physicist, showed that

$$C_D = \frac{24}{Re} \quad (20.5)$$

Now, as $Re = \frac{\rho_a u d}{\mu_a}$ where μ_a = dynamic viscosity of the fluid (Ns/m²),

$$C_D = \frac{24 \mu_a}{\rho_a u d}$$

Substituting for A_b and C_D equation (20.4) gives

$$\text{Drag} = \frac{24 \mu_a}{\rho_a u d} \frac{\pi d^2}{4} \rho_a \frac{u^2}{2} = 3 \pi \mu_a d u \quad \text{N} \quad (20.6)$$

As the particle accelerates downwards, its velocity, u , increases until the drag equals the downward force quantified in equation (20.3)

$$\frac{1}{6} \pi d^3 g (\rho_s - \rho_a) = 3 \pi \mu_a d u \quad \text{N} \quad (20.7)$$

At that point of dynamic equilibrium, the velocity of fall becomes constant and is renamed the **terminal velocity**, u_t . Equation (20.7) may now be rearranged as

$$u_t = \frac{d^2 g (\rho_s - \rho_a)}{18 \mu_a} \quad \text{m/s} \quad (20.8)$$

Equations (20.6 to 20.8) have all been referred to as **Stokes' Law**.

Stokes' Law applies with good accuracy to particles that are above the respirable range (5 microns). Smaller particles become sensitive to **slippage** and molecular forces. Stokes' Law is based on the assumption of laminar flow. If the terminal velocity is sufficiently high to cause the onset of a turbulent wake then the transfer of kinetic energy from the particle to the fluid (inertial effects) can no longer be ignored. The upper limit of Stokes' Law occurs at a Reynolds Number, Re , of about 0.1 which, for many mineral particles falling at their terminal velocity through air, is equivalent to geometric diameters of approximately 20 microns.

For larger particles at their terminal velocity, u_t , we may balance equations (20.3) and 20.4):

$$\frac{1}{6} \pi d^3 g (\rho_s - \rho_a) = C_D \frac{\pi d^2}{4} \rho_a \frac{u_t^2}{2}$$

giving

$$u_t = \sqrt{\frac{4 d g (\rho_s - \rho_a)}{3 C_D \rho_a}} \quad \text{m/s} \quad (20.9)$$

For dust particles in air, $\rho_s \gg \rho_a$ and the term $(\rho_s - \rho_a)$ is usually truncated to ρ_s . Flagan and Seinfeld (1988) suggest the approximations for coefficients of drag, C_D given in Table 20.1.

Reynolds' No., Re	C_D
< 0.1	$\frac{24}{Re}$ (Stokes' Law)
$0.1 < Re < 2$	$\frac{24}{Re} \left[1 + \frac{3}{16} Re + \frac{9}{160} Re^2 \ln(2Re) \right]$
$2 < Re < 500$	$\frac{24}{Re} \left[1 + 0.15 Re^{0.687} \right]$
$500 < Re < (2 \times 10^5)$	0.44

Table 20.1 Approximations for coefficients of drag for spherical particles (after Flagan and Senfeld, 1988)

20.2.1.2. Slip flow

Stokes' Law applies to dust particles that are large in comparison to the mean free path of the gas molecules. Hence, those particles see the gas as a continuum. As the particle size approaches the mean free path of the gas molecules this no longer holds. Two effects are then observable; first the jerky dislocations caused by molecular bombardment, known as Brownian motion and discussed in Section 20.2.2., and secondly, the drag force reduces as the small particle becomes more able to move or "slip" through intermolecular voids.

In order to quantify the very small distances now being considered, let us recall that the mean free path of a gas molecule is defined as the average distance it moves between collisions with other gas molecules. Although air is a mixture of gases, it is convenient to treat it as a single gas of equivalent molecular weight 28.966 and gas constant 287.04 J/kgK.

From the kinetic theory of gases it can be shown that the mean free path, λ , is given by

$$\lambda = \frac{\mu}{0.499 P (8 / \pi RT)^{\frac{1}{2}}} \quad \text{m} \quad (20.10)$$

where μ = dynamic viscosity of fluid (Ns/m²)
 P = pressure (N/m²)
 R = gas constant (J/kgK)
 and T = absolute temperature (K)

For air at $P = 100 \text{ kPa}$, $T = 293 \text{ K (20 °C)}$,
 $R = 287.04 \text{ J/kgK}$ and $\mu_a = 17.9 \times 10^{-6} \text{ Ns/m}^2$ (Section 2.3.3.),

$$\lambda = \frac{17.9 \times 10^{-6}}{0.499 \times 10^5 \{8 / (\pi 287.04 \times 293)\}^{\frac{1}{2}}} = 6.52 \times 10^{-8} \text{ m or } 0.0652 \text{ microns.}$$

When particle diameters fall below 5 microns, the effect of slippage becomes significant. In order to extend the applicability of Stokes' Law, a correction factor, C_c , can be introduced to reduce the calculated value of drag. Thus, for small particles equation (20.6) is corrected to

$$\text{Drag} = \frac{3 \pi \mu_a d u}{C_c} \quad \text{N} \quad (20.11).$$

A number of relationships between C_c and d have been suggested (e.g. Allen and Raabe, 1982), based mainly on a series of classical experiments on liquid aerosols carried out by Millikan between 1909 and 1923. Values of the slip correction factor for air at 25 °C and 101 kPa are given in Table 20.2.

d (microns)	0.01	0.05	0.1	0.5	1.0	5.0	10.0
C_c	22.7	5.06	2.91	1.337	1.168	1.034	1.017

Table 20.2. Slip correction factor for dust particles in air (after Flagan and Seinfeld, 1988).

The equation $C_c = \frac{9.56 \times 10^{-8}}{d^{1.045}} + 0.99$, with d expressed in metres, gives C_c within an accuracy of 2 percent.

Incorporating the slip correction factor into Stokes' Law for terminal velocity, equation (20.8) gives a relationship that can now be extended down to a particle size of 0.01 microns:

$$u_t = \frac{d^2 g(\rho_s - \rho_a) C_c}{18 \mu_a} \quad \text{m/s} \quad (20.12)$$

Figure 20.2 gives a graphical representation of this equation for particles of varying diameter and density falling through air of temperature 20°C. The curvature of the lines on this log-log plot is due to the effects of slippage.

Example

Determine the terminal velocities and time taken for particles of geometric equivalent diameter 0.1, 1, 10 and 100 microns to fall a distance of 2m through air of density $\rho_a = 1.1 \text{ kg/m}^3$ and dynamic viscosity, $\mu_a = 18 \times 10^{-6} \text{ Ns/m}^2$. The density of the dust material is 2000 kg/m^3 .

Solution

The terminal velocities for the 0.1, 1, and 10 micron particles can be estimated from the $\rho_s = 2000 \text{ kg/m}^3$ curve on Figure 20.2. For more precise values the slip corrected Stokes' equation (20.12) gives

$$u_t = \frac{d^2 g(\rho_s - \rho_a) C_c}{18 \mu_a} = \frac{9.81(2000 - 1.1) d^2 C_c}{18 \times 18 \times 10^{-6}} = 6.052 \times 10^7 d^2 C_c$$

Applying this relationship to each of the given particle diameters and reading corresponding values of C_c from Table 20.2 (remembering to multiply microns by 10^{-6} to convert diameters to metres) gives

d (microns)	0.1	1	10	100
Slip correction, C_c	2.91	1.168	1.017	1
u_t (m/s)				
calculated	1.761×10^{-6}	7.069×10^{-5}	6.155×10^{-3}	0.605
estimated from Figure 20.2	1.75×10^{-6}	7.1×10^{-5}	6.0×10^{-3}	out of range

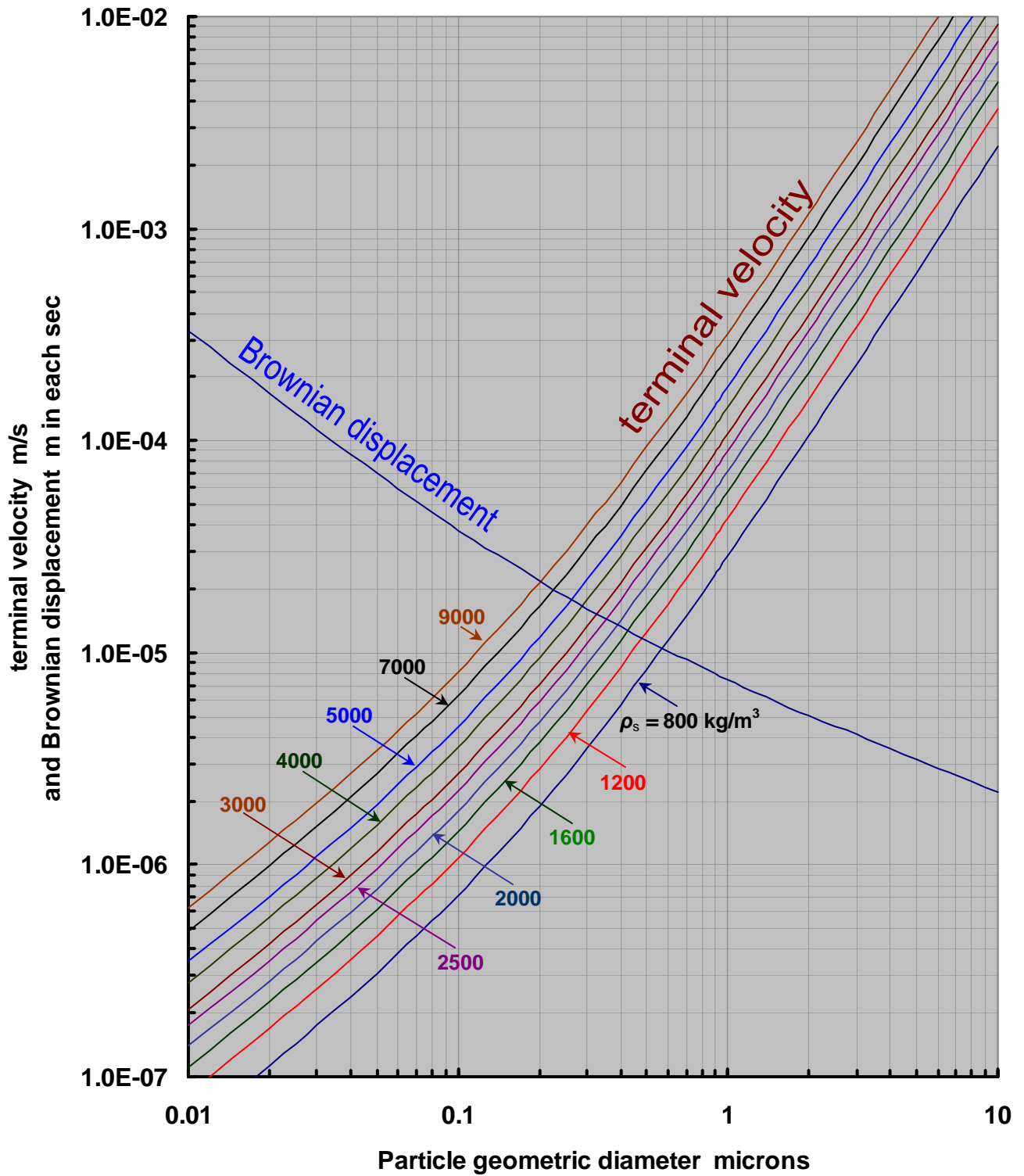


Figure 20.2 Slip corrected terminal velocities and Brownian displacements of dust particles falling through still air of viscosity $17.9 \times 10^{-6} \text{ Ns/m}^2$ (20°C). Based on equations (20.12) and (20.17 with barometric pressure of 100kPa and $g = 9.81 \text{ m/s}^2$).

These terminal velocities for the 0.1, 1.0 and 10 micron particles are acceptable as the diameters fall into the range of applicability of the slip-corrected Stokes' equation. The 100 micron particle, however, is well above the 20 micron limit for laminar flow and we must revert to the more general equation (20.9). This requires a value of coefficient of drag, C_D . Table 20.1 would allow us to calculate C_D if we knew the Reynolds' Number. Unfortunately, that depends upon the terminal velocity which we are trying to find. The problem can be solved iteratively, starting from the approximation $u_t = 0.605$ m/s given by the Stokes' equation, (20.8).

$$\begin{aligned} Re &= \frac{\rho_a d u_t}{\mu_a} = \frac{1.1 \times 100 \times 10^{-6} \times u_t}{18 \times 10^{-6}} = 6.111 u_t & (20.13) \\ &= 6.111 \times 0.605 = 3.7 \end{aligned}$$

Table 20.1 gives the appropriate expression for coefficient of drag as

$$C_D = \frac{24}{Re} (1 + 0.15 Re^{0.687}) = \frac{24}{3.7} (1 + 0.15 \times 3.7^{0.687}) = 8.882 \quad (20.14)$$

Equation (20.9) now gives an improved value of u_t

$$\begin{aligned} u_t &= \sqrt{\frac{4 dg(\rho_s - \rho_a)}{3 C_D \rho_a}} = \sqrt{\frac{4 \times 100 \times 10^{-6} \times 9.81(2000 - 1.1)}{3 \times 1.1 \times C_D}} \\ &= \frac{1.5417}{\sqrt{C_D}} = \frac{1.5417}{\sqrt{8.882}} = 0.517 \text{ m/s} & (20.15) \end{aligned}$$

Equations (20.13, 20.14 and 20.15) can readily be entered into a programmable calculator or spreadsheet software for iterative solution. The values of the variables over eight iterations are as follows.

u (m/s)	Re	C_D
0.605	3.70	8.88
0.517	3.16	10.10
0.485	2.96	10.66
0.472	2.89	10.90
0.467	2.85	11.00
0.465	2.84	11.05
0.464	2.84	11.06
0.463		

The procedure converges to $u_t = 0.463$ m/s
 The time taken for each of the particles to fall through 2 m can now be determined as $t = 2/u_t$.

diameter (microns)	u_t (m/s)	t
0.1	1.761×10^{-6}	315 hours
1.0	7.069×10^{-5}	7.9 hours
10	6.155×10^{-3}	5.41 minutes
100	0.463	4.32 seconds

It is clear from this example that little gravitational settlement of respirable dust (< 5 microns) can be expected within the retention times of ventilated areas underground. Coupled with the effects of Brownian motion, submicron particles can be considered to remain in permanent suspension. Indeed, Figure 20.2 indicates that for the 0.1 micron particle Brownian displacement is the dominant effect.

20.2.2 Brownian motion

For very small particles, the bombardment by fluid molecules is no longer balanced on all sides. The result is that the particles undergo random and jerky displacements. This is known as Brownian motion and can be seen under an optical microscope.

20.2.2.1. Brownian displacements

As Brownian movements are random, it is necessary to analyze their effect statistically on a complete population of particles. If we consider a vertical plane in still air of uniform dust concentration and with only Brownian motion causing horizontal movement of the particles, then the average displacement of particles moving through the plane in one direction ($+\bar{x}$) will be equal to the average displacement of particles in the opposite direction ($-\bar{x}$). Hence, the net displacement is zero - not a very useful result. However, if we square the displacements (positive or negative) then the sum is always a positive number. We can then quantify Brownian motion in terms of **mean-square displacement**, $(\bar{x})^2$

A relationship for mean-square displacement was first derived by Einstein in 1905¹ (see, also, Seinfeld, 1986) and has been verified by numerous observers:

$$(\bar{x})^2 = 2 \frac{MR}{A} T \frac{C_c}{3\pi\mu d} t \quad \text{m}^2 \quad (20.16)$$

where M = molecular weight of gas
 R = gas constant (J/kgK)
 (note that $MR = R_u =$ universal gas constant, 8314 J/K kg-mole, Section 3.3.1.)
 A = Avagadro's constant (6022×10^{23} molecules in each kg-mole)
 and t = time over which the displacement takes place (s)

(The ratio $\frac{R_u}{A} = \frac{8314}{6022 \times 10^{23}} = 1.381 \times 10^{-23} \frac{\text{J}}{\text{molecule K}}$ is known as **Boltzmann's constant**.)

For air at 20°C ($T = 293$ K), the viscosity is 17.9×10^{-6} Ns/m². Equation (20.16) can then be simplified to

$$(\bar{x})^2 = \frac{2 \times 1.381 \times 10^{-23} \times 293}{3\pi \times 17.9 \times 10^{-6}} \frac{C_c t}{d}$$

or

$$\bar{x} = 6.925 \times 10^{-9} \sqrt{\frac{C_c t}{d}} \quad \text{m} \quad (20.17)$$

Using the values of C_c given in Table 20.2 and $C_c = 1$ for $d > 10$ microns, equation (20.17) has been superimposed on Figure 20.2 with t set at 1 second. This allows the Brownian displacement to be compared with the terminal velocity curves. Inspection of the Figure indicates that at some point, as particle diameter decreases, Brownian displacement becomes predominant. This occurs within the range 0.2 to 0.6 microns, dependent upon the density of the material. At all lower diameters gravitational settlement is effectively nullified.

¹ Historical note: In 1905 Albert Einstein completed his doctoral thesis. It described his studies into the existence and behaviour of atoms and molecules. He rapidly applied this work to explain the phenomenon of Brownian motion. Later that same year he published his groundbreaking Theory of Special Relativity.

20.2.2.2. Brownian diffusivity

A consequence of random Brownian displacements is that migration of particles will occur from regions of higher to lower dust concentrations. We can describe the process as a form of diffusion and obeying Fick's Law:

$$N_b = D_b \frac{dc}{dx} \tag{20.18}$$

where

- N_b is the flux of particles through an area of 1 m² in one second [particles/(m² s)] by Brownian diffusion
- c is the concentration (particles/m³)
- x is distance (m) in the direction considered
- and D_b is a coefficient known as the **Brownian diffusivity** (m²/s).

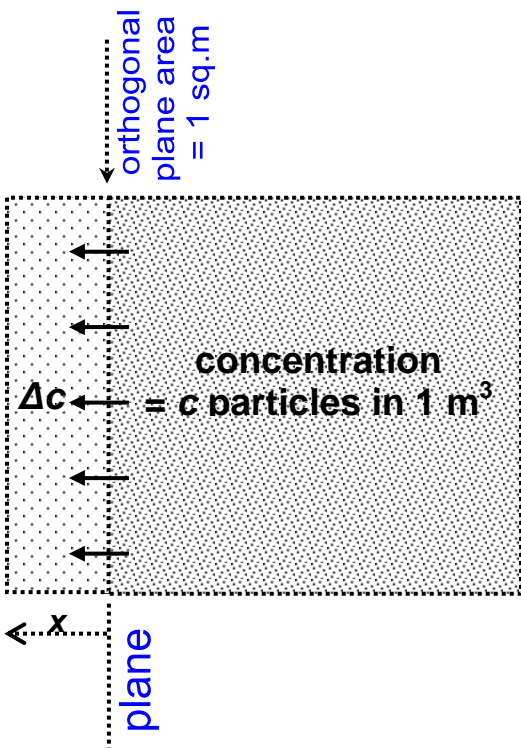


Figure 20.3 Δc particles diffuse from a concentration of c particles/m³ through an orthogonal area of 1 m² and over a Brownian dislocation distance of x metres.

Let us now attempt to find a relationship that will allow us to quantify the Brownian diffusivity. Consider the 1 metre cube shown on Figure 20.3. It contains c particles, i.e. a concentration of c particles/m³. In time Δt , a net number of those particles, Δc , will diffuse across a 1 m² plane by Brownian dislocations and as a consequence of the concentration gradient dc/dx .

Let us take the average Brownian dislocation, x , to be the distance through which the particles move in time Δt . Hence, their average velocity in the x direction will be $x/\Delta t$. Furthermore, the flux across the 1 m² plane will be the number of particles involved multiplied by their average velocity, i.e.

$$N_b = \Delta c \frac{x}{\Delta t} \frac{\text{particles}}{\text{m}^2 \text{ s}} \tag{20.19}$$

Combining equations (20.18) and (20.19)

gives
$$\Delta c \frac{x}{\Delta t} = D_b \frac{dc}{dx}$$

Now, over the very small distance of a Brownian dislocation, $x (= \bar{x})$, we can state that $\Delta c = dc$ and $\Delta t = dt$, giving $x dx = D_b dt$

Integrating both sides between corresponding boundary limits

$$\frac{x^2}{2} = D_b t \quad \text{m}^2 \tag{20.20}$$

As we chose the distance x to be the average Brownian dislocation, \bar{x} , we can combine with equation (20.16) to give

$$(\bar{x})^2 = 2D_b t = \frac{2MRT}{A} \frac{C_c}{3\pi\mu d} t \quad \text{m}^2 \quad (20.21)$$

from which

$$D_b = \frac{MRT}{A} \frac{C_c}{3\pi\mu d} \quad \text{m}^2/\text{s} \quad (20.22)$$

Again, for air at 20 °C, inserting the values

$$\begin{aligned} MR/A &= 1.381 \times 10^{-23} \text{ J/(molecule K)}, \\ T &= 293 \text{ K} \\ \text{and } \mu &= 17.9 \times 10^{-6} \text{ Ns/m}^2 \\ \text{gives} \end{aligned}$$

$$D_b = 2.398 \times 10^{-17} \frac{C_c}{d} \quad \text{m}^2/\text{s} \quad (20.23)$$

Note, also, from equation (20.20) that the mean dislocation is related to the Brownian coefficient of diffusion

$$\bar{x} = \sqrt{2D_b t} \quad \text{m} \quad (20.24)$$

20.2.3. Eddy diffusion

The previous two sections have considered the effects of gravity and molecular bombardment on dust particles. In ventilated areas, a larger influence is exerted on dust particles by the turbulent nature of the airflow. The transport of dust particles by eddies can also be described by a diffusion equation

$$N_e = \epsilon \frac{dc}{dx} \quad \frac{\text{particles}}{\text{m}^2 \text{ s}} \quad (20.25)$$

where

$$\begin{aligned} \epsilon &= \text{eddy diffusivity (m}^2/\text{s)} \\ \text{and } N_e &= \text{flux of particles through an area of } 1 \text{ m}^2 \text{ in one second (particles/m}^2 \text{ s)} \\ &\quad \text{by eddy diffusion.} \end{aligned}$$

The total rate of diffusion by both Brownian action and eddies is given by combining equations (20.18) and 20.25). Then

$$N = N_b + N_e = (D_b + \epsilon) \frac{dc}{dx} \quad \frac{\text{particles}}{\text{m}^2 \text{ s}} \quad (20.26)$$

[A glance back at equations (A15.2) and (A15.5) reveals the analogy with diffusion for both heat and momentum.]

The flux of particles passing from the turbulent core of an airflow through the buffer boundary layer to the laminar sublayer is of particular interest as these are particles that have a high probability of being deposited on the solid surfaces. Gravitational settlement will, of course, add to such deposition on floors or other upward facing surfaces. Eddy action can impart sufficient inertia to a dust particle to carry it into the laminar sublayer. Within the sublayer there are no such eddies. Hence only Brownian bombardment can superimpose further transverse forces. Ignoring any effects of re-entrainment, Brownian dislocations at the surface and *away* from the surface will be zero. Hence there will be a Brownian concentration gradient *towards* the surface. Coupled with the initial transverse inertia, this will tend to produce deposition of particles that enter the laminar

sublayer. As may be expected, this phenomenon is influenced by the same factors that affect the boundary layers of fluid flow through rough ducts, i.e. fluid density, viscosity and velocity (Reynolds' Number) as well as the roughness of the surface.

The average size of eddies grows from zero at the edge of the laminar sublayer to a maximum within the turbulent core and, hence, varies with distance, y , from the surface. In order to take the other variables into account, a *dimensionless distance*, y^* is defined as

$$y^* = y \frac{u}{2f} \frac{\rho}{\mu} \quad (20.27)$$

where y = actual distance from the surface (m)
 u = average velocity of fluid (m/s)
 f = coefficient of friction for the surface (dimensionless)
 ρ = fluid density (kg/m^3)
 and μ = dynamic viscosity (Ns/m^2)

Note that $yu\rho/\mu$ has the form of a Reynolds' Number. (The group $u/2f$ is sometimes referred to as the *friction velocity*.) Values of eddy diffusivity are suggested in Table 20.3.

Dimensionless distance from surface	Eddy diffusivity ϵ (m^2/s)
$0 < y^* < 5$ (laminar sublayer)	$0.001 \frac{\rho}{\mu} y_*^3$
$5 < y^* < 20$ (buffer layer)	$0.012 \frac{\rho}{\mu} [y_* - 1.6]^2$
$y^* > 20$ (turbulent core)	$0.4 \frac{\rho}{\mu} (y_* - 10)$

Table 20.3. Expressions for eddy diffusivity, ϵ , as a function of dimensionless distance from a surface, y^* (after Owen, 1969).

In order to track the combined Brownian and eddy transverse transportation of dust particles across an airway, it is necessary to carry out integrations of equation (20.26) across each of the zones specified in Table 20.3 (Bhaskar and Ramani, 1988). This is accomplished in a manner similar to that used for convective heat transfer in Appendix A15.3.

20.2.4. Other forms of dust transportation

The processes of sedimentation, Brownian and eddy diffusion, coupled with coagulation, are the predominant mechanisms leading to the deposition of dust particles. There are, however, other phenomena that play a secondary role in governing the behaviour of airborne dust.

Many particles gain an electrical charge during formation. The effects of frictional flow as air moves through a duct or airway can also induce electrical charges on dust particles. Even particles that are initially uncharged may gain dipole characteristics due to Van de Waal's forces. The primary effect of *electrostatic forces* is to increase rates of coagulation (Section 20.2.5).

Suppose a dust particle of charge, q , moves through an electrical field of strength E , then it will experience an electrostatic force, qE . This may occur particularly around electrical equipment. At equilibrium velocity, this force is balanced by fluid drag (equation (20.11) for laminar flow around the particle), giving

$$\frac{3\pi\mu_a d}{C_c} u_e = qE \quad \text{N} \quad (20.28)$$

where u_e = the electrical migration velocity relative to the air (m/s).

The induction of an electrical charge on dust particles to assist in deposition is utilized in electrostatic precipitators (Section 20.4.2.3.) and in the control of paint or powder sprays. However, the high voltages that are required impose a limit on the use of such devices in underground openings.

Phoretic effects refer to phenomena that impart a preferential direction to Brownian motion.

Thermophoresis is the migration of particles from a hotter to a cooler region of gas and is caused by the enhancement of Brownian displacement at higher temperatures (equation (20.16)). The dust particles are subjected to greater molecular bombardment from the side of higher temperature. The temperature gradient must be considerable to produce a significant effect and the phenomenon has little influence on dust deposition in mine airways. However, it is utilized in instruments such as the thermal precipitator (Section 19.4.2.).

Photophoresis occurs when an intense light beam or laser is employed in a dusty atmosphere. The absorption of light by the particle causes an uneven temperature field to exist around that particle. The resulting excitation of nearby gas molecules causes thermophoresis to occur in a direction that depends upon the induced temperature field around the surface of the particle.

An effect that encourages dust deposition on wet surfaces is *diffusiophoresis*. The migration of water vapour molecules away from an evaporating surface will result in a replacing flux of the more massive air molecules *towards* the surface. The result will be a net Brownian force on dust particles also towards the surface.

20.2.5. Coagulation

In any concentration of dust particles, collisions between the particles will occur due to Brownian motion, eddy action or differential sedimentation. Dependent upon the surface properties of any two such particles, they may adhere together to form a larger single particle. As the process continues, some particles will grow to the extent that their terminal velocity becomes significant and they will flocculate out of suspension. This phenomenon of *coagulation* is influenced by the number and size distribution of the particles (large particles are more likely to be struck by other particles), temperature and pressure of the air (governing Brownian displacements) and electrical charge distributions. The shape of the particles and the presence of adsorbed vapours on their surfaces also affect the probability of their adhering upon collision.

Analysis of coagulation is, again, an exercise in statistics. Consider, first, a concentration of n particles in 1m^3 . The average *frequency* of collisions (dn/dt particles involved in collisions per m^3 per second) clearly depends upon the number of particles in that space. We can write

$$\frac{dn}{dt} = -an \quad \frac{\text{particles}}{\text{sm}^3} \quad (20.29)$$

where a = the *probability* of any two particles colliding. (Negative as the number of discrete particles is *decreasing* with time.)

However, the probability of collision is itself proportional to the number of particles

$$a = Kn \quad 1/s \quad (20.30)$$

giving $\frac{dn}{dt} = -Kn^2$ $\frac{\text{particles}}{\text{sm}^3}$ (20.31)

K is known as the *coagulation coefficient* or *collision frequency function* ($\text{m}^3/(\text{particles}\cdot\text{s})$).

Equation (20.31) can be integrated readily:

$$\int \frac{dn}{n^2} = \int -K dt$$

$$\frac{1}{n} = Kt + \text{constant}$$

At $t = 0$, $n = n_o$ = original concentration of particles, giving

$$\text{constant} = \frac{1}{n_o} \text{ so that}$$

$$\frac{1}{n} = Kt + \frac{1}{n_o} \quad \left[\frac{\text{particles}}{\text{m}^3} \right]^{-1} \quad (20.31a)$$

i.e. at any given time, t , the particle concentration is given as

$$n = \frac{n_o}{n_o Kt + 1} \quad \frac{\text{particles}}{\text{m}^3} \quad (20.31b)$$

Values of the coagulation constant can be found for any given dust cloud by plotting the variation of particle concentration with respect to time. For Brownian coagulation of equal sized particles in a continuum, K is given by

$$K = \frac{8}{3} \frac{MR}{A} \frac{T}{\eta_a} \quad \frac{\text{m}^3}{\text{particles}\cdot\text{s}} \quad (\text{Flagan and Seinfeld, 1988}) \quad (20.32)$$

Hence for air at 20°C ,

$$\begin{aligned} MR &= 8314 \text{ J/K kg-mole}, & A &= 6022 \times 10^{-23}, \\ T &= 293 \text{ K and} & \mu_a &= 17.9 \times 10^{-6} \text{ Ns/m}^2 \end{aligned}$$

giving $K = 0.6 \times 10^{-15} \text{ m}^3/(\text{particle} \cdot \text{s})$ (20.33)

Ranges of size distribution and the other matters that influence coagulation result in considerable variations being found in observed values of the coagulation coefficient.

There is a further problem that limits the applicability of this analysis; not only has it taken no account of the differing sizes of particles, K changes as the agglomerates grow larger. A somewhat more sophisticated approach concentrates on one size range at a time and considers the appearance of particles of that size by agglomeration of smaller particles. Additionally, their progression out of the size range as they continue to grow should be taken into account. Let us assume, for the sake of explanation, that diameters are additive. (Actually, we should use particle volume rather than diameter.) Then, for example, particles of size 10 microns can appear by coagulation of smaller particles. If we employ subscripts to denote the size of particles, then

$$6_1 \quad \text{and} \quad 6_9 \quad \Rightarrow \quad 6_{10}$$

i.e. 6 (1 micron particles) agglomerating with 6 (9 micron particles) yields 6 (10 micron particles). Similar examples are

$$3_2 \quad \text{and} \quad 3_8 \quad \Rightarrow \quad 3_{10}$$

$$5_3 \quad \text{and} \quad 5_7 \quad \Rightarrow \quad 5_{10}$$

$$3_4 \quad \text{and} \quad 3_6 \quad \Rightarrow \quad 3_{10}$$

$$2_5 \quad \text{and} \quad 2_5 \quad \Rightarrow \quad 2_{10}$$

Totals: 38 particles collide to yield 19 particles of size 10 microns.

In each of these groups, the collisions result in the number of particles being halved. Using the concept of coagulation coefficient and the form of equation (20.31), we can write that the rate of *formation* of particle size k (10 microns in our example) is:

$$\frac{dn_k \text{ (formation)}}{dt} = \frac{1}{2} \sum_{i=1}^{k-1} K_{ij} n_i n_j \quad \frac{\text{particles formed}}{\text{m}^3 \text{ s}} \quad (20.34)$$

where K_{ij} is the particular coagulation coefficient for colliding particles of size i and j and n_k is the number of particles of size k that are formed from the collisions of n_i particles (size i) and an equal number of n_j particles (size j).

However, while all of this is going on, particles of size k are *disappearing* because further coagulation causes them to grow out of that size range. This can occur by each particle size k agglomerating with another particle of *any* size. In this case, we count the number of k size particles that are disappearing rather than being formed. Hence, we no longer require the factor of 1/2 and can write:

$$\frac{dn_k \text{ (disappearance)}}{dt} = - \sum_{m=1}^{\max} K_{km} n_m n_k \quad \frac{\text{particles lost}}{\text{m}^3 \text{ s}} \quad (20.35)$$

where max = largest size of particle to be considered relevant to the processes of coagulation

As n_k has a single value at any given time, t , it can be brought outside the summation sign.

Combining equations (20.34) and 20.35) gives the overall rate of change of concentration of particle size k :

$$\frac{dn_k}{dt} = \frac{1}{2} \sum_{i=1}^{k-1} K_{ij} n_i n_j - n_k \sum_{m=1}^{\max} K_{km} n_m \quad \frac{\text{particles}}{\text{m}^3 \text{ s}} \quad (20.36)$$

This result was reported by Chung (1981) but attributed to Smoluchowski. Even more complex analyses have been conducted for liquid aerosols involving not only particle size changes by coagulation but also by evaporation. These are of relevance in meteorology and surface atmospheric pollution.

20.2.6. Impingement and re-entrainment

The phenomena of impingement and re-entrainment become significant only in situations of high velocity or excessive turbulence such as may occur in and around ventilation shafts or fan drifts. In such cases, the momentum gained by some dust particles may cause them to be ejected from

the curved streamlines of eddies and impinge on the walls or other solid objects. Deposition by impaction of the particles on the walls can then occur. This is the principle employed in impact dust samplers such as the konimeter (Section 19.4.2.).

Impact deposition in mine airways is counteracted to some degree by re-entrainment in those same conditions of high velocity and turbulence. A particle on any surface and submerged within the laminar sublayer can be made to roll over the surface by viscous drag of the air when a sufficiently high velocity gradient exists across the sublayer. An accelerated rolling action may cause the particle to bounce until it momentarily escapes beyond the sublayer where capture by eddies can re-entrain it into the main airstream. Chaotic turbulence can have the same effect by transient thinning of the sublayer. The phenomena associated with these boundary layer effects are, again, influenced by Reynolds' Number and surface roughness. Re-entrainment can be analyzed by considering the drag and frictional forces on particles on or very close to solid surfaces (Ramani and Bhaskar, 1984).

20.2.7. Computer models of dust transport

The earlier mathematical models developed to describe dust transport in mine airways were empirical in nature (e.g. Hamilton and Walton, 1961). The growing availability of digital computers since the 1960's, combined with a better understanding of aerosol behaviour, led to the development of mathematical models to simulate the behaviour of dust particles in mine ventilation systems (Bhaskar and Ramani, 1988). Such a model may be based on a form of the convective diffusion equation

$$\frac{dc}{dt} = E_x \frac{\partial^2 c}{\partial x^2} - u \frac{dc}{dx} + \text{sources} - \text{sinks} \quad \frac{\text{particles}}{\text{m}^3 \text{ s}} \quad (20.37)$$

where c = concentration (particles/m³) t = time (s)
 x = distance along the airway (m) u = air velocity (m/s)
 and E_x = turbulent dispersion coefficient in the x direction (m²/s)

This can be solved numerically between given boundary limits of time and distance (Bandopadhyay, 1982) to track the temporal variations of dust concentration along a mine airway. The "sinks" term is determined from the relationships given in the preceding subsections and, in particular, the effects of gravitational settlement, Brownian motion, eddy diffusion and coagulation. The "sources" must be defined as a dust production - time curve or histogram that characterizes the make of dust from all significant sources along the length of airway considered.

20.3. THE PRODUCTION OF DUST IN UNDERGROUND OPENINGS

The majority of dust particles in mines are composed of mineral fragments. Oil aerosols may become significant when drilling operations are in progress. Diesel exhaust particulates can also form a measurable fraction of airborne dust in those mines that utilize internal combustion engines. However, in this Section we shall concentrate on the manner and processes through which mineral dusts are formed. Although the primary means of controlling mine dusts are discussed in detail in Section 20.4 we shall introduce some of these, for particular operations, in this Section.

20.3.1. The comminution process

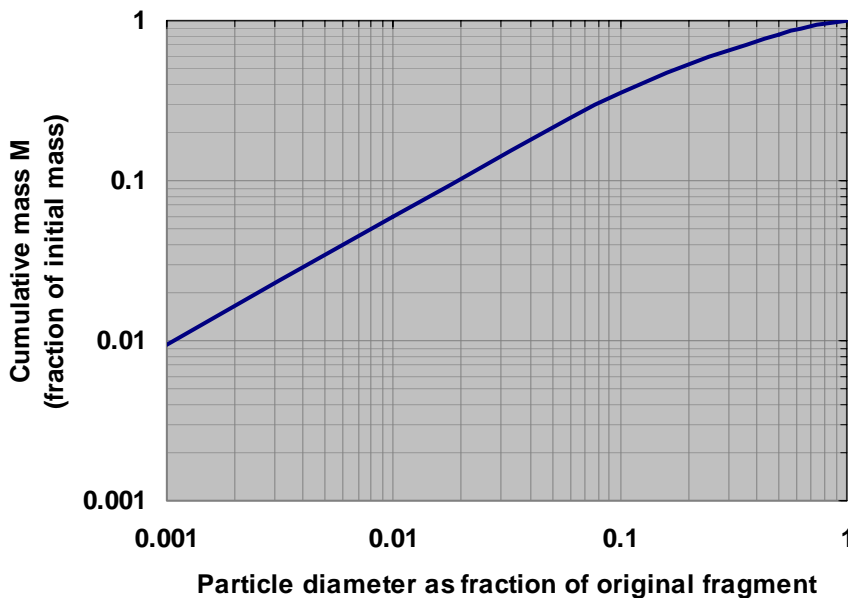
Mineral dusts are formed whenever any rock is broken by impact, abrasion, crushing, cutting, grinding or explosives. For any given material, the energy input required to break the rock is

proportional to the new surface area produced. As dust particles have a large surface area relative to their mass, it follows that any fragmentation process which produces an excessive amount of dust involves an inefficient use of energy. Before discussing specific operations that produce dust, a valuable insight into particles size distribution can be gained from a brief analysis of the comminution process.

Suppose a given brittle material is broken into fragments and the particles classified into a series of size ranges. Commencing with the mass of finest particles and progressively adding on the mass of each next coarser range, a table of cumulative "mass finer than" can be assembled. If this is plotted against particle diameter on a log-log basis (Figure 20.4) then a straight line is obtained for the smaller particles and curving over at larger sizes. The curve of Figure 20.4

follows an equation of the form
$$M = \left\{ 1 - \left[1 - \frac{x}{x_0} \right]^r \right\}^m \text{ kg} \quad (20.38)$$

- where x = particle diameter, (m) - we use x here, temporarily, in order not to confuse diameter with the differential operator, d
- x_0 = diameter of the initial fragment (m)
- M = cumulative mass finer than size x (kg)
- r is a constant that depends upon the particular comminution process and
- m is a characteristic of the material having values in the range 0.5 to 1 and varying only slightly with the method of comminution. (This is known as the Gaudin Meloy Schuhmann equation (Marshall, 1974; Gaudin and Meloy, 1962).)



If the term $[1 - x/x_0]^r$ is expanded by the binomial theorem, then for $x \ll x_0$

$$M = r \left[\frac{x}{x_0} \right]^m \text{ kg} \quad (20.39)$$

For dust particles, x is certainly very much smaller than x_0 . Equation (20.39) quantifies the straight line portion of Figure 20.4 and has been shown to hold for particle sizes down to 0.01 microns (National Research Council, 1980).

Figure 20.4 Typical size distribution graph of "cumulative mass finer than" against particle size.

Let us now try to find a means of determining (i) the mass and (ii) the number of particles in each size range:

(i) *mass*

Consider the mass, dM , of particles contained within the incremental range x to $x + dx$. Differentiating equation (20.39) gives

$$dM = \frac{r m}{x_0^m} x^{m-1} dx = C x^{m-1} dx \quad \text{kg} \quad (20.40)$$

where C = constant for that particular material, process and initial size.

Now let us take a finite size range from, say, $D/10$ to D (e.g. 0.5 to 5 microns). Then integrating equation (20.40) between those limits gives the corresponding mass for that range.

$$M(D/10 \text{ to } D) = \frac{C}{m} [x^m]_{D/10}^D = \frac{C}{m} D^m \left[1 - \frac{1}{10^m} \right]$$

$$\text{or } M(D/10 \text{ to } D) = \text{constant} \times D^m \quad (20.41)$$

As m is always positive this equation shows that the mass in each size range increases with particle diameter. In practice this means that only a small part of the total rock broken will be produced as dust particles. For coal, values in the range 5 to 9 kg per tonne (0.5 to 0.9 percent) of particles less than 7 microns have been reported (Qin and Ramani, 1989). However, *only a tiny fraction of this will become airborne as respirable dust.*

(ii) *number of particles*

Returning to our infinitely small increment of particle size range, x to $x + dx$, the volume of each particle is $\pi x^3 / 6$. If the material is of density, ρ , then the mass of each particle becomes

$\rho \pi x^3 / 6$. For dn particles in that range, the total mass becomes

$$\frac{\rho \pi x^3}{6} dn = dM = C x^{m-1} dx \quad (\text{from equation (20.40)})$$

$$\text{giving } dn = C' x^{m-4} dx \quad \text{particles} \quad (20.42)$$

where C' = constant for that material, process and initial size.

Integrating over the finite size range $D/10$ to D gives

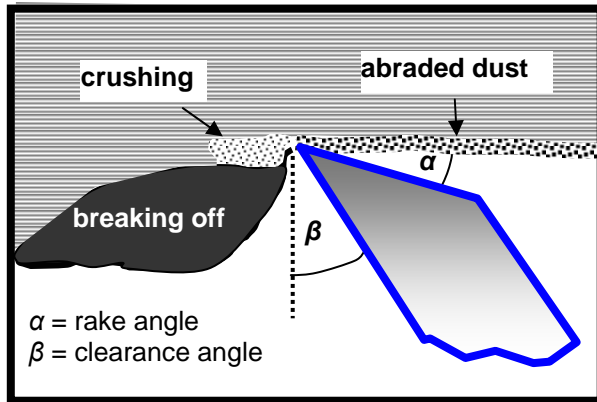
$$n(D/10 \text{ to } D) = \frac{C'}{m-3} [x^{m-3}]_{D/10}^D = \frac{C'}{m-3} D^{m-3} \left[1 - \frac{1}{10^{m-3}} \right]$$

i.e

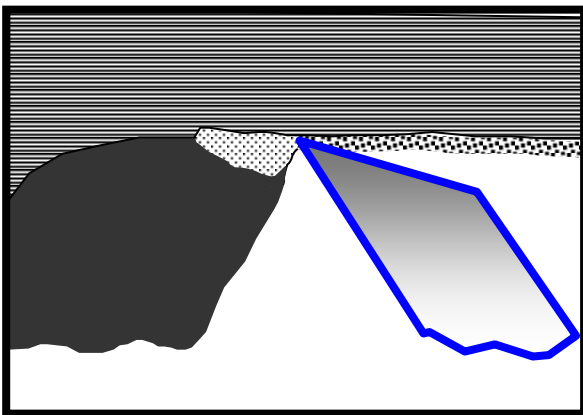
$$n(D/10 \text{ to } D) = \frac{\text{constant}}{D^{3-m}} \quad \text{particles} \quad (20.43)$$

As m lies in the range 0.5 to 1.0, this shows that *the number of particles rises logarithmically as the particle diameter decreases.*

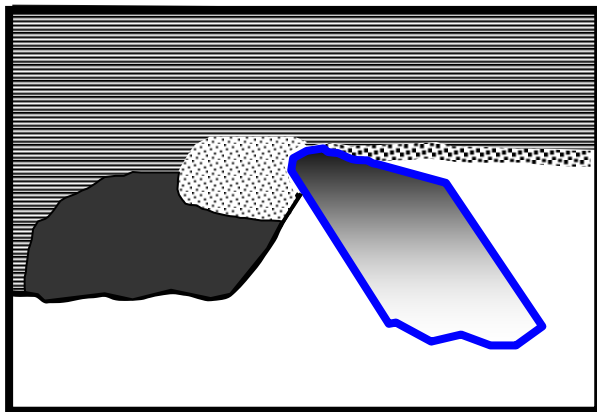
Equations (20.41) and (20.43) indicate that in any rock breaking process, the bulk of mass will appear as larger fragments. However, the number of fine dust particles produced may be enormous. Fortunately, most of those particles remain attached to the surfaces of larger fragments. The degree to which dust particles are dispersed into the air would seem to depend upon the nature of the rock as well as the comminution process. For brittle materials, the fragmentation becomes more 'explosive' in nature; the resulting surface vibration causes an enhanced dispersion of dust particles into the air. Hence, although comminution of softer materials may generate more dust particles, a greater proportion of those will remain adherent to the surfaces of larger particles and will not become airborne. The production of *airborne respirable dust* has been reported in the range 0.2 to 3.0 grams per tonne (Qin, 1989; Knight, 1985).



(a) Shallow cut



(b) Deep cut



(c) Blunt pick

Figure 20.5 A zone of pulverized rock forms ahead of a cutter pick.

20.3.2. Mechanised mining

Machines that break rock from the solid have the potential to be prolific sources of dust. These include longwall power loaders, continuous miners, roadheaders, tunnelling machines, raise borers and drills. Figure 20.5(a) illustrates a pick point acting against a rock face. Compressive forces induce a zone of pulverized material immediately ahead of the pick point. As the pick moves forward into that zone, the resultant wedging action produces tensile failure along a curved plane - a chip is broken away. The process is repeated continuously as the pick advances. The majority of the pulverized material is abraded onto the surfaces of the rock face and the chip. The amount of dust produced at the tensile failure plane itself may be quite small in homogeneous brittle material and is influenced by the presence of preformed dust in natural cleavage planes. However, the explosive nature of that tensile failure is a major factor in determining the amount of dust that is projected into the air.

A machine that takes a greater depth of cut will require higher torque and may be subject to greater vibration and bit breakage. However, a comparison of Figures 20.5(a) and (b) indicates that more of the broken material will be in the form of chips and, hence, the amount of dust produced in terms of *grams per tonne* will be reduced. The *specific energy* (per tonne mined) will also fall. Figure 20.5(c) shows that the greater area of contact given by a blunt pick will create additional dust in the pulverized zone. If such wear causes a significant reduction in the rake angle (Figure 20.5(a)) then the back of the bit will rub against the newly formed face, absorbing additional energy and producing further pulverized rock. Furthermore, as the clearance angle reduces, the chip may not be ejected efficiently but remain in place to be crushed against the unbroken rock. The design of a rock cutting bit is a compromise between the efficiency of cutting (energy absorbed per tonne), wear characteristics and dust production. Considerable diversity of opinion exists on preferred bit geometries for given machines and rock types.

Another factor that influences the proportion of dust which becomes airborne is the speed at which the pick moves. For any given depth of cut, an increased speed results in greater rate of comminution and, hence, dust production. Additionally, movement of the cutter drum causes a higher relative velocity to be induced between the local airstream and the material on the face (or fragments broken from the face). This assists in entrainment of dust particles into the air (Section 20.2.5.). The effect of pick speed on airborne dust is illustrated on Figure 20.6.

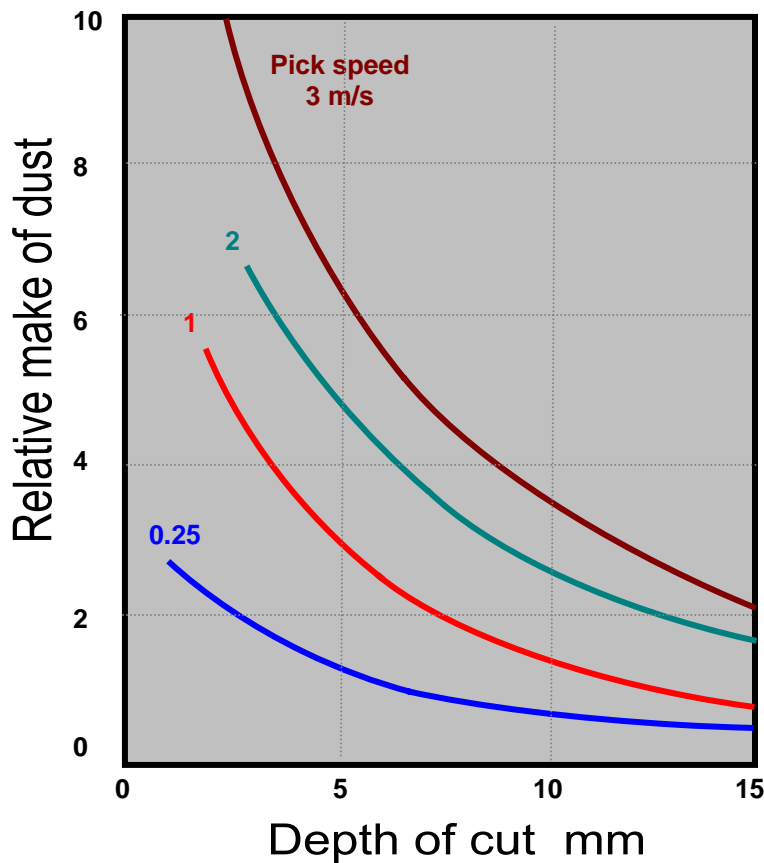


Figure 20.6 An illustration of the effects of pick speed and pick depth of cut. Actual dust makes also depend on other factors including sharpness of picks, effectiveness of dust suppression and air velocities around the cutting head.

20.3.3. Supports

Crushing of roof and floor strata by roof supports may liberate significant amounts of dust when the support is moved. This can be a particular problem on mechanized longwall faces that are equipped with powered hydraulic supports. As setting and yield loads of the supports increase so, also, does the amount of dust produced. The repeated lowering and raising of these supports can give a near continuous source of dust on longwall faces. Unless roof coal is left, this may be high in quartz content. The effect can be minimized by using wide-web roof beams or cushioning materials. Sheets of flexible material linking adjacent canopies have also been used to mitigate against roof dust.

20.3.4. Blasting

Drill and blast remains the predominant method of mining in metal (hardrock) mines. The peak concentrations of dust and gases (Section 11.3.4.) that are produced by the larger blasts are usually too high to be diluted effectively by the normal ventilating airflow. This necessitates the mine, or part of the mine, being evacuated of personnel for a *re-entry period* during and after the blast. The length of the re-entry period can vary from half an hour to several hours for stoping areas, dependent upon the layout of the ventilation network and the velocities of the air. This is a classical example of isolating personnel from the dust.

The amount of dust produced depends upon a number of factors including

- the mining method
- the type of rock
- the choice of explosive
- the charge density and drilling pattern and
- the type of stemming.

Blasts that eject the fragmented material into an air space (e.g. open stoping) will tend to produce sharper but shorter lived peaks of dust than caving techniques. However, the latter may result in

more pulverized material capable of being entrained into the airstream during subsequent loading and transportation operations. Water ampoules have been employed as stemming in an attempt to reduce dust emissions from blasting operations.

Another technique is to place very fine but high capacity water sprays (fog machines) upwind of the blast before and during the re-entry period. The combination of increased humidity and fine water droplets assists in the agglomeration and sedimentation of dust particles. Spraying the muckpiles produced by blasting is advisable before loading commences.

Secondary blasting also produces short peaks of dust concentration. This is yet one further reason for employing methods of mining that minimize the need for secondary blasting.

20.3.5. Loading operations

This is another part of some mining cycles that can produce a great deal of dust whether the loading operations are carried out by slushers, load-haul-dump (LHD) vehicles or loading machines in headings. The dust arises from a combination of particles produced previously from the mining process and held within the muckpile, and those that are generated by further comminution during loading.

In addition to adequate (but not excessive) airflows, the primary means of combatting dust from loading operations are water sprays and ensuring as little disturbance as possible to the loaded material. The air velocity should not be less than 0.5 m/s at loading points. Abrasion of the floor by heavy slusher buckets should be minimized. It is preferable to employ lighter buckets in tandem operating at a speed of some 0.6 m/s (Sandys and Quilliam, 1982). Spray bars should be located at intervals along slusher paths and, particularly, at points of transfer between buckets.

Muckpiles in headings should be sprayed with water continuously or frequently during mucking operations except where hygroscopic minerals inhibit the copious use of water. In hot mines, pre-chilling of this water produces cooling as well as dust suppression (Section 18.3.5.2.). Steam injection into muckpiles and the addition of wetting agents into the water has also been found to be beneficial in some cases (Knight, 1985). Exhaust auxiliary ventilation is preferred for dusty operations in headings, employing a force overlap, if necessary, to deal with gas emissions at the face (Section 4.4.2.).

The skill of the driver of an LHD can have considerable influence on dust production. Choosing the best point to insert the bucket into the muckpile will result in filling the bucket with a minimum number of thrusts and with least disturbance to the material. Similarly, at the dump point, the muck should be tipped gently and not dropped from a height. This should also be borne in mind during the design of tipping operations from rail-mounted dump cars. Cones and chutes at dump points should be designed to minimize impact forces on tipped material.

20.3.6. Transportation and crushing

Dust is produced throughout most mineral transportation routes, including conveyors, transfer points, bunkers, skips, airlocks and vehicular traffic. Dust on the surfaces of conveyors may be re-entrained into the air due to vibration of the belt as it passes over rollers. Spillage returning on the bottom belt, if not cleared, will generate dust as the material is crushed against rollers. Similarly, an excessive use of water can result in dust adhering to the belt surface. This may subsequently be deposited under the conveyor during the return journey of the bottom belt. Belt scraper devices or brushes at the drive heads should be properly maintained and all accumulations of debris or dust should regularly be cleaned from under the conveyor and at return rollers. Conveyor structure should be inspected routinely and attention paid to damaged idlers and centering devices.

Vehicle arrestors on rail transportation systems should incorporate deceleration devices in order to avoid impact loads on either the vehicles or the transported material. Tracks should be adequately maintained and not allowed to develop sudden changes in direction or gradient.

The mineral transportation routes and mine ventilation system should be planned together in order to avoid, wherever possible, minerals being transported through an airlock. The high velocities that can occur over belt conveyors at airlock leakage points can cause excessive production of dust. This can be minimized by employing side plates and attaching a length of flexible material (such as old belting) on the conveyor discharge side of the airlock so that it drags over the surface of the conveyed material.

Unless the mineral is hygroscopic, it should be kept damp throughout its transportation through the mine. Bunkers and, wherever possible, conveyor transfer points and stage loaders should be shrouded and fitted with internal sprays. It is also useful to duct the air from such shrouds directly into return airways. Sprays or dribbler bars onto conveyors some 5 to 10 m before a transfer point are often more effective than sprays actually at the transfer point itself.

Ore passes in metal mines should avoid lengthy segments of free fall. Air leakage at dump and draw points should be *into* the ore pass and, hence, pull dust laden air away from personnel. This can be arranged by an opening into the ore pass and connected either directly or via ducting to a return airway. If this is not practicable then dusty air drawn by a fan from an intermediate point in an ore pass can be filtered and returned to the intake system.

Crushers in any mine are prolific sources of dust. Here again, sprays may be used on the material before, during and after the crushing process. This is another situation where it is particularly valuable to draw air from the crusher enclosure and filter it.

20.3.7. Workshops

Aerosols produced in underground workshops are likely to occur as oil mists, diesel particulate matter and welding fumes. The latter may be handled by exhaust hoods extracting air from welding bays and directing it into a return airway. Indeed, all of the airflows through workshops should, preferably, pass into return airways. The general arrangements for diluting and removing airborne contaminants from workshops are discussed in Section 9.3.5.

20.3.8. Quartz dust in coal mines

The availability of instrumentation that can discern the quartz content of mine dusts within each of a range of particle sizes (Section 19.4.7.) has led to the observation that airborne dust in coal mines often has a quartz content that is significantly higher than that of the coal seam being worked. Furthermore, the percentage of quartz becomes particularly high in the finer sizes including the respirable range (Ramani et al, 1988; Padmanabhan and Mutmansky, 1989). Coupled with the special danger to health of quartz dust, this has led to research aimed at discovering the causes of such anomalous appearances of quartz in airborne dusts of coal mines.

There would appear to be at least two explanations. First, roof and floor strata usually have a higher quartz content than the coal seam. Hence any fragmentation of those strata will cause emissions of quartz dust. This can occur by rock-winning machines cutting into the roof or floor, cross-measures drilling for roof-bolting or other purposes, development drivages out of the seam or exceeding the height of the seam, hydraulic roof supports and fracturing of roof or floor strata.

A second, less obvious, cause of the apparently anomalous percentages of quartz in the dust of coal mines is hypothesized to be the different comminution characteristics of coal and quartz (Section 20.3.1.). Fragmentation of the stronger and more brittle quartz minerals may result in a greater proportion of that dust being ejected into the air than is the case for coal. The greater degree of entrainment would favour the finer particles.

20.4. CONTROL OF DUST IN MINES

The initial decisions that affect the severity of dust problems are made during the stages of design and planning for the mining of any geological deposit. The methods of working, rate of mineral production and equipment chosen all influence the amount of dust that is generated and becomes airborne. The layout of the mine, sizes and numbers of airways, and the efficiency of the ventilation system dictate the rate at which airborne contaminants, including dust, are diluted and removed from the mine.

For an existing mine, there are four main methods of controlling the production, concentration and hazards of airborne dust:

- **Suppression** - the prevention of dust becoming airborne
- **Filtration and scrubbing** - the removal of dust from the air
- **Dilution by airflow** , and
- **Isolation** - separation of personnel from the higher concentrations of dust.

In general, good management and housekeeping at a mine assist greatly in maintaining control of the dust problem. These measures include planned maintenance schemes for equipment, quantitative ventilation planning, cleaning up spillage, rock debris and local accumulations of dust, and adequate supervision of work practices.

20.4.1. Dust suppression

It is difficult and often expensive to remove respirable dust from the air. Hence, every attempt should be made to prevent it from becoming airborne in the first place. Methods of achieving this are known collectively as *dust suppression* and are discussed in this section.

20.4.1.1. Pick face flushing and jet-assisted cutting

Figure 20.5 gives a visual impression of how a rock face is pulverized in advance of a moving cutter pick. Pick face flushing involves directing a jet of water at the pick point during the cutting process. This has been found to give markedly improved dust suppression when compared to conventional water sprays on the drums of shearers, continuous miners or tunnelling machines. The water that feeds each jet can be channeled through conduits drilled in the bit holder and via a phasing valve that activates the jet only while the bit is cutting rock. Water filters are required to prevent blockage of the nozzles. A further advantage of pick face flushing is that the streak of incendiary sparks that often appears behind the pick in dry cutting is quenched. Hence, the incidence of frictional ignitions of methane is reduced greatly. Interlock switches may be employed to ensure that the machine cannot operate without the dust suppression water being activated.

A number of researchers have investigated the extension of pick face flushing to much higher water pressures, not only to further improve dust suppression but also in an attempt to produce a higher efficiency of rock cutting. The use of high pressure water jets alone, with or without the addition of abrasive particles, has had only limited success as a practical means of mining. However, combining the mechanism of cutter picks with high pressure water jets directed at the pick point has led to significant improvements in machine performance and the extension of mechanized mining to much harder material that, previously, could be mined only by drill and blast techniques. This technique is known as *jet assisted cutting*.

In addition to environmental enhancements, jet assisted cutting permits the same rate of comminution with reduced loading on the cutter pick. This results in a significant reduction in wear and, hence, less production time lost because of picks having to be changed. Furthermore, the total specific power (per tonne mined) required by the combination of a high pressure water pump and the cutting machine can be less than that of a conventional machine.

The benefits of jet assisted cutting are attainable by increasing the water pressure but reducing the nozzle size in order to keep the flow rate no greater than that employed in conventional pick face flushing. This can be important in hot mines or where floor strata react adversely to water. However, it has been reported that there is little apparent improvement in levels of airborne dust until the water pressure attains some critical value (Taylor et al, 1988). This would appear to be in the range 10 to 15 MPa for cutting coal. After the critical water pressure is attained, a dramatic reduction in airborne dust can be expected. However, this levels out again at water pressures in excess of 20 MPa. Indeed, if the velocities of the jet and resulting spray are too high then re-entrainment can exacerbate dust concentrations. Work continues on the preferred location of the jet. Distances as small as 2 mm between the nozzle and the pick point have been suggested (Hood et al, 1991).

The environmental and operational benefits of jet assisted rock cutting arise from at least seven mechanisms (Hood, 1991).

- (a) The pulverized rock immediately ahead of the pick point is wetted before it has an opportunity to become airborne.
- (b) The cooling action of the jet reduces wear: the bits remain sharp for significantly longer periods of time and bit breakage is less frequent.
- (c) Impact of the high velocity jet will produce an aerosol of very fine water droplets around the cutting head, thus enhancing the agglomeration and capture of airborne dust particles.
- (d) The washing action of the high-energy jet removes the cushion of pulverized material quite efficiently. This allows the pick point to act on a much cleaner surface. The effect of a cushion of pulverized rock is to distribute the force exerted by the pick over a broader front, i.e. similar to that of a blunt pick, Figure 20.5(c). It is to be expected that the total amount of finely crushed rock would be reduced.
- (e) Penetration of the water into natural cleavage planes in the material and ahead of the mechanical effect of the bit assists in pre-wetting dust particles that already exist within those planes.
- (f) Frictional ignitions of methane are virtually eliminated.
- (g) The total specific energy required for the rock cutting process may be reduced.

20.4.1.2. Water infusion

A technique of dust suppression that has been employed by some coal mining industries since the 1950's is pre-infusion of the seam by water, steam or foam. One or more boreholes are drilled into the seam in advance of the workings through which the fluid is injected. The migration of water through the natural fracture network of the coal results in pre-wetting of included dust particles. The success of the method is dependent upon the permeability of the seam and the type of coal-winning equipment employed. Good results have been reported where coal ploughs are used - these relying more upon coal breakage along natural cleavage than the cutting and grinding action of shearers or continuous miners (Heising and Becker, 1980).

In practice, some in-situ experimentation is usually necessary to determine the optimum injection pressure and flowrate, and the time period of injection. Water pressures in the range 2 to 34 MPa have been reported with water volumes of 7 to 20 litres per tonne in South African coal mines (Sandys and Quilliam, 1982). Best results are obtained at fairly modest pressures but applied over as long a period as possible. British experience in coals of limited permeability indicated water pressures of 1.5 to 2.5 MPa and flowrates of 0.2 to 2 litres/min. If too high a pressure is used then the water flows preferentially along major planes of weakness. Hydrofracturing may

occur, resulting in weakened roof conditions during mining and, possibly, backflow along bed separation routes to give water inflows at the current working faces. Water infusion is not recommended in areas of weak roof/floor strata or in the proximity of faults or other geological anomalies. Steam and wetting agents have been employed in attempts to improve pre-saturation of the zone. Water infusion must also be expected to influence the migration of strata gas (Section 12.3.2.3.). Holes drilled initially for in-seam methane drainage may subsequently be used for water infusion (Stricklin, 1987).

20.4.1.3. Wetting agents, foams and roadway consolidation

Worldwide experience of *surfactants* used as wetting agents in dust suppression water has been highly variable. The technique has been employed since at least 1940 (Hartman, 1940). In addition to the use of wetting agents to enhance the effects of water infusion, they may be employed to improve the performance of sprays and also, at sufficiently high concentration, to produce a *foam* around a rock fragmentation process.

Rocks vary considerably in their wettability characteristics. If surfactants added to muckpile sprays are to be effective then they must be at a high enough concentration to cause penetration of the fragmented material within an acceptable time period (Knight, 1985). The potential effects of such concentrations on mineral processing should be considered carefully. Wetting agents added to sprays are considered to have three beneficial effects. First, the reduced surface tension allows greater atomization of the water - the droplets are smaller and greater in number, hence, improving the probability of capturing dust particles (Section 20.4.2.1.). Secondly, the existence of a liquid coating on dust particles will improve the chances of coagulation when two particles collide. Third, the molecular structure of surfactants tends to counteract electrostatic forces that may keep particles apart (Wang, 1991).

If a wetting agent is in sufficient concentration within a spray directed at a rock cutting device then a foam can be formed that enshrouds the comminution process. This assists in coating the fragments with a wetting fluid and in inhibiting entrainment of the dust into the air. Again, this approach has met with mixed success (Bhaskar, 1991). It also interferes with ventilation of the cutting head and should be used with caution in gassy conditions.

Accumulations of dust on roadway floors used for travelling in both underground and surface mines can become airborne when disturbed by traffic. *Roadway consolidation* involves the use of water, hygroscopic salts and binders to encapsulate the dust and maintain the floor in a firm but moist state. Flakes of calcium chloride or magnesium chloride may be employed with lignin sulphonate as a binder. The process involves raking and levelling the surface dust, and spraying it lightly with water until it is wetted to a depth of some 2 to 3 cm. The addition of a wetting agent may be necessary. The total amount of water required can be of the order of 40 litres per m². Free-standing pools of water should be avoided. The hygroscopic salt should be spread evenly at a rate that depends upon the mean humidity of the air. For flake calcium chloride this will vary from about 3.8 kg/m² at a relative humidity of 40 percent down to 0.1 kg/m² for a relative humidity of 90 percent. It is advisable to apply three quarters of the salt during the initial application and the remainder about one week later. The treatment will normally last for about six months although re-spraying with water may be required after three months. Sodium chloride (common salt) will be effective while the relative humidity remains above 75 per cent. In all cases, care should be taken against corrosion of equipment and, in particular, within the vicinity of electrical apparatus.

20.4.2. Removal of dust from air

The larger dust particles will settle out by gravitational sedimentation in the air velocities typical of most branches in a mine ventilation system. Unfortunately, the more dangerous respirable particles will effectively remain in suspension. Removing these from the air for large flowrates can be expensive. The choice of a dust removal system is dictated by the size distribution and

concentration of particles to be removed, the air flowrate and the allowable dust concentration at outlet. The size of any unit is governed primarily by the air volume flow to be filtered. Operational costs can be determined from the product of the pressure drop and air flowrate through the unit, pQ (Section 5.5.), and the means of supplying and filtering water in the case of wet scrubbers. Where high efficiency is required for large flowrates over a wide range of particle sizes such as the emergency filters needed on nuclear waste repositories (Section 4.6.), two or more types of filters may be arranged in series, each taking out progressively smaller particles. This prevents the finer filters from becoming clogged quickly and, hence, prolongs the life of the system before cleaning or renewal of filters becomes necessary.

The efficiency of any dust removal facility, η , may be expressed either in terms of number of particles per m^3 of air:

$$\eta_p = \frac{\text{No. of particles in } /m^3 - \text{No. of particles out } /m^3}{\text{No. of particles in } /m^3} \quad (20.44)$$

or in terms of mass of particles:

$$\eta_m = \frac{\text{Mass of particles in } /m^3 - \text{Mass of particles out } /m^3}{\text{Mass of particles in } /m^3} \quad (20.45)$$

In both cases, it is usual to further restrict the count of particles or mass to a specified size range. Hence, for protection against pneumonconiosis, it is preferable to employ equation (20.45) for respirable particles only, i.e. less than 5 microns equivalent diameter.

Devices to remove dust from air may be fitted to other pieces of equipment such as rock cutting machinery, along transportation routes, within ventilation ducting or as free-standing units to filter dust from the general airstream. In this section, we shall discuss principles of the devices that are most commonly employed to reduce concentrations of airborne dust in mine atmospheres, namely, water sprays, wet scrubbers and dry filters or separators.

20.4.2.1. Water sprays

Water is by far, the most widely used medium for conditioning mine air, whether it be for cooling (Section 18.3), dust suppression or dust filtration. Open sprays can also be employed to direct, control or induce airflows in order to protect machine operators from unacceptable concentrations of dust (Section 20.4.4.).

The important parameters governing the efficiency of a spray can be highlighted through an analysis of the capture of dust particles by water droplets. Consider Figure 20.7 which illustrates air passing over a water droplet with a velocity *relative to the droplet* of u_r . The streamlines of air bend around the droplet. However, the inertia of dust particles causes them to cross those streamlines. Particles that lie closer to the centre line of motion will impact into the droplet and be captured by it.

We can conceive a flow tube of diameter y from which all particles are captured while particles that are further from the tube centreline will be diverted around the droplet. The efficiency of capture by a single droplet, E , can be defined as the ratio of the cross-sectional areas of the capture tube to the facing area of the droplet:

$$E = \frac{y^2}{D_w^2} \quad (20.46)$$

where D_w = droplet diameter (m)

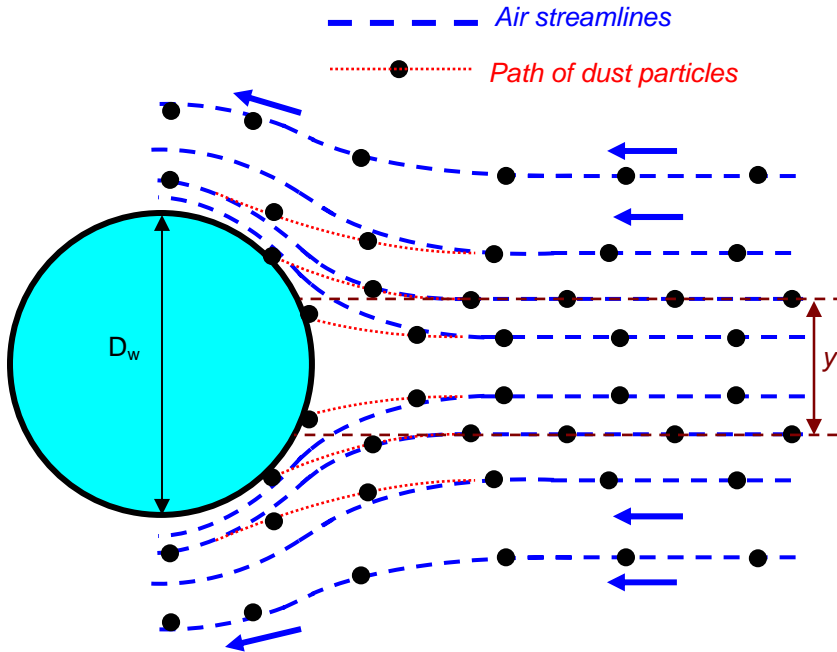


Figure 20.7 A water droplet of diameter D_w captures dust particles from a tube of air of diameter y . The relative velocity between the droplet and the air is u_r (m/s).

If there is a uniform dust concentration of n particles/ m^3 then the rate of capture of particles by one droplet of water is $n \times u_r \times$ area of capture tube

$$\frac{\text{particles}}{m^3} \frac{m}{s} m^2$$

or particles/s; that is:

$$\text{particles collected per droplet per second} = E n u_r \pi \frac{D_w^2}{4} \quad (20.47)$$

In order to maintain consistency with the definition of dust concentration that we are using here (particles/ m^3), it is preferable to restate this latter expression in terms of particles collected *per cubic metre* of air rather than particles captured per second. We can do this by dividing by the air flowrate Q (m^3/s).

Then rate of capture by *one* droplet (dn/dt = rate of change of dust concentration) becomes

$$-\frac{dn}{dt}(\text{one droplet}) = E n u_r \frac{\pi D_w^2}{4} \frac{1}{Q} \quad \frac{\text{particles}}{\text{droplet} \cdot s} \frac{s}{m^3} \quad \text{or} \quad \frac{\text{particles}}{\text{droplet} \cdot m^3} \quad (20.48)$$

where

$$t = \text{time (s)} \quad (\text{negative as concentration is falling}).$$

Now if water is dispersed in the spray at a volume flowrate of W (m^3/s) and the volume of each droplet is $\pi D_w^3 / 6$, m^3 , then the rate at which droplets are formed and pass through the spray is

$$\frac{W}{\pi D_w^3 / 6} = \frac{6W}{\pi D_w^3} \quad \frac{m^3 \text{ droplet}}{s \ m^3} = \frac{\text{droplets}}{s} \quad (20.49)$$

Multiplying by the particle capture for *one* particle, equation (20.48), gives the total rate at which particles are captured per cubic metre of air:

$$\begin{aligned} -\frac{dn}{dt}(\text{all droplets}) &= E n u_r \frac{\pi D_w^2}{4} \frac{1}{Q} \frac{6W}{\pi D_w^3} \quad \frac{\text{particles}}{\text{droplet} \ m^3} \frac{\text{droplets}}{s} \\ &= \frac{3}{2} E n u_r \frac{W}{D_w} \frac{1}{Q} \quad \frac{\text{particles}}{m^3 \ s} \end{aligned} \quad (20.50)$$

Now consider Figure 20.8. Dust particles and air pass each other effectively in counterflow with a relative velocity of u_r such that they move through a separation distance dx in time dt , i.e.

$$u_r = \frac{dx}{dt} \quad \frac{\text{m}}{\text{s}}$$

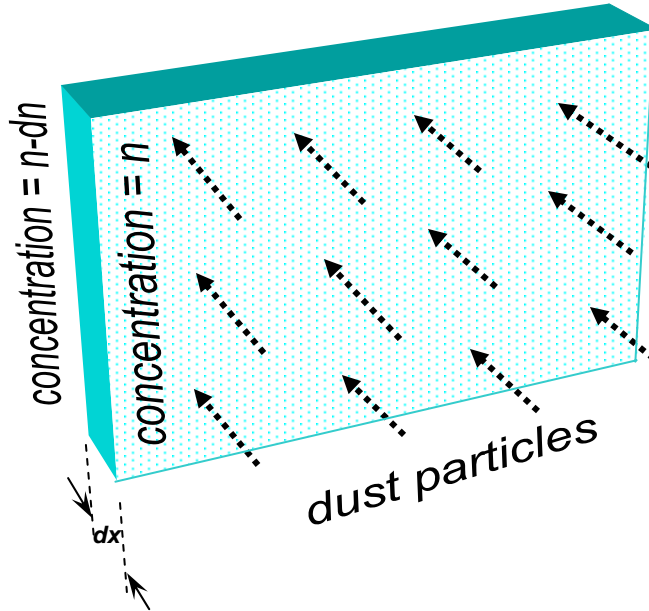


Figure 20.8 Section through a water spray. Dust particles and water droplets pass each other in counterflow with a relative velocity such that they move through a separation distance dx in time dt , over which the dust concentration falls by dn particles per m^3 of air.

During that time, the dust concentration changes from n to $n - dn$, i.e. the rate of change of dust concentration is $-dn/dt$ (particles/ m^3s).

But
$$-\frac{dn}{dt} = -\frac{dn}{dx} \frac{dx}{dt} = -\frac{dn}{dx} u_r \quad \frac{\text{particles}}{\text{m}^3 \text{s}}$$

Combining with equation (20.50) gives

$$-\frac{dn}{dt} = -\frac{dn}{dx} u_r = \frac{3}{2} E \frac{n}{D_w} u_r \frac{W}{Q} \quad \text{or} \quad dn = -\frac{3}{2} E \frac{n}{D_w} \frac{W}{Q} dx \quad \frac{\text{particles}}{\text{m}^3}$$

Integrating over the complete effective length of the spray, L (distance moved by particles plus distance moved by droplets (in counterflow) in the x direction), gives the total number of particles removed between the inlet concentration, N_{in} , and outlet concentration, N_{out} (particles/ m^3)

$$\int_{N_{in}}^{N_{out}} \frac{dn}{n} = -\frac{3}{2} \frac{E}{D_w} \frac{W}{Q} \int_0^L dx$$

$$\ln\{N_{out} / N_{in}\} = -\frac{3}{2} \frac{E}{D_w} \frac{W}{Q} L$$

$$\frac{N_{out}}{N_{in}} = \exp\left\{-\frac{3}{2} \frac{E}{D_w} \frac{W}{Q} L\right\} \quad (20.51)$$

Reference to equation (20.44) shows that the particle removal efficiency of the spray is given by

$$\eta_p = \frac{N_{in} - N_{out}}{N_{in}} = 1 - \frac{N_{out}}{N_{in}}$$

i.e.
$$\eta_p = 1 - \exp\left\{-\frac{3}{2} \frac{E}{D_w} \frac{W}{Q} L\right\} \quad (20.52)$$

Examination of this equation is most instructive in understanding the performance of sprays. The dust removal capacity of the spray increases with E , the **capture efficiency** of each droplet. To be precise, this depends upon the nature of the flow and the relative sizes of dust particles and water droplets. However, a coarse approximation for fully developed turbulence, based on work reported by Jones (1978), can be assessed as

$$E = 0.266 \ln(K) + 0.59 \quad (20.53)$$

over the range $0.2 < K < 4$ where \ln means natural logarithm and the dimensionless parameter K is:

$$K = \frac{u_r \rho D_p^2}{9 \mu D_w} \quad (20.54)$$

where ρ = particle density (kg/m^3)
 D_p = particle diameter (m)
 and μ = kinematic viscosity of the air (Ns/m^2).

In particular, the capture efficiency increases with the relative velocity between the dust particles and droplets (u_r), the diameter (D_p) and density (ρ) of the particles (these three governing particle inertia) and increases further as the water droplets become *smaller* (D_w).

Returning to equation (20.52) reinforces the fact that the overall efficiency of the spray improves with smaller water droplets. *A coarse spray of large water droplets will have very little effect on airborne respirable dust.*

A parameter of basic importance in equation (20.52) is the **water to air ratio** (W/Q). Values in the range 0.1 to over 2 litres of water per cubic metre of air have been reported. The lower values produce poor efficiency of dust capture. However, if too high a value is attempted then the concentration of droplets may become so large that coalescence occurs. The larger droplets then lead to decreased efficiency. A practical range of W/Q for sprays and wet scrubbers in mines is 0.3 to 0.6 litres/ m^3 . Tests on compressed air-powered atomizing nozzles have indicated an optimum W/Q value of 0.45 litres/ m^3 (Booth- Jones et al, 1984).

The last point to be gleaned from equation (20.52) is confirmation of the intuitive expectation that the spray efficiency is improved as the length (L) and, hence, time of contact between the air and the water droplets is increased.

In order to produce the finely divided sprays necessary to affect respirable dust, a number of methods are employed. The simplest technique is to supply high pressure water to the nozzles. Pressures of some 3000 to 4000 kPa applied across suitable nozzles give smaller droplets at

spray velocities high enough to cause air induction - surrounding dust laden air is drawn into the spray and thus improves the dust removal capacity of the unit. A variety of nozzle designs are available commercially. These control the shape as well as influencing the atomization of the spray. Full cone and hollow cone sprays have good air induction characteristics while fan shaped sprays are excellent at confining the dust clouds produced by shearers and continuous miners. Atomization is further improved in some nozzles by impinging the high velocity jet against an impact surface located facing and close to the orifice. Another arrangement causes the water to rotate rapidly around an orifice before ejection. In all cases, it is particularly important in mining that nozzle designs should mitigate against blockage from particles either in the water supply or (in the case of machine-mounted sprays), thrown forcibly against the jet from an external source.

Compressed air-assisted sprays can produce fine atomization with droplets in the respirable size range. The water feed is connected into the compressed air supply close to the nozzles. The water enters the compressed airstream either by its own applied pressure or by venturi action. It is advisable to insert non-return valves into the water line. The combination of very high turbulence at the nozzles and expansion of the compressed air into the ambient atmosphere produces fine droplets.

Compressed air-assisted sprays can be further enhanced by the addition of a sonic device to the nozzle (Schröder et al, 1985). Air expands through the nozzle into a facing resonator cup where it is reflected back to complement and amplify the initial shock wave at the mouth of the orifice. An intense field of sonic energy is focused in the gap between the nozzle and the resonator cup. Water droplets issuing from the nozzle and passing through the sonic field are further broken down to respirable sizes and, indeed, to submicron diameters. Similar effects can be achieved by high frequency oscillation of pairs of piezo-electric crystals.

A high degree of atomization can be achieved without high pipeline pressures through impingement devices. A free-standing "fog machine" of this type may consist of a stainless steel disc spinning at about 3000 rpm. A low pressure water supply is fed to the centre of the disc. Centrifugal action causes the water to flow outwards over the surface of the disc to impact at high velocity on a ring of stationary and closely spaced vanes around the perimeter. A fan impeller located on the upstream side of the disc projects the fog-laden airstream forward. The same principle is employed in wetted fan scrubbers and in some industrial humidifiers.

20.4.2.2. Wet scrubbers

As the name suggests, these are devices that also employ water to achieve dust removal. However, in this case the water streams (or sprays) and the airflow are controlled within an enclosure designed to maximize the parameters that improve the efficiency of dust capture (equation (20.52)). Wet scrubbers bring dust particles into intimate contact with wet surfaces and within a highly turbulent mixture of air, water droplets and dust. They have become popular for mining applications as they require less maintenance than most other dust filters and can achieve respirable dust capture efficiencies exceeding 90 per cent.

Here again, we shall restrict our discussion to the operating principles employed in the most common wet scrubbers. Many competing devices are marketed and manufacturers' literature should be consulted to match performance with required duties, and to compare capital and operating costs.

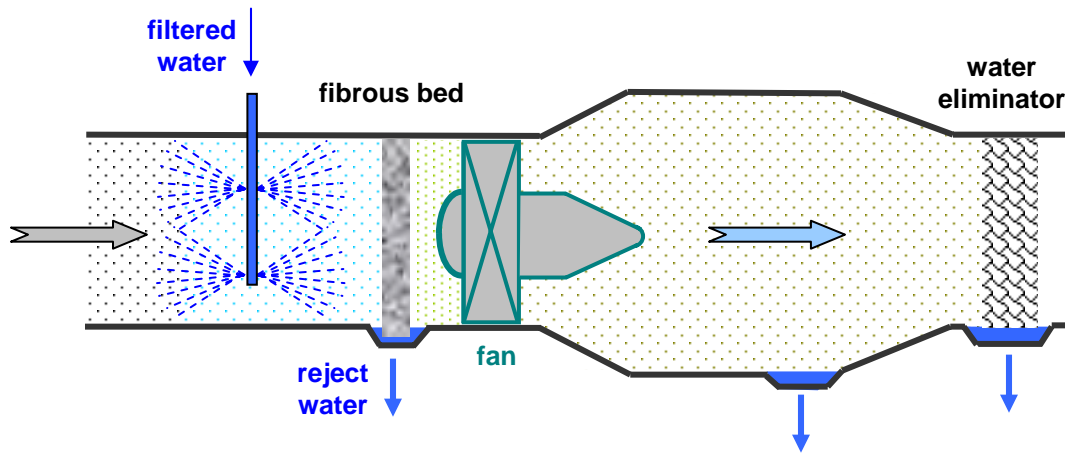


Figure 20.9 Fibrous (flooded) bed filter.

The *fibrous (or flooded) bed scrubber* illustrated on Figure 20.9 is one of the most widely used devices employed in mine dust collectors. Stainless steel or other non-corrosive material is used as the fibre material. Water is either admitted along the top of the fibrous bed and allowed to trickle downwards through it or, preferentially, the water sprayed directly into the air upstream from the fibrous bed. The air follows a tortuous path through the bed while the inertia of the dust particles causes them to strike and adhere to the wet fibres. The efficiency of dust removal increases with the fineness of the fibres, the thickness of the bed and the velocity of the air. This must be balanced by the resistance of the unit to airflow and, hence, the operating cost. Efficiencies exceeding 90 percent for respirable dust can be attained.

The dust laden water collects at the bottom of the fibrous bed from where it is drained, filtered and recycled. Arrangements must be made to remove the effluent sludge and to supply make-up water. In all cases, wet scrubbers can be supplied with chilled water to achieve simultaneous cooling and dust collection. Again, filtration within the chilled water cycle is necessary.

A water eliminator is required by most designs of wet scrubber in order to remove residual droplets of water. Several different systems of water elimination are available in practice including a second fibrous mat, a series of wavy or inclined plates, turning vanes to induce swirl into the air and, hence, throwing droplets outwards towards the duct walls, or an egg-tray arrangement. Here again, droplet removal is achieved by impingement.

Figure 20.10 illustrates the principle of the *wetted fan scrubber*. Sprays upstream and/or at the facing boss of a fan produce droplets that are mixed intimately and at high velocity with air across and around the fan impeller blades. The polluted water collects around the internal surface of the fan casing for removal and recycling. The addition of a fibrous bed downstream from the fan gives a powerful combination of dust collection devices. A disadvantage of wetted fan scrubbers is the pitting that may occur on the impeller blades and requiring additional fan maintenance. Designs employing centrifugal as well as axial fans have been developed. Wetted fan scrubbers are well suited to lower airflows and have an application as in-line dust collectors in auxiliary ventilation ducting.

The *venturi scrubber*, depicted on Figure 20.11, has no moving parts. Sprays are located upstream and/or at the throttled section of a venturi arrangement. Air velocities through the throat are typically in the range 60 to 120 m/s with a high degree of turbulent mixing. This encourages the impaction of dust particles into water droplets. Venturi scrubbers are compact, simple and rugged, and can reach efficiencies of more than 90 percent. However, it is costly in operating power and is suitable for limited airflows only.

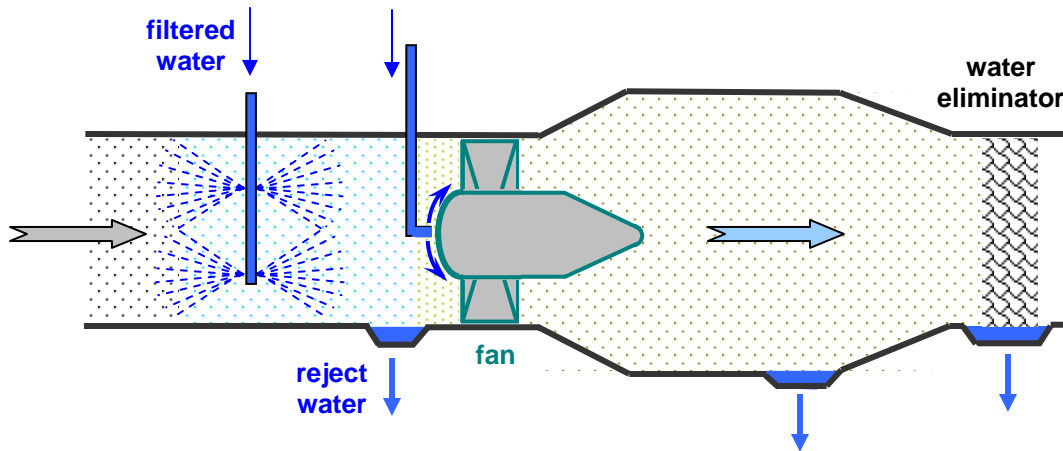


Figure 20.10 Wetted fan scrubber.

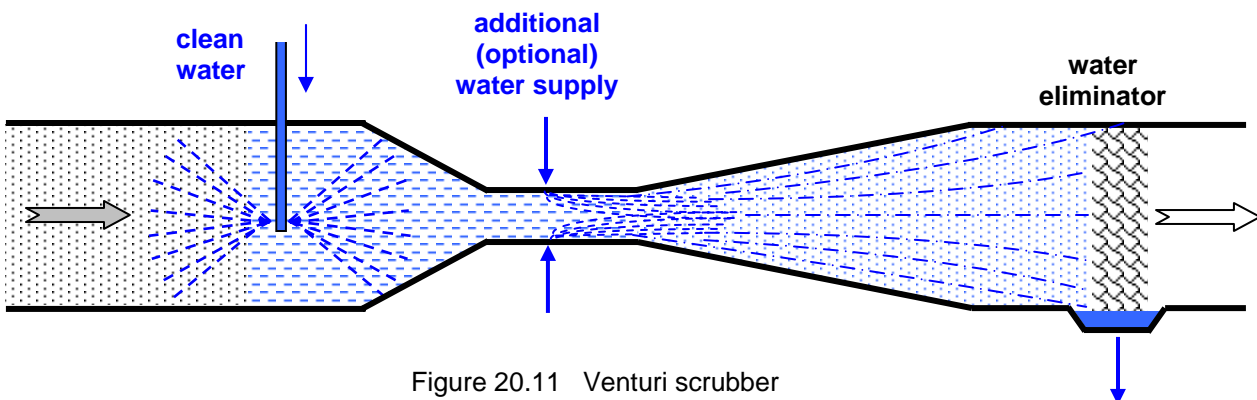


Figure 20.11 Venturi scrubber

The *flooded orifice scrubber*, illustrated on Figure 20.12, also has no moving parts and has the additional advantage that there are no nozzles that might become clogged. Air from the inlet duct flows outwards beneath a lip that is submerged in water. Movement of the air causes extreme agitation of the water and entrainment of droplets. Collection efficiencies of more than 80 percent can be achieved with this system.

The preferred location for a dust collection device is as close as practicable to the source of the dust. The types of wet scrubbers outlined in the previous paragraphs are suitable as free-standing units or within ventilation ducts. However, attempts to attach them to coal or rock winning machines have shown them to be somewhat bulky for that application and insufficiently robust to withstand the rigours of a working face. A device that met increasing favour for shearers and continuous miners through the 1980's was the simple *high pressure spray fan or induction tube* (Jones, 1978; Sartaine, 1985; James and Browning, 1988; Jayaraman et al, 1989). This is illustrated by Figure 20.13 and consists of a water jet spraying into a tube of some 100 mm diameter. The water is supplied at pressures in the range of 6 to 12 MPa through a nozzle of about 1.5 mm diameter. The momentum of the fine droplets induces an airflow through the tube and is very effective in removing dust. A single spray within a relatively small tube appears to be more effective than multiple nozzles within a larger induction tube. Furthermore, hollow cone sprays give a better performance than solid cone sprays.

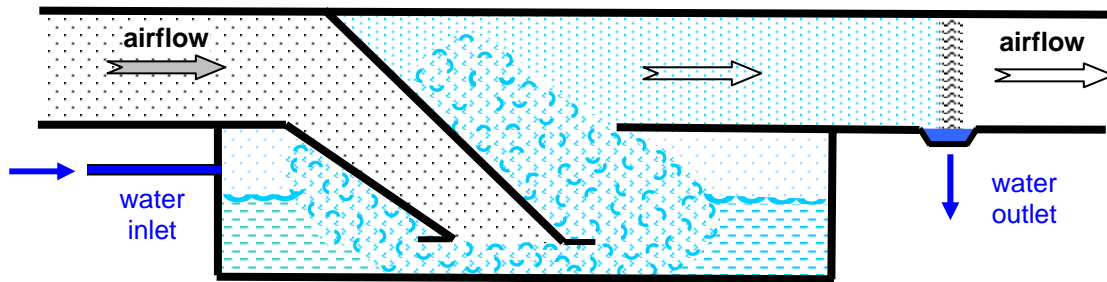


Figure 20.12 Principle of the flooded (or wet) orifice scrubber.

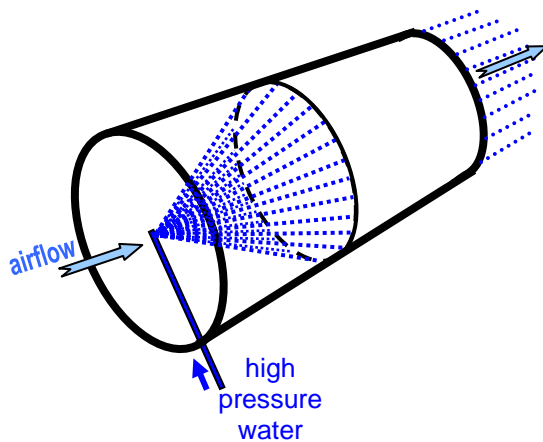


Figure 20.13 The high pressure spray fan or induction tube.

A series of 9 to 12 high pressure spray fans built into a longwall shearer drum is capable of promoting an airflow of up to $2 \text{ m}^3/\text{s}$ around the drum and can give reductions in airborne dust concentrations of 80 percent compared to conventional pick face flushing using the same amount of water (James and Browning, 1988).

The direction of induced airflow is away from the coal face and towards the travelling track. Hence, dust laden air is drawn around the cutter picks and down the face side to the tube inlets. At the outlet of the tubes, the dust-laden droplets are discharged against deflector plates and fall on to the conveyor. Similarly, a number of induction tubes can be mounted in parallel on the boom of a continuous miner (Jayaraman, 1989). When employed in headings, the air induction may cause local

recirculation and greatly improved ventilation of the cutter heads. Provided that adequate airflow is supplied to the face end of the heading, this will enhance the overall safety of the environment. However, legislative enforcement agencies should be consulted in industries where recirculation is prohibited.

The advantages of the high pressure spray induction tubes are that:

- they are simple, robust and have no moving parts
- they can be built into the machine structure
- they promote ventilation of the cutter heads as well as removing dust
- they give a good efficiency of dust capture and
- provided that the water pressure is maintained, there is little chance of blockage.

20.4.2.3. Dry filters and separators

There are many situations in subsurface ventilation systems where increasing the humidity of the air by the use of wet scrubbers is inadvisable. These include mines where heat and humidity is already a problem although cycling chilled water through wet scrubbers will reduce temperature, humidity and dust concentration simultaneously. Other difficulties that can arise from increases in humidity include clogging of hygroscopic minerals during transportation, roof control where the overlying strata is subject to rapid weathering, and where the mineral is subject to spontaneous combustion. In such circumstances, it may be preferable to employ dry filters to remove airborne dust.

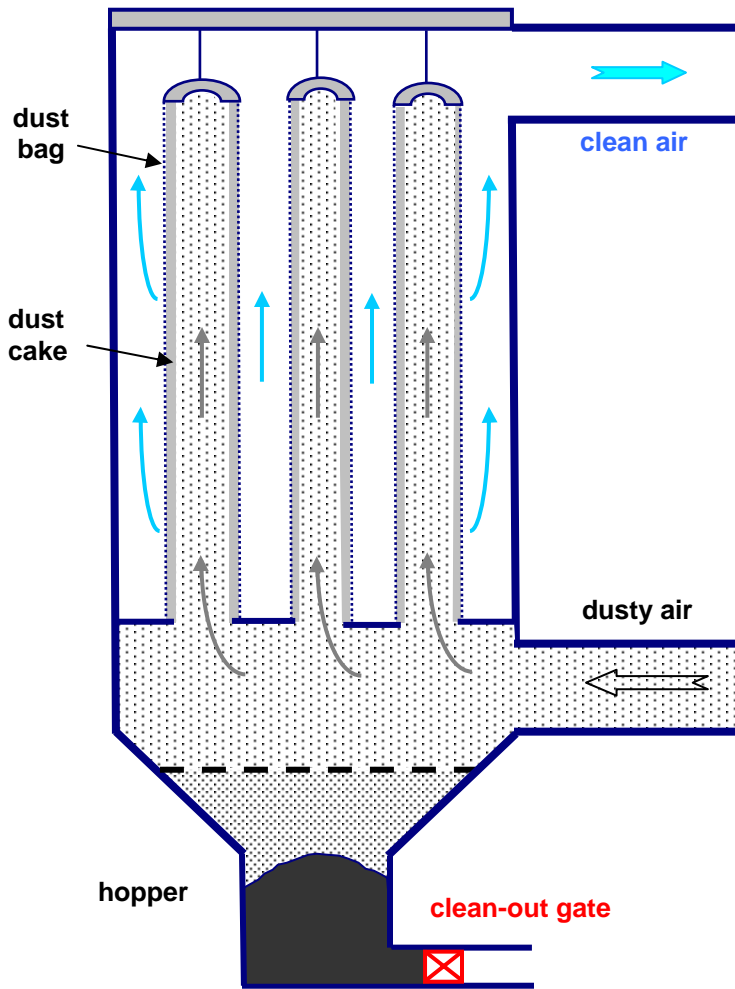


Figure 20.14 illustrates a *fabric filter*. The air passes through a fabric leaving dust particles adhering to the material or to the dust cake that builds up on the high pressure side. Air may flow from the inside to the outside of the bags as illustrated or in the *opposite* direction, in which case the bags are supported on an internal frame. The dust cake is dislodged at intervals of time by mechanical agitation or a reversed air pulse and falls to be collected in the hopper. The collected dust is either removed dry and bagged by a mechanical cleaning system or as a slurry produced by addition of water to the hopper.

The dust cake itself accomplishes most of the filtration and efficiencies of over 99 percent can be achieved in the submicron range. Airflow through the fine apertures of the dust cake is laminar. Hence, fabric dust collectors tend to follow a linear ($p = RQ$) relationship. The overall resistance of the unit arises from the combined effects of the dust-impregnated fabric and the dust cake. It is a straightforward matter to show that

Figure 20.14 Principle of a fabric filter.

$$R = R(\text{fabric}) + R(\text{cake}) = \frac{\mu}{A} \left\{ \frac{x}{k_f} + \frac{m}{k_c A \rho} \right\} \quad \frac{\text{Ns}}{\text{m}^5} \quad (20.55)$$

- where μ = dynamic viscosity of air (Ns/m²)
 A = surface area of filter (m²)
 x = thickness of fabric (m)
 k_f = permeability of dust-impregnated fabric (m²)
 k_c = permeability of dust cake (m²)
 m = mass of dust in the dust cake (kg)
 and ρ = density of the dust cake (kg/m³)

[The definition and units of permeability are explained in Section 12.3.2. However, manufacturers may assume a standard value of air viscosity and quote filter permeabilities in terms of m³/s of airflow through each (m² of area) for unit pressure gradient through the material (Pa/m), i.e. m³/s per m² per Pa/m.]

Equation (20.55) quantifies the increase in resistance as the thickness and, hence, mass of the dust cake builds up. This also increases the capture efficiency of the device. The pressure developed by the unit fan will rise and the air quantity will fall. An excessive pressure may cause rupturing of the filter fabric. The cake must, in any case, be dislodged before the airflow drops to an unacceptably low value. A backward curved (non-overloading) centrifugal fan operating on a steep pressure-quantity portion of its characteristic curve is advisable.

The simplest type of fabric cleaning mechanism is an electro-mechanical agitator. If operation of the unit can be interrupted every few hours (dependent upon dust loading) then the fan can automatically be switched off and the bags shaken by the agitator. More sophisticated units allow continuous operation by cycling the filtration and cleaning around several separate compartments.

Reverse flow cleaning involves a temporary reversal of air direction. This eliminates the mechanical linkages of the agitator system and is preferred for some types of fabric such as glass cloth where the severe flexing action of mechanical shaking may break the fibres. Pulsed jet reverse flow increases the efficiency of cleaning. Acoustic methods have also been employed to dislodge filter cakes.

The choice of fabric material usually lies between cotton weaves, felted fabrics or a synthetic such as polypropylene. The felted fabrics give an initially higher efficiency but synthetics are preferable where moist conditions or hygroscopic minerals may tend to produce a sticky dust cake. A newly installed bag will have a relatively low resistance. The initial mechanism is that dust particles will become lodged *within* the material. This increases both the resistance to flow and capture efficiency. Subsequent cleaning cycles will remove the dust cake but will have little effect on dust that has become impregnated in the material (more is dislodged from the smoother fibres of synthetic material). It follows that performance tests on a fabric dust collector should be delayed until dust impregnation of the material has reached steady state.

Two types of *cyclone* have been developed for dust removal, both of which can be operated dry or with the addition of water to improve capture efficiency. The *conical cyclone* operates by the dusty air being constrained into a helical vortex of reducing radius. Figure 19.4 was drawn to illustrate the conical cyclones used in dust samplers. Larger versions can be used as dust collectors. Dust particles are subjected to two opposing forces in a cyclone; the centrifugal force that tends to throw the particles out toward the wall, and drag of the air which tends to pull them inward toward the central air outlet tube. The greater the mass of the particle and the rotational velocity the more efficient the cyclone will become. Hence, the performance is enhanced for larger particles and as the physical size of the cyclone decreases. Cyclones are normally employed in groups for air cleaning. The centrifugal action is improved by arranging for the air to enter tangentially. It is essential to remove the dust from the base continuously in order to avoid re-entrainment. The finer particles that escape in the outlet air may be removed by a second cyclone or other filtration device connected in series.

The *cylindrical cyclone* imparts helical vortices to the airflow by means of turning vanes in a duct. The dust which concentrates and moves in helical fashion along the walls is collected and removed through an annulus formed by a second inner duct. The capital cost of cyclones is relatively low. They have no moving parts and are easy to maintain. However, the power requirements are such that they are constrained to applications of low airflow.

Electrostatic precipitators are used widely as air cleaners in buildings and for surface industrial applications such as the removal of fly ash from power station stacks or capturing aerosols in the chemical and metallurgical industries. Although a well designed electrostatic precipitator can reach capture efficiencies of over 99 percent in the submicron range, their need for high voltages prohibits their use in gassy mines and mitigates against their employment in other underground facilities.

The principle of operation of an electrostatic precipitator is that when an aerosol is passed through an electric field produced by a pair of electrodes then the particles will become charged and migrate towards one of those electrodes. For industrial applications, the active electrodes are charged to voltages between 20 and 60 kV while the dust collecting electrodes are earthed. The electric field is considerably enhanced in regions of sharp curvature on the electrode surfaces. For this reason, the active electrodes are often wires hanging vertically downward. The wires are usually charged negatively as this gives a more stable performance for heavy duty performance although ozone can be formed. High energy electrons are emitted from the negatively charged wires. Each electron collision with a gas molecule causes the ejection of two further electrons which go on to repeat the process. This escalating process produces an electron avalanche and is often accompanied by a visible glow; hence, the phenomenon is termed a *corona*. The gas molecules that have lost electrons become positive ions and migrate towards the negatively charged wires. However, further away from the active electrodes, the free electrons lose their kinetic energy to the extent that they are no longer capable of dislodging further electrons from gas molecules but are, instead, absorbed *into* those molecules. The electron avalanche ceases and the edge of the corona is reached.

The gas molecules are then negatively charged, i.e. negative ions, and migrate towards an earthed electrode. During that migration they become attached to dust particles which are also, therefore, drawn towards an earthed electrode and adhere by electrostatic attraction to the surface of that electrode. Upon contact, the particles begin to leak their charge to the earthed electrode. Other layers of charged particles arrive and build up progressively. They too will gradually give up their charge. However, the outermost layer of dust is always the most heavily charged and will be analogous to a skin compressing the underlying particles and causing the build-up of a dust cake. The dust can be dislodged into a lower hopper by rapping the earthed electrodes.

In *tube electrostatic precipitators*, a single wire forms the active electrode suspended in a metal cylinder which acts as the grounded electrode. However, for the larger flows found in industrial applications, the *plate precipitator* has become more common. This is illustrated in Figure 20.15. Air passes over the charged wire electrodes which are suspended between a series of grounded plates. The dust collects on the surfaces of the plates. For some applications, the mechanisms of dislodgment by rapping may be replaced by running a film of liquid down the plate surfaces or by periodically dipping the plates into a liquid bath.

The efficiency of an electrostatic precipitator can be determined by an equation first derived by W. Deutsch in 1922:

$$\eta = 1 - \exp\left\{-\frac{A u_e}{Q}\right\} \quad (20.56)$$

where A = area of plates (m^2)
 Q = airflow (m^3/s)
 and u_e = electrical (ion) migration velocity (m/s) (see equation (20.28))

The electrical migration velocity depends upon the type of dust and varies between 0.02 m/s for fly ash to 0.2 m/s for gypsum. Although theoretical procedures have been derived for quantification of the electrical migration velocity, tables of empirical values have, to this time, proved to be more reliable (ASHRAE, 1988).

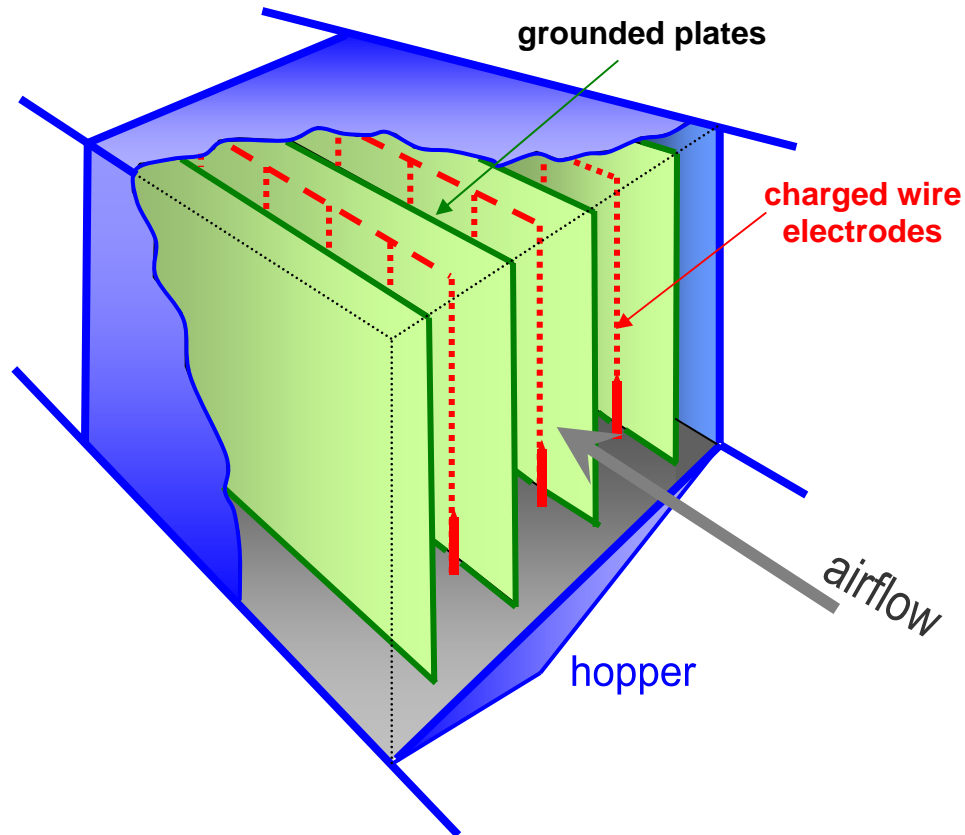


Figure 20.15 A plate electrostatic precipitator.

20.4.2.4. Personal respirators

Every effort should be made to maintain dust concentrations in subsurface workings within mandatory threshold limits and safe for the health of the workforce. A final line of defence is the *personal respirator* used to filter inhaled air. Two types are available. The first of these is a mask that fits around the nose and mouth. The filter is necessarily a compromise between dust removal efficiency and resistance. A respirator that requires more than about 150 Pa of pressure difference at normal breathing rates is unlikely to be tolerated by personnel. Furthermore, contact of the mask on the face can be irritating, especially in hot conditions. An improved version, sometimes called an airstream helmet, utilizes a belt-mounted battery to power a small fan. This passes air through a filter and up a tube to the helmet. The cleaned air flows downwards between a transparent visor and the face of the wearer. This device does not rely on breathing effort nor is there any direct face contact with the visor. It also provides eye protection with less visual impedance than that given by goggles or safety glasses.

20.4.3. Dilution and layout of the ventilation system

Despite the availability of dust collectors, dilution of mine dust by the mine ventilation system remains the primary method of controlling this hazard. The effects of airflow and air velocity have already been discussed in earlier chapters. Section 9.3.3 deals with airflow requirements for respirable and non-respirable dust while recommended air velocity limits are listed in Section 9.3.6. Exhaust systems of auxiliary ventilation are preferred for dust problems in headings (Section 4.4.) while overlap arrangements can also handle gas emissions. Furthermore, it is relatively straightforward to install in-line filters or dust collectors within ventilation ducts.

Controlled partial recirculation, where allowed by legislative authorities, coupled with dust filtration systems, can result in very significant reductions in general body dust concentrations (Section 4.5). The district ventilation systems discussed in Section 4.3 and designed to facilitate the dilution and removal of airborne pollutants in working zones apply equally well to respirable dust. Consideration might also be given to **homotropical ventilation** in which the airflow and mineral flow are in the same direction (Section 4.2.3.). As conveyors or other mineral transportation systems are then in return airways, any respirable dust they produce does not pass on to a working area. Furthermore, on a longwall face with uni-directional coal winning, few personnel need be on the downwind side of the machine. Despite these advantages, homotropical ventilation does have some drawbacks, particularly in mines with heavy gas emissions (Stevenson, 1985).

20.4.4. Separation of personnel and dust

In Section 20.3.4 we described the re-entry period after blasting in metal mines as a classical example of the separation of personnel from dust concentrations. Several other methods are available to reduce the exposure of individuals or groups to dust. The United States Bureau of Mines was active in developing this approach, particularly for the protection of the operators of longwall face equipment and continuous miners in room and pillar workings.

Airflow diverters of two types have been fitted to such machines. First, barriers have been added to shearers in order to divide the face airflow before it reaches the location of the cutting drum. This is positioned such that it provides a split of relatively clean air to the shearer operator. A great deal of research has been conducted into the use of spray fans to control the direction and flow of air at continuous miners and longwall shearers. Appropriate location and design of these triangular or cone shaped sprays not only assists in dust suppression but also ensures that airborne dust is diverted away from operators' positions (National Research Council, 1980).

Air curtains have also been employed to prevent dust clouds from reaching operators' positions, as well as assisting in the ventilation of cutter heads (Ford and Hole, 1984; Froger et al, 1984; James and Browning, 1988). The air curtains may be directed across the top, bottom and sides of the cutting zone. They are produced from tubes of about 10 mm diameter maintained at an air pressure of approximately 1.5 kPa. A 2.5 mm slot runs along the length of the tube with an attached guide plate angled such that air leaves the tube tangentially, clinging to the guide plate (the Coanda effect) until it is deflected into the required direction by a splitter. Entrainment of additional air assists in both the ventilating and dust control effects.

Another development that reduces dust exposure to machine operators has been the use of remote controls. These allow personnel to stand some distance from the mineral- winning machines while maintaining control by hand-held wireless units. Finally, studies leading to the reorganization of work practices have also promoted reduced dust exposure of face personnel (Tomb et al, 1990).

References

Allen, M.D. and Raabe, C.G. (1982). Re-evaluation of Milliken's oil drop data for the motion of small particles in air. *J. Aerosol Sci.* 13, pp 537-547.

ASHRAE (1988). American Society for Heating, Refrigerating and Air-conditioning Engineers, *Equipment Handbook*, Chapter 11, pp 11-12.

Bandopadhyay, S. (1982). Planning with diesel powered equipment in underground mines. Ph.D. thesis. The Pennsylvania State University.

- Bhaskar, R., Gong, R., and Jankowski, R.A. (1991).** Studies in underboom dust control to reduce operator exposure to dust. 5th U.S. Mine Ventilation Symp., W. Virginia, pp 197-206.
- Bhaskar, R. and Ramani, R.V. (1986).** Behavior of dust clouds in mine airways. Transactions of AIME, Vol. 280, pp 2051-2059.
- Booth-Jones, P.A., Annegarn, H.J. and Bluhm, S.J. (1984).** Filtration of underground ventilation air by wet dust-scrubbing, 3rd Int. Mine Ventilation Congress, Harrogate, U.K., pp 209-217.
- Chung, H.S. (1981).** Coagulation processes for fine particles. Ph.D. Thesis, The Pennsylvania State University.
- Flagan, R.C. and Seinfeld, J.H. (1988).** Fundamentals of air pollution engineering. Published by Prentice Hall, 542 pp.
- Ford, V.H.W. and Hole, B.J. (1984).** Air curtains for reducing exposure of heading machine operators to dust in coal mines, Ann. Occup. Hyg., Vol. 28, pp 93-106.
- Froger, C., Courbon, P. and Koniuta, A. (1984).** Dust-laden airflow control applied to worker protection: scale model study of a steep seam working, 3rd Int. Mine Ventilation Congress, Harrogate, U.K., pp 215-217.
- Gaudin, A.M. and Meloy, T.P. (1962).** Model and a comminution distribution equation for repeated fracture, Trans. AIME 223, pp 243-50.
- Hamilton, R.J. and Walton, W.H. (1961).** The selective sampling of respirable dust in inhaled particles and vapours (editor Davies), Pergamon Press, Oxford.
- Hartman, I. and Grenwald, H.P. (1940).** Use of wetting agents for allaying coal dust in mines, U.S. Bureau of Mines, IC-7131, 12 pp.
- Heising, C. and Becker, H. (1980).** Dust control in longwall workings, 2nd Int. Mine ventilation Congress, Reno, Nevada, pp 603-611.
- Hood, M. (1991).** Private communication on jet-assisted rock cutting.
- Hood, M., Knight, G.C. and Thimons, E.D. (1991).** A review of jet-assisted rock cutting. Trans. of ASME, Journal of Engineering for Industry.
- James, G.C. and Browning, E.J. (1988).** Extraction techniques for airborne dust control, 4th Int. Mine Ventilation Congress, Brisbane, Australia, pp 539-546.
- Jayaraman, N.I. et al (1989).** High pressure water-powered scrubbers for continuous miner dust control, 4th U.S. Mine Ventilation Symp., Berkeley, CA, pp 437-443.
- Jones, A.D. (1978).** Experimental and theoretical work on the use of a high pressure water spray to induce airflow in a tube and capture airborne dust. MRDE Report No. 73, National Coal Board, U.K.
- Jones, A.D. (1978).** Optimal design for water-powered dust extraction, M. Phil. Thesis, University of Nottingham, U.K.
- Knight, G. (1985).** Generation and control of mine airborne dust, 2nd U.S. Mine Ventilation Symp., Reno, NV, pp 139-150.
- Marshall., V.C. (1974).** Comminution, Chameleon Press Ltd., London.

- National Research Council (1980).** Measurement and control of respirable dust in mines, U.S. National Academy of Sciences, Washington, D.C., NMAB-363.
- Owen, P.R. (1969).** Dust deposition from a turbulent airstream (Aerodynamic capture of particles: editor, Richardson).
- Padmanabhan, S. and Mutmansky, J.M. (1989).** An analysis of quartz occurrence patterns in airborne coal mine dusts, 4th U.S. Mine Ventilation Symp., Berkeley, CA, pp 463-474.
- Prandtl, L. (1923).** Ergebnisse der aerodynamischen versuchsanstalt zu Gottingen; Oldenbourg, Munich and Berlin, p 29.
- Qin, J. and Ramani, R.V. (1989).** Generation and entrainment of coal dust in underground mines, 4th U.S. Ventilation Symp., Berkeley, CA, pp 454-462.
- Ramani, R.V. et al (1988).** On the relationship between quartz in the coal seam and quartz in the respirable airborne coal dust, 4th Int. Mine ventilation Congress, Brisbane, pp 519-526.
- Ramani, R.V. and Bhaskar, R. (1984).** Dust transport in mine airways, Proc. Coal Mine Dust Conference, W. Virginia University (ed. Peng), pp 198-205.
- Sandys, M.P.J., and Quilliam, J.H. (1982).** Sources and methods of dust control, Chap. 15, Environmental Engineering in South African Mines, Mine Ventilation Society of S. Africa.
- Sartaine, J.J. (1985).** The use of water-powered scrubbers on NMS Marietta drum miners, 2nd U.S. Mine Ventilation Symp., Reno, Nevada, pp 733-740.
- Schröder, H.H.E., Runggas, F.M. and Krüss, J.A.L. (1984).** Characterization of sonically atomized water-spray plumes, 3rd Int. Mine Ventilation Congress, Harrogate, U.K., pp 219-228.
- Seinfeld, J.H. (1986).** Atmospheric chemistry and physics of air pollution, Wiley, New York.
- Stevenson, J.W. (1985).** An operator's experience using antitropal and homotropal longwall face ventilation systems, 2nd U.S. Mine Ventilation Symp., Reno, Nevada, pp 551-557.
- Stricklin, J.H. (1987).** Longwall dust control at Jim Walters Resources, 3rd U.S. Mine Ventilation Symp., Penn. State, pp 558-563.
- Taylor, C.D., Kovscek, P.D. and Thimons, E.D. (1988).** Dust control on longwall shearers using water jet-assisted cutting, 4th Int. Mine Ventilation Congress, Brisbane, Australia, pp 547-553.
- Tomb, T.F. et al (1990).** Evaluation of longwall dust control on longwall mining operations, SME Annual Meeting, Salt Lake City, Utah, Feb., pp 1-10.
- Wang, Y.P. et al (1991).** Use of surfactants for dust control in mines, 5th U.S. Mine Ventilation Symp., W. Virginia, pp 263-270.

Part 5

Fires and Explosions

CHAPTER 21. SUBSURFACE FIRES AND EXPLOSIONS

21.1 INTRODUCTION	2
21.1.1. The fire triangle and the combustion process	3
21.1.2. Classification of mine fires	4
21.2 CAUSES OF IGNITIONS	4
21.2.1. Mechanized equipment	4
21.2.2. Electrical apparatus	5
21.2.3. Conveyors	5
21.2.4. Other frictional ignitions	6
21.2.5. Explosives	7
21.2.6. Welding	7
21.2.7. Smoking and flame safety lamps	7
21.3. OPEN FIRES	7
21.3.1. Oxygen-rich and fuel-rich fires	8
21.3.2. Effects of fires on ventilation	9
21.3.2.1. The choke effect	9
21.3.2.2. The buoyancy (natural draft) effect	10
21.3.3. Methods of fighting open fires	11
21.3.3.1. Firefighting with water	12
21.3.3.2. High expansion foam	13
21.3.4. Control by ventilation	14
21.3.4.1. Pressure control	14
21.3.4.2. Airflow reversal	15
21.4. SPONTANEOUS COMBUSTION	17
21.4.1. The mechanisms of spontaneous combustion in minerals	17
21.4.1.1. The phases of oxidation	17
21.4.1.2. The effects of water vapour	18
21.4.1.3. The path of a spontaneous heating.	19
21.4.2. Susceptibility to spontaneous combustion	19
21.4.3. Precautions against spontaneous combustion	20
21.4.4. Detection of a spontaneous heating	23
21.4.5. Dealing with a spontaneous heating	24
21.4.5.1. Excavating the fire	24
21.4.5.2. Burying the fire	24
21.4.5.3. Sealants	25
21.4.5.4. Localized pressure balancing	25
21.4.5.5. Flooding and sealing off	26
21.5. STOPPINGS, SEALS AND SECTION PRESSURE BALANCES FOR EMERGENCY SITUATIONS	27
21.5.1. Site selection of seals	28
21.5.2. Sequence of building seals	28
21.5.3. Construction of seals and stoppings	28
21.5.4. Re-opening a sealed area	30
21.5.5. Section pressure balances	31
21.6. THE USE OF INERT GASES	32
21.6.1. Carbon dioxide	32
21.6.2. Combustion gases	33
21.6.3. Nitrogen	33
21.6.4. Methods of application and control	33

21.7. FIRE GASES AND THEIR INTERPRETATION	35
21.7.1. The processes of burning and the gases produced	35
21.7.2. The detection and trend analysis of fire gases	36
21.7.3. Explosibility diagrams	39
21.8. EXPLOSIONS	45
21.8.1. Initiation of explosions	45
21.8.2. Mechanisms of explosions	46
21.8.2.1. Gas explosions	48
21.8.2.2. Coal dust explosions	48
21.8.2.3. Sulphide dust explosions	54
21.8.2.4. Dust explosibility tests	54
21.8.3. Suppression of mine explosions	54
21.8.3.1. Stonedust and water barriers	54
21.8.3.2. Triggered barriers and explosion detectors	55
21.8.4 Explosions in sealed areas.	56
21.8.4.1 Causes of explosions in abandoned areas.	56
21.8.4.2 Recognition of the hazard.	56
21.8.4.3 Approaches to the problem and the initial NIOSH Report.	56
21.8.4.4 Requirements of seals	58
21.9 PROTECTION OF PERSONNEL	61
21.9.1. Training and preparedness	61
21.9.2. Methods of warning and locating personnel	62
21.9.2.1. Stench warning systems	62
21.9.2.2. Ultra-low frequency radio signals.	63
21.9.2.3. More recent systems	63
21.9.2.4. Locating trapped persons	64
21.9.3. Self-rescuers	64
21.9.3.1. Filter self-rescuers (FSR's)	65
21.9.3.2. Self-contained self-rescuers (SCSR's)	65
21.9.4. Escapeways	66
21.9.5. Refuge chambers	68
21.10 EMERGENCY PROCEDURE AND DISASTER MANAGEMENT	68
21.10.1. Immediate response	69
21.10.2. Command centre	69
21.10.3. Disaster management	69
References	70

21.1 INTRODUCTION

The most feared of hazards in underground mines or other subsurface facilities are those of fires and explosions. Like airplane crashes, these do not occur often but, when they do, have the potential of causing disastrous loss of life and property as well as a temporary or permanent sterilization of mineral reserves. Furthermore, "near-misses" occur all too frequently. The incidence of mine fires appears not to be declining despite greatly improved methods of mine environmental design and hazard control. This is a consequence of several matters; first the growing variety of materials that are imported into modern mine workings, varying from resins and plastics to liquid fuels and hydraulic fluids. A second factor is the continuous increase in the employment of mechanized procedures, many of the machines involving flammable liquids and materials that can produce toxic fumes when over-heated.

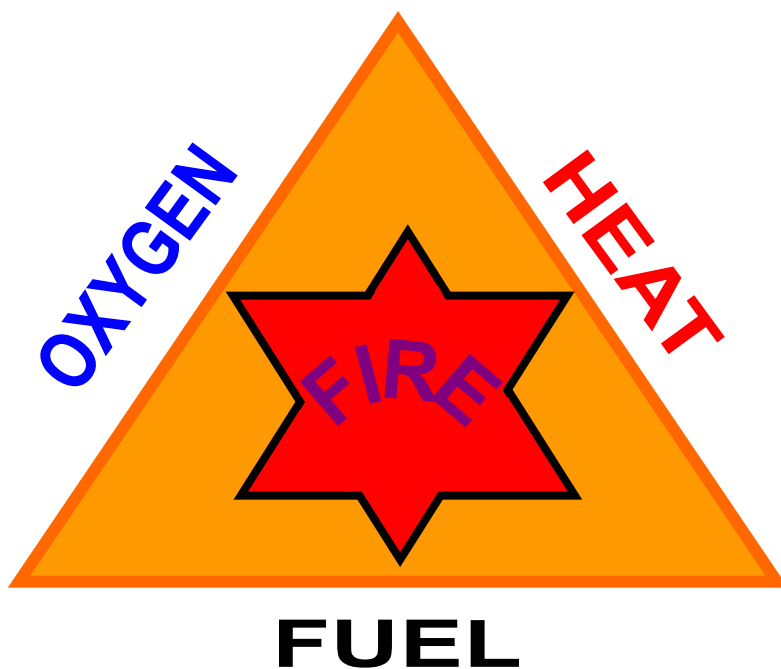
Although this chapter concentrates on technical considerations the incidence of mine disasters is greatly influenced by the priority afforded to safety and health by individual companies, states and countries. Mine disasters are more prevalent at times when market prices for minerals and fuels are high. Attention paid to mine safety is greatest in those countries that have active and well-funded research activities in this area and which maintain industry awareness through an ongoing output of reports and papers. Such work also assists in the promulgation of new or updated legislation.

These activities are often inter-related. A period of declining statistics of mine fatalities coupled with a period of limited research tends to create a laissez-faire attitude in both industry and legislative bodies or agencies. A boom market is then more likely to produce a spate of serious mine accidents. Public disquiet results in (often hasty) legislative action to promote new research investigations and the imposition of stricter standards and penalties on mining companies. Unfortunately, public memory tends to be short and history has shown the repetitive nature of this cycle. It is within that context that this chapter has been written.

The enormous loss of life due to mine fires and explosions during the eighteenth and nineteenth centuries preoccupied the minds of mining engineers and scientists of the time (Chapter 1). The majority of deaths arising from mine fires and explosions are caused, not by burning or blast effects, but by the inhalation of toxic gases, in particular, carbon monoxide. There are two major differences between underground fires and those that occur in surface structures. The first concerns the long distances, often several kilometres, that personnel might be required to travel in passageways that may be smoke-filled. Secondly, the ventilation routes are bounded by the confines of the airways and workings, causing closely coupled interactions between the ventilation and behaviour of the fire.

It is difficult for anyone who has not had the experience, to comprehend the sensations of complete isolation and disorientation involved in feeling one's way through a long smoke-filled mine airway in zero visibility. It is a cogent exercise to turn off one's caplamp in an unilluminated return airway and to walk just a few steps, even without the trauma of a highly polluted atmosphere.

It is, therefore, a matter of ongoing importance that all personnel involved in the design and operation of underground openings should have some knowledge pertaining to the prevention and detection of subsurface fires and explosions, as well as procedures of personnel warning systems, escapeways, firefighting, toxic gases, training, fire drills and the vital need for prompt response to an emergency situation. These are some of the topics that are discussed in this chapter.



21.1.1. The fire triangle and the combustion process

Perhaps the most basic precept in firefighter training is the *fire triangle* shown on Figure 21.1. This illustrates that the combustion process which we term "fire" requires three components: fuel, heat and oxygen. Remove any one of these and the fire will be extinguished. The *fuel* may be solids, liquids or gases. The liquids and gases might be introduced into the mine environment by natural or mining processes, or may be produced by heating solid materials. Whenever a combustible solid or liquid is *heated* to a sufficiently high temperature (*flashpoint*), it will produce a vapour that is capable of being ignited by a flame, spark or hot surface which has the required

Figure 21.1 The fire triangle.

concentration and duration of thermal energy. Gasoline has a flashpoint of -45°C while most commonly available solids require the application of a flame for them to reach flashpoint. The *ignition temperature* of any given substance is the lowest temperature at which sustained combustion is initiated. *Flaming* is the process of rapid oxidation of the vapours accompanied, usually, by the emission of heat and light. In the case of self-sustained burning, that heat is sufficient to raise the temperature of the newly exposed or surrounding areas of surface to flashpoint. However, combustion can continue at a slower rate without flaming through the process we know as *smouldering*. In this case, the oxidation process continues on the surface of the material and produces sufficient heat to be self sustaining, but not enough to cause the emission of vapours in the quantity required for flaming combustion.

The *oxygen* which forms the third side of the fire triangle is normally provided by the air. Flammable liquids such as the oil of a flame safety lamp will cease to burn when the oxygen content of the air is reduced to some 16 per cent (Section 11.2.2.). Flaming combustion of all kinds is extinguished at oxygen contents of 10 to 12 per cent while smouldering is usually terminated at oxygen concentrations below 2 per cent. However, some materials may contain sufficient inherent oxygen for slow combustion to continue at even further reduced levels of atmospheric oxygen. Coupled with the low values of thermal conductivity of crushed material, this can result in "hot spots" lying dormant in abandoned areas for long periods of time, but capable of re-ignition if a renewed air supply is admitted subsequently.

21.1.2. Classification of mine fires

Fires underground can be classified into two broad groups, *open and concealed fires*. Open fires occur in airways, faces and other openings that form part of the active ventilation system of the mine and, hence, affect the quality of the mine airflows quickly and directly. As the term might imply, open fires are often accompanied by flaming combustion because of the availability of oxygen and offer the possibility of direct attack by firefighting teams. Conversely, concealed fires occur in areas that are difficult or impossible to access such as caved or abandoned zones. These are usually, but not necessarily, initiated as a result of spontaneous combustion and can occur in both coal and sulphide ore minerals as well as within any imported organic matter such as paper, discarded fabrics (e.g. oily rags) or timbering in abandoned areas. The degree to which concealed fires propagate and pollute the mine atmosphere depends upon the rate at which air leaks through the areas affected. The matter of spontaneous combustion is discussed in further detail in Section 21.4.

21.2 CAUSES OF IGNITIONS

The variety of procedures, processes and materials used in modern mining provides many opportunities for the ignition of flammable materials. However, the most commonly reported causes of fires and explosions in mines are listed in the following subsections.

21.2.1. Mechanized equipment

Machines intended for use underground should be designed to operate with a high degree of safety in a harsh physical environment, and are subject to legal requirements and conditions in most mining countries. It is no surprise, therefore, that the majority of fires attributable to machines arise out of:

- misuse
- lack of proper maintenance
- removal or bypassing of safety features such as diagnostic devices, environmental monitors or thermal trip switches and
- running unattended for long periods of time.

Exhaust systems on diesel equipment should be fitted with particulate filters or water scrubbers that not only reduce airborne pollution (Section 11.3.2.), but also prevent the emission of incandescent particles. Furthermore, hoses, transmission or brake fluids and a variety of components made from synthetic materials on modern diesels may be capable of producing toxic gases when ignited. All vehicles or other diesel equipment should be fitted with on-board fire extinguishers.

It is particularly important that equipment containing significant quantities of oil, such as large transformers or air compressors, should be safeguarded by thermal trips, pressure relief valves and other devices necessary for automatic cut-off in the event of any abnormal condition. Such devices should be subjected to routine testing and maintenance. Wherever possible (and as may be required by law) non-mobile equipment should be located within enclosures with fire-resistant roof, floor and walls, and which are ventilated to a return airway. Again, fire extinguishers and, preferably, an automatic fire suppression system should be available within the chamber. In coal mines, the surroundings in adjacent airways should routinely be coated with stonedust (Section 21.8.3.1.).

21.2.2. Electrical apparatus

In addition to the general comments on mechanized equipment made in the preceding subsection, electrical gear can give rise to incendiary hazards from sparking and overheating. Switchgear or battery charging stations should be sited such that they are not affected by convergence or falls of roof. This is most liable to occur close to mineral winning areas. Furthermore, start switches should be protected against accidental operation by glancing blows from falling debris or passing traffic. Electrical sub-stations and battery charging chambers should be equipped with non-aqueous fire extinguishers.

Cables in airways should be hung in catenary fashion on cradles suspended from the roof. They should be located such that they will not be pinched by convergence or the yielding of roof supports, nor be impacted by vehicles. The insulation and type of sheathing must be suitable for the electrical load and rigours of the underground environment. All such cables should be inspected routinely for evidence of physical damage.

Electrical failures should result in immediate isolation of the power by means of overload and earth leakage protective devices. In gassy mines, all electrical motors and heavy current devices should be enclosed within flameproof casings so that any ignition of methane is contained within the equipment. Signalling or other light current apparatus should be certified as intrinsically safe, i.e. incapable of producing sparks of sufficient energy to ignite a methane:air mixture.

During non-working shifts, the electrical power supplied to each area of the mine should be isolated at the appropriate highest level control centre or substation. Precautions should be taken against power surges caused by lightning strikes on surface power lines, transformers, substations or any other lines that may conduct the surge to underground excavations. Similarly, particular care should be taken against electrical leakage in the vicinity of explosives or fuel storage areas.

21.2.3. Conveyors

Conveyor fires have been subjected to particular study because of the rapidity of fire propagation along the early rubber-based types of conveyor belting. Modern conveyor belting for underground use must be subjected to fire propagation tests (e.g. Verakis, 1991; Mutmansky et al, 2007). Three types of materials are used for mine conveyor belts, namely, styrene-butadiene rubber (SBR), neoprene (NP) and polyvinyl chloride (PVC). Composites of these materials are also employed. Following ignition of the belt material and removal of the igniting source, the fire should preferably fail to propagate or, if it does, move at a slow rate. However, it should be noted that heated belt material may produce hazardous fumes.

Numerous tests have indicated that fire propagation rates along conveyor belting are influenced by airspeed (e.g. Hwang et al, 1991). At a relative velocity of some 1.5 m/s between the belt surface and the

adjacent airstream, a phenomenon known as *flash over* attains its maximum effect. Flash over occurs when a flame front from the burning belt reaches forward over an unburned surface with an optimum angle and length such that the radiant effect on that surface reaches a maximum. This can cause flaming of the top layer of belting and a significant increase in flame propagation rate along the surface of the belt. Deeper layers in the weave of the material may or may not be ignited. The effect has been observed in belts of compositions including SBR, PVC, and SBR–neoprene combination (Verakis and Dalzell, 1988). Flashover involves a serious hazard as belt surface propagation rates may reach some 10 m/min. The spread of fire along mine conveyors is influenced strongly by the turbulence of the airflow. Hence, laboratory tests of small samples of belting can give misleading results. Large scale gallery tests are more reliable.

Conveyor fires are most likely to be initiated by friction. If the belt becomes staked (immobilized) at any point along its length and the drive rollers continue to turn, then high temperatures will be generated at the drive head. Temperature monitors or belt tension transducers can sense this condition. Such devices should be wired to isolate electrical power from the conveyor drive when an alarm condition is detected. Similarly, a seized idler or return roller can become red-hot from the friction of a belt moving over or around it. Conveyors should be patrolled regularly during operation in order to detect the development of faulty rollers. Worn bearings will often be noisy and may also be detected by the smell of heated surfaces. A further frictional hazard can occur if the conveyor becomes misaligned to the extent that the belt rubs against surrounding surfaces such as the conveyor structure or airway sides.

In all of these cases, a fire may be initiated when lubricants, coal dust or flammable debris reach their ignition points. It follows that dust or spillage should not be allowed to accumulate around and, particularly, underneath conveyors. A clean conveyor road is much more likely to be a safe one. In coal mines, conveyor entries should be well rock dusted

21.2.4. Other frictional ignitions

The main cause of methane ignitions on the working faces of coal mines is frictional sparking at the pick points of coal winning machinery. This occurs particularly when the machine cuts through sandstone or pyritic material. Two approaches have been taken to reduce this hazard. One is to ensure that there is sufficient ventilation around the cutting drum to provide rapid dilution of the methane as soon as it is emitted. It is, of course, important that the overall airflow at the working face is adequate to prevent methane layering (Section 12.4.2.) and that the layout of the system minimizes flushes of methane from worked-out areas (Section 4.3.2.). A number of devices have been employed to enhance air movement across the pick points of shearers and continuous miners (e.g. Browning, 1988). Unfortunately, these may exacerbate the dust problem unless combined with a wet scrubber (Section 20.4.2.2.).

The second approach to the incendiary streak of sparks that sometimes trails behind a cutter pick is to quench it with water. This technique combines the suppression of both dust and methane ignitions. It is achieved by pick face flushing and, even more efficiently, by jet assisted cutting (Section 20.4.1.1.).

Rope haulage systems have been the cause of some mine fires. Care should be taken that all pulleys and return wheels are routinely serviced and lubricated. Ropes should not be allowed to rub against solid surfaces such as the roof, sides or floor of airways and, particularly, timber supports. If haulage ropes must pass through holes in stoppings then, again, the ropes should not contact the sides of the orifices. Fluid couplings and enclosed gearings or direct drives are preferred to mechanical clutches, belts or V-drives for the transmissions of mining machinery. However, where the latter are employed then, again, regular inspections and maintenance are required to ensure their continued safe operation. Similarly, mechanical braking systems should be well looked after.

21.2.5. Explosives

The initiation of fires from explosives or igniter cord remains a danger in non-gassy mines. Incandescent particles from blasting operations may contain sufficient heat energy to ignite dry wood or combustible waste material. Igniter cord should never be hung on timber supports. A strict record should be maintained on all explosives and detonating devices at the times of issue and return to the stores. The relevant national or state legislation should be consulted for the conditions under which explosives may be stored or transported underground.

21.2.6. Welding

All welding operations that are permitted underground should be carried out under well-controlled conditions. Where there is any possibility of methane or other flammable gases being present then testing for those gases should be carried out before and, at intervals, during the welding operations. Hot slag and sparks from welding are easily capable of igniting combustible materials such as coal, wood, paper and waste rags. Wherever possible, such materials should be removed from the vicinity of welding operations and the remainder wetted down or coated by stonedust. Molten metal should not be allowed to drop on the floor. Slag pans should be used to capture hot run-off. This is particularly important in coal mines, in shafts and near timber supports. Fire extinguishers must be available at the sites of all welding operations.

Gas containers employed in oxy-acetylene cutting should be stored and used in a secure upright position. Gas bottles must never be stored or used in the vicinity of explosives or concentrations of flammable liquids.

21.2.7. Smoking and flame safety lamps

It is a sad fact that the use of smoking materials has been suspected as the cause of some fires and explosions in mines. In those mines that have been classified as gassy, carrying such materials (often known as *contraband*) into the subsurface is illegal. This law should be enforced with the utmost rigour. Through well chosen examples during training and refresher classes a workforce will, themselves, ensure compliance with non-smoking regulations.

In subsurface openings where smoking is permitted then, again, education, posters and warning signs should be employed as ongoing reminders of the possible disastrous consequences of careless disposal of smoking materials.

Damaged flame safety lamps have also been suspected of igniting a methane:air mixture. In the few places where these devices remain in use, they should be treated with care and subjected to inspection after each shift. When a high concentration of methane is detected by a blue flame spiralling rapidly within a flame safety lamp (Section 11.4.2.2.) then the lamp should be lowered gently and, if necessary, smothered inside one's clothing. Familiarity with the procedure should be gained through training and will counter the natural reaction of the untrained person to drop the lamp or to throw it away in panic. (Section 11.4.2.2)

21.3. OPEN FIRES

Fires that occur in mine airways usually commence from a single point of ignition. The initial fire is often quite small and, indeed, most fires are extinguished rapidly by prompt local action. Speed is of the essence. An energetic ignition that remains undetected, even for only a few minutes, can develop into a conflagration that becomes difficult or impossible to deal with. Sealing off the district or mine may then become inevitable.

The rate at which an open fire develops depends, initially, upon the heat produced from the igniting source. A fine spray of burning oil from a damaged air compressor can be like a flame thrower and ignite nearby combustibles within seconds. On the other hand, an earth leakage from a faulty cable may cause several hours of smouldering before flames appear. The further propagation of the fire depends upon the availability of fuel and oxygen (Figure 21.1). A machine fire in an untimbered metal mine airway will remain localized if there is little else to burn in the vicinity. Conversely, an airway that is heavily timbered or with coal surfaces in the roof, floor or sides will provide a ready path for speedy development and propagation of a fire.

When an open fire has developed to the extent of causing a measurable change in the temperature of the airflow then it can affect the magnitudes and distributions of flow within the mine ventilation system. Conversely, the availability of oxygen to the fire site controls the development of the fire. This Section discusses the coupled interaction between fire propagation and ventilation, and the means by which open fires in mines may be fought.

21.3.1. Oxygen-rich and fuel-rich fires

At the start of most open fires in ventilated areas, there is a plentiful supply of oxygen - more than sufficient for combustion of the burning material. Indeed, if the air velocity is brisk then heat may be removed at a rate greater than that at which it is produced. The heat side of the fire triangle is removed and the fire is "blown out". These are examples of *oxygen-rich fires*. Assuming that the fire continues to proliferate, it will consume increasing amounts of oxygen and, at the same time, produce greater volumes of distilled gases and vapours. The point may be reached when the heat of combustion produces temperatures that continue to remain high enough to distill gases and vapours from the coal, timber or other available fuels but with insufficient oxygen to burn those gases and vapours completely. The fire has then become *fuel-rich*.

The development of an oxygen-rich into a fuel-rich fire is a serious progression and produces a much more dangerous situation for firefighters. When flammable gases at temperatures exceeding their ignition point meet relatively fresh air then they will ignite along the gas:air interfaces. The added turbulence may produce intimate mixing of air and unburned gases resulting in explosions. These phenomena can occur downstream from an open fire if air leaks into the firepath from adjacent airways. Firefighters are then faced with a difficult decision. Leakage of air from adjacent airways must be *into* the firepath in order to prevent spread of the fire into those adjacent airways, yet the admittance of that air may cause explosions and propagation of the fire at a rate much greater than that allowed by burning of the solid material itself.

A similar effect occurs when buoyancy of the hot gases causes roll-back of smoke at roof level against the ventilating current (Section 21.3.2.2.). This can occur over the heads of workers who are fighting the fire from an upstream position. Again, burning of the gases along the air interface can occur, igniting coal or timber in the roof and producing the danger of explosion. Personnel involved in fighting a fuel-rich fire may become aware of pressure pulses or rapid fluctuations in the movement of the air. These are caused by rolling flames and "soft" explosions as gases ignite along gas:air mixing zones. The same phenomena can be observed following ignitions of methane (Section 1.2.). Such pulsations may be a precursor to a larger and more violent explosion.

It follows that every attempt should be made to prevent an oxygen-rich fire from developing into a fuel-rich fire. This underlines the need for early detection and prompt action. An intuitive reaction to a fire may be to restrict the air supply and, hence, remove the oxygen leg of the fire triangle. This can be accomplished by building stoppings or erecting brattice cloths upstream from an airway fire. However, consideration of the dangers inherent in fuel-rich fires indicates that restricting the airflow might be inadvisable. Analyses of gases downstream from fires can be interpreted to indicate whether a fire is oxygen-rich or fuel-rich (Section 21.7).

21.3.2. Effects of fires on ventilation

An open fire causes a sharp increase in the temperature of the air. The resulting expansion of the air produces two distinct effects. First the expansion attempts to take place in *both* directions along the airway. The tendency to expand *against* the prevailing direction produces a reduction in the airflow. This is known as the *choke or throttle effect*. Secondly, the decreased density results in the heated air becoming more *buoyant* causing local effects as well as changes in the magnitudes of natural ventilating energy.

21.3.2.1. The choke effect

Consider an airway before it is affected by a fire. Air flows along it at a mass flowrate of M kg/s and doing work against friction at a rate of F J/kg. The airpower dissipated against friction, P_{ow} , is the product of the two

$$P_{ow} = FM \quad \frac{\text{J kg}}{\text{kg s}} \quad \text{or} \quad \text{Watts} \quad (21.1)$$

The effect of a fire in the airway upon P_{ow} depends upon the reactions of fans, natural ventilating pressures and ventilation controls throughout the system. However, if no deliberate action is taken to change these factors, it is reasonable to estimate that it remains sensibly constant.

Equation (7.10) gave us

$$F = \frac{p}{\rho} = R_t Q^2 \quad \frac{\text{J}}{\text{kg}} \quad (21.2)$$

where p = frictional pressure drop (Pa)
 ρ = mean density of air (kg/m³)
 R_t = rational turbulent resistance of the airway (m⁻⁴)
 and Q = mean value of airflow (m³/s)

Combining equations (21.1) and 21.2) gives

$$P_{ow} = FM = R_t M Q^2$$

or $P_{ow} = R_t \frac{M^3}{\rho^2} \quad \text{W} \quad (21.3)$

as $Q = \frac{M}{\rho}$

Equation (21.3) may be written as

$$M = \left\{ \frac{P_{ow}}{R_t} \right\}^{1/3} \rho^{2/3} \quad \frac{\text{kg}}{\text{s}} \quad (21.4)$$

As P_{ow} and R_t are constants,

$$M \propto \rho^{2/3} \quad (21.5)$$

where \propto means 'proportional to'

Hence, as the fire causes the density of the air to decrease, the mass flow of air will also decrease for the same energy dissipation. This phenomenon produces the choke effect. It should be noted, however, that the *volume* flow exiting the airway has *increased*.

As $M = \rho Q$, proportionality (21.5) can be written as

$$Q \propto \frac{1}{\rho^{\frac{1}{3}}} \frac{\text{m}^3}{\text{s}} \quad (21.6)$$

Note, also, from $P_{ow} = FM = \text{constant}$, that as M decreases, the work done against friction per kg of air, F , must *increase* - a result of the increased volume flow and, hence, turbulence.

The choke effect is analogous to increasing the resistance of the airway. For the purposes of ventilation network analyses based on a standard value of air density, the raised value of this "pseudo resistance", R_t' , can be estimated in terms of the air temperature as follows:

From equation (21.3)

$$R_t = P_{ow} \frac{\rho^2}{M^3} \quad \text{m}^{-4}$$

Hence, for any standard (fixed) value of density and constant air power loss,

$$R_t' \propto \frac{1}{M^3}$$

But combining with proportionality (21.5) which represents the actual reduction in mass flow,

$$R_t' \propto \frac{1}{\rho^2}$$

For a given barometric pressure, the general gas law (Section 3.3.1.) gives

$$\rho \propto \frac{1}{T} \quad \text{where } T = \text{absolute temperature (K)}$$

Hence,

$$R_t' \propto T^2 \quad (21.7)$$

The value of the "pseudo-resistance" R_t' , increases with the square of the absolute temperature. However, it should be recalled that this somewhat artificial device is required only to represent the choke effect in an incompressible flow analysis.

Litton et al (1987) have also produced an estimate of the increased resistance in terms of the carbon dioxide evolved from a fire.

21.3.2.2. The buoyancy (natural draft) effect

The most immediate effect of heat on the ventilating air stream is a very local one. The reduced density causes the mixture of hot air and products of combustion to rise and flow preferentially along the roof of the airway. The pronounced buoyancy effect causes smoke and hot gases to form a layer along the roof and, in a level or descensional airway, will back up against the direction of airflow. The layering effect can be estimated using the method given in Section 12.4.2.

This phenomenon of **roll-back** creates considerable difficulties for firefighters upstream from the fire, particularly if the conflagration has become fuel-rich. The roll-back is visually obvious because of the smoke. However, it is likely to contain hidden but high concentrations of carbon monoxide. Furthermore, the temperatures of the roll-back may initiate roof fires of any combustible material above the heads of firefighters. The most critical danger is that tidal flames or a local explosion may occur throughout the roll-back, engulfing firefighters in burning gases.

One method of reducing roll-back is to increase the airflow in the airway. This, however, will increase the rate of propagation of the fire. Another method is to advance with **hurdle cloths** covering the lower 60 to 80 per cent of the airway (Section 12.4.2.). The increased air velocity at roof level will help to control the roll-back and allow firefighters to approach closer to the fire. However, this technique may also cause the roll-back gases to mix with the air and produce an explosive mixture on the forward side of the hurdle cloth. Furthermore, the added resistance of the hurdle cloth might reduce the total airflow to the extent that a fuel-rich situation is promoted. The behaviour of open fires is very sensitive to modifications to the airflow. Hence, any such changes should be made *slowly*, in small increments, and the effects observed carefully.

A third method of combatting roll-back is to direct **fog sprays** towards the roof. In addition to wetting roof material, the air induction effects of the sprays will assist in promoting airflow in the correct direction at roof level.

A more widespread effect of reductions in air density is the influence they exert in shafts or inclined airways. This was handled in detail under the name of natural ventilation in Section 8.3.1. The effect is most pronounced when the fire itself is in the shaft or inclined airway, promoting airflow if the ventilation is ascensional and opposing the flow in descensional airways. Indeed, in the latter case, the flow may be reversed and can result in uncontrolled recirculation of toxic atmospheres.

If the air temperatures can be estimated for paths downstream of the fire then the methods given in Section 8.3.1. may be employed to determine the modified natural ventilating pressures. Those temperatures vary with respect to

- size and intensity of the fire
- distance from the fire
- time
- leakage of cool air into the airways affected and
- heat transfer characteristics between the air and the surrounding strata.

At any given time, air temperatures tend to fall exponentially with respect to distance downstream from a fire. Climatic simulation models (Chapter 16) may also be employed to track the time transient behaviour of air temperatures downstream from a fire. However, in that case, two matters should be checked. One is that the limits of application of the program may be exceeded for the high temperatures that are involved. Secondly, the transient heat flux between the air and strata will be much quicker than for normal climatic variations. Hence, the virgin rock temperature (VRT) in the simulation input should be replaced by a "surrounding rock temperature" (SRT), this being an estimate of the mean temperature of the immediate envelope of rock around the airway before the fire occurs.

Having determined air temperatures in all paths downstream from the fire, the revised natural ventilation pressures for the mine can be determined. These may then be utilized in network analysis exercises to predict the changes in flow and direction that will be caused by a fire of given thermal output. A number of **fire simulation packages** have been developed to allow numerical modelling of mine fires (e.g. Trutwin et al (1992). Greuer, (1984); Greuer, 1988; Dziurzynski et al, (1988); Deliac et al, (1985); Stefanov et al, (1984); Wala (1998); Gillies et al (1995). Gillies A.D.S., et al (2004).

21.3.3. Methods of fighting open fires

The majority of open fires can be extinguished quickly if prompt action is taken. This underlines the importance of fire detection systems, training, a well-designed firefighting system and the ready availability of fully operational firefighting equipment. Fire extinguishers of an appropriate type should be available on vehicles and on the upstream side of all zones of increased fire hazard. These include storage areas and fixed locations of equipment such as electrical or compressor stations and conveyor gearheads.

Neither water nor foam should be used where electricity is involved until it is certain that the power has been switched off. Fire extinguishers that employ carbon dioxide or dry powders are suitable for electrical fires or those involving flammable liquids.

Deluge and sprinkler systems can be very effective in areas of fixed equipment, stores and over conveyors. These should be activated by thermal sensors rather than smoke or gas detectors in order to ensure that they are operated only when open combustion occurs in the near vicinity.

The two direct methods of firefighting introduced in this Section involve the application of water and high expansion foam. The additional or complementary means of fire management by adjustment of ventilation controls and the injection of an inert gas are discussed in Sections 21.3.4. and 21.6. respectively.

21.3.3.1. Firefighting with water

Except where electricity or flammable liquids are involved, water is the most common medium of firefighting. When applied to a burning surface, water helps to remove two sides of the fire triangle. The latent heat of the water as it vapourises and the subsequent thermal capacity of the water vapour assist in removing heat from the burning material. Furthermore, the displacement of air by water vapour and the liquid coating on cooler surfaces help to isolate oxygen from the fire.

Water is normally applied by hosepipes upstream from the fire. A difficulty in subsurface firefighting is the limited reach of water jets imposed by the height of the airway. This underlines the vital need for water to be available at adequate pressure and quantity in the firefighting range. In order for a water jet to reach some 30 m in a typical coal mine entry, water pressures should be in the range 800 to 1400 kPa (Mitchell, 1990) and capable of supplying up to five hoses from a manifold connected to a single hydrant. In practice, the range of water jets in mine airways may often be no greater than 10 m. The nozzles should preferentially be of the adjustable type to give either a jet or a fog spray.

Hard won lessons indicate the need for careful forethought in designing a mine firefighting water network. **The air and the water should flow in the same direction** so that firefighters do not become dependent on a water supply that passes through the fire before it reaches them. **Hydrants** should be located at strategic points with respect to areas of increased fire hazard, at intervals along airways and at cross-cuts with access doors. All fittings for hydrants and range components should be standardized throughout any given mine. Non-metallic caps should be used at hydrant outlets to minimize corrosion. However, these caps must always be removable by hand and without undue force. Supplies at firefighting stations should be inspected at set intervals to ensure their operational efficiency at all times. Range fittings should include tee-pieces, blank-off caps and manifolds. It is particularly important that hosepipes be unrolled and examined for deterioration on a planned maintenance schedule and that they should be stored according to manufacturers' recommendations.

If access can be gained to an airway that runs parallel to a fire then **fog sprays** can be directed through doors or holed stoppings into the path of the fire. This can be effective if the sprays are employed at an early stage and immediately downstream from the fire front. (see Fig 21.2). However, for a large conflagration or where the fire has become fuel-rich, it is likely to lose its effectiveness.

The **locations of pumps** and configuration of their power supplies should be considered carefully with respect to the layout of the mine. The pumps and routes of their cables should be chosen such that they are least likely to be disrupted by a fire. Dual power supplies via alternative routes may be considered. Furthermore, power for firefighting pumps should be capable of being maintained when electricity to working sections of the mine has to be isolated. Underground sumps can provide valuable water capacity. However, the firefighting system should also allow water to be supplied in adequate quantities from surface locations.

21.3.3.2. High expansion foam

Large volumes of water-based foam provide a valuable tool for fighting fires in enclosed spaces such as the basements of buildings or in the holds of ships. It has been employed for mine fires since at least 1956 (Eisner). The method is employed on large fires and, although it has had somewhat limited success in extinguishing mine fires, it can play a valuable role in cooling and quenching an area to an extent that allows firefighters with hoses to approach closer to the firefront. Even when sealing an area has become inevitable, valuable time for rescue operations can be bought by employing high expansion foam.

The bubbles are generated by a fan which blows air through a fabric net stretched across a diffuser. The net is sprayed continuously with a mixture of water and **foaming agent**. Bubbles can be produced at a rate of several cubic metres per second (Strang and MacKenzie-Wood, 1985). Compounds such as ammonium lauryl sulphate may be employed as the foaming agent while the addition of carboxymethylcellulose improves the stability of the bubbles (Grieg et al, 1975).

The objective is to form a plug of high expansion foam which fills the airway and is advanced on to the fire by the ventilating pressure. The **ratio of air to water** within the foam may be in the range 100:1 to 1000:1. As the foam advances, bubbles break around the perimeter of the airway when they touch a dry surface. However, the liquid that is released wets that surface and allows advancement of the following bubbles. Shrinkage of the foam occurs continuously at the leading edges and accelerates because of radiant effects as it approaches the burning material.

Control of the combustion process is achieved by two primary mechanisms. First, vapourization of the water removes heat from the site and, secondly, the increased concentration of water vapour may produce an extinguishing atmosphere. As the air within the bubbles is heated to 100°C it will expand by some 30 per cent. However, the vapourization of liquid water to a gas involves an expansion of about 1700:1. Assuming an air:water mix in the foam of 1000:1 a thousand litres of air expands to 1300 litres while 1 litre of water evaporates to become 1700 litres of water vapour giving 3000 litres of mixture. If the air originally had an oxygen content of 21 per cent then the evaporation of water will reduce that to

$$21 \times \frac{1300}{3000} = 9.1 \text{ percent which will extinguish flaming combustion.}$$

Despite these mechanisms, high expansion foam does have some drawbacks. First, it may be quite difficult to generate a foam plug that fills the airway completely. As the plug builds up, the air velocity will increase through the narrowing channel between the plug and the roof, tending to maintain the gap open. Judicious employment of brattice cloths may assist in forming a complete plug of foam. It is important to control the path of the foam and, in multi-entry systems, this can be problematic. The natural direction of movement of the foam is dictated by the ventilating pressure. Here again, brattice cloths or stoppings in cross-cuts to adjacent parallel entries can assist in controlling the direction of the foam. Major obstructions caused by roof falls are quite liable to occur during a large underground fire. A foam plug may not be able to climb over such obstructions with the ventilating pressure available.

The greatest danger of foam plugs is that the reduction in airflow may promote a fuel-rich fire with the attendant danger of explosion. Downstream gases should be monitored for the development of this condition. Both increases and decreases in combustible gases have been reported in differing fires when high expansion foam has been employed. The reduction in airflow will tend to raise the concentration of combustible gases. However, as the inert mixture of air and water progresses downstream, condensation of the water occurs, allowing the air fraction to increase and, hence, modifying the combustible gas concentrations.

After the application of high expansion foam has been initiated, it is important to maintain it in operation during fire fighting as intermittent production of foam can exacerbate the development of an explosive atmosphere. This underlines the need for good training so that operators are familiar with the equipment and procedure. Furthermore, care should be taken that sufficient supplies of foaming agent are available before the operation is started (Timko et al, 1988).

21.3.4. Control by ventilation

When contemplating changes to airflows and applied pressure differentials during a fire emergency, there are four types of effect that must be considered most carefully.

(a) The effect on the combustion process: The importance of avoiding the progression of an oxygen-rich fire into a fuel-rich fire has already been stressed in Section 21.3.1.

(b) The effect on direction and rate of propagation of the fire: Every attempt should normally be made to prevent an open fire from spreading into other airways. However, exceptions from this general rule may become necessary to guide products of combustion away from trapped personnel. An example may be the deliberate destruction of a stopping or air crossing to divert or short-circuit a fire path from an intake airway into an adjacent return. Again, any modifications of the airflow passing through the fire zone must seek to achieve a balance between speed of propagation and control of the combustion process.

(c) Effects on the distribution of products of combustion: This becomes a critical issue when personnel have become trapped in by the fire, particularly if their exact whereabouts are unknown. However, any steps that will improve atmospheric conditions in escapeways require to be investigated.

(d) Effects on airflow distributions in other parts of the mine: While the consequences of ventilation changes in the zone affected by the fire are of immediate concern, the effects of such changes throughout the rest of the mine should not be overlooked, particularly in a gassy mine or when personnel may still be evacuating other areas.

If a computer model of the mine ventilation network has been maintained up to date then this will prove invaluable in investigating the predicted effects of proposed changes to the ventilation system. With a modern network analysis package (Section 7.4.), a personal computer or terminal in the emergency control centre can produce such predictions within seconds. Nevertheless, the uncertainties inherent in a fire situation demand that actual changes to the airflow system be made incrementally while observing the reactions on distributions and gas concentrations. The following subsections discuss the practical strategies that may be employed to control a fire by ventilation.

21.3.4.1. Pressure control

Airways that are parallel and adjacent to the fire path will remain unpolluted provided they are maintained at a higher atmospheric pressure. These allow access for escape, firefighting, building or strengthening of stoppings in cross-cuts, or to apply water sprays into the fire path. In multi-entry workings, control of such pressure differentials can be achieved by the erection of brattice cloths in the adjacent airway as illustrated in Figure 21.2. Even if the pressure differential in the desired direction is not completely achieved, the reduced rate of toxic leakage may allow time for personnel to escape. If necessary, the brattice cloths may be advanced pillar by pillar to remove smoke sequentially from the adjacent airway. Devices such as the "parachute stopping" or "inflatable seal" have been developed to replace brattice cloths in such circumstances. These can be erected quickly and give improved seals around the perimeter of the airway (Kissell and Timko, 1991).

A consequence of this technique is that the airflow over the fire will be increased to an extent that depends upon the configuration and resistances of the local airways. Pressure differentials between airways can also be modified by the use of a temporary fan instead of a restriction in the adjacent airway. In this case, airflow over the fire will be reduced. The location and pressure developed by the fan must be selected with care in order to avoid recirculation of products of combustion. Where pressure differentials are small, even the few Pascals developed by a free-standing auxiliary fan can induce the desired effect (Section 4.4.3.).

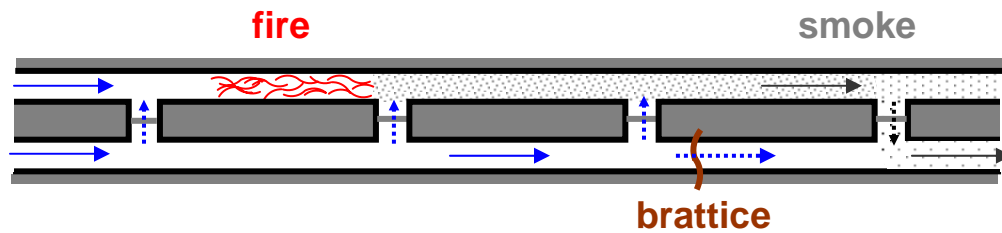


Figure 21.2 A brattice sheet in the adjoining airway clears smoke from that airway by promoting leakage into the firepath.

21.3.4.2. Airflow reversal

Many mines operate under a legislative requirement that the airflow provided by main fans must be capable of being reversed promptly. The background to such laws is the fear of a fire or other inundation of airborne pollutants occurring within a downcast shaft or main intake airway. Noxious and, possibly, flammable gases could then contaminate all, or most, of the ventilation system including working areas and return escapeways. If the fire is detected at an early stage then pollution of the complete system may be prevented by prompt reversal of the airflow. Even where contamination of the total network has occurred, air reversal may allow clearance of pollutants from return airways to the extent that a fresh air route may be established between surface and refuge chambers where personnel may be trapped. The decision to reverse a complete mine ventilation system is fraught with difficulties and has very seldom been taken in practice.

There are essentially three methods of achieving the reversal of airflow in a ventilation system. Where **axial impellers** are used on the main fans, then changing the direction of rotation will cause reversal of the airflow. This can be implemented electrically at the fan motor. However, axial fans operate efficiently in one direction only. The aerofoil section of each impeller blade is designed to give aerodynamic stability of flow through the fan. When operating in reverse, breakaway of the boundary layers over the blades occurs, resulting in high shock losses. The "lift" of the blades and, hence, the throughflow of air is greatly reduced (Section 10.3.2.). Similarly, fixed guide vanes, fan casings and evasees, all designed for a forward direction, will produce high shock losses when the airflow is reversed. The reversed air quantity may be reduced to less than 50 per cent of the normal forward flow (Dunn, 1982).

In the case of **centrifugal fans**, airflow reversal can be achieved only by means of reversal doors. The flow direction through the fan itself remains unchanged. For an exhausting centrifugal fan located at the mine surface, hydraulic or pneumatic activation of the reversal doors opens the fan inlet to the outside atmosphere and, simultaneously, diverts the fan exhaust into the mine shaft or slope. The opposite occurs for a forcing centrifugal fan. Where reversal doors are fitted as part of a surface fan installation, their operation should be checked routinely as part of a planned maintenance procedure.

Although the flow direction through a centrifugal fan remains unchanged, the shock losses incurred when air reversal doors are activated results in a reduced flow. The amount of the reduction is site specific and depends entirely upon the design and siting of the reversal doors, and the configuration of the fan with respect to the inlet and outlet duct arrangements. The possibility of requiring air reversal should be considered when designing the layout of airways and ventilation doors around an underground main fan. Such reversal should be attainable rapidly by opening or closing those doors.

During the course of ventilation network planning exercises (Chapter 9), it is often possible to design systems that allow rapid *reversal of airflow in one section of the mine*, or in a single airway, without total reversal at the main fans. This may be achieved by the strategic location of doors that can be opened or closed to permit airflow in either direction. Means of such **local reversal** might be considered, for example, for a conveyor route that is also to serve as an intake during normal operations.

Mandating the provision of air reversal facilities for an underground mine appears to be a reasonable safeguard. However, except in a clear-cut case such as a fire in or very close to a downcast shaft, the potential risks associated with reversing the airflow may be greater than those of maintaining the normal direction of flow, particularly in the short time period that may be available for making critical decisions.

The reasons that mine managements have very rarely decided to reverse ventilation during an emergency are both practical and also because of possible litigation should lives be lost as a consequence of the reversal. During the trauma of a major emergency involving changing conditions in air quality and possible disruptions of ventilation structures and communications, it may be impossible to know with certainty the locations, movements and dispersal of the workforce. Reversal of the airflow could then result in smoke and toxic gases being drawn over personnel who had assembled in a previously unpolluted zone. It may be expected that people who work routinely in a section of the mine will be familiar with the local ventilation system and, in case of an emergency, will act in accordance with that knowledge. Reversing the airflow could create additional uncertainty and confusion in their actions.

The majority of doors in airlocks or access paths between intakes and returns are designed to be self closing, assisted by the mine ventilating pressure. This may be a legislative requirement. In the event of airflow reversal, those doors will be blown open and create short circuits unless they are provided with self-locking devices. Even in the latter situation or where powered doors are employed, the proportion of air leakage must be expected to increase when the pressure differential across the door reverses. Hence, coupled with the diminution in overall flow caused by the reversal procedures, the reversed ventilation reaching the working areas must be expected to be much lower than the normal forward flow.

High temperatures usually preclude firefighting rescue teams from approaching a fire from the downstream side. If the airflow is reversed over a fire in an intake then firefighting teams must transport their equipment and materials to a fresh air base *inby* the fire.

The expansion of gases held in old workings or other voidage, and resulting from a drop in barometric pressure, is discussed in Section 4.2.2. In the case of a forcing fan being reversed to create an exhausting system, the rapid fall in barometric pressure throughout the system may cause large emissions of voidage gas. If these contain high concentrations of methane, passing it into the fire zone could result in a series of explosions propagating far back into the mine. Another possibility is that during the actual process of reversal, flammable gases from the strata or produced by incomplete combustion or volatilization of hydrocarbons may be drawn back over the fire, again, leading to the possibility of explosions.

Although there may be several hundred tonnes of moving air in a major subsurface structure, the braking effects of viscous shear and turbulence causes it to be a well-damped system. Hence, when a main fan stops, the effect is noticeable almost immediately at all places underground. In the majority of cases, natural (thermal) ventilating effects will maintain movement in the normal direction.

In the situation of forced reversal, the **transient effects** will exist for much longer time periods than for a simple stoppage of a main fan. This is because redistributions of the natural ventilating effects will not be completed until a new equilibrium of heat transfer has been established between the strata and the airflow. This may take several hours or even days. Furthermore, the fire itself will create thermally induced airflows with, perhaps, local reversals and recirculations. There is, therefore, some uncertainty concerning the speed at which reversal can be attained throughout the system and the stability of the reversed airflows. Research in Poland has indicated the efficacy of accelerating reversal by the use of intensive water sprays directed into the top of an upcast shaft (Trutwin, 1975).

21.4. SPONTANEOUS COMBUSTION

When air is allowed to percolate through many organic materials including coal then there will be a measurable rise in temperature. The same phenomenon can be observed in crushed sulphide ores and is caused by a progressive series of adsorptive, absorptive and chemical processes. These produce heat and an observable elevation in temperature. The percolating airflow will, therefore, remove that heat increasingly as the temperature of the material rises. If the leakage airflow is sufficiently high then a balanced equilibrium will be reached at which the rate of heat removal is equal to the rate at which heat is produced; the temperature will stabilize. The process will also reach an air-constrained equilibrium if the airflow is sufficiently low to inhibit the oxidation processes. However, between these two limits there is a dangerous range of percolating airflows that will encourage spontaneous heating.

Each material that is liable to spontaneous combustion has a critical temperature known as the minimum *self-heating temperature* (SHT). This is the lowest temperature that will produce a sustained exothermic reaction or *thermal runaway*. Hence, if the temperature reaches the SHT before thermal equilibrium is attained then the oxidation process will accelerate. The temperature will escalate rapidly, encouraging even higher rates of oxidation until the material becomes incandescent. At this stage, smoke and gaseous products of combustion appear in the subsurface ventilation system. The mine then has a *concealed fire*. The primary dangers of such occurrences are the evolution of carbon monoxide, the ignition of methane and combustion progressing into airways to produce open fires.

The phenomenon of spontaneous combustion has been recognized since at least the seventeenth century (PD-NCB, 1978). An early theory postulated that oxidation of pyritic material within coal provided centres of enhanced activity. Bacterial action is a factor in the initial natural heating of hay and other foodstocks. This can play a part in the spontaneous combustion of timber or organic waste material underground but is unlikely to contribute significantly to the self-heating of coal or other minerals. Similarly, while increases in the temperature of materials can be observed in ore passes (Section 15.3.6.), the gravitational energy of collapsing waste areas in mines produces temperature rises that are insufficient to promote spontaneous combustion. Current concepts of the initiation of self-heatings are discussed in the following subsection.

21.4.1. The mechanisms of spontaneous combustion in minerals

Although spontaneous combustion can occur in crushed or caved sulphide minerals and in heavily timbered areas within metal mines, the problem is most common in coal mines. Research in this area has concentrated on the spontaneous combustion of coals.

The development of self-heating requires a large surface area of crushed material combined with a slow migration of air through that material. Hence, the problem arises in goaf (gob) areas, caved zones, crushed pillar edges, fractured coal bands in roof or floor strata, stockpiles and tips on surface, and within abandoned sections of mines. The progressive stages of spontaneous combustion appear to be complex and not yet fully understood. Here, we shall examine the effects of *oxygen*, *elapsed time* and *water*.

21.4.1.1. The phases of oxidation

The oxidation processes of coal occur in four stages (Banerjee, 1985).

(a) *Physical adsorption* (Section 12.2.1.) of oxygen on coal commences at a temperature of about -80°C and is reversible but diminishes rapidly as the temperature increases to become negligible beyond 30 to 50°C . The process of adsorption produces heat as a by-product of the modified surface energy of the material. This causes the initial rise in temperature.

(b) *Chemical absorption* (known also as chemisorption or activated sorption) becomes significant at about 5°C . This progressively causes the formation of unstable compounds of hydrocarbons and oxygen known as peroxy-complexes.

(c) At a temperature which appears to approximate the self-heating temperature (SHT) of the coal, the **peroxy-complexes decompose** at an accelerating rate to provide additional oxygen for the further stages of oxidation. This occurs within the range of approximately 50 to 120°C with a typical value of 70°C. At higher temperatures, the peroxy-complexes decompose at a greater rate than they are formed (Chakravorty, 1960) and the gaseous products of chemical reaction appear - in particular, carbon monoxide, carbon dioxide, water vapour, and the oxalic acids, aromatic acids and unsaturated hydrocarbons that give the characteristic odour of "gobstink" (Section 21.4.4.).

(d) When the temperature exceeds some 150°C, the combustion process accelerates rapidly. Incineration of the coal occurs with escalating emissions of the gaseous products of combustion.

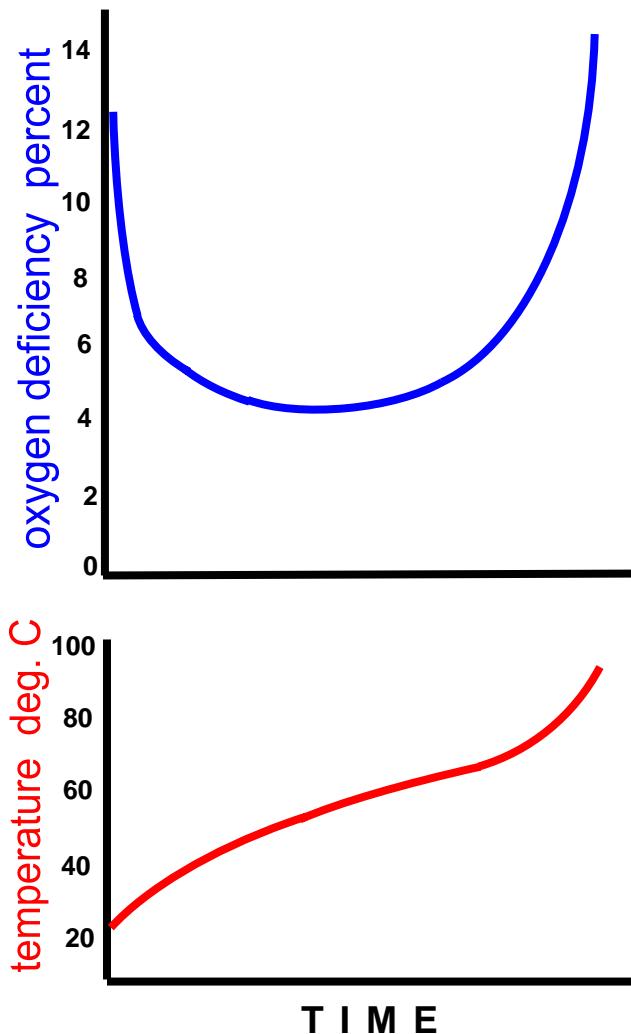


Figure 21.3 Examples of changes in oxidation rate and temperature with respect to time (developed from Muzyczuk, ref. Banerjee, 1985).

The time scale is omitted as this can vary from a few hours to many days depending upon the type and fineness of the coal, and the flowrate and psychrometric condition of the air.

The rate at which oxygen is consumed varies both with *time* and the *phase of oxidation* as illustrated in Figure 21.3. Oxygen is taken up rapidly in the earlier stages of chemisorption and as the peroxy-complexes are formed. However, this reduces with time and as the surfaces become coated (weathered) with those oxygen compounds. The temperature curve tends to level off and may reach equilibrium. However, if the SHT is reached, as illustrated in Figure 21.3, then both the rate of oxygen consumption and the temperature escalate rapidly.

21.4.1.2. The effects of water vapour

There are two processes involving *water* that act in opposite directions. First, the moisture content of the coal is driven off by evaporation during the early stages of heating. Hence, some of the heat is removed in the water vapour as latent heat of evaporation, tending to inhibit the temperature rise of the coal. The second process involves adsorption of water vapour *from* the air *by* the coal (Hodges and Hinsley, 1964). The heat of adsorption (sometimes called *heat of wetting*) produces an increase in the temperature of the material. It follows that the net effect depends on which of the two processes is dominant. Coal which is completely saturated with water is unlikely to increase in temperature due to heat of wetting. However, a dry crushed coal that is infiltrated by moist air can exhibit an initial rapid rise in temperature from this phenomenon.

Adsorption of water vapour adds considerably to the early stages of spontaneous heating of coal. It is significant that coal mines in dry climates tend to be less troubled by spontaneous combustion. However, it has been observed that re-ignition of coal frequently occurs on re-opening a mining area that has been flooded to extinguish a fire. This is thought to occur for two reasons. First, the flooding and subsequent drainage may produce further disintegration of the coal and the creation of new surfaces; and, secondly, it is probable that many points of higher elevation or entrapped gases may not be fully flooded and remain at a sufficiently high temperature (hot spots) to inhibit adsorption. When cooler air is admitted subsequently it will pick up water vapour as it progresses through the wet conditions. An initial short-lived cooling of the hot spots may be followed by rapid adsorption of water vapour and a renewed escalation of temperature.

21.4.1.3. The path of a spontaneous heating.

The processes of oxidation and adsorption do not occur uniformly throughout a mass of crushed combustible material. The rate and directions of air migration and the air:surface contact area depend upon the geometry of the zone, compaction from overlying strata and the fineness of the crushed material. Hence, the rapid escalation of temperature that characterizes the development of a concealed fire occurs first at discrete foci or "hot spots". The synergistic effects of iron pyrites are now thought to be caused by differential rates of expansion during the early stages of heating. The coal around the pyrites becomes more finely crushed and produces additional area for oxidation. Furthermore, the pyrite itself becomes oxidized, adding to the escalation in temperature. Green crystals of ferrous sulphate are formed which oxidize further to the yellow hydrated ferric oxide, a characteristic feature of zones in coal mines that have been involved in spontaneous combustion.

The migration of the heating again depends upon the rate and direction of air leakage. However, in contrast to open fires, **the tendency is for a spontaneous heating to propagate through crushed material against the airflow**, i.e. towards the intake airways.

21.4.2. Susceptibility to spontaneous combustion

A large number of tests and indices have been devised as suggested measures of the liability of differing coals and other materials to spontaneous combustion. These have involved:

- coal petrology and rank, the younger and lower ranks of coal being more susceptible
- rates of oxygen consumption or temperature rise at specified phases of the oxidation process
- self-heating temperatures (SHT) or other temperatures at specified stages of the heating process
- rates of heat production during isothermal or adiabatic tests.

No such test or index has been found to have universal application. The difficulty is that susceptibility to spontaneous combustion depends not only upon the material but also its physical state as well as the psychrometric condition and migration paths of the leakage airflows, the latter depending, in turn, upon the mining methods and layout. The matters of additional relevance are:

- ❖ amount and degree of comminution of crushed material left in the goaf (gob) area, these depending upon:
 - friability of coal
 - type of coal winning machine
 - efficiency of coal clearance (removal)
 - roof, floor or pillar coal left (percentage extraction)
 - thickness of seams and need for multi-lift or caving mining systems
 - depth and pre-stressing (microfracturing) of coal
 - geological disturbances

- ❖ methods of stowing and sealing of roadsides
- ❖ gradient of the seam and proximity of other seams
- ❖ length of face
- ❖ rate of face advance or retreat
- ❖ roof/floor stability and strata stresses in the vicinity of pillar edges, stoppings, air crossings and ventilation doors
- ❖ the air pressure differential across the affected area
- ❖ the layout and resistances of surrounding airways and faces, including obstructions
- ❖ degree of consolidation and, hence, resistance of the caved areas
- ❖ the relative moisture contents of the coal and air
- ❖ the reduction of oxygen content in the goaf (gob) areas by the emission of methane or other gases.

With this number and variety of factors it is not surprising that efforts to characterize the susceptibility of coals to spontaneous combustion purely on the basis of laboratory tests have met with rather limited success. An improved approach involves allocating weighted credit to each of the factors listed in an attempt to develop a site-specific indication of liability to spontaneous combustion (e.g. Banerjee, 1985; PD-NCB, 1978).

21.4.3. Precautions against spontaneous combustion

As with most potential hazards in the subsurface environment, *precautionary measures against spontaneous combustion at the time of planning and design of the mine*. Core samples of the seam or ore should be subjected to susceptibility tests discussed in the previous section. The layout of the ventilation network should be designed to minimize pressure differentials between adjoining airways and across caved areas. This might be arranged, for example, by favouring through-flow rather than U-tube arrangements (Section 4.3.1.). While design airflows must be sufficient to deal with gases or other airborne pollutants, consideration should be given to means of reducing those airflows such as methane drainage. Booster fans, where allowed by law, provide a powerful means of air pressure management and, coupled with the techniques of network analysis to investigate locations and fan duties, are most valuable in reducing incidences of spontaneous combustion. Branch resistances in the surrounding ventilation network should be kept as low as practicable by means of larger cross-sections or driving parallel entries. Furthermore, obstructions in those airways should be avoided.

The probability of spontaneous combustion can be reduced by minimizing the amount of coal, timber, paper, oily rags or other combustible materials that are left in gob areas. This may be inevitable if top coal must be left for the purposes of roof control. Nevertheless, efficient clearance of the fragmented coal from the face and good housekeeping should be practiced in mines that have a history of spontaneous combustion.

It is important for the mine ventilation engineer to be conscious of the *zones in which spontaneous combustion is most likely to occur*. Recalling that some leakage takes place through the strata around stoppings and doors, spontaneous heating may occur in coal which exists within that strata, whether it be in the roof, floor or sides. Good strata control and the liberal application of roadway sealants can help in such circumstances.

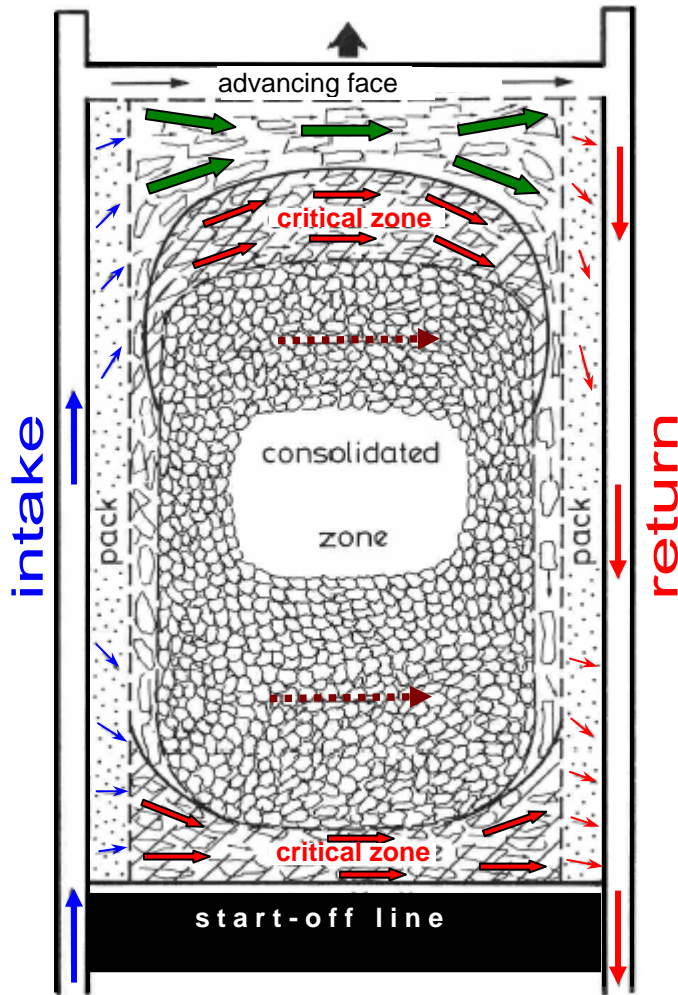
Pillars in coal mines should be designed large enough to minimize crushing at the edges and corners. Side bolts can help to maintain the integrity of pillars while the injection of low viscosity grouts might be used as a last resort. Here again, the application of surface sealants assists in preventing ingress of air. However, the most difficult types of spontaneous fires occur within caved zones and, in particular, in the goaf (gob) areas of coal mines.

Figure 21.4 illustrates the air migration paths and the zones most liable to spontaneous heating in the caved area of an advancing longwall. Those critical zones occur where the leakage airflows lie within that range which provides sufficient oxygen to promote continued oxidation of combustible material, but not enough to remove heat at the rate at which it is generated. There are two distinct zones. One of these lies along the original starting line of the face where incomplete consolidation allows a leakage path between intake and return. Within the central portion of the gob, consolidation allows little leakage. However, another critical zone occurs between the fully consolidated central core and the advancing face. This zone is not stationary but advances with the face. Recalling the time factor involved in the development of a spontaneous heating (Figure 21.3), it is clear that if the face is advanced continuously and at a sufficient rate then any potential heating may be "buried" by consolidation of the cave before it has had time to develop into a spontaneous fire. The most hazardous times occur at weekends and over holiday periods when additional precautions may be required. These include the application of **roadway sealants, grout injections into roadside packs**, and lowering the pressure differential across the gob by pressure balance techniques (Section 21.4.5.4.) In severe cases, injection of an inert gas into the gob may be considered (Section 21.6).

Figure 21.5 gives a similar illustration for a back-bleeder retreating longwall where the gob immediately behind the face is ventilated deliberately in order to prevent flushes of methane on to the faceline. Here again, the face start-up line and a moving zone trailing behind the face provide the critical zones most liable to spontaneous heatings. Despite the fact that the caved area is ventilated, less incidences of spontaneous heatings have been reported using this system than for advancing longwalls. As advancing or retreating systems tend to be favoured in separate geographical regions with differing coal seams and climates, there may be many reasons for this, as discussed in Section 21.4.2. Nevertheless, there are at least two features that may tend to mitigate against spontaneous heatings in back-bleeder layouts. First, there is likely to be a smaller pressure differential applied laterally across the gob area. This is particularly the case at the location of the starting line. Secondly, the fact that the area behind the face is actively ventilated may cause the critical zone between the ventilated and consolidated areas to be narrower and more quickly buried by the caving roof strata.

In mines with a history of spontaneous combustion, it is necessary to seal all abandoned workings. This is particularly important when those areas are adjacent to current workings and even more so when they exist within overlying strata. Spontaneous fires have resulted from undetected leakage airflows between current gob areas and workings that had existed in higher seams many years previously.

Following the completion and withdrawal of equipment from a section of a mine liable to spontaneous combustion, all entries into the section should be sealed and the atmospheric pressures applied to those seals balanced as far as it is practicable to do so. This may be accomplished simply by a re-arrangement of doors or by the dismantling of stoppings and air crossings. Active pressure balancing techniques may be employed as discussed in Section 21.5.5. The sites of seals should be prepared at strategic control points during the development of a section and should involve channels being excavated into the sides, and providing a nearby stock of building materials. This will facilitate sealing the district rapidly in the event of an uncontrollable fire.



Sufficient air to remove heat as it is produced.

Critical zones. Sufficient oxygen to promote oxidation but not enough to remove heat at the rate at which it is produced. The self-heating temperature may be reached.

Consolidation of material prevents enough oxygen to cause combustion that can reach self-sustaining temperature.

Figure 21.4 Zones showing liability to spontaneous combustion in the caved area behind a single entry advancing longwall face.

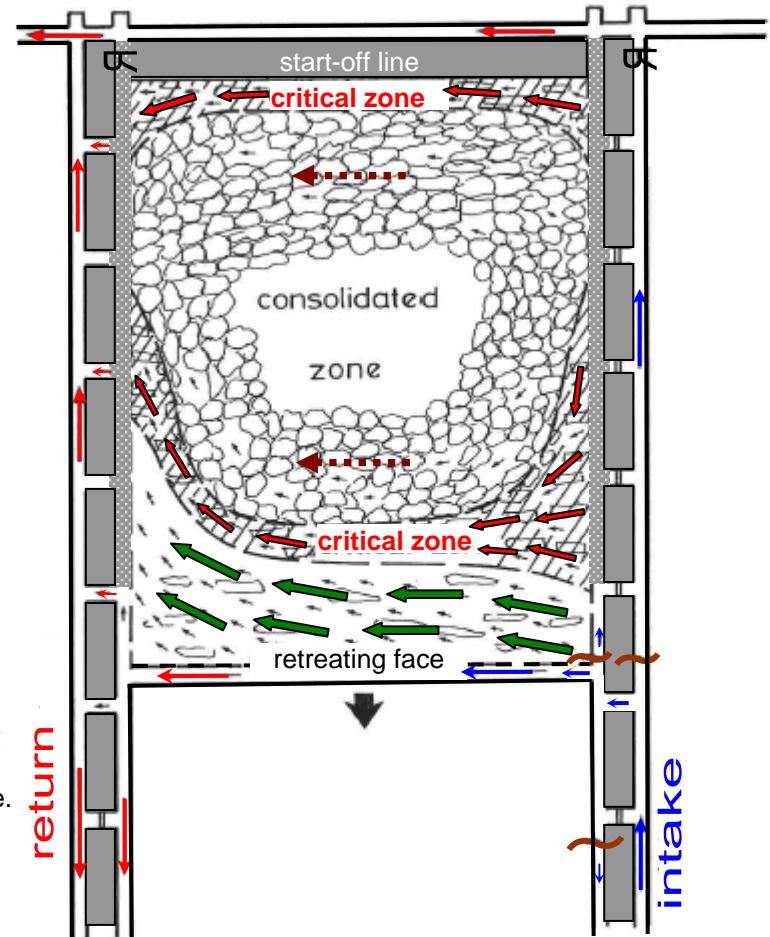


Figure 21.5 Zones showing liability to spontaneous combustion in a multiple entry retreating longwall with back bleeders.

21.4.4. Detection of a spontaneous heating

There are essentially three classes of detection for incipient or active spontaneous heatings. The oldest and, many would argue, still the most reliable is through the human senses. The aromatics and unsaturated hydrocarbon gases that are produced during the oxidation phases (Section 21.4.1.) give rise to an odour known colloquially as *gobstink*. This has been described variously as like "petroleum, the oil used in a flame-safety lamp and sterilizing liquid." Although, as with all odours, it can be described only by analogy it is, nevertheless, very distinctive and unlikely to be forgotten. Figure 21.6 illustrates the increasing strength of the smell with respect to gas concentrations and temperature of the oxidizing coal.

The odour is likely to be the first indication of a heating that can be detected by the human senses. The output of water vapour may also be observed either as a haze in the air or from beads of condensation on steel supports or other surfaces in locations where such condensation is unusual. At a later stage, the matter is put beyond doubt by the appearance of smoke.

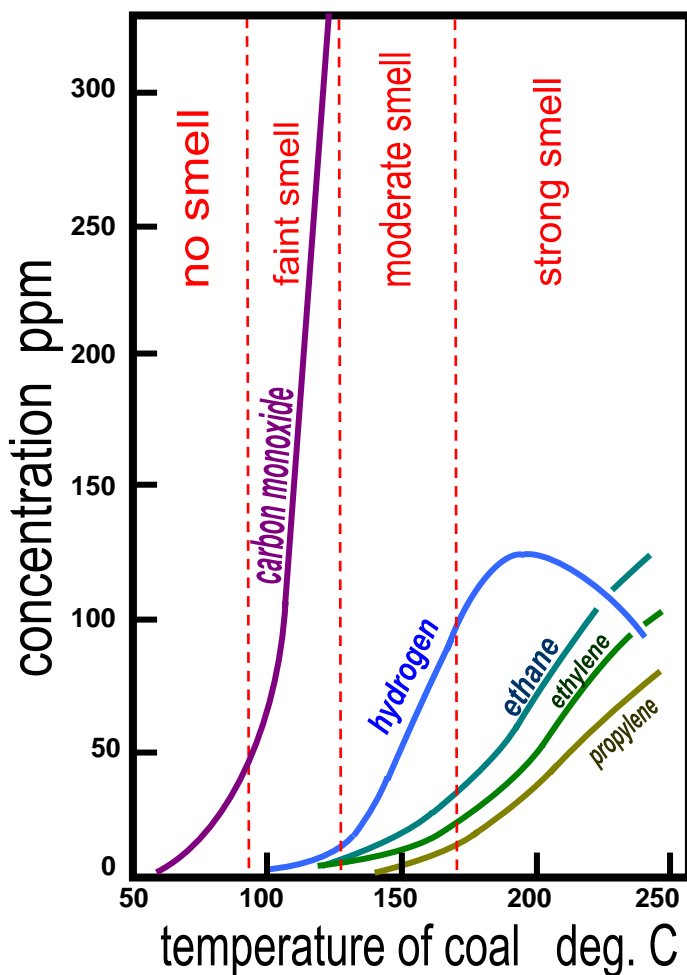


Figure 21.6 Example of the development of odour and gases from a medium-volatile bituminous coal. The relative positions of the gas curves will remain the same for other coals but the actual concentrations vary with the rank of coal and magnitude of leakage airflows.

The second class of detectors are *thermal devices* used to determine increases in temperature. Infra-red scans of roadway sides have been employed to identify the emission points of warm gases into airways and are useful for localized heatings in pillars or around stoppings (Chakravorty and Woolf, 1980). They are less useful as a permanent and continuous means of warning. Thermocouples or thermistors have been left in gob areas. However, they too have met with little success to the present time. First, their wiring is unlikely to withstand the mechanical stresses of an active caving zone, even when sheathed. Secondly, the thermal conductivity of crushed rock is low. Hence, the temperature even within a metre of an active centre of heating may indicate no abnormal condition.

The most widespread method of detecting the onset and development of a spontaneous heating is by monitoring *gas concentrations* in return airways (ref. Section 11.4.3). The gases that are evolved are indicated on Figure 21.6. The interpretation of the relative values and trends of these concentrations is discussed in detail in Section 21.7.

21.4.5. Dealing with a spontaneous heating

There is a procedure that should be followed when detection systems indicate that an active spontaneous heating is developing in a mine. First, a gas monitoring station should be set up downstream from the affected area and air samples taken at intervals of not more than 30 minutes. If an air monitoring system already exists in the mine then even greater detail of gas concentration trends can be followed. Personnel should be evacuated from all return airways affected and, if the condition is developing rapidly, also from the rest of the mine except for those involved in dealing with the situation.

Simultaneously, steps should be undertaken to identify the location of the fire. This may be obvious if smoke appears from discrete places in a close vicinity such as from a fire in leakage paths around a stopping or in the crushed corner of a pillar. The location of the fire is more difficult to detect if it occurs in a caved zone or inaccessible old workings. Whether or not smoke is present, it is useful to conduct a carbon monoxide survey. Measurements can be made by hand-held instruments or by stain tubes (Section 11.4.2.). Indicating the results on a mine map can assist in selecting the most probable sites of the fire.

Having located the fire, the next step is to decide how to control and, if possible, extinguish it. A variety of methods exist for this purpose. The injection of an *inert gas* as a practical and powerful method of dealing with both open and concealed fires in mines was developed through the 1980's and is discussed separately in Section 21.6. Other techniques of fighting concealed fires are introduced in the following subsections.

21.4.5.1. Excavating the fire

If the fire is known to be within a few metres of an airway then it may be possible to dig out, cool and remove the incandescent material. This can be the case for fires in pillars, around stoppings or air crossings, or for some gob fires. It may be necessary to drill holes into the zone in order to more accurately determine the site and extent of the fire. The excavation should commence from the upwind side of the fire to minimize the exposure of personnel to smoke and carbon monoxide. The airway should be wetted and/or coated in stonedust for a distance of some 10 m on either side of the excavation. Care should be taken to ensure control of the roof which may have become weakened by heat. Readings of methane and carbon monoxide concentrations should be taken frequently downstream from the site. As the fire is approached, it may be necessary to spray water on the workers to cool them. When the seat of the heating is exposed, it should be cooled by water jets applied around the periphery. Spraying water into the heart of a glowing carboniferous mass can result in the formation of water gas (Section 11.2.6.). The hot material should be loaded into metal conveyances and dampened thoroughly before transporting it out of the mine. When all of the incinerated material has been removed, the void should be cooled and, after some 24 hours to ensure no re-ignition, filled with an inert material such as limestone dust or gypsum-based wet fillers.

If it is impracticable to remove the fire physically then it becomes necessary to prevent ingress of air to the fire location. This leads us into the remaining techniques of dealing with a concealed fire.

21.4.5.2. Burying the fire

In some cases, it is possible to prevent or reduce access of air to the fire location by burying it under collapsed roof strata. Localized leakage through a roadside pack can be reduced by bringing the roof down in the airway, employing shotfiring if necessary, removing only a portion of the debris and compacting the remainder over the area to be sealed. The excavated roof must, of course, be well supported leaving the airway with an anticline.

If the heating occurs in the critical moving zone behind a longwall face (Figures 21.4 and 21.5) and is detected sufficiently early, then it is sometimes possible to bury it under consolidated caved material by a temporary increase in the rate of face advance (or retreat). This is likely to be successful only if the incipient heating has been detected by an early warning gas detection system and well before smoke appears.

21.4.5.3. Sealants

A variety of sealants have been employed on stoppings, airway surfaces, roadside packs and pillars in order to increase their resistance and, hence, reduce the access of leakage air. These may be applied on external surfaces or injected as grouts into the strata or packed material. While sealants that include resins or gels produce the lowest permeabilities and allow a degree of flexibility, the choice must often be made quickly and on the basis of local availability. Concrete and gypsum plasters can be sprayed quickly and effectively on to airway surfaces, as well as being useful for grouting and seal infills between stoppings. Water based slurries using mill tailings or other waste material have also been employed as grouts or for injecting into fire zones. These may be applied through boreholes drilled either from an underground location or from the surface. The injection of sodium silicate into coal pillars has been found to be effective (Banerjee, 1985).

While all known leakage paths connecting to the fire zone through roadsides should be sealed, it appears to be particularly advantageous to seal on the inlet or high pressure side. It is, however, often difficult to locate the relevant points of inward leakage on the inlet side. One way of doing this, where allowed by law, is to employ the techniques of pressure management (ref. following subsection) to intentionally and temporarily reverse the direction of leakage across the fire area. The appearance of smoke or elevated concentrations of carbon monoxide in the intake will identify the normal inlet points after which the flow reversal should be terminated or, better still, the leakage reduced to zero. This method should be employed with caution and only when adequate gas monitoring facilities are available in order to avoid unknown recirculation. The approval of governmental agencies should be sought if necessary.

21.4.5.4. Localized pressure balancing

If no differential pressure exists across a level permeable zone then there can be no air leakage through it. Pressure balancing involves raising the pressure on the return side or decreasing the pressure in the intake until the leakage flow is reduced to near zero. This principle can be applied to complete sections of abandoned workings as described in Section 21.5.5. or, in a more localized manner, to gain control of a gob fire without sealing the district.

Figure 21.7 shows the principle of this technique which can be applied to a variety of situations. In the example illustrated, a fire has commenced along the starting line of an advancing longwall. The pressure differential between intake and return in that vicinity has been reduced to near zero by the installation of a fan and regulator in the return airway. In cases of low normal pressure differentials, an induction fan without any surrounding brattice may be sufficient (Section 4.4.3.). The hydraulic gradients shown on the same figure illustrate the pressure differentials with and without the pressure balance. Where applicable, the method can be applied quickly and at low cost to arrest the development of a spontaneous heating and bring about an immediate reduction in carbon monoxide emissions. A pressure survey (Section 6.3.) may be run around the district to determine the effective fan pressure required. If there is convenient access, then a length of pressure tubing can be installed between the relevant points in the intake and return airways including an in-line pressure gauge. The regulator in the return airway can be adjusted until the pressure balance is achieved. Furthermore, an adjustable orifice within the short length of fan ducting can be used to modify the effective fan pressure. The locations of the fan and regulator may be changed in order to achieve finer control of the zone in which the pressure balance is applied.

The method of localized pressure balancing is very flexible and can achieve spectacular and speedy success in many scenarios. However, it requires skilled personnel to devise and control each installation. If applied inexpertly, it can result in partial recirculation of products of combustion. In any case, it is a prudent precaution to employ a carbon monoxide monitor in the intake to detect any reversal of leakage flows.

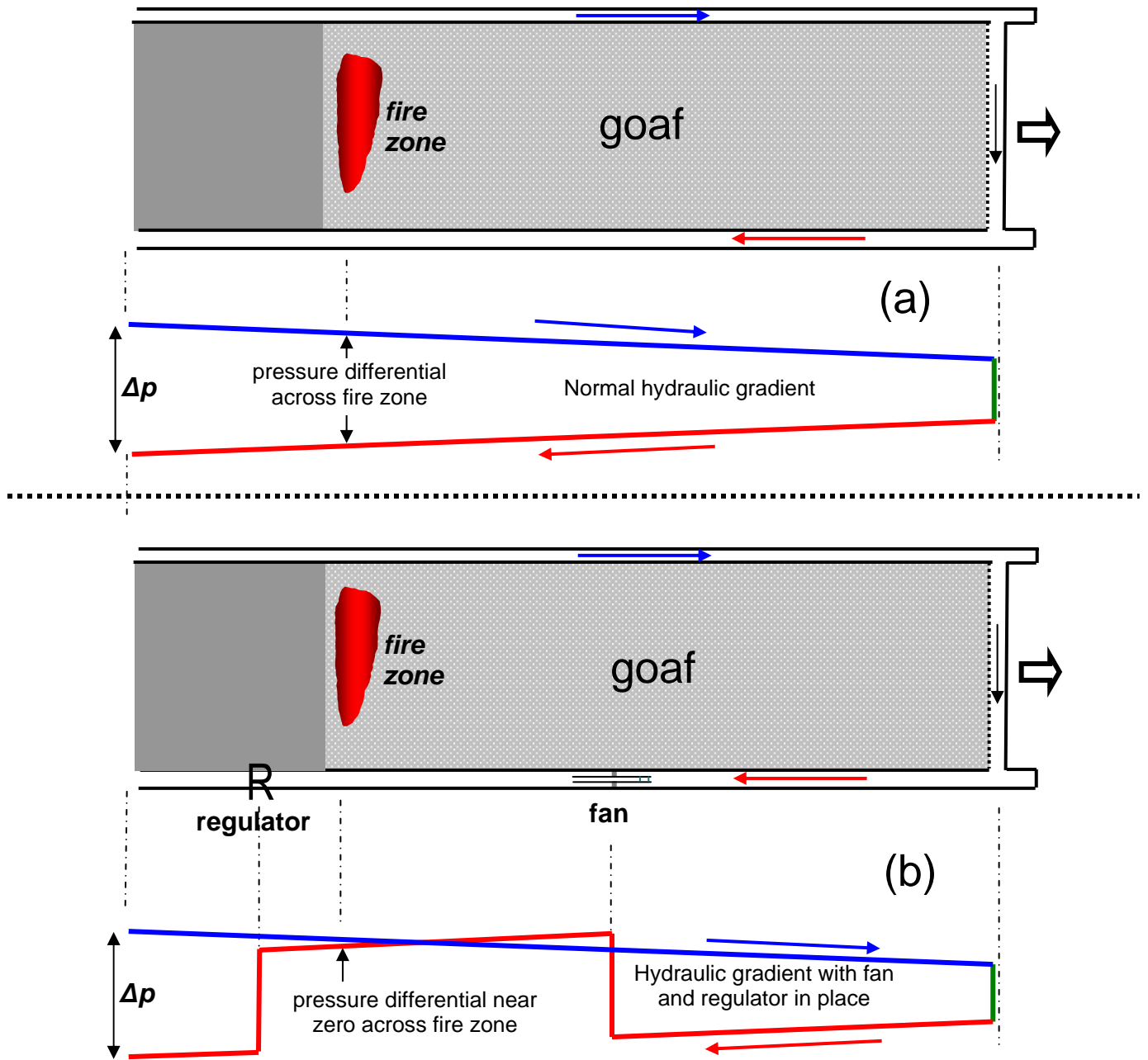


Figure 21.7 Example of localized pressure balancing to control a spontaneous heating in a goaf (gob) area.
 (a) without pressure balance (b) with pressure balance

21.4.5.5. Flooding and sealing off

Flooding can be used in two ways to extinguish concealed fires. First, if the affected zone lies to the dip of current workings then the fire itself can be flooded. This should be done in a controlled manner in order to be able to handle the products of combustion and other gases displaced by the water. Furthermore, if a previously flooded area is re-opened then it may rapidly re-ignite (Section 21.4.1.2.). The second use of flooding is to provide very effective seals in airways that have low-lying sections. The water penetrates fissures in the surrounding strata and provides a near perfect barrier against air leakage.

This brings us to the larger matter of building seals to control concealed fires in inby areas. While sealing a section of a mine is often considered as a last resort, it is important to recognize those situations in which it will become inevitable and then to seal quickly. This allows an inert atmosphere to build up and to extinguish active combustion. Re-entry and a resumption of mining may then be possible within a relatively short time. If, however, sealing-off has been delayed unduly, then the fire may have developed into such a large conflagration that the area could be sterilized indefinitely. The one situation in which sealing-off must be delayed is while there is the slightest possibility of rescuing trapped personnel. The procedures involved in constructing seals during a fire emergency are discussed in Section 21.5.

21.5. STOPPINGS, SEALS AND SECTION PRESSURE BALANCES FOR EMERGENCY SITUATIONS

This Section concentrates on the role of stoppings and seals in emergency situations involving fires or explosions. The routine use of these devices during normal mining operations is described in Section 4.2.1.2.

There is considerable divergence in differing geographical areas on the meaning of the terms *stoppings* and *seals*. In some regions, the two are regarded as synonymous while, in others, they are interpreted as quite different types of structures. To prevent confusion, we shall use the terms here according to the following definitions:

Temporary stopping: A light structure erected from brattice cloths, other fabrics or boarding but which will not withstand any significant physical loading.

Stopping: A single or double walled structure constructed from blocks, bricks, sandbags, prefabricated steel panels or from substantial boarding attached to tight roof supports. Stoppings are routinely employed as ventilation controls to minimize leakage between adjoining intake and return airways in active mining areas but are not intended to be explosion proof. It is to be expected, therefore, that stoppings will be destroyed or severely damaged in areas through which an explosion has passed.

Seal: A barrier designed to withstand mine explosions.

Temporary stoppings, often in the form of brattice cloths or quickly erected alternatives are employed during the fighting of open fires in order to regulate the airflow over the fire, change the air pressure in nearby airways (Section 21.3.4.1) or re-route airflows to assist in rescue operations.

Stoppings may also be used as a more substantial means of modifying and/or controlling the airflow paths in the event of a mine fire and to re-establish controlled ventilation during rescue operations.

Seals are used when alternative means of controlling a fire or spontaneous heating have been exhausted and inby rescue operations have been terminated. The purpose is to stop the flow of air and allow an inert atmosphere to build up within the affected zone. The decision on when to erect seals should be contingent on the particular circumstances. In the case of a deeply seated concealed fire seals may be erected in all entries to the area at a fairly early stage and before the heating reaches an open airway. The district may subsequently be re-entered for salvage of equipment or resumption of mining either after a cool-down period or when further arrangements have been made to control the heating. Sealing an airway fire should be carried out as soon as it becomes clear that the fire is out of control and rescue operations have been terminated.

21.5.1. Site selection of seals

It is important that all openings into an uncontrolled fire zone be sealed except for sampling pipes. Such openings may include boreholes and connections into old workings. In the shallower mines, there may be fractures extending through to the surface. The potential effects on surface structures and their inhabitants should be considered.

The sites should be selected to minimize the number of seals required. These are matters that should be taken into account during planning of the mine layout in order to facilitate rapid sealing of a section should that subsequently prove to be necessary. The precise locations should be in well supported areas with solid roof, floor and sides.

A well organized mine will have pre-prepared sites for seals at control points in each district and with a stock of the appropriate materials nearby (IME, 1985). In any case, those sites should allow ready access for the supply of further materials and, also, for the provision of ventilation to personnel involved in building the seal. The latter may necessitate a temporary duct and auxiliary fan. If the site is polluted by products of combustion then the construction must be undertaken by teams fitted with breathing apparatus. Where there is danger of an explosion or outrush of gases during construction, sites should be chosen that permit rapid escape of the personnel.

It is unlikely that locations will be found which satisfy all of these requirements. Site selection for stoppings and seals invariably requires compromises between optimum positions and practical considerations.

21.5.2. Sequence of building seals

In the case of concealed fires and where there is no imminent danger of explosion, it is preferable to complete intake seals first in order to terminate airflow into the fire zone, then to follow up quickly with closure of the return airways. However, in the case of an open fire, or where monitored gas concentrations indicate that an explosive atmosphere may develop then all stoppings or seals should be completed simultaneously and personnel evacuated from the mine for a period of 24 hours.

21.5.3. Construction of seals and stoppings

It is unlikely that explosions arising from fires in mines will generate pressure peaks of more than some 350 kPa gauge pressure¹ (50 psig²) on the faces of seals although considerably higher pressures have been measured in experimental explosions (Strang, 1985) and in explosions initiated by an ignition of methane. Hence, seals which (by our definition) should be explosion-proof must be able to withstand such dynamic pressure pulses. Figure 21.8 illustrates a typical seal. The end walls may be constructed from sandbags, masonry or any form of non-flammable blocks. The strength of the seal should be provided by the infill and any girders or other supports that may be employed in the intervening space. The length of seal is shown as 3 to 5 m but may be calculated as $\frac{\text{Airway width} + \text{height}}{2} + 0.6$ with a minimum length of 3 m (Hornsby et al, 1985) and should be chosen with reference to the condition of the surrounding strata and the type of infill available.

Construction of a seal in coal mines should commence by applying stonedust liberally to the airway inby the seal. Stonedust barriers may also be erected inby the seal to arrest an explosion before it reaches the face of the seal (Section 21.8.3.1.). Figure 21.8 illustrates the end walls recessed into the roof, floor and sides. This is considered to be good practice although it may not be necessary provided that the strata is competent, the length of seal adequate and a modern (quick-setting) wet infill is available. Conveyor

¹ Sometimes known as "overpressure"

² psig means pounds force per square inch gauge pressure. British Imperial units have been added as sections in this chapter are of particular interest in the United States following the Sago and Darby Mine explosions.

structure should be dismantled and cleared from the area. Similarly, pipes and cables should be dislocated and removed.

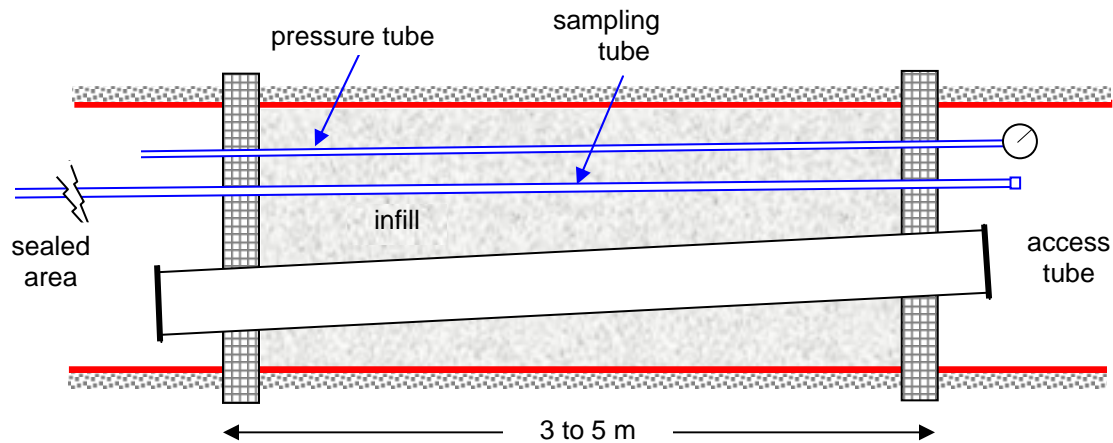


Figure 21.8 Example of an explosion proof seal where an active fire exists in the sealed area.

While dry material such as sand, stonedust or fly ash may be used for the infill, a better seal is obtained by employing a gypsum based plaster. This is pumped in as a liquid which penetrates immediate fractures in the surrounding strata then sets to a compact solid material. It is important that the infill completely blocks the seal to the roof.

The gas sampling pipe should extend at least 30 m in by the seal to allow for 'breathing' induced by fluctuations in barometric pressure. Three flexible tubes may be threaded through the metal sampling pipe in order to draw independent samples from roof, floor and middle of the sealed airway.

The steel access tube shown on Figure 21.8 has a number of purposes. First, it allows ventilation to be supplied to the fire while construction of the seal is in process. This tends to retard the development of a fuel-rich situation and, hence, reduces the risk of explosion whilst workers are still at the site. Despite the access tube, workers may be subjected to roll-back of smoke during construction of a seal. When each of the seals has been completed then all access tubes should all be blanked off *simultaneously* by strong steel plates both ends. All personnel must leave the mine for a period of 24 hours or until monitored signals of gas concentration indicate that an inert atmosphere has been attained.

Following the sudden cessation of airflow, significant changes take place within the sealed zone. The concentration of combustible gases increases while the oxygen content decreases. In the case of open fires, it is probable that the mixture of gases will pass through an explosive range (Section 21.7.). Meanwhile, convection effects will create movements of the changing atmosphere and, perhaps, rolling or 'tidal' flames. The combination of these effects may produce a series of explosions. These can be monitored by pressure transducers connected to the pressure tubes on the seals. An older but simpler method is to leave a glass U-tube containing mercury attached to a pressure tube. If the mercury is subsequently found to have been blown out then an explosion has occurred within the sealed zone.

A second reason for the access tube is to allow subsequent re-entry and inspection by rescue teams equipped with breathing apparatus. The outby end of the tube should be at a convenient height for this purpose. Should it become necessary, the access tube can be filled with infill material. This is the reason for the slight downward inclination of the tube towards the sealed area.

There is one major disadvantage to the type of seal we have been discussing - the time taken for its construction. In the case of an open fire in a timbered or coal-lined airway, rapid action is vital. It may be necessary to isolate the zone in a much shorter time period than that required to build an explosion proof seal. An alternative is to erect a stopping that contains a pressure-relief flap. This is a technique that has met with some success in the United States (Mitchell, 1990). Figure 21.9 illustrates such a *vented stopping*. Boards are attached firmly to two or three tight chocks (cribs) on both upstream and downstream sides except for the top quarter or third of the airway. A sealant can be sprayed over the boards. A weighted flap of conveyor belting is attached across the top of the outby side and held open by a cord which is tensioned by the weight of a canister of water. At the appropriate moment the canister at each site is punctured and all personnel leave the mine. The flaps close as the canisters empty.

Except for violent explosions, the structure of a vented stopping will remain intact. Lesser pulses simply blow open the flap which then falls back into place leaving the integrity of the stopping secure. Although the vented stopping does not have the structural strength or resistance of an explosion-proof seal, it provides a temporary expedient until permanent seals can be established, should those prove to be necessary.

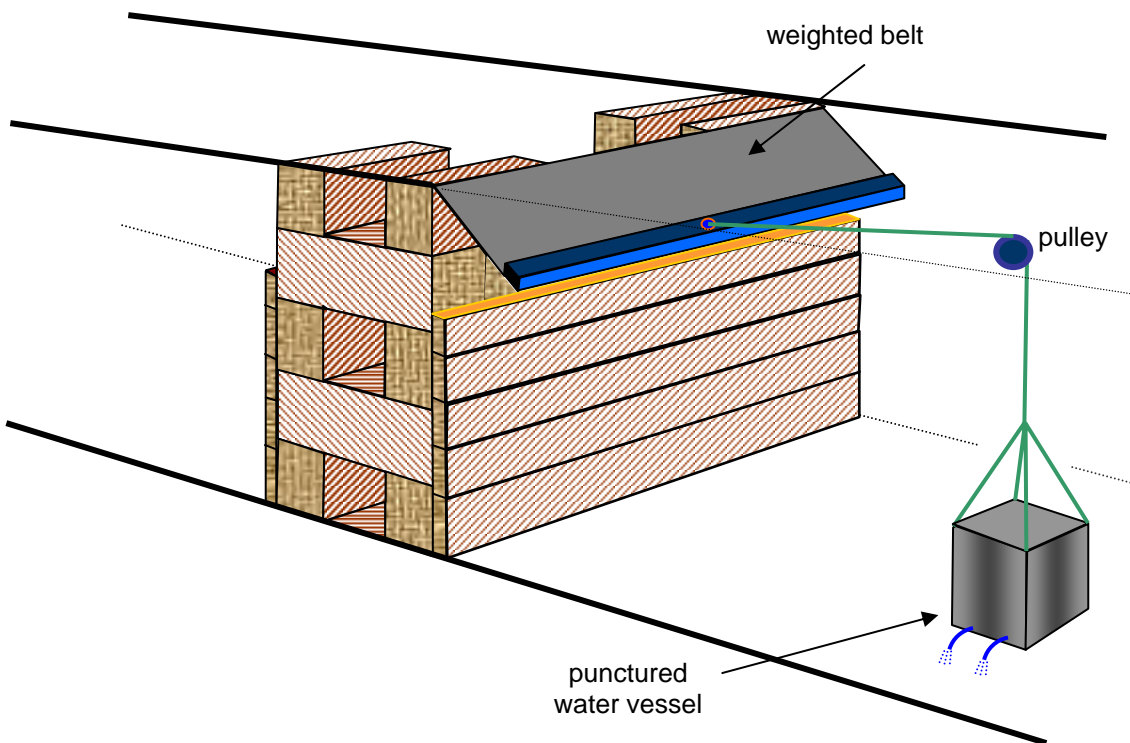


Figure 21.9 A vented emergency stopping.

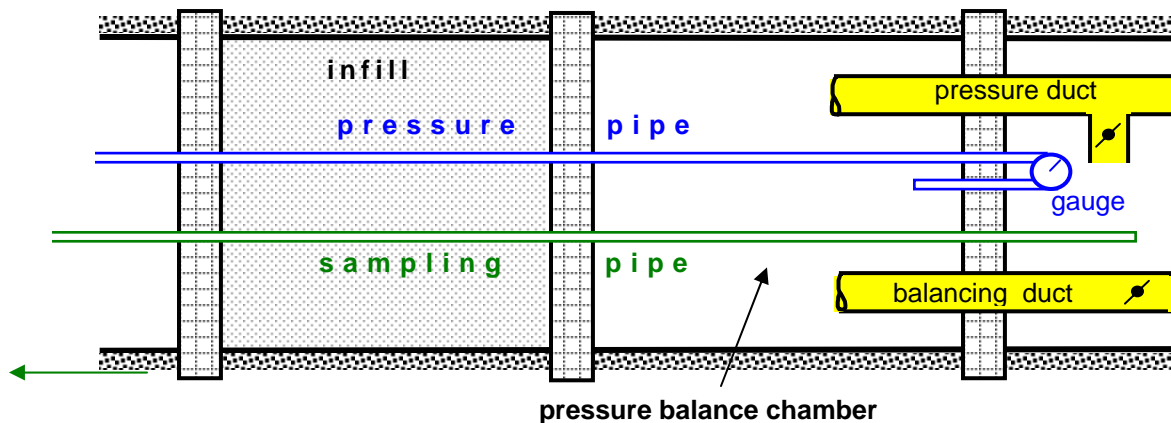
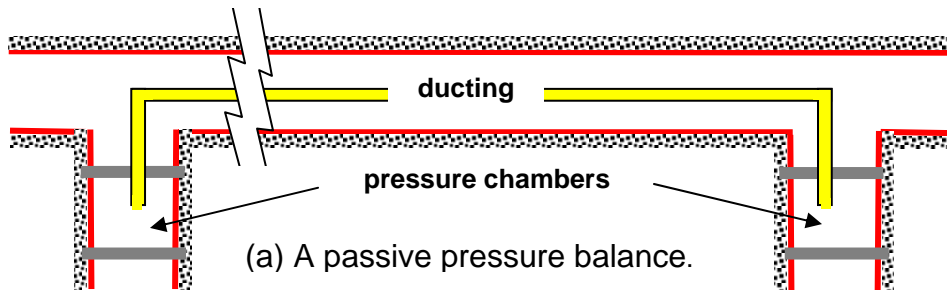
21.5.4. Re-opening a sealed area

The simple method of breaching stoppings or seals and re-establishing an air circuit suddenly is not one that can be recommended when a mine or section of a mine has been sealed because of a fire. Even when gas samples indicate that the fire is no longer active, hot spots may still remain that could result in re-ignition when supplied with oxygen. The preferred technique is first to send in rescue teams equipped with breathing apparatus to make a thorough inspection of the area and to take additional air samples. If the sealed area is extensive and, particularly, if the atmosphere will pass through an explosive range when mixed with fresh air, it may be necessary to re-ventilate in stages, building additional seals or stoppings further inby and closer to the original fire zone.

21.5.5. Section pressure balances

No stopping or seal in the subsurface has infinite resistance. Even if the stopping or seal itself were perfect, the potential for leakage still occurs in the surrounding strata. Such leakage can delay the extinction of a fire or, if serious, may maintain the fire indefinitely. Section 21.4.5.4. described how air pressure management can be employed to control the leakage airflows feeding a concealed fire. The same principle can be applied to complete sections of a mine.

The most rudimentary form of *pressure balancing* involves the re-arrangement of doors and air-crossings to ensure that each seal or stopping is exposed to return airway pressure. This reduces the pressure differential applied across the sealed district to the pressure drop over the length(s) of airway between the stoppings. Figure 21.10(a) illustrates an improved version. An additional wall is constructed some 3 to 5 metres in front of each main stopping or seal to form a *pressure chamber*. A duct of about 0.5 m diameter connects the chambers and, hence, equalizes their pressures. There is then no pressure differential applied across the sealed district, nor can there be any continuous flow around it. These are examples of *passive pressure balancing*.



(b) An active pressure balance chamber.

Figure 21.10 Passive and active pressure balance chambers.

The drawback to passive pressure balances is that they do not prevent "breathing" of the seals or stoppings during periods of changing barometric pressure. This can be overcome by employing an *active* (or powered) *pressure balance* system. This provides a means of equalizing the air pressures on the inner and outer faces of the same seal or stopping and is illustrated on Figure 21.10(b). Two ducts pass through the outer wall into the pressure chamber. One of these (the pressure duct) is supplied by a ventilating pressure either by a small fan or by laying the duct through a nearby door or stopping in order to utilize the mine ventilating pressure. The pressure chamber will be pressurized positively if the seal is on the return side of the main ventilation network and negatively if it faces an intake airway. The second

(balancing) duct simply passes through the outer wall. Both ducts are fitted with variable dampers to give a flexible means of fine adjustment to the pressure within the chamber.

Two tubes are employed to monitor air pressure, one passing completely through the seal and the other into the chamber. A gauge across these two tubes will indicate zero when there is no pressure differential between the chamber and the inby side of the seal. The duct dampers can be adjusted manually when the pressure gauge deviates from zero. The arrangement can be made automatic by employing an electronic pressure gauge which transmits an amplified signal to servo-motors on one or both of the duct dampers.

A number of special purpose adaptations to the principle of pressure chambers have been devised. One example may occur in a nuclear waste repository to ensure that leakage through an air lock takes place in one consistent direction at all times, irrespective of the direction of pressure differential across the airlock (Brunner et al, 1991). Another example, where permitted by legislation, is the use of compressed air to provide positive pressurization of the pressure chamber.

21.6. THE USE OF INERT GASES

The injection of inert gases to assist in the control of subsurface fires has been undertaken since, at least, the 1950's (Herbert, 1988). However, from 1974, significant developments in the deployment of nitrogen took place in Germany. The technique has become commonplace in coal mining areas where spontaneous combustion occurs frequently (Both, 1981). The overall purpose of injecting an inert gas is to reduce the oxygen content in order to prevent or inhibit combustion. The objectives may further be classified as follows:

- ❖ To prevent concealed heatings in zones that are highly susceptible to spontaneous combustion.
- ❖ To reduce the risk of explosions during sealing or stopping-off procedures.
- ❖ To accelerate the development of an inert atmosphere in a newly sealed zone and to prevent the creation of an explosive mixture when it is re-opened.
- ❖ To control the propagation of an open fire during rescue, firefighting and sealing operations.
- ❖ To prevent an explosive mixture forming due to "breathing" of a seal.

Three types of gases have been used in the procedure for which the term *inertization* has been coined; carbon dioxide, products of combustion and nitrogen. In this Section we shall discuss the employment of these gases in addition to methods of application and control.

21.6.1. Carbon dioxide

Carbon dioxide has a density of 1.52 relative to air (Table 11.1). This makes it particularly useful for the treatment of fires in low-lying areas such as dip workings or inclined drifts (Froger, 1985). However, the same property can render it difficult to control in horizontal workings. A 20 t tanker of liquid carbon dioxide will produce some 9000 m³ of cool gas. The liquid form may be piped into the area where it is required and expanded through an orifice or, indeed, injected directly into a localized heating. In both cases, the gas removes heat from the fire as well as promoting an inert atmosphere. However, piping the liquid carbon dioxide can give rise to freezing problems as well as difficulties in handling the pipes.

The use of carbon dioxide as an inerting gas has several other disadvantages. It is quite soluble in water and can suffer some loss in wet conditions. More significant perhaps, is the fact that it adsorbs readily on to coal and coked surfaces, even more so than methane (Figure 12.2(b)). When exposed to incandescent carboniferous surfaces it may be reduced to carbon monoxide. Furthermore, it is considerably more expensive than nitrogen.

21.6.2. Combustion gases

Following the sealing of a fire zone, gases produced by the combustion processes, combined with the consumption of oxygen, will produce an extinguishing atmosphere. However, it may be rich in combustible gases and become explosive if air is subsequently re-admitted (Section 21.7.3.). The products of full combustion, primarily mixtures of carbon dioxide, nitrogen and water vapour, have been employed as an injected inert gas. Flue gas from burning coal has been used in China (Sun, 1963) while modified jet engines have been employed in several countries including Poland, Russia and Czechoslovakia (Strang, 1985). The latter method involves burning kerosene at rates of some 0.7 kg/s to produce 30 m³/s of inert exhaust gases. These are cooled by large quantities of water and admitted into the fire zone. The engine produces a power output of about 30 MW which can be usefully employed. Where the law allows the underground use of a jet engine or where it can be employed on surface for a drift mine, then the large output of inert exhaust gases makes it attractive. However, it nullifies the employment of gas analysis as a means of following the progression of the fire, the capital cost is high and a highly specialized team is required to operate and maintain it.

21.6.3. Nitrogen

Liquid nitrogen is the basis for the majority of inertization schemes now employed for subsurface fires. Again, the liquid gas is supplied in tankers of, typically, 20 t capacity giving about 16500 m³ of gas. For continuous operation throughout a period of gas injection, the tankers may unload into a bulk storage vessel of up to 40 t capacity and which has been brought to the mine site.

Due to the low boiling temperature of nitrogen, the liquid must be evaporated before piping it into the mine. Figure 21.11 indicates the principle of a mobile evaporator which, again, has been brought to the mine for the emergency period. Typically, two water circuits are employed; a primary circuit using atmospheric heat and secondary heaters powered by electricity or liquid/gas fuels. The gaseous nitrogen passes through a bank of controllers before entering the mine pipeline. A subsidiary nitrogen line provides a feedback to maintain a constant pressure in the storage vessel. The maximum gas feed rate into the mine depends upon the duty of the evaporator but may, typically, be within the range 1 to 6 m³/s.

Liquid nitrogen is a by-product of the commercial production of oxygen and is much less expensive than liquid carbon dioxide. Furthermore, it is not as soluble as the latter, does not adsorb so readily on carbon surfaces and with a density approximating that of air, mixes readily without stratification.

21.6.4. Methods of application and control

In order to assess the volume flow of inert gas required, the rate of oxygen supply to the fire may be determined from the inlet oxygen concentration and a measured or estimated airflow. It is then a straightforward calculation to determine the flow rate of inert gas required to dilute the oxygen down to 10 per cent in order to extinguish flaming combustion, or to less than 2 per cent to suppress smouldering.

The inert gas may pass into the mine via water pipes or compressed air pipes commandeered for the purpose. Alternatively, gas feed boreholes may be drilled from the surface to intersect a fire zone (e.g. Zabrosky and Klinefelter, 1988). Perhaps the most difficult aspect of inertization is controlling dilution of the inert gas by air leakage. If leakage air enters in significant quantity between the gas injection point(s) and the fire, then the technique may fail. It follows that inertization is most likely to succeed where the fire is in a single entry with no leaking crosscuts or, in the case of a concealed fire, where the air inlet points have been well defined. Conversely, multi-entry systems offer a greater opportunity for

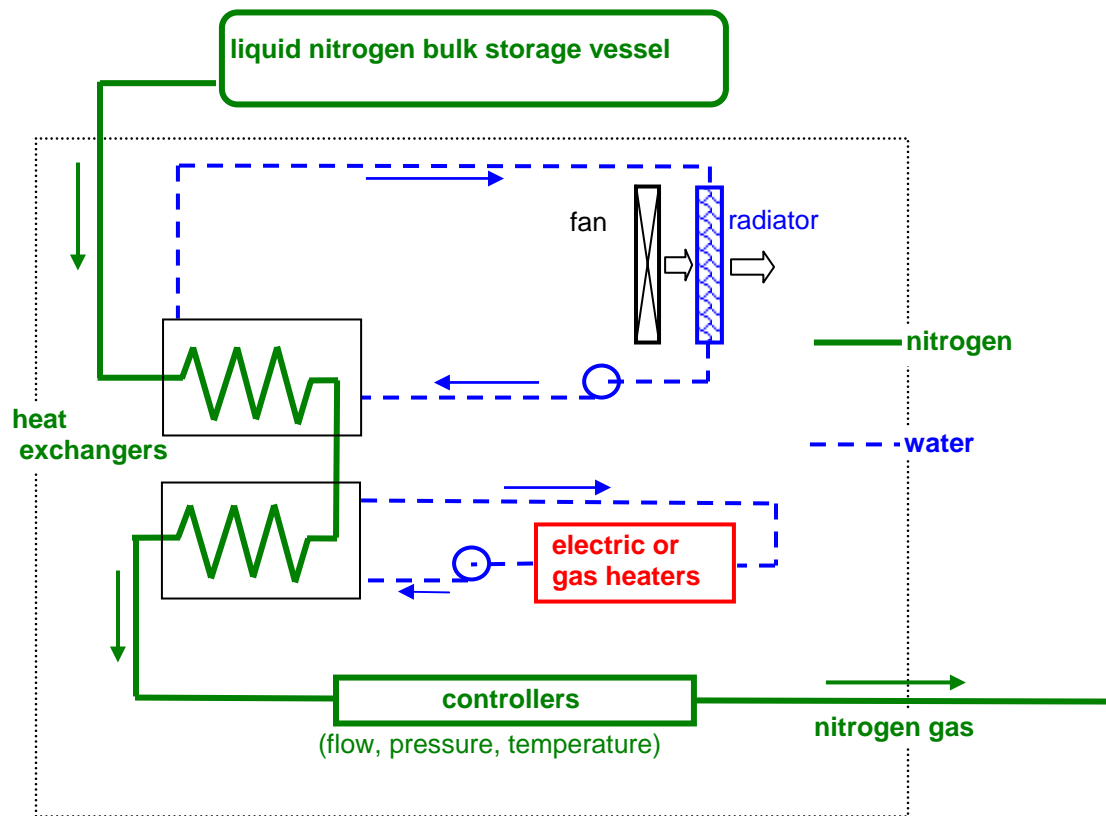


Figure 21.11 Simplified schematic of a mobile nitrogen evaporator.

dilution of the inert gas. Although the employment of inert gases can create difficulties in interpreting the analyses of gas samples taken downstream from the fire, it is usually possible to detect whether the fire is being suppressed. If there is no noticeable effect on an open fire within an hour or two then potential air leakage points should be investigated. Additional stoppings or pressure management techniques may be required to reduce the inward leakage.

For the control of spontaneous heatings in the goaf (gob) areas of longwall mines, the location of the fire and air entry points should first be established (Section 21.4.5.4.). Furthermore, a knowledge of air migration paths in goaf areas is invaluable (Figures 21.4 and 21.5). Injection pipes should be inserted from the airways or working face into the inlet zones, using boreholes if necessary. The volume flowrates of inert gas required are usually much lower for spontaneous heatings than for open fires. However, the reaction may be slower. Indeed, the monitored concentrations of carbon monoxide and methane may increase for up to 36 hours as the inert gas displaces those gases from the fire zone. A steady nerve is useful at such times. When the carbon monoxide concentration begins to fall, that can be used as a controlling guide to the required injection rate of the inert gas. Oxygen concentration in the return airways downstream from goaf (gob) inertization should be monitored to ensure that it remains above the relevant mandatory limits (19 to 19.5 per cent).

For coal mines with a history of recurring spontaneous combustion, the trend is towards establishing a permanent nitrogen "fixing" plant on the surface (e.g. BHP Billiton Sustainability Report, San Juan Coal Company, 2005). The lower grade of nitrogen that may be produced by this method is of little consequence for inertization. A permanent network of nitrogen pipelines throughout the working sections of the mine allows the gas to be fed at a relatively low rate but continuously into the caved zone.

Properly designed, this creates an inert atmosphere throughout the critical zones (Figures 21.4 and 21.5). As a further projection to future developments, the infrastructure is then in place for complete inertization of the working face if and when the techniques of automation and remote control make that cost effective.

Where inertization is having a beneficial effect it is important that it be maintained for as long as required. While a deeply seated fire can be controlled by an inert gas, it will seldom be cooled sufficiently to extinguish it. Hence, premature cessation of the operation may result in a rapid escalation of the fire. Similarly, injection into a sealed area should be continued until the oxygen content falls below 2 per cent.

21.7. FIRE GASES AND THEIR INTERPRETATION

In Section 11.3.3. we introduced the gases that are produced in the majority of underground fires. Other than use of the human senses, monitoring the quality of the air in a mine is the dominant method of detecting a fire or spontaneous heating. Sampling the air downstream from a fire or from within a newly sealed area and plotting the trends is the primary method of tracking the behaviour of the fire and the development of atmospheres that are, or may become, explosive. However, as the gases emitted vary with the phases of oxidation, time and temperature, it is necessary to employ skilled interpretation of those trends.

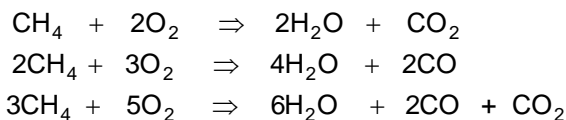
21.7.1. The processes of burning and the gases produced

When coal or timber are burning, three processes are in progress.

- distillation of gases from the solid material
- oxidation of the solid material on its surface with the emission of heat and light (this is why the surface glows more brightly when fanned with fresh air) and
- flaming combustion - the burning of combustible gases produced by the first two processes. Again heat and light are produced. Some of the heat passes back to the surface by radiation and convection to assist in the promotion of further distillation.

The fire gases and their relative proportions depend upon the contributions of each of these three processes. The gases of distillation from coal are carbon monoxide, carbon dioxide, hydrogen and water vapour. Methane and other hydrocarbon gases are also produced. Timber distills the same gases although the amount of hydrogen may be negligible. When flaming combustion occurs, the combustible gases burn to a degree that is governed by the availability of oxygen in the air. The final mixture leaving the fire zone is, therefore, a result of the gases of distillation and the extent to which the fire has become fuel-rich.

The complexity of the processes involved can be illustrated by considering just a few of the ways in which methane can burn:



Furthermore, secondary reactions may produce water gas and further reduction of carbon dioxide to carbon monoxide.

21.7.2. The detection and trend analysis of fire gases

For many purposes of analysis the sampled atmosphere is considered as comprised of air, combustibles and inerts (excess nitrogen and carbon dioxide). Figure 21.6 illustrates the combustible gases emitted as coal is heated in a limited air supply such as occurs in a spontaneous heating. It is clear that carbon monoxide is a leading indicator of the early stages of such a fire. However, the saturated hydrocarbons, in particular, ethylene, are useful indicators of burning coal. In general, as the fire develops into open combustion, the major gaseous product, carbon dioxide, forms an increasing proportion of the pollutant emission.

During any fire incident, running graphs should be maintained of the concentrations of the gases that are monitored or gained from the analysis of samples. Transmitting transducers installed downstream from the fire give a stream of near continuous data. However, in many cases, samples must still be obtained manually by means of evacuated chambers or hand pumps attached to sample containers. The sample vessels should be clean, dry and free from any lubricants that may contaminate the gas sample. A mobile laboratory should be available at the mine surface during any major incident to provide rapid analysis of samples. The rate of sampling must be dictated by the urgency of the situation and the speed at which conditions are changing.

Since the beginning of the twentieth century a number of ratios and composites of gas concentrations have been suggested to assist in the interpretation of fire gases. Table 21.1 indicates some of these.

Ratio	Name
$CO / \Delta O_2$	Graham's Ratio or Index for Carbon Monoxide (ICO)
$CO_2 / \Delta O_2$	Young's Ratio
$CO / (\text{Excess } N_2 + CO_2 + \text{combustibles})$	Willett's Ratio
$(CO_2 + 0.75CO - 0.25H_2) / \Delta O_2$	Jones and Trickett Ratio
CO / CO_2	Oxides of Carbon Ratio

Table 21.1. Gas ratios used in interpreting trends of gas concentrations produced by mine fires.

A feature of several of the ratios is the *oxygen deficiency*, ΔO_2 . This is a measure of the oxygen that has been consumed and is based on two assumptions; first, that the air has been supplied with 20.93 per cent oxygen and 79.04 per cent inert gases (excepting 0.03 per cent carbon dioxide). That 79.04 per cent contains traces of other gases but is referred to simply as nitrogen. Secondly, it is assumed that no nitrogen has been consumed or added (except from the air) through the area under consideration. If no oxygen is consumed, then the O_2/N_2 ratio would remain at $20.93/79.04 = 0.2648$ irrespective of the addition of other gases. For any *measured* values of O_2 and N_2 , the concentration of oxygen that was originally in place can be calculated as

$$\frac{20.93}{79.04} N_2$$

Hence, the amount of oxygen that has been consumed, or oxygen deficiency is given as

$$\Delta O_2 = \frac{20.93}{79.04} N_2 - O_2 \quad \text{per cent} \quad (21.8)$$

The oxidation of coal and the corresponding production of gases were studied by Dr. J.S. Haldane and others at the beginning of the 20th Century (e.g. Haldane and Meachen, 1898). By 1914, Ivon Graham had recognized the importance of carbon monoxide as an early indicator of the spontaneous heating of coal and the equally vital influence of the oxygen that was consumed. He first suggested using the index $CO/\Delta O_2$, now known as **Graham's Ratio** or the *Index for Carbon Monoxide (ICO)*.

Graham's Ratio is the most widely used indicator of an incipient heating in coal mines and has often given warnings several weeks before any odour could be detected. It has the significant advantage that it is almost independent of dilution by leakage of air as this affects both numerator and denominator equally. However, none of the indices listed in Table 21.1 is infallible and Graham's Ratio does have some drawbacks. First, its accuracy becomes suspect if very little oxygen has been consumed, i.e. Graham's Ratio is unreliable if the oxygen deficiency, ΔO_2 , is less than 0.3 per cent. This is a weakness shared by the other indices that involve oxygen deficiency. Secondly, it will be affected by sources of carbon monoxide other than the fire including the use of diesel equipment, or if the air supplied to the fire is not fresh. The latter can occur if the fire is fed, partially, by air that has migrated through old workings and contains blackdamp (de-oxygenated air). Again, like other trace gases or indices, a normal range of Graham's Ratio should be established for any given mine. This will usually be less than 0.5 per cent. Any consistently rising values in excess of 0.5 per cent is indicative of a heating.

Example

An air sample taken from a return airway yields the following analysis:

nitrogen,	N_2	=	79.22 per cent
oxygen,	O_2	=	20.05 per cent
carbon monoxide,	CO	=	18 ppm = 0.0018 per cent

Oxygen deficiency,	ΔO_2	=	$\frac{20.93}{79.04} \times 79.22 - 20.05$
		=	20.98 - 20.05 = 0.93 per cent

Graham's Ratio	=	$\frac{CO}{\Delta O_2} = \frac{0.0018}{0.93} \times 100$	=	0.19 per cent
----------------	---	--	---	---------------

The $CO_2/\Delta O_2$, or **Young's Ratio** is, again, nearly independent of dilution by fresh air. Carbon dioxide is the most prolific of the gases produced in mine fires. Hence, the values of $CO_2/\Delta O_2$ will be much higher than $CO/\Delta O_2$. As a fire progresses from smouldering to open flame, the burning of carbon monoxide will produce an increase in carbon dioxide. Hence a simultaneous rise in $CO_2/\Delta O_2$ and fall in $CO/\Delta O_2$ indicates further development of the fire. However, as both ratios have the same denominator, the straightforward plots of carbon dioxide and carbon monoxide show the same trends. Young's Ratio suffers from similar limitations to Graham's Ratio. Additionally, the concentration of carbon dioxide may have been influenced by adsorption, its solubility in water, strata emissions of the gas and other chemical reactions.

Willett's Ratio was introduced by Dr. H.L. Willett in 1951 with specific reference to situations where there is a higher than usual evolution of carbon monoxide by ongoing low temperature oxidation. In these cases, the gradual extinction of a fire in a sealed area may not be reflected well by the carbon monoxide trend alone but as a percentage of the air-free content of the sample.

The **Trickett or Jones-Trickett Ratio** is used as a measure of reliability of sample analysis and also as an indicator of the type of fuel involved. It can be used for the gaseous products of both fires and explosions. Typical values are shown on Table 21.2. Dilution by fresh air has no effect on the Jones-Trickett Ratio. However, it is subject to the limitations of oxygen deficiency.

The **Oxides of Carbon Ratio**, CO/CO_2 is a useful pointer to the progression of the fire, rising during the early stages and tending to remain constant during flaming combustion. However, the CO/CO_2 rises rapidly again as a fire becomes fuel-rich and is an excellent indicator of this condition. This ratio may also be favoured because it is unaffected by inflows of air, methane or injected nitrogen (Mitchell, 1990). It is, however, subject to variations in carbon monoxide and carbon dioxide that are not caused by the fire.

Fuel	Jones-Trickett Ratio
<i>Fires</i>	
methane	0.4 to 0.5
coal, oil, conveyor belting, insulation and polyurethanes	0.5 to 1.0
timber	0.5 to 1.0 0.9 to 1.6
<i>Explosions</i>	
methane	0.5
coal dust	0.87
methane and coal dust	0.5 to 0.87
no combustion process	< 0.4
impossible mixture (reliability check)	> 1.6

Table 21.2. Typical values of the Jones-Trickett Ratio (after Strang and MacKenzie-Wood, 1985).

It is clear that each gas and composite ratio has both strengths and weaknesses as a warning of impending fire or indicator of fire development. During any fire, it is recommended that spreadsheet and graphics software should be utilized to store all monitored data and sample analyses on a desk computer. This should be located in, or close to, the emergency control centre. All gas concentrations and preferred ratios should be made available as screen and hard-copy graphs plotted against time. These should be reviewed repeatedly as new data or analyses become available. The *trends* are more informative than the absolute values. Hence, repeated samples from a few set stations are preferred to samples taken at many different locations. The injection of inert gases will affect the gas analyses. The one exception is that the CO/CO_2 ratio is not influenced by the injection of nitrogen.

Gas concentrations and indices give pointers to the *average intensity* but not the size of the fire. In some cases, where there is limited leakage between the fire and sampling points, an estimate of the extent of the fire may be made from the flowrate of each of the gases. This is given as the product of the air flowrate and the relevant gas concentration.

The principles of gas detection and methods of sampling are discussed in Section 11.4. *Ionization smoke detectors* draw smoke particles through a chamber where they are charged by a radioactive source such as americium 241 or krypton 85. An ion collecting grid and amplifier produce an electrical output that is a function of the smoke concentration (e.g. Pomroy, 1988). Versions of this have been produced that can distinguish between smoke from a fire and diesel particulate matter (Lytton, 1988).

The improvements that have been made in electrochemical methods of detecting carbon monoxide (Section 11.4.2.5.) have led to this being a common method of fire detection as part of a mine environmental monitoring system. The employment of computer analysis allows filtering of false alarms from diesels or blasting operations that gave earlier versions a doubtful reputation (e.g. Eicker and Kartenberg, 1984). The filter program may be fairly simple such as ignoring short term peaks and giving audio visual alarms only when a significant upward trend is indicated. More sophisticated systems take

into account the time-variant generation of carbon monoxide between successive sensors distributed along an airflow path (Boulton, 1991).

The combination of computer controlled monitoring systems and ventilation network analysis programs allows the possibility of not only detecting the existence of a fire at an early stage, but also its probable location. This is facilitated by strategic location of the sensors (Pomroy and Laage, 1988). The employment of *tube bundle sampling* is particularly useful for detecting the early and slow development stages of a spontaneous heating. This technique is described in Section 11.4.3.2.

Temperature monitors, often known rather loosely as "heat sensors" have an application when mounted above fixed equipment and, particularly, when used to activate deluge or sprinkler systems (Section 21.3.3.). They are of somewhat limited use as fire detectors in airways as the air temperature drops rapidly downstream from a fire. Such sensors may be subjected to greater variations in air temperature from normal operations (such as passage of a diesel vehicle) than from the early stages of a fire. If made sufficiently sensitive, temperature sensors may lose credibility because of an excessive recurrence of false alarms.

21.7.3. Explosibility diagrams

When a fire becomes fuel-rich, there is a danger that explosive mixtures of gases will propagate away from the immediate fire zone. Furthermore, following sealing of a fire area, it frequently occurs that the rising concentration of combustible gases and falling concentration of oxygen produce mixtures that pass through an explosive range. Similarly, the dilution of combustible gases that occurs when a sealed area is re-opened may, again, result in passing through an explosive range. In order to be able to predict and control such circumstances, it is necessary to have an understanding of the flammability limits of gases and gas mixtures.

This subject was introduced in Section 11.2.4. and illustrated by the Coward diagram for methane shown in Figure 11.1. That diagram should be reviewed, if necessary, as a reminder of the concepts of upper and lower flammability and how these converge to a nose-limit as inert gases are added.

In many situations, the large majority of combustible gas is methane and Figure 11.1 may be employed to determine whether the mixture of oxygen, methane and inerts lies within the explosive triangle or is likely to do so in the near future. However, in other cases, the presence of carbon monoxide and/or hydrogen may cause significant changes in the Coward diagram (Coward, 1952, Strang J. and Mackenzie-Wood, 1990). Figure 21.12 shows the individual explosive triangles for all three of these combustible gases. The corresponding coordinate points are given in Table 21.3.

Gas	Flammable limits		Nose limits	
	lower	upper	gas	oxygen
methane	5.0	14.0	5.9	12.2
carbon monoxide	12.5	74.2	13.8	6.1
hydrogen	4.0	74.2	4.3	5.1

Table 21.3. Vertices of explosive triangles (percentages).

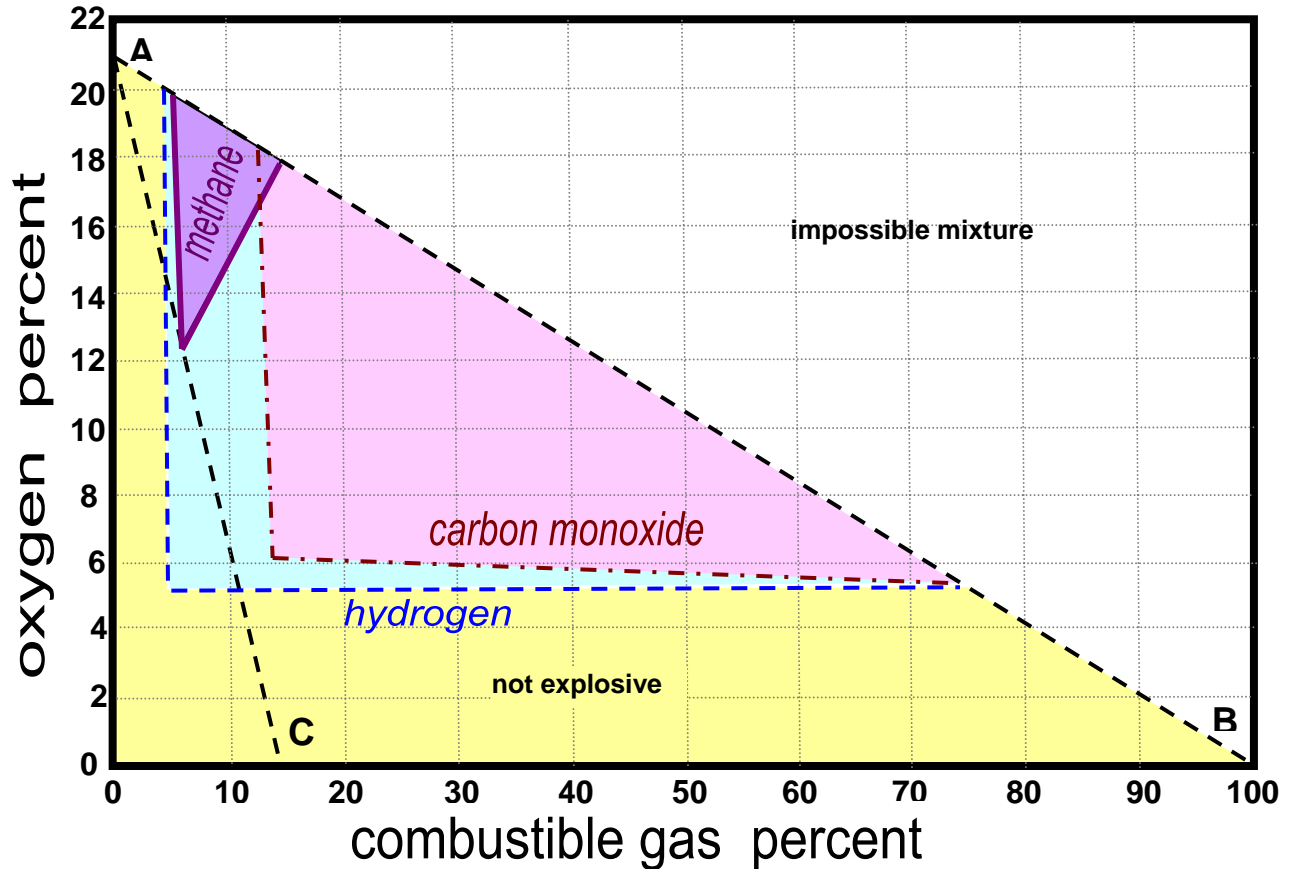


Figure 21.12 Coward explosive triangles for methane, carbon monoxide and hydrogen.

If the method of the Coward diagram is to be useful for mixtures involving more than one combustible gas then we must be able to quantify the explosive triangle for those composite mixtures. Let us attempt to do that.

A basic precept in the world of science and engineering is that if anything is done to upset the equilibrium of a system then that system will react in an attempt to reach a new equilibrium with the minimum adjustment of the component parts (Le Chatelier's Principle). Let us adopt subscripts 1, 2 and 3 for the three combustible gases and call their percentage concentrations p_1 , p_2 and p_3 respectively. If they do not react chemically with each other then the mixture will have a total combustible concentration of

$$p_t = p_1 + p_2 + p_3 \quad \text{percent} \quad (21.9)$$

Furthermore, Le Chatelier's Principle leads to the prediction that for gas flammability limits, L_1 , L_2 and L_3 (where these can be upper, lower or nose limits), the corresponding gas flammability limit of the mixture, L_{mix} , will be given by:

$$\frac{p_t}{L_{mix}} = \frac{p_1}{L_1} + \frac{p_2}{L_2} + \frac{p_3}{L_3} \quad (21.10)$$

Example

An air sample produces the following analysis:

CH_4 8 per cent

CO 5 per cent

H_2 3 per cent

Determine the lower flammability limit of this mixture.

Solution

The total percentage of combustible gases is

$$p_t = 8 + 5 + 3 = 16 \text{ percent.}$$

Using the individual gas lower flammability limits given in Table 21.3, together with equation (21.10) gives

$$\frac{16}{L_{mix}} = \frac{8}{5.0} + \frac{5}{12.5} + \frac{3}{4.0}$$

giving $L_{mix} = 5.82$ percent as the lower flammability limit of the mixture. A similar calculation may be used to determine the upper and nose flammability limits of the combustible content.

The upper and lower limits lie on the line AB on Figure 21.12 and, hence, are defined completely. However, the oxygen content at the nose limit remains to be found before we can construct the explosive triangle for the mixture. To find the oxygen content at the nose limit, we must first determine the excess inert gas (let us call it nitrogen) that has to be added in order to reach that nose limit.

Consider the situation for methane. If we start from *any* point on the line AB and add nitrogen then we shall move in a straight line towards the origin, O. The mixture will become extinctive when we cross the line AC. At that moment we shall have added an amount of nitrogen which, when expressed per unit volume of methane, is a *constant*. (This follows from the fact that both AB and AC are straight lines.) As we can commence at *any* position on AB, let us choose point B. On adding nitrogen and moving towards O, we shall cross the extinction line at point C where the methane concentration is 14.14 per cent. The remaining $(100 - 14.14) = 85.86$ percent is nitrogen. We have, therefore, added $85.86/14.14 = 6.07\text{m}^3$ of nitrogen for each m^3 of methane. A similar exercise can be carried out for carbon monoxide and hydrogen to give the values in Table 21.4.

Combustible gas	Nitrogen to be added to make mixture extinctive: (N^+ m^3 of nitrogen per m^3 of combustible gas)
methane	6.07
carbon monoxide	4.13
hydrogen	16.59

Table 21.4. Volumes of excess nitrogen to be added, N^+ , in order to make flammable gases extinctive.

This table gives the excess nitrogen to be added, N^+ , if the combustible content consisted of one gas only. For a mixture of combustible gases the excess nitrogen required, N_{ex} , is given as

$$N_{ex} = \frac{L_n}{p_t} \{N_1^+ p_1 + N_2^+ p_2 + N_3^+ p_3\} \text{ percent} \quad (21..11)$$

where L_n = percentage of combustible mixture at the nose [equation (21.10 with $L_{mix} = L_n$].

The required oxygen content at the mixture nose limit is then simply 20.93 per cent of the air fraction,

$$\text{i.e. Oxygen (nose limit)} = 0.2093 (100 - N_{ex} - L_n) \text{ percent} \quad (21.12)$$

Example

A sample taken from a sealed area yields the following analysis.

methane	8 per cent	}	p _t = 16 per cent
carbon monoxide	5 per cent		
hydrogen	3 per cent		
oxygen	6 per cent		
inerts	78 per cent		

Construct the Coward diagram for this condition.

Solution

(a) Using equation (21.10) and Table 21.3:

(i) lower flammability limit, L_{low} :

$$\frac{16}{L_{low}} = \frac{8}{5} + \frac{5}{12.5} + \frac{3}{4}$$

gives $L_{low} = 5.82$ percent combustible

(ii) upper flammability limit, L_{up} :

$$\frac{16}{L_{up}} = \frac{8}{14} + \frac{5}{74.2} + \frac{3}{74.2}$$

gives $L_{up} = 23.56$ percent combustible

(iii) nose flammability limit, L_n :

$$\frac{16}{L_n} = \frac{8}{5.9} + \frac{5}{13.8} + \frac{3}{4.3}$$

gives $L_n = 6.62$ per cent combustible

(b) Equation (21.11) and Table 21.4 give the excess nitrogen required for an extinctive atmosphere to be

$$N_{ex} = \frac{6.62}{16} \{ (6.07 \times 8) + (4.13 \times 5) + (16.59 \times 3) \} = 49.24 \text{ percent}$$

and, finally, oxygen content at the nose limit is given by equation (21.12) as

$$0.2093 (100 - 49.24 - 6.62) = 9.24 \text{ percent}$$

The explosive triangle has now been defined completely and has been constructed as Figure 21.13. The actual mixture point has also been entered on the diagram and illustrates that although the mixture is not explosive, it will become so if air is allowed to enter the area.

Coward diagrams are most useful in tracking trend directions of gas mixtures. They do, however, have a drawback. As each new sample analysis becomes available, the mixture point on the Coward diagram moves - but the explosive triangle also changes its shape and position. It is analogous to shooting at a moving target. Fortunately, the calculations are simple and a new triangle can be developed for each sample in order to follow actual trends. The complete process can readily be programmed for automatic

appearance of the updated Coward diagram and mixture point on a computer screen. Running through a set of consecutive data for any given sampling location produces a dynamic picture of explosive triangles and mixture points moving over the screen. This creates a strong visual impact of time-transient trends.

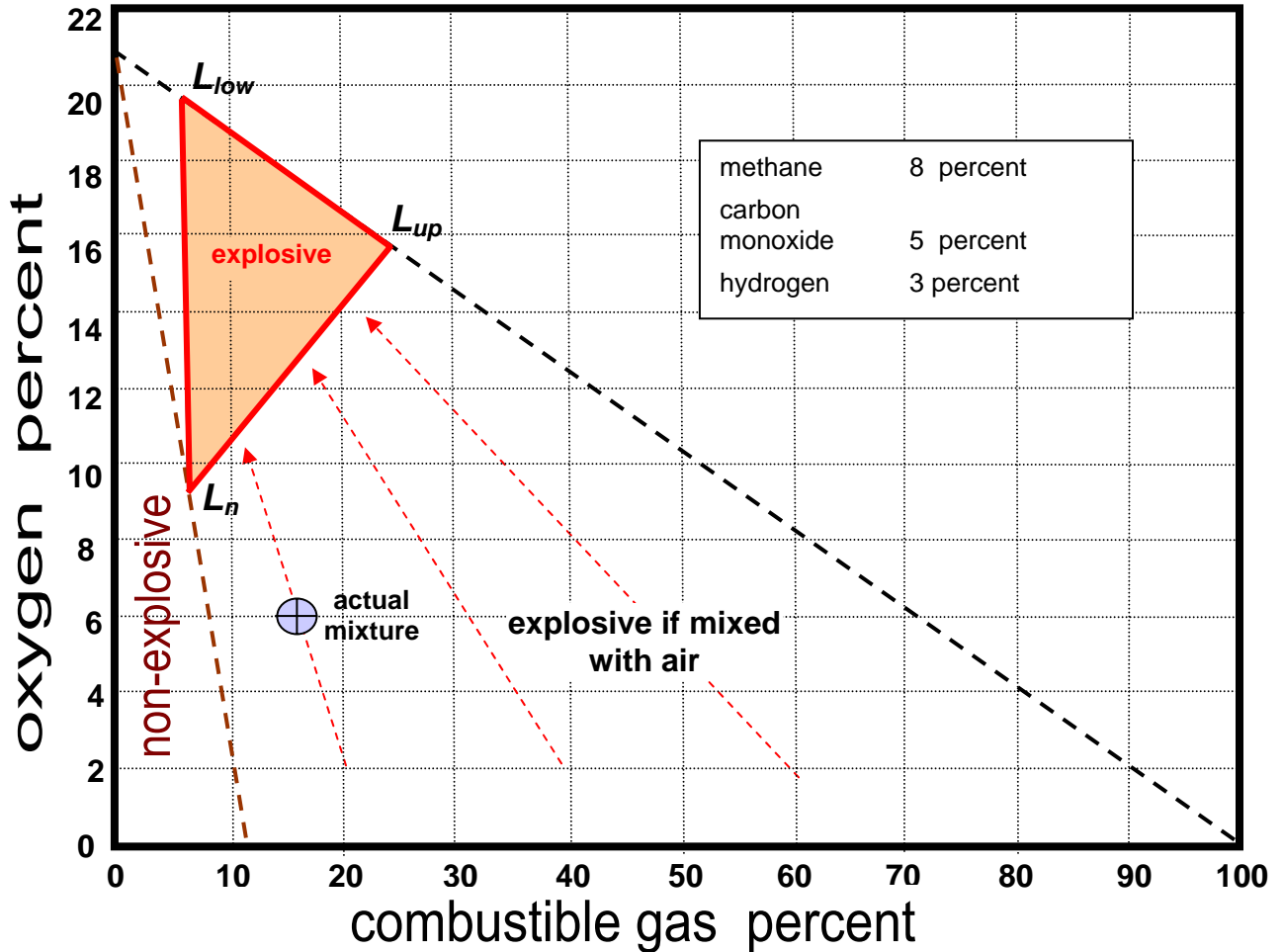


Figure 21.13 Coward diagram for mixture of gases in the example.

An older method of dealing with variations in gas mixtures is the U.S. Bureau of Mines composite diagram illustrated on Figure 21.14 and founded on earlier work by Zabetakis et al (1959). In this diagram, the y axis is an "effective combustible" defined by a weighted combination of the volumetric percentages of the three combustible gases. The weighting takes account of the explosibility of carbon monoxide and hydrogen compared with that of methane. The x axis is a combination of the excess nitrogen and 1.5 times the concentration of carbon dioxide, the 1.5 allowing for the greater extinctive power of carbon dioxide.

The "excess nitrogen" required here is the percentage of nitrogen in excess of that justified by the oxygen present.

$$\text{Excess nitrogen} = \text{actual } N_2 - O_2 \times \frac{79.04}{20.93}$$

The set of explosive triangles are approximations based on methane but adjusted for incremental combined additions of carbon monoxide and hydrogen.

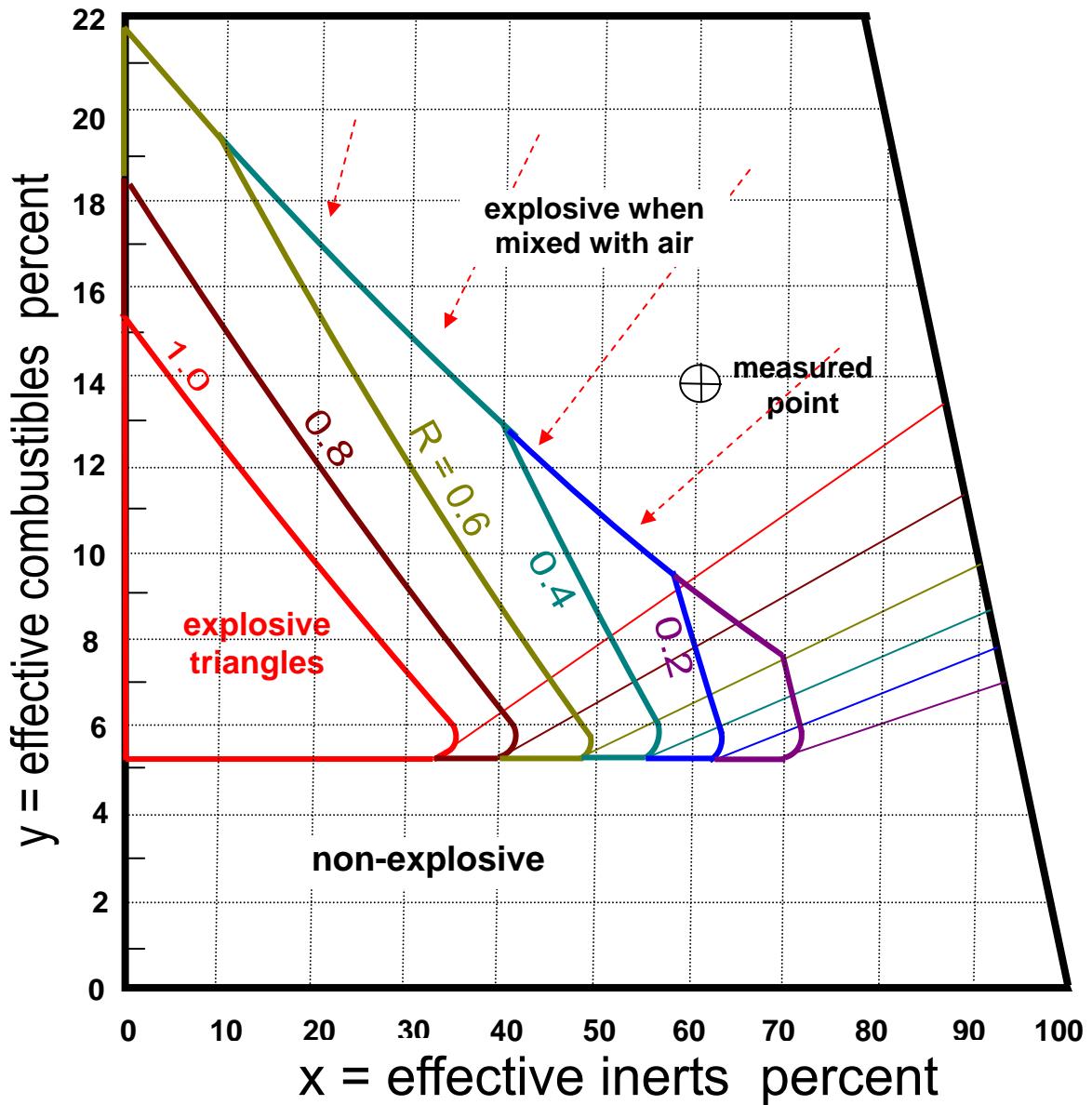


Figure 24.14 U.S. Bureau of Mines diagram.

Total combustible, p_t = methane + carbon monoxide + hydrogen

R = methane/ p_t

x = excess nitrogen + 1.5 x carbon dioxide

y = methane + 0.4 x carbon monoxide + 1.25 x hydrogen

All gases expressed in percentage by volume.

Example

Using a more detailed analysis of the sample used in the previous example gives

	methane	8 per cent
	carbon monoxide	5 per cent
	hydrogen	3 per cent
	oxygen	6 per cent
	nitrogen	68 per cent
and	carbon dioxide	10 per cent

Total combustibles, $p_t = 8 + 5 + 3 = 16$ per cent

$$\text{methane ratio } R = \frac{\text{methane}}{p_t} = \frac{8}{16} = 0.5$$

$$\text{excess nitrogen} = 68 - \left\{ 6 \times \frac{79.04}{20.93} \right\} = 45.3 \text{ per cent}$$

$$\text{effective inerts (x axis)} = 45.3 + (1.5 \times 10) = 60.3 \text{ per cent}$$

$$\text{effective combustibles (y axis)} = 8 + (0.4 \times 5) + (1.25 \times 3) = 13.75 \text{ per cent}$$

Plotting this point on Figure 21.14 shows that it lies above the $R = 0.5$ triangle, thus agreeing with the Coward diagram that this mixture is not explosive but will become so if air is added.

21.8. EXPLOSIONS

There has scarcely been a major mining industry that has not been traumatised by underground explosions of gases, dusts and mixtures of the two. The potential for disastrous loss of life when such an explosion takes place is very high. Fatality counts have too often been in the hundreds from a single incident. Fatalities and injuries produced by explosions arise from blast effects, burning and, primarily, from the carbon monoxide content of afterdamp - the mixture of gases produced by the explosion. In the dust explosion at Courrieres coal mine in France (1906), 1099 men lost their lives. One of the most catastrophic explosions on record occurred at Honkieko, Manchuria (1942) when over 1500 miners died. The carnage that took place in coal mines during the Industrial Revolution (Section 1.2.) was caused primarily by underground explosions and resulted in the start of legislation governing the operation of mines.

21.8.1. Initiation of explosions

For an explosion to occur, the same three components of the fire triangle must exist simultaneously; namely, a combustible material, oxygen and a source of ignition. However, there is a further condition for mine explosions; the combustible material must be a gas or finely divided dust mixed intimately with the air and in concentrations that lie between lower and upper flammability limits.

The majority of explosions in mines have been initiated by the ignition of methane. This, in itself, is a very dangerous occurrence. However, it becomes much worse when the shock wave raises combustible dust into the air such that it can be ignited by the flame of the burning methane. The resulting dust explosion is likely to be much more violent than the initial methane blast. Indeed, the majority of methane ignitions result in blue flames flickering backwards and forwards along the gas:air interface without developing into an explosion. It is only when the turbulence of the airflow or thermal effects produce a mixture within the explosive triangle (Section 21.7.3.) that the combustion accelerates into an explosion.

Finely divided particles of any combustible solid can become explosive, including metallic dusts, sulphide ores and most organic materials. Precautions must be taken against explosions in the manufacturing, processing and silo storage of many food stuffs including grain. However, in this Section, we shall confine ourselves to the igniting sources, mechanisms and suppression of explosions that occur in subsurface ventilation systems.

In Section 21.2. we classified the major igniting sources of fires and explosions in mines. Unfortunately, explosible mixtures of gases can be ignited by electrical sparks of energy levels as low as 0.3 millijoules, as illustrated by the tiny spark that ignites gas in a piezo-electric or induction coil cigarette

lighter. It is, therefore, prudent to give a little further attention to the initiation of explosions by sparking phenomena in addition to those sources of ignition discussed in Section 21.2.

Incendiary sparking arises from heat produced from a chemical reaction. The *thermite* process involves the reaction of aluminium powder with iron oxide.



This process produces so much heat that it has been used on small scale welding operations. A similar effect occurs when a surface consisting of aluminium, magnesium or their alloys collides with a rusted steel or iron surface. Incendiary sparks are produced that are well capable of igniting a methane:air mixture. It is prudent to prohibit the importation of any light alloys into gassy mines and, indeed, this is enforced by law in a number of countries.

Frictional sparking has been the cause of the increased incidence of methane ignitions on coal faces and which have accompanied the proliferation of mechanized mineral winning. This is discussed in Section 21.2.4.

In addition to sparking caused by the misuse or damage to electrical equipment, **electrostatic sparks** may also be capable of igniting a flammable mixture of gases. Electrostatic charges are built up on non-conducting (or poorly conducting) surfaces as a regular feature of many everyday operations and, particularly, at pointed or sharply curved regions on those surfaces. Electrical potentials of 10 000 volts are commonly generated. This phenomenon may occur, for example, where belts run over pulleys, at the nozzles of compressed air jets (particularly, if liquid or solid particles are entrained) and within non-conducting ventilation ducts. Even the charge that builds up on the human body in dry conditions can produce dangerous sparks (Strang and McKenzie- Wood, 1985). In such conditions, workers should not wear rubber- soled footwear.

All machines with moving parts should be adequately earthed against the build-up of electrostatic charges. Other devices that are liable to this phenomenon should be similarly protected. "Anti-static" materials are available for ducting, belts and pipes.

21.8.2. Mechanisms of explosions

An explosion may be defined as a process in which the rates of heat generation, temperature rise and pressure increase become very great due to the rapidity of combustion through the mixture. In a typical methane:air explosion, the temperature rises to some 2000 °C, i.e. by a factor of about seven. Even higher temperatures may be reached if the explosion is contained within a sealed volume. The speed of the process is so great that it is essentially adiabatic. The result is that the pressure in the immediate vicinity increases to a peak value very rapidly and is relieved by expansion of the air. This produces a **shock wave** that propagates in all available directions.

In a mine opening the expansion is constrained by the airway surfaces giving rise to high velocities of propagation. Initially, the **flame front** travels more slowly than the shock wave and the explosion is known as a **deflagration**. However, if the unburned zone ahead of the flame front becomes more conducive to combustion by approaching closer to stochastic condition (approximately 9.6 percent methane) then the flame front will accelerate and the peak pressure at the shock wave rises. Although the shock wave velocity also increases, the distance between the two narrows. This may continue until the flame front catches up with the shock wave (Figure 21.16). The explosion is then described as a **detonation**. The speed of the explosion and the peak pressure at the shock wave then escalate significantly. Conversely, if the unburned zone between the flame front and the shock wave moves away from stochastic conditions (e.g. by lack of fuel or the presence of stonedust) then the explosion will weaken.

At the actual site of the initial ignition the flame speed and rate of pressure rise are at their lowest. It is only as the shock wave and following flame front progress along the airway that their intensity increases, given the availability of both fuel and oxygen within the explosive range. It is for this reason that victims at the initiation site of an explosion often exhibit little blunt trauma but have succumbed to carbon monoxide poisoning. An ignition of a 10 per cent methane:air mixture in a heading may produce flame speeds of 660 m/s (twice the speed of sound) as it accelerates away from the face of the heading.

Figure 21.14A illustrates the passage of a **deflagrating explosion** that has been initiated at the face of a heading. Expansion of the gaseous products of combustion can proceed only away from the face of the heading. However, that expansion is resisted by the inertia of the outby atmosphere. The result is the development of the shock wave which is essentially the moving boundary between the normal mine atmosphere and the elevated pressure of the expanding explosion. Hence, there is a highly concentrated pressure gradient across the shock wave. It is this shock wave that causes "blast" effects and can inflict extremely high dynamic loads on objects that lie in the path of the explosion. The shock wave produces another effect. It causes intimate mixing of any accumulations of methane as it passes and will produce a continuous explosive path provided there is sufficient gas and oxygen to remain in the explosive range. Even worse, it raises dust into the air to produce concentrations which, if the dust is combustible, will themselves be explosive - resulting in even more favourable conditions for enriching the fuel path of the explosion.

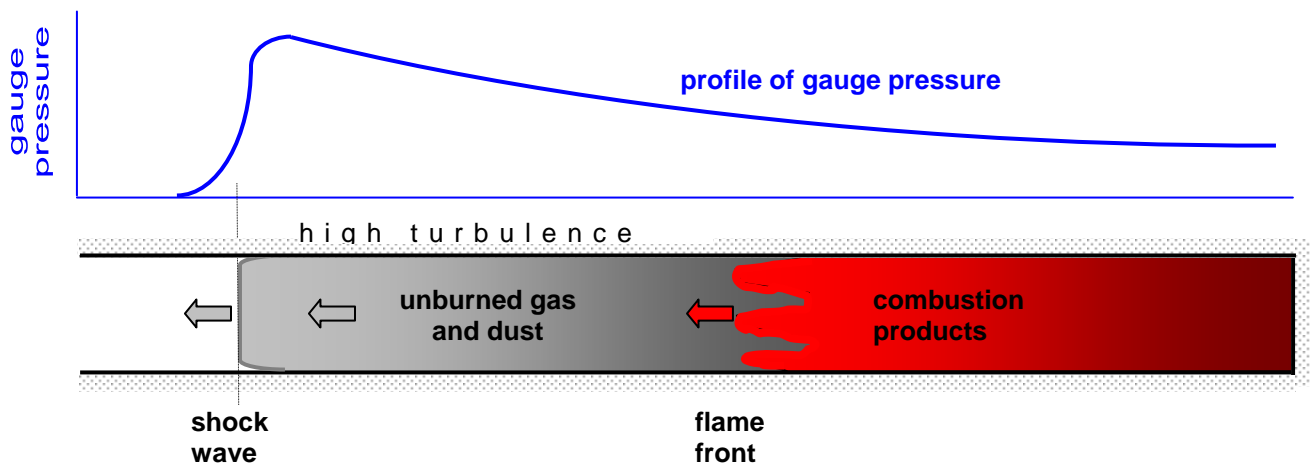


Figure 21.14A In an explosive deflagration the flame front is preceded by a shock wave.

The mixing process is further exacerbated by the highly turbulent conditions that exist between the flame front and the shock wave. Such turbulence, coupled with the high speed of the unburned mixture can result in scouring of the sides of the airway, especially if the coal is friable. The impact of flying debris can also result in significant erosion of the airway as well as dispersion of dust into the air.

If there is any obstruction that prevents the air being projected forward in front of the shock wave the peak pressure becomes greatly escalated. This occurs when the shock wave encounters a facing seal, stopping or any other ventilation control. Similarly, high pressures will be generated when a developed explosion enters a blind heading. In such circumstances victims are typically found to have suffered from blunt trauma in addition to severe burning. The latter is thought to be caused by swirling flames that exist until extinguished by lack of oxygen.

These are the basic mechanisms that drive explosions through subsurface ventilation networks. Bends, junctions, obstructions and the availability of fuel and oxygen all affect the rate of propagation. A mine

explosion is a highly dynamic phenomenon and seldom reaches steady-state even for a few milliseconds. For most of its life it is either proliferating or subsiding.

21.8.2.1. Gas explosions

Explosions of methane from coal are by no means confined to mines. Ignitions have too frequently occurred in storage silos and in coal cargo ships, causing great damage and loss of life. Methane concentrations of 40 per cent have been measured in such facilities. Layering phenomena and the production of explosive mixtures of methane and air make unloading operations particularly hazardous. Precautions against ignitions in these circumstances include good ventilation of the facility, monitoring for methane and the gaseous products of spontaneous combustion, ready availability of nitrogen or carbon dioxide cylinders for inertization, strict control of ignition sources and prohibition of smoking in the vicinity. Bacteria have also been used to convert the methane into carbon dioxide (Kolada and Chakravorty, 1987).

Incidences of **hydrogen explosions** at battery charging stations and ignitions of oil vapours from machines have been reported. However, the vast majority of gas explosions in mines have involved methane. Modern systems and standards of mine ventilation are successful in maintaining general body concentrations of methane at safe levels throughout the ventilated areas. However, strata emissions of gas are often at methane concentrations of over 90 per cent. It follows that between the points of emission and the general body of the airstream, zones of an explosive mixture must exist. The ventilation arrangements should ensure that these zones are as small as possible and, wherever practicable, maintained free from igniting sources. For example, the danger of methane, coal dust, air and sparks existing simultaneously at the pick-point of a coal winning machine can be reduced by pick-face flushing or jet-assisted cutting (Section 20.4.1.1.).

Dangerous accumulations of methane in roof cavities should be avoided by filling those cavities with an inert material. Air velocities should be sufficient to prevent methane layering (Section 12.4.2.) and longwall systems should be designed to maintain the gas:air interface within the goaf (gob) and without flushing on to the faceline. In appropriate circumstances, methane drainage will reduce the amount of gas that enters the mine ventilation system (Section 12.5.).

21.8.2.2. Coal dust explosions

The danger of coal dust being explosible in air depends upon a number of factors including:

- (a) *Concentration of the dust and presence of methane:* The flame of a dust deflagration is propagated by the combustion of each discrete particle in turn. If the particles are sufficiently far apart then the heat produced by a burning particle will be insufficient to ignite its closest neighbour. The flame will not propagate. The lower flammable limit is attained when the particles become sufficiently close to allow sequential ignition. At the other extreme, if the dust particles are too close together, there will be insufficient oxygen to allow complete combustion. The system will become internally fuel-rich and the rate of heat generation will fall. The upper flammability limit is attained when the temperature is reduced below the ignition point of the dust.

The lower flammability limit may be of the order of 50 g/m^3 with maximum explosibility at 150 to 350 g/m^3 depending upon the volatile content of the coal (Holding, 1982). The upper flammability limit might be as high as 5000 g/m^3 (Strang and McKenzie-Wood, 1985) but is dependent on the availability of oxygen. To put these flammability limits into perspective, it should be recalled that threshold limit values for respirable coal dust concentrations can be as low as *2 milligrams* per cubic metre (Table 19.2). A concentration of 50 g/m^3 produces a suffocating atmosphere. It is unlikely that such concentrations of airborne dust will exist under normal conditions in the active branches of a mine ventilation network. Nevertheless, in the absence of dust suppression, explosible dust concentrations might occur around the cutting heads of rock-breaking machines. Furthermore, a very thin coating of dust on the surfaces of airways or a conveyor can produce an explosive atmosphere when disturbed by a shock wave or highly turbulent conditions.



Figure 24.14B. The flame of a coal dust explosion emerging from a 2.5 m (8ft) high test gallery at the Barbara Mine, Poland

Coal dust and methane are synergistic in their explosibility characteristics. The flammability limits of each of them are widened in the presence of the other. The relationship between the two varies with the volatile content of the coal. A typical example, based on results reported for an Australian coal, is shown on Figure 21.15. It should be appreciated that when heated, coal emits its volatile content commencing with methane. Hence, a coal dust explosion involves the combustion of gaseous fuels as well as carbonaceous solid particles. It is common for partially de-volatilized coal dust to impact and adhere to solid surfaces during a coal dust explosion. This leaves coked material and carbon filaments on supports, equipment and airway surfaces which assist investigators tracing the role and path of coal dust in an explosion. On the other hand, a high velocity flame may leave little trace of coking.

(b) *Fineness of the dust:* There appears to have been little work done in establishing definitive relationships between explosibility and the size of dust particles. However, the increased surface area and more intimate mixing with the air given by the finer particles suggest that explosibility will increase as the average particle size decreases. An accepted assumption is that any combustible dust which can be raised into the air is explosible. This encompasses all particles of less than some 250 microns diameter.

(c) *Type of coal:* There is considerable evidence to show that coal dust explosibility increases with volatile content (e.g. Holden, 1982). Hence, low rank coals are more prone to dust ignitions. Anthracite dust is normally considered to be non-explosible in mining conditions. However, with a sufficiently high energy of initiation, low volatile coal dusts can produce violent explosions. The disastrous explosion in Manchuria (1942) occurred while mining a coal of volatile content 15 to 19 per cent. The explosibility of coal dust decreases with respect to ash and moisture content as well as with age. The latter factor is considered to be due to the coating

of a partially oxidized layer on older dust particles. It follows that coal dust on, or close to, a working face is more liable to ignitions.

(d) *Strength of initiating source:* The energy level of the initial ignition plays a large role in governing the rate of propagation and growth in power level of a dust explosion. The majority of coal dust explosions in mines have been initiated by a methane ignition, this providing the starting shock wave and flame front. However, any other igniting source of sufficient power can result in a dust explosion in the absence of a flammable gas. The Courrieres dust explosion (1906) is thought to have been caused in a methane-free atmosphere by a case of prohibited explosives (Cybulska, 1981).

To comprehend the power levels that can be attained by coal dust explosions, let us return to the matter of a spearheading shock wave driven by a more slowly advancing deflagrating flame front. A flame velocity of 50 m/s will produce a shock wave velocity of some 375 m/s. (A lower flame velocity is unlikely to propagate). However, Figure 21.16 shows that if the dust concentration and methane favour the growth of the explosion then the flame velocity will increase at a greater rate than that of the shock wave until both exceed some 1100 m/s. Beyond that, the process may develop further into a *detonation* when adiabatic compression in the shock wave can produce temperatures that exceed the ignition point of the fuel. Gas and dust particles no longer have to wait until they are ignited by a following flame. They ignite spontaneously. The flame front and shock wave then advance in unison and may reach speeds of over 2000 m/s (six times the speed of sound). It is little wonder that coal dust explosions are so feared throughout the world of mining.

Figure 21.16 also illustrates the dynamic pressure developed across the shock wave. Even at the lower end of this curve the pressures are sufficient to disrupt doors, stoppings and air-crossings, while the upper end explains the devastation that can be caused by a well-developed explosion.

During post-explosion inspections, the dominant path of the explosion may be deduced from the twisting of steel supports, the distortion of track rails, the direction of failure of strong stoppings and the dislocation of heavy equipment. The displacement of less sturdy objects may be misleading and can be caused by secondary deflections of the shock wave, particularly at bends or junctions. Furthermore, an explosion is often followed rapidly by an implosion of fresh air due to rapid cooling and contraction of the afterdamp gases. If open burning is in progress then the fresh air can initiate repeated explosions. These phenomena can also leave a confused picture for subsequent investigators.

The passage of an explosive flame is unlikely to ignite solid coal. However, paper, clothing and, especially, feeders of methane may be left burning if there is sufficient oxygen remaining in the area. This is most probable in the fringe areas of the explosion and can initiate further explosions of any methane that continues to be emitted into the area. The probability of such subsequent explosions is greatly increased if the initial explosion(s) have disrupted the ventilation system.



Figure 21.14C Photographs of post-explosion No.1 Surface Portal, dislodged and damaged steel arches, and remnants of ducting. *Westray Mine Public Inquiry, Exhibit No. 59 (Richard, 1997).*



Figure 21.14D Photographs of roof falls, dislodged steel arches, and damaged equipment.
Westray Mine Public Inquiry, Exhibit No. 59 (Richard, 1997).

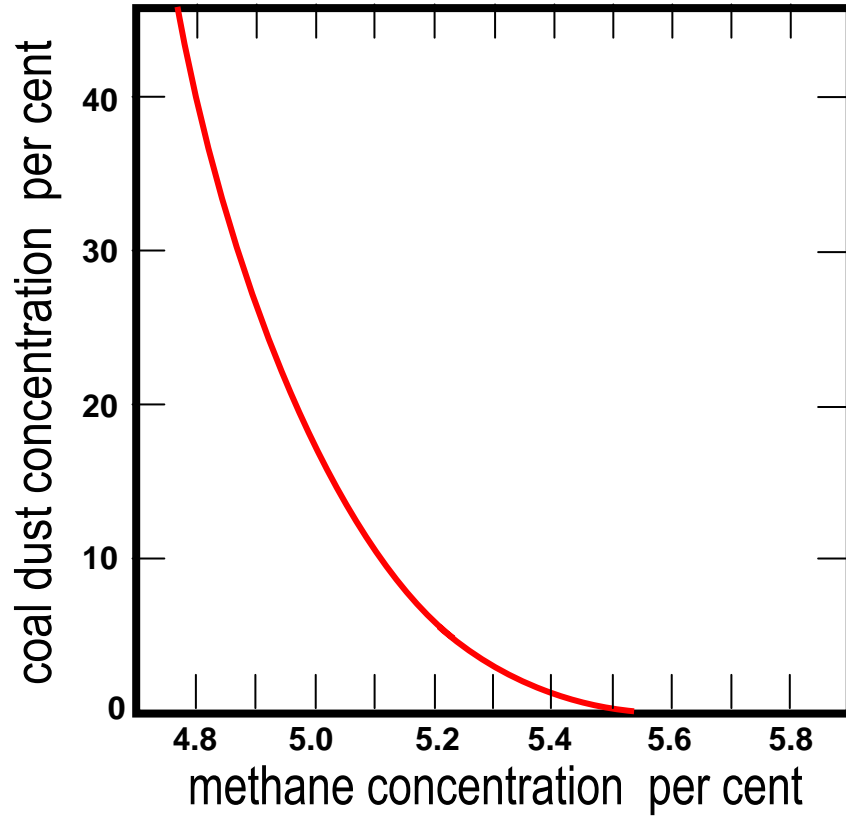


Figure 21.15 Example of the reduction in the lower flammability limit of coal in the presence of methane. Other curves vary according to the rank of the coal. (Based on work reported by Jensen et al (1989))

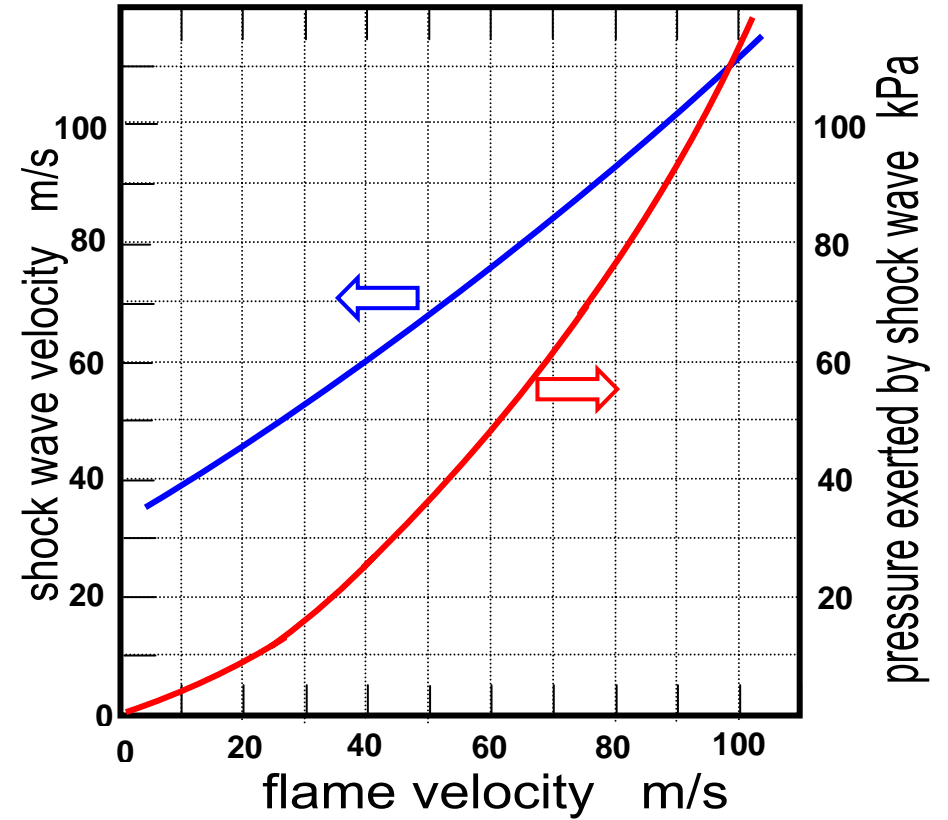


Figure 21.16 Variation of shock wave velocity and dynamic pressure with respect to flame velocity. (Developed from data reported by Strang and MacKenzie-Wood, 1985)

21.8.2.3. Sulphide dust explosions

Although explosions of sulphide ore dust are a hazard in some metal mines, they do not have the destructive power of coal dust explosions and have attracted much less attention by researchers (Holding, 1975). These explosions are initiated, primarily, during blasting operations of ores that contain more than 40 per cent sulphur. The main danger to life is production of the highly toxic sulphur dioxide gas which may be retained for several hours, particularly if ventilation controls have been disrupted. Furthermore, the gas reacts with water vapour causing corrosion problems from the sulphuric acid fumes that are produced. A number of precautionary measures have been suggested including hosing dust depositions from the walls of stopes prior to blasting and the use of water atomizers before and during blasting (Section 20.3.4.). Other techniques involve stemming the blast holes with water ampoules or powdered limestone and inserting explosive charges with zero-time detonators into bags of hydrated limestone powder suspended in the stopes. The latter technique fills the air with inert and suppressant dust particles immediately prior to detonation of the main round (Hall et al, 1989).

21.8.2.4. Dust explosibility tests

Explosibility tests for mine dusts vary considerably in the equipment and procedures employed. The essential sequence consists of producing a dust:air or dust:oxygen mixture and applying an igniting source, usually an electrical spark of constant energy level. The parameters that are varied include the dust concentration, the type of dust, added amounts of stonedust (usually powdered limestone) and methane concentration. The results may be recorded simply as "ignition" or "no ignition", or in the more sophisticated tests, the rates of increase of pressure and temperature and the peak values of those variables (Jensen et al, 1989).

Considerable variations occur in the reported explosibilities of similar dusts. These may be attributable, in part, to differences in test conditions. The results are influenced, for example, by variations in the uniformity of the dispersed dust, means of measuring dust concentration, strength of the igniting source and turbulence within the test chamber. This latter factor also indicates that whilst laboratory test results may provide valuable comparisons between differing dusts, they are not necessarily indicative of actual behaviour within the mine environment. Full scale galleries have been constructed in several countries for investigations into mine fires and explosions.

Indices of dust explosibility have been defined and referred to specific equipment and procedures in differing countries (e.g. Holding, 1982). While these produce useful relative information, caution should be applied when comparing one index with another.

21.8.3. Suppression of mine explosions

The primary safeguards against mine explosions are, once again, a well designed and operated ventilation system, planned maintenance of equipment and good housekeeping to control accumulations of combustible dust and to ensure adequate applications of stonedust. This brings us to the most widely used method of suppressing the propagation of mine explosions.

21.8.3.1. Stonedust and water barriers

Finely divided *limestone dust* serves at least two purposes when mixed intimately with coal dust in a mine airway. First, it will act as an inert diluent when the mixture becomes airborne, serving to increase the distance between combustible dust particles. Secondly, particles of stonedust will absorb heat and reduce the ability of airborne coal dust to propagate a flame. Provided that there is sufficient stonedust present, this technique provides an efficient means of suppressing the full development of an explosion.

It is important that the stonedust be mixed well with the coal dust. Tests have shown that strips of coal dust interspersed with strips of stonedust will sustain an explosion. Furthermore, combustible dust on a conveyor may propagate an explosion even when the airway is adequately stonedusted. Precautions should, therefore, be taken to ensure that the stonedust is spread on roof, floor and sides often and consistently. An efficient

means of doing this is to employ *trickle-dusters*. These are devices that emit stonedust into the air at a controlled rate. The stonedust mixes with the airborne coal dust and settles with it to produce a uniformly mixed deposition on all surfaces.

An additional means of using stonedust, particularly applicable to single entry longwall systems, involves *stonedust barriers*. These are boards supported on pivots across the airway, usually near the roof, and loaded with stonedust. Dust loadings vary from 30 to 60 kg per metre length of board. A number of boards are located close together within a short length of airway to form the complete stonedust barrier. The intention is that the boards and their contents will be dislodged by the shock wave of an explosion to produce a high concentration of airborne stonedust at the time the flame front arrives and, hence, prevent its further propagation.

The locations of stonedust barriers should be considered carefully. If they are too close to the seat of the explosion then the flame front may have passed before the stonedust has become adequately distributed; too far away then the stonedust will become too dispersed by the time the flame front arrives. A sensible arrangement is to have a lightly loaded (30 kg/m) barrier, that can more easily be displaced, located within some 200 m of face operations and more heavily loaded barriers further outby. While stonedust barriers may be sited in all district intakes and returns, conveyor entries are particularly recommended to be fitted with these devices.

Stonedust barriers do have some disadvantages. They must be inspected regularly to ensure that they remain capable of being dislodged - yet this renders them prone to accidental or mischievous disturbance. In damp conditions, moisture-proofed stonedust should be employed to ensure that the dust will be dispersed adequately by a shock wave. Stonedust barriers may fail to suppress methane explosions. Furthermore, if an explosion is allowed to develop into a detonation then it is unlikely to be halted by a stonedust barrier. Indeed, the objective of barriers is to suppress an explosion at an early stage of its development.

A *water barrier* is intended to serve the same purpose as a stonedust barrier. In this case, troughs holding some 40 to 90 litres of water are positioned across the airway and attached to roof supports. The troughs themselves are constructed from polystyrene foam or a similarly weak material so that they will disintegrate when subjected to a shock wave travelling at 100 m/s. The cross-section becomes filled with water droplets. Suppression of the flame is achieved by the cooling effect of evaporation and displacement of oxygen.

21.8.3.2. Triggered barriers and explosion detectors

Stonedust and normal water barriers both suffer from the disadvantage that they rely upon the shock wave to disperse the stonedust or water. Triggered barriers are designed to incorporate an internal power source. A typical design consists of an enclosed water tank connected to a concentrated array of nozzles along a short length of airway. A containment diaphragm prevents flow from the tank to the nozzles under normal operating conditions. A bottle of compressed nitrogen or carbon dioxide is located inside the water tank. The gas container is also fitted with a rupture disk.

Upon activation, a heater within the gas bottle causes the gas to expand and puncture the rupture disk. This causes very rapid pressurization of the water, breakage of the containment diaphragm and delivery of water at high pressure to the nozzles. Several hundred litres of water can be dispersed in less than one second. Some designs utilize a powdered flame suppressant in place of the water and a soft explosive instead of the gas container.

Activation of a triggered barrier is initiated by an electrical signal from a detector device located closer to the working area, where an explosion is more likely to commence. Infra-red, ultra-violet, temperature and pressure pulse sensors have all been employed as detection devices.

In addition to the active power source to disperse the fire suppressant, an advantage of the triggered barrier is that an optimum distance can be selected between the sensor and barrier. This ensures that the barrier will be activated at the correct moment with respect to the approaching flame front.

21.8.4 Explosions in sealed areas.

21.8.4.1 Causes of explosions in abandoned areas.

The majority of mine explosions are initiated by operations in the active zones of the mine, particularly arising from ignitions of methane at the pick points of mining machines. These explosions have sometimes caused damage to seals separating active mining zones from abandoned workings and allowing methane to flood into the current ventilation network. The fuel provided by this methane can add to the proliferation and violence of the explosion (for example, the Westray Mine explosion in Nova Scotia, 1992, Richard, K. P., 1997). It was for this reason that the designs of seals to unventilated old workings sought to be capable of withstanding explosion forces. It has now been accepted that explosions can occur *within* abandoned areas (example Sago Mine, West Virginia, 2006). It is difficult to determine with certainty the causes of such explosions. The possibilities include:

friction

The collapse of strata that contains quartz (particularly sandstones) is capable of producing incendiary sparks by friction of rock against rock or rock on steel (Powell, 1975, Nagy, 1960)

lightening

Lightening strikes on surface may be conducted for discharge in mine workings, including abandoned areas, via borehole casings, pipes, cables or any other conductive path (Sacks, H.K. and Novak, T., 2005).

adiabatic compression

The atmospheric pressures developed by sudden collapses of strata into sealed areas can cause rises in temperature to the ignition point of explosive mixtures (McPherson, 1995; Lin, W. 1997).

spontaneous combustion which reaches open areas. (See Section 21.4)

21.8.4.2 Recognition of the hazard.

Following the Sago Mine explosion (West Virginia, 2006, 12 fatalities) and Darby Mine explosion (Kentucky, 2006, five fatalities) urgent new research was initiated into safeguarding miners against the effects of explosions occurring in abandoned areas of coal mines. The National Institute for Occupational Safety and Health (NIOSH) in the United States reported that during the period 1986 to 2006 there were 12 incidents of explosions in sealed areas of mines in the United States (Zipf et al, NIOSH, 2007). In ten of those explosions seals were destroyed indicating that the U.S. design standard then in use 140 kPa (20 psig) was far from adequate. This contrasted with standards of the 345kPa (50psig) in the UK or 500kPa (73 psig) in Poland and Germany) where no seal failures due to explosions in old workings were reported in the same period.

One effect of the Sago Mine explosion was the issuance of a Mine Safety and Health Administration (MSHA) Emergency Temporary Standard that seals should be designed and constructed to withstand an explosion pressure of 345 kPa (50 psig) and that new research on mine seals be initiated (see Section 21.1). This provided the impetus for NIOSH to embark on such research. The first of their reports was issued in 2007 (Zipf et al) with the promise of further investigations to be conducted.

21.8.4.3 Approaches to the problem and the initial NIOSH Report.

An approach to the safety of abandoned workings has been either to ventilate those old workings continuously in order to remove methane or to seal them off and allow an inert atmosphere to be established. Both of those techniques have disadvantages. With regard to continuous ventilation, even when air passes slowly through caved areas it is still possible for pockets of methane and explosive mixtures to exist within those areas, particularly in inclined workings. Secondly, it is most unwise to pass air through old workings where the coal is prone to spontaneous combustion. And thirdly, recalling that ventilating fans are often the largest consumer of electrical power at a mine, the associated costs can become very high if airflows are used to ventilate increasing areas of abandoned workings.

With regard to sealing off an abandoned area, the intention is that an inert atmosphere be established in sealed areas by the combined effect of oxidation (replacing oxygen by carbon dioxide) and emissions of

methane. However, this can be effective only if the seals are designed to minimize leakage. Furthermore, recalling from Section 4.2.3 that the effective combined resistance, R_{eff} , of seals constructed essentially in parallel falls dramatically as their number increases it becomes important that the number of seals into the area is also minimized.

$$\left[R_{eff} = \frac{R}{n^2} \quad \text{where } R \text{ is the resistance of a single seal and } n = \text{number of seals.} \right]$$

An added complication is that seals will “breathe” as the external atmospheric pressure varies. (Section 4.2.2). The effect is that air will leak through or around seals during periods of a rising or falling barometric pressure. For these reasons an inert atmosphere may never be attained in all parts of an abandoned and sealed area. In particular, the breathing of seals can produce a time variant zone of explosive mixture immediately inby each seal.

The NIOSH Report of 2007 (Zipf et al) described a rigorous investigation involving laboratory (closed volume) tests, full scale gallery tests and the utilization of mathematical models. These tests examined

- the dependence of pressures developed by an explosion on the volume of explosive mixture,
- the case of products of combustion expanding into inert voidage and caved areas
- the case of gases resulting from the explosion venting into other active or inactive parts of the mine,
- the run-up distances through which an explosion can proliferate up to becoming a detonation (Section 21.8.2.2).

On the basis of their investigation, NIOSH suggested that if abandoned working are to be sealed rather than ventilated then mine management decide on a case-by case basis whether to

- (a) build unmonitored seals that will withstand most explosions within old workings, or
- (b) utilize lighter seals but to monitor continuously the atmosphere in a zone inby the seals.

Table 21.5 gives a synopsis of the applications of unmonitored and monitored seals that are described in more detailed in the NIOSH 2007 Report.

At the time of writing, NIOSH is continuing with its investigations. In particular, further work should provide guidance on the construction of seals.

Australia has already adopted regulations that consider the conditions under which unmonitored and monitored seals can be used (Oberholzer and Lyne, 2002). Monitoring is normally carried out by means of tube bundle systems (Section 21.7.2). Furthermore, in addition to monitoring, many Australian mines utilize inertization techniques to maintain an inert atmosphere inby the seals (Section 21.6).

Unmonitored	Design pressure	Monitored	Design pressure
<p>Panel and district seals. Length of sealed volume >50m. 100% filled with explosive mix, completely confined, unvented</p>	4400 kPa (640 psig)	<p>Panel and district seals. Length of sealed volume >50m in any direction . Monitoring ensures that that maximum length of explosive mix behind seal ≤ 5m and volume of explosive mix $\leq 40\%$ of total sealed volume. Some venting into inby inert atmosphere. (typical situation with breathing seals)</p>	345 kPa (50 psig)
<p>Panel, district and crosscut seals. Length of sealed volume ≤ 50m in any direction. Sealed area completely filled with explosive mix. Confined but can vent somewhat into gob</p>	800 kPa (120 psig)	<p>Panel , district and crosscut. seals. Length of sealed volume <50m in any direction Monitoring ensures that maximum length of explosive mix behind seal ≤ 5m Volume of explosive mix $\leq 40\%$total sealed volume.</p>	345 kPa (50 psig)

Table 21.5 A simplified synopsis of the design pressures recommended for unmonitored and monitored seals.

(Derived from Zipf et al. *Explosion pressure design criteria for new seals in U.S. coal mines. NIOSH IC 9500, 2007*)

Figures 21.17 and 21.18 show layouts that illustrate the possible locations for district, panel and cross-cut seals.

21.8.4.4 Requirements of seals

Due to the many uncertainties associated with atmospheric conditions and changing geometries within sealed areas it is difficult to know with any certainty the distributions and concentrations of gas mixtures much beyond the seal locations. Hence the conservative approach is to assume that well developed explosions can occur within the sealed area and to construct seals that can withstand such explosions . The requirements of such seals are:

- they be as leakproof as practicable, taking into account the number of seals to be built
- capable of withstanding repeated explosions
- explosion proof in both directions taking into account the shear strength of strata in the roof, floor and sides, and
- that they can withstand strata convergence over the long term.

It may prove difficult to design practicable and cost-effective single-wall seals that can meet all of these requirements. A wise objective of further investigations would be aimed at designing mine layouts that minimize the number of seals required and the utilization of double walled seals with an infill that is economically and readily available. Figure 21.19, with or without the sampling arrangements, illustrates the type of seal that has proved successful in meeting these listed requirements.

It is a prudent precaution to pre-prepare the sites of future seals as soon as practicable after excavation of the relevant airways. Such preparation should include cut-outs for the seal walls in airway sides and the storage of materials for construction of the seals. Such pre-preparation will prove invaluable in cases of emergency. Furthermore, airways should be liberally stone dusted both inby and outby the sites of seals.

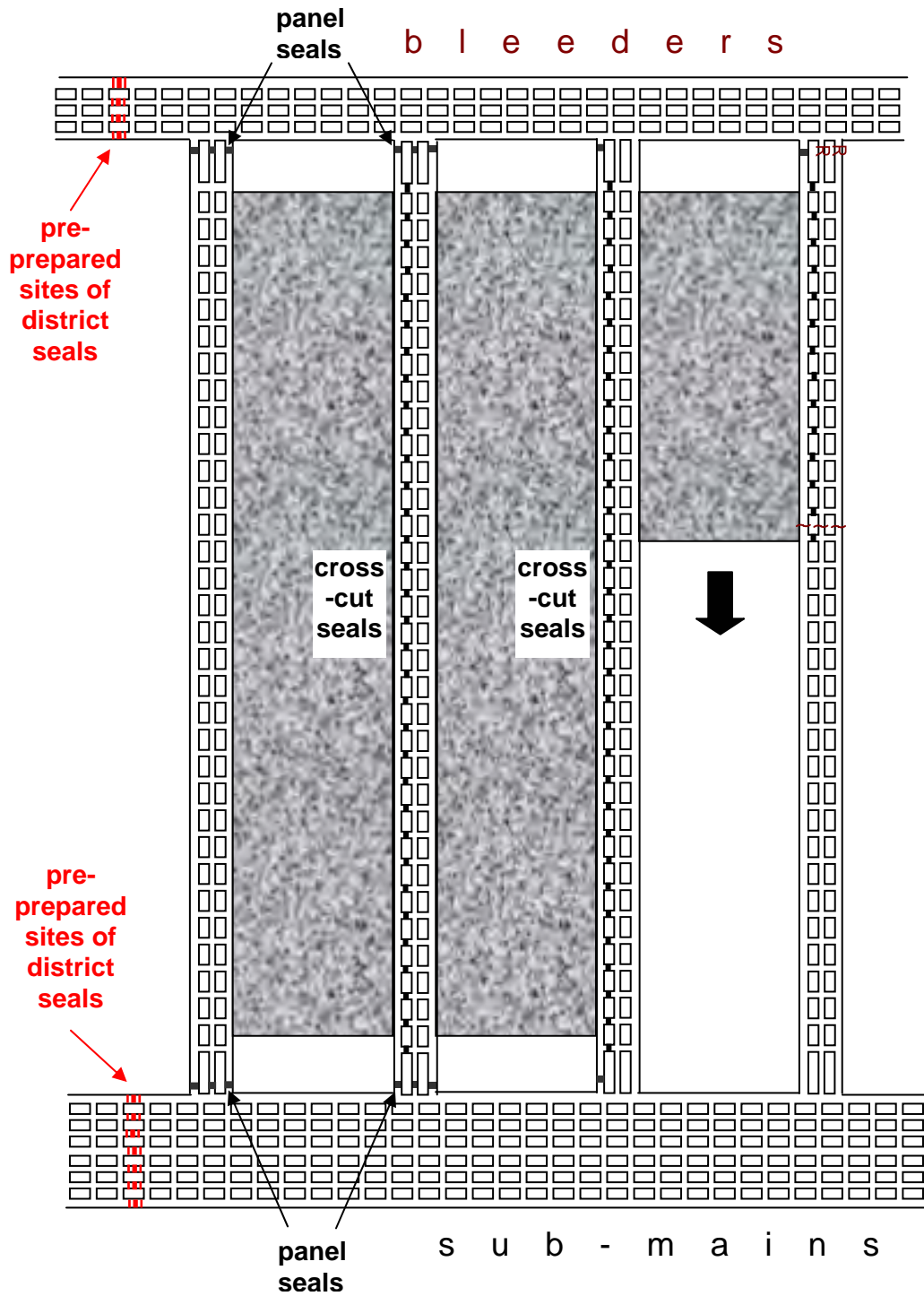


Figure 21.17 Panel extraction with panel and cross-cut seals. Multiple cross-cut seals are required.

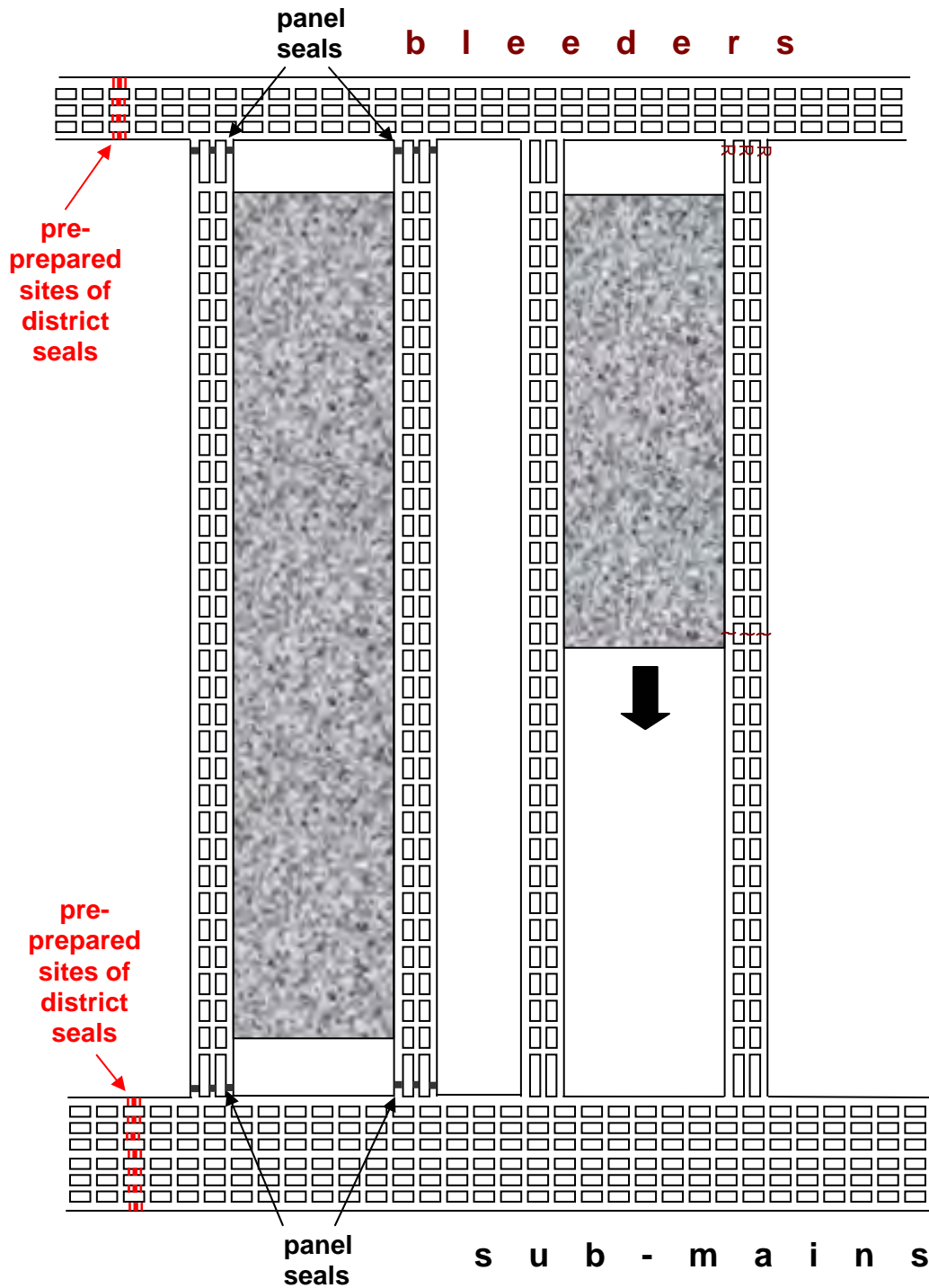


Figure 21.18 Barrier pillars left between panels (subject to rock mechanics considerations.)
No cross-cut seals required.

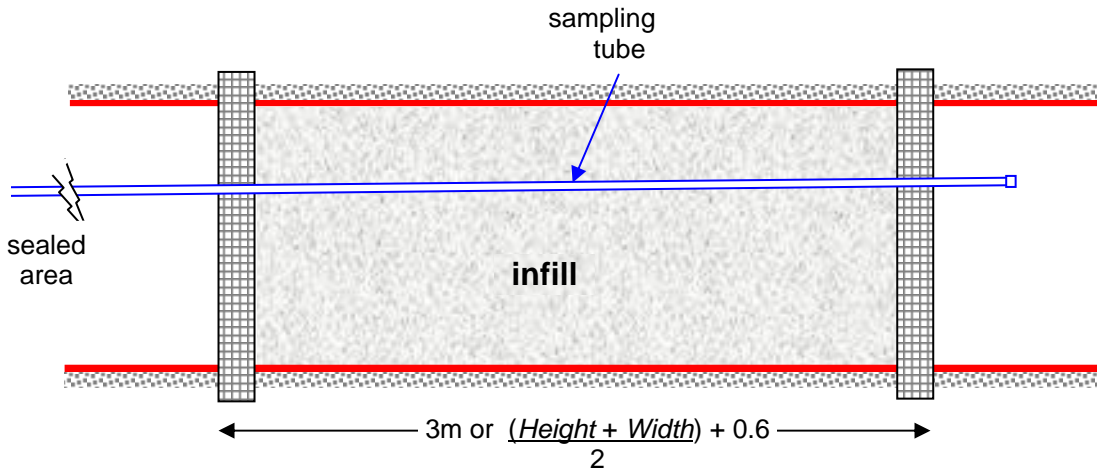


Figure 21.19 Example of an explosion proof seal.

21.9 PROTECTION OF PERSONNEL

21.9.1. Training and preparedness

In all underground emergencies, the first priority is the safety of personnel. The surest protection against the initiation and hazards of mine fires and explosions is training and practice of safety procedures. Classes and practical sessions should be held, not only for new recruits, but at regular intervals of time for all employees. These sessions should include discussions on the causes of fires and explosions and how they propagate. The elements of subsurface firefighting and operation of fire-suppression equipment should be outlined. It is prudent to ensure that supervisors and other selected members of the workforce should receive additional instruction and practice in firefighting. As in mine rescue work, competitions between teams can do much to foster interest. This further training may include the use of temporary stoppings, airflow control and air pressure management. However, training of all underground personnel should concentrate particularly on

- warning systems and location of trapped persons
- self rescuers
- escapeways and
- refuge chambers.

These four items are discussed in the following subsections.

Mine management plays a crucial role in minimizing the risks of fires and explosions, and in responding correctly when they do occur. In addition to matters of training, the planned arrangement of services dictates the efficiency of emergency response (Section 21.10.). Communications, routes of water pipes, cables, airflows and escapeways, availability and effectiveness of firefighting equipment, reliable environmental monitors and an integrated fire-protection policy (Sheer, 1988) can make the difference between a localized ignition that is quickly extinguished and disastrous loss of life. Ventilation and safety engineers should engage in mock scenarios and computer simulations of emergency situations. Such exercises assist in raising questions related to response strategies and mine preparedness such as establishing distances from work locations to refuge chambers and escapeways.

All underground workers should be required to engage in fire drills and emergency evacuation procedures at least once in each three months. These should involve leaving the mine by escapeways other than the normal travelling routes. Such drills should be accompanied by discussions on choices of escape routes and ventilation systems, and should also encourage familiarity with the layout of airways within the mine.

It is a useful exercise, as part of emergency preparedness, for mine management to establish prior friendly relationships with local police, fire, hospital and news agencies. This can be further facilitated by arranging occasional tours of the mine for such people.

21.9.2. Methods of warning and locating personnel

The rates at which mine fires can propagate and products of combustion spread throughout an underground network of airways make it vital that all personnel in the mine be warned of the emergency as quickly as possible. This can be difficult because of the distances involved and wide dispersal of the workforce, particularly in metal mines. Video cameras may be located at strategic locations although these might be obscured by smoke.

Most mining industries employ "firebosses, firemasters" (or similar titles) whose task is to patrol the mine before and, perhaps, during each working shift and following blasting operations to search for any indications of a fire. To ensure adequate and timely coverage of the mine, tags are left at strategic points showing the time and date of the last visit. Fire patrols should follow the direction of airflow in order to more easily locate the probable source of any smoke or fire odour.

Modern paging-type mine telephone systems enable voice warnings to be transmitted to main work areas and along major transport routes. These are particularly suitable for concentrated mining methods such as the longwall system. However, the extension of paging techniques along the several hundred kilometres of active airways in a large metal mine would be cost prohibitive. The methods that have been devised to transmit fire warnings to a widespread workforce in underground openings include:

- stench warning systems,
- radio signals and
- more recent systems

Following receipt of any form of fire warning, mine workers should immediately engage in the emergency evacuation or personnel protection procedures in which they should have been trained and practiced (Section 21.9.1.).

21.9.2.1. Stench warning systems

Versions of this technique have been employed in large metal mines since the 1930's. The procedure involves releasing a gas having a very distinctive odour into intake airways or compressed air systems. Having been exposed to low concentrations of the stench gas during training sessions, miners recognize the odour and can initiate emergency procedures. The gases used resemble those introduced into natural gas distribution systems. Ethyl mercaptan mixed into freon has been commonly employed. However, this can be toxic, corrosive and produce an unbearable stench at high concentrations. Furthermore, it may lose its potency when transported through steel pipes. A safer and healthier alternative is tetrahydrothiaphene (Ouderkerk et al, 1985).

A basic disadvantage of the stench warning technique is that it relies on the mine ventilation system. Transmission times of the stench depend upon the large range of air velocities that exist within a mine ventilation network. In openings of large cross-sectional area, travel times can

become dangerously high to serve as a fire warning system. Furthermore, the concentration of the odour will also vary from very high, close to the emission point, to barely detectable in remote areas of a complex ventilation network. To add to the difficulties, the ventilation system may have been modified or disrupted by the fire (Section 21.3.2.).

These drawbacks can be minimized by selecting multiple injection points in locations reasonably close to major work areas, in addition to downcast shafts or other primary inlets. Stench gas injector mechanisms should incorporate pressure balance arrangements and controlled release rates to prolong the warning and to avoid short peaks of excessively high concentration. Inby injectors should be capable of remote activation. The choice of injector sites and release rates should be made carefully. The objective is to carry a clearly detectable odour as rapidly as possible to all parts of the mine where personnel may be working. Ventilation network analysis packages that incorporate gas distribution modules are very helpful in selecting optimum locations and release rates (Section 7.4.4.).

21.9.2.2. Ultra-low frequency radio signals.

Many investigations have been conducted into the use of radio waves for warning mine personnel of an emergency condition and, also, for *locating* persons who have become trapped. High or medium frequency radio signals are limited to line-of-sight transmission or depend upon the existence of metal conductors such as pipes, cables or conveyor structure. For personnel warning or location, the radio signals must be capable of transmission through rock and of being detected by lightweight and low-powered personal receiver units.

Older developments in this area have involved ultra-low frequency devices. At frequencies in the range 630 to 2000 Hz and employing transmitting powers of 1 kW, rock penetration distances of over 1600 m have been achieved (Hjelmstad and Pomroy, 1990). This indicates that transmitters located on surface will be suitable for most mines, while underground transmission sites will serve for the deeper workings. The signal strength decays inversely with the cube of the distance through the rock.

The transmitter consisted of a radio (electromagnetic) signal generator, amplifier and antenna. The latter may be made from ten coils of insulated copper wire coiled into a loop of some 30 m diameter. The personal receiver units are small, intrinsically safe and may be powered by the wearer's caplamp battery. The pencil size receiver antenna is formed from a high-permeability ferrite core wound with copper wire and is very efficient in detecting electromagnetic radiation. More highly powered units can be fitted to vehicles or other equipment. The transmitter and receivers are tuned to a common resonant frequency to discriminate against electromagnetic noise or stray signals. The voltage produced by a receiver unit is amplified and may then be used to generate an audio-visual warning. Incorporation into the caplamp unit can produce on-off blinking of the light until nullified by operation of a switch. Research continues into the use of rock-penetrating radio waves for voice communication. Again, this will serve for both warning and personnel location purposes.

21.9.2.3. More recent systems

Following the Sago Mine explosion (West Virginia, 2006) a plethora of wireless tracking systems have been developed to locate persons in underground mines, particularly in Australia and the United States. These systems have included hand-held radios, leaky feeder and radio frequency devices. The first of these to be approved by the U.S. Mine Safety and Health Administration is normally energized via d.c. power cables with back-up battery power in case of failure of the cable system. (MSHA, 2008)³. The units can be used to track miners both before and after an emergency situation. Text messaging as well as gas detection can be added to the system to maintain communications between equipped miners and a central location where all such

³ Mine Tracer Miner Location System, Venture Design Services. Inc.

communications are logged . At the time of writing other tracking devices are under investigation for approval in U.S. mines.

21.9.2.4. Locating trapped persons

The situation has all too often arisen where miners have become trapped in locations that are inaccessible because of accumulations of gases, products of combustion, water or falls of roof. To facilitate rescue operations, it is necessary to identify the locations of the trapped personnel.

A very old method that has often led to life-saving operations is the seismic technique. An explosive charge or heavy hammer (pile-driver) blow on the mine surface may be heard or felt by personnel in relatively shallow mines. In deeper operations, similar seismic signals may be generated from underground locations. On hearing these signals, the trapped personnel respond by hammering on pipes, rails or, simply, the floor or walls. If this response is detected by the ears or geophones of rescue personnel then mine maps are consulted, if necessary, to select the probable location(s) of the trapped persons. Pilot boreholes may be drilled to those locations to supply food and air while rescue operations proceed.

21.9.3. Self-rescuers

An estimated 80 to 90 per cent of fatalities in mine fires or explosions are caused by carbon monoxide poisoning. Self- rescuers are compact versions of breathing apparatus and are intended to allow the wearers to pass through atmospheres that are contaminated by smoke or carbon monoxide. In many countries, it is mandatory for all persons who enter an underground mine to carry a self-rescuer. The lighter versions can be worn on the belt of each person who ventures underground while caches of the heavier self rescuers may be kept close to work areas and on vehicles. The purpose of self-rescuers is to allow the wearers to *escape* from or through contaminated atmospheres. Indeed, they are often known as escape breathing apparatus (EBA's). They are not intended for rescue operations or other type of work and should not be confused with the more specialized breathing equipment used by trained rescue teams.

The two essential features of self-rescuers are the types of atmosphere in which they are effective and the time they allow for escape. Their operational duration depends not only upon the type of self-rescuer but also:

- manual effort (e.g. speed of walking)
- breathing habits, experience, physical condition and mental state of the wearer, and
- environmental conditions.

Although many lives have been saved by self-rescuers, others have been lost even when such devices were available. In many of these cases, the error has been in failing to don the apparatus at the appropriate time. This matter should be stressed heavily during training sessions. In particular, self-rescuers should be put on as soon as it is suspected that the air is, or may become, contaminated, i.e. by means of telephone messages, personnel warning systems (Section 21.9.2.), shock waves or strong pulses in the ventilation, unusual odours or the appearance of smoke. Furthermore, during training, personnel should be required to practice unpacking and donning the apparatus. **Training versions** of the units are available for this purpose. Experience has shown that classroom instruction on the opening and donning of a self-rescuer is insufficient to emulate the physical and psychological conditions under which it may be used in an emergency. It is recommended that the procedure be practiced in a smoke-filled atmosphere or, at the very least, with closed eyes.

There are basically two types of self-rescuer units, the *filter* self-rescuer (FSR) and the *self-contained* self-rescuer (SCSR).

21.9.3.1. Filter self-rescuers (FSR's)

Each of these small and compact units fits inside a hermetically sealed plastic or stainless steel case which is worn on the belt. To use the device, the seal is broken by a lever arrangement, the mouthpiece inserted inside the lips and gripped by the teeth, and nose clips put on. The complete unit is held close to the face and chin by head straps. Air is drawn through three types of filter before passing through a heat exchanger to the mouthpiece. Exhaled air also traverses the heat exchanger and through a one-way valve to the external atmosphere.

The first level of filtration simply removes dust particles. The second filter is a drying agent - typically 9 per cent lithium chloride and 91 per cent calcium bromide impregnated into activated charcoal (Strang and MacKenzie-Wood, 1985). The activated charcoal assists in removing sulphur dioxide, hydrogen sulphide and oxides of nitrogen. The third level of filtration contains a catalytic mixture of granulated manganese dioxide, copper oxide and a little silver oxide. The mixture is known widely as *hopcalite*. This catalyst converts carbon monoxide into carbon dioxide with close to 100 per cent efficiency. It is, however, poisoned by water vapour. Indeed, the duration of the device is governed by the drying agent in the second level of filtration. The period of operation is, typically, about one hour for saturated conditions and carbon monoxide concentrations of up to 1.5 per cent.

Filter self-rescuers suffer from two disadvantages. First, they rely on there being at least 16 per cent oxygen in the ambient atmosphere (Section 11.2.2.). Secondly, both the drying filter and the hopcalite involve exothermic reactions. Indeed, the temperature of the inhaled air is an indication of the level of carbon monoxide present. At high concentrations, the temperature of the filtered air may exceed 90°C and cause great discomfort including blistering of the lips and mouth. However, removing the mouthpiece for temporary relief in such circumstances is likely to be fatal. The small heat exchanger close to the mouth piece absorbs heat from the filtered air and rejects it to the exhaled air. Because of these limitations it is prudent to replace filter self-rescuers by self-contained self-rescuers with the possible exception of small mines with ready access to the surface.

21.9.3.2. Self-contained self-rescuers (SCSR's)

As the name implies, these supply all the respiratory needs of the wearer and are independent of the gaseous constituents of the ambient atmosphere. A considerable variety of self-contained self-rescuers have been produced. The main disadvantage is their weight and bulk. Current generations of SCSR's vary from 2 to 5 kg and may not be sufficiently convenient for personal wear - hence, requiring caches of the units to be available close to active working areas. Research continues in attempts to develop a self-contained self-rescuer that is sufficiently light and compact to be worn on the belt while giving the 60 or 90 minute operating life that may be mandated by law. National and state legislation should be consulted for regulations that govern the requirement, types and operating durations of self-rescuers.

As with the FSR's, the self-contained versions are hermetically sealed in polypropylene or metal containers to ensure a long shelf life. However, if the seal is broken or damaged, the unit must be replaced. Periodic water bath tests should be carried out to ensure that the casings remain airtight. The units include noseclips, fitting straps and goggles. Two types of self-contained self-rescuers are in common use.

The *compressed oxygen SCSR* is a recirculating system. Expired air passes through a soda lime filter which removes carbon dioxide, then into a flexible "breathing bag" where it is enriched with oxygen from a compact gas cylinder. The oxygen may be supplied at a base rate of some 1.2 to 2 litres per minute but will be increased automatically if deflation of the breathing bag indicates a rising demand for air. The air passes to and from the mouthpiece via a flexible breathing tube. The unit is worn on the chest and supported by neck and waist straps.

The *chemical SCSRs* are lighter devices and develop oxygen from the reaction that occurs when water vapour and carbon dioxide from exhaled breath pass through potassium superoxide (KO_2). The oxygen in this compound contains an additional electron compared with free gaseous oxygen. This gives a fairly weak bond and free oxygen is released readily according to the following reactions:



and $KOH + CO_2 \rightarrow KHCO_3$

Exhaled air from the mouthpiece passes down the flexible breathing tube and through a bed of granulated potassium superoxide where oxygen is added and carbon dioxide removed. It is then collected in a breathing bag for re-inhalation. A heat exchanger can be incorporated to maintain the temperature of the inhaled air to no more than 45°C in most situations.

The chemical production of oxygen can be initiated simply by exhaling vigorously into the unit. However, there may be little or no time to accomplish this safely. Chlorate candles are incorporated into most chemical SCSR's to overcome this difficulty. The chlorate candle is started by percussion or other device when a ripcord is pulled. This provides some three to four litres of oxygen during the following few minutes and until the potassium superoxide reaction becomes effective.

Because of their vital role in cases of emergency, it is important that self-rescuers be inspected according to a timetable that may be imposed by regulations but should occur at intervals of no more than 3 months or after an SCSR has been carried or worn on the person of any individual. In particular the seal of each unit should be examined to ensure its integrity. A log should be maintained on inspections of each individual unit.

The bulk and weight of most current self-contained self rescuers may render them unsuitable for continuous wearing by a miner. Caches of SCSRs may be stored at underground locations. Such caches should be within a travel time of five to ten minutes, depending on the duties of any worker, preferably in a level intake airway but accessible from more than one entry. However, caches of SCSRs should be available at both the main gate and tail gate ends of a longwall panel and in designated escapeways. Caches of SCSRs should be checked as part of pre-shift inspections. These should be at least the number of SCSRs stored underground as the maximum number of personnel underground at any one time. Training should ensure that each miner knows the locations of SCSR caches. It is prudent to have self rescuer units on personnel transportation vehicles.

21.9.4. Escapeways

In any subsurface facility, certain paths should be selected as preferred evacuation routes in the event of an emergency. These *escapeways* should be highlighted during training sessions and fire drills. There are three matters of importance:

- selection of airways as escapeways
- preparation and maintenance, and
- protection and use of escapeways during an emergency.

The *choice* of escapeways commences by a pragmatic examination of the airflow routes, travel distances, geographical layout of airways, the physical state of those airways, directions of leakage through stoppings, and the locations of air crossings, doors and other ventilation controls that may be dislocated by a fire or explosion. The primary requirement is that escapeways should be maintained free from products of combustion for as long as possible following the outbreak of a fire.

At least two escapeways must be available from all areas of routine mineral extraction. This is usually mandated by law. In the case of single development headings or other special circumstances, legislation may limit the number of persons who may be allowed into those areas at any one time. For single entry longwall systems, the section intake and return airways must serve as the escapeways. However, even in multi-entry systems it is prudent to maintain at least one return as a escapeway. Incidents in the intakes or mineral extraction zone may prevent evacuation along intake escapeways. Depending upon air velocities and the efficacy of any barricades that may be erected, it might be possible to outpace the airflow and stay ahead of products of combustion along a well maintained return escapeway.

At least one (and preferably more) intake airway for each section of a mine should be maintained as an escapeway. Where two or more intakes are designated as escapeways then they should be truly independent ventilation routes as far back to the primary mine inlets as practicable. Two parallel airways, where one is ventilated by air that has passed through the other, are not independent ventilation routes and cannot be regarded as separate escapeways (MSHA, 1984). Strata stresses should also be considered in selecting escapeways. Routes that are subject to crushing will become excessively expensive to maintain in a good travelable condition and should not be chosen as escapeways.

Network analysis programs with pollutant distribution modules (Section 7.4.4.) can be employed to check and improve the selection of escapeways for any given fire scenario. Computer packages that simulate fire situations are particularly valuable for this purpose (Section 21.3.2.2). Even more specialized programs have been developed specifically for the identification of preferred escapeways (Barker-Read and Li, 1989). The reliability of escapeways can be subjected to objective tests through the techniques of fault-tree analysis through which the causes and consequences of events may be interlinked, tracked and analyzed (Goodman and Kissell, 1989).

The *preparation and maintenance of escapeways* should be carried out with careful consideration given to the potential conditions in which those escapeways may be used, i.e. in zero visibility by persons wearing self-rescuers and who are in a state of anxiety. Obstructions, patches of poor roof, uneven or tracked floors and unfenced junctions may create little difficulty during routine travel but can make the difference between life and death when the airway is filled with smoke.

Escapeways must be maintained in a condition suitable for unimpeded foot travel at all times. Signs and coloured reflectors should be employed to indicate directions of escape. However, here again, these visual indicators may be rendered invisible by smoke. Reflectors should, preferably, be located on the sidewalls rather than at the roof of airways as smoke is liable to be thickest at roof level. Some form of lifeline should extend throughout the length of an escapeway. This may simply be a water or compressed air pipe, a cable, wire line or part of the structure of a conveyor, but placed at a convenient height to be followed by hand contact. Such lifelines should also have cones or other devices at intervals to give a tactile indication of direction. It is prudent to deposit extra caches of self-rescuers in well-identified locations within escapeways.

Persons who work in any section of a mine should be completely familiar with the relevant escapeways. This can be promoted by using alternative exit routes during fire drills and displaying escapeway maps within the section and at other locations, such as shaft stations, where miners may congregate.

During an actual emergency, every attempt should be made to maintain escapeways free from products of combustion for as long as possible. This might be accomplished by the placement of brattice cloths or other devices to control pressure differentials between airways (Section 21.3.4.1.). Again, training classes and fire drills give the opportunity of imparting familiarity with procedures involved in evacuation through escapeways. These include the advisability of travelling in groups for mutual assistance and the use of lifelines.

21.9.5. Refuge chambers

When personnel have become trapped within underground workings and all escape routes have become inaccessible then refuge chambers provide a last resort to preserve life. These are lengths of airway or fire-resistant prefabricated chambers which might be portable and either rigid or inflatable within which miners may wait until they can be reached by rescue personnel. Blind headings or other single ended zones are the preferred locations. However, totally enclosed prefabricated chambers may be sited in through-flow airways or cross-cuts. The requirement, number and locations of refuge chambers may be mandated by legislation. Where used, they should be within reasonable access from active working sections (NIOSH, 2007).

Refuge chambers should be sized according to the maximum number of persons who work in that area of the mine and for an occupancy period of not less than two days. Assuming that each resting person has need of 0.15 litres of air per second (Table 11.2) gives an air requirement of 13 m³/day. However, this should be multiplied by a safety factor of 3 to allow for increased concentrations of exhaled carbon dioxide. Hence, if twenty persons are to be accommodated, then the chamber should have a minimum volume of $13 \times 2 \times 3 \times 20 = 1560\text{m}^3$. An opening of cross-sectional area of 15 m² would, therefore, require a length of $1560/15 = 104$ m if there is no additional air feed from a compressed air line or surface borehole.

Two types of refuge chamber have bought trapped miners vital waiting time. *Pre-prepared* and fully equipped refuge chambers should be considered for workings that are distant from surface connections, and in long development or exploration headings. They should ideally be equipped with water, compressed air, communication with the surface, gas and temperature monitors, sanitary arrangements, extra self-rescuers, food in sealed containers, first aid supplies, oxygen cylinders, emergency supplies of breathable air, and reading/writing materials (Halasz, 1985). The entrances to pre-prepared refuge chambers should be well marked. Routes leading to refuge chambers may be fitted with directional blinking lights (similar to Christmas tree lights) to assist miners traversing polluted airways. All underground workers and management should be trained in the maintenance and use of refuge chambers and be aware of the existence and locations of such chambers. Prefabricated chambers should be constructed from non-combustible and heat-resistant materials.

As a last resort, trapped personnel may be able to construct improvised refuge chambers provided that brattice cloths, timber, hammers, saws and nails are available. Leakage points may be sealed by clothing, rags, boards or, indeed, anything else that is available. In such cases, an active compressed air line into the zone is invaluable in maintaining the pressure above that of the connecting and, perhaps, polluted airways. If such barricades have to be erected within a continuous airway then attempts should be made to minimize the pressure differential applied across the ends. This may entail holing stoppings or opening doors in the immediate vicinity.

Following the NIOSH Report of Dec. 2007 the Mine Safety and Health Safety Administration of the United States published for public comment a Proposed Rule on Refuge Alternatives in American coal mines (MSHA, 2008). At the time of writing, it is intended that a Final Rule will be established by the end of 2008. This follows a period since 1969 when federal law allowed the regulatory agency to require that refuge chambers be installed in coal mines. Until 2008, however this authority was never exercised.

21.10 EMERGENCY PROCEDURE AND DISASTER MANAGEMENT

The manner in which a major fire or explosion in a mine is handled depends largely on the forethought and planning that has been expended on such an eventuality. The early stages of an emergency are often fraught with uncertainty, and chaos can easily occur. It is, therefore, vital that those in charge of subsurface operations should have established and documented a definitive

procedure to be followed when a dangerous condition is discovered. All key personnel should be very familiar with that procedure. This final Section discusses the three areas that should be addressed.

21.10.1. Immediate response

There are two sets of actions that should occur immediately and simultaneously when a major fire or an explosion takes place. First, all available warning systems for underground personnel should be activated; the numbers of persons underground and their work locations should be established, return airways should be evacuated, and responsible persons should be sent to inspect the affected area (as far as is possible). While this is in progress, telephone messages should be transmitted to key persons or agency representatives not already at the site. These include

- mine management and senior supervisory staff
- heads of mine specialist departments (e.g. ventilation, safety, electrical, mechanical)
- regional mine rescue centres and rescue stations at neighbouring mines
- government inspectorate or enforcement agencies
- union officials
- local police, fire and medical facilities.

A list of these persons or agencies and their telephone numbers should be posted permanently in a prominent position in the surface operations centre of the mine and updated whenever necessary. At all times, when people are in the mine, there must be a designated person on surface who has the authority and responsibility to initiate these immediate actions.

21.10.2. Command centre

An emergency command centre should be established in a surface office as rapidly as possible. This should be manned by a few key officials, normally the senior management of the mine and others with detailed and expert knowledge of firefighting and rescue operations. Those persons should have the authority to take part in decision making. However, they should be supported and advised by specialist engineers, other government officials and union representatives. Office accommodations equipped with desks, telephones, mine maps and stationery should be made available for these supplementary groups adjoining the command centre. Provision should also be made for rescue personnel and those involved in the analysis of gas samples.

It is important that the chain of command is firmly established. There should be one person in overall control. Decisions are usually arrived at after consultation and discussion. However, the final word lies with that one person. Instructions relating to firefighting, rescue and evacuation must be issued only from the command centre. Direct communication should be maintained between the command centre and the mine telephone system as well as to surface fans, power centres and pumping stations.

21.10.3. Disaster management

In addition to the operations that are conducted underground during an emergency, there are numerous other facets that require detailed organization and management. It is to be expected that many other people will arrive at the mine site throughout the emergency, including the news media, family and friends of underground workers and volunteers varying from willing but unskilled lay persons to specialist consultants. Police authorities should be asked to assume control of traffic and all access roads to the mine property including surface buildings and mine entrances. Medical facilities may require to be set up on the mine surface and vehicles made

readily available for transportation to hospitals. Medical personnel should be established on site and who must be able and willing to be escorted underground if necessary.

Accommodation may need to be found for immediate family members of trapped miners. This should, preferably, be close by but off the mine site. The presence of clergy and specialists in trauma reactions can be of tremendous assistance in those facilities. Responsible persons should be put in charge of continuous catering facilities and janitorial services.

Every effort should be made to establish good liaison with media personnel and to accommodate them with arrangements for interviews and telephones. One spokesperson for the mining company should be responsible for all statements to the press. As part of disaster preparedness, that person should have been trained in communicating through the media; in particular, making accurate and relevant statements and responses to questions within a 30 or 60 second television interview. It assists in maintaining good relationships with media personnel to keep them informed of the time of forthcoming statements.

Both company personnel and reporters should be aware of their mutual responsibilities. The latter have a duty to inform the public while, at the same time, they should not engage in any activities that will interfere with rescue or firefighting operations. As televised interviews can be broadcast immediately or within seconds, it is of great importance that information relating to individuals be given to concerned family members before being made available to the media. While the great majority of news people act in a responsible manner, there is the occasional renegade whose enthusiasm exceeds his/her common sense. In one such incident, a young reporter managed to evade the check-in procedures at the top of a mine shaft and reached an underground fresh-air base during rescue operations. He was brought out on a stretcher, having fainted at the scene.

References

Banerjee, S.C. (1985). Spontaneous combustion of coal and mine fires. CMRS, Dhanbad, India. Published by Balkema.

Barker-Read, G.R. and Li, H. (1989). Automatic selection of safe egress routes away from underground fires. *Mining Science and Technology*. Vol. 9, pp 289-308.

Bhowmick, B.C. et al (1991). Dynamic balancing of pressure - its relevance for control of fire in Indian coal mines. Indo- Polish Workshop on Mining Research and Mining Methods. Central Mining Research Station, Dhanbad, India, pp 1-15.

BHP Billiton Sustainability Report (2005). Safety Case Studies. Bleederless longwall ventilation at San Juan Underground Mine manages risk of fire and explosion.
<http://sustainability.bhpbilliton.com/2005/repository/safety/caseStudies/caseStudies14.asp>

Both, W. (1981). Fighting mine fires with nitrogen in the German coal industry. *The Mining Engineer*, U.K., May.

Boulton, J.R. (1991). Wave trend crossing - a new tool for detecting fires in a mine employing diesel equipment. 5th U.S. Mine Ventilation Symposium, W. Virginia, pp 9-17.

Browning, E.J. (1988). Frictional ignitions. 4th Int. Ventilation Congress, Brisbane, Australia, pp 319-326.

Brunner, D.J., Wallace, K.G. and Deen, J.B. (1991). The effects of natural ventilation pressure on the underground ventilation system at the Waste Isolation Pilot Plant. 5th U.S. Mine Ventilation Symp., W. Virginia, pp 593-604.

Chakravorty, R.N. and Woolf, R.L. (1980). Evaluation of systems for early detection of spontaneous combustion in coal mines. 2nd Int. Mine Ventilation Congress, Reno, Nevada, pp 429-436

Chakravorty, S.L. (1960). Auto-oxidation of Indian coals. Jnl. Min. Met. Fuels, Nos. 8, 9 and 11, pp 1 and 10.

Coward, H.F. and Jones, G.W. (1952). Limits of Flammability of Gases and Vapors. U.S. Bureau of Mines, Bulletin 503, US Government Printing Office, 153 pp.

Cybulska, R. (1981). Examples of coal dust explosions. Ignitions, Explosions and Fires (ed. A.J. Hargraves). Australian Inst. of Mining and Metallurgy, Illiwarra Symposium, pp 7.1-7.8.

Deliac, E.P. et al (1985). Development of ventilation software on personal computers in France and the application to the simulation of mine fires. 2nd U.S. Mine Ventilation Symposium, Reno, Nevada, pp 19-27.

Dunn, M.F. et al (1982). Main mine reverse performance characteristics. 1st U.S. Mine Ventilation Symp., Tuscaloosa, Alabama, pp 23-28.

Dziurzyński, W. Kruczkowski, J. (2007), Validation of the Mathematical Model Used in the Ventgraph Programme on the Example of the Introduction of New Headings to the Ventilation Network of Mine ARCHIVES OF MINING SCIENCES Poland VOL 52; PART 2, pages 155-170

Dziurzyński, W., Tracz, J. and Trutwin, W. (1988). Simulation of mine fires. 4th Int. Mine Ventilation Congress, Brisbane, Australia, pp 357-363.

Eicker, H. and Kartenburg, H.J. (1984). Investigation of methods for early detection of fires due to spontaneous combustion. 3rd Int. Ventilation Congress, Harrogate, U.K., pp 411-416.

Eisner, H.S. and Smith, P.B. (1956). Firefighting in underground roadways: experiments with foam plugs. S.M.R.E. Res. Rep. No. 130, U.K.

Froger, C.E. (1985). Firefighting expertise in French underground mines. 2nd U.S. Mine Ventilation Symp., Reno, Nevada, pp 3-10.

Gillies, A.D.S., Wala, A.M., Wu, H.W. (1995). Validation Study of the Mine Fire Simulation Model. Proc. 7th US Mine Vent. Symp. pp.199-206. 10th U.S. Mine Ventilation Symp, Anchorage, Alaska. pp 445-455.

Gillies A.D.S., Wala A.M. and Wu H.W., (May 2004). Case Studies from Application of Numerical Simulation Software to examining the effects of fires on mine ventilation systems, 10th US Mine Ventilation Symposium, Anchorage, Alaska, pp 445-455.

Goodman, G.V.R. and Kissell, F.N. (1989). Fault tree analysis of miner escape during mine fires. 4th U.S. Mine Ventilation Symp., Berkeley, CA, pp 57-65

Graham, J.I. (1914). Absorption of oxygen by coal. Trans. Inst. of Mining Engrs., U.K., Vol. 48, p 521.

Greuer, R.E. (1988). Computer models of underground mine ventilation and fires. U.S. Bureau of Mines, IC 9206 (Recent developments in metal and non-metal mine fire protection), pp 6-14.

Greuer, R.E. (1984). Transient-state simulation of ventilation systems in fire conditions. 3rd Int. Mine Ventilation Congress, Harrogate, U.K., pp 407-410.

Grieg, J.D., Lloyd, P.J.D. and Quail, R.W. (1975). Some aspects of the use of high-expansion foams in underground fire-fighting. 1st Int. Mine Ventilation Congress, Johannesburg, S. Africa, pp 239-245.

Halasz, L. (1985). Establishment and use of refuge bays at the Western Areas Gold Mining Company, Ltd., Chamber of Mines of S. Africa, Mine Safety Div., Vol. 4, No. 2.

Haldane, J.S. and Meachen, F. (1898). Oxidation and spontaneous combustion. Trans. Inst. of Mining Engrs., U.K., Vol. 16, p 457

Hall, A.E. et al (1989). Sulphide dust explosion studies at H-W mine of Westmin Resources, Ltd. 4th U.S. Mine Ventilation Symp., Berkeley, CA, pp 532-539.

Herbert, M.J. (1988). The use of nitrogen inertization in the British Isles. 4th Int. Mine Ventilation Congress, Brisbane, Australia, pp 327-335.

Hjelmstad, K.E. and Pomroy, W.G. (1990). Novel fire warning system for underground mines. Mining Engineering, U.S.A., Jan., pp 107-112.

Hodges, D.J. and Hinsley, F.B. (1964). The influence of moisture on spontaneous heating of coal. Trans. Inst. of Mining Engineers, U.K., Vol. 123, No. 40, pp 211-224.

Holding, W. (1982). Explosible dusts. Chapter 28, Environmental Engineering in South African Mines. Mine Ventilation Society of South Africa, pp 763-771.

Holding, W. (1975). An approach to the potential problem of sulphide dust ignitions at Prieska Copper Mine. 1st International Mine Ventilation Congress, Johannesburg, pp 207-211.

Hornsby C.D. et al. (1985). Memorandum of the Committee of Mining Engineers. United Kingdom.

Hwang, C.C. et al (1991). Modeling the flow-assisted flame spread along conveyor belt surfaces. 5th U.S. Mine Ventilation Symp., West Virginia, pp 39-45.

IME (1985). Sealing-off fires underground. Memorandum prepared by the Institution of Mine Engineers, Doncaster, England, pp 1-47.

Jensen, B. et al (1989). An experimental approach to the determination of explosible lean limits for coal dust and methane mixtures. 4th U.S. Mine Ventilation Symp., Berkeley, CA, pp 549-557.

Kissell, F.N. and Timko, R.J. (1991). Pressurization of intake escapeways with parachute stoppings to reduce infiltration of smoke. 5th U.S. Mine Ventilation Symp., West Virginia, pp 28-34.

Kolada, R.J. and Chakravorty, R.N. (1987). Controlling the hazard of methane explosions in coal storage facilities. 3rd U.S. Mine Ventilation Symp., Penn State, pp 334-339.

Lin, W. and McPherson, M.J. (1997). The Ignition of Methane and Coal Dust by Air Compression - The Experimental Proof. SME Annual Meeting, Denver, March, 1997.

Litton, C.D. (1988). Complexities of mine fire detection due to the use of diesel-powered equipment. 4th U.S. Mine Ventilation Symposium, Berkeley, California, pp 162-166.

Litton, C.D. et al (1987). Calculating fire-throttling of mine ventilation airflow. U.S. Bureau of Mines Report, RI 9076.

McPherson, M.J. (1995). The Adiabatic Compression of Air by Large Falls of Roof, 7th US Mine Ventilation Symposium, Lexington KY, pp 257-262.

Mitchell, D.W. (1990). Mine fires. Maclean Hunter, Chicago, Illinois, 167 pp.

MSHA (U.S. Mine Safety and Health Administration) (1984). Report of Investigation, Underground Coal Fire, Wilberg Mine, Utah.

MSHA (2008). News Release No. 08-126-NAT. Feb 1
<http://www.msha.gov/MEDIA/PRESS/2008/NR080131.asp>

MSHA, 2008. Proposed Rule on Refuge Chambers. U.S. Federal Register / Vol. 73, No. 116 / Monday, June 16, 2008 / Proposed Rules.

Nagy, J. and Kawenski, E.M. (1960). Frictional Ignition of Gas during a roof fall. U.S. Bureau of Mines, ROI 5548. pp 1-11.

NIOSH, (Dec, 2007). Research Report on refuge alternatives for underground coal mines.
<http://www.cdc.gov/niosh/mining/pubs/pubreference/outputid2643.htm>.

Mutmansky, J.M. et al (Dec. 2007). Report to the U.S. Dept. of Labor. Final Report of the Technical Study Panel on the utilization of belt air and the composition and fire retardant properties of belt materials in underground coal mining.
<http://www.msha.gov/BeltAir/BeltAirFinalReport122007.pdf>

Oberholzer J.W. and Lyne B.J. (2002). A review of the requirements for testing of the strength of ventilation structures to be used in Queensland mines. Proc. Queensland Mining Industry Health and Safety Conference, pp 105-112

Ouderkirk, S.J. et al (1985). Mine stench fire warning computer model development and in-mine validation testing. 2nd U.S. Mine Ventilation Symp., Reno, Nevada, pp 29-35.

PD-NCB Consultants (later British Mining Consultants) (1978). A review of spontaneous combustion problems and controls with application to U.S. coal mines. Report to the U.S. Dept. of Energy, ET-77-C-01-8965

Pomroy, W.H. (1988). Fire detection systems for non-coal underground mines. U.S. Bureau of Mines Information Circular IC 9206, pp 21-27.

Pomroy, W.H. and Laage, L.W. (1988). Real-time monitoring and simulation analysis of mine atmospheres to locate and characterize underground mine fires. 4th Int. Mine Ventilation Congress, Brisbane, Australia, pp 37-43.

Powell, F. and Billinge, K. (1975). The frictional ignition hazard associated with colliery rocks, The Mining Engineer, Institution of Mining Engineers, Vol. 134, No 174 pp 527-533.

Richard, K. P. 1997, "The Westray Story, A Predictable Path to Disaster", Four volumes, published by the Province of Nova Scotia, Canada.

Sacks, H.K. and Novak, T.(2005). Corona-discharge-initiated mine explosions Industry Applications, IEEE Transactions, Volume 41, Issue 5, pp 1316 – 1322.

Sheer, T.J. (1988). Safety precautions for the protection of miners against underground fires. 4th Int. Mine Ventilation Congress, Brisbane, Australia, pp 1-12.

Stefanov, T.P. et al (1984). Unsteady-state processes during an open fire in a ventilation network. 3rd Int. Mine Ventilation Congress, Harrogate, U.K., pp 417-420.

Strang, J. and MacKenzie-Wood, P. (1985). Mines Rescue, safety and gas detection. Weston Publishers, Kiama, Australia, 366 pp.

Strang J. and Mackenzie-Wood (1990). A Manual on Mines rescue, Safety and Gas Detection, Colorado School of Mines Press, 473 pp.

Sun, W.T. (1963). First industrial trial of fighting underground fires by combustion gases at Tchegan Colliery. Int. Mining Congress, Saltzburg, Germany.

Timko, R.J., Derick, R.L. and Thimons, E.D. (1988). Analysis of a fire in a Colorado coal mine. 4th Int. Mine Ventilation Congress, Brisbane, Australia, pp 345-353.

Trutwin, W. (1975). Reversal of airflow by means of water sprays in upcast shafts. Polish Academy of Sciences, Mining Archives Quarterly, Vol. 20, No. 4 (Published in Polish).

Trutwin, W., Dziurzyński W. and Tracz J., ((1992). Computer simulation of transients in mine ventilation. 5th Int. Mine Ventilation Congress, Johannesburg, South Africa, pp 193-200.

Verakis, H.C. (1991). Reducing the fire hazard of mine conveyor belts. 5th U.S. Mine Ventilation Symp., West Virginia, pp 69-73.

Verakis, H.C. and Dalzell, R.W. (1988). Impact of entry air velocity on the fire hazard of conveyor belts. 4th Int. Mine Ventilation Congress, Brisbane, Australia, pp 375-381.

Wala, A.M. (1998). Teaching the principles of mine fire using computer-aided instruction. Computer Applications in Engineering Education, Vol. 5, Issue 4 pp 249-255.

Wu H.W. and Gillies A.D.S. (2006). Queensland mine emergency level exercises assisted by fire simulation. 11th U.S./North American Mine Ventilation Symposium. pp.351-358.

Willett, H.L. (1951). Gas analysis behind stoppings. Trans. Inst. of Mining Engrs., Vol. 111, p 629.

Zabetakis, M.G. et al (1959). Determining the explosibility of mine atmospheres. U.S. Bureau of Mines, IC 7901, pp 11.

Zabrosky, C.E. and Klinefelter, G. (1988). Microcomputers assist in extinguishing a bituminous coal mine fire. 4th Int. Mine Ventilation Congress, Brisbane, Australia, pp 337-344.

Zipf, R.K., Sapko, M.J. and Brune, J.F. (2007). NIOSH Informational Circular 9500, Explosion pressure design criteria for new seals in U.S. coal mines. 76 pp.
<http://www.cdc.gov/niosh/mining/pubs/pubreference/outputid2477>.